Colorado River Environmental Models

Phase 2: Lake Travis

Final Report

Prepared for:

Lower Colorado River Authority

Austin, TX

Prepared by:

Anchor QEA, LLC

Austin, TX

In conjunction with:

Parsons Water and Infrastructure, Inc.

Austin, TX

March 18, 2009
Revised May 11, 2009

Colorado River Environmental Models

Phase 2: Lake Travis

Final Report

Prepared for:

Lower Colorado River Authority

Austin, TX

Prepared by:

Anchor QEA, LLC

Austin, TX

In conjunction with:

Parsons Water and Infrastructure, Inc.

Austin, TX

Job Number:

PARcrm:161

March 18, 2009
Revised May 11, 2009

Table of Contents

SECTION 1 INTRODUCTION 1-1
1.1 BACKGROUND 1-1
1.1.1 Lake Travis System 1-2
1.1.2 Relevant Ordinances 1-3
1.1.2.1 Highland Lakes Discharge Ban 1-3
1.1.2.2 Lake Travis Non-point Source Pollution Control Ordinance 1-3
1.2 SUMMARY OF THE PHASE 1 LAKE TRAVIS EFFORT 1-4
1.3 OBJECTIVES OF CREMS AND THE PHASE 2 LAKE TRAVIS EFFORT 1-5
1.4 OVERVIEW OF PHASE 2 REPORT 1-7

SECTION 2 MONITORING PROGRAM 2-1
2.1 OVERVIEW 2-1
2.2 PROGRAM 1: EXPANDED ROUTINE MONITORING 2-1
2.2.1 Expanded List of Parameters 2-3
2.2.1.1 Laboratory Parameters 2-3
2.2.1.2 Additional Field Parameters 2-4
2.2.2 Higher Resolution Sampling at Boundaries 2-5
2.2.3 Higher Resolution Sampling in the Lake 2-6
2.2.4 Additional Lake Stations 2-6
2.2.5 Additional Tributary Stations 2-6
2.2.6 Flow Rate in the Pedernales River 2-7
2.2.7 Expanded Vertical Sampling 2-7
2.2.8 Lower Detection Limits 2-8
2.3 PROGRAM 2: STORMWATER MONITORING 2-8
2.3.1 Storm Types and Sampling Frequency 2-9
2.3.2 Tributary and Lake Stations 2-10
2.4 PROGRAM 3: REMOTE MONITORING 2-11
2.4.1 Thermistor Chains 2-11
2.4.2 Automated Profilers 2-12
2.5 PROGRAM 4: SPECIAL MANUAL MONITORING 2-13
2.5.1 Boat-mounted Flow-through Data Collection 2-13
2.5.2 Phytoplankton Investigation Study 2-14
2.5.3 Sediment Characterization 2-14

SECTION 3 WATERSHED MODEL 3-1
3.1 INTRODUCTION 3-1
3.2 LAKE TRAVIS WATERSHED CONCEPTUAL MODEL 3-1
3.2.1 Spatial Domain and Model Development 3-1
3.3 MODEL OVERVIEW 3-3
3.3.1 Model Time Period and Timestep 3-4
3.3.2 Model Structure 3-5
3.3.2.1 Climatic Inputs and HRU Hydrologic Balance 3-5
3.3.2.2 Cropping, Management Inputs, and HRU Level Pollutant Losses 3-6
3.3.2.3 Flow and Pollutant Loss Routing 3-8
3.3.3 State Variables of Concern 3-8

3.4 MODEL INPUTS 3-9
3.4.1 Time Series Input Data 3-9
3.4.2 Geospatial Input Data 3-10
3.5 CALIBRATION 3-11
3.5.1 Hydrology Calibration Approach 3-12
3.5.2 Water Quality Calibration Approach 3-14
3.5.3 Calibration Results 3-16
3.6 WATERSHED MODEL SENSITIVITY ANALYSIS 3-22

SECTION 4 LAKE MODEL 4-1
4.1 INTRODUCTION 4-1
4.1.1 Spatial Domain and Model Segmentation 4-1
4.1.2 Model Time Period 4-2
4.1.3 General Processes Modeled 4-3
4.1.4 Calibration Metrics and Goals 4-4
4.2 MODEL OVERVIEW 4-4
4.2.1 State Variables of Concern 4-4
4.3 WATER BALANCE 4-6
4.3.1 Inputs 4-6
4.4 HYDRODYNAMICS AND TEMPERATURE MODEL DEVELOPMENT AND CALIBRATION 4-7
4.4.1 Model Inputs 4-7
4.4.1.1 Initial Conditions 4-7
4.4.1.2 Flows 4-7
4.4.1.3 Boundary Temperatures 4-8
4.4.2 Model Parameterization 4-9
4.4.3 Hydrodynamic and Temperature Calibration 4-10
4.4.3.1 Approach 4-10
4.4.3.2 Calibration Data 4-10
4.4.3.3 Calibration Results 4-10
4.5 WATER QUALITY MODEL DEVELOPMENT AND CALIBRATION 4-13
4.5.1 Model Inputs 4-13
4.5.1.1 Initial Conditions 4-13
4.5.1.2 Boundary Concentrations 4-14
4.5.1.3 Sediment Fluxes 4-19
4.5.2 Water Quality Calibration 4-20
4.5.2.1 Approach 4-20
4.5.2.2 Calibration Data 4-20
4.5.2.3 Calibration Results 4-21
4.5.3 MODEL PERFORMANCE IN COVES 4-32
4.6 WATER QUALITY MODEL SENSITIVITY ANALYSIS AND BOUNDING CALIBRATION 4-33
4.6.1 Sensitivity Analysis 4-33
4.6.2 Bounding Calibration 4-38

SECTION 5 MODEL LINKAGE 5-1
5.1 INTRODUCTION 5-1

5.2 MODEL SPATIAL LINKAGES 5-1
5.3 DECONVOLUTION OF SWAT TO CE-QUAL-W2 STATE VARIABLES 5-3
5.3.1 Inorganics 5-4
5.3.1.1 Inorganic Suspended Solids 5-4
5.3.1.2 Bioavailable Phosphorus 5-4
5.3.2 Nitrogen 5-5
5.3.2.1 Ammonia 5-5
5.3.2.2 Nitrate + Nitrite 5-6
5.3.3 Organic Matter 5-6
5.3.4 Algae 5-8
5.3.5 Dissolved Oxygen 5-9
5.3.6 Incorporating Deconvoluted Variables into the Lake Model 5-10

SECTION 6 SUMMARY 6-1

SECTION 7 REFERENCES 7-1

List of Tables

Table 2-1. Program 1 – RSS and expanded RSS monitoring locations.

Table 2-2. Program 1 – List of measured and calculated parameters.

Table 2-3. Program 2 – Storm monitoring locations and number of monitoring events.

Table 2-4. Program 2 – Summary of storm sampling.

Table 2-5. Program 3 – Summary of remote sampling.

Table 3-1. TCEQ permitted dischargers within the Lake Travis watershed.

Table 3-2. NOAA weather stations used in the Phase 2 watershed model.

Table 3-3. Calibration stations for Lake Travis watershed model.

Table 3-4. SWAT hydrologic calibration parameters.

Table 3-5. Uncertainty associated with rating curve predictions.

Table 3-6. SWAT water quality calibration parameters.

Table 3-7. Monthly hydrologic calibration model fit statistics for primary calibration stations.

Table 3-8. Hydrologic calibration for secondary calibration stations.

Table 3-9. Water quality calibration model fit statistics at Hammett's Crossing.

Table 3-10. Water quality calibration for secondary calibration stations.

Table 3-11. SWAT parameters selected for sensitivity analysis.

Table 3-12. Sensitivity metrics for each SWAT parameter tested.

Table 4-1. Summary of longitudinal segmentation for Lake Travis CE-QUAL-W2 model.

Table 4-2. List of CE-QUAL-W2 state variables used in Lake Travis model.

Table 4-3. Water temperature model performance metrics.

Table 4-4. Model parameters affecting hydrodynamic and thermal calibration.

Table 4-5. Measured water quality parameters at Lake Travis headwaters.

Table 4-6. Calibrated lake model parameters and default/recommended values.

Table 4-7. Water quality model performance metrics for surface layers (top third).

Table 4-8. Lake input parameters tested during sensitivity analysis.

Table 4-9. Root mean square errors for surface water at Mansfield Dam for the original and bounding calibrations.

Table 5-1. Relationship between lake model segments and watershed model subbasins.

List of Figures

Figure 2-1. Lake Travis study area with expanded sampling stations.

Figure 3-1. Lake Travis watershed model with major population centers.
Figure 3-2. Lake Travis watershed model showing upper and lower models.
Figure 3-3. Lake Travis watershed with Digital Elevation Model.
Figure 3-4. Phase 2 CREMs watershed model segmentation.
Figure 3-5. Lake Travis watershed NLCD land use.
Figure 3-6. Lake Travis watershed STATSGO soils.
Figure 3-7. Rating curves predicted by LOADEST for Big Sandy Creek.
Figure 3-8. Rating curves predicted by LOADEST for Cow Creek.
Figure 3-9. Rating curves predicted by QMLE for Bee Creek.
Figure 3-10. Rating curves predicted by LOADEST for the Pedernales River at Hammett's Crossing.
Figure 3-11. Monthly average flow comparison at Fredericksburg.
Figure 3-12. Monthly average flow comparison at Johnson City.
Figure 3-13. Flow cross plot at Fredericksburg.
Figure 3-14. Flow cross plot at Johnson City.
Figure 3-15. Flow comparison at Hammett's Crossing.
Figure 3-16. Total suspended solids comparison at Hammett's Crossing.
Figure 3-17. Total phosphorus comparison at Hammett's Crossing.
Figure 3-18. Orthophosphate comparison at Hammett's Crossing.
Figure 3-19. Organic phosphorus comparison at Hammett's Crossing.
Figure 3-20. Ammonia comparison at Hammett's Crossing.

Figure 3-21. Nitrate and nitrite comparison at Hammett's Crossing.
Figure 3-22. Organic nitrogen comparison at Hammett's Crossing.
Figure 3-23. Flow cross plot at Hammett's Crossing.
Figure 3-24. TSS cross plot at Hammett's Crossing.
Figure 3-25. Total phosphorus cross plot at Hammett's Crossing.
Figure 3-26. Orthophosphate cross plot at Hammett's Crossing.
Figure 3-27. Organic phosphorus cross plot at Hammett's Crossing.
Figure 3-28. Ammonia cross plot at Hammett's Crossing.
Figure 3-29. Nitrate and nitrite cross plot at Hammett's Crossing.
Figure 3-30. Organic nitrogen cross plot at Hammett's Crossing.
Figure 3-31. Influence of sensitivity parameters on flow.
Figure 3-32. Influence of sensitivity parameters on total nitrogen.
Figure 3-33. Influence of sensitivity parameters on total phosphorus.

Figure 4-1. Lake Travis model grid.
Figure 4-2. Conceptual model of Lake Travis water quality dynamics.
Figure 4-3. Model predicted water surface elevations compared to measured data at Mansfield Dam.
Figure 4-4. Temporals of constituent loads to Lake Travis from upstream.
Figure 4-5. Temporals of constituent loads to Lake Travis from Pedernales River.
Figure 4-6. Temporals of constituent loads to Lake Travis from Cow Creek.
Figure 4-7. Temporals of constituent loads to Lake Travis from Bee Creek.
Figure 4-8. Temporals of constituent loads to Lake Travis from Hurst Creek.
Figure 4-9. Temporals of constituent loads to Lake Travis from Big Sandy Creek.
Figure 4-10. Temporals of constituent loads to Lake Travis from Cypress Creek.
Figure 4-11. Temporals of constituent loads to Lake Travis from direct drainage.
Figure 4-12. Percentage contribution by source type for input constituent mass during calibration period.
Figure 4-13. Temporal of model versus data at Mansfield Dam (Segment 93) - Specific Conductivity.

Figure 4-14. Temporal of model versus data at Arkansas Bend (Segment 78) - Specific Conductivity.
Figure 4-15. Temporal of model versus data at Pace Bend (Segment 48) - Specific Conductivity.
Figure 4-16. Temporal of model versus data at Turkey Bend (Segment 28) - Specific Conductivity.
Figure 4-17. Temporal of model versus data at Sandy Creek (Segment 161) - Specific Conductivity.
Figure 4-18. Temporal of model versus data at Mansfield Dam (Segment 93) - Chloride.
Figure 4-19. Temporal of model versus data at Arkansas Bend (Segment 78) - Chloride.
Figure 4-20. Temporal of model versus data at Pace Bend (Segment 48) - Chloride.
Figure 4-21. Temporal of model versus data at Turkey Bend (Segment 28) - Chloride.
Figure 4-22. Temporal of model versus data at Sandy Creek (Segment 161) - Chloride.
Figure 4-23. Temporal of model versus data at Mansfield Dam (Segment 93) – Dissolved Oxygen.
Figure 4-24. Temporal of model versus data at Arkansas Bend (Segment 78) – Dissolved Oxygen.
Figure 4-25. Temporal of model versus data at Pace Bend (Segment 48) – Dissolved Oxygen.
Figure 4-26. Temporal of model versus data at Turkey Bend (Segment 28) – Dissolved Oxygen.
Figure 4-27. Temporal of model versus data at Sandy Creek (Segment 161) – Dissolved Oxygen.
Figure 4-28. Temporal of model versus data at Mansfield Dam (Segment 93) – Chlorophyll-a.
Figure 4-29. Temporal of model versus data at Arkansas Bend (Segment 78) – Chlorophyll-a.
Figure 4-30. Temporal of model versus data at Pace Bend (Segment 48) – Chlorophyll-a.
Figure 4-31. Temporal of model versus data at Turkey Bend (Segment 28) – Chlorophyll-a.
Figure 4-32. Temporal of model versus data at Sandy Creek (Segment 161) – Chlorophyll-a.
Figure 4-33. Comparison of summertime predicted and measured chlorophyll-a concentrations.
Figure 4-34. Temporal of model versus data at Mansfield Dam (Segment 93) – Total Organic Carbon.

Figure 4-35. Temporal of model versus data at Arkansas Bend (Segment 78) – Total Organic Carbon.
Figure 4-36. Temporal of model versus data at Pace Bend (Segment 48) – Total Organic Carbon.
Figure 4-37. Temporal of model versus data at Turkey Bend (Segment 28) – Total Organic Carbon.
Figure 4-38. Temporal of model versus data at Sandy Creek (Segment 161) – Total Organic Carbon.
Figure 4-39. Temporal of model versus data at Mansfield Dam (Segment 93) – Total Kjeldahl Nitrogen.
Figure 4-40. Temporal of model versus data at Arkansas Bend (Segment 78) – Total Kjeldahl Nitrogen.
Figure 4-41. Temporal of model versus data at Pace Bend (Segment 48) – Total Kjeldahl Nitrogen.
Figure 4-42. Temporal of model versus data at Turkey Bend (Segment 28) – Total Kjeldahl Nitrogen.
Figure 4-43. Temporal of model versus data at Sandy Creek (Segment 161) – Total Kjeldahl Nitrogen.
Figure 4-44. Temporal of model versus data at Mansfield Dam (Segment 93) – Ammonia.
Figure 4-45. Temporal of model versus data at Arkansas Bend (Segment 78) – Ammonia.
Figure 4-46. Temporal of model versus data at Pace Bend (Segment 48) – Ammonia.
Figure 4-47. Temporal of model versus data at Turkey Bend (Segment 28) – Ammonia.
Figure 4-48. Temporal of model versus data at Sandy Creek (Segment 161) – Ammonia.
Figure 4-49. Temporal of model versus data at Mansfield Dam (Segment 93) – Nitrate+Nitrite.
Figure 4-50. Temporal of model versus data at Arkansas Bend (Segment 78) – Nitrate+Nitrite.
Figure 4-51. Temporal of model versus data at Pace Bend (Segment 48) – Nitrate+Nitrite.
Figure 4-52. Temporal of model versus data at Turkey Bend (Segment 28) – Nitrate+Nitrite.
Figure 4-53. Temporal of model versus data at Sandy Creek (Segment 161) – Nitrate+Nitrite.
Figure 4-54. Temporal of model versus data at Mansfield Dam (Segment 93) – Total Phosphorus.

Figure 4-55. Temporal of model versus data at Arkansas Bend (Segment 78) – Total Phosphorus.
Figure 4-56. Temporal of model versus data at Pace Bend (Segment 48) – Total Phosphorus.
Figure 4-57. Temporal of model versus data at Turkey Bend (Segment 28) – Total Phosphorus.
Figure 4-58. Temporal of model versus data at Sandy Creek (Segment 161) – Total Phosphorus.
Figure 4-59. Temporal of model versus data at Mansfield Dam (Segment 93) – Orthophosphate.
Figure 4-60. Temporal of model versus data at Arkansas Bend (Segment 78) – Orthophosphate.
Figure 4-61. Temporal of model versus data at Pace Bend (Segment 48) – Orthophosphate.
Figure 4-62. Temporal of model versus data at Turkey Bend (Segment 28) – Orthophosphate.
Figure 4-63. Temporal of model versus data at Sandy Creek (Segment 161) – Orthophosphate.
Figure 4-64. Sensitivity of chlorophyll-a predictions at Mansfield Dam, Lake Travis to 18 input parameters of the CE-QUAL-W2 model during summer months in surface waters.
Figure 4-65. Sensitivity of orthophosphate predictions at Mansfield Dam, Lake Travis to 18 input parameters of the CE-QUAL-W2 model during summer months in surface waters.
Figure 4-66. Sensitivity of chlorophyll-a predictions at Mansfield Dam, Lake Travis to 6 loading inputs of the CE-QUAL-W2 model during summer months in surface waters.
Figure 4-67. Sensitivity of orthophosphate predictions at Mansfield Dam, Lake Travis to 6 loading inputs of the CE-QUAL-W2 model during summer months in surface waters.
Figure 4-68. Temporal of model versus data at Mansfield Dam (Segment 93) – Specific Conductivity – Bounding calibration.
Figure 4-69. Temporal of model versus data at Mansfield Dam (Segment 93) – Chloride – Bounding calibration.
Figure 4-70. Temporal of model versus data at Mansfield Dam (Segment 93) – Dissolved Oxygen – Bounding calibration.

Figure 4-71. Temporal of model versus data at Mansfield Dam (Segment 93) – Chlorophyll-a – Bounding calibration.
Figure 4-72. Temporal of model versus data at Mansfield Dam (Segment 93) – Total Organic Carbon – Bounding calibration.
Figure 4-73. Temporal of model versus data at Mansfield Dam (Segment 93) – Total Kjeldahl Nitrogen – Bounding calibration.
Figure 4-74. Temporal of model versus data at Mansfield Dam (Segment 93) – Ammonia – Bounding calibration.
Figure 4-75. Temporal of model versus data at Mansfield Dam (Segment 93) – Nitrate+Nitrite – Bounding calibration.
Figure 4-76. Temporal of model versus data at Mansfield Dam (Segment 93) – Total Phosphorus – Bounding calibration.
Figure 4-77. Temporal of model versus data at Mansfield Dam (Segment 93) – Orthophosphate – Bounding calibration.

Figure 5-1. Watershed and lake model segmentation for Lake Travis.

List of Appendices

Appendix A. Colorado River Environmental Models Lake Travis Phase II Monthly In-Field Chlorophyll-a Measurements.
Appendix B. Seasonal Phytoplankton – Zooplankton Dynamics in Lake Travis, Texas.
Appendix C. Tarrant Soils in Upper Pedernales Watershed.
Appendix D. Statistical Analysis of Lake Travis Water Quality to Assist CREMs Modeling.
Appendix E. Lake Travis CE-QUAL-W2 Model Review.
Appendix F. CE-QUAL-W2 Upstream Loading.
Appendix G. SWAT – CE-QUAL-W2 Linkages.
Appendix H. Water Quality Calibration Metrics for the Lake Travis CE-QUAL-W2 Model.
Appendix I. Summary of Selected USGS Phytoplankton Studies on Lake Travis to Assist CREMs Modeling.

Appendix J. Vertical Profiles of Water Temperature, Specific Conductivity, Chloride, Dissolved Oxygen, and Algal Limiting Factor at Mansfield Dam, Arkansas Bend, Pace Bend, Turkey Bend, and Sandy Creek.

List of Acronyms

AG	Algal Growth
AME	Absolute Mean Error
APHA	American Public Health Association
ASAE	American Society of Agricultural Engineers
BASINS	Better Assessment Science Integrating Point and Nonpoint Sources
BIOMIX	Biological Mixing Efficiency
BMP	Best Management Practice
CBOD	Carbonaceous Biochemical Oxygen Demand
CN	Curve Number
COA	City of Austin
CREMs	Colorado River Environmental Models
DEM	Digital Elevation Model
DO	Dissolved Oxygen
EComm	Ecological Communications Corp.
EPCO	Plant Uptake Compensation Factor
EPSC	Evapotranspiration Potential for Plants
ESCO	Soil Evaporation Compensation Factor
ET	Evapotranspiration
GPS	Global Positioning System
HRU	Hydrologic Response Unit
HUC	Hydrologic Unit Code
HUMUS	Hydrologic Unit Model of the United States
ISS	Inorganic Suspended Solids
LCRA	Lower Colorado River Authority
LD	Labile Dissolved

LOADEST	Load Estimator
LOB	Line of Business
LP	Labile Particulate
LTI	Limno Tech, Inc.
MDL	Method Detection Limit
ME	Mean Error
Mg/L	Milligrams per Liter
ML	Milliliters
MUD	Municipal Utility District
MUMAX	Maximum Specific Algal Growth Rate
MUSLE	Modified Universal Soil Loss Equation
NCDC	National Climatic Data Center
NH_3	Ammonia
NLCD	National Land Cover Dataset
NO_2	Nitrite
NO_3	Nitrate
NOAA	National Oceanic and Atmospheric Administration
NO_x	Nitrate + Nitrite
NPS	Non-point Source
NRCS	Natural Resource Conservation Service
OrgN	Organic Nitrogen
OrgP	Organic Phosphorus
P_UPDIS	Phosphorus Uptake Distribution Parameter
PO_4	Orthophosphate
PSP	Phosphorus Availability Index
PVC	Polyvinyl Chloride
QEA	Quantitative Environmental Analysis, LLC (now Anchor QEA, LLC)
QMLE	Quasi-Maximum Likelihood Estimator
RD	Refractory Dissolved
RI	Reliability Index
RMSE	Root Mean Square Error

ROC	River Operations Center
RP	Refractory Particulate
RSS	Reservoir and Stream Sampling
SLSUBBSN	Average Slope Length
SOD	Sediment Oxygen Demand
STATSGO	State Soil Geographic (Database)
SWAT	Soil and Water Assessment Tool
TCEQ	Texas Commission on Environmental Quality
TKN	Total Kjeldahl Nitrogen
TMDL	Total Maximum Daily Load
TN	Total Nitrogen
TOC	Total Organic Carbon
TP	Total Phosphorus
TSS	Total Suspended Solids
TWC	Texas Water Commission
USACE	United States Army Corp of Engineers
USDA	United States Department of Agriculture
USEPA	United States Environmental Protection Agency
USGS	United States Geological Survey
USLE	Universal Soil Loss Equation
USLE_P	Universal Soil Loss Equation Support Practice Factor
WWTP	Wastewater Treatment Plant

ACKNOWLEDGEMENTS

The Lake Travis Phase 2 model development project was a team effort. Angela Rodriguez, formerly with the Lower Colorado River Authority (LCRA), led the initial Soil and Water Assessment Tool (SWAT) watershed model development. Ruben Solis, also formerly of LCRA, developed the grid segmentation, water balance, and initial hydrodynamic model for the CE-QUAL-W2 model. The final watershed model development and calibration was conducted by Parsons Water and Infrastructure (Parsons). Anchor QEA developed and calibrated the lake water quality model. Monitoring conducted to support the modeling effort was led by LCRA with assistance from Ecological Communications (EComm). Mimi Wallace and Richard Kiesling of the United States Geological Survey (USGS) conducted monitoring of algae and sediment flux in the system. Dr. Scott Wells of Portland State University and Dr. R. Srinivasan of Texas A&M University provided assistance in the calibration of the hydrodynamic model and development of the watershed model, respectively. LCRA staff, including Lisa Hatzenbuehler, John Wedig, Bryan Cook, Dave Bass, Karen Bondy, and Suzanne Zarling, provided guidance and feedback throughout the project.

SECTION 1
INTRODUCTION

1.1 BACKGROUND

The Lower Colorado River Authority (LCRA) initiated development of mathematical models to support water quality management of the Lower Colorado River system. This project, referred to as the Colorado River Environmental Models (CREMs) project, was designed to help diagnose existing water quality problems and issues, discern water quality trends, and predict the consequences of various management decisions and associated actions on the water quality of the Highland Lakes, Lower Colorado River, and its tributaries. The modeling tools are being designed to provide the information needed by LCRA staff and management to support policy decisions that proactively and effectively protect the integrity of the water resources in the Lower Colorado River basin.

The CREMs project has three phases: Phases 1 and 2 focus on Lake Travis, which was selected during the prioritization process described in the *CREMs Master Plan* (CH2MHill 2002). Phase 3, which commenced in 2008, focuses on Lakes LBJ, Inks, and Marble Falls. The selection of Lake Travis for Phases 1 and 2 was based on the need to support the evaluation of the Lake Travis non-point source (NPS) pollution control ordinance and to address community questions regarding the effectiveness of the Texas Commission on Environmental Quality's (TCEQ) wastewater discharge ban (also known as the point source discharge ban or the Highland Lakes discharge ban). Phase 1 assessed Lake Travis water quality using existing data to develop a simplified model of the reservoir and watershed. Details on the Phase 1 work can be found in the *Phase 1 Lake Travis Model Report* (LCRA 2004). Phase 2 involves acquiring additional water quality data and developing refined watershed and water quality models of the lake.

1.1.1 Lake Travis System

Lake Travis is the fifth in a series of six reservoirs on the Lower Colorado River known as the Highland Lakes and was created by the construction of Mansfield Dam in 1941 (Figure 1-1). Lake Travis is a flood control reservoir, but it also provides drinking water, power, and recreation for Central Texas and irrigation water for agriculture on the Texas coast.

At a conservation pool elevation of 681 feet (ft.; 206 m) above mean sea level, Lake Travis holds 1,132,172 acre-feet (1.4 x 109 cubic meters [m^3]) of water and covers an area of 18,622 acres (75 square kilometers [km^2]). It is a sinuous lake, winding roughly 62 river miles (100 km) through the central Texas Hill Country. It is less than 0.1 miles (161 meters [m]) wide in the upper reaches of the lake and widens to more than 1.3 miles (2160 m) near Mansfield Dam. When it is at its conservation pool elevation, the deepest point is more than 180 ft. (55 m) in the thalweg near Mansfield Dam. Depths decrease to nearly 150 ft. (46 m) at Arkansas Bend, 90 ft. (27 m) at Pace Bend, 60 ft. (18 m) at Turkey Bend, and 40 ft. (12 m) at the headwaters near Max Starcke Dam. The drainage area between Mansfield Dam and Max Starcke Dam covers 1,751 mi^2 (4,535 km^2). Mean annual rainfall across the drainage basin varies from nearly 32 inches (in.; 0.8 m) at Mansfield Dam to approximately 21 in. (0.5 m) in the upper reaches of the basin in West Texas.

Lake Travis water quality is ranked among the best for Texas reservoirs. The lake provides swimming, boating, fishing, wind-surfing, and scuba diving recreation, and supplies drinking water for the City of Austin (COA) and other municipalities. It discharges into Lake Austin, which in turn discharges to Lady Bird Lake, both small reservoirs with short retention times that the COA uses as a source of drinking water. Lake Austin and Lady Bird Lake are prime recreational attractions for Austin residents and visitors. Until 2007, Lady Bird Lake also provided cooling water for the Holly Power Plant, one of the city's electric generation facilities, now retired.

Lake Travis is an oligo-mesotrophic system with relatively low to moderate levels of algae. Average chlorophyll-*a* concentrations in the epilimnion (upper layer of the stratified reservoir) are well below 0.01 milligrams per liter (mg/L) year-round. Nutrient concentrations

are similarly low with measured epilimnetic orthophosphate concentrations generally below the method detection limit (currently 0.01 mg/L). Historically, algal blooms occurred in Lake Travis particularly following storm events, but these blooms were typically short in duration and isolated to the cove regions of the reservoir. However, over the last several spring and summer seasons, algae blooms have become more frequent and severe.

1.1.2 Relevant Ordinances

One of the primary missions of LCRA is to ensure that water quality of the Lower Colorado River tributaries and reservoirs will support fishing, swimming, and public water supply uses with no degradation in key indicators from 1998 levels. Reservoir and watershed management approaches to protecting Lake Travis water quality include TCEQ's ban on point source discharges and LCRA's implementation of the NPS pollution ordinance. Water quality modeling is critical to understanding important processes in Lake Travis relevant to protecting water quality and to evaluating the benefits provided by the Lake Travis and Highland Lakes discharge ban and NPS pollution ordinances.

1.1.2.1 Highland Lakes Discharge Ban

In order to protect and maintain the existing water quality of the Highland Lakes, the Texas Water Commission (TWC; a predecessor to TCEQ) adopted regulations in October 1986 prohibiting new or expanded discharges of wastewater treatment plant (WWTP) effluent into the Highland Lakes or their tributaries within 10 stream miles of the lakes. Details of the discharge ban to Lake Travis can be found in Chapter 311, Subchapter A of the Texas Administrative Code.

1.1.2.2 Lake Travis Non-point Source Pollution Control Ordinance

LCRA responded to the threat of pollution resulting from a construction boom around the Highland Lakes in the early 1990's with a NPS pollution control ordinance. The ordinance was the first in the state to be implemented by a river authority to address NPS pollution or

stormwater runoff, targeting three key pollutants: total suspended solids, total phosphorus, and oil and grease. The Lake Travis NPS Pollution Control Ordinance (also referred to as the Highland Lakes Watershed Ordinance), enacted in February 1990, requires from 70% to 90% removal of pollutants from NPS runoff from the Lake Travis watershed in Travis County. It is a performance-based ordinance, meaning that developers and landowners must show that the water quality standards will be met before proceeding with a project. The ordinances apply to all new construction; property platted before the ordinance went into effect is exempt.

1.2 SUMMARY OF THE PHASE 1 LAKE TRAVIS EFFORT

The principal objective of the Phase 1 Lake Travis modeling effort was to develop a mathematical tool to project long-term and large-scale water quality impacts associated with changes in watershed land use. The watershed model was a derivative of PLOAD (see BASINS documentation for an explanation of PLOAD; United States Environmental Protection Agency [USEPA] 2001) and used simplified approaches to estimate watershed hydrologic and pollutant loadings. The reservoir model consisted of a custom, nine-segment model that simulates nitrogen, phosphorus, and chlorophyll-*a* dynamics in a simplified kinetic framework (LCRA 2004).

The Phase 1 data analysis and modeling effort provided the following insights into the Lake Travis system:

- Data:
    - the Phase 1 dataset has limitations with regard to model development (e.g., lack of: storm event data, on-lake wind information, light attenuation measurements, phytoplankton speciation, phytoplankton photosynthesis and respiration data, and cove, metalimnion, and phytoplankton bloom data);
    - low concentrations of nutrients and phytoplankton (many below the method detection limits) complicate the discernment of spatial and temporal trends;
    - certain land use types and areas disproportionately contribute to NPS loadings; and

- additional monitoring data were necessary to support the Phase 2 modeling effort.

- Model:
  - upstream source loads are important water quality drivers;
  - the Phase 1 model was not sufficiently refined to detect temporally and spatially localized water quality impacts of existing nutrient loads; and
  - Lake Travis experiences both nitrogen and phosphorus limitations, as well as co-limitation.

The Phase 1 model can be used to predict long-term, system-wide changes in phytoplankton concentration as a result of changes in land use. However, it cannot be used to predict changes in the duration, extent, and severity of phytoplankton blooms, nor can the Phase 1 model discern what is occurring in the coves of Lake Travis. Algal blooms within the coves are potentially more important to stakeholders than overall lake average phytoplankton concentrations, as the public strongly associates blooms with degradation of water quality and impairment of recreational opportunities. Hence, while the Phase 1 modeling effort provided valuable insights into the relationships between watershed land use changes and Lake Travis water quality as well as preliminary quantification of hydrologic and nutrient budgets, it lacked the spatial resolution to define localized water quality impacts of potential watershed land use changes. The Phase 2 modeling effort was designed to address these shortcomings.

1.3 OBJECTIVES OF CREMS AND THE PHASE 2 LAKE TRAVIS EFFORT

The principal goal of the Phase 2 Lake Travis modeling effort was to develop a comprehensive, linked watershed and water quality modeling tool of the Lake Travis system. The model will ultimately be applied to investigate system responses (both lake and watershed) to projected growth and/or proposed water quality management practices. Specifically, the Phase 2 model was developed to:

- evaluate the effectiveness of the NPS ordinance in protecting Lake Travis water quality;

- assess the effectiveness of the TCEQ point source discharge ban in protecting Lake Travis water quality;
- identify and quantify trends in specific water quality indicators (long-term, seasonal, and short-term);
- quantify differences in water quality between the main body of Lake Travis and its coves;
- evaluate the impacts of land use changes on the quality and quantity of runoff and resulting impacts on the lake and watershed;
- assess the impacts of existing point source discharges on the water quality of Lake Travis;
- evaluate the relative contribution of anthropogenic and natural background sources of nutrients to observed water quality trends;
- predict the impacts of potential water quality restoration projects;
- assess the impacts of water quality changes on recreational uses of the lakes;
- predict the impacts of various basin-wide best management practice (BMP) implementation strategies;
- evaluate post-flood water quality and recovery;
- identify tributaries with the highest nutrient loadings;
- evaluate water quality trends with respect to drinking water source issues;
- assist in spill and response planning for source water protection;
- provide an understanding of the sedimentation processes and changes in watershed stream morphology associated with land use changes or management practices;
- supply information to facilitate the identification of locations for water intakes;
- assist in the regulatory establishment of nutrient standards;
- aid in assessments of trihalomethane precursors, chemical spills and releases, and pathogens;

- support river/lake operations;
- evaluate the impact of the Pedernales River brush control project on the Lake Travis water balance and water quality;
- expand competency of internal LCRA staff with respect to watershed and water quality management and modeling issues; and
- identify and guide potential future water quality protection and restoration projects on the Highland Lakes.

Various LCRA lines of business (LOBs) have established many of these issues as high priority items, as documented in the CREMs Master Plan (CH2M Hill 2002). As such, the Lake Travis Phase 2 model is a valuable tool for providing information to guide management decisions that are central to the LCRA's mission statement and operational goals. In the short term, the priority application of the models was to understand the effects of the NPS ordinance and TCEQ's Highland Lakes Discharge Ban on water quality (see Anchor QEA and Parsons 2009 for a discussion of the predicted water quality impacts should these two policies change), although these other long-term objectives were considered throughout model development and application.

1.4 OVERVIEW OF PHASE 2 REPORT

The purpose of this report is to describe the Phase 2 program, including Lake Travis monitoring, model development, and model calibration. It contains five additional sections. Section 2 summarizes the Phase 2 sampling efforts on Lake Travis, including sampling conducted by LCRA and the United States Geological Survey (USGS). Sections 3 and 4 discuss the model development and calibration for the watershed and lake models, respectively. Each section also includes analyses performed with regard to model sensitivity and uncertainty. Section 5 provides the details on the linkage of the two models. Section 6 summarizes the work and provides conclusions. Several appendices are included that further document the field studies (Appendices A, B, and I), data analyses/model set-up (Appendices C, D, F, and G), and model review (Appendices E, H, and J).

SECTION 2
MONITORING PROGRAM

2.1 OVERVIEW

The purpose of the Phase 2 monitoring effort was to develop a more complete dataset for supporting the development and calibration of the Lake Travis watershed and water quality models. The Phase 2 monitoring supplemented the existing data record (and existing monitoring program) by providing information to develop and calibrate a more complex model of Lake Travis and its surrounding watershed than was able to be developed under the Phase 1 modeling effort. For Phase 2, four monitoring programs were designed and implemented: 1) expanded routine monitoring; 2) storm event monitoring; 3) special remote monitoring studies; and 4) special manual sampling studies. Each program started after the completion of Phase 1 in 2004 and ended before the development and calibration of the Phase 2 model, with varying durations of each monitoring program. Details of each monitoring program are presented in this section. Additional details on the monitoring can be found in the *Lake Travis Phase 2 Work Plan* (Quantitative Environmental Analysis, LLC [QEA] et al. 2003).

2.2 PROGRAM 1: EXPANDED ROUTINE MONITORING

The Phase 2 ambient sampling and analysis program was an expansion of the current Reservoir and Stream Sampling (RSS) program, which provides a long-term record and satisfies LCRA and state requirements independent of the CREMs program. From 1982 to the early 1990's, data were collected monthly in the LCRA basin through the RSS program. The existing RSS program includes collection of water samples and field data at five stations in Lake Travis every other month (Figure 2-1), as well as measurements of field parameters at two additional stations and collection of water samples and field data at three stations at the model boundaries. Similar to the existing RSS program, the expanded routine monitoring program was limited to regularly scheduled sampling (i.e., it did not target high flow events). Specific components of the expanded monitoring included measuring additional parameters, increasing the sampling

temporal resolution at the boundaries and in the lake, and sampling additional stations in the lake and the tributaries. The expanded routine monitoring program started in January 2004 and ended in December 2006 after which the existing RSS program sampling regime resumed.

As part of CREMs Phase 2, data were collected at an additional seven sites within the lake and five sites within its tributaries (Figure 2-1). Table 2-1 lists sampling stations that were monitored during Phase 2. These additional sites are discussed in Section 2.2.4 and 2.2.5.

Table 2-1. Program 1 – RSS and expanded RSS monitoring locations.

Site	Site ID[5]	RSS	Expanded RSS	Number of Sampling Events (during the Phase 2 monitoring period; 2004-2006)
LAKE				
Travis at Mansfield Dam	12302	x		35
Travis at Cypress Creek Cove	12304		x	36
Travis at Sandy/Lime Creeks	12307	x		36
Travis at Starnes Island	LC901		x	36
Travis at Arkansas Bend	12309	x		36
Travis at Hurst Creek Cove	15428		x	36
Travis at Anderson Bend	12311	x[1]		37
Travis at Bee Creek Cove	LC902		x	36
Travis at Thurman Bend	LC903		x	36
Travis at Pace Bend	12313	x		36
Travis at Cow Creek Cove	LC909		x	37
Travis at Pedernales Bend	LC908		x	36
Travis at Carpenter Bend	12315	x[1]		36
Travis at Turkey Bend	12316	x		36
BOUNDARY				
Travis at Headwaters[2]	12318	x		186
Pedernales at Hammett's Crossing	12369	x		152
Lake Austin at Tail Race	12300	x		152
TRIBUTARY				
Cypress Creek	15429		x	36
Sandy Creek	LC905		x	19
Hurst Creek	LC904		x	36
Bee Creek[3]	LC907		x	17
Cow Creek	LC906		x	35

Notes:
[1] Field parameters measured only.
[2] Site is considered a boundary site for this report, but it is also considered to be within the main lake.
[3] Site dry most of 2005.
[4] Lake and tributary sites sampled monthly; boundary sites sampled weekly. Sampling frequency at Lake Austin at Tail Race increased to weekly during Phase 2.
[5] See Figure 2-1 for map of monitoring locations.

Throughout this monitoring program, the main lake and tributary stations (including coves) were sampled at the top (0.33 m from the water surface) and bottom (1 m above the sediments) of the water column, as the existing protocols state. In addition, when a defined thermocline was present, an additional water quality sample was collected at that location (Section 2.2.7). Tributary stations were sampled once at mid-depth.

2.2.1 Expanded List of Parameters

2.2.1.1 Laboratory Parameters

Two laboratory parameters, dissolved organic carbon and dissolved phosphorus, were added to the suite of parameters being analyzed under the routine monitoring program (Table 2-2). These were added so that the dynamics between the particulate and dissolved forms of organic matter could be defined better within the lake model. Ideally, particulate organic carbon and particulate nitrogen would also be measured directly (particulate phosphorus is difficult to measure directly), but due to limited resources, their concentrations were calculated as the difference between the measured total and measured dissolved concentrations. For the measurement of dissolved constituents, filtration followed the procedures outlined in Standard Methods (American Public Health Association [APHA] 1998). The data were reported as low as the method detection limit (MDL), which varies for each laboratory calibration of the analytical instrument (Table 2-2).

Table 2-2. Program 1 – List of measured and calculated parameters.

Parameter[1,2]	STORET	Units	Detection or Precision[3]
MEASURED IN FIELD			
Light extinction	L1001	μmol s^{-1} m^{-2}	0.4%
Oxygen, dissolved	00300	mg/L	0.20
Oxygen, % saturation	00301	%	-
pH	00400	SU	0.20
Secchi depth	00078	m	-
Solar radiation (total)	-	Wm^{-2}	-
Specific conductance	00094	μS/cm	1%
Temperature, air	00020	°C	0.20
Temperature, water	00010	°C	0.05
Turbidity	82078	NTU	1%
Wind direction	L1003	°	-
Wind speed	L1002	mph	-
MEASURED IN LABORATORY			
Alkalinity, total	00410	mg/L	0.32
Chloride	00940	mg/L	0.08
Chlorophyll-a	70953	μg/L	0.02
Ammonia, nitrogen	00610	mg/L	0.005
Nitrite plus nitrate, nitrogen	00630	mg/L	0.004
Organic carbon, dissolved	00681	mg/L	0.03
Organic carbon, total	00680	mg/L	0.03
Pheophytin	32113	μg/L	0.5
Kjeldahl nitrogen, dissolved	00623	mg/L	0.006
Kjeldahl nitrogen, total	00625	mg/L	0.006
Phosphorus, dissolved	00666	mg/L	0.005
Phosphorus, ortho	00671	mg/L	0
Phosphorus, total	00665	mg/L	0.005
Sulfate	00945	mg/L	0.02
Suspended solids, total	00530	mg/L	0.5
CALCULATED			
Dissolved solids, total	70952	mg/L	-
Nitrogen, particulate	-	mg/L	-
Organic carbon, particulate	-	mg/L	-
Phosphorus, particulate	-	mg/L	-

Notes:
[1] Parameters added in Expanded RSS shown in bold italics.
[2] Bacteria were collected only in even months to support routine monitoring.
[3] The MDL for each laboratory analyte may vary each time the analytical instrument is calibrated.

2.2.1.2 Additional Field Parameters

Three field parameters – solar radiation, wind direction, wind speed – were added to the suite of parameters measured under the routine monitoring program (Table 2-2). Concentrations for one additional parameter, total dissolved solids, were calculated from the lake specific relationship with specific conductance developed by LCRA.

Solar radiation controls photosynthesis and the temperature cycle of the lake and is a forcing function for the hydrodynamic and water quality calculations in the lake model. Light penetration must also be known and is described by two factors: 1) the fraction of light absorbed/reflected in the surface layer; and 2) the light extinction through the water column. Both of these were measured using a light probe (e.g., the LCRA's Li-Cor LI-189 probe). Light was measured above the water surface, immediately below the water surface (at 0.33 m depth), and at one meter intervals through the water column down to 10 m concurrently with samples collected in the reservoir (solar radiation data were not needed in the tributaries).

Due to the importance of wind speed and direction on mixing in Lake Travis, wind data were obtained concurrently with all field samples. This allowed for a point estimate of wind conditions at the time of sampling. These measurements provided information on spatial wind patterns and sheltering over Lake Travis and helped to decrease the uncertainty in specifying wind energy at the lake surface. Wind data were collected with a portable field sensor at 2 m above the water surface concurrently with all water samples collected in the reservoir (collection of wind data in the tributaries was not needed).

2.2.2 Higher Resolution Sampling at Boundaries

The refined temporal resolution of the Phase 2 model required high resolution data at the model boundaries; the two most important boundaries are the upstream boundary and the Pedernales River. The upstream boundary condition was specified using data collected below Max Starcke Dam (Station 12318, Travis Reservoir at the Headwaters). These data were used to specify the upstream boundary to the reservoir model (Section 4.5.1.1.2). The Pedernales River boundary to the reservoir model was specified in the watershed model, which used data from Station 12369 (Pedernales River at FM 962 [Hammett's Crossing]) as a calibration target (Section 3.5.2). Because of the importance of these two stations, weekly sampling was implemented there. Weekly data were also collected at the headwaters of Lake Austin (Station 12300, Lake Austin at Tail Race).

2.2.3 Higher Resolution Sampling in the Lake

To improve the characterization of water quality in Lake Travis, the sampling frequency was increased from bimonthly to monthly at all non-boundary stations. This allowed for a more complete understanding of seasonal trends in water quality throughout the lake.

2.2.4 Additional Lake Stations

Seven new lake sampling stations were added to the program (Table 2-1). Four of these sites were located in different coves of the lake (Cypress Creek Cove, Hurst Creek Cove, Bee Creek Cove, and Cow Creek Cove), two stations were situated in the main body of Lake Travis (Starnes Island and Thurman Bend), and one station was located in the arm of the Pedernales River (Pedernales Bend). The cove stations were located in the Lake Travis pool. Data from these stations facilitated the quantification of water quality in previously unsampled areas of the lake and improved the resolution for calibration of the lake model. For each of these stations, water samples were collected and analyzed for the expanded suite of water quality parameters (Table 2-2) on a monthly basis, in tandem with the other sampling on Lake Travis.

These stations were selected to quantify differences in water quality between the main body of Lake Travis and the most developed coves (e.g., Lakeway which drains into Hurst Cove). Coves further upstream were not selected, as they were assumed to have less significant water quality deviations from the main body of the lake.

2.2.5 Additional Tributary Stations

To improve the quantification of base flow loadings to Lake Travis, the following five tributary stations were added to the sampling program: Cypress Creek, Sandy Creek, Hurst Creek, Bee Creek, and Cow Creek. These stations corresponded with the cove sampling program described above.

The locations of these stations were upstream of the Lake Travis pool, but as far downstream as practicable, given accessibility and flooding constraints. Because these stations were also used as storm event sampling stations (discussed in Section 2.3), they needed to be positioned in areas where they could be safely accessed and protected from loss (vandalism, flooding, etc.). For Cow Creek, the water quality station was co-located with the existing flow gage.

For stations without an established flow gage (similar to the existing Hydromet flow stations), the automated stormwater samplers (Section 2.3) were equipped to determine stream stage. Stage height was measured every ten minutes; site-specific rating curves were used to determine flow from the stage height data. Because these tributaries were not expected to have as high loadings as upstream of Lake Travis or the Pedernales River, water quality sampling occurred monthly in conjunction with the cove sampling. Sampling included the expanded suite of water quality parameters (Table 2-2).

2.2.6 Flow Rate in the Pedernales River

Flow rates of the Pedernales River at Hammett's Crossing were prorated from daily flows measured at the USGS Pedernales River gage at Johnson City using the drainage areas of the two watershed basins contributing to each station (Section 3.5.1).

2.2.7 Expanded Vertical Sampling

The routine monitoring program was expanded to include metalimnion sampling. The metalimnion field data were collected by first identifying the depth at which a half degree Celsius or greater temperature change was measured over a one meter depth interval. A sample of the water in the metalimnion was collected one meter below this point.

2.2.8 Lower Detection Limits

For a number of water quality parameters, lower method detection limits were applied to the Phase 2 monitoring programs compared to those used historically. This was done to facilitate temporal and spatial trend analysis and to support lake model calibration. Table 2-2 contains the parameter specific MDL.

2.3 PROGRAM 2: STORMWATER MONITORING

Storm loadings in flood prone areas such as central Texas can account for a large percentage of the total annual loading to a water body. Such loadings are difficult to quantify due to their transient nature and the level of effort required for collecting samples. Due to the lack of historical storm event data on Lake Travis, such sampling comprised a significant portion of the Phase 2 monitoring effort. Table 2-3 lists the storm monitoring locations and the number of monitoring events.

Table 2-3. Program 2 – Storm monitoring locations and number of monitoring events.

Site	Site ID [1]	Number of Storm Monitoring Events [2]
LAKE		
Travis at Mansfield Dam	12302	5
Travis at Cypress Creek Cove	12304	7
Travis at Sandy/Lime Creeks	12307	7
Travis at Starnes Island	LC901	3
Travis at Arkansas Bend	12309	3
Travis at Hurst Creek Cove	15428	8
Travis at Anderson Bend	12311	4
Travis at Bee Creek Cove	LC902	10
Travis at Thurman Bend	LC903	3
Travis at Pace Bend	12313	3
Travis at Cow Creek Cove	LC909	6
Travis at Pedernales Bend	LC908	11
Travis at Carpenter Bend	12315	5
Travis at Turkey Bend	12316	3
BOUNDARY		
Travis at Headwaters	12318	10
Pedernales at Hammett's Crossing	12369	24
Lake Austin at Tail Race	12300	2
TRIBUTARY		
Cypress Creek	15429	47
Sandy Creek	LC905	21

Site	Site ID [1]	Number of Storm Monitoring Events [2]
Hurst Creek	LC904	32
Bee Creek	LC907	31
Cow Creek	LC906	21

Notes:
[1] See Figure 2-1 for map of monitoring locations.
[2] Multiple monitoring events happened during a single storm.

2.3.1 Storm Types and Sampling Frequency

From August 2004 to July 2006, storm event monitoring captured two types of storms – Type 1 and Type 2. Type 1 storms were defined as small events producing localized runoff over a small time scale. Only the affected tributaries and coves were sampled, as no lake-wide impacts were expected. Type 2 storms were those that were expected to affect most of the Lake Travis watershed and had the potential to produce substantial in-lake changes in water quality because of the large runoff volume (e.g., >2 in. of rain over at least 25% of the Lake Travis watershed). As summarized in Table 2-4, seventeen Type 1 and one Type 2 storm events were captured.

Table 2-4. Program 2 - Summary of storm sampling.

Storm Type	Storm Start Date	Storm Duration (hours)	Approx. Total Rainfall (inches)	Number of Stations Monitored		Number of Samples Collected Over All Stations
				Tributary	Lake	
1	10/2/2004	11	1.7	3	2	15
1	10/23/2004	3	1.6	2	0	8
1	10/26/2004	3	2.5	1	1	4
1	11/1/2004	7	1.4	4	0	15
1	11/15/2004	2	0.6	4	0	4
2	11/17/2004	22	5.7	4	16	137
1	5/9/2005	19	1.2	1	0	1
1	6/1/2005	2	1.0	1	0	2
1	7/27/2005	4	1.2	1	0	3
1	8/5/2005	1	1.0	1	0	1
1	3/20/2006	5	0.8	1	0	1
1	3/28/2006	2	1.8	2	0	8
1	4/20/2006	7	2.7	5	3	22
1	4/29/2006	9	1.2	8	0	4
1	5/4/2006	30	2.9	2	1	47
1	6/17/2006	3	1.1	1	0	11
1	7/4/2006	2	2.1	2	0	3

Sampling of each storm type followed a different protocol. During a Type 1 storm, only tributaries and coves impacted by the storm were sampled. Sampling occurred at 12-hour intervals for the first day and first two days of the storm, respectively. The impacted tributaries were also sampled daily for the next four days. During a Type 2 storm, sampling in coves occurred daily for the first four days and at seven and 14 days following the triggering event. Sampling in tributaries took place daily for the first five days and also seven and 14 days after the storm began. A second sample was also collected during the first day at Cypress, Sandy, Hurst, and Bee Creeks. The main body of the lake was only sampled during a Type 2 storm, with all sites being sampled immediately after reaching the storm trigger level, and then seven and 14 days thereafter.

Starting in August 2004, tributary sampling was initiated based on a prescribed change from base flow that is characteristic of storm events. Immediately after the trigger level was reached, automated storm samplers collected the first flush and then flow composite samples until stream flow returned to pre-storm values. The flow composite method was abandoned after 2004 due to difficulty selecting an appropriate flow volume trigger, which resulted in poor sampling performance. A low trigger level during large storms filled all of the bottles in the automated sampler before the entire hydrograph was sampled, while a higher trigger level caused an under-sampling of smaller storms. As a result, after the November 2004 flood, the automated samplers were programmed to collect first flush samples followed by hourly discrete samples. Based on professional judgment, the number of hourly samples varied depending on the severity of the storm. Between 4 and 16 hourly discrete samples were collected per storm event. In addition, meteorological conditions (a major flood event occurred in November 2004, followed by a drought in 2005 and 2006), coupled with the difficulties in determining and refining a tributary's trigger level for optimal sampling, resulted in the sampling of essentially all rainfall events greater than one inch.

2.3.2 Tributary and Lake Stations

Tributary sampling stations for the storm event monitoring program were co-located with the five tributary monitoring locations in the expanded routine monitoring program described in

Section 2.2.4. This allowed for a comparison between storm and base flow data. Sampling was performed using an ISCO® (or equivalent) automated sampler as well as via grab sampling at boundary locations. Tributary samples were analyzed for the expanded suite of water quality parameters (Table 2-2).

Lake samples (both cove and main body) were collected manually during storm events and were analyzed for the expanded suite of water quality parameters (Table 2-2).

2.4 PROGRAM 3: REMOTE MONITORING

Remote monitoring using automatic sampling devices collect data in a continuous manner over time, which is difficult to accomplish by field teams. The objective of this sampling program was to provide detailed data for the lake model calibration.

Remote data collection equipment was deployed at selected locations to serve a number of purposes. These purposes included helping in the calibration of the Phase 2 models; quantifying the short-circuiting of flood flows and plunging of inflows; measuring stratification and mixing; providing an early warning system to identify algal blooms; and quantifying the occurrence, duration, and intensity of algal blooms. The two types of remote monitoring units used were thermistor chains and automated profilers.

2.4.1 Thermistor Chains

Thermistor chains measure water temperature at multiple depths in the water column. One thermistor chain was installed at each of the stations listed in Table 2-5. The majority of the chains were installed in July 2004 (within the first four months of sampling) and were left in place between one and two years, depending on site location. The units measured temperature every two meters depth at Turkey Bend (12316), Pace Bend (12313), Arkansas Bend (12309), Mansfield Dam (12302), and Sandy/Lime Creeks (12307); at the other stations, only surface temperature was measured. The chains measured temperature each hour. Unfortunately, several thermistor chains were lost to vandalism, entanglement with lake debris, and storm events. In

fact, at all deployment locations except for Pace Bend, the field crew had to replace missing thermistor chains over the course of the monitoring program.

Table 2-5. Program 3 - Summary of remote sampling.

Site	Site ID[1]	Vertical Spacing (m)	Average Water Depth at Site (m)	Number of Thermistors per Chain
Mansfield Dam	12302	2	51	26
Sandy/Lime Creeks	12307	2	20	10
Arkansas Bend	12309	2	42	22
Pace Bend	12313	2	25	13
Turkey Bend	12316	2	16	9
Headwaters	12318	-	1	1
Hammett's Crossing	12369	-	1	1
Cypress Creek	15429	-	0.3	1
Sandy Creek	LC905	-	0.3	1
Hurst Creek	LC904	-	0.3	1
Bee Creek	LC907	-	0.3	1
Cow Creek	LC906	-	0.3	1

Notes:
[1] *See Figure 2-1 for map of monitoring locations.*

2.4.2 Automated Profilers

Automated profilers are remotely programmable field stations with probes suitable for measuring standard field parameters as well as chlorophyll-*a* and turbidity. These systems are also capable of sampling a vertical profile through the water column, not just at a fixed depth. Two automated profilers were installed for this monitoring program, one near Mansfield Dam and one in Sandy/Lime Creek Cove. The one near Mansfield Dam was established to provide information on flow patterns at the dam; stratification, thermocline development, and turnover; oxygen consumption in the hypolimnion; and diurnal fluctuations of dissolved oxygen and pH. The one stationed in Sandy/Lime Creek Cove was set to help identify smaller scale (in both space and time) phytoplankton blooms that have been reported to occur in Lake Travis. The two autoprofilers measured a full vertical profile (every meter) of field parameters, including chlorophyll-*a*, generally every day from February 9, 2005 to February 11, 2007 near Mansfield Dam and February 18, 2005 to December 28, 2006 for Sandy/Lime Creek Cove. Unfortunately, because of the lack of confidence in the data collected by the autoprofilers due to instrumentation issues, the data collected by the automated profilers were not used in the lake model calibration.

An autoprofiler was also planned to be used as an early warning system to trigger manual sampling of blooms and to provide high-resolution sampling during the blooms. When an autoprofiler reported an increase in chlorophyll-*a* levels above background levels, a field crew was to be mobilized to the location and take manual samples. This manual sampling was to occur every 24 hours for the duration of the bloom and include all water quality parameters (Table 2-2). The manual sampling, however, did not occur due to instrumentation problems and other limitations, as well as a lack of substantial algal blooms on the lake during Phase 2 monitoring.

2.5 PROGRAM 4: SPECIAL MANUAL MONITORING

To further constrain the Lake Travis water quality model, special manual field and laboratory studies were conducted. These included boat-mounted, flow-through chlorophyll-*a* monitoring; a phytoplankton investigation study; and sediment characterization.

2.5.1 Boat-mounted Flow-through Data Collection

Measurements of lake-wide phytoplankton distribution occurred monthly from March through June 2006 at 14 locations in Lake Travis. Chlorophyll-*a* was measured in the surface water (up to 1 meter below the water surface) using a Turner Model 10-AU-005-CE portable fluorometer. In addition, for each day in the field, a single water sample was collected for laboratory verification, stored on ice, and analyzed by the LCRA's environmental laboratory. The laboratory results were then used to develop a correction factor that was then applied to the fluorometer measurements collected the same day as the lab sample. The sample sites included Turkey Bend, Carpenter Bend, Pedernales Bend (in the Pedernales River), Cow Creek Cove (in Cow Creek), Pace Bend, Thurman Bend, Bee Creek Cove, Anderson Bend, Hurst Creek Cove, Arkansas Bend, Sandy Creek Cove, Starnes Island, Cypress Creek Cove, and Mansfield Dam. A summary of the sampling and data are provided in Appendix A.

2.5.2 Phytoplankton Investigation Study

The USGS conducted a phytoplankton investigation in Lake Travis between April 2005 and December 2006. Surface water plankton was collected on a monthly basis from six thalweg sites and one cove site (12307) in the reservoir. The six thalweg sites included: 12302 (Mansfield Dam); LC901 (Starnes Island); 12309 (Arkansas Bend); 12313 (Pace Bend); 12315 (Carpenter Bend); and 12316 (Turkey Bend). Phytoplankton composition and abundance and phytoplankton nutrient-dependent growth rates were investigated. More details can be found in the memorandum summarizing the study (Appendix B).

2.5.3 Sediment Characterization

Phase 1 data analysis suggested that sediment diagenesis may be a significant source of internal nutrient loading to Lake Travis. Based on these results, a sediment characterization study was completed by the USGS in October 2006. Sediment box cores were collected from three sites on Lake Travis (12302 [Mansfield Dam], 12307 [Sandy/Lime Creeks], 12309 [Arkansas Bend]) using a Wildco stainless steel box corer (model 191-A12; box size: 150 x 150 x 230 millimeters [mm]) fitted with an acrylic sleeve. Deployed using a small crane fitted with a cable retrieve, the box corer was lowered to approximately 2 to 3 meters above the surface of the sediment and then allowed to free-fall into the sediment. This method permitted full penetration into the soft sediments of the lake while maintaining 4 to 6 cm of overlying water. Cores were brought onto the deck of the boat and immediately sub-sampled using polycarbonate push cores. Four replicate push cores were collected simultaneously from each box core, sealed with polyvinyl chloride (PVC) caps, and stored on ice in an upright position for transport to the laboratory.

In the laboratory, overlying water was sampled with replacement for initial ammonia concentrations. Cores were incubated for 24 hours in the dark under ambient temperature conditions and then the overlying water was sampled for changes in ammonia concentrations. Flux rates were calculated from the average concentrations from the four replicate samples. After being sampled at 24 hours, overlying water was re-filled with 50 milliliters (mL) of

de-ionized water and the cores were incubated for an additional 72 or 96 hours with the overlying water of two of the four replicates sampled at each of the time intervals. Maximum flux rates were calculated from the ammonia concentrations in the overlying de-ionized water. Data from this study are summarized in Appendix C.

SECTION 3
WATERSHED MODEL

3.1 INTRODUCTION

The management tool under development through CREMs consists of a hydrodynamic and water quality model of Lake Travis based upon the U.S. Army Corps of Engineers (USACE) CE-QUAL-W2 model described in Section 4. To effectively use the lake model to meet the modeling objectives identified in Section 1, accurate tributary loadings under a myriad of watershed management scenarios must be specified. This was accomplished through the development and calibration of a mathematical model of the Lake Travis watershed. The watershed model selected for the Phase 2 Lake Travis work is the Soil and Water Assessment Tool (SWAT) model. The watershed model is capable of simulating the constituent loads arising from the watershed and accounting for the various land uses and associated activities. The model is also capable of predicting changes in constituent loads to Lake Travis arising from changes in land use and practices within the watershed and providing a mechanism to tie activities in the Lake Travis watershed to resultant water quality in the lake.

3.2 LAKE TRAVIS WATERSHED CONCEPTUAL MODEL

3.2.1 Spatial Domain and Model Development

The Lake Travis watershed is comprised of the Colorado River watershed from Max Starke Dam to Mansfield Dam, including the main tributary to Lake Travis, the Pedernales River. The watershed is approximately 1,750 square miles (44,030 km^2) and includes a number of incorporated cities and towns. Watershed land use is characterized as predominantly rural and agricultural.

The decision of which watershed model to employ in CREMs was based only in part upon the characteristics of the Lake Travis watershed because the goal of CREMs is to develop

models capable of representing the full spectrum of LCRA's aquatic resources. Ideally, a single watershed model would be used for all of the subject water bodies. A variety of potential modeling frameworks were considered. In some cases, a simple scoping model can be applied to provide general estimates of the risk posed to water quality. Simple models are often useful to estimate runoff flows and contaminant loads to assess relative magnitudes and target areas of greatest risk. In a situation where a high degree of accuracy is not required, this type of modeling can be more cost-effective than monitoring. As an example, simple procedures such as the use of loading coefficients can aid in identifying areas where runoff is greatest, and areas which are likely to generate the largest loads of a particular pollutant. Such modeling is particularly useful for obtaining initial estimates of NPS loads because monitoring non-point runoff flow and pollutant loads is particularly difficult and expensive. However, to meet the objectives of the CREMs project, the watershed and water quality models must be of sufficient resolution to predict future conditions. One of the primary functions of the models developed for CREMs is to aid in evaluating different water quality management options.

The two main sources of NPS loading in the Travis watershed are urban runoff and non-urban runoff. Non-urban areas dominate the land use of the Lake Travis watershed; however, land use area alone does not determining NPS loads. Other factors including land slope, soil characteristics, and ground cover are important determinants of non-point source watershed nutrient and solids loadings. In addition, there are some point sources in the watershed.

The dominant characteristic of urban areas is a high percentage of impervious land cover. Rather than percolating into the soil, precipitation runs off directly from impervious surfaces, which significantly affects the transport of constituents. A common and more sophisticated, yet still simple, approach to estimating pollutant loads generated by urban areas is the use of buildup-wash off models. This approach is predicated on the observation that almost all runoff from urban areas comes from the paved or impervious area, and that most of the polluting material carried in runoff accumulates within 1 m of curbs. In the interval between precipitation events, material accumulates along the curbs. In addition to an increase with time, buildup may be correlated with other variables as well. The amount of wash off of material that occurs in

response to a precipitation event, correlated with rainfall intensity, and the amount of available accumulated solids must be represented in the watershed model.

Non-urban sources of runoff and pollution include agriculture, forestry, and other rural land uses that are generally characterized by pervious surfaces into which water infiltrates. Pollutant loading is often separated into a dissolved component moving with the flow of water, and a sediment associated component that moves with the erosion of sediment. Overland runoff is often estimated with the Natural Resource Conservation Service (NRCS) Curve Number (CN) method. This method relates runoff volume to precipitation volume, antecedent soil moisture conditions, and a NRCS CN. CN is taken from tables compiled by NRCS and depends on land use, land cover, and the hydrologic soil group characteristic of the predominant surface soil.

Erosion from non-urban pervious surfaces is often estimated using the Universal Soil Loss Equation (USLE) or one of its many modifications. The USLE includes factors for rainfall erosivity, soil erodibility, slope length and steepness, and land cover and management. The USLE is designed to predict long-term average rates of soil losses from fields and other land uses. However, the rate of soil loss is not the same as the yield of eroded sediment because a substantial amount of the eroded soil may be trapped or redeposited before reaching a water body. Therefore, in watershed models, the USLE is usually coupled with an estimate of fraction of sediment delivery (delivery ratio).

In many watersheds, delivery of dissolved nutrients via groundwater flux is also significant, particularly for nitrogen. At the simple process-model level, simple mass balance models of precipitation infiltration and groundwater delivery to streams are often used to account for groundwater loading.

3.3 MODEL OVERVIEW

Numerous watershed models were considered for the CREMs project. The domination of non-urban land uses and associated runoff processes in the LCRA watershed led to the selection of the SWAT model. SWAT is a basin-scale, continuous time watershed model that currently

operates on a daily timestep. The model is designed to predict the impact of management on water, sediment, and agricultural chemical yields. The model is physically (and empirically) based, computationally efficient, and capable of continuous simulation over long time periods. The major model components of the model include weather, hydrology, soil temperature and properties, plant growth, nutrients, pesticides, bacteria and pathogens, and land management. In SWAT, a watershed is divided into multiple subwatersheds, which are then further subdivided into hydrologic response units (HRUs) that consist of homogeneous land use, management, and soil characteristics. The HRUs represent percentages of the subwatershed area and are not identified spatially within a SWAT simulation. Alternatively, a watershed can be subdivided into subwatersheds that are characterized by dominant land use, soil type, and management. A full description of the SWAT model and its simulated processes can be found in Neitsch et al. (2005).

SWAT has a long history of application including many applications in Texas. The United States Department of Agriculture (USDA) research center in Temple, Texas is the "keeper" of the model and has consequently applied SWAT to numerous watersheds throughout the state. It is currently employed in a number of Total Maximum Daily Load (TMDL) projects in Texas, as well as in the rest of the country (see Gassman et al. 2007 for a full list of SWAT applications). One of the first major applications performed with SWAT was in the Hydrologic Unit Model of the U.S. (HUMUS) modeling system, which was implemented to support USDA analyses of the U.S. Resources Conservation Act Assessment of 1997 for the conterminous United States. The system was used to simulate the hydrologic and/or pollutant loss impacts of agricultural and municipal water use, tillage and cropping system trends, and other scenarios within each of the 2,149 USGS 8-digit Hydrologic Unit Code (HUC) watersheds.

3.3.1 Model Time Period and Timestep

A daily timestep was employed with SWAT over the 23-year modeling period extending from 1984 to 2006. This period was chosen to simulate instream water quality for Lake Travis with the lake model. SWAT was run for an additional four-year period from January 1, 1980 through 1984 to provide a four-year "spin-up" time for the model to equilibrate and the effects of

the specification of initial model conditions to dampen. Output from SWAT was only produced for the 1984 to 2006 period to serve as input to the lake model.

3.3.2 Model Structure

3.3.2.1 Climatic Inputs and HRU Hydrologic Balance

Climatic inputs used in SWAT include daily precipitation, maximum and minimum temperature, solar radiation data, relative humidity, and wind speed data, which can be input from measured records and/or generated. Relative humidity is required if the Hargreaves (Hargreaves 1975) or Priestley-Taylor (Priestley and Taylor 1972) evapotranspiration (ET) routines are used; wind speed is only necessary if the Penman Monteith (Monteith 1965) method is used. Measured or generated sub-daily precipitation inputs are required if the Green Ampt infiltration method (Green and Ampt 1911) is selected. For this analysis, the Penman Monteith potential evapotranspiration method was chosen, because a relative humidity time series were not available and the Priestley-Taylor method tends to underpredict in semi-arid climates. Additionally, the NRCS CN method of infiltration, runoff, and routing estimation was selected rather than the Green Ampt infiltration method, which requires precipitation on a finer scale than data could reliably provide.

The average air temperature is used to determine if precipitation should be simulated as snowfall. The maximum and minimum temperature inputs are used in the calculation of daily soil and water temperatures. Generated weather inputs are calculated from tables consisting of 13 monthly climatic variables, which are derived from long-term measured weather records. Customized climatic input data options include:

- simulation of up to 10 elevation bands to account for orographic precipitation and/or for snowmelt calculations;
- adjustments to climate inputs to simulate climate change; and
- forecasting of future weather patterns, which is a new feature in SWAT2005.

The overall hydrologic balance is simulated for each HRU, including canopy interception of precipitation, partitioning of precipitation, snowmelt water, and irrigation water between surface runoff and infiltration, redistribution of water within the soil profile, evapotranspiration, lateral subsurface flow from the soil profile, and return flow from shallow aquifers. Estimation of areal snow coverage, snowpack temperature, and snowmelt water is based on the approach described by Fontaine et al. (2002).

Three options exist in SWAT for estimating surface runoff from HRUs; these are combinations of daily or sub-hourly rainfall and the NRCS CN method (NRCS 1986) or the Green Ampt method. Canopy interception is implicit in the CN method, while explicit canopy interception is simulated for the Green Ampt method. A storage routing technique is used to calculate redistribution of water between layers in the soil profile. Bypass flow can be simulated, as described by Neitsch et al. (2005), for soils characterized by cracking, such as Vertisols. SWAT2005 also provides a new option to simulate perched water tables in HRUs that have seasonal high water tables. As cited above, the NRCS CN method was chosen for this analysis.

3.3.2.2 Cropping, Management Inputs, and HRU Level Pollutant Losses

Crop yields and/or biomass output can be estimated for a wide range of crop rotations, grassland/pasture systems, and trees with the crop growth submodel. New routines in SWAT2005 allow for simulation of forest growth from seedling to mature stand. Planting, harvesting, tillage passes, nutrient applications, and pesticide applications can be simulated for each cropping system with specific dates or with a heat unit scheduling approach. Residue and biological mixing are simulated in response to each tillage operation. Nitrogen and phosphorus applications can be simulated in the form of inorganic fertilizer and/or manure inputs. An alternative automatic fertilizer routine can be used to simulate fertilizer applications, as a function of nitrogen stress. Biomass removal and manure deposition can be simulated for grazing operations. SWAT2005 also features a new continuous manure application option to reflect conditions representative of confined animal feeding operations, which automatically simulates a specific frequency and quantity of manure to be applied to a given HRU.

The type, rate, timing, application efficiency, and percentage application to foliage versus soil can be accounted for in simulations of pesticide applications. Selected conservation and water management practices can also be simulated in SWAT. Conservation practices that can be accounted for include terraces, strip cropping, contouring, grassed waterways, filter strips, and conservation tillage. Simulation of irrigation water on cropland can be simulated on the basis of five alternative sources: stream reach, reservoir, shallow aquifer, deep aquifer, or a water body source external to the watershed. The irrigation applications can be simulated for specific dates or with an auto-irrigation routine, which triggers irrigation events according to a water stress threshold. Subsurface tile drainage is simulated in SWAT2005 with improved routines that are based on the work performed by Du et al. (2005) and Green et al. (2006). The simulated tile drains can also be linked to new routines that simulate the effects of depressional areas (potholes). Water transfer can also be simulated between different water bodies, as well as "consumptive water use," in which removal of water from a watershed system is assumed. HRU level and instream pollutant losses can be estimated with SWAT for sediment, nitrogen, phosphorus, pesticides, and bacteria. Sediment yield is calculated with the Modified Universal Soil Loss Equation (MUSLE) developed by Williams and Berndt (1977). The original USLE estimates are output during a model simulation for comparative purposes only.

The transformation and movement of nitrogen and phosphorus within an HRU are simulated in SWAT as a function of nutrient cycles consisting of several inorganic and organic pools. Losses of both nitrogen and phosphorus from the soil system in SWAT occur by crop uptake and in surface runoff in the solution phase and on eroded sediment. Simulated losses of nitrogen can also occur in percolation below the root zone, in lateral subsurface flow including tile drains, and by volatilization to the atmosphere. Accounting of pesticide fate and transport includes degradation and losses by volatilization, by leaching, on eroded sediment, and in the solution phase of surface runoff and later subsurface flow. Bacteria surface runoff losses are simulated in both the solution and eroded phases with improved routines in SWAT2005.

3.3.2.3 Flow and Pollutant Loss Routing

Flows are summed from all HRUs to the subwatershed level, and then routed through the stream system using either the variable rate storage method (Williams 1969) or the Muskingum method (Neitsch et al. 2005), which are both variations of the kinematic wave approach. Sediment, nutrient, pesticide, and bacteria loadings or concentrations from each HRU are also summed at the subwatershed level, and the resulting losses are routed through channels, ponds, wetlands, depressional areas, and/or reservoirs to the watershed outlet. Contributions from point sources and urban areas are also accounted for in the total flows and pollutant losses exported from each subwatershed. Sediment transport is simulated as a function of peak channel velocity in SWAT2005, which is a simplified approach relative to the stream power methodology used in previous SWAT versions. Simulation of channel erosion is accounted for with a channel erodibility factor. Instream transformations and kinetics of algae growth, nitrogen and phosphorus cycling, carbonaceous biological oxygen demand, and dissolved oxygen are performed on the basis of routines developed for the QUAL2E model (Brown and Barnwell 1987). Degradation, volatilization, and other instream processes are simulated for pesticides, as well as decay of bacteria. Routing of heavy metals can be simulated; however, no transformation or decay processes are simulated for these pollutants. The variable rate storage method was chosen for this analysis.

3.3.3 State Variables of Concern

The primary purpose of the SWAT model developed for CREMs is the calculation of watershed loads to be applied to the receiving water model, in this case the CE-QUAL-W2 based Lake Travis model. As a result, the state variables chosen for simulation in SWAT reflect the needs of the lake water quality model. State variables simulated in SWAT to be passed to the Lake Travis model include:

- flow;
- total suspended solids (TSS);
- total nitrogen (TN);

- ammonia (NH_3);
- nitrate (NO_3);
- nitrite (NO_2);
- organic nitrogen (OrgN);
- total phosphorus (TP);
- mineral phosphorus (minP)[1];
- organic phosphorus (OrgP);
- carbonaceous biochemical oxygen demand (CBOD);
- dissolved oxygen (DO); and
- chlorophyll-*a*.

3.4 MODEL INPUTS

3.4.1 Time Series Input Data

The SWAT model requires several data time series of various types, depending upon the modeling option selected in the model. For the Lake Travis watershed simulations, the two main types of time series input required are meteorology and point source input. The point source input was developed from TCEQ Discharge Monitoring Report records for the permitted dischargers shown in Table 3-1. The meteorology for the simulation period of 1980 – 2006 was developed from meteorological data for 17 National Oceanic and Atmospheric Administration (NOAA) National Climatic Data Center (NCDC) stations shown in Table 3-2. Most of the stations listed in Table 3-2 are cooperative stations (as indicated by the Program Code listed in Table 3-2) owned and operated by entities other than NOAA.

[1] This is the state variable assumed to represent orthophosphate for the purpose of calibration and model linkage.

Table 3-1. TCEQ permitted dischargers within the Lake Travis watershed.

Permittee	Permit Number	County
Travis Vista	11531-001	Travis
City of Burnet	10793-002	Burnet
City of Johnson City	10198-001	Blanco
City of Fredericksburg	10171-001	Gillespie

Table 3-2. NOAA weather stations used in the Phase 2 watershed model.

Station Name	Program Code	COOP ID	County
Andice 2 SW	B COOP COOP-A	410246	Williamson
Austin Mueller Municipal Airport	ASOS-NWS AB ASOS COOP	410428	Travis
Bertram 3 ENE	B COOP COOP-A	410738	Burnet
Blanco	AB COOP COOP-A	410832	Blanco
Burnet	COOP-A COOP AB	411250	Burnet
Cottonwood	COOP-A COOP B	412040	Gillespie
Fredericksburg	COOP-A COOP AB	413329	Gillespie
Gold	B COOP-A COOP	413605	Gillespie
Harper 1w	B COOP COOP-A	413954	Gillespie
Johnson City	COOP-A COOP AB	414605	Blanco
Round Mountain	COOP B	417787	Blanco
Spicewood	COOP-A COOP B	418531	Burnet
Teague Rch	B COOP-A COOP	418877	Gillespie

3.4.2 Geospatial Input Data

The spatial extent of the Lake Travis SWAT model is the drainage basin of the Colorado River from Mansfield Dam upstream to Max Starcke Dam. Lake Travis is impounded between these two dams. The upstream input to the Lake Travis CE-QUAL-W2 model was derived from observed data taken at Starcke Dam; therefore, this SWAT model is only required to simulate the watershed of Lake Travis that either drains directly to the lake or drains to one of the tributaries of the lake. The modeled Lake Travis watershed is shown in Figure 3-1. The bulk of the modeled watershed is comprised of the Pedernales River watershed that enters Lake Travis from the west.

For operational considerations, the Lake Travis SWAT model is actually two interconnected SWAT models, as shown in Figure 3-2. The upper model encompasses the

Pedernales River watershed upstream of Johnson City. The output from the upper model is passed to the lower model that incorporates the remainder of the Lake Travis watershed.

These watersheds were derived from available 30-meter USGS Digital Elevation Models (DEMs) of the area. Watershed delineation techniques were employed to ascertain the extent of the area that drains, eventually, to Lake Travis. The DEMs along with the USGS National Hydrography Dataset were used to determine the stream network that would be incorporated into the SWAT models. The DEM coverage and resultant stream network are shown in Figure 3-3.

Figure 3-4 shows the subwatersheds into which each of the models are divided. The upper model is composed of 27 subwatersheds, while the lower model is composed of 76 subwatersheds. As explained previously, the actual calculation unit for SWAT is the HRU. Each of the 103 subwatersheds is comprised of varying numbers of HRUs, because each HRU constitutes a unique combination of land use and underlying soils. The HRUs were created for each subwatershed based upon the intersection of the year 2000 version of the USGS/USEPA National Land Cover Dataset (NLCD), shown in Figure 3-5 and the NRCS State Soil Geographic (STATSGO) soils database, shown in Figure 3-6. Additional information concerning the STATSGO soils database for the Lake Travis watershed can be found in Appendix C.

3.5 CALIBRATION

Calibration of the SWAT model consists of adjusting the model parameters described above so that the model accurately reproduces observed data. The time period for which the model was calibrated was from the start of 1984 through the end of 2005. Although the model now simulated up to and including 2006, because the watershed model needed to be calibrated in advance of the lake model, the 2006 data were not available at the time the watershed model was being calibrated. The stations used in the calibration are outlined in Table 3-3 (see Figures 2-1 and 3-4 for stations locations).

Table 3-3. Calibration stations for Lake Travis watershed model.

Sampling Site	Type of Station	Period of Record for Hydrology	Type of Water Quality Station	Approximate Number of Days Sampled for Water Quality	Type of Calibration Station
Fredericksburg (USGS 08152900)	USGS	1/1/1984 – 12/31/2006	Routine	n/a	Hydrology (Primary)
Johnson City (RSS 12372)	LCRA RSS/USGS	1/1/2984 – 12/31/2006	Routine	n/a	Hydrology (Primary)
Hammett's Crossing (RSS 12369)	LCRA RSS	n/a	Routine	265	Water Quality (Primary) Hydrology* (Secondary)
Sandy Creek (LC905)	Hydromet	7/23/2003 – 12/31/2006	CREMs Storm	19	Hydrology and Water Quality (Secondary)
Cow Creek (LC906)	Hydromet	4/15/2003 – 12/31/2006	CREMs Storm	20	Hydrology and Water Quality (Secondary)
Bee Creek (LC907)	Hydromet	10/30/2004 – 12/31/2006**	CREMs Storm	29	Hydrology and Water Quality (Secondary)

Notes:

* *To compare measured flow to simulated flow at Hammett's Crossing, the measured flow at Johnson City was prorated to Hammett's Crossing by using the ratio of the two subbasin sizes.*

** *Bee Creek hydrology is not always continuous, for 71 days there were no recorded flows in the 793 day period of record. Statistics in this model-to-data comparison only use data on days for which flow was recorded in the LCRA database*

3.5.1 Hydrology Calibration Approach

The initial step in model calibration was to calibrate the hydrology of the model so that the model reproduces hydrographs measured during the calibration time period. Once the model accurately reproduced the measured runoff amounts from the watershed, the water quality simulation was calibrated. The water quality calibration was achieved by adjustment of various parameters affecting constituent concentrations in the routed runoff.

Table 3-4 illustrates the model parameters that were adjusted to calibrate the hydrologic portion of SWAT. The table briefly describes each parameter and gives both the default and calibrated values. For the factors CH_N and ALPHA_BF, adjustment of these factors during calibration resulted in the confirmation of the default values.

The calibration parameter values were derived through iterative runs of the model while implementing small changes in this suite of model parameters and using both statistical and graphical evaluations of the model's agreement with measured data. These statistical and graphical methods are presented below. Additionally, as a part of the project, LimnoTech, Inc. (LTI) examined the extent and characterization of Tarrant-series soils in the Pedernales River watershed. LTI reviewed available STATSGO and SSURGO datasets to identify the extent of Tarrant-series soils, and also reviewed descriptions of the various soil series in these areas (Appendix C). As a result of their evaluation, the hydrologic soil group used in SWAT for the Tarrant series was changed from D to C and subsequent model parameters related to this designation were updated to reflect hydrologic soil group C soils.

Table 3-4. SWAT hydrologic calibration parameters.

Parameter	Description	Default Value	Calibrated Value
SURLAG	Surface runoff lag coefficient	4	2
ESCO	Soil evaporation compensation factor	0.95	0.125
CH_N(2)	Manning's coefficient for the main channel	0.014	0.014
ALPHA_BF	Base flow recession constant	0.048	0.048

The hydrologic calibration was primarily performed based upon data available at two gage locations, the Pedernales River at Fredericksburg and the Pedernales River at Johnson City. For the water quality calibration, the only station with enough available data of sufficient quality that encompasses enough of the watershed to make calibration meaningful was the Pedernales River at Hammett's Crossing. Therefore, the water quality calibration was performed mainly based upon data available at this location. Three other stations (on Bee, Cow, and Sandy Creeks) that drained smaller subbasins were used as "secondary" calibration stations to assess model performance at a smaller scale. These three stations had continuous flow information and some storm sampling collected during the CREMs storm sampling effort (see Section 2).

3.5.2 Water Quality Calibration Approach

In order to perform model-to-data comparisons, representations of the loading time series on the monitored tributaries and the Pedernales River were necessary. Because these datasets only represent "event" data (i.e., the smaller tributaries were only measured periodically and during storms; the Pedernales River was monitored routinely, but not during storms), they are not a continuous record, which is necessary for model calibration. Consequently, an empirical model was developed to produce a continuous time-series to which the simulated time-series was compared for calibration. The USGS LOAD ESTimator (LOADEST; Runkel et al. 2004), a FORTRAN program for estimating constituent loads in streams and rivers, was used to develop watershed-specific constituent regression models (i.e., rating curves) for those tributaries where sufficient stream flow and constituent concentrations were available. Given a stream flow time-series and constituent concentration, LOADEST develops a regression model for the estimation of the constituent loads. For instances where sufficient stream flow or constituent concentration data were not available to estimate loads using LOADEST, quasi-maximum likelihood estimator (QMLE) was used (Ferguson 1986).

Stream flow data were available from LCRA's Hydromet stations at Big Sandy Creek and Cow Creek, LCRA CREMs sampling site at Bee Creek, and the USGS Pedernales River gage at Johnson City during the constituent sampling periods of record.[2] Sufficient constituent concentration data were not available at Johnson City to develop reliable Pedernales River rating curves. The stream flow at Johnson City was prorated using the watershed drainage area ratio to Hammett's Crossing (the furthest downstream Pedernales sampling location where sufficient constituent concentration data were available) and used to develop a continuous time-series at Hammett's Crossing. The contributing area at Hammett's Crossing is 27% larger than that at Johnson City, thus the flow at the USGS gage at Johnson City was increased by 27% (Figure 3-2). Figures 3-7 through 3-10 present the rating curves for TSS, OrgN, OrgP, NO_x, ammonia, PO_4, and TP at each of the four locations: Big Sandy Creek, Cow Creek, Bee Creek,

[2] Note that Hurst and Cedar Creek, although sampled during storm events (see Section 2), did not have a continuous stream flow record, which prohibited the development of full times-series at these two locations.

and Pedernales River at Hammett's Crossing (CREMs monitoring stations LC905, LC906, LC907, and 12369, respectively).

Daily loads for each of the constituents were then estimated for each of the four locations using the average, continuous daily flow data (Table 3-3) and the rating curve predictions. The simulated loads were compared to these time-series of load estimates for each constituent during watershed model calibration. Table 3-5 presents the standard errors calculated associated with the rating curve predictions for each station and constituent.

Table 3-5. Uncertainty associated with rating curve predictions in kg/day.

Station	Parameter	Mean Load	Standard Error
LC905 Sandy Creek	TSS	1536	733
	Organic N	10.83	2.18
	Organic P	1.05	0.39
	NO_x	3.18	0.29
	Ammonia	0.61	0.14
	PO_4 *	0.028	0.024
	TP	1.09	0.36
LC906 Cow Creek	TSS	961	412
	Organic N	15.02	3.92
	Organic P	0.88	0.24
	NO_x	5.12	2.1
	Ammonia	0.81	0.48
	PO_4 *	0.039	0.003
	TP	0.91	0.25
LC907 Bee Creek	TSS *	107	19
	Organic N *	3.24	1.95
	Organic P *	11.58	11.5
	NO_x *	1.16	0.14
	Ammonia *	0.28	0.21
	PO_4 *	0.008	0.003
	TP *	2.21	2.06
12369 Pedernales at Hammett's Crossing	TSS	241,897	123,452
	Organic N	883	186
	Organic P	197.13	121.77
	NO_x	323.99	100.61
	Ammonia	36.11	9.94
	PO_4 *	8.23	2.25
	TP	160.85	79.82

*Notes: * QMLE was used for load estimation due to insufficient data to run LOADEST.*

Table 3-6 illustrates the model parameters that were adjusted to calibrate the water quality in SWAT. The table briefly describes each parameter, indicates the location in the SWAT input and gives both the default and calibrated values. These values were derived through iterative runs of the model while implementing small changes in this suite of model parameters and using both statistical and graphical evaluations of the model's agreement with measured data (see Section 3.5.1 regarding measured data for water quality). These statistical and graphical methods are presented in Section 3.5.2

Table 3-6. SWAT water quality calibration parameters.

Parameter	Description	Location in SWAT Input	Default Value	Calibrated Value
RCN	Concentration of nitrogen in rainfall (mg N/L)	basins.bsn	1	0.0
P_UPDIS	Phosphorus uptake distribution parameter	basins.bsn	20	60
PHOSKD	Phosphorus soil partitioning coefficient (m^3/Mg)	basins.bsn	175	300
PSP	Phosphorus availability index	basins.bsn	0.4	0.8
RSDCO	Residue decomposition coefficient	basins.bsn	0.05	0.0
SPCON	Linear parameter for calculating the maximum amount of sediment that can be re-entrained during channel sediment routing	basins.bsn	0.0001	0.0006
MUMAX	Maximum specific algal growth rate at 20º C (day^{-1})	basin.wwq	2	1
P_N	Algal preference factor for ammonia	basin.wwq	0.5	0.01
SLSUBBSN	Average slope length (m)	*.hru	50	40.815 to 41.489
ESCO	Soil evaporation compensation factor	*.hru		0.125
EPCO	Plant uptake compensation factor	*.hru		0.2
BIOMIX	Biological mixing efficiency	*.mgt	0.2	0.05
USLE_P	USLE equation support practice factor	*.mgt	1	0.5

3.5.3 Calibration Results

The hydrologic calibration of the SWAT model was based upon monthly average flow rates available at Fredericksburg and Johnson City. Figure 3-11 shows the results for Fredericksburg, and Figure 3-12 shows the results for Johnson City. The model matches the

measured data well, although the model tends to display higher peak values particularly at Fredericksburg.

Another way to look at the calibration data is with the aide of a cross plot. Figures 3-13 and 3-14 are cross plots of the hydrodynamic calibration at Fredericksburg and Johnson City, respectively. The data points plotted on the cross plot are measured values with the corresponding model prediction plotted with the measured value as the abscissa and the predicted value as the ordinate. Also shown is a linear regression line between the measured and predicted values and the corresponding coefficient of determination. When plotted where the abscissa and ordinate have equal ranges, a perfect fit regression line would lie atop a diagonal from the origin to the range, shown here in green. As evidenced in both cross plots, the fit is good, particularly at Johnson City, which encompasses far more of the watershed than Fredericksburg, which is near the headwaters of the watershed.

Table 3-7 includes some statistical descriptors of the monthly hydrologic calibration. The Nash-Sutcliffe efficiency coefficient measures how much better a model predicts observed values than the average of the observed values. A value of 1 indicates a perfect match, whereas a value of 0 or negative indicates that the model performs no better at predicting observed values than the average of the observed values. Again, the fit is good, particularly at Johnson City. A comparison of the measured versus simulated averages indicates the model is performing well at both stations, on average.

Table 3-7. Monthly hydrologic calibration model fit statistics for primary calibration stations.

Location	Measured Monthly Average (m^3/s)	Predicted Monthly Average (m^3/s)	Cumulative Measured Averages	Cumulative Predicted Averages	Root Mean Square Error	Nash-Sutcliffe Efficiency Coefficient
Fredericksburg	2.07	2.21	427.8	583.1	2.87	0.47
Johnson City	7.17	7.16	1893.7	1759.74	5.77	0.82

Note: These statistics use the period of record of January 1, 1984 to December 31, 2005.

Table 3-8 compares the measured and simulated average flows at the three smaller subbasins. Traditionally, modeling small subbasins with a daily timestep is difficult when model

adjustments are made at a basin-wide scale (Benaman et al. 2005). Consequently, as expected, the performance of the model at these smaller stations is not as good as at the primary calibration stations. The results at Sandy and Bee Creeks are about 50% to 100% higher than the measured, on average, but still within a factor of two of the measured data. The performance at Cow Creek is within 10% of the observed average hydrology, indicating a relatively good representation on the smaller subbasins.

Table 3-8. Hydrologic calibration for secondary calibration stations.

Sampling Site	Average Flow (m^3/s)	
	Measured	**Predicted**
Sandy Creek (LC905)	0.19	0.37
Cow Creek (LC906)	0.27	0.30
Bee Creek (LC907)	0.03	0.05

Note: These statistics use the period of record indicated in Table 3-3.

These calibration results for SWAT in the Lake Travis watershed compare to other SWAT applications. In a Northeastern study, Cho et al. (1995) reported monthly Nash-Sutcliffe values ranging from 0.57 to 0.83 for a small forested watershed in the Delaware River basin. A previous study in the Midwest (Srinivasan et al. 1998) obtained monthly Nash-Sutcliffe values of 0.87 and 0.84. Another Midwest project applied SWAT to three Illinois watersheds, resulting in monthly Nash-Sutcliffe values of 0.63, 0.78, and 0.95 for basin sizes of 122, 246, and 188 km^2, respectively (Arnold and Allen 1996). More recently, modeling efforts in Texas were completed; the first effort obtained calibrated flow volume monthly Nash-Sutcliffe values of 0.80 and 0.89 for two subbasins of 926 and 2997 km^2, respectively (Santhi et al. 2001). The second effort obtained Nash-Sutcliffe values of 0.12 and 0.72 for two USGS flow stations in a 4552 km^2 watershed (Santhi et al. 2006). A recent review of many SWAT applications throughout the world, including many in Texas, show monthly Nash-Sutcliffe values ranging from 0.3 to above 0.95 (Gassman et al. 2007). The Santhi et al. (2001) study assumed an 'acceptable calibration' for hydrology at a monthly Nash-Sutcliffe > 0.6.

Similar plots were prepared for the flow and water quality calibration at Hammett's Crossing. Figures 3-15 through 3-22 are the comparisons between the measured and predicted values for eight modeled parameters and Figures 3-23 through 3-30 are the cross plot comparisons for the same parameters. Table 3-9 depicts the statistical descriptors of the hydrological and water quality calibration for eight parameters at the Hammett's Crossing station. For TSS, the model comes within a factor of 2 of the observed TSS, which is considered good performance for this constituent in watershed modeling (Benaman et al. 2005). The Lake Travis SWAT model produces a percent difference for TSS of approximately 47%. Santhi et al. (2001) considered SWAT's simulations of sediment loading acceptable with percent differences of –16% and –20% (Santhi et al. 2001). An application of SWAT in the Texas Gulf basin compared SWAT simulated annual sediment loads to loads estimated from data using sediment rating curves. The simulated annual sediment loads for six different basins displayed percent differences from the rating curve estimates ranging from 35% to 130%. The smallest absolute difference (6%) was for a 13,000 km^2 basin (Arnold et al. 1999). Srinivasan et al. (1998) also performed a sediment calibration in Texas and came within 2% of the measured annual sediment loads. Although the review of 37 different SWAT applications across many different basins does not report percent differences in their summary, they indicate Nash Sutcliffe values that are negative up to above 0.8 (Gassman et al. 2007). Gassman et al. (2007) and Benaman et al. (2005) also document weaknesses in sediment erosion and transport simulation that make it difficult to simulate sediments in SWAT.

Table 3-9. Water quality calibration model fit statistics at Hammett's Crossing.

Parameter	Measured Average	Predicted Average	Measured Total	Predicted Total	% Diff. in Average	Monthly Nash-Sutcliffe Efficiency Coefficient
TSS (MT/d)	241.9	334.8	2,032,173	2,812,584	38.4	0.56
Total P (kg/d)	160.9	165.4	1,351,327	1,389,619	2.8	0.35
Ortho P (kg/d)	8.23	4.6	69,162	38,332	-44.6	0.533
Organic P (kg/d)	197.1	160.8	1,656,057	1,351,287	-18.4	0.31
Ammonia (kg/d)	36.1	51.2	303,388	430,454	41.9	-2.83
Nitrate+Nitrite (kg/d)	324.0	2,399	2,721,684	20,150,732	640	-20.17
Organic N (kg/d)	882.5	275.4	7,413,863	2,313,619	-69	0.06

Note: These statistics use the period of record of January 1, 1984 to December 31, 2006.

For the nutrient series, the model fits are fair; in particular, the phosphorus series is simulated relatively well, on average. Indeed, the watershed model calibration process focused on optimizing the phosphorus calibration due to the control this nutrient exerts on lake productivity.[3] The model performs well, on average, in predicting the inorganic phosphorus, which is the phosphorus available for algae growth (within a factor of 2). The challenges of using a rating curve to define the "measured" time series is shown with the measured average phosphorus series. The total phosphorus should be the sum of orthophosphate and organic phosphorus, but uncertainties in the rating curves result in the two average species not adding up to the average total. The uncertainties in the LOADEST phosphorus time-series (see Table 3-5) may account for some of the differences between "measured" and predicted.

The model does not perform well for the nitrogen series, with large discrepancies between the "measured" and predicted loads for all three species, particularly nitrate plus nitrite, that cannot be fully explained by the uncertainties in the LOADEST-estimated time-series (see Table 3-5). During calibration, a good calibration could not be achieved for both phosphorus and nitrogen. Therefore, the calibration focused on optimizing model-data comparisons for the phosphorus series, considering the importance of this constituent in controlling algae growth in the summer and the uncertainties of the "measured" loadings. Nonetheless, as described in Section 4, a reasonable lake model calibration was obtained for the different nitrogen species using the watershed derived loadings and in-lake nitrogen process parameterization within accepted ranges. This additional constraint on the watershed loads suggest that the differences between "measured" and predicted nitrogen may be due, at least in part, to uncertainties in the "measured" loads.

Modeling the nutrient series in SWAT is challenging and requires adjustment of multiple parameters, which describe land side processes (including erosion and plant uptake) and instream kinetic processes. Typically, little site-specific data are available to guide the modeler as to which parameters should be adjusted. Consequently, literature values and professional judgment are used to perform the calibration. Gassman et al. (2007) summarized SWAT model

[3] Although the lake shows both phosphorus and nitrogen limitation, as well as co-limitation, early sensitivity analyses on the lake model indicated the model responded more to changes in phosphorus loads.

performance in nutrient simulations for various studies and found that SWAT performed acceptably to "poorly." To compare the Lake Travis results, Santhi et al. (2001) and Santhi et al. (2006), which were two studies performed in Texas, show percent differences for the phosphorus series of -18% and -3% for orthophosphate, on average. Santhi et al. (2001) also reported a 7% over-prediction in organic phosphorus. In both of these Santhi et al. studies, it seems that their nitrogen calibration results were less reliable than their phosphorus calibration results, just as seen here on Lake Travis. In both studies, the mineral nitrogen (i.e., ammonia plus nitrite+nitrate) was over-predicted by about 45%. Another study in upstate New York showed phosphorus percent differences of about 6 to 41% (Tolson and Shoemaker 2007).

Table 3-10 shows the results of the water quality simulations at the three smaller stations. When originally constructed, this SWAT model was intended to focus upon the watershed as a whole, and not specifically on any small watersheds. The model is therefore composed of relatively few slope categories, sufficient to categorize the entire Lake Travis watershed. Many of the small watersheds, particularly the ones with sampling data, have large areas with slopes much steeper than the general categories used in the model. As a result, the model does not perform well when simulating the loads from individual small watersheds, but does a relatively good job predicting the load of the watershed, as a whole. Increasing the resolution of the slope categories was considered, but because these categories must apply to the entire model, this would drastically increase the numbers of HRUs, the size of the models, and the required runtime.

Table 3-10. Water quality calibration for secondary calibration stations.

Sampling Site	TSS (kg/d)		TP (kg/d)		PO_4 (kg/d)		Org P (kg/d)		NH_3 (kg/d)		NO_2+NO_3 (kg/d)		Org N (kg/d)	
	Obs	Pred	Obs	Pred	Obs	Pred	Obs	Pred	Obs	Pred	Obs	Pred	Obs	Pred
Sandy Creek	1,540	99,965	1.1	11.2	0.03	0.04	1.05	11.1	0.6	12.0	3.2	5.13	10.8	62.6
Cow Creek	960	408,941	0.9	10.1	0.04	0.07	0.9	10.0	0.8	17.5	5.1	5.86	15.0	55.6
Bee Creek	110	137,895	0.2	1.6	0.004	0.003	0.09	1.6	0.07	2.4	1.04	0.2	1.3	8.7

Note: These statistics use the period of record indicated in Table 3-3.

Of particular concern are the sediment predictions on these smaller watersheds, which are grossly overpredicted by the model. It is felt that this is a direct consequence of the slope categories limitation. Previous sensitivity analyses on SWAT have shown that the sediment predictions are very sensitive to the land-based parameters such as slope length and slope (Benaman 2003). Consequently, use of this model on such a fine scale is not suggested to predict sediment loadings from small watersheds. However, for predictions of orthophosphate, which will be the constituent most likely to control algae growth, the smaller subbasins perform acceptably (within a factor of two for all three subbasins).

Care should be taken when interpreting these model-to-data comparisons, as they are actually comparing a model to another "model". Because continuous water quality modeling is typically prohibitive due to costs and logistics, these model-to-data comparisons cannot be viewed in the same way as the hydrologic calibration, for which a continuous measured time series is available for assessing model performance. This water quality calibration is being compared to a time series that was established using rating curves (see Section 3.5.1), which, in and of themselves, have significant uncertainty (see Table 3-5). In fact, for many of the stations, barely enough non-detect data were available to establish a concentration versus flow curve that was then used to estimate a continuous load record using the continuous flow record at each station. Consequently, the model performance should be assessed in light of the uncertainty in the calibration time series, as well as the inherent difficulty, in general, of modeling erosion and instream water quality processes.

3.6 WATERSHED MODEL SENSITIVITY ANALYSIS

Sensitivity analysis relates how the variation (uncertainty) in the output of a mathematical model can be apportioned, qualitatively or quantitatively, to different sources of variation in both model input data and, more commonly, the various parameters in the model that affect the performance or calibration of the model. In general, both uncertainty and sensitivity analyses investigate the robustness of a model. While uncertainty analysis evaluates the overall uncertainty in the conclusions of the model, sensitivity analysis tries to identify what source of uncertainty weighs more on the model output or conclusions.

Choosing the appropriate uncertainty analysis/sensitivity analysis method is often a matter of trading off between the amount of information one wants from the analyses and the computational difficulties of the analyses. These computational difficulties are often inversely related to the number of assumptions one is willing or able to make about the shape of a model's response surface (Pascual et al. 2003).

Considering the computational difficulty of running the SWAT models in an iterative or Monte Carlo fashion to facilitate uncertainty analysis, a one-at-a-time sensitivity analysis was performed in three steps. The initial step was to select the parameters and their ranges to test in the one-at-a-time sensitivity analysis. Table 3-11 illustrates the parameters chosen for sensitivity analysis. The table shows the calibrated value for the parameter and the range evaluated in the sensitivity analysis. Ranges were developed using professional judgment, taking into account information available in the literature pertaining to the ranges for these parameters where possible.

Table 3-11. SWAT parameters selected for sensitivity analysis.

Parameter	Description	Location in SWAT Input	Calibrated Value	Sensitivity Range
RCN	Concentration of nitrogen in rainfall (mg N/L)	basins.bsn	0.0	0.01 to 2.0
P_UPDIS	Phosphorus uptake distribution parameter	basins.bsn	60	1.0 to 80.0
PHOSKD	Phosphorus soil partitioning coefficient (m^3/Mg)	basins.bsn	300	200 to 400
PSP	Phosphorus availability index	basins.bsn	0.8	0.1 to 0.9
RSDCO	Residue decomposition coefficient	basins.bsn	0.0	0.0 to 0.05
SPCON	Linear parameter for calculating the maximum amount of sediment that can be re-entrained during channel sediment routing	basins.bsn	0.0006	0.0001 to 0.01
MUMAX	Maximum specific algal growth rate at 20º C (day^{-1})	basin.wwq	1	0.5 to 3.0
P_N	Algal preference factor for ammonia	basin.wwq	0.01	0.01 to 1.0
SLSUBBSN	Average slope length (m)	*.hru	40.815 to 41.489	8.195 – 8.298 to 81.629 – 82.978
ESCO	Soil evaporation compensation factor	*.hru	0.125	0.01 to 1.0
EPCO	Plant uptake compensation factor	*.hru	0.2	0.01 to 1.0
BIOMIX	Biological mixing efficiency	*.mgt	0.05	0.01 to 0.5
USLE_P	USLE equation support practice factor	*.mgt	0.5	0.05 to 5.0

For each parameter selected, step 2 of the procedure involved changing the model input to the low value of the range specified in Table 3-11 and running the model. This was repeated using the high value of the range. In this one-at-a-time manner, the two results are used in step 3 in the presentation and evaluation of the sensitivity analysis for each of the eight major state variables of the model including:

- flow (m^3/s);
- total suspended solids (tons/d);
- total phosphorus (kg/d);
- orthophosphate (kg/d)[4];
- organic phosphorus (kg/d);
- ammonia (kg/d);
- nitrate + nitrite (kg/d); and
- organic nitrogen (kg/d).

Changing parameters one-at-a-time ignores correlations between parameters and, consequently, introduces a limitation of this approach. However, given the desired study outcomes and the restricted time and resources, a one-at-a-time sensitivity approach aided in narrowing down the list of parameters efficiently. The results from this approach should not supersede professional judgment or previous analyses.

The principle function of the SWAT model is to generate nutrient loadings for the Lake Travis model. As a result, the main focus of the sensitivity analyses centered on the nitrogen and phosphorus series. Table 3-12 shows the results of the sensitivity analyses on the eight major state variables in the model. The table shows the difference between the high run and the low run for each parameter for each state variable, the average between the high and low runs, and the difference expressed as a percentage of the average. Results for three of the state variables – flow, TN, and TP – are also graphically illustrated in Figures 3-31 through 3-33, respectively.

[4] This is based on the state variable mineral phosphorus (minP) in SWAT.

Table 3-12. Sensitivity metrics for each SWAT parameter tested.

Parameter	Metric	Flow m^3/s	TSS tons/d	TP kg/d	PO_4 kg/d	Org P kg/d	NH3 kg/d	NO_2+NO_3 kg/d	Org N kg/d
SPCON	Delta	0.0	672.2	0.0	0.0	0.0	0.0	0.0	0.0
	Average	866220.3	399.0	203.9	8.3	195.7	51.6	3482.0	328.1
	% of Average	**0.0**	**168.5**	**0.0**	**0.0**	**0.0**	**0.0**	**0.0**	**0.0**
BIOMX	Delta	-8414.2	2.7	35.8	-7.1	42.9	36.5	775.8	175.2
	Average	862925.8	355.6	232.3	6.4	225.9	67.4	3866.5	411.5
	% of Average	**1.0**	**0.8**	**15.4**	**111.4**	**19.0**	**54.2**	**20.1**	**42.6**
EPCO	Delta	-227846.0	-132.4	21.3	-3.0	24.3	68.8	-761.0	66.6
	Average	906798.2	389.2	224.7	8.7	216.1	92.1	3626.1	367.7
	% of Average	**25.1**	**34.0**	**9.5**	**34.4**	**11.2**	**74.8**	**21.0**	**18.1**
ESCO	Delta	-227846.0	-132.4	21.3	-3.0	24.3	68.8	-761.0	66.6
	Average	906798.2	389.2	224.7	8.7	216.1	92.1	3626.1	367.7
	% of Average	**25.1**	**34.0**	**9.5**	**34.4**	**11.2**	**74.8**	**21.0**	**18.1**
MUMAX	Delta	0.0	0.0	-3.5	-27.5	24.0	8.1	83.4	29.5
	Average	866220.3	354.8	209.7	19.6	190.1	51.7	3493.4	320.9
	% of Average	**0.0**	**0.0**	**1.7**	**140.4**	**12.6**	**15.6**	**2.4**	**9.2**
P_N	Delta	0.0	0.0	0.0	0.0	0.0	-2.1	-36.0	0.0
	Average	866220.3	354.8	203.9	8.3	195.7	52.7	3500.0	328.1
	% of Average	**0.0**	**0.0**	**0.0**	**0.1**	**0.0**	**4.1**	**1.0**	**0.0**
P_UPDIS	Delta	10605.9	4.6	-58.9	-13.8	-45.1	-6.1	7.3	-48.4
	Average	860923.2	352.5	225.4	13.6	211.8	54.2	3469.8	346.2
	% of Average	**1.2**	**1.3**	**26.1**	**101.3**	**21.3**	**11.2**	**0.2**	**14.0**
PSP	Delta	10605.9	4.6	-58.9	-13.8	-45.1	-6.1	7.3	-48.4
	Average	860923.2	352.5	225.4	13.6	211.8	54.2	3469.8	346.2
	% of Average	**1.2**	**1.3**	**26.1**	**101.3**	**21.3**	**11.2**	**0.2**	**14.0**
RCN	Delta	0.0	0.0	0.0	0.0	0.0	0.0	0.0	0.0
	Average	866220.3	354.8	203.9	8.3	195.7	51.6	3482.0	328.1
	% of Average	**0.0**	**0.0**	**0.0**	**0.0**	**0.0**	**0.0**	**0.0**	**0.0**
RSDCO	Delta	0.0	0.0	0.0	0.0	0.0	0.0	0.0	0.0
	Average	866220.3	354.8	203.9	8.3	195.7	51.6	3482.0	328.1
	% of Average	**0.0**	**0.0**	**0.0**	**0.0**	**0.0**	**0.0**	**0.0**	**0.0**
SLSUBBSN	Delta	-129899.5	159.4	108.1	0.7	107.5	5.8	779.5	172.5
	Average	913080.6	311.1	202.2	8.5	193.7	58.1	3720.6	320.9
	% of Average	**14.2**	**51.2**	**53.5**	**7.7**	**55.5**	**10.0**	**21.0**	**53.8**
SPCON	Delta	0.0	672.2	0.0	0.0	0.0	0.0	0.0	0.0
	Average	866220.3	399.0	203.9	8.3	195.7	51.6	3482.0	328.1
	% of Average	**0.0**	**168.5**	**0.0**	**0.0**	**0.0**	**0.0**	**0.0**	**0.0**
USLE_P	Delta	314.2	223.9	43.2	0.2	43.0	28.6	533.0	110.1
	Average	866183.4	308.9	190.4	8.2	182.1	41.0	3332.2	291.6
	% of Average	**0.0**	**72.5**	**22.7**	**2.9**	**23.6**	**69.9**	**16.0**	**37.8**

Notes: Delta = the difference between the results of the High and Low runs

Average = the average of the results for the High and Low runs.

Phosphorus uptake distribution parameter (P_UPDIS) and the phosphorus availability index (PSP). P_UPDIS controls plant uptake of phosphorus from the different soils. The importance of the phosphorus uptake distribution parameter lies in its control over the maximum amount of soluble P removed from the upper soil layers. Because the top 10 mm of the soil interacts with surface runoff, the phosphorus uptake distribution parameter influences the amount of labile phosphorus available for transport in surface runoff. The equilibration between the soluble and active mineral pool for phosphorus is governed by the PSP. This index specifies the fraction of fertilizer P that is in solution after an incubation period or the rapid reaction period. These two factors relate to the amount of phosphorus available especially in the upper layers of the soil. Phosphorus is also quite sensitive to USLE_P, the universal soil loss equation support practice factor. USLE_P is defined as the ratio of soil loss with a specific support practice to the corresponding loss with up-and-down slope culture. Support practices include contour tillage, strip-cropping on the contour, and terrace systems and pertain to the potential for erosion of phosphorus laden soils. Additionally, phosphorus is quite sensitive to SLSUBBSN, the average slope length. This is the distance that sheet flow is the dominant surface runoff flow process and is also directly related to erosive potential.

With the exception of the two specific parameters, PSP and P_UPDIS, nitrogen is sensitive to most of the same factors as phosphorus. Nitrogen concentrations are sensitive to the USLE_P and SLSUBBSN factors since nitrogen compounds are contained in the eroded soils as well as phosphorus. Nitrogen concentrations are also sensitive to ESCO, the soil evaporation compensation factor and EPCO, the plant uptake compensation factor. The ESCO coefficient modifies the depth distribution used to meet the soil evaporative demand to account for the effect of capillary action, crusting and cracks and is related to soil nitrogen availability. EPSC is related to the evapotranspiration potential for plants in the model and is, therefore, directly related to nitrogen uptake by plants.

The four SWAT parameters (BIOMIX, MUMAX, P_UPDIS, PSP) that were tested and found to be most sensitive with respect to orthophosphate were carried forward into the lake model sensitivity analysis (Section 4.6).

SECTION 4
LAKE MODEL

4.1 INTRODUCTION

The lake model selected for the Phase 2 Lake Travis work is CE-QUAL-W2 (version 3.5), a two-dimensional laterally averaged hydrodynamic and water quality model developed and maintained by the USACE Waterways Experiment Station. Model selection was based on the model evaluation section in the Master Plan (CH2M Hill 2002), results from the Phase 1 work, and discussions within the project team. CE-QUAL-W2 is best suited for relatively long and narrow water bodies, such as Lake Travis, that exhibit longitudinal and vertical water quality gradients. The model has been applied to rivers, lakes, reservoirs, and estuaries across the United States (Cole and Wells 2006). In addition, the SWAT and CE-QUAL-W2 models have been successfully linked for other sites such as the Cedar Creek Reservoir, Texas (Debele et al. 2006). This section describes the development and calibration of the CE-QUAL-W2 for Lake Travis. Additional information about the ambient water quality of Lake Travis, including spatial and temporal trends can be found in Appendix D.

4.1.1 Spatial Domain and Model Segmentation

The lake model domain consists of the waters that form Lake Travis and its main branches (i.e., tributaries; Figure 4-1, top panel). These waters are modeled in CE-QUAL-W2 in two dimensions: in the longitudinal direction (i.e., spatially, in the direction of flow) and in the vertical direction (i.e., at depth). The longitudinal segmentation for the main body of the lake begins at Max Starcke Dam and ends at Mansfield Dam (Figure 4-1, top panel). The model also includes the Pedernales River, Cow Creek, Bee Creek, Hurst Creek, Big Sandy Creek, and Cypress Creek as tributaries to the model. The lake model domain captures the major coves of Lake Travis by extending several miles upstream of the confluence of these tributaries with Lake Travis. Table 4-1 summarizes the model segmentation for Lake Travis and its tributaries. Dimensions appearing in Table 4-1 are referenced to a water surface elevation of 203.45 m (677.49 ft.), the elevation on January 1, 1984 at Mansfield Dam. The entire model domain

consists of a total of 164 longitudinal divisions. Each longitudinal segment extends from "bank to bank" and therefore, represents laterally averaged conditions.

Table 4-1. Summary of longitudinal segmentation for Lake Travis CE-QUAL-W2 model.

Water Body	Number of Longitudinal Model Segments	Length (km)	Average Width (m)	
			At Elevation of 203.45 Meters	At Depth
Lake Travis	92	83.5	1,047	543
Pedernales River	15	9.5	394	240
Cow Creek	11	4.6	313	162
Bee Creek	7	3.3	588	239
Hurst Creek	11	3.2	556	306
Big Sandy Creek	20	10.2	576	337
Cypress Creek	8	3.8	447	252
Total	**164**	**118.2**	---	---

The Lake Travis CE-QUAL-W2 model was segmented vertically into 32 layers, each with a thickness of two meters. During a model simulation, the number and thickness of vertical segments remain fixed and the vertical segments become variably wet (i.e., active) or dry (i.e., inactive) depending on the water surface elevation of the lake. A side view of the model grid is depicted in the bottom panel of Figure 4-1.

4.1.2 Model Time Period

The lake model was developed and calibrated using data from January 1, 1984 through December 31, 2006, matching the time period of the output from the watershed model calibration and extended data collection (Sections 2 and 3). CE-QUAL-W2 internally calculates the timestep necessary for the model to maintain hydrodynamic numerical stability. The minimum timestep specified was one second. The maximum timestep allowed was set to 360 seconds for the majority of the calibration period; this maximum timestep was occasionally reduced to 10 seconds to maintain numerical stability. The model provided daily output for the simulated parameters for each model segment.

4.1.3 General Processes Modeled

The Lake Travis water quality model represents the major hydrodynamic, water column nutrient cycling, and sediment processes controlling water quality in the lake (Figure 4-2). The hydrodynamic component of the model simulates temperature as well as vertical and horizontal mixing processes. The water column component of the model describes the major water column processes affecting lake water quality, including nitrification, organic matter decomposition, algal photosynthesis, respiration, and nutrient uptake as well as particulate settling to the sediment bed. The sediment component of the model represents the conversion of particulate organic material to dissolved nutrients and the concurrent consumption of oxidized compounds from the overlying water column. These fluxes are approximated by zero-order processes.

For hydrodynamics and associated constituent transport, CE-QUAL-W2 uses laterally averaged equations of fluid motion, namely equations for continuity and for conservation of momentum. Included in these equations are velocity, acceleration, gravity, pressure, and turbulent shear stresses. Additional governing equations incorporated are the equation of state, which relate density to temperature and concentration of dissolved substances and to the equation of free water surface, which integrates continuity over the depth of the water column. For details on the hydrodynamic and constituent transport processes that CE-QUAL-W2 simulates, see Appendix A of the CE-QUAL-W2 User Manual (Cole and Wells 2006).

For water quality, CE-QUAL-W2 computes the concentrations of user-specified state variables such as algae, dissolved oxygen, organic matter, and sediment for each model segment and each timestep using constituent-specific rate equations that account for sources and sinks associated with biological and chemical processes. The user can specify any number of generic constituents, suspended solids groups, CBOD groups, algal groups, macrophyte groups, zooplankton groups, and epiphyton groups. A full list of state variables available in CE-QUAL-W2 is presented in Table 4-2 in section 4.2.1, along with those selected for representation of Lake Travis water quality. For detailed descriptions of all water quality processes simulated by CE-QUAL-W2, see Appendix B of the model's user manual (Cole and Wells 2006).

4.1.4 Calibration Metrics and Goals

To evaluate model performance, it is typical to set calibration metrics that compare simulated constituents with measured data. Calibration metrics typically used for CE-QUAL-W2 were evaluated and are summarized in Appendix H. Throughout this chapter, various model-to-data goodness-of-fit measures are provided with the calibration results. Particular attention is given to the absolute mean error (AME) goodness-of-fit measure, for which system-wide average CE-QUAL-W2 calibration goals were found from other CE-QUAL-W2 modeling efforts (Appendix H; Table 2).

4.2 MODEL OVERVIEW

The Lake Travis model calibration effort was performed in two distinct steps. First, the hydrodynamics were calibrated to predict water transport including flows, dispersion, depths, velocities, water surface elevations, temperature, and conservative constituents. After satisfactory completion of the hydrodynamic calibration, model water quality was calibrated against observed data to simulate the major processes of eutrophication kinetics. After water quality calibration, hydrodynamics were checked again as parameters such as suspended solids affect light penetration and therefore potentially affect water temperature, density, and movement.

4.2.1 State Variables of Concern

The state variables chosen to represent the water quality dynamics of Lake Travis along with the rationale for those state variables not chosen are presented in Table 4-2.

Table 4-2. List of CE-QUAL-W2 state variables used in Lake Travis model.

Constituent Name	Include in Lake Travis Model?	Comments
Generic constituents	Yes	Included chloride, specific conductivity; water age.
Inorganic suspended solids (ISS)	Yes	One class included.
Phytoplankton	Yes	One group included.
Epiphyton	No	Epiphyton are not expected to impact other state variables in Lake Travis significantly due to the lake's variable stage and depth.
Carbonaceous biochemical oxygen demand (CBOD)	No	Modeled as organic matter groups.
Ammonium (NH_4)	Yes	
Nitrite+nitrate (NO_2+NO_3)	Yes	
Bioavailable phosphorus (e.g., PO_4)	Yes	
Labile dissolved organic matter (LDOM)	Yes	
Refractory dissolved organic matter (RDOM)	Yes	
Labile particulate organic matter (LPOM)	Yes	
Refractory particulate organic matter (RPOM)	Yes	
Total inorganic carbon	No	Total inorganic carbon is not an issue of management concern and does not significantly impact other state variables.
Alkalinity	No	Alkalinity is not an issue of management concern and does not significantly impact other state variables.
Total iron	No	Iron is included in CE-QUAL-W2 primarily as a sorption site for PO_4. This mechanism is not expected to be significant in Lake Travis.
Dissolved oxygen (DO)	Yes	
Organic sediments	No	Organic sediments were not specified because the method selected for simulation uses a constant release and demand instead of using a sediment compartment to accumulate organic sediments and allow their decay.
Gas entrainment	No	The extent of Lake Travis is large – oxygen entrainment from Max Starcke Dam is expected to have a negligible impact on the overall oxygen levels.
Macrophytes	No	Macrophytes were not considered a concern in the Phase 2 modeling effort.
Zooplankton	No	Parameterized as mortality rate of algae.
Labile dissolved organic matter-phosphorus (LDOM-P)	Yes	
Refractory dissolved organic matter-phosphorus (RDOM-P)	Yes	
Labile particulate organic matter-phosphorus (LPOM-P)	Yes	
Refractory particulate organic matter-phosphorus (RPOM-P)	Yes	
Labile dissolved organic matter-nitrogen (LDOM-N)	Yes	
Refractory dissolved organic matter-nitrogen (RDOM-N)	Yes	
Labile particulate organic matter-nitrogen (LPOM-N)	Yes	
Refractory particulate organic matter-nitrogen (RPOM-N)	Yes	

4.3 WATER BALANCE

Together the SWAT watershed model and CE-QUAL-W2 lake model represent the Colorado watershed from Max Starcke Dam to Mansfield Dam. A water balance was developed for this watershed, based on the available hydrology, lake elevation, lake evaporation, and meteorological records. Because the establishment of the water balance occurred before the full development and calibration of the SWAT model and because the numerical stability of CE-QUAL-W2 is highly sensitive to the water balance, the water balance was used as input to the lake model instead of the SWAT predicted flows. See Section 5.3.6 for details on the watershed to lake model linkage.

4.3.1 Inputs

LCRA staff originally developed and ran the program that retrieved the data, performed quality control checks, and calculated resultant flows for the water balance. The results of this analysis were used in the initial hydrodynamic calibration. Several data were required including:

- Tributary Inflow Data
  - Lake Marble Falls flow data at Max Starcke Dam; and
  - Pedernales River flow data from USGS Gage 0815350.
- Meteorological Data
  - precipitation time series for local stations; and
  - evaporation data for the area.
- Lake Travis Data
  - time series of water surface elevations;
  - area/capacity curves; and
  - time series of releases at Mansfield Dam.

The water balance tool integrated this information and closed the flow balance with a rule-based reconciliation routine that enforced a mass balance by attributing surpluses or deficits

to the ungaged drainage area. See Appendix A of the Phase 1 Lake Travis Model Report for more details concerning the water balance (LCRA 2004). During the course of model development for Phase 2, the modeling team used this tool developed by LCRA to extend the period of record for the water balance through 2006.

4.4 HYDRODYNAMICS AND TEMPERATURE MODEL DEVELOPMENT AND CALIBRATION

4.4.1 Model Inputs

Hydrodynamic and temperature inputs to the lake model include initial conditions, flows, boundary temperatures, and meteorological data.

4.4.1.1 Initial Conditions

For each model element (longitudinal and vertical), the initial water temperature was set to 14.9° Celsius (C) based on the bottom temperature at the end of 1983 at station 12303 (adjacent to Windy Point) as this was the closest station to Mansfield Dam with available data for 1983.

4.4.1.2 Flows

The lake model input files for flow were based on the water balance (Section 4.3). Incoming flows to the model domain included flows from upstream, the Pedernales River, five major creeks (Cow, Bee, Hurst, Big Sandy, and Cypress Creeks), and direct runoff into the lake. Outgoing flows from the model domain consisted of flows over Mansfield Dam, which included both hydropower flows and flood flows. Precipitation and evaporation were simulated by adjusting the flow over Mansfield Dam. Each of these flow files was specified as a daily time series.

4.4.1.3 Boundary Temperatures

Boundary water temperatures for flows from upstream, the Pedernales River, other major creeks, and all other direct drainage, as well as temperature of the sediment bed, were needed for model input. The only two locations with sufficient data and at appropriate locations were LCRA site No. 12318 (Travis Reservoir at the Dam) and LCRA site No. 12369 (Pedernales River at Hammett's Crossing). Other boundary temperatures were estimated as described below.

Upstream Water Temperatures

Daily water temperatures for flow from upstream were computed from data collected at LCRA site No. 12318 (Travis Reservoir at the Dam). Measurements at this station were generally made monthly from 1984 through mid-1989, every two months from mid-1989 to 2003, and weekly from 2004 through 2006. Linear interpolation between measurements was performed to obtain temperature values for days without data.

Pedernales River and Major Creeks Water Temperatures

Daily water temperatures for the Pedernales River were computed from data collected at LCRA site No. 12369 (Pedernales River at Hammett's Crossing). Measurements at this station were generally made monthly from 1984 through mid-1989, every two months from mid-1989 to 2003, and weekly from 2004 through 2006. Linear interpolation between measurements was performed to obtain temperature values for days without data.

Water temperature data for Cow, Bee, Hurst, Big Sandy, and Cypress Creeks were not available. Consequently, the daily temperatures for these creeks were assumed equal to the Pedernales River.

Direct Drainage Water Temperature

Water temperature data for direct drainage from the watershed were not available. As a result, the daily temperatures for direct drainage were assumed identical to the Pedernales River.

Sediment Bed Temperature

The temperature of the sediment bed was set to 13.5°C, which is approximately the average bottom temperature at station 12302 for the calibration period (13.7°C).

Meteorological Data

Hourly cloud cover, wind speed and direction, and air and dew point temperature data were obtained from the NCDC for Austin Mueller Municipal Airport (January 1, 1984 to May 23, 1999) and Austin Bergstrom International Airport (May 24, 1999 to December 31, 2006). Model inputs were created using hourly values.

For cloud cover, the values in the NCDC dataset range from 0 to 8 oktas representing eighths of the total celestial dome covered by clouds (i.e., 0 oktas for clear to 8 oktas for fully overcast). The input to the lake model required cloud cover on a scale of 0 to 10 rather than 0 to 8, therefore each NCDC value was multiplied by 1.25. For times with no data, the value from the previous observation was used. NCDC values of 9 or 10 were reported to represent partial but indeterminate obscuration; model values for these times were interpolated from observations with quantified cloud cover, imposing a minimum value of 5. Because many consecutive days were missing data between July 1995 and August 1996, interpolation was not performed for this time period; instead, historical monthly averages for cloud cover were used. Daily solar radiation was computed internally in the model from cloud cover for Lake Travis and position on the earth (latitude: 30.40°, longitude: 97.89°).

4.4.2 Model Parameterization

Model parameter values considered during the hydrodynamic and thermal calibration process were largely based on recommended values cited in the CE-QUAL-W2 manual. The primary calibration parameters included the time variable wind sheltering coefficient and the spatially variable shading coefficient.

4.4.3 Hydrodynamic and Temperature Calibration

4.4.3.1 Approach

The calibration of the hydrodynamics portion of the lake model involved fitting the model prediction of water surface elevation to data collected at Mansfield Dam and temperature to data collected at various stations throughout the lake for the time period from January 1, 1984 to December 31, 2006.

4.4.3.2 Calibration Data

Water surface elevation was recorded daily by the LCRA River Operations Center (ROC) at Mansfield Dam for the entire simulation period.

Water temperatures were measured at depth by LCRA generally on a monthly or bi-monthly basis at Mansfield Dam during the calibration period. From May 1984 through June 1989 and in 2004 through 2006, temperatures were recorded every month. From July 1989 through December 2004, water temperatures were measured every other month. For each sampling event, measurements were taken at the surface (approx. 0.3 meters below the surface) and at depth at generally 2-m intervals for the entire depth of the water column.

4.4.3.3 Calibration Results

The comparison of predicted water surface elevation to measured data at Mansfield Dam (lake model Segment 93) is shown in Figure 4-3. The model prediction tracks the data well. This is expected because the water balance used to create the flow inputs to the model preserved the volume of water in the lake as calculated using these measured daily lake elevations and an area/capacity table (LCRA 2004).

Temperature calibration of the model consisted primarily of adjustment of the wind sheltering coefficient. This parameter varied from 0.3 to 1.3 with an average value of 0.8. The

solar shading parameter was also adjusted during calibration. The shading coefficient was adjusted to 0.65 for the main branch of Lake Travis from Arkansas Bend to Mansfield Dam (Segments 77 through 93). Figure J-1 of Appendix J shows predicted temperature profiles and measured data at Mansfield Dam (lake model Segment 93) for each simulation year; temperature profiles for the four other stations are included in Figures J-2 through J-5. The model prediction agrees well with the data both seasonally and at depth. Starting in the spring and continuing into the summer and early fall, the lake becomes thermally stratified with the top-most layer (epilimnion) having higher temperatures than the deeper hypolimnion, typically by about 10 to 15 degrees. During late fall and early winter, the lake "turns over" as surface water cooled by lower air temperatures becomes more dense and sinks. This exchange of surface and bottom waters is enhanced by wind-induced mixing, which maintains generally uniform water temperatures during the winter over the entire water depth.

To evaluate the model performance numerically, four goodness-of-fit parameters were calculated for temperature across three water depths. These parameters (described in Appendix H) were the mean error (ME), AME, root mean square error (RMSE), and reliability index (RI). These performance metrics are given in Table 4-3. The metrics show that on average, the model does a good job of reproducing temperature observations. This is especially evident in the RI, which are all close to 1.0 (perfect agreement). The calibration performance for system-wide water temperature is on target with applications of CE-QUAL-W2 on other systems (see Table 2 of Appendix H).

Table 4-3. Water temperature model performance metrics.

	Water Depth	Segment	ME	AME*	RMSE	RI
Water Temperature (°C)	Surface (top third)	28	0.38	0.68	0.90	1.05
		48	0.43	0.74	0.98	1.05
		78	0.80	1.07	1.51	1.07
		93	1.03	1.10	1.41	1.07
		161	0.56	0.88	1.28	1.06
	Middle (middle third)	28	1.03	1.28	1.84	1.09
		48	1.38	1.61	2.24	1.12
		78	1.27	1.55	2.09	1.12
		93	1.34	1.45	1.92	1.11
		161	1.13	1.44	2.04	1.11
	Bottom (bottom third)	28	1.55	1.81	2.51	1.14
		48	1.26	1.66	2.28	1.13
		78	0.87	1.17	1.57	1.10
		93	0.62	0.93	1.22	1.08
		161	1.48	1.95	2.73	1.15

*Notes: *The system-wide average calibration goal using AME for water temperature is 1 °C (see Table 2 in Appendix H).*

Besides the wind sheltering coefficient and solar shading parameter, some of the hydraulic and bottom heat exchange coefficients were different from the model recommended values during the calibration (Table 4-4). The values for the interfacial friction factor and TSEDF set by LCRA modelers during the initial simulations most likely were taken from the DeGray Reservoir example provided with the CE-QUAL-W2 code. The bottom friction solution was selected as Manning's formulation.

The treatment of the vertical eddy viscosity in the longitudinal momentum equation was treated as explicit as recommended by the CE-QUAL-W2 manual for reservoirs. The maximum recommended value for the vertical eddy viscosity for the explicit scheme is 0.001 (Cole and Wells 2006).

Table 4-4. Model parameters affecting hydrodynamic and thermal calibration.

Parameter	Calibration Value	Default/Recommended Value	Units	Description
AX	1.0	1.0	$m^2\ sec^{-1}$	Longitudinal eddy viscosity
DX	1.0	1.0	$m^2\ sec^{-1}$	Longitudinal eddy diffisivity
CBHE	0.3	0.3	$W\ m^{-2}\ sec^{-1}$	Coefficient of bottom heat exchange
TSED	13.5	---	°C	Sediment temperature
FI	0.0	0.01	---	Interfacial friction factor
TSEDF	0.0	1.0	---	Heat lost to sediments that is added back to water column
FRICC	MANN	CHEZY	---	Bottom friction solution, MANN or CHEZY
FRICT	0.04	0.035	---	Manning's N
AZC	W2	W2	---	Form of vertical turbulence closure algorithm, NICK, PARAB, RNG, W2, W2N, or TKE
AZSLC	EXP	EXP	---	Specified either implicit, IMP, or explicit, EXP, treatment of the vertical eddy viscosity in the longitudinal momentum equation
AZMAX	1.0E-3	1.0E-3	$m^2\ s^{-1}$	Maximum value for vertical eddy viscosity
WSC	0.3 to 1.3	---	---	Wind sheltering coefficient
BETA	0.45	0.45	---	Solar radiation absorbed in surface layer
EXH2O	0.25	0.25 or 0.45	m^{-1}	Extinction coefficient for pure water
EXSS	0.01	0.01	m^{-1}	Extinction due to inorganic suspended solids
EXOM	0.2	0.2	m^{-1}	Extinction due to organic suspended solids
EXA	0.2	0.2	m^{-1}/gm^{-3}	Algal light extinction

4.5 WATER QUALITY MODEL DEVELOPMENT AND CALIBRATION

4.5.1 Model Inputs

Water quality inputs to the lake model include initial conditions, boundary conditions, and sediment fluxes.

4.5.1.1 Initial Conditions

Initial conditions for each state variable were set using earliest available data from 1984 measured at Station 12302 at the deepest depth. Organic matter parameters were assumed to be 100% refractory as initial conditions. As with the upstream boundary conditions, some measured water quality parameters needed to be deconvoluted into state variables because the measured parameters did not directly correspond to the variables required by the model.

4.5.1.2 Boundary Concentrations

Boundary conditions for the Lake Travis water quality model were established using two methodologies. For the upstream boundary, data collected at the Lake Travis headwaters station were converted into a time series of model state variable concentrations. For the other tributary boundaries, the calibrated watershed model output was used to specify time variable boundary concentrations.

Upstream Water Column Concentrations

Data collected at Station 12318 (Travis at Headwaters) were used in creating input representing upstream water quality concentrations. Prior to processing, data below detection were set to half of the detection limit. A temporary change in the method detection limit occurred in 1997 corresponding to a change in laboratories used for the sample analyses. At LCRA's recommendation, non-detect values that occurred during this time were treated as non-detected at a more typical detection limit.

The measured parameters at the upstream stations are shown in Table 4-5. In order to use these measured data in the model for boundary conditions, many needed to be deconvoluted to the state variables simulated in CE-QUAL-W2 (see Table 4-2). The converted state variables, discussed in detail below and in Appendix F, included:

- inorganics (inorganic suspended solids [ISS], PO_4);
- nitrogen (NH_3, $NO_2 + NO_3$);
- organic matter (labile and refractory, dissolved and particulate);
- algae; and
- DO.

Table 4-5. Measured water quality parameters at Lake Travis headwaters.

Abbreviation	Description*	Years Available
DO	**Dissolved Oxygen**	**1984-2006**
TOC	**Total Organic Carbon**	**1984-2006**
DOC	**Dissolved Organic Carbon**	**2004-2006**
CHLA	**Chlorophyll-a**	**1984-2006**
PHEO	**Pheophytin-a**	**1984-2006**
NOX	**Nitrite + Nitrate**	**1984-2006**
NH4	**Ammonia**	**1984-2006**
TKN	**Total Kjeldahl Nitrogen**	**1984-2006**
DKN	**Dissolved Kjeldahl Nitrogen**	**2004-2006**
TP	**Total Phosphorus**	**1984-2006**
DP	**Dissolved Phosphorus**	**2004-2006**
PO4	**Orthophosphate**	**1984-2006**
TSS	**Total Suspended Solids**	**1984-2006**
TDS	**Total Dissolved Solids**	**1984-2006**
VSS	Volatile Suspended Solids	1984-1990, 2004
ALK	Total Alkalinity	1984-2004
CHLR	**Chloride**	**1984-2004**
COND	**Specific Conductance**	**1984-2004**
SULF	Sulfate	1984-2004
TURB	Turbidity	2000-2004
FCOL	Fecal Coliform	1984-2001
ECOL	E. Coli	1994-2001
TEMP	**Temperature****	**1984-2004**
PH	pH	1984-2004

*Notes: *Parameters in bold represent those needed directly or via deconvolution for CE-QUAL-W2 primary state variables, while non-bolded parameters were not needed to set boundary conditions.*
*** Temperature boundary conditions are described in Section 4.4.1.3.*

Daily input concentration values were generated by interpolating between days with data for days without data. The resulting daily upstream loads (the product of upstream concentration and flow releases over Max Starcke Dam) of organic matter, algae, nitrogen, and phosphorus for the calibration period are shown in Figure 4-4.

Algae

Measured chlorophyll-*a* concentrations were converted from chlorophyll-*a* to organic matter by multiplying by the stoichiometric equivalent between the two.

$$ALG = CHLA_{(data)} * ACHLA \quad (4\text{-}1)$$

where:

CHLA = chlorophyll-*a* concentration based on data [mg/L]; and

ACHLA = algal biomass to chlorophyll-*a* ratio; set to 120 based on analysis of USGS phytoplankton studies.

Inorganic suspended solids

ISS is the inorganic portion of total suspended solids. It was calculated by subtracting the organic (living and non-living) portion from the total using the following equations:

$$ISS = TSS_{(data)} - (ALG + NLOSS) \quad (4\text{-}2)$$

$$NLOSS = (POC - ALG * AC)/OC \quad (4\text{-}3)$$

$$POC = TOC_{(data)} - DOC_{(data)} \quad (4\text{-}4)$$

where:

TSS = total suspended solids concentration based on data [mg/L];

NLOSS = non-living organic carbon concentration [mg/L];

POC = particulate organic carbon concentration [mg/L];

AC = algal carbon to biomass ratio; set to 0.45 (recommended CE-QUAL-W2 value);

OC = detrital carbon to biomass ratio; set to 0.45 (recommended CE-QUAL-W2 value);

TOC = total organic carbon concentration based on data [mg/L]; and

DOC = dissolved organic carbon concentration based on data [mg/L].

Bioavailable phosphorus

The deconvolution of orthophosphate data to CE-QUAL-W2 variables was not necessary.

Ammonia

The deconvolution of ammonia data to CE-QUAL-W2 variables was not necessary.

Nitrate + Nitrite

The deconvolution of nitrate and nitrite data to CE-QUAL-W2 variables was not necessary.

Organic matter

Organic matter was represented as three types in the lake model based on nutrient: organic carbon, organic nitrogen, and organic phosphorus. The following equations were used to convert the data to inputs to CE-QUAL-W2:

$$OM = (TOC - ALG * AC) / OC \quad (4\text{-}5)$$

$$OM\_N = TON - ALG * AN \quad (4\text{-}6)$$

$$OM\_P = TOP - ALG * AP \quad (4\text{-}7)$$

$$TON = TKN_{(data)} - NH4_{(data)} \quad (4\text{-}8)$$

$$TOP = TP_{(data)} - PO4_{(data)} \quad (4\text{-}9)$$

where:

TON	=	total organic nitrogen concentration [mg/L];
TOP	=	total organic phosphorus concentration [mg/L];
AN	=	algal nitrogen to biomass ratio; set to 0.042 based on analysis of USGS phytoplankton studies;
AP	=	algal phosphorus to biomass ratio; set to 0.0027 based on analysis of USGS phytoplankton studies;
TKN	=	total Kjeldahl nitrogen concentration based on data [mg/L];
NH_4	=	ammonia nitrogen concentration based on data [mg/L];
TP	=	total phosphorus concentration based on data [mg/L]; and
PO_4	=	total orthophosphate concentration based on data [mg/L].

For the carbon, nitrogen, and phosphorus it was necessary to establish the dissolved and particulate components of each organic matter group. The percentages of dissolved organic matter were based on data when available. When dissolved data were not available, the average percent dissolved of available data were applied to the appropriate organic matter group. The average was 98% for carbon, 63% for nitrogen, and 25% for phosphorus. The labile/refractory split of upstream organic matter was used as a calibration parameter because no measured information was available. The calibration established each organic matter group as 100% refractory.

Dissolved Oxygen (DO)

The deconvolution of DO data to CE-QUAL-W2 variables was not necessary.

Non-point (including Pedernales River) Water Quality Concentrations

Non-point sources to Lake Travis include inflows from the Pedernales River and five major creeks, as well as runoff (direct drainage) from each of the upgradient watershed subbasins that was not a "major creek". Non-point source inflow concentrations were specified from results from the calibrated watershed model. The output from the SWAT model, which was used for the nutrient series, organic matter, and algae, were deconvoluted for the lake model (see Section 5.3 for SWAT\CE-QUAL-W2 model linkage, including deconvolution) and input as a daily time series into the lake model by the specification of a flow file and a concentration file for each watershed subbasin. In order to preserve the water balance (Section 4.3), the flow incoming into the lake from each watershed subbasin was set to a very low constant rate of 0.001 cubic meters per second (m^3/s). The concentrations from each subbasin were then calculated by dividing the deconvoluted and spatially-appropriate loadings from the watershed model by this artificial flow rate. In this manner, the loadings predicted by the watershed model were preserved as they were input into the lake model without changing the water balance. Daily watershed loads of organic matter, algae, nitrogen, and phosphorus for the calibration period are shown in Figures 4-5 through 4-11. Non-point source organic matter groups were set as 75% refractory (Debele, Srinivasan, and Parlange 2006).

Inflow concentrations for specific conductivity, chloride, and dissolved oxygen for the five major creeks, the Pedernales River, and direct drainage were set based on data collected at the Pedernales River. Specific conductivity and chloride concentrations measured at the Pedernales River at Hammett's Crossing (Station 12369) were linearly interpolated for days without data. Because specific conductivity and chloride measurements were not available prior to April 18, 1984 and October 9, 1990, respectively, for days from the beginning of the modeling period (January 1, 1984) up to the first day with data, specific conductivity and chloride concentrations were set equal to those measured on the first day with available data. Similarly, at the time this report was written, the latest specific conductivity and chloride data downloaded and interpolated were through August 10, 2006 and July 27, 2006, respectively. These values were repeated in the model input through December 31, 2006. These substitutions for missing data did not affect the model results greatly. DO concentrations for the Pedernales River were calculated from temperature measurements at Hammett's Crossing, assuming 100% saturation. Temperature values were linearly interpolated for days without measurements.

Figure 4-12 shows the proportion of total mass over the calibration period input from SWAT into the lake model from upstream, the Pedernales River, the major creeks (Bee, Cow, Cypress, Hurst, and Sandy), and direct drainage. Upstream loads and the Pedernales River contribute the majority of constituent mass compared to the five major creeks and direct drainage.

4.5.1.3 Sediment Fluxes

CE-QUAL-W2 allows for sediment fluxes of ammonia (source), orthophosphate (source), nitrates (sink) and dissolved oxygen (sink). Sediment oxygen demand (SOD) was parameterized during calibration as a spatially variable anaerobic zero-order process. Sediment fluxes of NH_3 and PO_4 are based on SOD as constant multipliers of the SOD rate. Sediment flux of nitrates is modeled as a zero-order process. More details on the kinetic formulations of sediment fluxes are given in Appendix B of the CE-QUAL-W2 User Manual (Cole and Wells 2006). Model parameters associated with these fluxes were determined through calibration.

4.5.2 Water Quality Calibration

4.5.2.1 Approach

The calibration of the water quality portion of the lake model involved fitting the model predictions of nutrients, chlorophyll-*a*, and dissolved oxygen to data collected at Turkey Bend, Pace Bend, Arkansas Bend, Mansfield Dam, and Big Sandy Creek for the time period from January 1, 1984 through December 31, 2006. Model parameters were adjusted to match observed water quality concentrations, generally following the sequence:

- specific conductivity and chloride;
- total organic carbon and dissolved oxygen;
- total phosphorus and total Kjeldahl nitrogen; and
- chlorophyll-*a* and inorganic nutrients.

This approach is useful as it targets the water quality parameters with the simplest kinetics first, proceeding up in complexity. Using this approach as a guide, model calibration required iteration of the above steps until final parameterization was reached.

The majority of water quality parameters were measured at the surface and at one additional hypolimnion depth. For these parameters, calibration focused on matching temporal trends in surface concentrations (top two meters for chlorophyll-*a*; otherwise, top one third of the water column excluding data measured below 10 meters (approximate starting depth of the metalimnion)) with secondary consideration to bottom concentrations (bottom one third of water column). For DO, specific conductivity, and chloride, measurements were available at multiple depths throughout the water column, so calibration focused on matching observed vertical profiles.

4.5.2.2 Calibration Data

The lake model was calibrated to water quality data collected between 1984 and 2006 as part of the LCRA RSS program and the Phase 2 sampling (see Section 2 for details). The five

primary calibration locations were at Turkey Bend (Segment 28), Pace Bend (Segment 48), Arkansas Bend (Segment 78), Mansfield Dam (Segment 93), and Big Sandy Creek (Segment 161; see top panel of Figure 4-1 for locations).

4.5.2.3 Calibration Results

Several model parameters were changed during model calibration (Table 4-6). Of particular interest is the reduction of the maximum algal growth rate (AG) from the default/recommended value of 2 per day to 1.1 per day. The rate of 2 per day is typically used in eutrophication models. The 1.1 per day rate was verified by reviewing 19 CE-QUAL-W2 applications where AG was set from 0.9 to 9.0 per day with a median value of 1.9. The model requires the maximum gross production rate uncorrected for respiration, mortality, excretion, or sinking (Cole and Wells 2006). The lab incubations of epilimnetic waters from Lake Travis by the USGS did not measure AG, but instead were based on the rate of change in the daily algal fluorescence (thereby incorporating algal respiration). The USGS measurement of 0.45 per day was, therefore, a maximum net growth rate and required adjustment prior to use as a rate coefficient in the lake model.

The measured algal growth rate of 0.45 per day is likely too low because it incorporates mortality and respiration, but a growth rate of 2 per day is probably too high for Lake Travis. A range of 1.1 to 1.5 was considered during calibration as it is within the range of coefficients used in other CE-QUAL-W2 models, but not completely inconsistent with the measured data. For comparison, a rate of 1.1 per day was used for algae in a CE-QUAL-W2 model of Lake Houston (Liscum and East 2000), and values of 0.9, 1.3, and 2.1 were used for blue-green, green algae, and diatoms in a CE-QUAL-W2 model of Lake Waco (Flowers et al. 2001). Other algal parameters were adjusted during calibration to maintain a reasonable net growth rate.

Algal stoichiometry was determined based on analysis of 2005-2006 data collected by USGS and LCRA (Appendix I). Average C:N, C:P, and C:Chl-a ratios were calculated at Mansfield Dam for particulate matter. Assuming a C:Algae ratio (ALGC) of 0.45, ALGN, ALGP, and ALCHLA were estimated at 0.042, 0.0027, and 120 respectively. The N and P

stoichiometric values differ from the CE-QUAL-W2 recommended values (0.08 and 0.005, respectively) by about 50%. For oligotrophic lakes such as Lake Travis, low algal nutrient content is not uncommon. The CE-QUAL-W2 manual cites minimum elemental content of 0.034 N and 0.001 P for cyanobacteria. The recommended values of 0.08 N and 0.005 P are more typical of optimal growing conditions.

Table 4-6. Calibrated lake model parameters and default/recommended values.

Category	Parameter	Calibration Value	Default/Recommended Value	Units	Description	Basis
Algal Rates	AG	1.1	2	day^{-1}	Maximum algal growth rate	Calibration parameter
	AR	0.15	0.04	day^{-1}	Maximum algal respiration rate	Calibration parameter
	AE	0.04	0.04	day^{-1}	Maximum algal excretion rate	
	AM	0.11	0.1	day^{-1}	Maximum algal mortality rate	CE-QUAL-W2 recommends value of less than 10% of AG
	AS	0.05	0.1	m day^{-1}	Algal settling rate	Calibration parameter
	AHSP	0.001	0.003	G m^{-3}	Algal half-saturation for phosphorus limited growth	Calibration parameter
	AHSN	0.010	0.014	G m^{-3}	Algal half-saturation for nitrogen limited growth	Calibration parameter
	ASAT	100	75	W m^{-2}	Light saturation intensity at maximum photosynthetic rate	Calibration parameter
Algal Temperature Rate Coefficients	AT1	5	5	deg C	Lower temperature for algal growth	
	AT2	25	25	deg C	Lower temperature for maximum algal growth	
	AT3	35	35	deg C	Upper temperature for maximum algal growth	
	AT4	40	40	deg C	Upper temperature for algal growth	
	AK1	0.1	0.1	---	Fraction of algal growth rate at AT1	
	AK2	0.99	0.99	---	Fraction of maximum algal growth rate at AT2	
	AK3	0.99	0.99	---	Fraction of maximum algal growth rate at AT3	
	AK4	0.1	0.1	---	Fraction of algal growth rate at AT4	

Category	Parameter	Calibration Value	Default/Recommended Value	Units	Description	Basis
Algal Stoichiometry	ALGP	0.0027	0.005	---	Stoichiometric equivalent between algal biomass and phosphorus	USGS particulate C,N measurements; LCRA TP,PO_4 measurements
	ALGN	0.042	0.08	---	Stoichiometric equivalent between algal biomass and nitrogen	USGS particulate C,N measurements
	ALGC	0.45	0.45	---	Stoichiometric equivalent between algal biomass and carbon	
	ALCHLA	120	145	---	Ratio between algal biomass and chlorophyll-*a*	USGS particulate C,N measurements; LCRA chlorophyll-*a* measurements
	ALPOM	0.8	0.8	---	Fraction of algal biomass that is converted to particulate organic matter when algae die	
	ANEQN	2	2	---	Equation number for algal ammonium preference (either 1 or 2)	
	ANPR	0.001	0.001	---	Algal half saturation constant for ammonium preference	
Dissolved Organic Matter	LDOMDK	0.1	0.1	day^{-1}	Labile DOM decay rate	
	RDOMDK	0.001	0.001	day^{-1}	Refractory DOM decay rate	
	LRDDK	0.01	0.01	day^{-1}	Labile to refractory DOM decay rate	
Particulate Organic Matter	LPOMDK	0.08	0.08	day^{-1}	Labile POM decay rate	
	RPOMDK	0.001	0.001	day^{-1}	Refractory POM decay rate	
	LRPDK	0.01	0.01	day^{-1}	Labile to refractory POM decay rate	
	POMS	1	0.1	m day^{-1}	POM settling rate	Calibration parameter
Organic Matter Stoichiometry	ORGP	0.0027	0.005	---	Stoichiometric equivalent between organic matter and phosphorus	Same as ALGP
	ORGN	0.042	0.08	---	Stoichiometric equivalent between organic matter and nitrogen	Same as ALGN
	ORGC	0.45	0.45	---	Stoichiometric equivalent between organic matter and carbon	

Category	Parameter	Calibration Value	Default/Recommended Value	Units	Description	Basis
Organic Matter Temperature Rate Multipliers	OMT1	4	4	deg C	Lower temperature for organic matter decay	
	OMT2	25	25	deg C	Upper temperature for organic matter decay	
	OMK1	0.1	0.1	---	Fraction of organic matter decay rate at OMT1	
	OMK2	0.99	0.99	---	Fraction of organic matter decay rate at OMT2	
Inorganic phosphorus	PO4R	0.0015	0.001	fraction of SOD	Sediment release rate of phosphorus	Calibration parameter
Ammonium	NH4R	0.025	0.001	fraction of SOD	Sediment release rate of ammonium	Calibration parameter
	NH4DK	0.06	0.12	day^{-1}	Ammonium decay rate	Calibration parameter
Ammonium Temperature Rate Multipliers	NH4T1	5	5	deg C	Lower temperature for ammonia decay	
	NH4T2	25	25	deg C	Lower temperature for maximum ammonia decay	
	NH4K1	0.1	0.1	---	Fraction of nitrification at NH4T1	
	NH4K2	0.99	0.99	---	Fraction of nitrification at NH4T2	
Nitrate	NO3DK	0.03	0.03	day^{-1}	Nitrate decay rate	
	NO3S	0.35	1	m day^{-1}	Denitrification rate from sediments	Calibration parameter
Nitrate Temperature Rate Multipliers	NO3T1	5	5	deg C	Lower temperature for nitrate decay	
	NO3T2	25	25	deg C	Lower temperature for maximum nitrate decay	
	NO3K1	0.1	0.1	---	Fraction of denitrification rate at NO3T1	
	NO3K2	0.99	0.99	---	Fraction of denitrification rate at NO3T2	
Oxygen Stoichiometry	O2NH4	4.57	4.57	---	Oxygen stoichiometry for nitrification	
	O2OM	1.4	1.4	---	Oxygen stoichiometry for organic matter decay	
Oxygen Stoichiometry 2	O2AR	1.1	1.1	---	Oxygen stoichiometry for algal respiration	
	O2AG	1.4	1.4	---	Oxygen stoichiometry for algal primary production	

Category	Parameter	Calibration Value	Default/Recommended Value	Units	Description	Basis
Oxygen limit	KDO	0.1	0.1	g m^{-3}	Dissolved oxygen half-saturation constant or concentration at which aerobic processes are at 50% of their maximum	
Sediment compartment	SEDC	OFF	OFF		Switch to turn on/off first order sediment compartment	
SOD temperature rate multipliers	FSOD	1	1	---	Fraction of the zero-order SOD rate used	
	SODT1	4	4	deg C	Lower temperature for zero-order SOD or first-order sediment decay	
	SODT2	25	25	deg C	Upper temperature for zero-order SOD or first-order sediment decay	
	SODK1	0.1	0.1	---	Fraction of SOD or sediment decay rate at lower temperature	
	SODK2	0.99	0.99	---	Fraction of SOD or sediment decay rate at upper temperature	
Zero-Order Sediment Oxygen Demand	SOD	1.0 to 1.6	---	g O_2 m^{-2} day^{-1}	Zero-order sediment oxygen demand for each segment	Calibration parameter

Notes: Default/recommended values reported in Cole and Wells (2006).

Conservatives Constituents (Specific Conductivity and Chloride)

Figures J-6 through J-10 of Appendix J show the monthly specific conductivity vertical profiles at the five main water quality stations. Generally, specific conductivity does not vary much over the depth of the lake, a feature also reproduced by the model. Figures 4-13 through 4-17 show the temporal plots at these same stations. Overall, the model does a good job in reproducing the specific conductivity throughout the lake. The model performs best at the most upstream stations (Segments 28 and 48). The slight overprediction that occurs at the downstream stations is most likely due to the approximation that the inputs from other tributaries and direct drainage have the same conductivity as the Pedernales. Also of particular interest is the large salt pulse that occurred during 1989 to 1991 due to saline water released from the Natural Dam Salt Lake in 1987 to 1989 (Raines 1999); the model tracks lake response to this accurately at the different locations. The most upstream location (Segment 28) shows gradual

increases from 1987 to a peak in 1990 and a subsequent decline from 1990 to 1992. The conductivity and chloride concentrations at this location are much more responsive to the salt water inputs than at Mansfield Dam. At the Dam, the concentrations are much more attenuated. The rise in concentrations is more gradual and delayed. Peak concentrations are not reached until 1991. Concentrations gradually decline until late in 1991 when a large flood restores the lake back to typical concentrations. The fact that the model reproduced these responses well indicates that the hydrodynamic and thermal model accurately represents lake advection and dispersion.

Figures J-11 through J-15 of Appendix J show the vertical and temporal profiles of chloride throughout the lake. As with conductivity, the model reproduces the chloride levels well.

Dissolved Oxygen

The main drivers of oxygen levels in the lake are surface reaeration, SOD, and to a somewhat lesser degree, algal growth/respiration and organic matter decay. Figures 4-18 through 4-27 and Figures J-16 through J-20 of Appendix J show the dissolved oxygen levels at various stations simulated by the model. Inspection of the temporal plots shows that the model does a good job of capturing the seasonal dynamics of oxygen at surface, middle, and bottom depths. One important feature that the model captures well is the onset and duration of bottom hypoxia (bottom panels, Figures 4-23 through 4-27). The model tends to underpredict oxygen levels at the surface and middle depths during the winter months, especially during the later years of calibration. This may be due to the model not predicting the levels of algae observed during the winter months (see below).

Algae

Figures 4-28 through 4-32 show temporals of the surface (i.e., top two meters depth) chlorophyll-*a* concentrations throughout the lake. The data show that generally algal concentrations are highest upstream and decline toward Mansfield Dam. The model does a good job of reproducing this spatial trend. The model also performs reasonably in predicting average chlorophyll-*a* levels, although it is not able to reproduce the intra-seasonal variability that is

observed. Short-term algal blooms are generally not captured. The model also shows a much stronger seasonal dependence of algae than is observed in the data. The CE-QUAL-W2 model could not produce the standing levels of algae that are observed in the winter. For this reason, the primary calibration of chlorophyll-*a* focused on reproducing average chlorophyll-*a* concentrations during the months of maximum standing algal density (i.e., summer season). Figure 4-33 shows the model to data comparison of the summer (June - September) mean surface chlorophyll-*a* concentrations. Along the main lake stations, the model matches the average summer algal concentrations well.

In order to understand the factors controlling algal growth throughout Lake Travis, it is useful to examine the algal growth limitation factors. Figures J-21 through J-25 of Appendix J show monthly vertical profiles of the algal limiting factor at locations corresponding to the primary sampling stations. These plots show that the maximum algal growth typically occurs in a photic zone with a width of about 4 to 8 m at a depth 0 to 4 m below the surface. Below this zone, low light levels limit algal growth. At the surface, light often limits algal growth by photo-inhibition, whereby strong light (above the saturation intensity) can reduce photosynthetic capacity. Within the photic zone, both the availability of nitrogen and phosphorus can limit the algal growth. Lake-wide, algal growth is limited almost equal amounts of the time by both nutrients. The upper lake (Segments 28 and 48) is phosphorus-limited (38% of the time P-limited and 32% N-limited) more of the time, and the lower lake (Segments 78, 93, and 161) is more nitrogen limited (29% of the time P-limited and 40% N-limited). Seasonally, the lake is somewhat limited more of the time by phosphorus in the summer and limited by nitrogen more in the winter. These nutrient limitations are verified by the performance of the model in capturing the surface orthophosphate and nitrate (despite the apparent overprediction of nitrates from the watershed model) levels throughout the lake (see below).

Organic Matter (Total Organic Carbon)

Figures 4-34 through 4-38 show the model to data comparisons of total organic carbon (TOC). TOC is observed to be relatively constant throughout the lake at 3 to 5 mg/L in the upper lake and 2 to 4 mg/L in the lower lake. The model does well at capturing this general behavior. The main factors controlling TOC levels in the lake are particulate settling, labile and refractory

decay. In order to calibrate to the observed TOC levels, the incoming organic matter from all sources was set to be 100% refractory in nature.

Nitrogen

Total Kjeldahl Nitrogen (TKN) is shown in Figures 4-39 through 4-43. TKN remains at relatively low concentrations (< 1.0 mg/L) throughout the lake. The model reproduces these levels well. The data show more variability in TKN at the upstream and cove locations with occasional spikes, and a more constant signal towards Mansfield Dam. This feature is also reproduced by the model although TKN spikes are not captured, individually. At the deeper locations in the lake, a late summer increase occurs in bottom TKN that is due to the release of ammonia under hypolimnetic anoxic conditions. The model also does well to capture that increase.

Ammonia levels in surface (i.e., top one-third depth) waters throughout Lake Travis are generally very low (below 0.2 mg/L) as seen in Figures 4-44 through 4-48. The model also generates comparably low ammonia values. As stated above, some of the deeper parts of the lake will accumulate higher bottom ammonia levels, up to 0.8 mg/L, due to ammonia releases from the sediment during the times of the year that the lake bottom waters go anoxic. The model does well to simulate the timing and magnitude of these releases at these locations. There also appears to be a pulse of somewhat higher (0.2 mg/L) surface ammonia concentrations that occurs in 1997-1998. The model does not capture this period of higher ammonia.

Figures 4-49 through 4-53 show the nitrate and nitrite levels throughout the lake. Observed levels are generally low (<0.5 mg/L). The model does well to reproduce the surface NO_x levels, and most importantly, reproduces the NO_x depletion that typically occurs from late spring through summer. Nitrate and nitrite levels at Pace Bend (Segment 48) are overpredicted. The high concentrations generated by the model at that location arise from the high levels coming in from the Pedernales River. Another feature of the data is the accumulation of nitrate and nitrite at the lake bottom during the winter. Although the model also shows an increase during these months, the magnitude of this increase is underestimated in the downstream portions of the lake. Although the watershed model seemed to grossly overpredict the nitrate and

nitrite levels (see Section 3), the lake model does not suffer correspondingly. This may indicate that the levels produced by the SWAT model represent the actual loads better than suggested by the watershed model-data comparisons. That is, the data used to calibrate the SWAT model may have been biased low due to lack of storm data. Denitrification is the only other sink that could compensate for an overestimated watershed nitrate and nitrite load. However, denitrification within the water and sediments were calibrated at reasonable values (0.03/d and 0.35 m/d, respectively).

Phosphorus

Figures 4-54 through 4-58 show the total phosphorus observed with the model calibration. The primary factor in the model controlling TP levels in the lake is particulate settling of organic phosphorus (algal and/or detrital). CE-QUAL-W2 does not simulate the sorption and subsequent settling of orthophosphate that can occur in water bodies. TP is generally low throughout the lake, with a large number of samples being below detection limit. There is a trend of decreasing TP from upstream to downstream. The model reproduces these values and trends well. Occasional isolated high values (above detection limit) are observed at various locations; these are not typically reproduced by the lake model. There are also marked elevated TP concentrations throughout the lake from fall 1993 to spring 1995; the model also captures this phenomenon, although it does not simulate this increase until spring 1994. During fall 1993, the observed TP concentrations at the boundary are nearly the same at the next downstream station (Segment 28). This may be indicative of a higher proportion of dissolved organic phosphorus during this time. The model also seems to underestimate the high TP levels at the Mansfield Dam during 1993-1995, as well as other occasional subsequent elevated spikes. Inspection of the data shows that during these times, TP levels in the lake often increase from upstream to downstream. This may be due to high phosphorus levels coming in from local watersheds downstream of the Pedernales River not predicted by the watershed model or possibly an in-lake process not represented in the water quality model.

Orthophosphate model calibration is shown in Figures 4-59 through 4-63. Surface PO_4 concentrations are typically below detection limit in Lake Travis. Consequently, no observable patterns are visible. The model also produces surface PO_4 levels that generally remain below

detection limits. The model simulates very low limiting values of PO_4 during the summer, but it cannot be verified against observations as the detection limit for the majority of calibration is above typical half-saturation values for PO_4 limitation. As with ammonia, PO_4 levels will rise at the deeper areas of the lake in summertime due to the accumulation of PO_4 released from the sediments to the hypolimnion under hypoxic condition. This can be seen most dramatically at segments 78 and 93 at the lower end of the lake. The model simulates the magnitude of this increase of PO_4 reasonably well at all main lake locations.

Goodness-of-fit statistics were calculated for all surface water quality parameters. These performance metrics are given in Table 4-7. The metrics for conservative constituents (specific conductivity and chloride) are good, with only a small overprediction by the model. RI is close to 1.0 at all locations. The model also performs well for dissolved oxygen. Model performance for chlorophyll-*a* is acceptable, with the RI between 2.4 and 3.6. The model underpredicts somewhat at the most upstream location (segment 28), but does not show significant bias in the rest of the lake. TOC metrics are good throughout the lake. Model performance for various nutrients (nitrogen and phosphorus) are reasonable, with the RI routinely between 2.8 and 4.0 for most parameters (TKN performance is better at ~1.9). These higher values are due to the high variability of the data and may be compounded by the high frequency of TP and PO_4 data at detection limit. On average, TKN, NH_4, and TP are underpredicted by the model, while the inorganics (NO_x and PO_4) are on average overpredicted. High values of the RMSE can occur because this index is strongly influenced by occasionally observed extremely high concentrations that are not reproduced. While the RMSE was the preferred metric used for the evaluation of model performance, it should be noted that the values for AME are similar to values for system-wide water quality in other reservoirs modeled using CE-QUAL-W2 (see Table 2 of Appendix H). One exception is for TP, where the AME is slightly higher compared to applications of the model on other systems; the higher deviations from data could be due to the higher variability of the data as well as much data being reported at the detection limit. The values in Table 2 of Appendix H are average AME's for the system as a whole and may not be met at all places and times.

Table 4-7. Water quality model performance metrics for surface layers (top third).

Parameter	Segment	ME	AME	RMSE	RI
Specific Conductivity (µmhos/cm)	28	-8	34	62	1.11
	48	-17	33	48	1.10
	78	-18	35	43	1.09
	93	-26	37	45	1.09
	161	-23	37	46	1.09
Chloride (mg/L)	28	-2.6	5.9	8.9	1.15
	48	-5.7	7.5	10.6	1.22
	78	-3.7	5.9	8.2	1.17
	93	-4.5	6.6	10.0	1.18
	161	-3.6	6.2	8.7	1.18
Dissolved Oxygen (mg/L)	28	0.24	0.65	0.90	1.12
	48	0.40	0.75	0.96	1.15
	78	0.33	0.74	0.93	1.14
	93	0.46	0.89	1.08	1.17
	161	0.79	0.87	1.05	1.14
Chlorophyll-*a** (µg/L) (SA AME = 4)	28	2.12	5.72	8.95	2.40
	48	-3.15	6.00	8.47	2.68
	78	-4.15	5.13	6.90	3.18
	93	-1.16	3.35	4.81	3.13
	161	-3.87	4.99	6.73	3.64
TOC (mg/L) (SA AME = 0.6)	28	0.04	0.71	0.97	1.28
	48	0.17	0.73	1.05	1.32
	78	0.19	0.63	0.81	1.29
	93	0.27	0.65	0.85	1.30
	161	0.14	0.59	0.78	1.28
TKN (mg/L) (SA AME = 0.4)	28	0.16	0.26	0.44	1.94
	48	0.16	0.25	0.57	1.92
	78	0.08	0.18	0.33	1.90
	93	0.09	0.16	0.28	1.79
	161	0.07	0.19	0.35	1.87
NH_4 (µg/L) (SA AME = 30)	28	17.8	28.8	56.7	3.22
	48	9.0	24.1	41.2	3.01
	78	7.9	23.3	52.1	3.01
	93	11.8	23.8	48.2	3.01
	161	9.5	27.8	58.4	3.33
NO_x (mg/L) (SA AME = 0.1)	28	-0.02	0.07	0.13	2.95
	48	-0.20	0.24	0.83	4.02
	78	-0.07	0.11	0.18	3.40
	93	-0.04	0.08	0.13	3.18
	161	-0.05	0.09	0.14	3.29
TP (µg/L) (SA AME = 20)	28	20.3	32.2	114.3	2.80
	48	7.7	33.3	84.2	3.06
	78	3.84	32.4	84.7	3.30
	93	9.80	37.6	90.6	3.48
	161	-2.3	27.6	54.1	3.43

Parameter	Segment	ME	AME	RMSE	RI
PO_4 (µg/L) (SA AME = 10)	28	-2.15	6.86	10.37	3.05
	48	-6.05	9.82	15.46	3.28
	78	-9.33	10.76	13.25	3.58
	93	-8.53	10.52	13.45	3.48
	161	-7.87	10.85	17.99	3.55

Surface water is considered as top one-third of water column except for chlorophyll-a (top two meters of water column). Data in the top one-third depth are excluded if measured below 10 meters (approximate starting depth of metalimnion

SA AME = System-wide average absolute mean error calibration goal

**Note: Chlorophyll-a statistics are for summer (Jun-Sept) only*

4.5.3 MODEL PERFORMANCE IN COVES

As indicated in Section 1.3, one of the objectives for the Phase 2 work was to quantify differences in water quality between the main body of Lake Travis and its coves. Phase 2 included the modeling of Cow, Bee, Hurst, Big Sandy, and Cypress Creeks. Because monitoring at all but one of the cove sampling stations started in 2004 with the expanded sampling program (Table 2-1), the evaluation of model performance in the coves focused on Big Sandy Creek, which contains a station (RSS site 12307) with a sampling period encompassing the model calibration period.

For the hydrodynamic component, the model largely captured the trends in specific conductivity, chloride, DO, and temperature data measured in Big Sandy Creek over the calibration period (Figures 4-17, 4-22, 4-27, J-5, J-10, J-15, and J-20). It performed as well there as it did at the main lake stations. The goodness-of-fit statistics of ME, RMSE, and RI for water temperature show that good agreement exists between model predictions and observations at the cove location (Table 4-3). Values for all three metrics at the Big Sandy Creek location are within the range of values calculated for the four main lake stations except for temperature predictions in the bottom third of the water column, where the model-data agreement is marginally worse when comparing RMSE and RI.

For the water quality component, the model generally captured the trends in nutrient data measured in Big Sandy Creek over the calibration period (Figures 4-32, 4-38, 4-43, 4-48, 4-53, 4-58, and 4-63). For almost all water quality parameters, it also performed as well at Big Sandy Creek as it did at the main lake stations. The performance metrics of ME, RMSE, and RI calculated for all surface water quality parameters compare well to those computed for the main lake stations (Table 4-7). In most cases, the metrics at Big Sandy Creek were within the range of those for the lake stations. The ME is slightly worse for DO, the RI is marginally worse for chlorophyll-a, and the RMSE and RI are slightly worse for NH4. These differences are likely not significant and therefore, the model can be as reliably used for Big Sandy Creek (and other coves) as it can for the main lake.

4.6 WATER QUALITY MODEL SENSITIVITY ANALYSIS AND BOUNDING CALIBRATION

The lake modeling included the evaluation of the sensitivity of model predictions to SWAT and CE-QUAL-W2 input parameters and external loadings. With a few exceptions, the sensitivity analysis involved a one-at-a-time parameter change for each input variable analyzed. Model uncertainty was addressed through the establishment of a bounding calibration. With this approach, another acceptable model calibration was established to give an upper-bound prediction of summertime chlorophyll-*a* and therefore yield insights to the uncertainty associated with the model predictions (QEA 1999). This approach was necessary because long model run times prohibited iterative model runs such as those performed in a Monte Carlo simulation. In this case, another acceptable model calibration was established to give an upper-bound prediction of summertime chlorophyll-*a*.

4.6.1 Sensitivity Analysis

Two sets of sensitivity analyses were performed for the lake model: 1) sensitivity to SWAT and CE-QUAL-W2 model parameters and 2) sensitivity to external loadings (i.e., from upstream or from the watershed). For the first set, the sensitivity analyses entailed a one-at-a-time parameter change for each lake model input parameter modified from the recommended

value during model calibration and for the four watershed model parameters found to be most sensitive with respect to orthophosphate (Section 3.6). The exceptions to the one-at-a-time testing were for the maximum algal growth rate (maximum algal mortality rate was kept at 10% of the tested algal growth rate) and percent dissolved carbon, nitrogen, and phosphorus from upstream and from the watershed (all three constituents were changed to their low value and run and then all three were changed to their high value and run). Table 4-8 lists the 14 lake model parameters tested and their values; most parameters were adjusted ±50% of their base value and were confirmed that they were within bounds found in literature (Bowie et al. 1985; Cole and Wells 2006). Watershed model outputs from the watershed sensitivities related to SWAT parameters BIOMIX, MUMAX, P_UPDIS, and PSP were linked and passed as inputs to the lake model; see Table 3-10 for the parameter ranges tested for the watershed model input parameters.

Table 4-8. Lake input parameters tested during sensitivity analysis.

Parameter	CE-QUAL-W2 Code	Parameter Values Tested				Comments
		Base	Low	High	Units	
Maximum algal growth rate	AG	1.1	0.55	1.65	1/d	maximum algal mortality rate, AM, kept at 10% of AG during testing
Algal settling rate	AS	0.05	0.025	0.075	m/d	
Algal half-saturation for phosphorus limited growth	AHSP	0.001	---	0.003	g/m^3	non-linear function; base is at minimum recommended value in manual
Algal half-saturation for nitrogen limited growth	AHSN	0.010	0.005	0.015	g/m^3	
Maximum algal respiration rate	AR	0.150	0.075	0.225	1/d	
Light saturation intensity at maximum photosynthetic rate	ASAT	100	50	150	W/m^2	non-linear function, but kept at ±50% because found not to have much impact during calibration
Particulate organic matter settling rate	POMS	1	0.5	1.50	m/d	
Sediment release rate of phosphorus	PO4R	0.0015	0.0008	0.0023	fraction of SOD	
Sediment release rate of ammonium	NH4R	0.025	0.0125	0.0375	fraction of SOD	
Ammonium decay rate	NH4DK	0.06	0.03	0.09	1/d	
Denitrification rate from sediments	NO3S	0.35	0.175	0.525	m/d	
% refractory organic matter (from watershed)	---	75	37.5	100	%	high value capped at 100%
% dissolved C, N, and P (from upstream)	---	98 / 63 / 25	49 / 21.5 / 12.5	100 / 94.5 / 37.5	%	all three constituents varied at once; high value capped at 100%
% dissolved C, N, and P (from watershed)						all three constituents varied at once; high value capped at 100%
non-Pedernales watershed	---	84 / 33 / 8	42 / 16.5 / 4	100 / 49.5 / 12	%	
Pedernales watershed		91 / 52 / 13	45.5 / 26 / 6.5	100 / 78 / 19.5	%	

Notes: Parameters varied ±50% from base (calibration) value unless otherwise indicated. C = carbon, N = nitrogen, P = phosphorus

The second set of sensitivities included a one-at-a-time change for the following external loadings:

- PO_4 from the watershed;
- NO_X from the watershed;
- Organic P from the watershed;
- PO_4 from upstream;
- NO_X from upstream; and
- Organic P from upstream.

These parameters were adjusted ±50% of their base loadings. Fifty percent was arbitrarily chosen, merely to vary each loading in the same way for direct comparison of sensitivity analysis results.

Due to the lengthy model run time, the sensitivity analyses were conducted only on the last seven years (2000-2006) of the calibration period. Initial conditions were set as the depth-averaged model predictions from the calibration run for January 1, 2000. The base case was a similarly shortened run using the calibration parameters. The shortened base run was compared to the 2000-2006 portion of the full calibration run. Except for the first few months of the simulation, the shortened run reproduced the full calibration almost identically.

The model predictions used to assess model sensitivity were average chlorophyll-*a* in the top two meters and average PO_4 in the top third depth at Mansfield Dam (segment 93) during summer months (June-Sept). For each constituent, a sensitivity index was calculated as the maximum difference between the sensitivity and base model results for each parameter set divided by the change in input parameter (equation 4-10). The change in input parameter was included as part of the metric because not all inputs were adjusted the same percentage.

$$SI = \max\left(\left|\frac{result_{low} - result_{base}}{P_{low}}\right|, \left|\frac{result_{high} - result_{base}}{P_{high}}\right|\right) \quad (4\text{-}10)$$

where:

$result_{low}$ = average model prediction for sensitivity using the low value for the input parameterl;

$result_{high}$ = average model prediction for sensitivity using the high value for the input parameter;

$result_{base}$ = average model prediction using the base case value for the input parameter;

P_{low} = percent change in input value from base case value to low value; and

P_{high} = percent change in input value from base case value to high value.

The input parameters were then sorted by descending ranking index; the higher the index, the more sensitive the model output. Figures 4-64 and 4-65 show the changes to the model output variables in relation to the change in input parameters; the most sensitive parameters are listed first.

The most sensitive lake model parameters for summertime surface chlorophyll-*a* were found to be maximum algal growth rate, particulate organic matter settling rate, and % refractory organic matter from the watershed. For summertime surface PO_4, the same three parameters were among the most sensitive in addition to the phosphorus availability index (SWAT). Within the range of values and time period tested, these inputs had at least a 0.7 µg/L impact on predicted summertime surface chlorophyll-*a* concentration and more than a 3.5 µg/L impact on predicted summertime surface PO_4 concentration.

Figures 4-66 and 4-67 show the changes in the model results in relation to the changes to the external loadings. Of the six loadings tested, the most sensitive were found to be the organic P loading from the watershed and NO_X loading from the watershed. The results for this set of sensitivity analyses are in-line with the relative contributions of loadings to the system (Figure 4-12).

4.6.2 Bounding Calibration

Based on the sensitivity analysis, three input parameters were adjusted to achieve an upper bound calibration for summertime chlorophyll-*a* for the full calibration period. These parameters were maximum algal growth rate, particulate organic matter settling rate, and refractory percentage from watershed. A lower value for each of these parameters equates to higher chlorophyll-*a* concentrations. All three parameters were reduced equally by 20%. This reduction was the maximum value that preserves approximately the same degree of accuracy to data observations as measured by the RMSE performance metric. This set of parameter values represent a bounding limit of key parameters that still would provide an acceptable calibration. Figures 4-68 through 4-77 show temporal plots of the surface water quality concentrations at Mansfield Dam. The figures include the measured data, the original model calibration, and the bounding calibration. Root mean square errors for the base and bounding calibrations are presented in Table 4-9.

Table 4-9. Root mean square errors for surface water at Mansfield Dam for the original and bounding calibrations.

Parameter	Root Mean Square Error	
	Original Calibration	Bounding Calibration
Specific Conductivity (µmhos/cm)	45	45
Chloride (mg/L)	10.0	10.0
Dissolved Oxygen (mg/L)	1.08	1.15
Chlorophyll-*a** (µg/L)	4.81	5.78
TOC (mg/L)	0.85	0.84
TKN (mg/L)	0.28	0.27
NH_4 (µg/L)	48.2	48.7
NO_x (mg/L)	0.13	0.16
TP (µg/L)	90.6	91.0
PO_4 (µg/L)	13.45	18.40

Surface water is considered as top one-third of water column except for chlorophyll-a (top two meters of water column). Data in the top one-third depth are excluded if measured below 10 meters (approximate starting depth of metalimnion).

**Note: Chlorophyll-a statistics are for summer (Jun-Sept) only.*

The bounding calibration was used to assess uncertainty in summertime surface chlorophyll-*a* predictions under different future scenarios (Anchor QEA and Parsons 2009).

SECTION 5
MODEL LINKAGE

5.1 INTRODUCTION

The watershed model was joined to the lake model through a custom intermediary program that connected and converted the output files from the watershed model to appropriate input files for the lake model. The linkage was performed in two steps: 1) spatially relating each lake model segment to the appropriate watershed model subbasin; and 2) deconvoluting SWAT state variables to CE-QUAL-W2 state variables. These two steps are described in Sections 5.2 and 5.3, respectively. More information on the variable deconvolution can be found in Appendix G.

5.2 MODEL SPATIAL LINKAGES

Figure 5-1 shows the lake model segments and the nearby subbasins of watershed model. Due to the nature of the subbasin delineation, each lake model segment is spatially related to a watershed model subbasin in one of two ways: either it is contained within a watershed subbasin or it is the receiving segment of an adjacent upstream watershed.

Determination of the spatial relationship of each lake model segment to a watershed model subbasin is important because the relationship indicates the proper watershed model output file to use for linkage between the models. The two SWAT model output files used for the linkage were output.sub and output.rch. The former file contains summary information for each subbasin in the watershed or the loadings coming directly from the land surface into the lake segment; the latter file contains summary information for each routing reach in the watershed or the loadings once SWAT has routed the nutrients down the stream. If the lake segment is contained within a watershed subbasin, the information from output.sub is used. If the lake segment is the receiving segment of an adjacent upstream watershed, the information from output.rch is used. In other words, the nutrient kinetics for portions of the lake being

represented as a segment in the lake model are modeled in CE-QUAL-W2 using the loads from the appropriate subbasin of the watershed model. For portions of the lake not being represented as a segment in the lake model (i.e., smaller tributaries feeding into the main body of the lake), the output from the reach is used as input to the lake model because it contains cumulative results from water quality processes within all upstream watershed subbasins at the point where the reach intersects and empties into the lake. Table 5-1 shows the relationship between the lake model segments and watershed model subbasins and indicates the type of output file used.

Table 5-1. Relationship between lake model segments and watershed model subbasins.

Branch	Watershed Subbasin Number	Output Type	Receiving Lake Model Segment Number	
			Upstream	Downstream
Lake Travis	6	SUB	2	6
Lake Travis	5	RCH	6	
Lake Travis	8	SUB	6	7
Lake Travis	7	RCH	7	
Lake Travis	12	SUB	7	8
Lake Travis	11	RCH	8	
Lake Travis	16	SUB	9	10
Lake Travis	15	RCH	10	
Lake Travis	14	SUB	11	16
Lake Travis	13	RCH	17	
Lake Travis	17	SUB	17	19
Lake Travis	18	RCH	19	
Lake Travis	26	SUB	20	23
Lake Travis	25	RCH	23	
Lake Travis	27	SUB	23	25
Lake Travis	28	RCH	25	
Lake Travis	33	SUB	26	33
Lake Travis	34	RCH	33	
Lake Travis	37	SUB	34	40
Pedernales	38	SUB	96	110
Pedernales	45	RCH	96	
Pedernales	46	RCH	96	
Lake Travis	30	SUB	40	48
Cow Creek	23	SUB	113	116
Cow Creek	73	RCH	113	
Cow Creek	29	SUB	116	123
Cow Creek	24	RCH	116	
Lake Travis	47	SUB	48	70
Bee Creek	48	SUB	126	132
Bee Creek	71	RCH	126	
Lake Travis	49	SUB	70	71
Lake Travis	50	RCH	71	
Lake Travis	43	SUB	71	76
Hurst Creek	70	RCH	135	
Hurst Creek	44	SUB	135	145
Lake Travis	35	SUB	77	86

Branch	Watershed Subbasin Number	Output Type	Receiving Lake Model Segment Number	
			Upstream	Downstream
Big Sandy	19	RCH	148	
Big Sandy	20	RCH	149	
Big Sandy	22	SUB	149	150
Big Sandy	21	RCH	150	
Big Sandy	31	SUB	151	160
Big Sandy	32	RCH	160	
Big Sandy	36	SUB	161	
Lake Travis	39	SUB	86	89
Cypress Creek	72	RCH	170	
Cypress Creek	40	SUB	170	177
Lake Travis	74	SUB	89	93

Notes: See Figure 5-1 for a map showing the segmentation.

5.3 DECONVOLUTION OF SWAT TO CE-QUAL-W2 STATE VARIABLES

The custom intermediary program not only needed information for spatially linking the two models, but also required some output processing because several variables output by SWAT were not directly translatable to inputs to CE-QUAL-W2. The output from SWAT became the input to CE-QUAL-W2 through the creation of post-processors that read in the SWAT output files and produced inputs in the format required by CE-QUAL-W2. This transformation required the deconvolution of SWAT state variables. The converted state variables used in CE-QUAL-W2 are:

- inorganics (ISS, PO_4);
- nitrogen (NH_3, $NO_2 + NO_3$);
- organic matter (labile and refractory, dissolved and particulate);
- algae; and
- DO.

In the following discussions, equations pertaining to the deconvolution of variables in the output.rch file are on the left side of the page; equations using variables in output.sub are on the right side of the page.

5.3.1 Inorganics

5.3.1.1 Inorganic Suspended Solids

ISS was calculated by subtracting the particulate portion of organic matter from the sediment that is transported out of a reach or sediment transported into a subbasin and converting to the appropriate units. If ISS was negative, it was set to zero.

$$ISS = \frac{SED\_OUT - LPOM - RPOM}{timestep} \qquad ISS = \frac{SYLD \times AREA - LPOM - RPOM}{timestep} \qquad (5\text{-}1)$$

where:

SED_OUT	=	sediment transported with water out of reach during timestep (mass); from SWAT output.rch;
LPOM	=	labile particulate organic matter (see organic matter below);
RPOM	=	refractory particulate organic matter (see organic matter below);
SYLD	=	sediment yield (mass/area); sediment from the subbasin that is transported into the reach during the timestep; from SWAT output.sub;
AREA	=	area of subbasin (length squared); from SWAT output.sub; and
timestep	=	watershed model timestep.

5.3.1.2 Bioavailable Phosphorus

Orthophosphate is the form of phosphorus that is bioavailable. Except for the conversion to appropriate units, deconvolution of SWAT variables to CE-QUAL-W2 variables was not necessary for orthophosphate.

$$PO_4 = \frac{MINP\_OUT}{timestep} \qquad PO_4 = \frac{(SOLP + SEDP) \times AREA}{timestep} \qquad (5\text{-}2)$$

where:

MINP_OUT = mineral phosphorus transported with water into reach during timestep (mass); from SWAT output.rch;

SOLP = soluble *P* yield (mass/area); phosphorus that is transported by surface runoff into the reach during the timestep; from SWAT output.sub;

SEDP = mineral *P* yield (mass/area); mineral phosphorus attached to sediment that is transported by surface runoff into the reach during the timestep; from SWAT output.sub;

AREA = area of subbasin (area); from SWAT output.sub; and

timestep = watershed model timestep.

5.3.2 Nitrogen

5.3.2.1 Ammonia

Except for the conversion to appropriate units, deconvolution of SWAT variables to CE-QUAL-W2 variables was not necessary for the model elements receiving ammonia from upstream reaches. Ammonia is not tracked in subbasins and therefore, ammonia levels from the land surface were set to zero in the lake model input file.

$$NH4 = \frac{NH4\_OUT}{timestep} \qquad NH4 = 0 \qquad (5\text{-}3)$$

where:

NH4_OUT = ammonium transported with water out of reach during timestep (mass); from SWAT output.rch; and

timestep = watershed model timestep.

5.3.2.2 Nitrate + Nitrite

Except for the conversion to appropriate units, deconvolution of SWAT variables to CE-QUAL-W2 variables was not necessary for nitrate plus nitrite.

$$NO3 = \frac{NO3\_OUT + NO2\_OUT}{timestep} \qquad NO3 = \frac{NSURQ \times AREA}{timestep} \qquad (5\text{-}4)$$

where:

NO3_OUT	=	nitrate transported with water out of reach during timestep (mass); from SWAT output.rch;
NO2_OUT	=	nitrite transported with water out of reach during the timestep (mass); from SWAT output.rch;
NSURQ	=	nitrate in surface runoff (mass/area); nitrate transported by the surface runoff into the reach during the timestep; from SWAT output.sub;
AREA	=	area of subbasin (area); from SWAT output.sub; and
timestep	=	watershed model timestep.

5.3.3 Organic Matter

Organic matter in CE-QUAL-W2 is divided into four categories: 1) labile dissolved (LD); 2) labile particulate (LP); 3) refractory dissolved (RD); and 4) refractory particulate (RP). For each of these categories, the following equations were used to convert the carbon form of organic matter to the appropriate value for input into CE-QUAL-W2.

$$OM_x = \frac{f_{xOM} \times CBOD\_OUT \times R_{co}}{R_{com}} \qquad OM_x = \frac{f_{xOM} \times CBODU \times SURQ \times AREA \times R_{co}}{timestep \times R_{com}} \qquad (5\text{-}5)$$

where:

f_{XOM} *(x = LD, LP, RD, RP)* = fraction of a particular type of organic matter;

CBOD_OUT = carbonaceous biochemical demand of material transported out of reach during timestep (mass oxygen); from SWAT output.rch;

R_{co} = stoichiometric equivalent between carbon and oxygen;

R_{com} = stoichiometric equivalent between carbon and organic matter;

CBODU = carbonaceous biochemical demand of material transported out of subbasin during timestep (mass oxygen); from SWAT output.sub; the SWAT model code was modified by Temple-Blacklands to output this variable for this project (Sammons 2007);

SURQ = surface runoff contribution to stream flow during timestep (mm); from output.sub;

AREA = area of subbasin (area); from SWAT output.sub; and

timestep = watershed model timestep.

It was necessary to convert the CBOD values from SWAT reaches from units of mass oxygen to units of mass organic matter by using two stoichiometric equivalents, R_{co} and R_{com}. The values assumed for these stoichiometric equivalents were 0.32 and 0.45, respectively.

A portion of organic matter is organic phosphorus and a portion is organic nitrogen. The following equations were used to convert the SWAT output for organic phosphorus and organic nitrogen to inputs to CE-QUAL-W2.

$$OM_x\_P = \frac{f_{xOM} \times ORGP\_OUT}{timestep} \qquad OM_x\_P = \frac{f_{xOM} \times ORGP \times AREA}{timestep} \qquad (5\text{-}6)$$

$$OM_x\_N = \frac{f_{xOM} \times ORGN\_OUT}{timestep} \qquad OM_x\_N = \frac{f_{xOM} \times ORGN \times AREA}{timestep} \qquad (5\text{-}7)$$

where:

f_{XOM} *(x = LD, LP, RD, RP)* = fraction of a particular type of organic matter;

ORGP_OUT = organic phosphorus transported with water out of reach during timestep (mass P); from SWAT output.rch;

ORGP = organic phosphorus yield (mass/area); organic phosphorus transported with sediment into the reach during the timestep; from SWAT output.sub;

ORGN_OUT = organic nitrogen transported with water out of reach during timestep (mass N); from SWAT output.rch;

ORGN = organic nitrogen yield (mass/area); organic nitrogen transported out of the subbasin and into the reach during the timestep; from SWAT output.sub;

AREA = area of subbasin (area); from SWAT output.sub; and

timestep = watershed model timestep.

The labile fraction of organic matter (carbon, nitrogen, and phosphorus) was set to 0 during model calibration. The dissolved fractions for the carbon, nitrogen, and phosphorus forms of organic matter from watersheds contributing to the Pedernales River were set to 0.91, 0.52, and 0.13, respectively. These percentages were computed based on average constituent concentrations measured at Hammett's Crossing (Station 12369) from 2004 through 2006. For all other watersheds, the dissolved fractions of organic matter were set to 0.84 for carbon, 0.33 for nitrogen, and 0.08 for phosphorus. These percentages were calculated from constituent concentrations measured at Bee, Cow, Cypress, Hurst, and Big Sandy Creeks from 2004 through 2006.

5.3.4 Algae

Values for algal biomass from SWAT reaches needed to be converted from units of mass chlorophyll-*a* to units of mass organic matter by using a stoichiometric equivalent between organic matter and chlorophyll-*a*, ACHLA. The value assumed for this stoichiometric equivalent was 120. Algae from the watershed subbasins was assumed to be negligible,

therefore, algae from the subbasins were set to zero in the lake model input file. A cap corresponding to 300 µg/L was imposed on the SWAT output on several dates when the watershed model predicted unrealistically high chlorophyll-*a* concentrations.

$$ALG = \frac{ALGAE\_OUT \times ACHLA}{timestep} \qquad ALG = 0 \qquad (5\text{-}8)$$

where:

ALGAE_OUT = algal biomass transported with water out of reach during timestep (mass chlorophyll-*a*); from SWAT output.rch;

ACHLA = stoichiometric equivalent between organic matter and chlorophyll-*a*; and

timestep = watershed model timestep.

5.3.5 Dissolved Oxygen

The SWAT reach output for DO was converted to the appropriate units and used in the lake model. DO from the SWAT subbasins (i.e., the land surface) was calculated from the temperatures specified in the lake model input (see Section 4.3.1.3), assuming 100% saturation.

$$DO = \frac{DISOX\_OUT}{timestep} \qquad DO = 100\% \text{ saturation using input temperatures} \qquad (5\text{-}9)$$

where:

DISOX_OUT = amount of dissolved oxygen transported out of reach during timestep (mass oxygen); from SWAT output.rch; and

timestep = watershed model timestep.

5.3.6 Incorporating Deconvoluted Variables into the Lake Model

Flows predicted by SWAT were not directly used in CE-QUAL-W2. Because the establishment of the water balance occurred before the full development and calibration of the SWAT model and because the numerical stability of CE-QUAL-W2 is highly sensitive to the water balance, the water balance was used as input to the lake model instead of the SWAT predicted flows. The water balance is based on a robust data set that includes daily water surface elevations, flow releases, and USGS flows (Section 4.3). The watershed model is calibrated hydrologically, meaning that it tracks the same flow-related data that was used in the water balance; therefore, the use of the water balance as input to the lake model instead of the SWAT predicted flows should have little effect on the calibration or future management scenarios.

Loadings predicted by the watershed model were input as a daily time series into the lake model by the specification of a flow file and a concentration file for each watershed subbasin. The flow incoming into the lake from each watershed subbasin was set to a very low constant rate of 0.001 m^3/s. The concentrations from each subbasin were then calculated by dividing the deconvoluted and spatially appropriate loadings from the watershed model by this artificial flow rate. To accommodate the additional 0.001 m^3/s for each of the 47 watershed subbasins, the input flow file for direct runoff was decreased by 0.047 m^3/s. In this manner, the loadings predicted by SWAT were preserved in the water quality model.

SECTION 6
SUMMARY

The Phase 2 Lake Travis modeling effort consisted of three components: enhanced system monitoring, watershed modeling, and lake water quality modeling. An extended monitoring program that included enhanced ambient monitoring in Lake Travis, its major creeks, and its upstream boundary was conducted to support the modeling project. The monitoring also included storm sampling to capture high flow measurements in order to establish a continuous times series of water quality in the tributaries for calibration of the watershed model. Additionally, the monitoring effort encompassed special studies aimed at defining algae growth and speciation as well as sediment fluxes within the lake.

The watershed model chosen to model the Lake Travis system was SWAT, a widely accepted semi-lumped watershed model that has been widely applied in Texas. The model development encompassed a significant watershed size (1750 km^2) and included simulation of flow, sediment erosion and transport, and nutrient transport and instream processes. Model calibration focused on the Pedernales River, which drains close to two-thirds of the entire lake basin. Secondary stations on smaller creeks were used to assess the model performance on the smaller basins. Calibration results indicate that the model represents flow in the basin well, with monthly Nash-Sutcliffe efficiencies at the two primary stations along the Pedernales River at approximately 0.5 and 0.8. Sediment loads at the primary water quality station on the Pedernales River was acceptable, coming within 40% of the loads estimated from a rating curve of measured data. For the nutrient series, the model performed well, on average, for the phosphorus series. The average result for the total phosphorus was good, coming within 3% of the estimated total loads. For organic P and orthophosphate, the model underpredicted the data by about 18% and 45%, respectively. The performance of the model on the nitrogen series was fair to poor, with gross over-predictions in the nitrite+nitrate loads at the primary station. Because the lake model calibration to the nitrogen series was achieved without having to compensate by overestimating in-lake nitrogen sinks (parameters used for model calibration were within accepted ranges), the over-prediction may be a product of comparing modeled loads to loads estimated from rating curves developed with little high flow data. For the smaller basins, the simulation of flow was

good, on average, and the simulation of the phosphorus series was acceptable. As with the larger basin, the nitrogen series on the smaller subbasins were over-estimated; the over-prediction, however, was for organic nitrogen; the model performed relatively well for nitrite+nitrate. Of particular note on the smaller subbasins was the model's poor performance capturing the sediment loads. The model over-predicted these loads, which is believed to be a result of both a focus on a basis-wide calibration (instead of a subbasin-by-subbasin calibration) and the setting of a single slope class during early development of the model. In the end, the model's representation of the sediment loads on this small scale is relatively unreliable, illustrating the challenges in simulating sediment transport and erosion on a small basin.

A two-dimensional time-variable water quality model was developed for Lake Travis using the USACE CE-QUAL-W2 modeling framework. The model simulates important hydrodynamic and water quality processes including: advection, dispersion, sedimentation, algal dynamics (growth, respiration, mortality, excretion, and settling), atmospheric reaeration, nutrient cycling (uptake, organic decomposition, and nitrification/denitrification), and water-sediment interactions (SOD, anaerobic nutrient releases, and denitrification). Calibration of the model occurred in two steps, hydrodynamics and water quality. Hydrodynamic/thermal calibration focused on matching observed lake water levels at Mansfield Dam as well as vertical and temporal profiles of temperature and conservative constituent concentrations at the five primary water quality stations (four main lake: Turkey Bend, Pace Bend, Arkansas Bend, and Mansfield Dam; one cove: Big Sandy Creek). Hydrodynamic/thermal calibration was generally good at reproducing observed spatial and temporal trends in temperature. Of primary importance, the model reproduced the location, depth, and timing of thermal stratification that occurs during the summer months. Water quality calibration focused on matching epilimnetic and hypolimnetic temporal profiles of chlorophyll-*a*, DO, TP, TOC, TKN, NO_x, NH_4, and PO_4 at the five stations. The model accurately simulated DO levels throughout the epilimnion and hypolimnion. The reproduction of hypoxic conditions observed frequently during the summer in the hypolimnion of the deeper parts of the lake was a good indicator of the strength of the model calibration. Surface algal levels during the summer months were reasonably well reproduced along with the decreasing trend from upstream to downstream observed in the data. One limitation of the model is that it does not predict sufficient algal levels during the winter months.

This is not seen as a major limitation as it is anticipated that the primary utility of the model will be its prediction of algal productivity during the summer periods. Nutrient levels were generally well reproduced, particularly the low limiting concentrations of inorganic nutrients (NO_x and PO_4) that occur in the epilimnion during the periods of high algal growth. The model predictions generally followed the data trends well at the four lake locations and one cove location evaluated during calibration. Overall, good calibration was achieved using parameterization based on adjustment of a limited number of model coefficients. Therefore, the lake water quality model can be used for predicting lake-wide responses as well as responses in coves to potential future changes in nutrient loadings to the lake. Special studies conducted for LCRA were used when available (i.e., algal growth studies) and recommended values provided by the CE-QUAL-W2 authors were used regularly in the absence of data.

Sensitivity analyses were performed for both the watershed and water quality models. With a few exceptions, the sensitivity analyses involved one-at-a-time model parameter changes to a "low" value and a "high" value. Values were chosen using available literature or professional judgment. Thirteen model input parameters were tested for the watershed model and eighteen (four were passed from the watershed sensitivity analysis) were evaluated for the water quality model. The analysis for the lake water quality model also included the assessment of the sensitivity of model results to changes in loadings from upstream and the watershed. For the values tested and output evaluated, the most sensitivity parameters for predictions of summertime surface chlorophyll-*a* were found to be model input parameters for the lake water quality model. Because long model run times prohibited iterative model runs such as those performed in a Monte Carlo simulation, uncertainty was assessed through the establishment of a bounding calibration. The three most sensitive parameters – maximum algal growth rate, particulate organic matter settling rate, and refractory % from the watershed – were adjusted to increase the model prediction of summertime surface chlorophyll-*a*, but keeping the model within the range of the data (i.e., keeping the model calibration line reasonable, given the data). This represents an upper-prediction to help assess model uncertainty in summertime surface chlorophyll-*a* predictions under different future scenarios.

The Lake Travis water quality models developed under the CREMs project provide predictive tools to facilitate proactive watershed and reservoir management decisions. The Phase 2 watershed and water quality models can be used to evaluate the water quality and quantity effects of a wide range of management policies such as the NPS pollution ordinance, the TCEQ point source discharge ban, and land use changes. In addition, the Phase 2 effort has strengthened LCRA's understanding of the Lake Travis system through enhanced sampling and data analysis and expanded the expertise of LCRA staff with respect to watershed and water quality management and modeling issues. In conclusion, CREMs not only provides valuable insights into the relationships between Lake Travis water quality and its surrounding watershed, but the means to quantify the positive or negative impacts of proposed management activities.

SECTION 7
REFERENCES

American Public Health Association, American Water Works Association, and Water Environment Federation, 1998. *Standard Methods for the Examination of Water and Wastewater*, 20th Edition.

Anchor QEA, LLC and Parsons Water and Infrastructure, Inc. (Parsons) 2009. *Final Scenario Memo.* March 18, 2009, revised May 11, 2009.

Arnold J.G. and P.M. Allen, 1996. Estimating hydrologic budgets for three Illinois watersheds. *J. Hydrology* 176(1996):57-77.

Arnold, J.G., R. Srinivasan, T.S. Ramanarayanan, and M. DiLuzio, 1999. Water resources of the Texas Gulf Basin. *Water Science Tech.* 39(3):121-133.

Benaman, J., 2003. *Uncertainty and Sensitivity Analyses for Watershed Models: Hydrology and Sediment Transport Modeling on the Cannonsville Reservoir System.* Ph.D. Dissertation. Department of Civil and Environmental Engineering, Cornell University, Ithaca, NY.

Benaman, J., C.A. Shoemaker, and D.A. Haith, 2005. Calibration and validation of soil and water assessment tools on an agricultural watershed in Upstate New York. *Hydrologic Enginr*. 10(5):363-374.

Bowie, G.L., W.B. Mills, D.B. Porcella, C.L. Campbell, J.R. Pagenkopt, G.L. Rupp, K.M. Johnson, P.W.H. Chan, and S.A. Gherini, 1985. *Rates, Constants, and Kinetics Formulations in Surface Water Quality Modeling (Second Edition).* EPA/600/3-85/040. United States Environmental Protection Agency (USEPA), Environmental Research Laboratory, Athens, GA.

Brown, L.C., and T.O. Barnwell, 1987. *The enhanced stream water quality models QUAL2E and QUAL2E-UNCAS: Documentation and user manual*. USEPA, Office of Research and Development, Athens, GA; EPA/600/3-87/007; May 1987.

CH2M Hill, 2002. *Master Plan for the Colorado River Environmental Models Program*. Lower Colorado River Authority (LCRA), Austin, TX.

Cho, S., G.D. Jennings, C. Stallings, and H.A. Devine, 1995. *GIS-based water quality model calibration in the Delaware River Basin.* American Society of Agricultural Engineers Meeting Presentation: Microfiche No. 95-2404.

Cole, T.M., and S.A. Wells, 2006. *CE-QUAL-W2: A Two-Dimensional, Laterally Averaged, Hydrodynamic and Water Quality Model, Version 3.5*. United States Army Corps of Engineers (USACE). Draft Instruction Report EL-06-1.

Debele, B., R. Srinivasan, and J.-Y. Parlange, 2006. Coupling upland watershed and downstream waterbody hydrodynamic and water quality models (Soil Water Assessment Tool [SWAT] and CE-QUAL-W2) for better water resources management in complex river basins. *Environ Model Assess,* DOI 10.1007/s10666-006-9075-1.

Du, B., J.G. Arnold, A. Saleh, and D.B. Jaynes, 2005. Development and application of SWAT to landscapes with tiles and potholes. *Trans. ASAE* 48(3):1121−1133.

Ferguson, R.I., 1986. River loads underestimated by rating curves. *Water Resources Research*, 22(1):74-76.

Flowers, J.D., L.M. Hauck, and Kiesling, R.L., 2001. W*ater Quality Modeling of Lake Waco using CE-QUAL-W2 for Assessment of Phosphorus Control Strategies*. Publication TR0114. Texas Institute for Applied Environmental Research, Tarleton State University, Stephenville, Texas, December 2001.

Fontaine, T.A., T.S. Cruickshank, J.G. Arnold, and R.H. Hotchkiss, 2002. Development of a snowfall-snowmelt routine for mountainous terrain for the SWAT. *J. Hydrology* 262(1-4):209-223.

Gassman, P.W., M.R. Reyes, C.H. Green, and J.G. Arnold, 2007. The soil and water assessment tool: Historical development, applications, and future research directions. *Trans. ASABE* 50(4):1211-1250.

Green, C.H., M.D. Tomer, M.Di Luzio, and J.G. Arnold, 2006. Hydrologic evaluation of the Soil and Water Assessment Tool for a large tile-drained watershed in Iowa. *Trans. ASABE* 49(2):413-422.

Green, W.H., and G.A. Ampt, 1911. Studies on soil physics, 1. The flow of air and water through soils. *J. Ag. Sciences* 4:11-24.

Hargreaves, G.L., G.H. Hargreaves, and J.P. Riley, 1985. Agricultural benefits for Senegal River Basin. *J. Irrig. and Drain.Engr.* 111(2):113-124.

LCRA, 2004. *Phase 1 Lake Travis Model*. Austin, TX.

Liscum, F., and East, J.W., 2000. *Estimated Effects on Water Quality of Lake Houston from Interbasin Transfer of Water from the Trinity River, Texas*. United States Geological Survey (USGS) Water Resources Investigation Report 00-4082. Austin, TX.

Monteith, J.L., 1965. Evaporation and the Environment. In *The State and Movement of Water in Living Organisms.* 19th Symposium of the Society for Experimental Biology. Cambridge University Press. London, U.K.

Natural Resources Conservation Service, 1986. *National Engineering Manual Section 4, Hydrology.* A division of the United States Department of Agriculture (USDA). (Also known as National Engineering Manual Part 620.)

Neitsch, S.L., and M. DiLuzio, 1999. *ArcView Interface for SWAT 99.2.* USDA Agricultural Research Center, and Texas A&M University Agricultural Experiment Station.

Neitsch, S.L., J.G. Arnold, J.R. Kiniry, and J.R. Williams, 2005. *Soil and Water Assessment Tool Theoretical Documentation: Version 2005*. USDA Agricultural Research Center and Texas A&M University Agricultural Experiment Station.

Pascual, P., N. Stiber, and E. Sunderland, 2003. *Draft Guidance on the Development, Evaluation, and Application of Regulatory Environmental Model.* USEPA Office of Science Policy, Council for Regulatory Environmental Modeling, Washington, D.C.; November 2003.

Priestley, C.H.B., and R.J. Taylor, 1972. On the assessment of surface heat flux and evaporation using large-scale parameters. *Mon. Weather Rev*. 100:81-92.

Quantitative Environmental Analysis, LLC (QEA), Parsons Engineering Science, and Ecological Communications Corp, 2003. *Lake Travis Phase 2 Work Plan*. LCRA, Austin, TX.

QEA, 1999. *PCBs in the Upper Hudson River: Volume 2, A Model of PCB Fate, Transport, and Bioaccumulation*. General Electric, Montvale, NJ

Raines, T.H., and W. Rast, 1999. *Characterization and Simulation of the Quantity and Quality of Water in the Highland Lakes, Texas, 1983–92*. USGS Report 99–4087.

Runkel, R.L., C.G. Crawford, and T.A. Cohn, 2004. *Load Estimator (LOADEST): A FORTRAN Program for Estimating Constituent Loads in Streams and Rivers*. USGS Techniques and Methods Book 4, Chapter A5. Reston, VA.

Sammons, N., 2007. Personal communication with Jennifer Benaman.

Santhi, C., J.G. Arnold, J.R. Williams, W.A. Dugas, R. Srinivasan, and L.M. Hauck, 2001. Validation of the SWAT model on a large river basin with point and nonpoint sources. *J. Am. Water Resources Assn.* 37(5):1169-1188.

Santhi, C., R. Srinivasan, J.G. Arnold, and J.R. Williams, 2006. A modeling approach to evaluate the impacts of water quality management plans implemented in a watershed in Texas. *Environmental Modeling and Software* 21:1141-1157.

Srinivasan, R., T.S. Ramanarayanan, J.G. Arnold, and S.T. Bednarz, 1998. Large area hydrologic modeling and assessment, Part II: Model application. *J. Am. Water Resources Assn.* 34(1):91-101.

Tolson, B.A., and C.A. Shoemaker, 2007. Cannonsville reservoir watershed SWAT2000 model development, calibration, and validation. *J. Hydrology* 337:68-86.

USEPA, 2001. *PLOAD version 3.0, User's Manual, An Arc View GIS Tool to Calculate Nonpoint Sources of Pollution in Watershed and Stormwater Projects*. January 2001.

Williams, J.R., 1969. Flood routing with variable travel time or variable storage coefficients. *Trans. ASAE* 12(1):100-103.

Williams, J.R., and H.D. Berndt, 1977. Sediment yield prediction based on watershed hydrology. *Trans. ASAE* 20(6): 1100-1104.

FIGURES

ANCHOR QEA

PARSONS

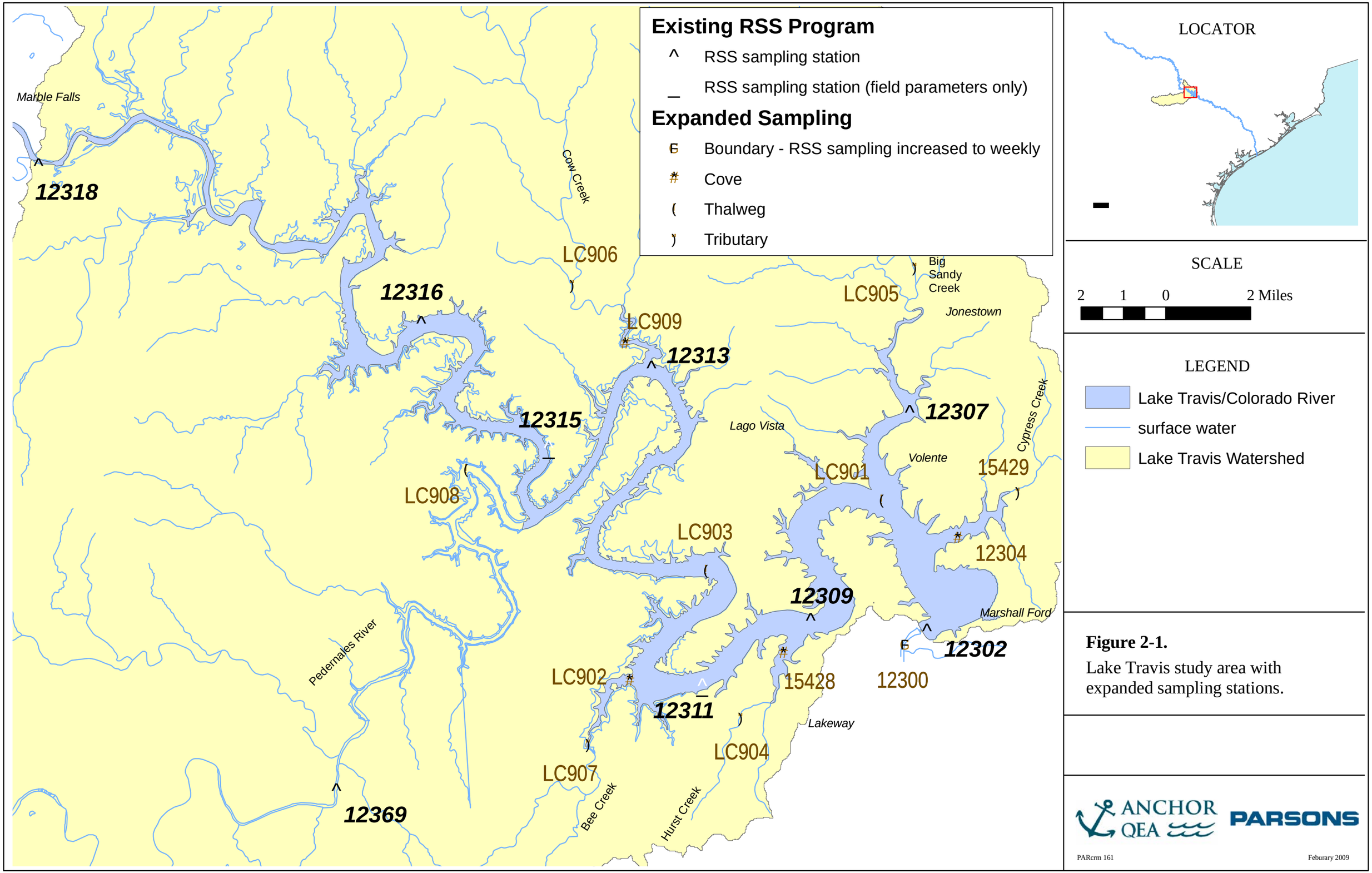

Figure 2-1.
Lake Travis study area with expanded sampling stations.

\\Emily\d_drive\PARcrm\GIS\Lake_Travis_Phase2\sampling_loc\lake_travis_sampling_stations_20090303.mxd

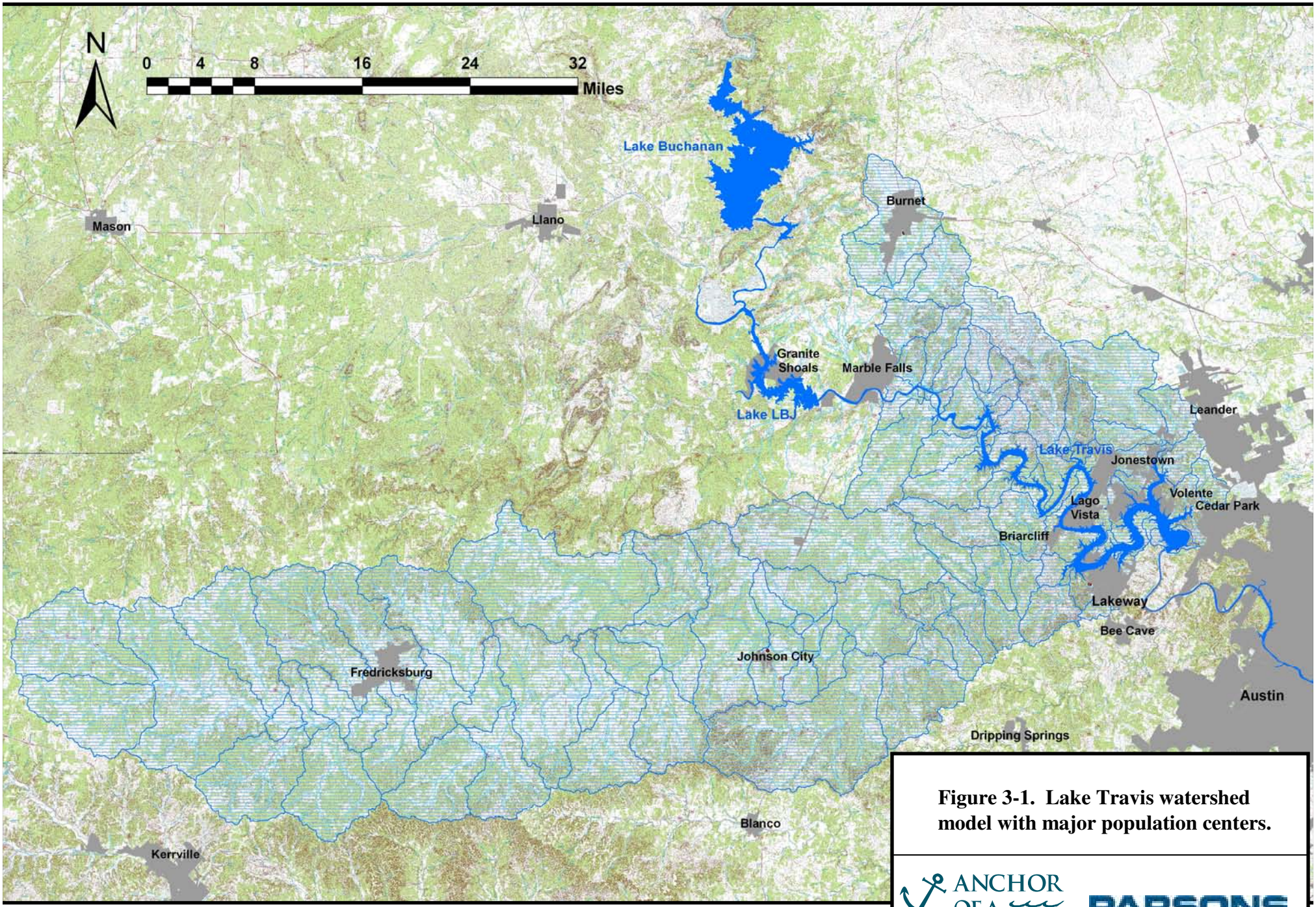

Figure 3-1. Lake Travis watershed model with major population centers.

ANCHOR QEA

PARSONS

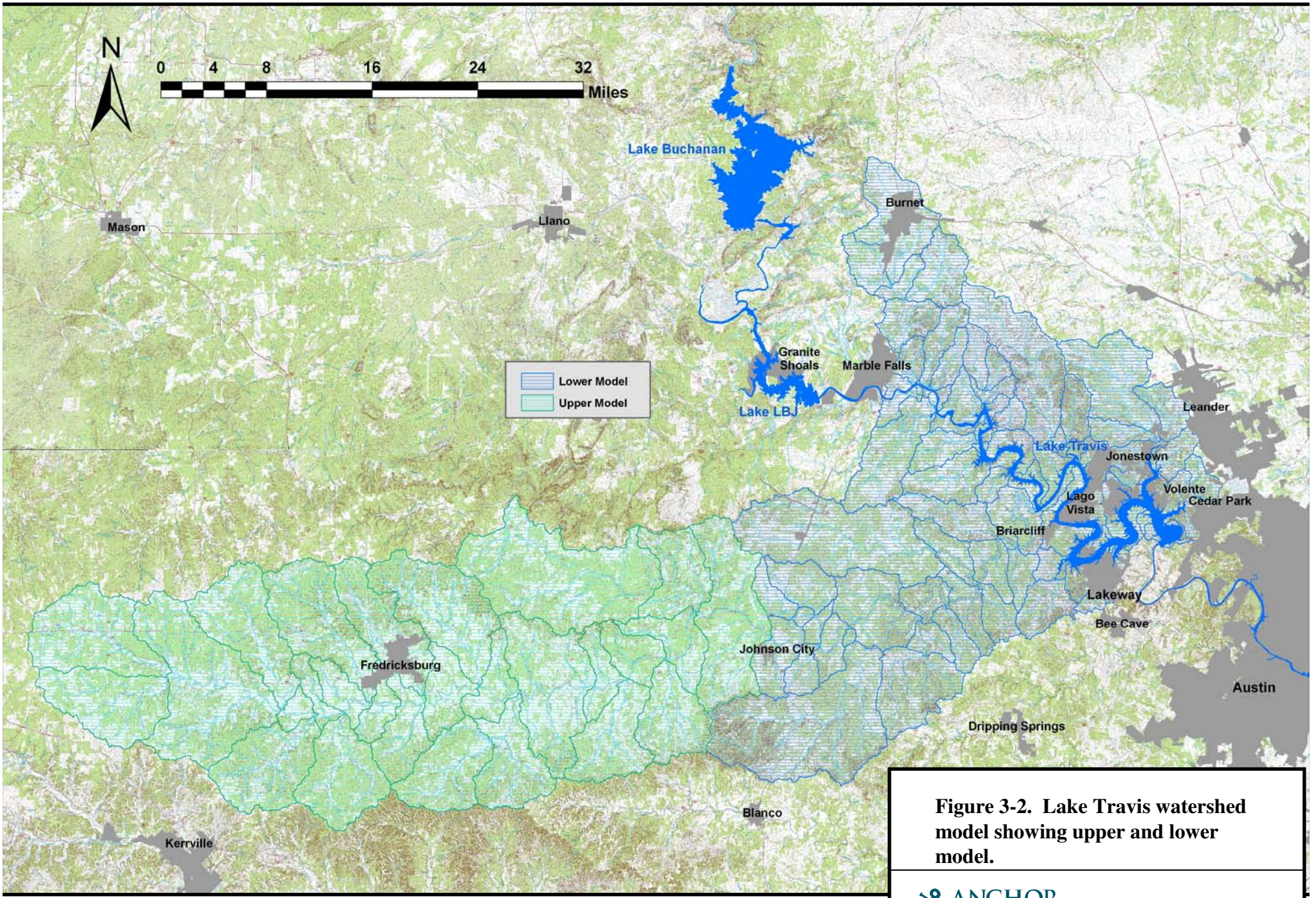

Figure 3-2. Lake Travis watershed model showing upper and lower model.

ANCHOR QEA

PARSONS

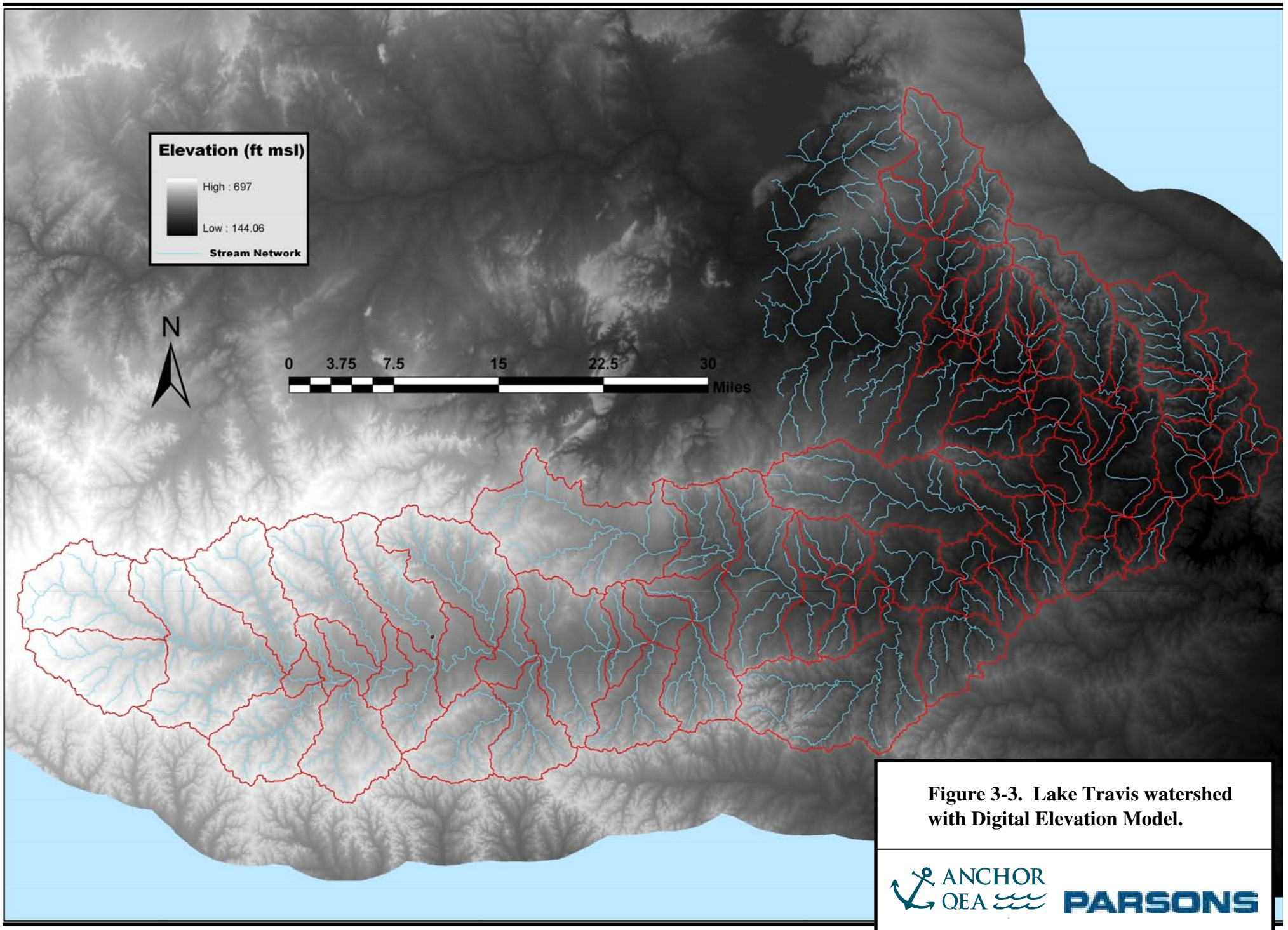

Figure 3-3. Lake Travis watershed with Digital Elevation Model.

ANCHOR QEA

PARSONS

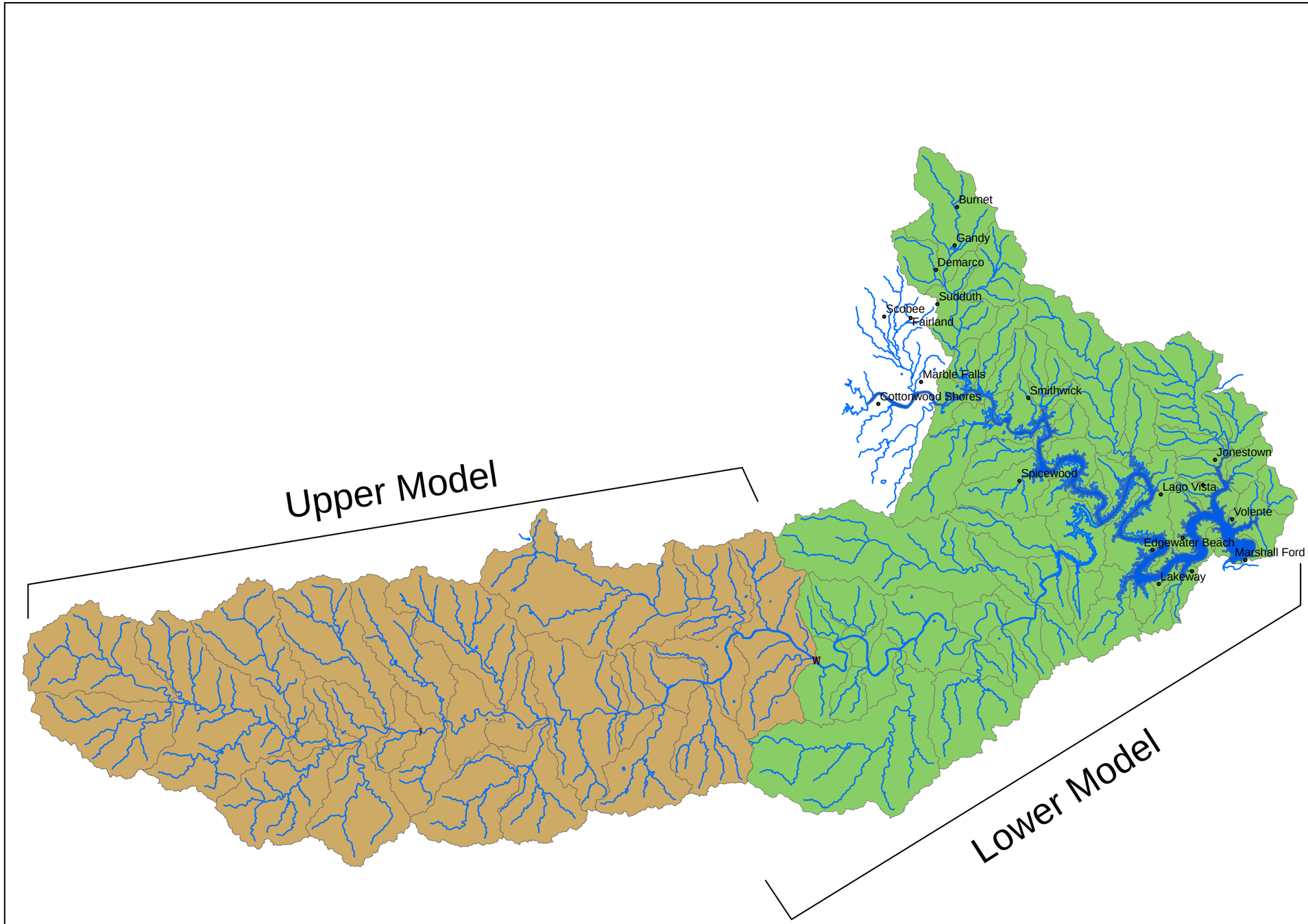

LOCATOR

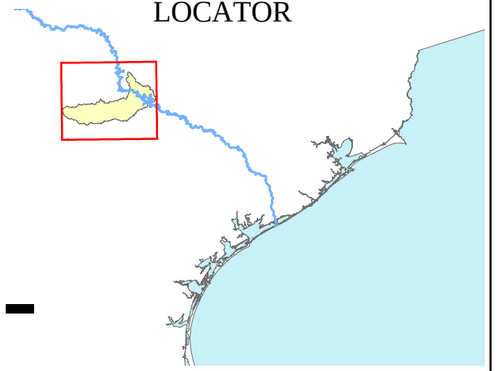

SCALE

10 5 0 10 Miles

LEGEND

- Fredericksburg (USGS 08152900)
- Johnson City (RSS 12372)
- towns
- Lake Travis
- surface water
- upper model subbasins
- lower model subbasins

Figure 3-4.
Phase 2 CREMS
watershed model segmentation

ANCHOR QEA PARSONS

PARcrm 161 February 2009

\\Emily\d_drive\PARcrm\GIS\Lake_Travis_Phase2\SWATsubbasins\fig3-4_lake_travis_watershed_segonly_20090206.mxd

N

0 3.75 7.5 15 22.5 30

Miles

NLCD Landuse

- Water
- Low Intensity Residential
- High Intensity Residential
- Commercial/Industrial/Transportation
- Bare Rock/Sand/Clay
- Quarries/Strip Mines/Gravel Pits
- Deciduous Forest
- Evergreen Forest
- Mixed Forest
- Shrubland
- Orchards/Vineyards/Other
- Grasslands/Herbaceous
- Pasture/Hay
- Row Crops
- Small Grains
- Urban/Recreational Grasses
- Emergent Herbaceous Wetlands

Figure 3-5. Lake Travis watershed NLCD land use.

ANCHOR QEA PARSONS

N

0 3.75 7.5 15 22.5 30

Miles

Soils - STATSGO MUID

TX071	TX371
TX144	TX388
TX151	TX521
TX155	TX542
TX227	TX546
TX309	TX592
TX360	

Figure 3-6. Lake Travis watershed STATSGO soils.

ANCHOR QEA

PARSONS

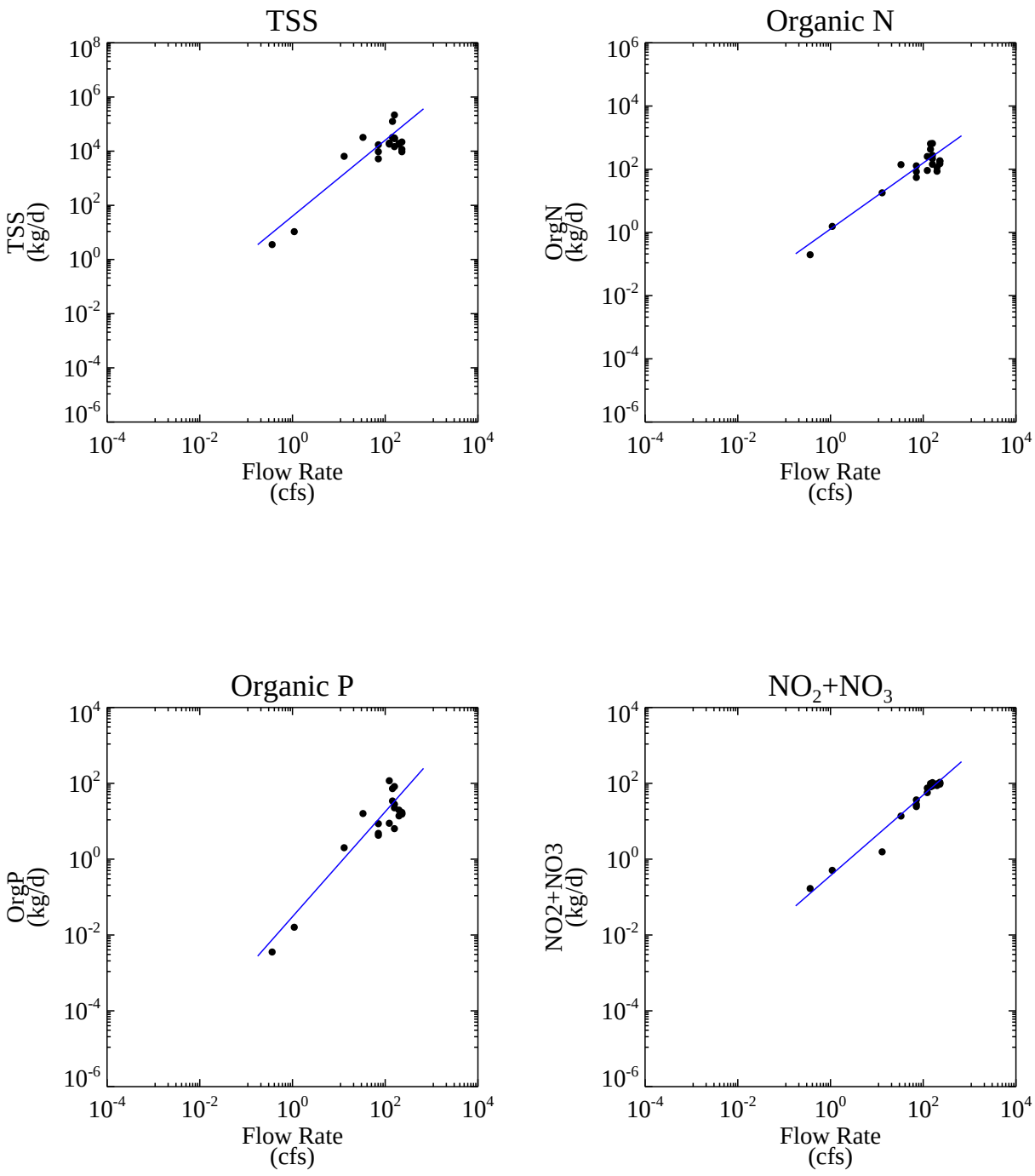

Figure 3-7a. Rating curves predicted by LOADEST for Big Sandy Creek.

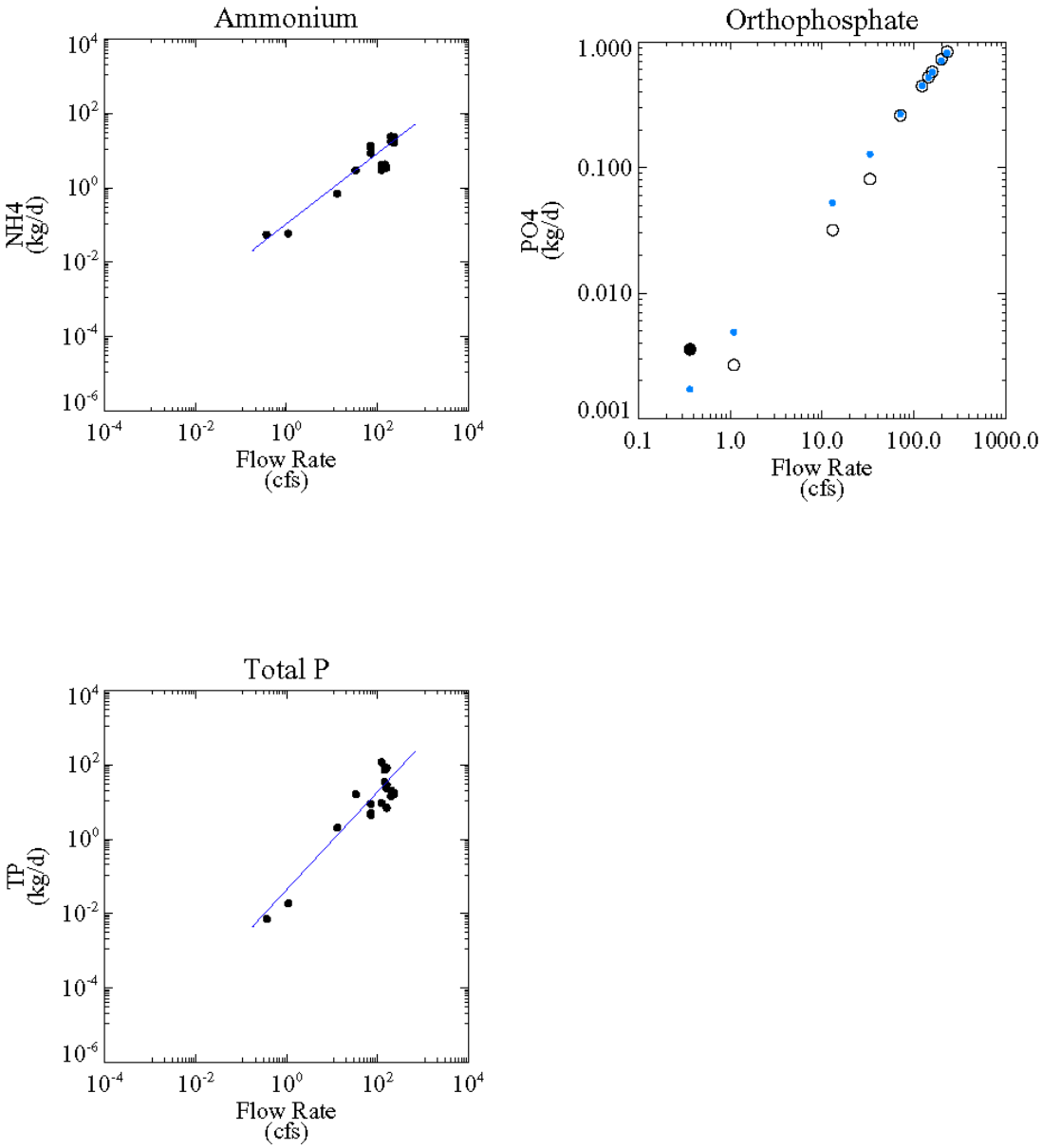

Figure 3-7b. Rating curves predicted by LOADEST for Big Sandy Creek.

Orthophosphate rating curve (blue dots) established using QMLE.
Open circles indicate non-detect data and are shown at half the detection limit.

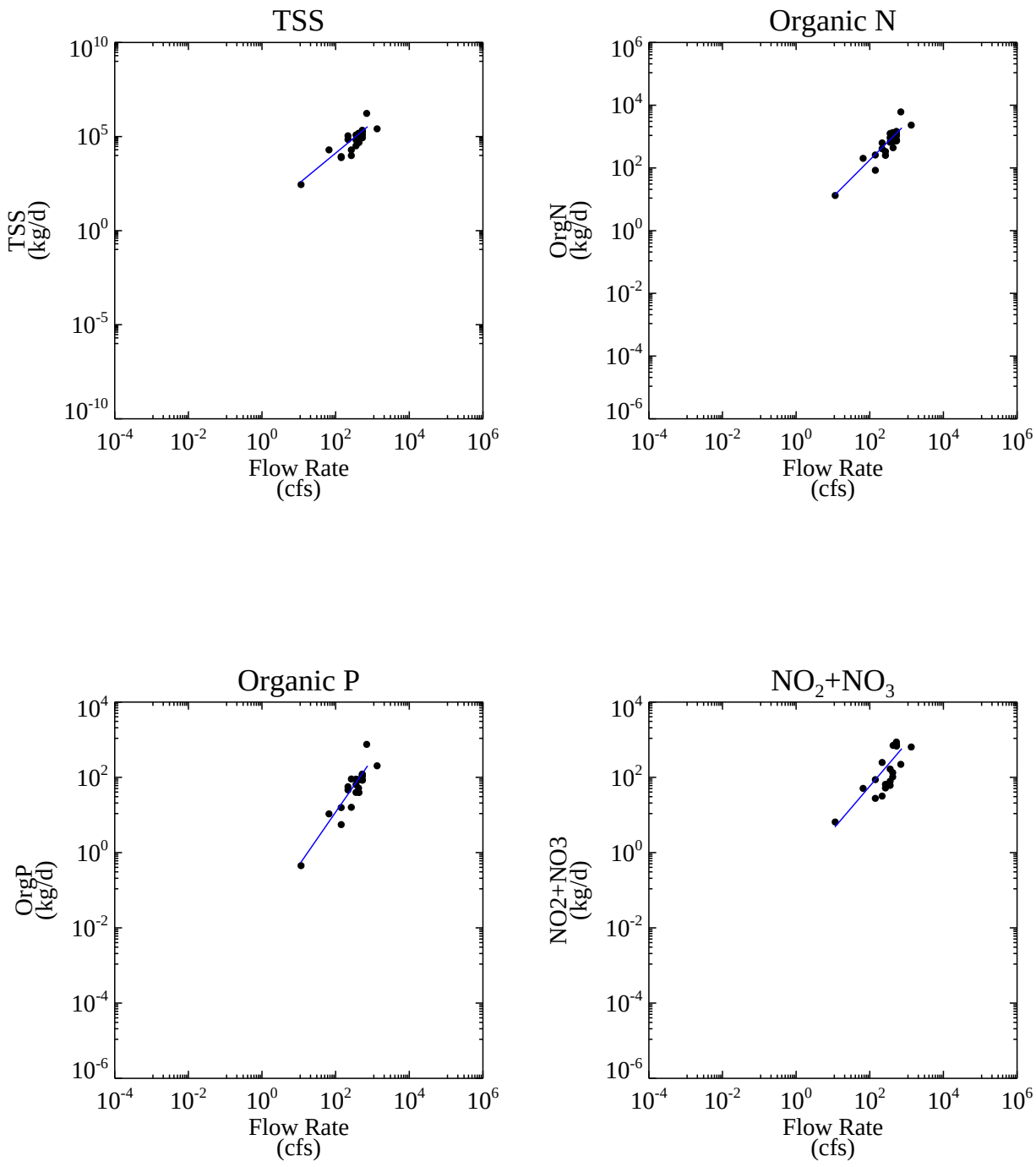

Figure 3-8a. Rating curves predicted by LOADEST for Cow Creek.

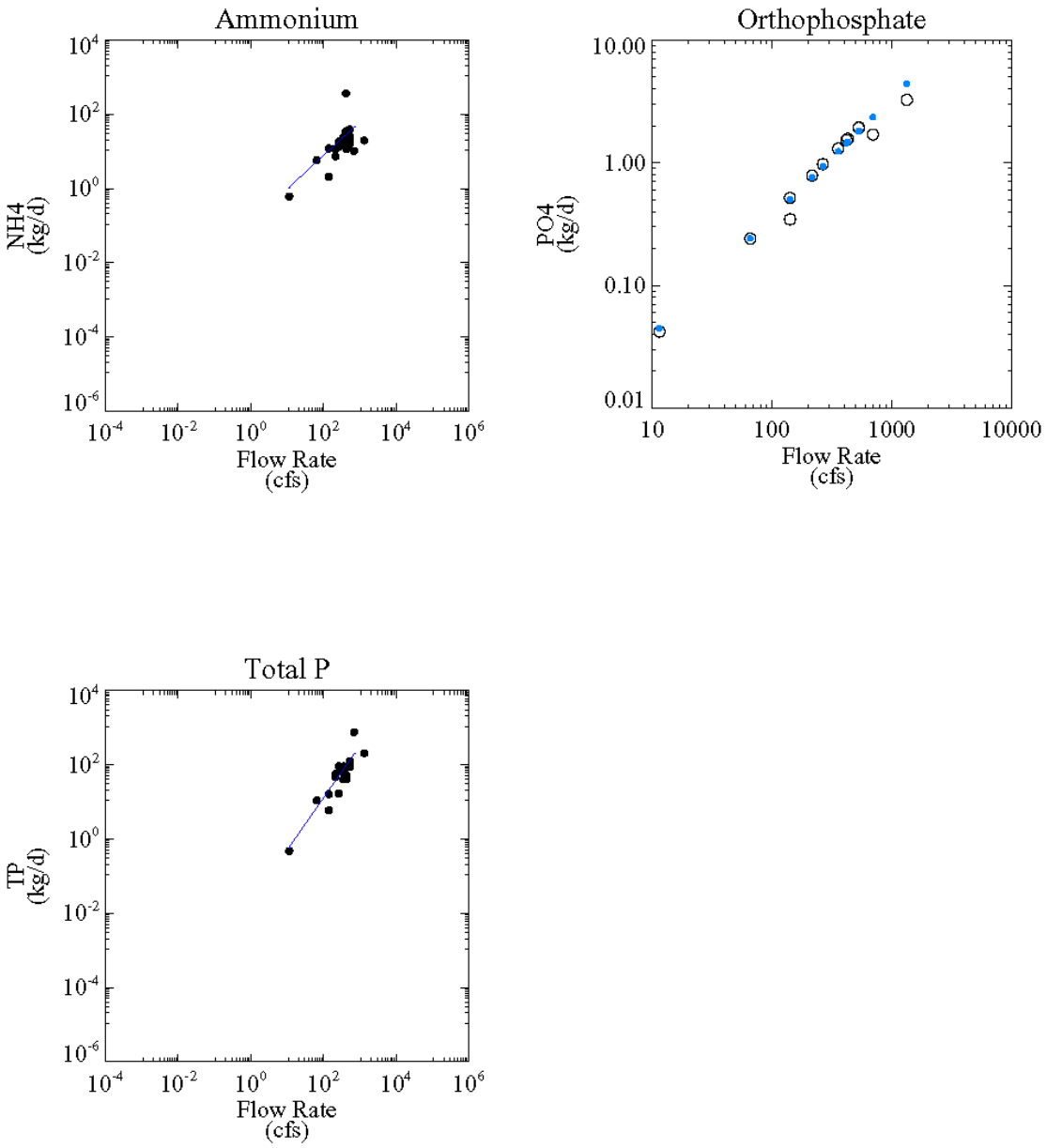

Figure 3-8b. Rating curves predicted by LOADEST for Cow Creek.

Orthophosphate rating curve (blue dots) established using QMLE.
Open circles indicate non-detect data and are shown at half the detection limit.

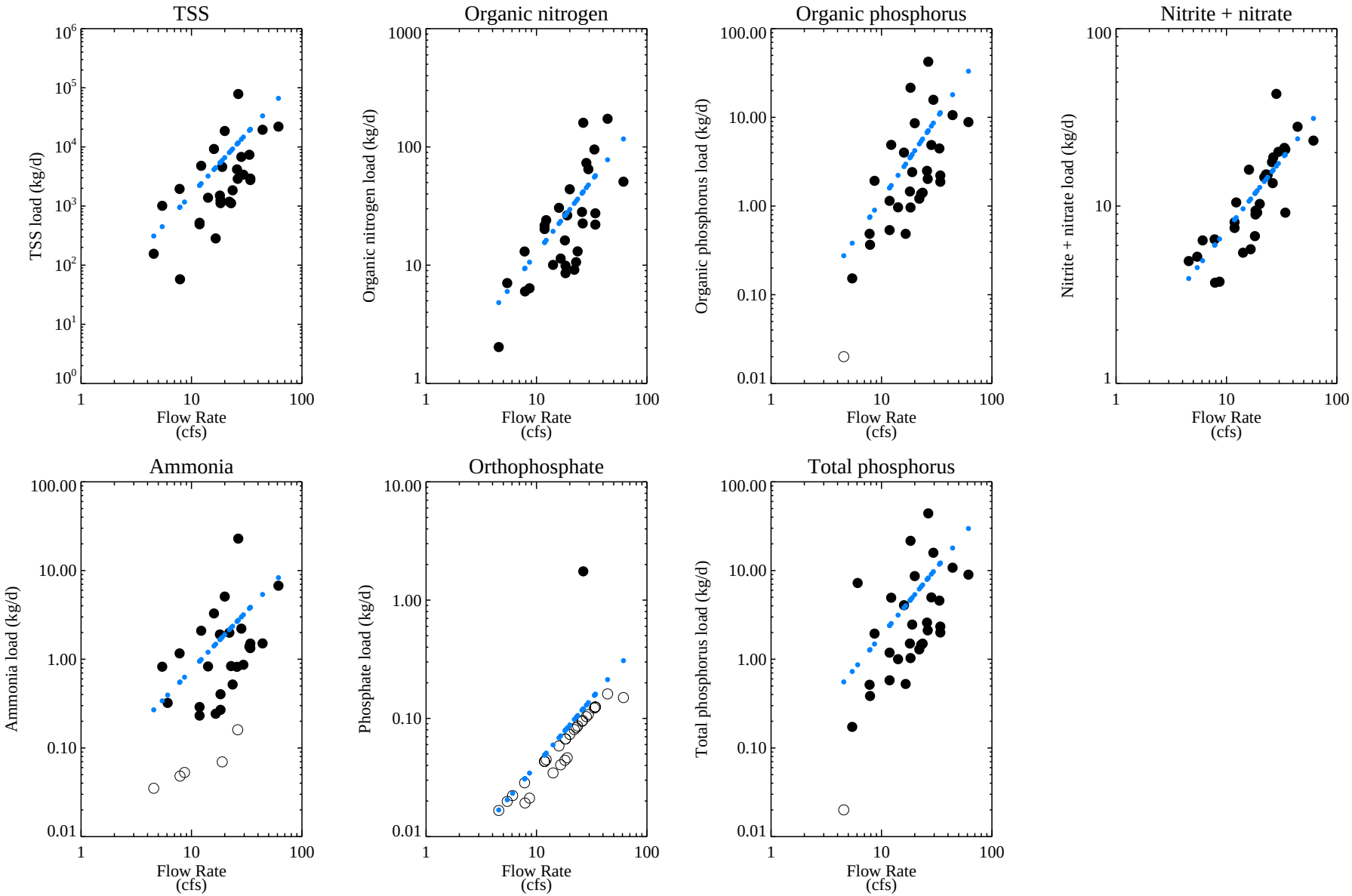

Figure 3-9. Rating curves predicted by QMLE for Bee Creek.

Open symbols indicate non-detects - reported as half the method detection limit.
Smaller blue symbols are the QMLE estimated load concentrations using the rating curve.

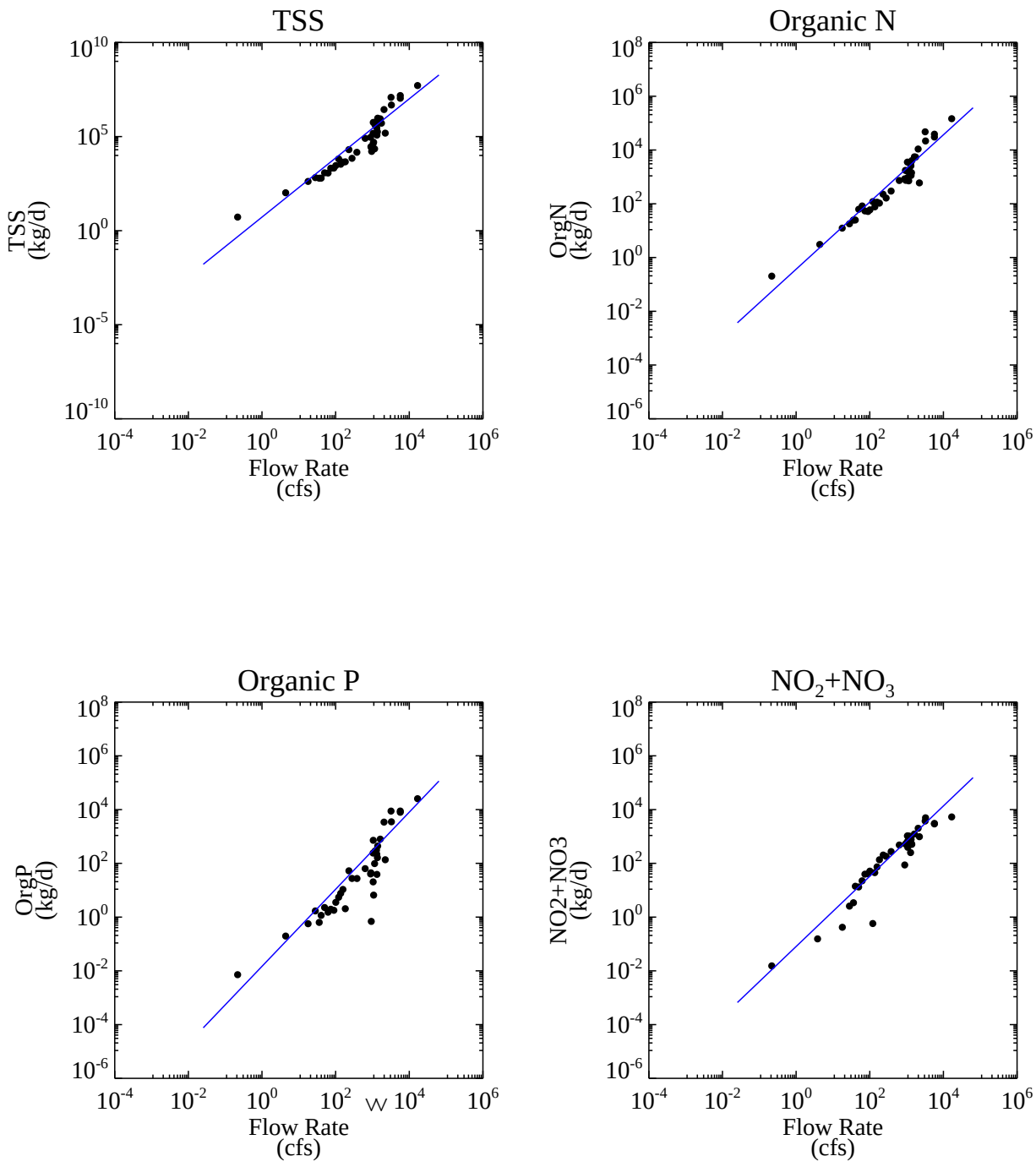

Figure 3-10a. Rating curves predicted by LOADEST for the Pedernales River at Hammett's Crossing.

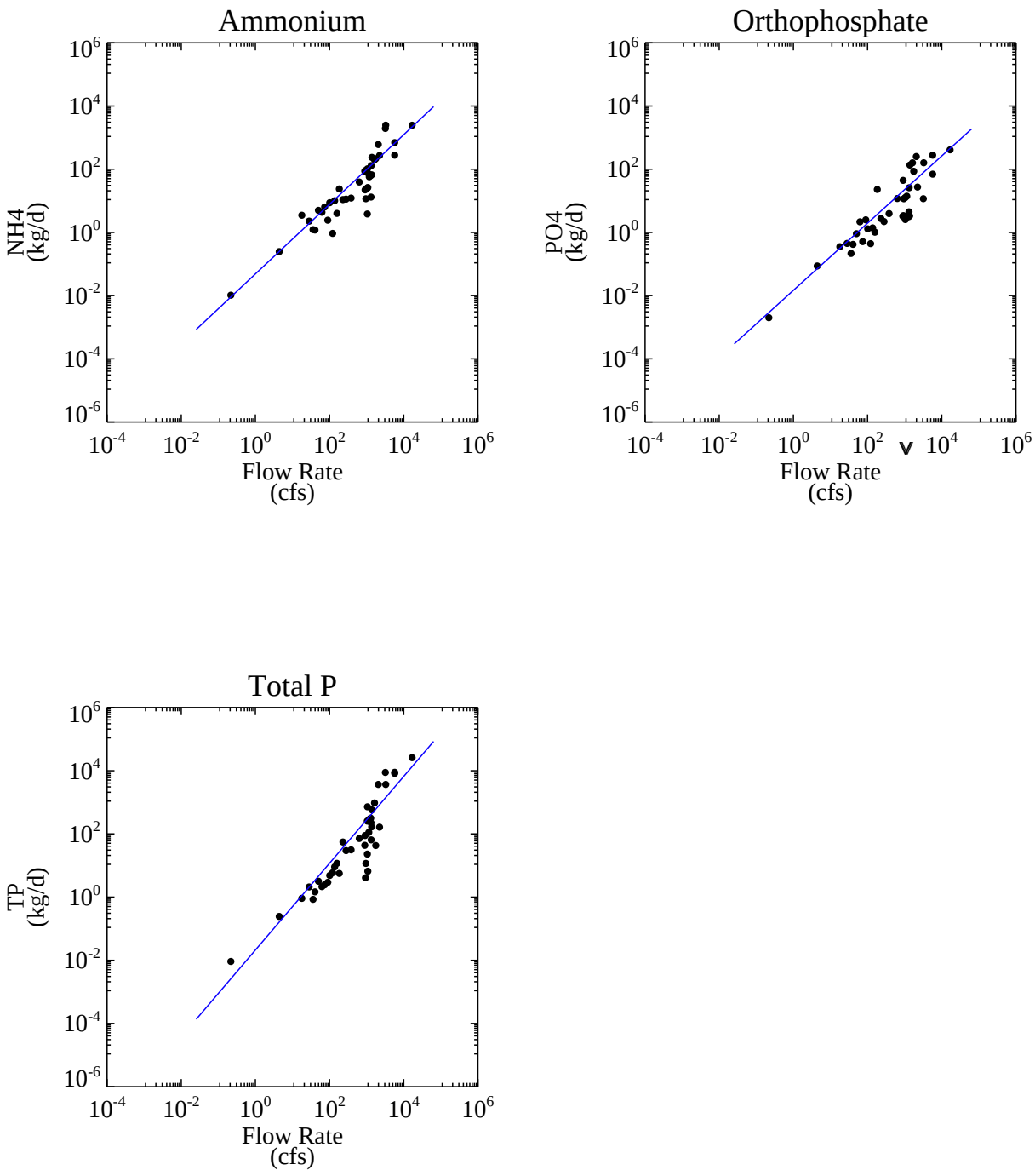

Figure 3-10b. Rating curves predicted by LOADEST for the Pedernales River at Hammett's Crossing.

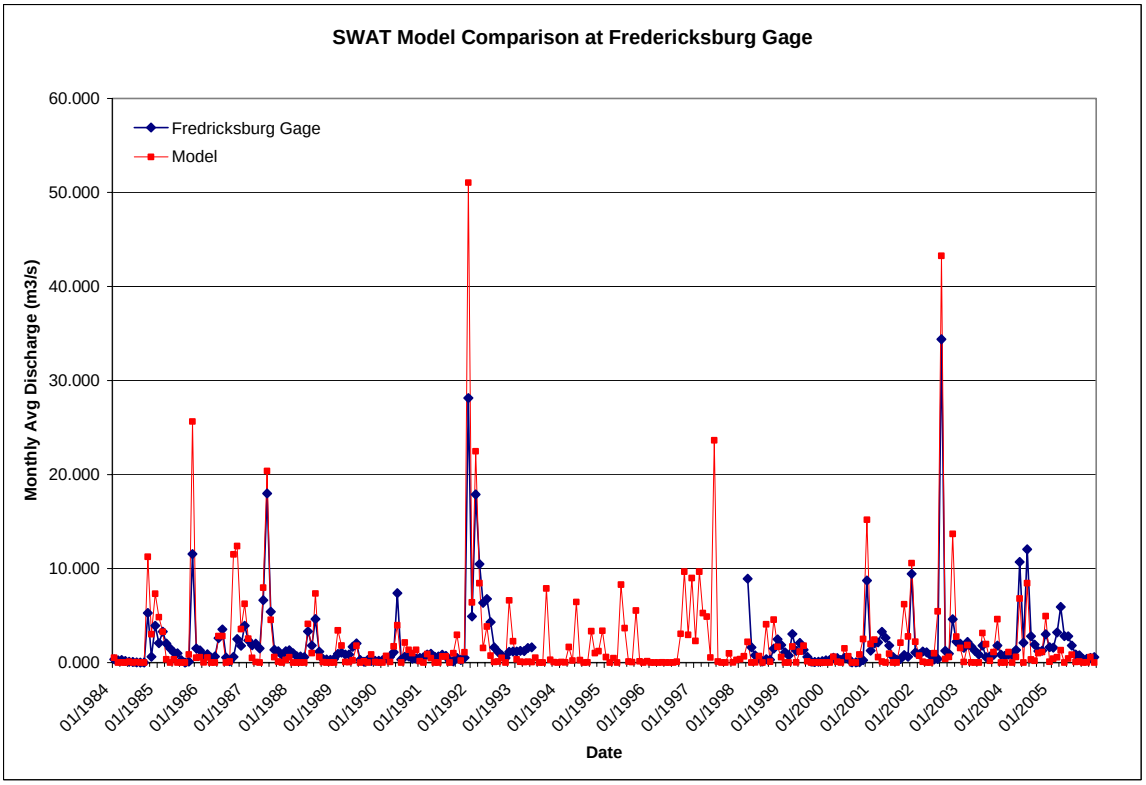

Figure 3-11. Monthly average flow comparison at Fredricksburg.

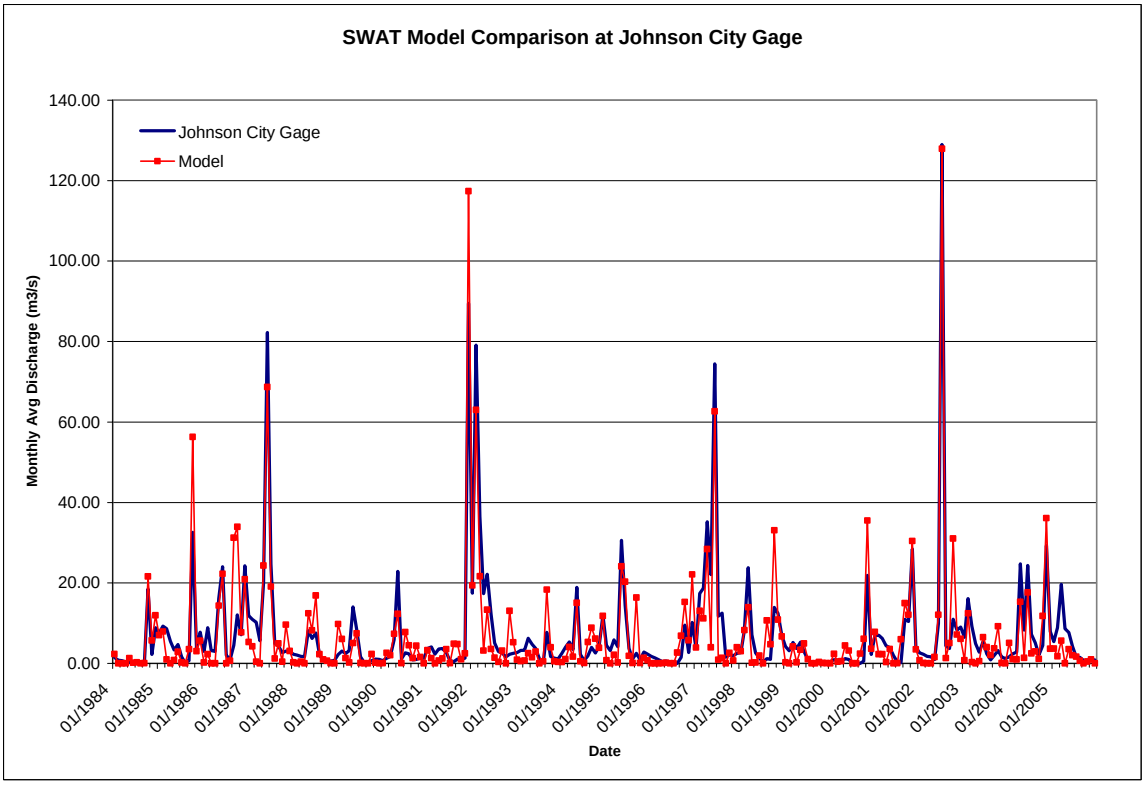

Figure 3-12. Monthly average flow comparison at Johnson City.

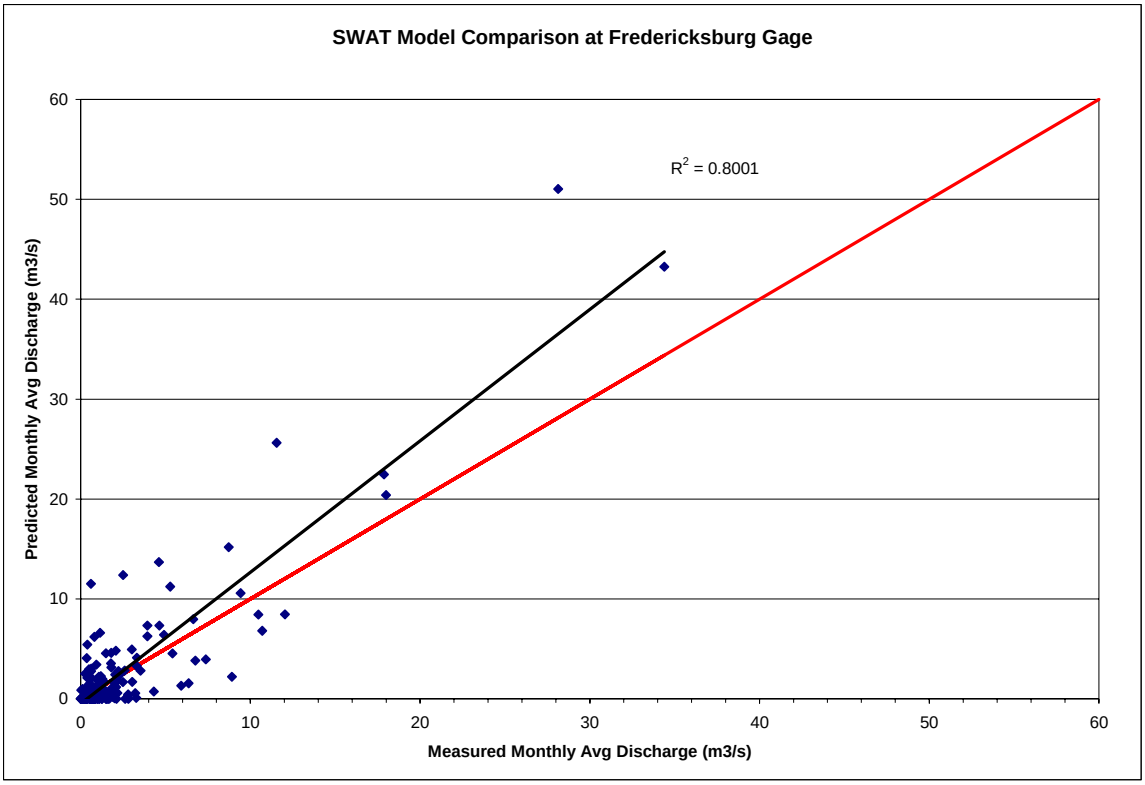

Figure 3-13. Flow cross plot at Fredricksburg.

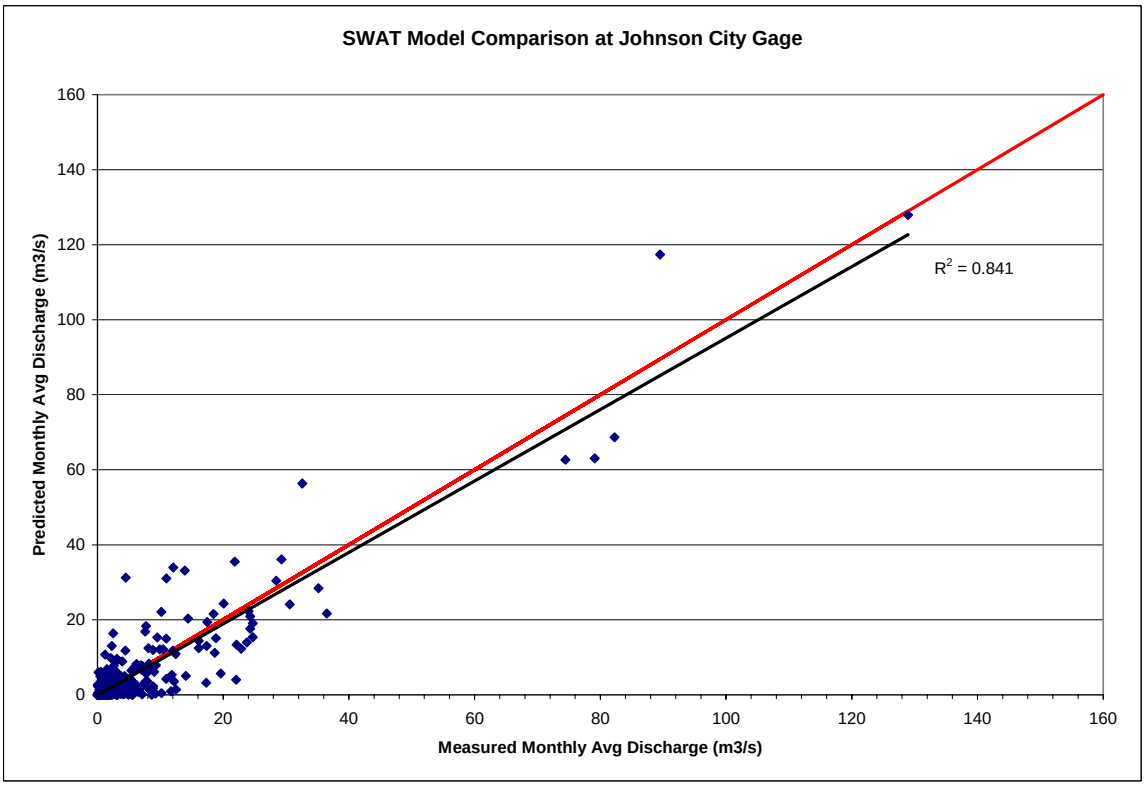

Figure 3-14. Flow cross plot at Johnson City.

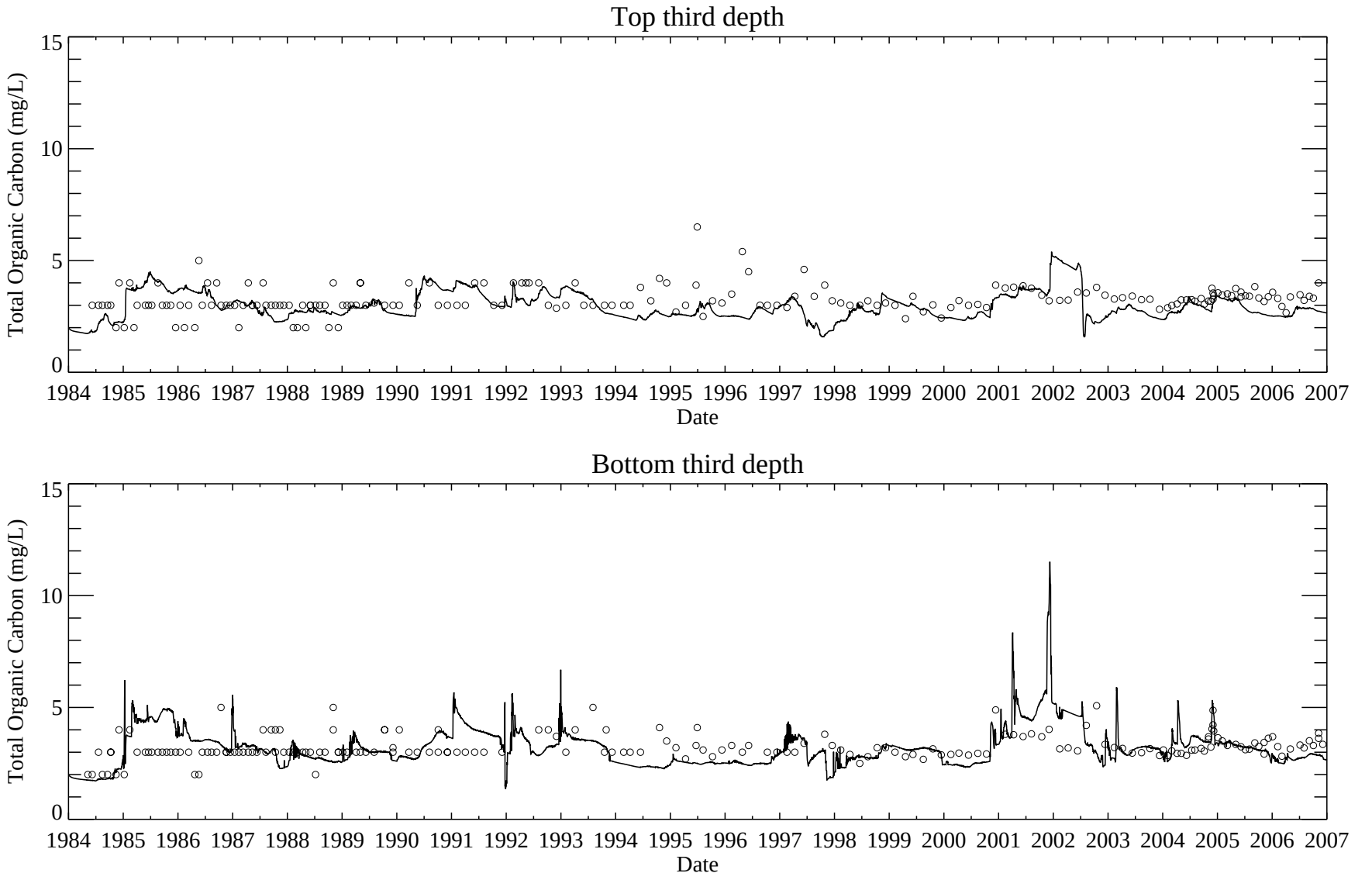

Figure 4-34. Temporal of model versus data at Mansfield Dam (Segment 93) - Total Organic Carbon.

Top third depth, Bottom third depth
When HAAWQ and CREMS data were measured on the same day, only CREMS data are shown. Non-detects plotted at detection limit.
Each data point is a discrete measurement except when multiple measurements were taken on the same day at the same depth (average shown).
Data in 'top third depth' excluded if collected below 10 meters (approximate starting depth of metalimnion).

haz/ec - A:\Jobs\PARcrm\model\Phase2_Travis\CE-QUAL-W2\postprocess\travis_temporal_forPh2rpt.pro
Wed Apr 08 14:50:21 2009

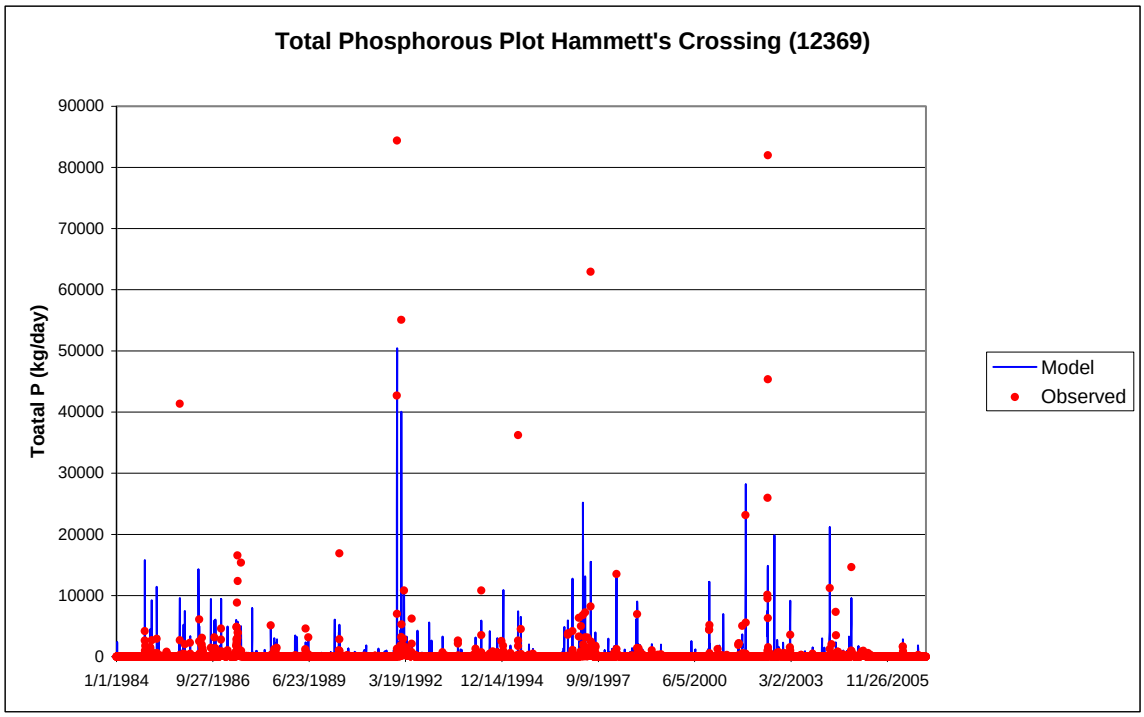

Figure 3-17. Total phosphorus comparison at Hammett's Crossing.

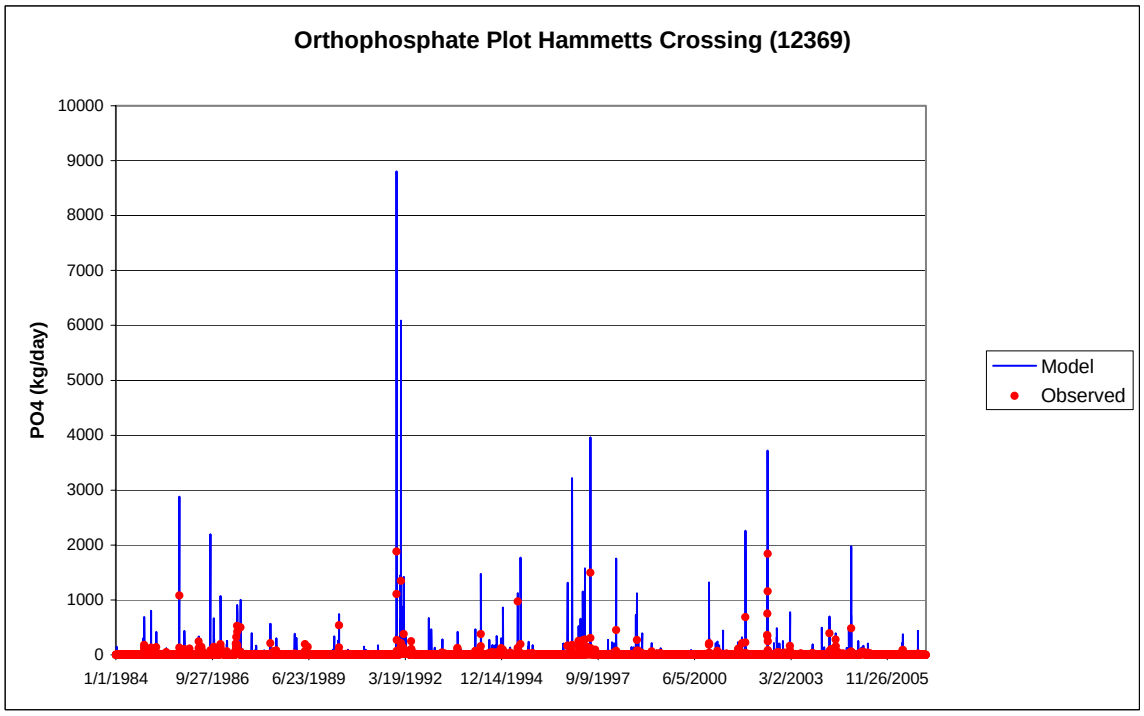

Figure 3-18. Orthophosphate comparison at Hammett's Crossing.

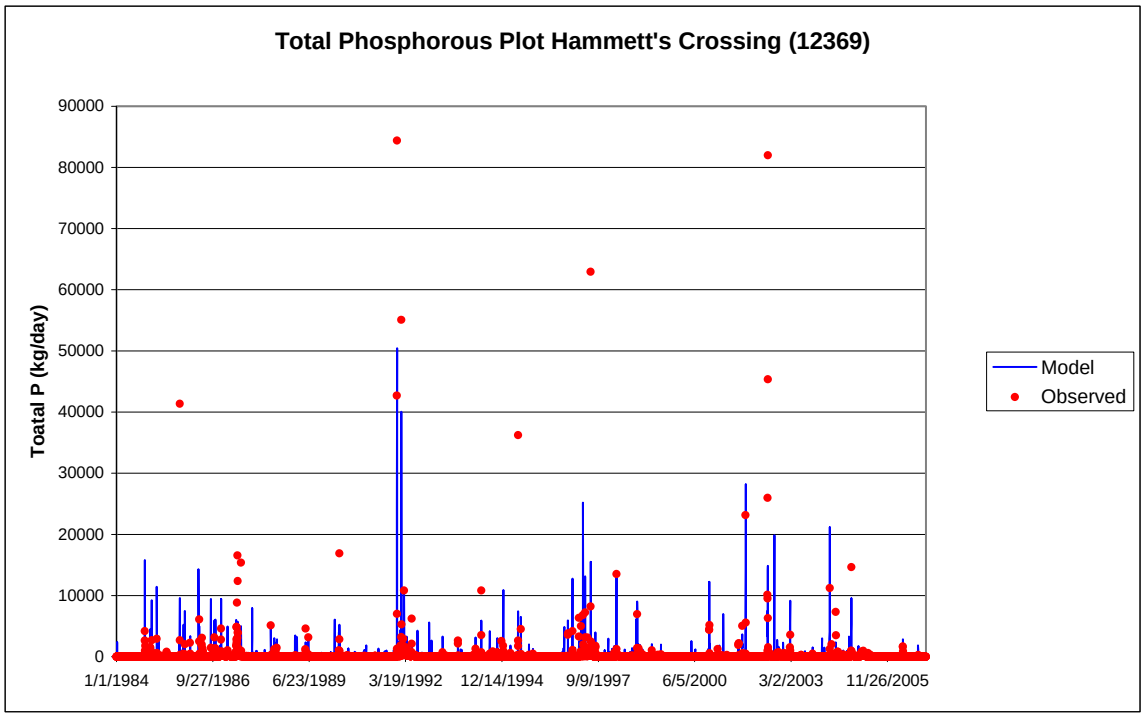

Figure 3-19. Organic phosphorus comparison at Hammett's Crossing.

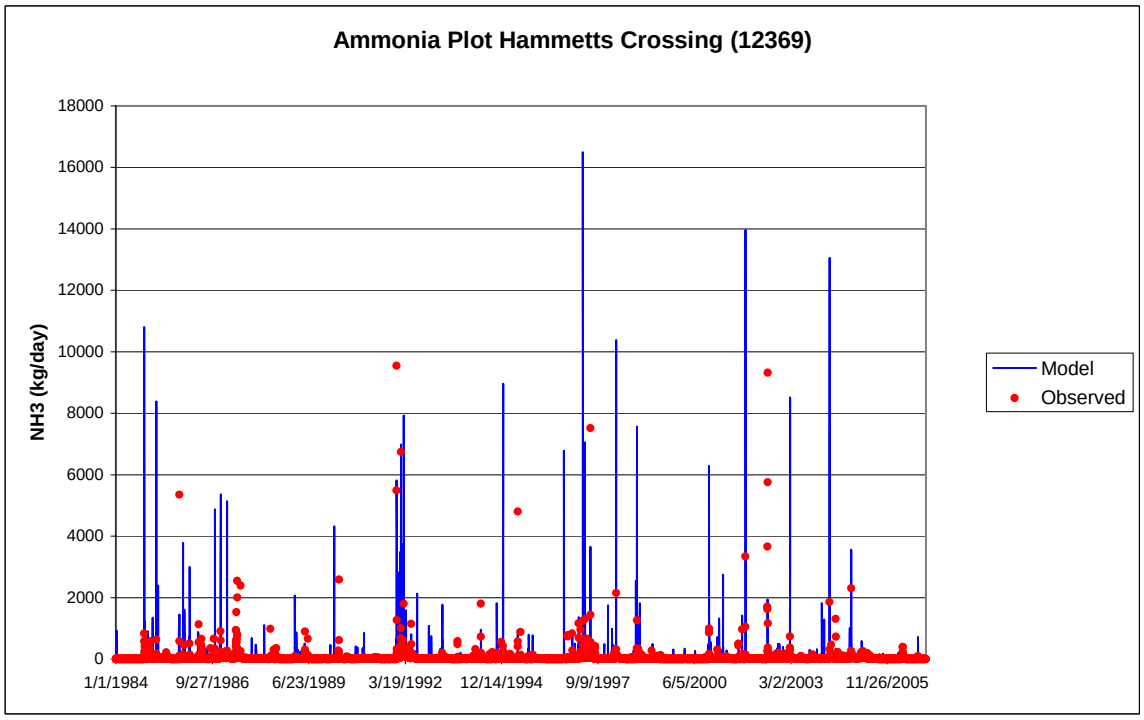

Figure 3-20. Ammonia comparison at Hammett's Crossing.

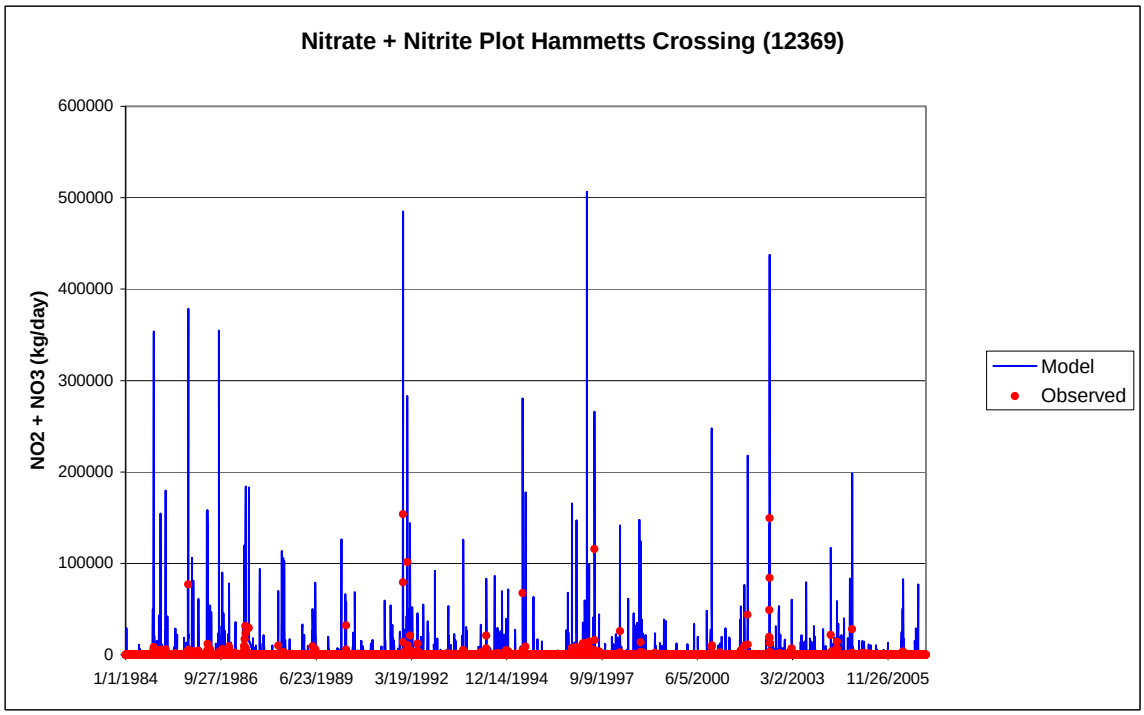

Figure 3-21. Nitrate and nitrite comparison at Hammett's Crossing.

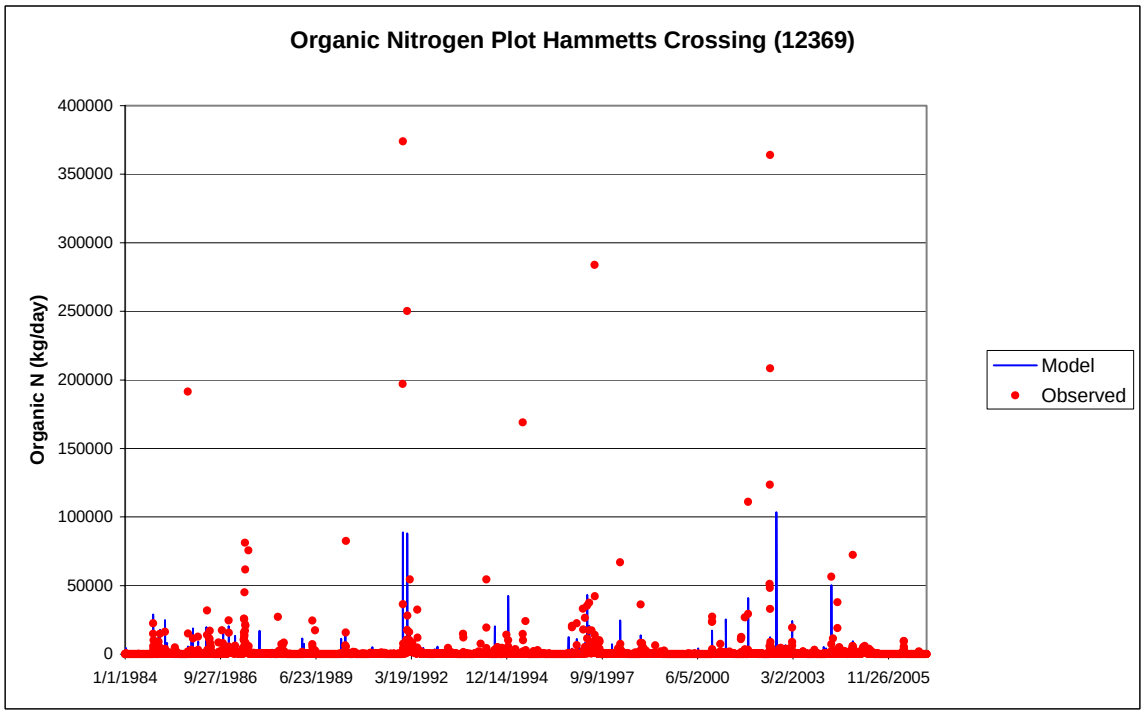

Figure 3-22. Organic nitrogen comparison at Hammett's Crossing.

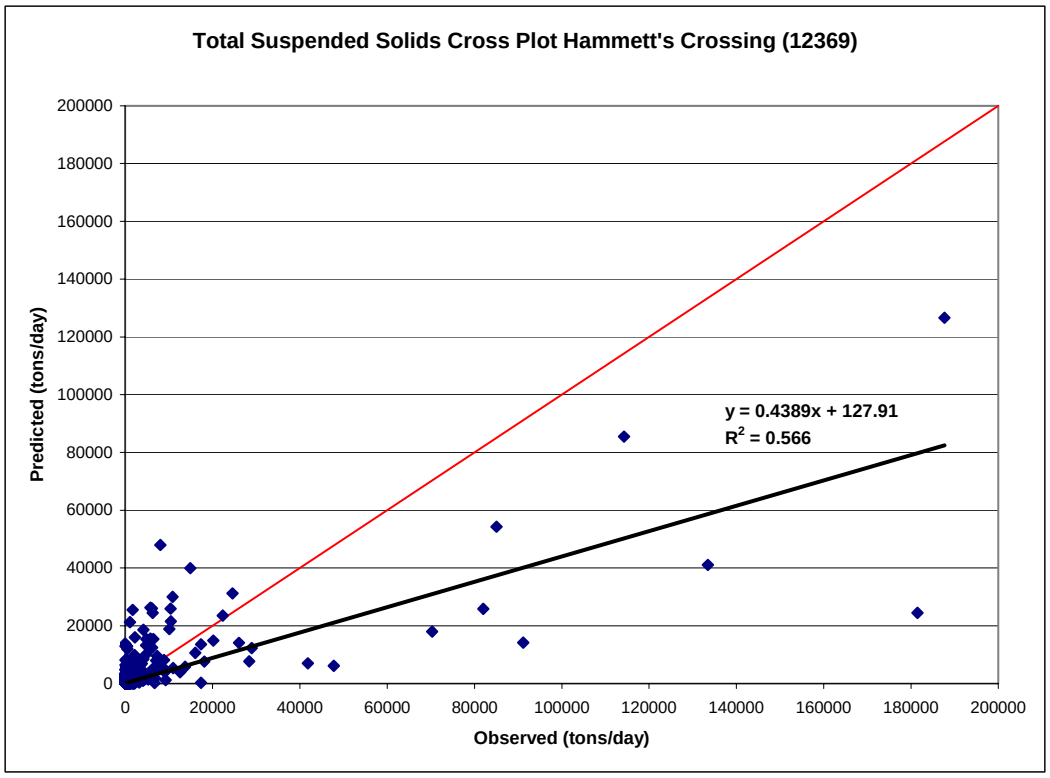

Figure 3-23. Flow cross plot at Hammett's Crossing.

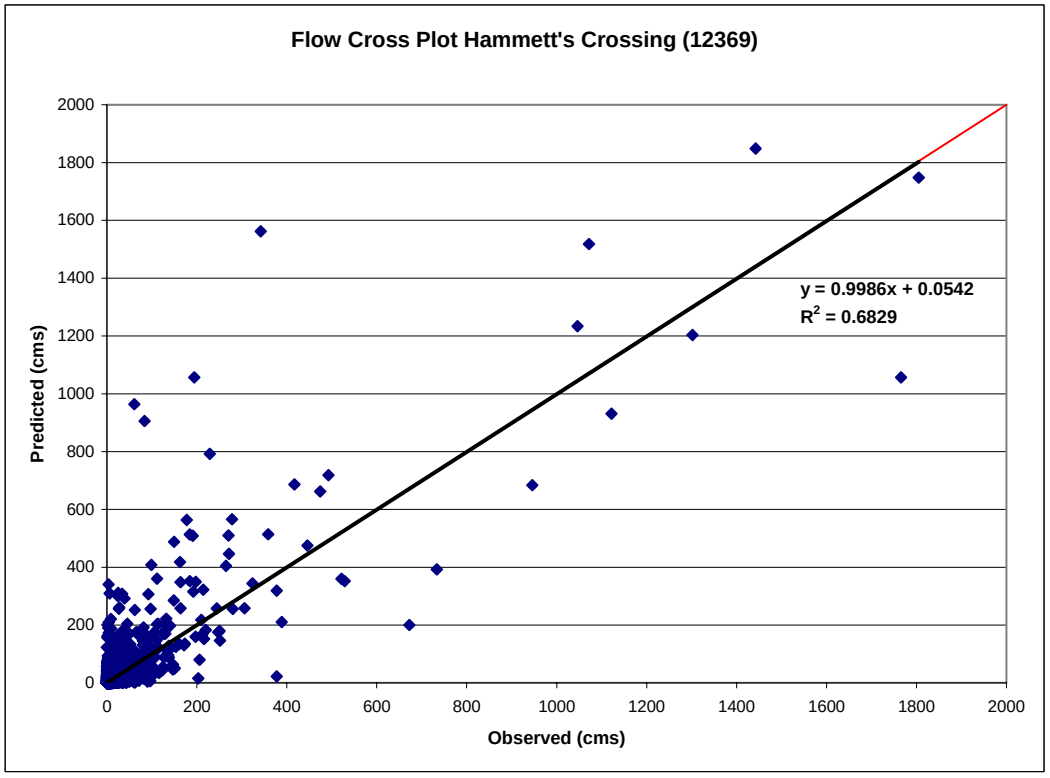

Figure 3-24. Total suspended solids cross plot at Hammett's Crossing.

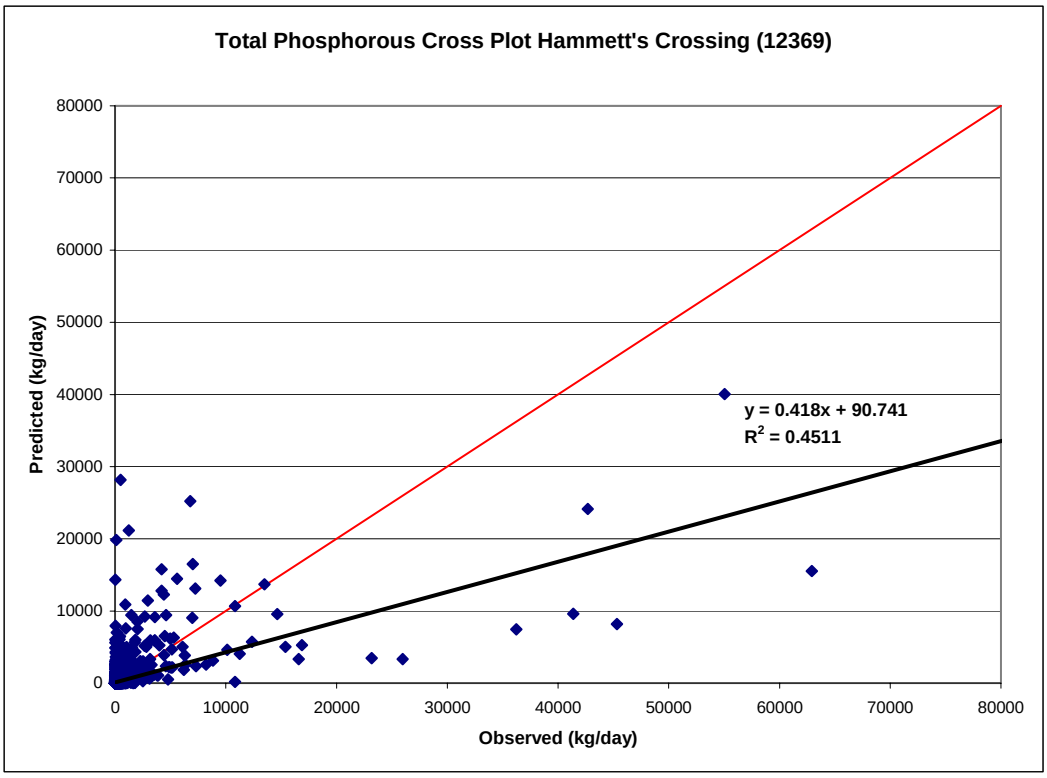

Figure 3-25. Total phosphorus cross plot at Hammett's Crossing.

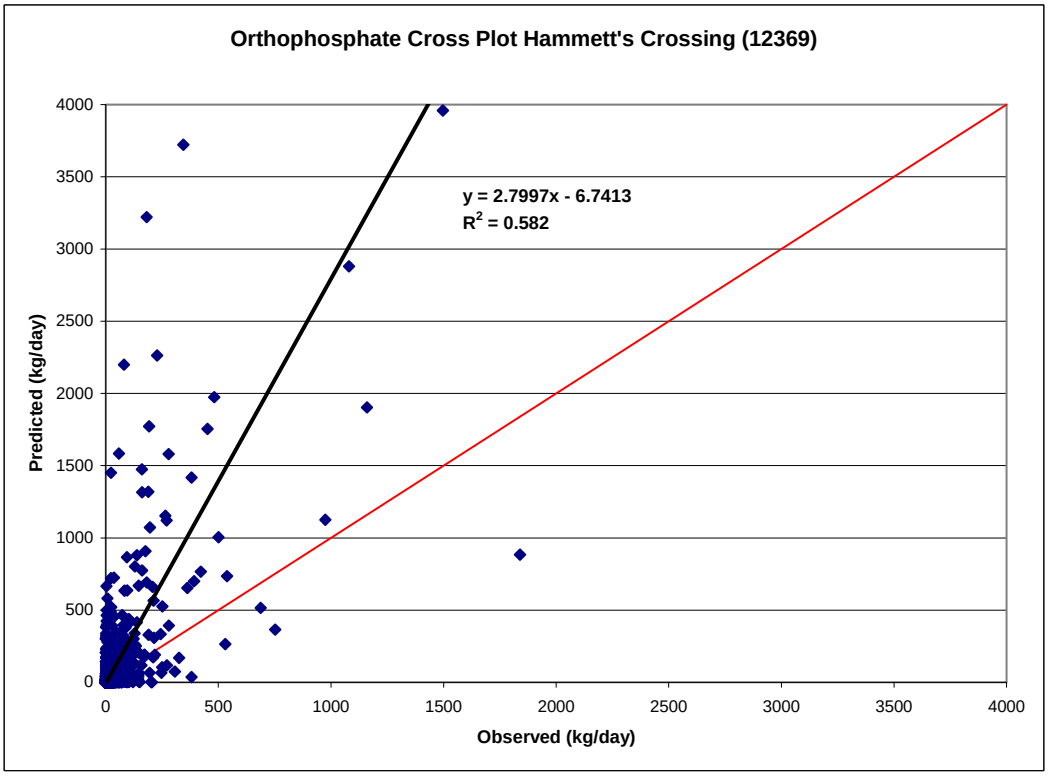

Figure 3-26. Orthophosphate cross plot at Hammett's Crossing.

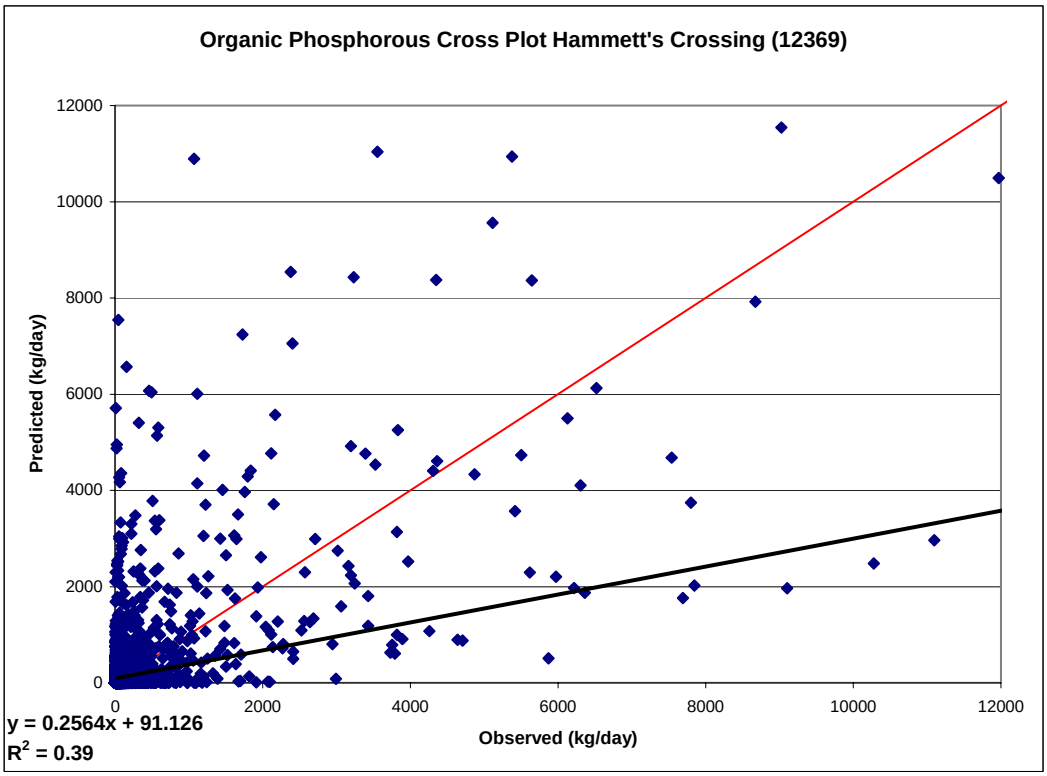

Figure 3-27. Organic phosphorus cross plot at Hammett's Crossing.

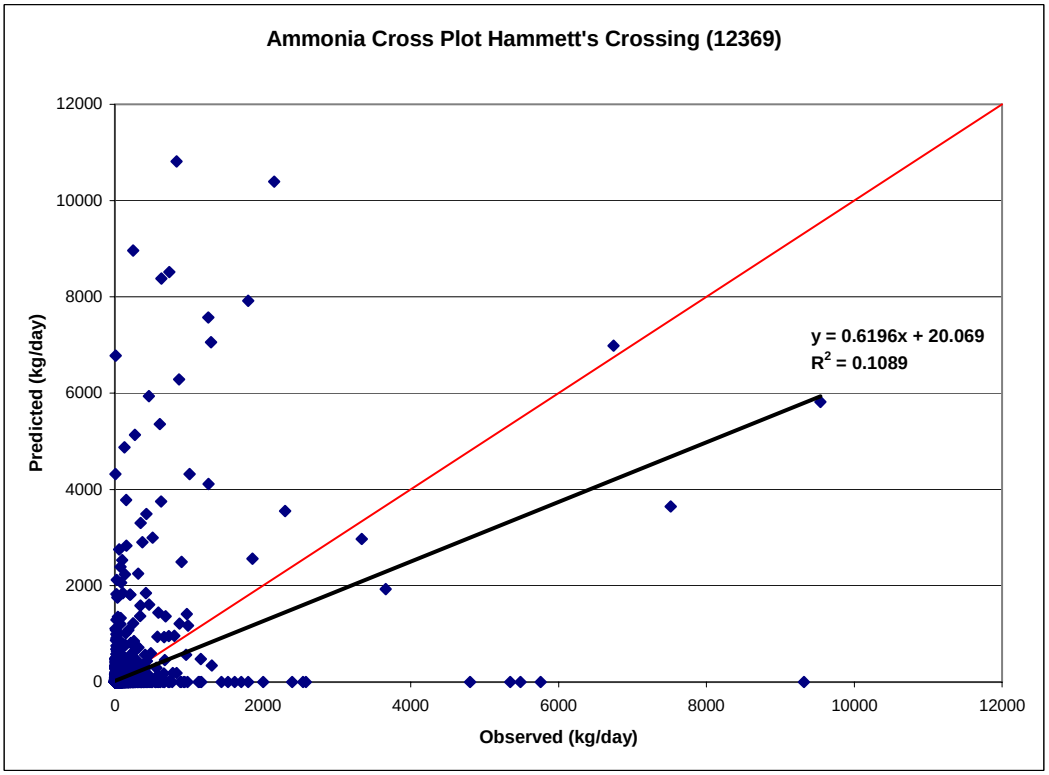

Figure 3-28. Ammonia cross plot at Hammett's Crossing.

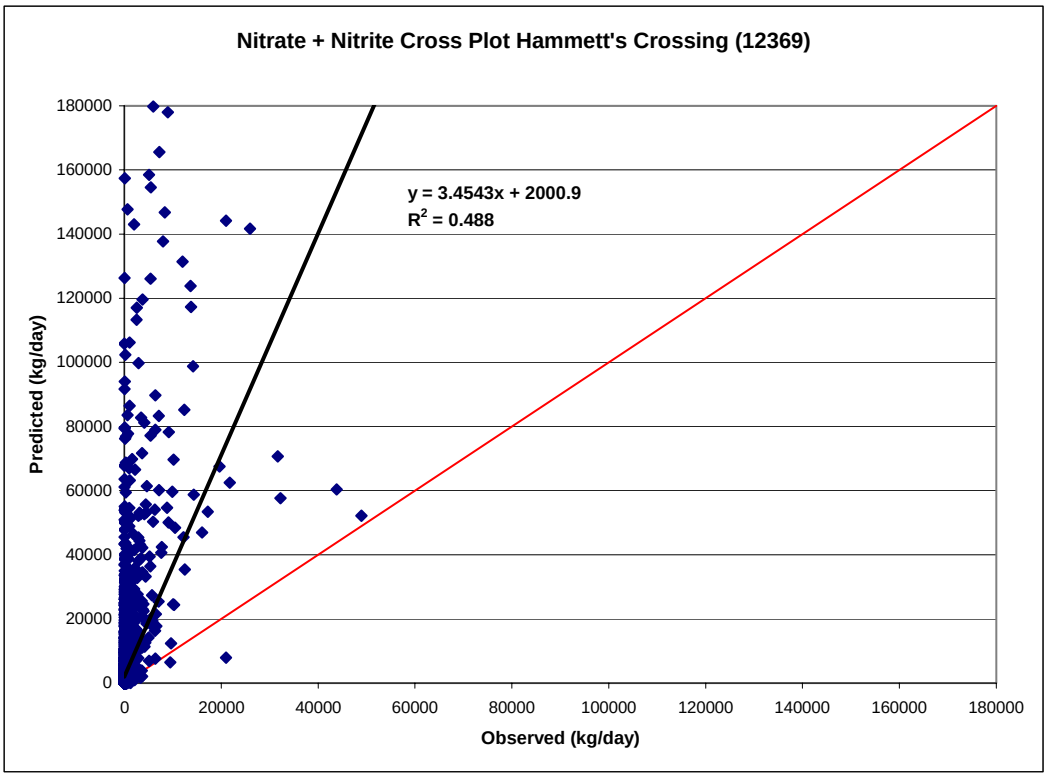

Figure 3-29. Nitrate and nitrite cross plot at Hammett's Crossing.

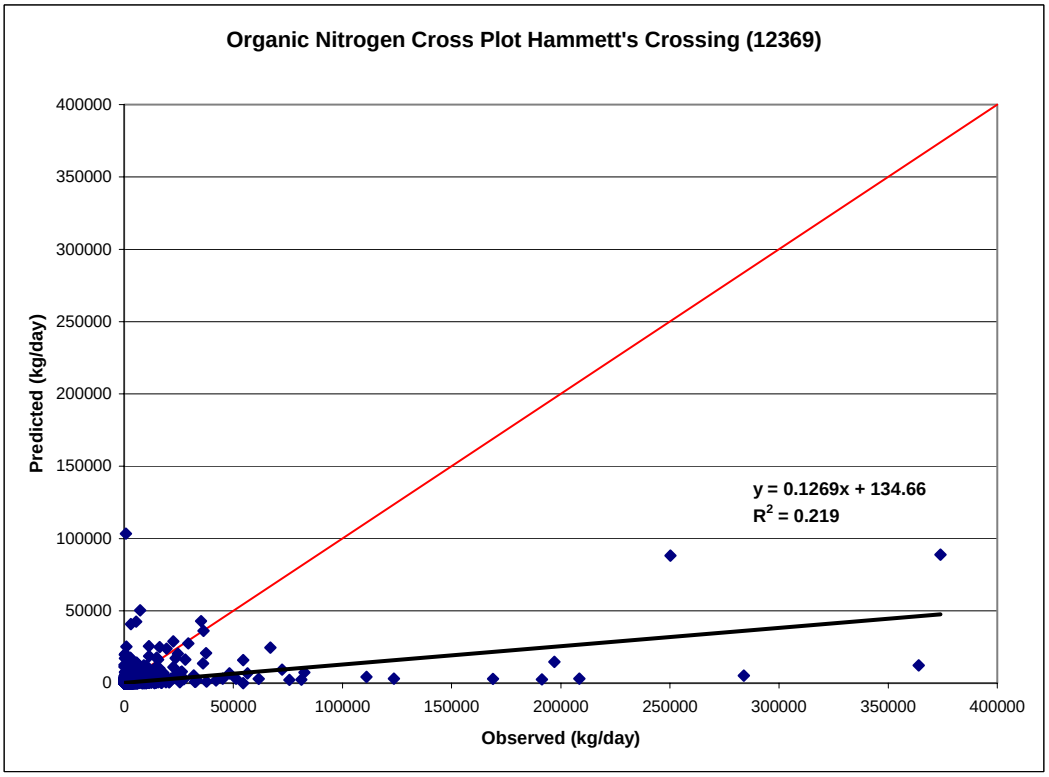

Figure 3-30. Organic nitrogen cross plot at Hammett's Crossing.

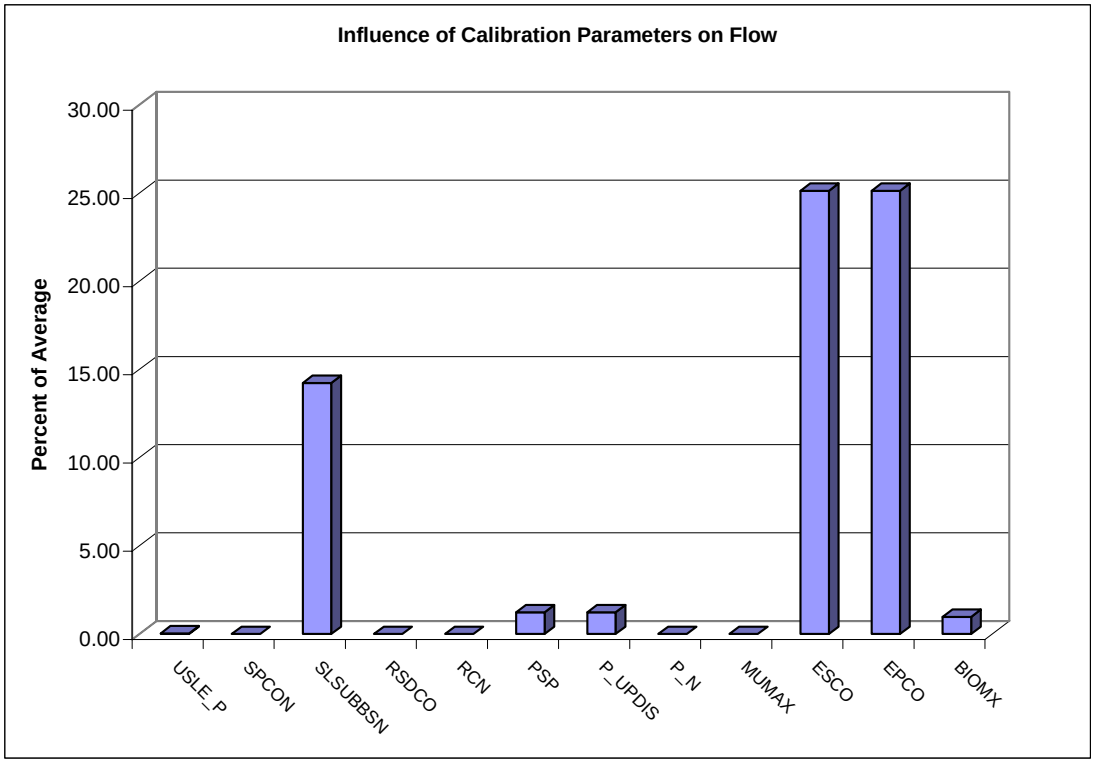

Figure 3-31. Influence of sensitivity parameters on flow.

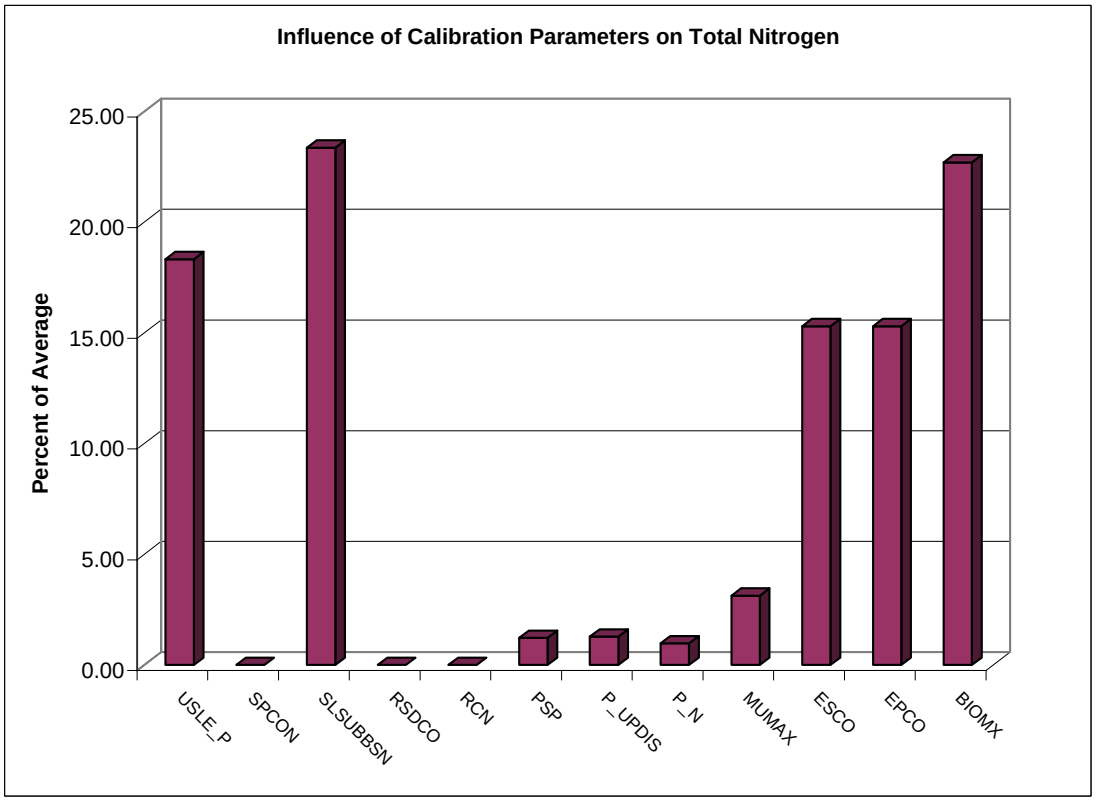

Figure 3-32. Influence of sensitivity parameters on total nitrogen.

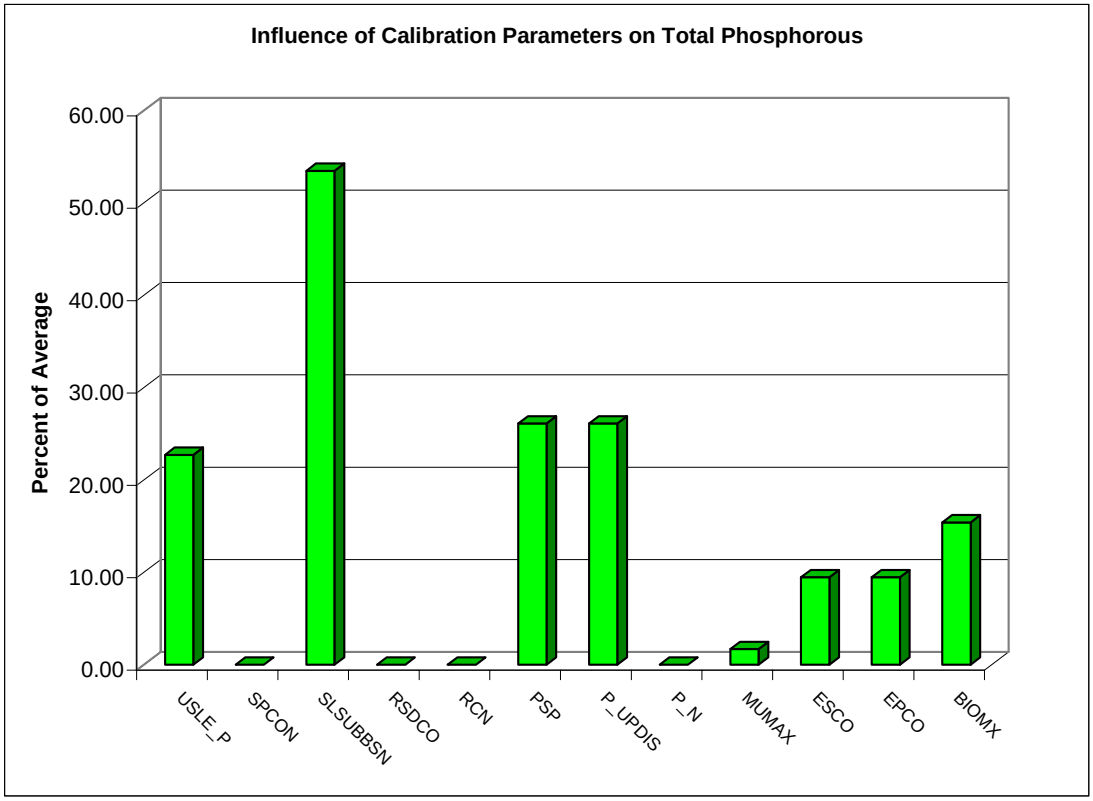

Figure 3-33. Influence of sensitivity parameters on total phosphorus.

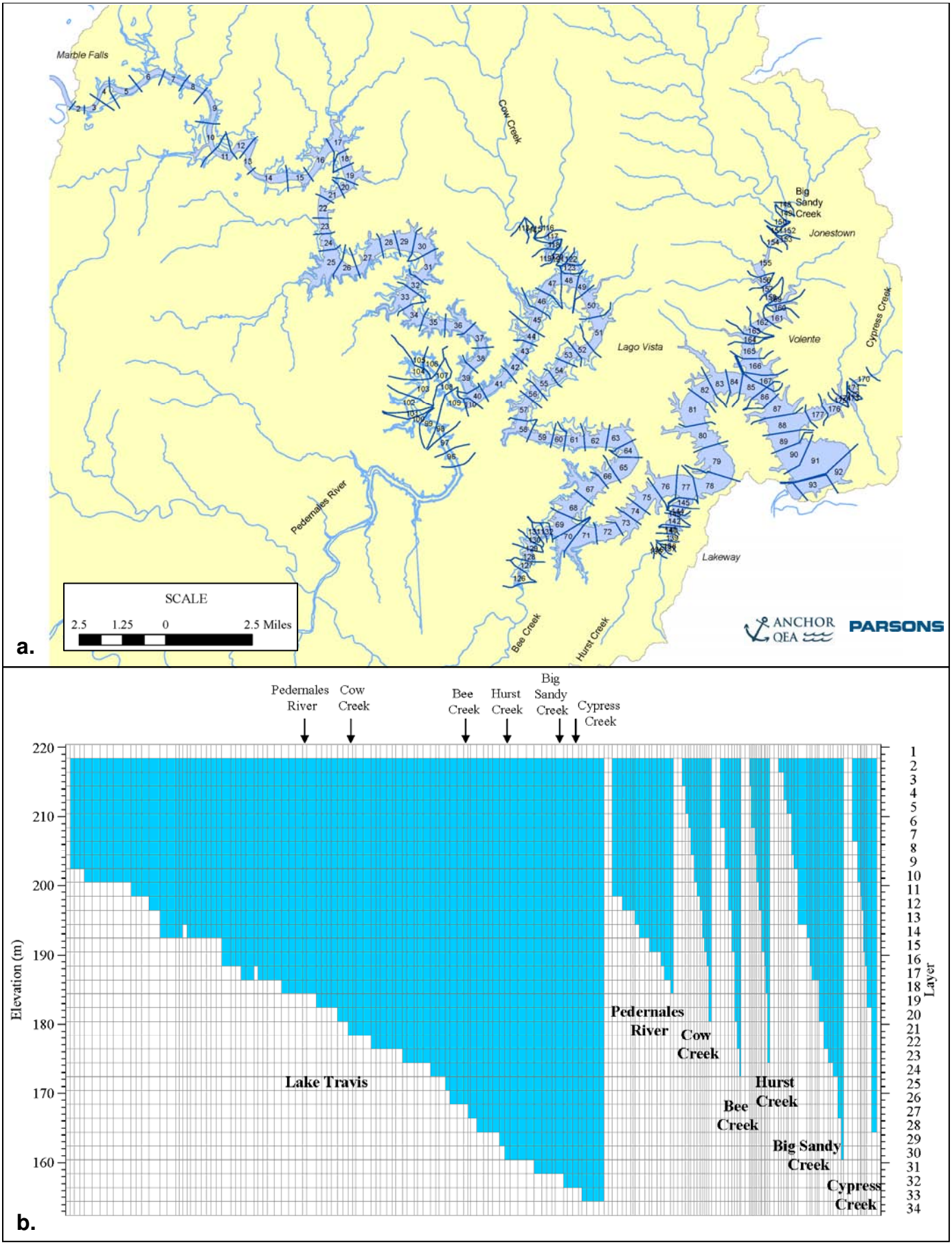

Figure 4-1. Lake Travis model grid.

Panel a. depicts overhead model view. Panel b. depicts side-view of model grid. Locations where tributaries enter Lake Travis indicated above figure.

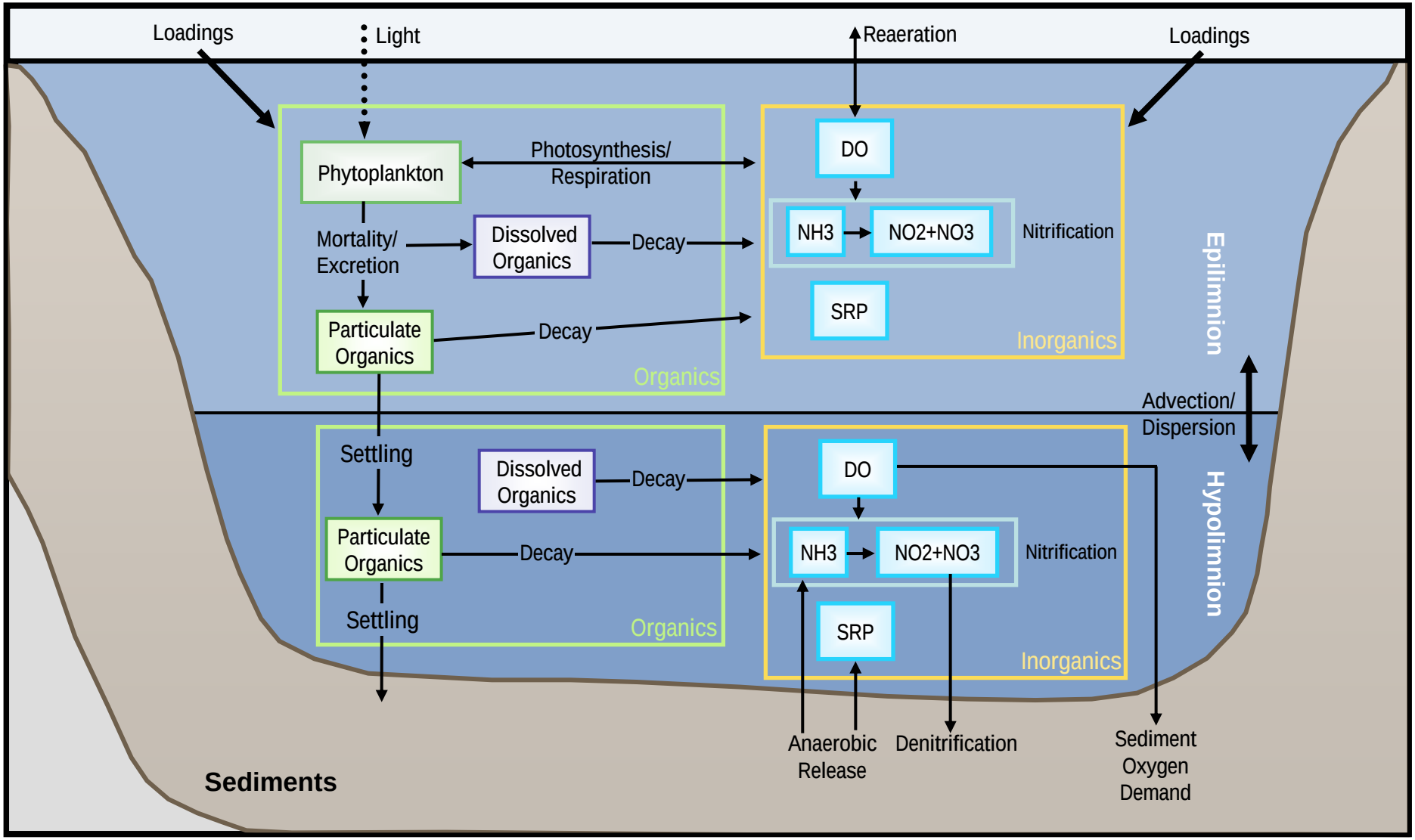

Figure 4-2. Conceptual model of Lake Travis water quality dynamics.

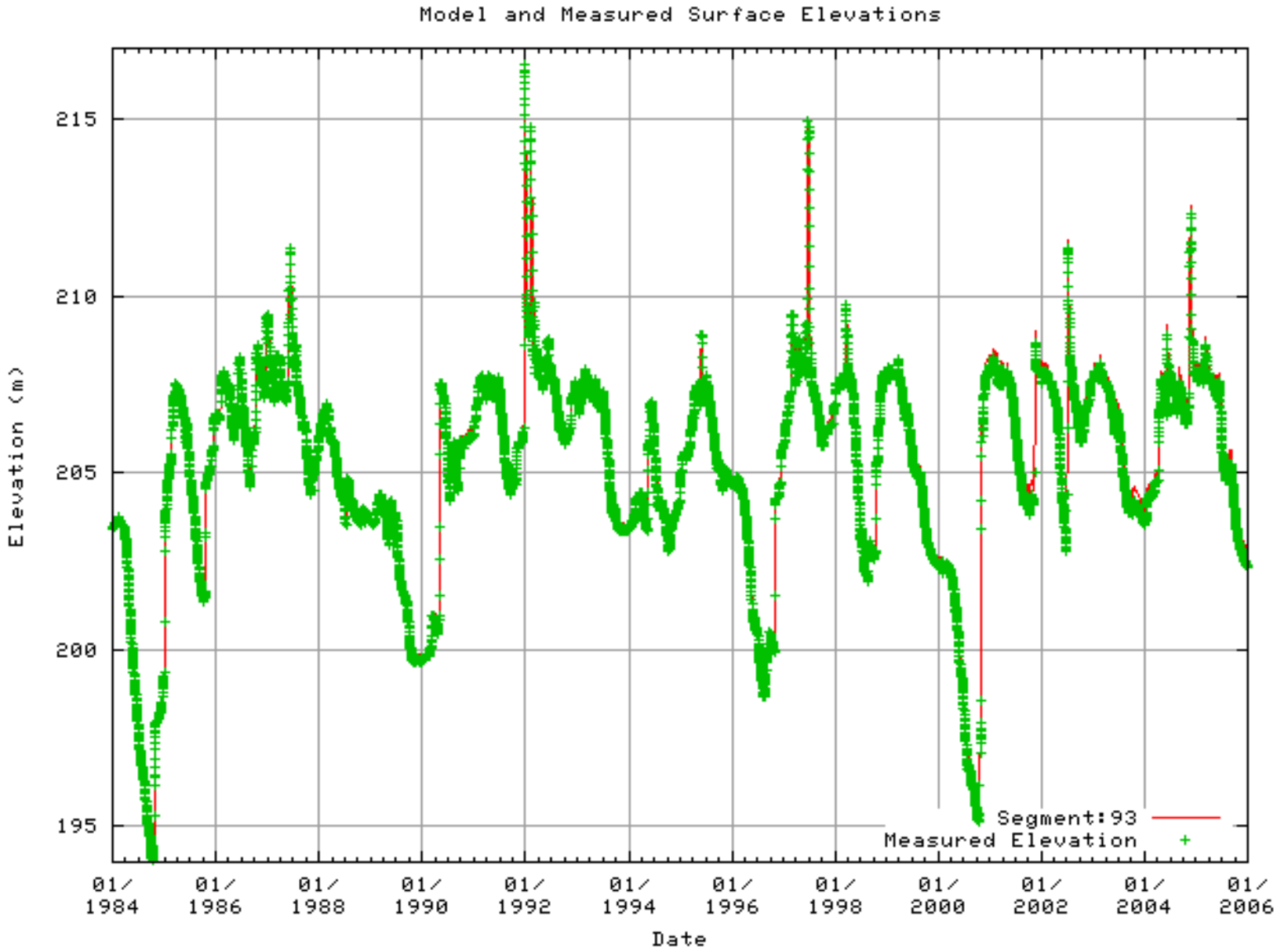

Figure 4-3. Model predicted water surface elevations compared to measured data at Mansfield Dam.

The model calibration period is 1/1/1984 through 12/31/2006. This figure was not updated to include the 2006 comparisons after the extension of the model.

\\EC\d_drive\PARcrm\Documents\reports\Lake_Travis_Phase2\figures\fig4-3_elev_cw0709-08_071015.ppt

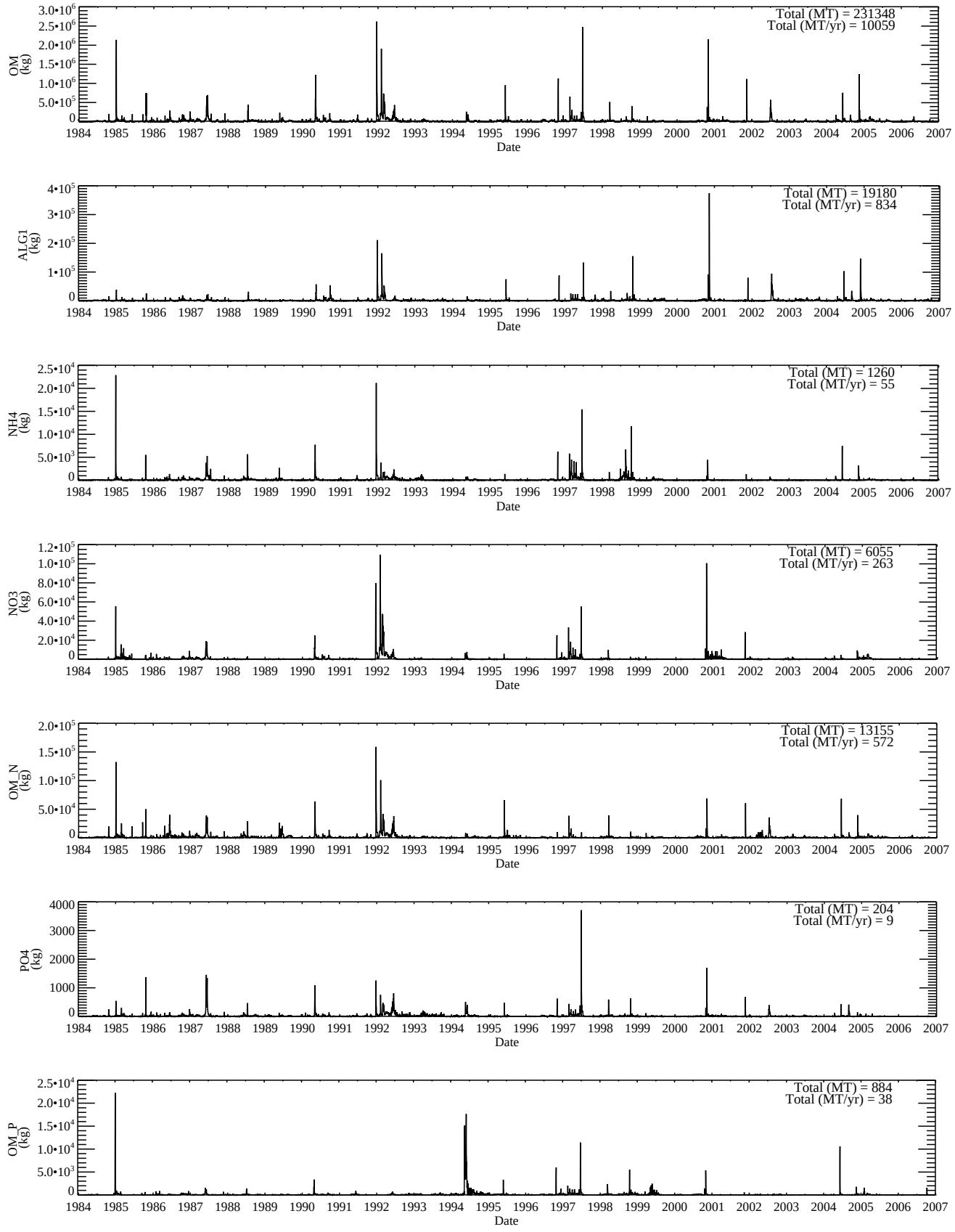

Figure 4-4. Temporals of constituent loads to Lake Travis from upstream.

Model time period: 1984 to 2006

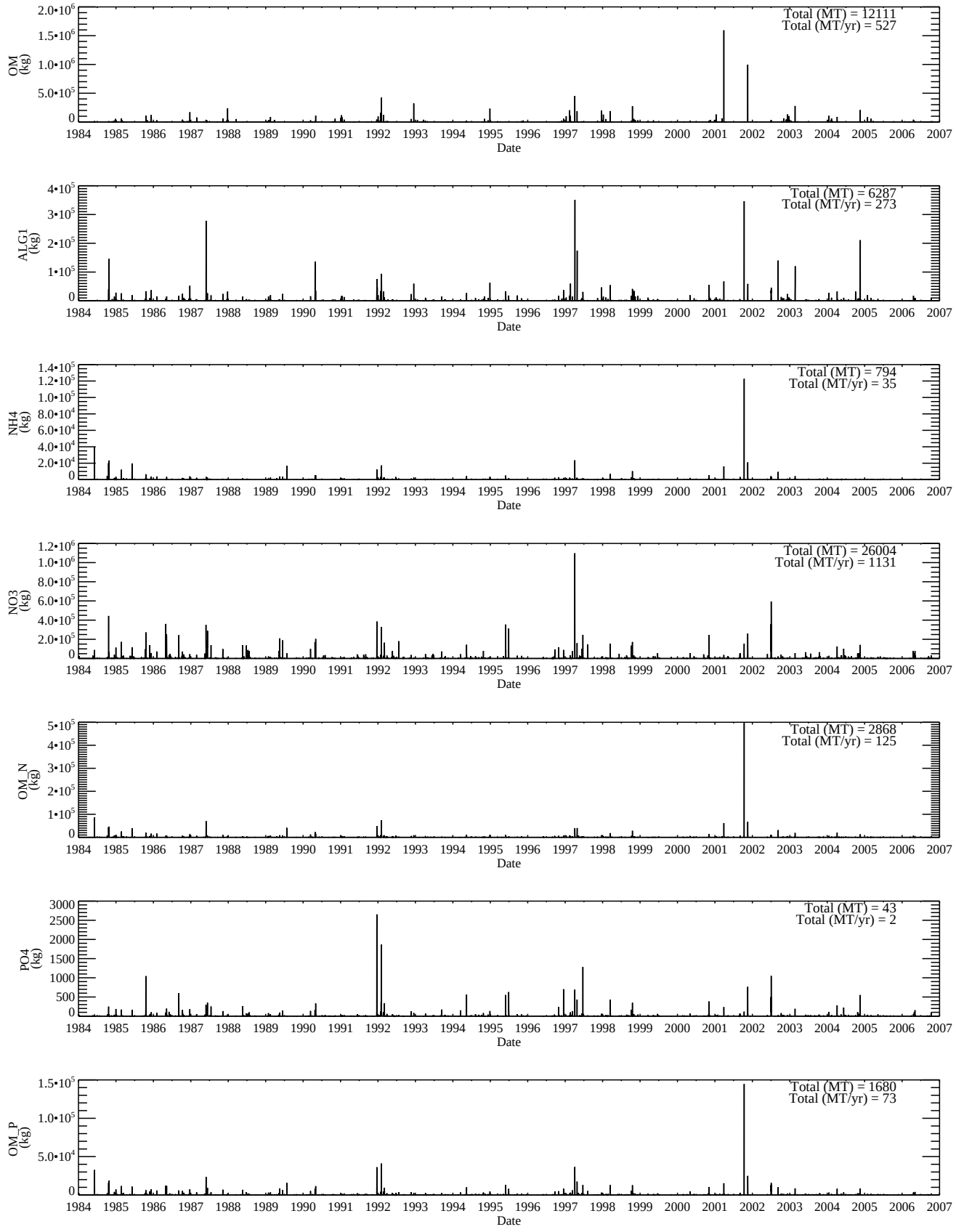

Figure 4-5. Temporals of constituent loads to Lake Travis from Pedernales River.

Model time period: 1984 to 2006

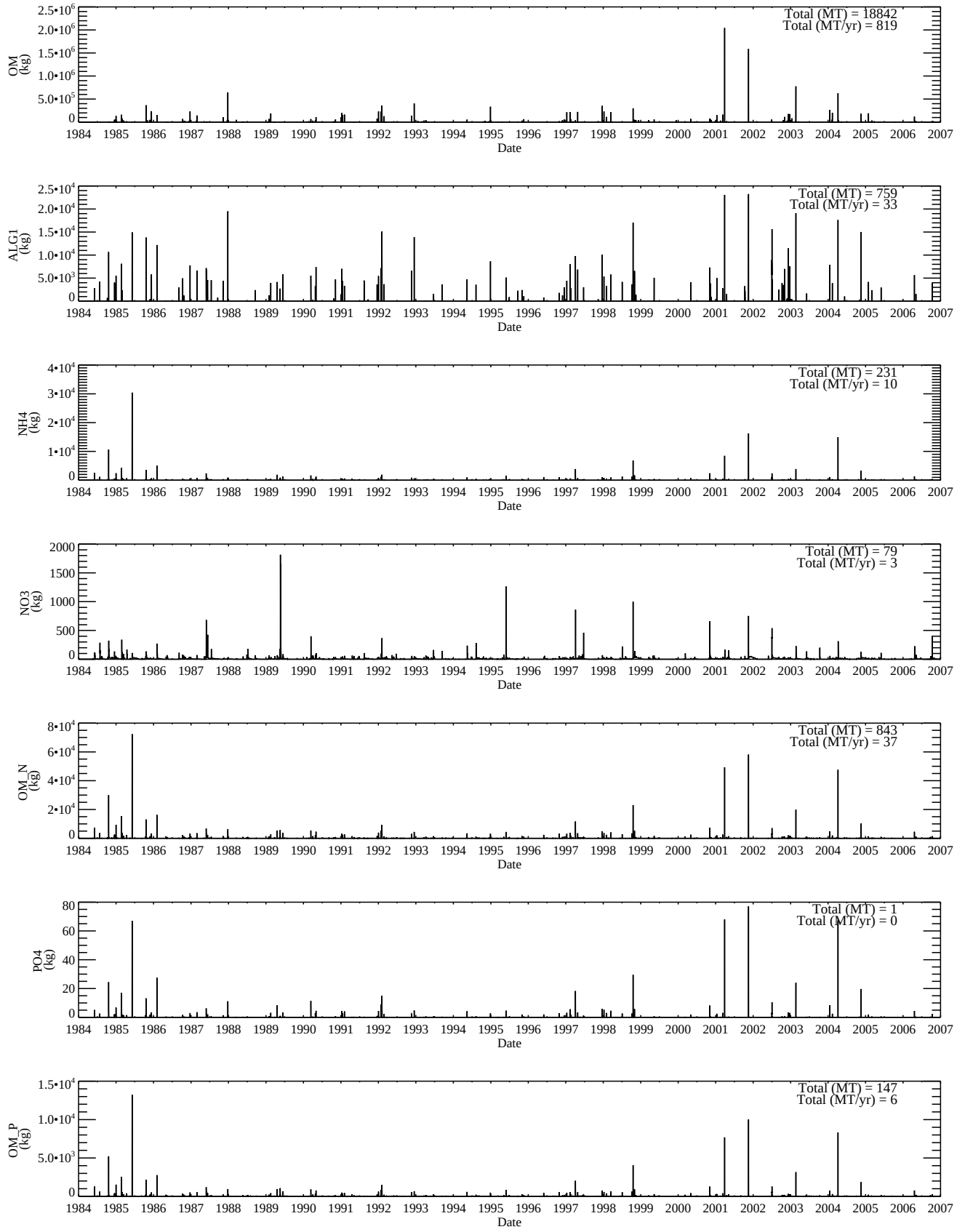

Figure 4-6. Temporals of constituent loads to Lake Travis from Cow Creek.

Model time period: 1984 to 2006

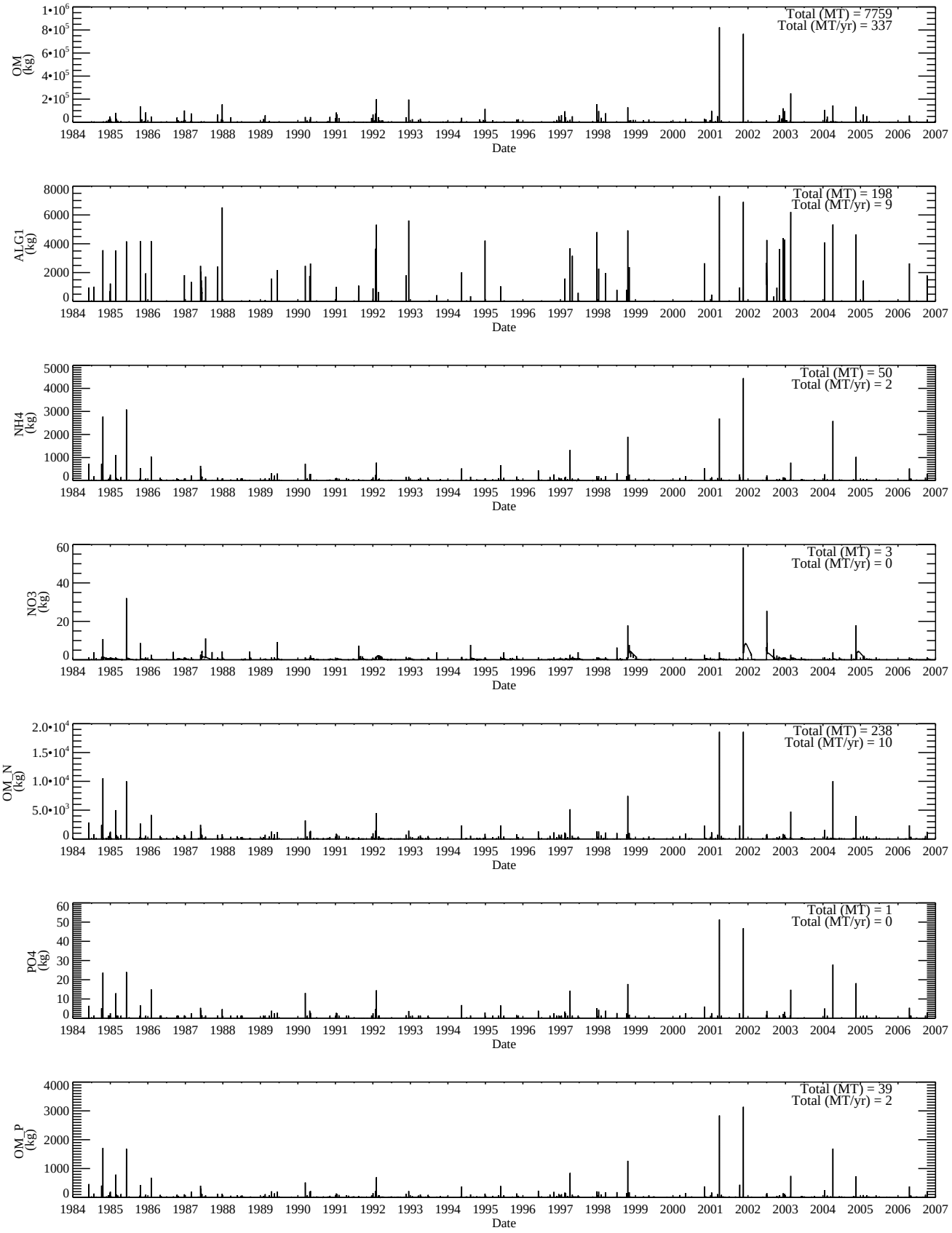

Figure 4-7. Temporals of constituent loads to Lake Travis from Bee Creek.

Model time period: 1984 to 2006

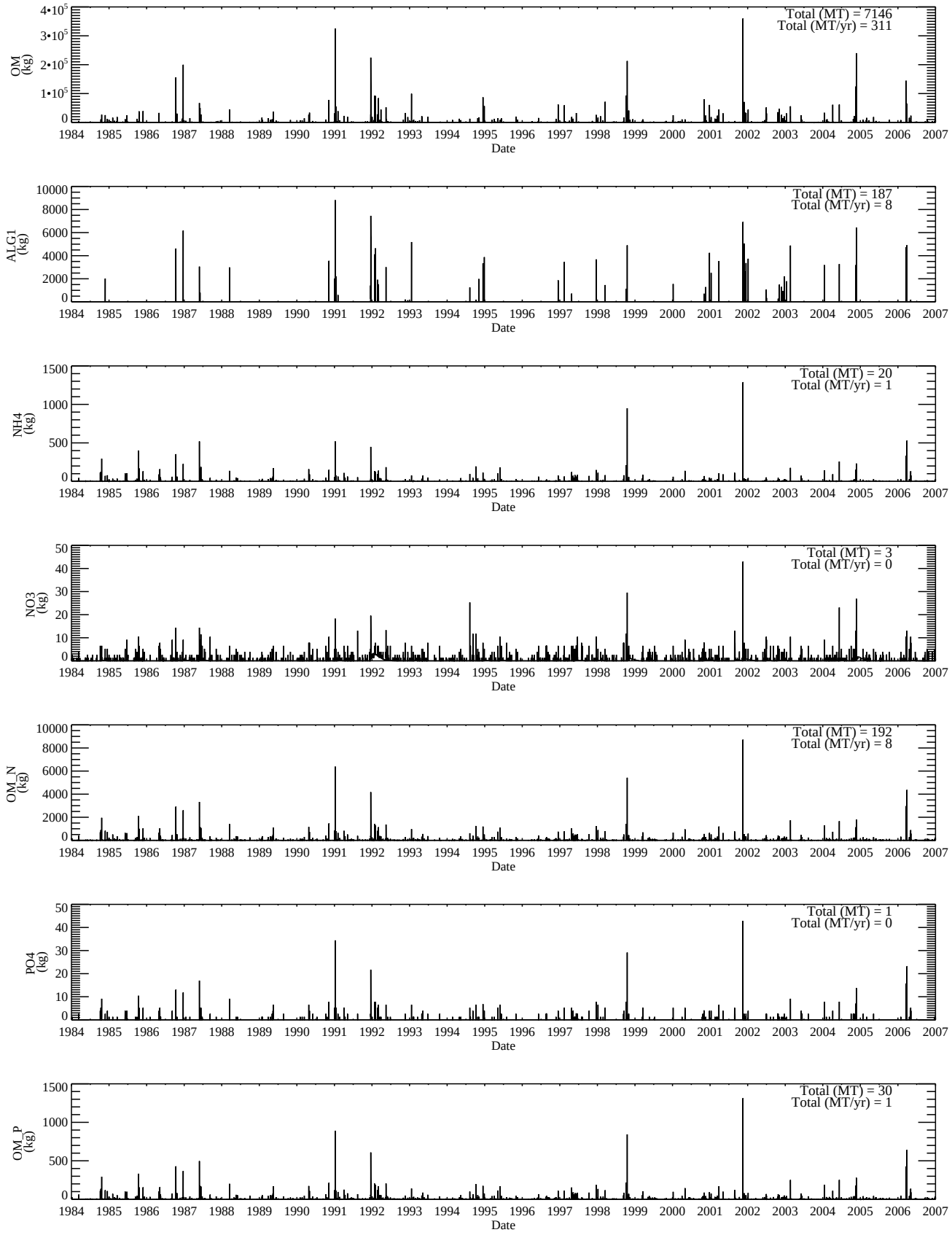

Figure 4-8. Temporals of constituent loads to Lake Travis from Hurst Creek.

Model time period: 1984 to 2006

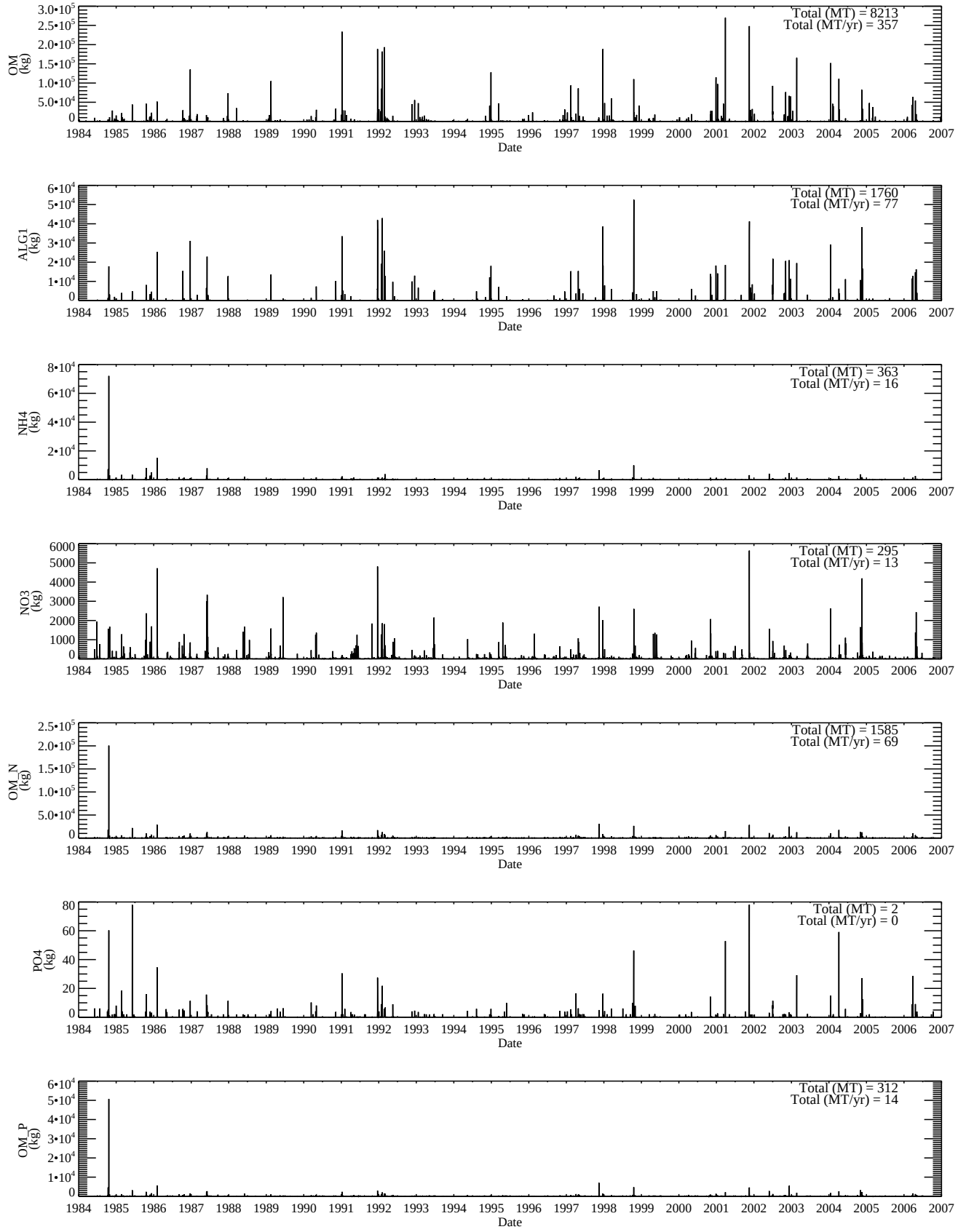

Figure 4-9. Temporals of constituent loads to Lake Travis from Big Sandy Creek.

Model time period: 1984 to 2006

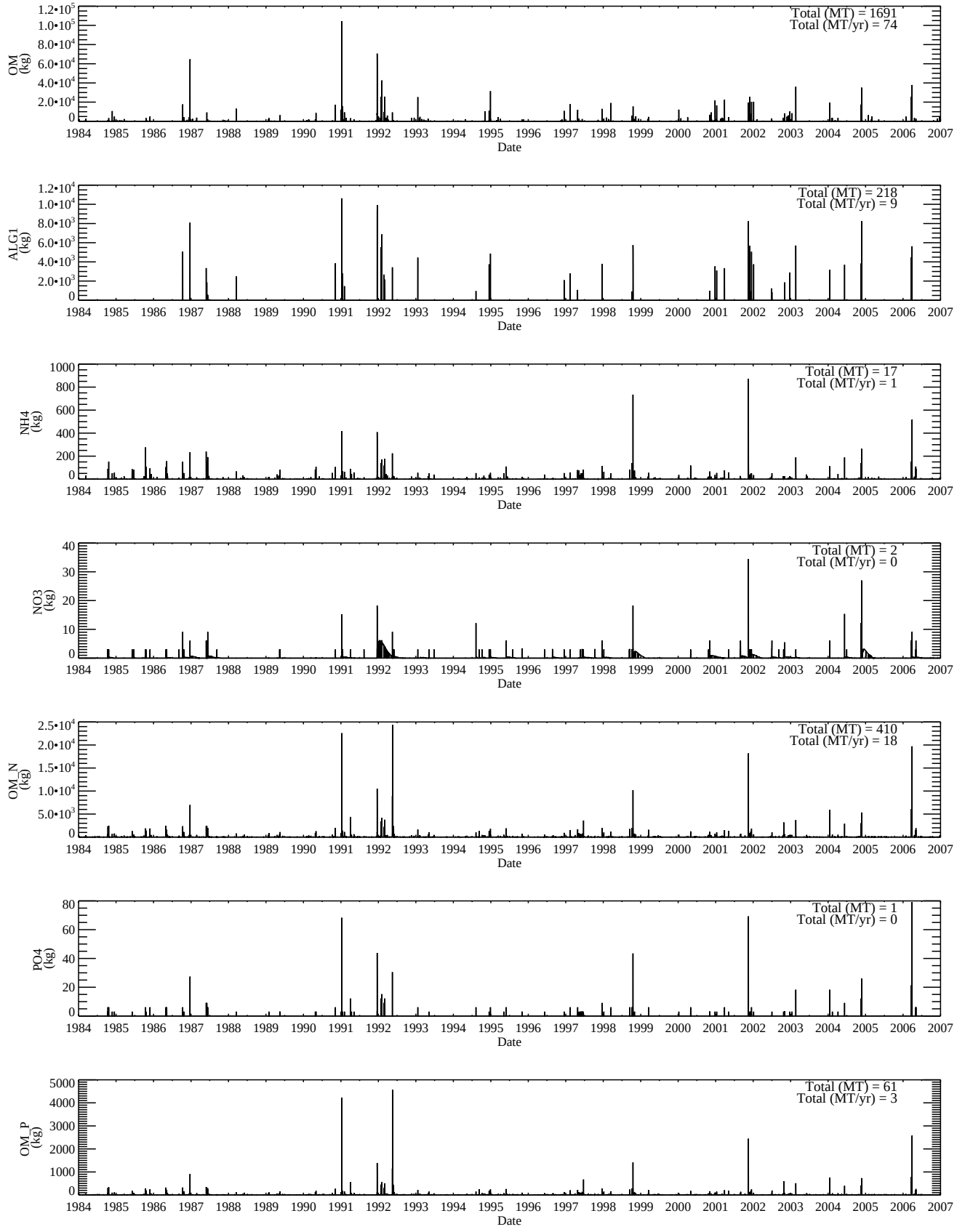

Figure 4-10. Temporals of constituent loads to Lake Travis from Cypress Creek.

Model time period: 1984 to 2006

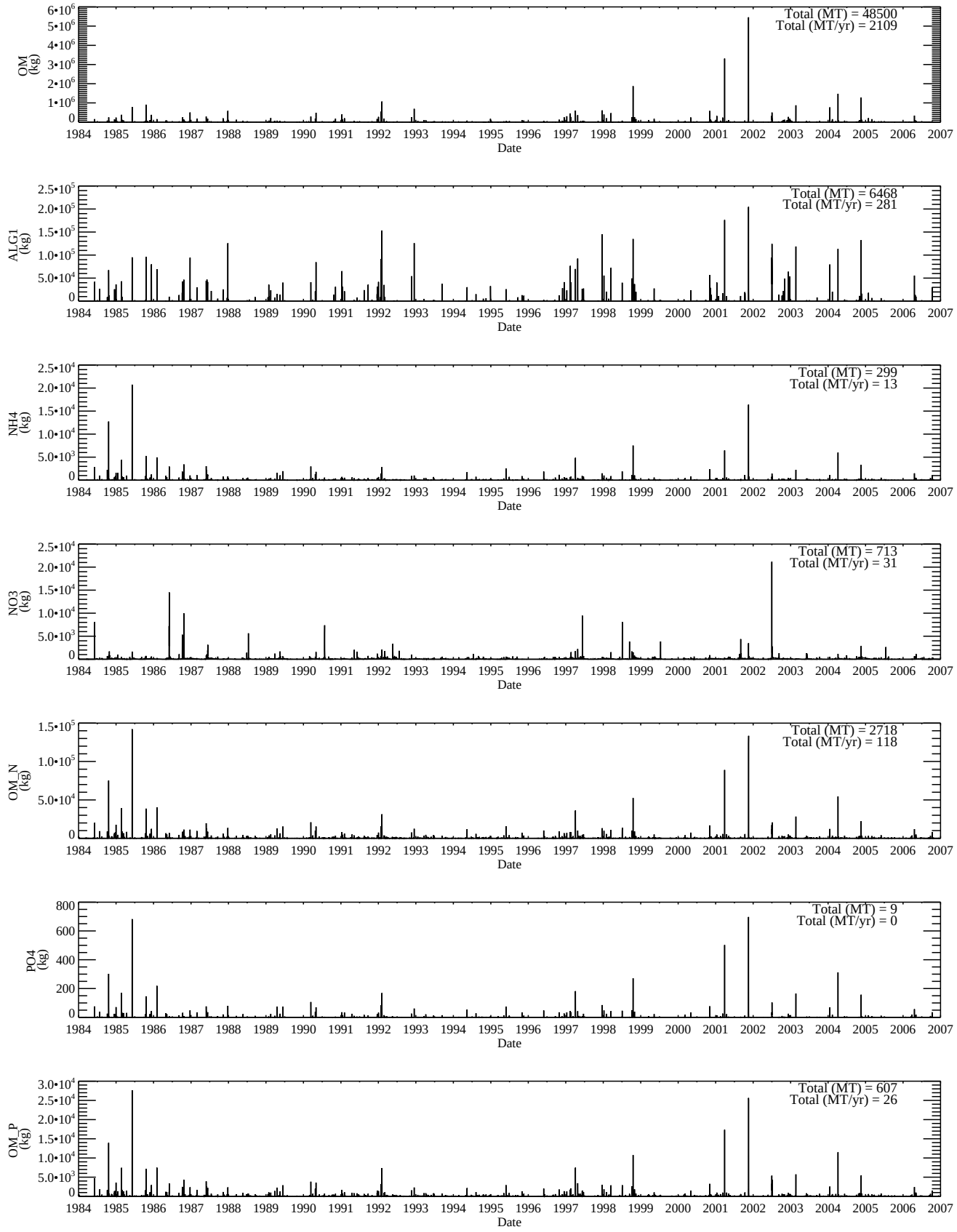

Figure 4-11. Temporals of constituent loads to Lake Travis from direct drainage.

Model time period: 1984 to 2006

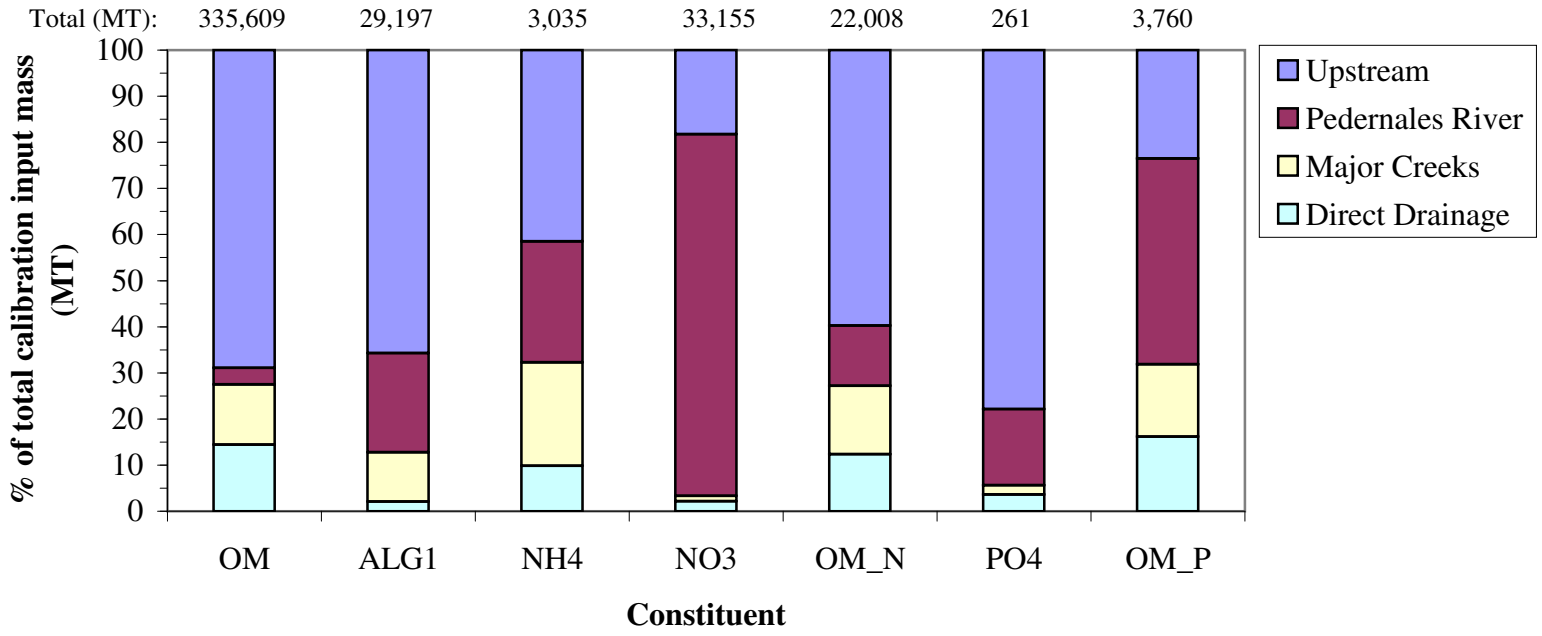

Figure 4-12. Percentage contribution by source type for input constituent mass during calibration period.
Calibration period: 1/1/1984 through 12/31/2006
Major creeks are Bee, Cow, Cypress, Hurst, Sandy.
Upstream inputs based on data.
Watershed inputs (Pedernales River, major creeks, direct drainage) calculated from watershed model results.

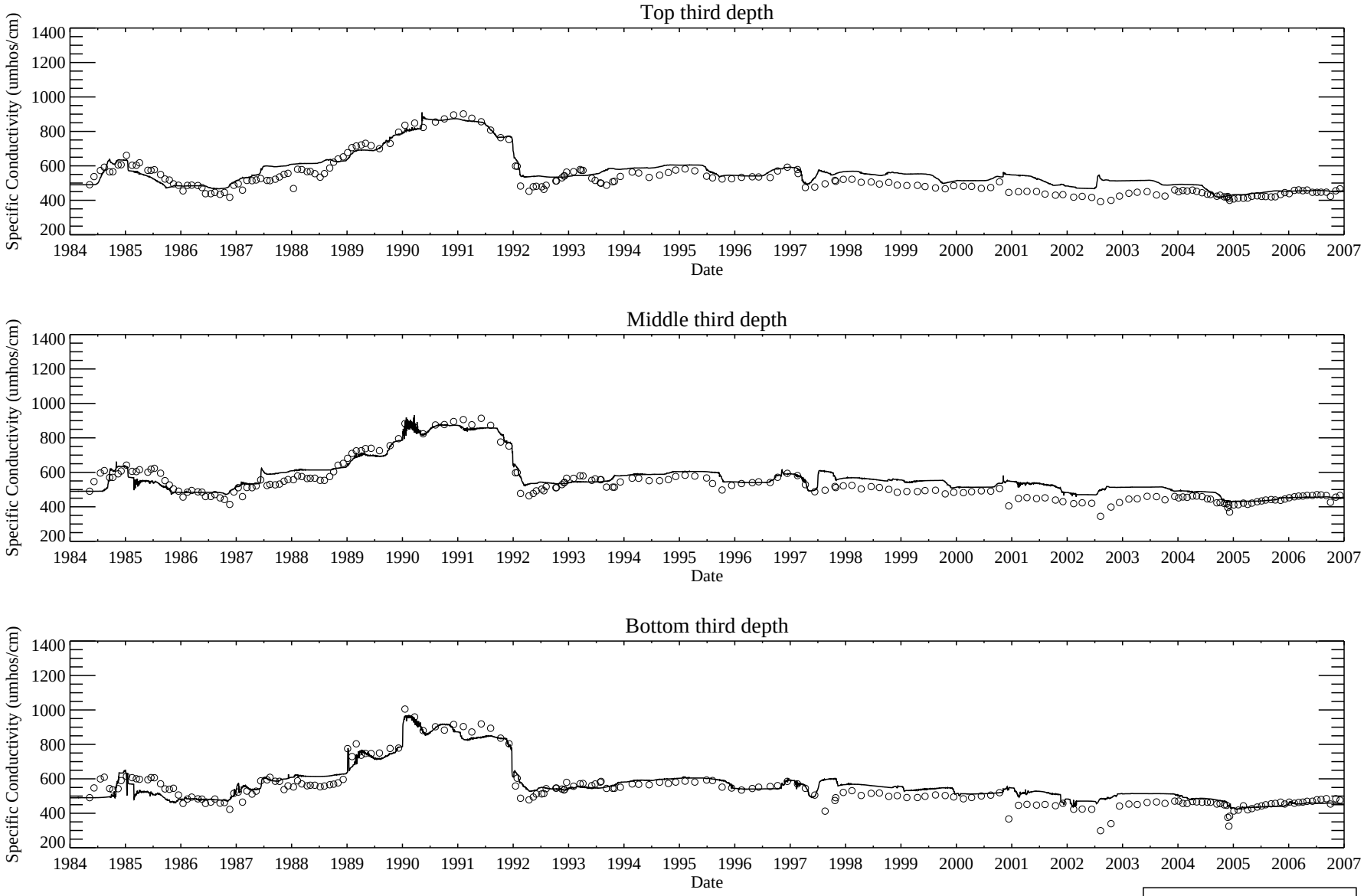

Figure 4-13. Temporal of model versus data at Mansfield Dam (Segment 93) - Specific Conductivity.

Top third depth, Middle third depth, Bottom third depth
When HAAWQ and CREMS data were measured on the same day, only CREMS data are shown. Non-detects plotted at detection limit.
Data averaged over water column depths shown.

haz/ec - D:\PARcrm\Model\Phase2_Travis\CE-QUAL-W2\postprocess\travis_temporal_forPh2rpt.pro
Thu Jan 29 14:02:13 2009

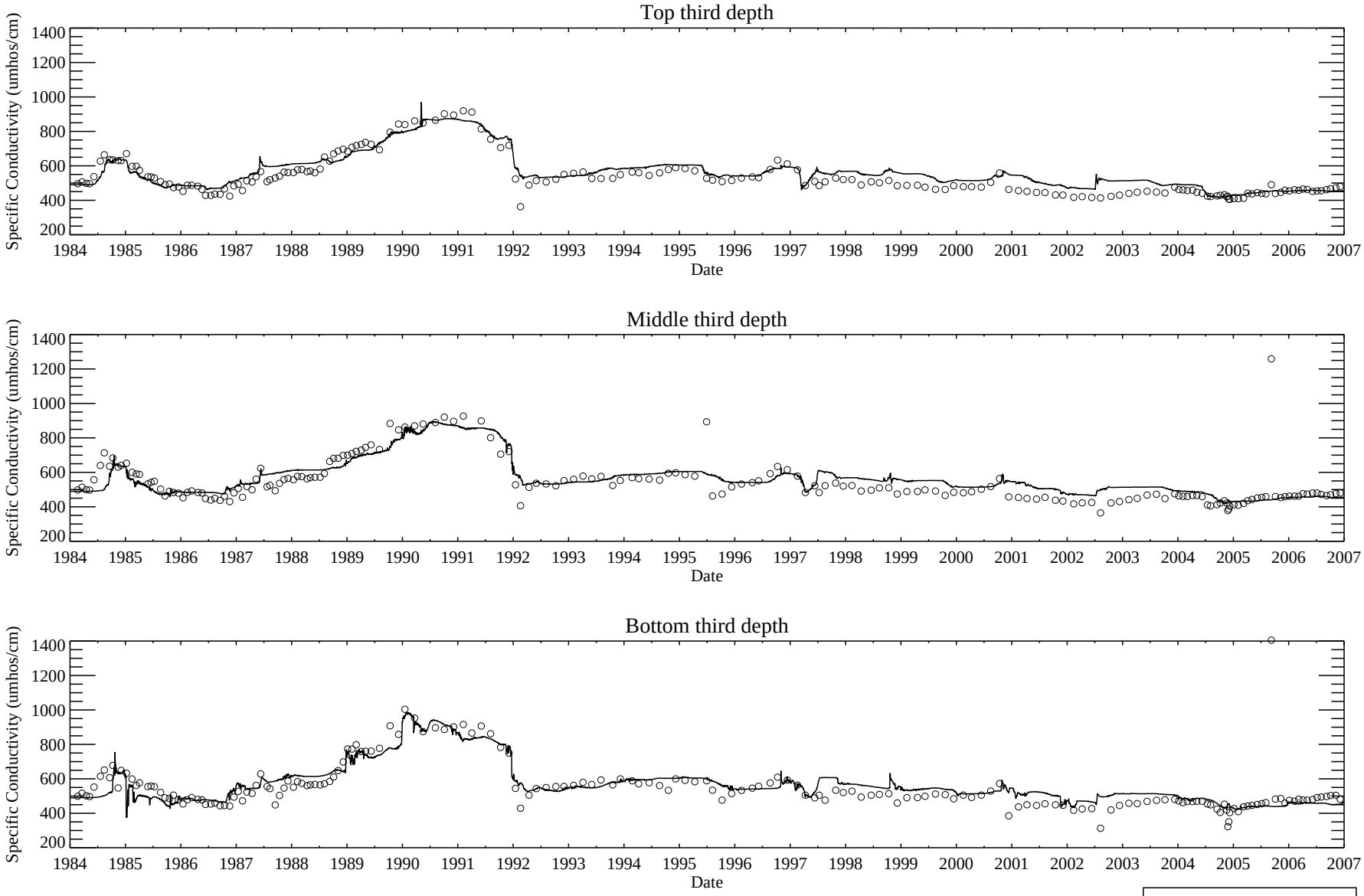

Figure 4-14. Temporal of model versus data at Arkansas Bend (Segment 78) - Specific Conductivity.

Top third depth, Middle third depth, Bottom third depth
When HAAWQ and CREMS data were measured on the same day, only CREMS data are shown. Non-detects plotted at detection limit.
Data averaged over water column depths shown.

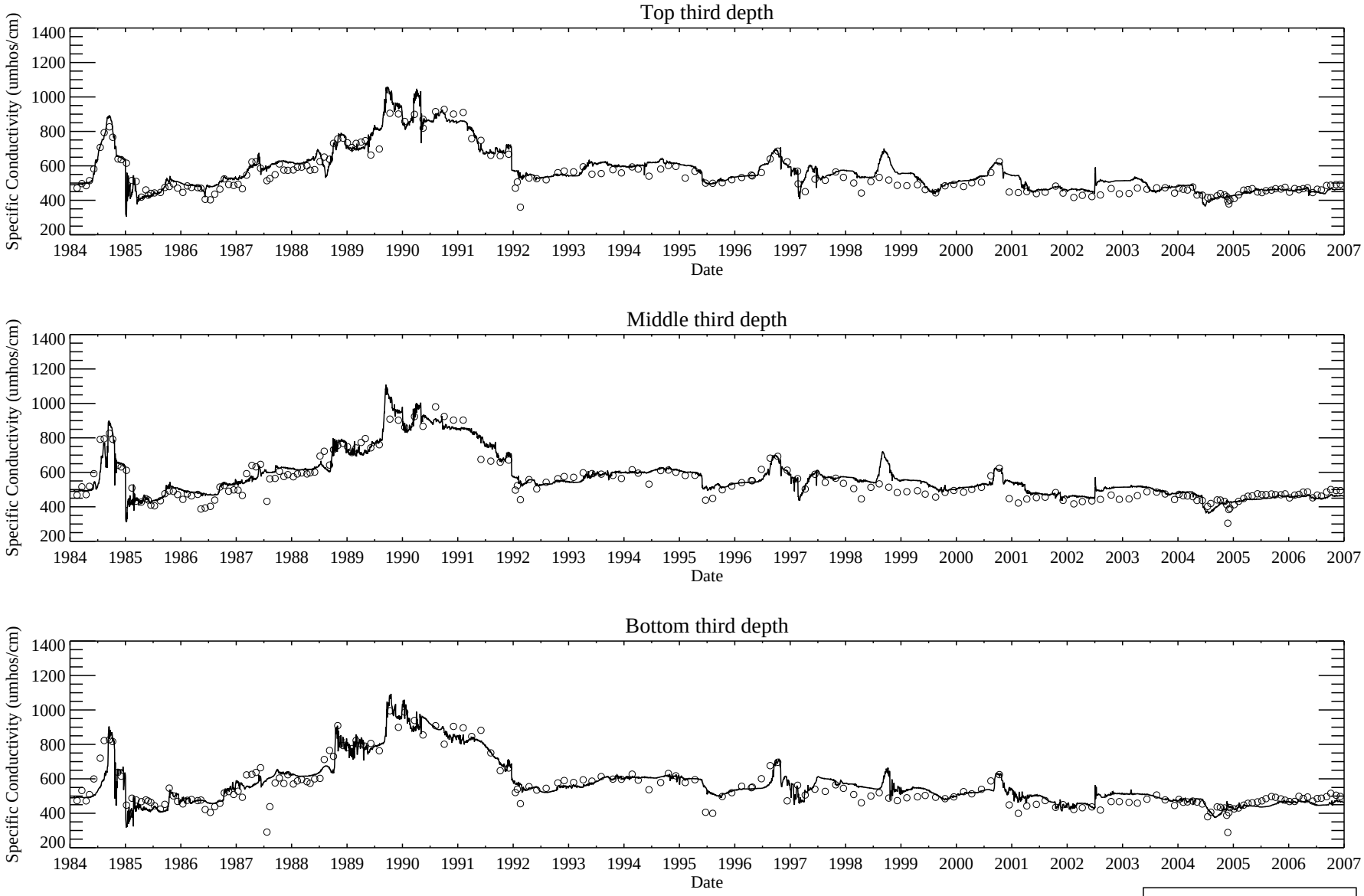

Figure 4-15. Temporal of model versus data at Pace Bend (Segment 48) - Specific Conductivity.

Top third depth, Middle third depth, Bottom third depth
When HAAWQ and CREMS data were measured on the same day, only CREMS data are shown. Non-detects plotted at detection limit.
Data averaged over water column depths shown.

haz/ec - D:\PARcrm\Model\Phase2_Travis\CE-QUAL-W2\postprocess\travis_temporal_forPh2rpt.pro
Thu Jan 29 13:56:41 2009

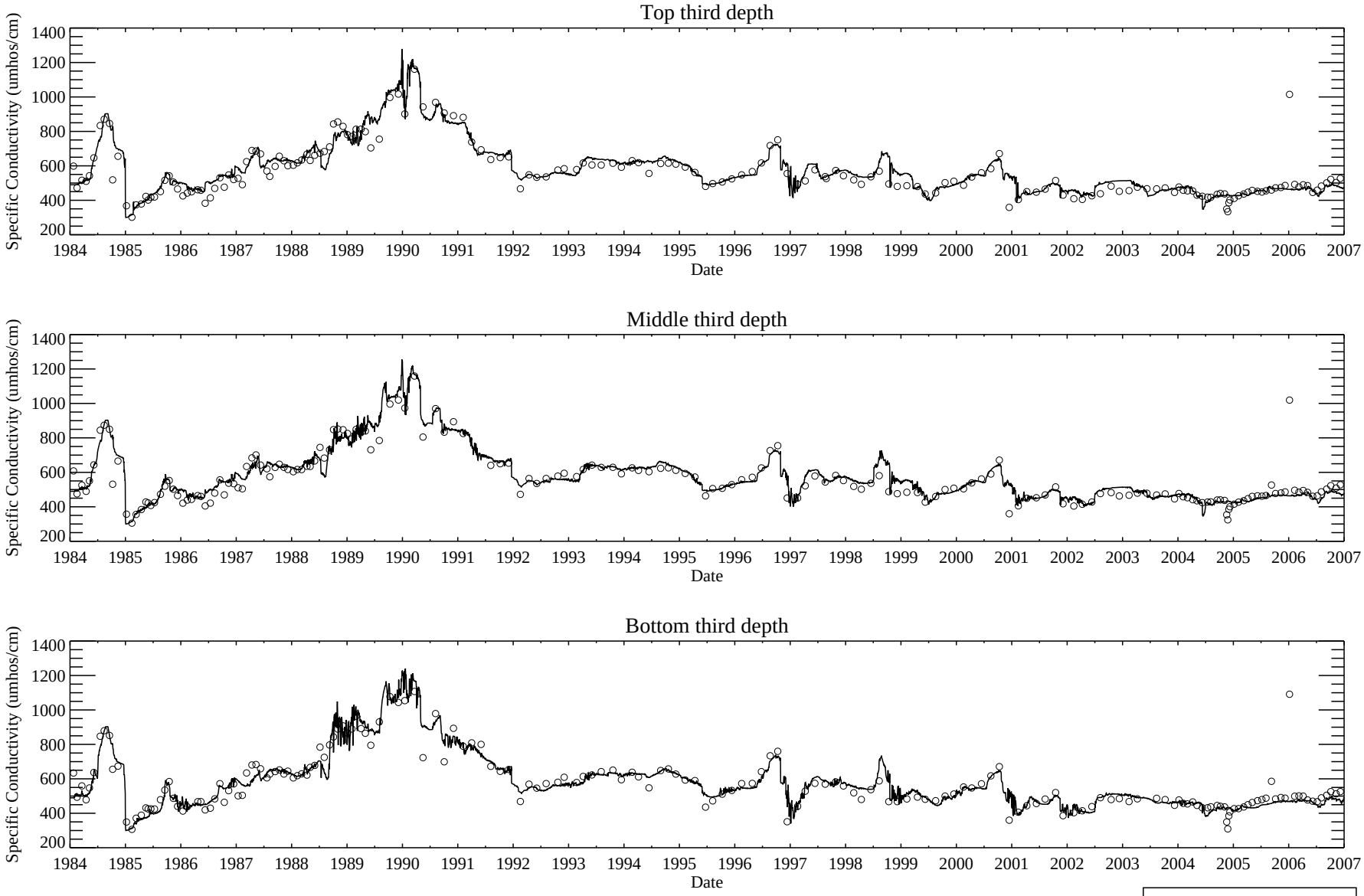

Figure 4-16. Temporal of model versus data at Turkey Bend (Segment 28) - Specific Conductivity.

Top third depth, Middle third depth, Bottom third depth
When HAAWQ and CREMS data were measured on the same day, only CREMS data are shown. Non-detects plotted at detection limit.
Data averaged over water column depths shown.

haz/ec - D:\PARcrm\Model\Phase2_Travis\CE-QUAL-W2\postprocess\travis_temporal_forPh2rpt.pro
Thu Jan 29 13:55:03 2009

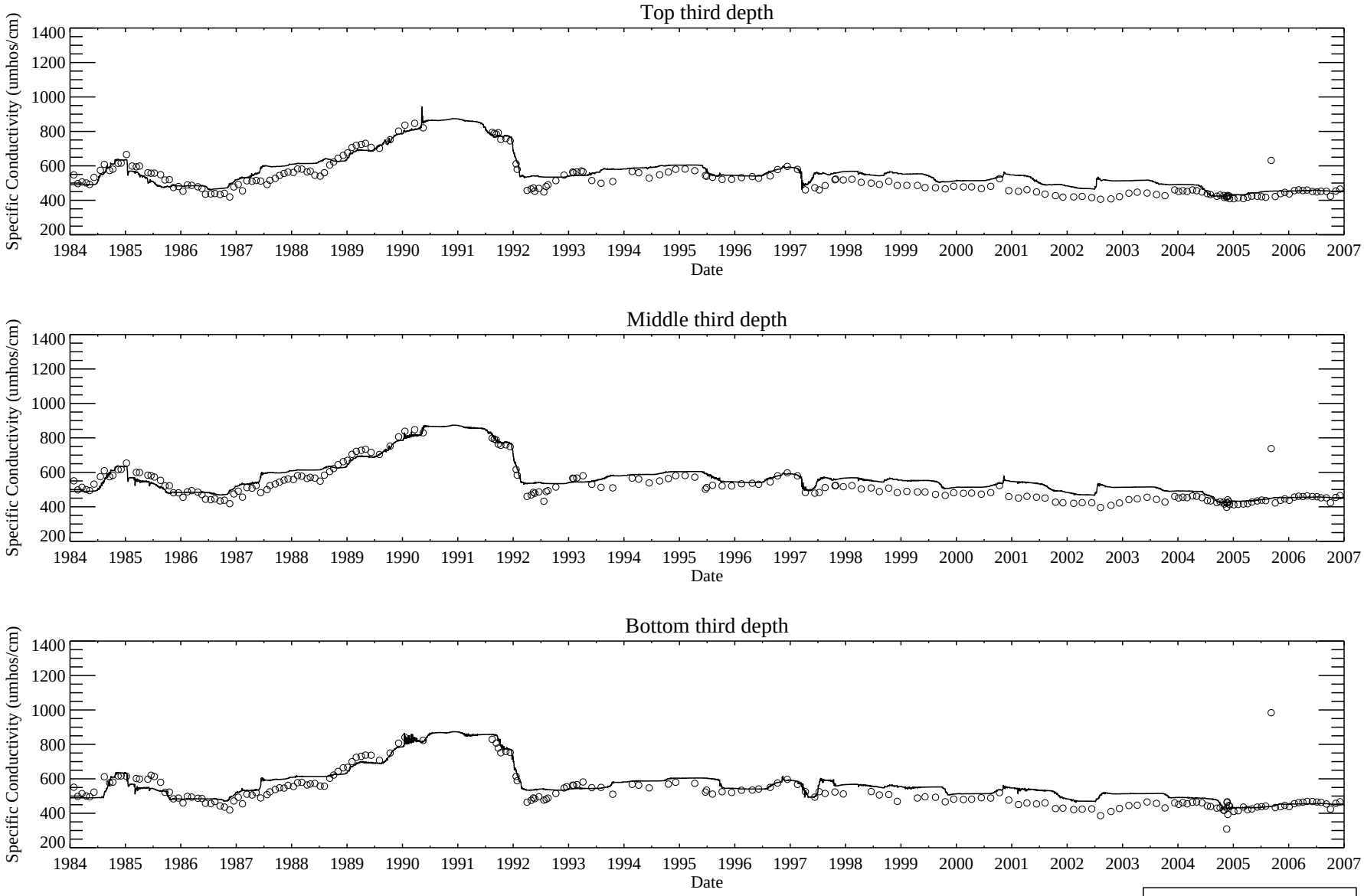

Figure 4-17. Temporal of model versus data at Sandy Creek (Segment 161) - Specific Conductivity.

Top third depth, Middle third depth, Bottom third depth
When HAAWQ and CREMS data were measured on the same day, only CREMS data are shown. Non-detects plotted at detection limit.
Data averaged over water column depths shown.

haz/ec - D:\PARcrm\Model\Phase2_Travis\CE-QUAL-W2\postprocess\travis_temporal_forPh2rpt.pro
Thu Jan 29 14:03:44 2009

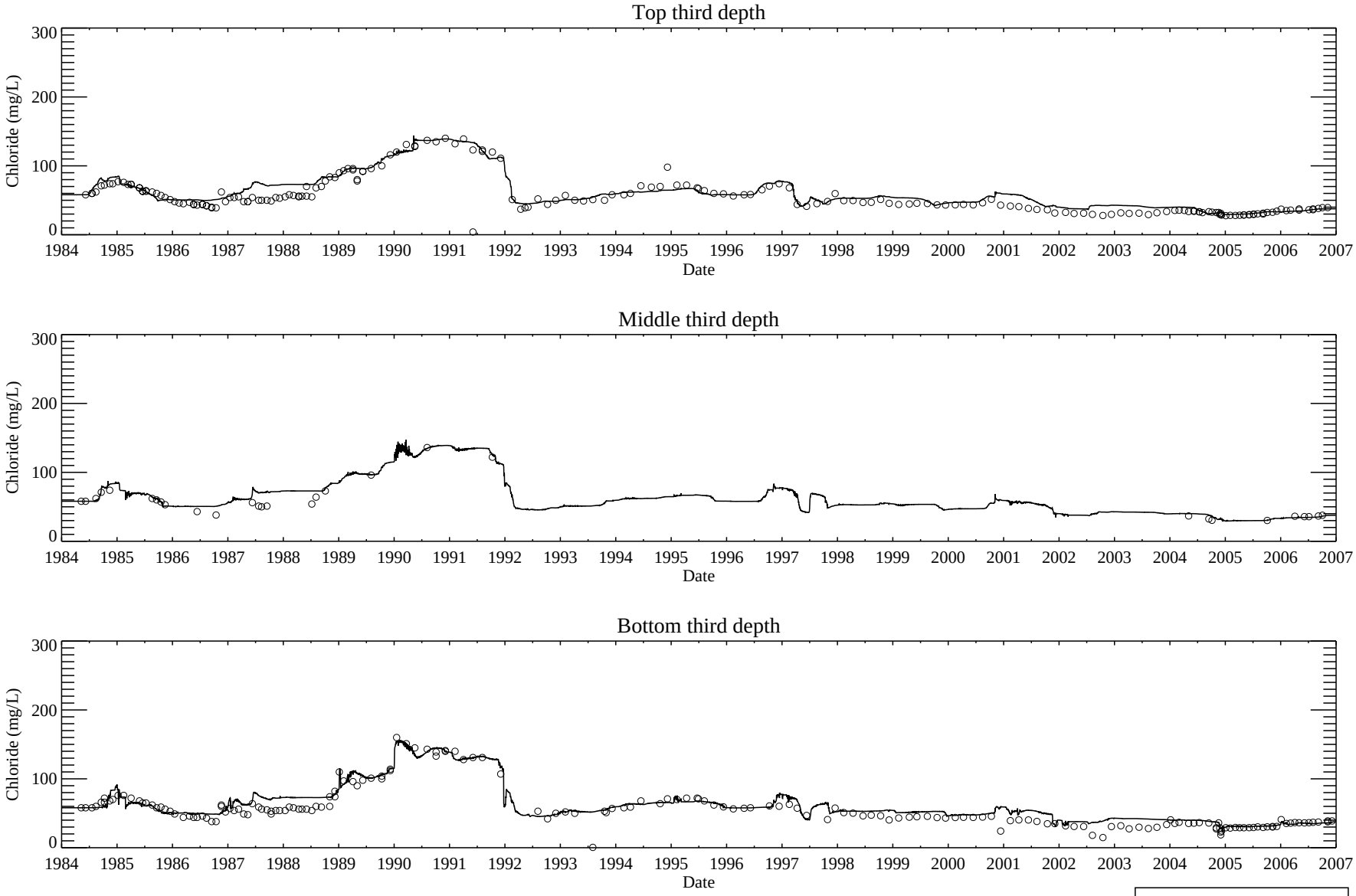

Figure 4-18. Temporal of model versus data at Mansfield Dam (Segment 93) - Chloride.

Top third depth, Middle third depth, Bottom third depth
When HAAWQ and CREMS data were measured on the same day, only CREMS data are shown. Non-detects plotted at detection limit.
Each data point is a discrete measurement except when multiple measurements were taken on the same day at the same depth (average shown).

haz/ec - D:\PARcrm\Model\Phase2_Travis\CE-QUAL-W2\postprocess\travis_temporal_forPh2rpt.pro
Thu Jan 29 13:52:31 2009

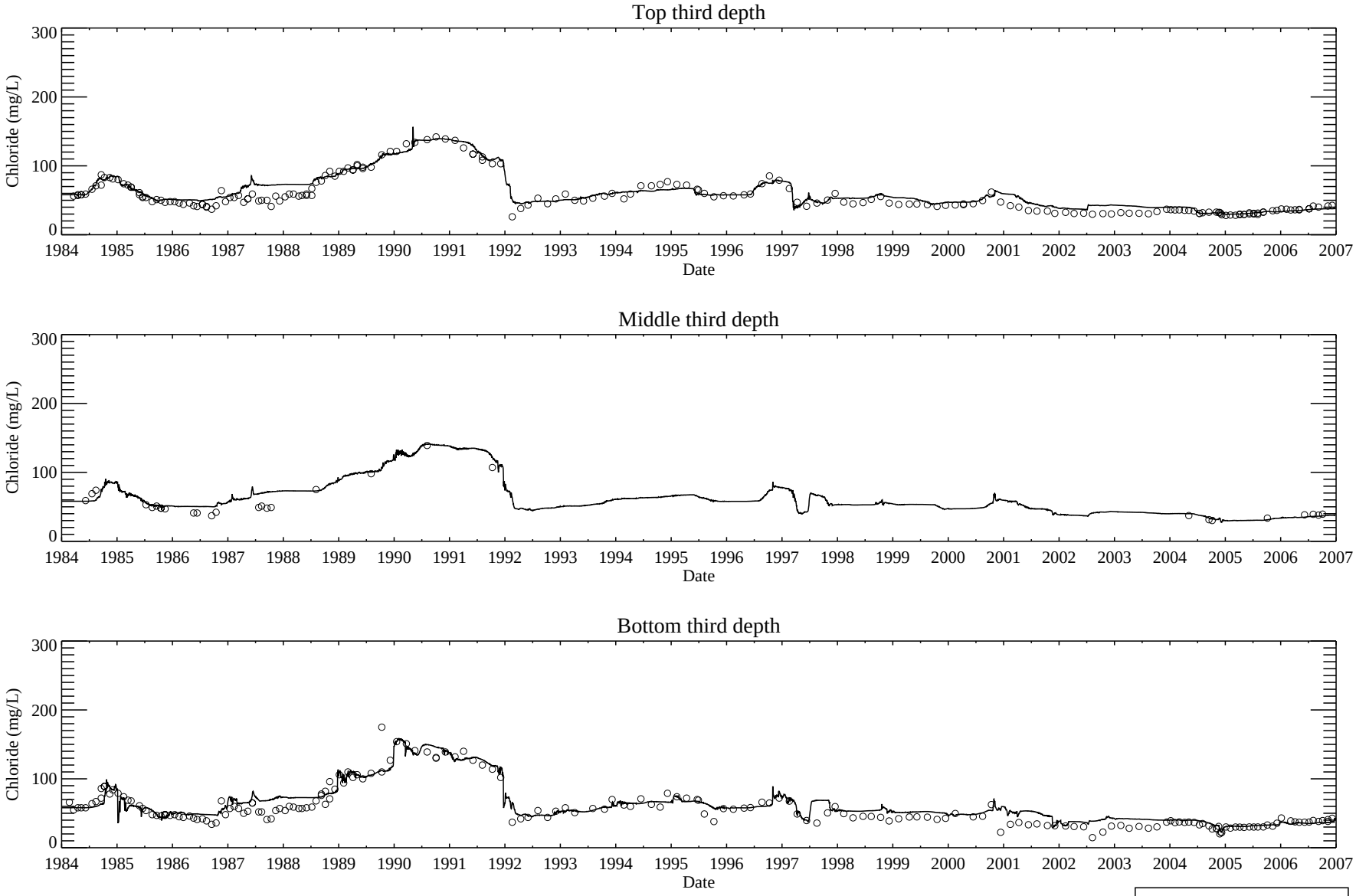

Figure 4-19. Temporal of model versus data at Arkansas Bend (Segment 78) - Chloride.

Top third depth, Middle third depth, Bottom third depth
When HAAWQ and CREMS data were measured on the same day, only CREMS data are shown. Non-detects plotted at detection limit.
Each data point is a discrete measurement except when multiple measurements were taken on the same day at the same depth (average shown).

haz/ec - D:\PARcrm\Model\Phase2_Travis\CE-QUAL-W2\postprocess\travis_temporal_forPh2rpt.pro
Thu Jan 29 13:49:34 2009

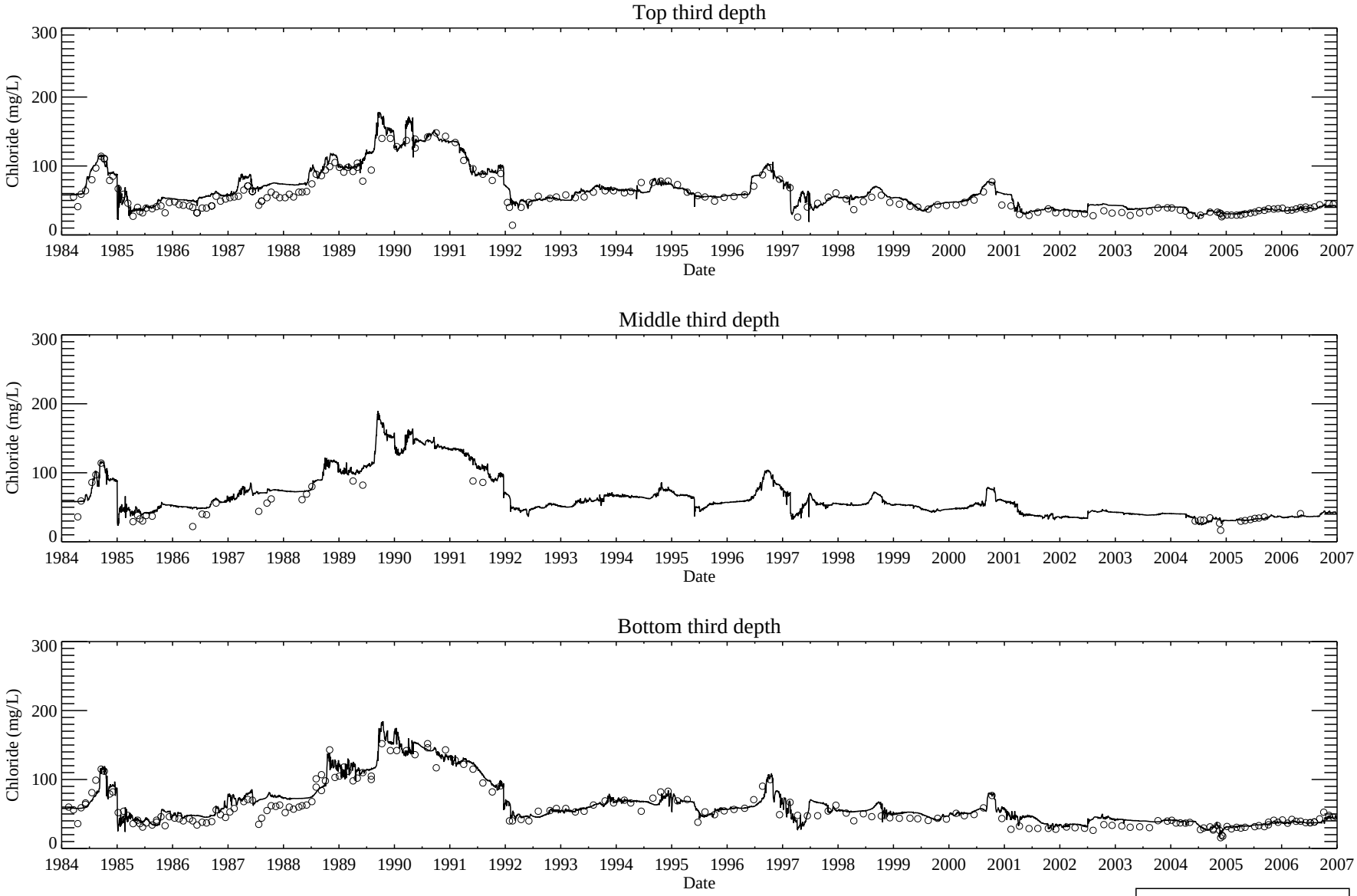

Figure 4-20. Temporal of model versus data at Pace Bend (Segment 48) - Chloride.

Top third depth, Middle third depth, Bottom third depth
When HAAWQ and CREMS data were measured on the same day, only CREMS data are shown. Non-detects plotted at detection limit.
Each data point is a discrete measurement except when multiple measurements were taken on the same day at the same depth (average shown).

haz/ec - D:\PARcrm\Model\Phase2_Travis\CE-QUAL-W2\postprocess\travis_temporal_forPh2rpt.pro
Thu Jan 29 13:46:57 2009

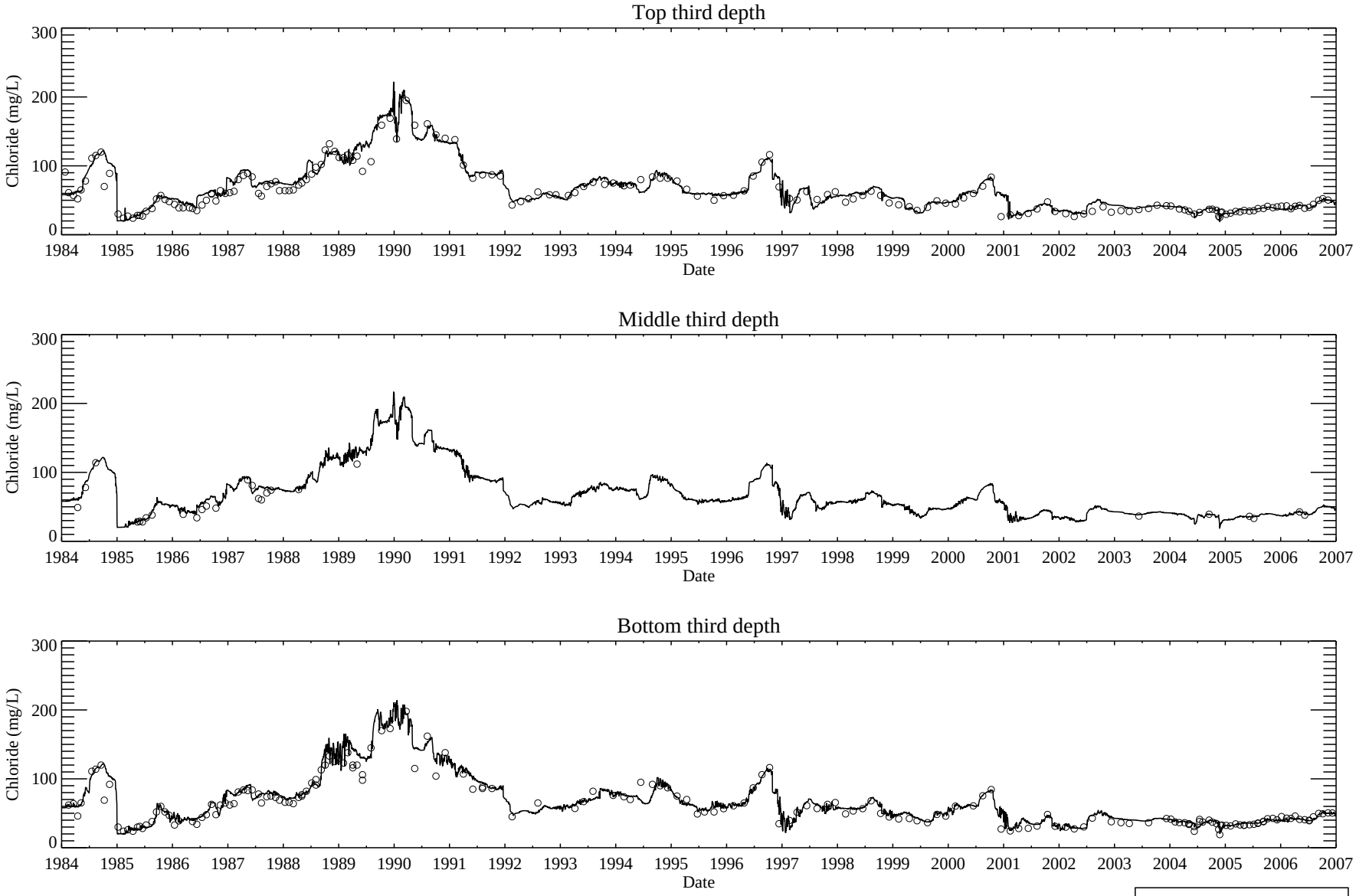

Figure 4-21. Temporal of model versus data at Turkey Bend (Segment 28) - Chloride.

Top third depth, Middle third depth, Bottom third depth
When HAAWQ and CREMS data were measured on the same day, only CREMS data are shown. Non-detects plotted at detection limit.
Each data point is a discrete measurement except when multiple measurements were taken on the same day at the same depth (average shown).

haz/ec - D:\PARcrm\Model\Phase2_Travis\CE-QUAL-W2\postprocess\travis_temporal_forPh2rpt.pro
Thu Jan 29 13:45:19 2009

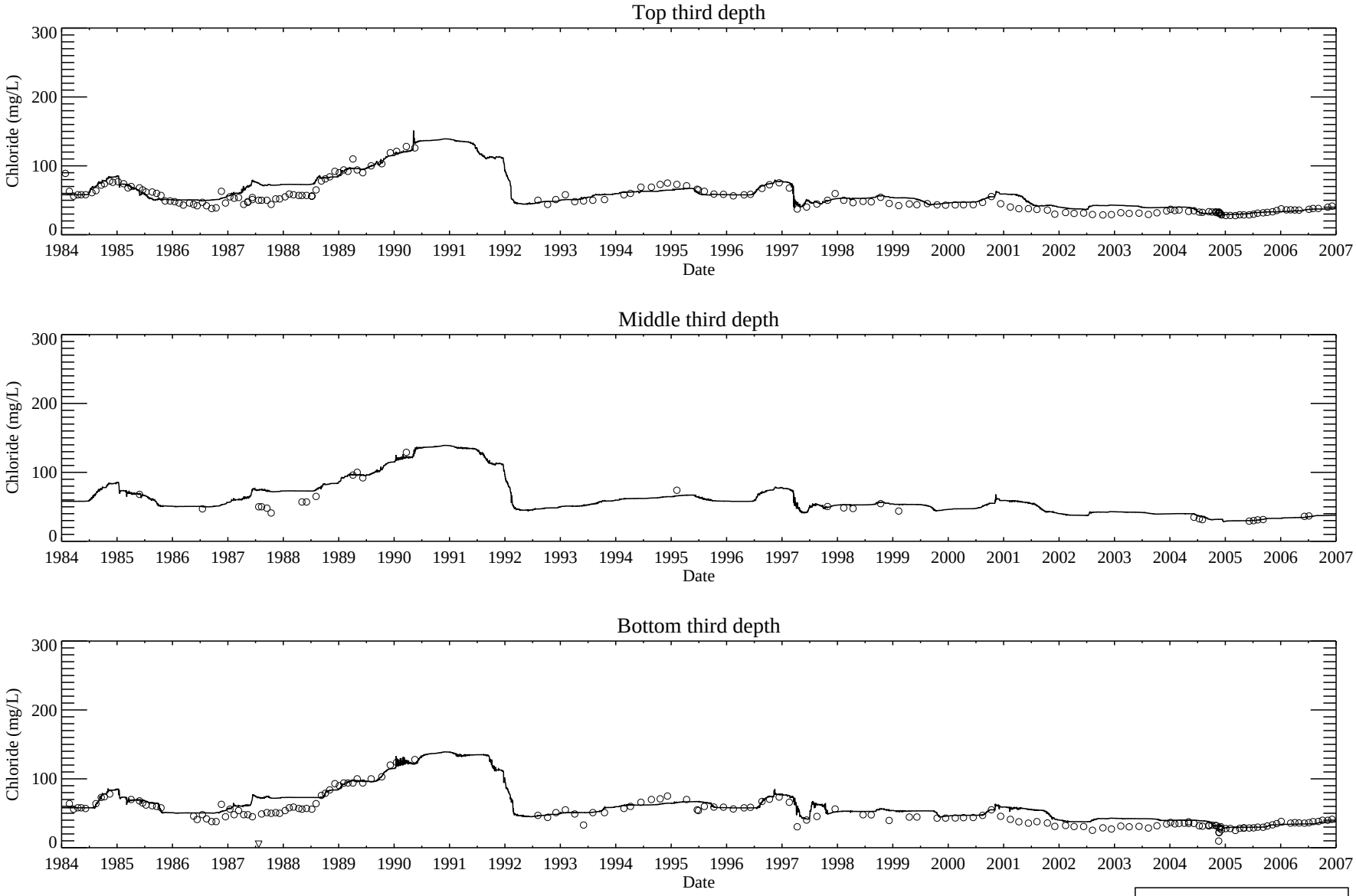

Figure 4-22. Temporal of model versus data at Sandy Creek (Segment 161) - Chloride.

Top third depth, Middle third depth, Bottom third depth
When HAAWQ and CREMS data were measured on the same day, only CREMS data are shown. Non-detects plotted at detection limit.
Each data point is a discrete measurement except when multiple measurements were taken on the same day at the same depth (average shown).

haz/ec - D:\PARcrm\Model\Phase2_Travis\CE-QUAL-W2\postprocess\travis_temporal_forPh2rpt.pro
Thu Jan 29 13:54:00 2009

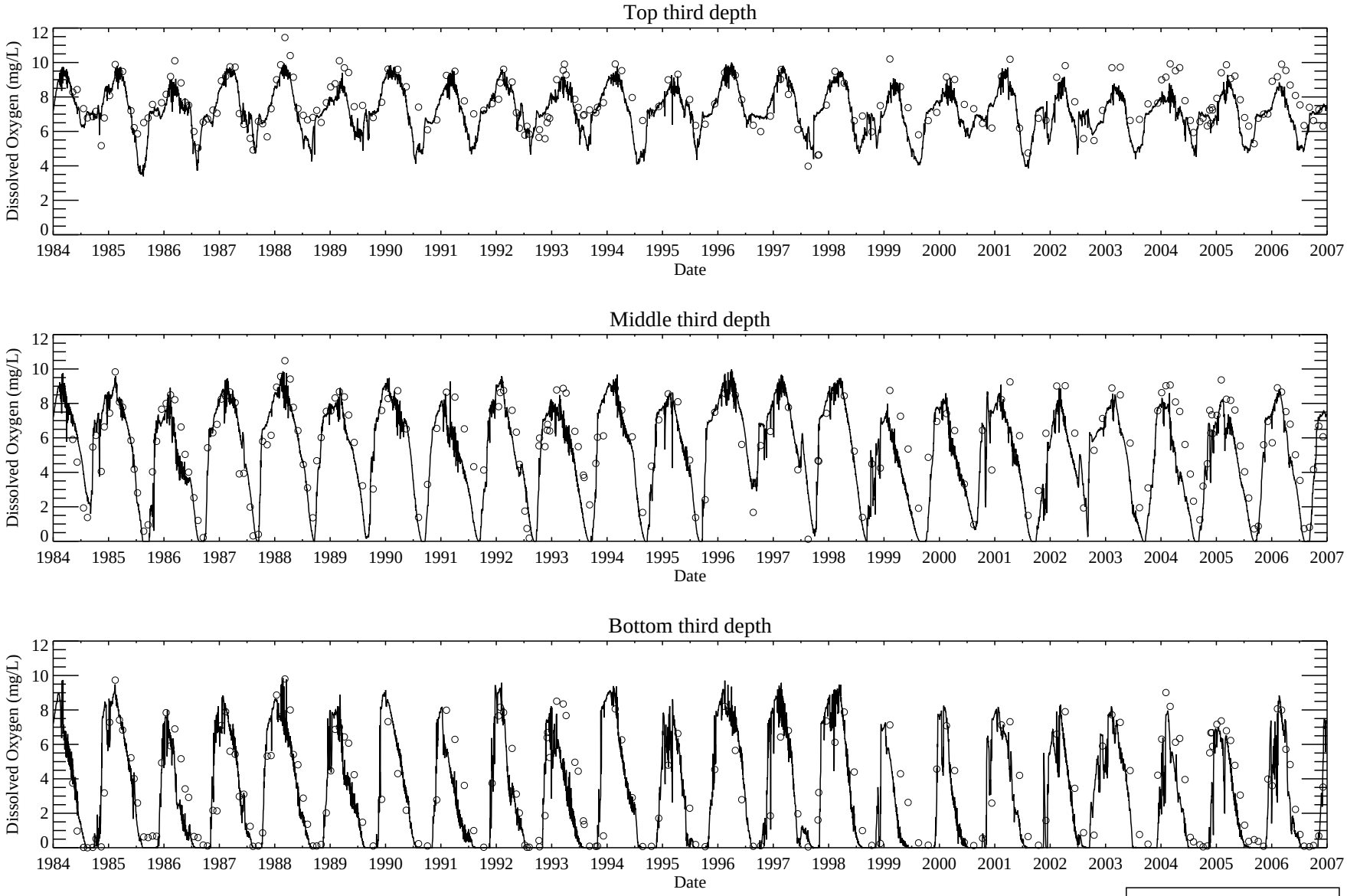

Figure 4-23. Temporal of model versus data at Mansfield Dam (Segment 93) - Dissolved Oxygen.

Top third depth, Middle third depth, Bottom third depth
When HAAWQ and CREMS data were measured on the same day, only CREMS data are shown. Non-detects plotted at detection limit.
Data averaged over water column depths shown.

haz/ec - D:\PARcrm\Model\Phase2_Travis\CE-QUAL-W2\postprocess\travis_temporal_forPh2rpt.pro
Thu Jan 29 13:03:34 2009

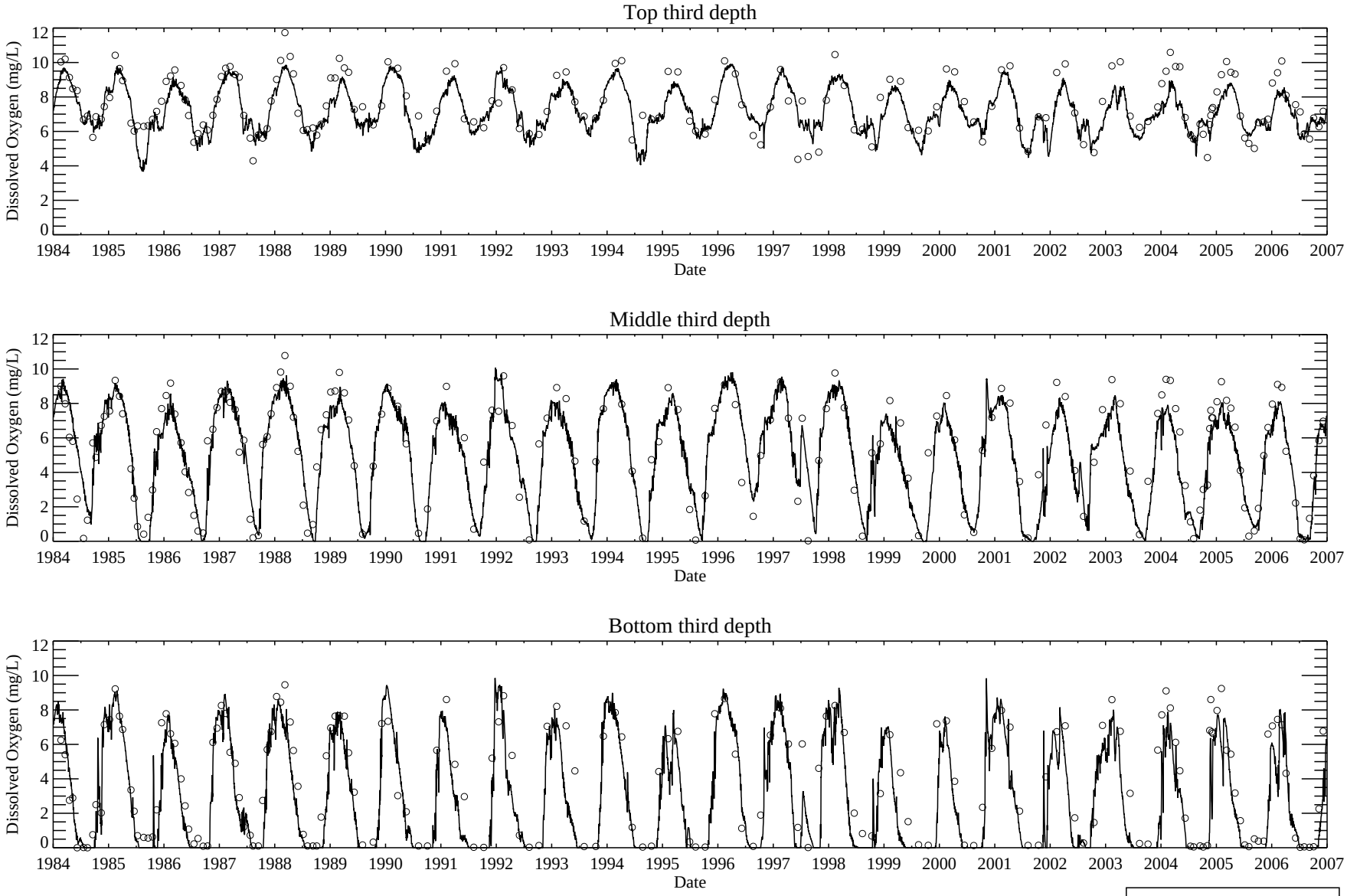

Figure 4-24. Temporal of model versus data at Arkansas Bend (Segment 78) - Dissolved Oxygen.

Top third depth, Middle third depth, Bottom third depth
When HAAWQ and CREMS data were measured on the same day, only CREMS data are shown. Non-detects plotted at detection limit.
Data averaged over water column depths shown.

haz/ec - D:\PARcrm\Model\Phase2_Travis\CE-QUAL-W2\postprocess\travis_temporal_forPh2rpt.pro
Thu Jan 29 13:00:36 2009

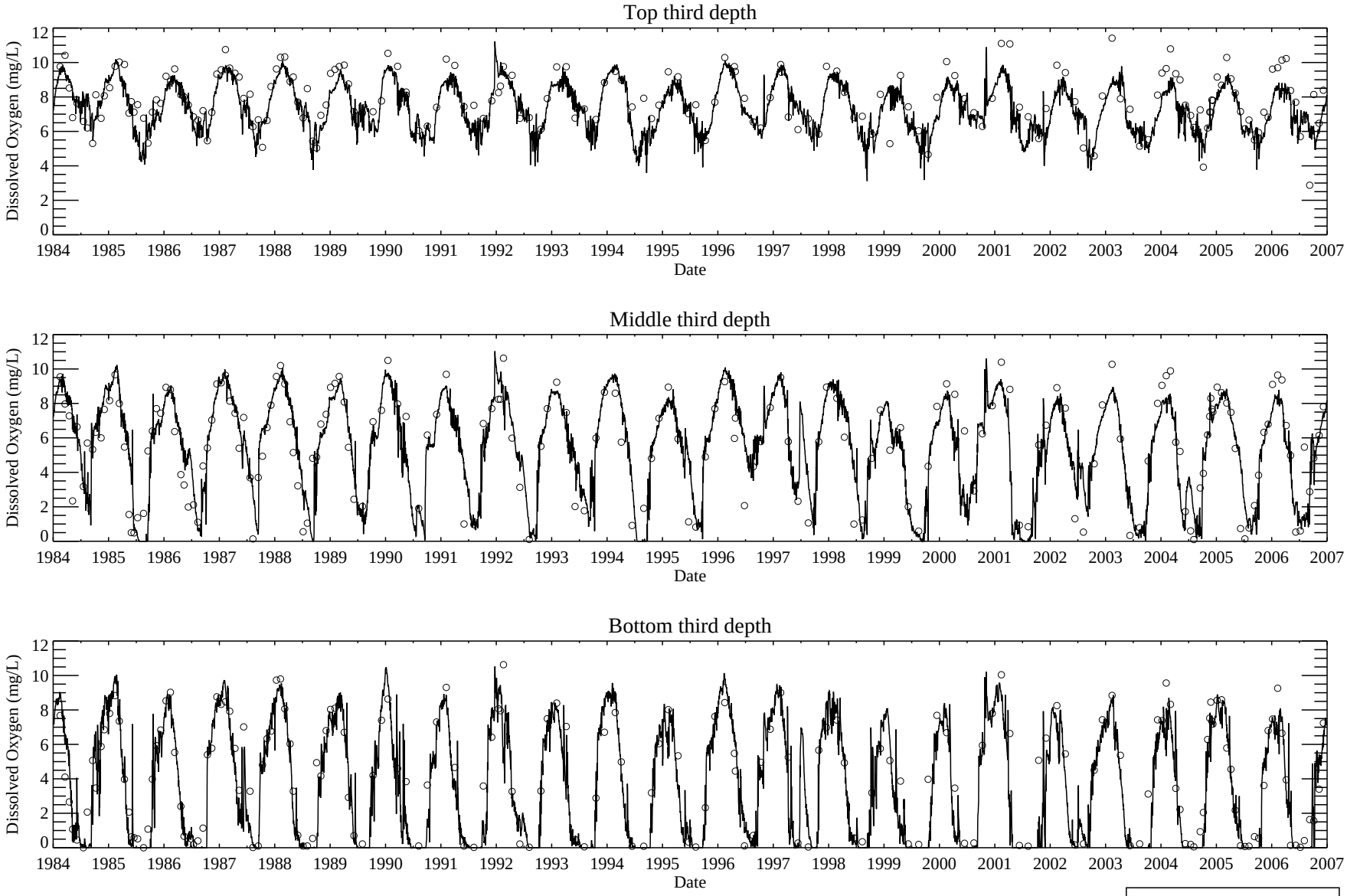

Figure 4-25. Temporal of model versus data at Pace Bend (Segment 48) - Dissolved Oxygen.

Top third depth, Middle third depth, Bottom third depth
When HAAWQ and CREMS data were measured on the same day, only CREMS data are shown. Non-detects plotted at detection limit.
Data averaged over water column depths shown.

haz/ec - D:\PARcrm\Model\Phase2_Travis\CE-QUAL-W2\postprocess\travis_temporal_forPh2rpt.pro
Thu Jan 29 12:58:01 2009

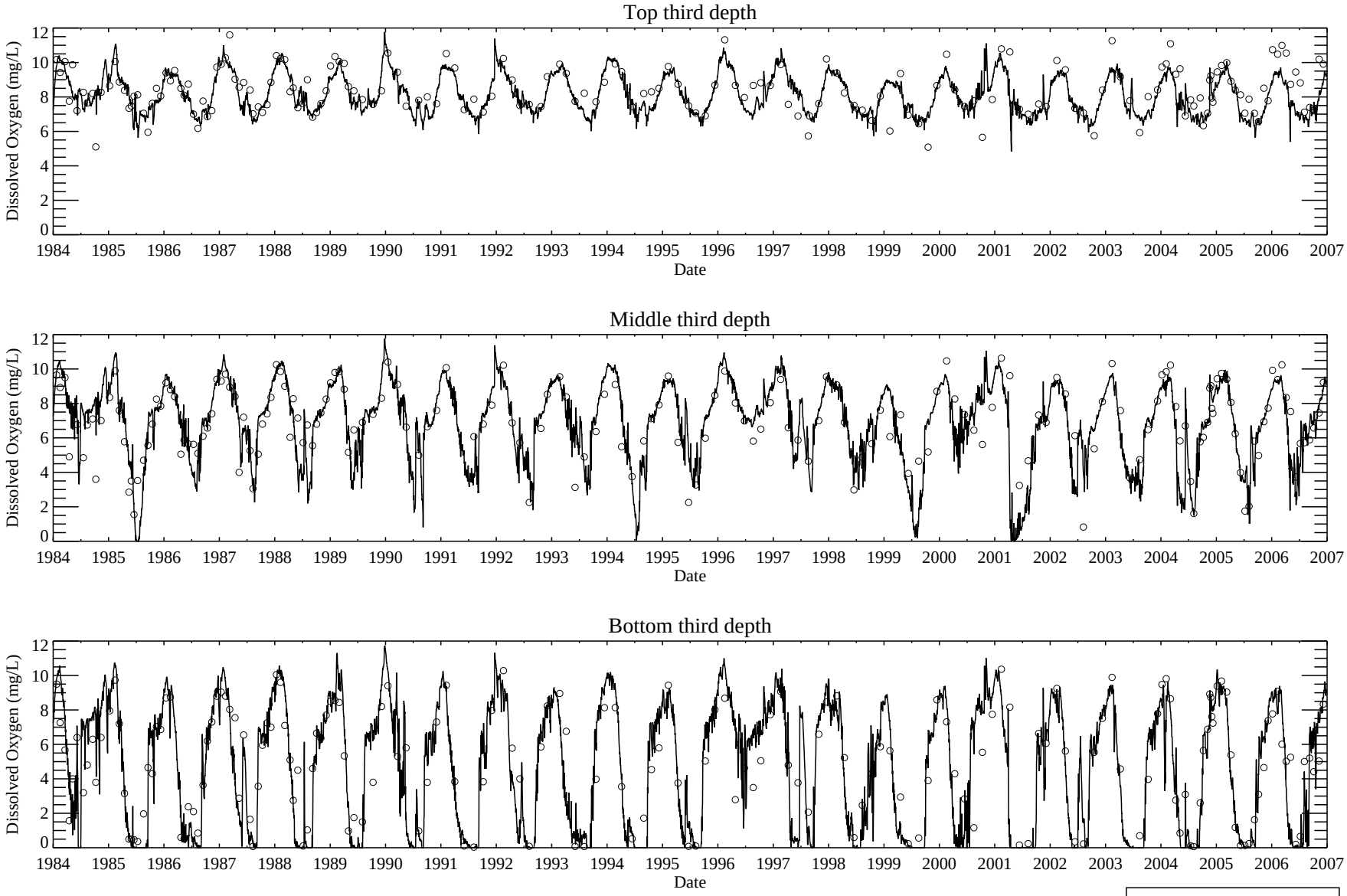

Figure 4-26. Temporal of model versus data at Turkey Bend (Segment 28) - Dissolved Oxygen.

Top third depth, Middle third depth, Bottom third depth
When HAAWQ and CREMS data were measured on the same day, only CREMS data are shown. Non-detects plotted at detection limit.
Data averaged over water column depths shown.

haz/ec - D:\PARcrm\Model\Phase2_Travis\CE-QUAL-W2\postprocess\travis_temporal_forPh2rpt.pro
Thu Jan 29 12:56:23 2009

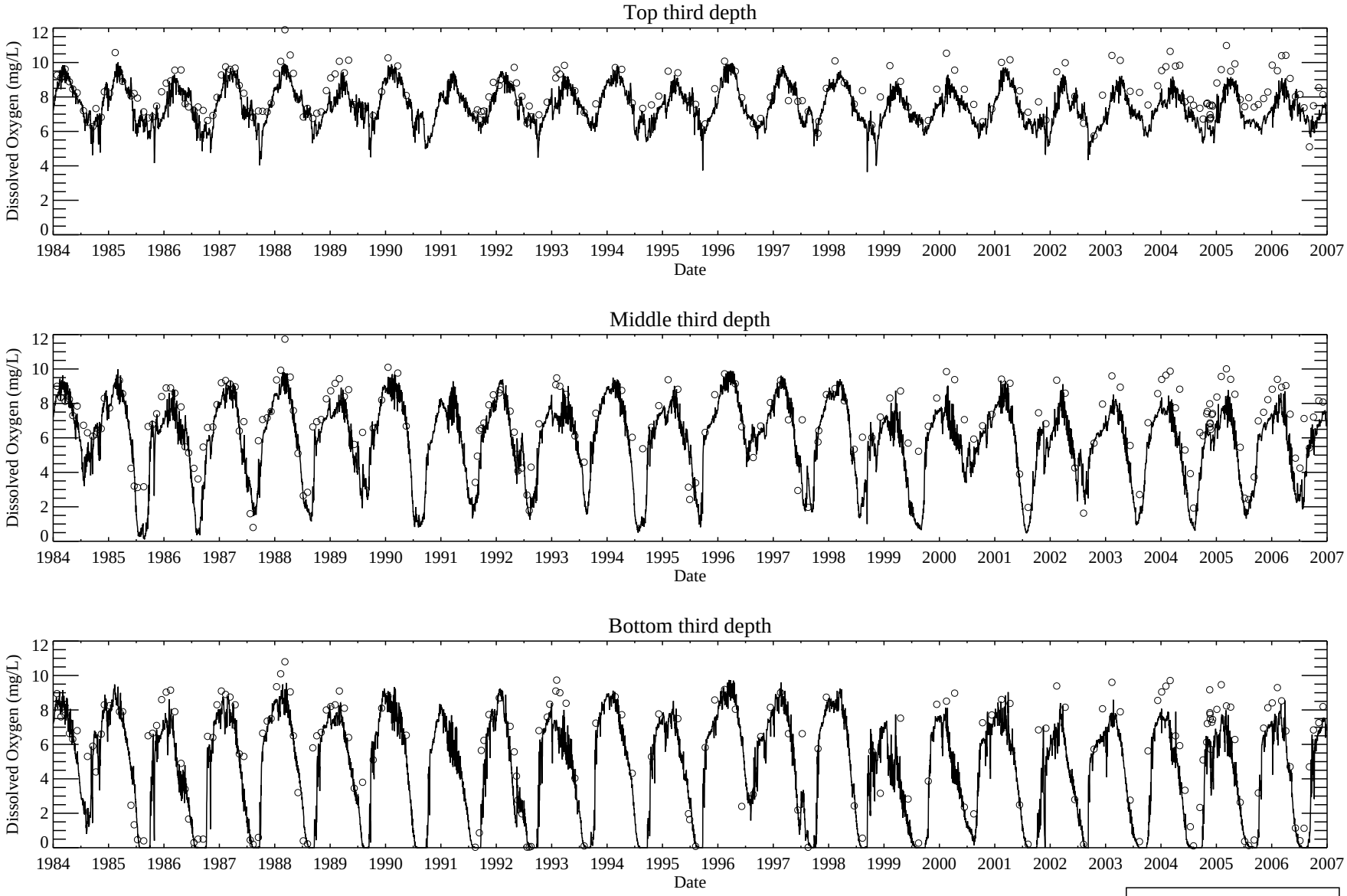

Figure 4-27. Temporal of model versus data at Sandy Creek (Segment 161) - Dissolved Oxygen.

Top third depth, Middle third depth, Bottom third depth
When HAAWQ and CREMS data were measured on the same day, only CREMS data are shown. Non-detects plotted at detection limit.
Data averaged over water column depths shown.

haz/ec - D:\PARcrm\Model\Phase2_Travis\CE-QUAL-W2\postprocess\travis_temporal_forPh2rpt.pro
Thu Jan 29 13:05:04 2009

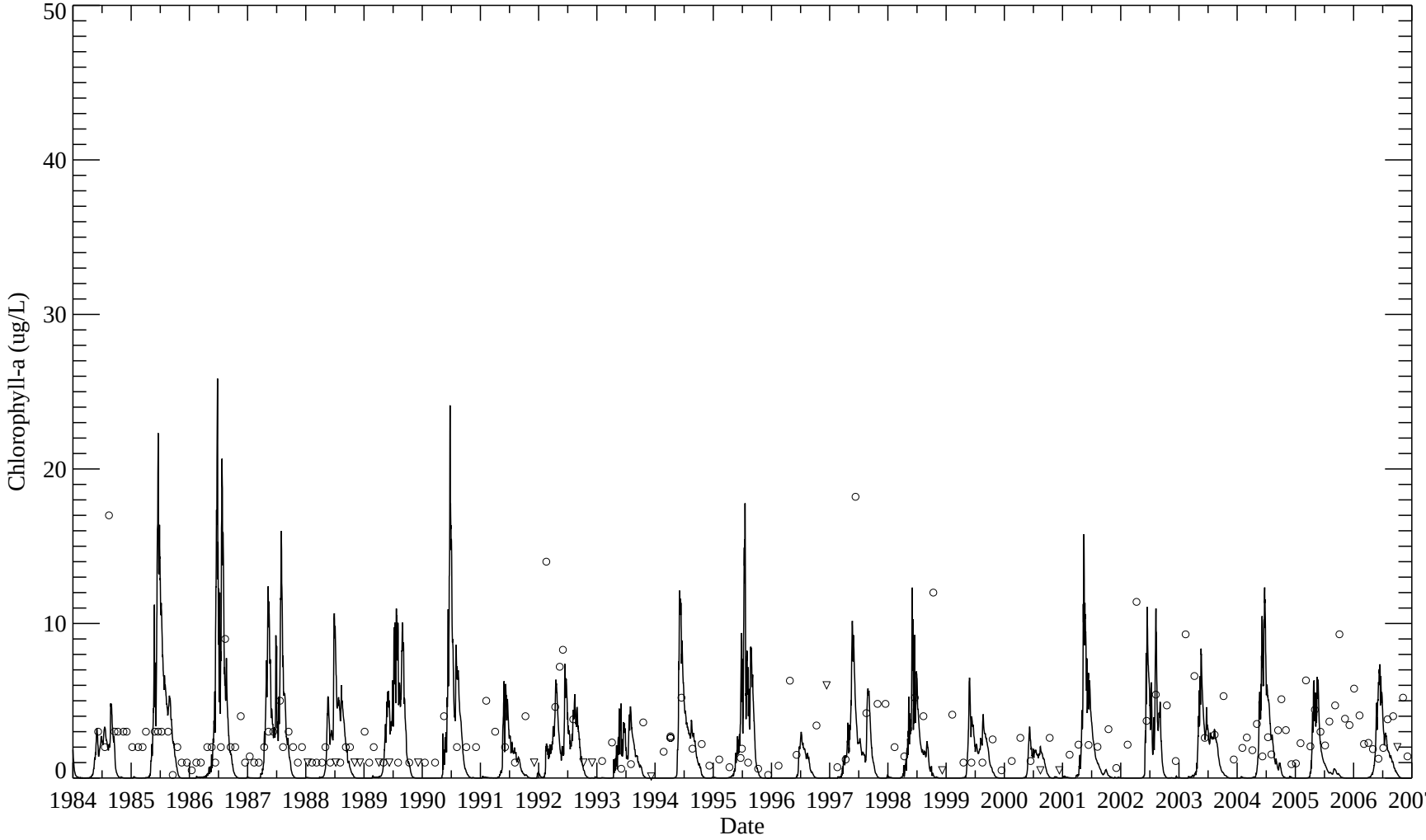

Figure 4-28. Temporal of model versus data at Mansfield Dam (Segment 93) - Chlorophyll-a.

Top 0 to 2 meters
When HAAWQ and CREMS data were measured on the same day, only CREMS data are shown. Non-detects plotted at detection limit.
Each data point is a discrete measurement except when multiple measurements were taken on the same day at the same depth (average shown).

haz/ec - D:\PARcrm\Model\Phase2_Travis\CE-QUAL-W2\postprocess\travis_temporal_forPh2rpt.pro
Thu Jan 29 12:55:17 2009

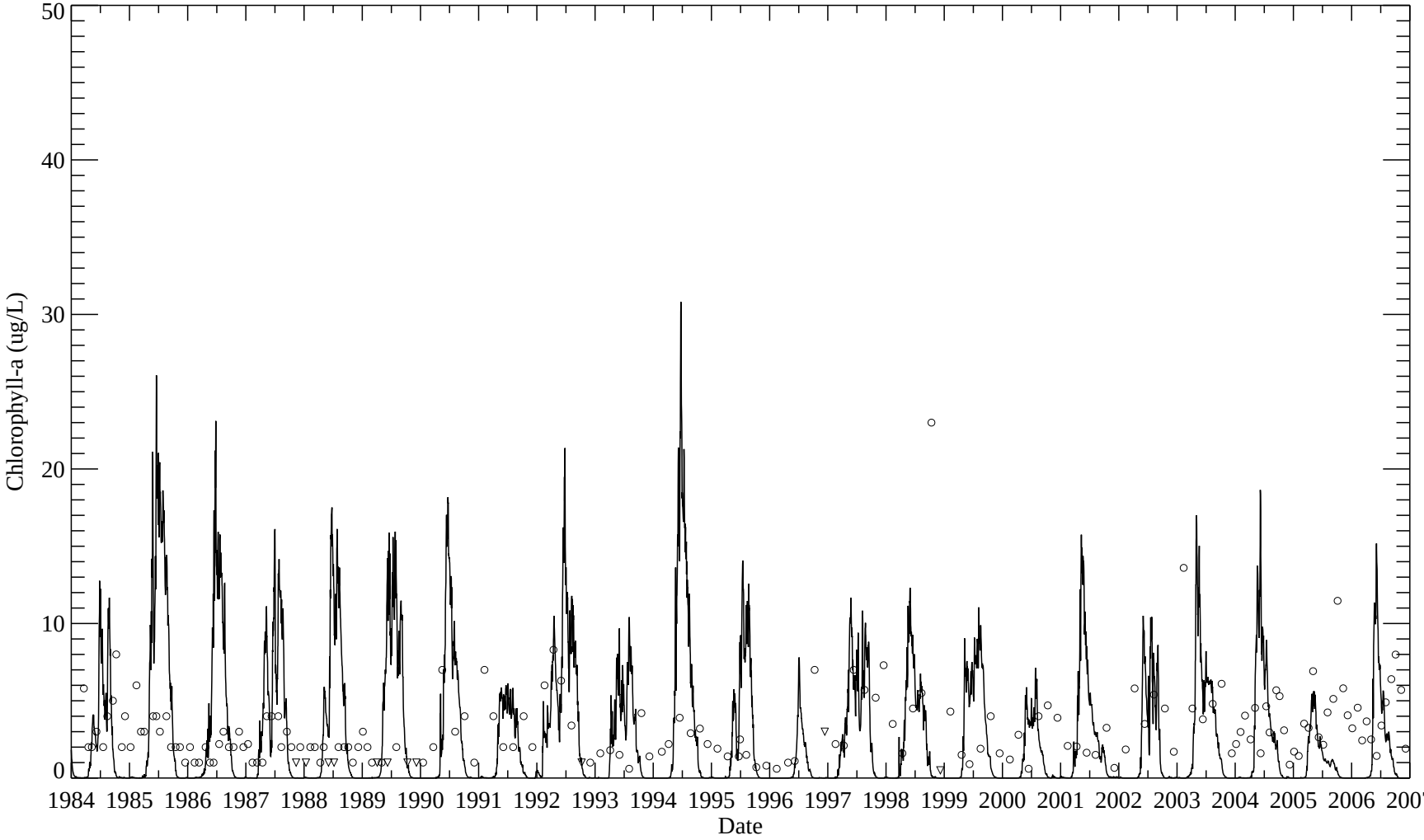

Figure 4-29. Temporal of model versus data at Arkansas Bend (Segment 78) - Chlorophyll-a.

Top 0 to 2 meters
When HAAWQ and CREMS data were measured on the same day, only CREMS data are shown. Non-detects plotted at detection limit.
Each data point is a discrete measurement except when multiple measurements were taken on the same day at the same depth (average shown).

haz/ec - D:\PARcrm\Model\Phase2_Travis\CE-QUAL-W2\postprocess\travis_temporal_forPh2rpt.pro
Thu Jan 29 12:55:14 2009

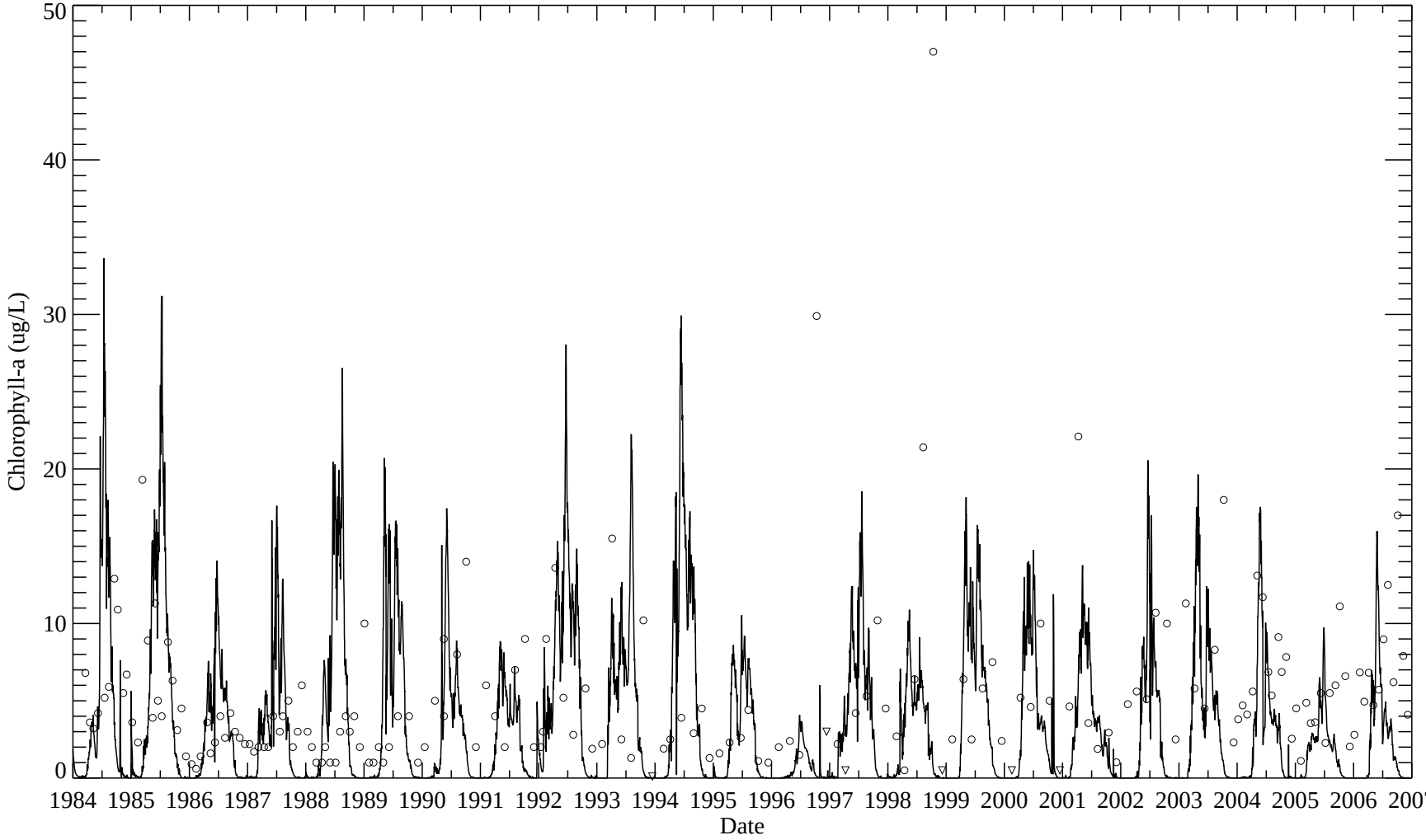

Figure 4-30. Temporal of model versus data at Pace Bend (Segment 48) - Chlorophyll-a.

Top 0 to 2 meters
When HAAWQ and CREMS data were measured on the same day, only CREMS data are shown. Non-detects plotted at detection limit.
Each data point is a discrete measurement except when multiple measurements were taken on the same day at the same depth (average shown).

haz/ec - D:\PARcrm\Model\Phase2_Travis\CE-QUAL-W2\postprocess\travis_temporal_forPh2rpt.pro
Thu Jan 29 12:55:11 2009

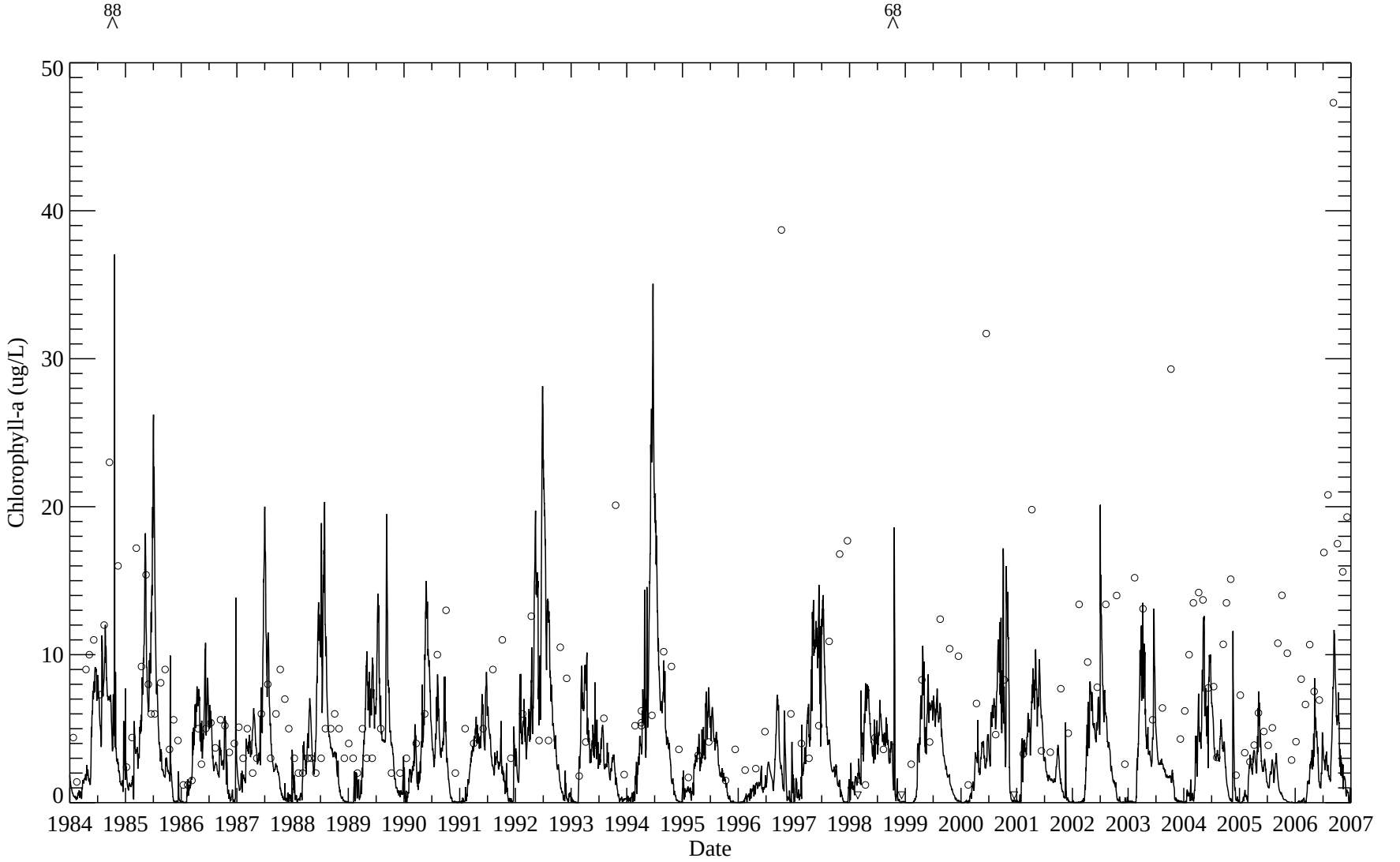

Figure 4-31. Temporal of model versus data at Turkey Bend (Segment 28) - Chlorophyll-a.

Top 0 to 2 meters
When HAAWQ and CREMS data were measured on the same day, only CREMS data are shown. Non-detects plotted at detection limit.
Each data point is a discrete measurement except when multiple measurements were taken on the same day at the same depth (average shown).

haz/ec - D:\PARcrm\Model\Phase2_Travis\CE-QUAL-W2\postprocess\travis_temporal_forPh2rpt.pro
Thu Jan 29 12:55:09 2009

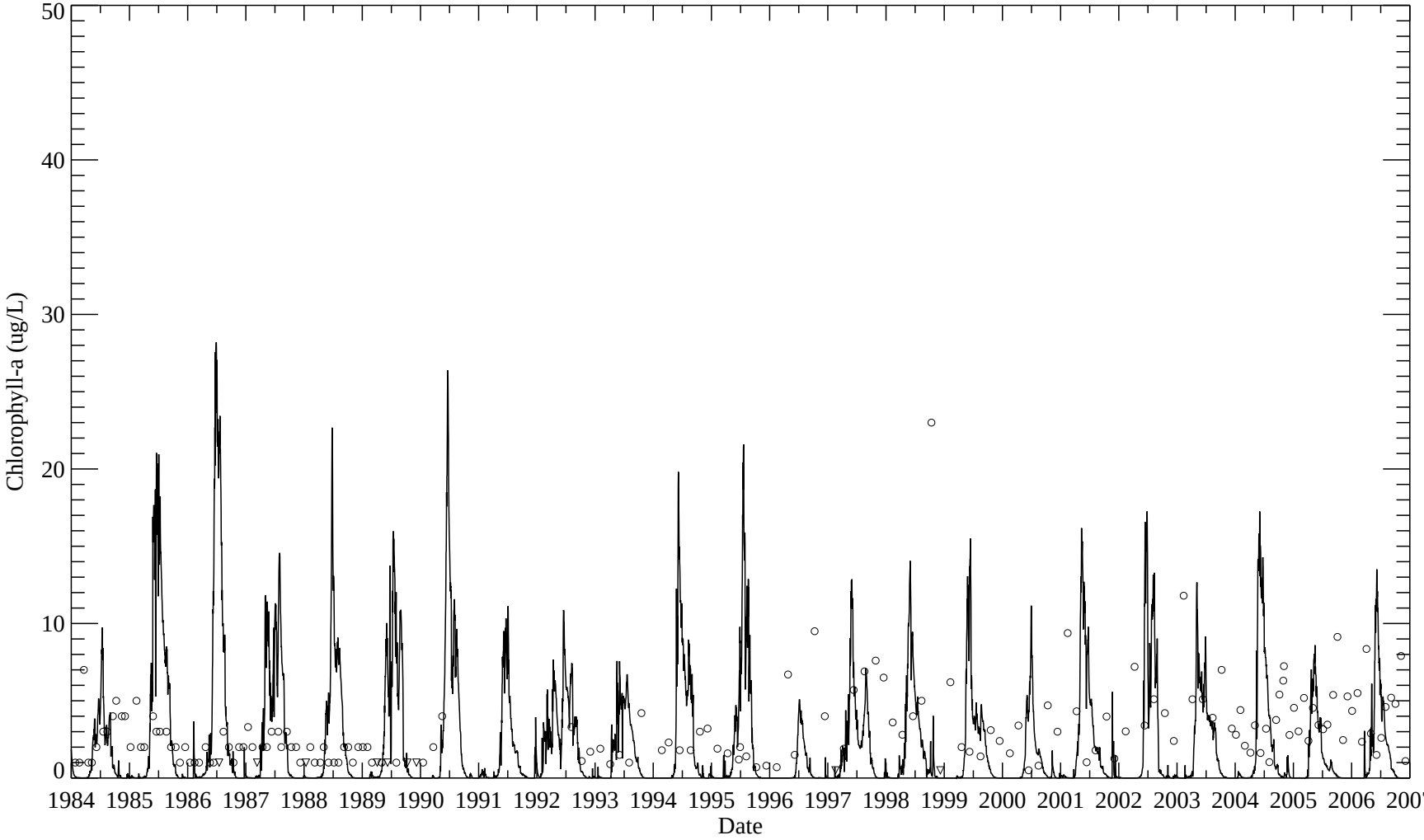

Figure 4-32. Temporal of model versus data at Sandy Creek (Segment 161) - Chlorophyll-a.

Top 0 to 2 meters
When HAAWQ and CREMS data were measured on the same day, only CREMS data are shown. Non-detects plotted at detection limit.
Each data point is a discrete measurement except when multiple measurements were taken on the same day at the same depth (average shown).

haz/ec - D:\PARcrm\Model\Phase2_Travis\CE-QUAL-W2\postprocess\travis_temporal_forPh2rpt.pro
Thu Jan 29 12:55:20 2009

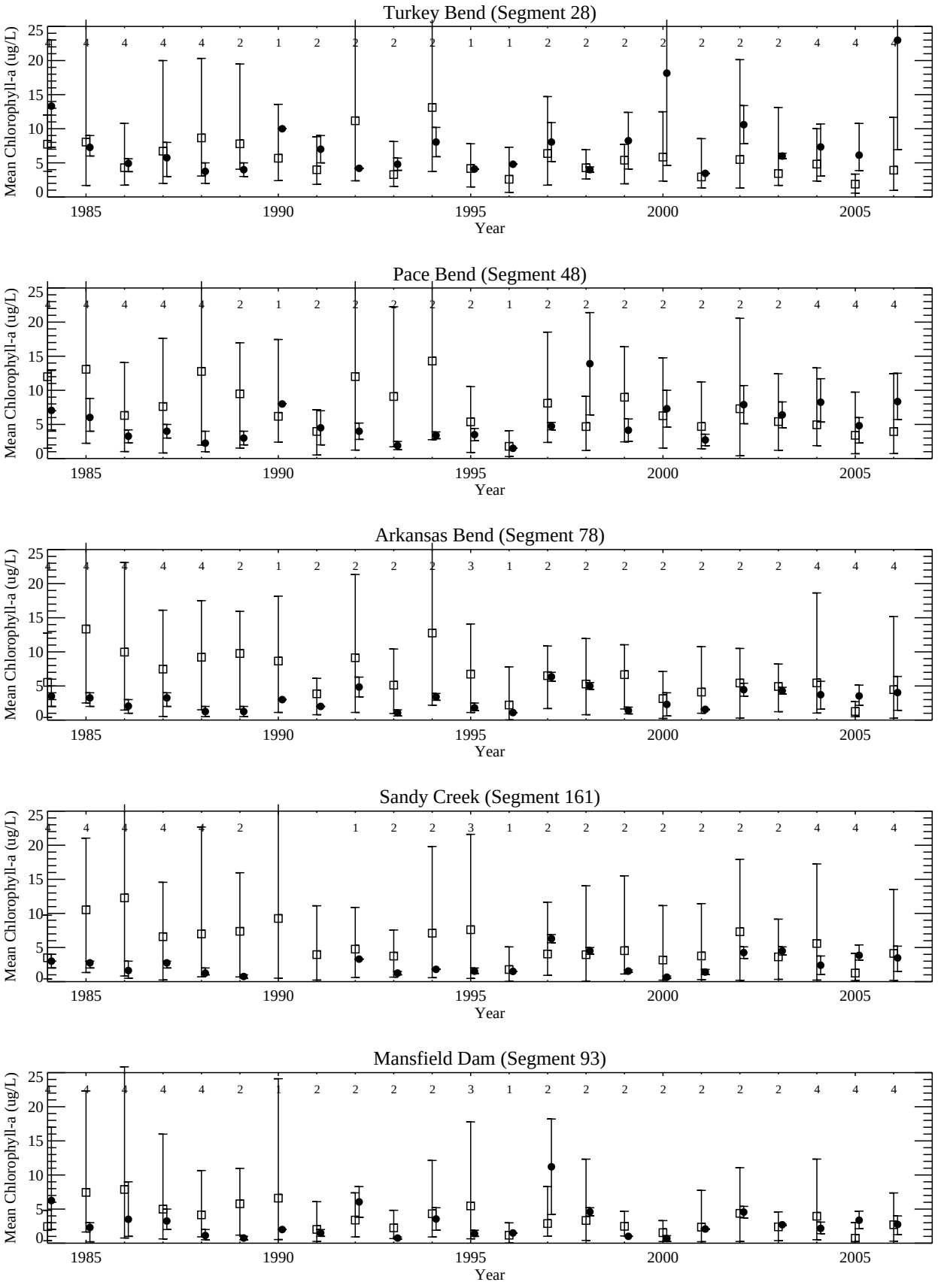

Figure 4-33. Comparison of summertime predicted and measured chlorophyll-a concentrations.

Top 0 to 2 meters; error bars = 2 standard errors.
Start month: 6, end month: 9; all data within these months and depth interval averaged together (# observations labeled along top of panel).
Data below detection set to one half the detection limit prior to averaging. Data offset to right by 0.1 year for presentational purposes.

ec - D:\PARcrm\Model\Phase2_Travis\CE-QUAL-W2\postprocess\model_vs_data_seasonal_forPh2rpt.pro
Thu Jan 29 14:15:50 2009

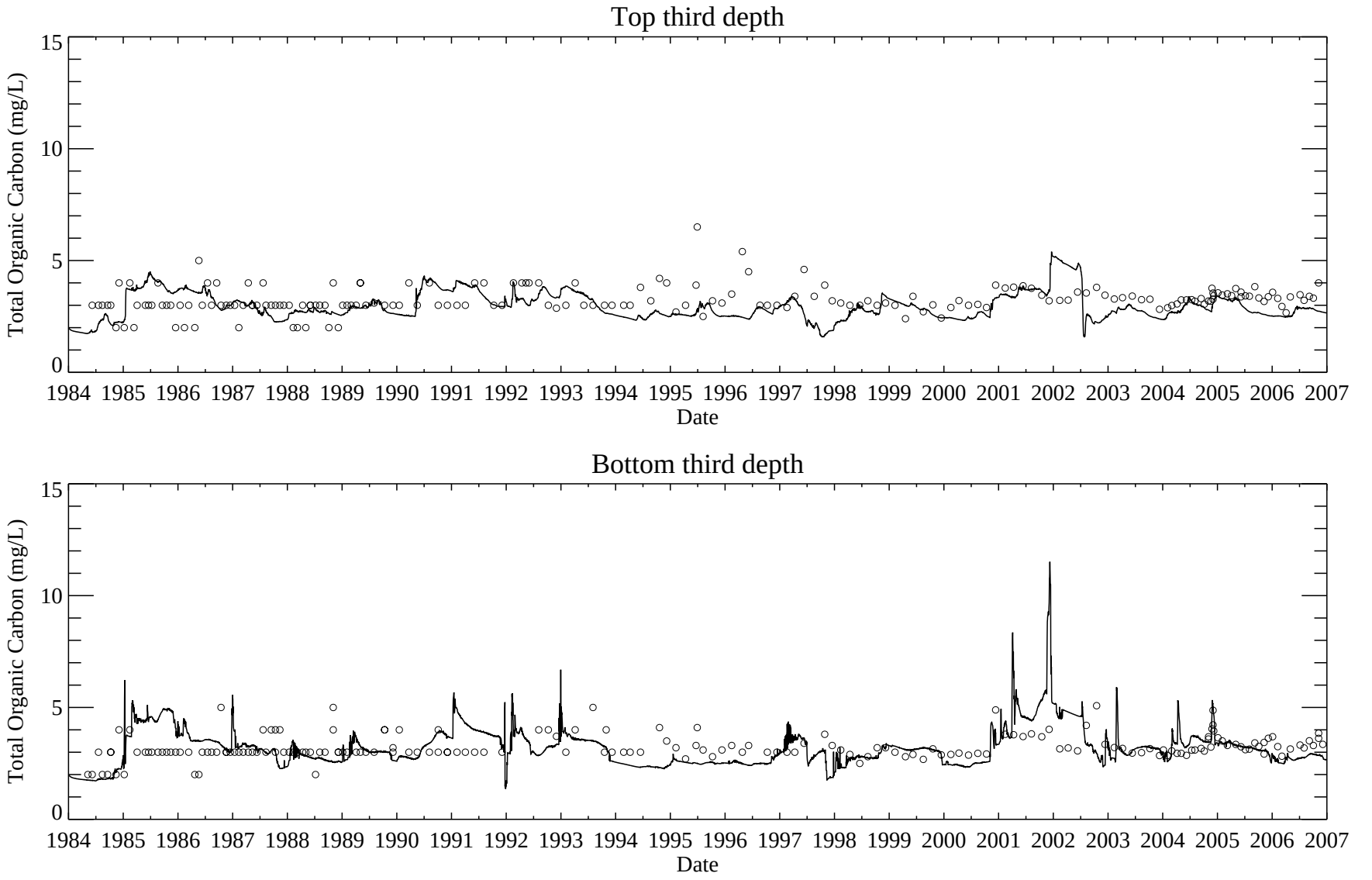

Figure 4-34. Temporal of model versus data at Mansfield Dam (Segment 93) - Total Organic Carbon.

Top third depth, Bottom third depth
When HAAWQ and CREMS data were measured on the same day, only CREMS data are shown. Non-detects plotted at detection limit.
Each data point is a discrete measurement except when multiple measurements were taken on the same day at the same depth (average shown).
Data in 'top third depth' excluded if collected below 10 meters (approximate starting depth of metalimnion).

haz/ec - A:\Jobs\PARcrm\model\Phase2_Travis\CE-QUAL-W2\postprocess\travis_temporal_forPh2rpt.pro
Mon Apr 13 10:46:41 2009

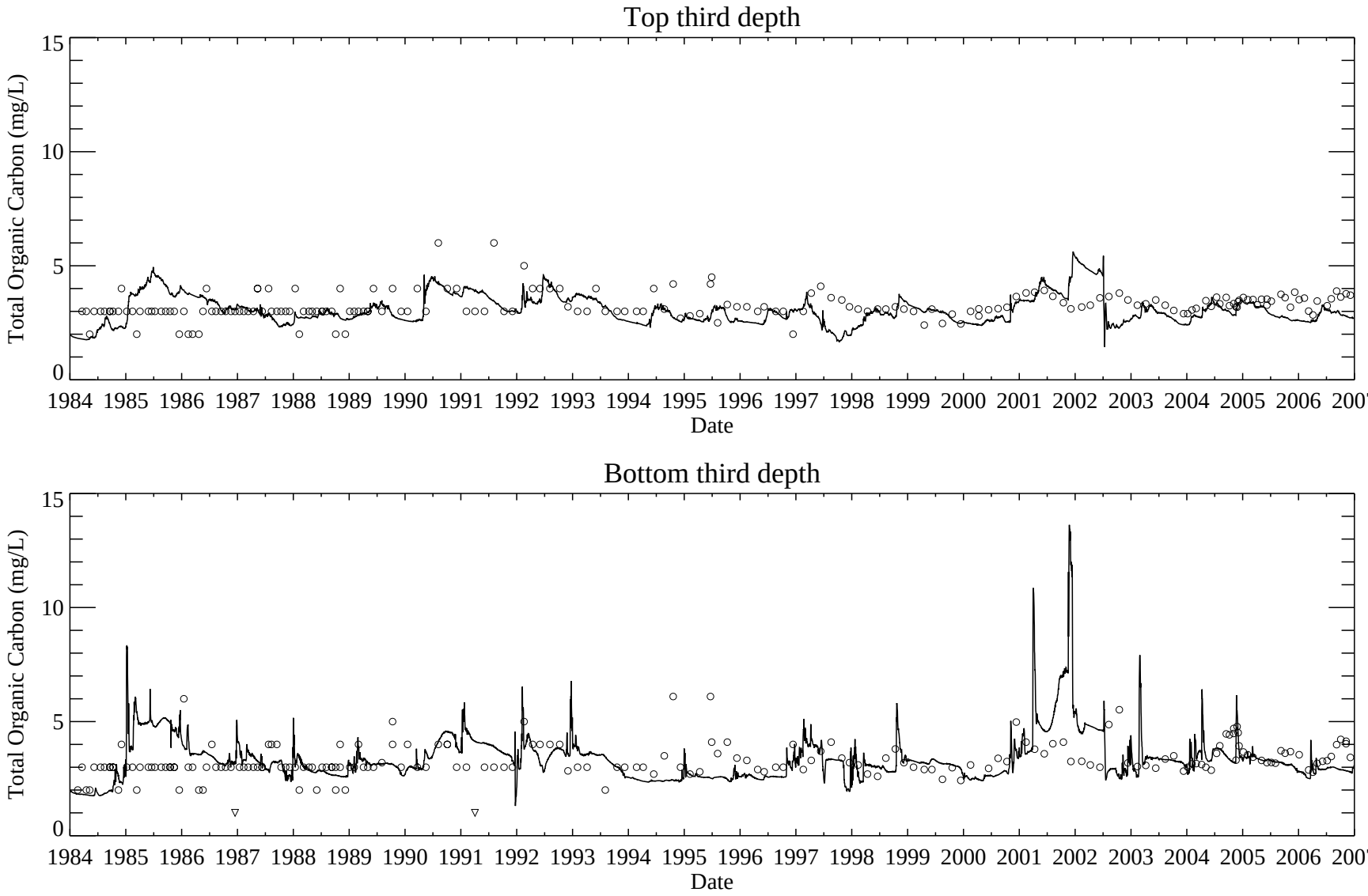

Figure 4-35. Temporal of model versus data at Arkansas Bend (Segment 78) - Total Organic Carbon.

Top third depth, Bottom third depth
When HAAWQ and CREMS data were measured on the same day, only CREMS data are shown. Non-detects plotted at detection limit.
Each data point is a discrete measurement except when multiple measurements were taken on the same day at the same depth (average shown).
Data in 'top third depth' excluded if collected below 10 meters (approximate starting depth of metalimnion).

haz/ec - A:\Jobs\PARcrm\model\Phase2_Travis\CE-QUAL-W2\postprocess\travis_temporal_forPh2rpt.pro
Mon Apr 13 10:39:49 2009

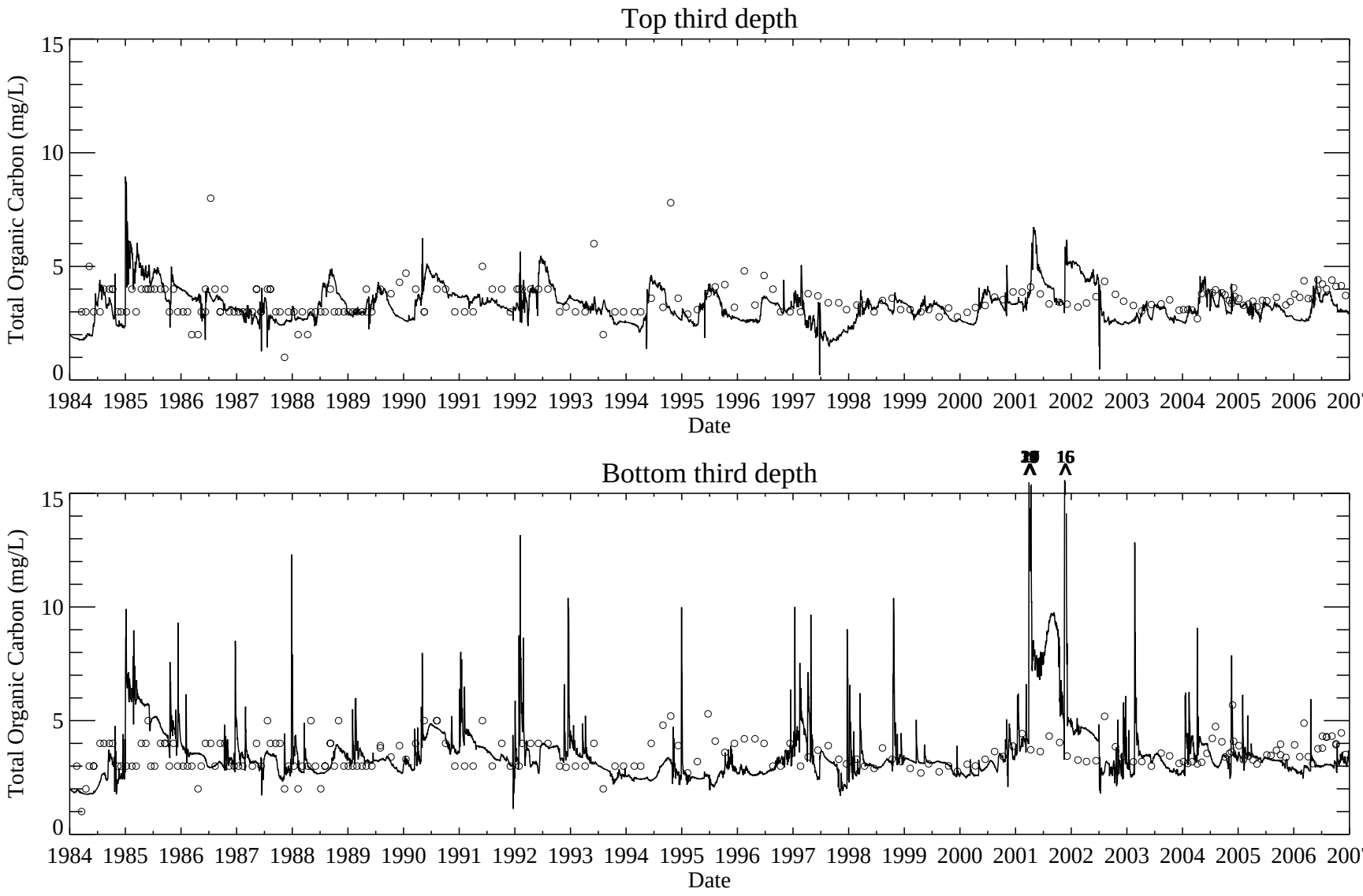

Figure 4-36. Temporal of model versus data at Pace Bend (Segment 48) - Total Organic Carbon.

Top third depth, Bottom third depth
When HAAWQ and CREMS data were measured on the same day, only CREMS data are shown. Non-detects plotted at detection limit.
Each data point is a discrete measurement except when multiple measurements were taken on the same day at the same depth (average shown).

haz/ec - D:\PARcrm\Model\Phase2_Travis\CE-QUAL-W2\postprocess\travis_temporal_forPh2rpt.pro
Thu Jan 29 13:13:21 2009

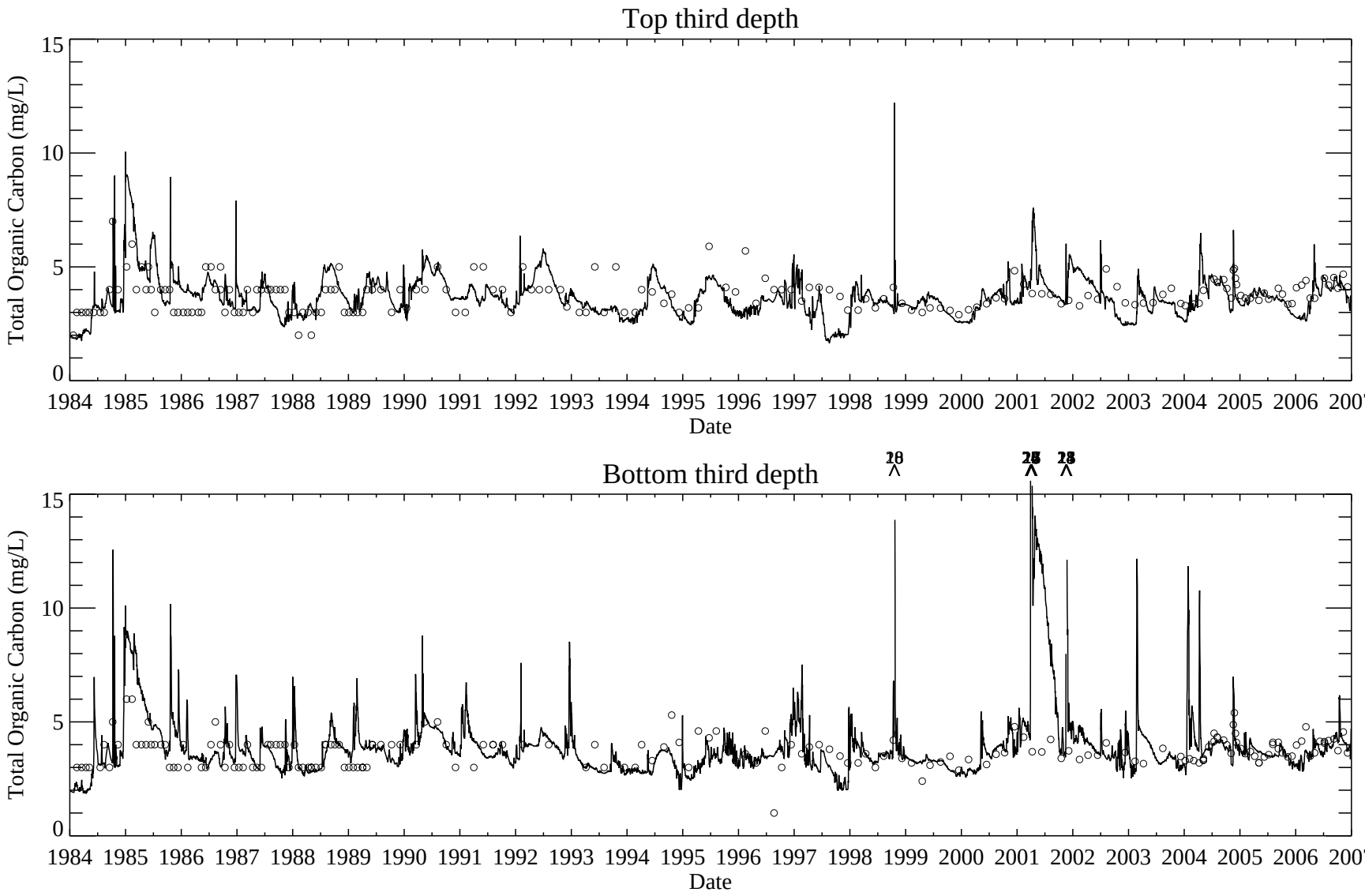

Figure 4-37. Temporal of model versus data at Turkey Bend (Segment 28) - Total Organic Carbon.

Top third depth, Bottom third depth
When HAAWQ and CREMS data were measured on the same day, only CREMS data are shown. Non-detects plotted at detection limit.
Each data point is a discrete measurement except when multiple measurements were taken on the same day at the same depth (average shown).

haz/ec - D:\PARcrm\Model\Phase2_Travis\CE-QUAL-W2\postprocess\travis_temporal_forPh2rpt.pro
Thu Jan 29 13:12:16 2009

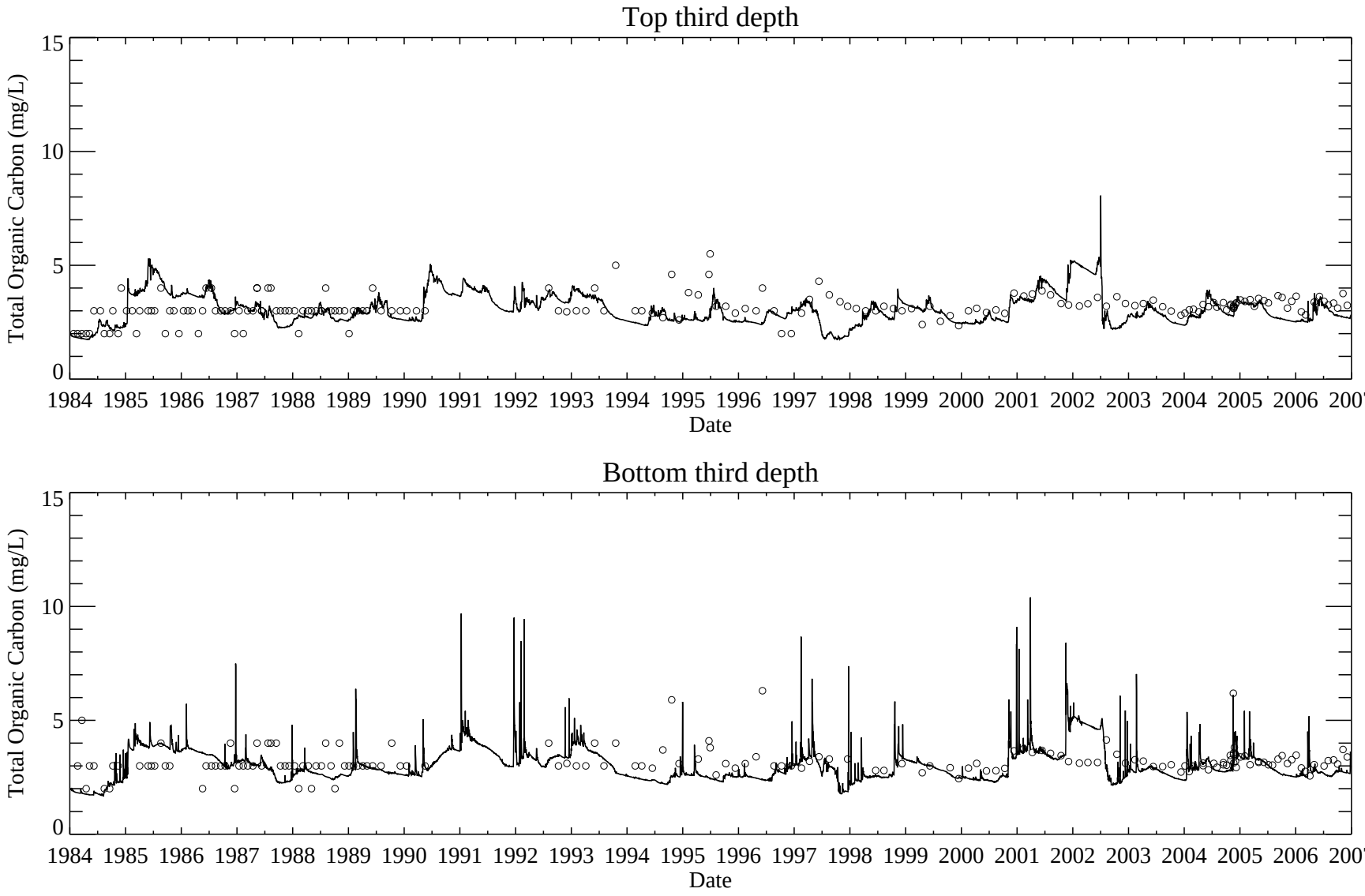

Figure 4-38. Temporal of model versus data at Sandy Creek (Segment 161) - Total Organic Carbon.

Top third depth, Bottom third depth
When HAAWQ and CREMS data were measured on the same day, only CREMS data are shown. Non-detects plotted at detection limit.
Each data point is a discrete measurement except when multiple measurements were taken on the same day at the same depth (average shown).

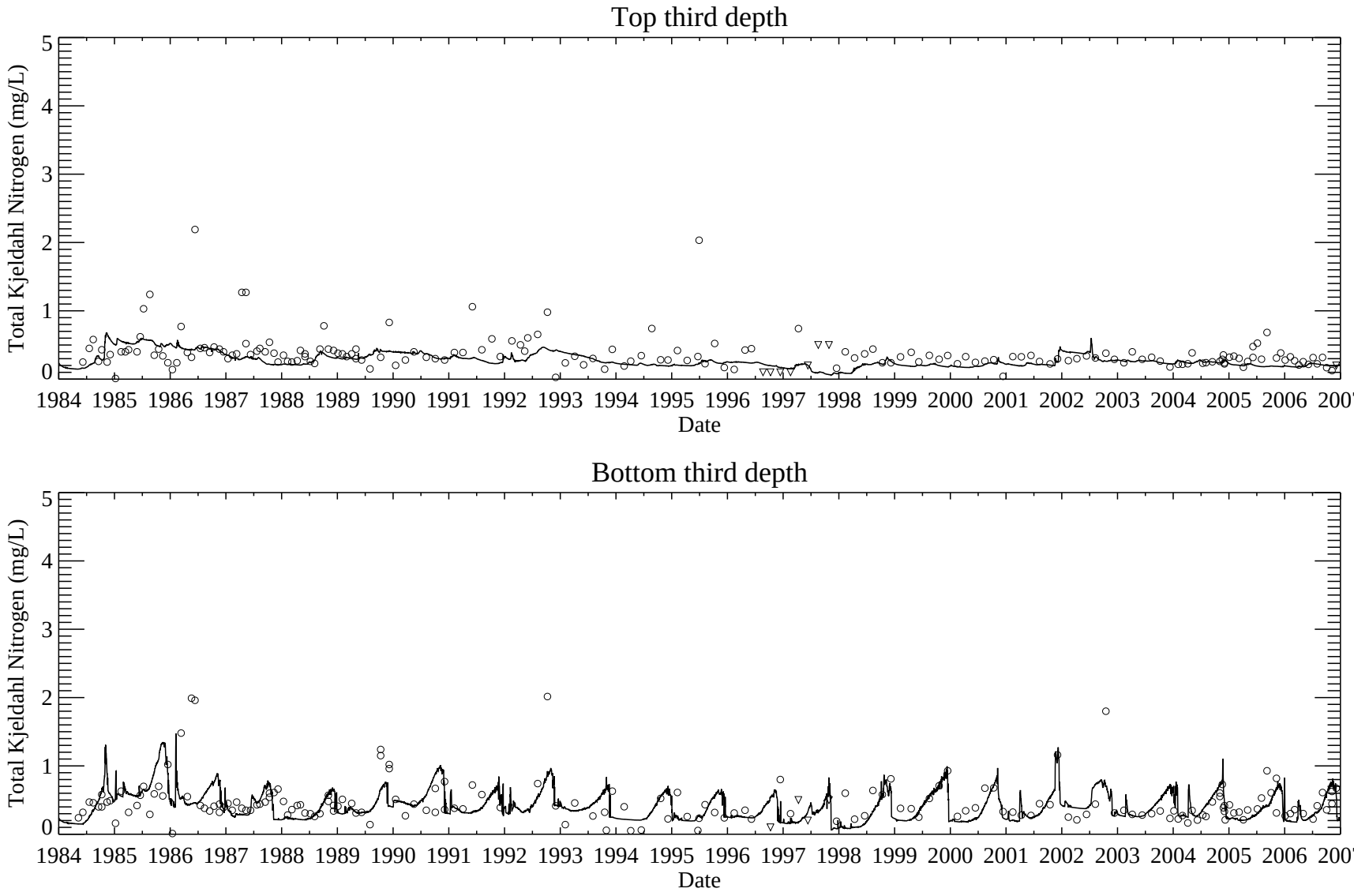

Figure 4-39. Temporal of model versus data at Mansfield Dam (Segment 93) - Total Kjeldahl Nitrogen.

Top third depth, Bottom third depth
When HAAWQ and CREMS data were measured on the same day, only CREMS data are shown. Non-detects plotted at detection limit.
Each data point is a discrete measurement except when multiple measurements were taken on the same day at the same depth (average shown).
Data in 'top third depth' excluded if collected below 10 meters (approximate starting depth of metalimnion).

haz/ec - A:\Jobs\PARcrm\model\Phase2_Travis\CE-QUAL-W2\postprocess\travis_temporal_forPh2rpt.pro
Wed Apr 08 14:54:08 2009

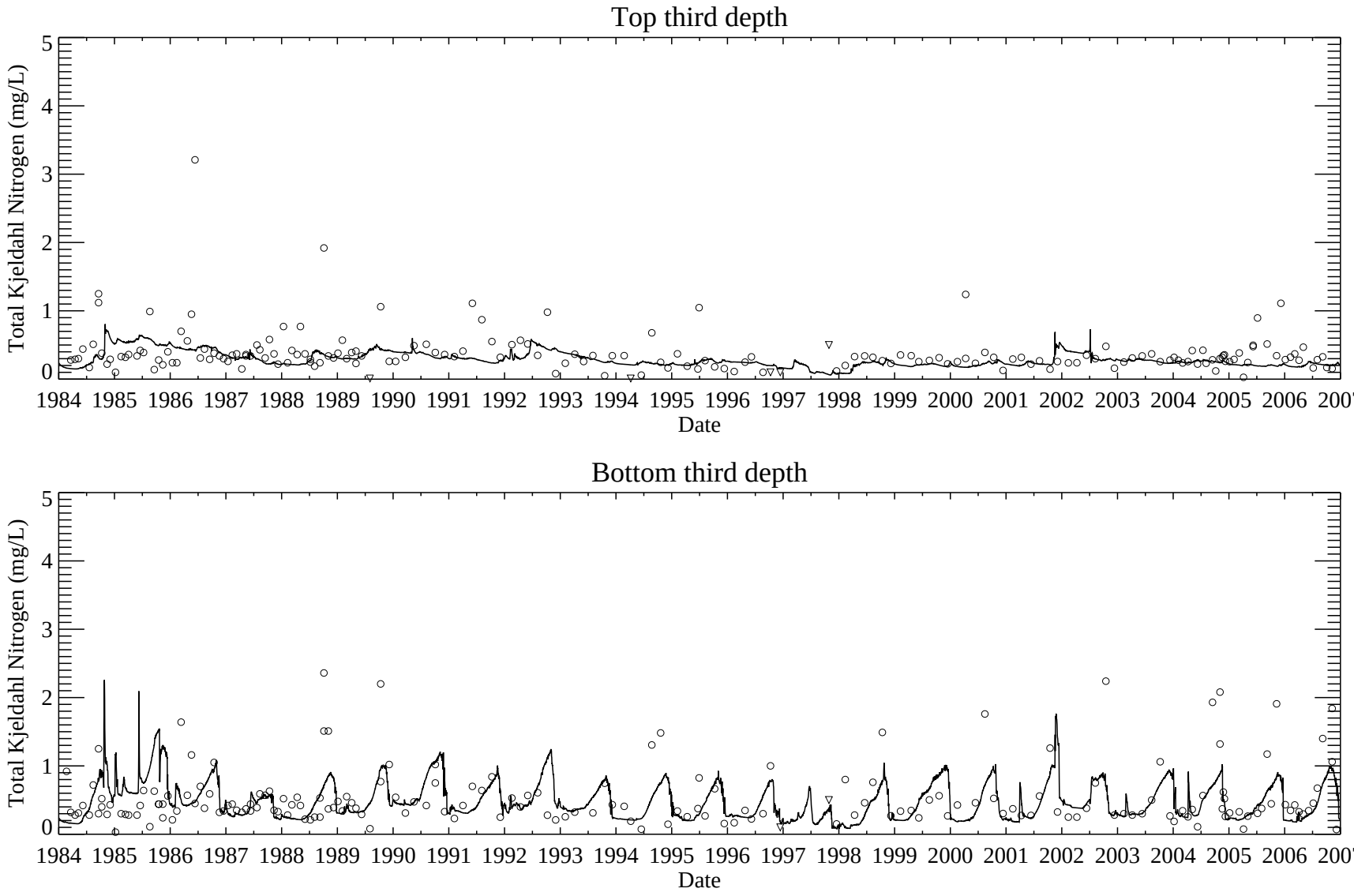

Figure 4-40. Temporal of model versus data at Arkansas Bend (Segment 78) - Total Kjeldahl Nitrogen.

Top third depth, Bottom third depth
When HAAWQ and CREMS data were measured on the same day, only CREMS data are shown. Non-detects plotted at detection limit.
Each data point is a discrete measurement except when multiple measurements were taken on the same day at the same depth (average shown).
Data in 'top third depth' excluded if collected below 10 meters (approximate starting depth of metalimnion).

haz/ec - A:\Jobs\PARcrm\model\Phase2_Travis\CE-QUAL-W2\postprocess\travis_temporal_forPh2rpt.pro
Mon Apr 13 10:43:05 2009

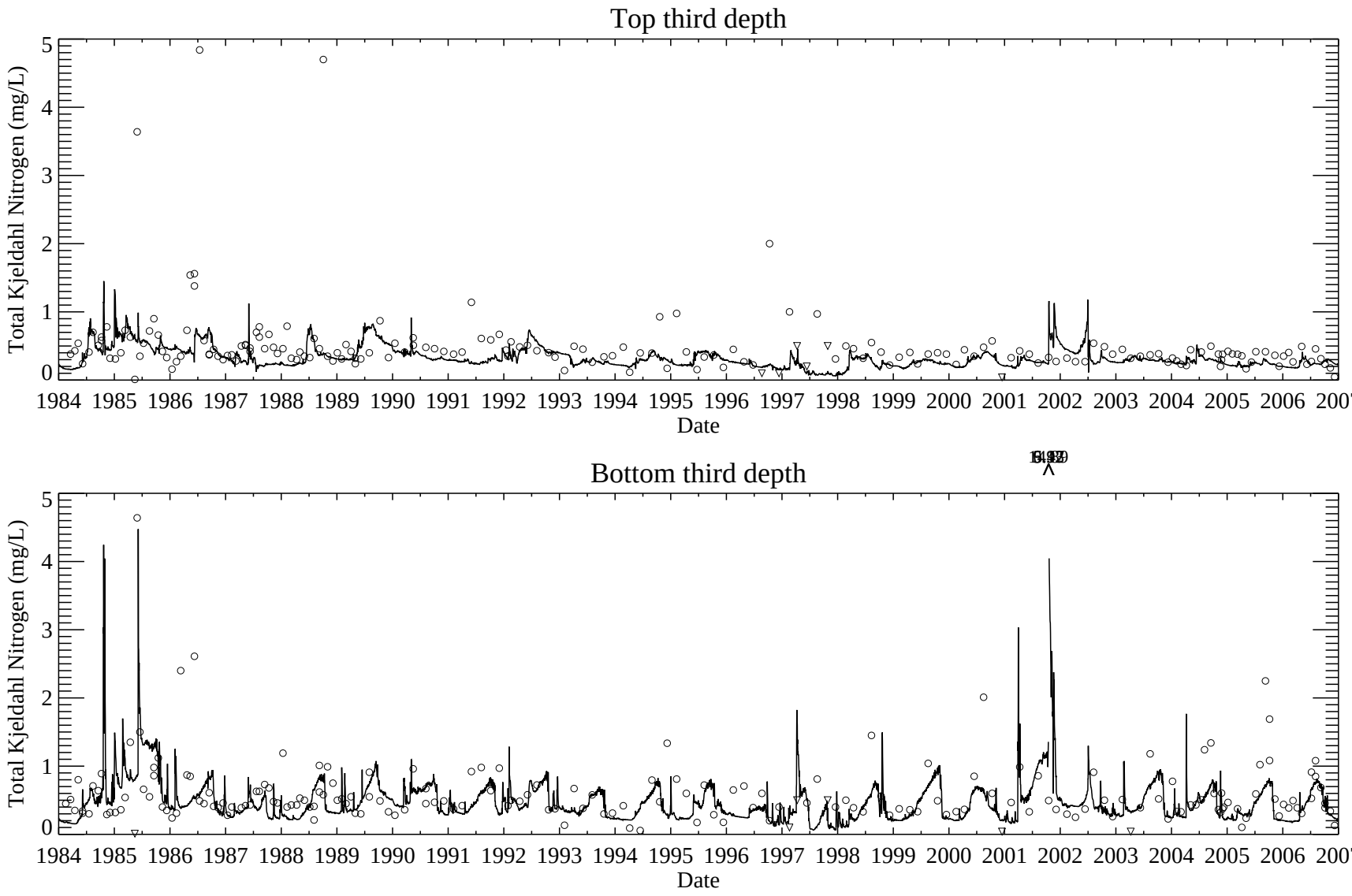

Figure 4-41. Temporal of model versus data at Pace Bend (Segment 48) - Total Kjeldahl Nitrogen.

Top third depth, Bottom third depth
When HAAWQ and CREMS data were measured on the same day, only CREMS data are shown. Non-detects plotted at detection limit.
Each data point is a discrete measurement except when multiple measurements were taken on the same day at the same depth (average shown).

haz/ec - D:\PARcrm\Model\Phase2_Travis\CE-QUAL-W2\postprocess\travis_temporal_forPh2rpt.pro
Thu Jan 29 14:07:39 2009

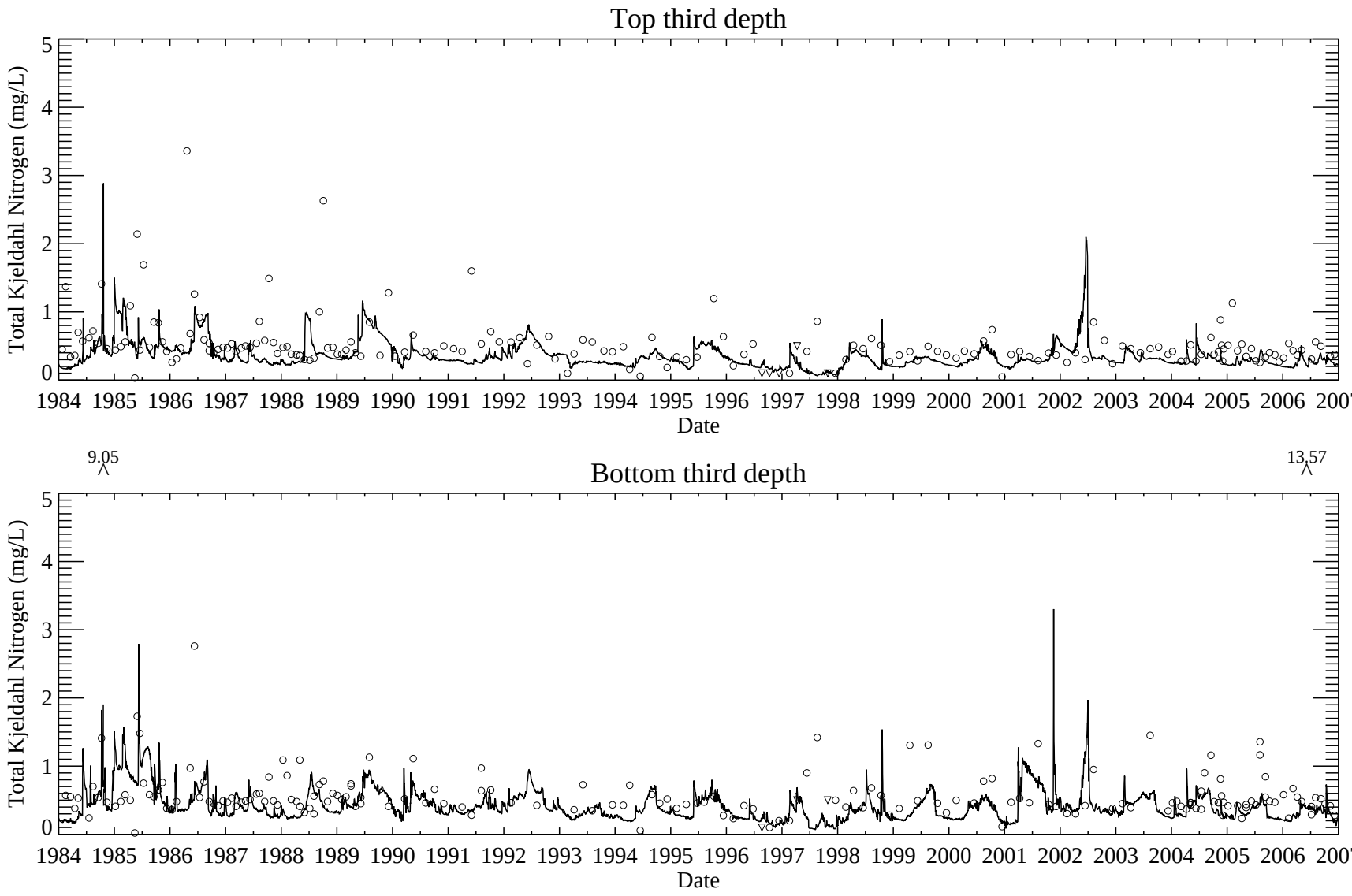

Figure 4-42. Temporal of model versus data at Turkey Bend (Segment 28) - Total Kjeldahl Nitrogen.

Top third depth, Bottom third depth
When HAAWQ and CREMS data were measured on the same day, only CREMS data are shown. Non-detects plotted at detection limit.
Each data point is a discrete measurement except when multiple measurements were taken on the same day at the same depth (average shown).

haz/ec - D:\PARcrm\Model\Phase2_Travis\CE-QUAL-W2\postprocess\travis_temporal_forPh2rpt.pro
Thu Jan 29 13:31:50 2009

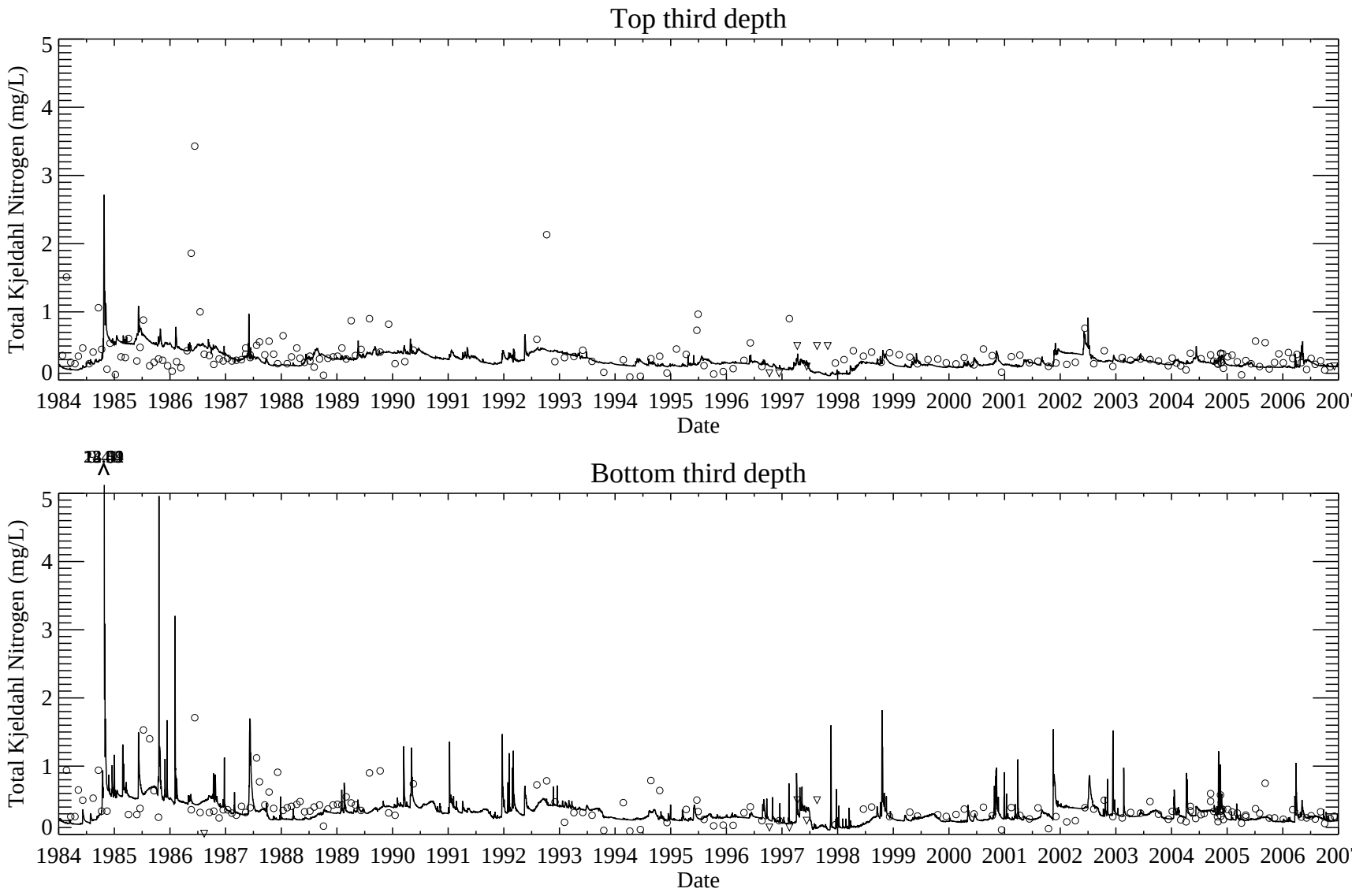

Figure 4-43. Temporal of model versus data at Sandy Creek (Segment 161) - Total Kjeldahl Nitrogen.

Top third depth, Bottom third depth
When HAAWQ and CREMS data were measured on the same day, only CREMS data are shown. Non-detects plotted at detection limit.
Each data point is a discrete measurement except when multiple measurements were taken on the same day at the same depth (average shown).

haz/ec - D:\PARcrm\Model\Phase2_Travis\CE-QUAL-W2\postprocess\travis_temporal_forPh2rpt.pro
Thu Jan 29 13:37:43 2009

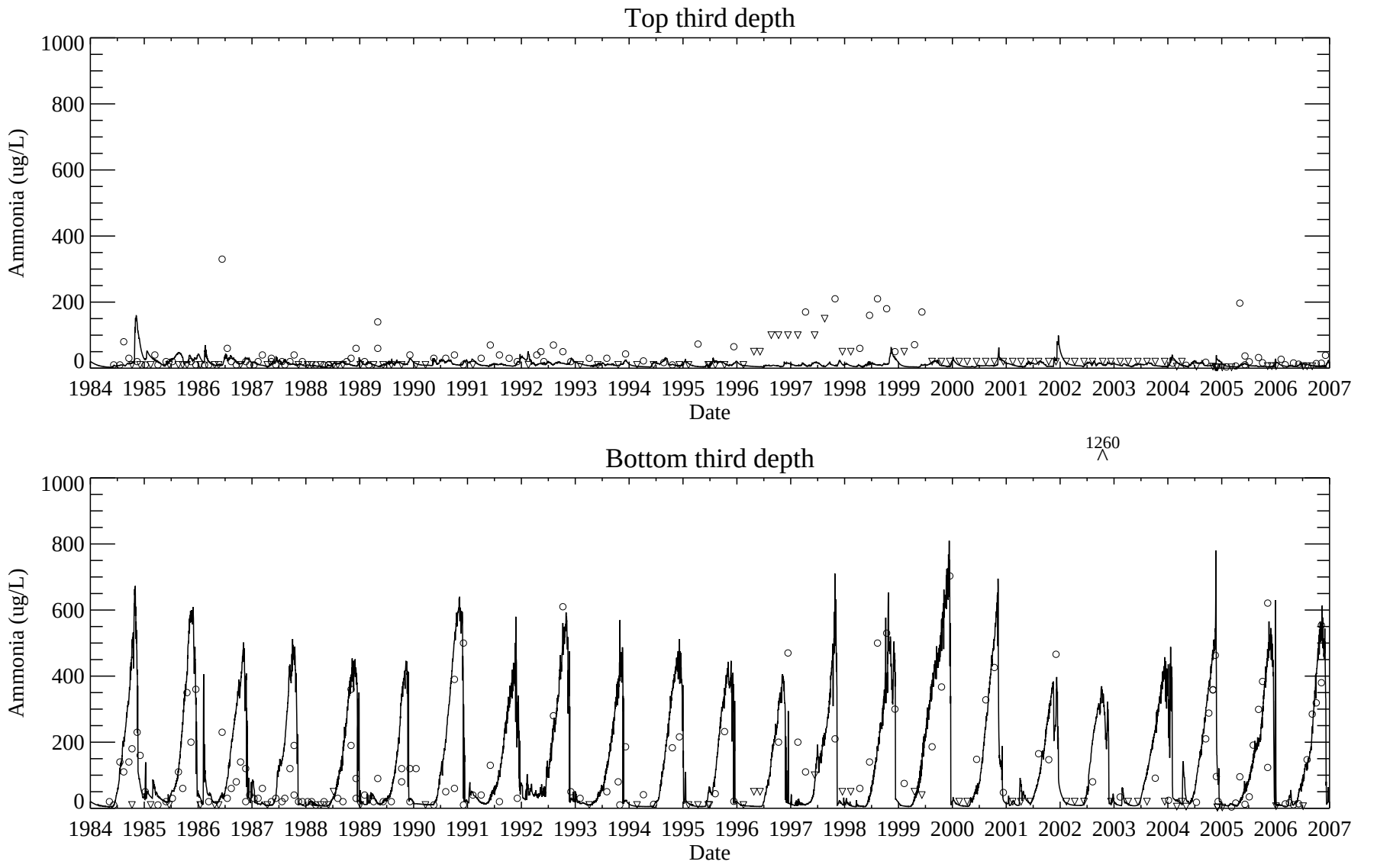

Figure 4-44. Temporal of model versus data at Mansfield Dam (Segment 93) - Ammonia.

Top third depth, Bottom third depth
When HAAWQ and CREMS data were measured on the same day, only CREMS data are shown. Non-detects plotted at detection limit.
Each data point is a discrete measurement except when multiple measurements were taken on the same day at the same depth (average shown).
Data in 'top third depth' excluded if collected below 10 meters (approximate starting depth of metalimnion).

haz/ec - A:\Jobs\PARcrm\model\Phase2_Travis\CE-QUAL-W2\postprocess\travis_temporal_forPh2rpt.pro
Wed Apr 08 14:55:23 2009

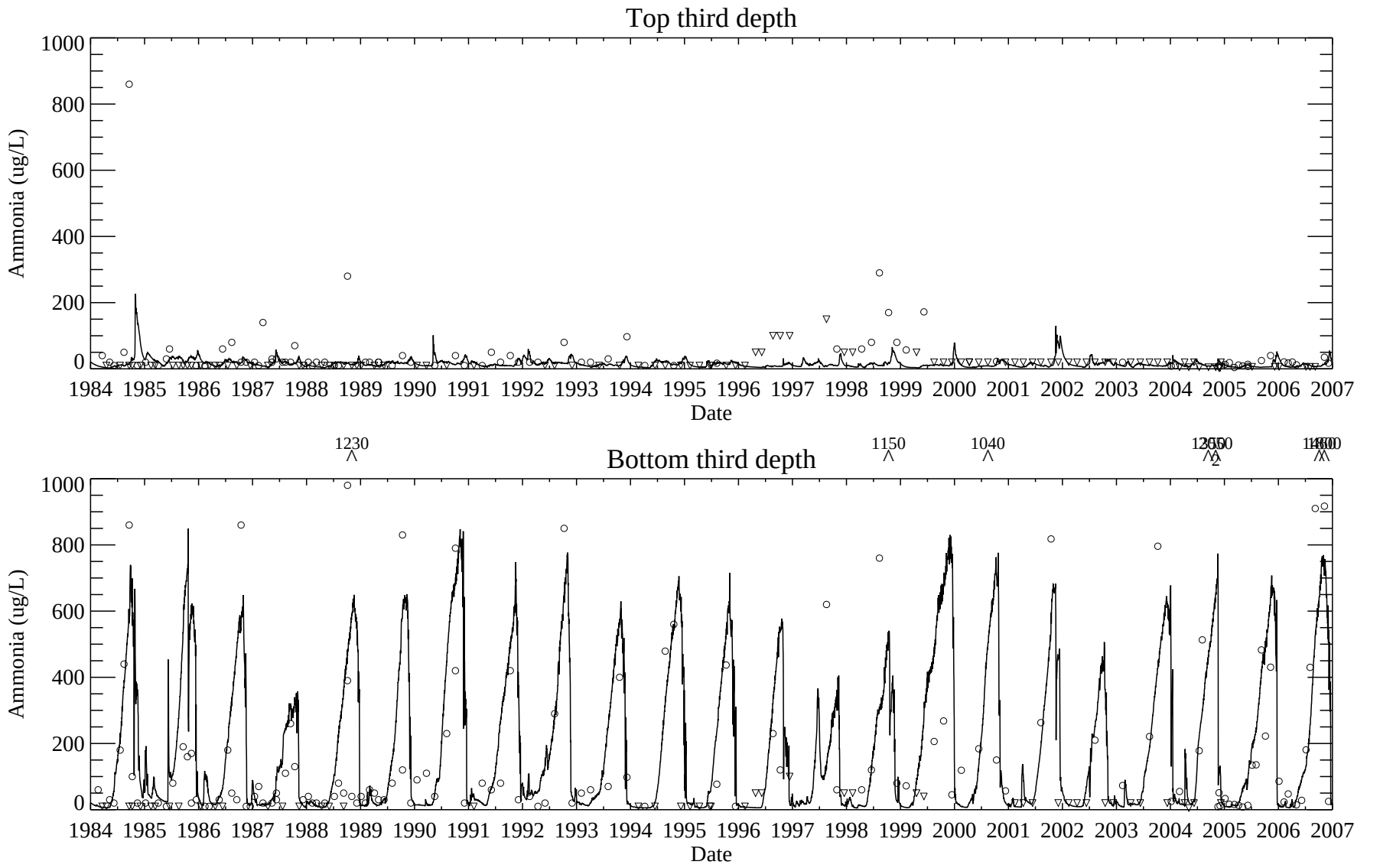

Figure 4-45. Temporal of model versus data at Arkansas Bend (Segment 78) - Ammonia.

Top third depth, Bottom third depth
When HAAWQ and CREMS data were measured on the same day, only CREMS data are shown. Non-detects plotted at detection limit.
Each data point is a discrete measurement except when multiple measurements were taken on the same day at the same depth (average shown).
Data in 'top third depth' excluded if collected below 10 meters (approximate starting depth of metalimnion).

haz/ec - A:\Jobs\PARcrm\model\Phase2_Travis\CE-QUAL-W2\postprocess\travis_temporal_forPh2rpt.pro
Mon Apr 13 10:44:08 2009

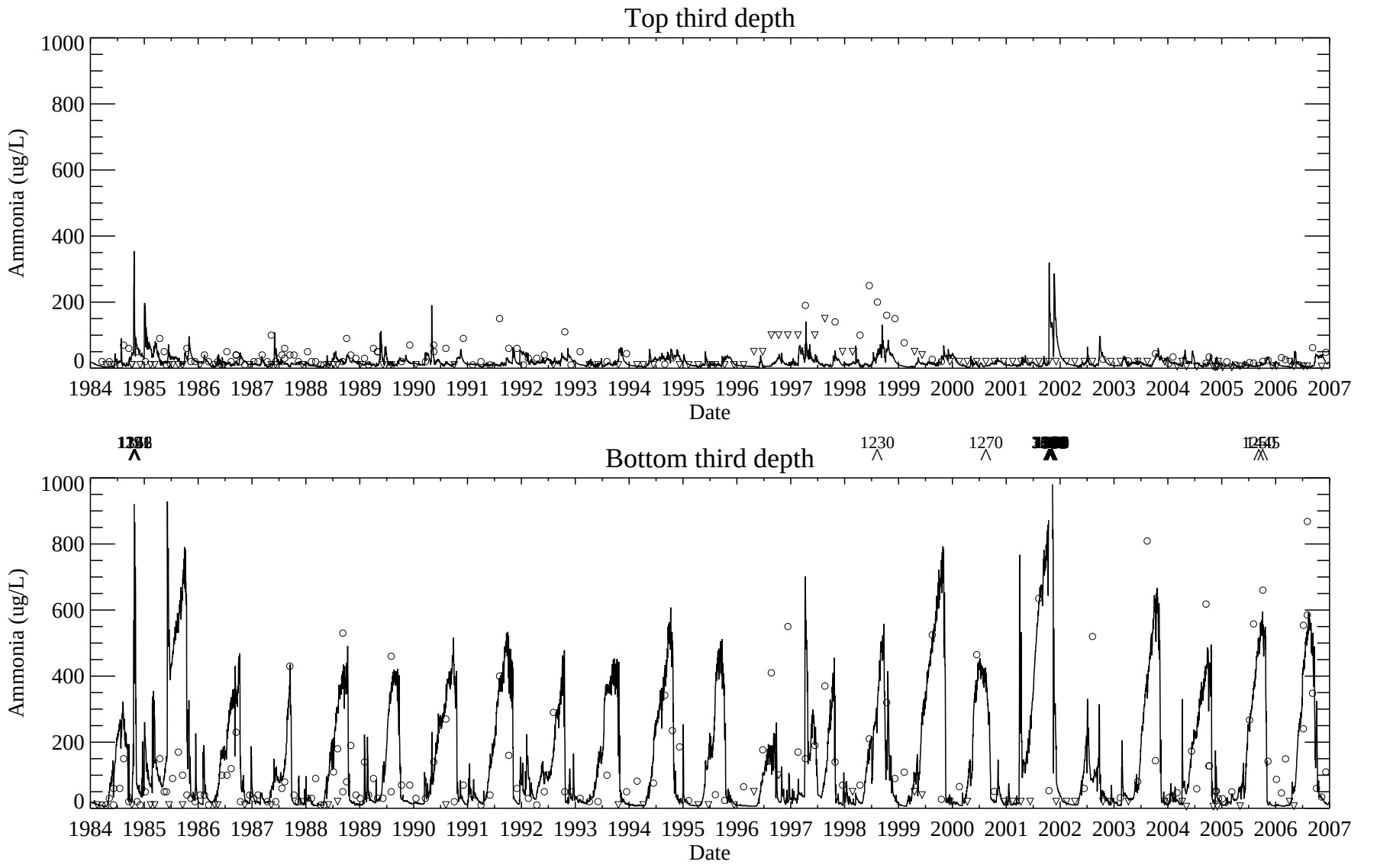

Figure 4-46. Temporal of model versus data at Pace Bend (Segment 48) - Ammonia.

Top third depth, Bottom third depth
When HAAWQ and CREMS data were measured on the same day, only CREMS data are shown. Non-detects plotted at detection limit.
Each data point is a discrete measurement except when multiple measurements were taken on the same day at the same depth (average shown).

haz/ec - D:\PARcrm\Model\Phase2_Travis\CE-QUAL-W2\postprocess\travis_temporal_forPh2rpt.pro
Thu Jan 29 13:39:31 2009

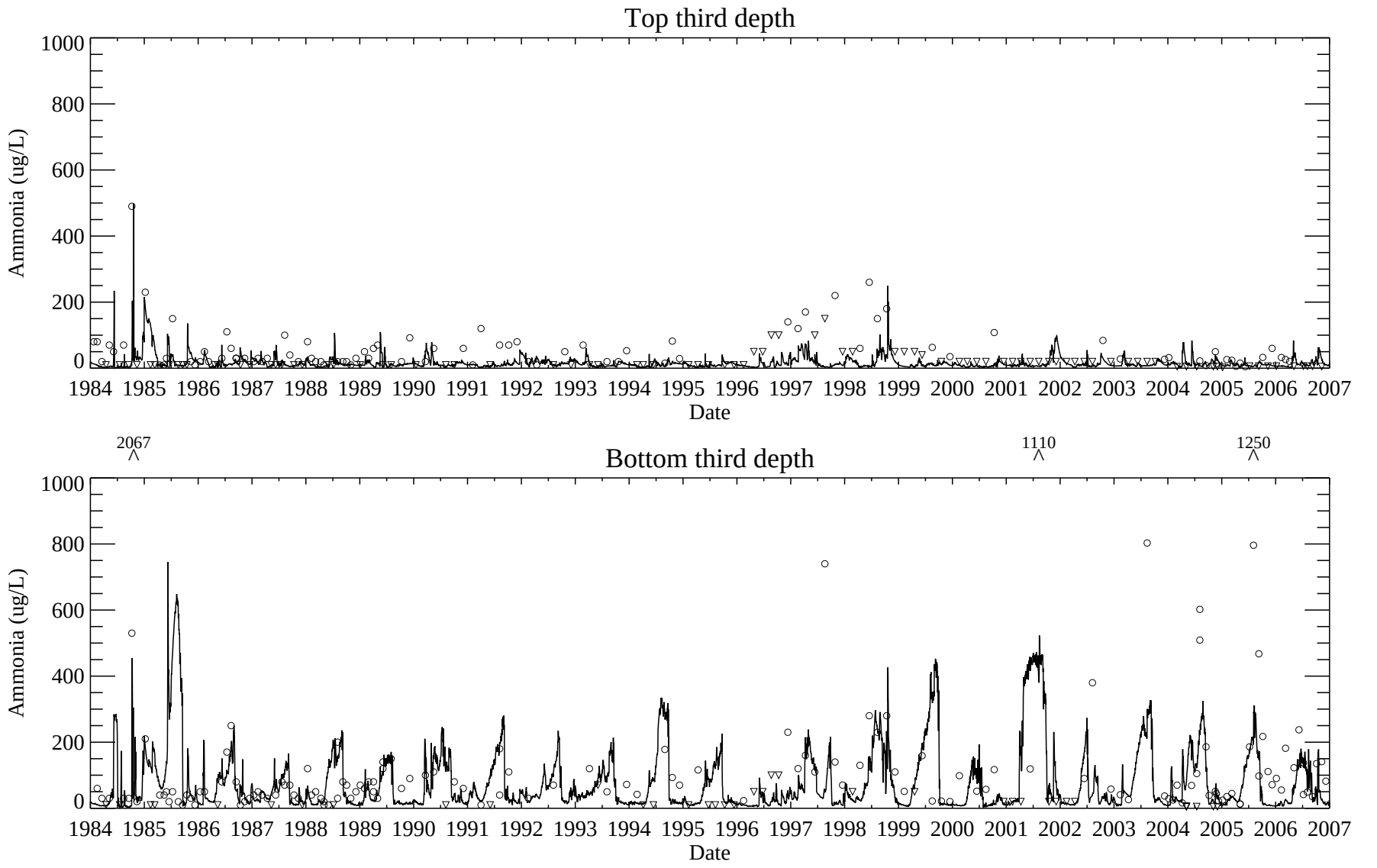

Figure 4-47. Temporal of model versus data at Turkey Bend (Segment 28) - Ammonia.

Top third depth, Bottom third depth
When HAAWQ and CREMS data were measured on the same day, only CREMS data are shown. Non-detects plotted at detection limit.
Each data point is a discrete measurement except when multiple measurements were taken on the same day at the same depth (average shown).

haz/ec - D:\PARcrm\Model\Phase2_Travis\CE-QUAL-W2\postprocess\travis_temporal_forPh2rpt.pro
Thu Jan 29 13:38:25 2009

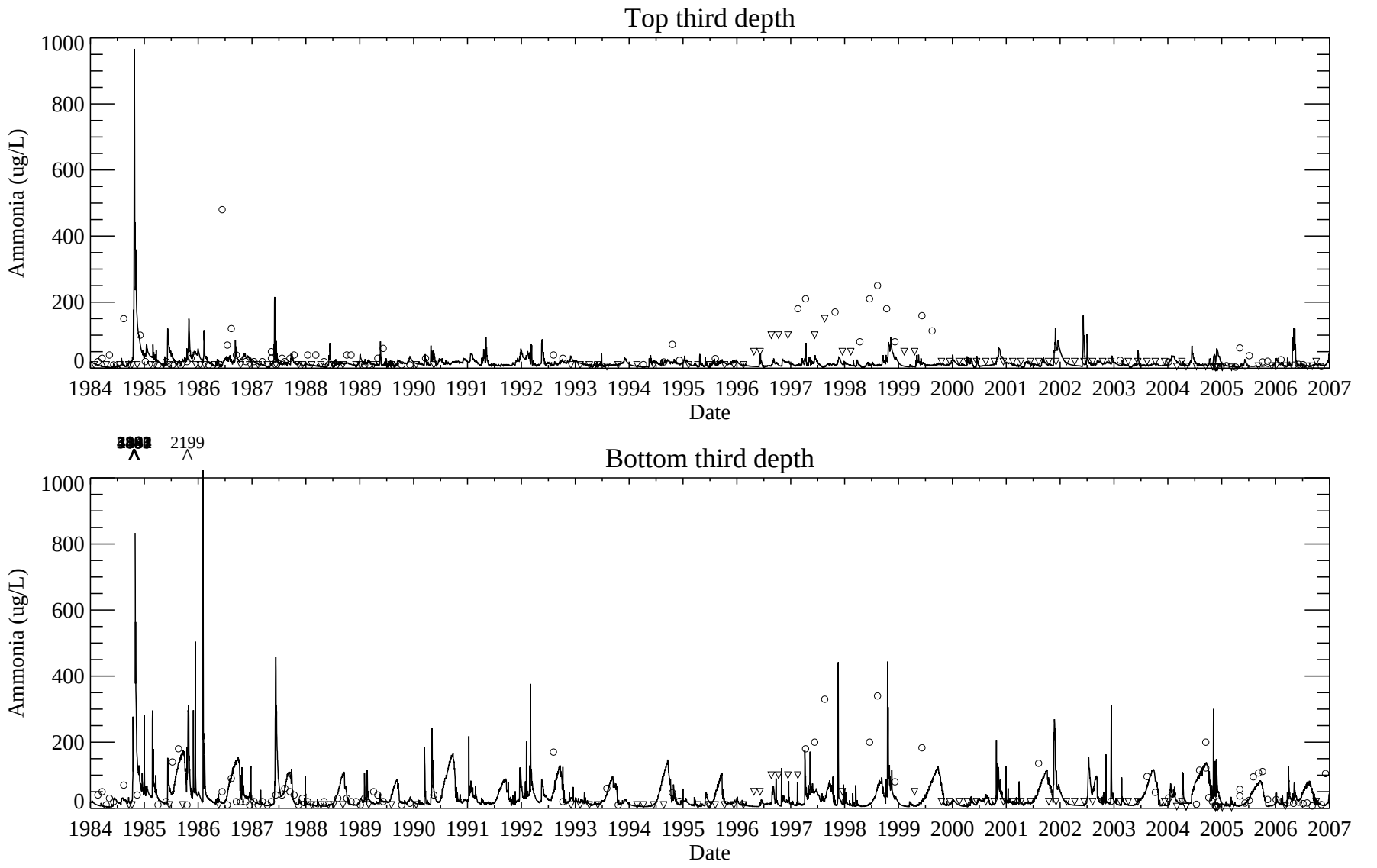

Figure 4-48. Temporal of model versus data at Sandy Creek (Segment 161) - Ammonia.

Top third depth, Bottom third depth
When HAAWQ and CREMS data were measured on the same day, only CREMS data are shown. Non-detects plotted at detection limit.
Each data point is a discrete measurement except when multiple measurements were taken on the same day at the same depth (average shown).

haz/ec - D:\PARcrm\Model\Phase2_Travis\CE-QUAL-W2\postprocess\travis_temporal_forPh2rpt.pro
Thu Jan 29 13:44:15 2009

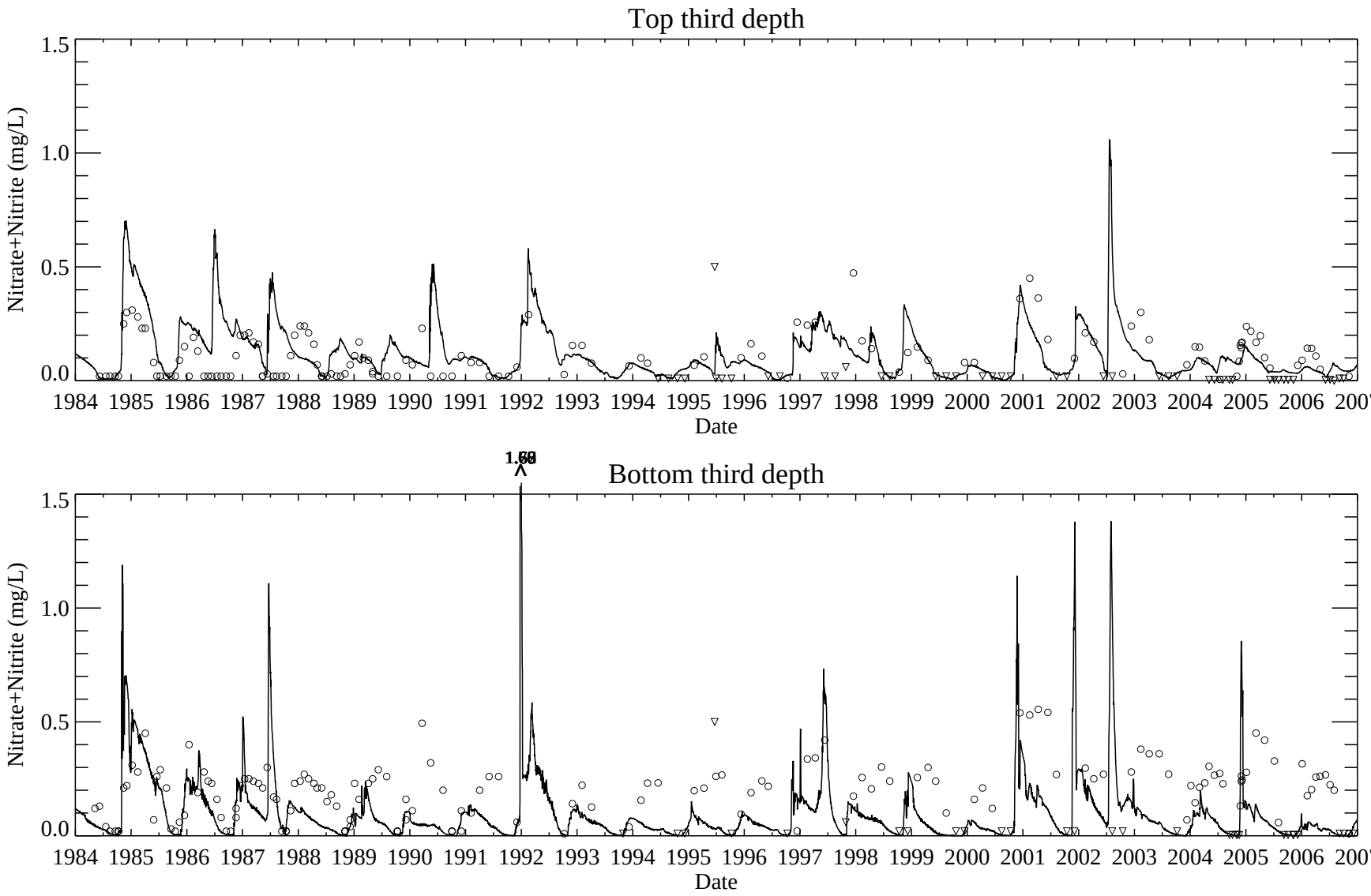

Figure 4-49. Temporal of model versus data at Mansfield Dam (Segment 93) - Nitrate+Nitrite.

Top third depth, Bottom third depth
When HAAWQ and CREMS data were measured on the same day, only CREMS data are shown. Non-detects plotted at detection limit.
Each data point is a discrete measurement except when multiple measurements were taken on the same day at the same depth (average shown).
Data in 'top third depth' excluded if collected below 10 meters (approximate starting depth of metalimnion).

haz/ec - A:\Jobs\PARcrm\model\Phase2_Travis\CE-QUAL-W2\postprocess\travis_temporal_forPh2rpt.pro
Wed Apr 08 14:51:35 2009

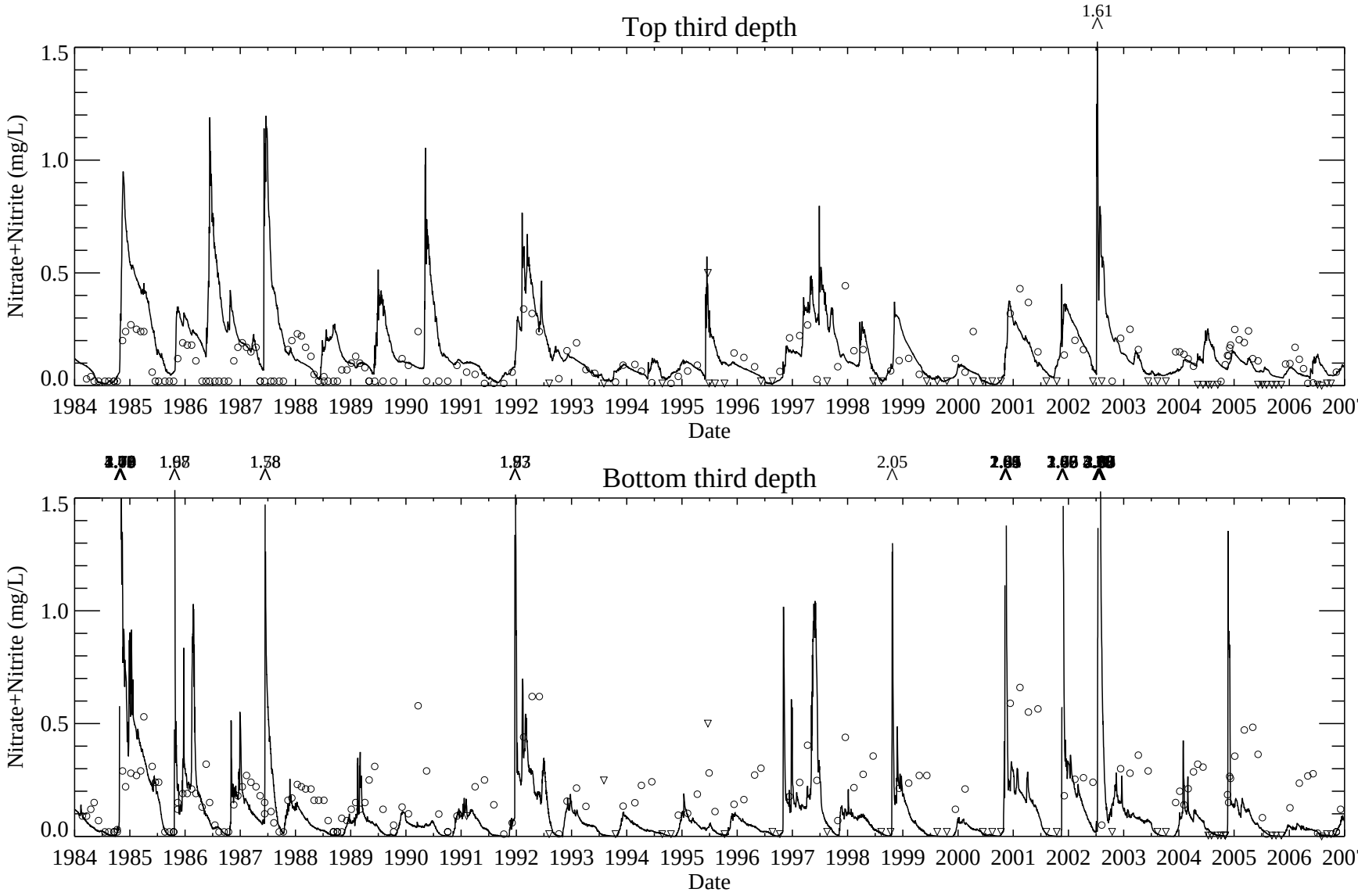

Figure 4-50. Temporal of model versus data at Arkansas Bend (Segment 78) - Nitrate+Nitrite.

Top third depth, Bottom third depth
When HAAWQ and CREMS data were measured on the same day, only CREMS data are shown. Non-detects plotted at detection limit.
Each data point is a discrete measurement except when multiple measurements were taken on the same day at the same depth (average shown).
Data in 'top third depth' excluded if collected below 10 meters (approximate starting depth of metalimnion).

haz/ec - A:\Jobs\PARcrm\model\Phase2_Travis\CE-QUAL-W2\postprocess\travis_temporal_forPh2rpt.pro
Mon Apr 13 10:40:54 2009

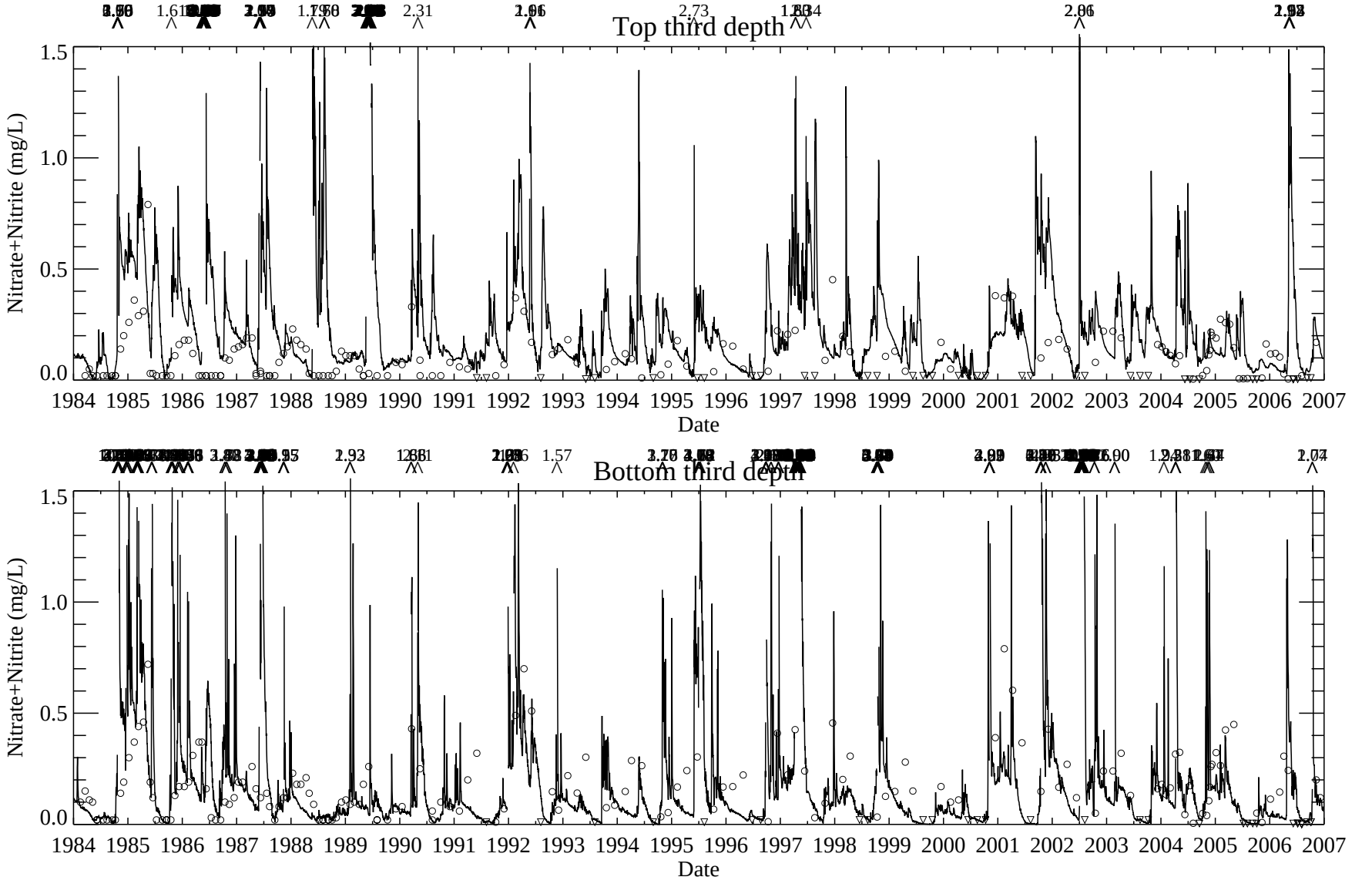

Figure 4-51. Temporal of model versus data at Pace Bend (Segment 48) - Nitrate+Nitrite.

Top third depth, Bottom third depth
When HAAWQ and CREMS data were measured on the same day, only CREMS data are shown. Non-detects plotted at detection limit.
Each data point is a discrete measurement except when multiple measurements were taken on the same day at the same depth (average shown).

haz/ec - D:\PARcrm\Model\Phase2_Travis\CE-QUAL-W2\postprocess\travis_temporal_forPh2rpt.pro
Thu Jan 29 13:19:49 2009

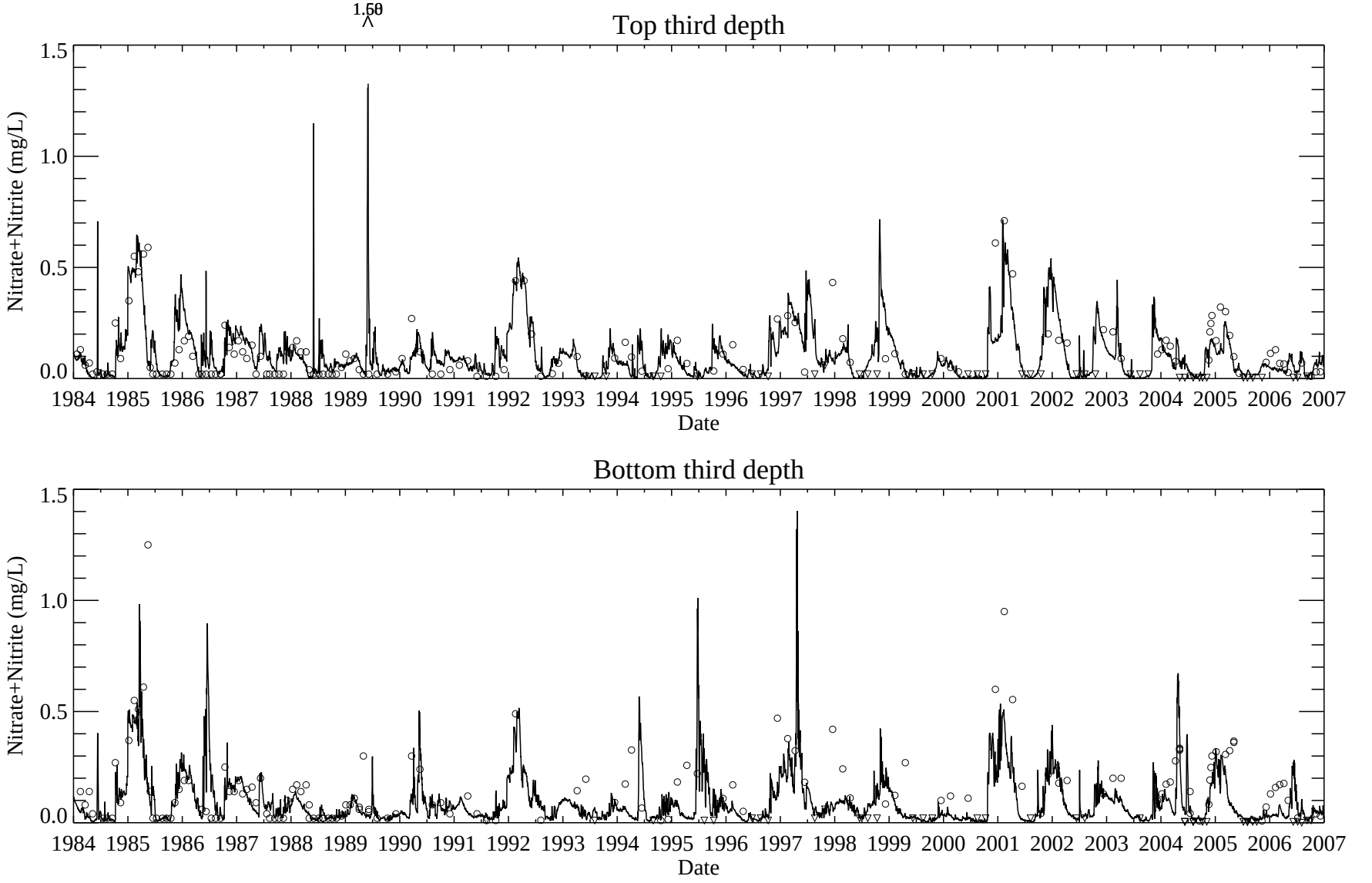

Figure 4-52. Temporal of model versus data at Turkey Bend (Segment 28) - Nitrate+Nitrite.

Top third depth, Bottom third depth
When HAAWQ and CREMS data were measured on the same day, only CREMS data are shown. Non-detects plotted at detection limit.
Each data point is a discrete measurement except when multiple measurements were taken on the same day at the same depth (average shown).

haz/ec - D:\PARcrm\Model\Phase2_Travis\CE-QUAL-W2\postprocess\travis_temporal_forPh2rpt.pro
Thu Jan 29 13:18:44 2009

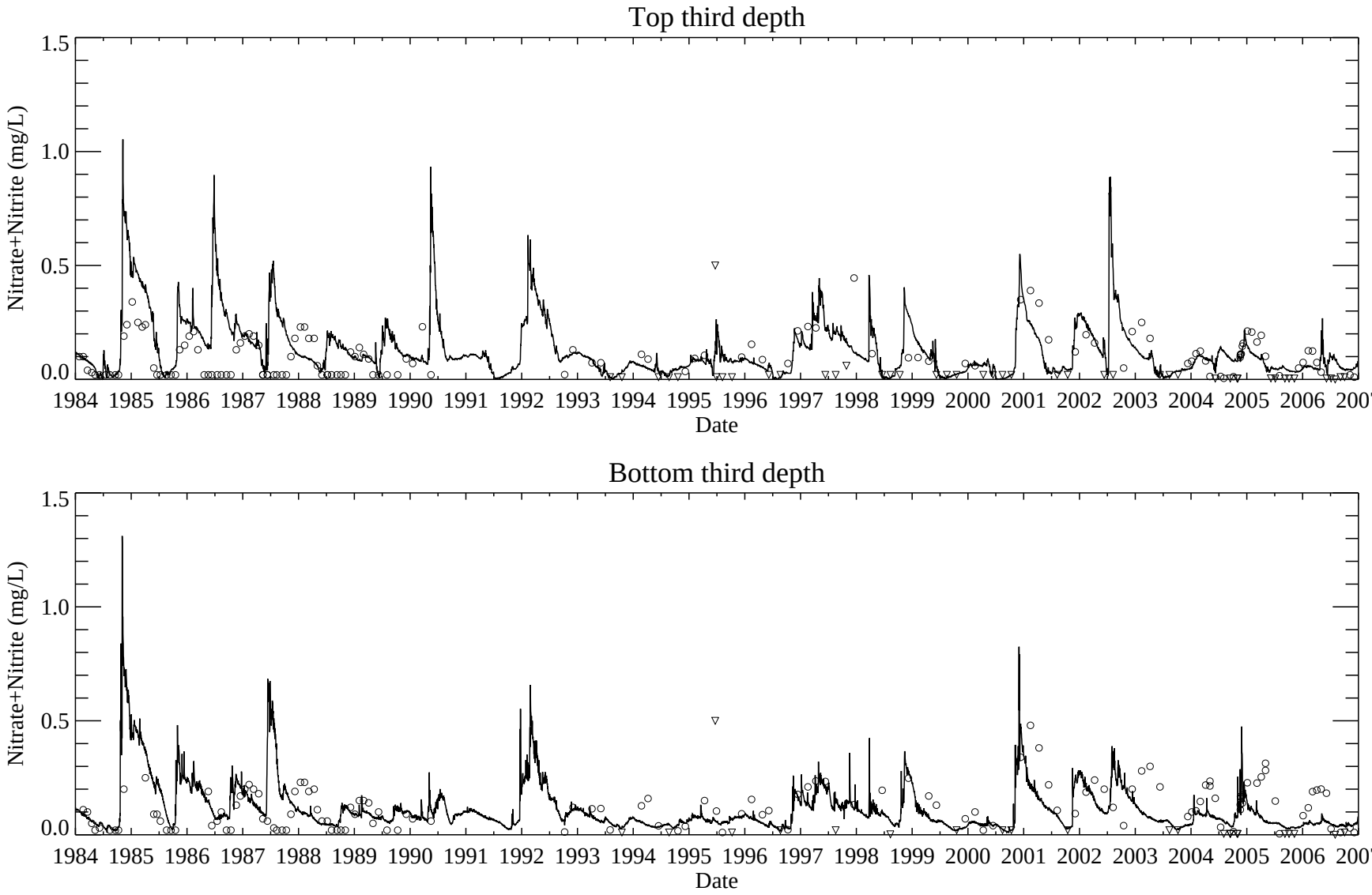

Figure 4-53. Temporal of model versus data at Sandy Creek (Segment 161) - Nitrate+Nitrite.

Top third depth, Bottom third depth
When HAAWQ and CREMS data were measured on the same day, only CREMS data are shown. Non-detects plotted at detection limit.
Each data point is a discrete measurement except when multiple measurements were taken on the same day at the same depth (average shown).

haz/ec - D:\PARcrm\Model\Phase2_Travis\CE-QUAL-W2\postprocess\travis_temporal_forPh2rpt.pro
Thu Jan 29 13:24:34 2009

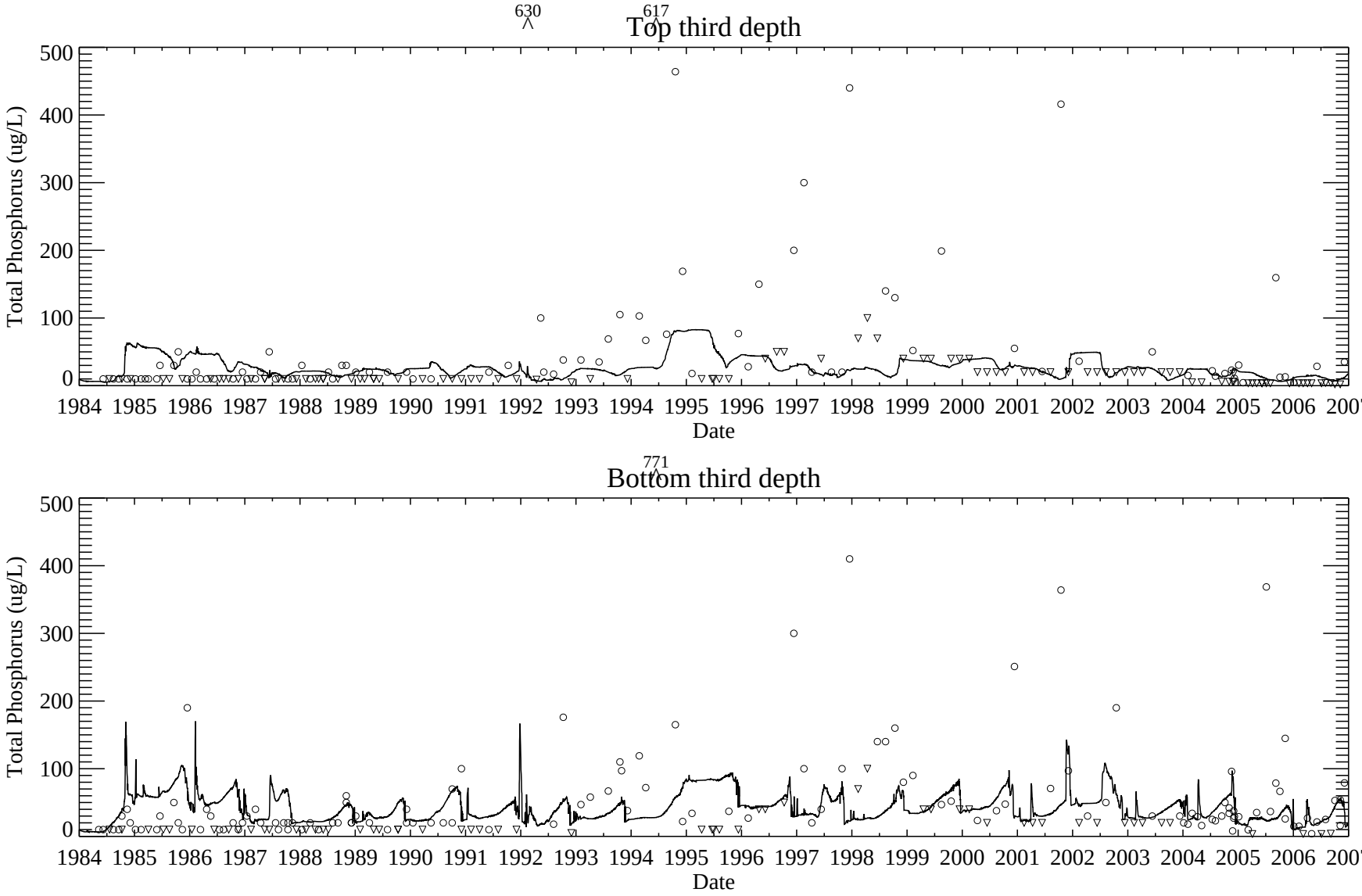

Figure 4-54. Temporal of model versus data at Mansfield Dam (Segment 93) - Total Phosphorus.

Top third depth, Bottom third depth
When HAAWQ and CREMS data were measured on the same day, only CREMS data are shown. Non-detects plotted at detection limit.
Each data point is a discrete measurement except when multiple measurements were taken on the same day at the same depth (average shown).
Data in 'top third depth' excluded if collected below 10 meters (approximate starting depth of metalimnion).

haz/ec - A:\Jobs\PARcrm\model\Phase2_Travis\CE-QUAL-W2\postprocess\travis_temporal_forPh2rpt.pro
Wed Apr 08 14:52:52 2009

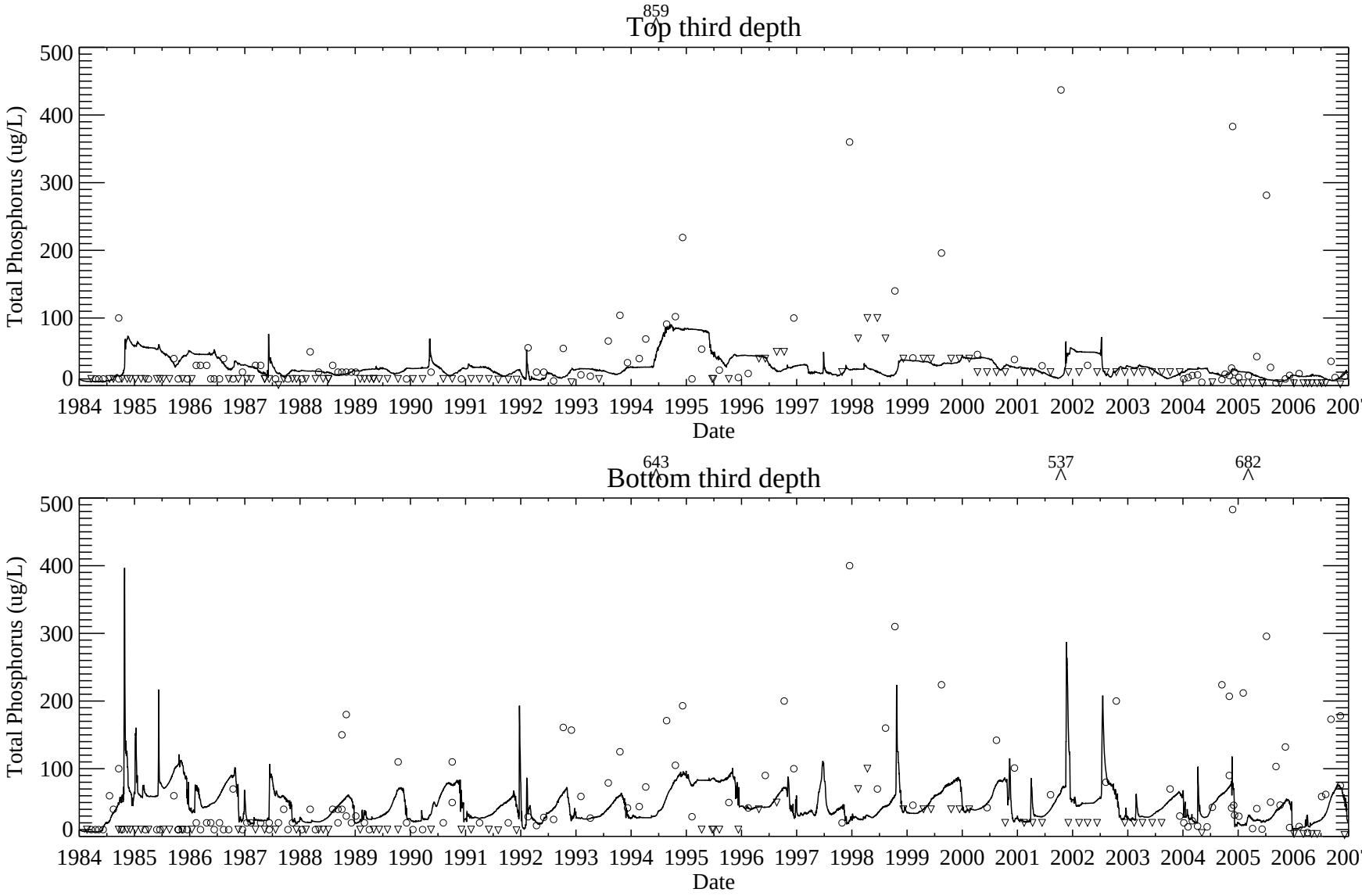

Figure 4-55. Temporal of model versus data at Arkansas Bend (Segment 78) - Total Phosphorus.

Top third depth, Bottom third depth
When HAAWQ and CREMS data were measured on the same day, only CREMS data are shown. Non-detects plotted at detection limit.
Each data point is a discrete measurement except when multiple measurements were taken on the same day at the same depth (average shown).
Data in 'top third depth' excluded if collected below 10 meters (approximate starting depth of metalimnion).

haz/ec - A:\Jobs\PARcrm\model\Phase2_Travis\CE-QUAL-W2\postprocess\travis_temporal_forPh2rpt.pro
Mon Apr 13 10:41:59 2009

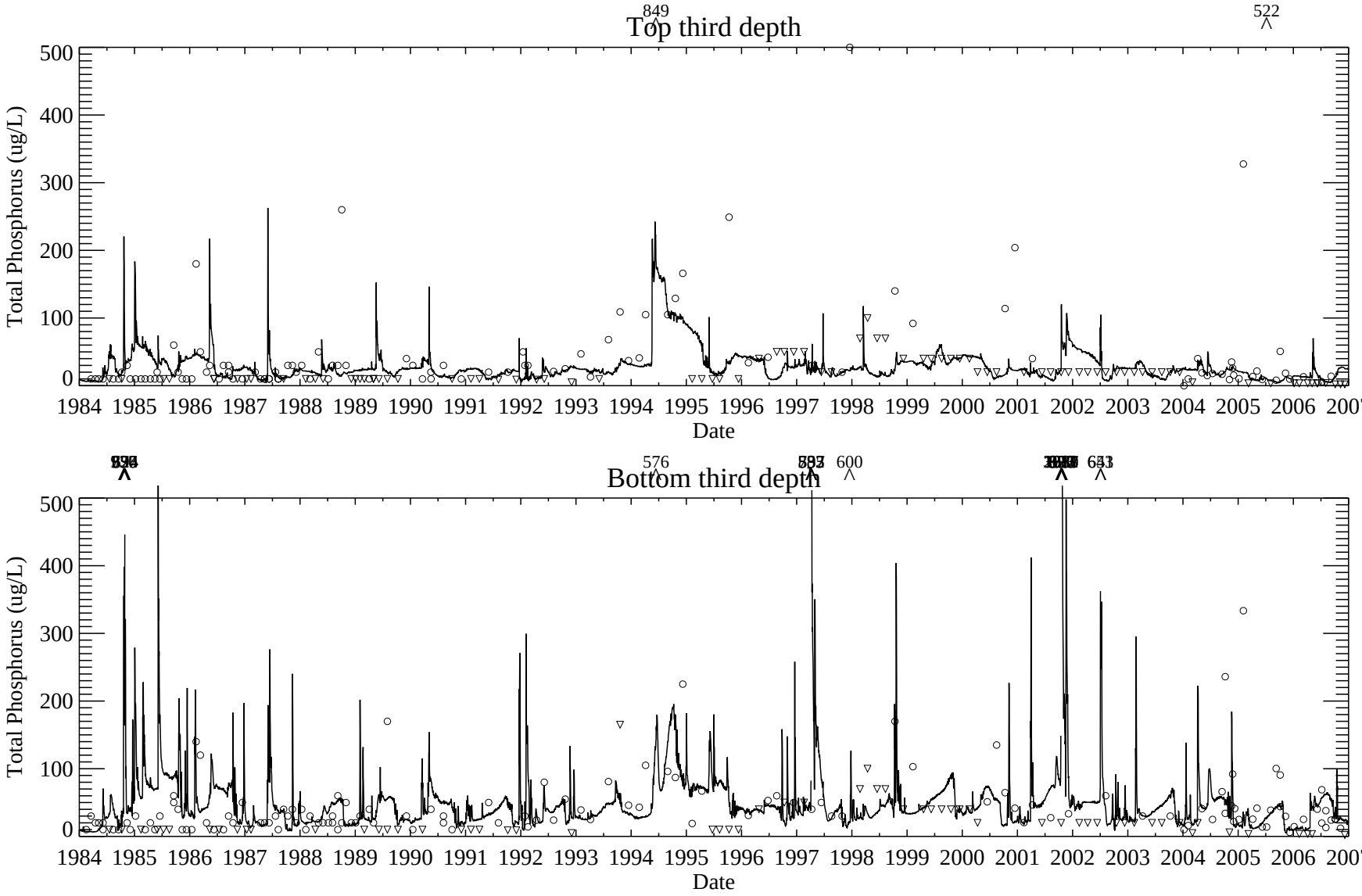

Figure 4-56. Temporal of model versus data at Pace Bend (Segment 48) - Total Phosphorus.

Top third depth, Bottom third depth
When HAAWQ and CREMS data were measured on the same day, only CREMS data are shown. Non-detects plotted at detection limit.
Each data point is a discrete measurement except when multiple measurements were taken on the same day at the same depth (average shown).

haz/ec - D:\PARcrm\Model\Phase2_Travis\CE-QUAL-W2\postprocess\travis_temporal_forPh2rpt.pro
Thu Jan 29 13:26:22 2009

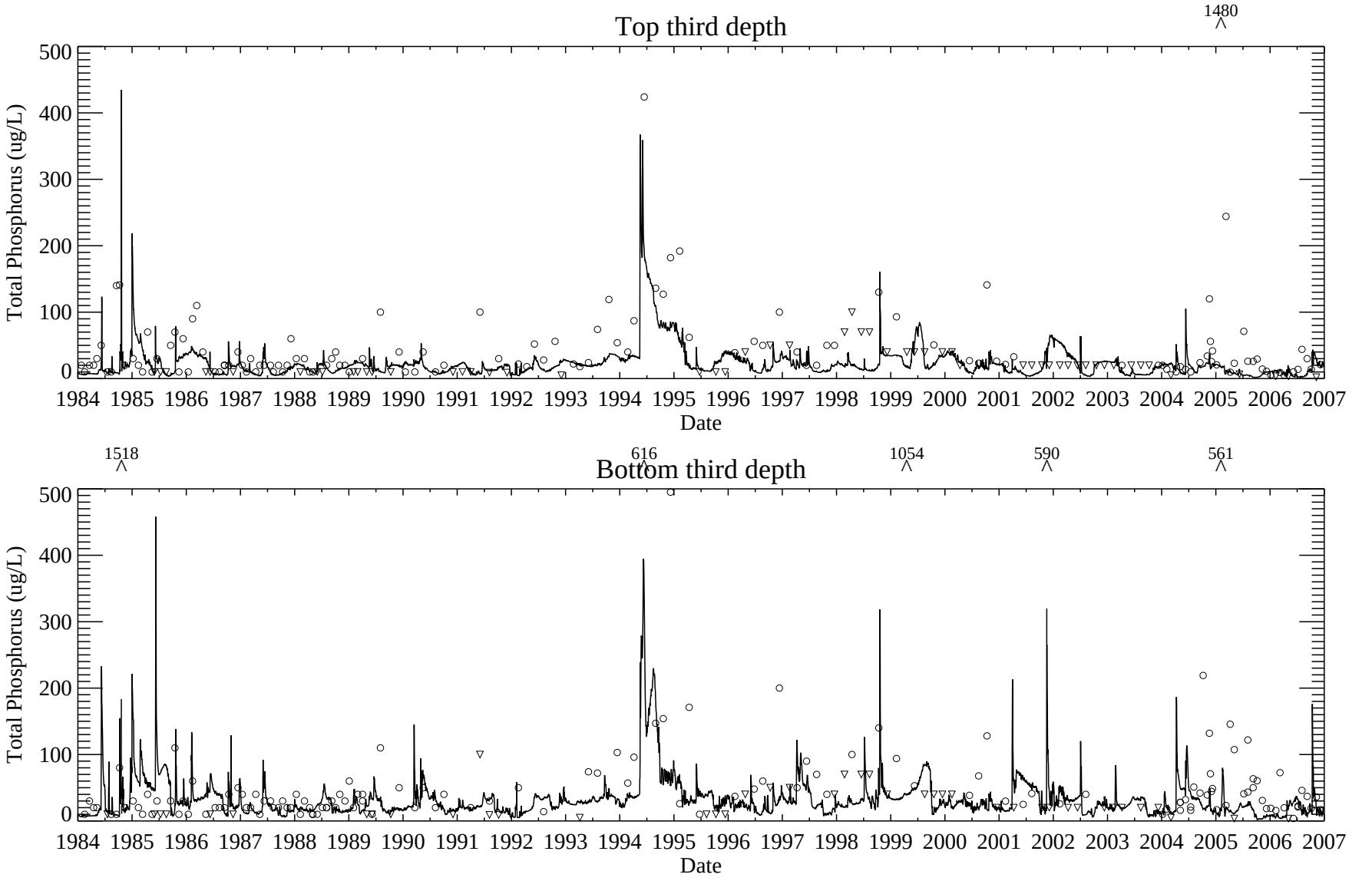

Figure 4-57. Temporal of model versus data at Turkey Bend (Segment 28) - Total Phosphorus.

Top third depth, Bottom third depth
When HAAWQ and CREMS data were measured on the same day, only CREMS data are shown. Non-detects plotted at detection limit.
Each data point is a discrete measurement except when multiple measurements were taken on the same day at the same depth (average shown).

haz/ec - D:\PARcrm\Model\Phase2_Travis\CE-QUAL-W2\postprocess\travis_temporal_forPh2rpt.pro
Thu Jan 29 13:25:16 2009

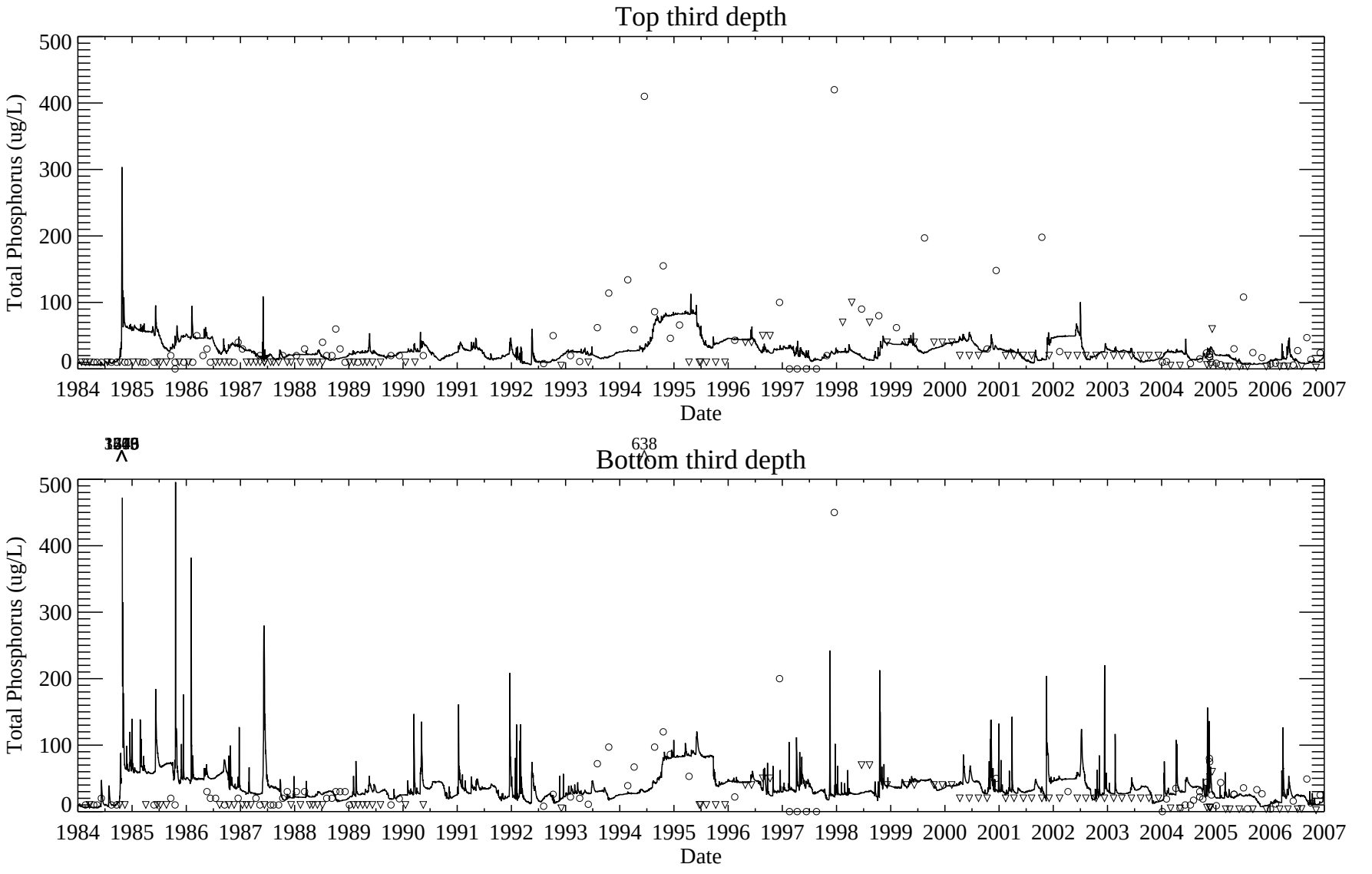

Figure 4-58. Temporal of model versus data at Sandy Creek (Segment 161) - Total Phosphorus.

Top third depth, Bottom third depth
When HAAWQ and CREMS data were measured on the same day, only CREMS data are shown. Non-detects plotted at detection limit.
Each data point is a discrete measurement except when multiple measurements were taken on the same day at the same depth (average shown).

haz/ec - D:\PARcrm\Model\Phase2_Travis\CE-QUAL-W2\postprocess\travis_temporal_forPh2rpt.pro
Thu Jan 29 13:31:07 2009

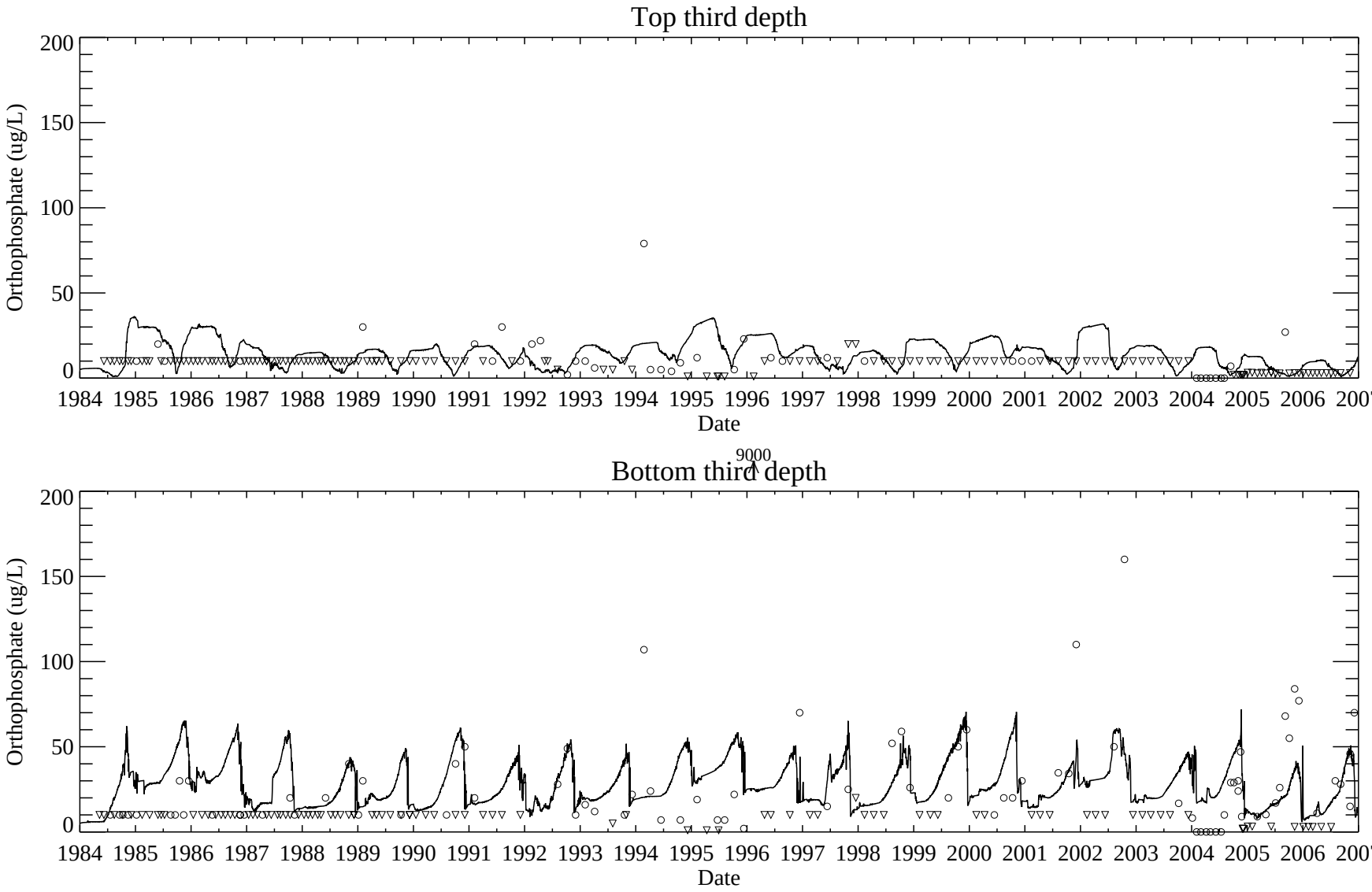

Figure 4-59. Temporal of model versus data at Mansfield Dam (Segment 93) - Orthophosphate.

Top third depth, Bottom third depth
When HAAWQ and CREMS data were measured on the same day, only CREMS data are shown. Non-detects plotted at detection limit.
Each data point is a discrete measurement except when multiple measurements were taken on the same day at the same depth (average shown).
Data in 'top third depth' excluded if collected below 10 meters (approximate starting depth of metalimnion).

haz/ec - A:\Jobs\PARcrm\model\Phase2_Travis\CE-QUAL-W2\postprocess\travis_temporal_forPh2rpt.pro
Wed Apr 08 14:49:07 2009

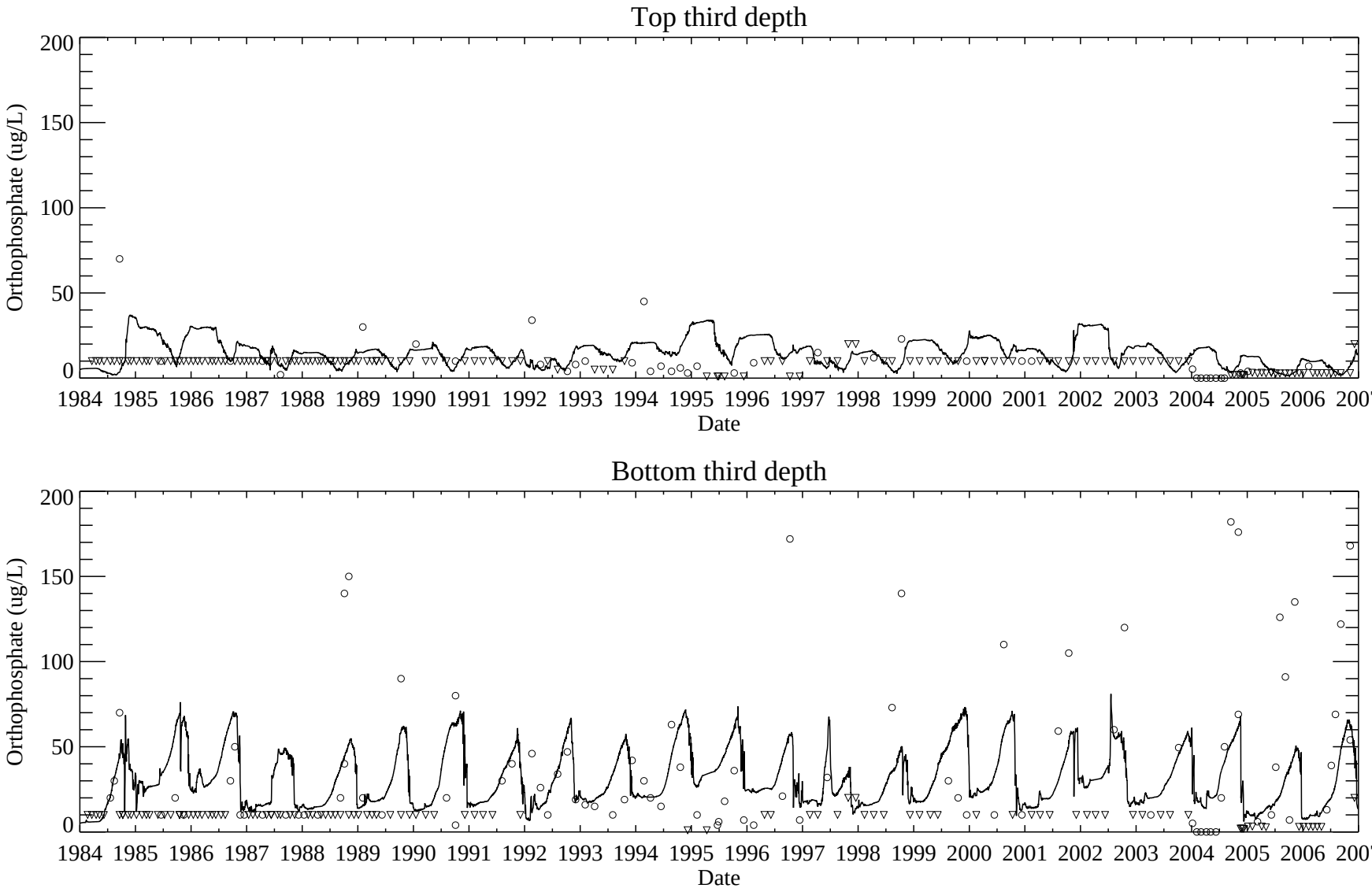

Figure 4-60. Temporal of model versus data at Arkansas Bend (Segment 78) - Orthophosphate.

Top third depth, Bottom third depth
When HAAWQ and CREMS data were measured on the same day, only CREMS data are shown. Non-detects plotted at detection limit.
Each data point is a discrete measurement except when multiple measurements were taken on the same day at the same depth (average shown).
Data in 'top third depth' excluded if collected below 10 meters (approximate starting depth of metalimnion).

haz/ec - A:\Jobs\PARcrm\model\Phase2_Travis\CE-QUAL-W2\postprocess\travis_temporal_forPh2rpt.pro
Mon Apr 13 10:38:45 2009

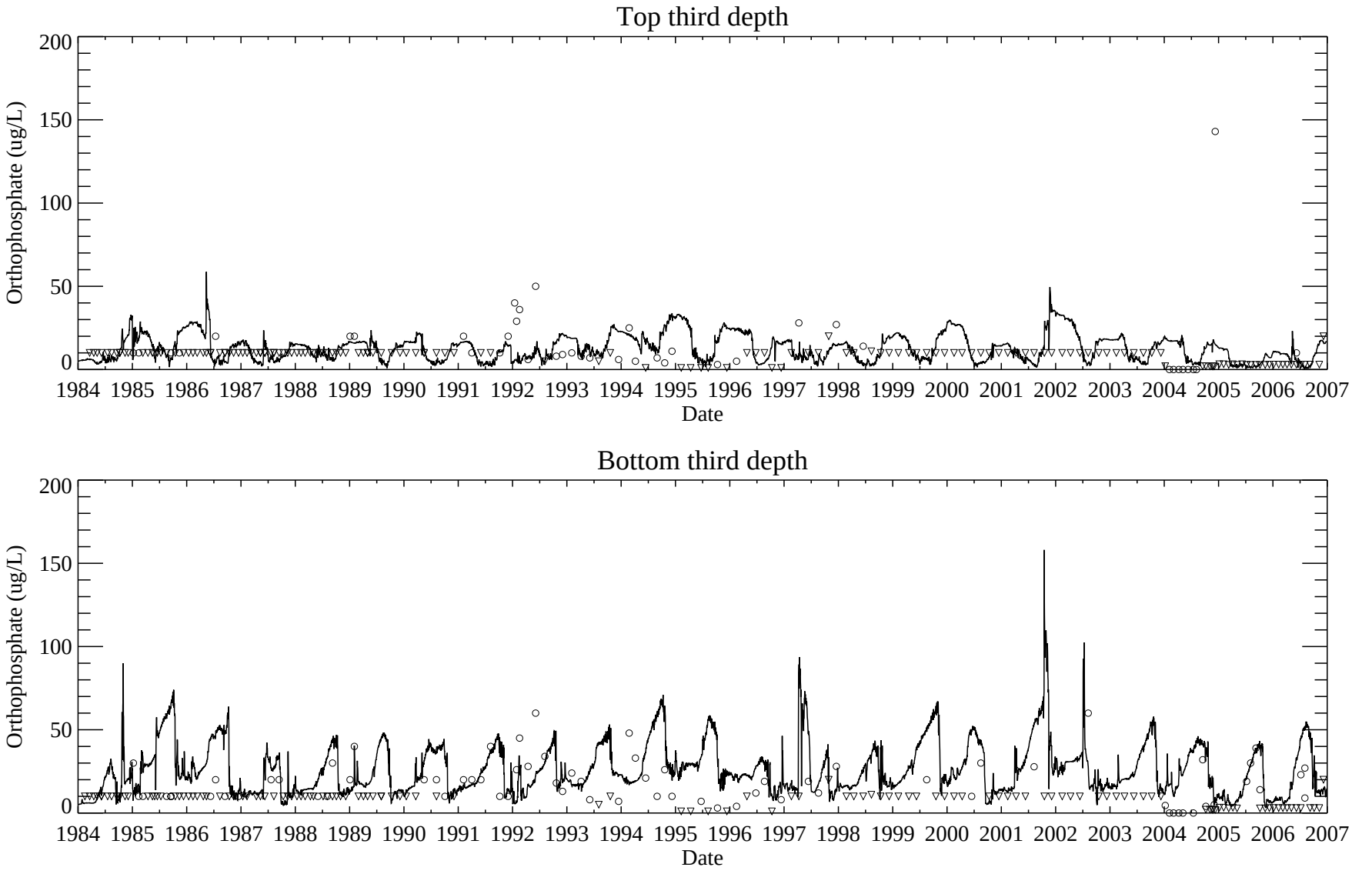

Figure 4-61. Temporal of model versus data at Pace Bend (Segment 48) - Orthophosphate.

Top third depth, Bottom third depth
When HAAWQ and CREMS data were measured on the same day, only CREMS data are shown. Non-detects plotted at detection limit.
Each data point is a discrete measurement except when multiple measurements were taken on the same day at the same depth (average shown).

haz/ec - D:\PARcrm\Model\Phase2_Travis\CE-QUAL-W2\postprocess\travis_temporal_forPh2rpt.pro
Thu Jan 29 13:06:52 2009

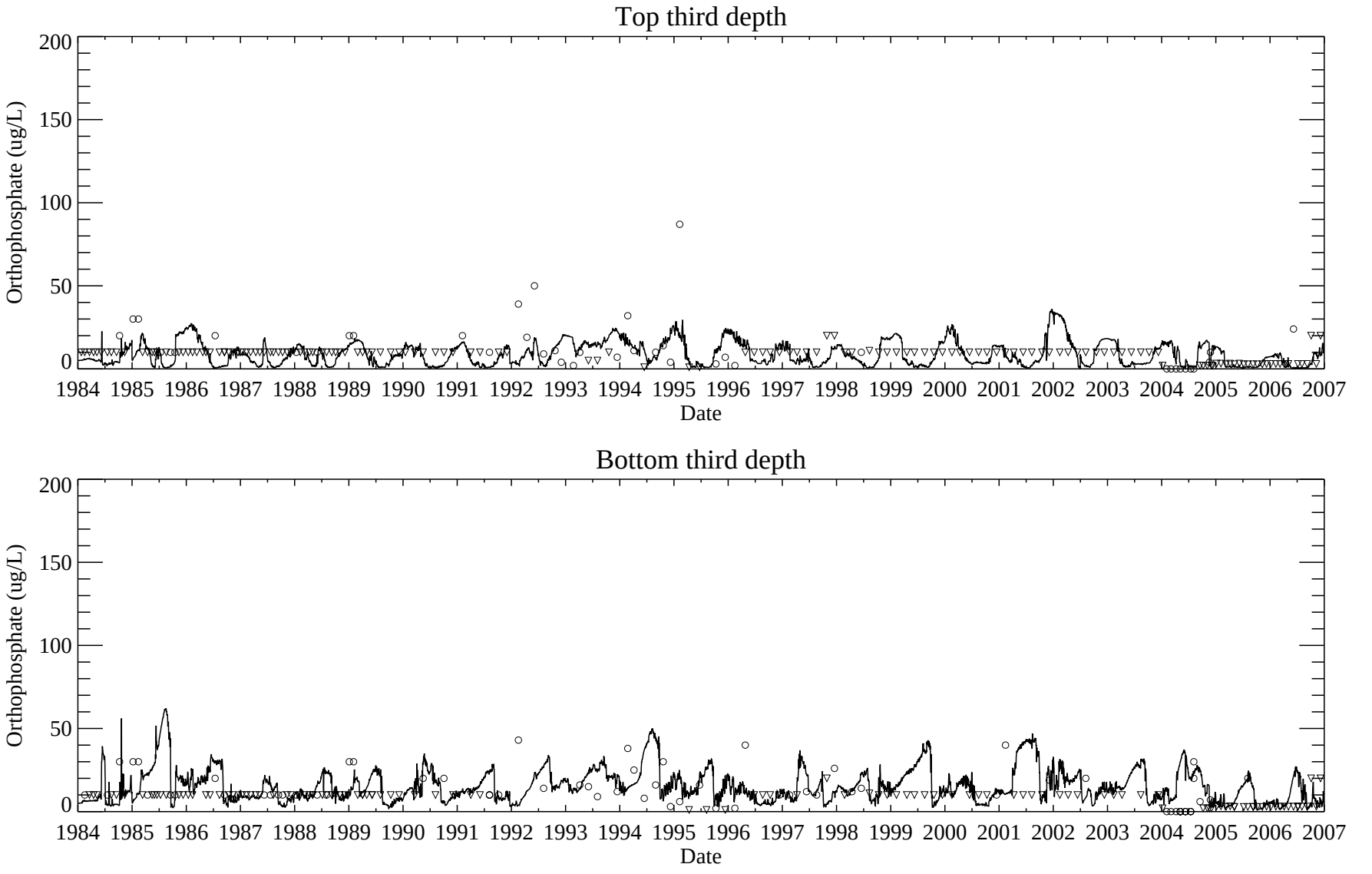

Figure 4-62. Temporal of model versus data at Turkey Bend (Segment 28) - Orthophosphate.

Top third depth, Bottom third depth
When HAAWQ and CREMS data were measured on the same day, only CREMS data are shown. Non-detects plotted at detection limit.
Each data point is a discrete measurement except when multiple measurements were taken on the same day at the same depth (average shown).

haz/ec - D:\PARcrm\Model\Phase2_Travis\CE-QUAL-W2\postprocess\travis_temporal_forPh2rpt.pro
Thu Jan 29 13:05:46 2009

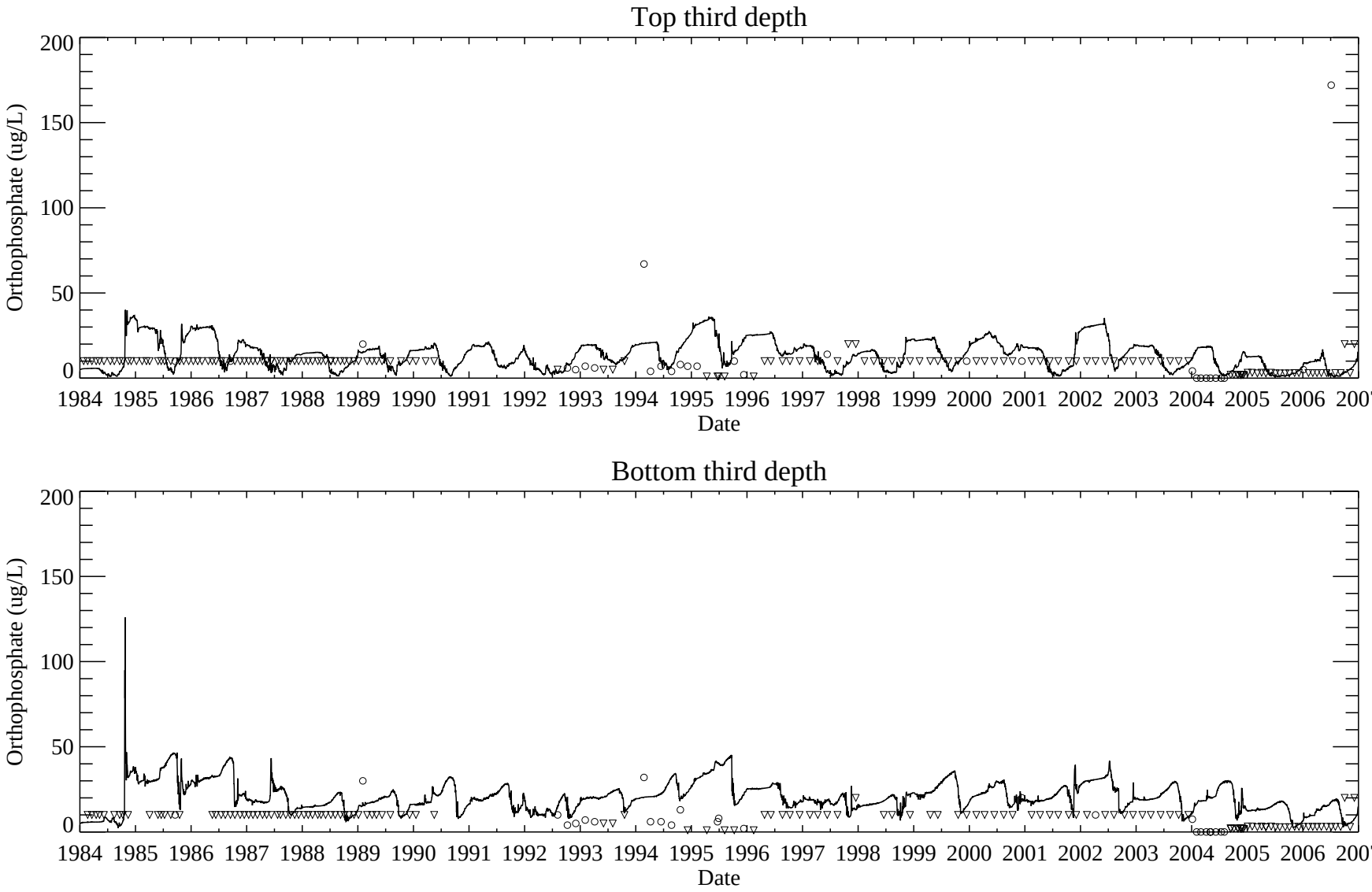

Figure 4-63. Temporal of model versus data at Sandy Creek (Segment 161) - Orthophosphate.

Top third depth, Bottom third depth
When HAAWQ and CREMS data were measured on the same day, only CREMS data are shown. Non-detects plotted at detection limit.
Each data point is a discrete measurement except when multiple measurements were taken on the same day at the same depth (average shown).

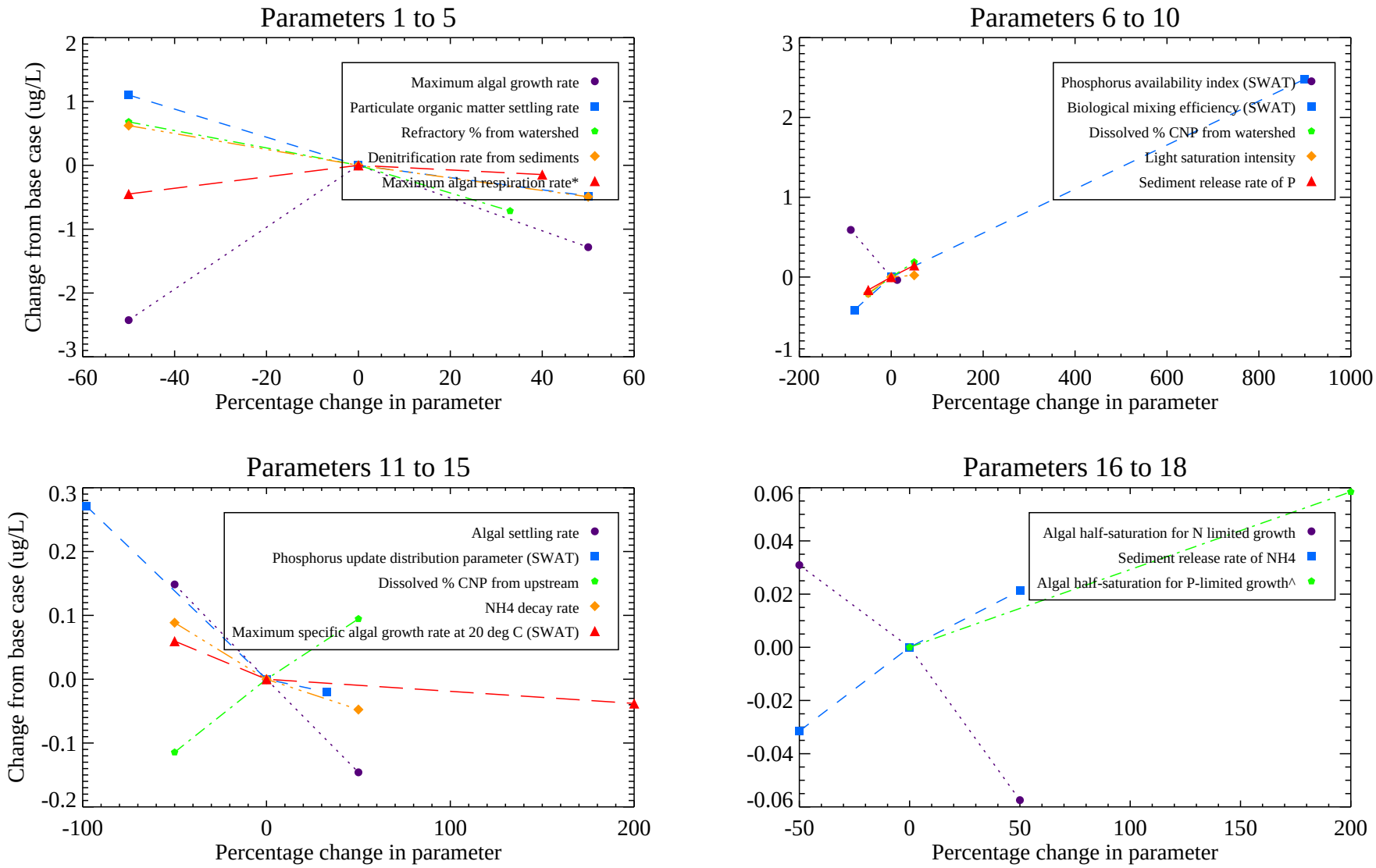

Figure 4-64. Sensitivity of chlorophyll-a predictions at Mansfield Dam, Lake Travis to 18 input parameters of the CE-QUAL-W2 model during summer months in surface waters.

Surface = 0.00 to 2.00 m; summertime = months 6 through 9.

Parameters plotted by highest ranking index (maximum of absolute slope differences between two sensitivity cases and base case).

Parameters changed one-at-a-time except for algal growth (mortality kept at 10% of growth) and dissolved % of carbon, nitrogen, and phosphorus (CNP; all varied at once).

**For high case, value changed to +40% due to model instability with +50%.*

^Only tested for high case because base case value is same as low value.

EC - D:\PARcrm\Model\Phase2_Travis\CE-QUAL-W2\postprocess\spiderplots_TravisW2sens.pro
Sun Feb 22 21:59:28 2009

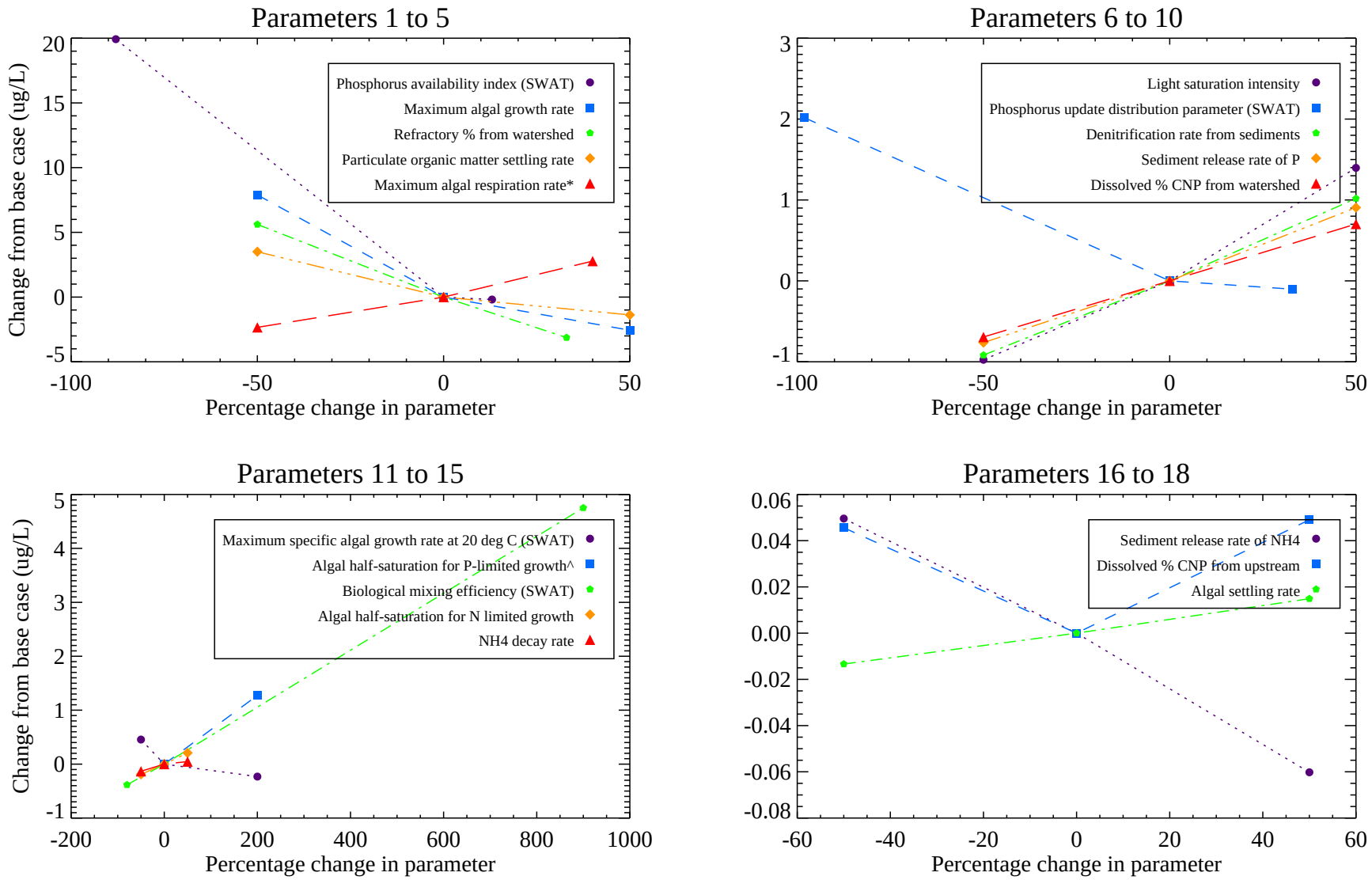

Figure 4-65. Sensitivity of orthophosphate predictions at Mansfield Dam, Lake Travis to 18 input parameters of the CE-QUAL-W2 model during summer months in surface waters.

Surface = top third depth; summertime = months 6 through 9.

Parameters plotted by highest ranking index (maximum of absolute slope differences between two sensitivity cases and base case).

Parameters changed one-at-a-time except for algal growth (mortality kept at 10% of growth) and dissolved % of carbon, nitrogen, and phosphorus (CNP; all varied at once).

**For high case, value changed to +40% due to model instability with +50%.*

^Only tested for high case because base case value is same as low value.

EC - D:\PARcrm\Model\Phase2_Travis\CE-QUAL-W2\postprocess\spiderplots_TravisW2sens.pro
Sun Feb 22 21:59:19 2009

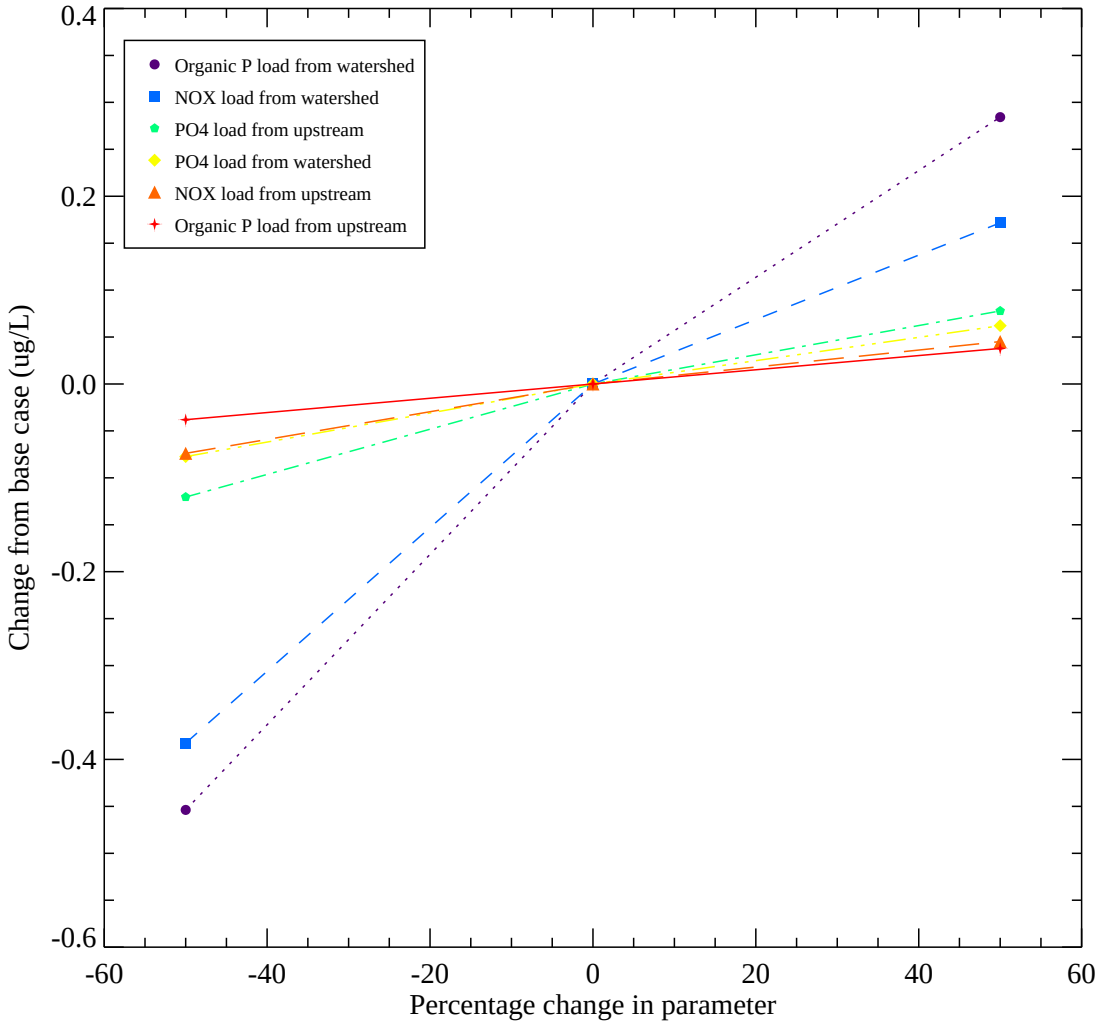

Figure 4-66. Sensitivity of chlorophyll-a predictions at Mansfield Dam, Lake Travis to 6 loading inputs of the CE-QUAL-W2 model during summer months in surface waters.

Surface = 0.00 to 2.00 m; summertime = months 6 through 9.

Parameters plotted by highest ranking index (maxiumum of absolute differences between two sensitivity cases and base case).

EC - D:\PARcrm\Model\Phase2_Travis\CE-QUAL-W2\postprocess\spiderplots_TravisW2sens_load.pro
Sun Feb 22 22:01:21 2009

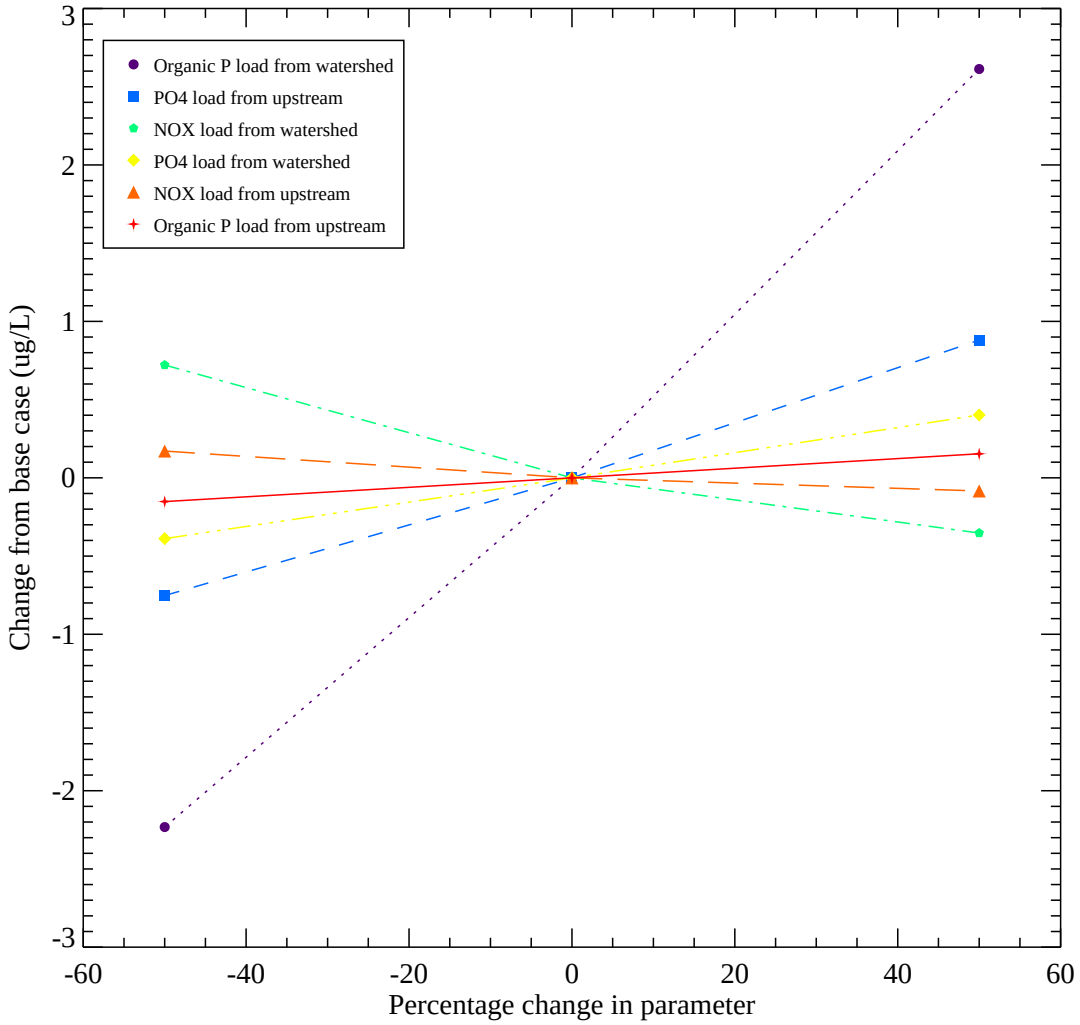

Figure 4-67. Sensitivity of orthophosphate predictions at Mansfield Dam, Lake Travis to 6 loading inputs of the CE-QUAL-W2 model during summer months in surface waters.

Surface = top third depth; summertime = months 6 through 9.

Parameters plotted by highest ranking index (maxiumum of absolute differences between two sensitivity cases and base case).

EC - D:\PARcrm\Model\Phase2_Travis\CE-QUAL-W2\postprocess\spiderplots_TravisW2sens_load.pro
Sun Feb 22 22:01:14 2009

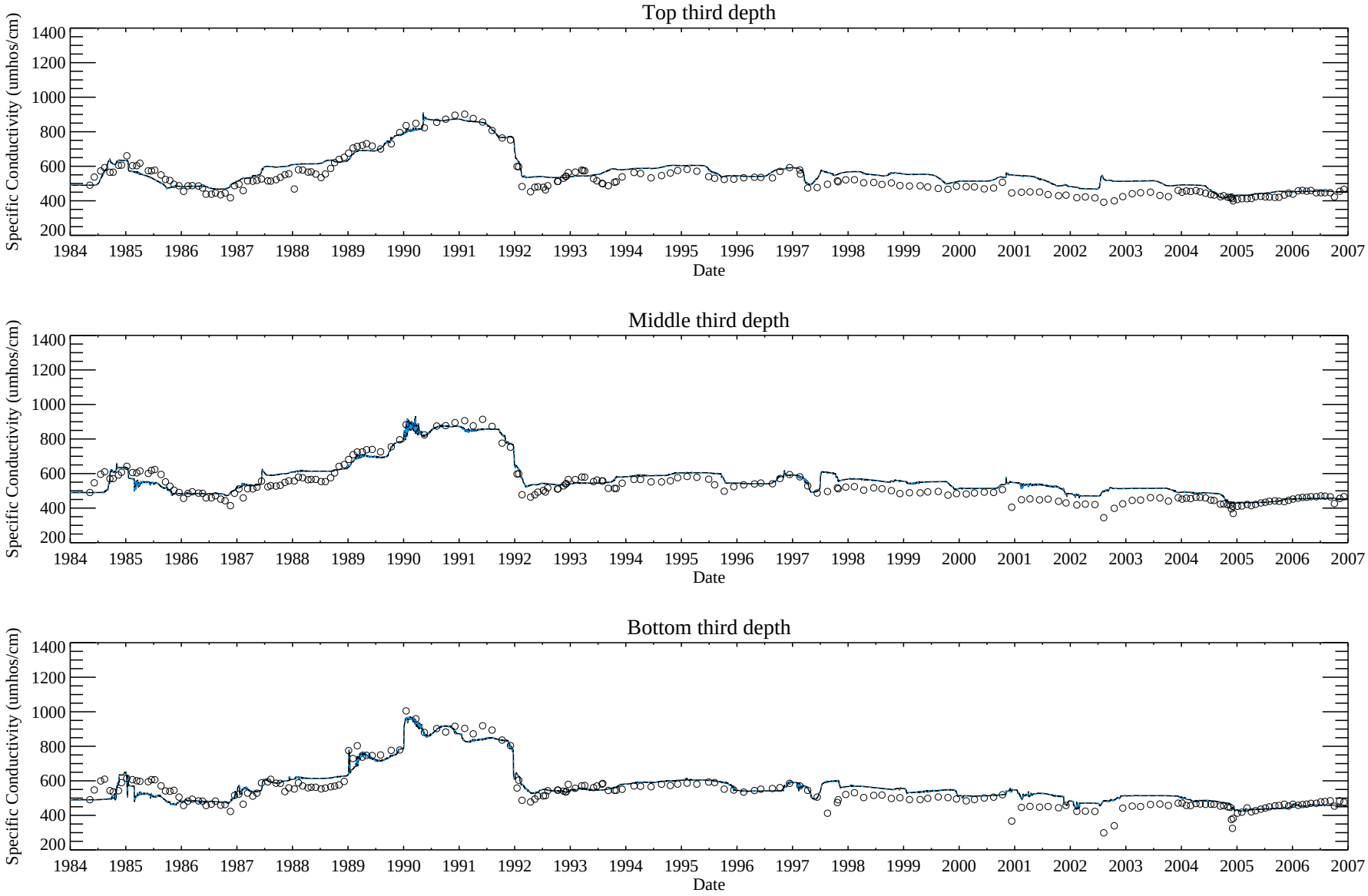

Figure 4-68. Temporal of model versus data at Mansfield Dam (Segment 93) - Specific Conductivity - Bounding calibration.

Top third depth, Middle third depth, Bottom third depth
When HAAWQ and CREMS data were measured on the same day, only CREMS data are shown. Non-detects plotted at detection limit.
Data averaged over water column depths shown.

haz/ec - D:\PARcrm\Model\Phase2_Travis\CE-QUAL-W2\postprocess\travis_temporal_forPh2rpt.pro
Sun Feb 22 21:53:40 2009

Bounding calibration Calibration Data (detect) Data (non-detect)

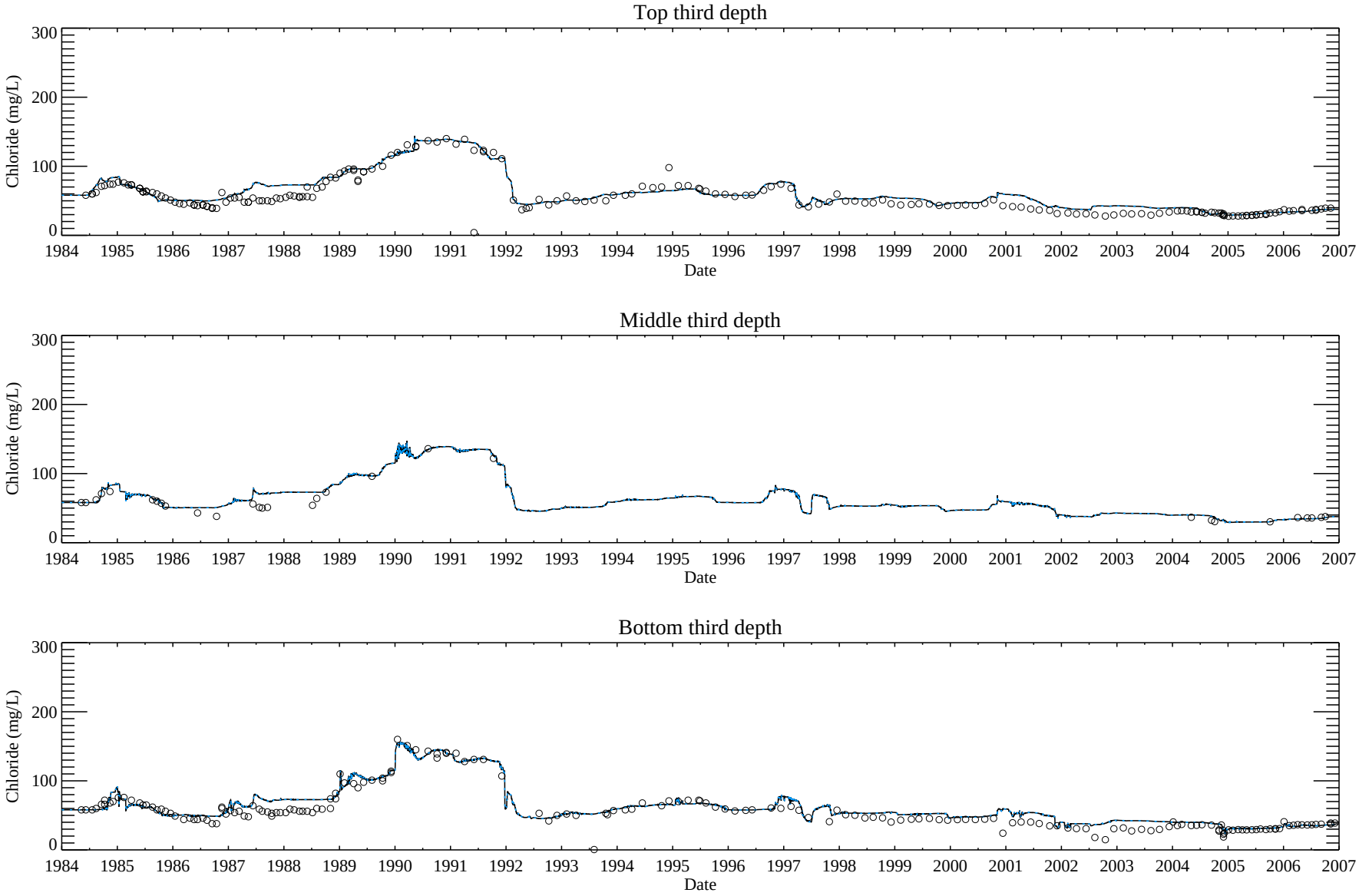

Figure 4-69. Temporal of model versus data at Mansfield Dam (Segment 93) - Chloride - Bounding calibration.

Top third depth, Middle third depth, Bottom third depth
When HAAWQ and CREMS data were measured on the same day, only CREMS data are shown. Non-detects plotted at detection limit.
Each data point is a discrete measurement except when multiple measurements were taken on the same day at the same depth (average shown).

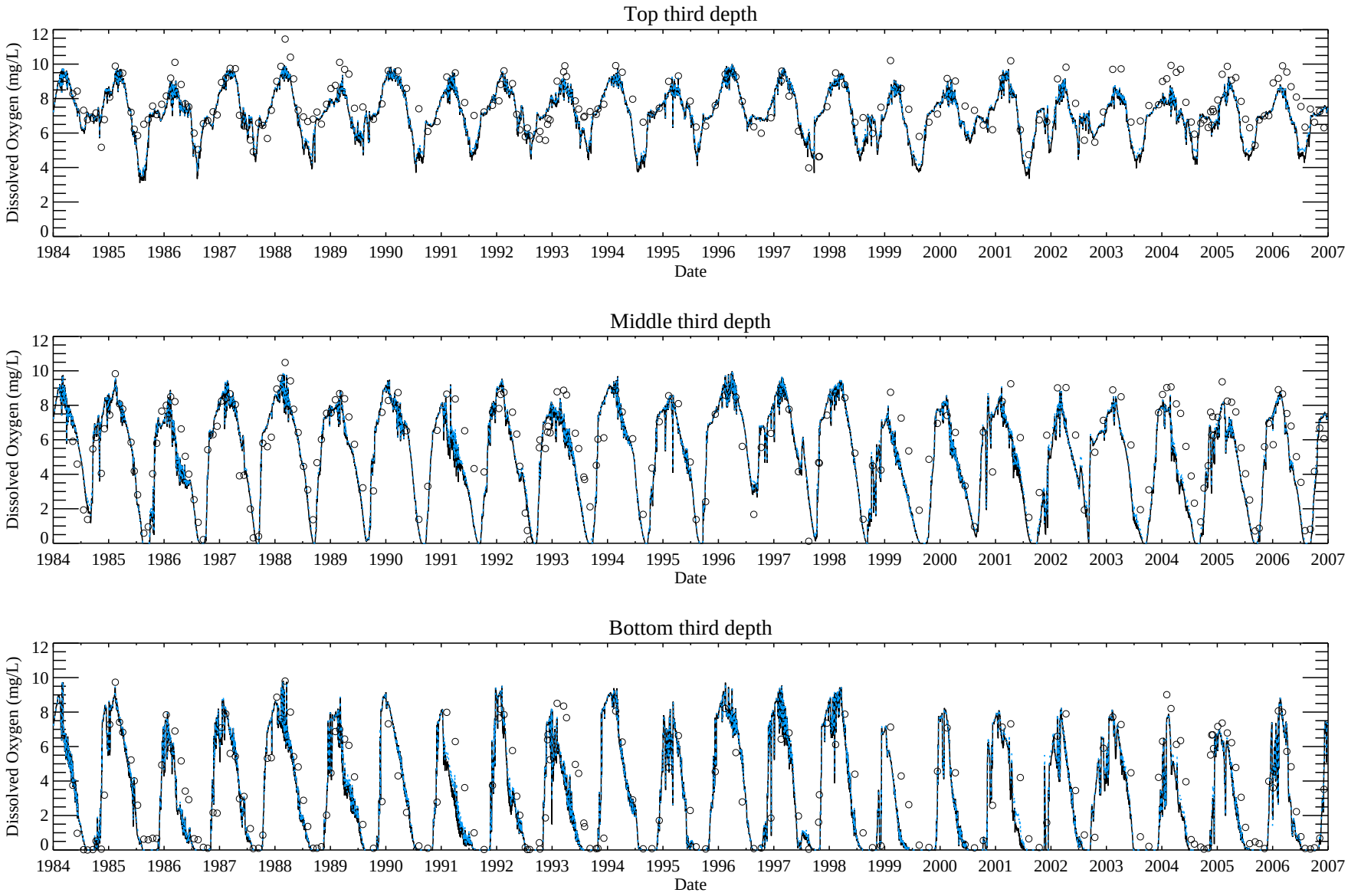

Figure 4-70. Temporal of model versus data at Mansfield Dam (Segment 93) - Dissolved Oxygen - Bounding calibration.

Top third depth, Middle third depth, Bottom third depth
When HAAWQ and CREMS data were measured on the same day, only CREMS data are shown. Non-detects plotted at detection limit.
Data averaged over water column depths shown.

haz/ec - D:\PARcrm\Model\Phase2_Travis\CE-QUAL-W2\postprocess\travis_temporal_forPh2rpt.pro
Sun Feb 22 21:31:40 2009

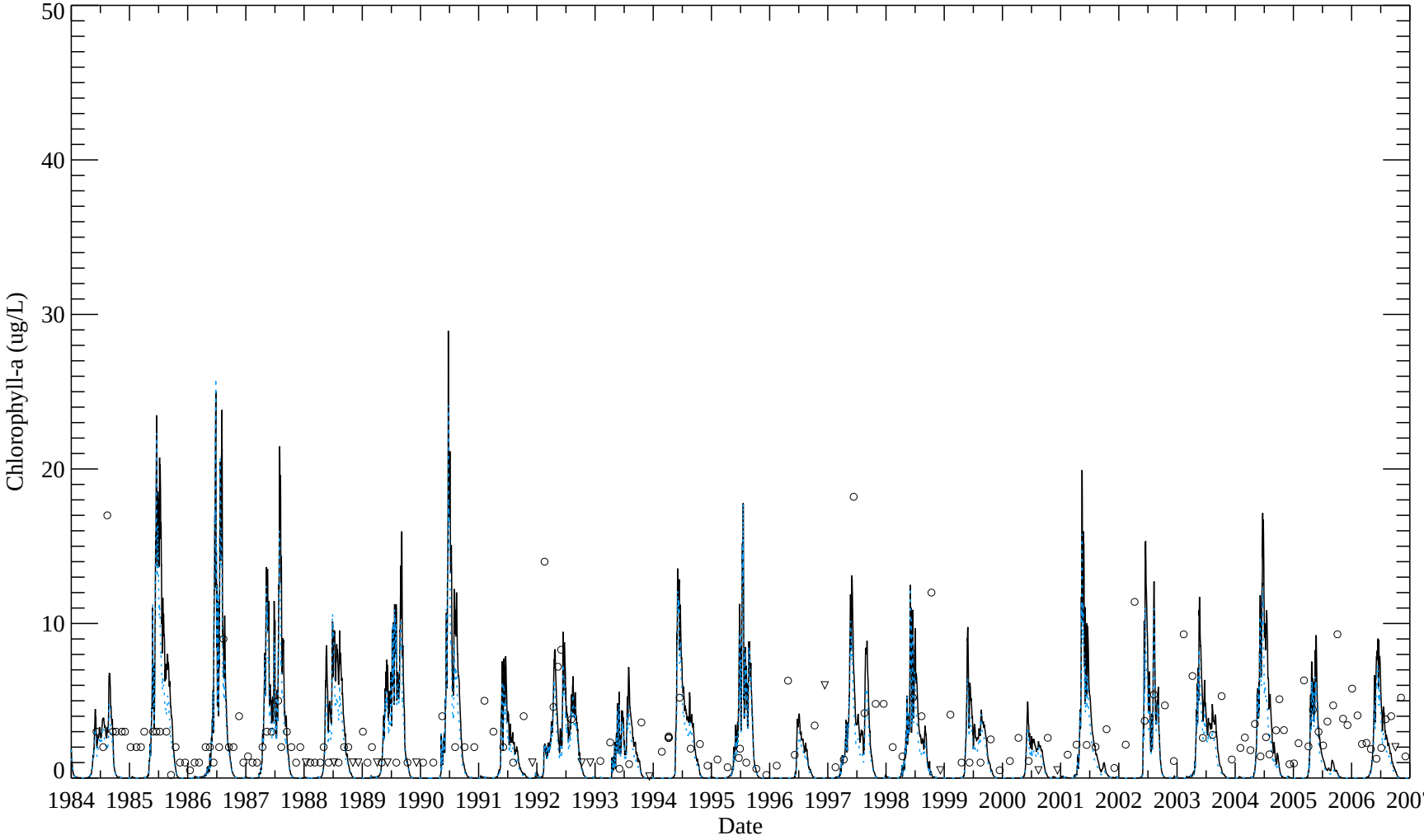

Figure 4-71. Temporal of model versus data at Mansfield Dam (Segment 93) - Chlorophyll-a - Bounding calibration.

Top 0 to 2 meters
When HAAWQ and CREMS data were measured on the same day, only CREMS data are shown. Non-detects plotted at detection limit.
Each data point is a discrete measurement except when multiple measurements were taken on the same day at the same depth (average shown).

haz/ec - D:\PARcrm\Model\Phase2_Travis\CE-QUAL-W2\postprocess\travis_temporal_forPh2rpt.pro
Sun Feb 22 21:28:00 2009

Bounding calibration Calibration Data (detect) Data (non-detect)

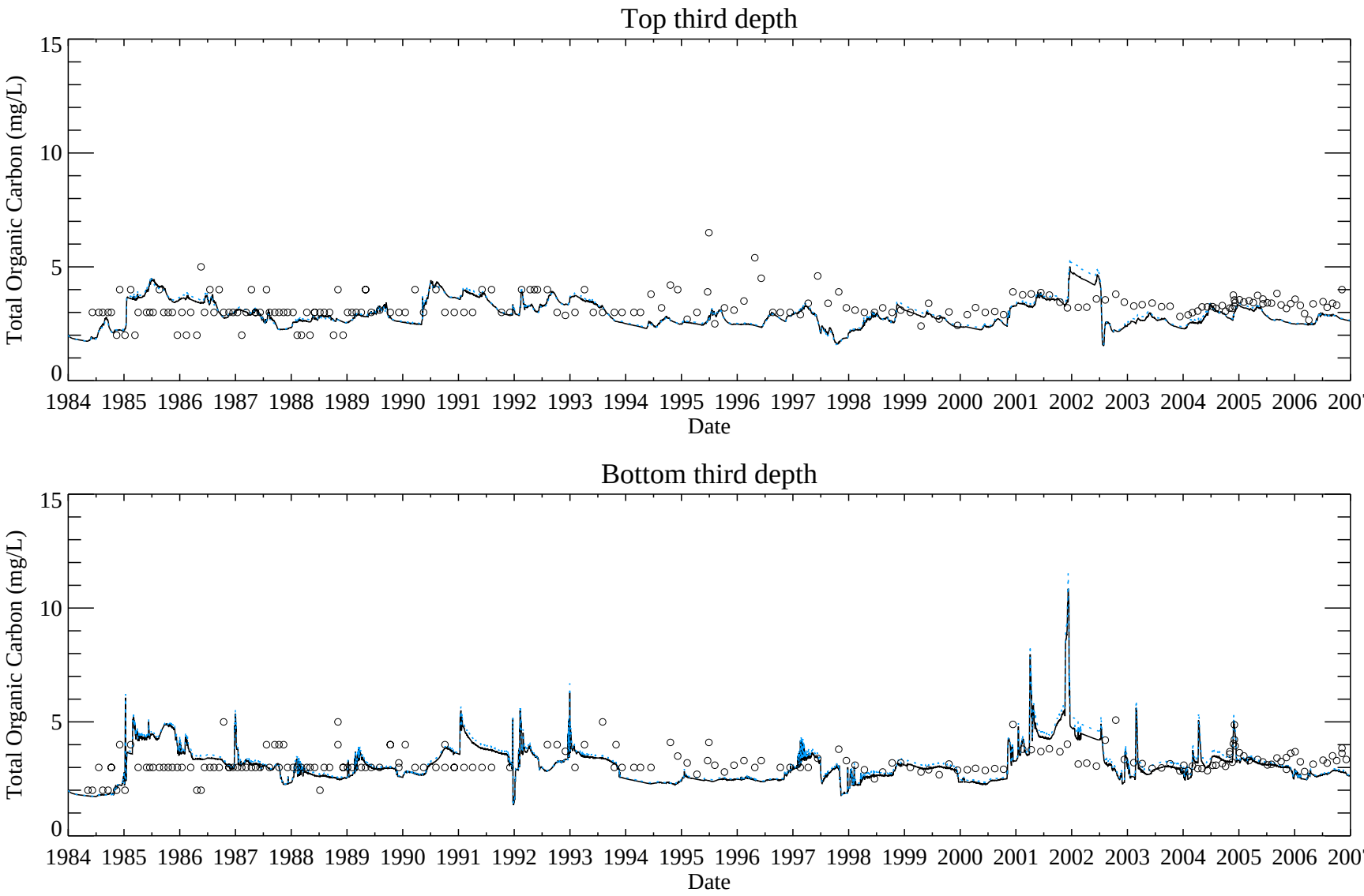

Figure 4-72. Temporal of model versus data at Mansfield Dam (Segment 93) - Total Organic Carbon - Bounding calibration.

Top third depth, Bottom third depth
When HAAWQ and CREMS data were measured on the same day, only CREMS data are shown. Non-detects plotted at detection limit.
Each data point is a discrete measurement except when multiple measurements were taken on the same day at the same depth (average shown).
Data in 'top third depth' excluded if collected below 10 meters (approximate starting depth of metalimnion).

haz/ec - A:\Jobs\PARcrm\model\Phase2_Travis\CE-QUAL-W2\postprocess\travis_temporal_forPh2rpt.pro
Mon Apr 13 11:15:47 2009

Bounding calibration Calibration Data (detect) Data (non-detect)

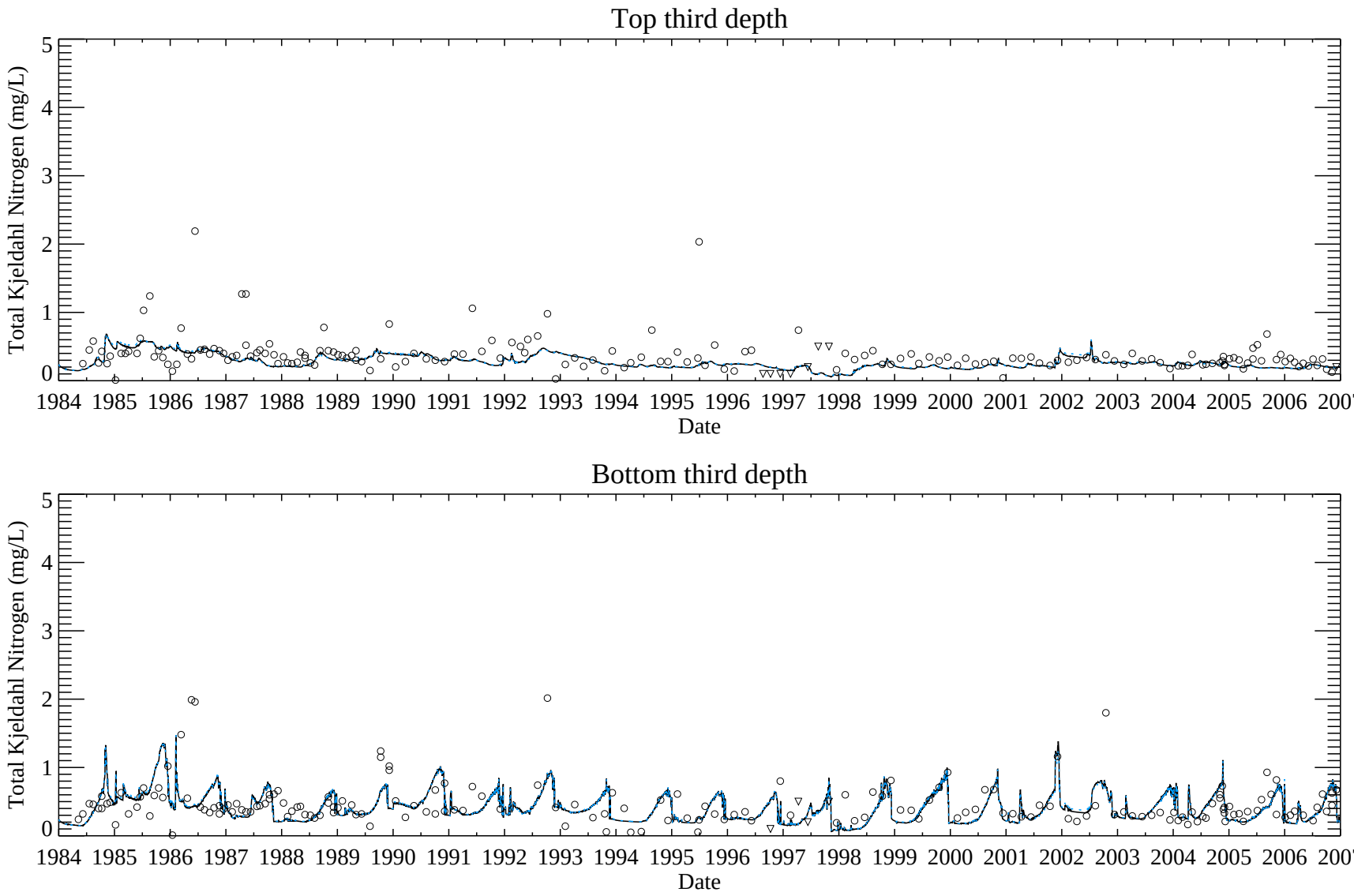

Figure 4-73. Temporal of model versus data at Mansfield Dam (Segment 93) - Total Kjeldahl Nitrogen - Bounding calibration.

Top third depth, Bottom third depth
When HAAWQ and CREMS data were measured on the same day, only CREMS data are shown. Non-detects plotted at detection limit.
Each data point is a discrete measurement except when multiple measurements were taken on the same day at the same depth (average shown).
Data in 'top third depth' excluded if collected below 10 meters (approximate starting depth of metalimnion).

haz/ec - A:\Jobs\PARcrm\model\Phase2_Travis\CE-QUAL-W2\postprocess\travis_temporal_forPh2rpt.pro
Mon Apr 13 11:23:03 2009

Bounding calibration Calibration Data (detect) Data (non-detect)

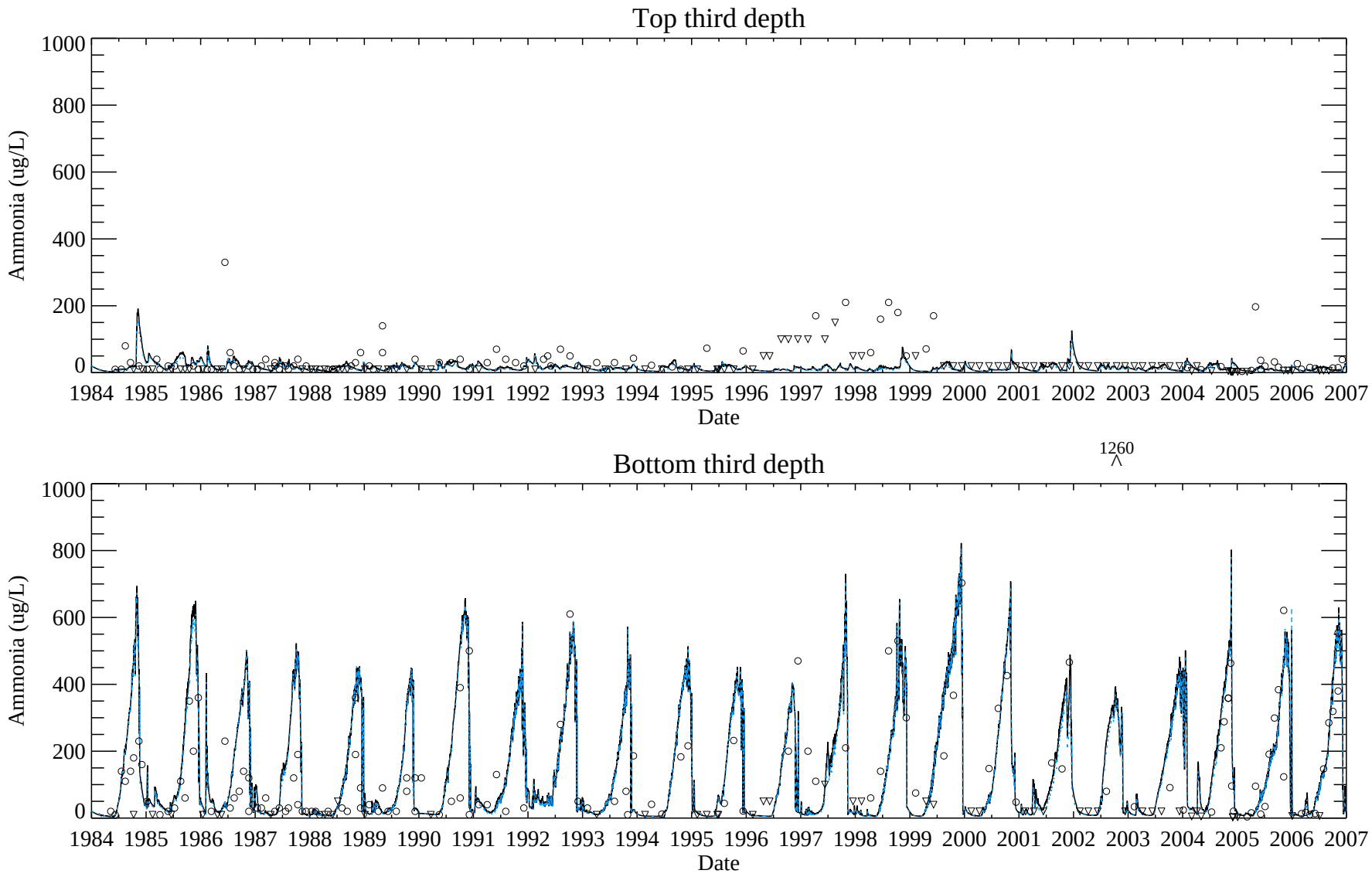

Figure 4-74. Temporal of model versus data at Mansfield Dam (Segment 93) - Ammonia - Bounding calibration.

Top third depth, Bottom third depth
When HAAWQ and CREMS data were measured on the same day, only CREMS data are shown. Non-detects plotted at detection limit.
Each data point is a discrete measurement except when multiple measurements were taken on the same day at the same depth (average shown).
Data in 'top third depth' excluded if collected below 10 meters (approximate starting depth of metalimnion).

haz/ec - A:\Jobs\PARcrm\model\Phase2_Travis\CE-QUAL-W2\postprocess\travis_temporal_forPh2rpt.pro
Mon Apr 13 11:25:26 2009

Bounding calibration Calibration Data (detect) Data (non-detect)

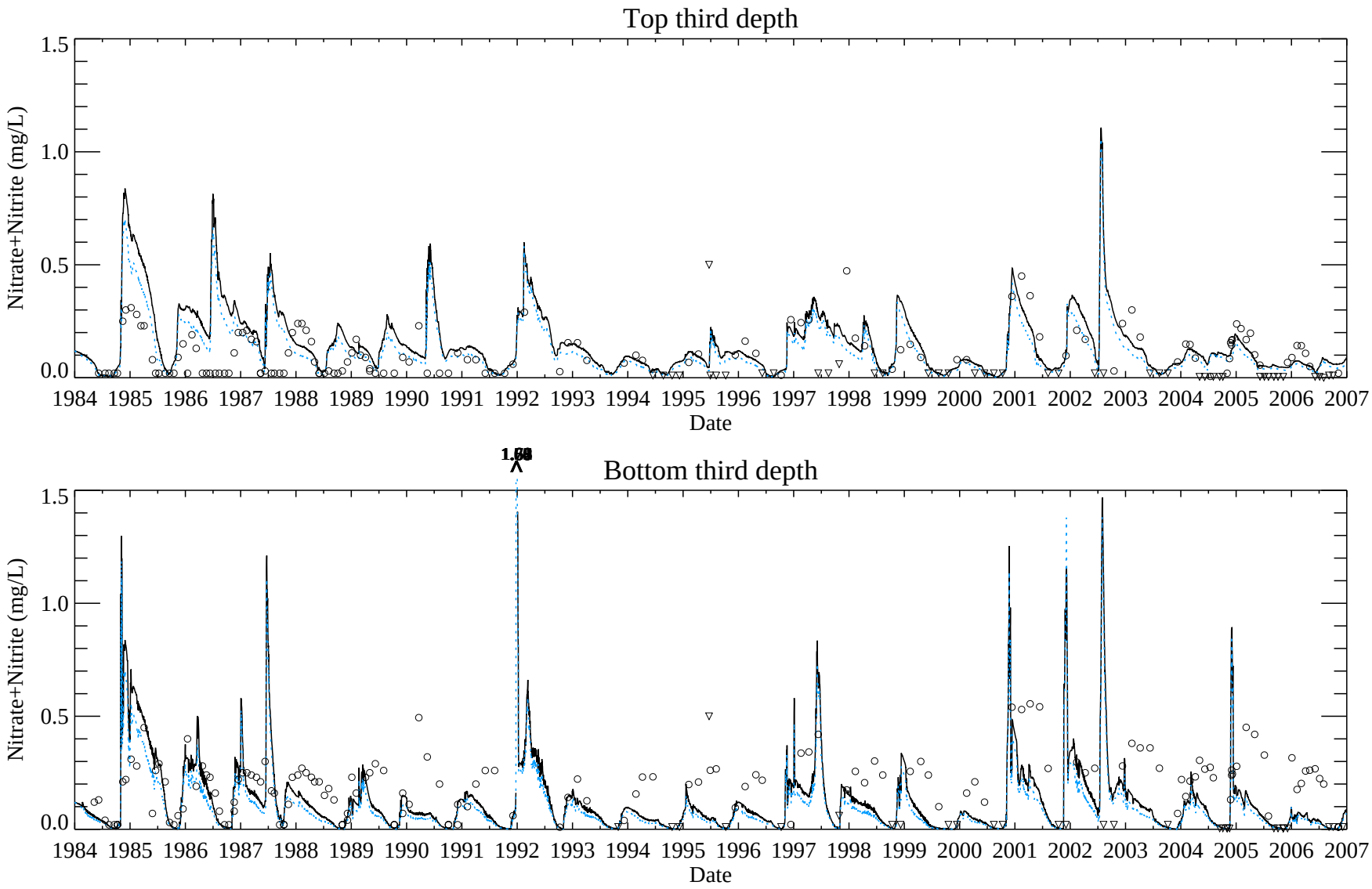

Figure 4-75. Temporal of model versus data at Mansfield Dam (Segment 93) - Nitrate+Nitrite - Bounding calibration.

Top third depth, Bottom third depth
When HAAWQ and CREMS data were measured on the same day, only CREMS data are shown. Non-detects plotted at detection limit.
Each data point is a discrete measurement except when multiple measurements were taken on the same day at the same depth (average shown).
Data in 'top third depth' excluded if collected below 10 meters (approximate starting depth of metalimnion).

haz/ec - A:\Jobs\PARcrm\model\Phase2_Travis\CE-QUAL-W2\postprocess\travis_temporal_forPh2rpt.pro
Mon Apr 13 11:18:16 2009

Bounding calibration Calibration Data (detect) Data (non-detect)

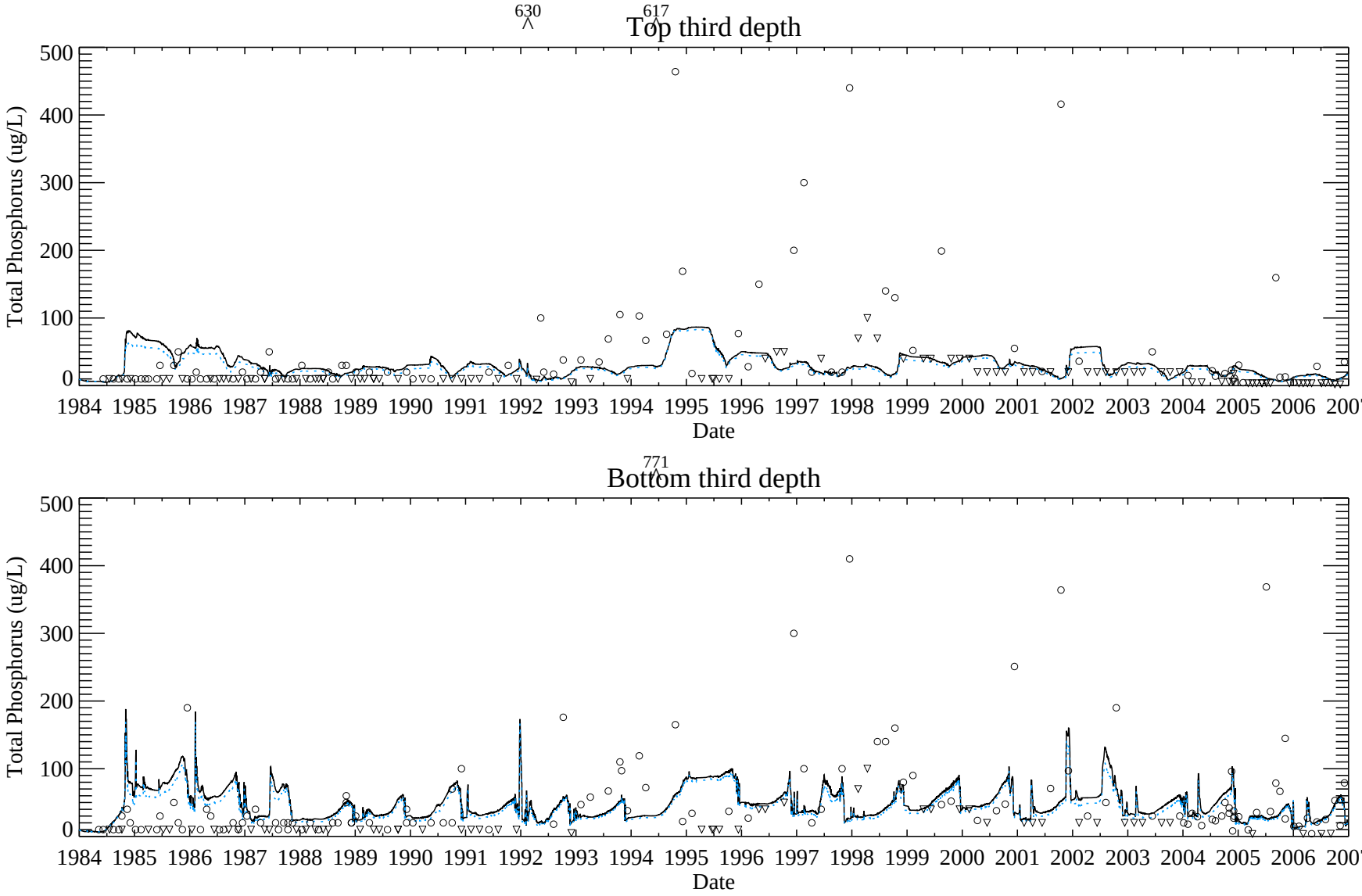

Figure 4-76. Temporal of model versus data at Mansfield Dam (Segment 93) - Total Phosphorus - Bounding calibration.

Top third depth, Bottom third depth
When HAAWQ and CREMS data were measured on the same day, only CREMS data are shown. Non-detects plotted at detection limit.
Each data point is a discrete measurement except when multiple measurements were taken on the same day at the same depth (average shown).
Data in 'top third depth' excluded if collected below 10 meters (approximate starting depth of metalimnion).

haz/ec - A:\Jobs\PARcrm\model\Phase2_Travis\CE-QUAL-W2\postprocess\travis_temporal_forPh2rpt.pro
Mon Apr 13 11:20:38 2009

Bounding calibration Calibration Data (detect) Data (non-detect)

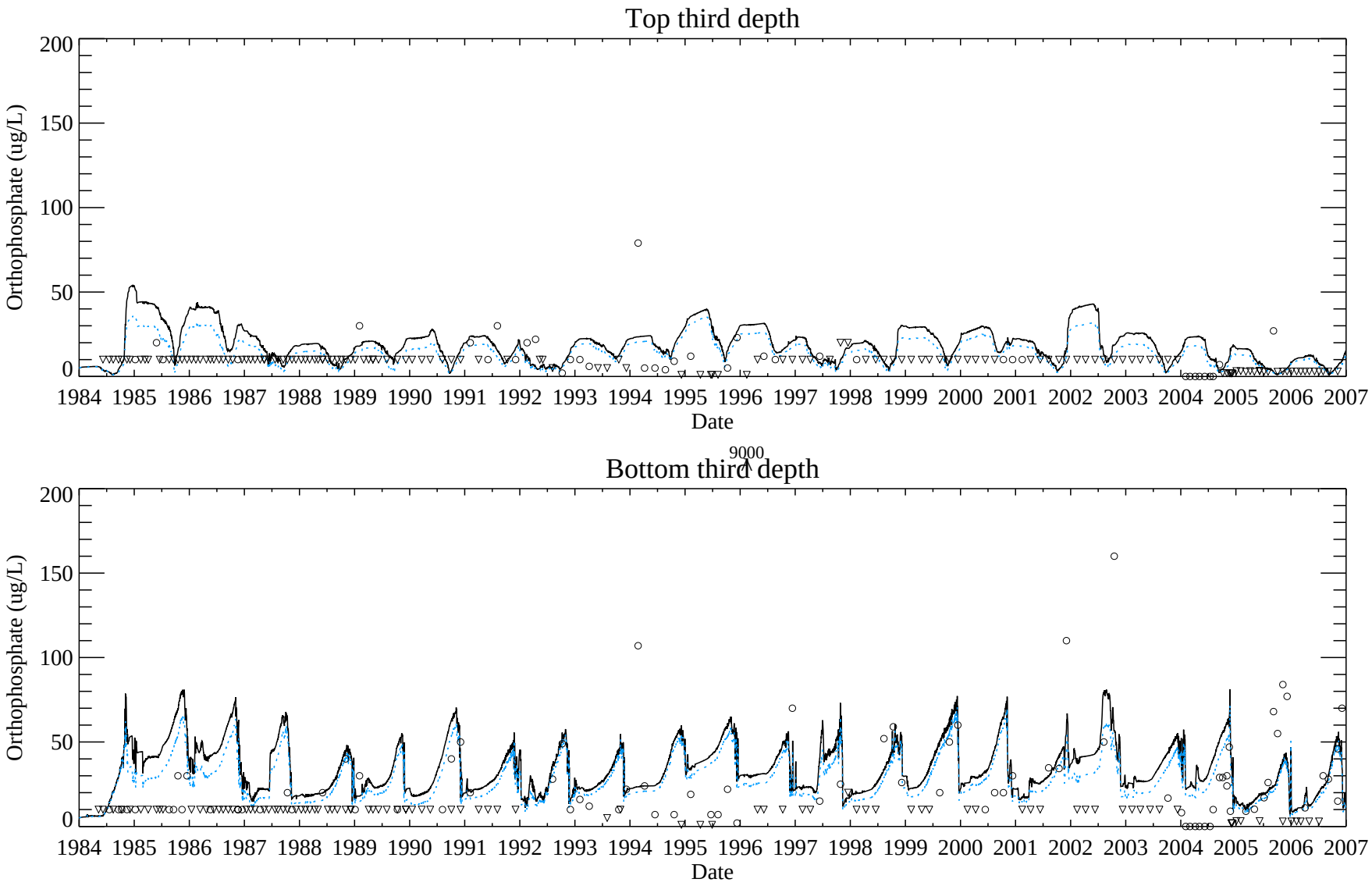

Figure 4-77. Temporal of model versus data at Mansfield Dam (Segment 93) - Orthophosphate - Bounding calibration.

Top third depth, Bottom third depth
When HAAWQ and CREMS data were measured on the same day, only CREMS data are shown. Non-detects plotted at detection limit.
Each data point is a discrete measurement except when multiple measurements were taken on the same day at the same depth (average shown).
Data in 'top third depth' excluded if collected below 10 meters (approximate starting depth of metalimnion).

haz/ec - A:\Jobs\PARcrm\model\Phase2_Travis\CE-QUAL-W2\postprocess\travis_temporal_forPh2rpt.pro
Mon Apr 13 11:13:23 2009

Bounding calibration Calibration Data (detect) Data (non-detect)

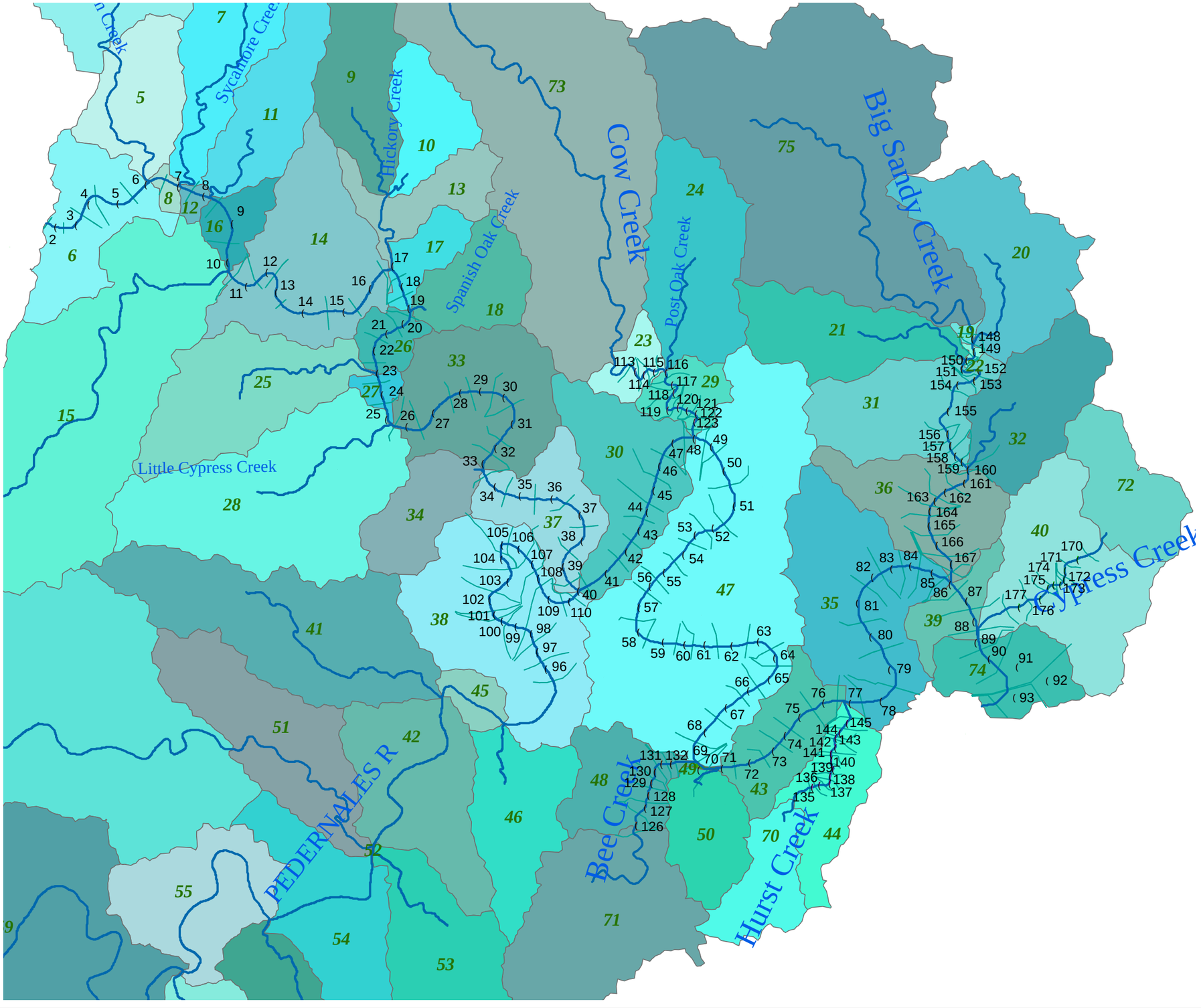

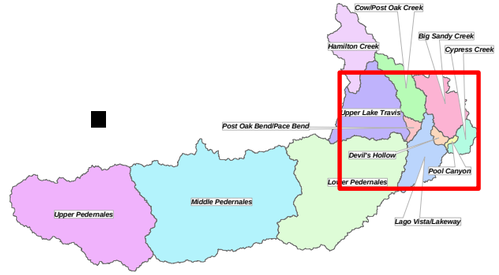

2 1 0 2 Miles

Legend

- Surface water
- Cross-section lines
- Cypress Creek segment numbers
- Hurst Creek segment numbers
- Bee Creek segment numbers
- Big Sandy Creek segment numbers
- Cow Creek segment numbers
- Pedernales River segment numbers
- Lake Travis segment numbers

Figure 5-1.

Watershed and lake model segmentation for Lake Travis.

ANCHOR QEA PARSONS

PARcrm:161 **February 2009**

EC - \\Emily\d_drive\PARcrm\GIS\Lake_Travis_Phase2\SWATsubbasins_CEQUALW2segments\lake_travis_model_segmentation_20090206.mxd

APPENDIX A

Colorado River Environmental Models
Lake Travis Phase II
Monthly In-Field Chlorophyll-*a* Measurements

ANCHOR QEA

PARSONS

Colorado River Environmental Models
Lake Travis Phase II
Monthly In-Field Chlorophyll *a* Measurements

The Lower Colorado River Authority (LCRA) contracted with Ecological Communications Corporation (EComm), in association with Parsons Water and Infrastructure (PARSONS), to collect monthly chlorophyll *a* data at 14 locations in Lake Travis. All data were collected from the surface water (depth to one meter) using a Turner Model 10-AU-005-CE portable fluorometer. In addition, for each day in the field, a single laboratory verification sample was collected, stored on ice, and analyzed by the LCRA's environmental laboratory. The laboratory results were then used to develop a correction factor that was applied to the fluorometer measurements collected the same day as the lab sample. The sample sites included Turkey Bend, Carpenter Bend, Pedernales Bend (in the Pedernales River), Cow Creek Cove (in Cow Creek), Pace Bend, Thurman Bend, Bee Creek Cove, Anderson Bend, Hurst Creek Cove, Arkansas Bend, Sandy Creek Cove, Starnes Island, Cypress Creek Cove, and Mansfield Dam (Figure 1).

All field fluorometry measurements, correction factors, and the associated adjusted measurements for each sample run are presented in tables found in the Appendices at the end of this report. Table 1 represents a summary of these data (giving the mean chlorophyll *a* measurement at each site for each month), while Figure 2 gives a graphical representation of this same summary data. It should be noted that a "zero" was entered in the summary table for any raw fluorometry measurements that measured in the negative numbers. Upon discussions with LCRA staff, it was determined that when there is virtually no chlorophyll *a* to fluoresce, aberrant readings on the flourometer may occur.

Table 1. Mean Chlorophyll *a* values, after application of laboratory correction factor, for 14 stations in Lake Travis, Texas.

Site #	**Site Location**	**Mean Chl *a* (ug/L)**			
		March 2006	**April 2006**	**May 2006**	**June 2006**
1	Turkey Bend	5.1	5.3	28.6	8.7
2	Carpenter Bend	8.2	5.7	11.2	1.2
3	Pedernales Bend	8.4	12.2	21.4	12.4
4	Cow Cr. Cove	8.2	0.0	26.75	5.6
5	Pace Bend	8.0	0.0	10.6	0.0
6	Thurman Bend	2.9	0.0	0.1	0.0
7	Bee Cr. Cove	2.9	0.0	3.9	1.5
8	Anderson Bend	2.5	2.7	1.1	0.0
9	Hurst Cr. Cove	2.5	1.9	0.1	0.0
10	Arkansas Bend	2.3	1.6	0.8	0.0
11	Sandy Cr. Cove	2.8	0.4	0.4	0.0
12	Starnes Island	2.5	0.4	1.7	0.0
13	Cypress Cr. Cove	3.6	1.1	0.0	0.0
14	Dam	1.8	1.3	0.0	0.0

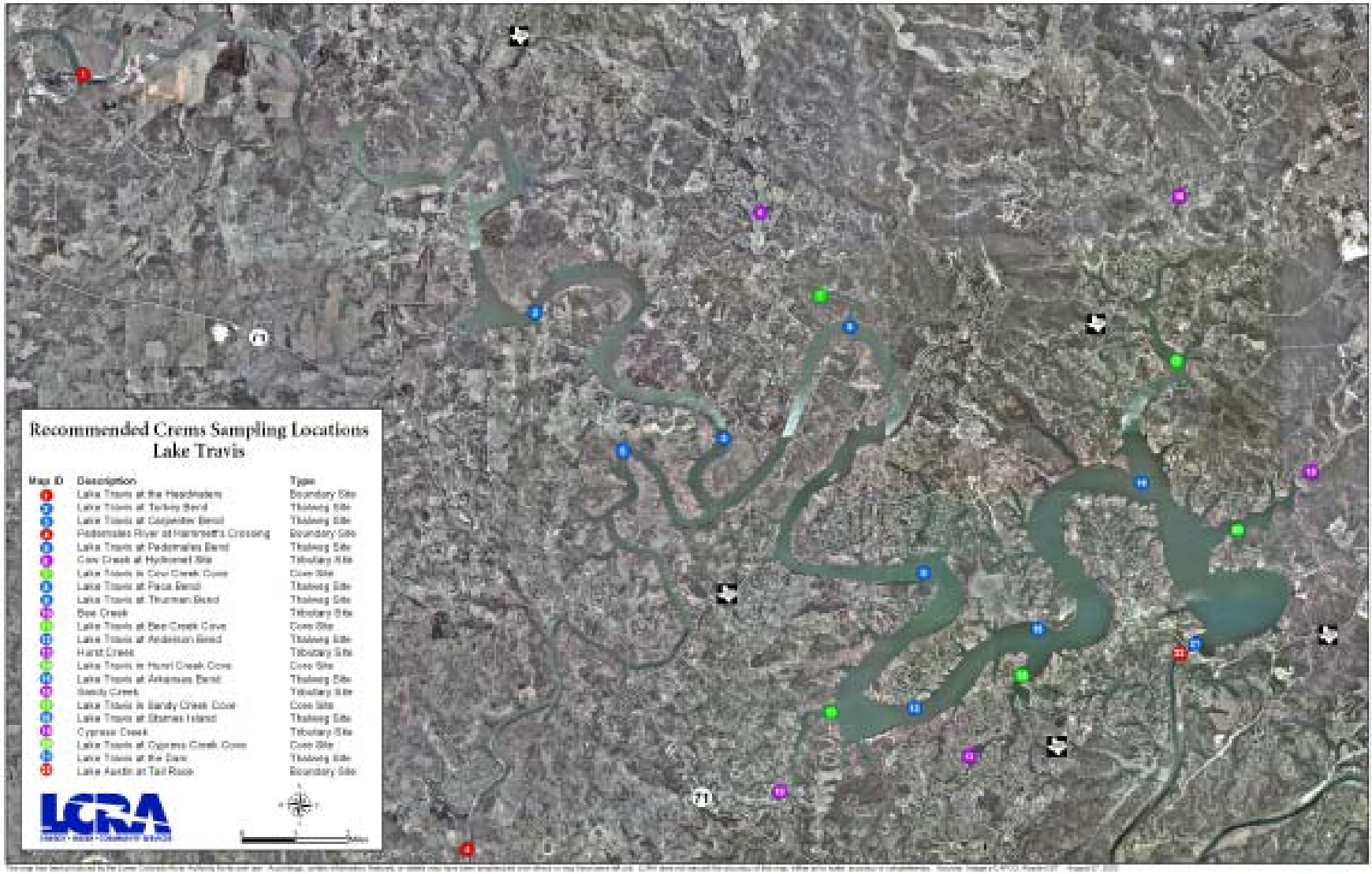

Figure 1. Lake Travis sample locations. Chlorophyll *a* samples were taken only at those locations depicted with green or blue dots.

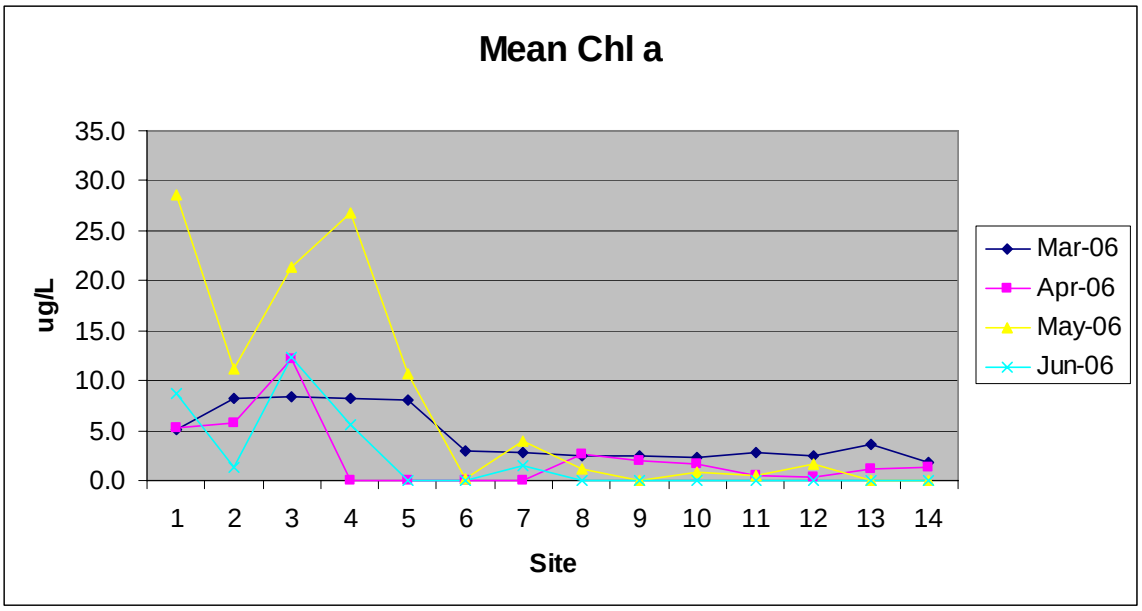

Figure 2. Mean Chlorophyll *a* values, after application of laboratory correction factor, for 14 stations in Lake Travis, Texas. (Site #'s locations are identified in Table 1.)

Such aberrant reading on the fluorometer appeared to occur at several sites during April, May, and June. During the same time period, LCRA staff observed sechhi depths in excess of 25 m, lending credence to the low fluorometry readings.

Notable Observations to Date

Chlorophyll *a* measurements were consistently higher in the upper regions of the lake than at locations closer to the Dam throughout the duration of the study. Nevertheless, data collected on May 17 for the upper lake locations (Turkey Bend, Carpenter Bend, Pedernales, Pace Bend, Cow Creek, and Thurman Bend) appeared to be substantially higher in comparison to the other sample dates (with the exception of June 14, 2006). One possible cause may be that the laboratory analyses for the May 17 sample was significantly higher than the field measurement (26.5 ug/L and 2.59 ug/L, respectively). Thus the correction factor for the field measurements (10.2) was higher than any other sample date, including those locations sampled the following day (May 18, 2006).

In general, Chlorophyll *a* samples were highest in March, fell slightly in April, went up substantially in the upper regions of the lake but went down in the lower regions of the lake during May, and were, overall, lowest in most locations in June. The highest readings were consistently found at the Pedernales location.

The correction factors seem to escalate over time, ranging from 1.0 on the first sample date to 19.5 on the last (Table 2), even though the fluorometer was recalibrated at the start of the May sample period. The correction factors for May 17, 2006 and June 14, 2006 appear particularly high. Interestingly, the flourometer readings in the field (see Appendicies) for adjacent sample dates (May 17 and 18, and June 13 and 14) do not appear to vary in a similar fashion.

Table 2. Correction Factors for each of the sample dates (Correction factors were calculated by dividing the laboratory result by the associated field measurement.

Sample Date	Correction Factor
March 21, 2006	1.0
March 22, 2006	1.5
April 11, 2006	5.0
April 12, 2006	4.5
May 17, 2006	10.2
May 18, 2006	7.0
June 13, 2006	8.2
June 14, 2007	19.5

APPENDIX B

Seasonal Phytoplankton – Zooplankton Dynamics in Lake Travis, Texas

ANCHOR QEA

PARSONS

Seasonal Phytoplankton – Zooplankton Dynamics in Lake Travis, Texas

CD-ROM Data Report Overview

By

M. A. Wallace
USGS Biologist

And

Richard L. Kiesling
USGS Hydrologist

U. S. Geological Survey
Water Science Center

8027 Exchange Drive
Austin, Texas
78754

January 2007

Seasonal Phytoplankton – Zooplankton Dynamics in Lake Travis, Texas

The U. S. Geological Survey (USGS), in cooperation with Lower Colorado River Authority (LCRA), conducted reservoir-specific, community-level experiments to estimate phytoplankton growth rates and zooplankton grazing rates from June 2005 through September of 2006. Lake Travis is one of the main reservoirs in the Highland Lakes system located on the Colorado River and is managed by the LCRA for hydropower and drinking water supply. LCRA is currently involved in a quantitative water quality modeling effort of the Colorado River and its tributaries – termed Colorado River Environmental Modeling System (CREMS) (LCRA 2002; QEA 2003). Although reservoir-specific phytoplankton growth rates and biomass loss estimates by zooplankton are useful in modeling efforts for water quality monitoring in Lake Travis, another, broader context for this study is how phytoplankton communities respond to nutrient loads, inflows, and temperature stratification, relative to reservoir trophic status and water residence time (Soballe and Kimmel 1987, and references therein).

This study provides a foundation for an ecosystem-level understanding of food web interactions in Lake Travis and associated variations in trophic status by coupling abiotic factors such as temperature and nutrients with phytoplankton growth rates and mortality estimates through zooplankton grazing (collectively termed *plankton dynamics*; Pinto-Coelho et al. 2005). The trophic levels included in this study are phytoplankton microzooplankton (e.g. protists, rotifers, and copepod nauplii), and mesozooplankton (e.g. cladocerans and copepods).

Methods

Phytoplankton Nutrient-enrichment Bioassays

Nutrient-dependent phytoplankton growth bioassays were conducted on a monthly basis from June 2005 - September 2006. Surface water plankton was collected from five main stem sites and one tributary site (12307) in the reservoir by LCRA Environmental Services. These six sites include: 12302 (Mansfield Dam); 12307 (Sandy Creek); 12309 (Lakeway); 12313 (Cow Creek); 12315 (Carpenter Bend); and 12316 (Turkey Bend) (Figure 1). A comprehensive physical profile was performed at each of these sites including incident light profiles to 10 M, chlorophyll-*a* (from 2-3 depths according to stratification), and dissolved and total N and P. Vertical zooplankton net tows (64 μM mesh size) were taken from the mid-column depths and preserved in 10% formalin. Additional surface water and net tow samples (February – October 2006) were collected for zooplankton grazing experiments.

For the bioassays, five 1L bottles of water were collected from the surface of each site, and stored in a cooler containing an ice-bath slurry to keep water samples cool and dark. Samples were transported to the USGS laboratory in Austin, Texas within 24h of collection. All 1L sample bottles were allowed to warm to room temperature and thoroughly mixed to form a composite. Composite samples were split into four 500 ml treatments that consisted of four treatments with four replicates of each. Treatments included: control or ambient; Nitrogen (N) - as NO_3; Phosphorus (P) – as hydrated-PO_4; and a combined N+P. Nutrient additions of N and P were made according to DYIII media (refer to the CCMP web site) with sodium nitrate (FW = 84.99) and sodium glycerophosphate penta-hydrate (FW = 268.7).

The composite samples from each site and treatment were transferred into sterile 50ml borosilicate culture tubes and placed into the incubator directly beneath the lights at ambient reservoir temperature (14:10 & 12:12 light:dark cycle during the summer & winter months, respectively.) Incubation light intensity was approximately 10% of natural irradiance, which is generally accepted to be sufficient for algal photosynthesis.

Initial and final chlorophyll-*a* (Sterner 1994, Leboulanger et al. 2006 and others) and daily *in vivo* fluorescence (IVF) (Leboulanger et al. 2006) were measured to determine algal biomass and growth. Each replicate was mixed by a vortex Genie® to suspend settled cells prior to IVF readings with a Turner 10-AU fluorometer. The natural log of the daily IVF values versus time were plotted to determine phytoplankton intrinsic growth rate rates. To avoid potential "container effects," bioassay incubations were short-term (5-7 d).

Phytoplankton samples were preserved in Lugols Iodine for enumeration of the initial ambient and final treatments. Chlorophyll-*a* concentrations were measured on initial ambient and final treatments by filtration of two replicates onto GF/F filters, extracted in absolute methanol overnight at 4°C (Wetzel and Likens 1990), and measured with a Turner-700 fluorometer with the appropriate excitation and emission filters. Total particulate Carbon and Nitrogen (TPCN) concentrations were determined for ambient surface water (experimental controls) and for final treatments from two experiments. In addition, total organic Carbon (TOC) was determined from the ambient surface water from all sites by the USGS National Water Quality Lab.

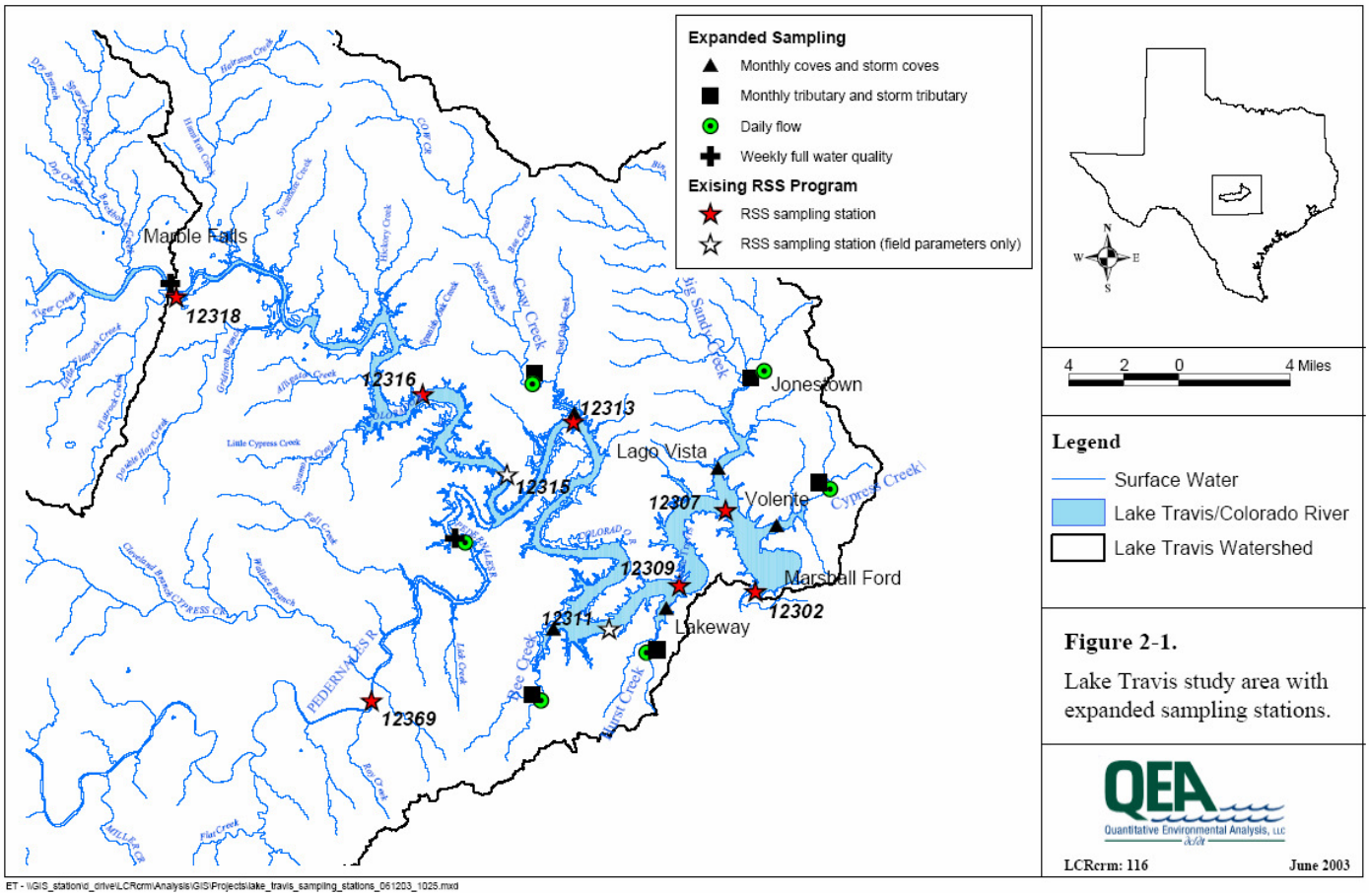

Figure 1. Lake Travis sampling sites (QEA 2003).

Mesozooplankton grazing experimental procedure

Mesozooplankton grazing experiments were performed in winter 2005 and spring through summer 2006 with surface plankton collected at the same sites in Lake Travis as the bioassays (Figure 1). Mesozooplankton were collected by vertical tows to 20 M from two lacustrine sites (12302 & LC901 - listed as 12307 in Fig. 1) with a large diameter 64 μM net and gently transferred into 4L carboys with ~ 2L surface water added for oxygen consumption and transported to the USGS - Austin Water Science Center (WSC). Zooplankton transfers were made within 24 hr to allow the net algae to settle. Upon experimentation, zooplankton were transferred gently to 250 - 1000 ml graduated cylinders to concentrate them into relative 1X, 2X, & 3X proportions, and finally, added to the 30 ml culture tubes containing surface water.

Zooplankton grazing experiments are based on the assumption that the major loss factor of phytoplankton biomass accumulation is a direct result of grazing mortality by mesozooplankton in the experimental treatment. Therefore, phytoplankton growth (as measured by IVF-based and initial/final Chl-*a*) is measured as an indicator of grazing. The relative change in phytoplankton growth was monitored by IVF using a Turner 10-AU fluorometer during short-term incubations (0-48 hrs.) under ambient temperatures. Controls were not covered and experimental treatments were covered after 48 hrs. A grazer density-gradient (Lehman and Sandgren 1985) was constructed in 50ml borosilicate culture tubes by adding increased amounts of grazers (mesozooplankton) to the natural algal assemblage from each site (starting volume ~ 30ml) with one to two replicates per treatment (1X ~ 5; 2X ~ 10-15; and 3X ~ 20-30 grazers, respectively). Upon termination, the 2 & 3X treatments were sieved and the >200 μM fraction was

preserved with 10% formalin for zooplankton enumeration. All treatments, including controls were then filtered for fluorometric Chl-*a* analysis. Grazing results of all experimental treatments and controls (no additional mesozooplankton) were calculated (based on either the IVF-based or the fluorometric-based Chl-*a*) with the following growth equation:

$$[(\mathrm{LN}(\text{final Chl-}a) - \mathrm{LN}(\text{initial Chl-}a))/\text{day}].$$

Linear regression were performed on the growth estimates versus zooplankton density, whereby the slope of the regression line estimates the grazing rate, thus negative when grazing occurs.

Microzooplankton grazing experimental procedure

Microzooplankton grazing experiments (Landry and Hassett 1982) were performed on one to five sites in winter, spring, and summer 2006 with surface plankton collected from the same six sites in Lake Travis with the exception of LC 901 (labeled as 12307 in Fig. 1). Surface water was gently sieved through 153 µM Nitex® screen (termed *whole lake water*) to exclude mesozooplankton upon collection and transported under ambient conditions to the USGS – WSC. A portion of the water from each site was ultra-filtered by a peristaltic pump with pre-cleaned silicone tubing and pre-rinsed capsule filters to 0.45 µM (termed *diluent*). Sterile or pre-cleaned, polycarbonate tissue culture flasks were used for the dilution series and two replicates each of 25%, 40%, and 100% whole lake water were combined with the diluent (total volume = 320 ml). Nutrients were initially added at the same concentrations used for the algal bioassays (April – May 2006), but the algal growth response to N and P overwhelmed the grazing signal in several experiments.

Thus, as these experiments progressed, one replicate with nutrient additions and another without additions were conducted in June 2006. In the most recent set of experiments (September 2006), N and P were added at half the bioassay doses (i.e. final: 117 μM [N] and 15 μM [P]) to all. The dilution experiments were incubated under ambient temperature with similar light conditions as described in Section I methods. Growth was monitored by daily IVF and by initial and final extracted Chl-*a*.

Calculations were made using the same equation described above for mesozooplankton, though initial values were corrected for each dilution. Linear regression were performed on the growth estimates versus dilution, whereby the slope of the regression estimates the micro-grazing rate, thus negative when grazing occurs, and the y-intercept estimates the intrinsic (or maximum) growth rate of the algal community.

Results

Monthly Ambient Phytoplankton Growth Rates

Monthly phytoplankton growth rates in the ambient (control) treatment from early-summer 2005 to mid-summer 2006 were generally low. Ambient growth rates ranged from 0.000 to 0.227 (Figure 2). The highest growth rates were in December 2005, while the lowest growth rates were in March 2006 following a period of low inflows into the reservoir. The elevated growth rates in December 2005 may have been due to a small-sized non-filamentous diatom observed as the dominant phytoplankton species.

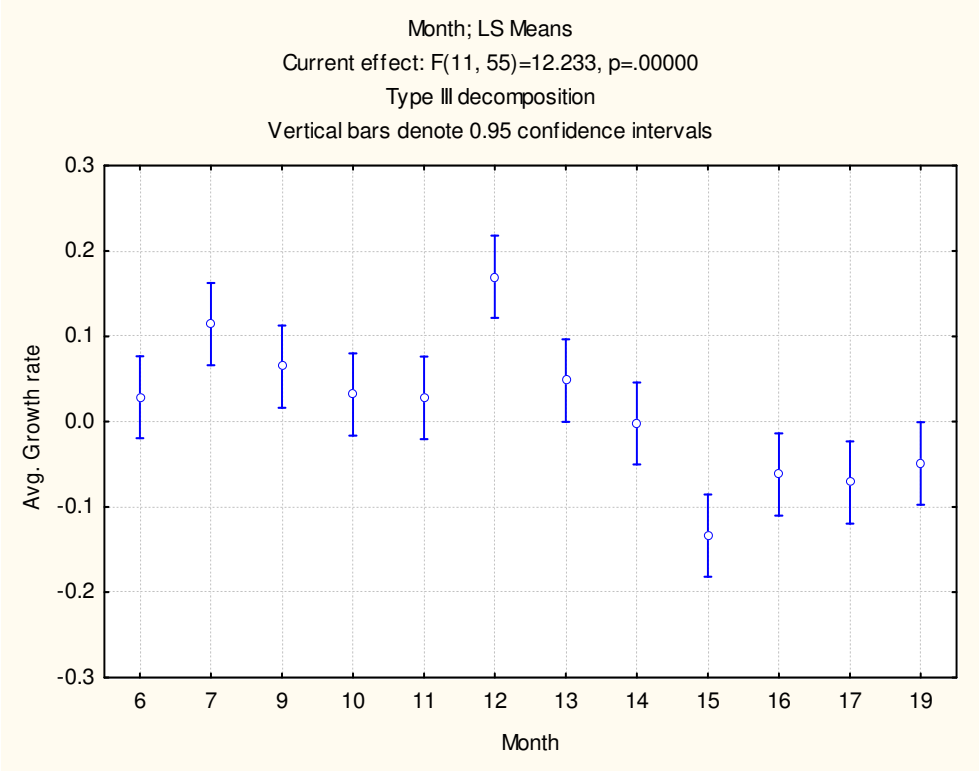

Figure 2. Least Square Means of Lake Travis ambient phytoplankton growth rates for all four replicates and all six sites by month beginning in June 2005. X-Axis labeled 13-19 corresponds to January through September 2006.

Spatial Patterns in Ambient Phytoplankton Growth Rates

Phytoplankton growth rates did not differ significantly between the lacustrine and riverine zones of the reservoir from June 2005 to September 2006 in the monthly ambient (control) treatments. This is most likely a result of the large degree of overlap in the 95% confidence intervals between sites, as there is a slight increase in growth rates from the transition (site 12309) to the riverine (site 12316) zones of the reservoir (Figure 3).

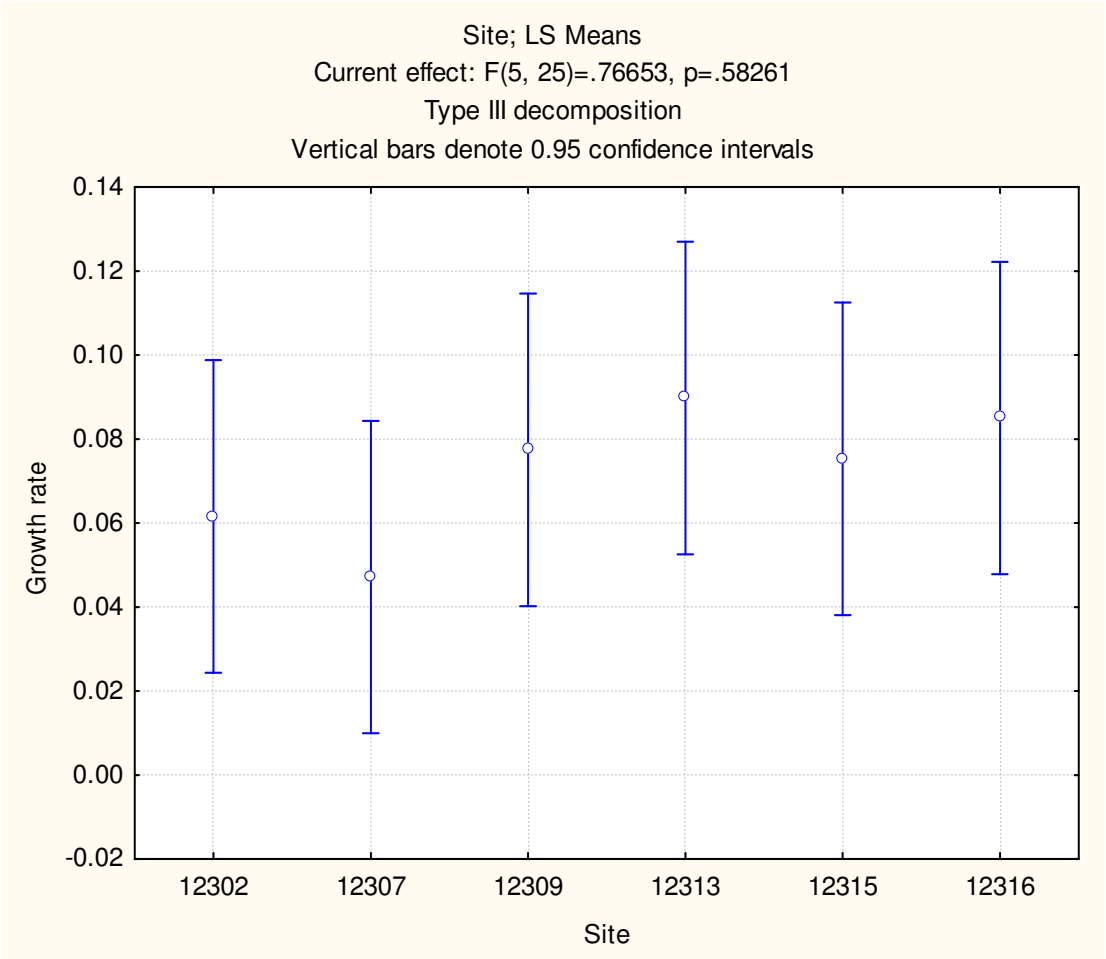

Figure 3. Least Square Means of Lake Travis ambient phytoplankton growth rates for all months (2005-2006) sampled from each site.

Nutrient Enrichment Effects on Phytoplankton Growth

Average growth rates combined for all months and sites differed significantly when compared to individual nutrient treatments (Figure 4; p=0.00). The combined nutrient enrichment treatment (NP) increased phytoplankton growth rates with the exception of two months in 2006 when P and NP treatments were similar (Figure 4). Relative to controls, phosphorus enrichment resulted in increased phytoplankton growth rates from December 2005 to May 2006 followed by increased growth rates with nitrogen enrichment (Figure 4). When monthly average growth rates were combined for each site and compared by treatment (Figure 5), P-enrichment increased growth rates at the lacustrine and first riverine site (12315). Alternatively, N-enrichment increased growth rates at the farthest riverine site (12316). Overall, the treatment and station interaction term was significant (Figure 5).

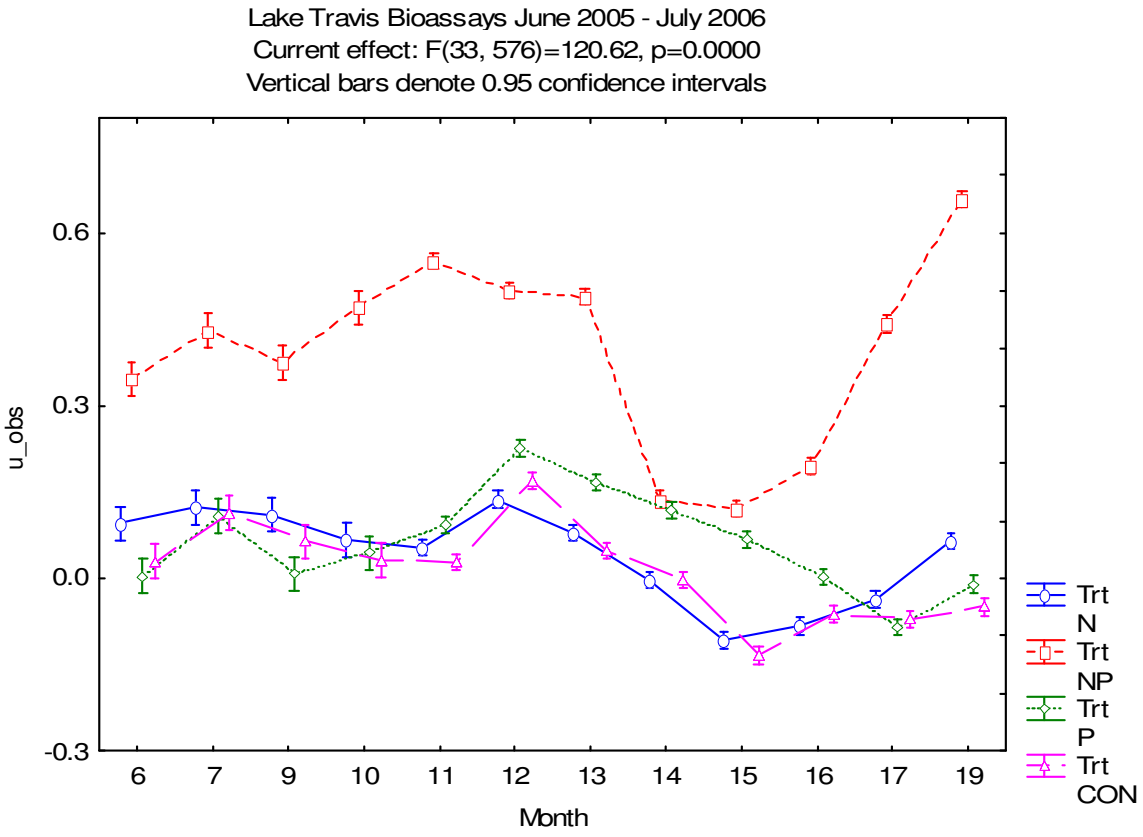

Figure 4. Monthly average Lake Travis phytoplankton growth rates of each treatment and all sites combined. X-Axis labeled 13-19 corresponds to January through September 2006.

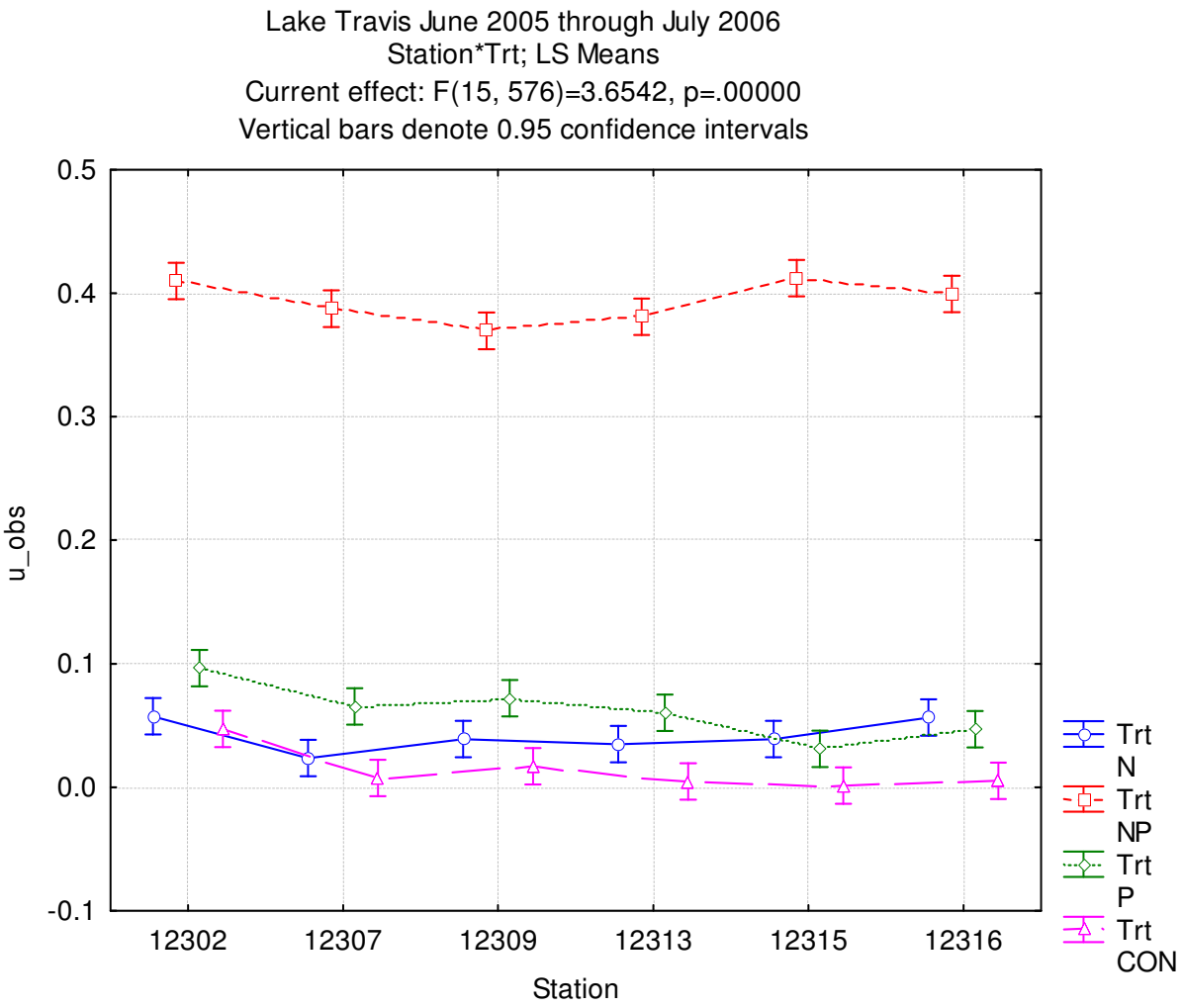

Figure 5. Monthly average Lake Travis phytoplankton growth rates for each treatment at each site (2005-2006).

While further analysis is necessary, Lake Travis epilimnetic phytoplankton communities appear to be co-limited in growth potential for the macro-nutrients nitrate and phosphate during periods of low inflow such as during 2005 - 2006. N- limitation was documented during this study in Lake Travis and in previous studies in two other subtropical reservoirs, Canyon and Waco (Groeger and Kiesling personal communication), which may be of importance relative to phytoplankton growth dynamics, and for agencies tasked with establishing nutrient criteria for these reservoirs.

Mesozooplankton Grazing Rates

Mean spring mesozooplankton grazing rate estimates were 0.26 day $^{-1}$ in February - May 2006, as estimated from surface water taken from three to six sites along the longitudinal axis of the reservoir (i.e. grazing experiments were conducted on all six sites in March – May). This estimate is approximately twice the ambient phytoplankton growth rate as determined from the bioassays, indicating strong top-down control by mesozooplankton on the phytoplankton community during the period sampled. Note that these results will be analyzed separately and presented individually in subsequent publications. The results were combined here to indicate the overall grazing rate in this reservoir that was consistently in the range of 0.2 to 0.26 day $^{-1}$.

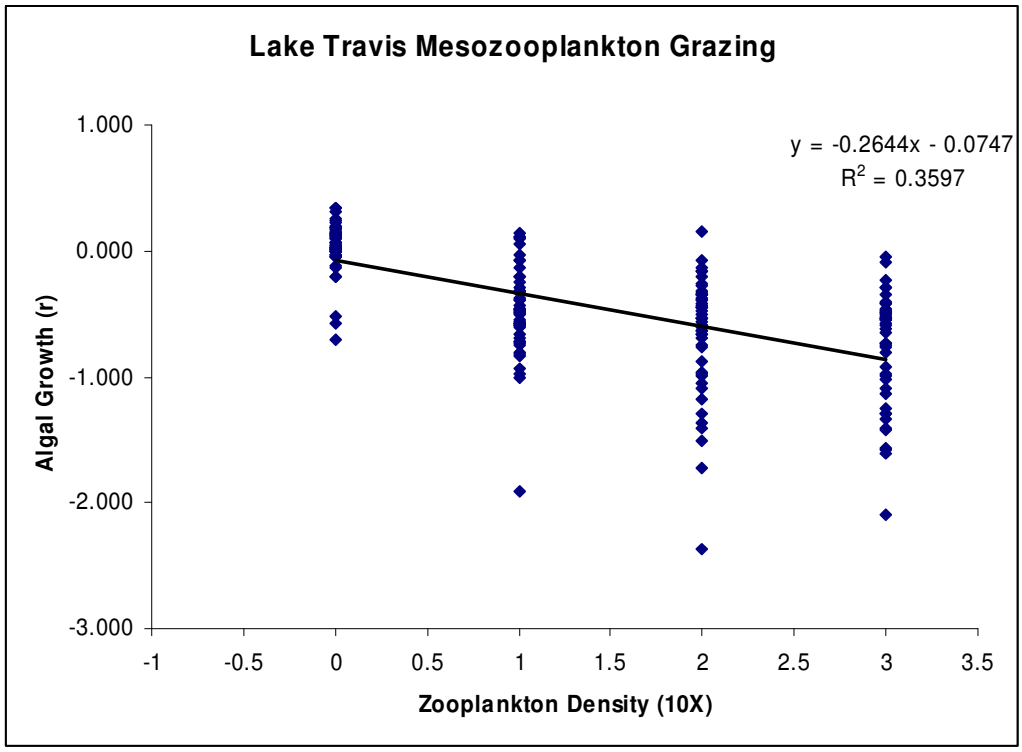

Figure 6. Lake Travis mesozooplankton grazing rate estimates for 2006. Each set of symbols represent individual experiments.

Microzooplankton Grazing Rates

Microzooplankton grazing rate estimates were variable between months and sites. While further statistical analysis is necessary, a summary of 2006 phytoplankton growth rates and microzooplankton grazing rates is provided (Figure 7). In general, phytoplankton growth rates exceeded micro-grazing rates with the following exceptions in March 2006: 12302 (dock) (growth and grazing equal); 12307; and 12316. Microzooplankton grazing exceeded phytoplankton growth at LC901 in April 2006, and at 12302 in May (both sites are lacustrine).

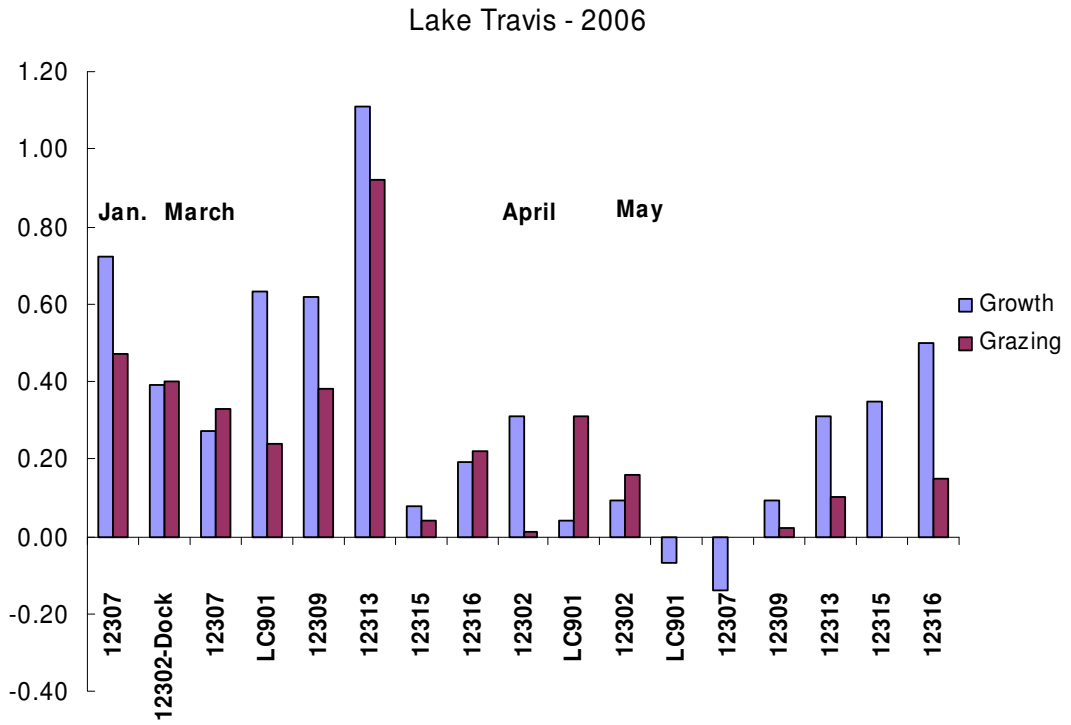

Figure 7. Lake Travis phytoplankton growth and microzooplankton grazing rates estimates by site and month in 2006. Sites are in order from the lacustrine to riverine zones.

Overall, the epilimnetic phytoplankton community in Lake Travis experienced strong top-down control by mesozooplankton and only consumed periodically and to a lesser extent by microzooplankton in the early months (during cooler reservoir temperatures). Based upon live water sample observations, micro-grazing activity does occur at all times during the year, thus the microzooplankton may be grazing predominantly upon bacteria (Sanders 1989), suggesting that these microzooplankton grazing rates likely are an underestimate of the total grazing magnitude of this functional group (Hansen et al. 1994; Hansen et al. 1997).

Relative to the regulation of the Lake Travis phytoplankton community, there appeared to be regulation of growth and biomass accumulation from both the bottom-up (macronutrient co-limitation) and the top-down (zooplankton grazing pressure) during 2005 – 2006.

Literature Cited

Hansen, J., P. K. Bjornsen, and B. W. Hansen. 1994. The Size Ratio Between Planktonic Predators and Their Prey. Limnol. Oceanogr. 39(2): 395 – 403.

Hansen, J., P. K. Bjornsen, and B. W. Hansen. 1997. Zooplankton Grazing and Growth: Scaling Within the 2-2,000 μM Body Size Range. Limnol. Oceanogr. 42(4): 687 – 704.

Landry, M. R., and R. P. Hassett. 1982. Estimating the grazing impact of marine microzooplankton. Mar. Biol. 67: 283-288.

LCRA. 2002. Colorado River Environmental Models Projects Charter. 3 pp.

Leboulanger, C., C. Quiblier, and P. Dufour. 2006. Rapid assessment of multiple-limiting factors of phytoplankton biomass: bioassays, *in vivo* chlorophyll-*a* fluorescence, and factorial design. Arch. Hydrobiol. 166(2): 261-287.

Lehman, J. T., and C. D. Sandgren. 1985. Species-specific rates of growth and grazing loss among freshwater algae. Limnol. Oceanogr. 30(1): 34-36.

Pinto-Coelho, R., B. Pinel-Alloul, G. Methot, and K. E. Havens. 2005. Crustacean zooplankton in lakes and reservoirs of temperate and tropical regions: variation with trophic status. Can. J. Fish. Aquat. Sci. 62: 348-361.

QEA, LLC. 2003. Colorado River Environmental Modeling System: Phase 2 Work Plan. 83 pp.

Sanders, R. W. 1989. Seasonal patterns of bacterivory by flagellates, ciliates, rotifers and cladocerans in a freshwater plankton community. Limnol. Oceanogr. 34: 673-687.

Soballe, D. M. and B. L. Kimmel. 1987. A large-scale comparison of factors influencing phytoplankton abundance in rivers, lakes, and impoundments. Ecology 68(6): 1943-1954.

Sterner, R. W. 1994. Seasonal and spatial patterns in macro- and micronutrient limitation in Joe Pool Lake, Texas. Limnol. Oceanogr. 39: 535-550.

Wetzel, R. G. and G. E. Likens. 1991. Limnological Analyses, 2nd edn. Springer, Berlin Heidelberg New York.

APPENDIX C

Tarrant Soils in Upper Pedernales Watershed

ANCHOR QEA

PARSONS

LimnoTech
Water | Environment | Scientists | Engineers

MEMORANDUM

DATE: 20 July 2007

FROM: Tad Slawecki, Brian Busiek

PROJECT: CREMS2

TO: Jennifer Benaman (QEA)
John Weddig (LCRA)

CC: Lara Jarrett (CH2M)

SUBJECT: Tarrant soils in Upper Pedernales watershed - DRAFT

Summary

In response to a request from Jennifer Benaman at QEA on behalf of LCRA, LimnoTech has examined the extent and characterization of Tarrant-series soils in the Pedernales River watershed. The examination was prompted in part by initial difficulties on the part of LCRA in achieving a satisfactory calibration to data at the Fredericksburg USGS gage using the SWAT model.

LimnoTech reviewed available STATSGO and SSURGO datasets to identify the extent of Tarrant-series soils, and also reviewed descriptions of the various soil series in these areas. LimnoTech found that:

1) The STATSGO soil maps combine Tarrant soils with Purves and Eckrant soils, and may therefore overstate the area in the Tarrant series.

2) The SSURGO soil maps are more detailed, and break STATSGO's Tarrant-Purves-Eckrant features into many individual series.

3) The default soil characteristics in SWAT for Tarrant assign it to hydrologic soil group D, which is not consistent with the official description the series.

Two actions are recommended to improve the quality of the calibration to data at the Fredericksburg gage:

1) Change the hydrologic soil group used in SWAT for the Tarrant series from D to C. (Easier)

2) Use SSURGO soil data in place of STATSGO. (Potentially more difficult if soil characterizations for SWAT are not available for all SSURGO soil series present in the watershed)

501 Avis Drive
Ann Arbor, MI 48108
734-332-1200
Fax: 734-332-1212
www.limno.com

Background

LCRA is currently engaged in the development of an integrated water quality assessment tool for Lake Travis that links a watershed model (SWAT) – capable of simulating changes in watershed loads due to development – to a water quality model (CE-QUAL-W2) – usable for detailed predictions of water quality impacts from those loading changes. LCRA staff, assisted by QEA and LimnoTech, have been working on the setup and calibration of these complex models.

One of the major contributors to Lake Travis loadings is the Pedernales River. LCRA has been working to calibrate hydrology and water quality measures for the Pedernales River watershed with particular attention to flow at USGS gage locations near Fredericksburg and Johnson City. Although SWAT modeled daily flow has compared well to measured flow at Johnson City, results have been less promising at the Fredericksburg gage. As seen in Figure 1, modeled flows (red line) are flashier than observed flows (blue line) at Fredericksburg.

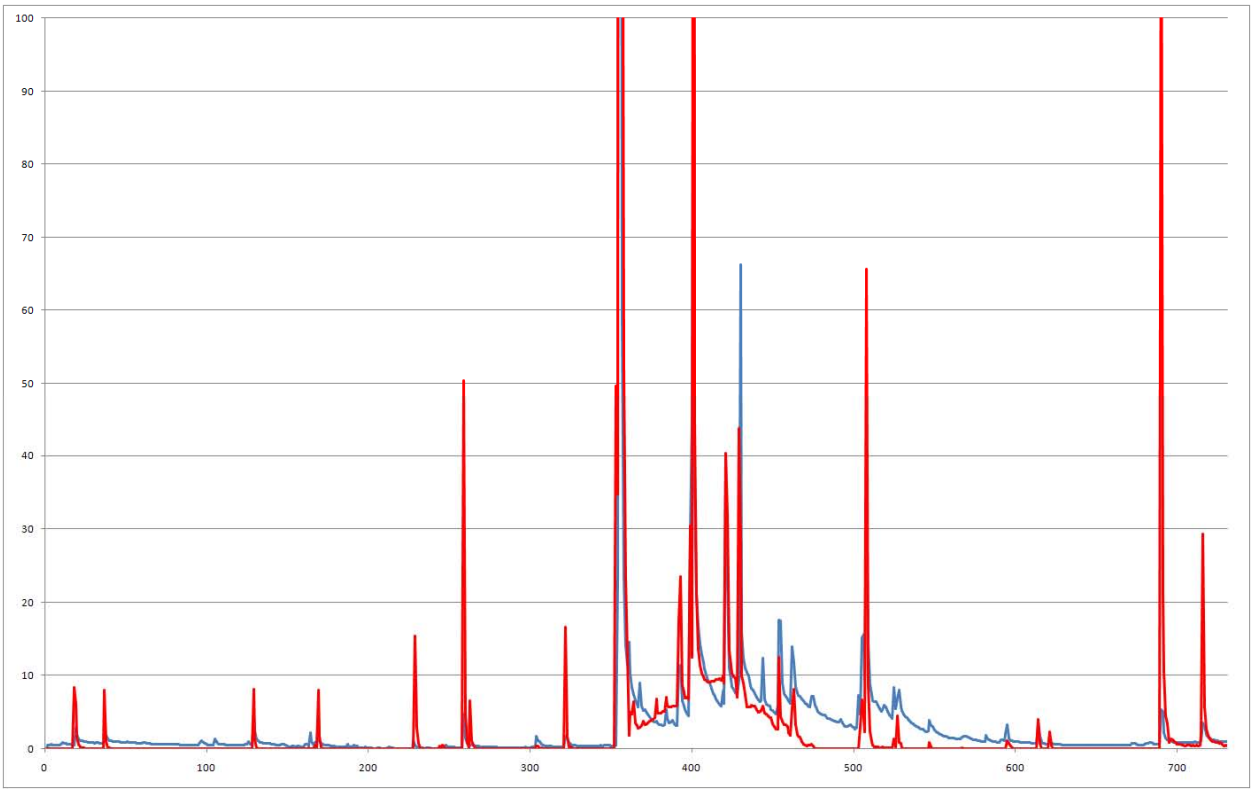

Figure 1. Comparison of preliminary SWAT modeled flow to observed flows at Fredericksburg for 1991-1992.

The flashiness suggested that runoff is overestimated by SWAT for the drainage area above the Fredericksburg gage. After a number of attempts to reduce runoff through adjustment of groundwater parameters, LCRA and LimnoTech identified the Tarrant series soil as the largest contributor to runoff. A qualitative test of sensitivity to the Tarrant series soils was performed by running SWAT with all Tarrant series soils "replaced" with Luckenbach series soils. The annual

and monthly regression and Nash-Sutcliffe coefficients were markedly improved. At this point, LimnoTech recommended more detailed investigation of soils issues, particularly for the Tarrant series.

Investigation

Two lines of investigation were undertaken to see if the Tarrant series might be mischaracterized in the SWAT model. First, the STATSGO datasets used in LCRA's preliminary calibration efforts were compared to the SSURGO datasets for the study area. Two findings of note were made in this first step:

1) The STATSGO soil maps combine Tarrant soils with Purves and Eckrant soils into a single Tarrant-Purves-Eckrant complex, and may therefore overstate the area actually in the Tarrant series.
2) Comparison to SSURGO maps shows that the "Tarrant" series in STATSGO actually covers a wide range of series. Figure 2 shows that many areas identified as Tarrant in STATSGO are identified differently in SSURGO (blue areas). Table 1 lists other soil series in SSURGO that had been identified in STATSGO as Tarrant.

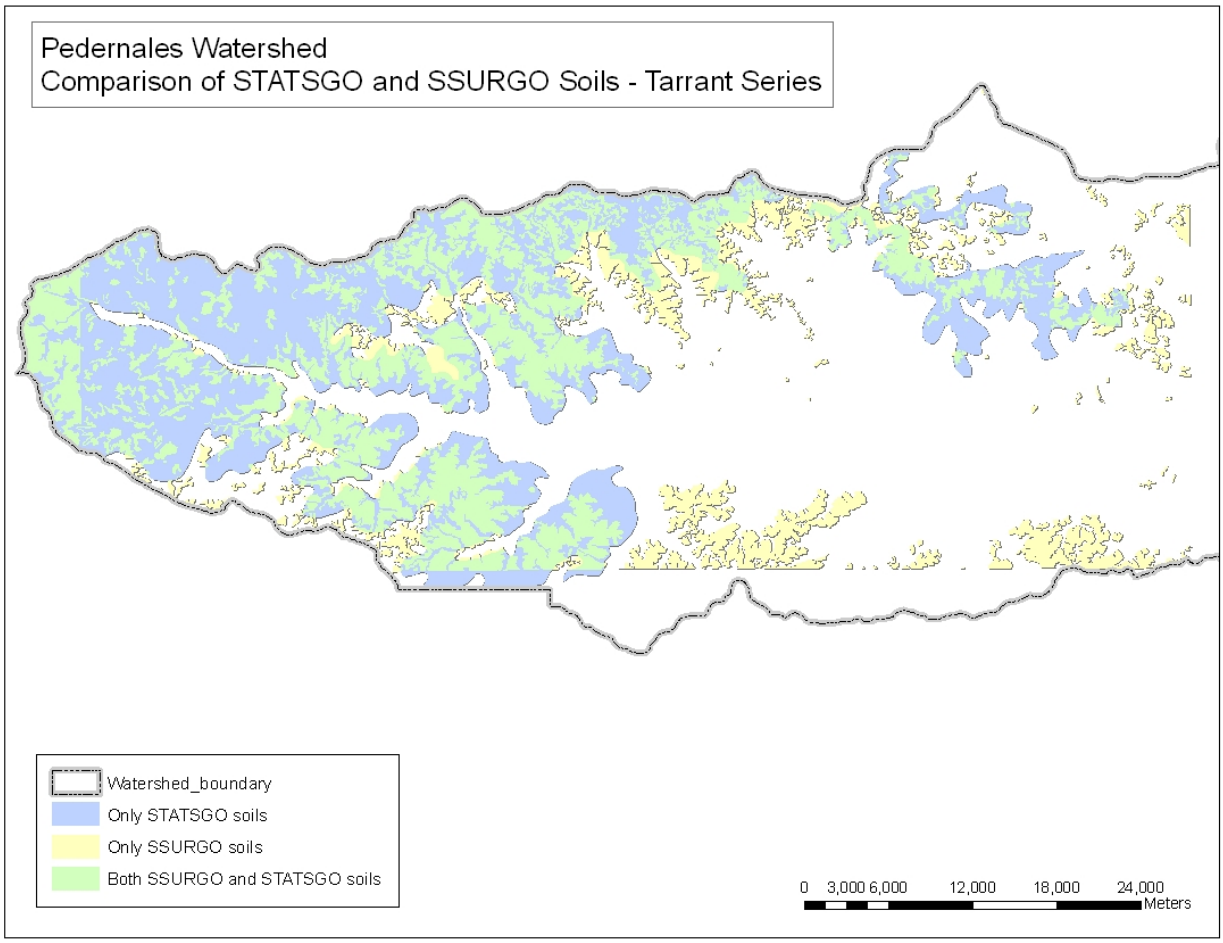

Figure 2. Comparison of STATSGO and SSURGO Tarrant series soils

Table 1. SSURGO-Identified Soil Series Listed as Tarrant in STATSGO For Study Area

MUSYM	Mapunit Name
PuC	Purves soils, undulating
SsD	Tarpley clay, stony, 1 to 8 percent slopes
Gr	Boerne and Oakalla soils, channeled, frequently flooded
DoC	Doss silty clay, 1 to 5 percent slopes
BrE	Brackett soils, hilly
TpB	Topia clay, 1 to 3 percent slopes
DnB	Denton silty clay, 1 to 3 percent slopes
LnD	Lindy cobbly clay loam, 1 to 8 percent slopes
DsC2	Doss soils, 1 to 5 percent slopes, eroded
BrC	Brackett soils, undulating
DnC	Denton silty clay, 3 to 5 percent slopes
Fr	Frio silty clay loam, occasionally flooded
KuC	Krum silty clay, 3 to 5 percent slopes
TRC	Tarpley-Roughcreek association, gently undulating
ECC	Eckrant-Comfort association, gently undulating
KuB	Krum silty clay, 1 to 3 percent slopes
SpC	Tarpley clay, 1 to 4 percent slopes
DsC	Doss silty clay, 1 to 5 percent slopes
DnC2	Denton silty clay, 3 to 5 percent slopes, eroded
SpB	Speck clay loam, 0 to 3 percent slopes
ERG	Eckrant-Rock outcrop association, steep
TpC	Topia clay, 3 to 5 percent slopes
LuB	Luckenbach clay loam, 1 to 3 percent slopes
HnD	Hensley loam, 3 to 8 percent slopes
LeA	Lewisville clay loam, 0 to 1 percent slopes
PeC	Pedernales fine sandy loam, 3 to 5 percent slopes
Bk	Luckenbach clay loam
VaB	Valera clay, 1 to 3 percent slopes
De	Dev very gravelly loam, frequently flooded
DpB	Depalt silty clay loam, 0 to 3 percent slopes
LeB	Lewisville clay loam, 1 to 3 percent slopes
LuC	Luckenbach clay loam, 3 to 5 percent slopes
KrB	Krum silty clay, 1 to 3 percent slopes
W	Water
KrC	Krum silty clay, 3 to 5 percent slopes
PeB	Pedernales fine sandy loam, 1 to 3 percent slopes
HsB	Hensley soils, 1 to 3 percent slopes
Gu	Pedernales-Gullied land complex, strongly sloping
Oa	Oakalla silty clay loam
BaC	Bastrop loamy fine sand, 1 to 5 percent slopes
AlC	Altoga silty clay, 3 to 5 percent slopes
LeC	Lewisville clay loam, 3 to 5 percent slopes
He	Heaton loamy fine sand
BoC	Bonti loamy sand, 3 to 5 percent slopes
LuC2	Luckenbach clay loam, 2 to 5 percent slopes, eroded
OB	Orif-Boerne association, frequently flooded
DeC	Loneoak fine sand, 1 to 5 percent slopes
VaC	Campair loamy fine sand, 1 to 5 percent slopes
Gp	Boerne loam, occasionally flooded
VhB	Campair fine sandy loam, 1 to 3 percent slopes
To	Tobosa clay

LimnoTech also reviewed available online descriptions of the Tarrant, Eckrant, and Purves series:

http://ortho.ftw.nrcs.usda.gov/osd/dat/T/TARRANT.html

DRAINAGE AND PERMEABILITY: Well drained. Runoff is negligible on 0 to 1 percent slopes. Very low on 1 to 3 percent slopes, low on 3 to 5 percent slopes, medium on 5 to 20 percent slopes and high on 20 to 50 percent slopes. Permeability is moderately slow.

http://ortho.ftw.nrcs.usda.gov/osd/dat/E/ECKRANT.html

DRAINAGE AND PERMEABILITY: Well drained. Runoff is negligible on 0 to 1 percent slopes, very low on 1 to 3 percent slopes, low on 3 to 5 percent slopes, medium on 5 to 20 percent slopes and high on 20 to 60 percent slopes. Permeability is moderately slow.

http://ortho.ftw.nrcs.usda.gov/osd/dat/P/PURVES.html

DRAINAGE AND PERMEABILITY: Well drained. Runoff is slow to medium. Permeability is moderately slow

All three of these series are described as "Well drained", which is inconsistent with the general description of Hydrologic Soil Group D as "Poorly drained, clay soils with high swelling potential, permanent high water table, claypan, or shallow soils over nearly impervious layer(s)." (from http://www.emrl.byu.edu/gsda/data_tips/tip_soiltype_table.html).

LimnoTech therefore recommends:

1) Modifying the description in SWAT of the Tarrant series to change the hydrologic soil group from "D" to "C"

And/or

2) Switching to the use of SSURGO soil series delineations instead of STATSGO.

APPENDIX D

Statistical Analysis of Lake Travis Water Quality to Assist CREMS Modeling

ANCHOR QEA

PARSONS

MEMORANDUM

TO:	Lisa Hatzenbuehler, LCRA John Wedig, LCRA Angela Rodriguez, LCRA Jorge Izaguirre, LCRA Bryan Cook, LCRA	**DATE:**	April 25, 2007
FROM:	Kirk Dean, Parsons	**RE:**	Statistical analysis of Lake Travis water quality to assist CREMS modeling
CC:	Harry Zahakos, QEA Randy Palachek, Parsons Jennifer Benaman, QEA Jim Patek, Parsons	**JOB#:**	PARcrm

Introduction

Ambient water quality data from Lake Travis were analyzed to provide insight to the major spatial and temporal trends and patterns in water quality, and elucidate the main factors influencing water quality. This work was performed to support development of a CE-QUAL-W2 model of Lake Travis as part of the CREMS project. Additionally, efforts were made to quantify model parameters that could be estimated from the ambient data. Only a portion of the total analyses and graphics performed will be presented here, and these represent only a portion of the possible questions that could result after review of the data. Due to space and time restrictions, these additional analyses will be performed on an *ad hoc* basis upon request of the CREMS team.

Methods

Water quality data were compiled from the LCRA HAAWQ ambient water quality monitoring database and the CREMS project databases, and subjected to a data quality review prior to data analysis. Only data from Lake Travis were included in the analysis. In most analyses and figures, all data collected between 1982 and early August 2006 were included, although long-term trends were analyzed as separate explanatory variables in statistical models. The dataset included a relatively constant number of observations (a unique combination of a station, date, time, and depth at which one or more measurements were taken or a sample was collected) from 1983 to 2003, then a large increase in 2004 (Figure 1).

Values below Detection Limits

In most cases when reported concentrations were below detection limits, the detection limit was used in lieu of a measured value. However, in cases with a large fraction of non-detect values, the data were not analyzed.

Figure 1. Observations by year for CREMS and "routine" sampling programs.

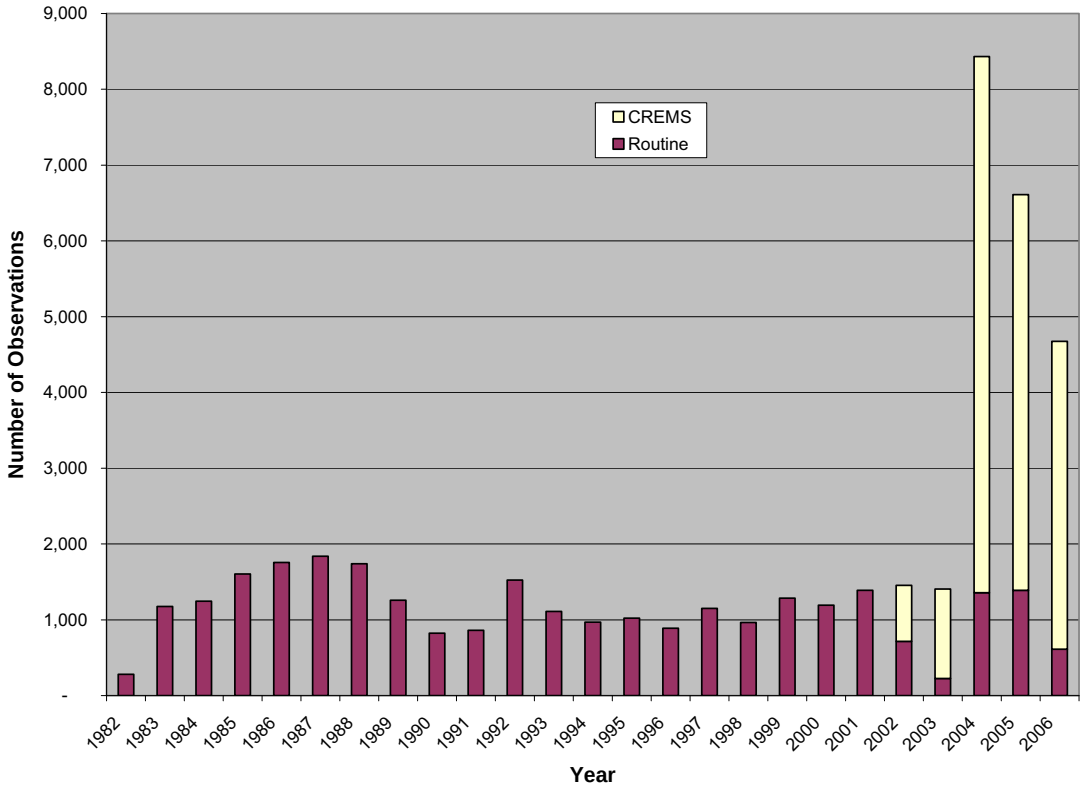

Spatial Analysis

Lake Travis is a linear feature, albeit a very curvy and somewhat branching one, so the linear distance upstream from Mansfield Dam is the primary metric of spatial variation. As a deep and stratified reservoir, depth is a second important spatial dimension. A third spatial characteristic considered was whether the sampling station was on the main thalweg of the lake or in a cove, most of which are flooded tributaries. The cross-channel spatial variations were ignored as they are not considered in the model. The characteristics of the water quality stations are provided in Table 1.

Temporal Analysis

In addition to date and time, other temporal properties were added to each observation to facilitate temporal analysis, including month, year, season, and monthlag. To calculate the ordinal variable "season," winter (with a value of 1) was assigned to the months of December, January, and February; spring (2) was assigned to March, April,

and May; summer (3) was June, July, and August; and fall (4) was September, October, and November. "Monthlag" is a temporal indicator of seasonality with July (mid-summer) as the starting value. Values were calculated as the absolute value of the number of months between the measurement month and July, so all values were integers between 0 (for July) and 6 (for January). Some variables were also classified into categorical interval ranges to facilitate display.

Table 1. Characteristics of water quality monitoring stations.

TNRCC ID	Site Description	km upstream of dam	Site Type
12302	Lake Travis near dam at LCRA Travis County Park	0.1	thalweg
12303	Lake Travis mid-lake, adjacent to Windy Point	3.6	thalweg
12304	Lake Travis Cypress Creek Arm, 0.6 miles from confluence with main lake	6.4	cove
LC901	Lake Travis at Starnes Island	6.7	thalweg
12305	Lake Travis in Cypress Creek Cove, at confluence with Long Hollow Creek	7.8	thalweg
12307	Lake Travis in Big Sandy Creek Cove 1.25 km downstream of the confluence with Lime Creek	11.3	cove
12309	Lake Travis at Arkansas Bend	15.0	thalweg
15428	Lake Travis in the Hurst Creek Arm	16.2	cove
12311	Lake Travis mid-lake adjacent to Lakeway	20.2	thalweg
LC902	Lake Travis at Bee Creek Cove	22.4	thalweg
LC903	Lake Travis at Thurman Bend	28.5	thalweg
12312	Lake Travis at Baldwin Bend	33.2	thalweg
12313	Lake Travis mid-lake at confluence with Cow Creek Arm at Pace Bend	42.0	thalweg
LC909	Lake Travis at Cow Creek Cove	44.3	cove
12315	Lake Travis mid-lake, 0.8 miles above confluence of Pedernales River Arm at Post Oak Bend	52.5	thalweg
LC908	Lake Travis at Pedernales Bend	56.0	cove
12314	Lake Travis Pedernales River Arm, at Old Ferry Rd Crossing	58.4	cove
12316	Lake Travis near Spicewood	61.9	thalweg
12317	Lake Travis mid-lake, 2 miles upstream from Spicewood Beach Landing Strip	65.0	thalweg
12318	Lake Travis at headwaters	89.7	thalweg

Statistical Analysis

Statistical analyses were performed using S-PLUS and Statistica software. In most cases, analyses were performed using generalized linear models. Some analyses were performed with mixed categorical and numeric variables. Some regressions were performed using stepwise regression to identify significant relationships.

Box-and-whisker plots were developed using S-PLUS software. The upper and lower boundaries of the box define the 75th and 25th percentiles of measured values, also known as the interquartile range (IQR), which contains half of the observations. The

line across the box represents the median, or 50th percentile. In some cases, the thickness of the median line indicates the 95 percent confidence interval for the median. The whiskers are the vertical lines at the top and bottom of the box, which represent the range of the data, after excluding outliers. Outliers, if present, are displayed as dots above and/or below the whiskers. Outliers are defined as values greater than the 75th percentile plus 1.5 times the IQR, or less than the 25th percentile minus 1.5 times the IQR. When several boxes are displayed together for comparative purposes, the width of the bar indicates the relative number of data points.

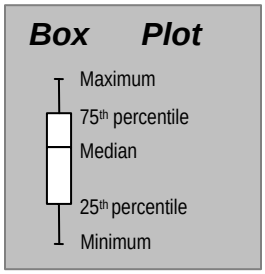

Results

Results will be presented on a parameter-by-parameter basis, except that two closely related parameters may be presented together. The following Table of Contents and Lists of Tables and Figures are designed to facilitate rapid access to pertinent sections of the memorandum.

Table of Contents

Introduction 1
Methods 1
Values below Detection Limits 2
Spatial Analysis 2
Temporal Analysis 2
Statistical Analysis 3
Results 4
Chlorophyll-a 9
Spatial Patterns 9
Temporal Trends 11
Chlorophyll-a Model 13
Water Clarity 14
Spatial Patterns 14
Temporal variation 14
Secchi Depth Model 18
Independent variable 18
t-value 18
p-value 18
Model Coefficient 18
pH 18
Spatial Patterns 18
Temporal Variation 20
pH Model 22
Ammonia nitrogen 23
Spatial Variation 23
Temporal Variation 23
Nitrate/Nitrite Nitrogen 26
Spatial variation 26
Temporal variation 26
Nitrate+Nitrite Nitrogen Model 30
Total Kjeldahl Nitrogen 30
Spatial Analysis 30

Temporal Analysis *31*
TKN Model *32*
Dissolved Kjeldahl Nitrogen *33*
Phosphorus 35
Dissolved Phosphorus *38*
Dissolved Oxygen 42
Spatial Analysis *42*
Temporal Analysis *42*
Dissolved Oxygen Model *47*
Suspended Solids 47
Spatial Analysis *47*
Temporal Analysis *47*
Suspended Solids Model *50*
Volatile Suspended Solids *51*
Organic Carbon 52
Spatial Analysis *52*
Temporal Analysis *52*
Dissolved fraction *52*
Light Penetration and Extinction with Depth 55

List of Tables

Table 1. Characteristics of water quality monitoring stations. 3

List of Figures

Figure 1. Observations by year for CREMS and "routine" sampling programs. 2
Figure 2. Chlorophyll-a concentration vs. distance upstream from Mansfield Dam... 9
Figure 3. Chlorophyll-a concentration vs. distance upstream from Mansfield Dam for thalweg and cove sites..... 10
Figure 4. Chlorophyll-a concentration vs. depth..... 10
Figure 5. Chlorophyll-a concentration vs. year..... 11
Figure 6. Chlorophyll-a concentration vs. month..... 12
Figure 7. Chlorophyll-a concentration vs. time of day. 12
Figure 8. Secchi depth vs. distance upstream from Mansfield Dam. 14

Figure 9. Turbidity vs. distance upstream from Mansfield Dam 15
Figure 10. Comparison of Secchi depth in thalweg and cove sites. 15
Figure 11. Secchi depths vs. month. 16
Figure 12. Turbidity vs. month. 16
Figure 13. Secchi depth vs. year. 17
Figure 14. Turbidity vs. year. 17
Figure 15. pH vs. distance upstream from Mansfield Dam. 19
Figure 16. pH vs. depth. 19
Figure 17. pH vs. time of day. 20
Figure 18. pH vs. month. 21
Figure 19. pH vs. year. 21
Figure 20. pH vs. dissolved oxygen 23
Figure 21. Ammonia nitrogen vs. distance upstream from Mansfield Dam. 24
Figure 22. Ammonia nitrogen vs. depth. 24
Figure 23. Ammonia nitrogen vs. year. 25
Figure 24. Ammonia nitrogen vs. time of day. 25
Figure 25. Ammonia nitrogen vs. month. 26
Figure 26. Nitrate+nitrite nitrogen vs. distance upstream from Mansfield Dam. 27
Figure 27. Nitrate+nitrite nitrogen in cove vs. thalweg sites. 27
Figure 28. Nitrate+nitrite nitrogen vs. depth. 28
Figure 29. Nitrate+nitrite nitrogen vs. month. 28
Figure 30. Nitrate+nitrite nitrogen vs. time of day. 29
Figure 31. Nitrate+nitrite nitrogen vs. year. 29
Figure 32. Total Kjeldahl nitrogen vs. distance upstream from Mansfield Dam. 31
Figure 33. Total Kjeldahl nitrogen vs. depth. 31
Figure 34. Total Kjeldahl nitrogen vs. month. 32
Figure 35. Total Kjeldahl nitrogen vs. year. 32
Figure 36. DKN/TKN ratio vs. depth. 34
Figure 37. DKN/TKN ratio vs. TSS concentration. 34
Figure 38. DKN/TKN ratio vs. chlorophyll-a concentration. 35
Figure 39. Total phosphorus vs. distance upstream from Mansfield Dam. 36
Figure 40. Total phosphorus vs. depth. 36
Figure 41. Total phosphorus vs. year. 37

Figure 42. Total phosphorus vs. month. 37
Figure 43. Total phosphorus vs. time of day. 38
Figure 44. Dissolved: total phosphorus ratio for cove and thalweg sites. 39
Figure 45. Dissolved: total phosphorus ratio vs. depth. 39
Figure 46. Dissolved: total phosphorus ratio vs. TSS. 40
Figure 47. Dissolved: total phosphorus ratio vs. distance upstream from Mansfield Dam. 40
Figure 48. Dissolved orthophosphate: dissolved phosphorus ratio for cove and thalweg sites. 41
Figure 49. Dissolved orthophosphate: total phosphorus ratio for cove and thalweg sites. 41
Figure 50. Dissolved orthophosphate: total phosphorus ratio vs. TDS. 42
Figure 51. Surface dissolved oxygen concentrations vs. distance upstream from Mansfield Dam. 43
Figure 52. Surface dissolved oxygen concentration for cove and thalweg sites. 43
Figure 53. Dissolved oxygen concentrations vs. depth. 44
Figure 54. Surface dissolved oxygen concentration vs. month. 44
Figure 55. Benthic dissolved oxygen concentration vs. month. 45
Figure 56. Dissolved oxygen concentration vs. time of day. 45
Figure 57. Dissolved oxygen concentration vs. year. 46
Figure 58. Dissolved oxygen concentration vs. year for individual years. 46
Figure 59. Total suspended solids vs. distance upstream from Mansfield Dam. 48
Figure 60. Total suspended solids in cove and thalweg sites. 48
Figure 61. Total suspended solids vs. depth. 49
Figure 62. Total suspended solids concentration vs. month. 49
Figure 63. Total suspended solids concentration vs. year. 50
Figure 64. Volatile vs. total suspended solids. 52
Figure 65. Total organic carbon vs. distance upstream from Mansfield Dam. 53
Figure 66. Total organic carbon vs. depth. 53
Figure 67. Total organic carbon vs. year. 54
Figure 68. Total organic carbon vs. month. 54
Figure 69. Dissolved fraction of organic carbon for cove and thalweg sites. 55

Chlorophyll-a

Spatial Patterns

Figure 2 shows that chlorophyll-a levels tend to be lowest, generally in the 1 to 4 µg/L range, near the dam. In upstream reaches, the chlorophyll-a levels tend to be in the 3 to 9 µg/L range. Figure 3 indicates that there is no substantial difference in chlorophyll-a levels between the main channel and coves. Chlorophyll-a levels tend to decline with depth in the water column (Figure 4).

Figure 2. Chlorophyll-a concentration vs. distance upstream from Mansfield Dam.

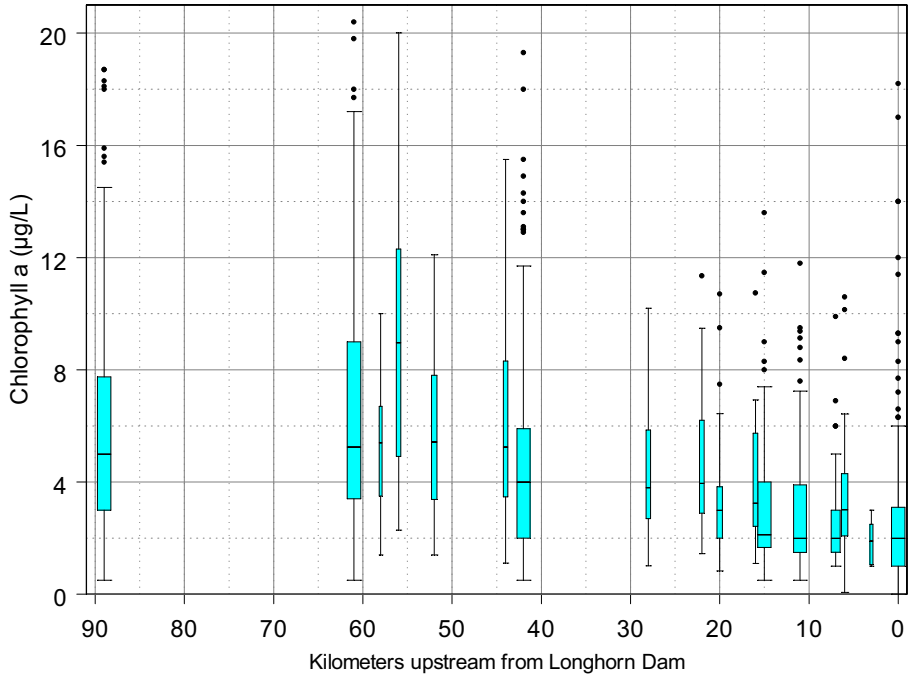

Figure 3. Chlorophyll-a concentration vs. distance upstream from Mansfield Dam for thalweg and cove sites.

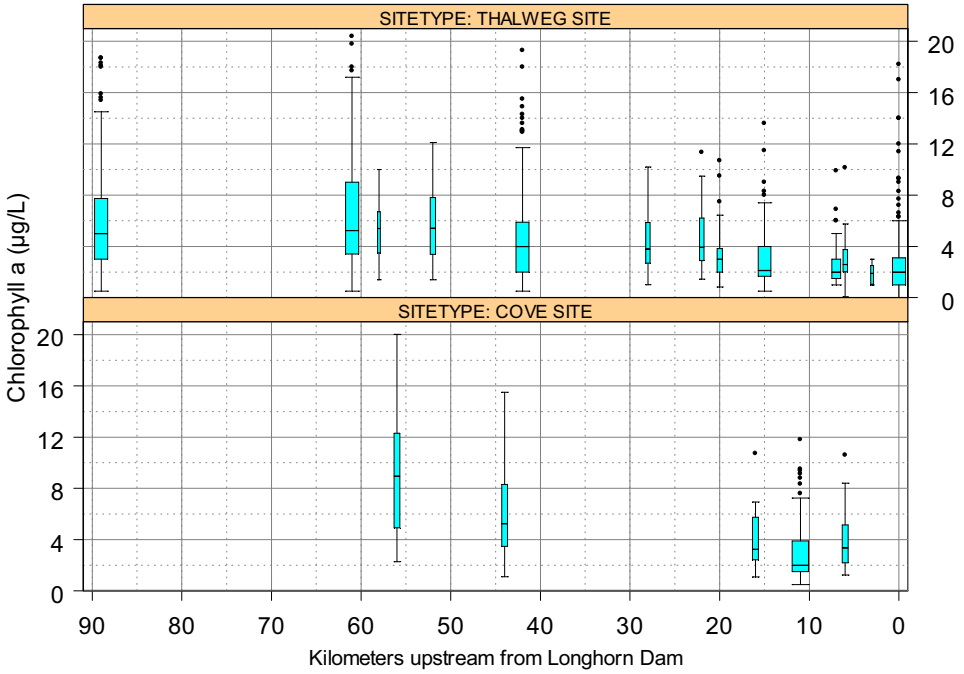

Figure 4. Chlorophyll-a concentration vs. depth.

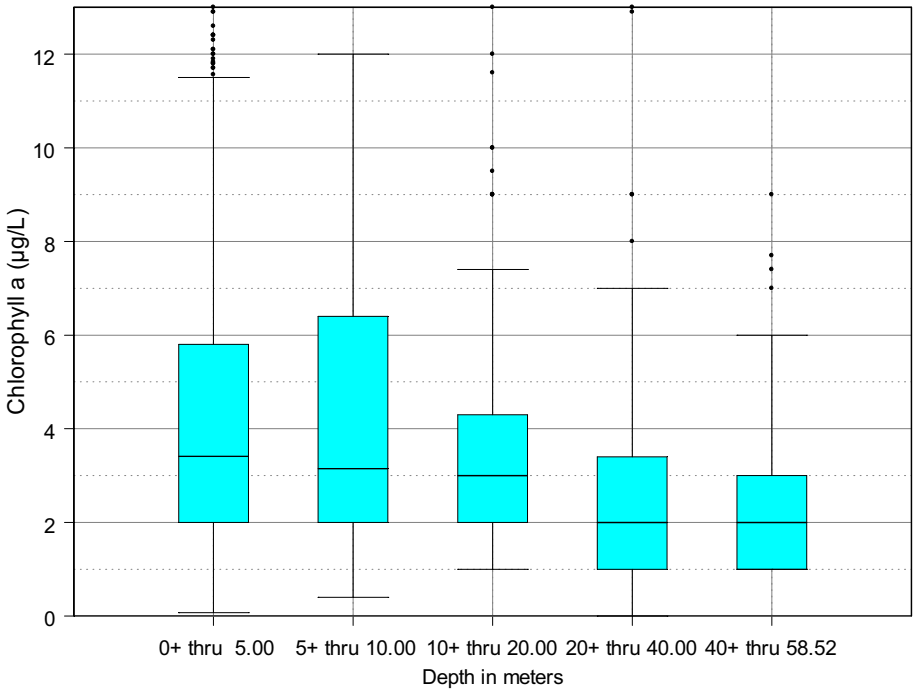

Temporal Trends

Figure 5 indicates that chlorophyll-a levels have tended to increase with time. Median lakewide chlorophyll-a levels increased from approximately 3 µg/L in the 1980s to approximately 5 µg/L, currently. This increase has been observed throughout the lake, but it is not known if changes in sampling or measurement methods may be responsible for all or part of this apparent increase.

Figure 6 shows that chlorophyll-a levels tend to increase from winter through fall, peaking in October then declining in November and December to the lowest levels of the year. Chlorophyll-a levels also tend to increase with time of day, though most of the measurements have been made in the late morning hours (Figure 7).

Figure 5. Chlorophyll-a concentration vs. year.

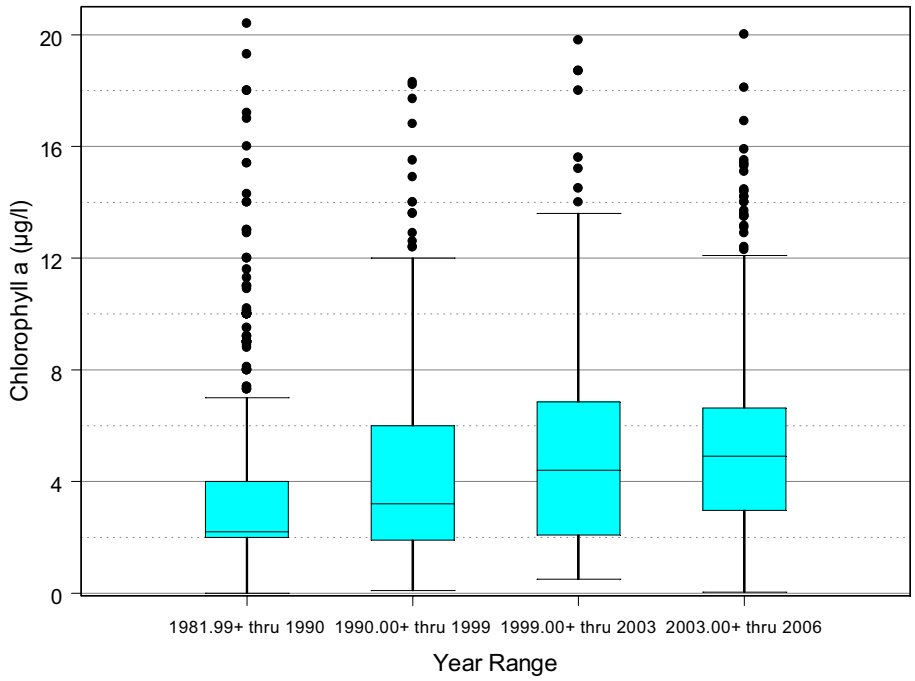

Figure 6. Chlorophyll-a concentration vs. month.

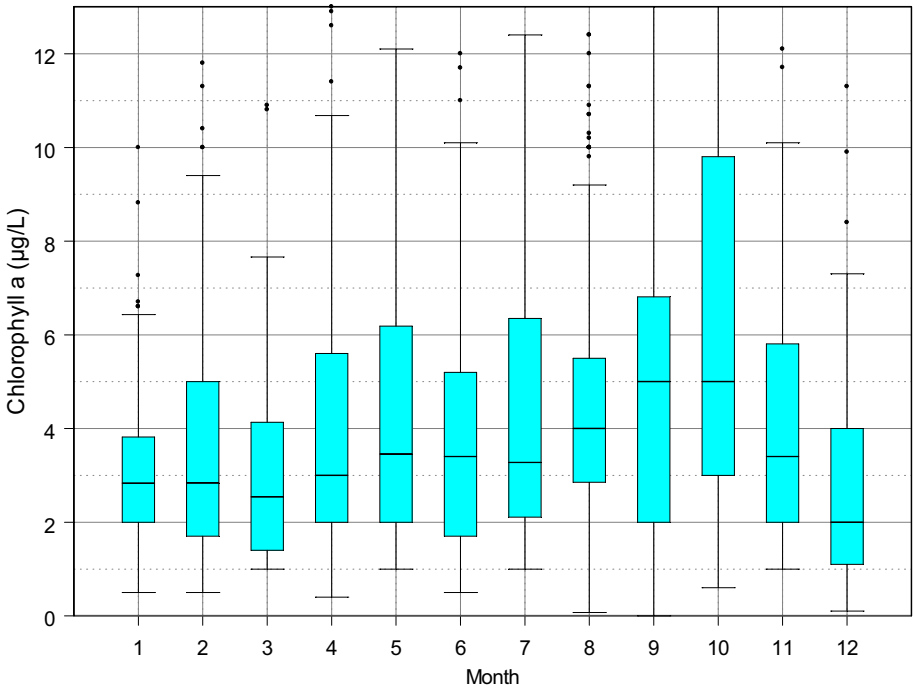

Figure 7. Chlorophyll-a concentration vs. time of day.

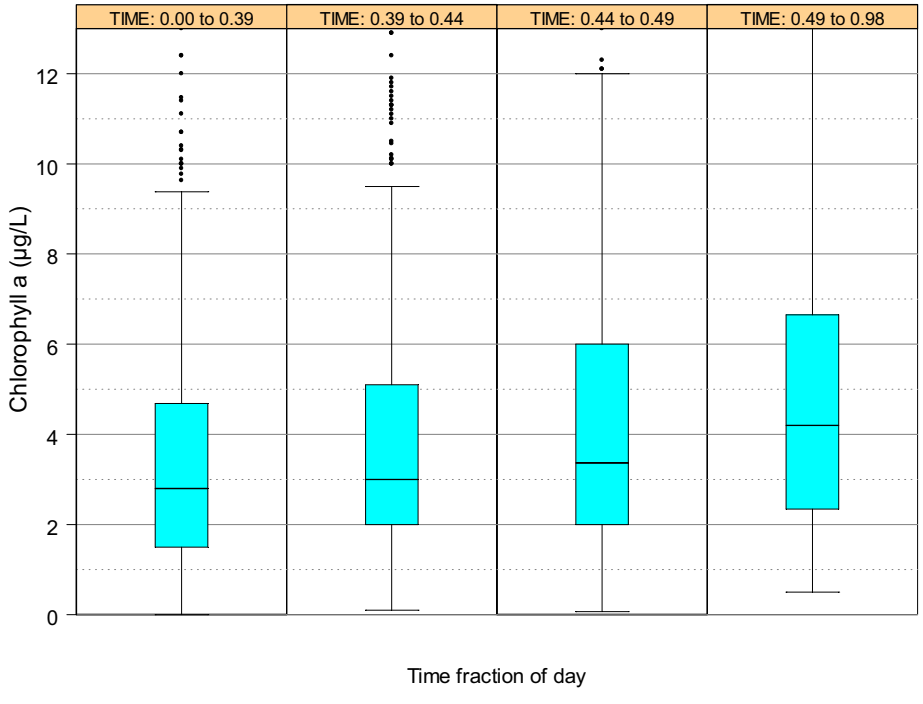

Chlorophyll-a Model

A generalized linear model was developed to explain observed variance in chlorophyll-a levels. Although this simple statistical model only accounts for approximately 23 percent of the observed variance in chlorophyll-a concentrations, it should provide the best estimates of Lake Travis chlorophyll-a concentrations at any point in time and space and elucidates some of the significant factors that may influence chlorophyll-a concentrations that should be accounted for in the CE-QUAL-W2 water quality model. It should be emphasized that a significant statistical relationship, or lack thereof, does not imply causation. Also, temporal and spatial interactions with nutrient levels were not accounted for in this simple model.

Independent variable	t-value	p-value	Model Coefficient
Intercept	-8.22	<0.0001	-182.8
Distance (0.1-90)	13.32	<0.0001	0.0426
Season (1-4)	11.75	<0.0001	1.147
Ammonia nitrogen mg/L	9.94	<0.0001	20.39
Year (1980-2006)	8.06	<0.0001	0.0902
Time of day (0-1)	3.55	0.0004	5.165
Nitrate/nitrite nitrogen mg/L	2.82	0.0048	2.582

The model indicates that chlorophyll-a levels

- increase with distance upstream from the dam at an average rate of 0.043 µg/L per kilometer after other significant factors have been accounted for such as changes in nitrogen concentrations;
- increase from winter through spring and summer to fall at an average rate of 1.15 µg/L per season;
- increase with ammonia nitrogen and, to a much lesser extent, nitrate+nitrite concentrations (but only after other factors are considered);
- have increased annually at a rate of approximately 0.09 µg/L since 1982 (total range 1.7 µg/L) after other significant factors are accounted for (notably some declines in nitrogen concentrations);
- increase with time during each day (though almost all of the data were collected in the late morning hours); and
- are not significantly related to total Kjeldahl nitrogen, total phosphorus, or dissolved orthophosphorus concentrations.

Water Clarity

Spatial Patterns

Secchi depth tends to decrease with distance upstream from the dam in Lake Travis, with median values ranging from less than a meter at the headwaters to 4 meters at the dam (Figure 8). Turbidity exhibited similar patterns, except that turbidities at the headwaters were not as high as those in middle reaches of the lake (Figure 9). Secchi depths in cove sites were similar to, although perhaps slightly less than, those at thalweg sites at similar distances from the dam (Figure 10).

Temporal variation

Water clarity, as indicated by both Secchi depth and turbidity, exhibits a seasonal pattern, with lowest clarity in winter, followed by a spring clear water phase in March and April, relatively good clarity in the summer, and declining clarity in the fall (Figures 11 and 12). Water clarity seasonal patterns correlate well with those of chlorophyll-a.

Figure 13 indicates that Secchi depths may have been declining since the 1990s, which is perhaps related to the increases in algal populations, as reflected by chlorophyll-a levels. While field turbidity measurements (Figure 14) do not reflect this trend, it is inappropriate to perform long-term trend analysis on the turbidity measurements because they were seldom measured before 1999 and most measurements were collected between 2003 and 2005.

Figure 8. Secchi depth vs. distance upstream from Mansfield Dam.

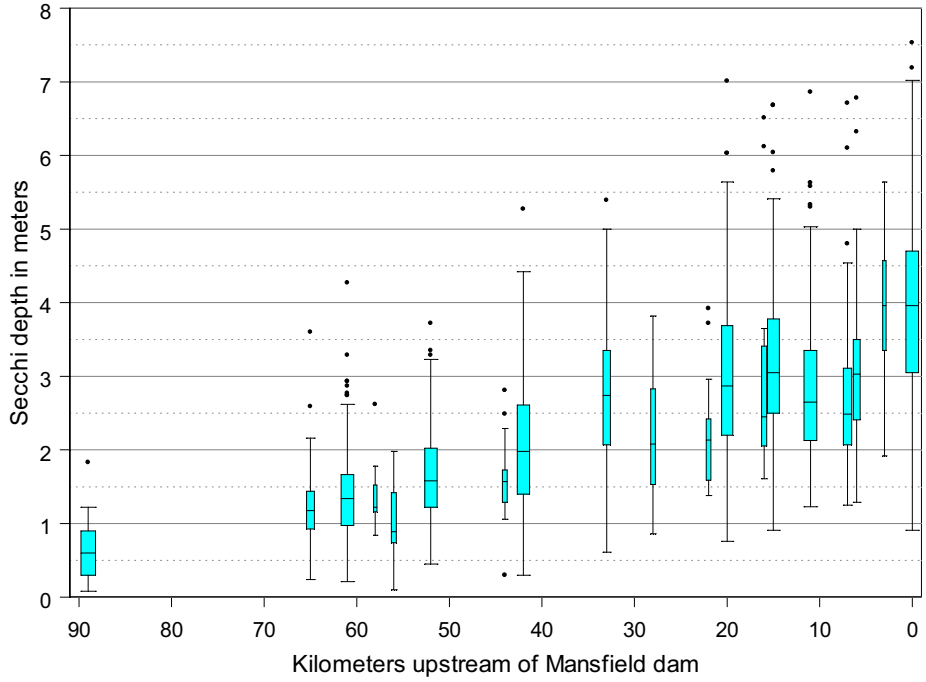

Figure 9. Turbidity vs. distance upstream from Mansfield Dam

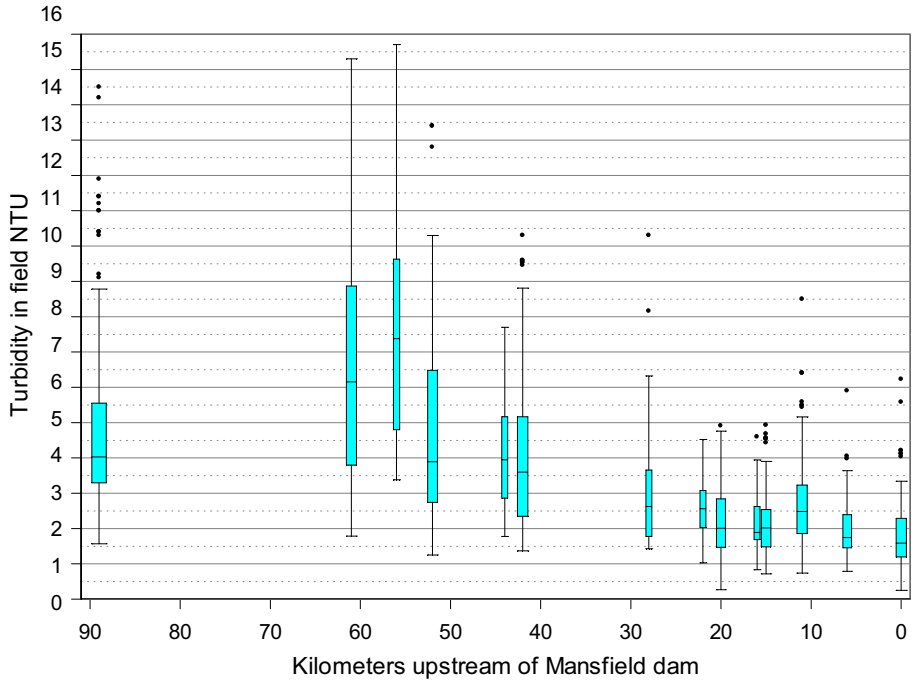

Figure 10. Comparison of Secchi depth in thalweg and cove sites.

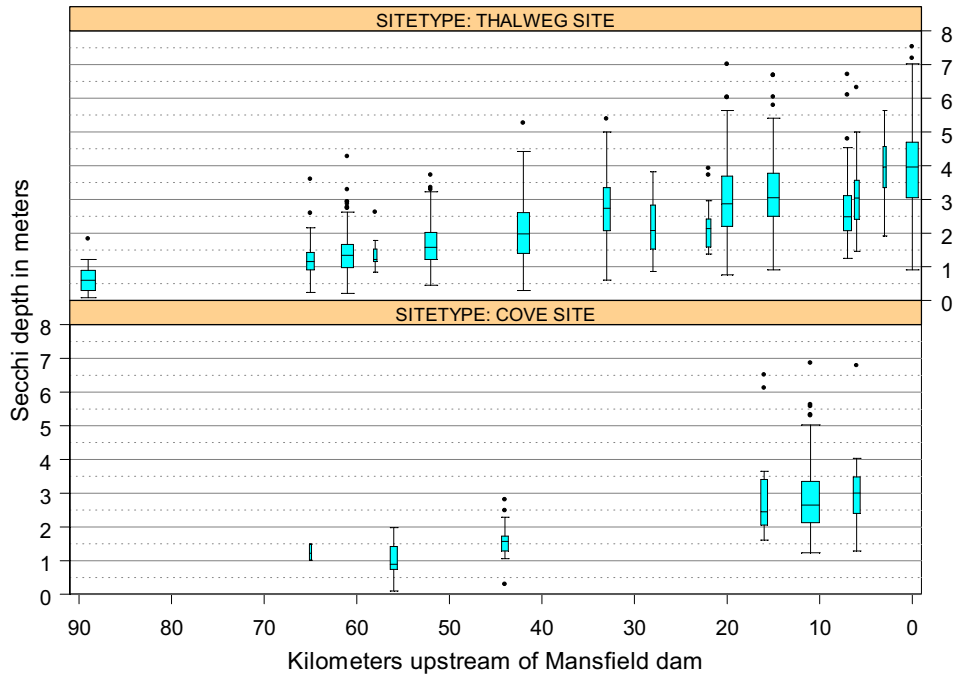

Figure 11. Secchi depths vs. month.

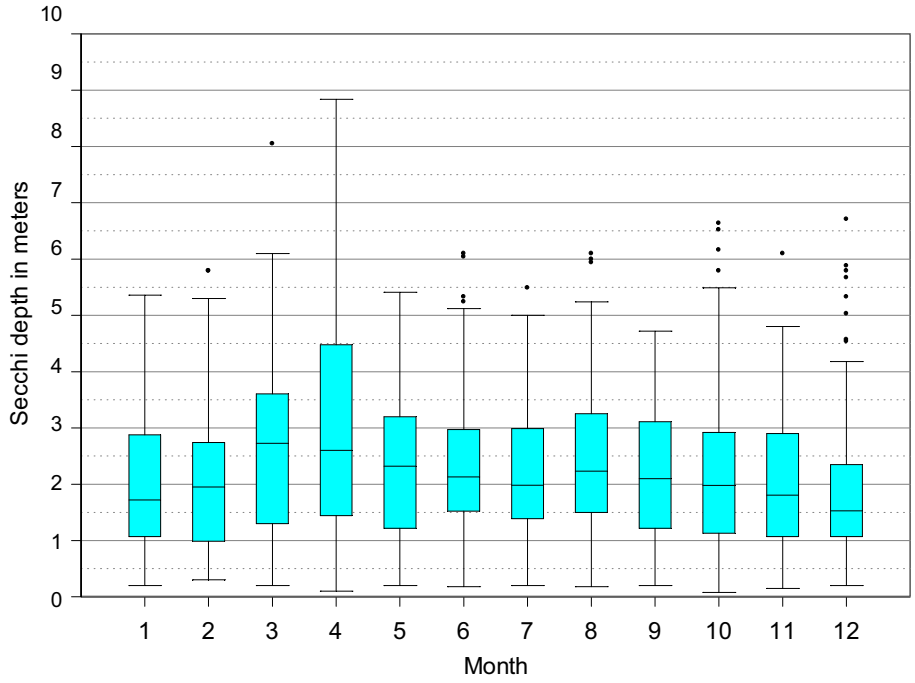

Figure 12. Turbidity vs. month.

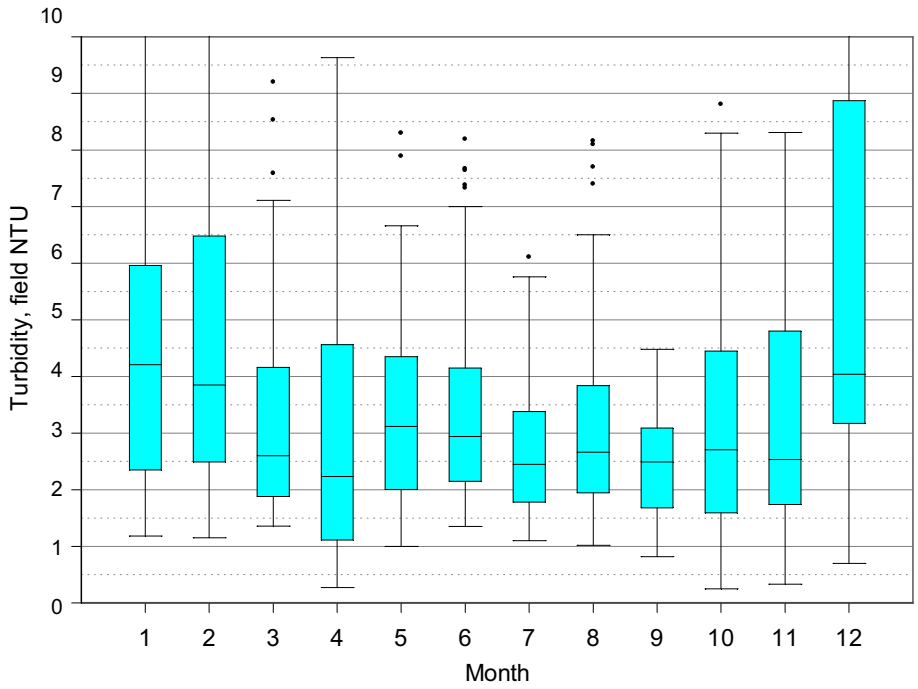

Figure 13. Secchi depth vs. year.

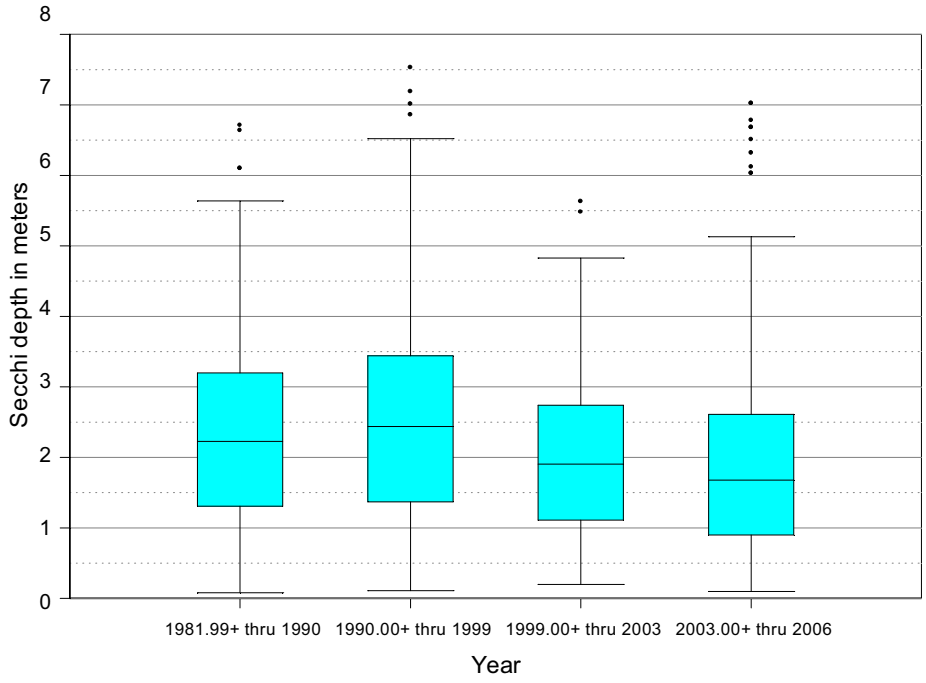

Figure 14. Turbidity vs. year.

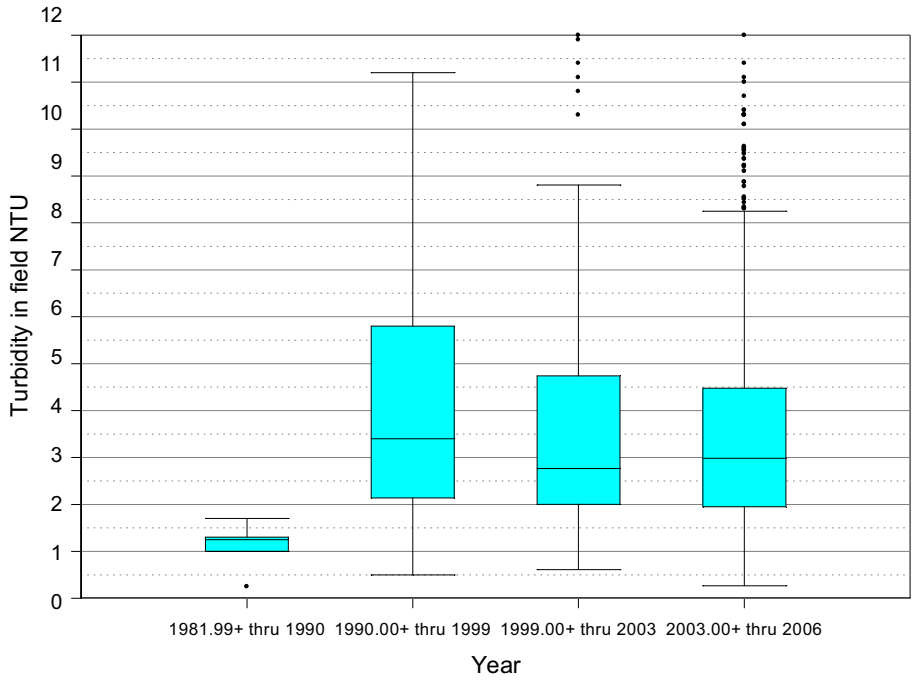

Secchi Depth Model

A generalized linear model was developed to explain observed variance in Secchi depth.

This simple statistical model accounts for approximately 62 percent of the observed variance in Secchi depths. It elucidates some of the significant factors, which may influence Secchi depths, that should be accounted for in the CE-QUAL-W2 water quality model. It should be emphasized that a significant statistical relationship, or lack thereof, does not imply causation. Also, temporal and spatial interactions with chlorophyll-a and suspended solids levels were not accounted for in this simple model.

Independent variable	t-value	p-value	Model Coefficient
Intercept	4.51	<0.0001	25.22
Distance	36.86	<0.0001	-0.0305
Time	-6.69	<0.0001	-2.432
Month (July lag)	-6.37	<0.0001	-0.0868
Chlorophyll-a	-5.08	<0.0001	-0.0336
Year	-3.62	0.0003	-0.0102
Total suspended solids	-3.33	0.0009	-0.0117

The model indicates that Secchi depths:

- decline with distance upstream from the dam at an average rate of 0.03 meters per kilometer (total range 2.7 meters), after other significant factors have been accounted for,
- decrease with time during each day (though almost all of the data were collected in the late morning hours),
- decline with months distant from July at an average rate of 0.087 meters per month (total range 0.52 meters),
- decrease with chlorophyll-a concentration,
- have decreased annually since 1982, and
- decrease with total suspended solids (TSS)concentrations.

pH

Spatial Patterns

The pH values are slightly alkaline in Lake Travis, with median values around 8; these values seldom fall outside the range between 7.5 and 8.5. Any spatial variation with distance from Mansfield Dam cannot be visually detected from Figure 15. pH does

appear to decline with depth (Figure 16), most likely due to the ratio of active photosynthesis to respiration.

Figure 15. pH vs. distance upstream from Mansfield Dam.

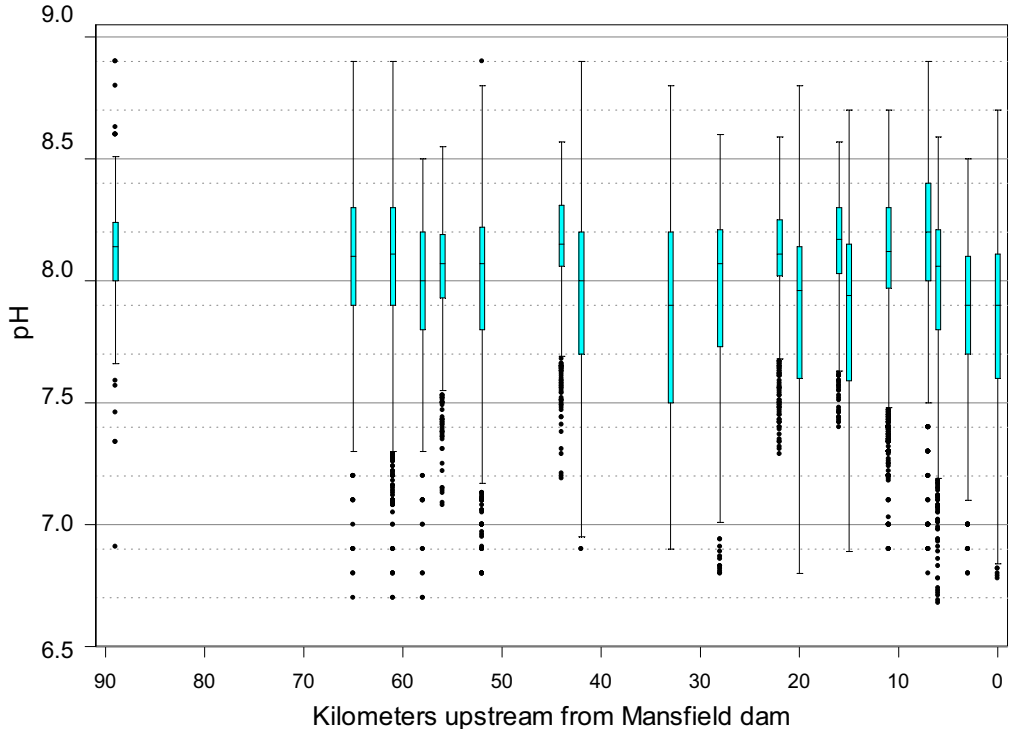

Figure 16. pH vs. depth.

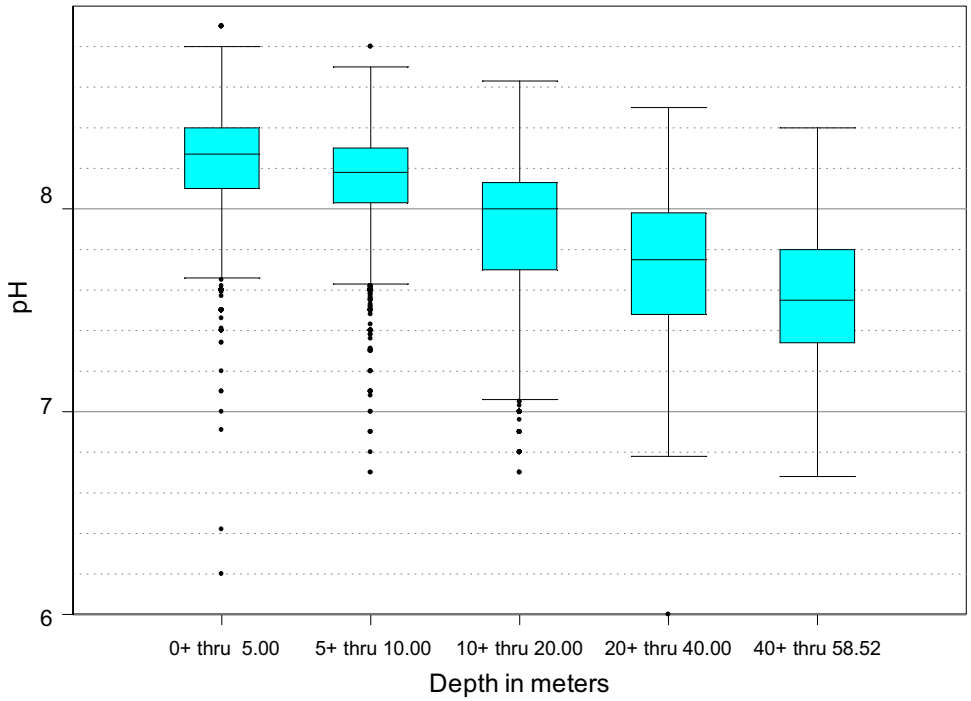

Temporal Variation

Figure 17 indicates that pH values may vary slightly during the day due to photosynthesis and respiration. Median pH values in the morning for the reservoir as a whole are less than 8, but greater than 8 in the afternoon.

Figure 18 indicates that pH values also appear to vary seasonally, with median values declining during the summer months.

No long-term trend in median pH values is apparent (Figure 19), though the range of measured pH values has been declining. This may reflect improvements in measurement technology or increased buffering of lake water.

Figure 17. pH vs. time of day.

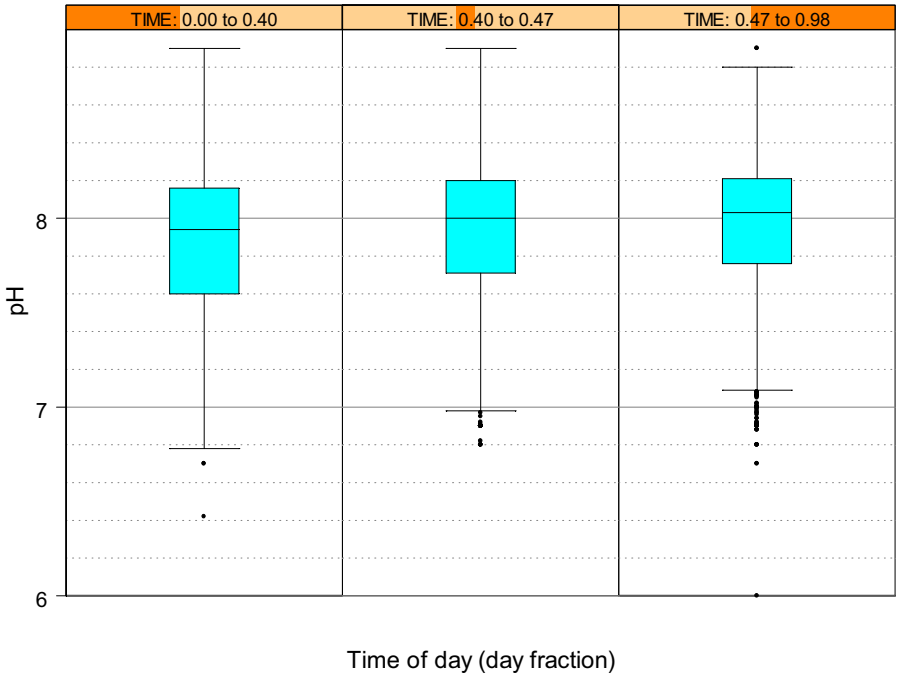

Figure 18. pH vs. month.

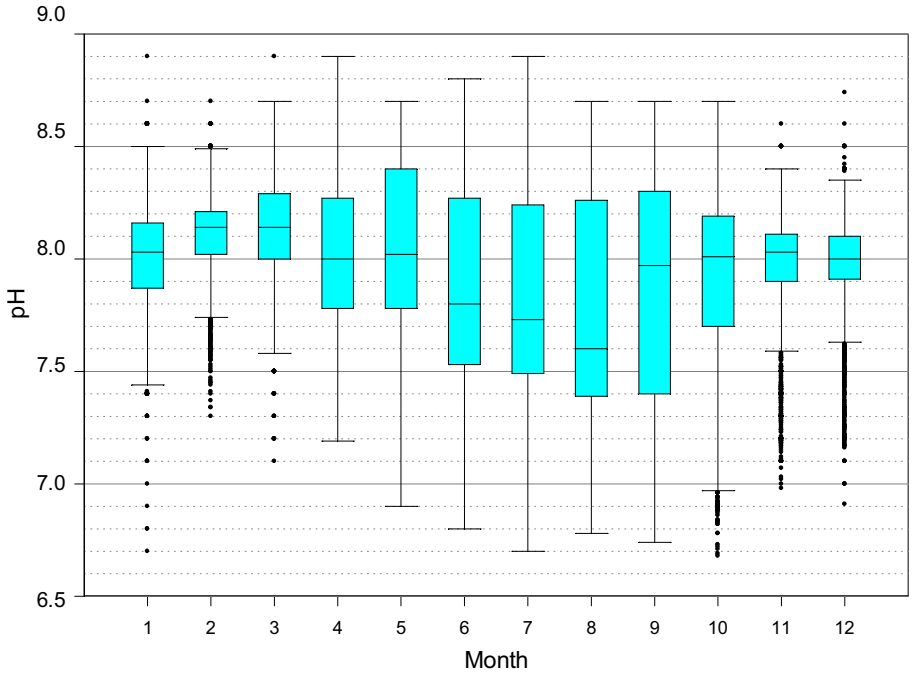

Figure 19. pH vs. year.

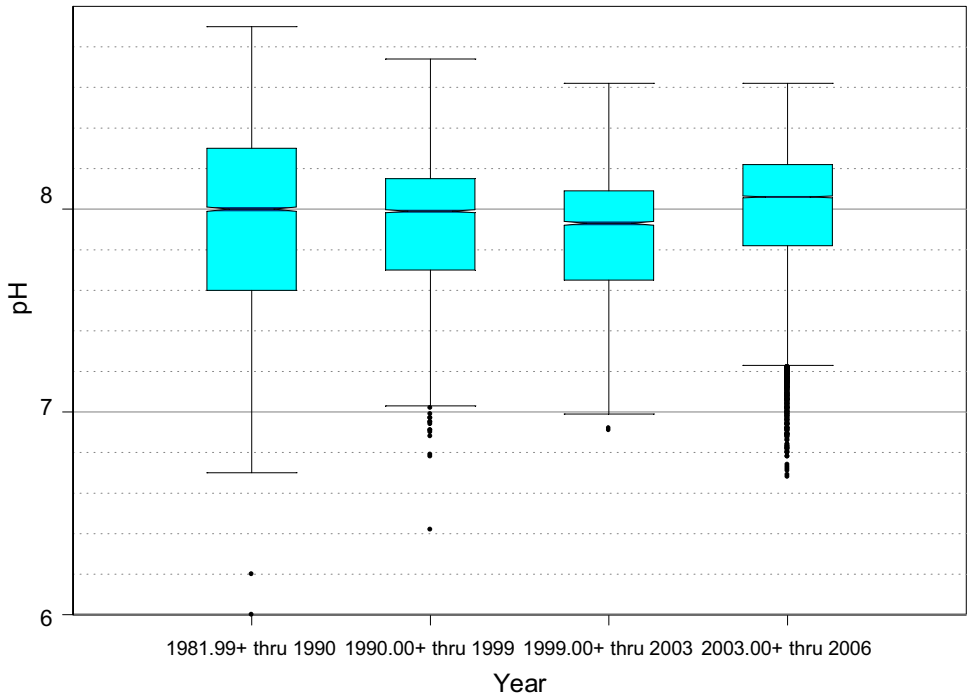

pH Model

A generalized linear model was developed to explain observed variance in pH. The standard error of this statistical model is 0.16 s.u., and it accounts for approximately 80 percent of the observed variance in pH. It should provide good estimates of Lake Travis pH values at any point in time and space, and elucidates some of the significant factors that may influence pH that should be accounted for in the CE-QUAL-W2 water quality model. It should be emphasized that a significant statistical relationship, or lack thereof, does not imply causation. Also, interactions between predictive variables were not accounted for in this simple model.

Independent variable	t-value	p-value	Model Coefficient
Intercept	18.8	<0.0001	3.68
Dissolved oxygen	268.4	<0.0001	0.101
Water Temperature	96.7	<0.0001	0.0190
Month (July lag)	-25.4	<0.0001	-0.0161
Distance	-12.6	<0.0001	-0.00052
Depth	-24.1	<0.0001	-0.00229
Year	17.2	<0.0001	0.0017

The model indicates that pH values are increased by primary production and reduced by respiration, with peaks in the upper water column in the summertime and lower values in the deeper water layers that are respiration-dominated. pH values

- are correlated most strongly with dissolved oxygen concentrations,
- are seasonal – varying with water temperature and month,
- decline with depth,
- decline with distance upstream from the dam at a small, but significant average rate of 0.00052 standard units per kilometer (total range 0.05 s.u.), after other significant factors have been accounted for, and
- have increased annually at a small rate of approximately 0.0017 s.u. per year since 1982 (total range 0.04 s.u.), after other factors have been accounted for.

Figure 20 illustrates the strong relationship between pH and dissolved oxygen, indicating the importance of photosynthesis and respiration on pH levels.

Figure 20. pH vs. dissolved oxygen

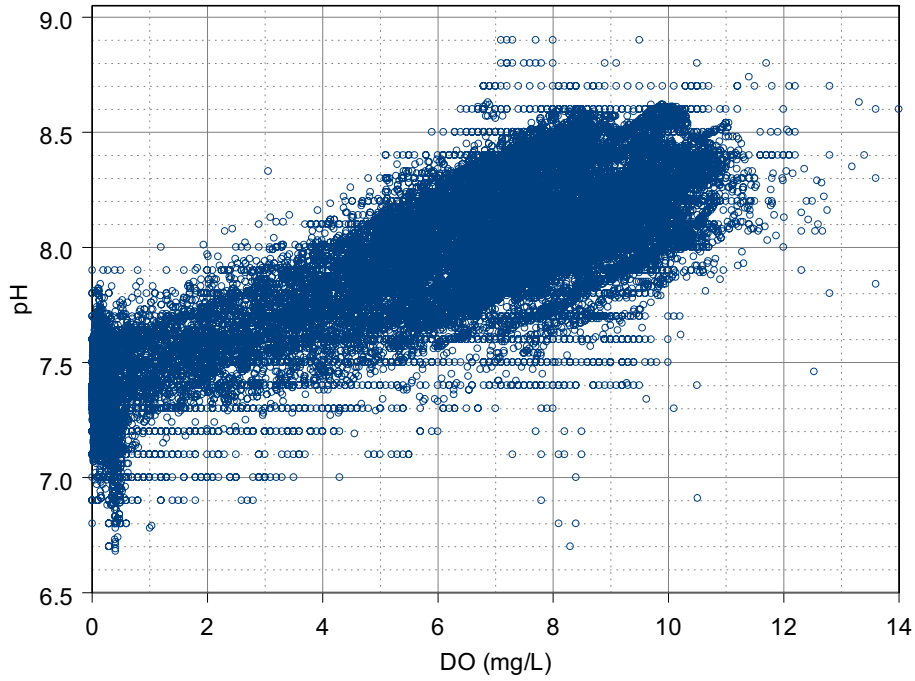

Ammonia Nitrogen

Spatial Variation

Analysis revealed few systematic trends in ammonia nitrogen concentrations. Many of the values were reported as below a detection limit, which confounded the analysis. Detection limits were typically about 0.01 mg/L.

Figure 21 illustrates no trends in ammonia concentration with distance from Mansfield Dam. Ammonia does exhibit a small trend with depth, with lowest values near the surface and highest values near the bottom (Figure 22). There was no apparent difference in ammonia nitrogen concentrations between cove and thalweg sites.

Temporal Variation

No long-term temporal trend with year was apparent for ammonia (Figure 23), as the analysis was confounded by values below detection limits. At the opposite time scale, no variation was apparent for ammonia with time of day (Figure 24), which may indicate that organic matter decay rates are slow and/or nitrification rates are rapid. Seasonal variation in ammonia levels was minimal, although levels may have been higher in late summer and fall (Figure 25).

Figure 21. Ammonia nitrogen vs. distance upstream from Mansfield Dam.

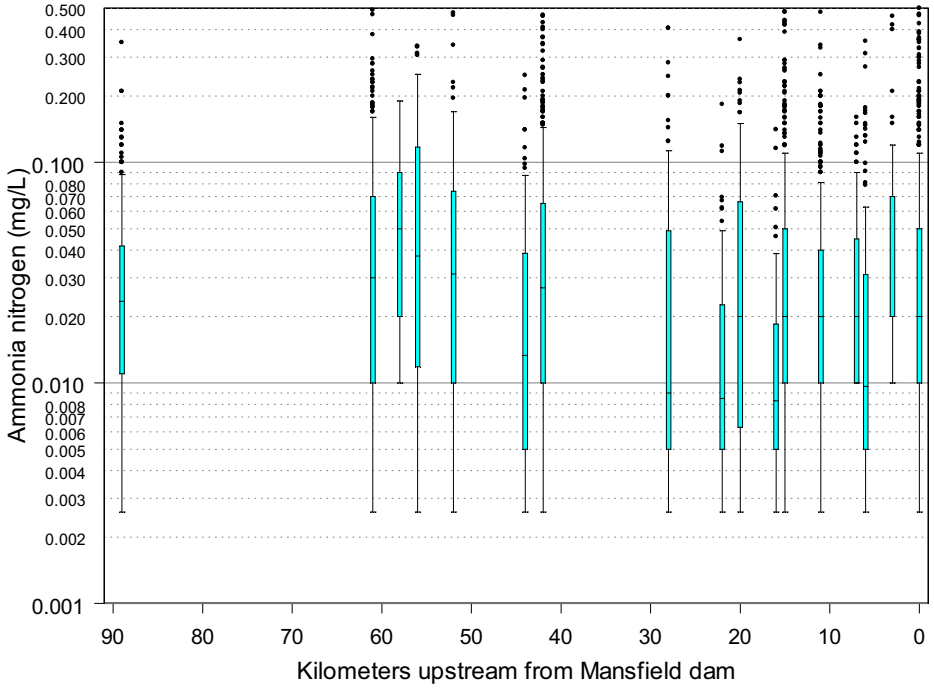

Figure 22. Ammonia nitrogen vs. depth.

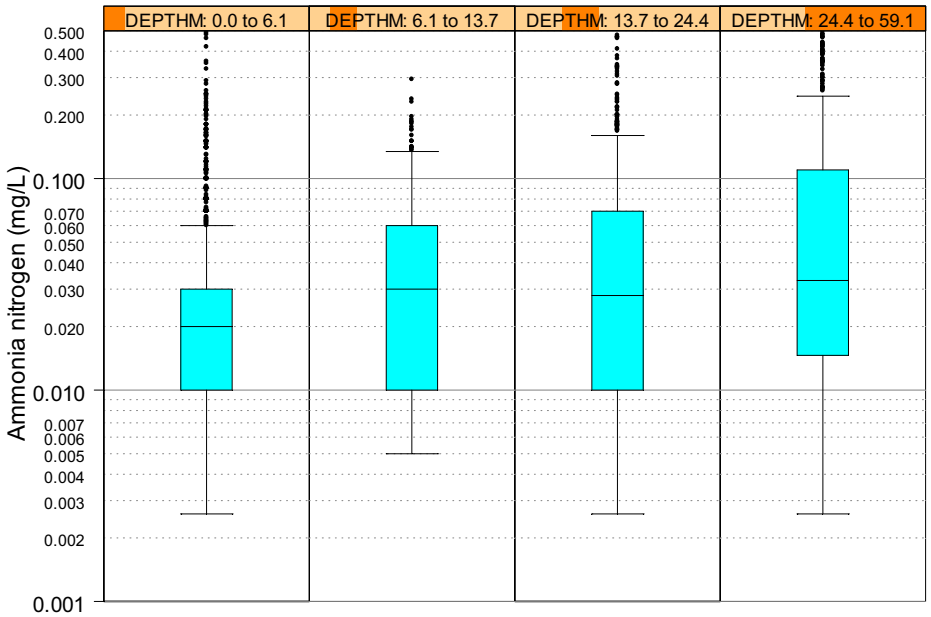

Figure 23. Ammonia nitrogen vs. year.

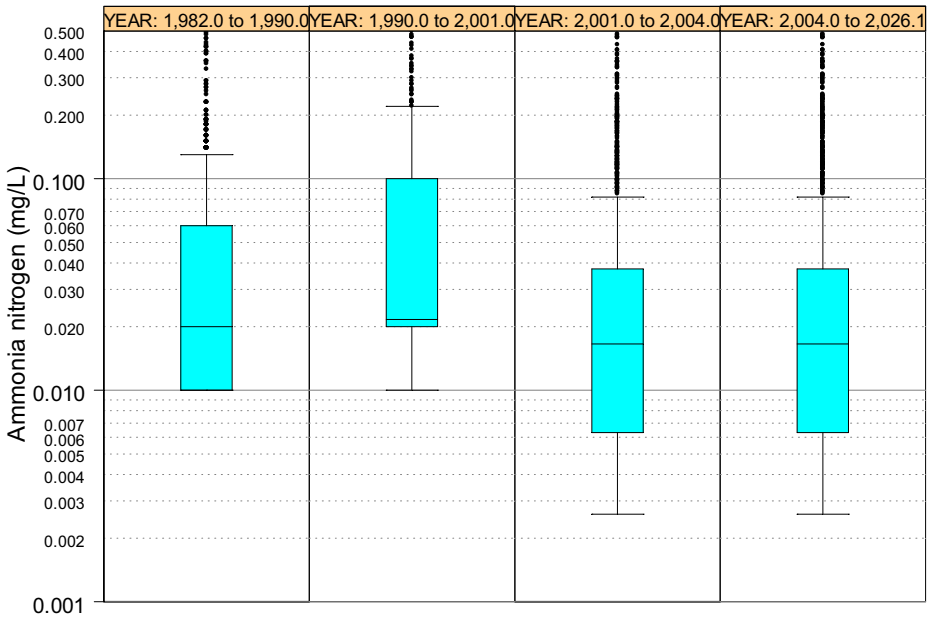

Figure 24. Ammonia nitrogen vs. time of day.

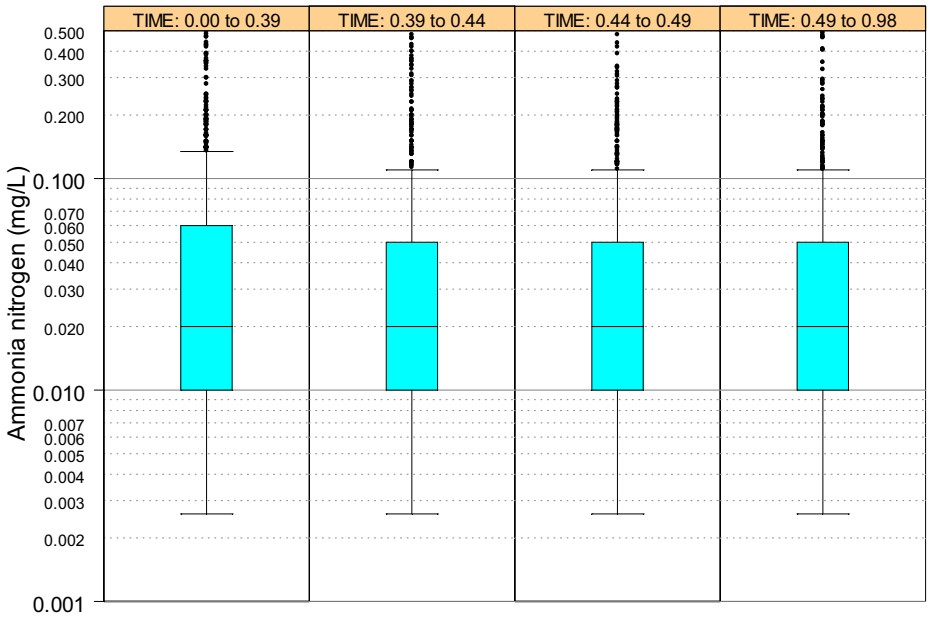

Figure 25. Ammonia nitrogen vs. month.

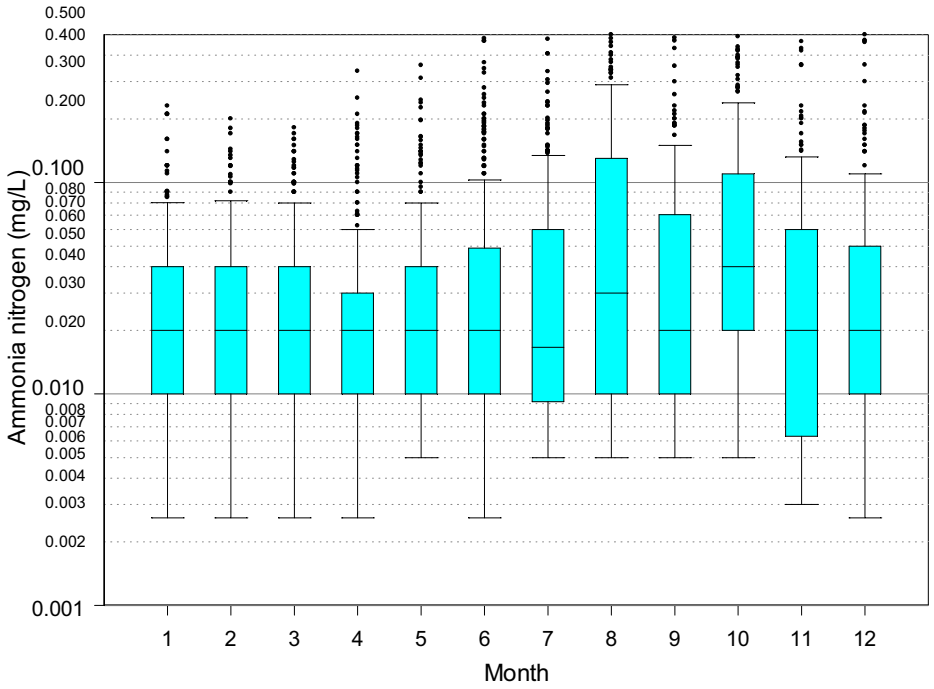

Nitrate/Nitrite Nitrogen

Spatial Variation

Nitrate+nitrite nitrogen did not appear to vary significantly with distance upstream (Figure 26). Nitrate nitrogen also did not appear to vary between cove and thalweg sites (Figure 27). Nitrate did appear to vary slightly with depth (Figure 28), with minimum values in the 5 to 10-meter depth range that may be due to uptake by growing algae.

Temporal Variation

Nitrate+nitrite levels exhibit seasonality, with concentrations declining in late spring to minimum values in the summer, and increasing in the fall (Figure 29). This may be due to uptake by algae and/or reduced inputs from inflows, and/or increased denitrification at higher temperatures. Nitrate levels did not appear to vary significantly with time of day (Figure 30). There appears to be a small long-term increasing trend in nitrate+nitrite levels since the 1980s (Figure 31).

Figure 26. Nitrate+nitrite nitrogen vs. distance upstream from Mansfield Dam.

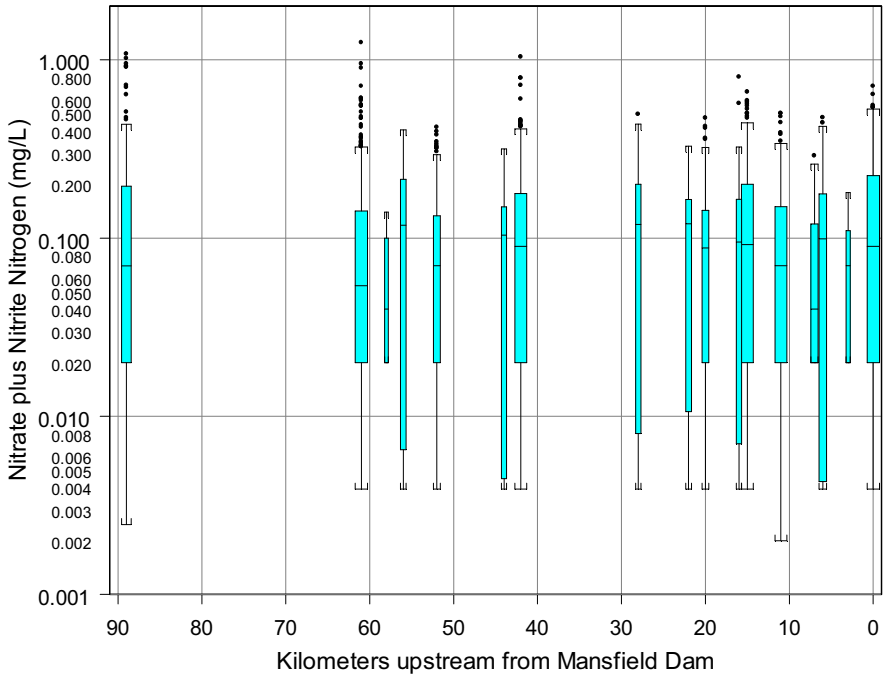

Figure 27. Nitrate+nitrite nitrogen in cove vs. thalweg sites.

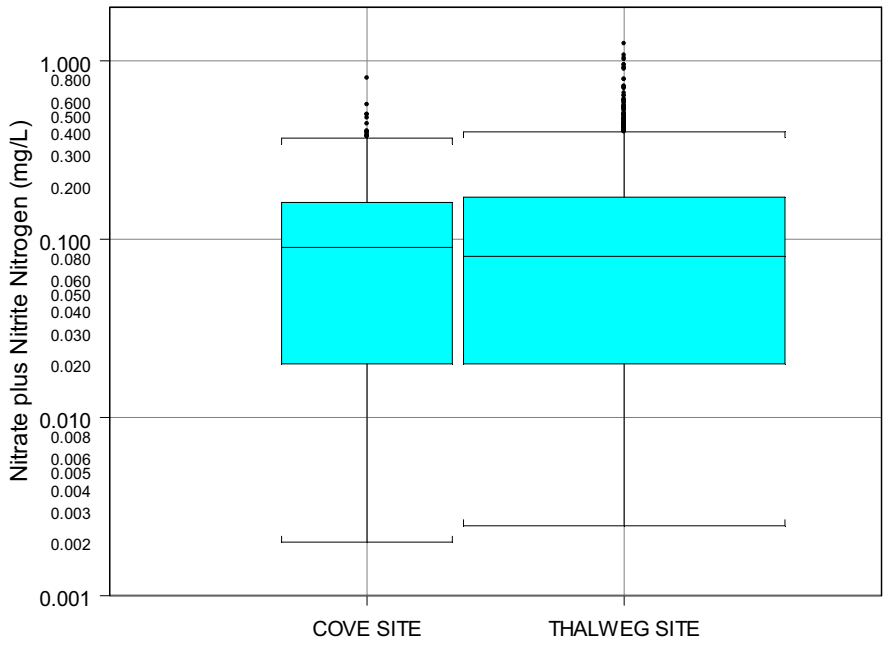

Figure 28. Nitrate+nitrite nitrogen vs. depth.

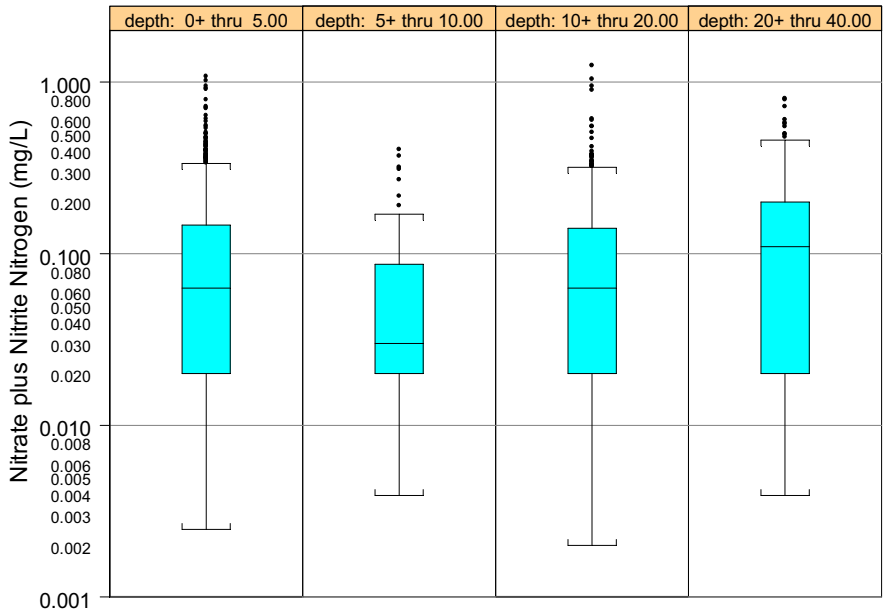

Figure 29. Nitrate+nitrite nitrogen vs. month.

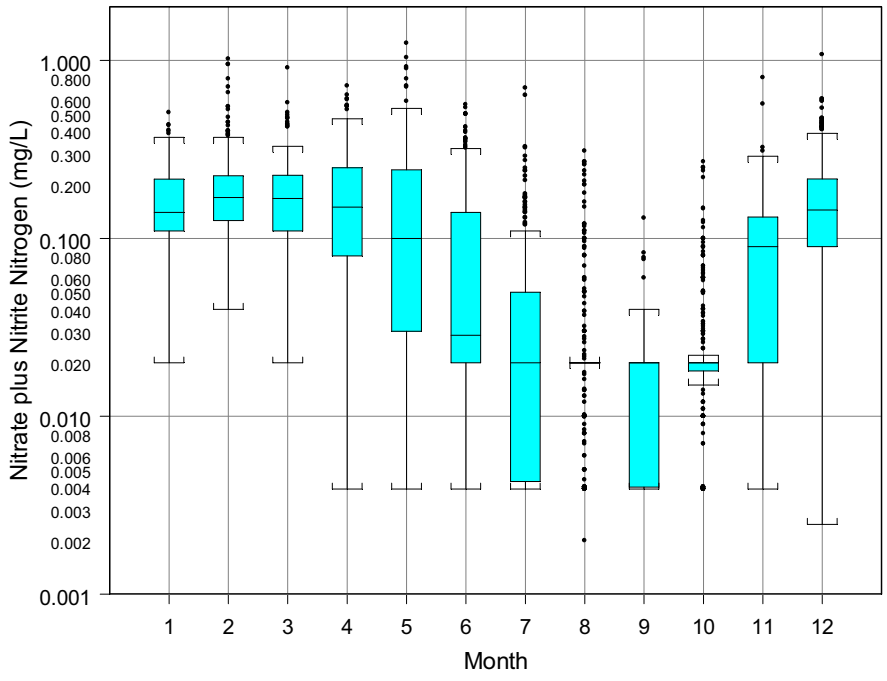

Figure 30. Nitrate+nitrite nitrogen vs. time of day.

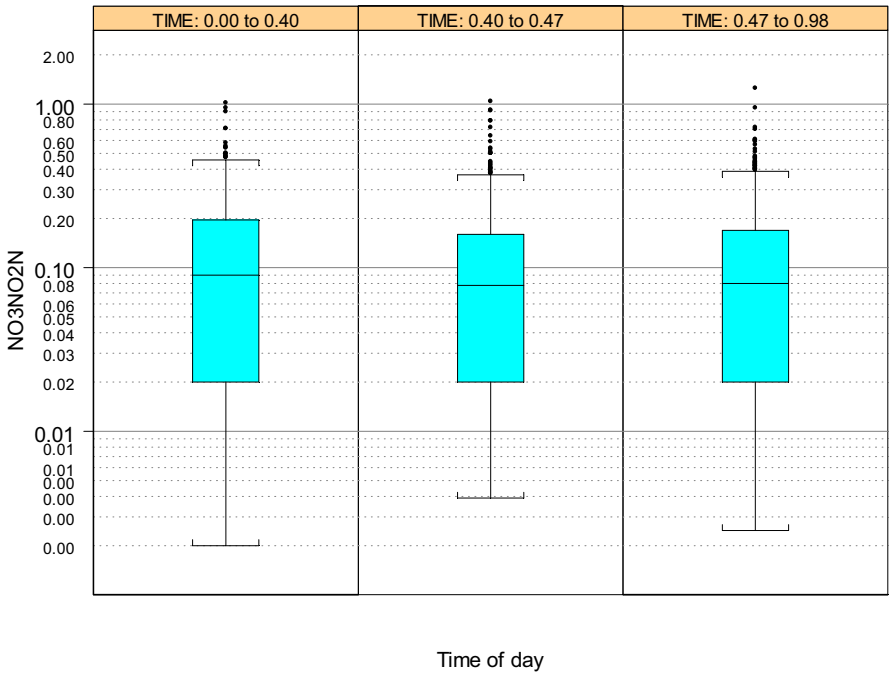

Figure 31. Nitrate+nitrite nitrogen vs. year.

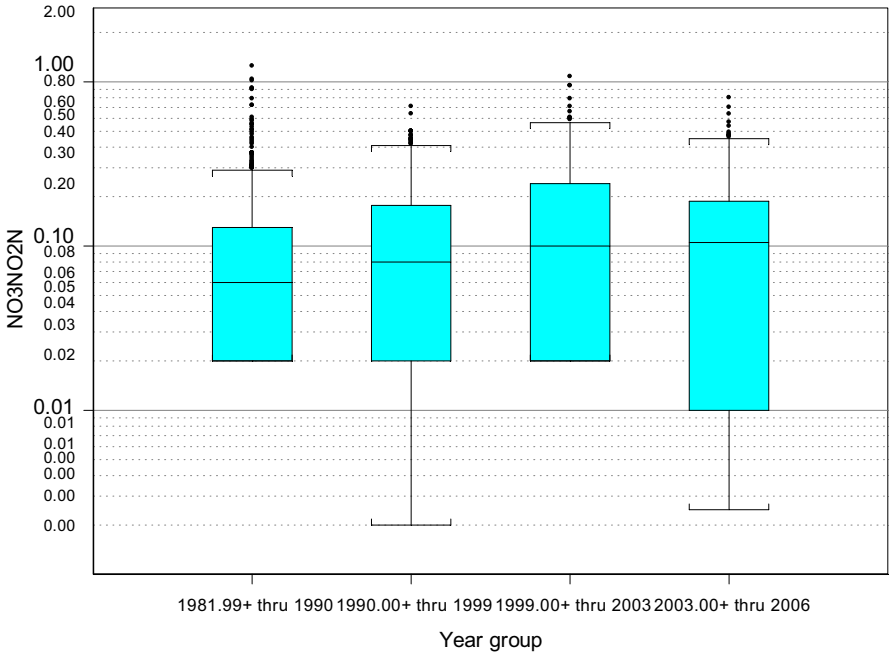

Nitrate+Nitrite Nitrogen Model

A generalized linear model was developed to explain observed variance in nitrate+nitrite nitrogen. The model accounts for approximately 56 percent of the observed variance. It should provide reasonable estimates of Lake Travis pH values at any point in time and space, and elucidate some of the significant factors that may influence nitrate that should be accounted for in the CE-QUAL-W2 water quality model. It should be emphasized that a significant statistical relationship, or lack thereof, does not imply causation. Also, interactions between predictive variables were not accounted for in this simple model.

Independent variable	t-value	p-value	Model Coefficient
Intercept	3.9	0.0001	0.237
Water temperature (°C)	-37.4	<0.0001	-0.1387
Ammonia nitrogen (mg/L)	-18.8	<0.0001	-2.216
Season	-8.2	<0.0001	-0.164
Distance (km)	6.1	<0.0001	0.0038

The model indicates that nitrate+nitrite values:

- are strongly seasonal, as indicated by the relationships with season and water temperature;
- are related to ammonia nitrogen levels;
- increase with distance from Mansfield Dam, after accounting for other factors (although this is not apparent from a univariate model); and
- are not related to depth, although this is probably because nitrate levels are higher at the surface and near the bottom, and lower in the middle, which is not accounted for in this type of model.

Total Kjeldahl Nitrogen

Spatial Analysis

Total Kjeldahl nitrogen (TKN) appears to be higher in the upstream reaches of Lake Travis where concentrations are typically between 0.4 and 0.5 mg/L, than in the lower reaches, where concentrations are typically between 0.3 and 0.4 mg/L (Figure 32). Concentrations do not appear to differ between cove and thalweg sites. TKN appears to vary with depth, with lowest levels near the surface and near the bottom, and higher levels in between (Figure 33).

Figure 32. Total Kjeldahl nitrogen vs. distance upstream from Mansfield Dam.

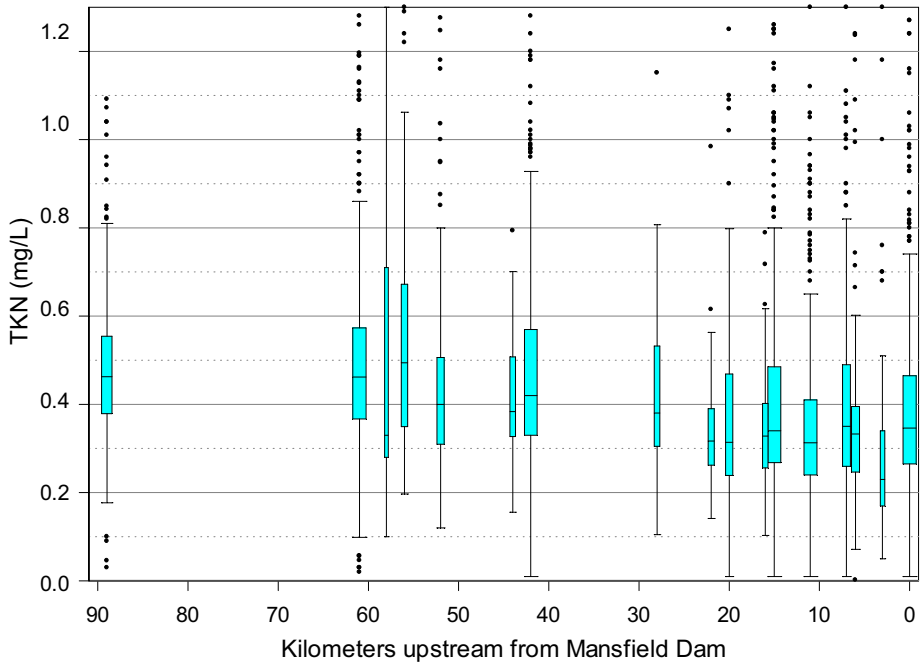

Temporal Analysis

TKN levels appear to vary seasonally, reaching peak values in late summer and early fall (Figure 34). TKN levels did not vary with time of day. TKN levels do not appear to have changed in a systematic way from year to year since the early 1980s (Figure 35).

Figure 33. Total Kjeldahl nitrogen vs. depth.

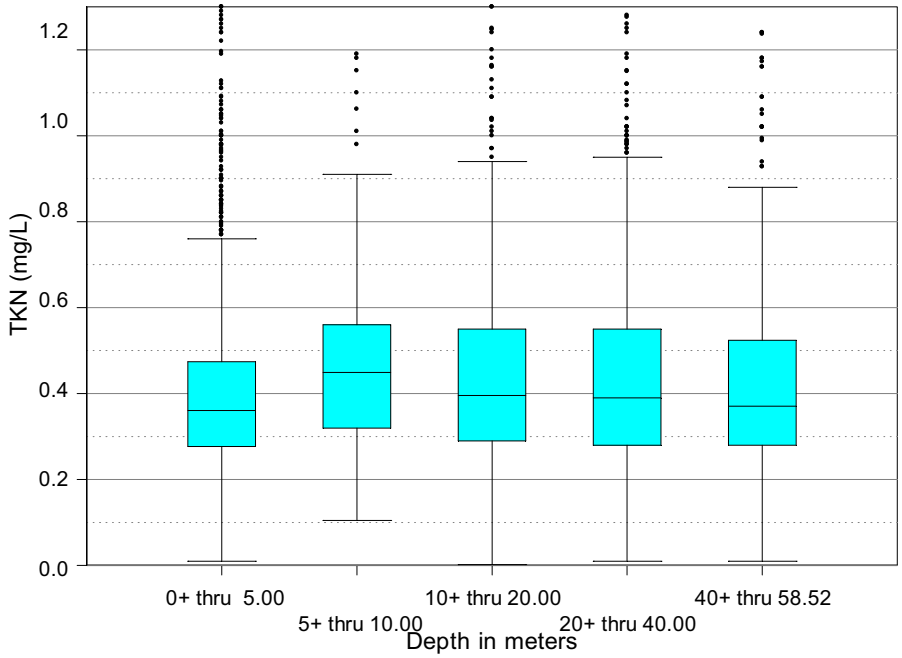

Figure 34. Total Kjeldahl nitrogen vs. month.

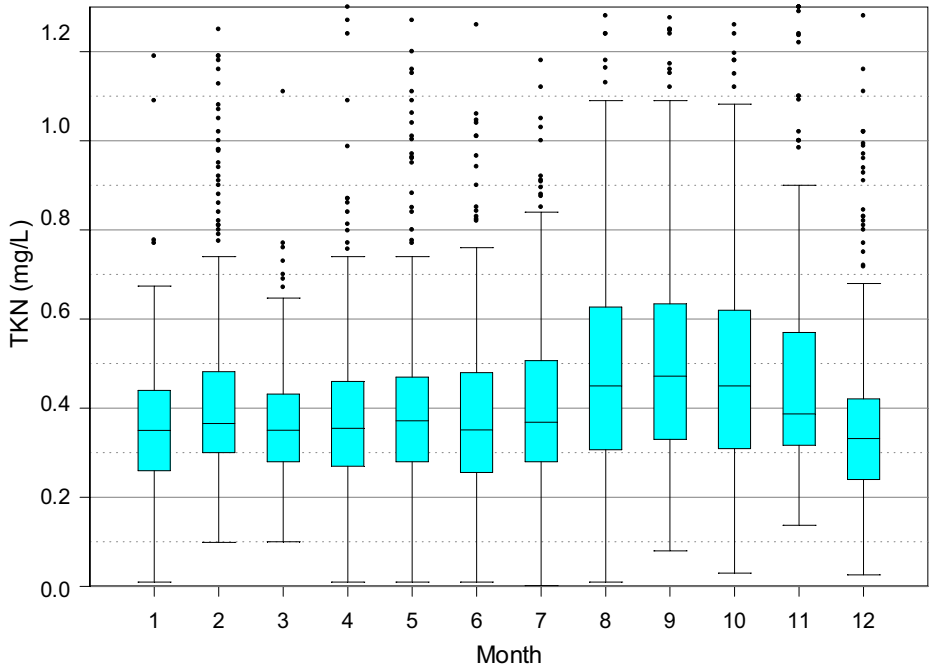

Figure 35. Total Kjeldahl nitrogen vs. year.

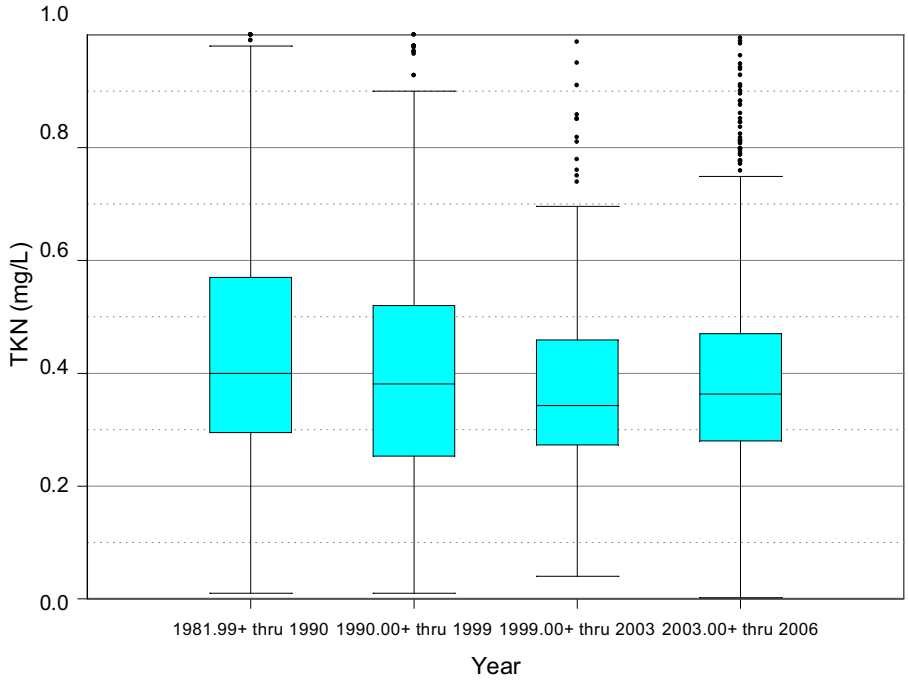

TKN Model

A generalized linear model was developed to explain observed variance in TKN. More than any other parameter, TKN levels were relatively constant and unrelated to other

parameters. The model accounts for only 13 percent of the observed variance. It should be emphasized that a significant statistical relationship, or lack thereof, does not imply causation. Also, interactions between predictive variables were not accounted for in this simple model.

Dependent variable: log TKN

Independent variable	t-value	p-value	Model Coefficient
Intercept	6.3	<0.0001	21.29
Distance (km)	10.0	<0.0001	0.0054
Year	7.0	<0.0001	-0.0019
log nitrate+nitrite nitrogen	-5.6	<0.0001	-0.0649
Depth (m)	5.4	<0.0001	0.0092
log total phosphorus (mg/L)	3.7	0.0002	0.1507
Chlorophyll-a	3.3	0.0010	0.0125
pH	3.0	0.0028	0.1656

The model indicates that TKN values:

- are only weakly related to other variables;
- increase with distance from Mansfield Dam;
- on average, have decreased with year since the early 1980s;
- were negatively related to nitrate+nitrite concentrations;
- increase with depth; and
- are positively related to total phosphorus, chlorophyll-a, and pH levels.

Dissolved Kjeldahl Nitrogen

The dissolved pool of Kjeldahl nitrogen typically comprises 75 to 80 percent of TKN. This ratio is proportional to chlorophyll-a and total suspended solids concentrations, and is lowest in the lower epilimnion where primary production peaks (Figures 36 to 38). Ratios may exceed 1 due to analytical uncertainty and detection limit issues.

Figure 36. DKN/TKN ratio vs. depth.

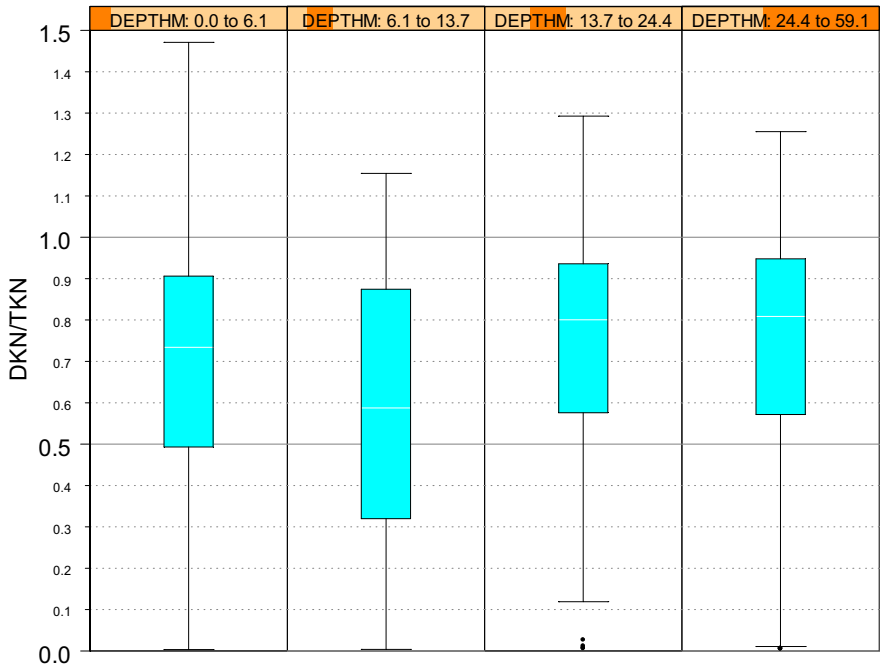

Figure 37. DKN/TKN ratio vs. TSS concentration.

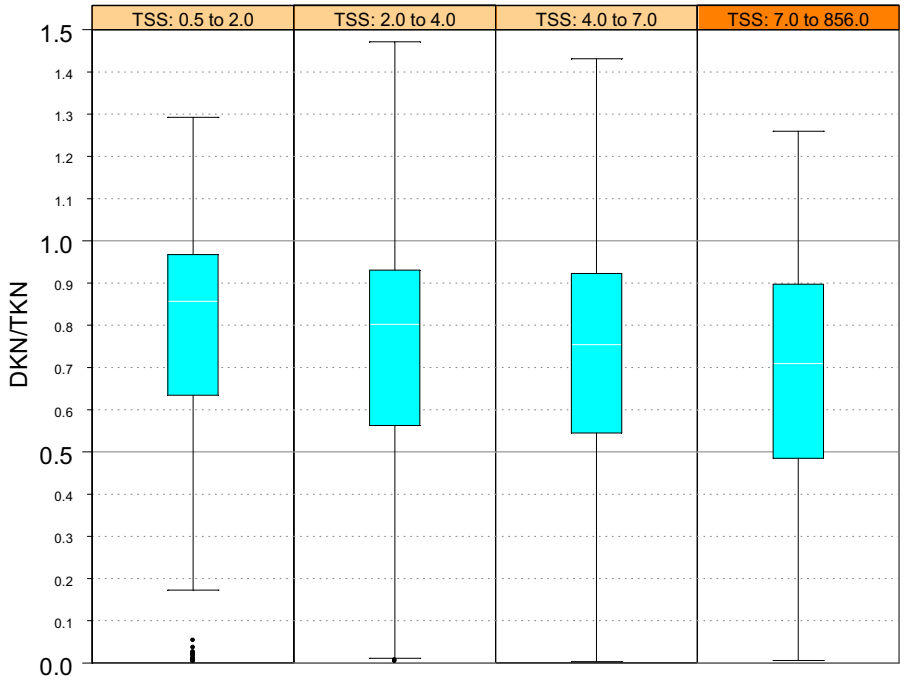

Figure 38. DKN/TKN ratio vs. chlorophyll-a concentration.

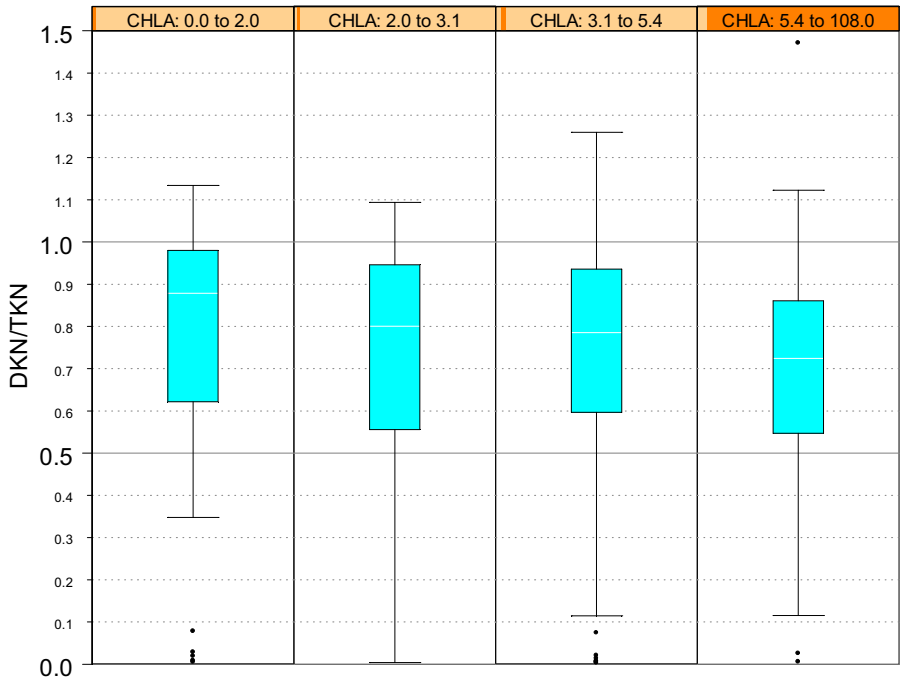

Phosphorus

Spatial and temporal analysis of total phosphorus concentrations were confounded by low levels of phosphorus and varying detection limits. The analysis was affected more by the detection limit than any other factor. For this reason, we do not attempt to interpret or model the results, but present several figures (39-43).

Figure 39. Total phosphorus vs. distance upstream from Mansfield Dam.

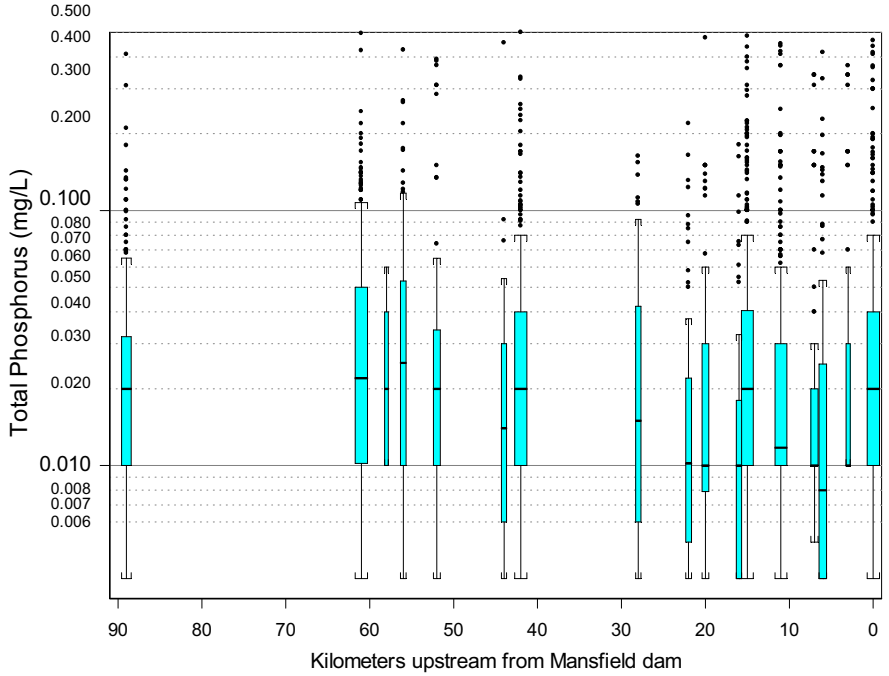

Figure 40. Total phosphorus vs. depth.

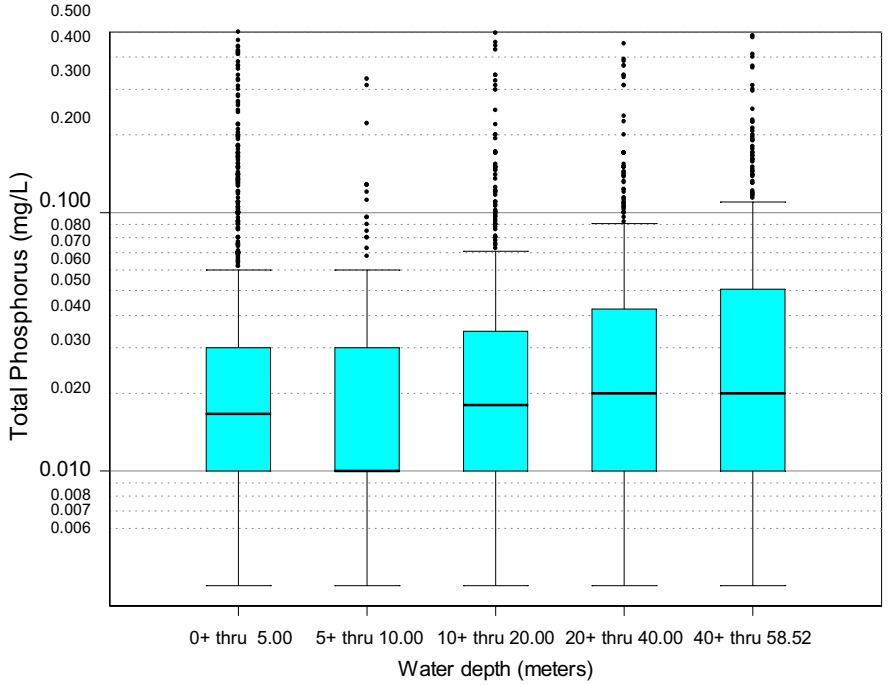

Figure 41. Total phosphorus vs. year.

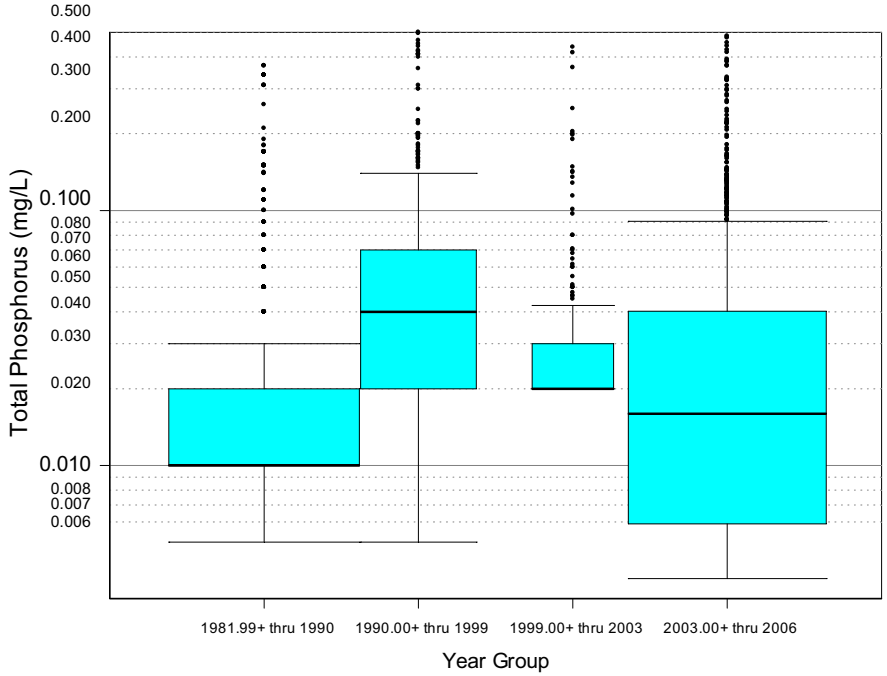

Figure 42. Total phosphorus vs. month.

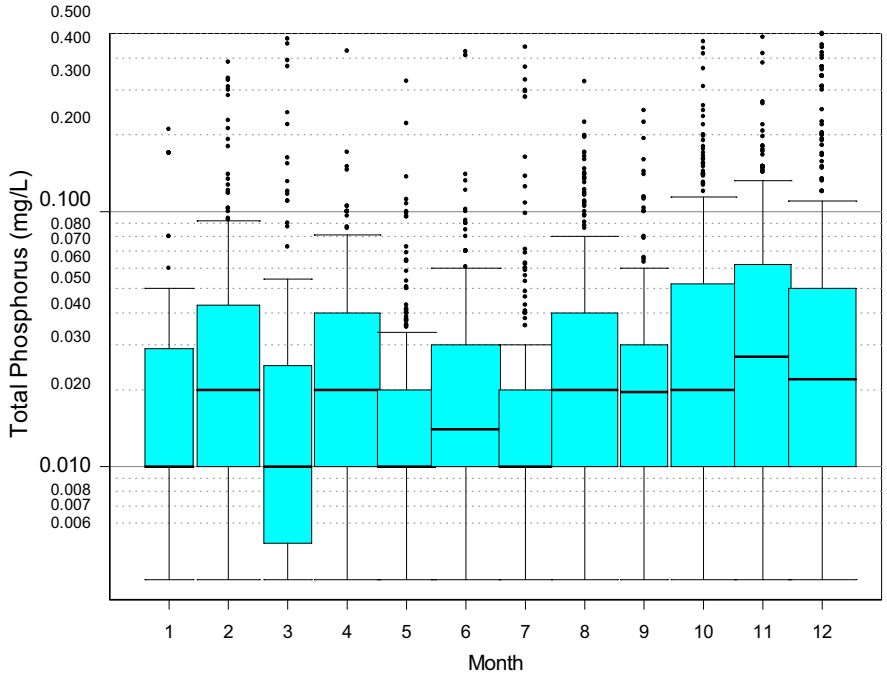

Figure 43. Total phosphorus vs. time of day.

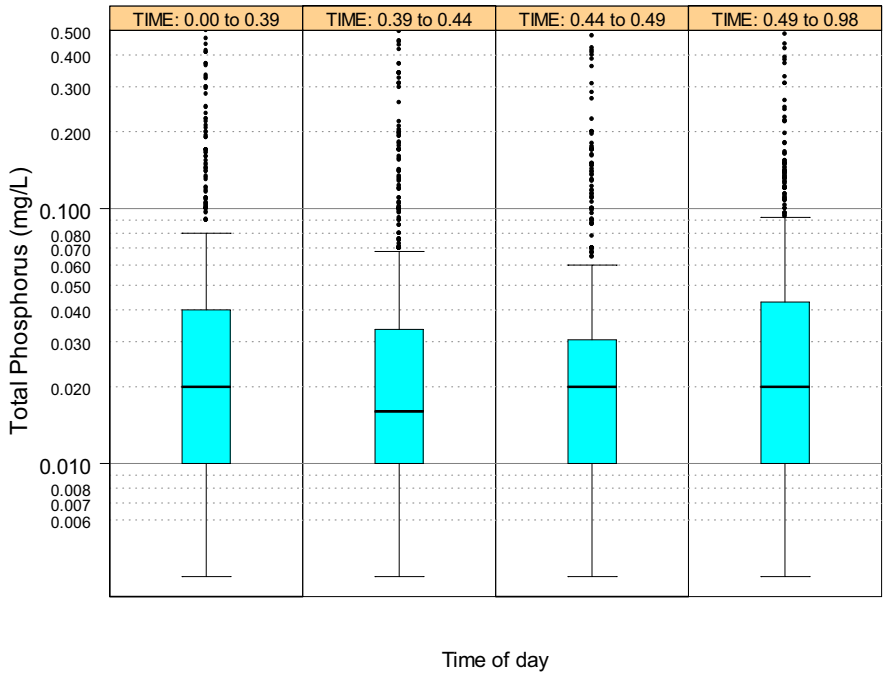

Dissolved Phosphorus

On average, approximately 65 to 70 percent of total phosphorus is in the dissolved pool, but the fraction is highly variable. The dissolved fraction does not appear to differ between cove and thalweg sites (Figure 44). The dissolved fraction tends to be highest near the surface and the bottom, and lower in between (Figure 45). The dissolved fraction declines with increasing suspended solids concentrations (Figure 46) and tends to increase with distance from Mansfield Dam (Figure 47).

Figure 48 indicates that, on average, from 30 to 40 percent of the dissolved phosphorus pool is present as orthophosphate, with the balance presumed to be primarily dissolved organic forms. The ratio is quite variable, and may be slightly higher at thalweg sites than cove sites.

Given that, on average, 65 to 70 percent of total phosphorus is dissolved, and 30 to 40 percent of the dissolved pool is orthophosphate, it seems reasonable to expect the ratios of dissolved orthophosphate to total phosphorus to be less than those of orthophosphate to dissolved phosphorus, and in the range of 20 to 25 percent. However, Figure 49 shows that dissolved orthophosphate comprises on average 30 to 40 percent of total phosphorus, similar to the fraction of dissolved phosphorus. Figure 50 illustrates how this ratio increases with total dissolved solids levels.

Figure 44. Dissolved: total phosphorus ratio for cove and thalweg sites.

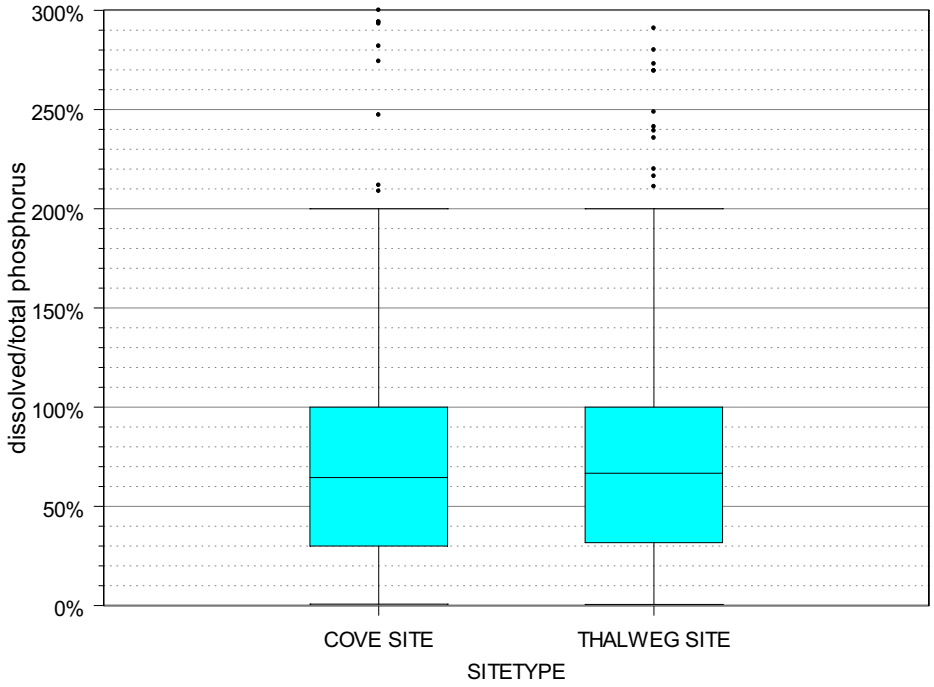

Figure 45. Dissolved: total phosphorus ratio vs. depth.

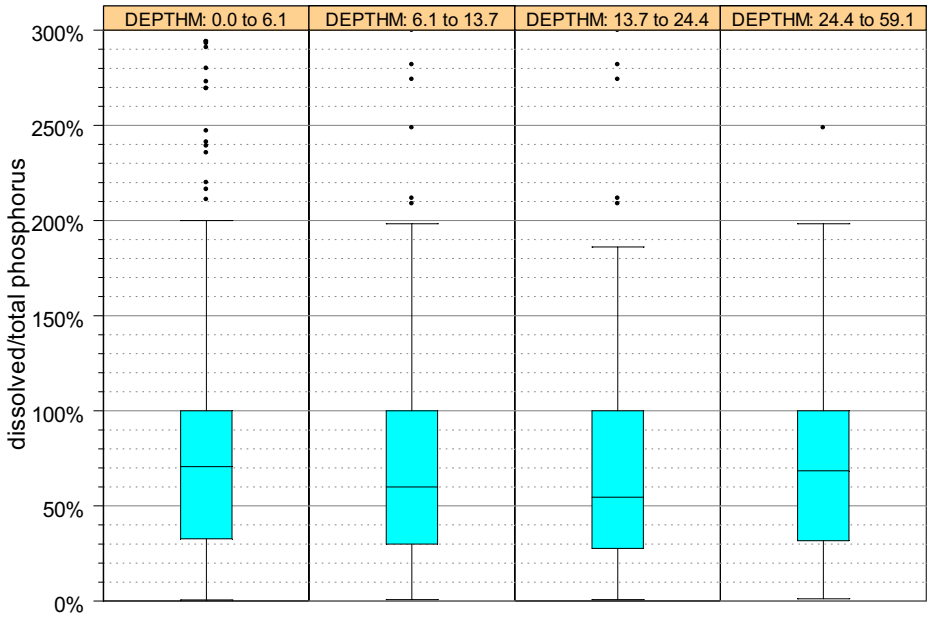

Figure 46. Dissolved: total phosphorus ratio vs. TSS.

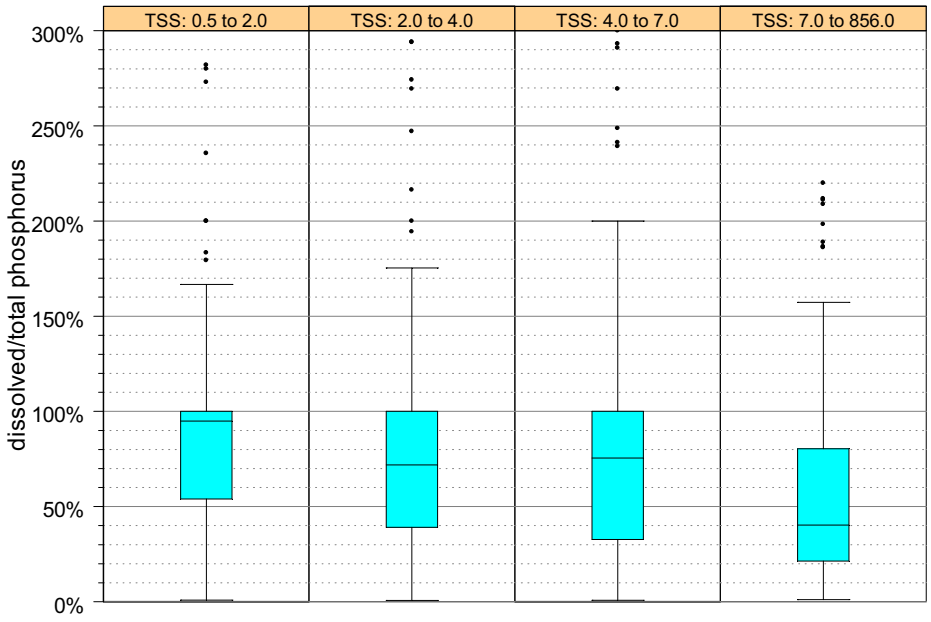

Figure 47. Dissolved: total phosphorus ratio vs. distance upstream from Mansfield Dam.

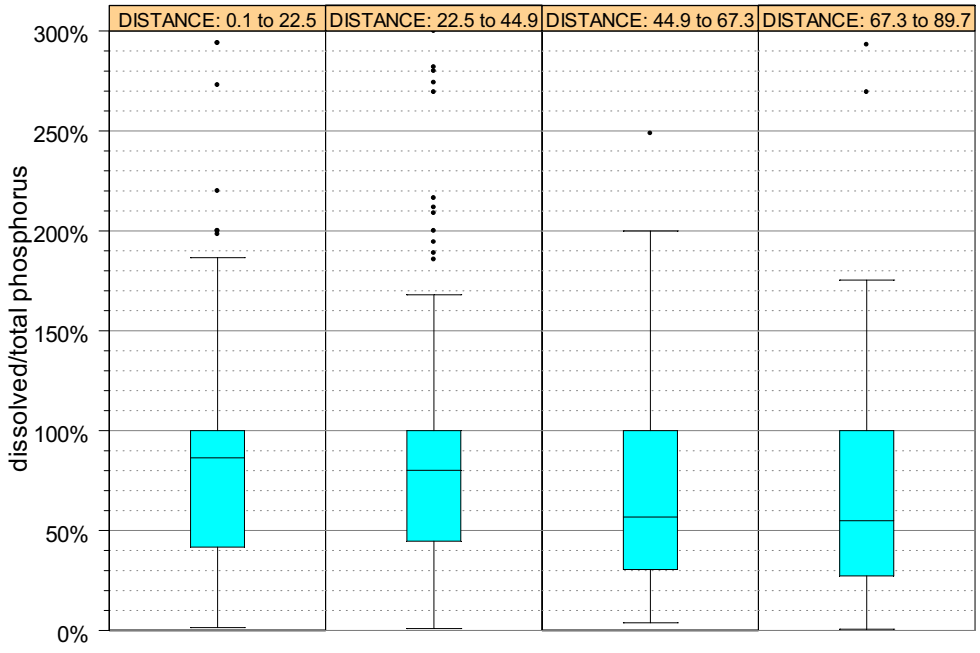

Figure 48. Dissolved orthophosphate: dissolved phosphorus ratio for cove and thalweg sites.

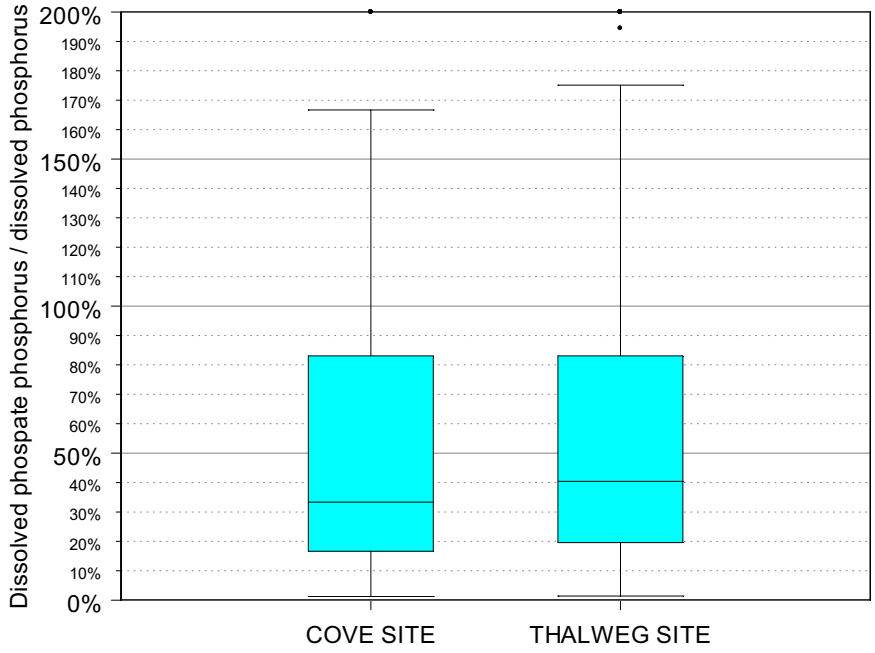

Figure 49. Dissolved orthophosphate: total phosphorus ratio for cove and thalweg sites.

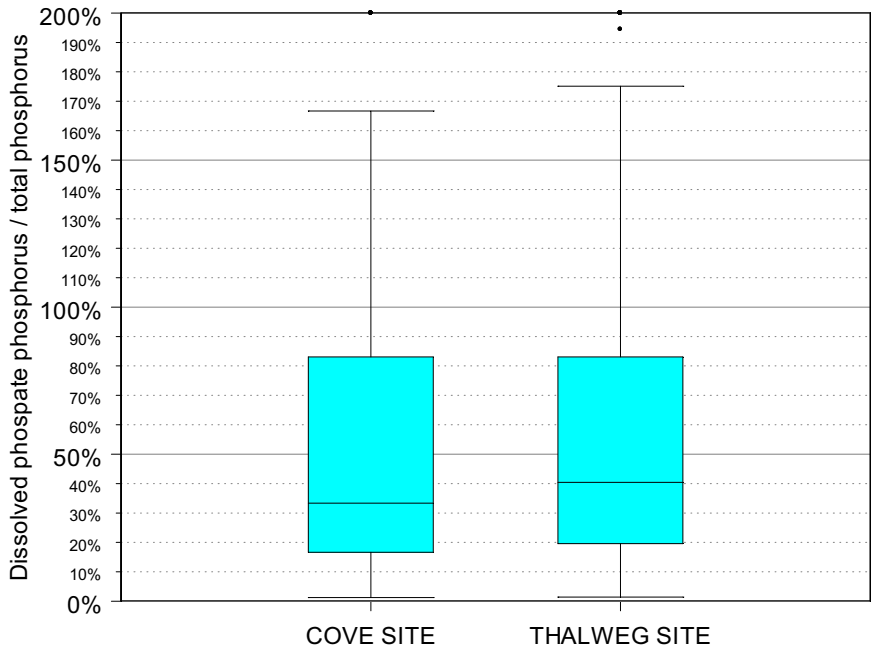

Figure 50. Dissolved orthophosphate: total phosphorus ratio vs. TDS.

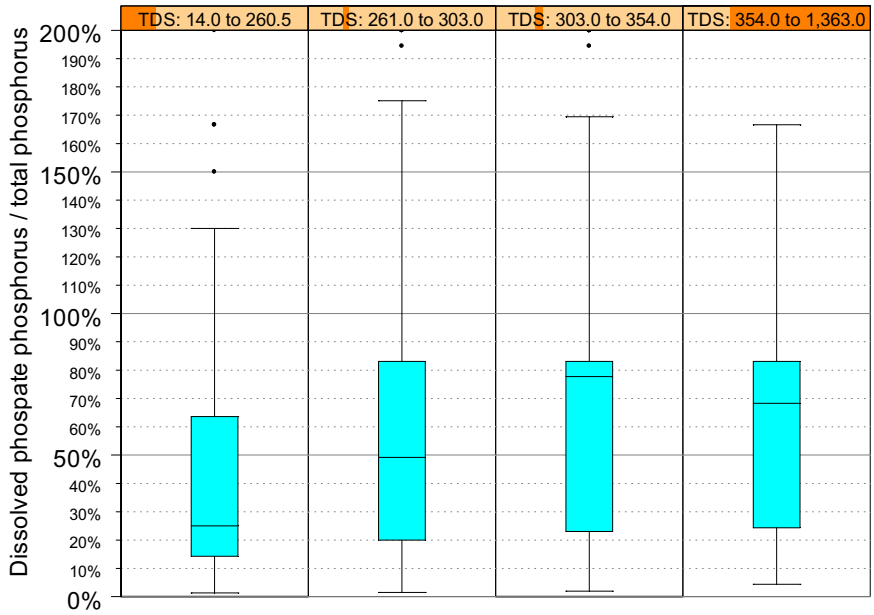

Dissolved Oxygen

Spatial Analysis

No spatial variations in surface dissolved oxygen concentrations were apparent (Figure 51), nor were systematic patterns apparent at greater depths. Surface dissolved oxygen concentrations were routinely high, with most values ranging between 7 and 10 mg/L reflecting seasonal variations in oxygen solubility in water with temperature. A few low (<4 mg/L) dissolved oxygen concentrations were measured in middle and upstream reaches of the reservoir. Figure 52 illustrates that there is no significant difference in average surface dissolved oxygen concentration for cove and thalweg sites, although the variance is slightly greater in thalweg sites. Figure 53 illustrates the variation of dissolved oxygen with depth.

Temporal Analysis

Figure 54 illustrates the seasonal pattern of surface (depth <5 meters) dissolved oxygen concentrations due to the temperature effect on oxygen solubility. Figure 55 shows seasonal patterns of dissolved oxygen concentrations in deep waters (depth >30 meters), illustrating seasonal hypolimnetic anoxia. Hypolimnetic oxygen is typically depleted in July and recovers in November. Median dissolved oxygen levels appear to exhibit only slight diel cycles, although most measurements were taken in late morning (Figure 56). Long-term dissolved oxygen trends indicate slight increases with time since the early 1980s (Figure 57). Closer inspection of the long-term oxygen variation indicates a cyclical pattern that appears to be related to water temperature (Figure 58).

Figure 51. Surface dissolved oxygen concentrations vs. distance upstream from Mansfield Dam.

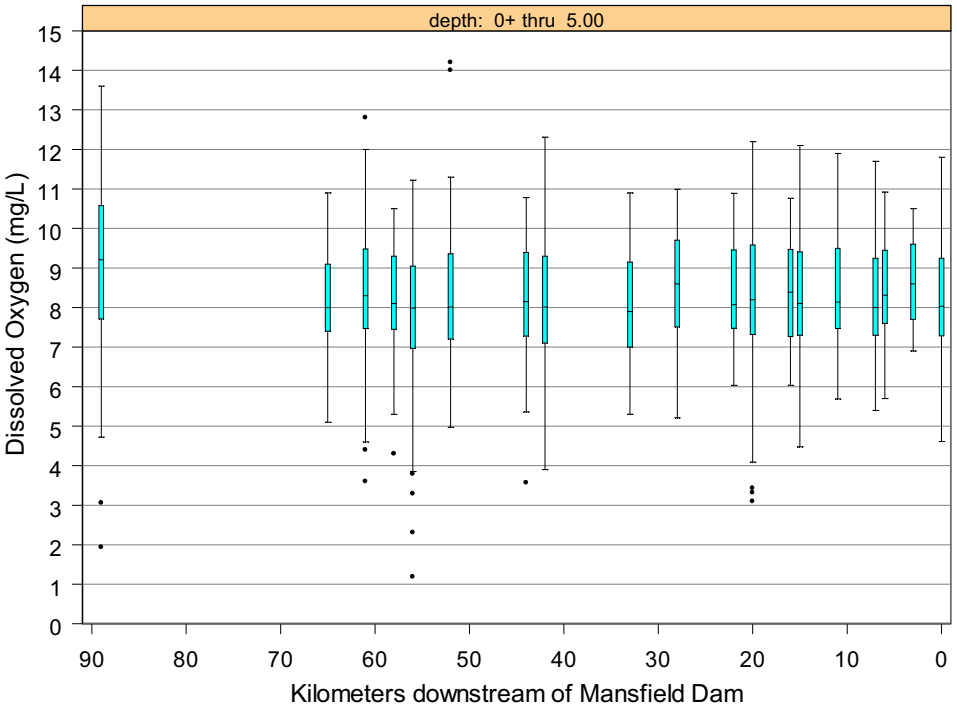

Figure 52. Surface dissolved oxygen concentration for cove and thalweg sites.

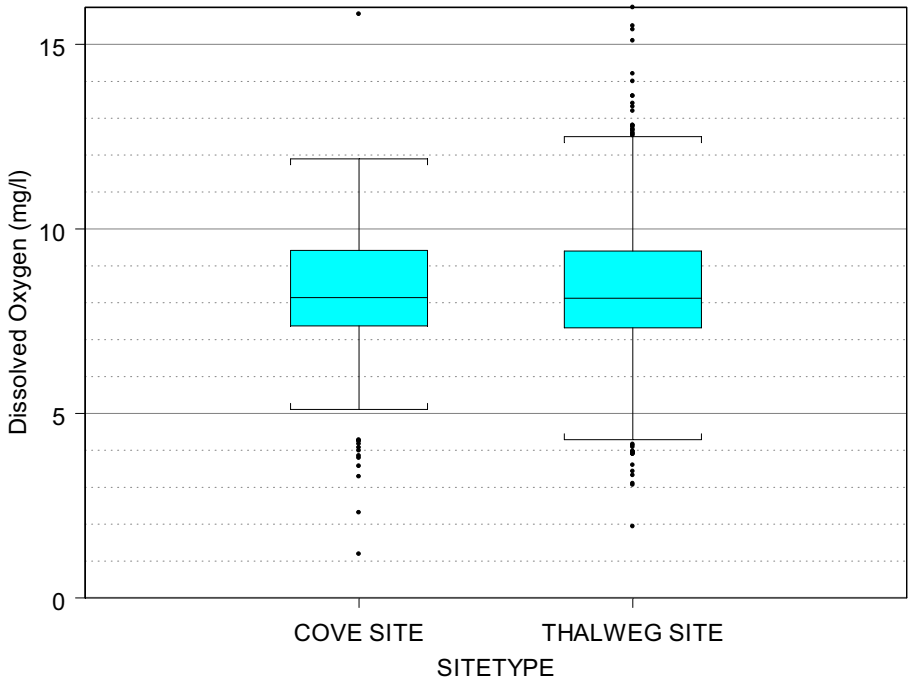

Figure 53. Dissolved oxygen concentrations vs. depth.

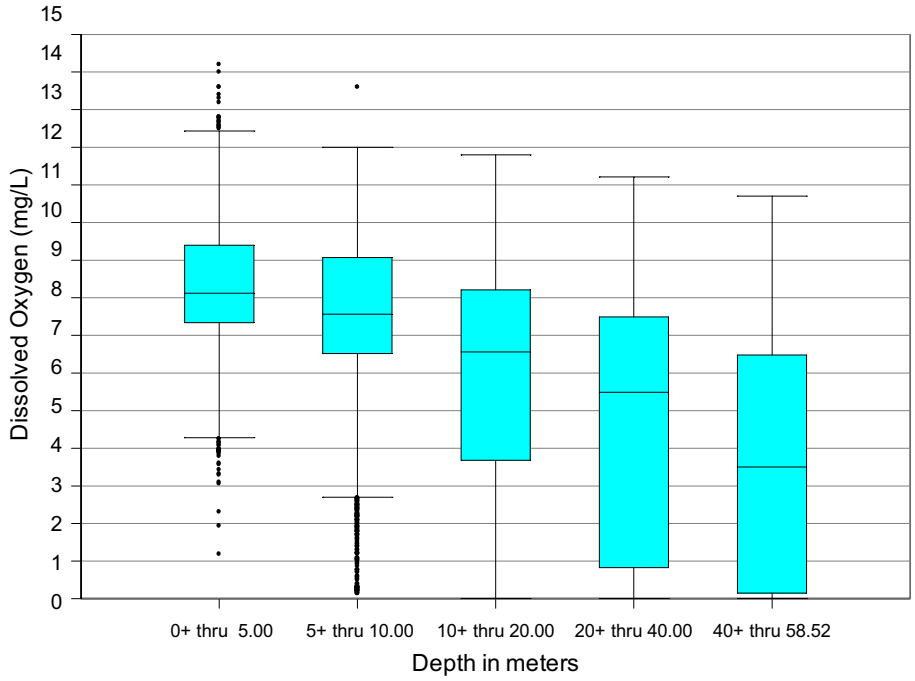

Figure 54. Surface dissolved oxygen concentration vs. month.

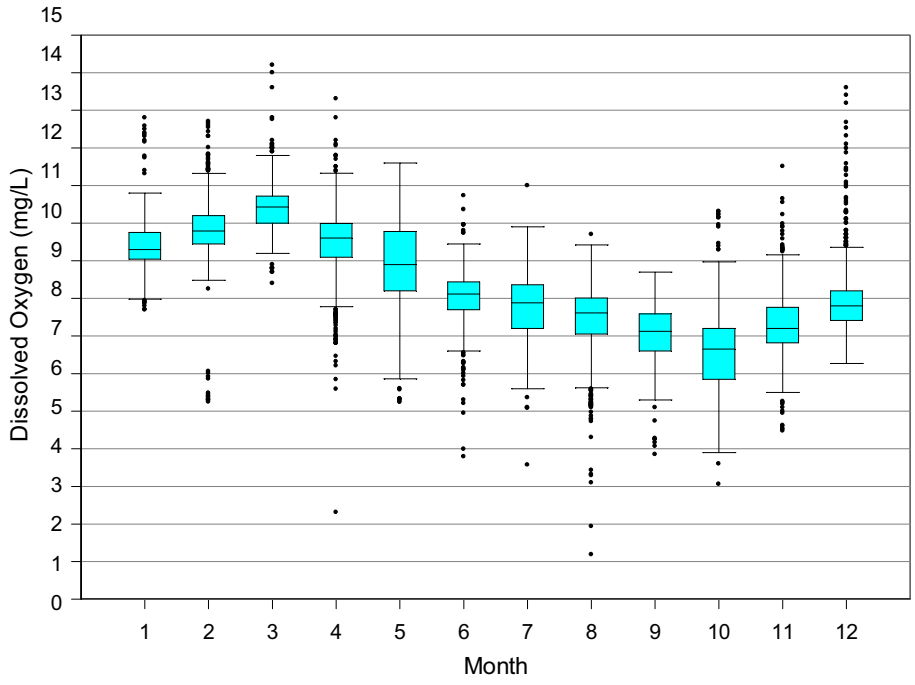

Figure 55. Benthic dissolved oxygen concentration vs. month.

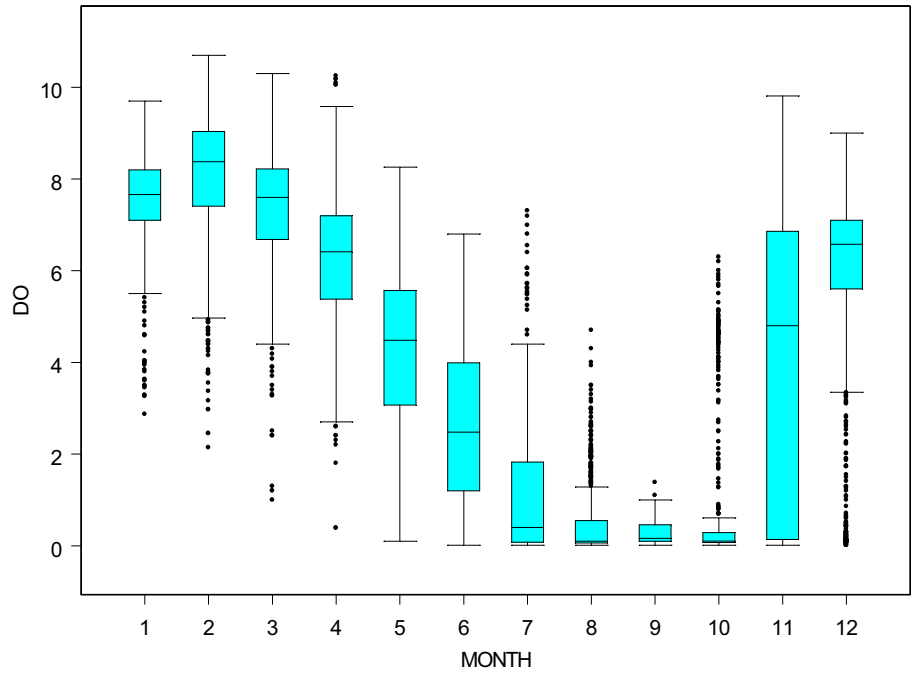

Figure 56. Dissolved oxygen concentration vs. time of day.

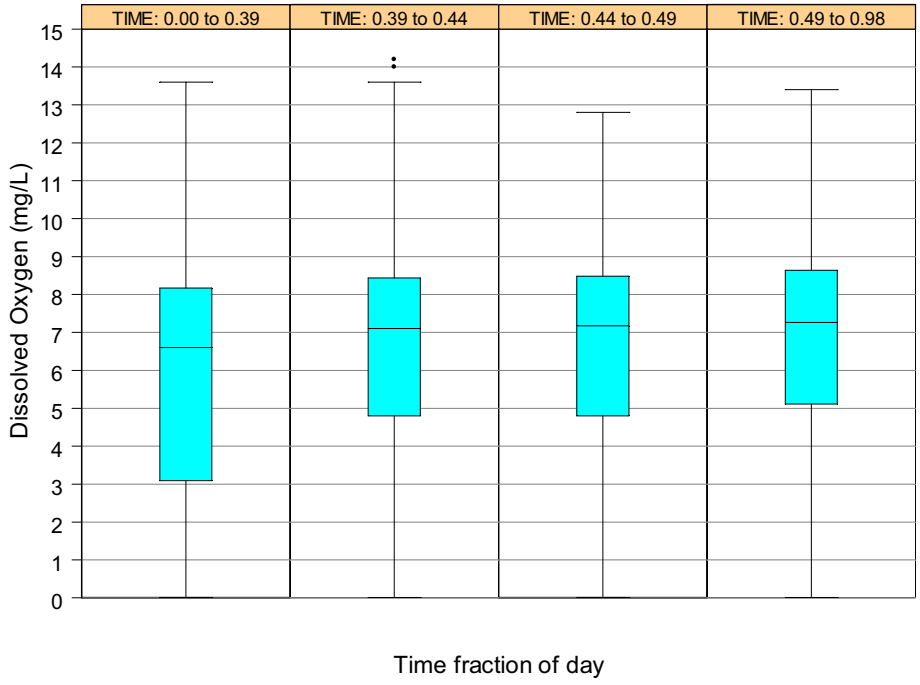

Figure 57. Dissolved oxygen concentration vs. year.

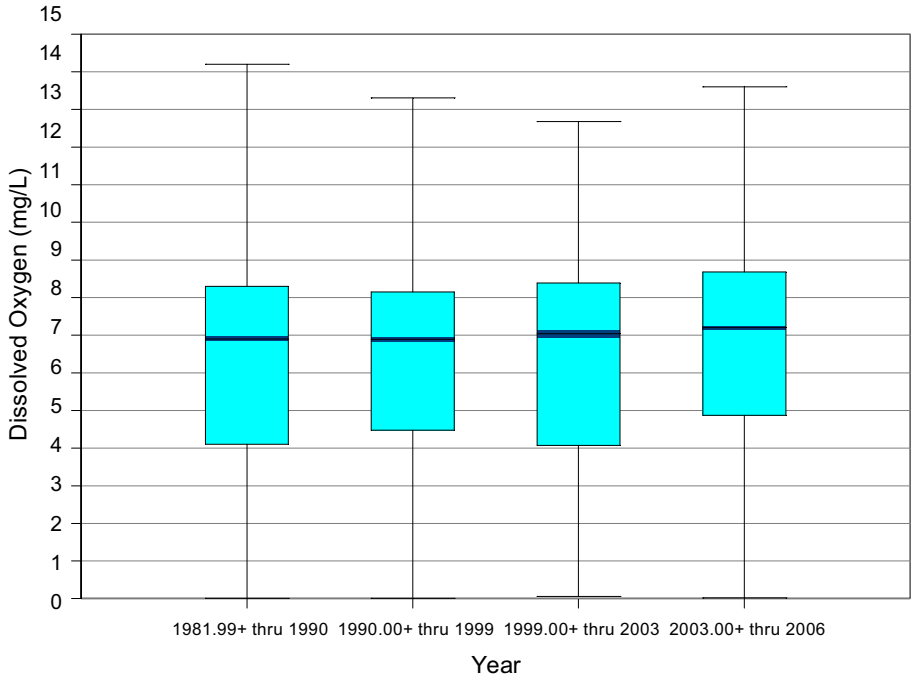

Figure 58. Dissolved oxygen concentration vs. year for individual years.

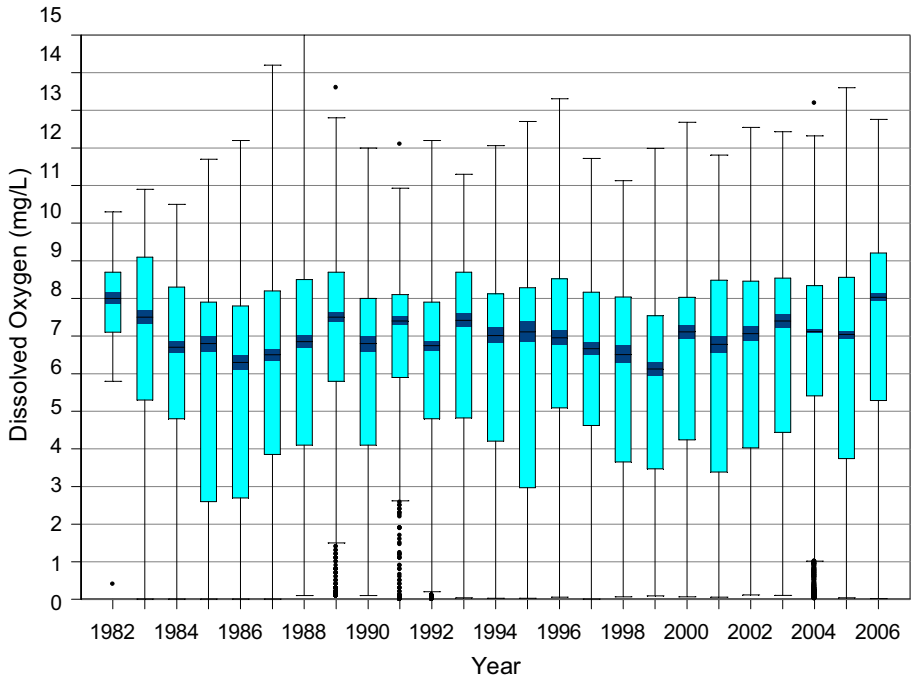

Dissolved Oxygen Model

A generalized linear model was developed to explain observed variance in dissolved oxygen (DO). The standard error of this statistical model is 1.3 mg/l, and it accounts for approximately 97percent of the observed variance in DO. It should provide good estimates of Lake Travis DO values at any point in time and space, and elucidates some of the significant factors that may influence DO that should be accounted for in the CE-QUAL-W2 water quality model. It should be emphasized that a significant statistical relationship, or lack thereof, does not imply causation. Also, interactions between predictive variables were not accounted for in this simple model.

Independent variable	t-value	p-value	Model Coefficient
pH	241	<0.0001	5.61
Year	-203	<0.0001	-0.0195
Month (July lag)	185	<0.0001	0.684
Month	102	<0.0001	-0.185
Depth	-32	<0.0001	-0.02

The model indicates that DO values are increased by primary production and reduced by respiration, with peaks in the upper water column in the summertime, and lower values in the deeper water layers that are respiration-dominated DO values

- are correlated most strongly with pH;
- are seasonal – and a combination of month and monthlag is required to simulate the seasonal cycle;
- decline with depth; and
- have declined annually at a small rate of approximately 0.02 mg/L per year since 1982, after other factors have been accounted for. Note, however, that this is very confounded by changes in pH.

Suspended Solids

Spatial Analysis

Total suspended solids (TSS) tend to increase with distance from Mansfield Dam, except for the headwaters where levels are low (Figure 59). TSS levels are not significantly different between cove and thalweg sites (Figure 60). The TSS relationship with depth is complex; it varies from site to site and is seasonal. At most sites and times, there is a subsurface TSS maximum in the 5-20 meter depth range. Surface concentrations are often among the lowest measured. Figure 61 illustrates the overall average relationship with depth.

Temporal Analysis

The seasonal variation in TSS appears to be governed more by allocthonous inputs of solids in runoff than by autochthonous production, because TSS levels are lowest

during the typically dry summertime (Figure 62). Figure 63 indicates no long-term trend in TSS concentrations.

Figure 59. Total suspended solids vs. distance upstream from Mansfield Dam.

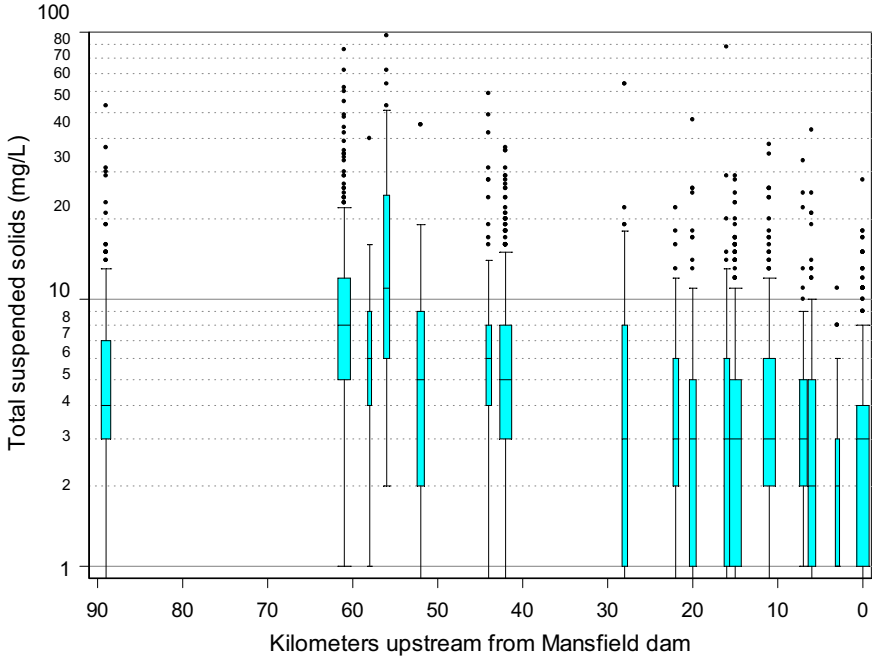

Figure 60. Total suspended solids in cove and thalweg sites.

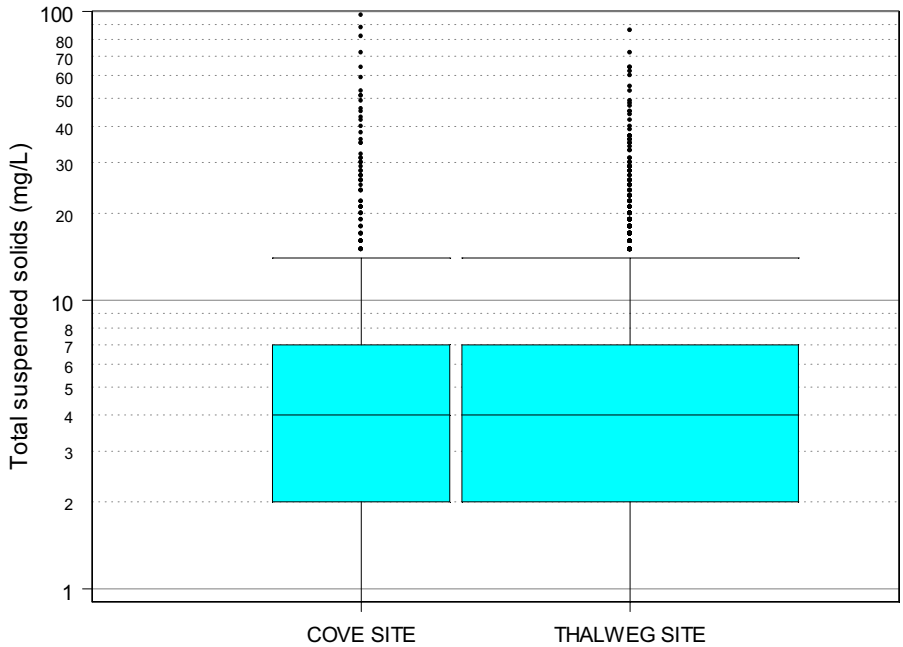

Figure 61. Total suspended solids vs. depth.

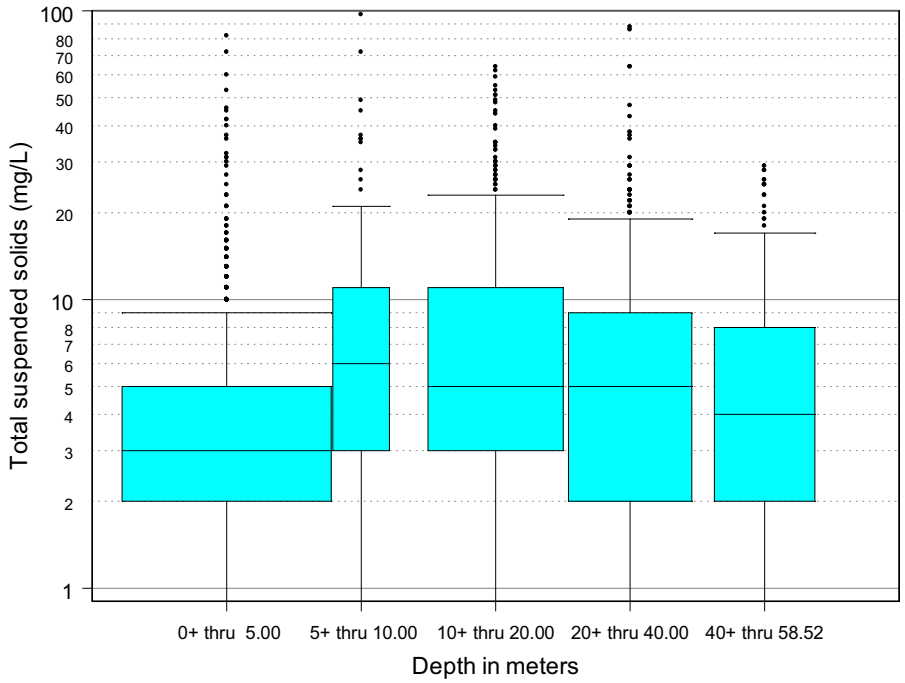

Figure 62. Total suspended solids concentration vs. month.

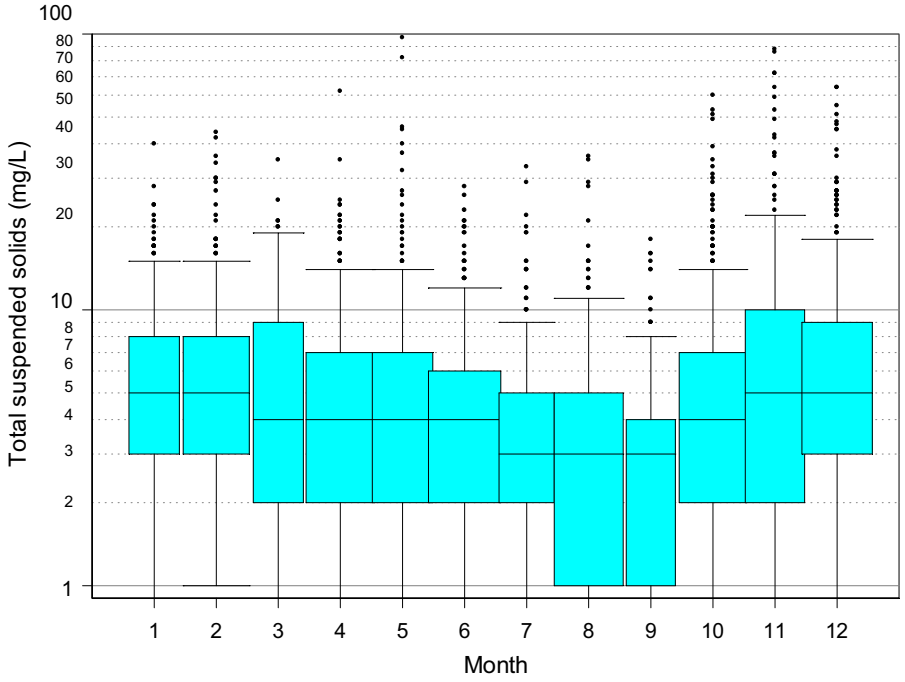

Figure 63. Total suspended solids concentration vs. year.

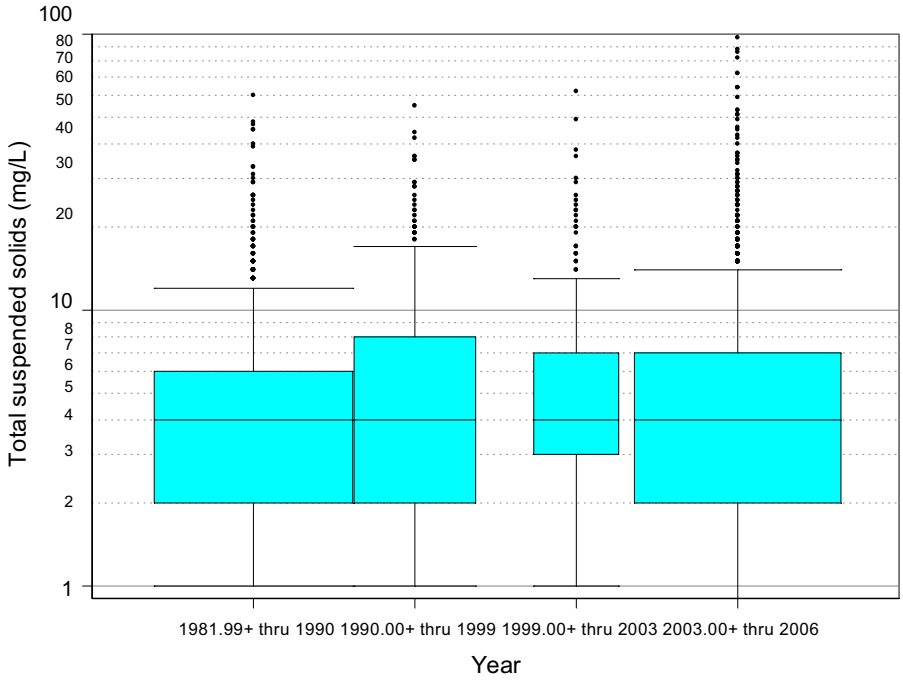

Suspended Solids Model

A generalized linear model was developed to explain observed variance in TSS. The model accounts for only approximately 24 percent of the observed variance in TSS. It should be emphasized that a significant statistical relationship, or lack thereof, does not imply causation. Also, interactions between predictive variables were not accounted for in this simple model.

Dependent variable: ln(TSS)

Independent variable	t-value	p-value	Model Coefficient
Intercept	9.8	<0.0001	0.3544
Distance (kilometers)	30.6	<0.0001	0.0173
Depth (meters)	20.6	<0.0001	0.0192
Month (July lag)	12.1	<0.0001	0.0961
Site Type (cove=0, thalweg=1)	-10.0	<0.0001	-0.1732

The model indicates that TSS values increase with distance from the dam, with increasing depth and in accordance with the number of months from July. The model also indicates that, after considering other factors, cove sites have slightly higher TSS levels on average than thalweg sites.

Volatile Suspended Solids

At high levels of suspended solids, the volatile (organic) fraction of the suspended solids concentration is relatively constant at 8 to 10 percent. However, at lower and more typical levels of suspended solids, the relationship is much more variable (Figure 64) but the volatile mass fraction tends to be higher. A simple linear regression fit is:

$$VSS = 1.53 + 0.0823 * TSS$$

where $r^2 = 0.714$

This relationship explains 71 percent of the variation in VSS, and has a residual standard error of 1.3 mg/L. However, this least-squared regression procedure is heavily weighted toward the larger suspended solids concentrations. Another regression procedure that is less sensitive to the extreme values (robust least-trimmed squares) gives the result that approximately 30 percent of the suspended mass is volatile:

$$VSS = 0.304 * TSS$$

Where $r^2 = 0.703$

Finally, a log-log regression that is relatively insensitive to the magnitude of TSS gives the result that approximately 40 percent of the solids are volatile (organic).

$$\log_{10}VSS = 0.3865 * \log_{10}TSS$$

where $r^2 = 0.635$

In any case, it is apparent that more than half of the solid particulate matter is inorganic in nature, probably fine clays.

A simple statistical model indicates that VSS levels are proportional to TSS levels, specific conductance, and inversely proportional to the temporal distance from July. The relationship with conductivity likely reflects the impact of runoff.

Dependent variable: ln(VSS)

Independent variable	t-value	p-value	Model Coefficient
ln(TSS)	34.0	<0.0001	0.421
Month (July lag)	-5.4	<0.0001	-0.0371
Specific Conductance	2.4	0.0172	0.0000999

Figure 64. Volatile vs. total suspended solids.

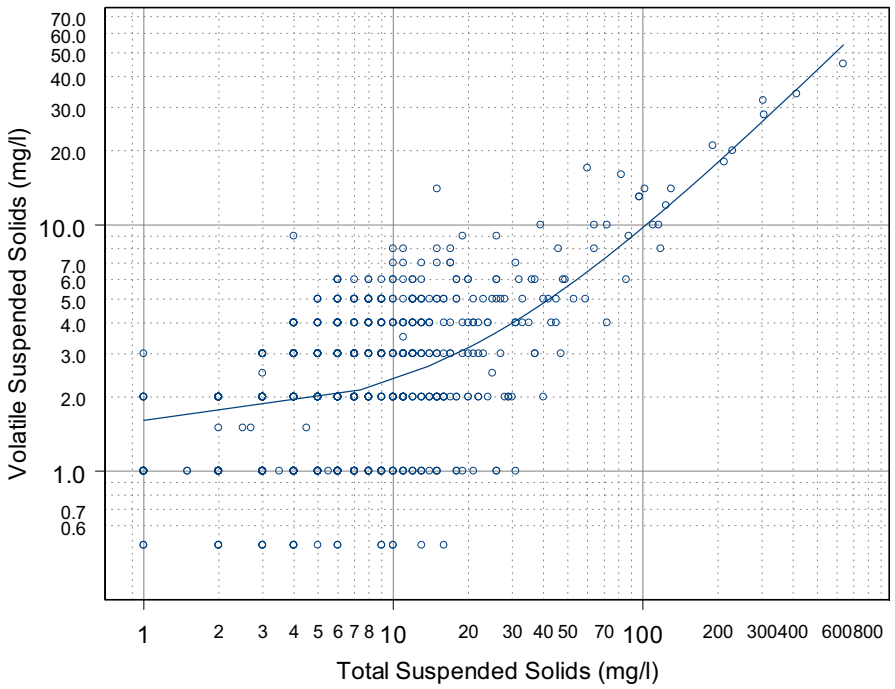

Organic Carbon

Spatial Analysis

Total organic carbon (TOC) levels typically range between 3 and 4 mg/L in Lake Travis, increasing with distance from Mansfield Dam. A small decline in TOC with depth is also evident.

Temporal Analysis

Year to year variation in TOC levels is apparent, but not a long-term trend in concentration. On average, the highest TOC levels are observed in the summer and early fall.

Dissolved Fraction

With the exception of a few outlier measurements, the dissolved fraction comprises more than 80 percent of the organic carbon pool. On average, the dissolved fraction comprises approximately 96 percent of the organic carbon pool. Thalweg sites have on average a slightly higher dissolved fraction than cove sites.

Figure 65. Total organic carbon vs. distance upstream from Mansfield Dam.

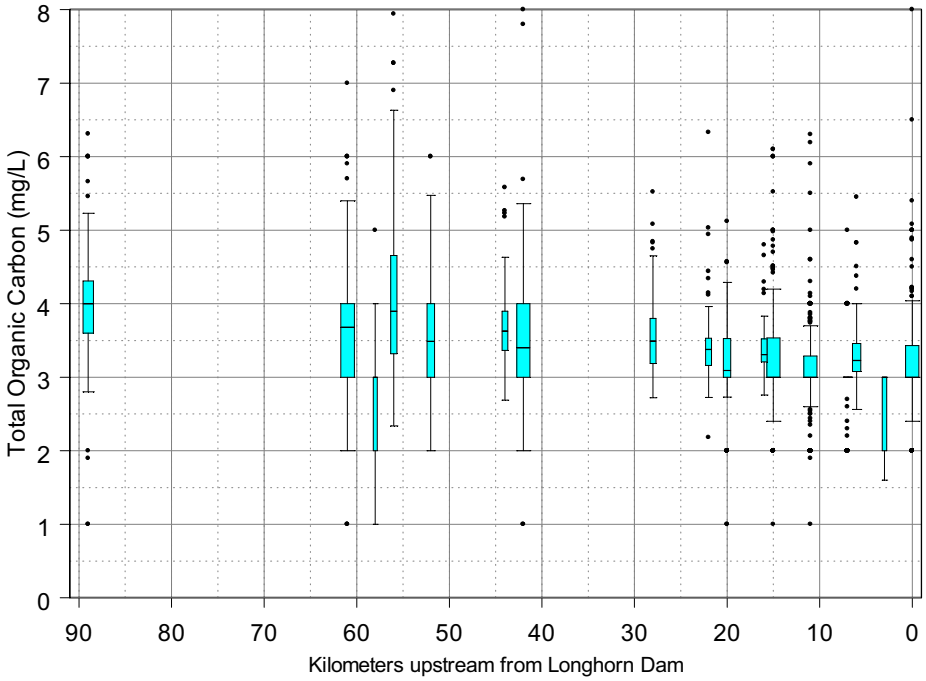

Figure 66. Total organic carbon vs. depth.

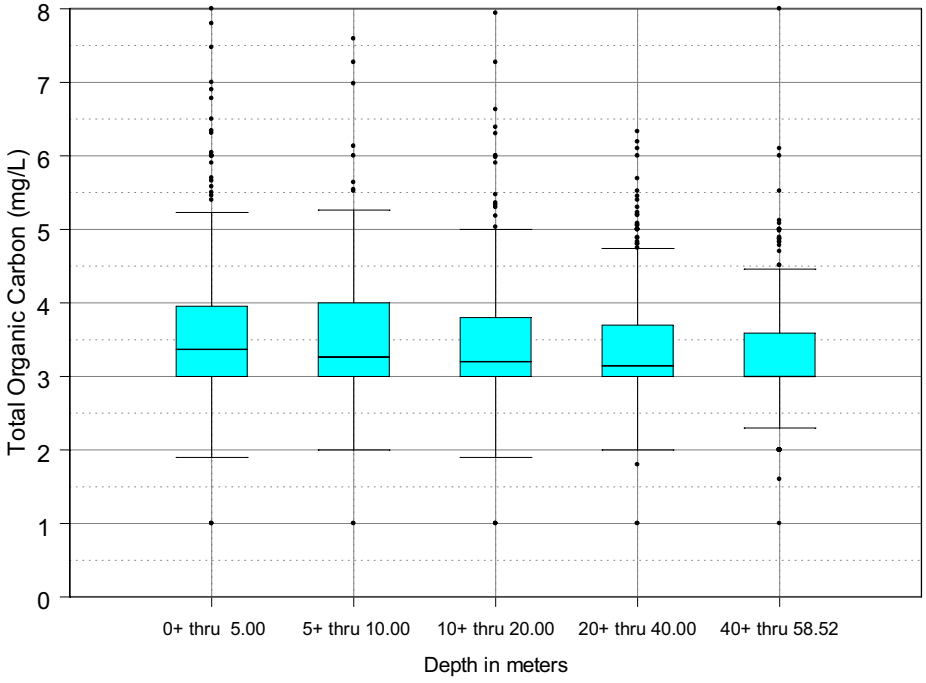

Figure 67. Total organic carbon vs. year.

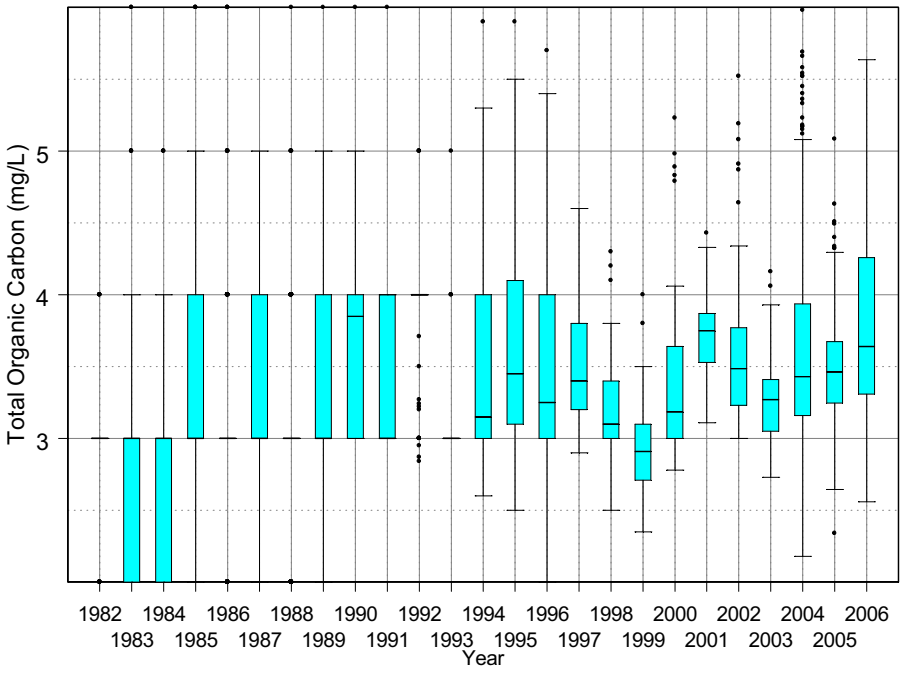

Figure 68. Total organic carbon vs. month.

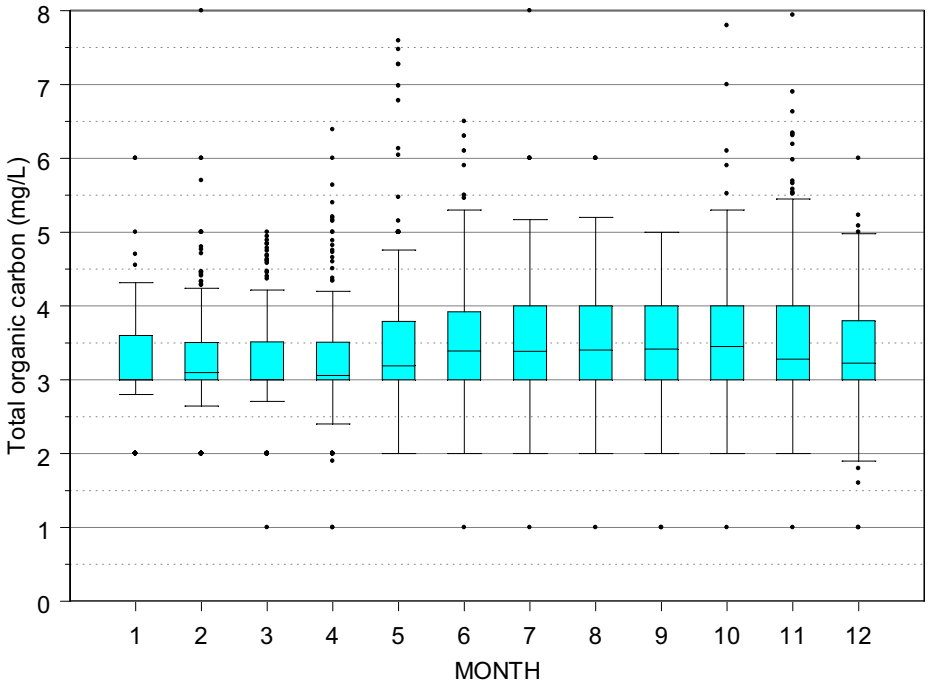

Figure 69. Dissolved fraction of organic carbon for cove and thalweg sites.

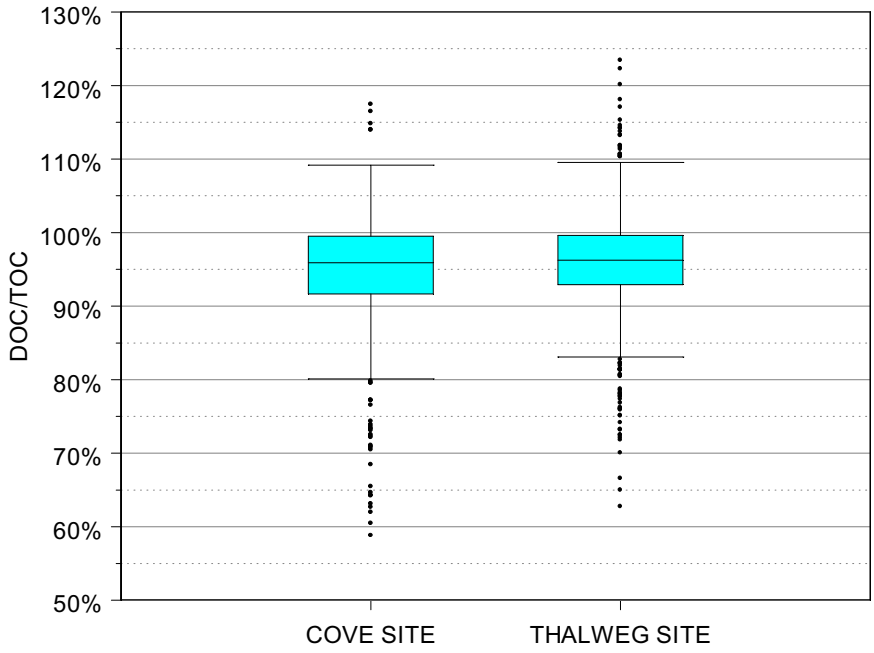

Light Penetration and Extinction with Depth

Light levels decline with depth in the water column as described by the relationship

$$I_z = I_0 e^{-\eta z}$$

or

$$\ln(I_0/I_z)=\eta z$$

where I_z = light irradiance at depth z,

I_0 = irradiance at the lake surface, and

η = the extinction coefficient.

The extinction coefficient as used here is for all light wavelengths and is influenced by scattering and absorption due to the water molecules themselves, as well as absorption by suspended particles, dissolved and colloidal colored molecules, and chlorophyll-a. Scattering of light can change seasonally due to the incident angle of irradiation, as well as due to wave action. CE-QUAL-W2 allows light extinction coefficients to vary seasonally and also includes separate extinction coefficients for water (EXH2O), inorganic suspended solids (EXSS), organic suspended solids (EXOM), and algae (EXA).

The bulk extinction coefficient can be considered to be a sum of each of these extinction coefficients:

$$\eta = \eta_{h20} + \eta_{ss} + \eta_{om} + \eta_a$$

where: η_{ss} = EXSS*[TSS],

η_{om} = EXOM*[OM] and

η_a = EXA*[algae] = EXA*[ChlA]*[algae]/[ChlA].

We attempted to extract several of the various extinction coefficients by simulating field-measured data using general linear models. The most basic model of light penetration includes only a seasonally and spatially invariant bulk extinction coefficient:

$$\ln(I_0/I_z) = \eta z$$

where: η = 0.7077,

r^2 = 0.889, and

p = 0.0000.

This model explains 88 percent of the variation in observed data. If we allow the bulk extinction coefficient to vary seasonally, we get a model that performs slightly better:

$$\ln(I_0/I_z) = \eta z + 0.1971*\text{MONTHLAG}$$

where: η = 0.6223,

r^2 = 0.903, and

p = 0.0000.

If we ignore seasonal variation but split up the bulk extinction coefficient into separate terms to account for variations in suspended solids and algae (chlorophyll-a) concentrations, we get a better model:

$$\ln(I_0/I_z) = 0.474z + 0.0427*[\text{TSS}]*z + 0.0197*[\text{Chla}]*z$$

where r^2 = 0.929 and

p = 0.0000.

EXH2O = 0.474 m^{-1}

EXSS = 0.0427 m^2/g

EXA cannot be derived without the algal biomass to chlorophyll-a ratio, but an extinction coefficient due to chlorophyll-a is estimated as 0.0197 m^2/mg chlorophyll-a

A separate extinction term for organic matter (as measured by total organic carbon) did not improve the model, and could not be determined with any confidence.

If we add the seasonal variation component back into this model, we can account for a slightly larger percentage of variance in the observed data:

$$\ln(I_0/I_z) = 0.396z + 0.0391*[\text{TSS}]*z + 0.0219*[\text{Chla}]*z + 0.1815*\text{MONTHLAG}$$

where r^2 = 0.940

p = 0.0000

EXH2O = 0.396 m^{-1}

EXSS = 0.0391 m^2/g

EXA cannot be derived without the algal biomass to chlorophyll-a ratio, but an extinction coefficient due to chlorophyll-a is estimated as 0.0219 m^2/mg chlorophyll-a.

The ranges of extinction coefficient values that have been used by others in CE-QUAL-W2 models are listed below. For the most part, these are not measured values.

EXH2O: 0.18 – 0.5 m^{-1}

EXSS: 0 – 0.1 m^2/g

EXA: 0.1 – 0.3 m^2/g

EXOM: 0.08 – 0.4 m^2/g

APPENDIX E

Lake Travis CE-QUAL-W2 Model Review

ANCHOR QEA

PARSONS

Lake Travis CE-QUAL-W2 Model Review

DRAFT

Prepared for QEA

by

Scott A. Wells, Ph.D., P.E.

March 1, 2007

Table of Contents

Table of Contents ii
List of Figures ii
List of Tables ii
Introduction 1
Model Review 1
Preprocessor Model Check 1
Model Orientation and Bathymetry 2
Model Input Files 5
W2 control file 6
Water Level Simulations on a PC 7
Water Level Simulations on a Linux Workstation 9
Summary 9

List of Figures

Figure 1. Model grid using the V3.2 W2 control program to visualize the grid. 3
Figure 2. Water level predictions of W2 model compared to field data between 1984 and 1998 8

List of Tables

Table 1. Segments and widths adjusted for model stability considerations. 3
Table 2. Comparison of volume-elevation curves after segment widths were adjusted as shown in Table 1. 4
Table 3. Model input files for 1984-1998 simulation. 5
Table 4. W2 control file parameters. 6
Table 5. Model runs exploring ways to decrease model run time. 9

Introduction

The CE-QUAL-W2 Lake Travis model was set up for 15 years between 1984-1998. The model files that were received from QEA included files for each year individually, as well as a set of files for the entire 15 year period. The model matched water levels well year-by-year, but when the model was run for the entire 15-year period the model became unstable. The CE-QUAL-W2 model used was version 3.2 using the generic code for a Linux workstation. The model was compiled on a Linux workstation using the Intel Linux FORTRAN 8 compiler with the following settings: `"ifort w2_generic.f90 -o w2"`. Hence the purpose of this review was to resolve the 15-year model run issue and to provide a quick review of the current model set-up and recommendations.

Model Review

The files were evaluated on a PC initially prior to running on a Linux workstation. The review process followed these steps:

1. Set-up files for 15 year run and check preprocessor
2. Review grid orientation and bathymetry file
3. Review dynamic boundary condition input files
4. Review w2_con.npt file
5. Set-up files to run on a PC, reproduce problem, debug problem on PC
6. Test model on Linux workstation
7. Provide recommendations

Preprocessor Model Check

The model files that were provided included input files for each year and files for the 15 year period. These files included files for inflow temperature, flow, and meteorological conditions. A control file (w2_con.npt), bathymetry file, shade file, initial condition file (vpr.npt), and wind sheltering file were assembled for the 15 year simulation based on files for the 1984 simulation. The model file, graph.npt, was apparently a V3.1 graph.npt file. Since the format was changed from V3.1 to V3.2, a new graph.npt file was prepared. Once these files were ready, the W2 preprocessor was run (pre.exe). The preprocessor ran fine with no errors and gave the following warnings(pre.wrn):

```
Wind speed [WIND= 23.100] > 20 m/s on day 4896.929 in met.npt
Wind speed [WIND= 23.100] > 20 m/s on day 4896.931 in met.npt
Constituent 2 is " ON", but distributed tributary inflow constituent
concentration is "OFF" for branch 1
Water surface elevation is below bottom elevation at segment 112
Water surface elevation is below bottom elevation at segment 113
Water surface elevation is below bottom elevation at segment 114
Water surface elevation is below bottom elevation at segment 115
Water surface elevation is below bottom elevation at segment 125
```

```
Water surface elevation is below bottom elevation at segment 126
Water surface elevation is below bottom elevation at segment 134
Water surface elevation is below bottom elevation at segment 135
Water surface elevation is below bottom elevation at segment 136
Water surface elevation is below bottom elevation at segment 137
Water surface elevation is below bottom elevation at segment 147
Water surface elevation is below bottom elevation at segment 148
Water surface elevation is below bottom elevation at segment 149
Water surface elevation is below bottom elevation at segment 150
Water surface elevation is below bottom elevation at segment 151
Water surface elevation is below bottom elevation at segment 152
Water surface elevation is below bottom elevation at segment 169
Water surface elevation is below bottom elevation at segment 170
```

None of these warnings were critical to the running of the model. These warnings showed that:

1. There were 2 dates of high wind speed, but these may be realistic if there were high winds on those days.
2. The model was using only 1 active water quality variable, a conservative tracer. There was no conservative tracer given in the distributed inflow file, which seems reasonable.
3. The initial water surface elevation on January 1, 1984 was below the elevation of some of the bottom elevations of some model segments. This meant that these segments were not in the model domain initially.

Model Orientation and Bathymetry

The model grid orientation is shown in Figure 1. This agrees with the layout of the physical system. The bathymetry was reviewed to see if there were any ‘orphan’ segments with deep holes and if there were any narrow segments that could affect model stability.

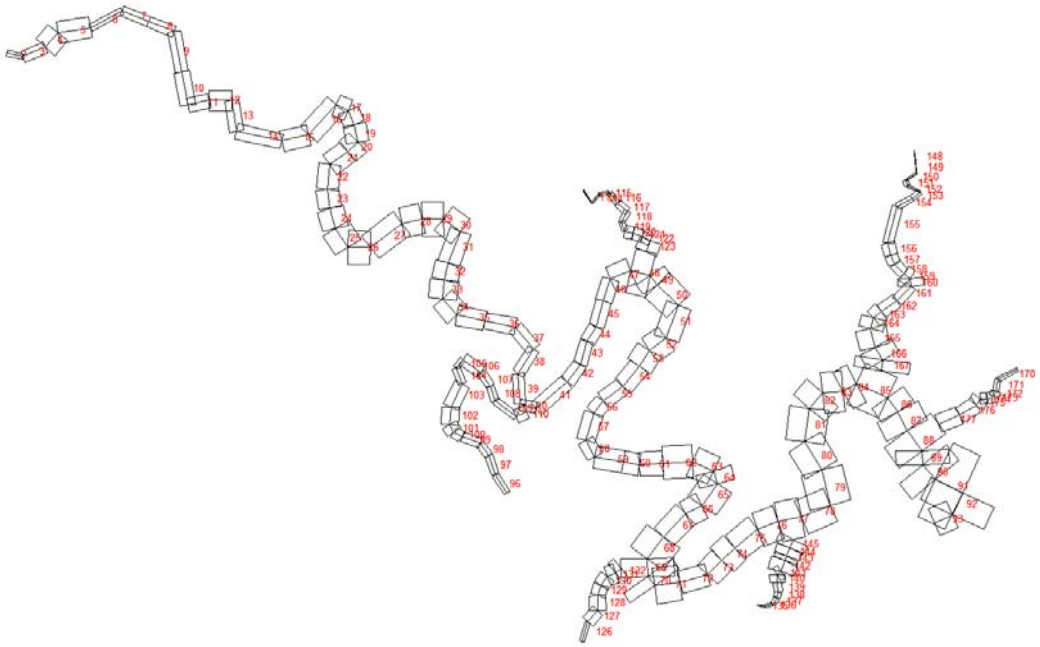

Figure 1. Model grid using the V3.2 W2 control program to visualize the grid.

Most of the flow was coming through the main branch, hence any model segments where there was only one layer hydrated were candidates for "adjustment". This became more critical when changing the minimum hydrated layers from NL=2 to NL=1 in the control file, w2_con.npt. We recommend using NL=1 if possible for the best resolution of the volume-elevation curve of the reservoir. When we ran the model at NL=1, many of the warnings in the w2.wrn file were for segments 8-14. With TIMESTEP VIOLATIONS turned on in the SNP output, segment 12 layer 14 had the most violations of any grid cell. This meant that the minimum time step for stability was controlled by these cells. Narrow widths at segments 8-14 were enlarged to allow the time step for stability to be increased. The model results though were unchanged even without making these adjustments – the only issue was decreased model run times. The grid segments that were recommended to be modified to allow a higher average time step during the simulation were shown in Table 1.

Table 1. Segments and widths adjusted for model stability considerations.

Segment	Layer	Old width	New width
5	10	10.64	20.64
6	10	10.64	20.64
7	10	10.64	20.64
8	10	10.64	20.64
9	10	11.10	21.1
11	11	11.56	21.56
12	11	12.91	22.91
14	12	8.86	20.86

This did little to change the volume elevation curve and allowed the average model time step to be raised such that the model run times were reduced. A comparison of volume-elevation curves before and after the width adjustment is shown in Table 2.

Table 2. Comparison of volume-elevation curves after segment widths were adjusted as shown in Table 1.

Elevation	Layer	Original volume, m^3*10^6	Volume after width adjustment, m^3*10^6	% difference
216.41	2	2186.135	2186.332	-0.0090
214.41	3	1983.593	1983.79	-0.0099
212.41	4	1795.989	1796.186	-0.0110
210.41	5	1621.737	1621.934	-0.0121
208.41	6	1460.064	1460.261	-0.0135
206.41	7	1310.082	1310.279	-0.0150
204.41	8	1170.503	1170.7	-0.0168
202.41	9	1042.586	1042.783	-0.0189
200.41	10	926.054	926.25	-0.0212
198.41	11	819.326	819.401	-0.0092
196.41	12	721.766	721.807	-0.0057
194.41	13	633.053	633.053	0.0000
192.41	14	552.29	552.29	0.0000
190.41	15	478.843	478.843	0.0000
188.41	16	412.354	412.354	0.0000
186.41	17	352.663	352.663	0.0000
184.41	18	298.93	298.93	0.0000
182.41	19	251.383	251.383	0.0000
180.41	20	209.277	209.277	0.0000
178.41	21	171.941	171.941	0.0000
176.41	22	139.734	139.734	0.0000
174.41	23	112.018	112.018	0.0000
172.41	24	88.785	88.785	0.0000
170.41	25	69.081	69.081	0.0000
168.41	26	52.461	52.461	0.0000
166.41	27	38.342	38.342	0.0000
164.41	28	26.795	26.795	0.0000
162.41	29	17.524	17.524	0.0000
160.41	30	10.102	10.102	0.0000
158.41	31	4.718	4.718	0.0000
156.41	32	1.638	1.638	0.0000
154.41	33	0.226	0.226	0.0000

The model vertical grid spacing was set at 2 m. This is considered coarse resolution for capturing vertical variations in temperature and water quality variations in the reservoir. I would recommend changing this to 1 m (or even to 0.61 m).

The model longitudinal grid spacing was unequal varying from 177 m to 1506 m. Attempts should usually be made to have equal grid spacing within a branch if possible since the numerical accuracy of the simulation is degraded slightly by unequal grid spacing. If there are reasons though for using unequal grid spacing, then this can be OK,

but grid refinement studies should show that the current grid resolution does not affect the model results.

Model Input Files

Comments on some of the boundary condition files are shown in Table 3.

Table 3. Model input files for 1984-1998 simulation.

File	Comment
graph.npt	Revised and updated to V3.2
qin_Bee_Creek.npt	Often there were periods of negative flow, implying a withdrawal.
qin_Cow_Creek.npt	Often there were periods of negative flow, implying a withdrawal.
qin_Cypress_Creek.npt	Often there were periods of negative flow, implying a withdrawal.
qin_Hurst_Creek.npt	Often there were periods of negative flow, implying a withdrawal.
qin_Sandy_Creek.npt	Often there were periods of negative flow, implying a withdrawal.
shd.npt	No shading – OK for a large reservoir without topographic shading.
tdt_br1.npt	Inflow temperature of 22.2^{o}C at the beginning in January 1988 – seems too warm for January – but you have negative flow during this period so it may not matter.
tin_Bee_Creek.npt	Inflow temperature of 22.2^{o}C at the beginning in January 1988 – seems too warm for January – but you have negative flow during this period so it may not matter.
tin_Cow_Creek.npt	Inflow temperature of 22.2^{o}C at the beginning in January 1988 – seems too warm for January – but you have negative flow during this period so it may not matter.
tin_Cypress_Creek.npt	Inflow temperature of 22.2^{o}C at the beginning in January 1988 – seems too warm for January – but you have negative flow during this period so it may not matter.
tin_Hurst_Creek.npt	Inflow temperature of 22.2^{o}C at the beginning in January 1988 – seems too warm for January – but you have negative flow during this period so it may not matter.
tin_Marble_Falls.npt	Inflow temperature of 22.2^{o}C at the beginning in January 1988 – seems too warm for January – but you have negative flow during this period so it may not matter.
tin_Pedernales.npt	Inflow temperature of 22.2^{o}C at the beginning in January 1988 – seems too warm for January – but you have negative flow during this period so it may not matter.
tin_Sandy_Creek.npt	Inflow temperature of 22.2^{o}C at the beginning in January 1988 – seems too warm for January – but you have

File	Comment
	negative flow during this period so it may not matter.
wsc.npt	WSC varied from 0.7 to 1.2. This parameter depends on where the wind data were taken. This should be used as a calibration parameter for the temperature profile calibration.

W2 control file

The control file, w2_con.npt, was reviewed. Comments on some of the parameters are noted below in Table 4.

Table 4. W2 control file parameters.

Variable	Description	Value in control file	Comment
DLTMAX	Maximum time step	3600	Even though it was reduced during some periods, this is a very high time step, especially with flow interpolation being OFF (see below). For the 1984 year, the model average DLT was 325 s, hence a lower value may contribute to a more stable simulation without making the run time any longer.
NDLT	# of time step periods	1	I used just one value for the entire simulation. One could add several periods to raise and lower DLTMAX if necessary.
DTLF	Fraction of maximum time step	0.9	If a model run is running unstable, or if the number of model violations is high, reduce DTLF. I would use for your system 0.8 to 0.7 as insurance against the model going unstable. But if DLTMAX is reduced sufficiently this may not be necessary.
EVC	Evaporation control	OFF	Be careful that evaporation is being included in your water balance since it is OFF in the model.
NL	Number of active vertical layers before layer subtraction/addition	2	Recommend using NL=1 for better grid resolution
CBHE	Coefficient of bottom heat exchange	0.7E-07	This is an old value from V3.1. It should be changed to 0.3 in V3.2 because of code changes correcting an earlier error.

Variable	Description	Value in control file	Comment

QINC	Inflow interpolation	OFF	This is usually ON to allow smooth transition between inflows. For example in the inflow file for the main branch, there are the following lines:
			`JDAY Q`
			`657.500 0.000`
			`658.500 643.860`
			With QINC=OFF, the flow instantly goes from 0 to 643.86 m^3/s rather than linearly increasing over a day. This affects model stability and the time step for stability. I would recommend that this be ON unless there is a good reason for the step function inflows.

DTRIC	Distributed inflow interpolation	OFF	This is usually ON to allow smooth transition between inflows.
SLHTC	Heat balance model	ET	I always recommend TERM since it is more accurate, but similar results can be obtained with ET as with TERM.
AZMAX	Maximum vertical eddy viscosity	1E-5	It should be 1E-3 if using the EXP scheme.
STRIC	Structure outflow interpolation	OFF	This is usually ON to allow smooth transition between outflows.
EXH20	Extinction for water	0.25	When no water quality is being simulated, this often is set to 0.45 to account for water quality induced turbidity.
SNPF	Snapshot frequency	1.0	I changed this to 60 to reduce the huge size of the file.
CST PRINT	Print of Water quality constituents	ON/OFF	Many of these were ON for constituents that were not being simulated – I would turn them OFF except for the tracer that you are simulating.
SEDPRC	Print control for sediment model	ON	Turn OFF if not simulating water quality.

Water Level Simulations on a PC

The problem of the model going unstable for the multi-year simulation was reproduced on a PC without making any adjustments to the model files. The maximum time step DLTMAX set at 3600 was too high. This was seen by examining the water mass balance in the SNP file that showed that the mass error was over 70%. The following model changes were made:

1. Lowered DLTMAX to 360 s
2. Changed NL=1
3. Adjusted slightly the bathymetry of segments 5-14 as shown in Table 1
4. Changed AZMAX=1E-3 and CBHE=0.3

The water level data provided by QEA was compared to the simulation results in Figure 2 over the 15 year period. The model predicted water surface elevation was close to the measured data, but the distributed inflow file needs further adjustment to match water levels.

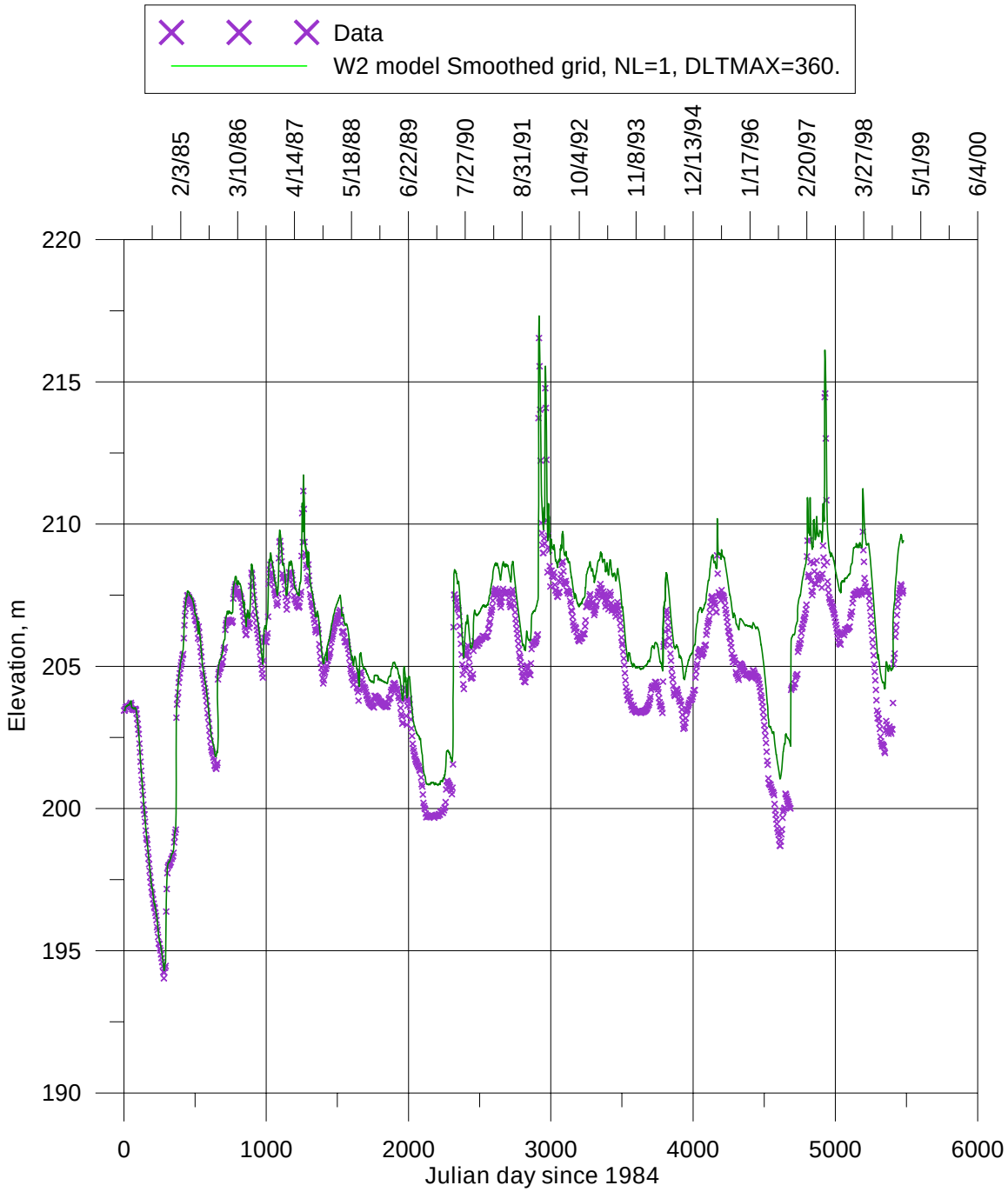

Figure 2. Water level predictions of W2 model compared to field data between 1984 and 1998.

Several model runs were made looking at ways to decrease model run time. These runs all resulted in similar water levels as those shown in Figure 2. In all these runs, the mass

balance for water was to machine accuracy of about 1E-8% to 1E-9% error. The PC system was an Intel Core 2 Duo E6700. The effect of these runs on model run time were summarized in Table 5.

Table 5. Model runs exploring ways to decrease model run time.

Run	Smoothed bathymetry	Interpolation ON/OFF	DLTMAX	DTLF	Average Δt, s, during 15 year simulation	CPU time, min, on PC for 15 year simu-lation
1	YES	OFF	360	0.7	233	127.2
2	YES	ON	3600	0.7	242	122.2
3	YES	ON	600	0.9	287	102.2

Water Level Simulations on a Linux Workstation

Using the same revisions as noted for the PC, the same results as the PC were obtained on a Linux workstation using the following compiler options for Intel Linux FORTRAN 9 compiler: `"ifort w2_generic.f90 -o w2".` The model was also compiled using `"ifort w2_generic.f90 –r8 -o w2".` Using the "-r8" option assigns all real variables to double precision. This would then be compatible with the release version of the W2 executable on a PC and improves the numerical accuracy of the computations, even though it results in a slightly slower model simulation. The PC simulation (Core 2Duo E6700) actually was much faster (about 2X) compared to the Linux workstation simulation (Opteron 252 system). We have found that the Intel compiler itself generates executables that are still slower (by up to 40% on a comparable platform) than the older CVF PC compiler that we use for our PC executables.

Summary

The model files for the CE-QUAL-W2 V3.2 model of Lake Travis were reviewed. The model was able to run the entire 15 year simulation without going unstable on both a PC and a Linux workstation. The following suggestions were made:

- Use the new graph.npt file if you want to run on a PC
- Adjust the following parameters as a minimum:
  - DLTMAX
  - NL
  - AZMAX
  - CBHE
- Adjust the bathymetry as noted in Table 1

- Change to interpolation for inflows and outflows if appropriate
- Compile using the –r8 option on the Linux workstation ti improve numerical accuracy
- Consider other changes and comments made throughout this review. One of the more important would be to change the grid from 2 m to 1 m resolution.

The water balance still needs some adjustments to match the field data. A set of input files for the 1984-1998 model run were compiled for a PC and for a Linux workstation for the V3.2 model used in the simulations.

The files for a PC are included in the PC.zip file which includes the following files (including output files from the preprocessor and model run):

```
02/23/2007  01:25 PM            86,150 bth.npt
02/16/2007  05:16 PM             7,109 cin_br1.npt
02/16/2007  05:16 PM             7,109 cin_br2.npt
02/16/2007  05:16 PM             7,109 cin_br3.npt
02/16/2007  05:16 PM             7,109 cin_br4.npt
02/16/2007  05:16 PM             7,109 cin_br5.npt
02/16/2007  05:17 PM             7,109 cin_br6.npt
02/16/2007  05:17 PM             7,109 cin_br7.npt
10/04/2005  09:45 AM             5,815 graph.npt
12/21/2006  03:47 PM         7,636,626 met.npt
02/16/2007  04:46 PM         2,007,163 pre.exe
03/05/2007  08:33 PM           194,768 pre.opt
03/05/2007  08:33 PM             1,550 pre.wrn
12/21/2006  02:47 PM           104,126 qdt_br1.npt
12/21/2006  02:47 PM           104,126 qin_Bee_Creek.npt
12/21/2006  02:47 PM           104,126 qin_Cow_Creek.npt
12/21/2006  02:47 PM           104,126 qin_Cypress_Creek.npt
12/21/2006  02:47 PM           104,126 qin_Hurst_Creek.npt
12/21/2006  02:47 PM           104,126 qin_Marble_Falls.npt
12/21/2006  02:47 PM           104,126 qin_Pedernales.npt
12/21/2006  02:47 PM           104,126 qin_Sandy_Creek.npt
12/21/2006  02:47 PM           104,126 qot_Mansfield_Dam.npt
12/08/2006  05:19 PM             3,255 shd.npt
02/23/2007  03:48 PM         6,230,246 snp_wb1.opt
12/21/2006  04:27 PM           104,107 tdt_br1.npt
12/21/2006  04:27 PM           104,107 tin_Bee_Creek.npt
12/21/2006  04:27 PM           104,107 tin_Cow_Creek.npt
12/21/2006  04:27 PM           104,107 tin_Cypress_Creek.npt
12/21/2006  04:27 PM           104,107 tin_Hurst_Creek.npt
12/21/2006  04:27 PM           104,107 tin_Marble_Falls.npt
12/21/2006  04:27 PM           104,107 tin_Pedernales.npt
12/21/2006  04:27 PM           104,107 tin_Sandy_Creek.npt
02/23/2007  03:48 PM           724,042 tsr_wb1_1.opt
12/20/2006  02:03 PM             1,079 vpr.npt
02/23/2007  03:28 PM           604,995 w2.wrn
02/23/2007  01:34 PM            40,209 w2_con.npt
06/30/2006  10:30 AM         2,011,136 w2_cvf.exe
02/16/2007  05:20 PM            24,524 wsc.npt
```

The files for the Linux box are the same input files, except that the source codes for the W2 model and Preprocessor are included rather than executables. These fiels are included in the file Linux.zip:

```
02/23/2007  01:25 PM            86,150 bth.npt
02/16/2007  05:16 PM             7,109 cin_br1.npt
02/16/2007  05:16 PM             7,109 cin_br2.npt
02/16/2007  05:16 PM             7,109 cin_br3.npt
02/16/2007  05:16 PM             7,109 cin_br4.npt
02/16/2007  05:16 PM             7,109 cin_br5.npt
02/16/2007  05:17 PM             7,109 cin_br6.npt
02/16/2007  05:17 PM             7,109 cin_br7.npt
10/04/2005  09:45 AM             5,815 graph.npt
12/21/2006  03:47 PM         7,636,626 met.npt
03/05/2007  10:50 PM           319,042 pre.f90
12/21/2006  02:47 PM           104,126 qdt_br1.npt
12/21/2006  02:47 PM           104,126 qin_Bee_Creek.npt
12/21/2006  02:47 PM           104,126 qin_Cow_Creek.npt
12/21/2006  02:47 PM           104,126 qin_Cypress_Creek.npt
12/21/2006  02:47 PM           104,126 qin_Hurst_Creek.npt
12/21/2006  02:47 PM           104,126 qin_Marble_Falls.npt
12/21/2006  02:47 PM           104,126 qin_Pedernales.npt
12/21/2006  02:47 PM           104,126 qin_Sandy_Creek.npt
12/21/2006  02:47 PM           104,126 qot_Mansfield_Dam.npt
12/08/2006  05:19 PM             3,255 shd.npt
12/21/2006  04:27 PM           104,107 tdt_br1.npt
12/21/2006  04:27 PM           104,107 tin_Bee_Creek.npt
12/21/2006  04:27 PM           104,107 tin_Cow_Creek.npt
12/21/2006  04:27 PM           104,107 tin_Cypress_Creek.npt
12/21/2006  04:27 PM           104,107 tin_Hurst_Creek.npt
12/21/2006  04:27 PM           104,107 tin_Marble_Falls.npt
12/21/2006  04:27 PM           104,107 tin_Pedernales.npt
12/21/2006  04:27 PM           104,107 tin_Sandy_Creek.npt
12/20/2006  02:03 PM             1,079 vpr.npt
02/23/2007  01:34 PM            40,209 w2_con.npt
06/30/2006  10:21 AM           517,021 w2_generic.f90
02/16/2007  05:20 PM            24,524 wsc.npt
```

APPENDIX F

CE-QUAL-W2 Upstream Loading

ANCHOR QEA

PARSONS

Quantitative Environmental Analysis, LLC
$\partial c/\partial t$

TECHNICAL MEMORANDUM

TO:	Ruben Solis, LCRA	**DATE:**	May 2, 2006
FROM:	Harry Zahakos	**RE:**	CE-QUAL-W2 Upstream Loading
CC:	Angela Rodriguez, LCRA Jennifer Benaman, QEA	**JOB#:**	PARcrm:140

The development of the CE-QUAL-W2 (W2) Lake Travis water quality model as described in the CREMS Phase 2 Work Plan (QEA 2003) requires the specification of the upstream loading. Routine monitoring data collected from 1984 to 2006 at the Lake Travis Headwaters (Station 12318) by LCRA as part of the HAAWQ and CREMS sampling programs will provide the basis for these upstream loadings.

The W2 model state variables are shown in Table 1. Table 2 shows the list of water quality parameters measured by LCRA. While some of the water quality state variables measured match those used in W2, there are many variables that do not exactly correspond. Measured parameters are often a combination of distinct components. For example, Total Kjeldahl Nitrogen (TKN) is a measure of the sum of organic and ammonia nitrogen. Therefore the TKN is a convolution of organic and ammonia nitrogen. Convolved parameters such as this require deconvolution (separation of components) for specifying the individual constituent loadings.

Table 1. CE-QUAL-W2 primary state variables.

Abbreviation	Description
Φ_{TDS}	Total dissolved solids
Φ_{ISS}	Inorganic suspended solids
Φ_{P}	Bioavailable Phosphorus (e.g., PO4)
Φ_{NH4}	Ammonia
Φ_{NOx}	Nitrate+Nitrite
Φ_{LDOM}	Labile Dissolved Organic Matter
Φ_{RDOM}	Refractory Dissolved Organic Matter
Φ_{LPOM}	Labile Particulate Organic Matter
Φ_{RPOM}	Refractory Particulate Organic Matter
Φ_{CBOD}	CBOD
Φ_{a}	Algae
Φ_{DO}	Dissolved Oxygen

www.qeallc.com

305 West Grand Avenue
Suite 300
Montvale, NJ 07645
(201) 930-9890
(201) 930-9805 *fax*

290 Elwood Davis Road
Suite 230
Liverpool, NY 13088
(315) 453-9009
(315) 453-9010 *fax*

80 Glen Street
Suite 2
Glens Falls, NY 12801
(518) 792-3709
(518) 792-3719 *fax*

800 Brazos Street
Suite 1040
Austin, TX 78701
(512) 707-0090
(512) 275-0915 *fax*

Table 2. Measured Water Quality Parameters at Lake Travis Headwaters.

Abbreviation	Description*	Years Available
DO	**Dissolved Oxygen**	**1984-2006**
TOC	**Total Organic Carbon**	**1984-2006**
DOC	**Dissolved Organic Carbon**	**2004-2006**
CHLA	**Chlorophyll-a**	**1984-2006**
PHEO	**Pheophytin-a**	**1984-2006**
NOX	**Nitrite and Nitrate**	**1984-2006**
NH4	**Ammonia**	**1984-2006**
TKN	**Total Kjeldahl Nitrogen**	**1984-2006**
DKN	**Dissolved Kjeldahl Nitrogen**	**2004-2006**
TP	**Total Phosphorus**	**1984-2006**
DP	**Dissolved Phosphorus**	**2004-2006**
PO4	**Orthophosphorus**	**1984-2006**
TSS	**Total Suspended Solids**	**1984-2006**
TDS	**Total Dissolved Solids**	**1984-2006**
VSS	Volatile Suspended Solids	1984-1990, 2004
ALK	Total Alkalinity	1984-2004
CHLR	Chloride	1984-2004
COND	Specific Conductance	1984-2004
SULF	Sulfate	1984-2004
TURB	Turbidity	2000-2004
FCOL	Fecal Coliform	1984-2001
ECOL	E. Coli	1994-2001
TEMP	Temperature	1984-2004
PH	pH	1984-2004

**Parameters in bold represent those needed for deconvolution to CE_QUAL-W2 primary state variables*

Additionally, the measured water quality parameters are measured at various frequencies ranging from weekly to bi-monthly. It is assumed that the parameter deconvolution will be performed for each day that parameters are measured and that the resulting state variable concentrations will be interpolated between these days to provide continuous daily values to be input to the W2 model.

The biggest differences between W2 state variables and measured parameters are the organic constituents. W2 models non-living organic matter as LDOM, RDOM, LPOM, RPOM, and multiple CBOD groups. Each of these W2 organic matter systems has a fixed N and P stoichiometry. In contrast, the measured organic carbon, nitrogen, and phosphorus do not occur in fixed ratios.

305 West Grand Avenue
Suite 300
Montvale, NJ 07645
(201) 930-9890
(201) 930-9805 *fax*

290 Elwood Davis Road
Suite 230
Liverpool, NY 13088
(315) 453-9009
(315) 453-9010 *fax*

80 Glen Street
Suite 2
Glens Falls, NY 12801
(518) 792-3709
(518) 792-3719 *fax*

800 Brazos Street
Suite 1040
Austin, TX 78701
(512) 707-0090
(512) 275-0915 *fax*

In order prepare the upstream W2 model inputs, equations need to be developed that will deconvolute the measured parameters. This conversion needs to be prepared in such a way that balances the mass inventory of all constituents involved (especially nutrients), as well as preserving the transport and kinetic characteristics of each.

Organic Constituents

Before specifying the various forms of upstream organic matter, the organic component of nitrogen and phosphorus must first be calculated from the measured parameters. While TOC and DOC are measured directly, Total Organic Nitrogen (TON) and Dissolved Organic Nitrogen (DON) are calculated from measured parameters as follows:

$$TON = TKN - NH4 \quad (1)$$

$$DON = DKN - NH4 \quad (2)$$

Similarly, Total Organic Phosphorus (TOP) and Dissolved Organic Phosphorus (DOP) are calculated from:

$$TOP = TP - PO4 \quad (3)$$

$$DOP = DP - PO4 \quad (4)$$

For these calculations, and all calculations involving the difference of measured parameters, care must be given to ensure no negative values arise. One method of dealing with this is to set all negative values to zero and adjust the differencing values to be equal. They can be set to either one of the parameter values or the average of the two values.

Algae

W2 can accommodate multiple algal groups. While it is expected that eventually the Phase 2 lake model will simulate multiple algal groups, it is proposed that the initial model be set up with one algal group until data becomes available that characterizes the algae. Thus, the model input for algae is just the living portion of the measured chlorophyll-a converted to total algal mass:

$$\Phi_a = (CHLA - PHEO) * r_{a\lg - chla} \quad (5)$$

Where $r_{alg\text{-}chla}$ is the algal biomass to chlorophyll-a ratio. This value can range from 50-250 mg-algae/mg-chla, with the higher range typically observed in oligotrophic systems because less chlorophyll-a is required when higher solar radiation is available. Analysis of the algal characterization studies should be performed to determine the average observed ratio. The W2

305 West Grand Avenue
Suite 300
Montvale, NJ 07645
(201) 930-9890
(201) 930-9805 *fax*

290 Elwood Davis Road
Suite 230
Liverpool, NY 13088
(315) 453-9009
(315) 453-9010 *fax*

80 Glen Street
Suite 2
Glens Falls, NY 12801
(518) 792-3709
(518) 792-3719 *fax*

800 Brazos Street
Suite 1040
Austin, TX 78701
(512) 707-0090
(512) 275-0915 *fax*

default value of 145 mg-algae/mg-chla is sufficient as an initial estimate. When the multiple algal groups are added to the lake model, additional analyses should be done to examine the spatial and temporal variability of the algal mixture, specify the W2 algal groups, and determine the best way to apportion the upstream chlorophyll-a to these algal groups.

Non-Living Organic Matter

Because the upstream organic carbon, nitrogen, and phosphorus are measured independently, it is not possible to use the fixed stoichiometric W2 organic matter (OM) groups to account for the mass of all three nutrients. Future versions of W2 (v3.5) will allow for multiple OM groups each with their own stoichiometry that can accommodate arbitrary inputs of nutrients. Until that model becomes available, it is suggested that these systems be input to the W2 model using the multiple W2 CBOD groups. Three CBOD groups will be necessary:

- CBOD1: Pure carbonaceous BOD with no Nitrogen (N) or Phosphorus (P);
- CBOD2: CBOD with a high ratio of N and no P; and
- CBOD3: CBOD with a high ratio of P and no N.

The advantage of this method is that it allows for the proper accounting of all the nutrient fluxes from the upstream source; any combination of organic carbon, nitrogen, and phosphorus measured can be input to W2. As these three nutrients typically co-exist as organic complexes, it is also suggested that the CBOD kinetic parameters (namely, the 5-day decay rate, temperature coefficient, and ultimate to 5-day ratio) be the same for all three groups.

Another advantage of this method is that it obviates the need to distinguish between dissolved and particulate forms of organic constituents. Because there have only been measurements of DOC, DKN, and DP for 2004-06 (Table 1), there is no need to make assumptions regarding the upstream dissolved/particulate components of inputs for the 1984-2003 simulations.

Using this method, the proposed CBOD stoichiometry to be used in the W2 model is given in Table 3.

Table 3. Recommended W2 CBOD stoichiometry.

	P/CBOD	N/CBOD	C/CBOD
CBOD1	0	0	$r_{c\text{-}o}$
CBOD2	0	1.0	$r_{c\text{-}o}$
CBOD3	1.0	0	$r_{c\text{-}o}$

305 West Grand Avenue
Suite 300
Montvale, NJ 07645
(201) 930-9890
(201) 930-9805 *fax*

290 Elwood Davis Road
Suite 230
Liverpool, NY 13088
(315) 453-9009
(315) 453-9010 *fax*

80 Glen Street
Suite 2
Glens Falls, NY 12801
(518) 792-3709
(518) 792-3719 *fax*

800 Brazos Street
Suite 1040
Austin, TX 78701
(512) 707-0090
(512) 275-0915 *fax*

Where r_{c-o} is the carbon to oxygen stoichiometry for CBOD. It is recommended that this value be set to 0.375 (the stoichiometry of Carbon to Oxygen in CO_2), although the W2 users manual recommends 0.32.

Accordingly, the equations to link the measurements to W2 for non-living organic matter are given below. Note that in all the following formulations, the living algal component of organic matter generated by equation (5) is subtracted from the total organic measurement to yield the non-living component.

$$\Phi_{CBOD2} = TON - \Phi_a * r_{n-a\lg} \tag{6}$$

$$\Phi_{CBOD3} = TOP - \Phi_a * r_{p-a\lg} \tag{7}$$

$$\Phi_{CBOD1} = \frac{TOC - \Phi_a * r_{c-a\lg}}{r_{c-o}} - (\Phi_{CBOD2} + \Phi_{CBOD3}) \tag{8}$$

Where $r_{n\text{-}alg}$, $r_{p\text{-}alg}$, and $r_{c\text{-}alg}$ represent the nitrogen, phosphorus, and carbon (respectively) to biomass stoichiometry for algae. The respective default values for these parameters in W2 are 0.08, 0.005, and 0.45. Analysis of the algal characterization study should yield better estimates of stoichiometry.

Using the CBOD groups, the W2 organic matter inputs will all be set to zero:

$$\Phi_{LDOM} = \Phi_{RDOM} = \Phi_{LPOM} = \Phi_{RPOM} = 0 \tag{9}$$

One disadvantage of this approach is that in the current version of W2 (v3.2), the CBOD groups represent only dissolved CBOD (i.e. there is no settling of CBOD). Generally this may cause an inaccuracy of determining the fate of incoming nutrients to a water body if the loss rate due to settling is on the same time scale as the CBOD decay rate. To investigate the impact of this potential drawback in the Lake Travis model, an analysis is performed on total and dissolved organic carbon, nitrogen, and phosphorus levels at the Lake Travis Headwaters. Figure 1 shows the relationship of measured TOC to DOC. The DOC at the headwaters is well correlated to TOC (correlation coefficient, R=0.87) and represents the majority (95%) of organic carbon. Figure 2 shows the similar plot for nitrogen. The TON/DON correlation is much weaker (R=0.44) and on average DON only represents 63% of TON. There is almost no correlation (R=0.05) between TOP and DOP (Figure 3) and on average DOP is only 38% of the TOP. It should be noted that a large part of the TP, DP, and PO4 measurements were below detection limits (26%, 60%, and 100% respectively). Another caveat is that all of these data were

305 West Grand Avenue
Suite 300
Montvale, NJ 07645
(201) 930-9890
(201) 930-9805 *fax*

290 Elwood Davis Road
Suite 230
Liverpool, NY 13088
(315) 453-9009
(315) 453-9010 *fax*

80 Glen Street
Suite 2
Glens Falls, NY 12801
(518) 792-3709
(518) 792-3719 *fax*

800 Brazos Street
Suite 1040
Austin, TX 78701
(512) 707-0090
(512) 275-0915 *fax*

collected as part of LCRA routine monitoring programs and may not be representative of the composition of organic matter during high runoff events. Similar analyses should be conducted with storm water data.

Based on these analyses, the assumption of no settling of upstream nutrients may potentially have a significant impact on model results when available phosphorus is the limiting factor of algal growth and if the settling speed of particulate phosphorus is fast enough to remove organic phosphorus from the epilimnion before decay can occur. However, for the initial modeling, the CBOD approach for upstream non-living organic matter is recommended because it ensures the mass balance these constituents. Model sensitivity should be performed to assess the impact of this assumption. Eventually, LCRA may want to include settling of this material by switching to the OM groups of W2 v3.5 when this model becomes available, or alternatively, by modifying the W2 code to allow for CBOD settling.

Another potential issue is whether the incoming watershed organic matter is labile or refractory. Unfortunately, no data was readily available to assess the decay rates of this material. A similar modeling effort on the Bosque River (Flowers et al 2001) assumed a refractory/labile split of 75% and 25%, respectively; however no data was presented to support this assumption. If future studies reveal a refractory component of the organic matter from the lake headwaters, it is suggested that the number of CBOD groups be expanded to six (three labile and three refractory).

Inorganic Constituents

The majority of the inorganic constituent measurements correspond to W2 model systems. No deconvolution is necessary for orthophosphate, ammonia, nitrates, oxygen, and total dissolved solids.

$$\Phi_P = PO4 \tag{10}$$

$$\Phi_{NH4} = NH4 \tag{11}$$

$$\Phi_{NOx} = NOX \tag{12}$$

$$\Phi_{DO} = DO \tag{13}$$

$$\Phi_{TDS} = TDS \tag{14}$$

The calculation of inorganic suspended solids (ISS) is more involved. The measurement of TSS must be adjusted to subtract out the organic component of suspended solids. Organic suspended solids are a combination of the living (algal) and non-living (detrital) solids. The living

305 West Grand Avenue
Suite 300
Montvale, NJ 07645
(201) 930-9890
(201) 930-9805 *fax*

290 Elwood Davis Road
Suite 230
Liverpool, NY 13088
(315) 453-9009
(315) 453-9010 *fax*

80 Glen Street
Suite 2
Glens Falls, NY 12801
(518) 792-3709
(518) 792-3719 *fax*

800 Brazos Street
Suite 1040
Austin, TX 78701
(512) 707-0090
(512) 275-0915 *fax*

component is calculated in equation (5) above. The non-living portion can be estimated from the non-living particulate organic carbon. This method is shown in the calculation below:

$$\Phi_{ISS} = TSS - \Phi_a - \frac{(TOC - DOC - \Phi_a * r_{c-a\lg})}{r_{c-om}} \quad (15)$$

Where $r_{c\text{-}om}$ is the carbon to total mass stoichiometry for detrital organic matter. A typical value for $r_{c\text{-}om}$ is 0.4. If it is assumed that the carbon to total mass stoichiometries are equal for algae and detritus, equation (15) simplifies to:

$$\Phi_{ISS} = TSS - \frac{(TOC - DOC)}{r_{c-om}} \quad (16)$$

References

Flowers, J.D., L.M. Hauck, and R.L. Kiesling, 2001. *Water quality modeling of Lake Waco using CE-QUAL-W2 for assessment of phosphorus control strategies.* Texas Institute for Applied Environmental Research, Stephenville, TX.

QEA, LLC, 2003. *Colorado River Environmental Modeling System Lake Travis Phase 2 Work Plan.* Lower Colorado River Authority, Austin, TX.

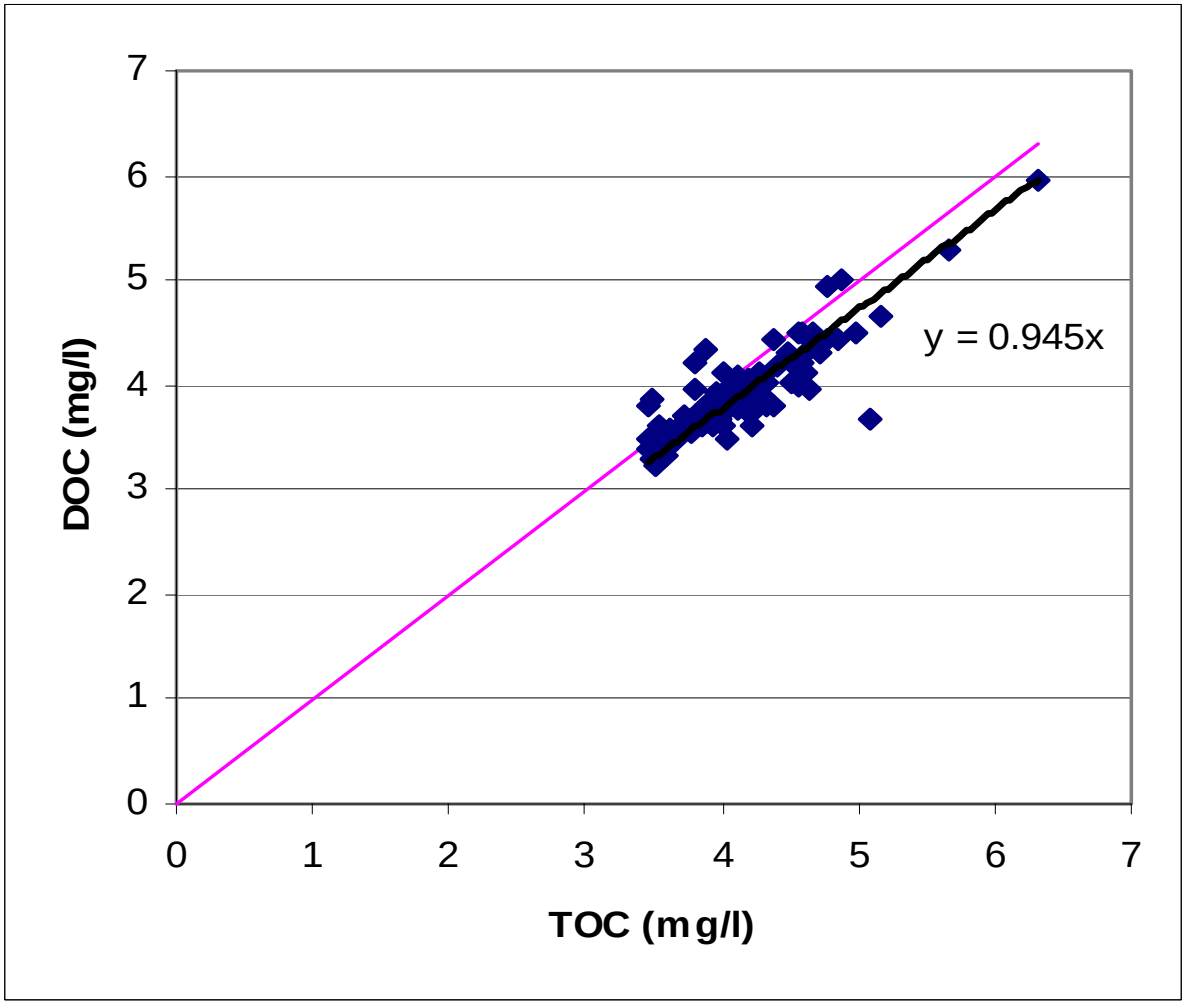

Data source: LCRA Phase 2 Sampling Program (2004-06)

Figure 1. Total to dissolved organic carbon relationship at Lake Travis Headwaters (Station 12318)

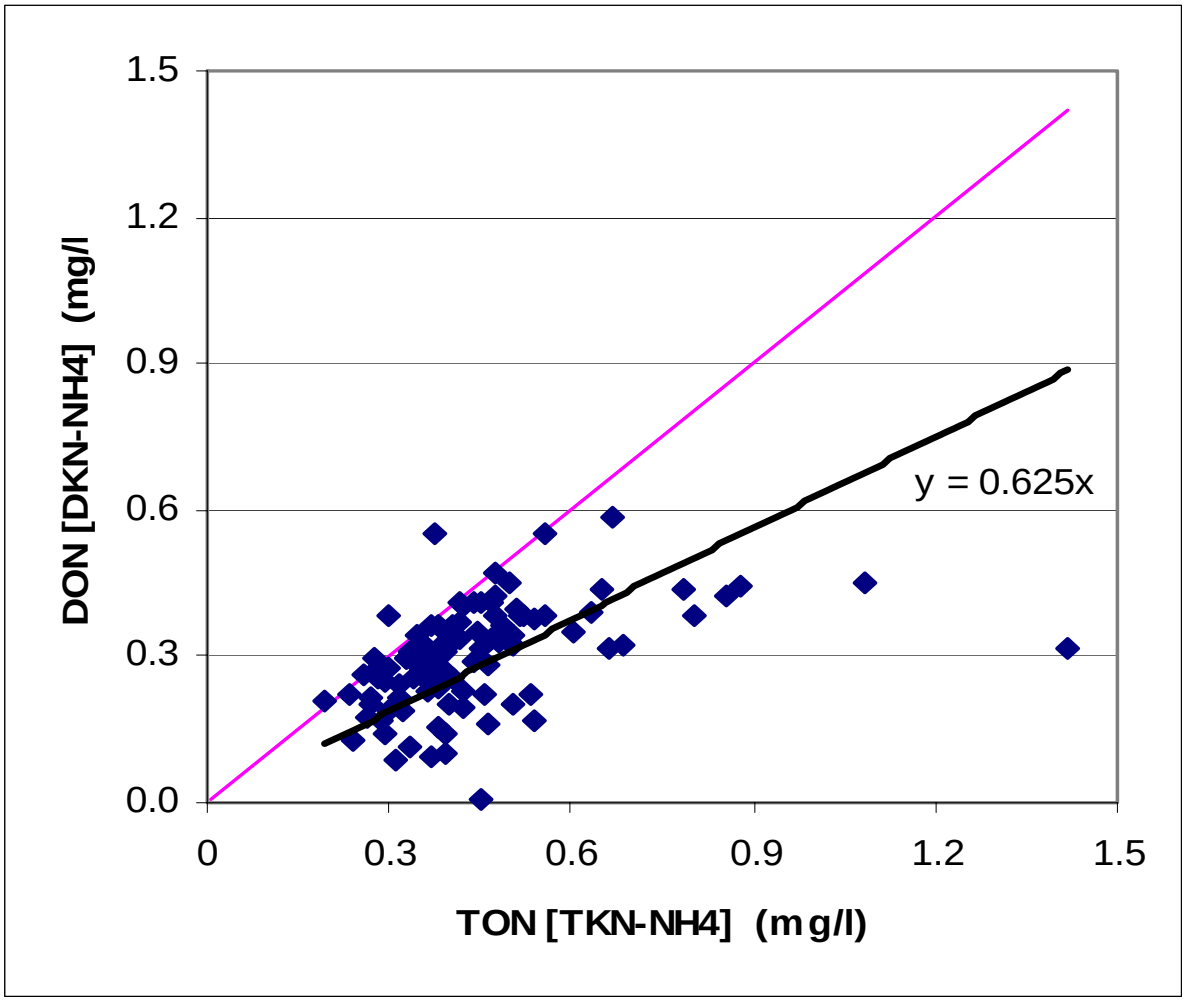

Data source: LCRA Phase 2 Sampling Program (2004-06)

Figure 2. Total to dissolved organic nitrogen relationship at Lake Travis Headwaters (Station 12318)

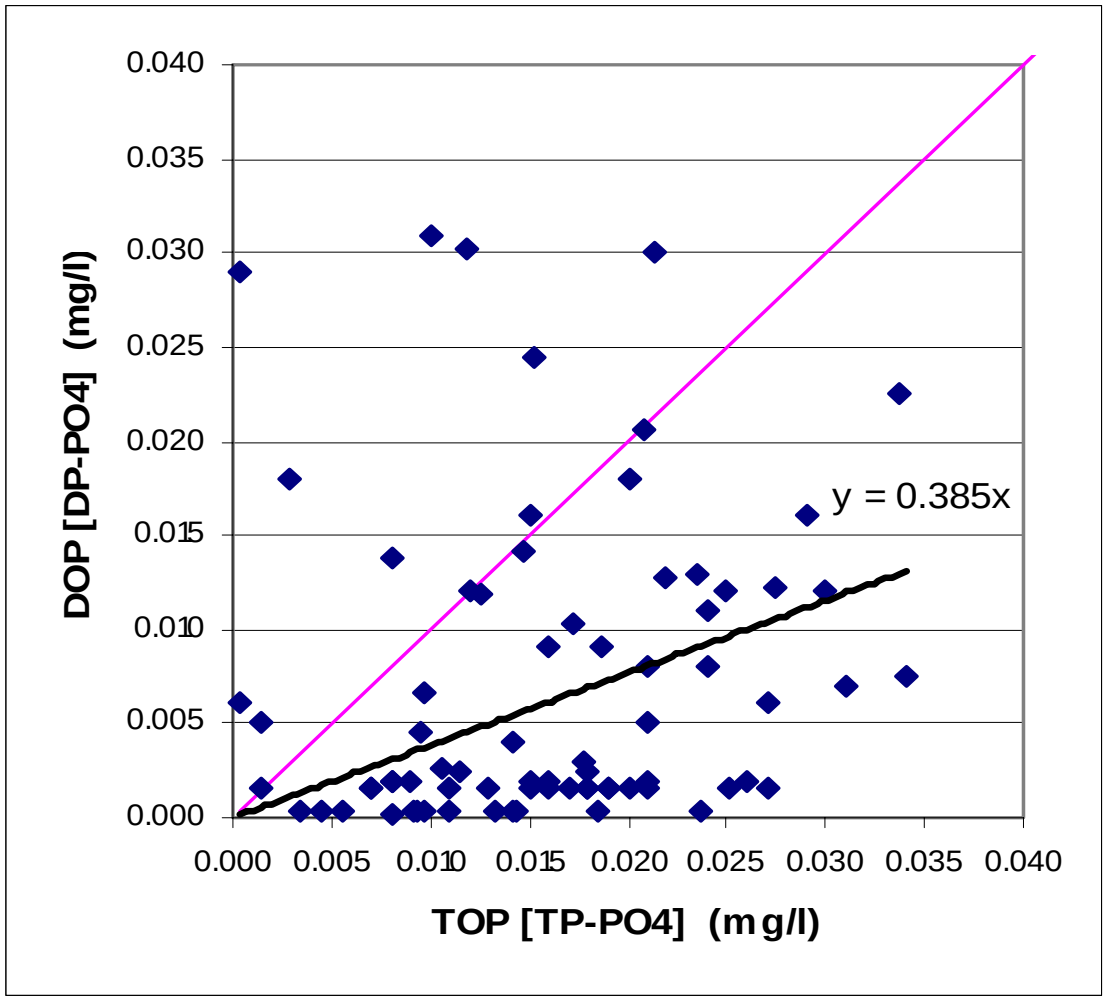

Data source: LCRA Phase 2 Sampling Program (2004-06)
All values less than detection limit are set to one-half detection limit

Figure 3. Total to dissolved organic phosphorus relationship at Lake Travis Headwaters (Station 12318)

APPENDIX G

SWAT – CE-QUAL-W2 Linkages

ANCHOR QEA

PARSONS

Quantitative Environmental Analysis, LLC
$\partial c/\partial t$

TECHNICAL MEMORANDUM

TO:	Ruben Solis, LCRA	**DATE:**	March 9, 2006
FROM:	Harry Zahakos	**RE:**	SWAT – CE-QUAL-W2 Linkages
CC:	Angela Rodriguez	**JOB#:**	PARcrm:111

The development of an integrated watershed management tool for Lake Travis as described in the CREMS Phase 2 Work Plan (QEA 2003) requires the linking of the Soil and Water Assessment Tool (SWAT) watershed model with the CE-QUAL-W2 (W2) water quality model. SWAT uses the equations from the instream model QUAL2E to predict state variables listed in Table 1. The W2 model is based on a different set of equations to predict state variables shown in Table 2. Although many of the water quality state variables output by SWAT match those used in CE-QUAL-W2, there are many variables that do not exactly correspond and require the model coupling to include variable deconvolution.

Table 1. SWAT primary state variables.

Abbreviation	Description
FLOW	Average daily streamflow
EVAP	Average daily rate of water loss from reach by evaporation
TLOSS	Average daily rate of water loss from reach by transmission through streambed
SED	Sediment
ORGN	Organic nitrogen
ORGP	Organic phosphorus
NO_3	Nitrate
NH_4	Ammonium
NO_2	Nitrite
MINP	Mineral phosphorus
ALGAE	Algal biomass
CBOD	Cabonaceous biochemical oxygen demand
DISOX	Dissolved oxygen

305 West Grand Avenue
Suite 300
Montvale, NJ 07645
(201) 930-9890
(201) 930-9805 *fax*

290 Elwood Davis Road
Suite 230
Liverpool, NY 13088
(315) 453-9009
(315) 453-9010 *fax*

80 Glen Street
Suite 2
Glens Falls, NY 12801
(518) 792-3709
(518) 792-3719 *fax*

800 Brazos Street
Suite 1040
Austin, TX 78701
(512) 707-0090
(512) 275-0915 *fax*

Table 2. CE-QUAL-W2 primary state variables.

Abbreviation	Description
Φ_{TDS}	Total dissolved solids
Φ_{ISS}	Inorganic suspended solids
Φ_{P}	Bioavailable Phosphorus (e.g., PO4)
Φ_{NH4}	Ammonia
Φ_{NOx}	Nitrate+Nitrite
Φ_{LDOM}	Labile Dissolved Organic Matter
Φ_{RDOM}	Refractory Dissolved Organic Matter
Φ_{LPOM}	Labile Particulate Organic Matter
Φ_{RPOM}	Refractory Particulate Organic Matter
Φ_{CBOD}	CBOD
Φ_{a}	Algae
Φ_{DO}	Dissolved Oxygen

The most notable difference between state variables is that SWAT models non-living organic matter as ORGN, ORGP, and CBOD, whereas W2 models non-living organic matter as LDOM, RDOM, LPOM, RPOM, and multiple CBOD groups. Each of these W2 organic matter systems has a fixed N and P stoichiometry.

In order to link the two models, equations need to be developed that will deconvolute the SWAT state variables. This conversion needs to be prepared in such a way that balances the mass inventory of all constituents (especially nutrients) involved, as well as preserving the transport and kinetic characteristics of each.

Organic Constituents

Algae

SWAT predicts only total algae; however W2 can accommodate multiple algal groups. While it is expected that eventually the Phase 2 lake model will simulate multiple algal groups, it is proposed that the initial model be set up with one algal group until data becomes available that characterizes the algae. Thus, the model coupling is one-to-one:

$$\Phi_{a} = ALGAE \tag{1}$$

After completion of the algal characterization studies, analysis will be done to examine the spatial and temporal variability of the algal mixture and determine the best way to apportion the total algae predicted by SWAT to W2 algal groups.

305 West Grand Avenue
Suite 300
Montvale, NJ 07645
(201) 930-9890
(201) 930-9805 *fax*

290 Elwood Davis Road
Suite 230
Liverpool, NY 13088
(315) 453-9009
(315) 453-9010 *fax*

80 Glen Street
Suite 2
Glens Falls, NY 12801
(518) 792-3709
(518) 792-3719 *fax*

800 Brazos Street
Suite 1040
Austin, TX 78701
(512) 707-0090
(512) 275-0915 *fax*

Non-Living Organic Matter

Because the Org-N, Org-P, and CBOD output by the SWAT model are independent systems, it is not possible to use the fixed stoichiometric W2 organic matter groups to account for the mass of all three nutrients. It is proposed that these systems be input to the W2 model using the multiple W2 CBOD groups. Three CBOD groups will be necessary:

CBOD1: Pure carbonaceous BOD with no Nitrogen (N) or Phosphorus (P)

CBOD2: CBOD with a high ratio of N and no P

CBOD3: CBOD with a high ratio of P and no N

The advantage of this method is that it allows for the proper accounting of all the nutrient fluxes from SWAT to W2; any combination of ORGN, ORGP, and CBOD output by the SWAT model can be input to W2. As these three nutrients typically co-exist as organic complexes, it is also suggested that the CBOD kinetic parameters (namely, the 5-day decay rate, temperature coefficient, and ultimate to 5-day ratio) be the same for all three groups.

The proposed CBOD stoichiometry to be used in the W2 model is given in Table 3.

Table 3. Recommended W2 CBOD stoichiometry.

	P/CBOD	N/CBOD	C/CBOD
CBOD1	0	0	$r_{c\text{-}o}$
CBOD2	0	1.0	$r_{c\text{-}o}$
CBOD3	1.0	0	$r_{c\text{-}o}$

Where $r_{c\text{-}o}$ is the carbon to oxygen stoichiometry for CBOD. It is recommended that this value be set to 0.375 (the stoichiometry of Carbon to Oxygen in CO_2), although the W2 users manual recommends 0.32.

Accordingly, the equations to link the SWAT output to W2 for organic matter are:

$$\Phi_{CBOD2} = ORGN \tag{2}$$

$$\Phi_{CBOD3} = ORGP \tag{3}$$

$$\Phi_{CBOD1} = CBOD - (ORGN + ORGP) \quad (4)$$

Using the CBOD groups, the W2 organic matter inputs will all be set to zero:

$$\Phi_{LDOM} = \Phi_{RDOM} = \Phi_{LPOM} = \Phi_{RPOM} = 0 \quad (5)$$

One drawback of this approach is that in the current version of W2 (v3.2), the CBOD groups represent only dissolved CBOD (i.e. there is no settling of CBOD). Generally this may cause an inaccuracy of determining the fate of incoming nutrients to a water body if the loss rate due to settling is of the same order of the CBOD decay rate. To investigate the impact of this potential drawback in the Lake Travis, model, an analysis was performed on available Total (TOC) and Dissolved Organic Carbon (DOC) data collected by LCRA at the headwaters as well as tributaries. It was observed that the large majority of the TOC was in dissolved form (see Figure 1). The TOC for the headwaters, Pedernales, Sandy Creek and Bee Creek was about 94% dissolved. This number was lower (~85%) for Hurst Creek and Cow Creek. As a result, this assumption of no settling should have a minimal impact on the model results. However, it should be noted that all of this data was collected as part of the LCRA routine monitoring program and may not be representative of the composition of organic matter during high runoff events. Similar analyses should be conducted with storm water data.

Another potential issue is whether the incoming watershed organic matter is labile or refractory. Unfortunately, no data was readily available to assess the decay rates of this material. A similar modeling effort on the Bosque River (Flowers et al 2001) assumed a refractory/labile split of 75% and 25%, respectively; however no data was presented to support this assumption. If future studies reveal a refractory component of the organic matter from the watersheds, it is suggested that the number of CBOD groups be expanded to six (three labile and three refractory).

Inorganic Constituents

The majority of the inorganic constituents are the same in both models. Thus model coupling is relatively straightforward for orthophosphate, ammonia, nitrates, and oxygen.

$$\Phi_P = MINP \quad (6)$$

$$\Phi_{NH4} = NH_4 \quad (7)$$

$$\Phi_{NOx} = NO_2 + NO_3 \tag{8}$$

$$\Phi_{DO} = DISOX \tag{9}$$

No variable related to total dissolved solids (TDS) is output by the SWAT model. TDS is treated conservatively in W2 (i.e no direct kinetic interactions with other systems) and only will affect water density and ionic strength. Because of this and the fact that the values of TDS observed are not expected to cause large changes in water density, it is suggested that this value be set to a constant value based on available data.

$$\Phi_{TDS} = Const \tag{10}$$

Inorganic suspended solids (ISS) is little more problematic. SWAT total suspended solids (SED) is estimated using the Modified Universal Soil Loss Equation and includes an organic matter component. This organic matter component is included as part of CBOD. One method to calculate the ISS from SED is to subtract the particulate organic component. This particulate organic matter component can be estimated from CBOD:

$$\Phi_{ISS} = SED - CBOD * (1 - f_d) * r_{c-o} / r_{c-om} \tag{11}$$

Where f_d is the ratio of dissolved to total organic carbon (DOC/TOC) and a constant value can be estimated for each watershed from analyses similar to those shown in Figure 1; $r_{c\text{-}om}$ is the carbon to total mass stoichiometry for organic matter. A typical value for $r_{c\text{-}om}$ is 0.4.

References

Flowers, J.D., L.M. Hauck, and R.L. Kiesling. 2001. *Water quality modeling of Lake Waco using CE-QUAL-W2 for assessment of phosphorus control strategies.* Texas Institute for Applied Environmental Research, Stephenville, TX.

QEA. 2003. *Colorado River Environmental Modeling System Lake Travis Phase 2 Work Plan.* Lower Colorado River Authority, Austin, TX.

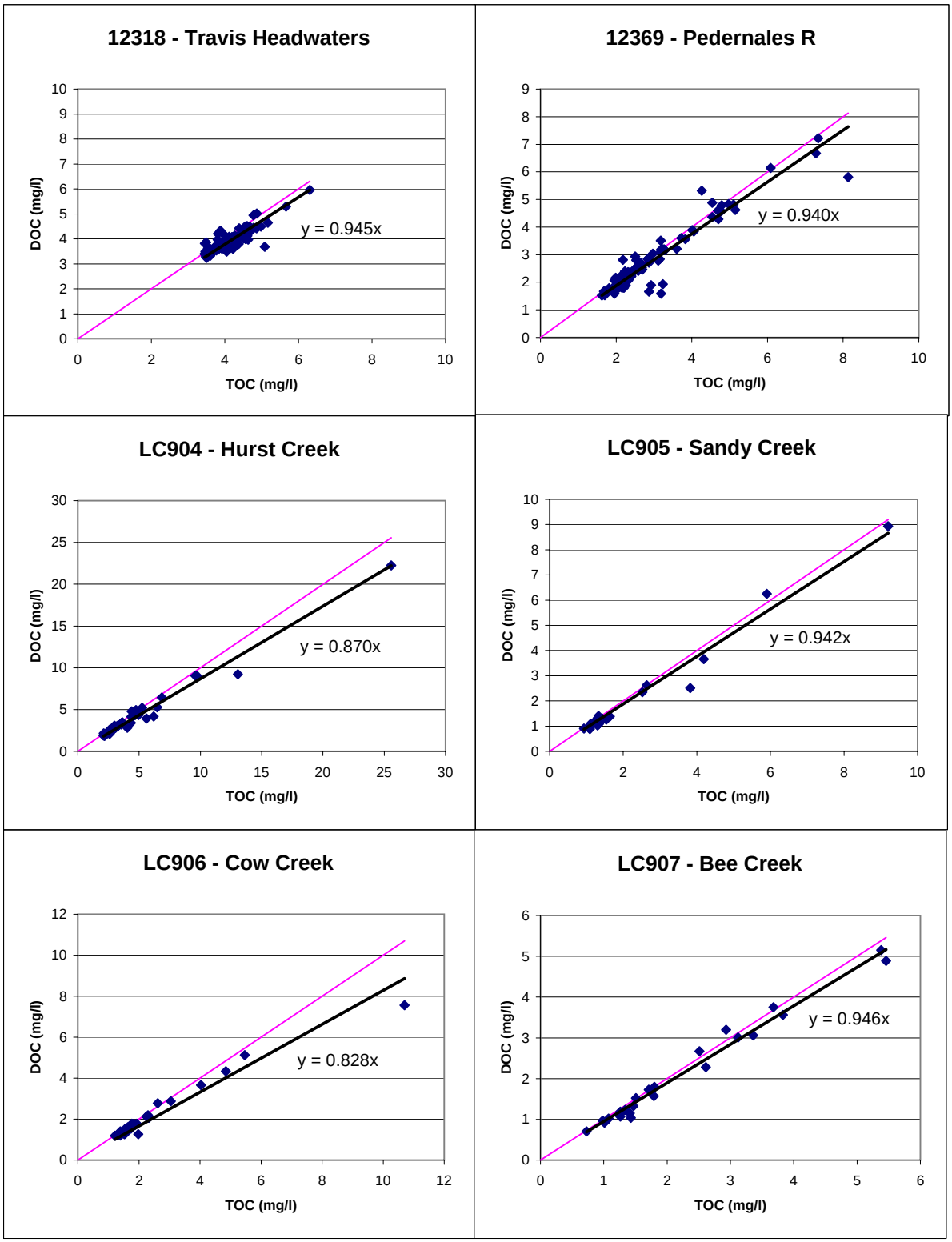

Figure 1. Dissolved to total organic carbon correlations for Lake Travis headwaters and monitored tributaries.

Data Source: LCRA CREMS Phase 2 Sampling Program (2004-06)

APPENDIX H

Water Quality Calibration Metrics for the Lake Travis CE-QUAL-W2 Model

ANCHOR QEA

PARSONS

MEMORANDUM

TO:	CREMS Lake Travis Team	**DATE:**	4/13/2007
FROM:	Kirk Dean, Parsons	**RE:**	Water quality calibration metrics for the Lake Travis CE-QUAL-W2 model
CC:		**JOB#:**	PARcrm

This memorandum discusses several issues pertinent to the calibration of the Lake Travis water quality model. Recommendations are made regarding the most suitable approaches for the Lake Travis model for CREMS.

Manual Calibration or Numerical Optimization?

One key decision is whether to utilize 1) a formal numerical optimization procedure or 2) statistical and graphical comparisons between model predictions and observations in a manual trial and error approach, with the modeler providing interpretation and judgment as to the optimum calibration. The latter is the more common approach. However, as the number of interacting parameters simulated increases, the model calibration becomes more complex because varying one parameter affects many others. Because a eutrophication model includes multiple biological responses to multiple chemical and physical driving parameters, it can be difficult and time-consuming for a modeler to find the optimum values of model calibration parameters. Thus, a numerical optimization procedure may be recommended. However, numerical optimization procedures should not be considered 'black boxes' that feed out the ultimate answer, but should be used as a tool with statistical and graphical analysis by an experienced modeler.

Formal numerical optimization procedures can be of several types. For a small number of parameters, an optimum numerical solution may be obtained by minimizing an objective function using calculus-based solver algorithms. UCODE uses nonlinear regression, with a modified Gauss-Newton method to adjust parameter values to minimize the weighted least-squares objective function. PEST is a similar program using the Marquardt-Levenburg method of nonlinear parameter estimation. Either of these tools will work with most models. These programs may, however, have problems with numerical instability when fitting functions do not vary smoothly.

Another option would be to run a Monte Carlo analysis. In Monte Carlo analysis, key parameters are varied within a range of potential values; the model is run with each

combination of parameter values, and model goodness of fit is judged with one or more statistics until a best fit is identified.

More recently, genetic algorithms (GAs) have been used commonly in model calibration. They are based on the biological principles of natural selection, with optimal combinations of parameters selected from a "population" of potential values through many "generations" of variations. In each generation, combinations of parameters that improve the model fit tend to be more favored for selection in the next generation. GA's tend to be more stable and robust than calculus-based numerical algorithms, and tend to converge to a solution more efficiently than Monte Carlo analysis. Mulligan and Brown (1998) report use of a genetic algorithm to calibrate Streeter-Phelps and QUAL2E stream models. Pelletier et al. (2006) applied a publicly-available GA (PIKAIA) to calibrate a QUAL2Kw eutrophication model. Ostfeld and Salomons (2005) report application of a hybrid genetic algorithm to calibrate a CE-QUAL-W2 model. In this report, the efficiency of the genetic algorithm was enhanced using hurdle-race and k-nearest neighbor algorithms to eliminate most of the excess computational effort.

Although the numerical optimization methods offer certain advantages, many modelers feel more comfortable with a manual trial-and error approach based on statistical and graphical analysis. Given the time required to develop a numerical optimization program, the manual approach is recommended for the Lake Travis model.

Calibration then Verification or Combined Calibration/Verification?

Typically, it is recommended that models should be calibrated to one dataset, then verified using an independent dataset. Often, this is performed by splitting the available dataset in half, using the first half for calibration and the second half for verification. If the model fits the verification dataset well (without adjusting the calibrated model parameters), it lends confidence in model predictions of future conditions. Cole and Wells (2002) point out, however, that the separation between calibration and verification is a false one, because if the verification run does not fit well, then the model calibration coefficients will inevitably be adjusted until the model fits both calibration and verification periods. Thus, they recommend that the model should be calibrated to all available data continuously, i.e. not broken into separate runs by years or seasons. However, the model should exhibit good fit to all periods, including individual years, droughts, and flood periods. Ideally, the calibration data set should encompass the full range of variations and extreme conditions that might be anticipated in the future.

Measures of Model Goodness of Fit

While some modelers do not use statistical measures of goodness of fit (GOF), choosing to rely instead on graphical illustration of GOF, it is generally recommended (Reckhow et al. 1990) that one or more quantitative measures of GOF be used in calibration and verification/confirmation of models. Numerous statistical measures of model goodness of fit (GOF) are available, and some are listed below and summarized in Table 1. The similarly of most of these measures is readily noticeable when they are expressed using common notation. The table lists the number of times each GOF statistic was used in a brief review of modeling reports.

Several authors recommend that several GOF measures be used, to quantify 1) model bias, 2) absolute error, and 3) relative error. This may lead to situations where different calibrations show improved performance with respect to some GOF statistics, but poorer performance for others. For this reason, it is recommended that acceptable ranges of GOF statistics are decided in advance, as well as a hierarchy of importance of GOF statistics. To facilitate calibration, an automated or semi-automated method should be implemented to calculate and summarize the various GOF statistics, compare them to acceptable ranges, and calculate an overall calibration score.

Cole and Wells (2002) recommend using the absolute mean error (AME) as an indicator of CE-QUAL-W2 model accuracy, since it is simply calculated and directly interpretable, i.e., it is in the same units as the measurement. A similar statistic is the root mean square error (RMSE), with the difference that it provides an extra penalty for the outlying predictions that are very different from observations. The RMSE is commonly used in the objective minimization functions of parameter optimization algorithms. Neither the AME nor RMSE provide information on model bias, as deviations in either direction from observed values are penalized equally. For quantification of the bias of model predictions, the mean error (ME) or mean percent error (M%E) are recommended.

The reliability index (RI) of Leggett and Williams (1981) has been used by many CE-QUAL-W2 modelers to evaluate model performance. Wlosinski (1984) considered the RI to be the best statistic for reporting aggregate model performance for CE-QUAL-R1, the predecessor to CE-QUAL-W2. The RI indicates the average factor by which model predictions differ from observations. A RI of 1.0 indicates a perfect fit. If all predicted values are one-half order of magnitude apart, a RI of 5 will result. RI values of less than 3 are generally considered to be acceptable for most parameters. RI values of greater than 10 usually indicate extremely low values near detection limits, as often found with some nutrient species, or highly variable parameters, such as algae biomass. One of the weaknesses of the RI is that the values are difficult to interpret since they are unitless and their range is expected to vary by parameter. The RI should be used with other measures of absolute and relative error.

The modeling efficiency (MEF) measures how much better a model predicts observed values than the average of the observed values. A value of 1 indicates a perfect match, whereas a value of 0 indicates that the model performs no better at predicting observed values than the average of the observed values.

Theil's inequality coefficient is similar to a correlation coefficient, but is a measure of distance instead of similarity. One advantage of Theil's inequality coefficient is that it can be decomposed into bias, variance, and fit quality components (Smith and Rose, 1995). However, the interpretation of these quantities may not be as straightforward as the more direct measures.

While the modeler has substantial leeway in selecting GOF statistics, we recommend using mean error (ME) to evaluate bias, root mean square error (RMSE) to evaluate absolute error, and Leggett and Williams' (1981) reliability index (RI). These are straightforward to calculate and interpret. Since they have been used in other modeling studies, it will facilitate comparison of model performance with other studies.

Table 1. Summary of model goodness of fit statistics and their characteristics

Statistic	Statistic name	Use‡	Measure of?	Penalizes outliers?	Units?	Range†,*
ME	mean error	9	absolute bias	N	Same as observation	-∞ — +∞ 0*
M%E	mean percent error	2	relative bias	N	Unitless % of observation	-∞ — +∞ 0*
MSE	mean square error	2	absolute error	Y	Square of observation	0* — ∞
MAE	mean absolute error	10	absolute error	N	Same as observation	0* — ∞
MA%E	mean absolute percent error	2	relative error	N	Unitless % of observation	0* — ∞
RMSE	root mean square error	11	absolute error	Y	Same as observation	0* — ∞
RMAE	relative mean absolute error	1	relative error	N	Unitless % of observation	0* — ∞
GSD	general standard deviation	1	relative error	Y	Unitless % of observation	0* — ∞
U	Theil's inequality coefficient	1	fit quality index	Y	unitless	0* — 1
E	Nash-Sutcliffe coefficient of efficiency	1	fit quality index	Y	unitless	-∞ — 1*
E′	modified coefficient of efficiency	1	fit quality index	N	unitless	-∞ — +∞ 1*
J	Janus quotient	1	fit quality index	Y	unitless	0* — ∞
R^2	coefficient of determination	8	fit quality index	Y	unitless	0 —1*
d	index of agreement	1	fit quality index	Y	unitless	0 —1*
d′	modified index of agreement	1	fit quality index	N	unitless	0 —1*
L_k	likelihood function	1	fit quality index	Y	Square root of observation	0* — ∞
k_g or RI	reliability index	6	fit quality index	Y	unitless	1* — ∞
d	functional distance	1	fit quality index	N	logarithm of y	0* — ∞
MEF	modeling efficiency	1	fit quality index	Y	unitless	-∞ — 1*

† assuming observed data are positive numbers ‡ number of modeling reports and papers using this statistic

*asterisk indicates value for a perfect model fit to observed data

Model Verification and Confirmation

For model confirmation, several authors recommend that statistical hypothesis tests should be used in lieu of, or as a supplement to, descriptive GOF statistics. If model predictions fall within confidence limits of measured data, the model cannot be said to differ from the real system and confidence in model predictions is increased, even in the case of poor GOF statistics commonly observed for highly variable or near-detection limit parameters. To evaluate model predictive capacity, one can test the hypothesis that average prediction errors are, for example, less than 1 mg/l for dissolved oxygen

and less than 10 µg/l for chlorophyll a. Many hypothesis tests, such as the t-test, Wilcoxon-Mann-Witney test, or the Kolmogorov-Smirnov test are capable. All of these tests require independent samples drawn from a population, but water quality model simulations are typically very strongly autocorrelated with respect to time and location. Reckhow et al. (1990) describe methods to adjust for this autocorrelation. The t-test also requires normally distributed values, which is unusual for most environmental parameters but may be achievable through log-transformation.

Cole and Wells (2002) do not provide guidelines regarding a priori acceptable levels of error for CE-QUAL-W2. Ultimately, acceptable levels of error should be based on model uncertainty versus water quality prediction requirements of lake managers. However, based on a review of reported model errors in other systems, we can identify calibration goals for some parameters that may be achievable. These are average absolute mean errors for the system as a whole, and may not be met at all places and times.

Table 2. Calibration goals for system-wide average absolute mean error, based on CE-QUAL-W2 modeling results in other systems

water level	0.2 meters	total Kjeldahl nitrogen	0.4 mg/l
water temperature	1°C	ammonia nitrogen	0.03 mg/l
pH	0.3 su	nitrate nitrogen	0.1 mg/l
total organic carbon	0.6 mg/l	total phosphorus	0.02 mg/l
chlorophyll a	4 µg/l	orthophosphate phosphorus	0.01 mg/l

Model Goodness of Fit Statistic Formulas

In these formulas:

- y_i represents a measured value at point i in time and space
- $\hat{y}_i$ represents a model predicted value at point i in time and space
- i represents a point in time and space
- n represents the number of observations
- $\bar{y}$ represents the average measured value
- $\bar{\hat{y}}$ represents the average predicted value

Mean error $$ME = \left(\sum_{i=1}^{n} (y_i - \hat{y}_i) \right) / n$$

Mean % error $$M\%E = 100 \left[\sum_{i=1}^{n} (y_i - \hat{y}_i) / y_i) \right] / n$$

Mean square error $$MSE = \left[\sum_{i=1}^{n} (y_i - \hat{y}_i)^2 \right] / n$$

Mean absolute error $$MAE = \left(\sum_{i=1}^{n} |y_i - \hat{y}_i| \right) / n$$

Mean absolute % error $$MA\%E = 100 \left[\sum_{i=1}^{n} (|y_i - \hat{y}_i| / |y_i|) \right] / n$$

Root mean square error $$RMSE = \left\{ \left[\sum (y_i - \hat{y}_i)^2 \right] / n \right\}^{0.5}$$

Relative mean absolute error $$RMAE = \left(\sum_{i=1}^{n} |y_i - \hat{y}_i| \right) / (n * \bar{y}) = MAE / \bar{y}$$

General standard deviation $$GSD = RMSE / \bar{y}$$

Theil's inequality coefficient (Theil, 1966) $$U = \sqrt{\left[\sum_{i=1}^{n} (y_i - \hat{y}_i)^2 \right] / \sum_{i=1}^{n} y_i^{\,2}}$$

$$U_{bias} = \left[\bar{y} - \bar{\hat{y}} \right]^2 / \left[(1/n) \sum_{i=1}^{n} (y_i - \hat{y}_i)^2 \right]$$

$$U_{\text{var}iance} = \left[s - \hat{s} \right]^2 / \left[(1/n) \sum_{i=1}^{n} (y_i - \hat{y}_i)^2 \right]$$

where $\hat{s} = \sqrt{\frac{1}{n} \sum_{i=1}^{n} (\hat{y}_i - \bar{\hat{y}})^2}$ and $s = \sqrt{\frac{1}{n} \sum_{i=1}^{n} (y_i - \bar{y})^2}$

$$U_{\text{cov}ariance} = \left[2(1 - r_{y\hat{y}}) * s * \hat{s} \right] / \left[(1/n) \sum (y_i - \hat{y}_i)^2 \right]$$

Nash-Sutcliffe coefficient of efficiency (Nash and Sutcliffe 1970)

$$E = 1 - \sum_{i=1}^{n} (y_i - \hat{y}_i)^2 / \sum_{i=1}^{n} (y_i - \bar{y})^2$$

Modified coefficient of efficiency reduces the impact of outliers:

$$E' = 1 - \sum_{i=1}^{n}(y_i - \hat{y}_i) / \sum_{i=1}^{n}(y_i - \bar{y})$$

Janus quotient (Gadd and Wold, 1964) $J^2 = \left\{\sum_{i=1}^{m}(y_i - \hat{y}_i)^2 / m\right\} / \left\{\sum_{i=1}^{n}(y_i - \hat{y}_i)^2 / n\right\}$

Coefficient of determination $r^2 = \left\{\dfrac{\sum_{i=1}^{n}(y_i - \bar{y})(\hat{y}_i - \bar{\hat{y}})}{\left[\sum_{i=1}^{n}(y_i - \bar{y})^2\right]^{0.5} * \left[\sum_{i=1}^{n}(\hat{y}_i - \bar{\hat{y}})^2\right]^{0.5}}\right\}^2$

Index of Agreement (Willmott et al., 1985) $d = 1 - \dfrac{\sum_{i=1}^{n}(y_i - \hat{y}_i)^2}{\sum_{i=1}^{n}\left(|\hat{y}_i - \bar{y}| + |y_i - \bar{y}|\right)^2}$

Modified index of agreement $d' = 1 - \dfrac{\sum_{i=1}^{n}(y_i - \hat{y}_i)}{\sum_{i=1}^{n}\left(|\hat{y}_i - \bar{y}| + |y_i - \bar{y}|\right)}$

Likelihood function for parameter k $L_k = \sqrt{\dfrac{1}{n_k} * \sum_{i=1}^{n_k}\dfrac{(\hat{y}_{i,k} - y_{i,k})^2}{y_{i,k}}}$

Reliability index (Leggett and Williams 1981) $k_g = \dfrac{1 + \sqrt{\frac{1}{n}\sum_{i=1}^{n}\left[\frac{1-(y_i/\hat{y}_i)}{1+(y_i/\hat{y}_i)}\right]^2}}{1 - \sqrt{\frac{1}{n}\sum_{i=1}^{n}\left[\frac{1-(y_i/\hat{y}_i)}{1+(y_i/\hat{y}_i)}\right]^2}}$

Functional distance $d = \sqrt{\sum_{i=1}^{n}(\ln y_i - \ln \hat{y}_i)^2 / n}$

Modeling efficiency $$MEF = \frac{\sum_{i=1}^{n}(y_i - \bar{y})^2 - \sum_{i=1}^{n}(\hat{y}_i - y_i)^2}{\sum_{i=1}^{n}(y_i - \bar{y})^2}$$

Autocorrelation coefficient for time lag k $$r_k = \frac{\mathrm{cov}\,ar[y_i, y_{i+k}]}{s(y_i) * s(y_{i+k})}$$

References

Berger, C.J., R.L. Annear, Jr., and S.A. Wells. 2003. "Upper Spokane River Model: Model Calibration, 2001". Technical Report EWR-1-03, Department of Civil and Environmental Engineering, Portland State University, Portland, OR, 89 pages.

Cole, T.M., and S.A. Wells. 2002. CE-QUAL-W2: A two-dimensional, laterally averaged, hydrodynamic and water quality model, version 3.1: user manual. Instruction report EL-02-1. U.S. Army Corps of Engineers, Washington DC, August 2002.

Gadd, A., and H. Wold. 1964. The Janus coefficient: a measure for the accuracy of prediction. In H. Wold (ed.) *Econometric model building: essays on the causal chain approach*. North Holland, Amsterdam, pp. 229-235.

Leggett, R.W., and L.R. Williams. 1981. A reliability index for models. *Ecological Modelling*, 13: 303-312.

Mulligan, A.E., and L.C. Brown. 1998. Genetic algorithms for calibrating water quality models. *Journal of Environmental Engineering*, 124: 202-211.

Nash, J.E., and J.V. Sutcliffe. 1970. River flow forecasting through conceptual models part 1: a discussion of principles. *Journal of Hydrology*, 10: 282-290.

Ostfeld, A. and S. Salomons. 2005. A hybrid genetic-instance based learning algorithm for CE-QUAL-W2 calibration. *Journal of Hydrology*, 310: 122-142.

Pelletier, G.J., S.C. Chapra, and H. Tao. 2006. QUAL2Kw – A framework for modeling water quality in streams and rivers using a genetic algorithm for calibration. *Journal of Environmental Modeling and Software*, 21: 419-425.

Reckhow, K.H., J.T. Clements, and R.C. Dodd. 1990. Statistical evaluation of mechanistic water-quality models. *Journal of Environmental Engineering*, 116: 250-268.

Smith, E.P., and K.A. Rose. 1995. Model goodness-of-fit analysis using regression and related techniques. *Journal of Ecological Modelling*, 77:49-64.

Theil, H. 1966. Applied Econometric Forecasting. North Holland, Amsterdam, 474 pp.

Willmott, C.J., S.G Ackleson, R.E. Davis, J.J. Feddema, K.M. Klink, D.R. Legates, J. O'Donnell, and C.M. Rowe. 1985. Statistics for the evaluation and comparison of models. *Journal of Geophysical Research*, 90: 8995–9005.

Wlosinski, J.H. 1984. Evaluation techniques for CE-QUAL-R1 – a one-dimensional reservoir water quality model. Miscellaneous Paper E-84-1. U.S. Army Corps of Engineers Waterways Experiment Station, Vicksburg, MS.

APPENDIX I

Summary of Selected USGS Phytoplankton Studies on Lake Travis to Assist CREMS Modeling

ANCHOR QEA

PARSONS

MEMORANDUM

To:	Lisa Hatzenbuehler, LCRA John Wedig, LCRA Angela Rodriguez, LCRA Jorge Izaguirre, LCRA Bryan Cook, LCRA
cc:	Harry Zahakos, QEA Randy Palachek, Parsons, Jennifer Benaman, QEA Jim Patek, Parsons
From:	Monica Suarez, Parsons
Subject:	Summary of selected USGS phytoplankton studies on Lake Travis to assist CREMS modeling – Revision 1
Date:	September 8, 2008

This document presents a summary of results of a phytoplankton investigation in Lake Travis conducted by the USGS between April 2005 and December 2006. The main purpose of this document is to quantify several algal-related model parameters in support of the development of a CE-QUAL-W2 model of the lake as part of the CREMS project.

Phytoplankton Abundance and Distribution of Major Algal Groups

Surface water plankton was collected on a monthly basis from six thalweg sites and one cove site (12307) in the reservoir between April 2005 and December 2006 by LCRA Environmental Services (see Figure 1 for sampling locations). The six thalweg sites include: 12302 (Mansfield Dam); LC901 (Starnes Island); 12309 (Arkansas Bend); 12313 (Pace Bend); 12315 (Carpenter Bend); and 12316 (Turkey Bend). Identification and enumeration of major algal groups were performed at the USGS Water Quality Lab (NWQL). Figure 2 shows the spatial distribution of the relative contribution of the various groups to total cell counts. As can be seen, cyanobacteria (blue-green algae) were the most abundant group in all but one location, with the highest average contribution at Station 12313 (km 42). There were no discernible spatial trends for any of the algal groups.

Figure 3 shows that cyanobacteria represent the highest percent of algal counts during the summer months (June-August) and November-December, while diatoms are more abundant in January-February and September-October. Flagellates were the most abundant species in April and May, closely followed by cyanobacteria.

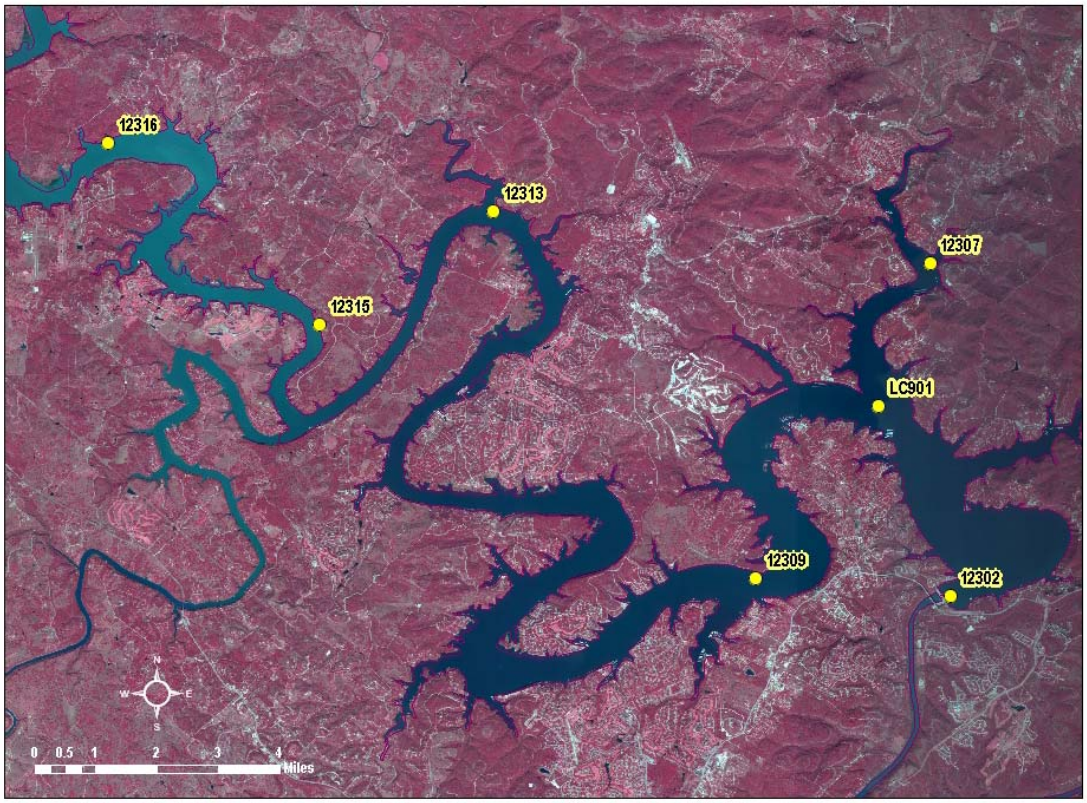

Figure 1. Travis Lake locations sampled during phytoplankton study

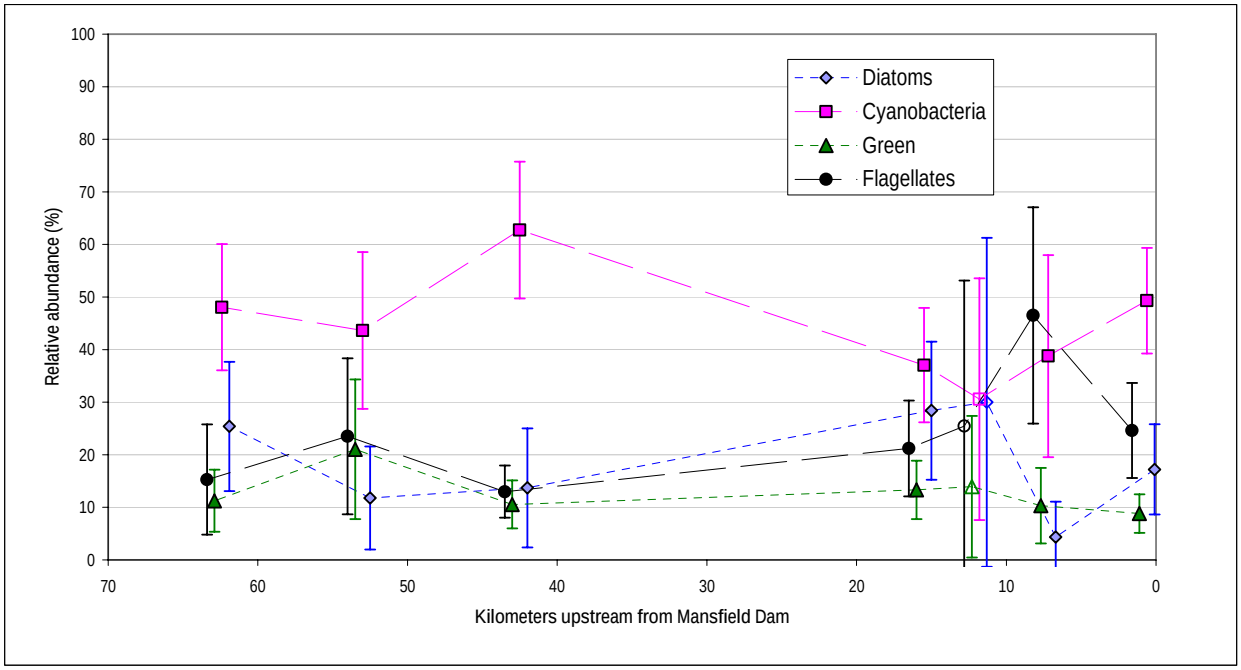

Error bars denote 95% confidence intervals
Open symbols correspond to the cove site (12307)

Figure 2. Algal abundance vs. distance upstream from Mansfield dam (Apr 2005-Dec 2006)

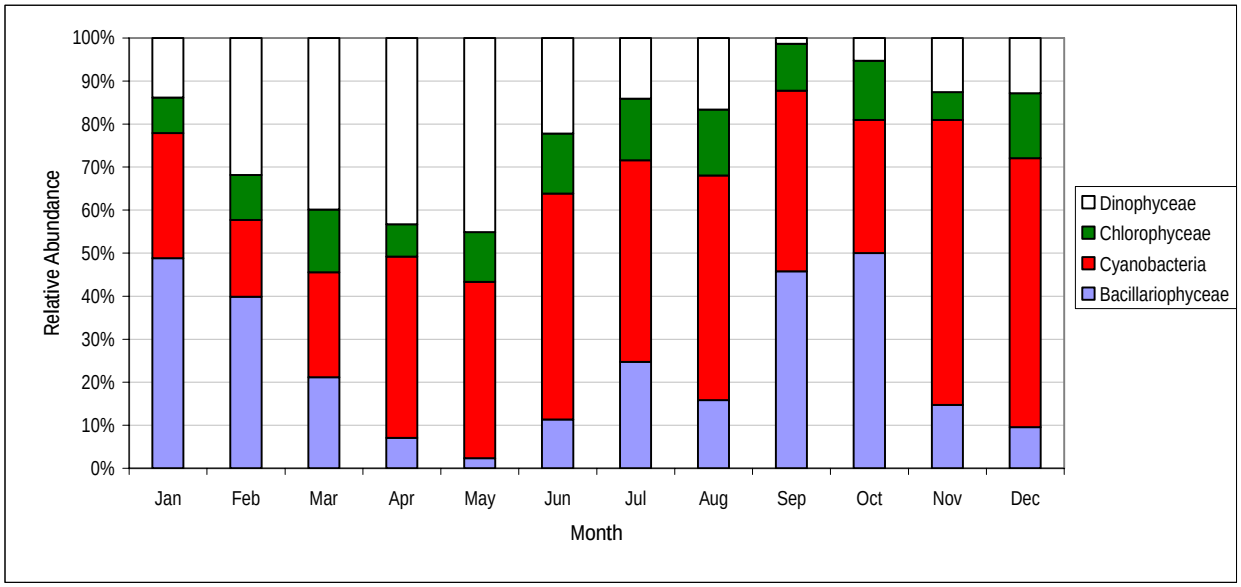

Values shown are averages by month

Figure 3. Relative abundance of major algal classes by month

Cell counts were converted to biovolumes using average values for each species used in a Lake Waco study (McFarland et. al, 2001). A summary of average biovolume for each algal group is included in Table 1.

Table 1. Algal volume by major group

Group	Mean Biovolume (μm^3/cell)
Diatoms	2,826
Cyanobacteria	
- filamentous	281.5
- coccoid	508.9
Green	1,766
Flagellates	81.8

Cyanobacteria had the highest relative abundance (45%, range 31 to 63%, Table 2), but diatoms had the highest relative biovolume (46%, range 21 to 57%, Table 2). Green algae had the second highest relative biovolume (28%, Table 2).

Figure 4 shows that diatoms had the highest contribution to biovolume for all months but April, May and December, with values between 19 and 77%. Green algae had the highest contribution to biovolume in April and May (35 and 52%, respectively), while cyanobacteria presented the highest contribution in December (44%). Figure 5 shows that diatoms represent the highest contribution to total biovolume in fall, winter, and summer; while in spring green algae had the highest contribution. Flagellate relative biovolumes are usually low, with the highest contribution in spring compared to the remaining seasons.

Table 2. Average phytoplankton abundance and biovolume by station (%)

Site	Diatoms		Cyanobacteria		Green		Flagellates	
	Abundance	Biovolume	Abundance	Biovolume	Abundance	Biovolume	Abundance	Biovolume
12302	17	42	49	28	9	25	25	4
LC901	4	21	39	24	10	41	47	14
12307	30	45	31	13	14	27	25	15
12309	28	57	37	14	13	27	21	2
12313	14	42	63	25	11	31	13	2
12315	12	32	44	19	21	44	24	5
12316	25	55	48	21	11	21	15	2
Mean	21	46	45	21	12	28	22	5

It is noted that lake levels during the sampling period were comparable to long-term averages as shown in Figure 6a. However, monthly average flows during the sampling period (April 2004 to December 2006) were significantly lower than long-term averages, as indicated by data collected at USGS gage 8153500 - Pedernales River near Johnson City (Figure 6b). Monthly average flows during the study period were as low as 9% of the long-term average flows for the month of September, while they were at comparable values in May.

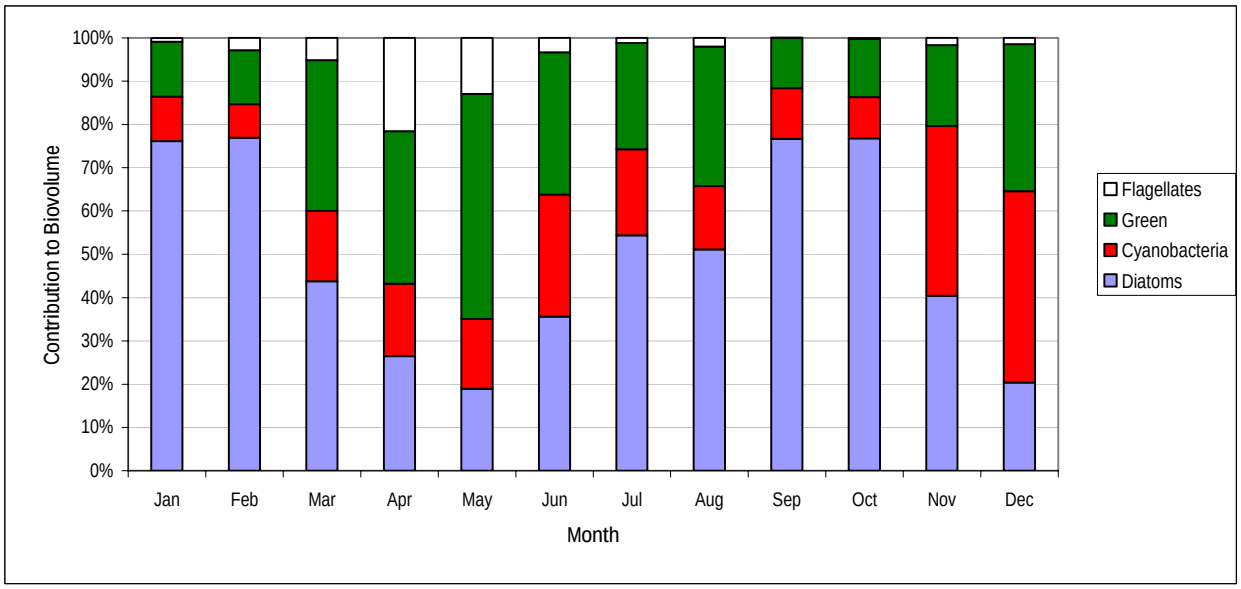

Values shown are averages by month

Figure 4. Relative biovolume of major algal classes by month

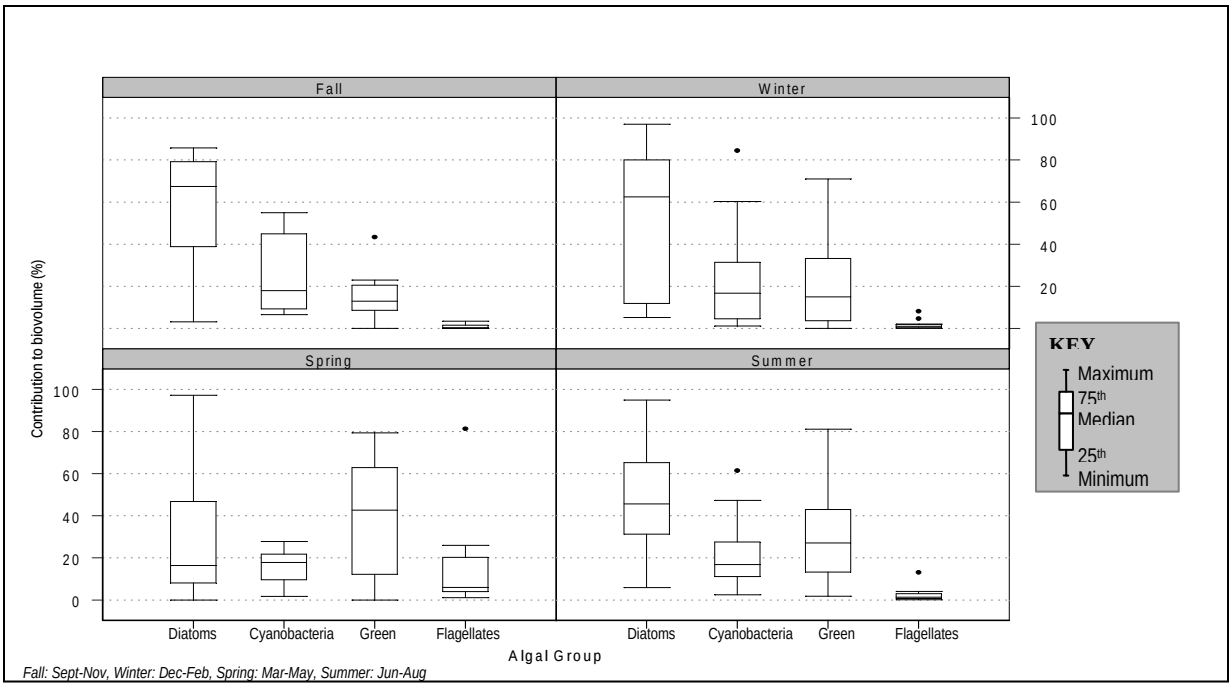

Figure 5. Relative biovolume of major algal classes by season

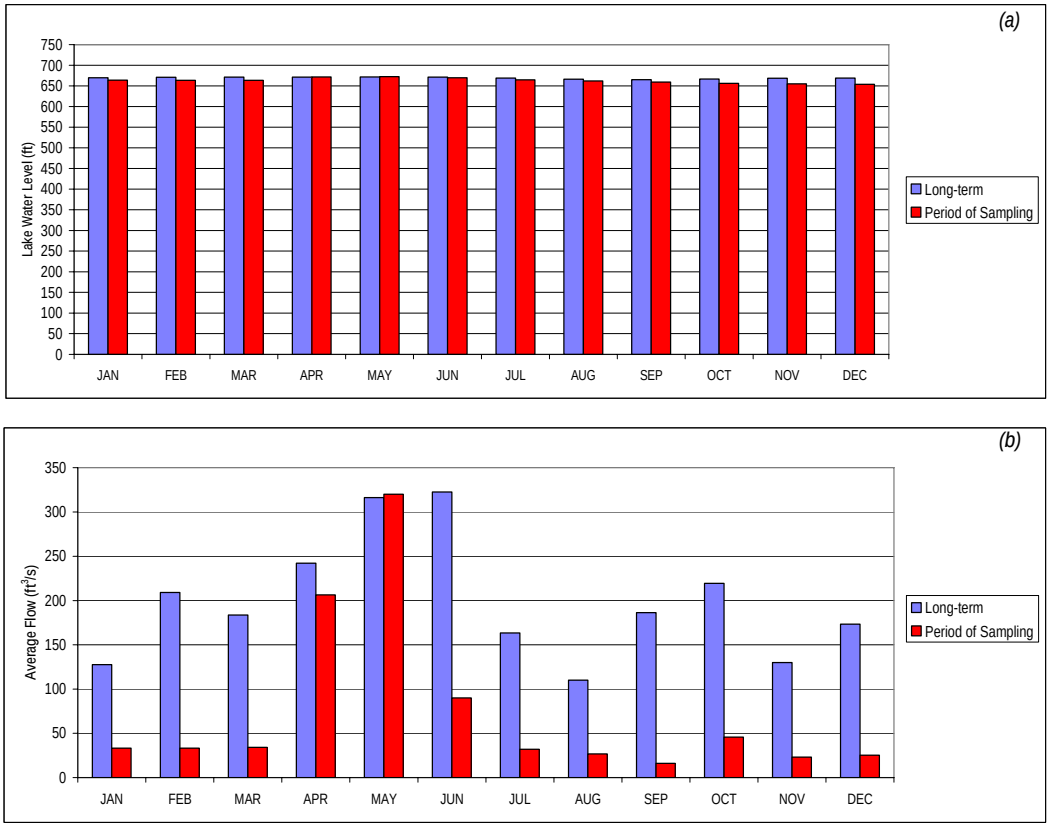

(a) Monthly average reservoir levels for Lake Travis. Source: http://www.lcra.org/water/XML_historical.html?type=print
(b) Monthly average flows in Pedernales River near Johnson City. Source: http://tx.usgs.gov/

Figure 6. Average Monthly Flow and Reservoir Levels

Phytoplankton Nutrient-Enrichment Bioassays

Nutrient-dependent phytoplankton growth bioassays were conducted on a monthly basis from June 2005 to August 2006. Surface water plankton was collected from five sites and one cove site (12307) in the reservoir by LCRA Environmental Services. These six sites include: 12302 (Mansfield Dam); 12307 (Sandy Creek Cove); 12309 (Arkansas Bend); 12313 (Pace Bend); 12315 (Carpenter Bend); and 12316 (Turkey Bend). Growth rates were measured under four treatment conditions:

1. control or ambient (CON) – no nutrients added;
2. Nitrogen (N) – $NaNO_3$ was added for a total of 3.29 mg/L of N;
3. Phosphorus (P) – $Na_2HPO_4 \cdot 7H_2O$ was added for a total of 0.93 mg/L of P; and
4. combined N+P addition.

Bioassays were incubated at reservoir ambient temperatures (between 15 and 29°C, as measured at the dam on the day of sample collection) for 5 to 7 days with a 14:10 & 12:12 light:dark cycle during the summer and winter months, respectively. Incubation light intensity was approximately 10% of natural irradiance, which is generally accepted to be sufficient for algal photosynthesis. Table 3 presents summary statistics for the measured growth rates.

Figure 7 shows that the observed growth rates for the N+P enriched bioassays did not vary significantly during the first six months of the study; they then experienced a decrease in February and March 2006 and finally exhibited a consistent increasing trend during the remaining months. Variations in rates for the N and P treatments were much less marked and patterns were not consistent among the different stations. The ambient bioassays (CON) resulted in some negative rates.

Figure 8 indicates that the growth rates did not vary significantly with location, but nevertheless were highest at the dam. Overall growth rates (mean±95% confidence interval) were 0.41±0.03, 0.03±0.01, 0.06±0.01, and -0.003±0.01 day^{-1} for the NP, N, P, and ambient bioassays, respectively (Table 3).

Further seasonal analysis was conducted for the non-nutrient limiting bioassays (i.e. N+P treatment) since they yielded the maximum growth rates, which will be used for setting up the CE-QUAL-W2 model for the lake. Figure 9 shows that growth rates are the lowest in February and March then increase to their peak in August, drop in September to finally increase during fall until January. It is apparent that the rates are significantly different among seasons.

Table 3. Summary of measured growth rates (day^{-1})

Station ID	Statistic	CON	N	P	NP
12302 (Mansfield Dam)	n	40	40	40	40
	min	-0.06	-0.11	-0.09	0.14
	max	0.15	0.16	0.25	0.79
	mean	0.04	0.06	0.09	0.46
	st dev	0.05	0.06	0.10	0.21
12307 (Sandy Creek Cove)	n	40	40	40	40
	min	-0.13	-0.15	-0.22	0.03
	max	0.17	0.12	0.25	0.80
	mean	-0.01	0.02	0.07	0.41
	st dev	0.08	0.08	0.12	0.24
12309 (Arkansas Bend)	n	40	40	40	40
	min	-0.35	-0.15	-0.10	0.10
	max	0.34	0.15	0.17	0.69
	mean	0.00	0.03	0.08	0.40
	st dev	0.15	0.09	0.08	0.20
12313 (Pace Bend)	n	36	36	36	36
	min	-0.17	-0.19	-0.14	0.00
	max	0.30	0.25	0.40	0.72
	mean	-0.01	0.01	0.06	0.38
	st dev	0.12	0.12	0.15	0.22
12315 (Carpenter Bend)	n	40	40	40	40
	min	-0.16	-0.16	-0.12	0.06
	max	0.16	0.17	0.25	0.86
	mean	-0.03	0.02	0.03	0.44
	st dev	0.10	0.09	0.09	0.21
12316 (Turkey Bend)	n	36	36	36	36
	min	-0.20	-0.16	-0.11	0.06
	max	0.21	0.21	0.32	0.70
	mean	-0.01	0.02	0.05	0.38
	st dev	0.11	0.10	0.12	0.16
Overall	n	232	232	232	232
	min	-0.35	-0.19	-0.22	0.00
	max	0.34	0.25	0.40	0.86
	mean	-0.003	0.03	0.06	0.41
	st dev	0.11	0.09	0.11	0.21

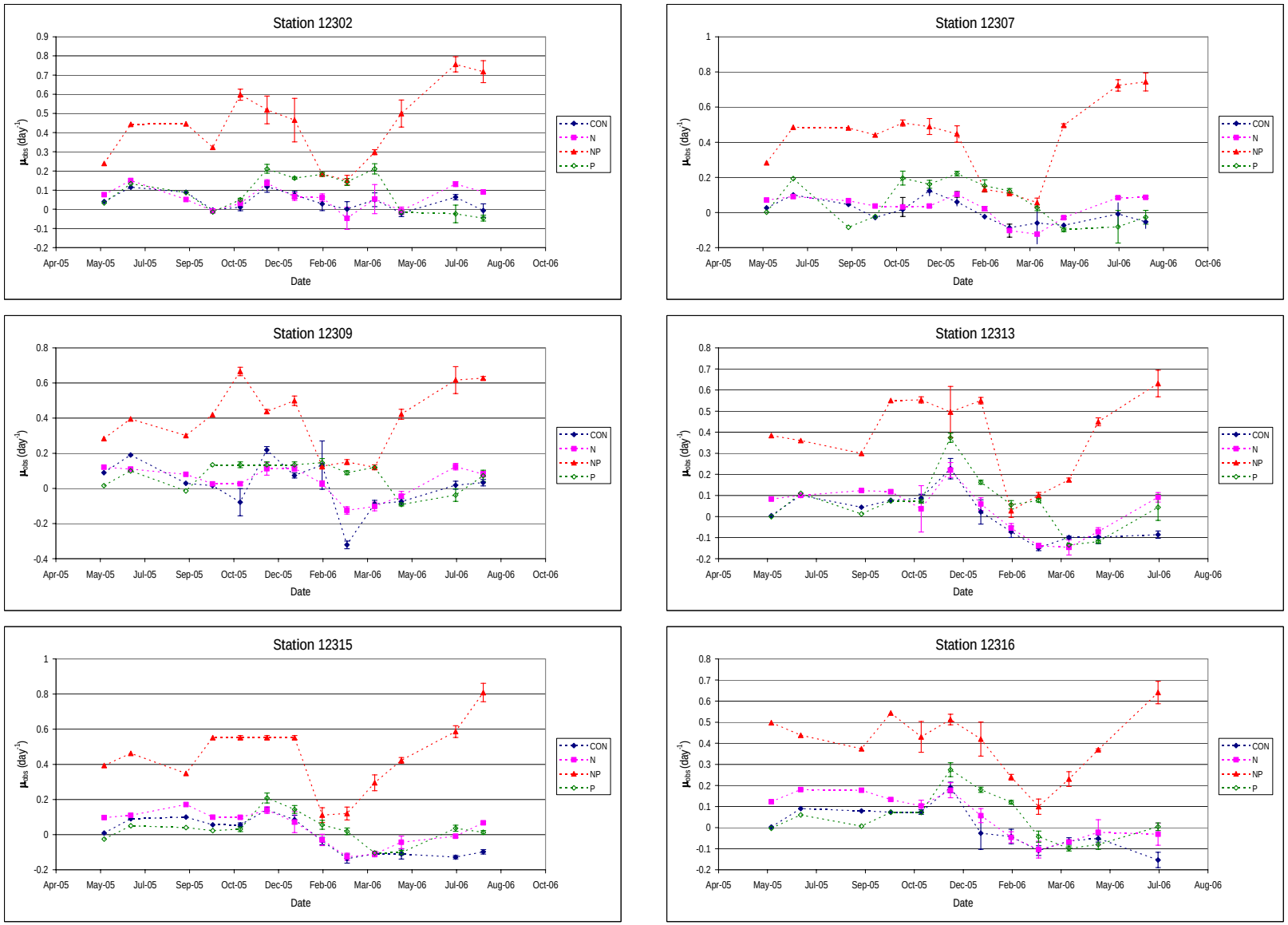

Error bars denote 95% confidence intervals

Figure 7. Average growth rates

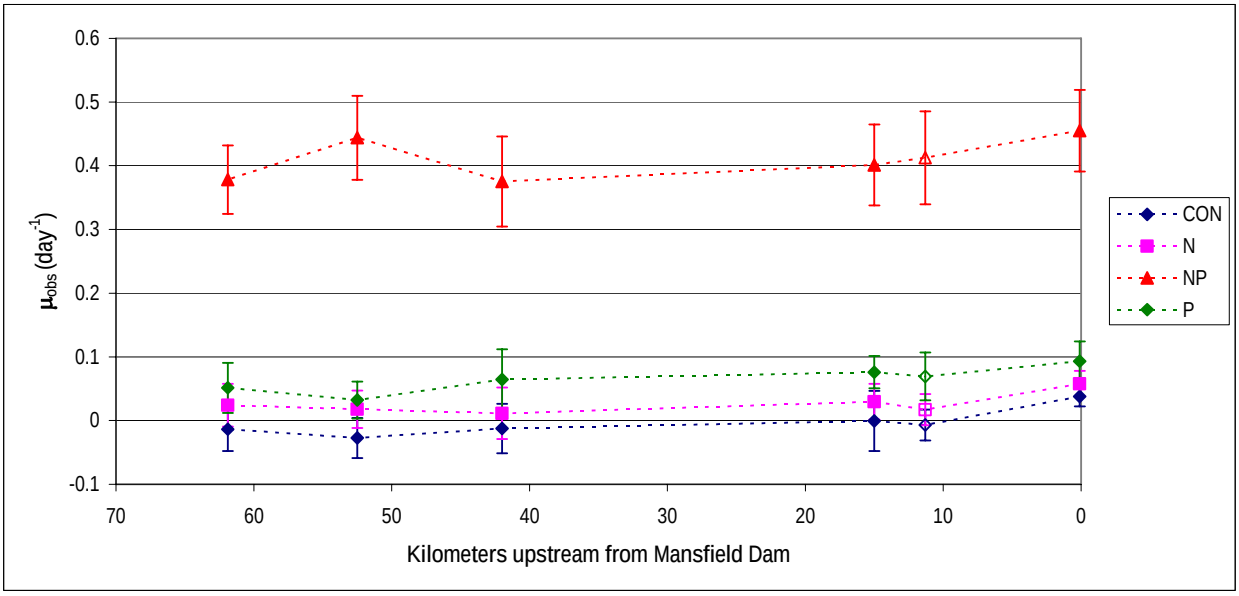

Error bars denote 95% confidence intervals
Open symbols correspond to the cove site (12307)

Figure 8. Average growth rate vs. distance upstream from Mansfield Dam

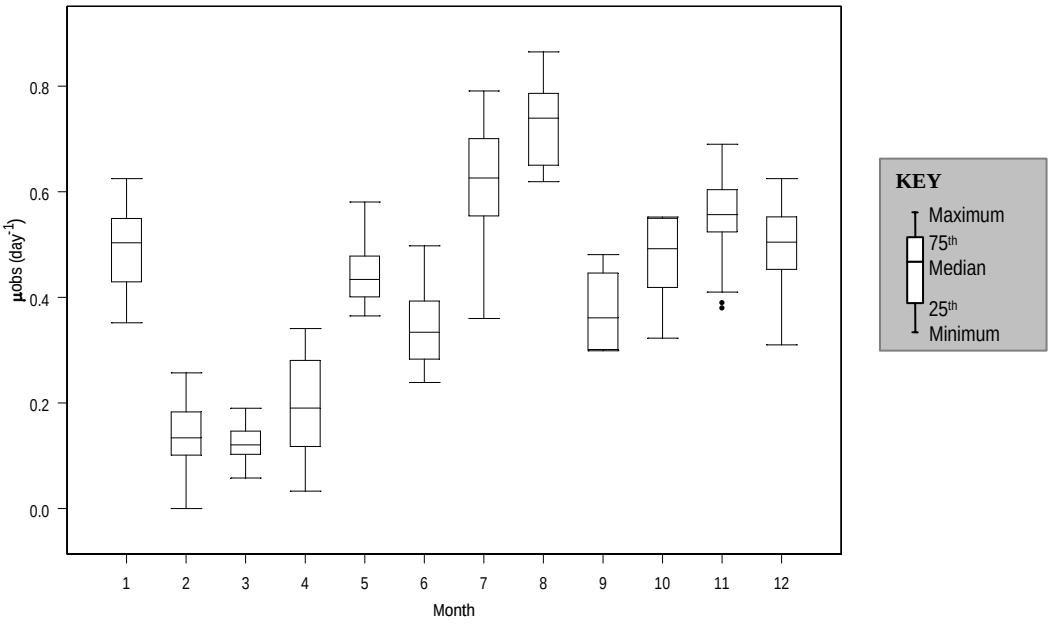

Figure 9. Maximum growth rates (N+P bioassays) vs. month

Carbon to Nutrient Ratios

Figure 10 indicates that the C:N ratios (range 8-12) tended to decrease upstream of the dam and presented their highest average value at the cove site (11302, open symbols on Figure 10). C:P ratios (range 168-311), on the other hand, presented an increasing trend

upstream of the dam. Figure 11 indicates that C:P ratios tended to be higher in April, whereas the highest C:N ratios were observed in October. October also corresponded to the month with the lowest measured C:P ratios.

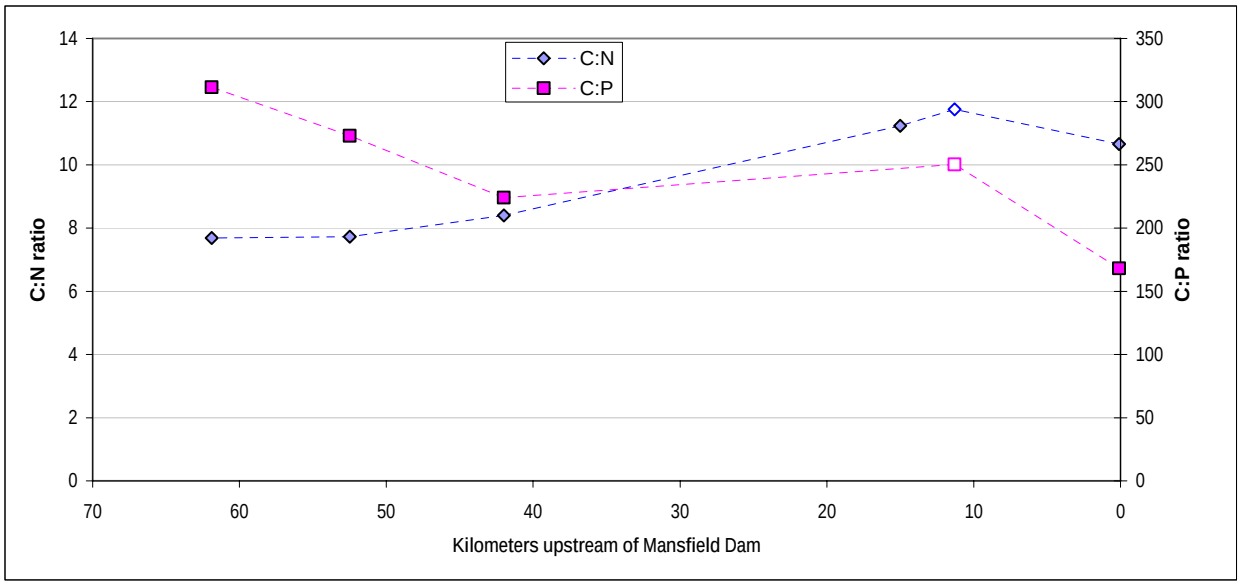

Error bars denote 95% confidence intervals
Open symbols correspond to the cove site (12307)

Figure 10. Carbon to nutrient ratios vs. distance

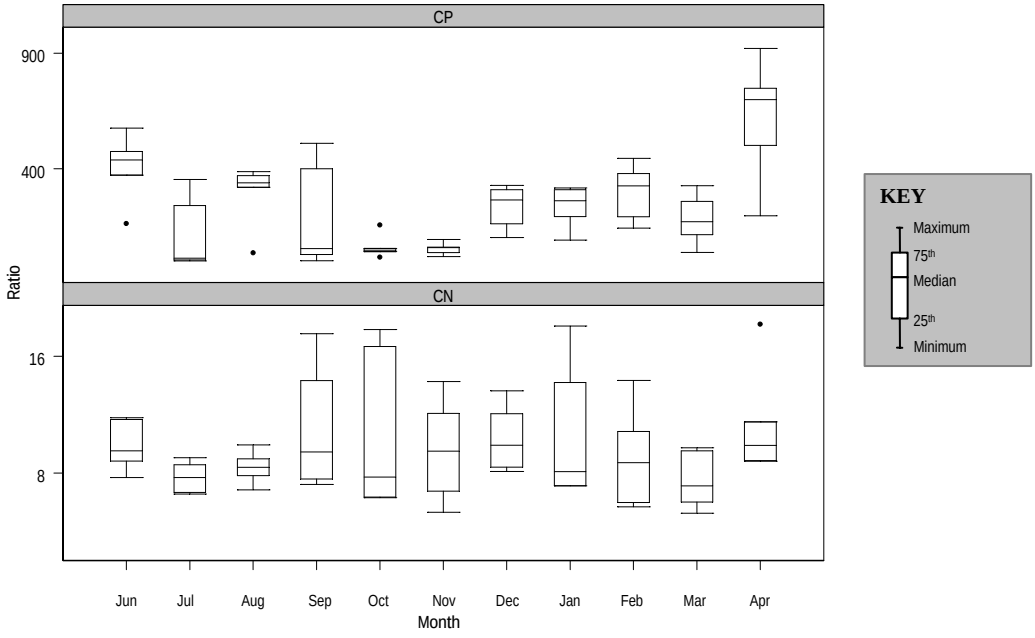

Figure 11. Carbon to nutrient ratios vs. month

Mesozooplankton grazing experiments

Mesozooplankton grazing experiments were performed in winter 2005 and spring through summer 2006 with surface plankton collected at the same sites in Lake Travis as the bioassays. The experiments were based on the assumption that the major loss factor of phytoplankton biomass accumulation is a direct result of grazing mortality by mesozooplankton in the experimental treatment. A grazer density-gradient was constructed in 50ml borosilicate culture tubes by adding increased amounts of grazers (mesozooplankton) to the natural algal assemblage from each site (starting volume ~ 30mL) with one to two replicates per treatment (1X ~ 5; 2X ~ 10-15; and 3X ~ 20-30 grazers, respectively). Grazing results of all experimental treatments and controls (no additional mesozooplankton) were calculated using an exponential model (first-order decay). Subsequently, linear regression were performed on the growth estimates versus zooplankton density, whereby the slope of the regression line estimates the grazing rate, thus negative when grazing occurs. As shown in Figure 12, the estimated grazing rate was 0.26 day^{-1}/X.

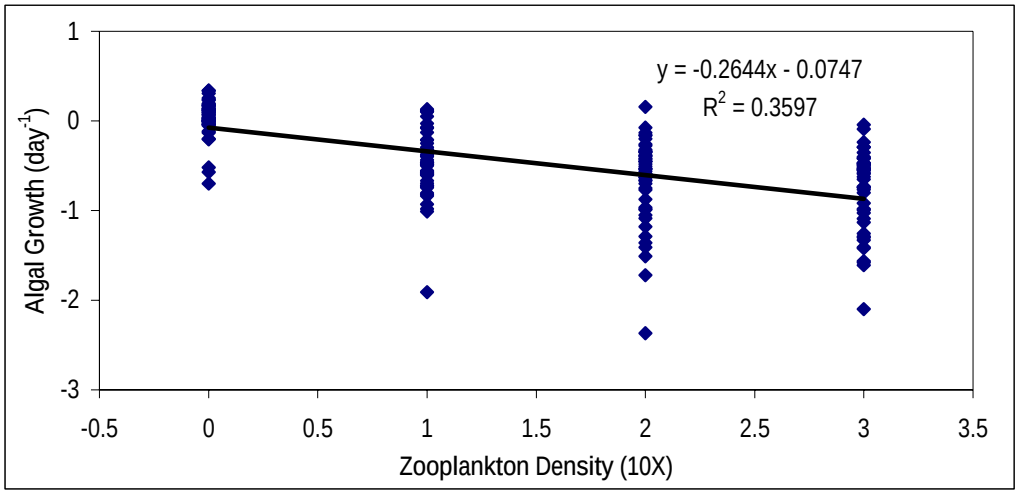

Figure 12. Mesozooplankton grazing

Table 4 summarizes zooplankton density measurements performed monthly between April 2005 and January 2006 at the same stations were grazing experiments were conducted. Overall, between 0 and 877 organisms/L were measured in Lake Travis samples, with an average of 190 organisms/L. Table 4 also includes zooplankton densities normalized to 30mL, which is the volume used for the grazing experiments. It is recognized that the reported counts for deep sites may underestimate the concentration of organisms due to dilution. Nevertheless, the reported ranges were used in this document to estimate grazing rates in units of 1/day. As mentioned earlier, for the grazing experiments, 1X and 3X are equal to 5 and 20-30 grazers per 30 m, respectively. Thus, overall zooplankton densities in Lake Travis varied between 0 and 3X, with an average of 1X. This means that the grazing rates can be estimated to range from 0 to 0.78 day^{-1}, with an average value of 0.26 day^{-1}.

Table 4. Summary of zooplankton counts

Station ID	n	Range (org/L)	Mean (org/L)	Range (org/30mL)	Mean (org/30mL)
12302	13	1-414	159	0-12	5
12307	4	0-171	95	0-5	3
12309	10	1-412	130	0-12	4
12313	7	1-496	244	0-15	7
12315	13	1-877	290	0-26	9
12316	3	2-248	99	0-7	3
Overall	50	0-877	190	0-26	6

CE-QUAL-W2 MODEL PARAMETERS

Three main groups of algal-related kinetic coefficients are required by the CE-QUAL-W2 model for Lake Travis. If field measurements were available to determine the model parameters (i.e., growth rates, half-saturation concentrations, and stoichiometric ratios), the values were determined by algal group using either regressions or proportioning assumptions. For a substantial number of model parameters, there were no site-specific data and, thus, literature values are provided as starting points for calibration.

Algal Rates

Maximum algal growth rate [AG] for major algal groups

Values for this parameter were obtained using data from the bioassays with N+P treatment. Observed growth rates were paired with average biovolume data measured at a given location during the same month of the bioassay sample collection. Growth rates for individual groups were estimated assuming the following model:

- At a given time, *t*, the total biomass is equal to

$$C_t = C_0 e^{\mu_{obs} t} \quad (1)$$

  where μ_{obs} is the bulk observed growth rate measured in the bioassays and

  C_0 is the initial biomass concentration, which is equal to the sum of biomass concentrations per algal group.

- Assuming that the relative contribution to biomass by group is equal to the relative contribution to biovolume (in other words, equal density):

$$C_0 = B_1 C_0 + B_2 C_0 + B_3 C_0 + B_4 C_0 \quad (2)$$

  where B_1, B_2, B_3, and B_4 are the percent biovolumes for diatoms, cyanobacteria, green algae, and flagellates, respectively.

- The total biomass at time t can also be calculated as

$$C_t = C_0 e^{\mu_{obs} t} = B_1 C_0 e^{k_1 t} + B_2 C_0 e^{k_2 t} + B_3 C_0 e^{k_3 t} + B_4 C_0 e^{k_4 t} \quad (3)$$

  where k_1, k_2, k_3, and k_4 are the growth rates for diatoms, cyanobacteria, green algae, and flagellates, respectively.

- By simplification equation 3 becomes

$$e^{\mu_{obs}t} = B_1 e^{k_1 t} + B_2 e^{k_2 t} + B_3 e^{k_3 t} + B_4 e^{k_4 t} \quad (4)$$

Thus, if a time *t* is assumed, the growth rates by algal group can be calculated using a multiple non-linear regression. For the purpose of this document, a time equal 5 days was assumed and regressions were performed using S-PLUS 2000.

An initial regression including the entire dataset yielded a zero growth rate coefficient for flagellates. However, large residuals were observed for the summer months, when the bulk rates were the highest (See Figure 8). Thus, an additional regression was completed for those months in an attempt to estimate a growth rate for flagellates at high temperatures. To do so, the rates calculated using the initial multiple regression (0.5, 0.64, and 0.57 day^{-1} for diatoms, cyanobacteria, and green algae, respectively) were incorporated in Equation 4 and a non-linear regression was run with data for June to August to estimate k_4. The resulting equation is:

$$e^{\mu_{obs}t} - B_1 e^{0.5t} - B_2 e^{0.61t} - B_3 e^{0.57t} = B_4 e^{k_4 t} \quad (5)$$

This regression yielded a summer growth rate for flagellates of 1.39±0.02 day^{-1} (mean ± standard error). Incorporation of a non-zero value for k_4 at temperatures higher than 25°C significantly improved the model fit for the entire dataset (the model was able to predict 57% of the total variance and the standard residual error was reduced from 14.2 to 9.5). A summary of the estimated rates and statistics parameters for the "two-step" model is shown in Table 5.

Table 5. Summary of estimated maximum growth rates [AG]

Group	Temperature (°C)[a]	Rate (day^{-1})	Std. error (day^{-1})	t-value	Residual std. error
Diatoms	15-30	0.498	0.040	12.3	9.5
Cyanobacteria	15-30	0.612	0.054	11.3	
Green	15-30	0.569	0.054	10.5	
Flagellates	15-25	0	-	-	
	25-30	1.391	0.024	58.1	

[a] The range of temperatures in the bioassays was 15-30°C

Table 6 indicates that the calculated rates are within the range of rates reported in the literature for the range of average temperatures in Lake Travis (15 to 30°C).

Table 6. Calculated maximum growth rates vs. literature reported values

Group	Calculated rates (day^{-1})	Range of rates reported in literature (day^{-1})[a]
Diatoms	0.50	0.34-3.4
Cyanobacteria	0.61	0.17-5.04
Green algae	0.57	0.56-4.1
Flagellates	1.39	0.2-2.1

[a] Rates reported in CE-QUAL-W2 Manual corresponding to temperatures in the range 15-30°C

Mortality rates [AM]

The grazing experiments yielded and average rate of 0.26 day^{-1}, which could be used in the model under the assumption that grazing is the major biomass loss factor. The calculated rate, however, seems high when compared to the rates used in other CE-QUAL-W2 studies (Table 7). A general rule of thumb is that the maximum algal mortality rate [AM] should be less than 10% of the maximum algal growth rate [AG] as indicated in the CE-QUAL-W2 Manual. Thus, Table 7 also includes upper limits for mortality rates that were estimated using 10% of the growth rates for the various algal groups, which are the recommended values for use in the model.

Table 7. Range of values for mortality rates [AM]

Algal group	Values used in other CE-QUAL-W2 studies (day^{-1})[a]	Calculated (day^{-1})[b]
Diatoms	0.04-0.09	0.05
Cyanobacteria	0-0.02	0.06
Green	0.04-0.1	0.06

[a] For the most part, these are not measured values

[b] Calculated as 10% of the maximum growth rates derived from bioassays (Table 5)

Additional rates

CE-QUAL-W2 requires additional input for respiration, excretion, and settling rates, as well as saturating light intensity. Because no site-specific were available to derive such coefficients, literature values are suggested for input to the model as summarized in Table 8. Values reported in seventeen CE-QUAL-W2 studies compiled for this project are also included in Table 8.

Table 8. Range of values for additional algal coefficients

Parameter	Algal group	Literature values[a]	Values used in other CE-QUAL-W2 studies[b]
Maximum algal respiration rate, day^{-1} [AR]	Diatoms	0.05-0.59	0.02-0.1
	Cyanobacteria	0.10-0.92	0.01-0.02
	Green	0.01-0.16	0.02-0.08
	Flagellates		0.005-0.15[c]
Maximum algal excretion rate, day^{-1} [AE]	Diatoms		0.02-0.04
	Cyanobacteria		0.01-0.02
	Green	0.014-0.044	0.02-0.04
	Flagellates	0.036	0.005-0.15[c]
Algal settling rate, m/day [AS]	Diatoms	0.02-30.2	0.1-0.35
	Cyanobacteria		0-0.03
	Green		0.05-0.25
	Flagellates	0.31-6.1	0.01-0.4[c]
Saturating light intensity, W/m^2 [ASAT]	Diatoms	86	50-130
	Cyanobacteria	10-61	25-100
	Green	24	75-125
	Flagellates	12-36	40-150[c]

[a] From CE-QUAL-W2 Manual

[b] For the most part, these are not measured values

[c] No data were available for flagellates, so the range of values for studies not reporting specific groups are presented

Half-saturation constants

Half-saturation concentrations, K_s, are being developed by USGS using the maximum observed growth rates from bioassays (N+P treatments) and a Lineweaver-Burke plot (i.e., linear form of the Monod function). Ranges of K_s estimates will be added to this Memorandum when data become available.

Algal Temperature Rate Coefficients

CE-QUAL-W2 allows two different approaches for implementing the effect of temperature on maximum algal growth rates. One approach is to use a temperature coefficient for algal growth (AGTC). In this approach, growth would increase exponentially with temperature. More commonly, four temperature coefficients are used to specify an optimum temperature range for maximum growth, with reduced rates above and below this range. The ranges of algal temperature rate coefficients that have been used by others in CE-QUAL-W2 models for the second approach are listed in Table 9. These values are calibrated (not measured but adjusted during calibration) values for the most part.

Table 9. Algal temperature rate coefficients used in other modeling studies

Parameter	Description	Diatoms	Cyano-bacteria	Green algae	Flagellates
AT1	Lower temperature for algal growth, ^oC	1-3	5-0	5-24	8-10
AT2	Lower temperature for maximum algal growth, ^oC	3-24.5	12-10	20-25	30
AT3	Upper temperature for maximum algal growth, ^oC	12-26.5	16-20	25-35	35
AT4	Lower temperature for algal growth, ^oC	24-29	30	35-40	40
AK1	Fraction of algal growth rate at AT1	0.1	0.1	0.1-0.5	0.1-0.2
AK2	Fraction of algal growth rate at AT2	0.6-0.99	0.6-0.9	0.99	0.99
AK3	Fraction of algal growth rate at AT3	0.99	0.9-0.99	0.99	0.99
AK4	Fraction of algal growth rate at AT4	0.01	0.01-0.1	0.1	0.1-0.3

A linear regression was developed to explain observed variance in growth rates using bioassay data. The model is statistically significant at the 97% confidence level and accounts for approximately 47 percent of the observed variance. The regression coefficients are summarized below:

Dependent variable: μ_{obs} (day^{-1})

Independent variable	t-value	p-value	Model coefficient
Intercept	-2.13	0.03	-0.112
Temperature (^oC)	10.8	<0.0001	0.026

The model indicates that the rates increase with temperature at a rate of 0.026 day^{-1} per °C. This factor could be used to determine the difference of fraction algal growth between AT2 and AT3, assuming the maximum growth rate is observed at AT3 (i.e.

AK3=1). So if, for example, the optimum temperature range (AT2-AT3) for diatoms growth were 20-25°C, then AK2 would be equal to (0.50-5*0.026)/0.5=0.74.

As mentioned in the [AG] calculation section, the model that yielded the best fit assumed that growth rate for flagellates was zero for temperatures below 26°C. Thus, the values suggested for AT1, AT2, AT3, and AT4 are 25, 26, 30, and 31, respectively. The corresponding fractions of algal growth rates AK1, AK2, AK3, and AK4 would respectively be 0.01, 0.99, 0.99, and 0.01.

Algal Stoichiometry

The percent biovolume by algal group was used to partition the algal biomass estimates - the chlorophyll a and total particulate phosphorus (TPP) data from LCRA and the total particulate carbon (TPC) and total particulate nitrogen (TPN) data from the USGS NWQL. Because biomass concentration values were not available, it was assumed that TPC is equal to 45% of the biomass concentrations (i.e. AC coefficient in the model is 0.45, which is the default value). It is noted that because the factors used to partition TPC, TPP, and TPN concentrations are the same for a given group, the biomass to phosphorous and biomass to nitrogen stoichiometric ratios do not vary among groups and are equal to 45% of the inverse of the C:P and C:N ratios reported previously. Similarly, the biomass to chlorophyll a ratio is constant among groups. Table 10 summarizes the ranges of stoichiometric ratios obtained from field data.

Table 10. Algal stoichiometric ratios from field data

Parameter	Description	Range of values	Mean±SE
AP	Stoichiometric equivalent between algal biomass and phosphorous (ratio of TPP to algal biomass)	0.0005-0.3556	0.0154±0.0071
AN	Stoichiometric equivalent between algal biomass and nitrogen (ratio of TPN to algal biomass)	0.0247-0.0859	0.0516±0.0018
ACHLA	Ratio between algal biomass and chlorophyll a	103.8-991.1	371.7±34.6

REFERENCES

McFarland, A., R. Kiesling, and C. Pearson. 2001. *Characterization of a Central Texas Reservoir with Emphasis on Factors Influencing Algal Growth*. Texas Institute for Applied Environmental Research, Tarleton State University, Stephenville, Texas, TR0104, (April 2001).

APPENDIX J

Vertical Profiles of Water Temperature, Specific Conductivity, Chloride, Dissolved Oxygen, and Algal Limiting Factor at Mansfield Dam, Arkansas Bend, Pace Bend, Turkey Bend, and Sandy Creek

ANCHOR QEA

PARSONS

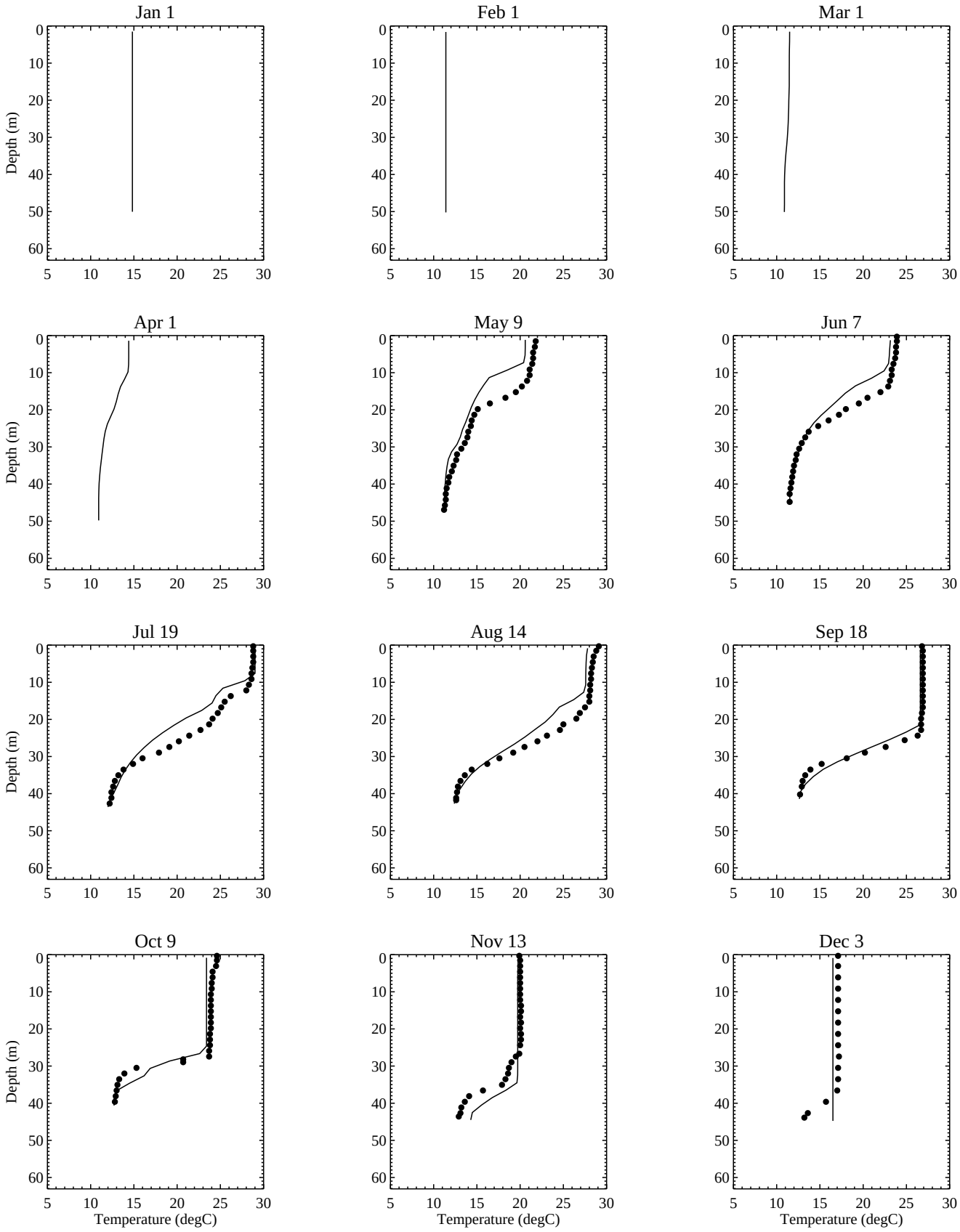

Figure J-1. Vertical profiles of model versus data at Mansfield Dam (Segment 93) - Temperature - 1984.

Profiles shown for dates with available data else model results for first day of month shown.

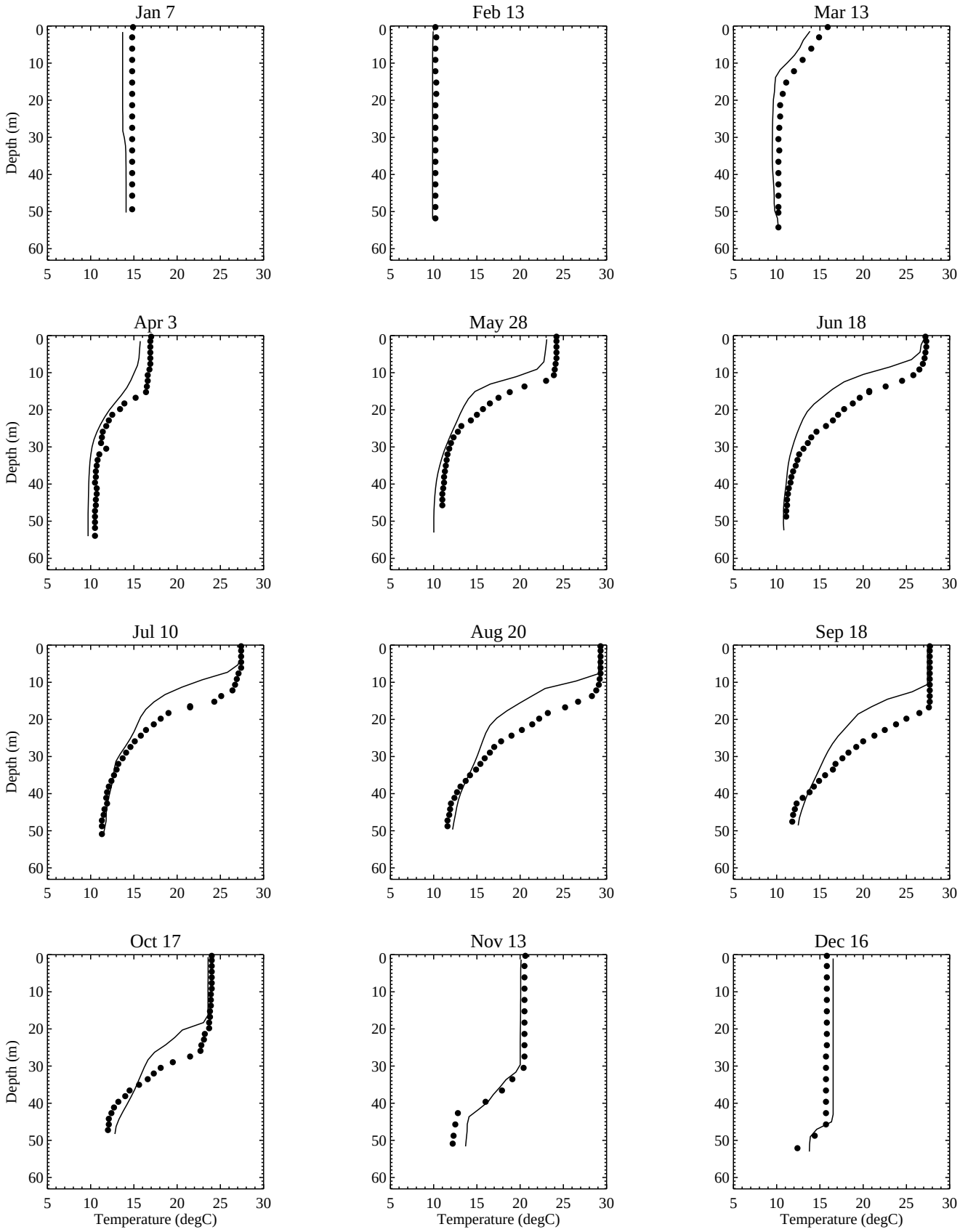

Figure J-1. Vertical profiles of model versus data at Mansfield Dam (Segment 93) - Temperature - 1985.

Profiles shown for dates with available data else model results for first day of month shown.

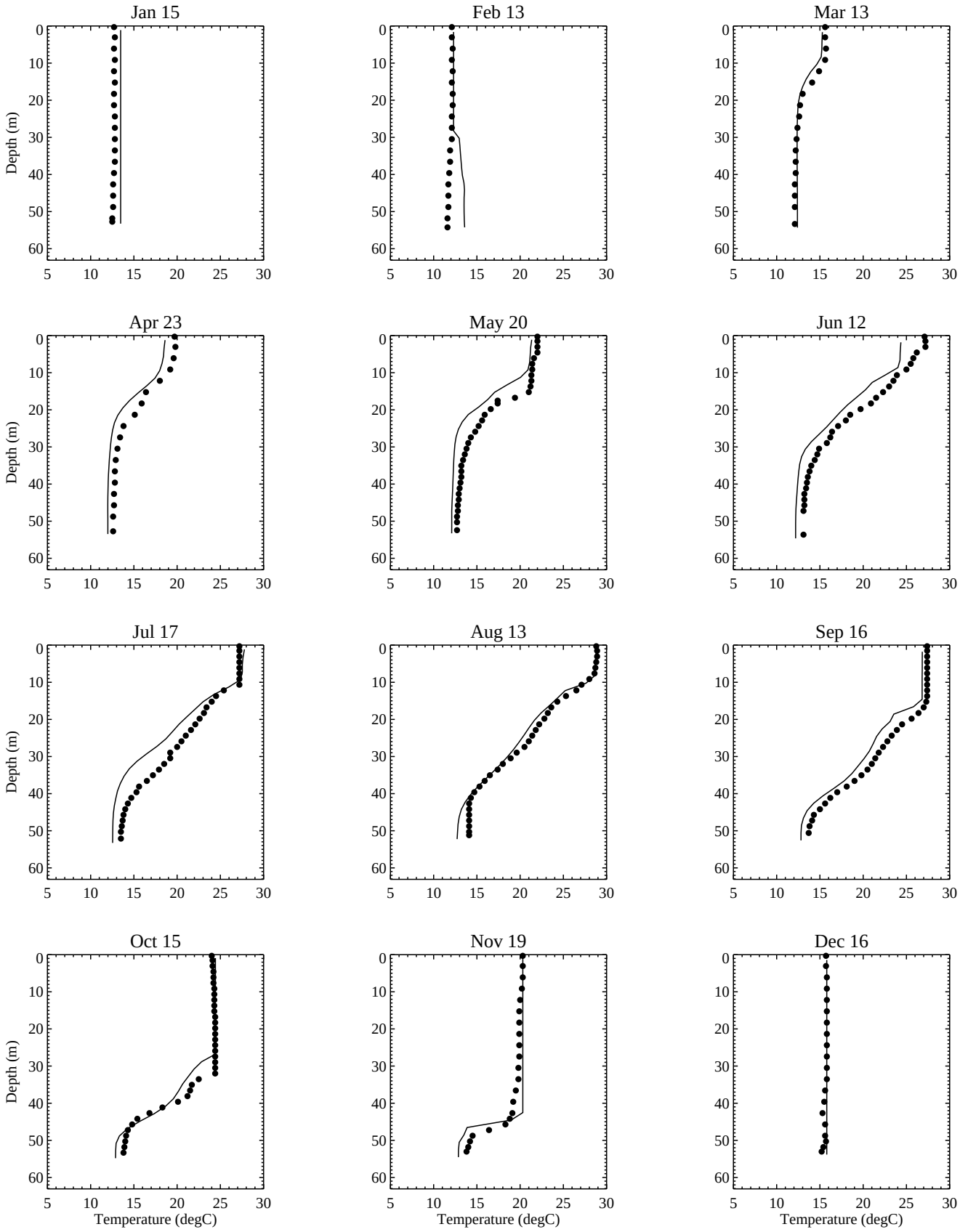

Figure J-1. Vertical profiles of model versus data at Mansfield Dam (Segment 93) - Temperature - 1986.

Profiles shown for dates with available data else model results for first day of month shown.

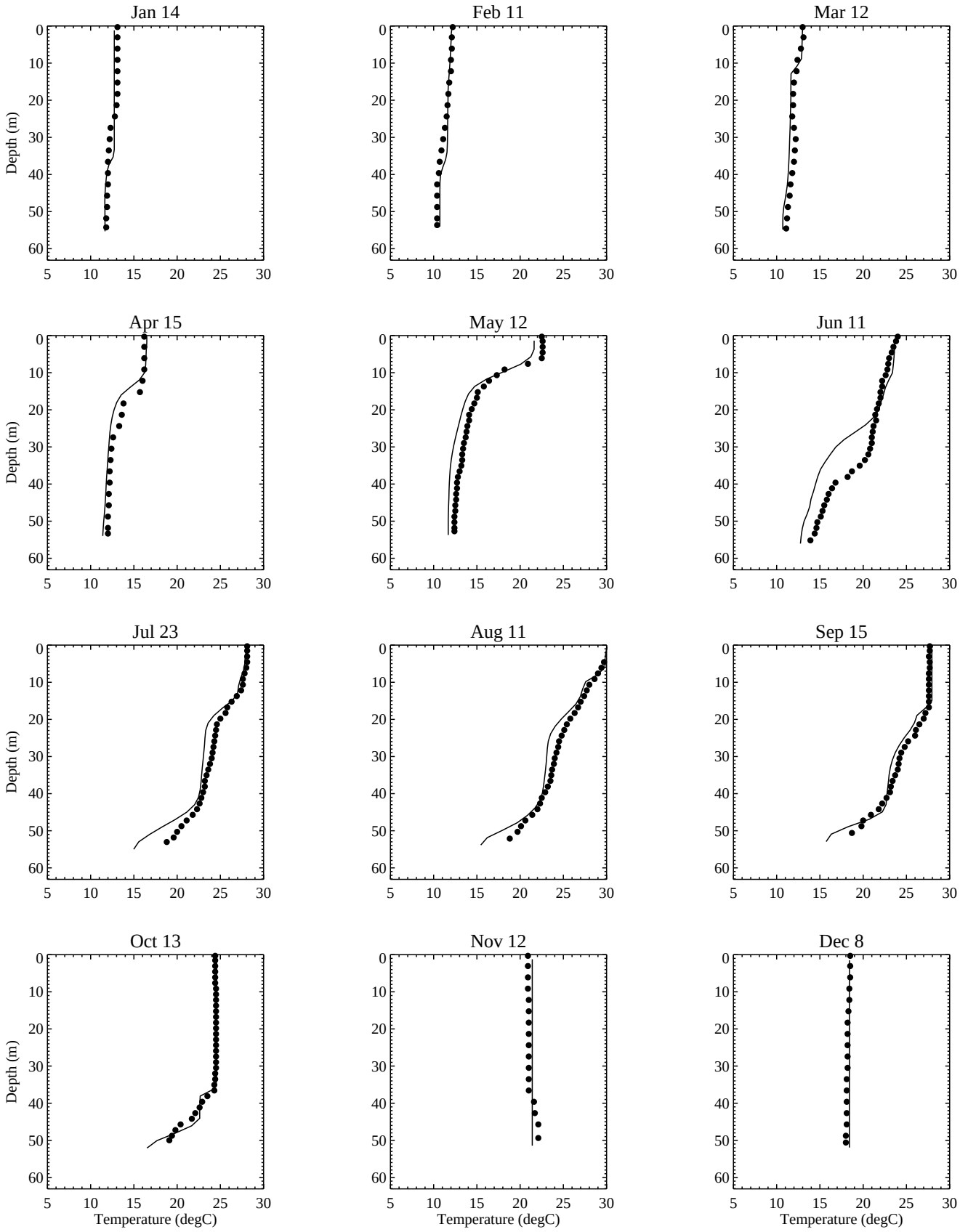

Figure J-1. Vertical profiles of model versus data at Mansfield Dam (Segment 93) - Temperature - 1987.

Profiles shown for dates with available data else model results for first day of month shown.

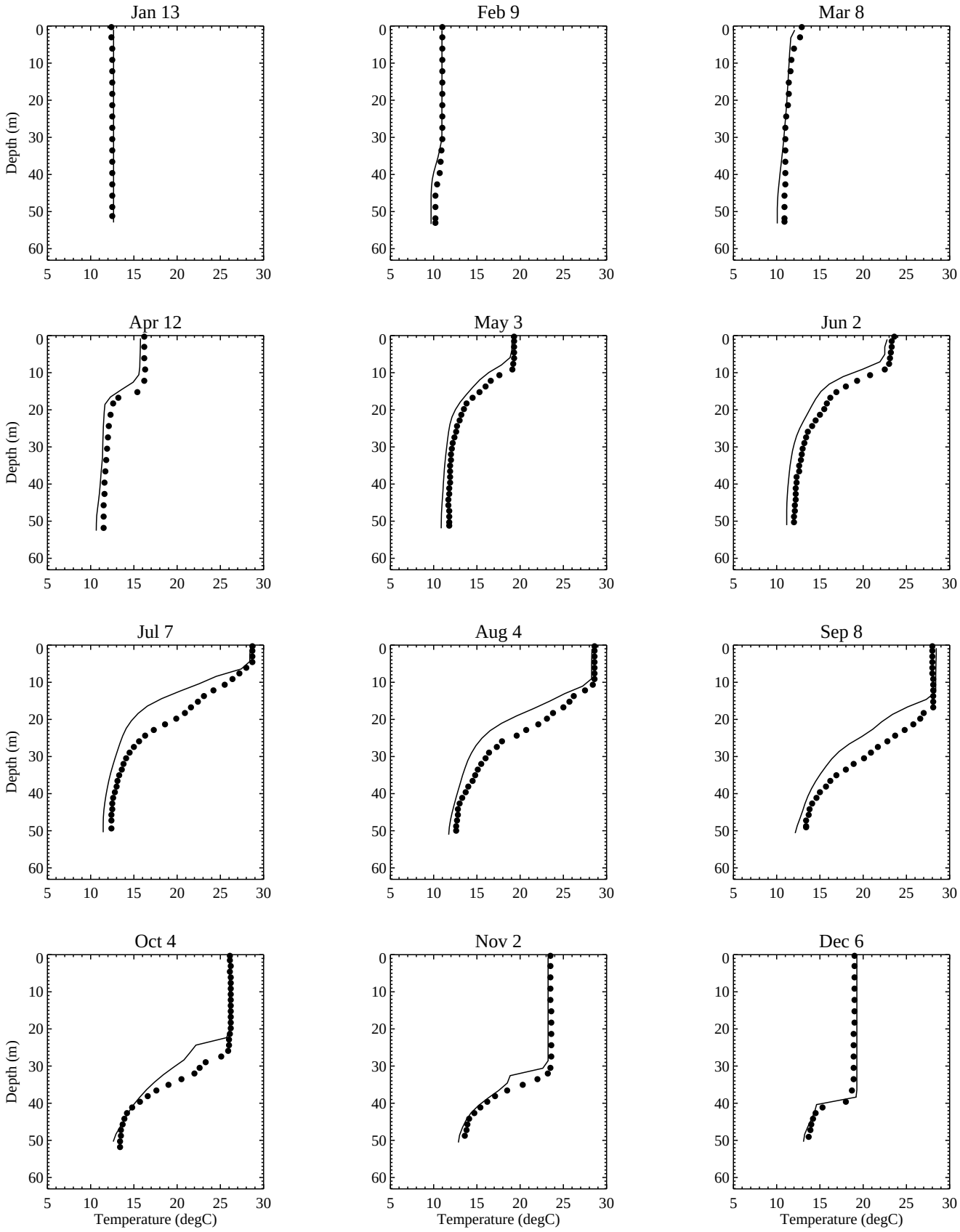

Figure J-1. Vertical profiles of model versus data at Mansfield Dam (Segment 93) - Temperature - 1988.

Profiles shown for dates with available data else model results for first day of month shown.

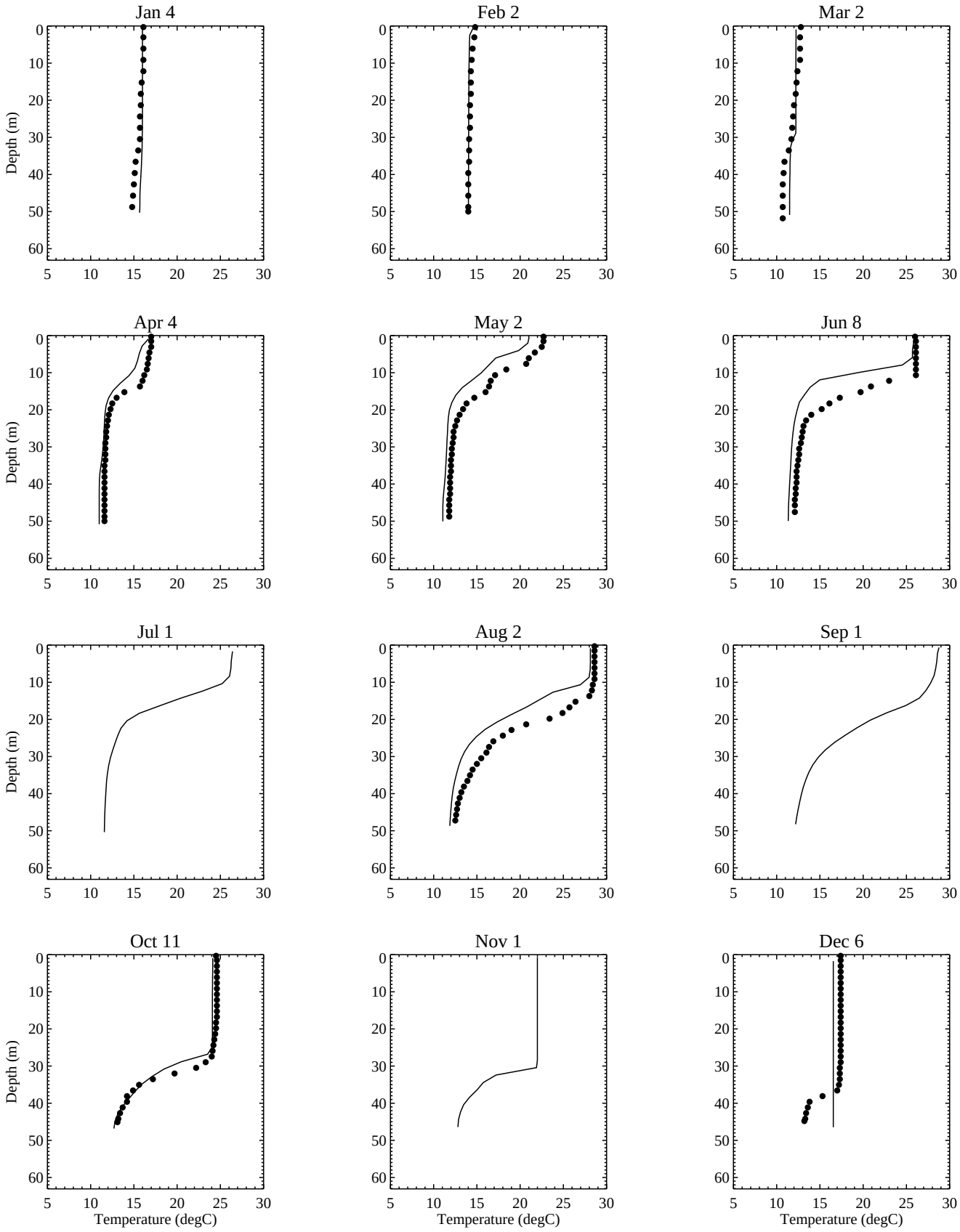

Figure J-1. Vertical profiles of model versus data at Mansfield Dam (Segment 93) - Temperature - 1989.

Profiles shown for dates with available data else model results for first day of month shown.

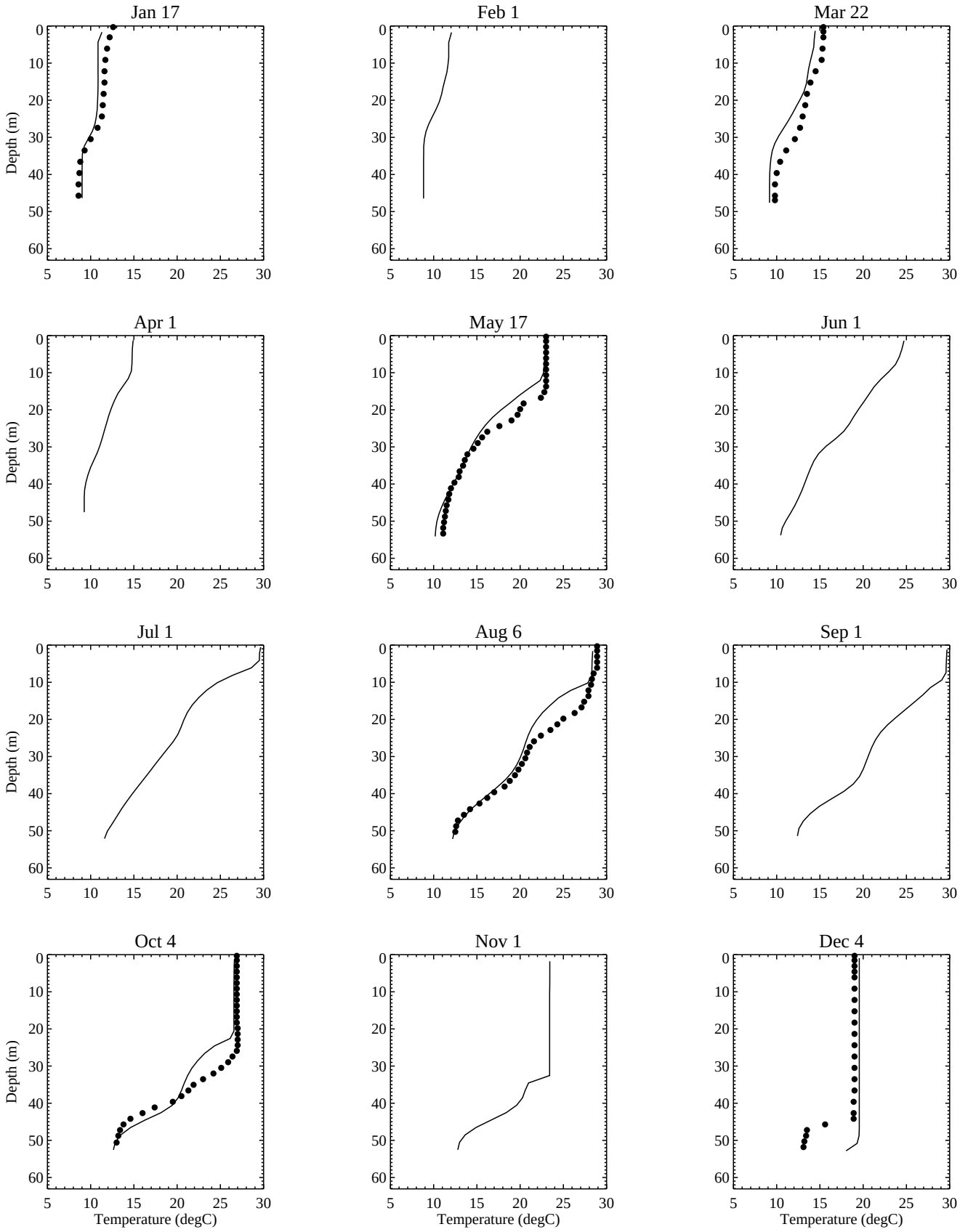

Figure J-1. Vertical profiles of model versus data at Mansfield Dam (Segment 93) - Temperature - 1990.

Profiles shown for dates with available data else model results for first day of month shown.

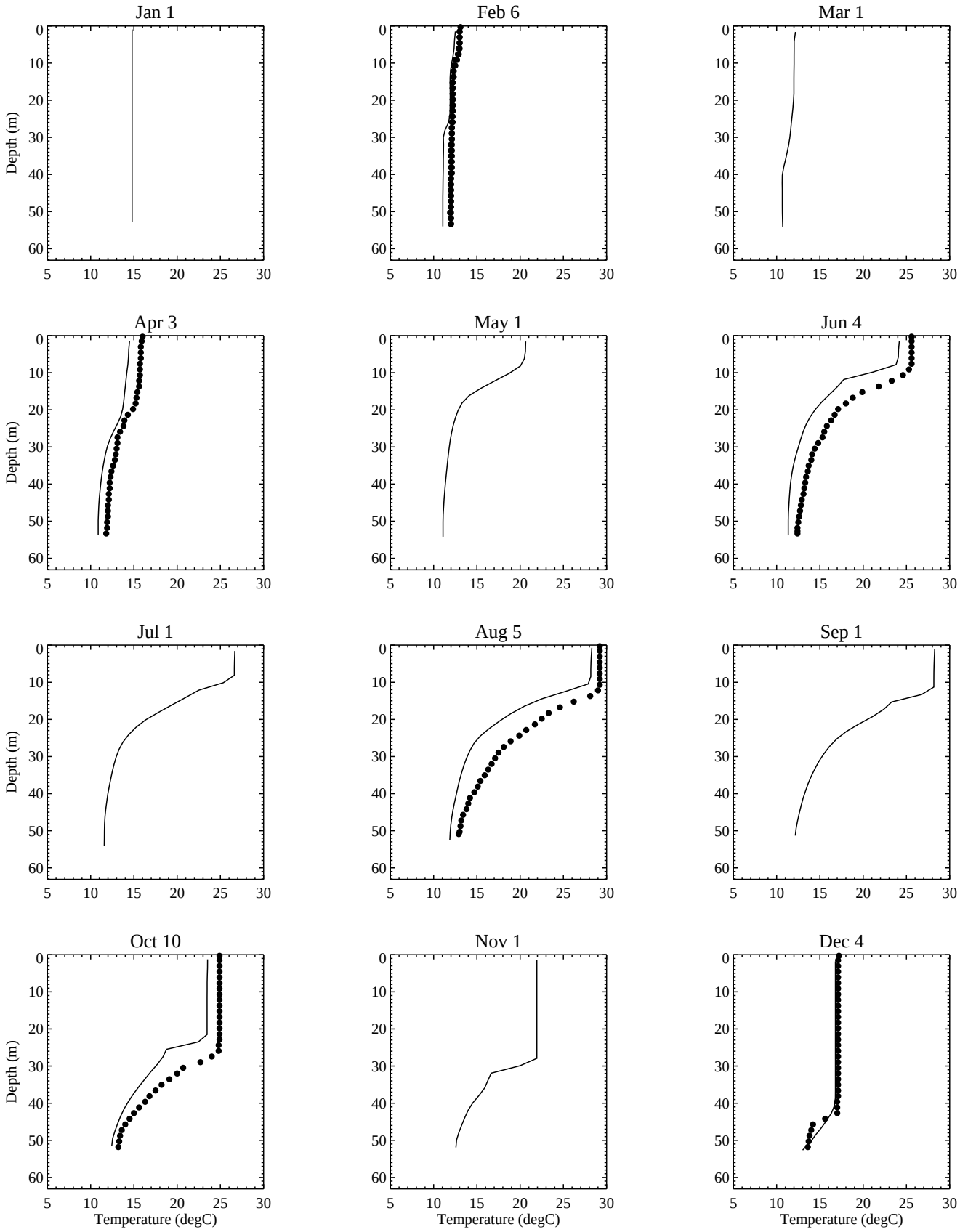

Figure J-1. Vertical profiles of model versus data at Mansfield Dam (Segment 93) - Temperature - 1991.

Profiles shown for dates with available data else model results for first day of month shown.

Model Data

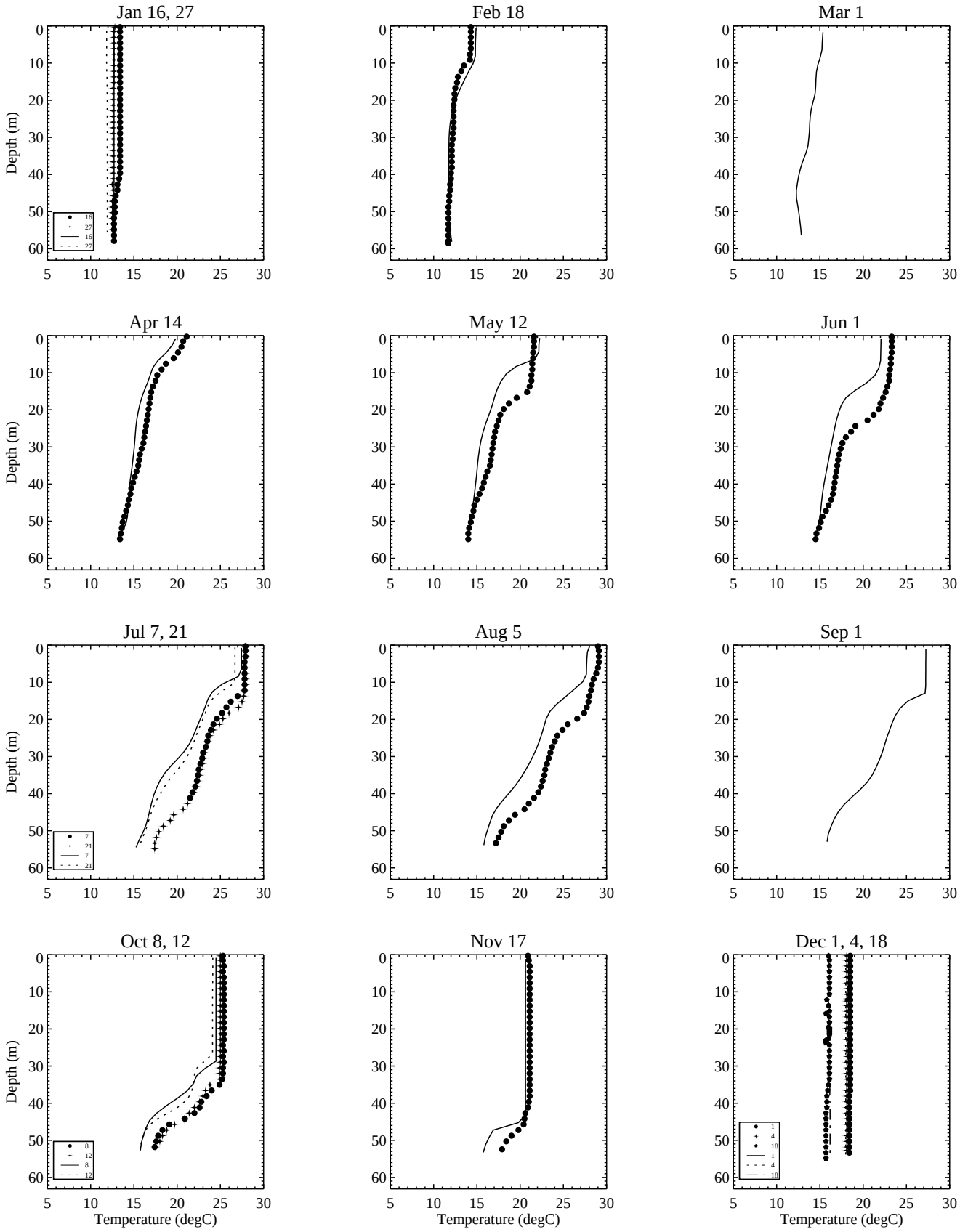

Figure J-1. Vertical profiles of model versus data at Mansfield Dam (Segment 93) - Temperature - 1992.

Profiles shown for dates with available data else model results for first day of month shown.

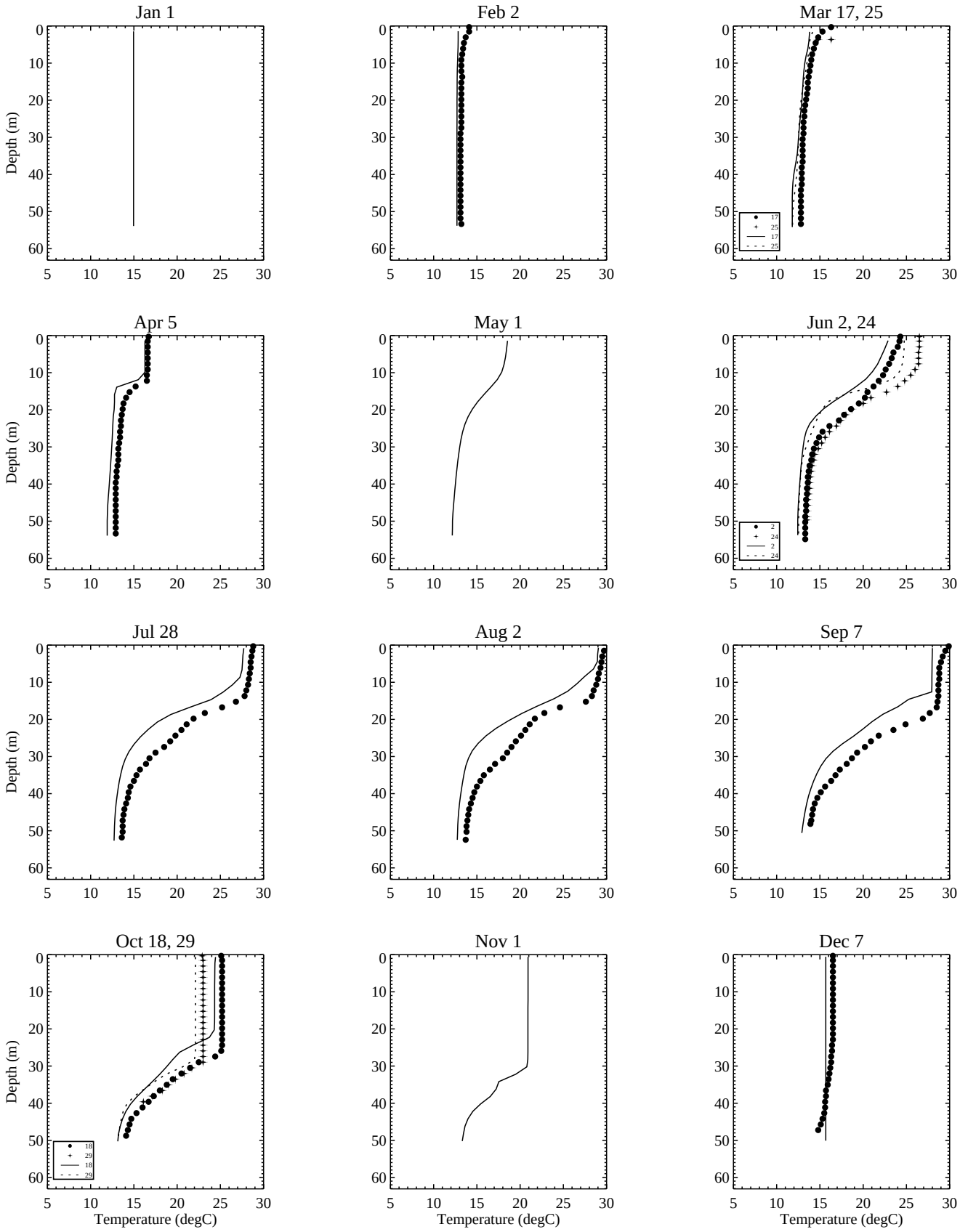

Figure J-1. Vertical profiles of model versus data at Mansfield Dam (Segment 93) - Temperature - 1993.

Profiles shown for dates with available data else model results for first day of month shown.

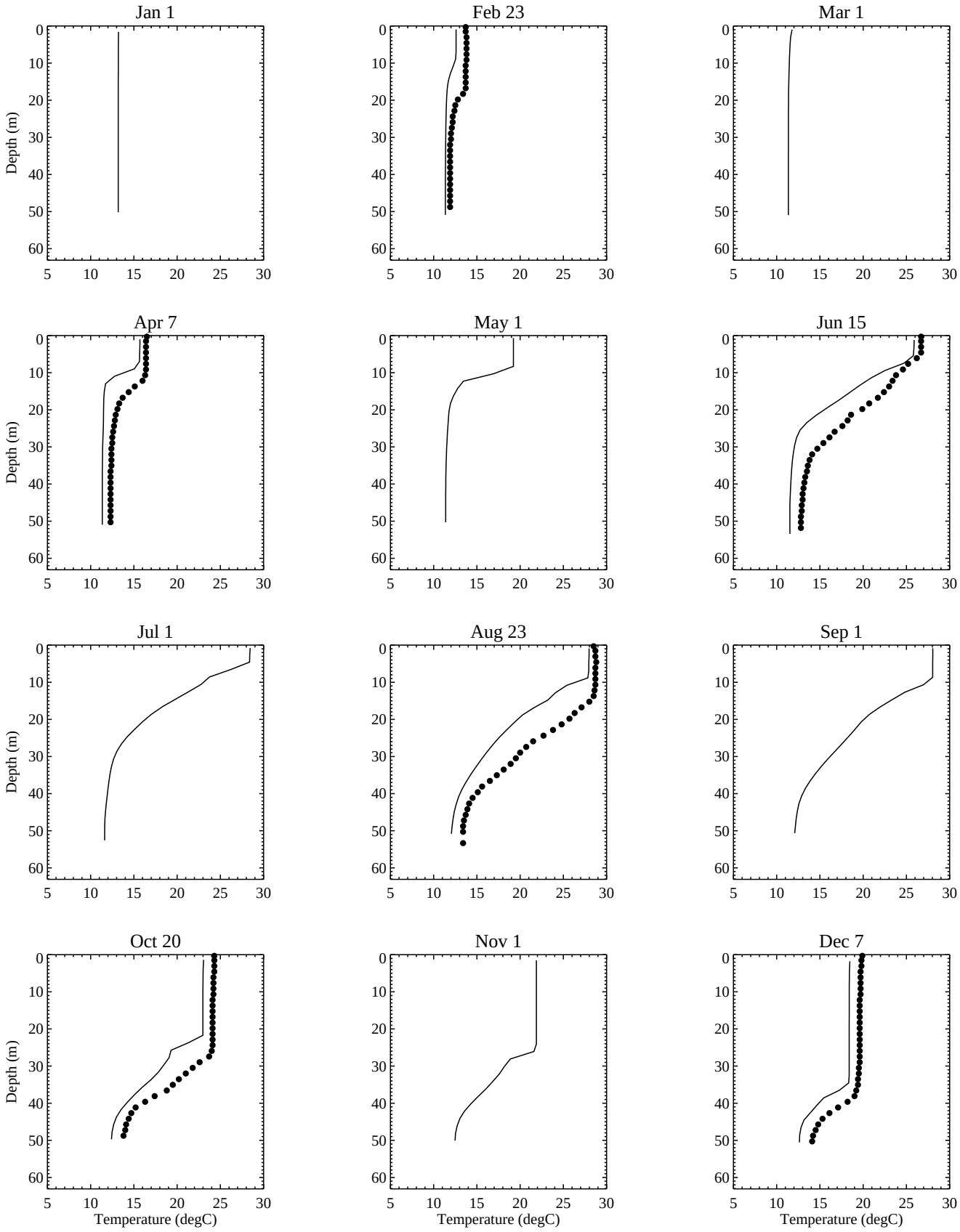

Figure J-1. Vertical profiles of model versus data at Mansfield Dam (Segment 93) - Temperature - 1994.

Profiles shown for dates with available data else model results for first day of month shown.

Model Data

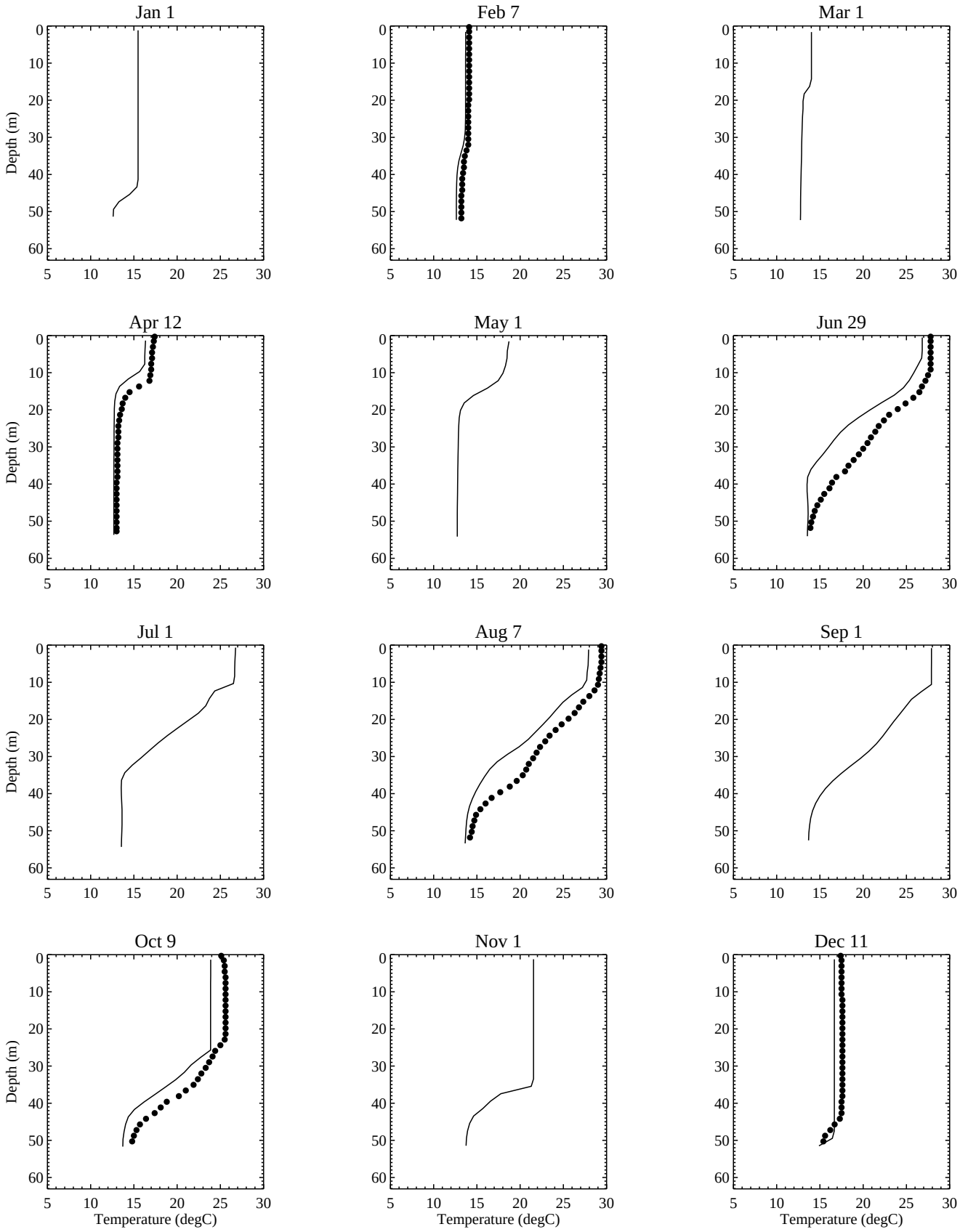

Figure J-1. Vertical profiles of model versus data at Mansfield Dam (Segment 93) - Temperature - 1995.

Profiles shown for dates with available data else model results for first day of month shown.

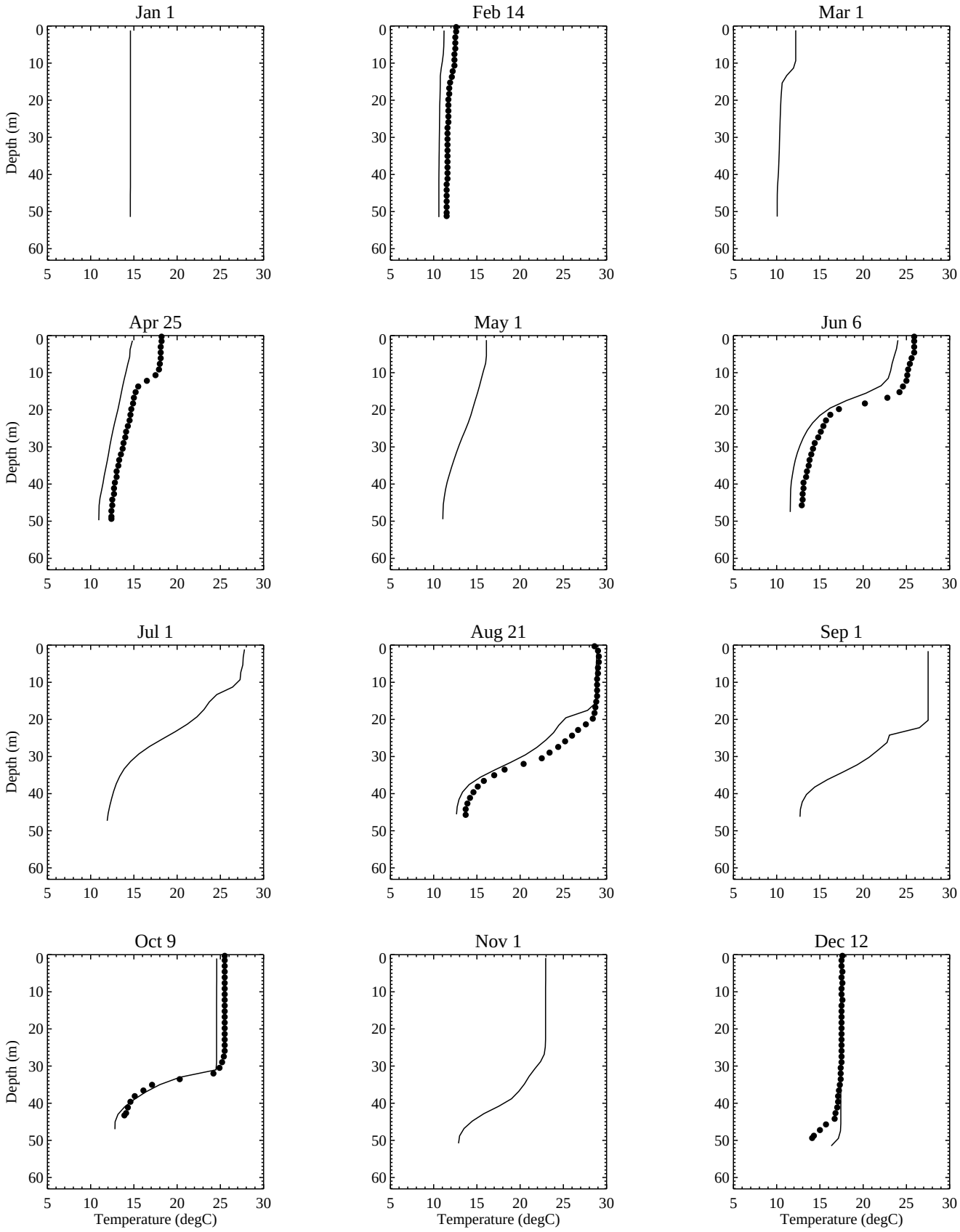

Figure J-1. Vertical profiles of model versus data at Mansfield Dam (Segment 93) - Temperature - 1996.

Profiles shown for dates with available data else model results for first day of month shown.

Model Data

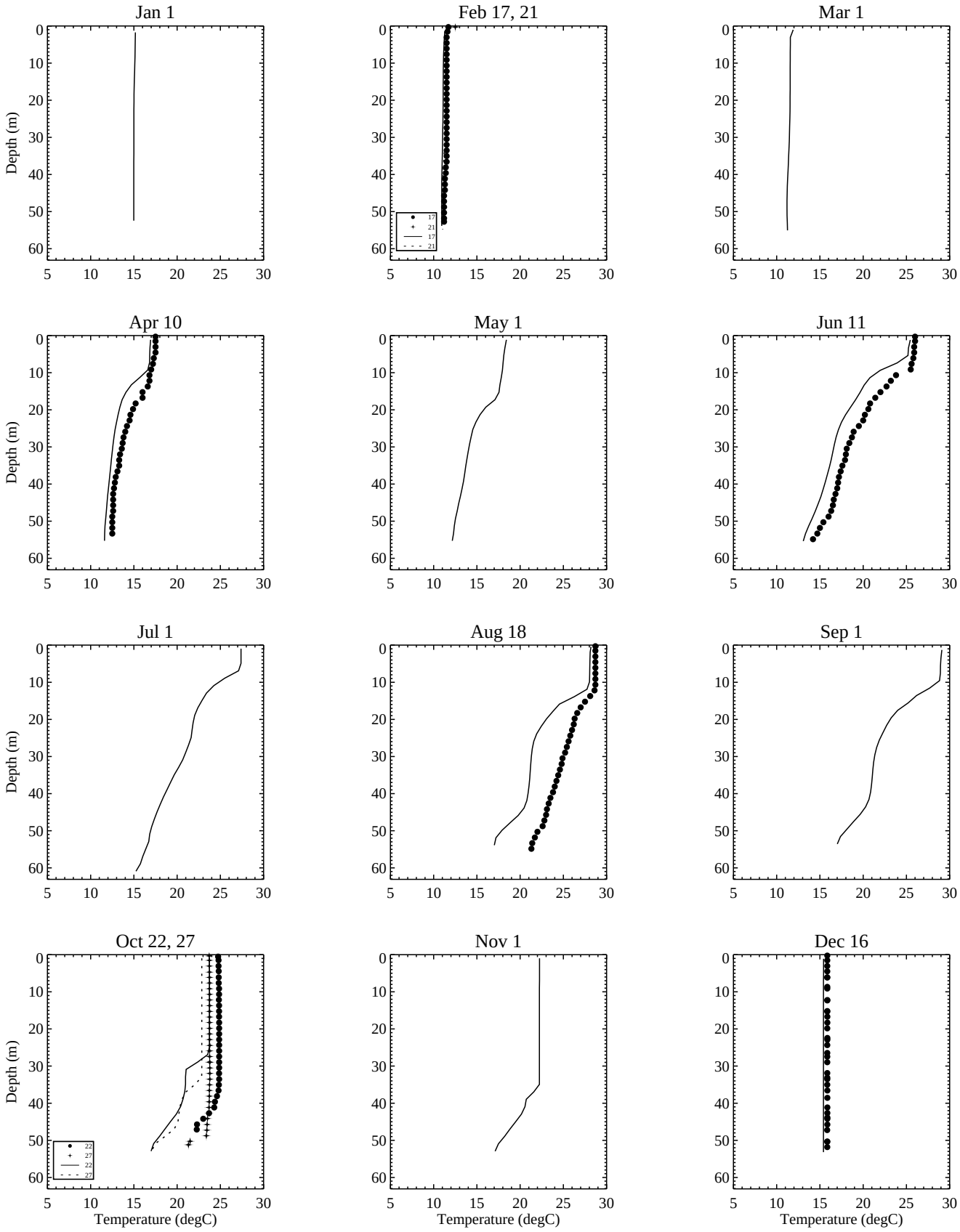

Figure J-1. Vertical profiles of model versus data at Mansfield Dam (Segment 93) - Temperature - 1997.

Profiles shown for dates with available data else model results for first day of month shown.

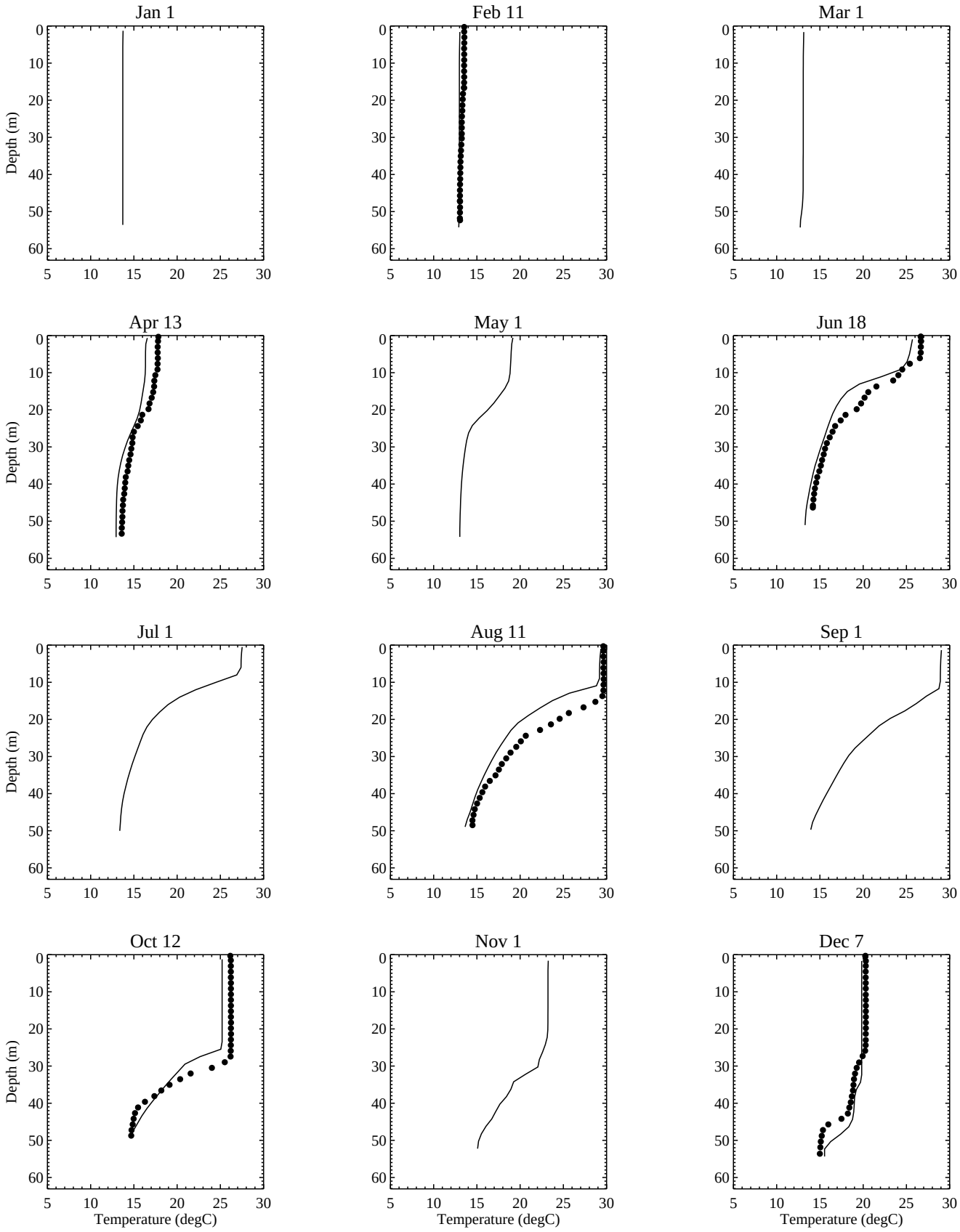

Figure J-1. Vertical profiles of model versus data at Mansfield Dam (Segment 93) - Temperature - 1998.

Profiles shown for dates with available data else model results for first day of month shown.

Model Data

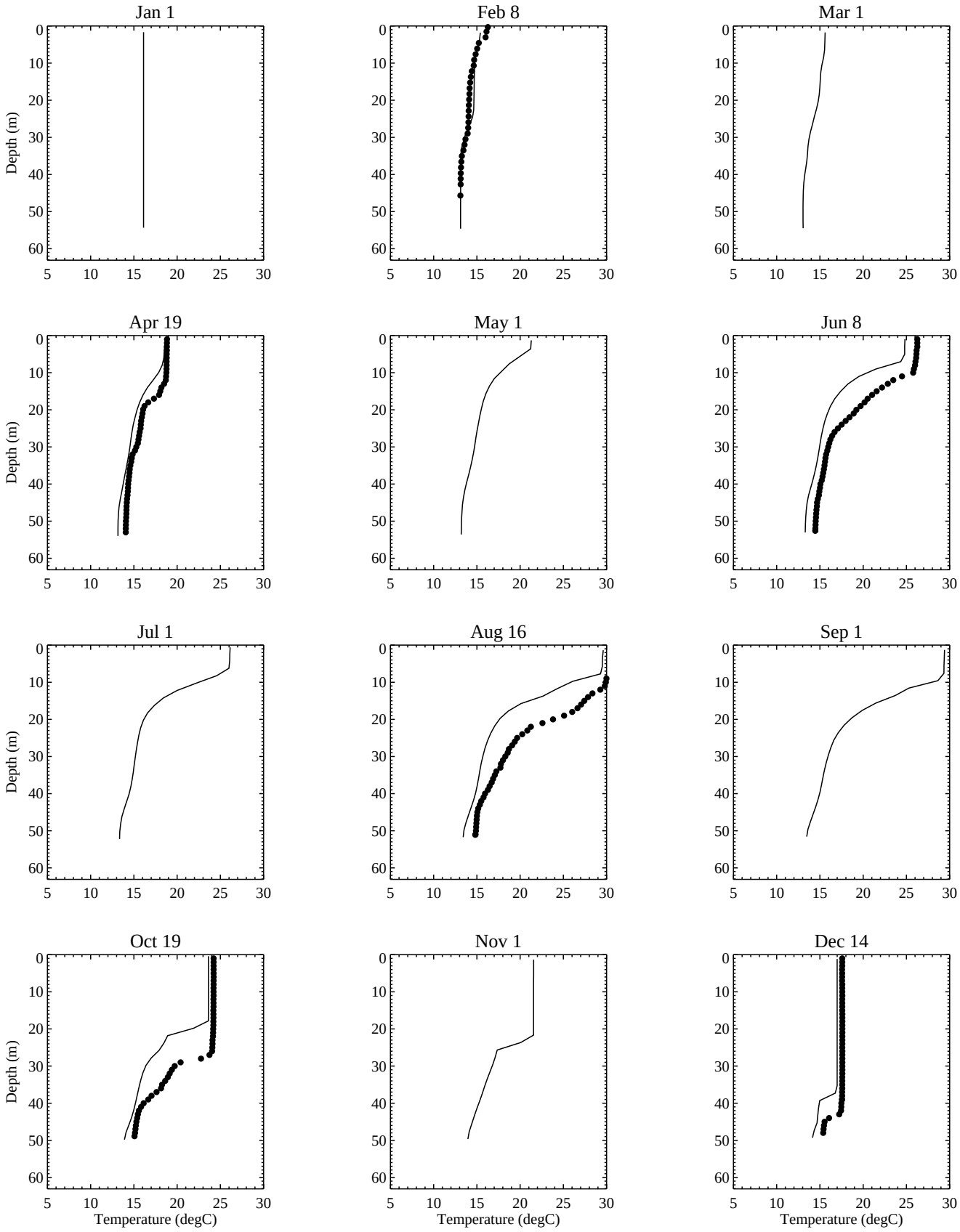

Figure J-1. Vertical profiles of model versus data at Mansfield Dam (Segment 93) - Temperature - 1999.

Profiles shown for dates with available data else model results for first day of month shown.

Model Data

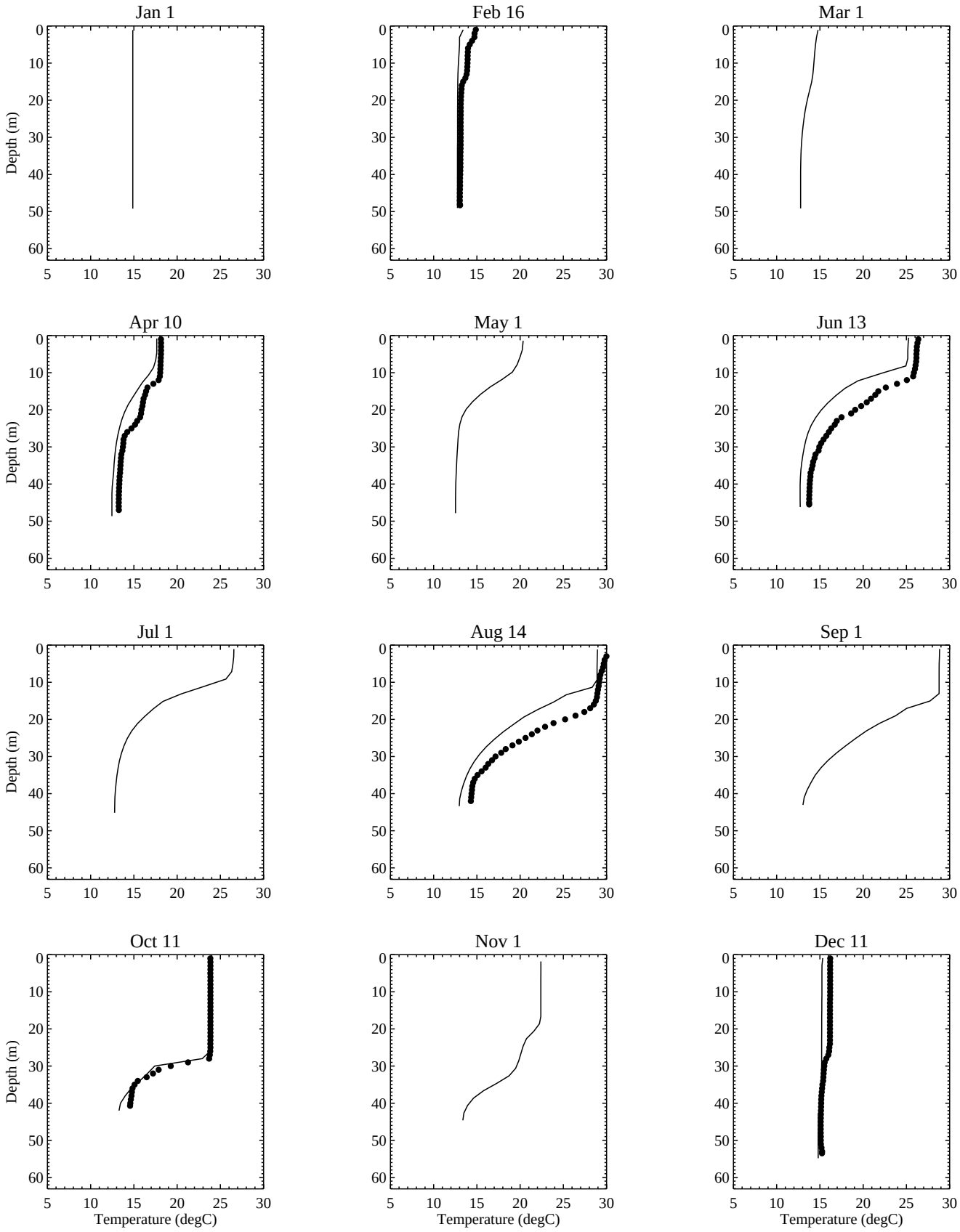

Figure J-1. Vertical profiles of model versus data at Mansfield Dam (Segment 93) - Temperature - 2000.

Profiles shown for dates with available data else model results for first day of month shown.

Model ● Data

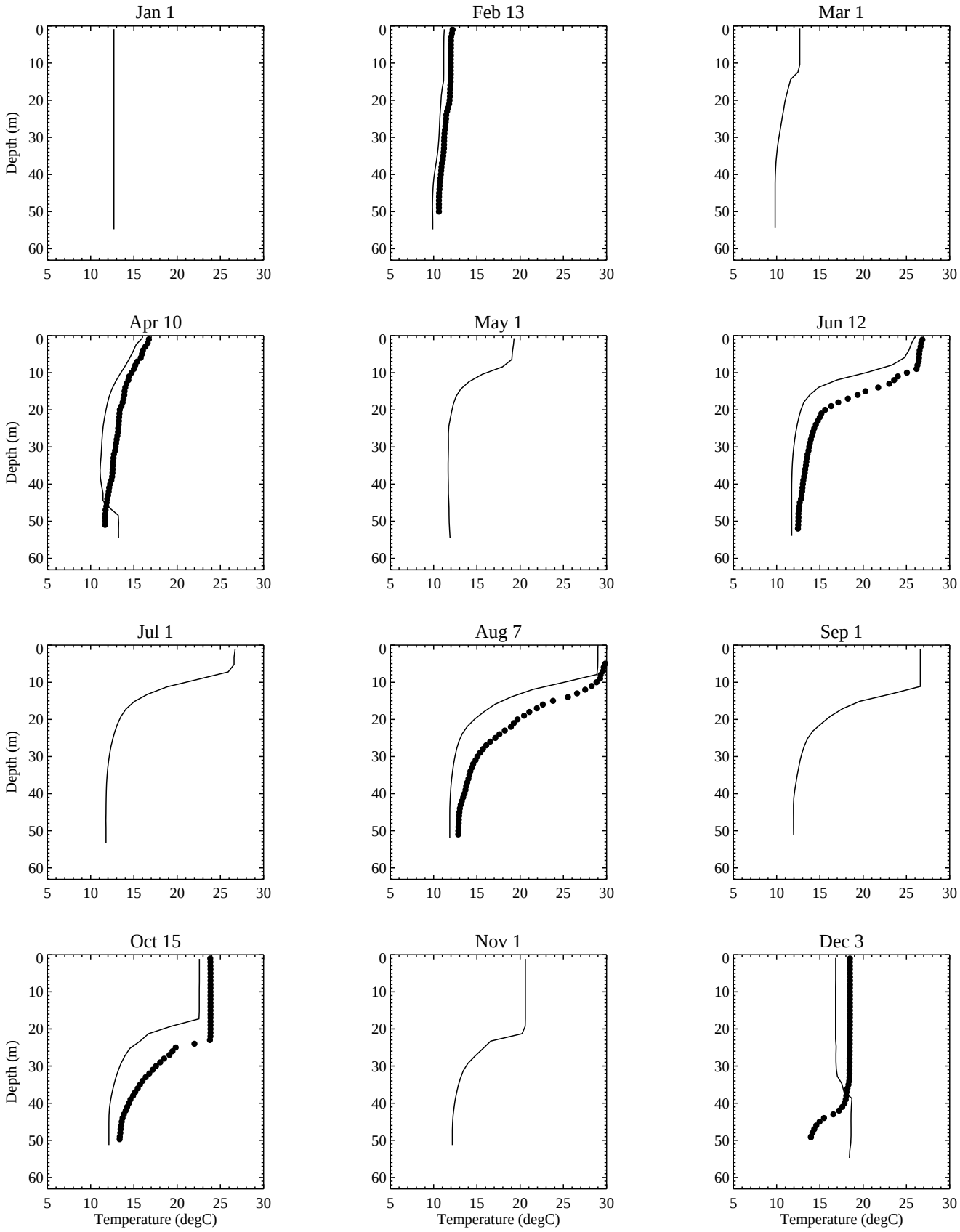

Figure J-1. Vertical profiles of model versus data at Mansfield Dam (Segment 93) - Temperature - 2001.

Profiles shown for dates with available data else model results for first day of month shown.

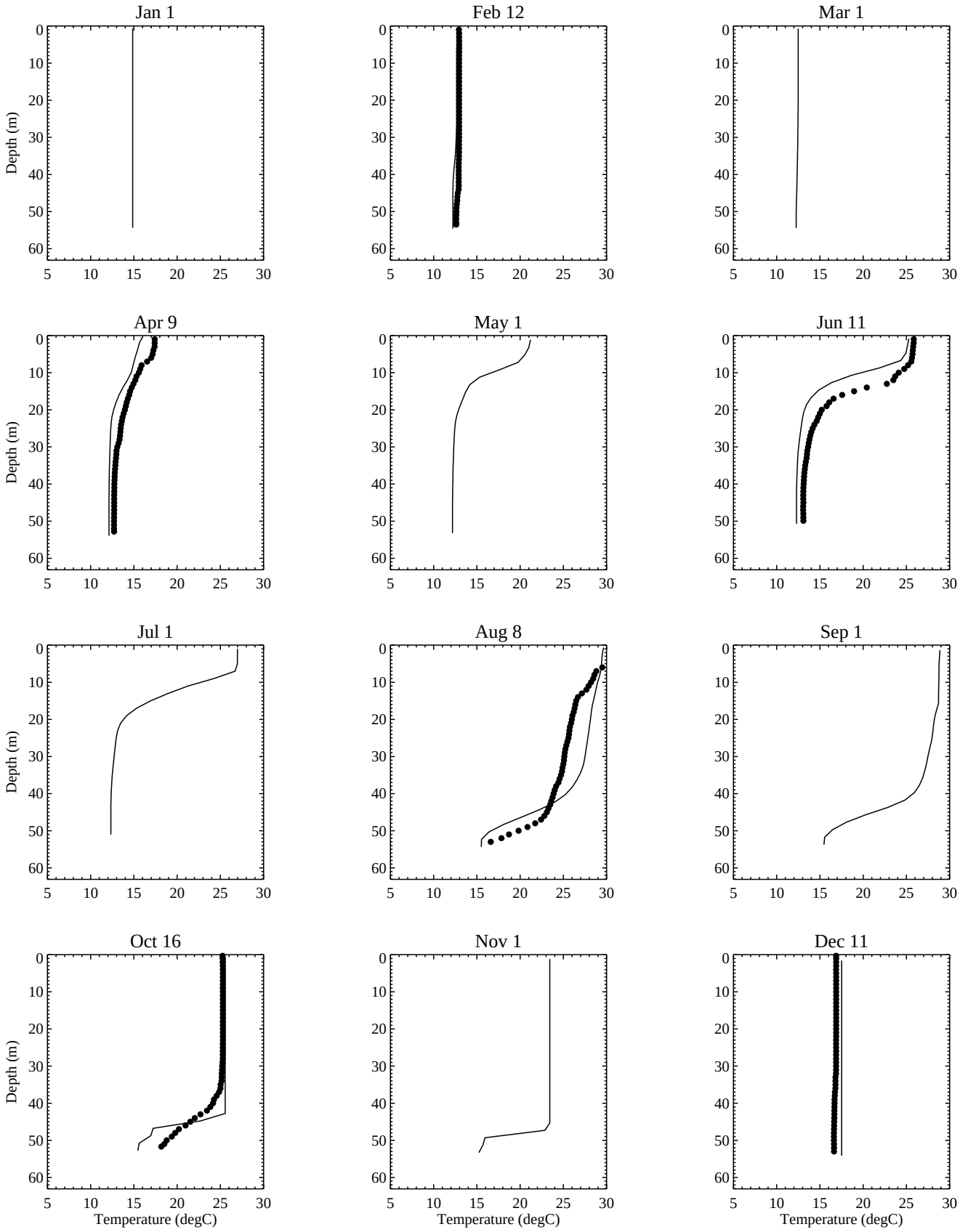

Figure J-1. Vertical profiles of model versus data at Mansfield Dam (Segment 93) - Temperature - 2002.

Profiles shown for dates with available data else model results for first day of month shown.

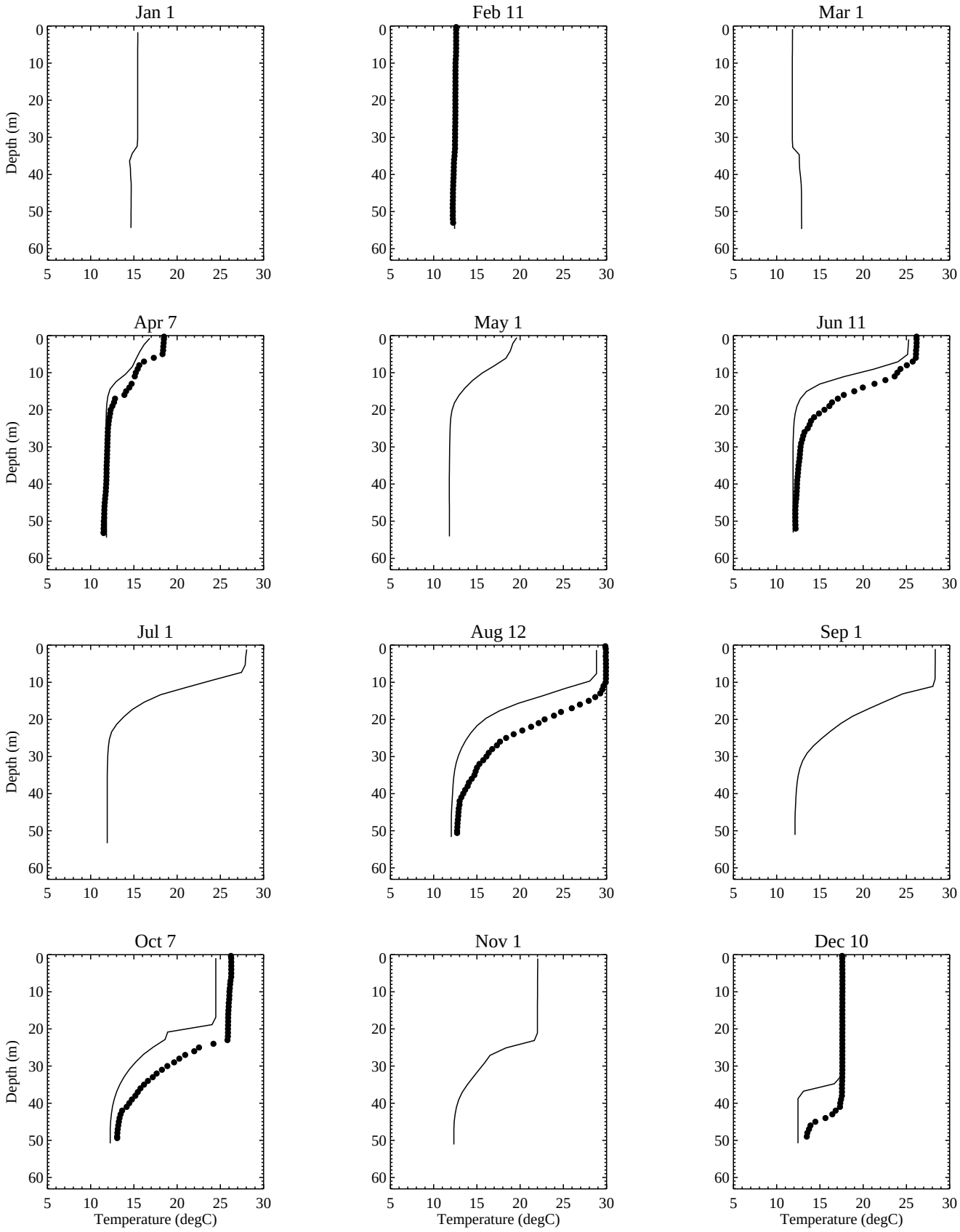

Figure J-1. Vertical profiles of model versus data at Mansfield Dam (Segment 93) - Temperature - 2003.

Profiles shown for dates with available data else model results for first day of month shown.

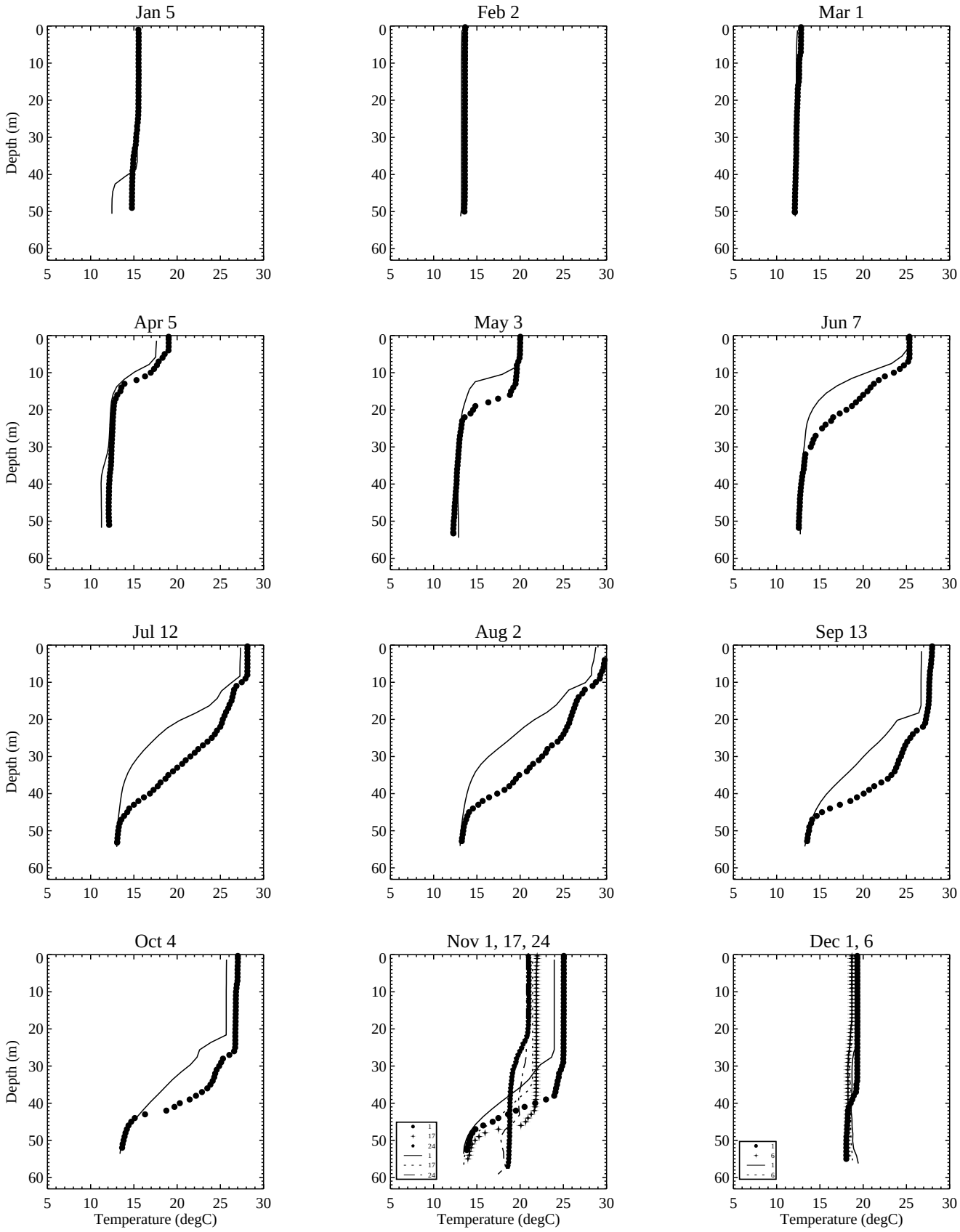

Figure J-1. Vertical profiles of model versus data at Mansfield Dam (Segment 93) - Temperature - 2004.

Profiles shown for dates with available data else model results for first day of month shown.

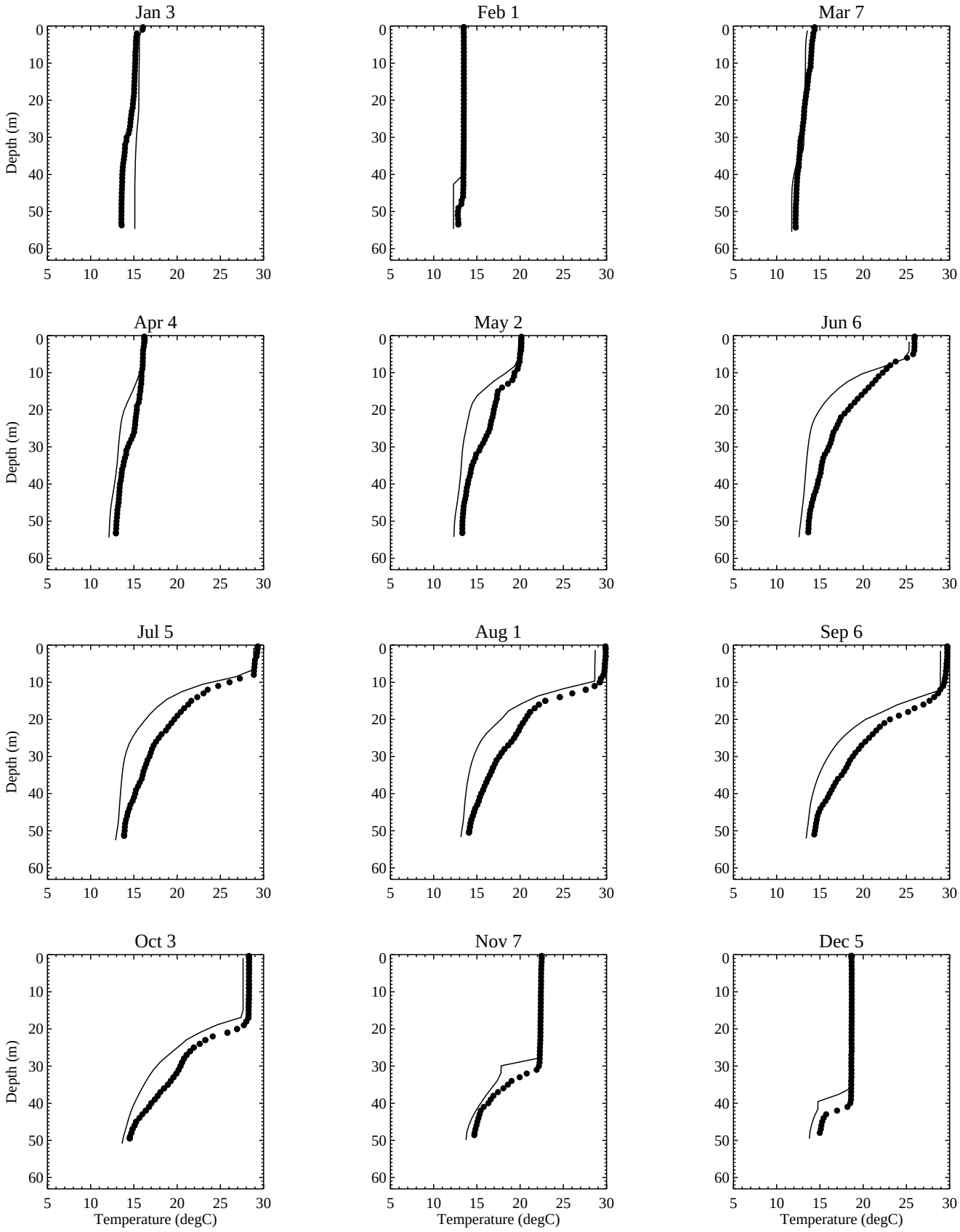

Figure J-1. Vertical profiles of model versus data at Mansfield Dam (Segment 93) - Temperature - 2005.

Profiles shown for dates with available data else model results for first day of month shown.

Model Data

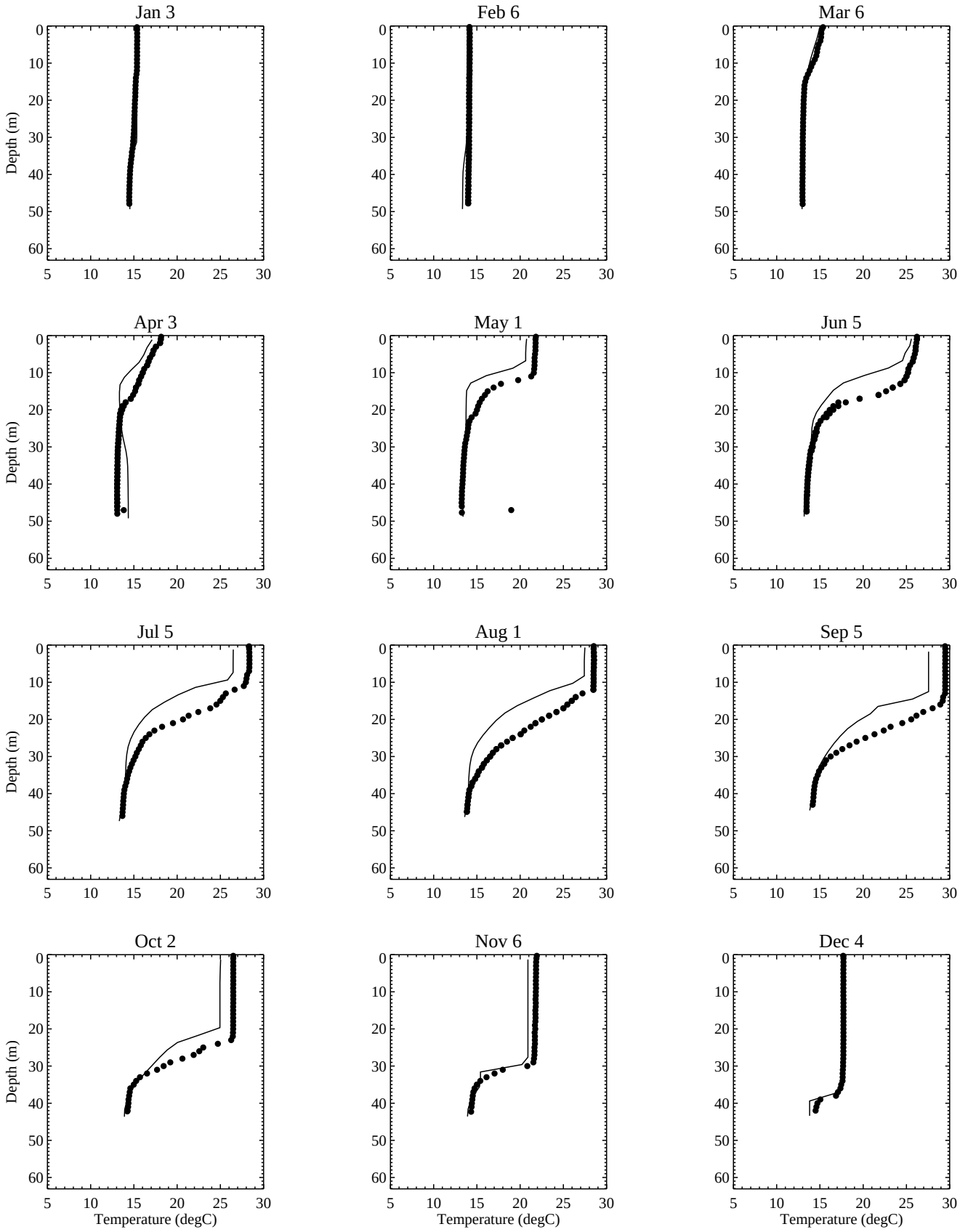

Figure J-1. Vertical profiles of model versus data at Mansfield Dam (Segment 93) - Temperature - 2006.

Profiles shown for dates with available data else model results for first day of month shown.

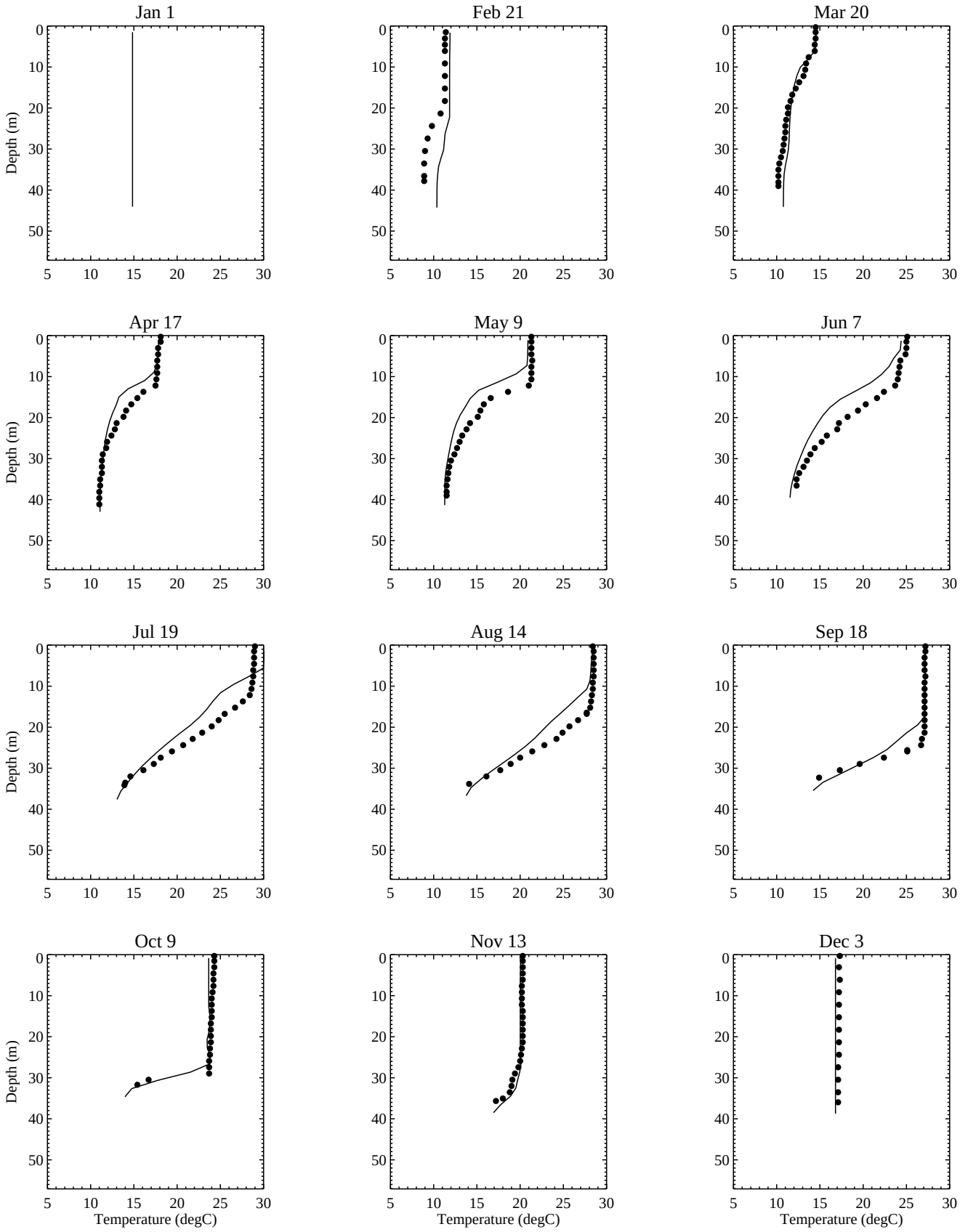

Figure J-2. Vertical profiles of model versus data at Arkansas Bend (Segment 78) - Temperature - 1984.

Profiles shown for dates with available data else model results for first day of month shown.

Model Data

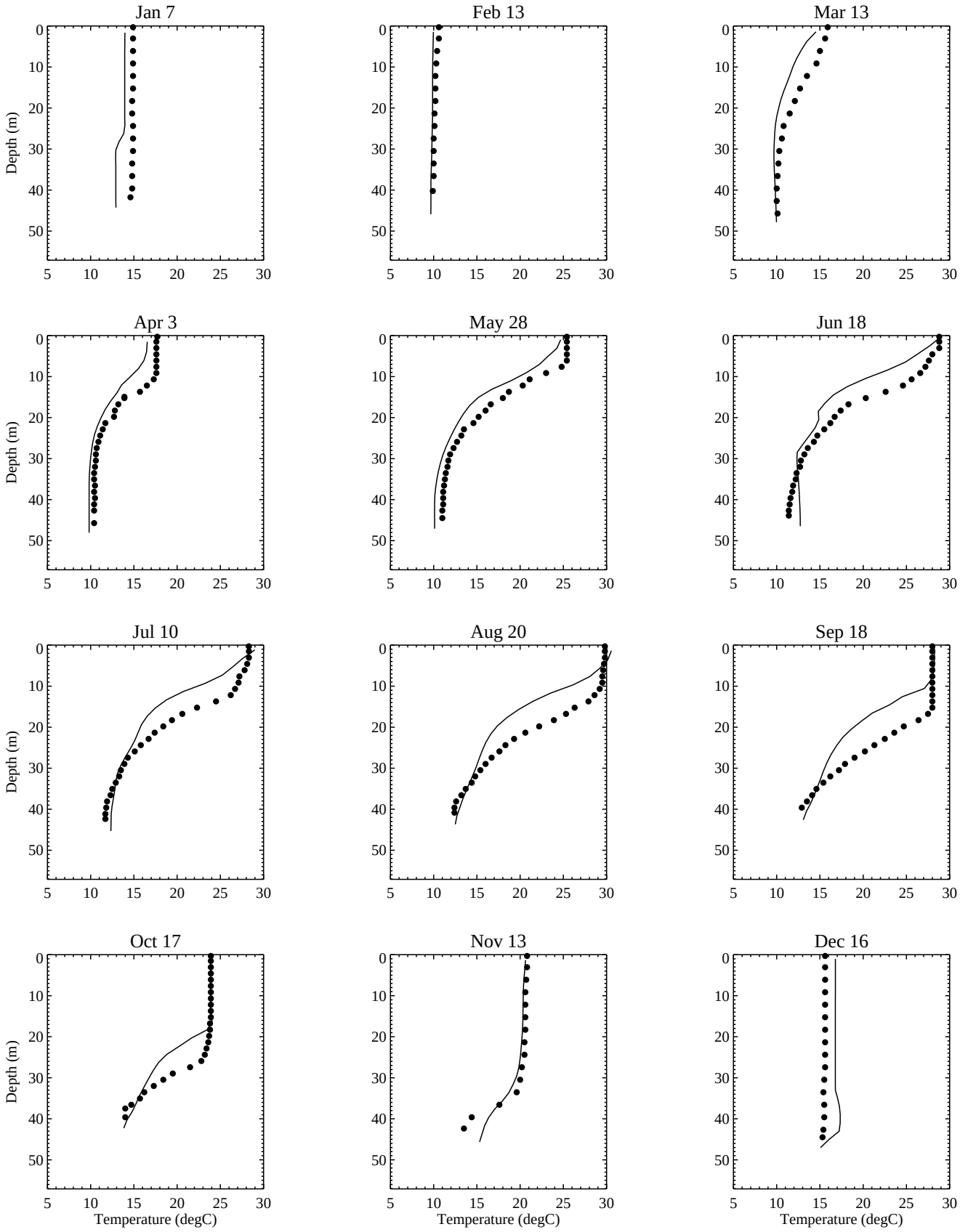

Figure J-2. Vertical profiles of model versus data at Arkansas Bend (Segment 78) - Temperature - 1985.

Profiles shown for dates with available data else model results for first day of month shown.

Model Data

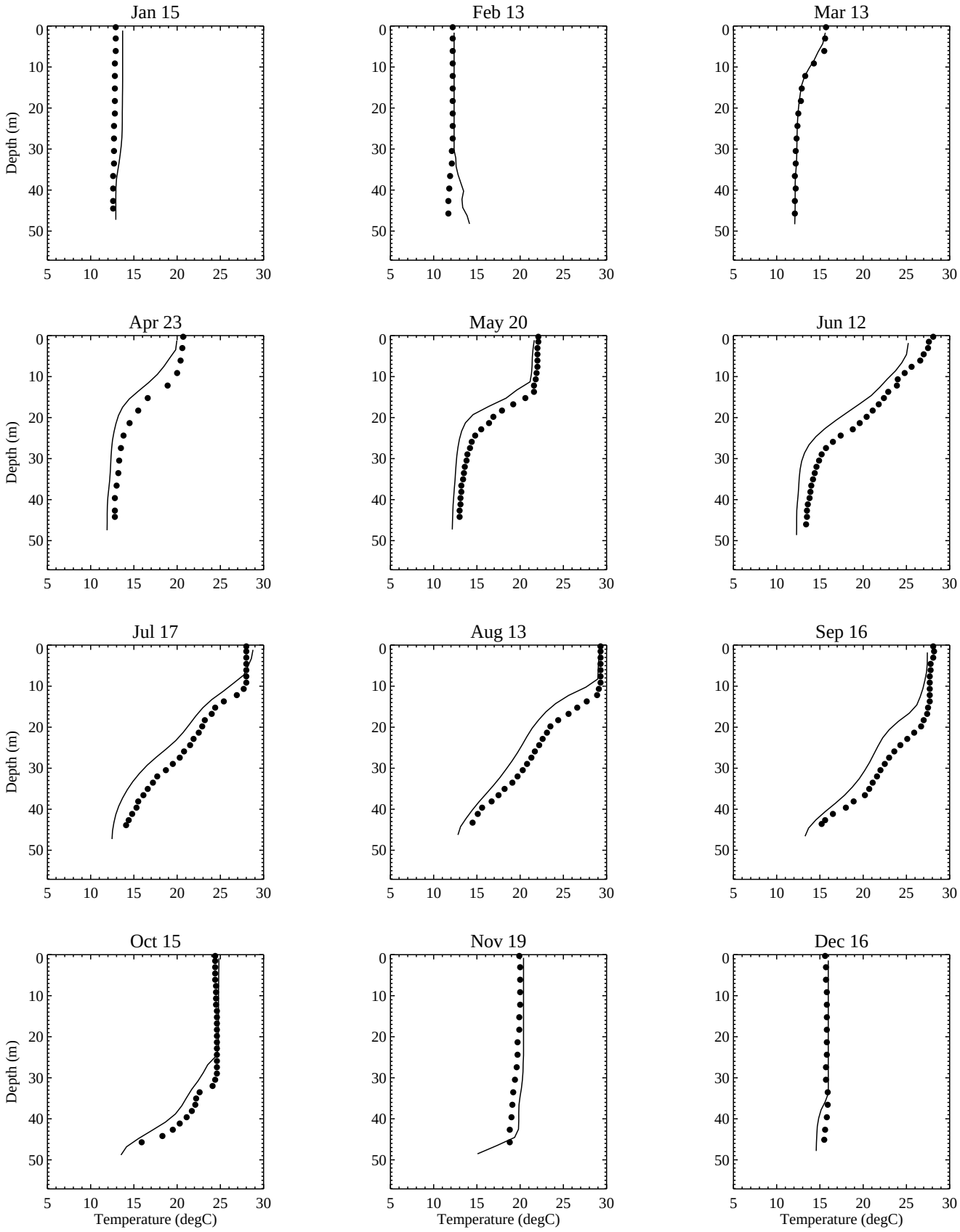

Figure J-2. Vertical profiles of model versus data at Arkansas Bend (Segment 78) - Temperature - 1986.

Profiles shown for dates with available data else model results for first day of month shown.

Model Data

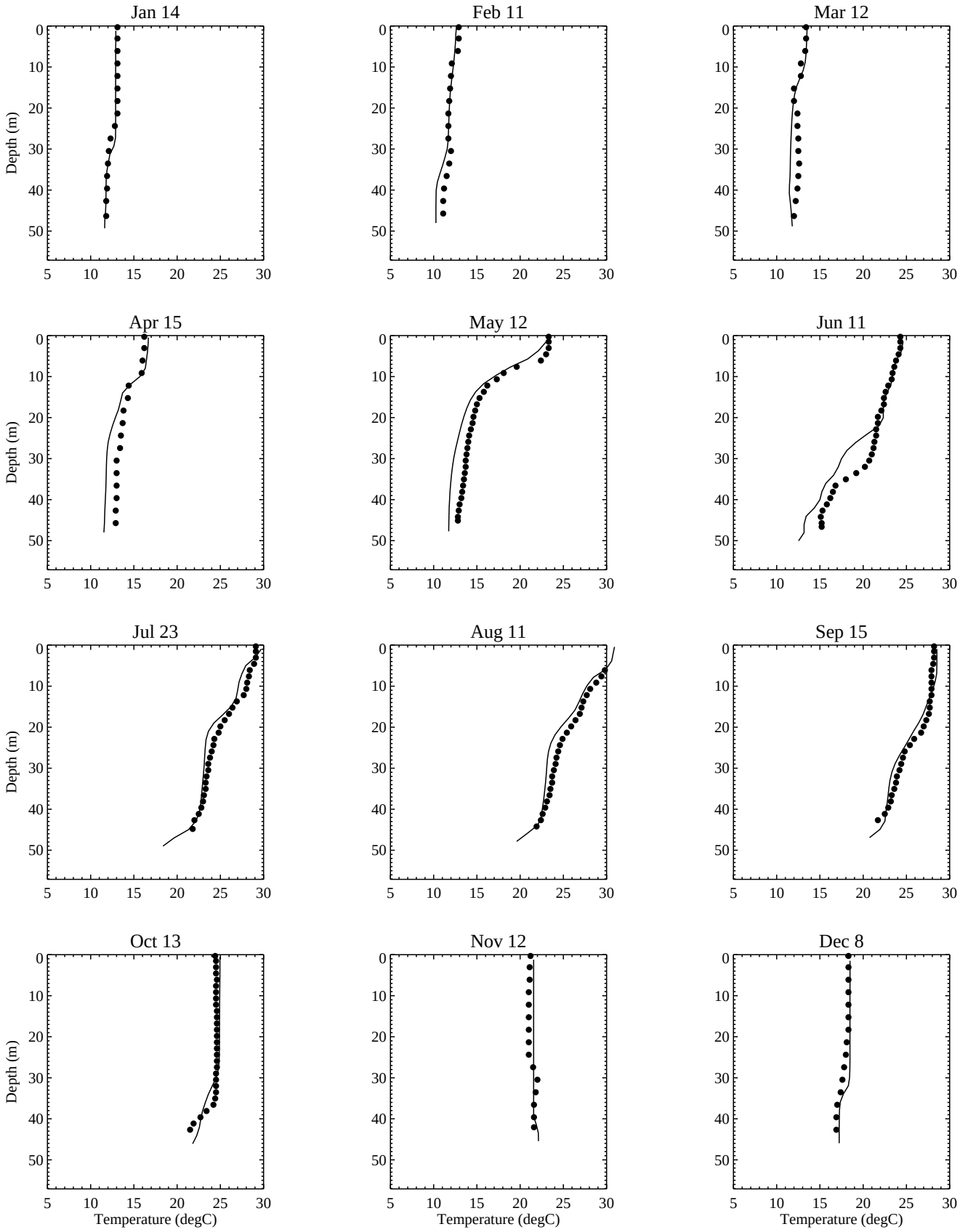

Figure J-2. Vertical profiles of model versus data at Arkansas Bend (Segment 78) - Temperature - 1987.

Profiles shown for dates with available data else model results for first day of month shown.

Model Data

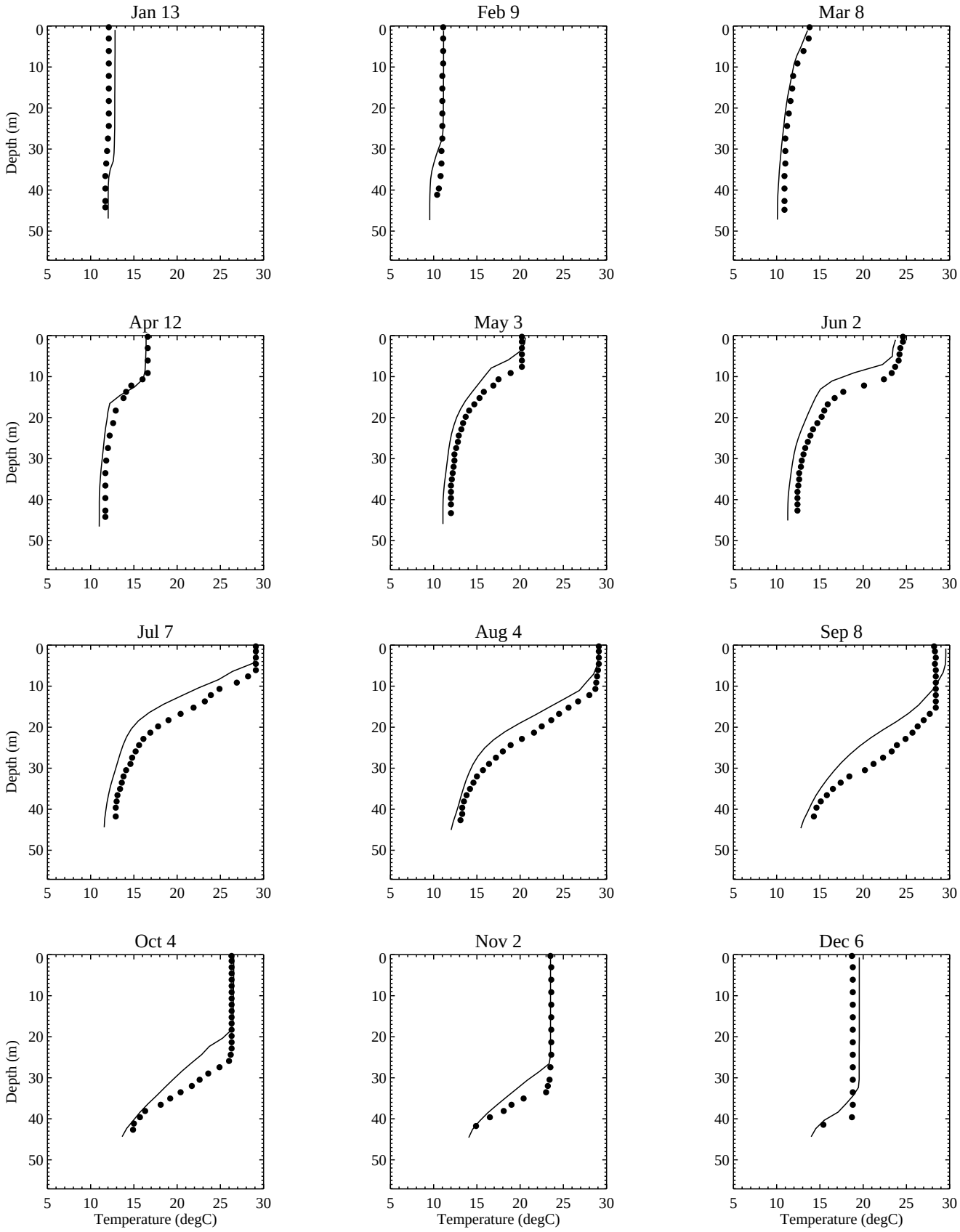

Figure J-2. Vertical profiles of model versus data at Arkansas Bend (Segment 78) - Temperature - 1988.

Profiles shown for dates with available data else model results for first day of month shown.

Model Data

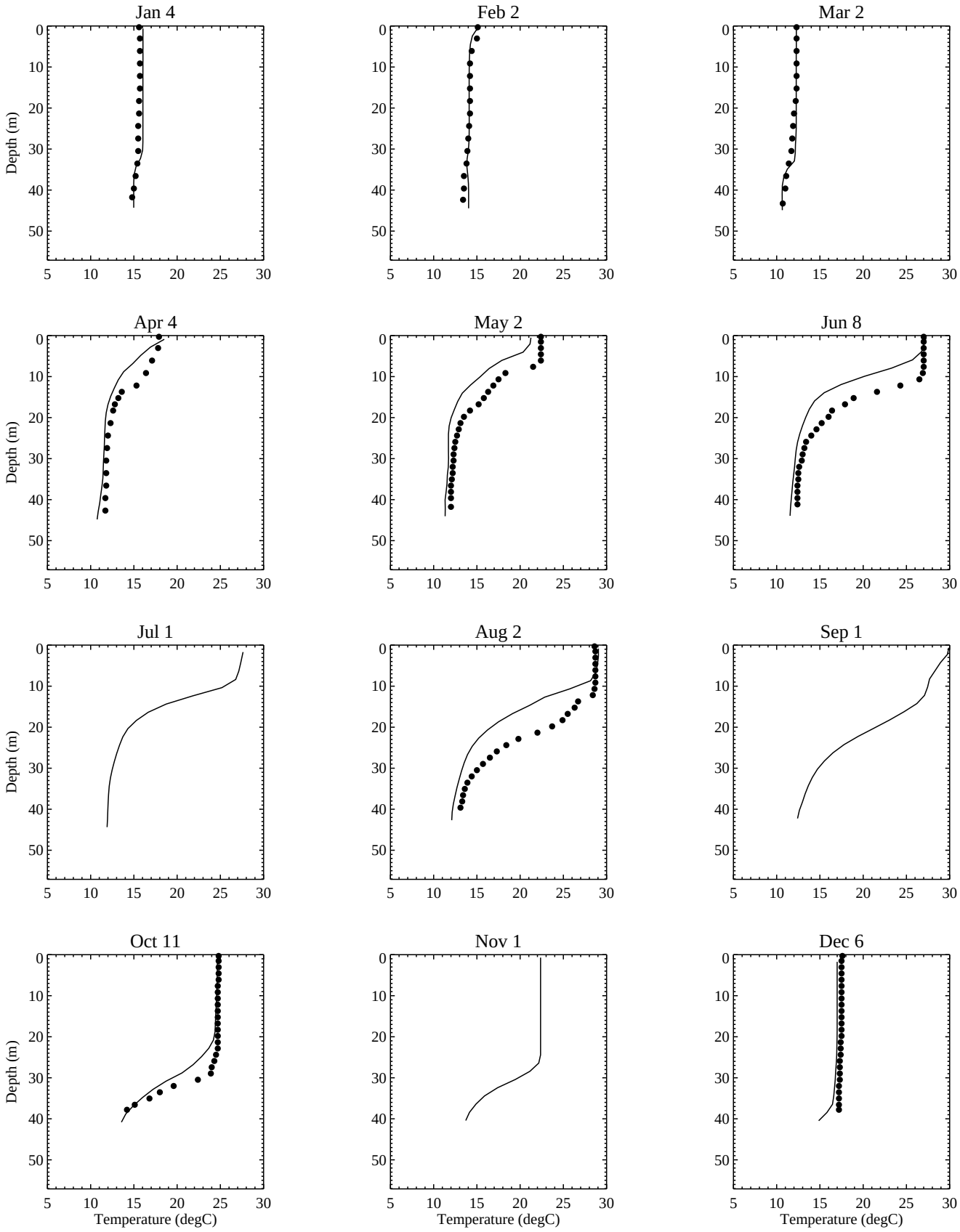

Figure J-2. Vertical profiles of model versus data at Arkansas Bend (Segment 78) - Temperature - 1989.

Profiles shown for dates with available data else model results for first day of month shown.

Model Data

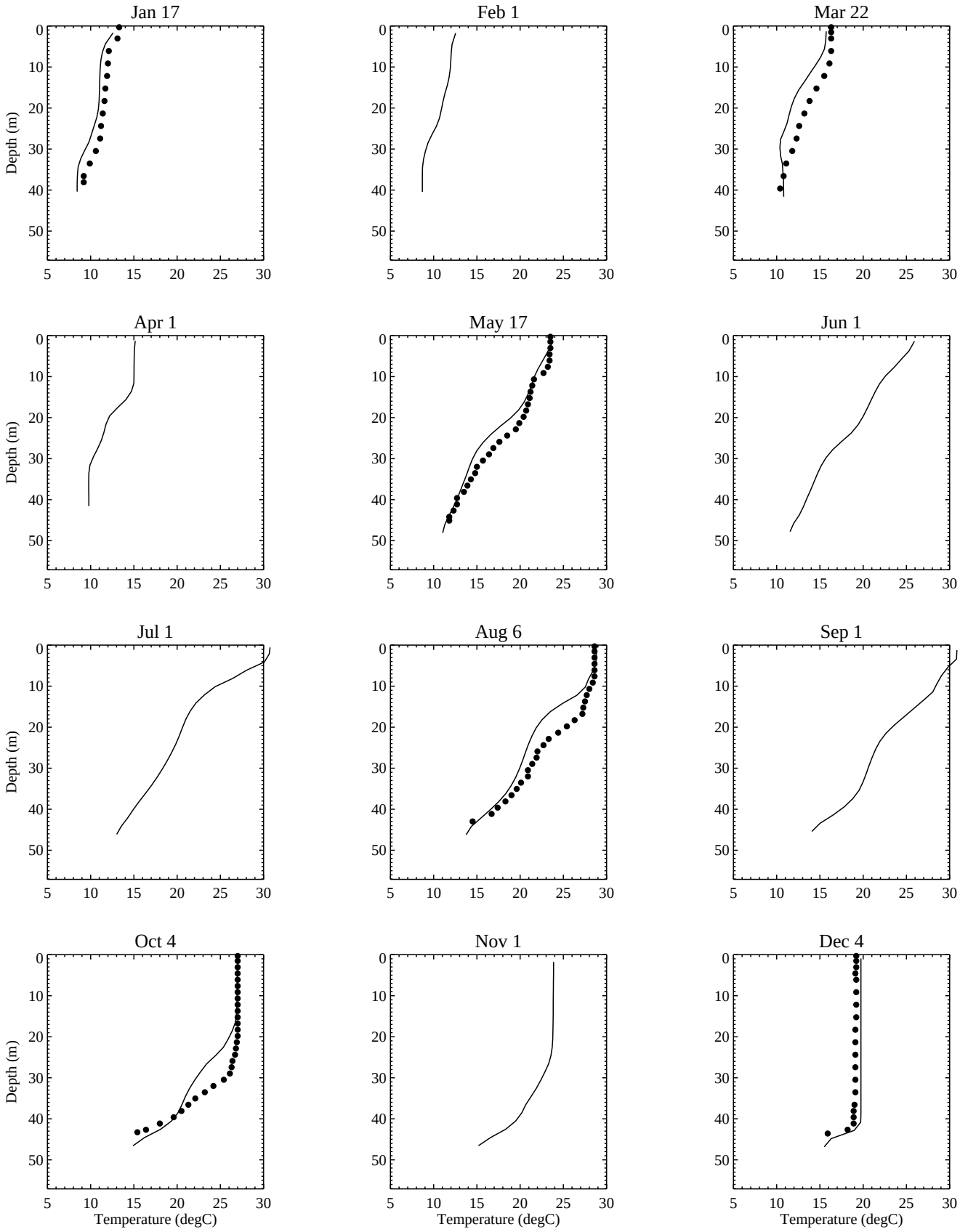

Figure J-2. Vertical profiles of model versus data at Arkansas Bend (Segment 78) - Temperature - 1990.

Profiles shown for dates with available data else model results for first day of month shown.

Model Data

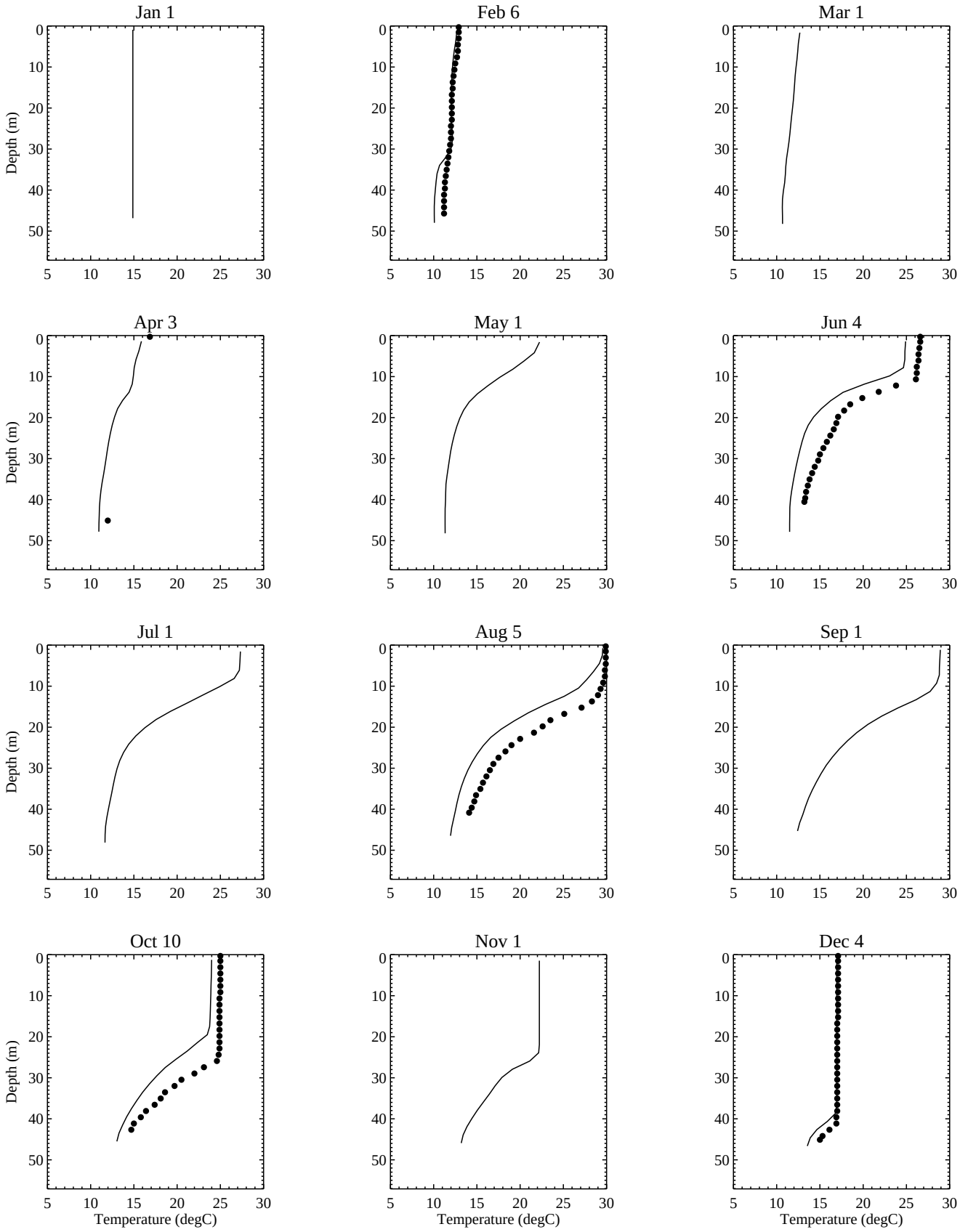

Figure J-2. Vertical profiles of model versus data at Arkansas Bend (Segment 78) - Temperature - 1991.

Profiles shown for dates with available data else model results for first day of month shown.

Model Data

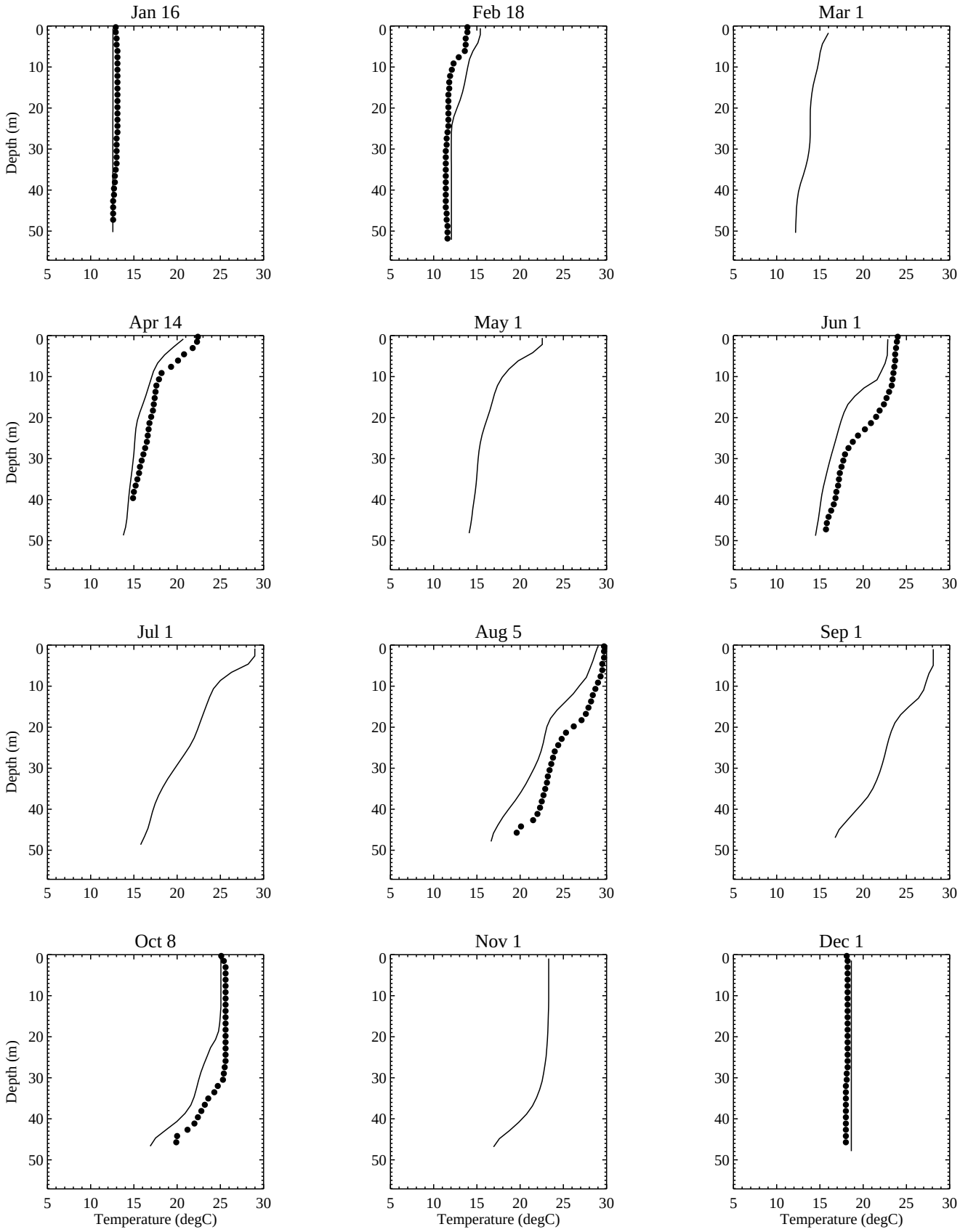

Figure J-2. Vertical profiles of model versus data at Arkansas Bend (Segment 78) - Temperature - 1992.

Profiles shown for dates with available data else model results for first day of month shown.

Model Data

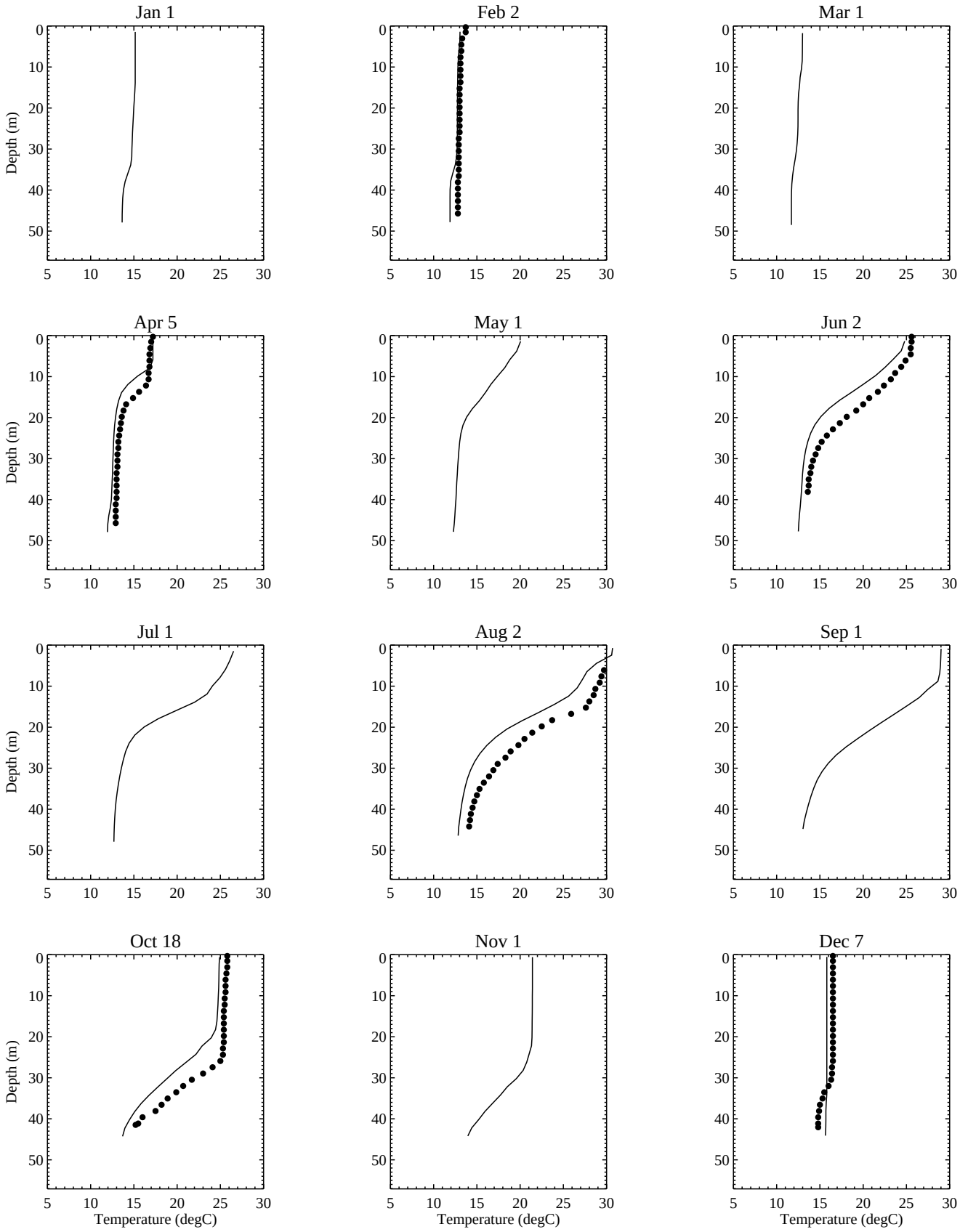

Figure J-2. Vertical profiles of model versus data at Arkansas Bend (Segment 78) - Temperature - 1993.

Profiles shown for dates with available data else model results for first day of month shown.

Model Data

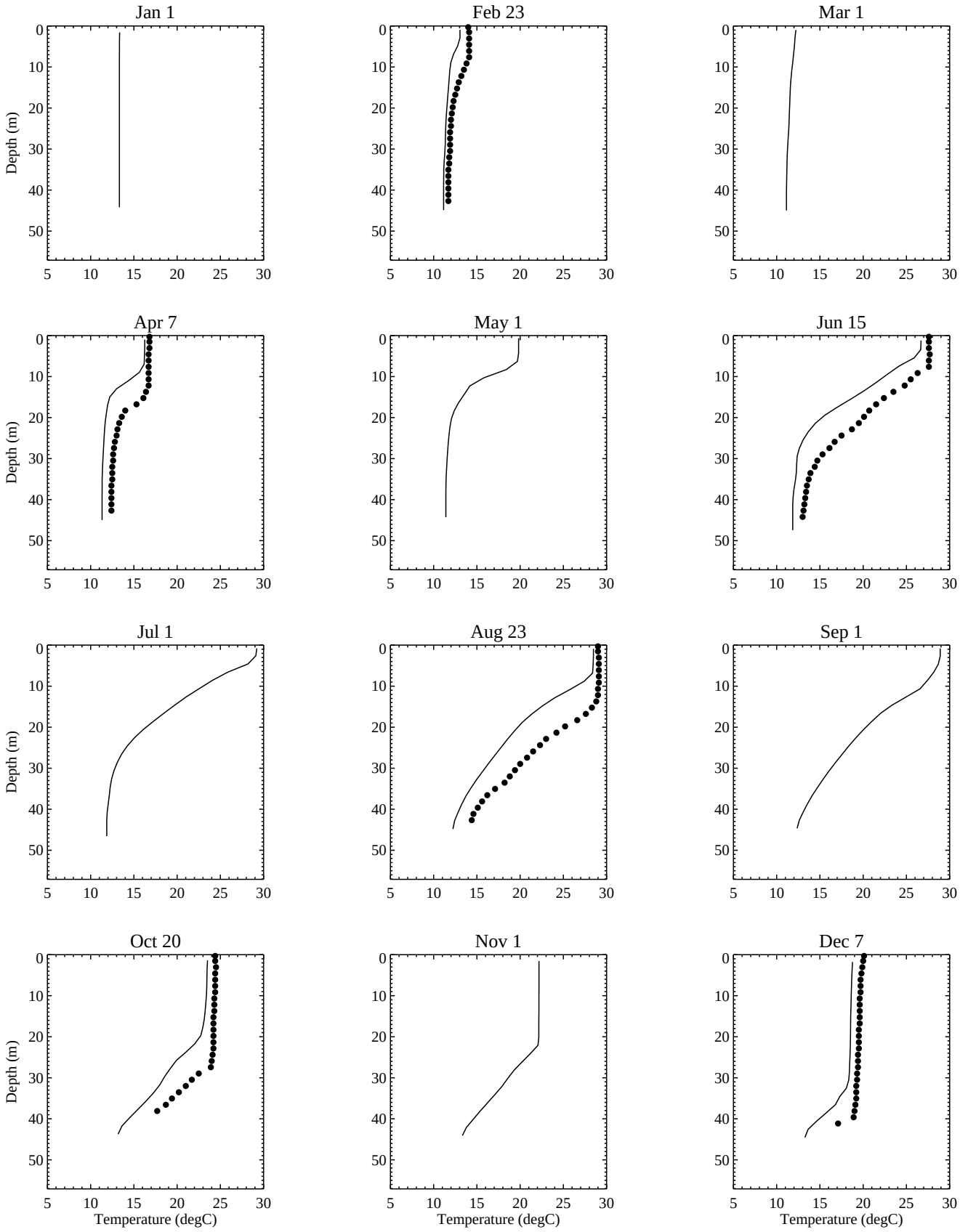

Figure J-2. Vertical profiles of model versus data at Arkansas Bend (Segment 78) - Temperature - 1994.

Profiles shown for dates with available data else model results for first day of month shown.

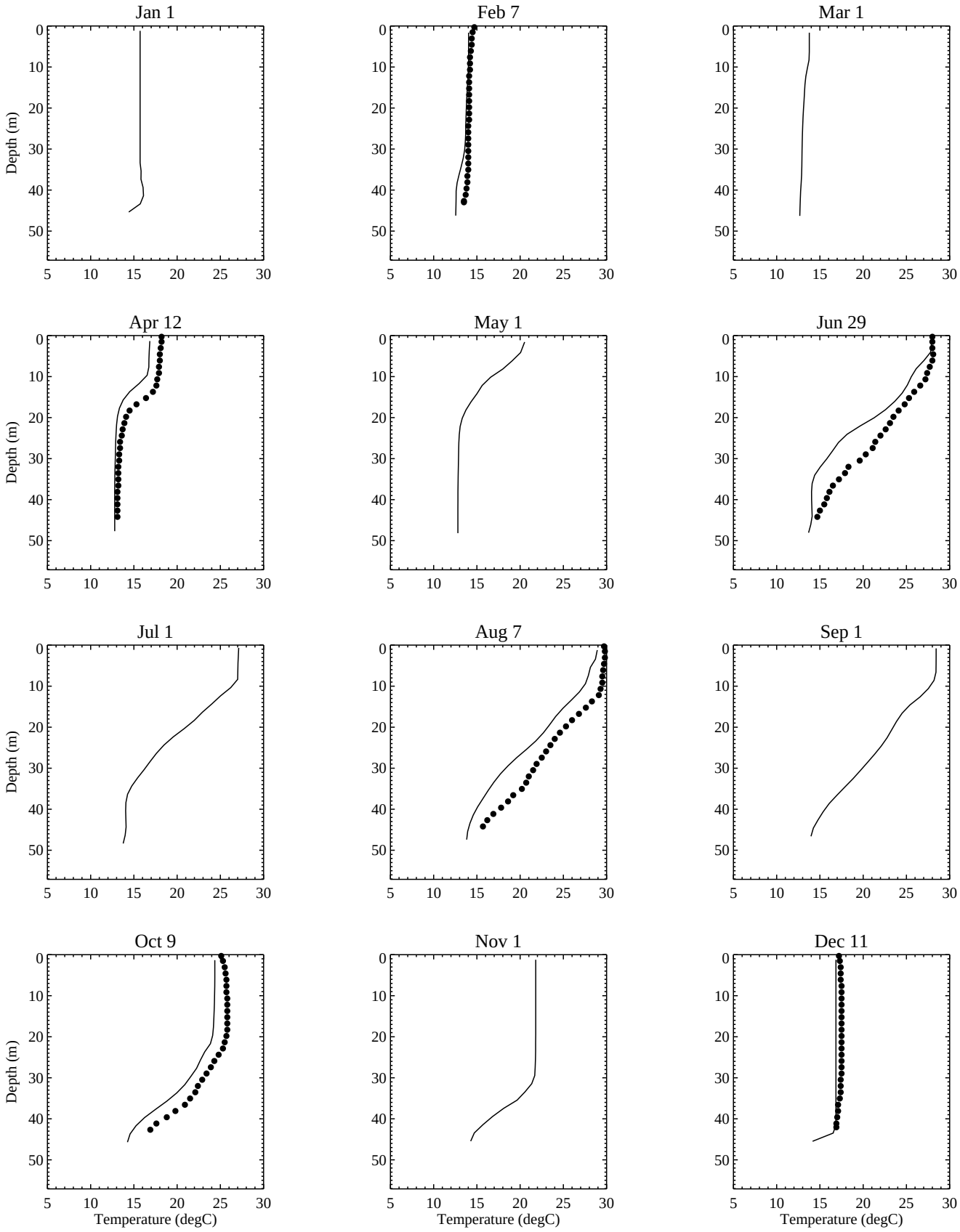

Figure J-2. Vertical profiles of model versus data at Arkansas Bend (Segment 78) - Temperature - 1995.

Profiles shown for dates with available data else model results for first day of month shown.

Model Data

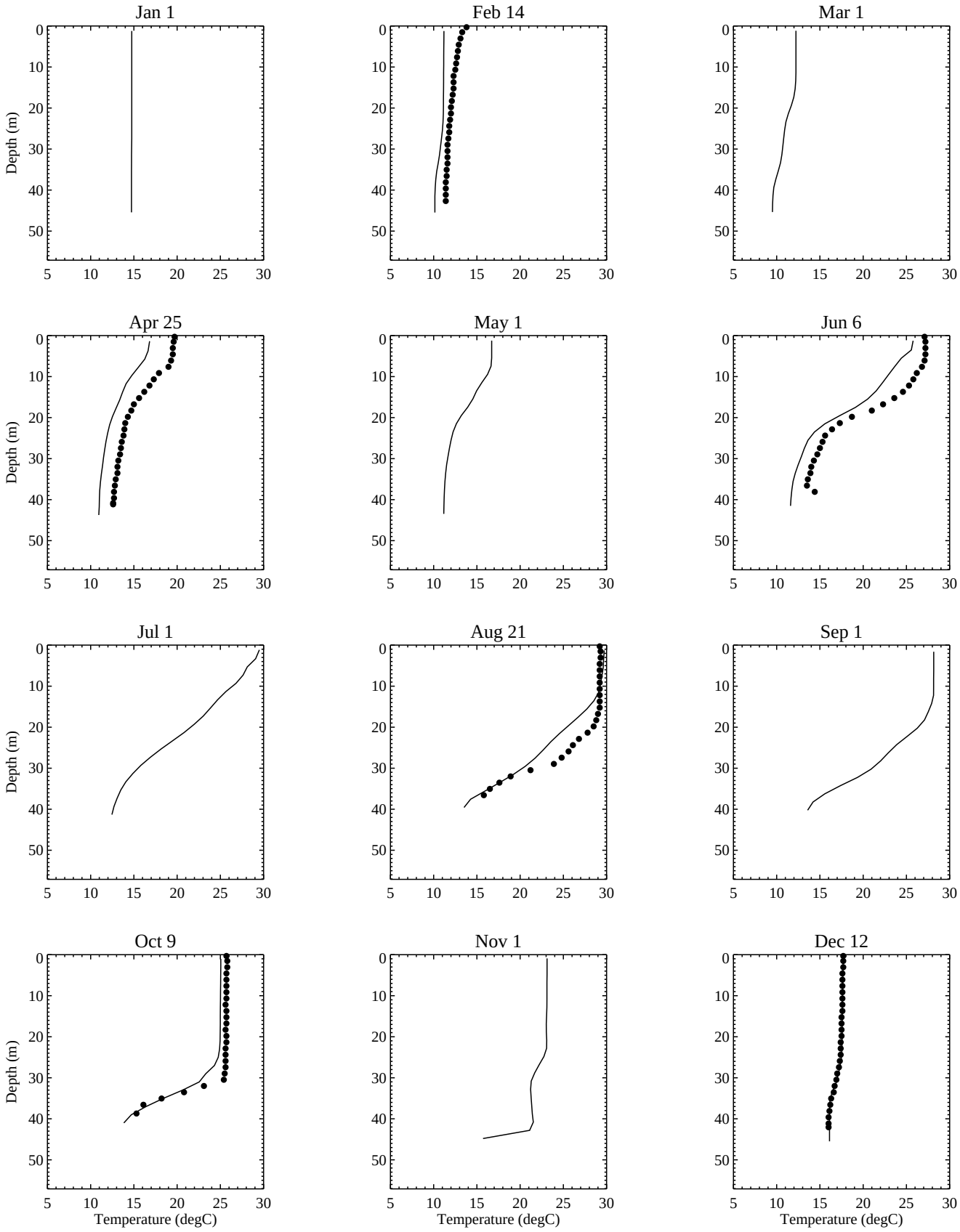

Figure J-2. Vertical profiles of model versus data at Arkansas Bend (Segment 78) - Temperature - 1996.

Profiles shown for dates with available data else model results for first day of month shown.

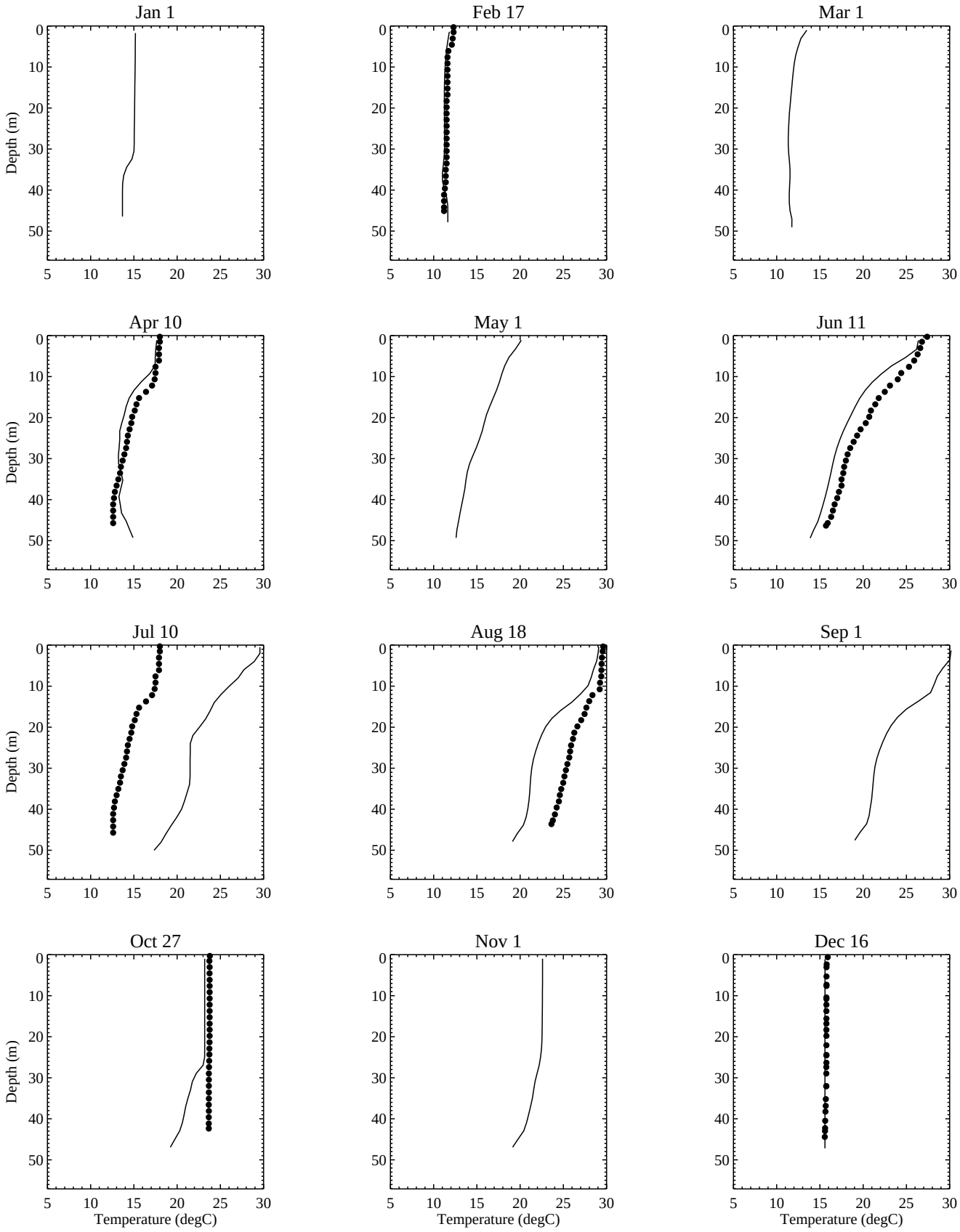

Figure J-2. Vertical profiles of model versus data at Arkansas Bend (Segment 78) - Temperature - 1997.

Profiles shown for dates with available data else model results for first day of month shown.

Model Data

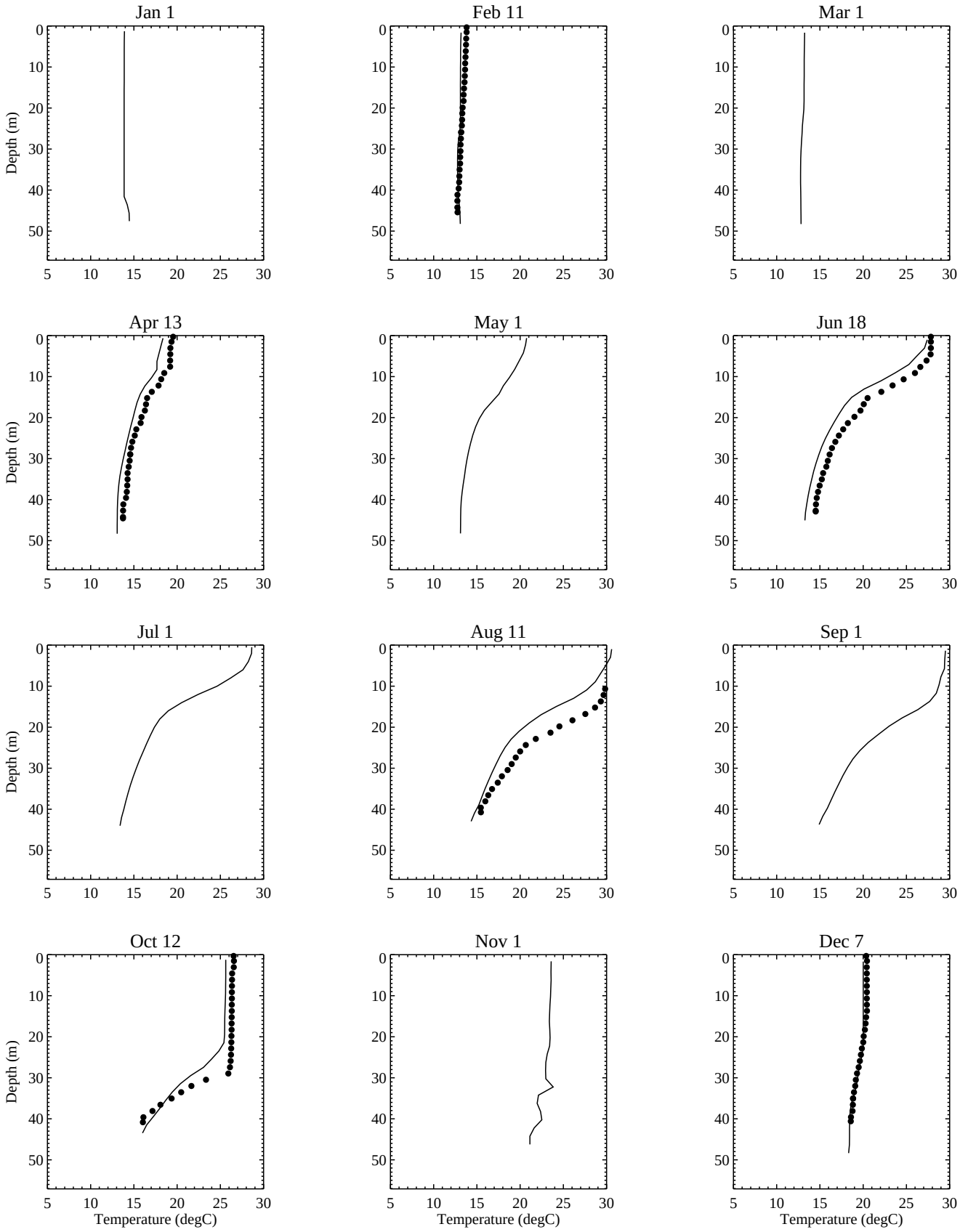

Figure J-2. Vertical profiles of model versus data at Arkansas Bend (Segment 78) - Temperature - 1998.

Profiles shown for dates with available data else model results for first day of month shown.

Model Data

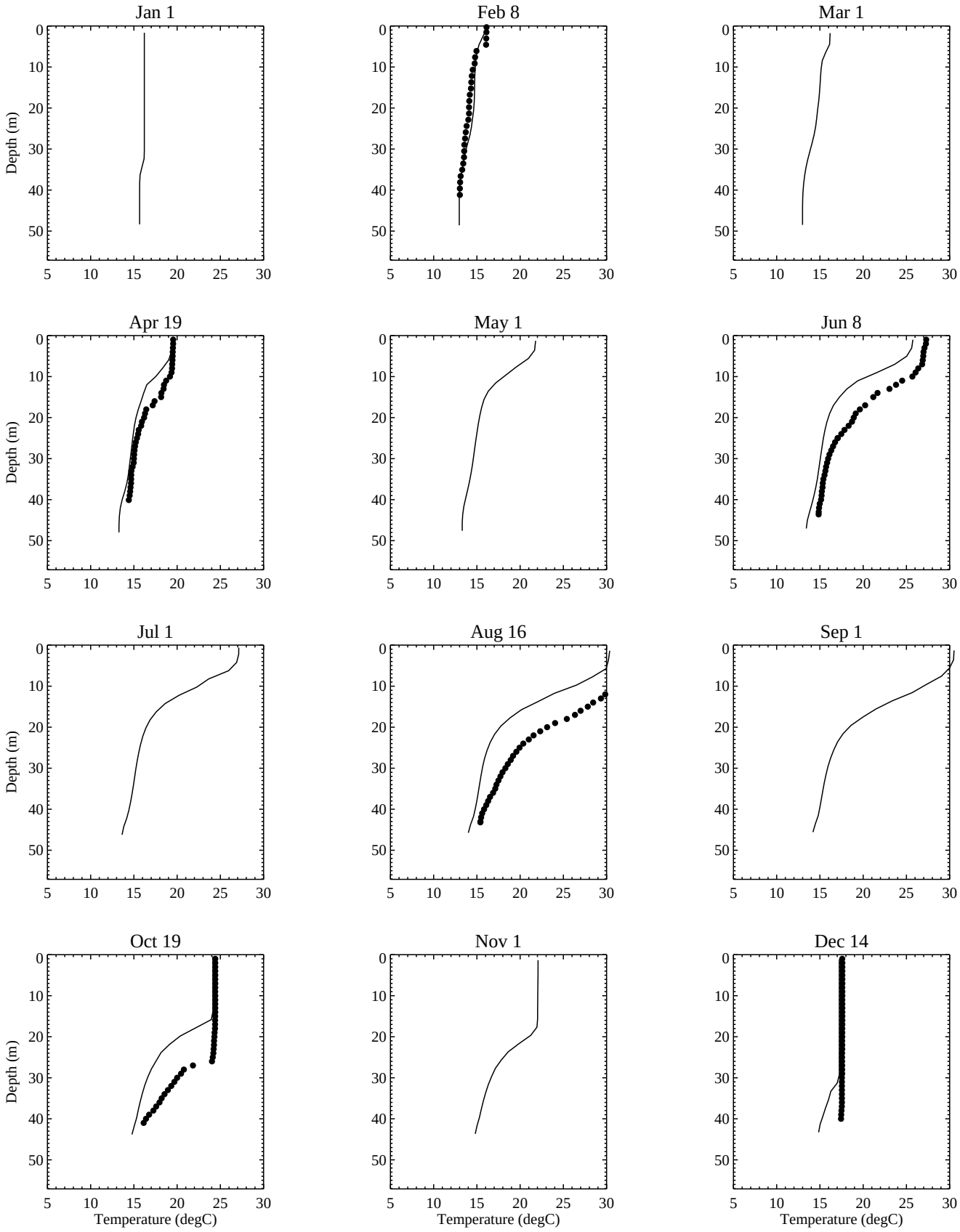

Figure J-2. Vertical profiles of model versus data at Arkansas Bend (Segment 78) - Temperature - 1999.

Profiles shown for dates with available data else model results for first day of month shown.

Model Data

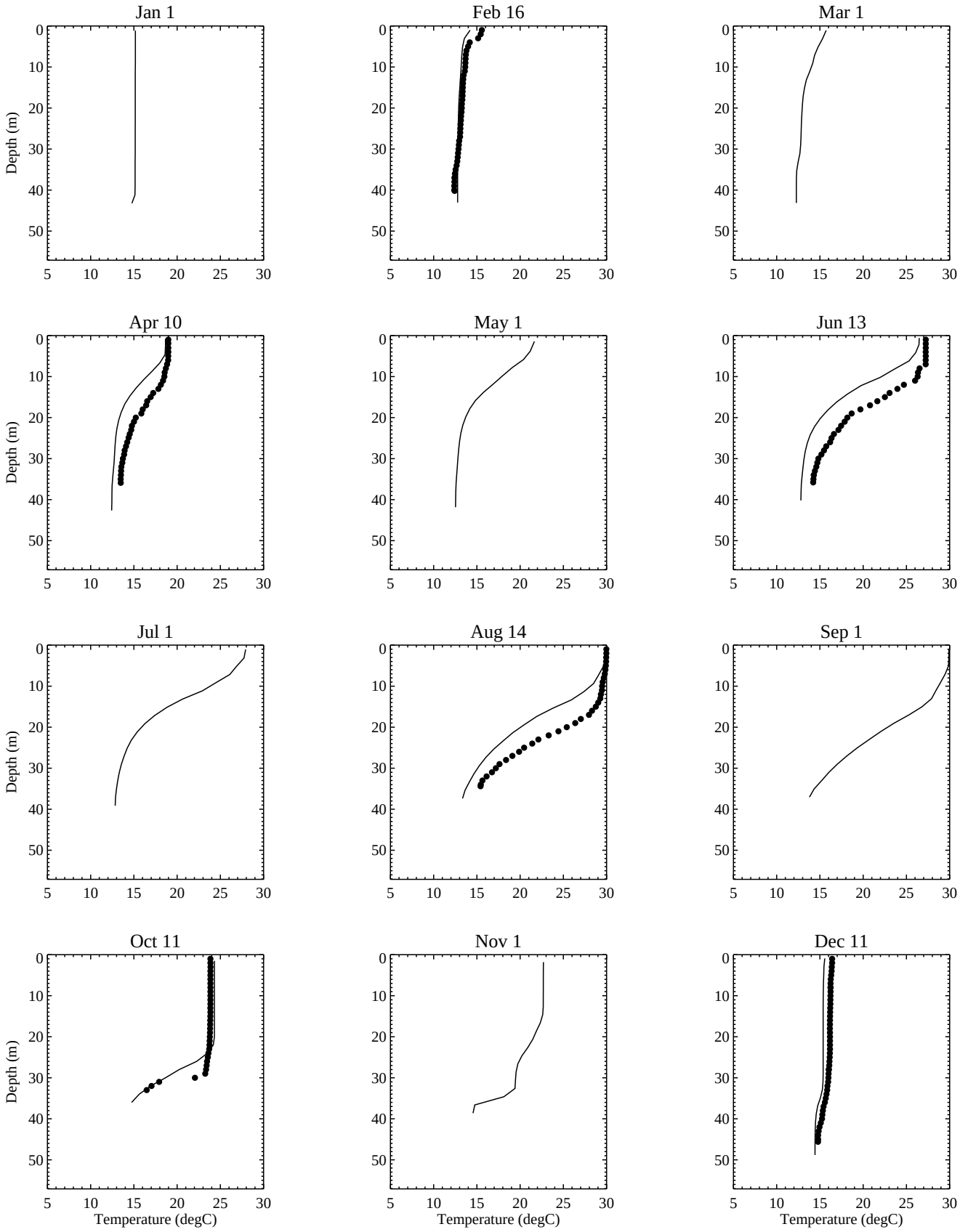

Figure J-2. Vertical profiles of model versus data at Arkansas Bend (Segment 78) - Temperature - 2000.

Profiles shown for dates with available data else model results for first day of month shown.

Model Data

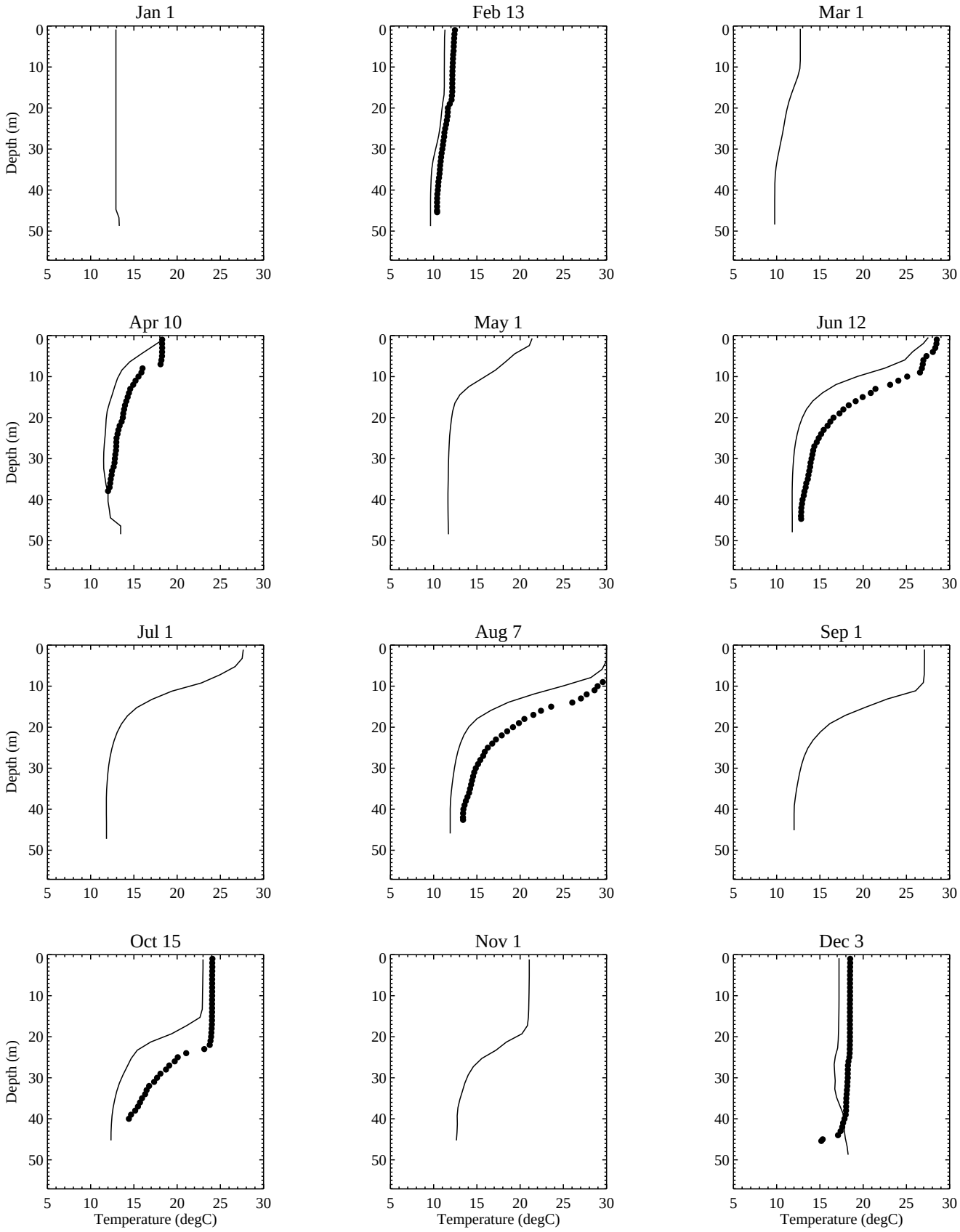

Figure J-2. Vertical profiles of model versus data at Arkansas Bend (Segment 78) - Temperature - 2001.

Profiles shown for dates with available data else model results for first day of month shown.

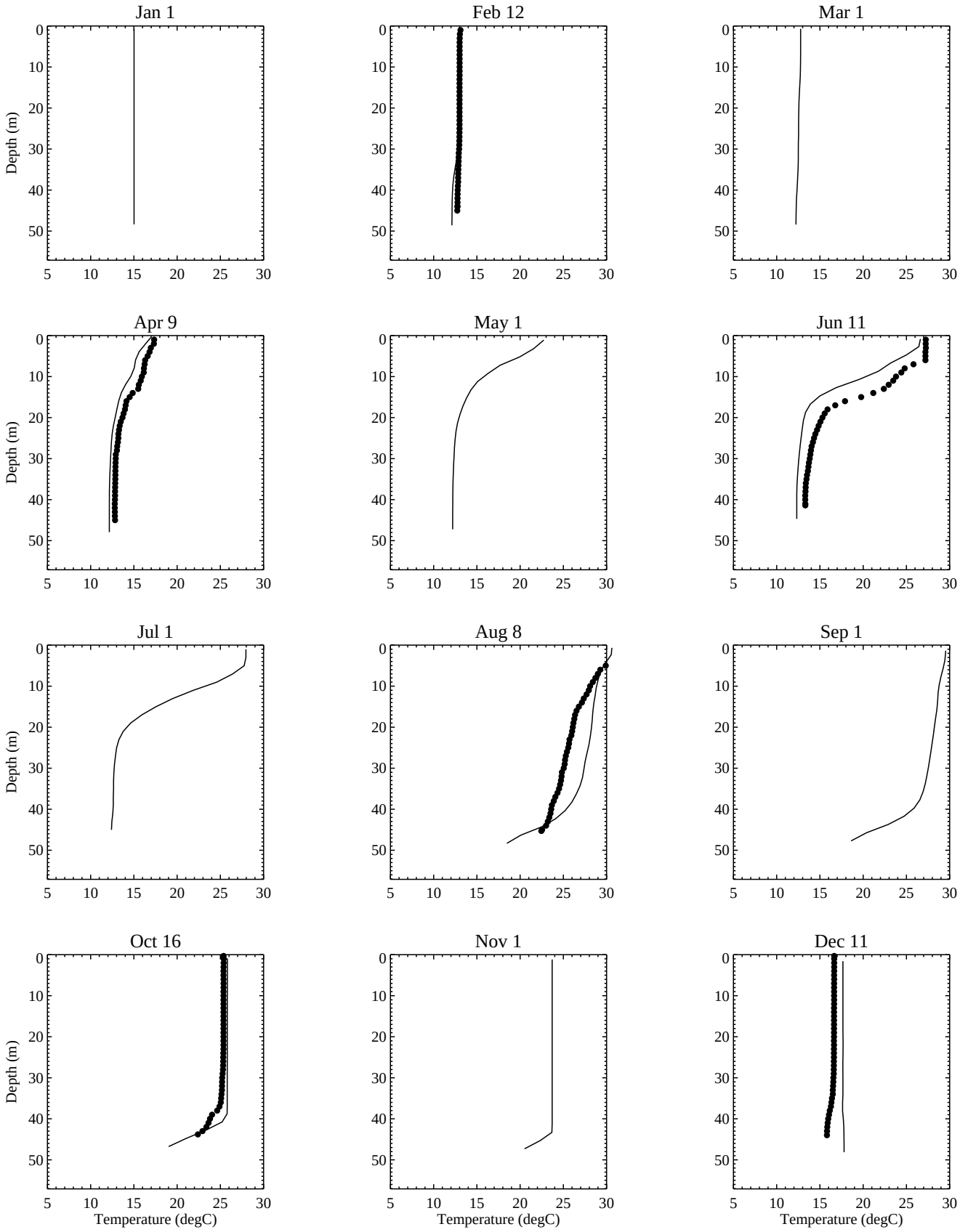

Figure J-2. Vertical profiles of model versus data at Arkansas Bend (Segment 78) - Temperature - 2002.

Profiles shown for dates with available data else model results for first day of month shown.

Model Data

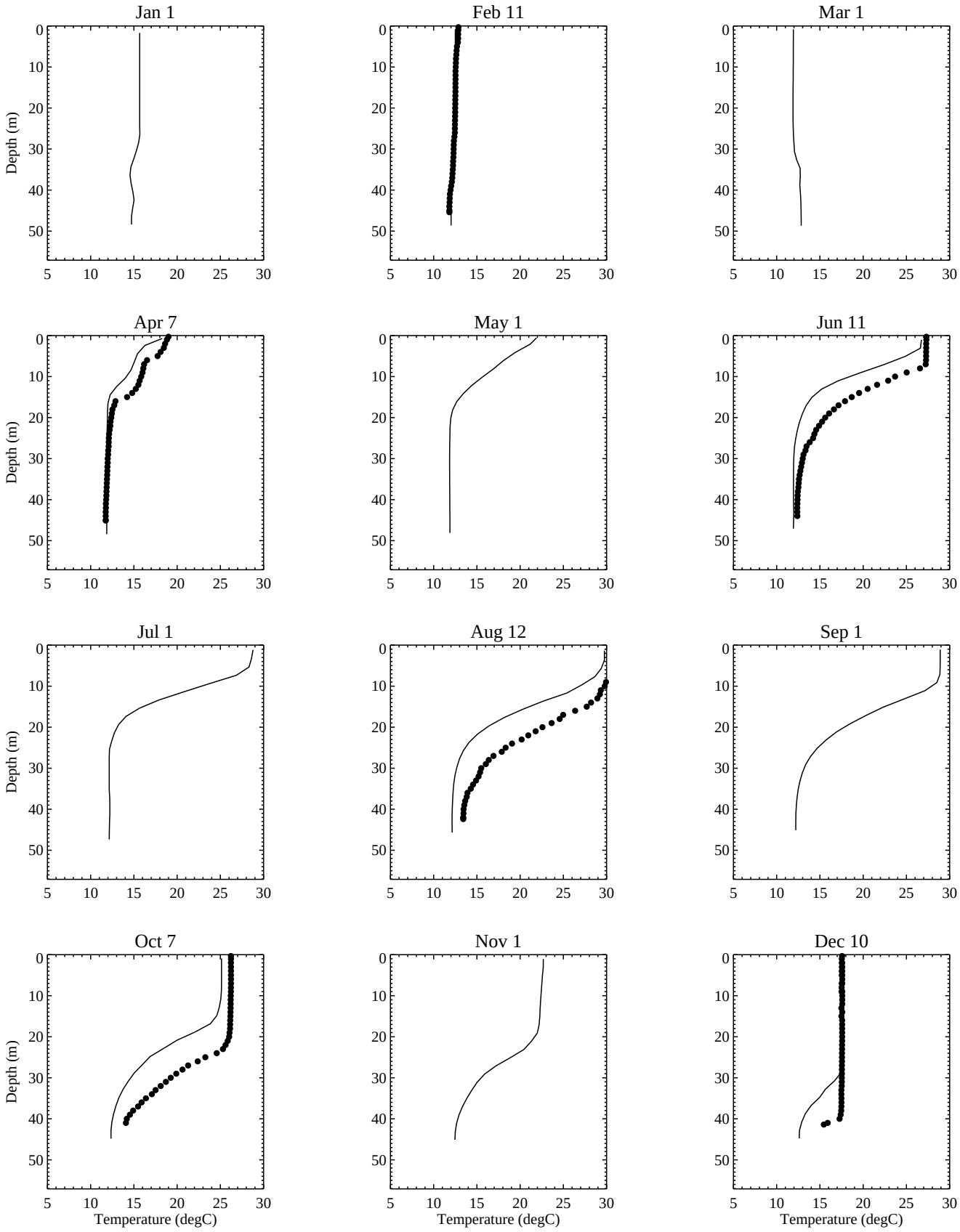

Figure J-2. Vertical profiles of model versus data at Arkansas Bend (Segment 78) - Temperature - 2003.

Profiles shown for dates with available data else model results for first day of month shown.

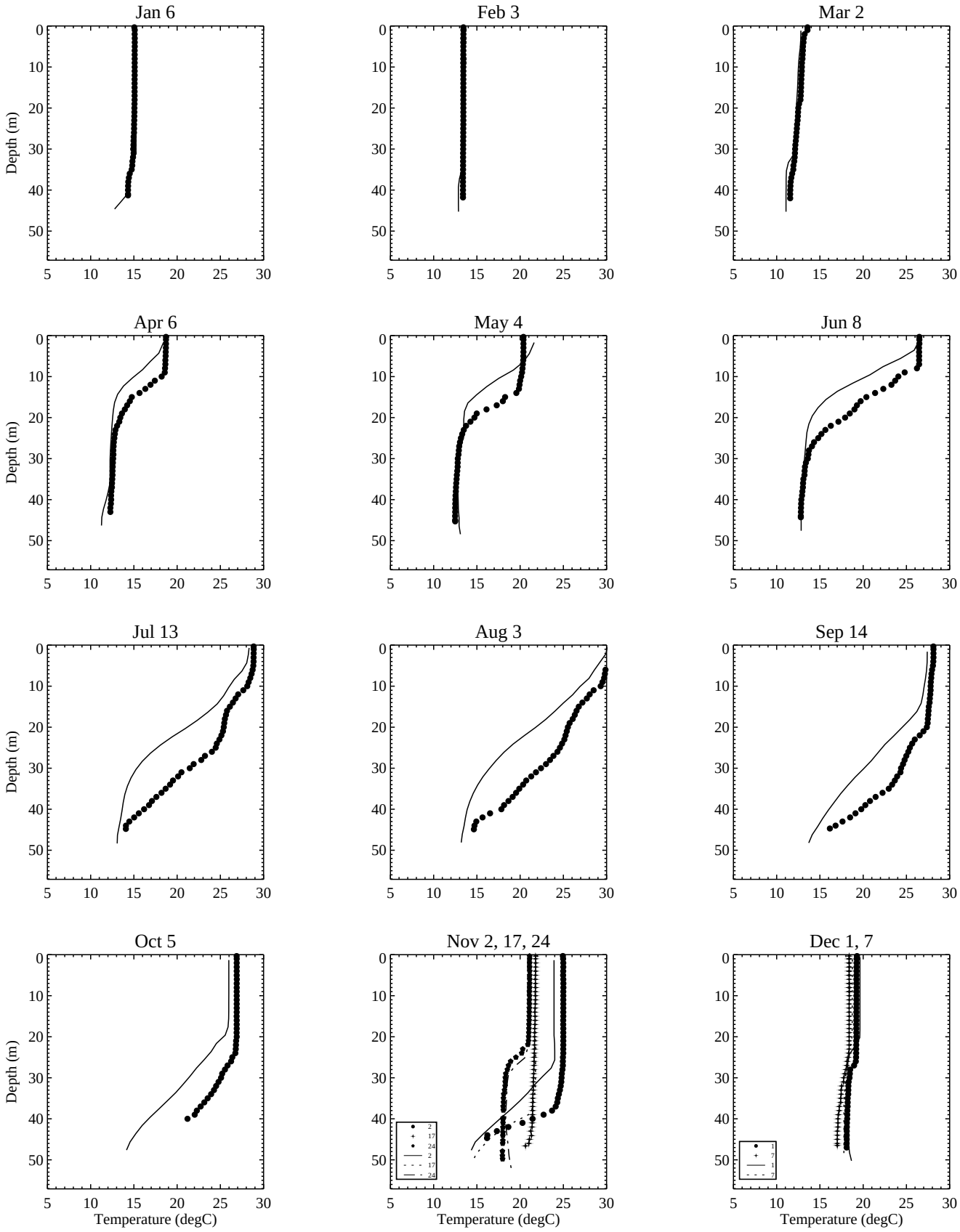

Figure J-2. Vertical profiles of model versus data at Arkansas Bend (Segment 78) - Temperature - 2004.

Profiles shown for dates with available data else model results for first day of month shown.

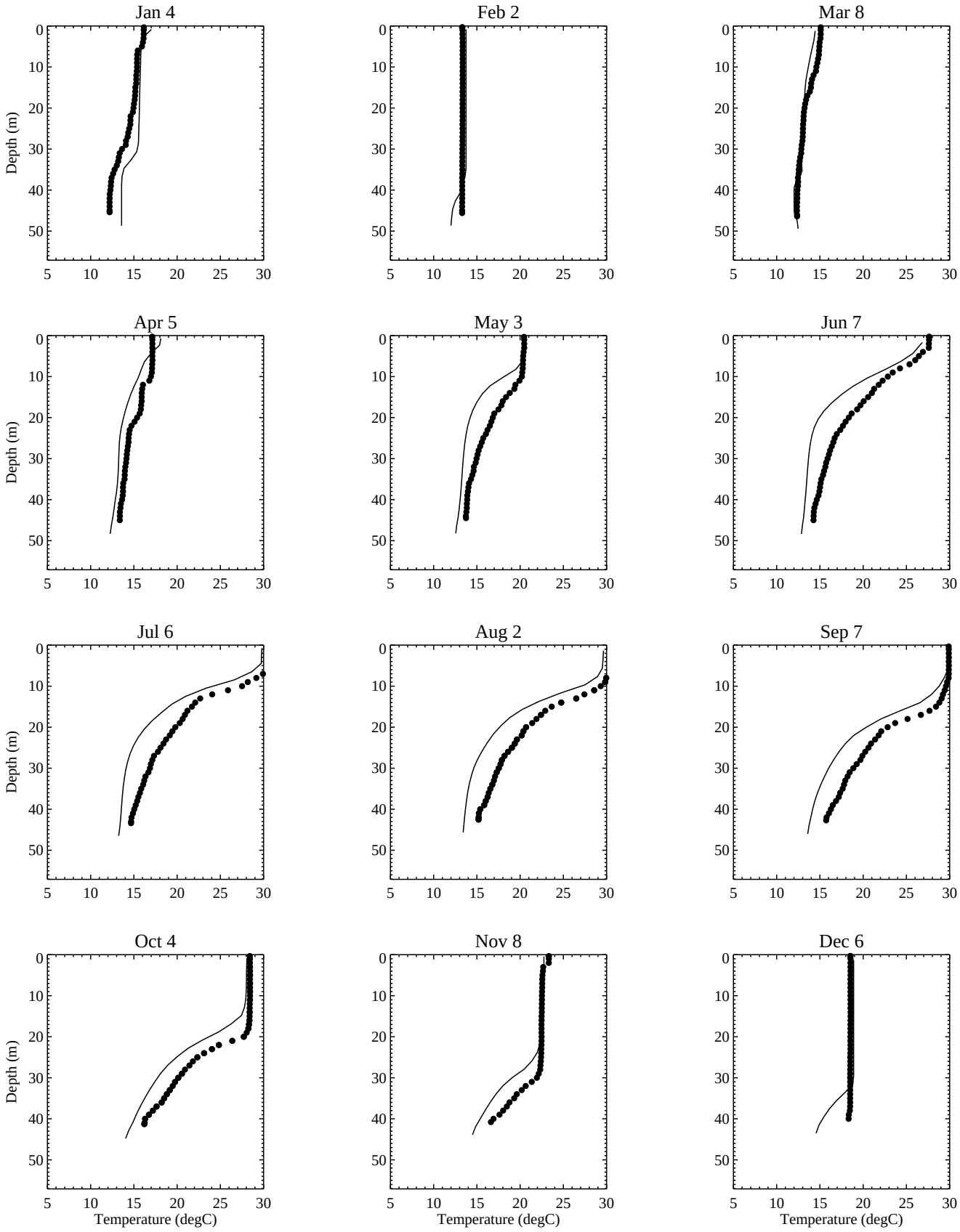

Figure J-2. Vertical profiles of model versus data at Arkansas Bend (Segment 78) - Temperature - 2005.

Profiles shown for dates with available data else model results for first day of month shown.

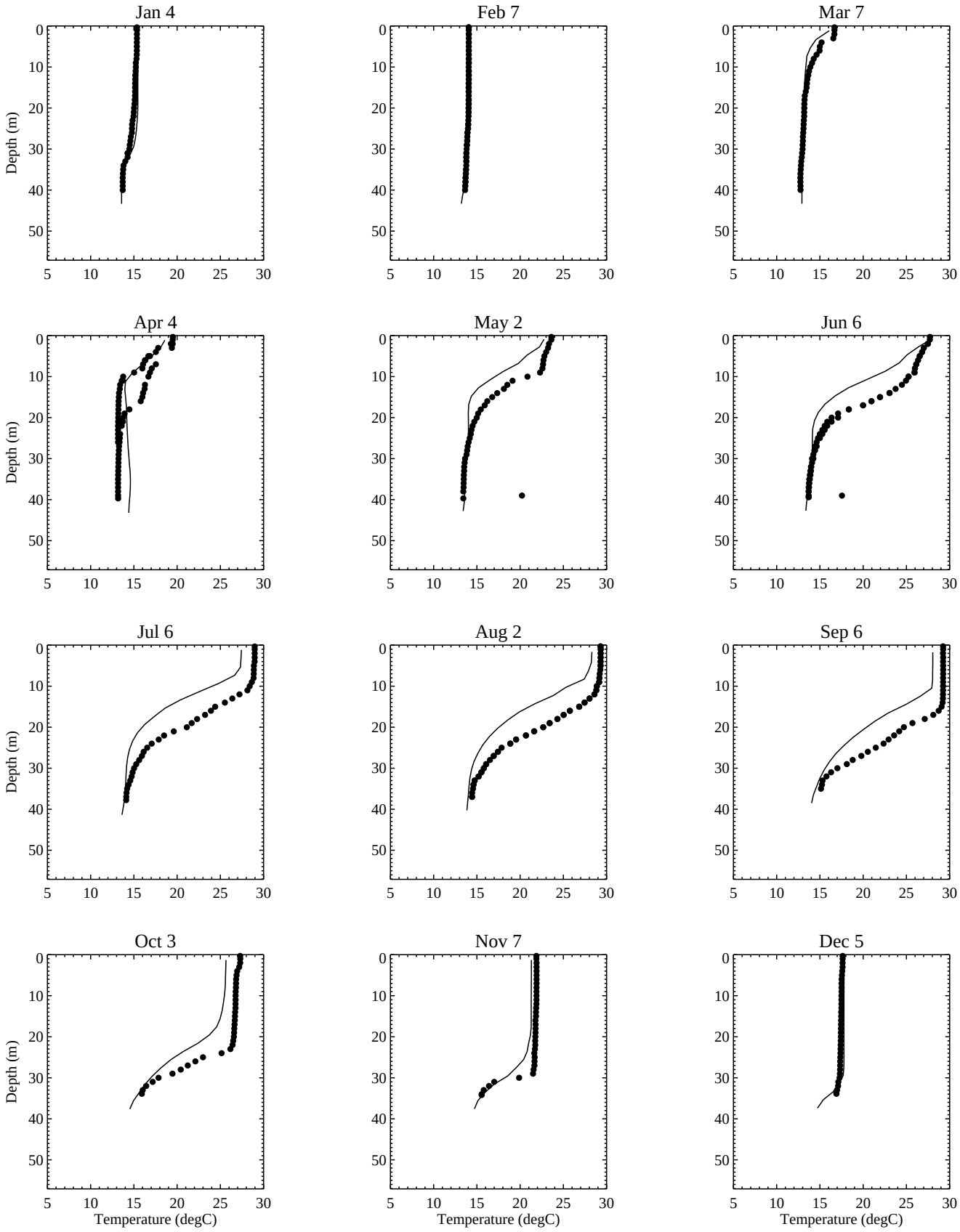

Figure J-2. Vertical profiles of model versus data at Arkansas Bend (Segment 78) - Temperature - 2006.

Profiles shown for dates with available data else model results for first day of month shown.

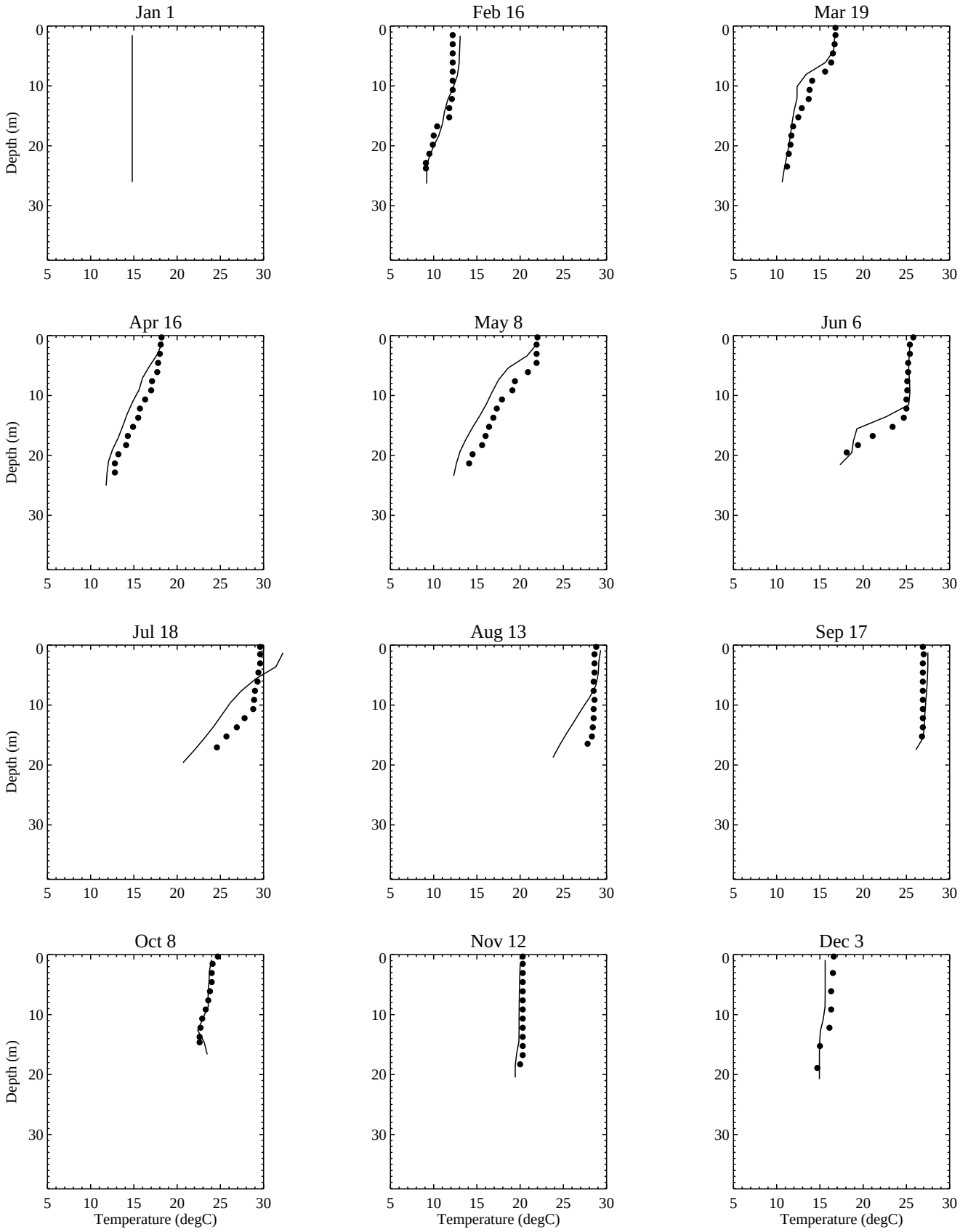

Figure J-3. Vertical profiles of model versus data at Pace Bend (Segment 48) - Temperature - 1984.

Profiles shown for dates with available data else model results for first day of month shown.

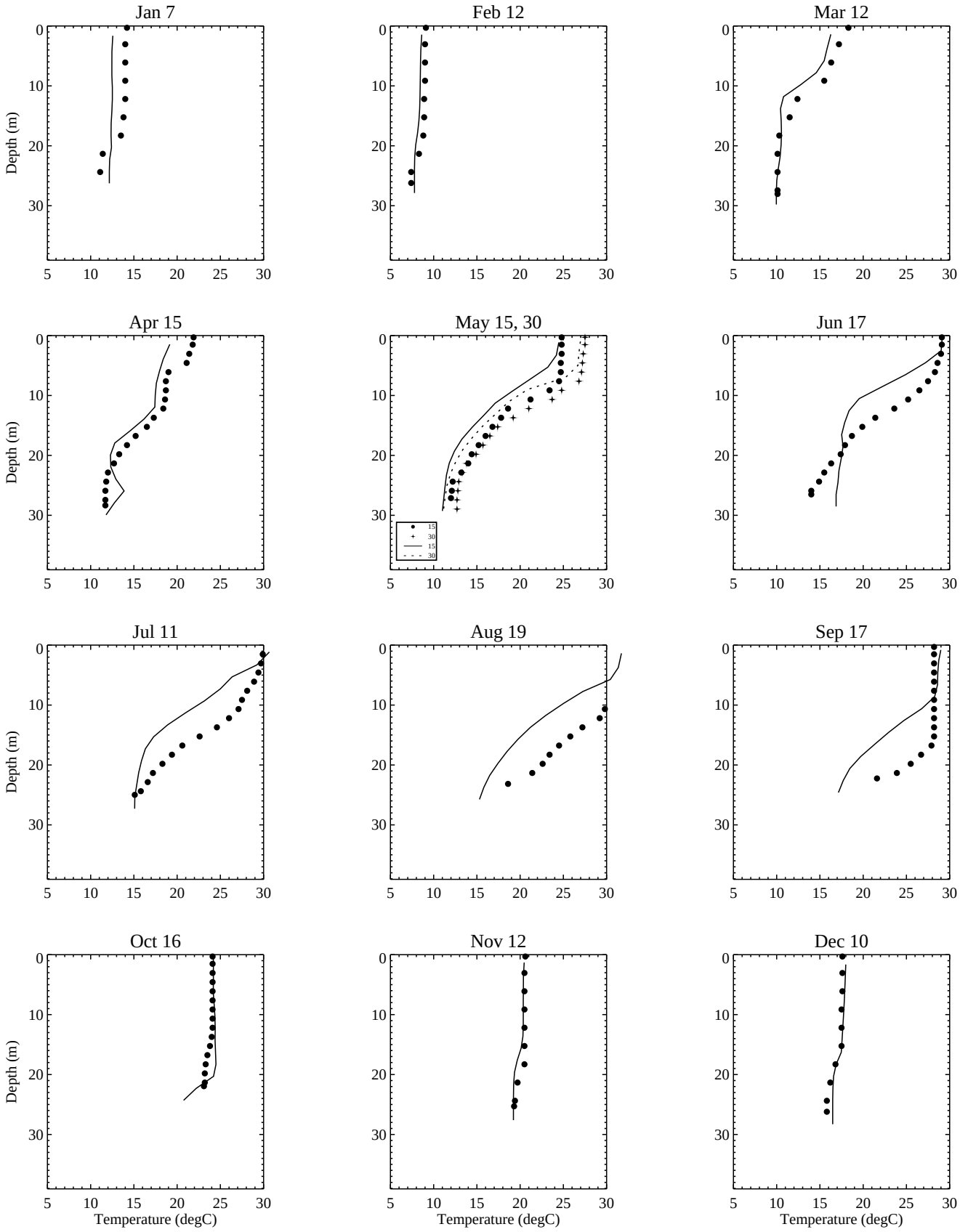

Figure J-3. Vertical profiles of model versus data at Pace Bend (Segment 48) - Temperature - 1985.

Profiles shown for dates with available data else model results for first day of month shown.

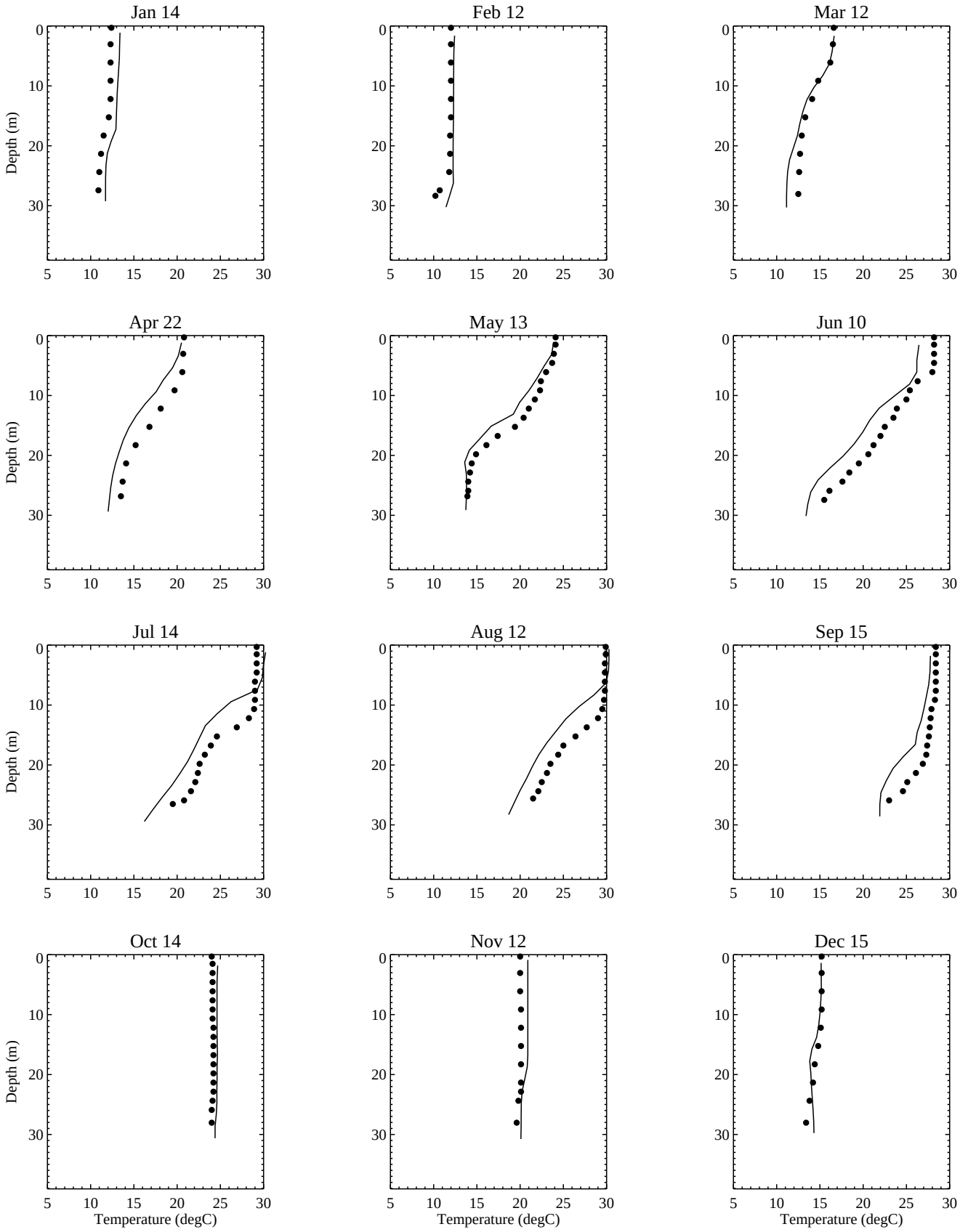

Figure J-3. Vertical profiles of model versus data at Pace Bend (Segment 48) - Temperature - 1986.

Profiles shown for dates with available data else model results for first day of month shown.

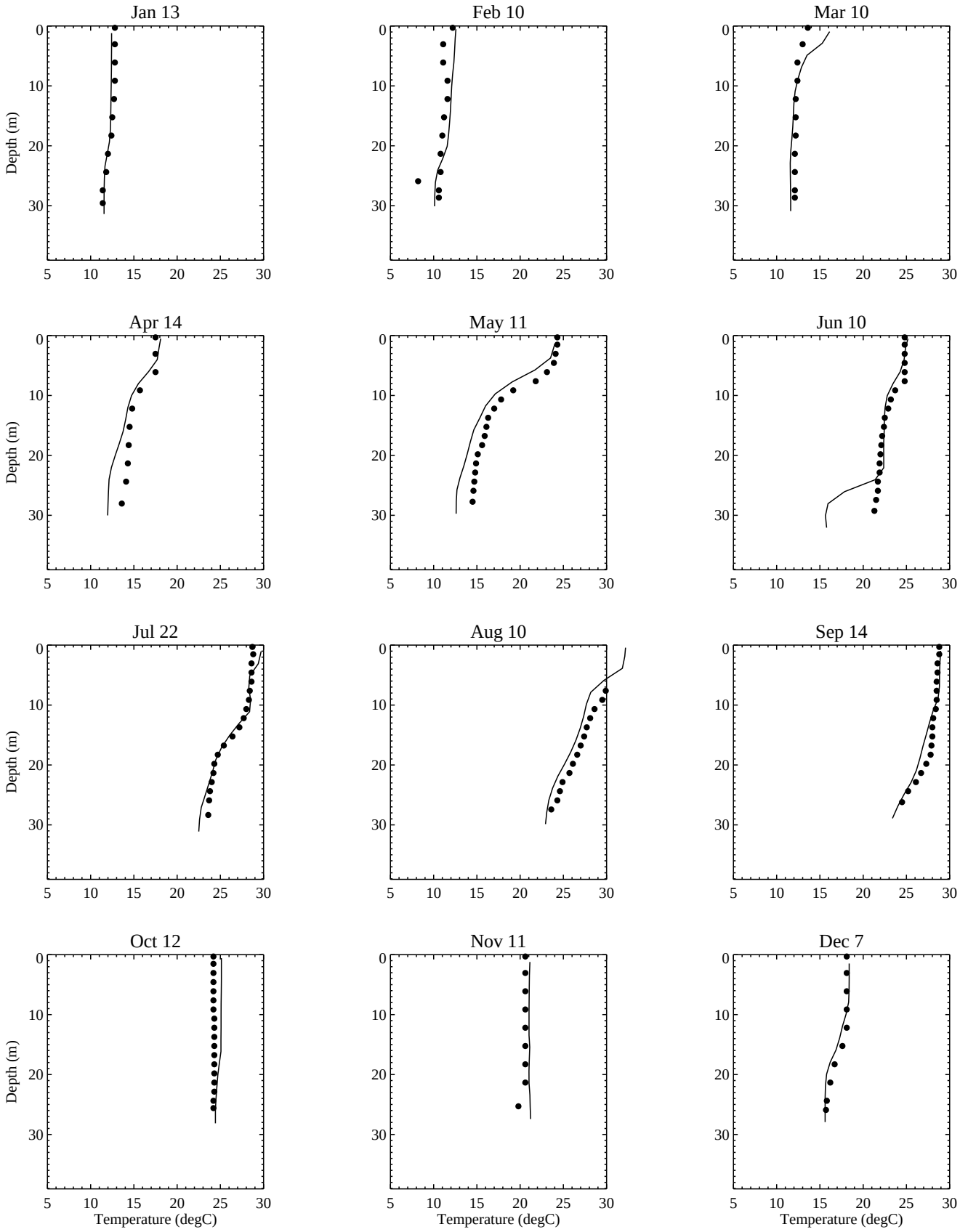

Figure J-3. Vertical profiles of model versus data at Pace Bend (Segment 48) - Temperature - 1987.

Profiles shown for dates with available data else model results for first day of month shown.

Model Data

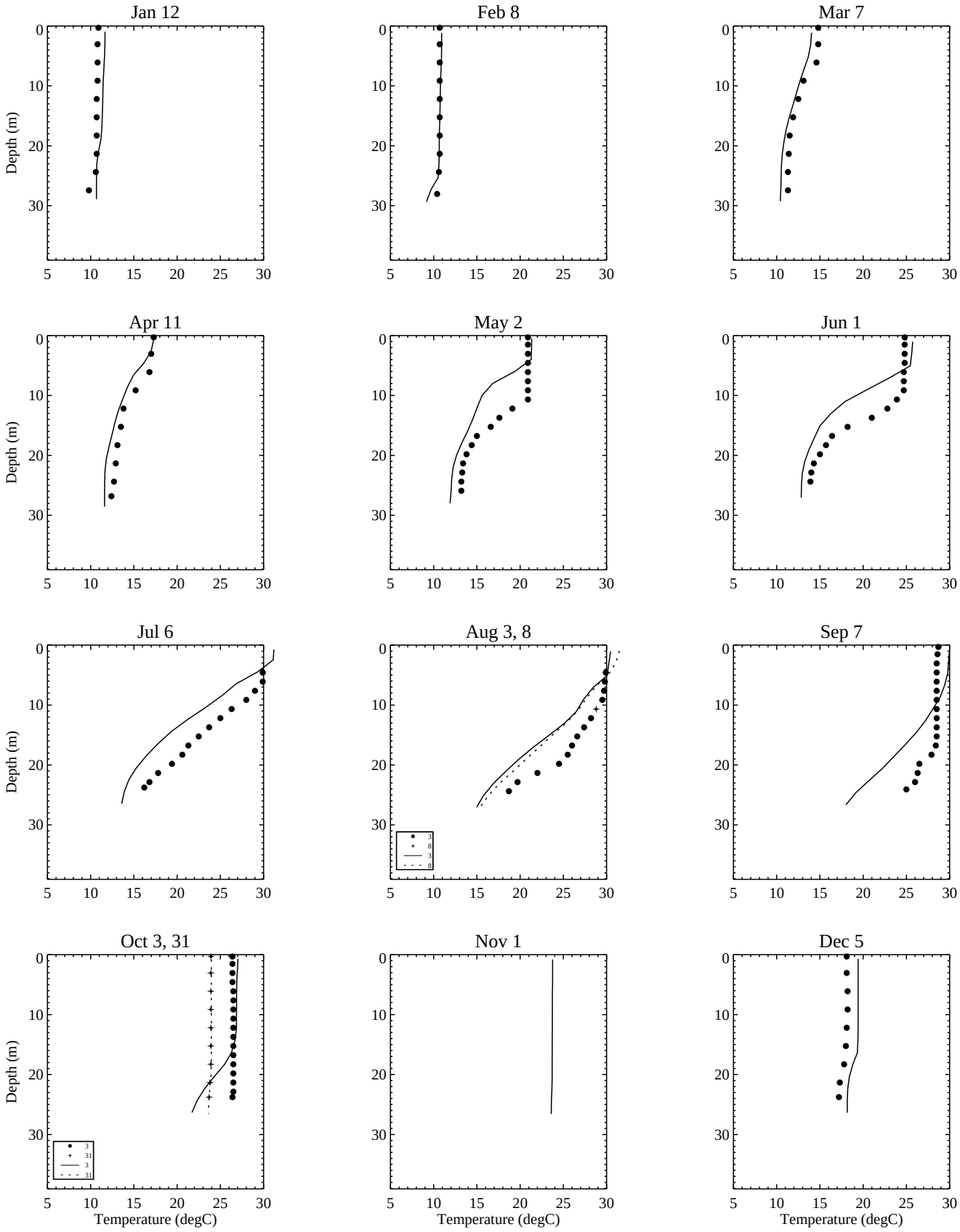

Figure J-3. Vertical profiles of model versus data at Pace Bend (Segment 48) - Temperature - 1988.

Profiles shown for dates with available data else model results for first day of month shown.

Model Data

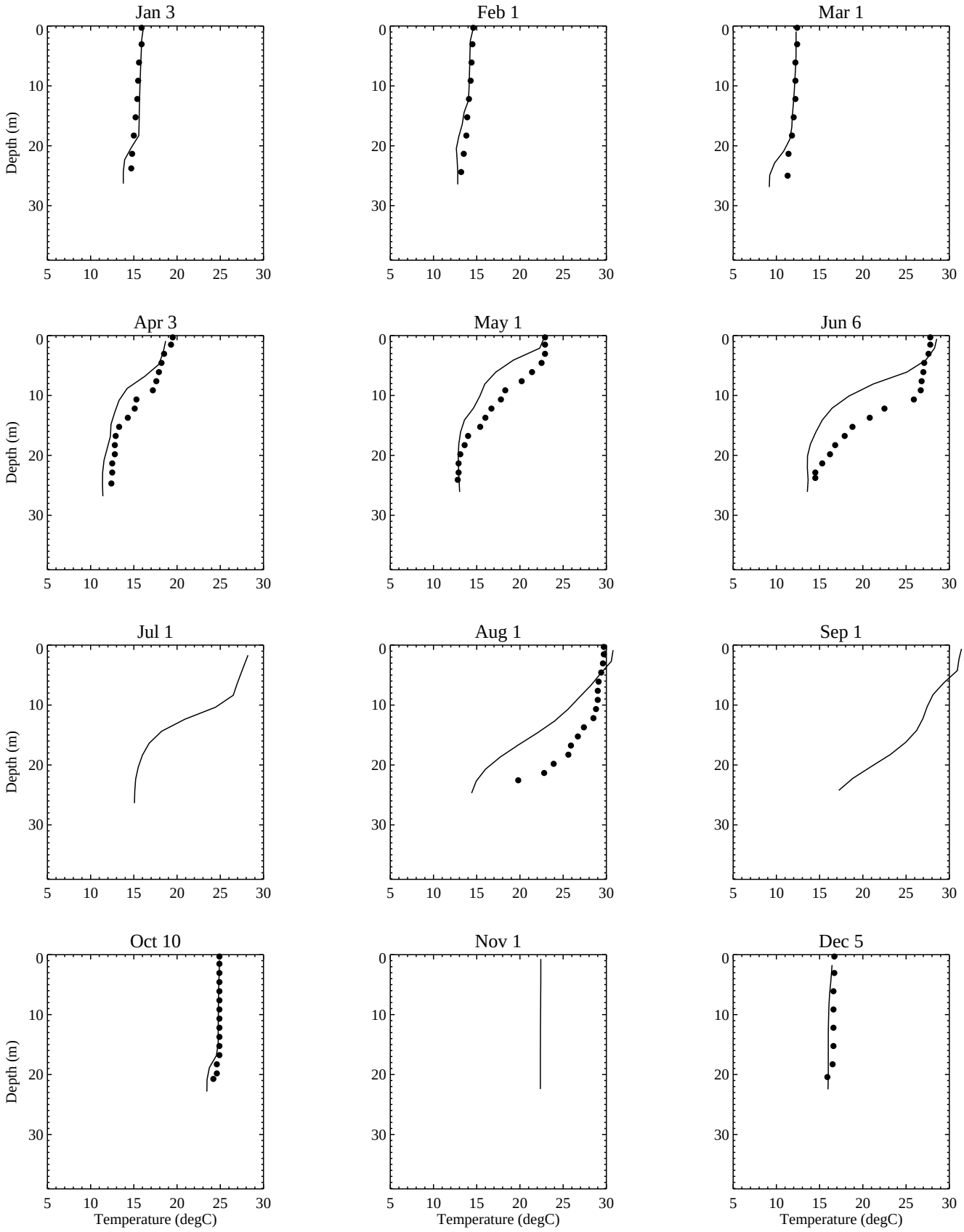

Figure J-3. Vertical profiles of model versus data at Pace Bend (Segment 48) - Temperature - 1989.

Profiles shown for dates with available data else model results for first day of month shown.

Model Data

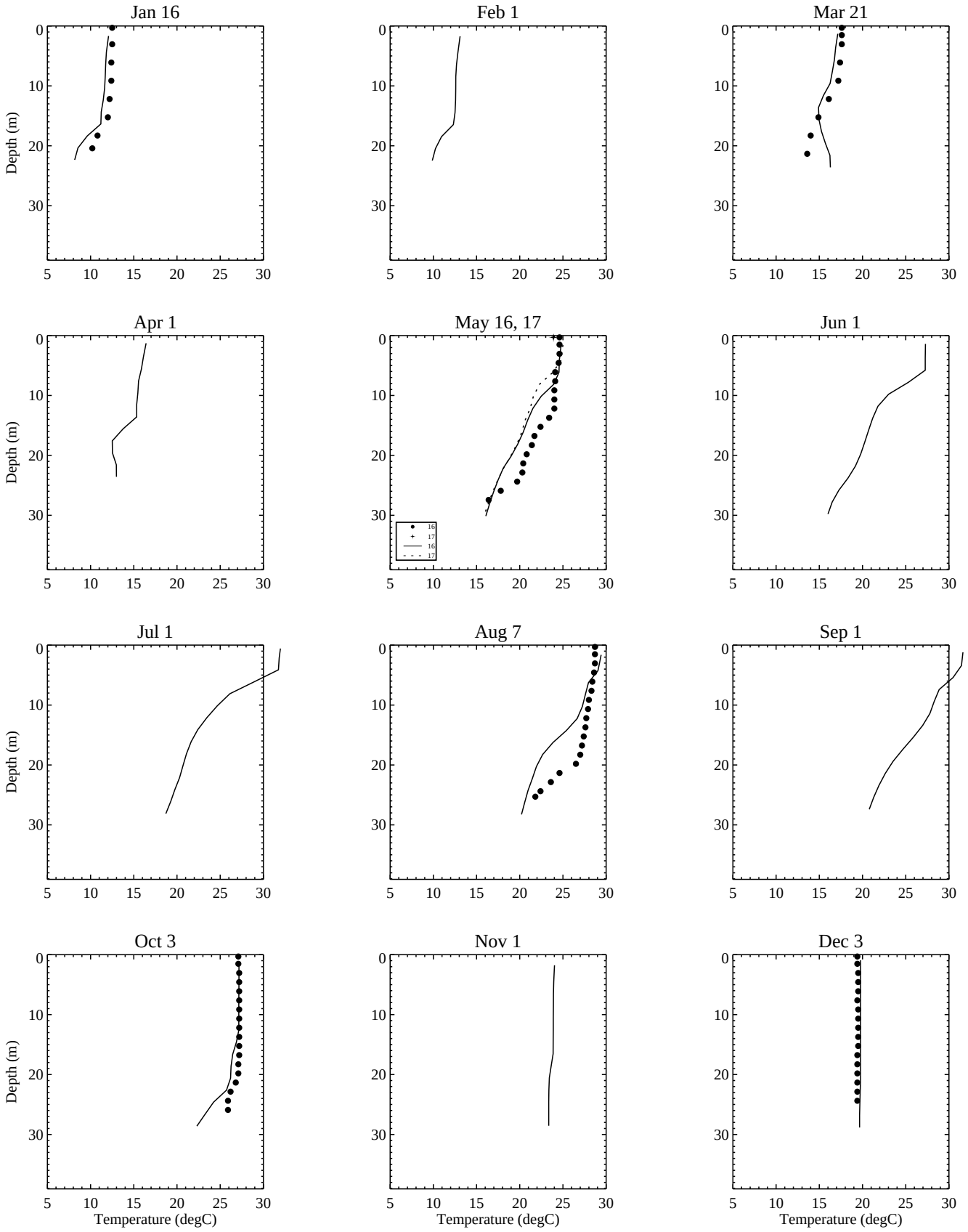

Figure J-3. Vertical profiles of model versus data at Pace Bend (Segment 48) - Temperature - 1990.

Profiles shown for dates with available data else model results for first day of month shown.

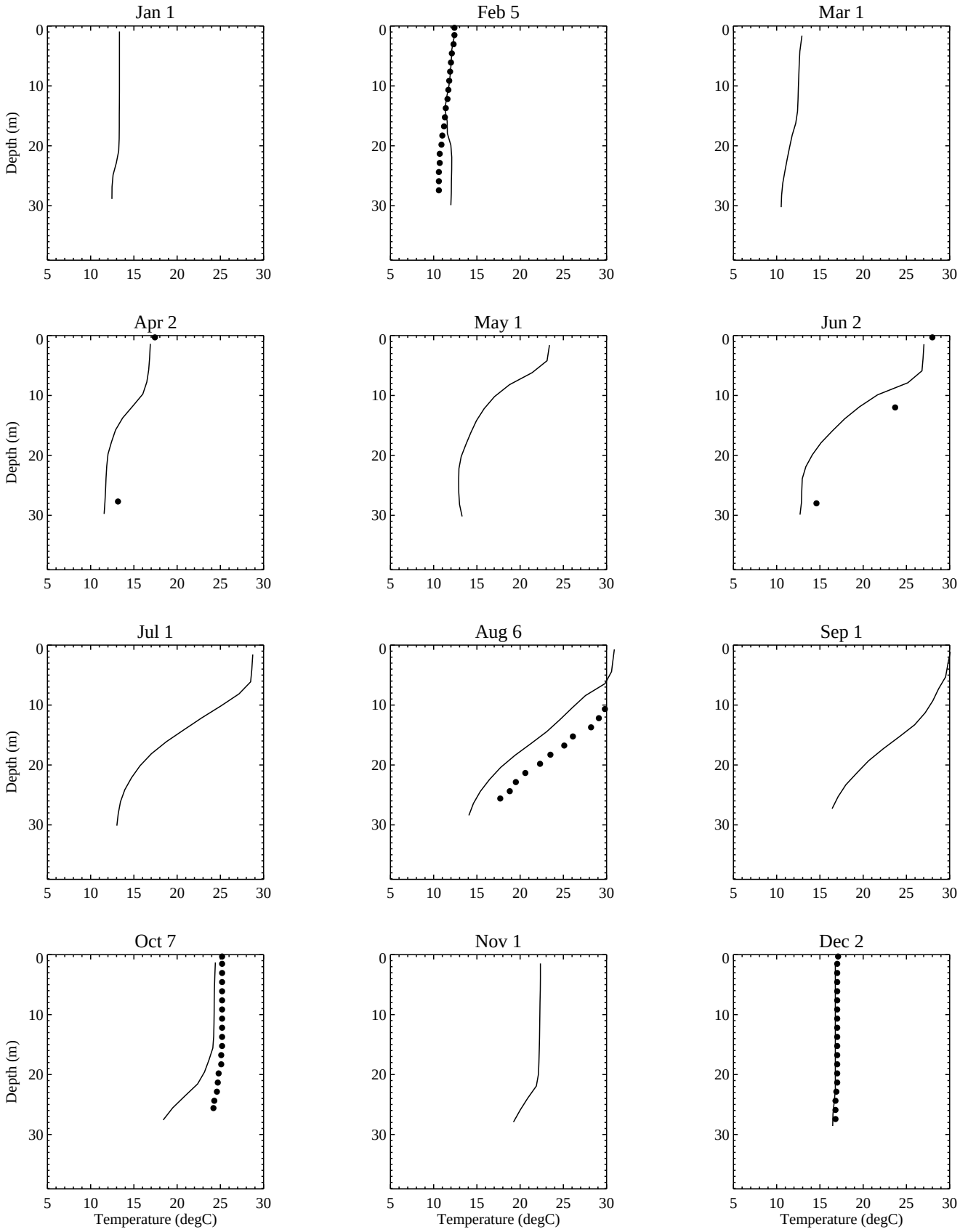

Figure J-3. Vertical profiles of model versus data at Pace Bend (Segment 48) - Temperature - 1991.

Profiles shown for dates with available data else model results for first day of month shown.

Model Data

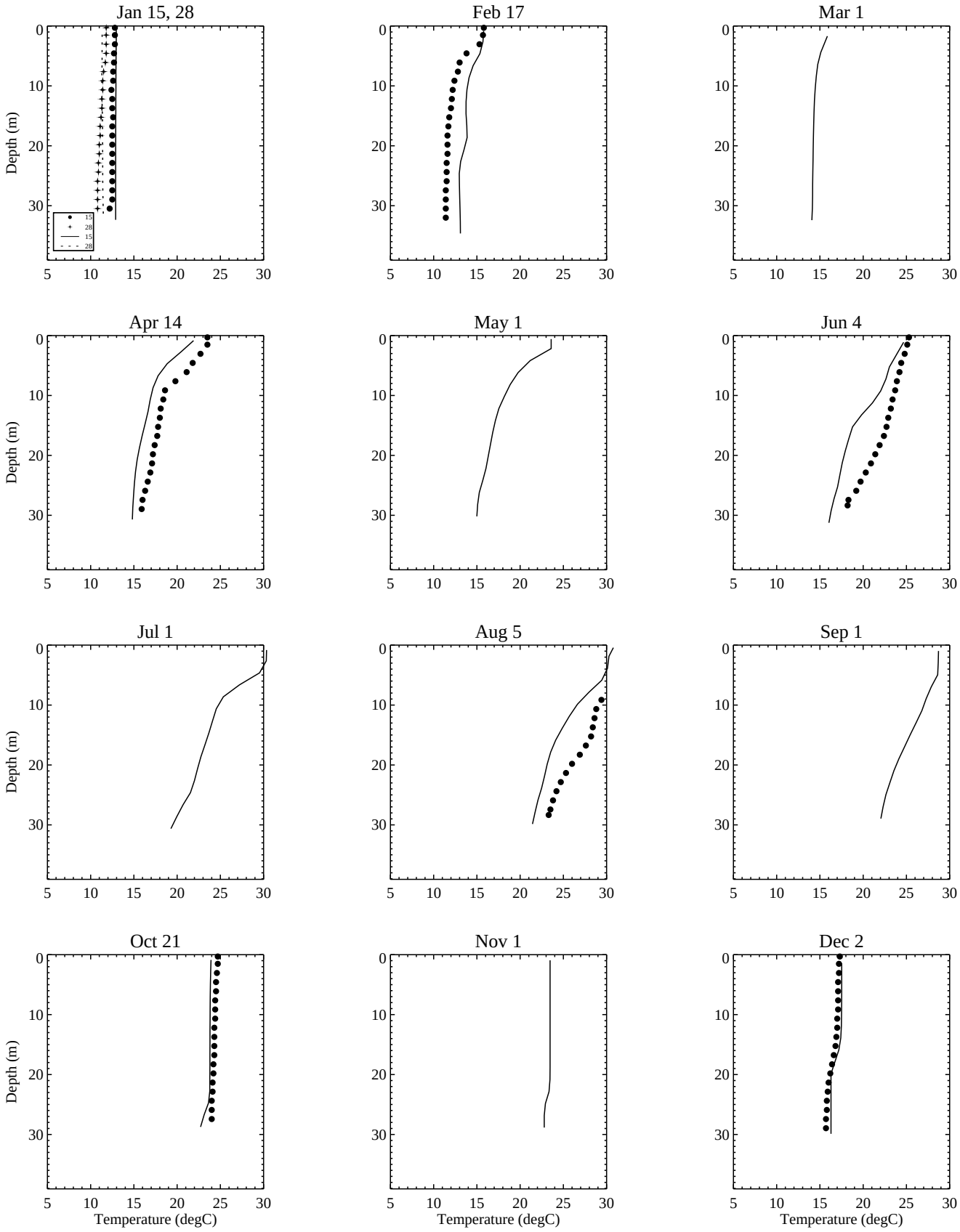

Figure J-3. Vertical profiles of model versus data at Pace Bend (Segment 48) - Temperature - 1992.

Profiles shown for dates with available data else model results for first day of month shown.

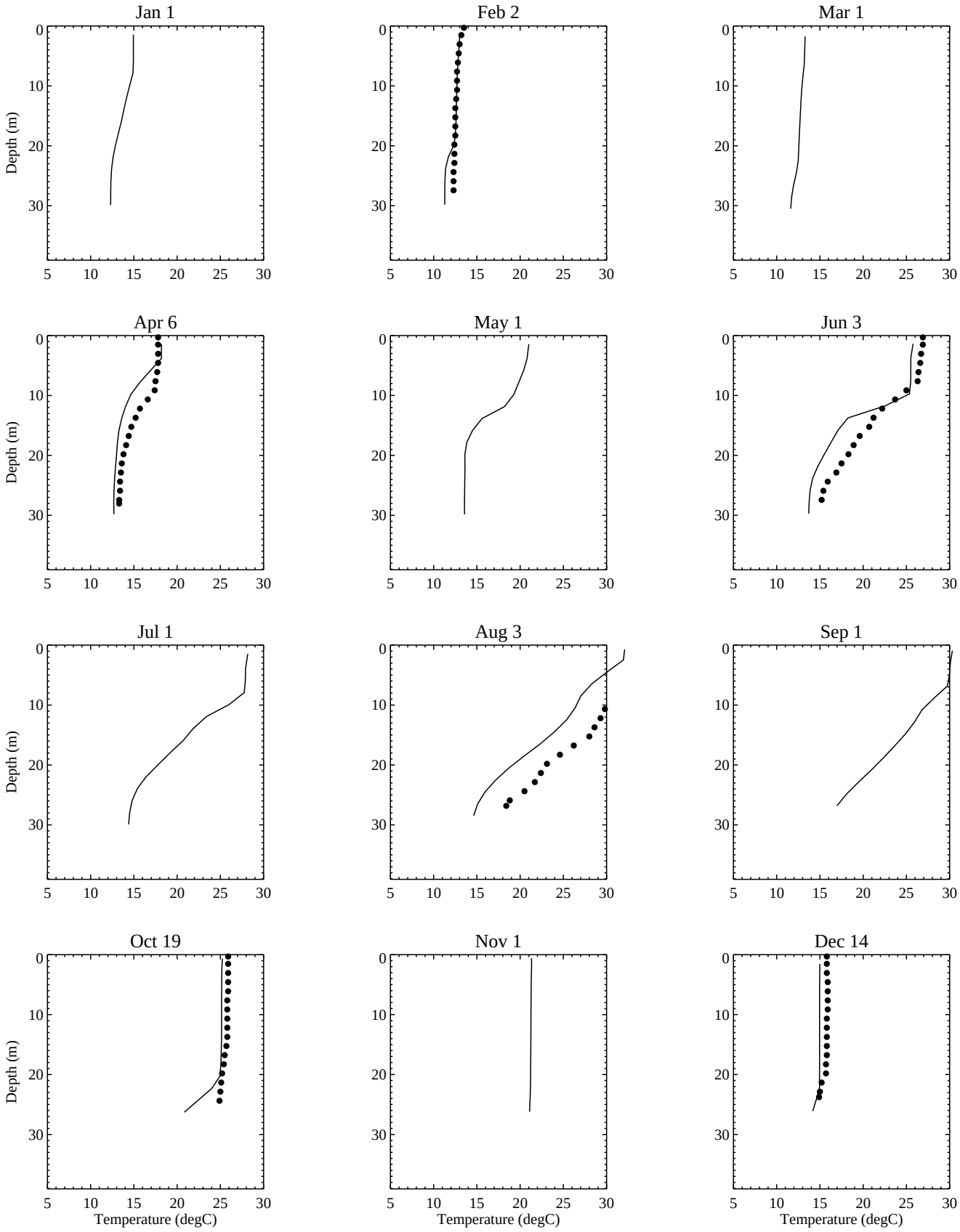

Figure J-3. Vertical profiles of model versus data at Pace Bend (Segment 48) - Temperature - 1993.

Profiles shown for dates with available data else model results for first day of month shown.

Model Data

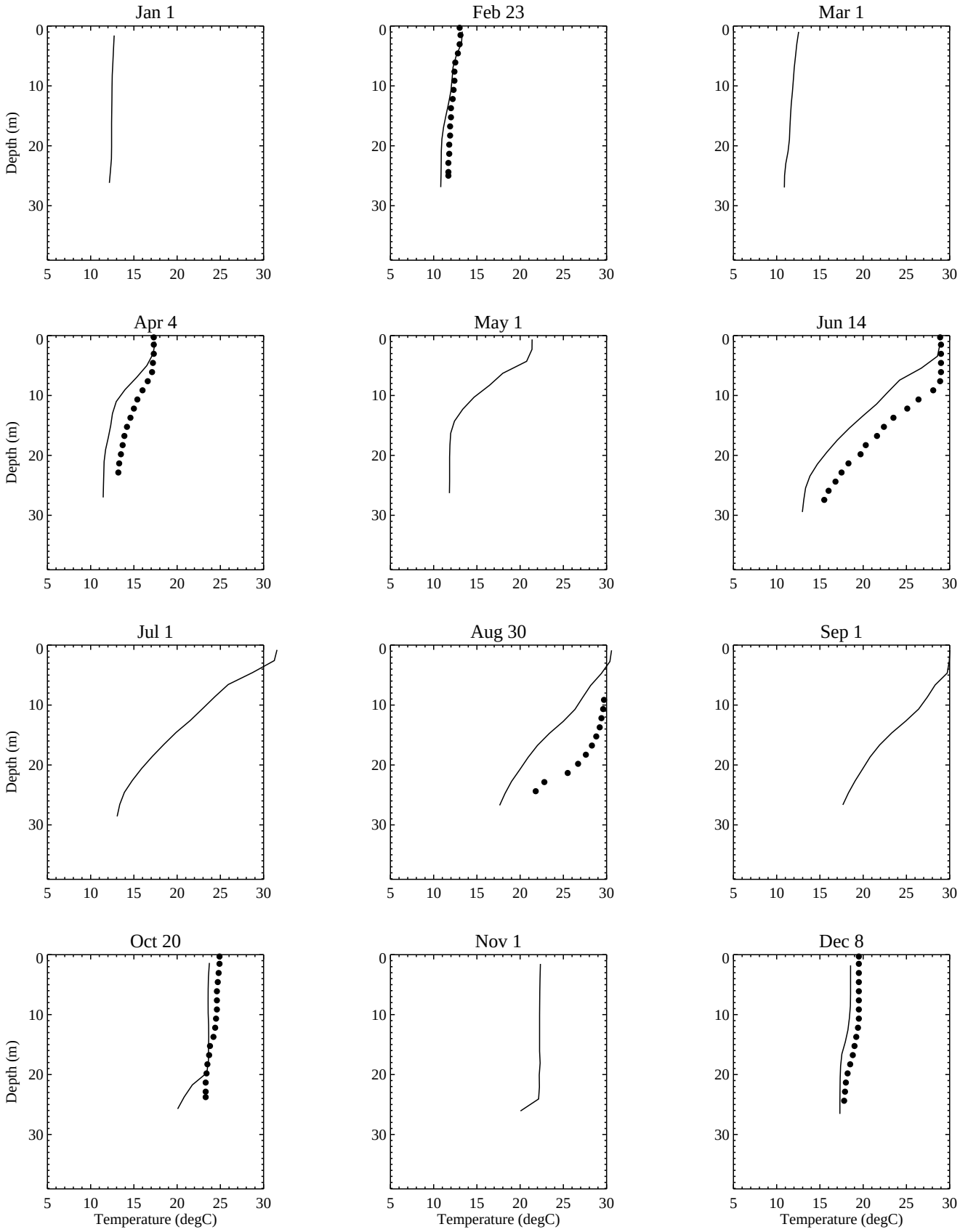

Figure J-3. Vertical profiles of model versus data at Pace Bend (Segment 48) - Temperature - 1994.

Profiles shown for dates with available data else model results for first day of month shown.

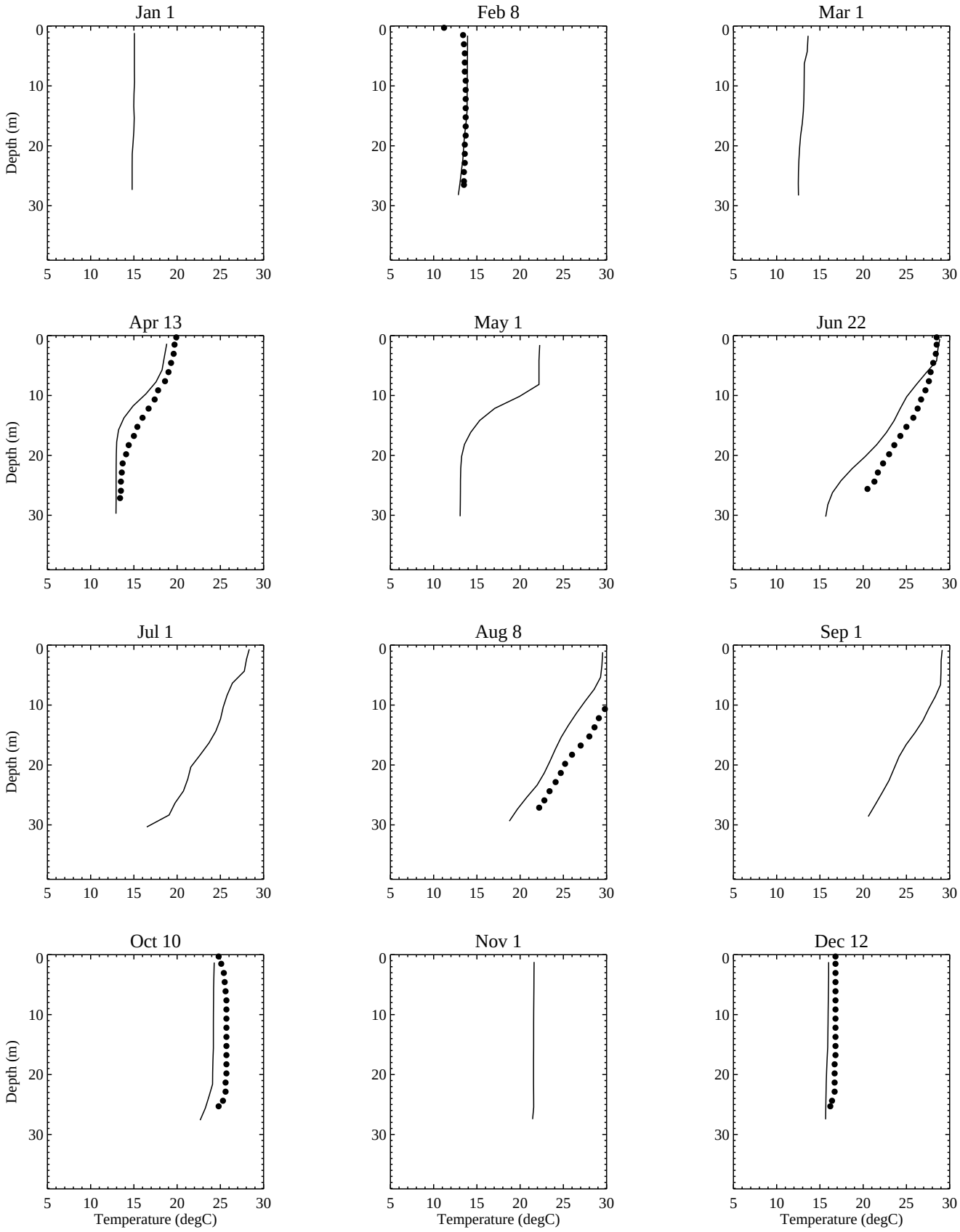

Figure J-3. Vertical profiles of model versus data at Pace Bend (Segment 48) - Temperature - 1995.

Profiles shown for dates with available data else model results for first day of month shown.

Model Data

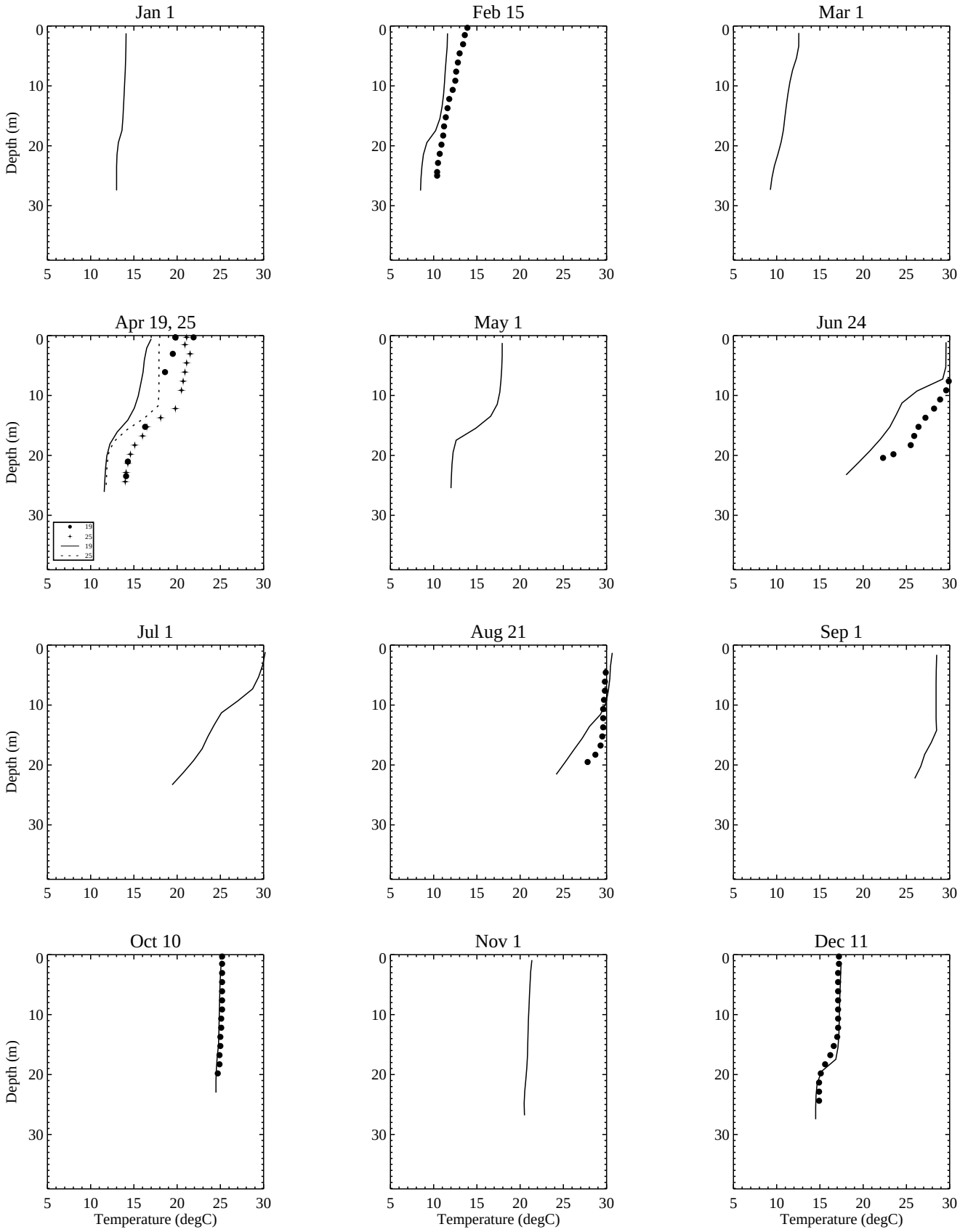

Figure J-3. Vertical profiles of model versus data at Pace Bend (Segment 48) - Temperature - 1996.

Profiles shown for dates with available data else model results for first day of month shown.

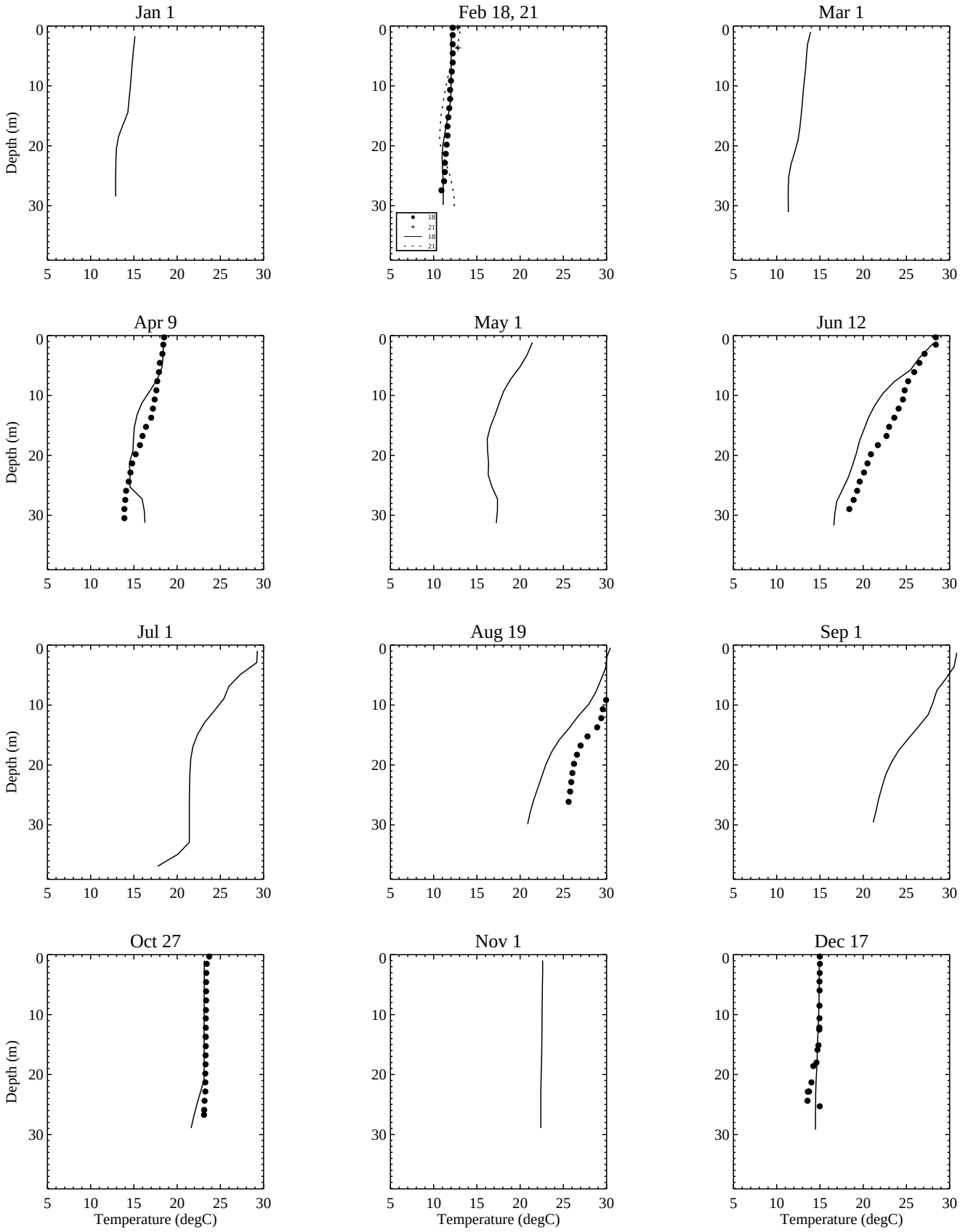

Figure J-3. Vertical profiles of model versus data at Pace Bend (Segment 48) - Temperature - 1997.

Profiles shown for dates with available data else model results for first day of month shown.

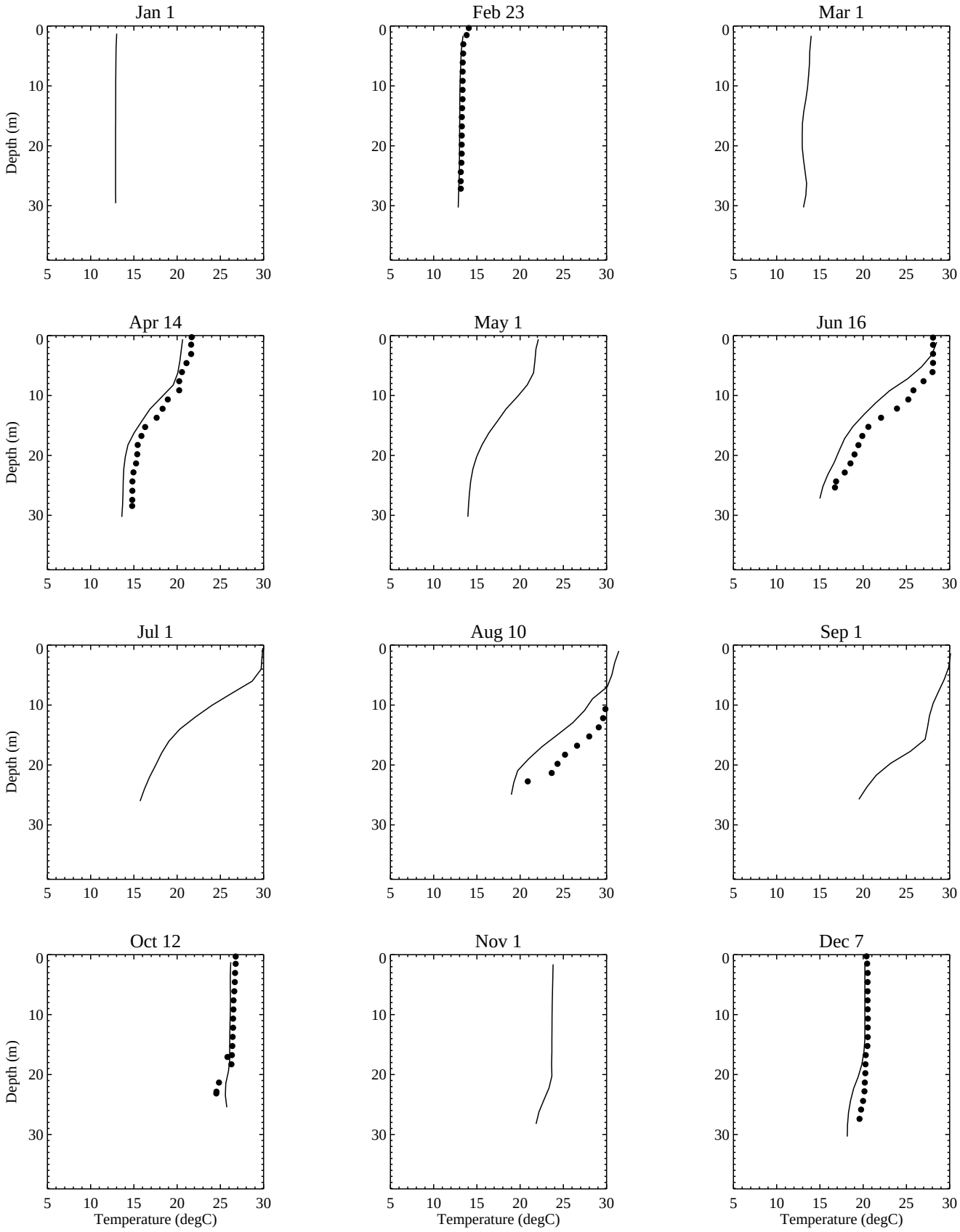

Figure J-3. Vertical profiles of model versus data at Pace Bend (Segment 48) - Temperature - 1998.

Profiles shown for dates with available data else model results for first day of month shown.

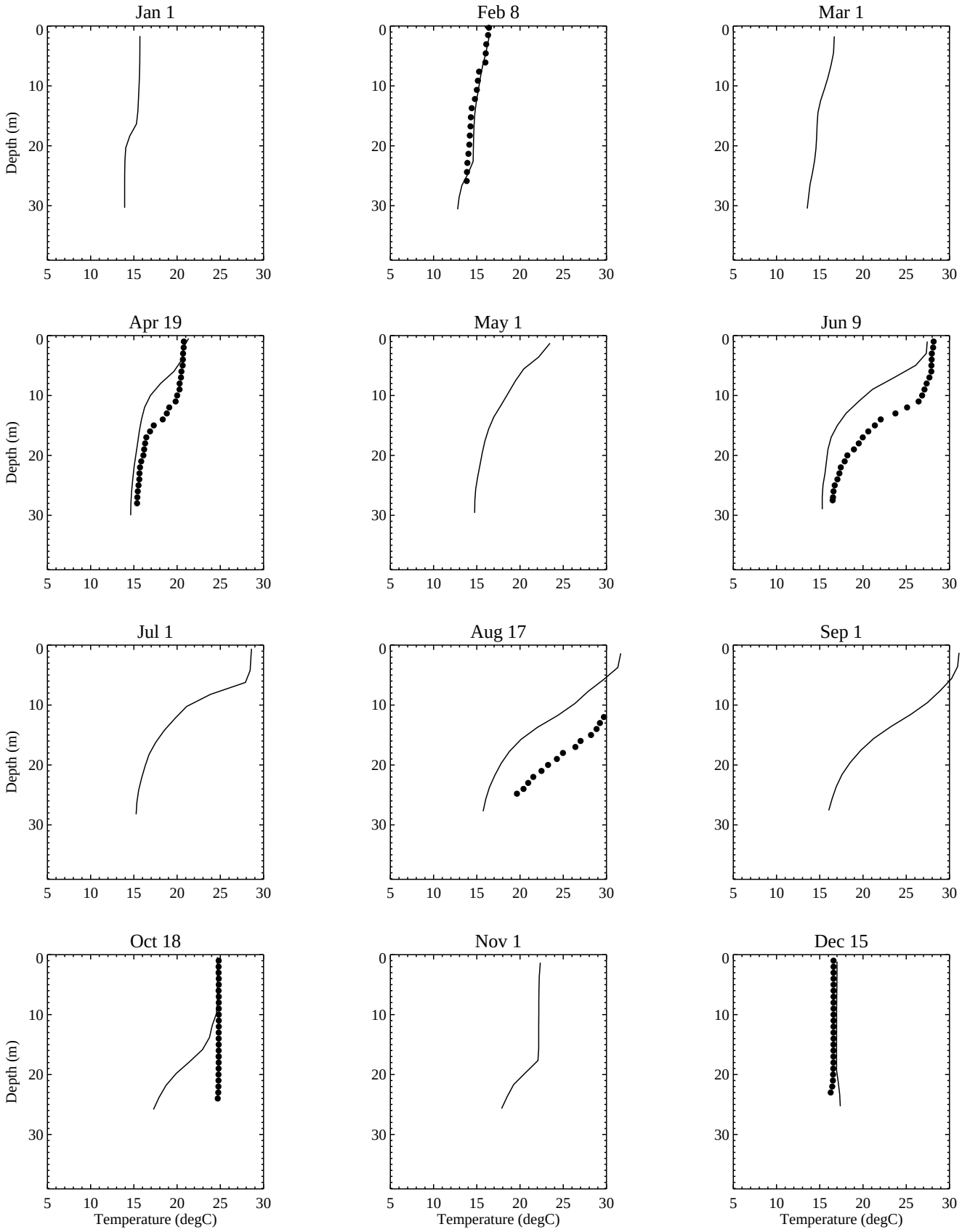

Figure J-3. Vertical profiles of model versus data at Pace Bend (Segment 48) - Temperature - 1999.

Profiles shown for dates with available data else model results for first day of month shown.

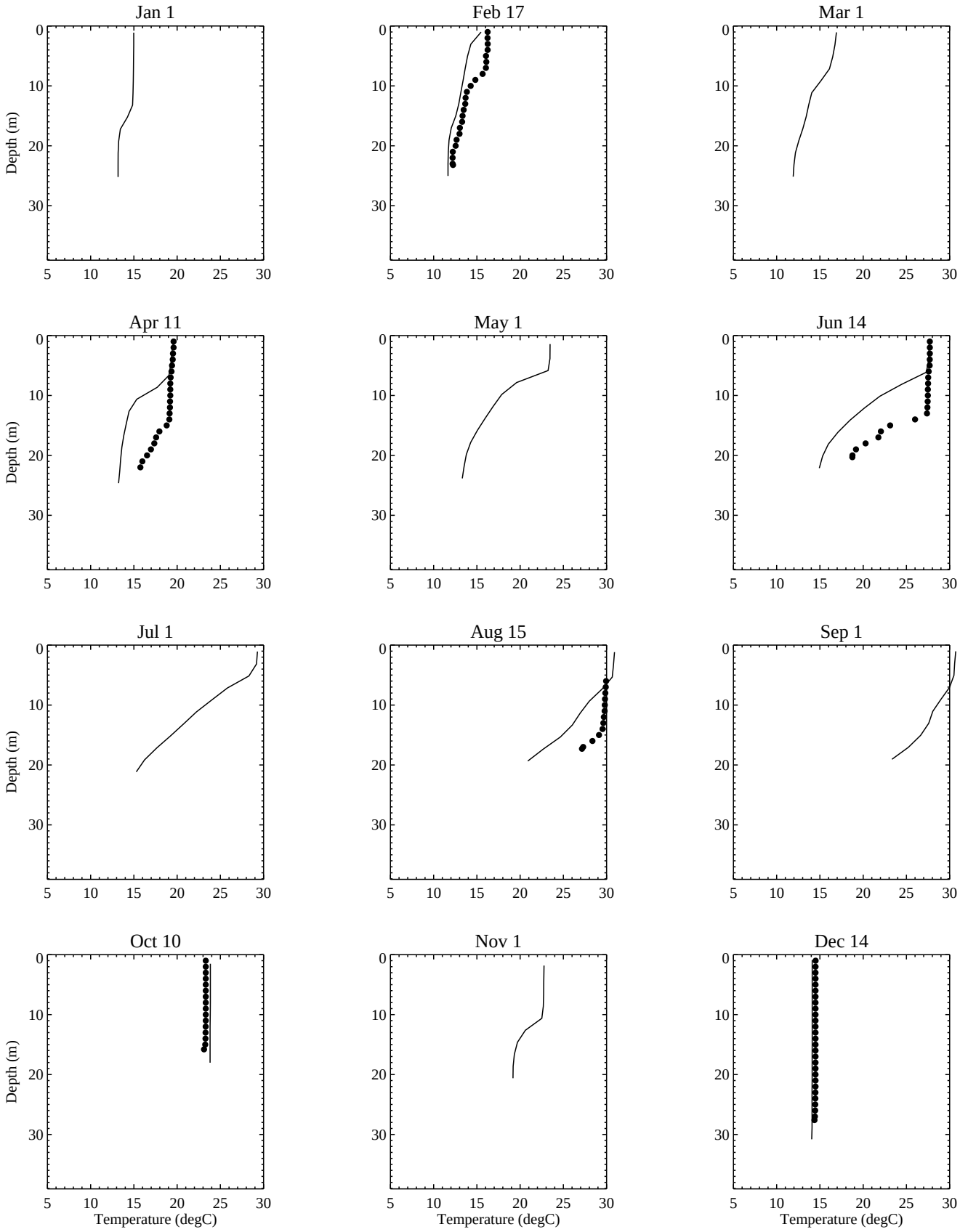

Figure J-3. Vertical profiles of model versus data at Pace Bend (Segment 48) - Temperature - 2000.

Profiles shown for dates with available data else model results for first day of month shown.

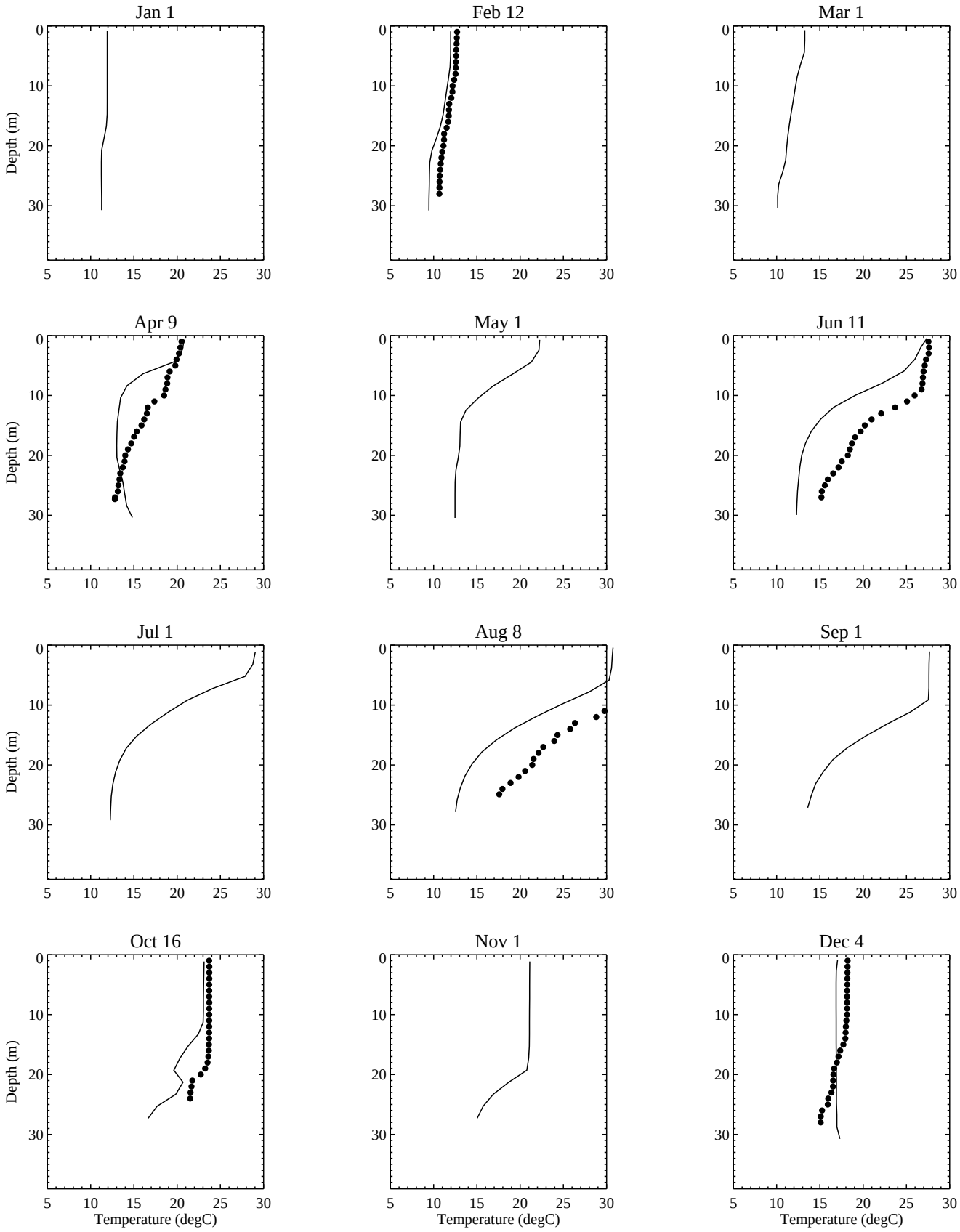

Figure J-3. Vertical profiles of model versus data at Pace Bend (Segment 48) - Temperature - 2001.

Profiles shown for dates with available data else model results for first day of month shown.

Model Data

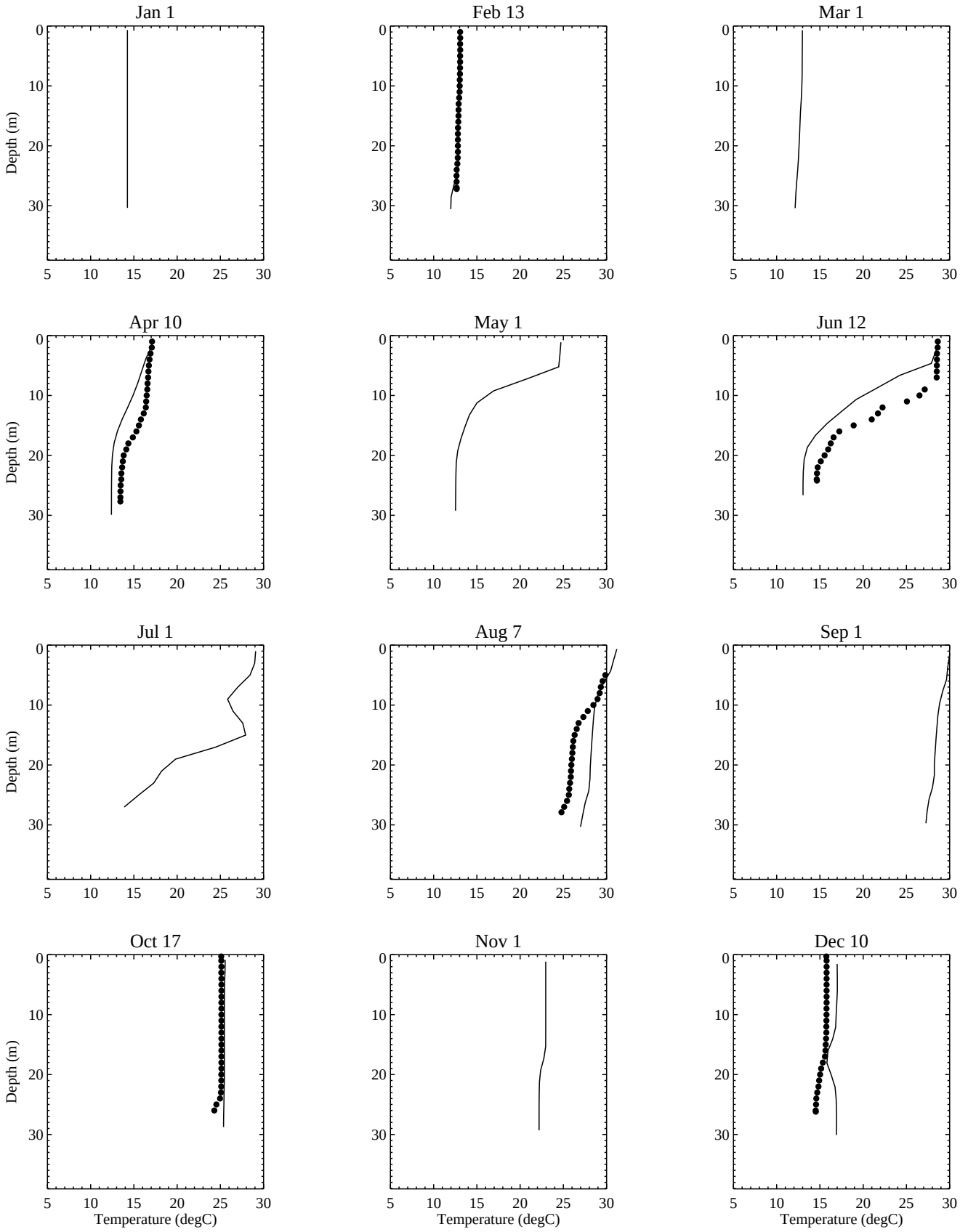

Figure J-3. Vertical profiles of model versus data at Pace Bend (Segment 48) - Temperature - 2002.

Profiles shown for dates with available data else model results for first day of month shown.

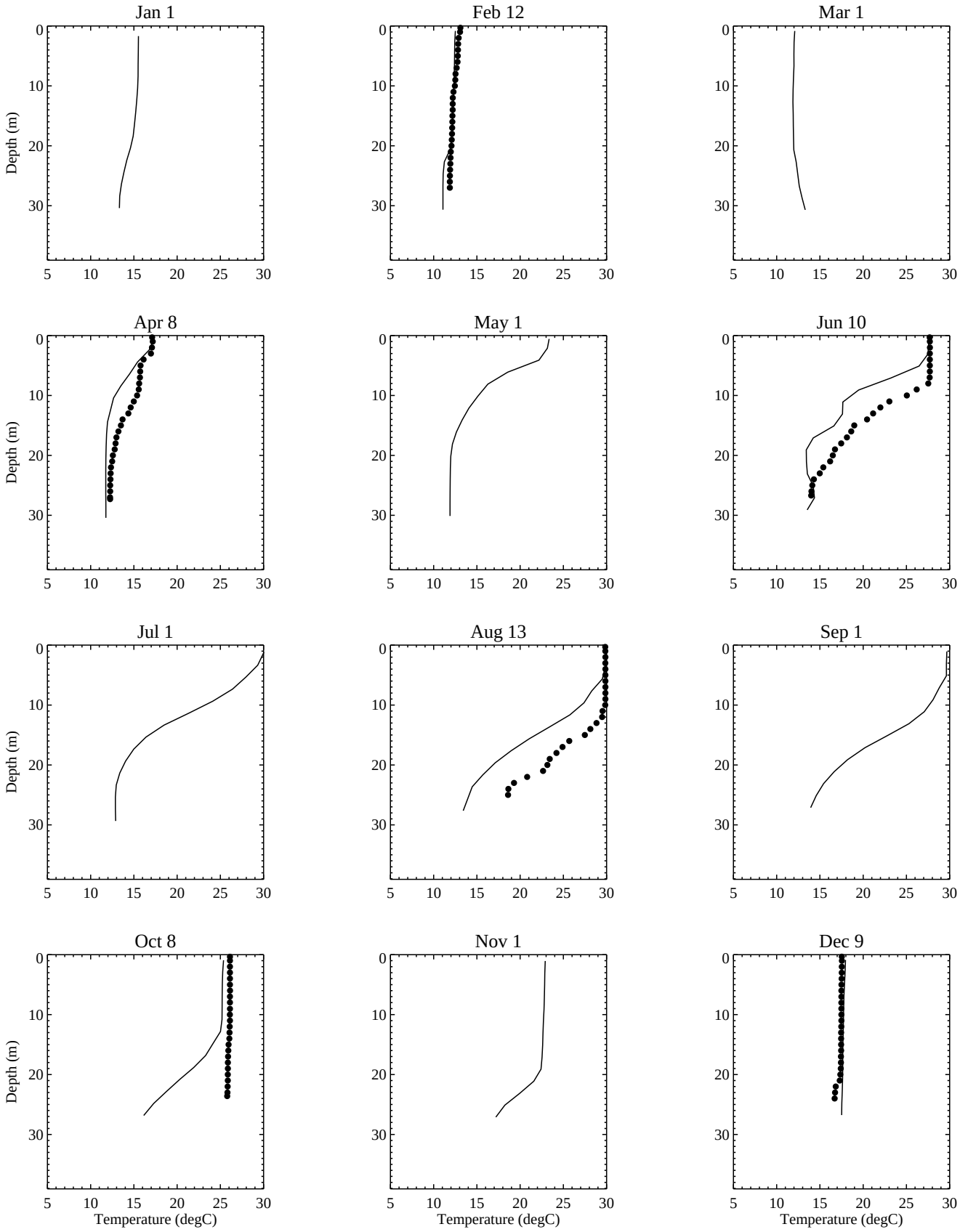

Figure J-3. Vertical profiles of model versus data at Pace Bend (Segment 48) - Temperature - 2003.

Profiles shown for dates with available data else model results for first day of month shown.

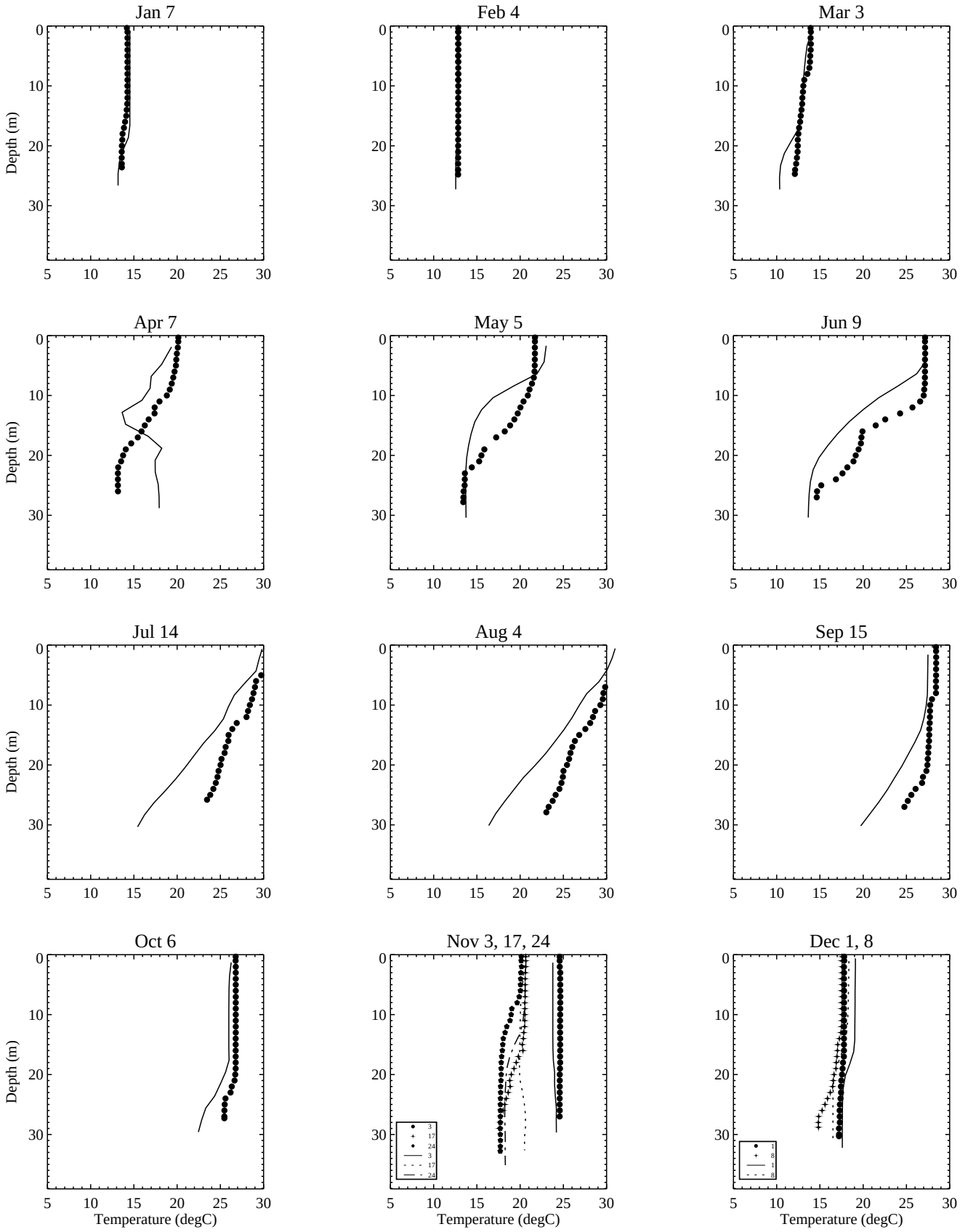

Figure J-3. Vertical profiles of model versus data at Pace Bend (Segment 48) - Temperature - 2004.

Profiles shown for dates with available data else model results for first day of month shown.

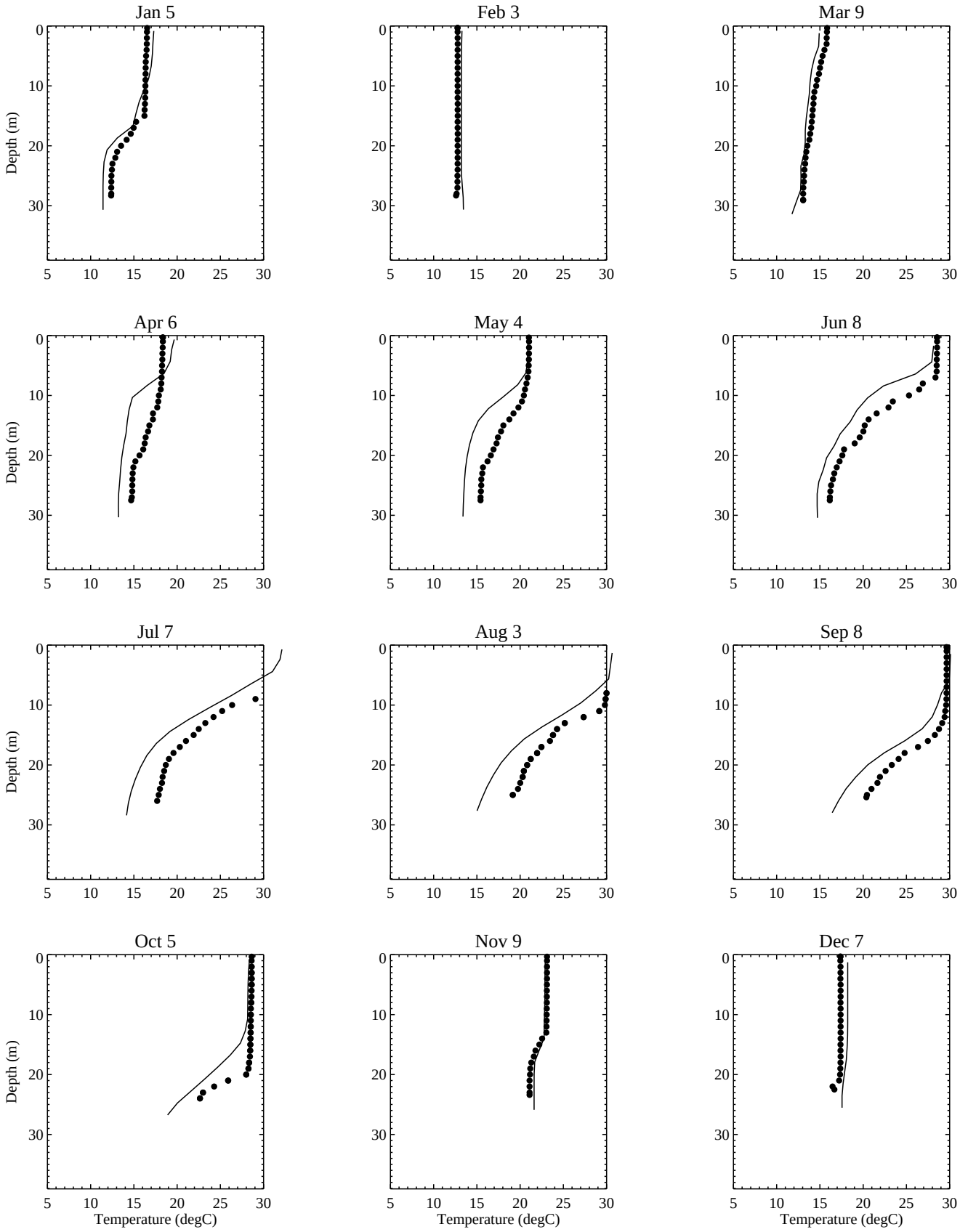

Figure J-3. Vertical profiles of model versus data at Pace Bend (Segment 48) - Temperature - 2005.

Profiles shown for dates with available data else model results for first day of month shown.

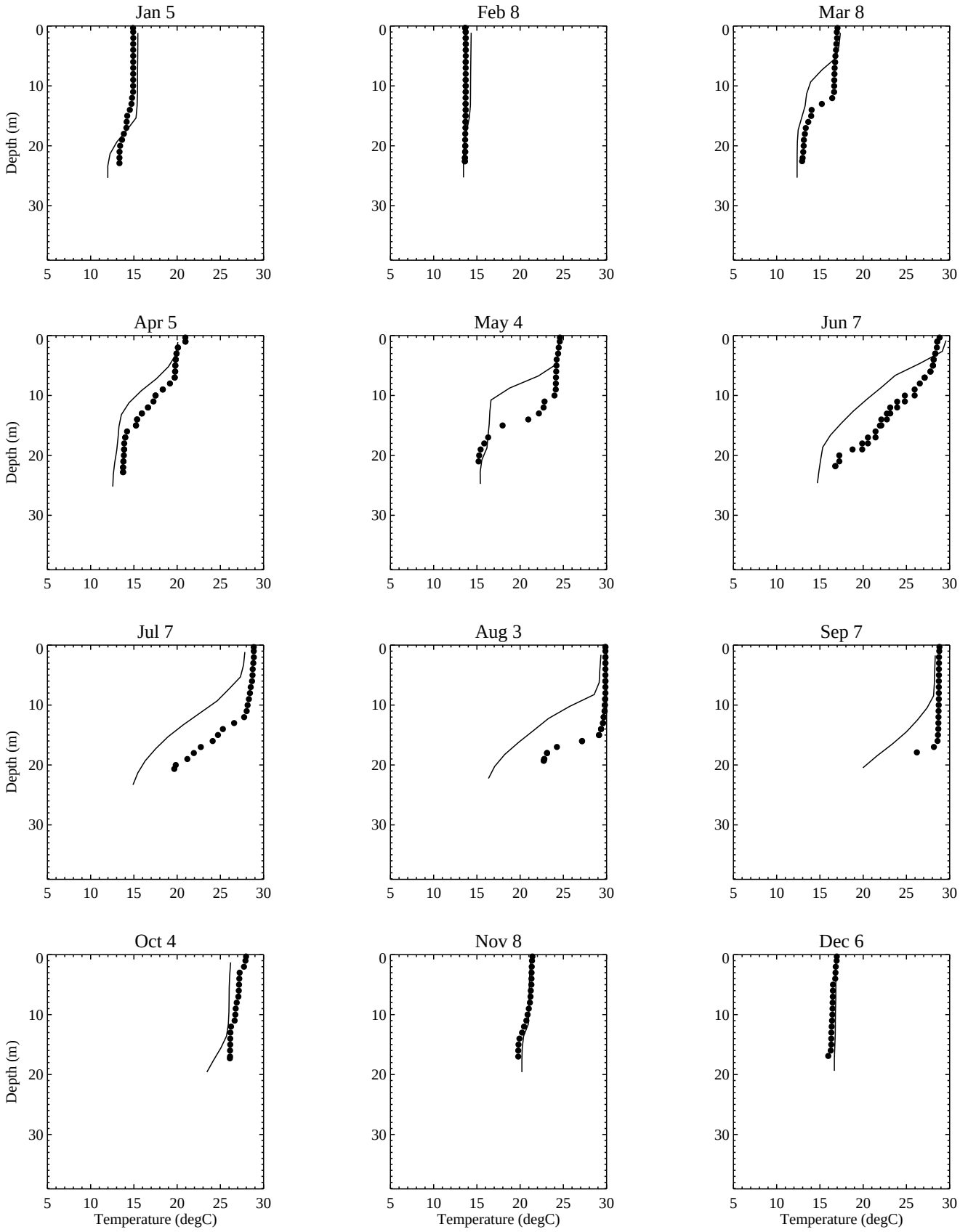

Figure J-3. Vertical profiles of model versus data at Pace Bend (Segment 48) - Temperature - 2006.

Profiles shown for dates with available data else model results for first day of month shown.

Model Data

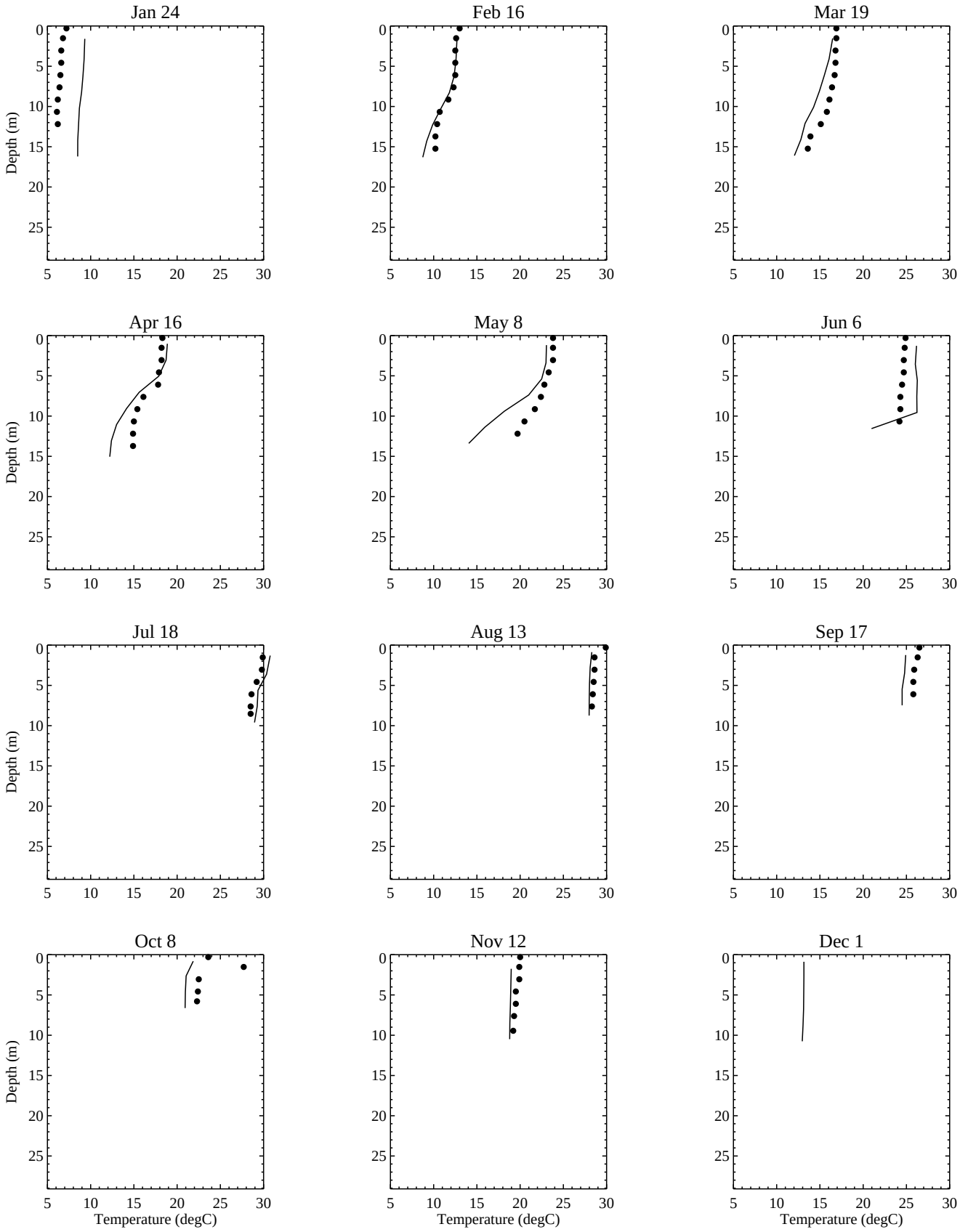

Figure J-4. Vertical profiles of model versus data at Turkey Bend (Segment 28) - Temperature - 1984.

Profiles shown for dates with available data else model results for first day of month shown.

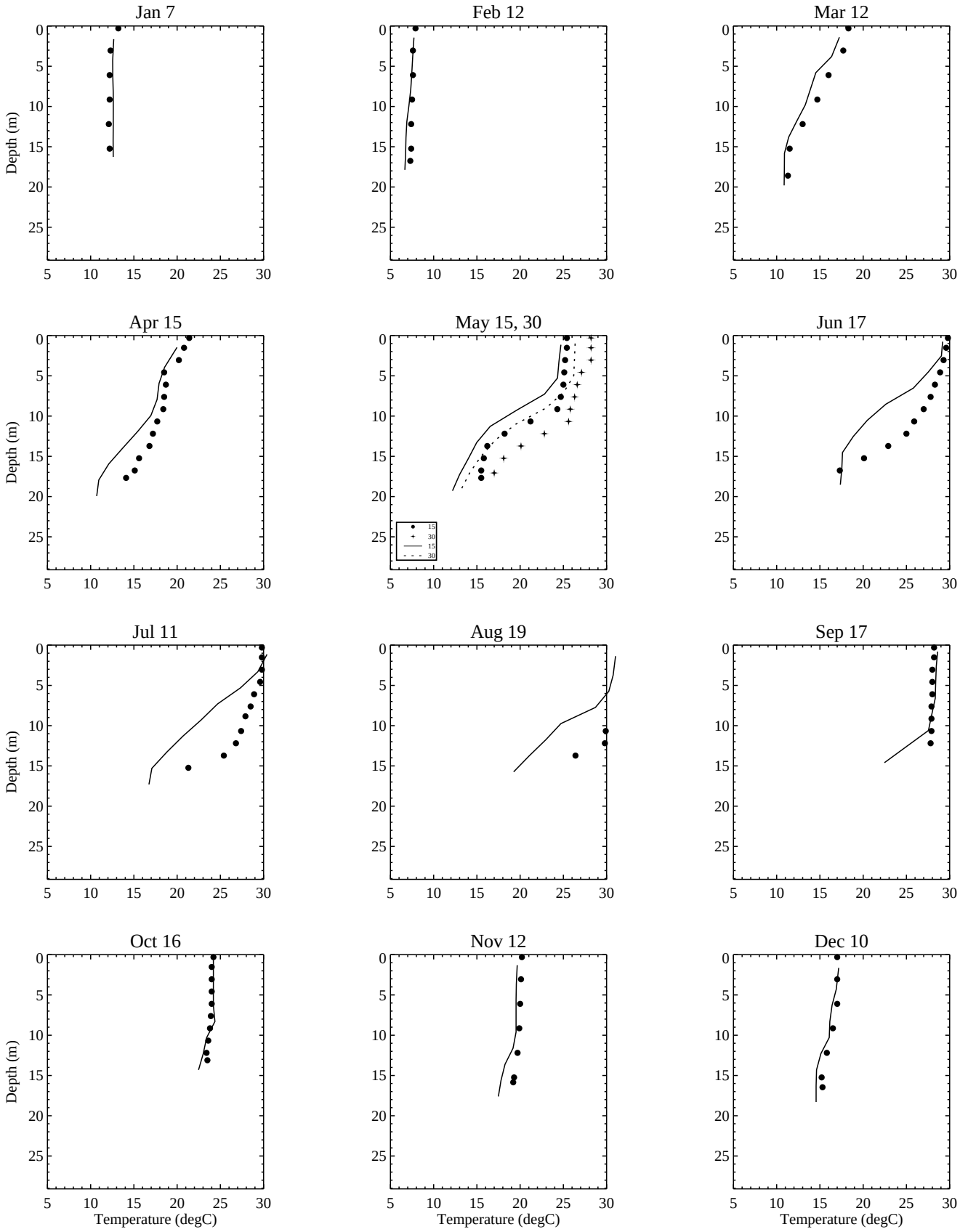

Figure J-4. Vertical profiles of model versus data at Turkey Bend (Segment 28) - Temperature - 1985.

Profiles shown for dates with available data else model results for first day of month shown.

Model Data

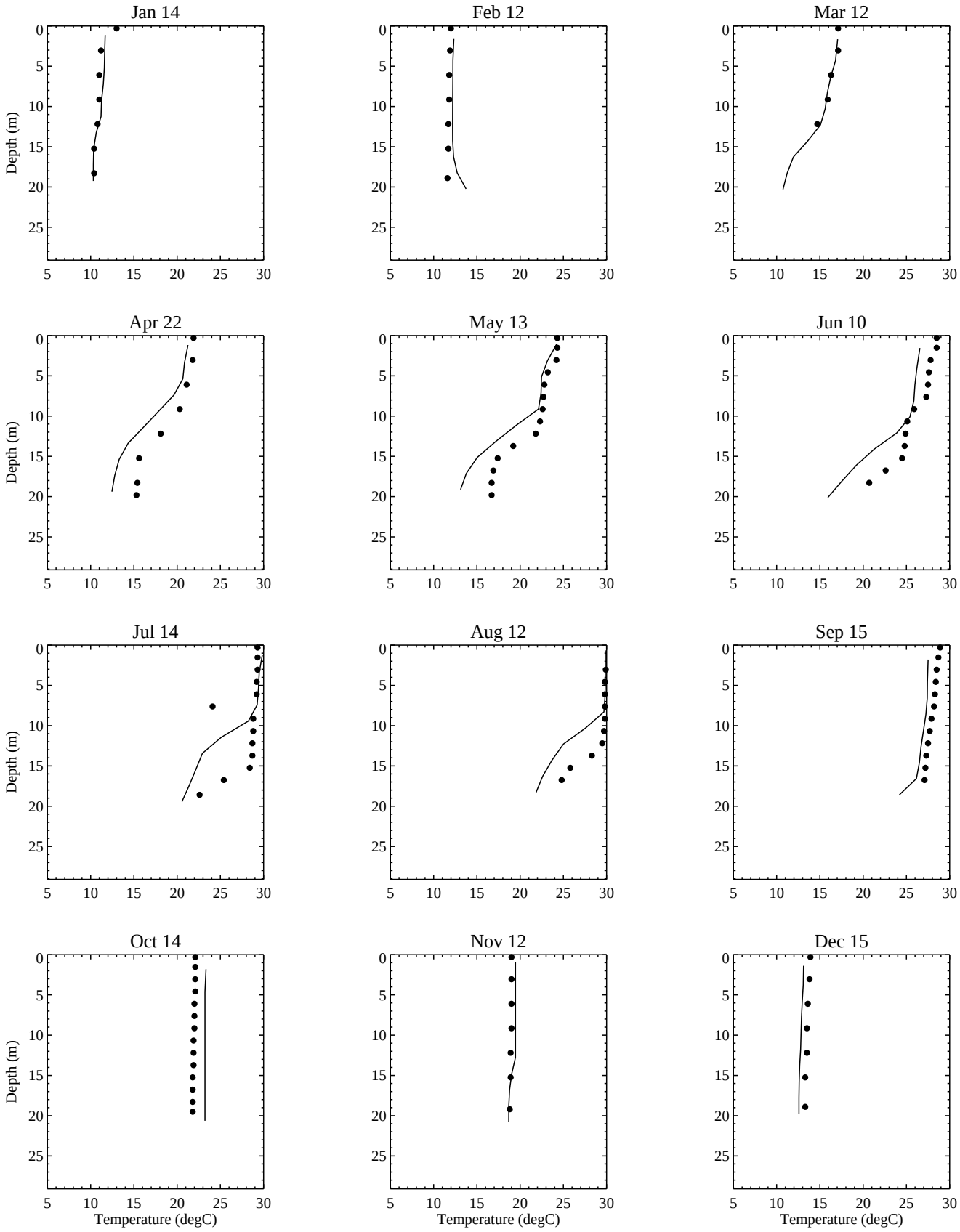

Figure J-4. Vertical profiles of model versus data at Turkey Bend (Segment 28) - Temperature - 1986.

Profiles shown for dates with available data else model results for first day of month shown.

Model Data

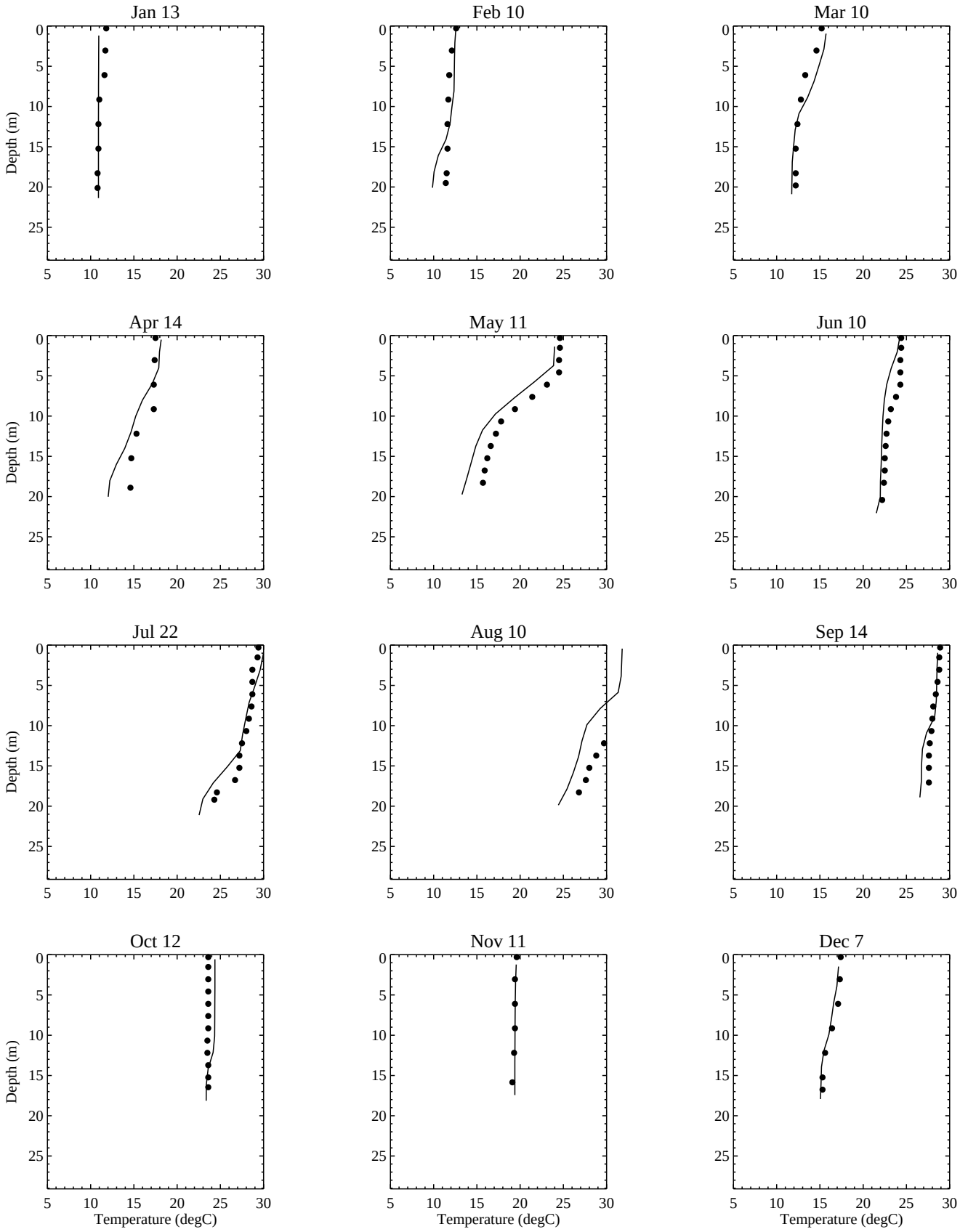

Figure J-4. Vertical profiles of model versus data at Turkey Bend (Segment 28) - Temperature - 1987.

Profiles shown for dates with available data else model results for first day of month shown.

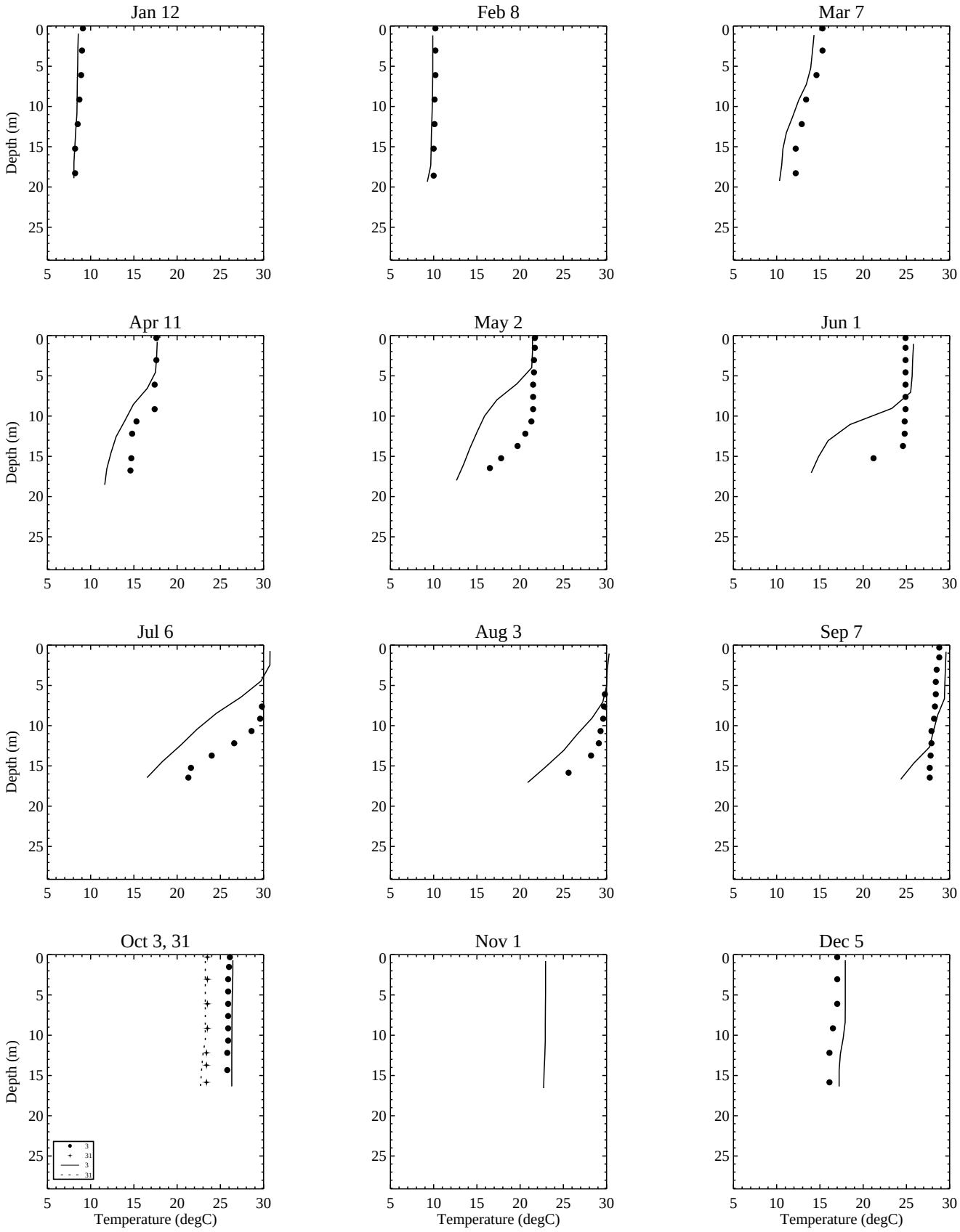

Figure J-4. Vertical profiles of model versus data at Turkey Bend (Segment 28) - Temperature - 1988.

Profiles shown for dates with available data else model results for first day of month shown.

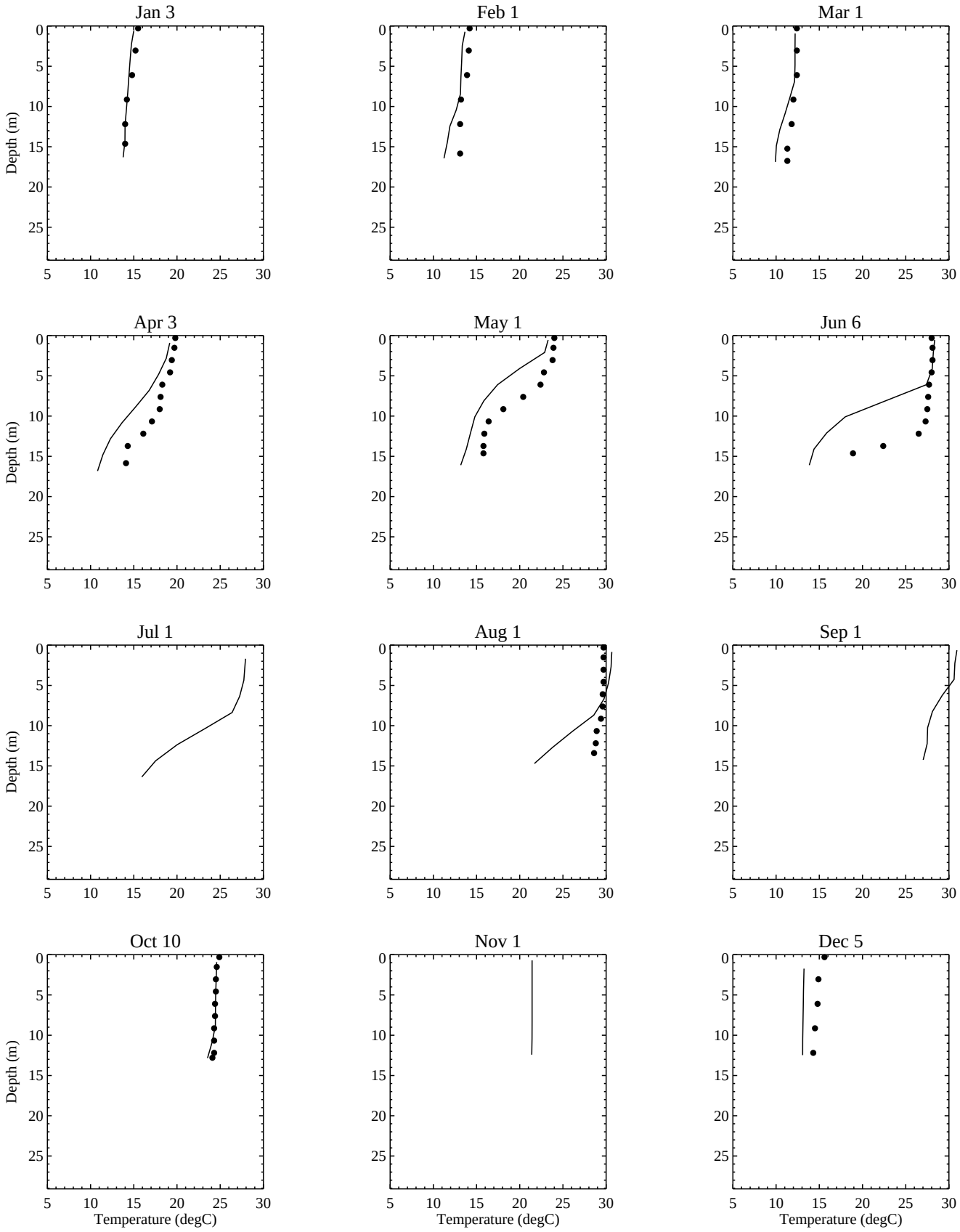

Figure J-4. Vertical profiles of model versus data at Turkey Bend (Segment 28) - Temperature - 1989.

Profiles shown for dates with available data else model results for first day of month shown.

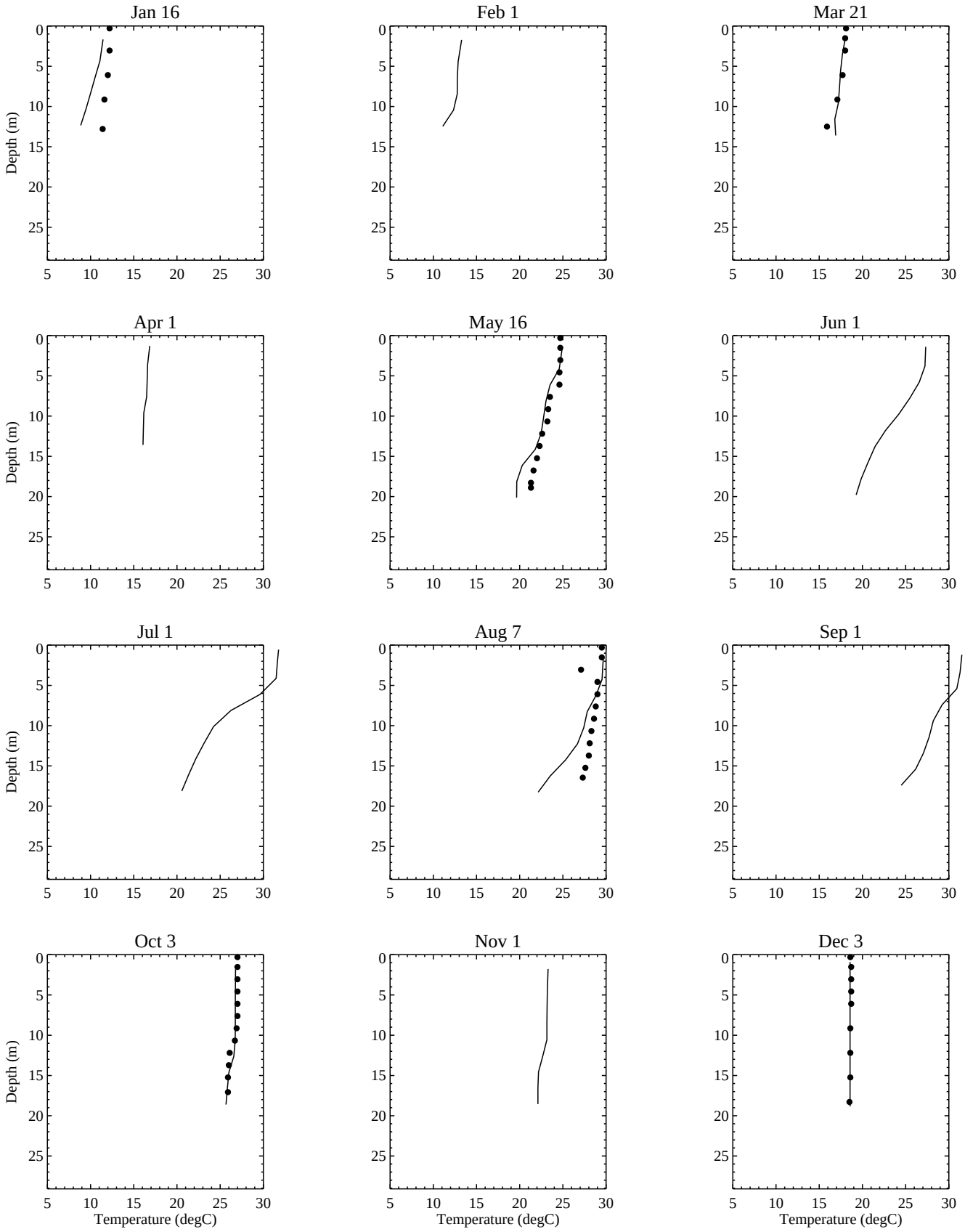

Figure J-4. Vertical profiles of model versus data at Turkey Bend (Segment 28) - Temperature - 1990.

Profiles shown for dates with available data else model results for first day of month shown.

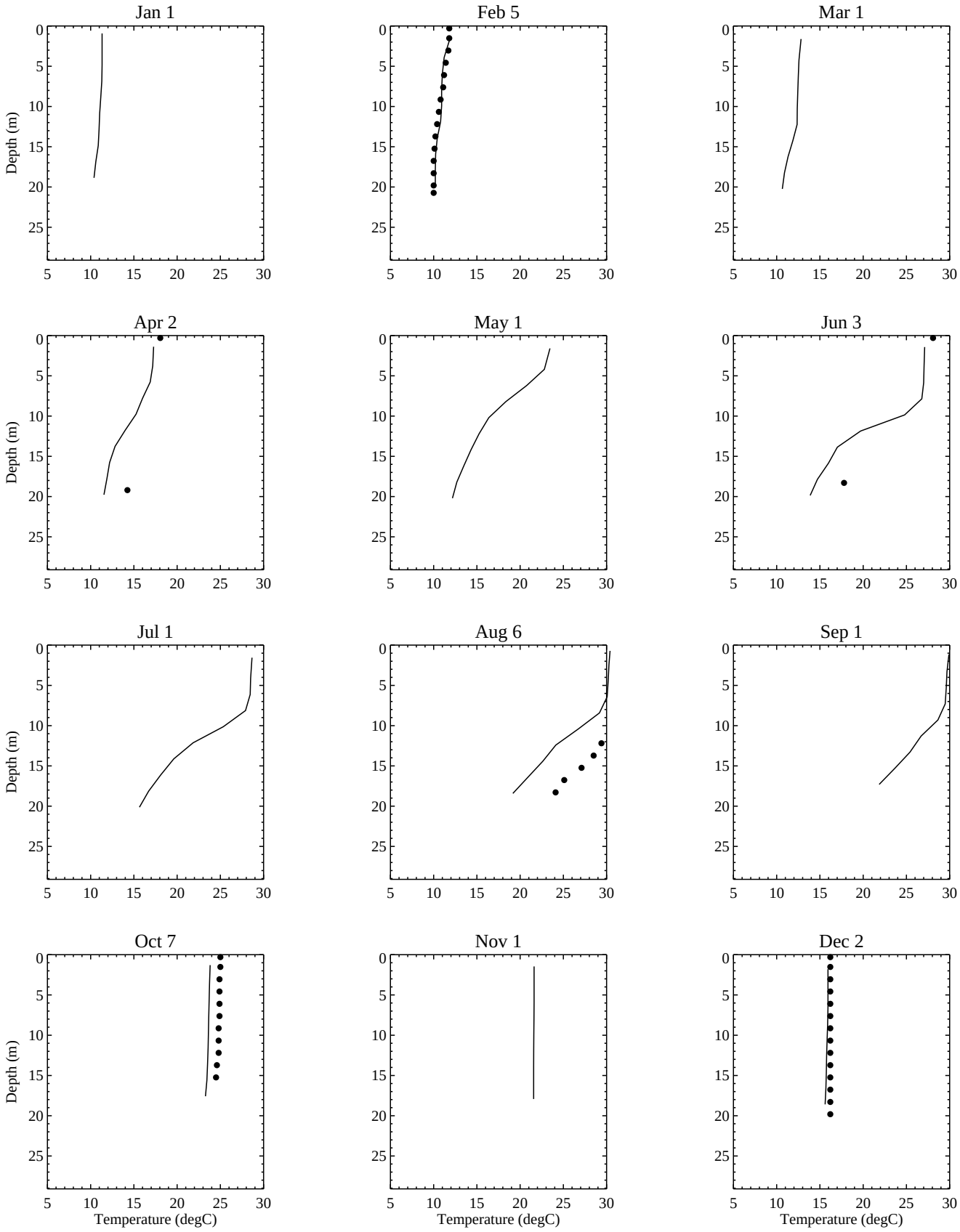

Figure J-4. Vertical profiles of model versus data at Turkey Bend (Segment 28) - Temperature - 1991.

Profiles shown for dates with available data else model results for first day of month shown.

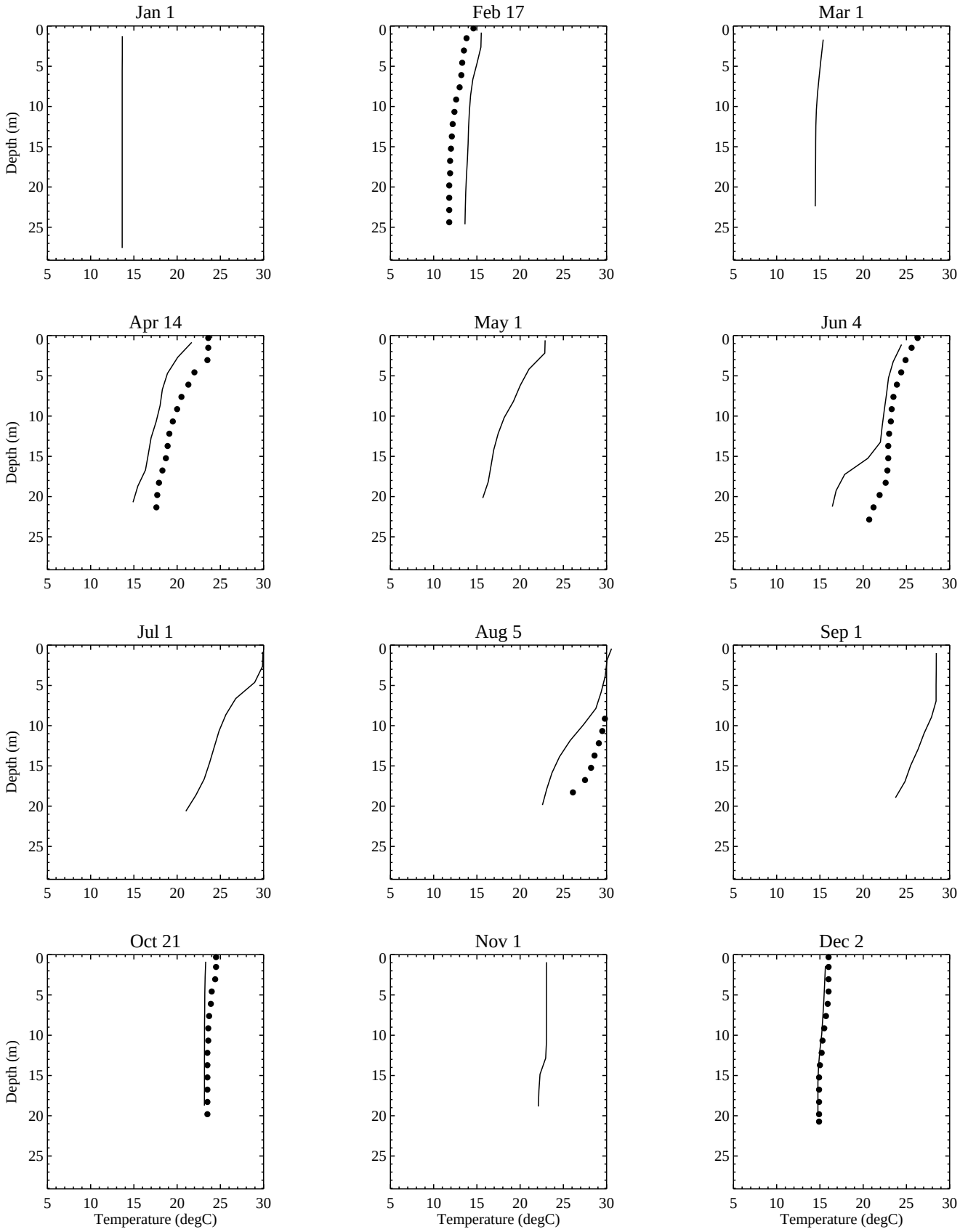

Figure J-4. Vertical profiles of model versus data at Turkey Bend (Segment 28) - Temperature - 1992.

Profiles shown for dates with available data else model results for first day of month shown.

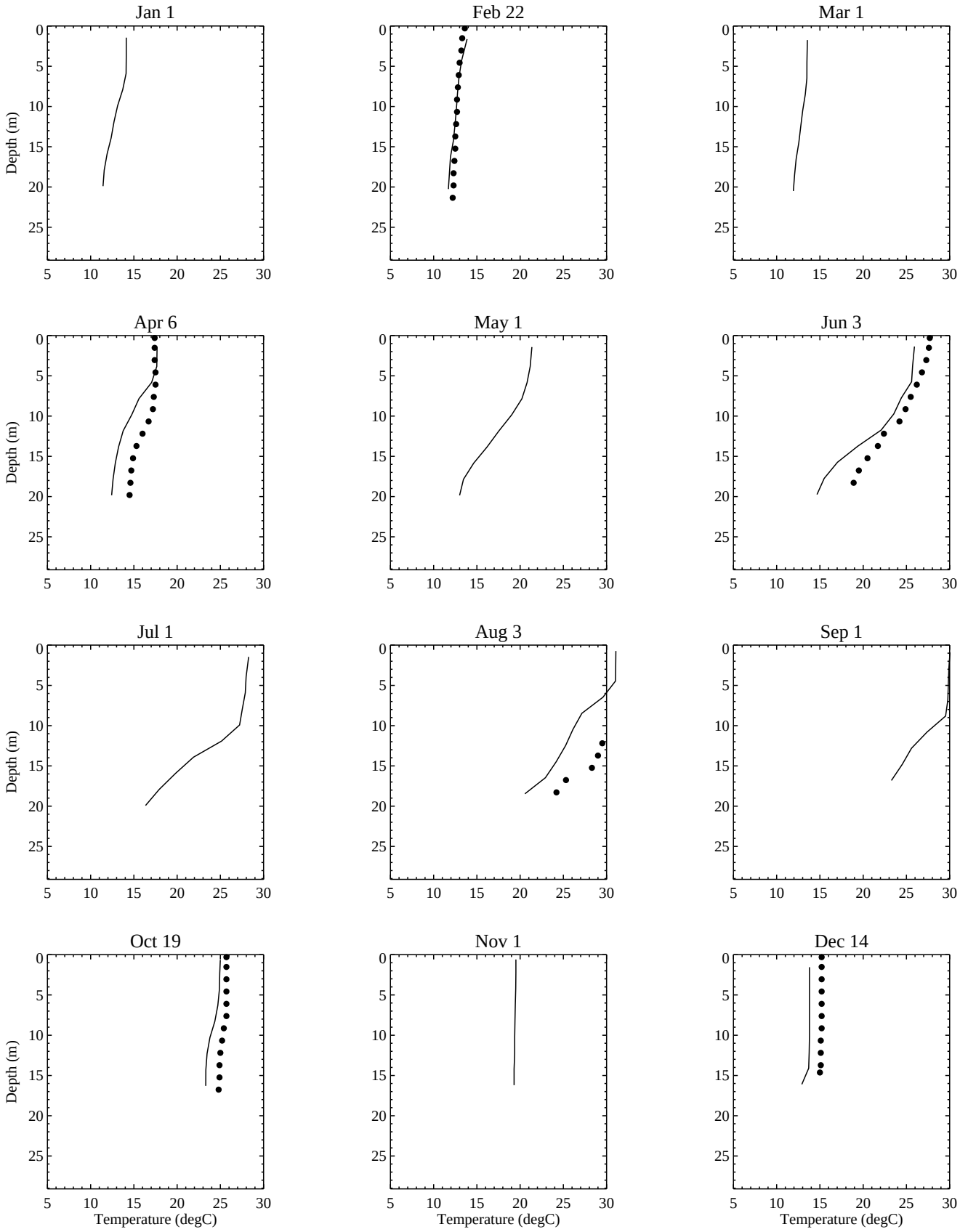

Figure J-4. Vertical profiles of model versus data at Turkey Bend (Segment 28) - Temperature - 1993.

Profiles shown for dates with available data else model results for first day of month shown.

Model Data

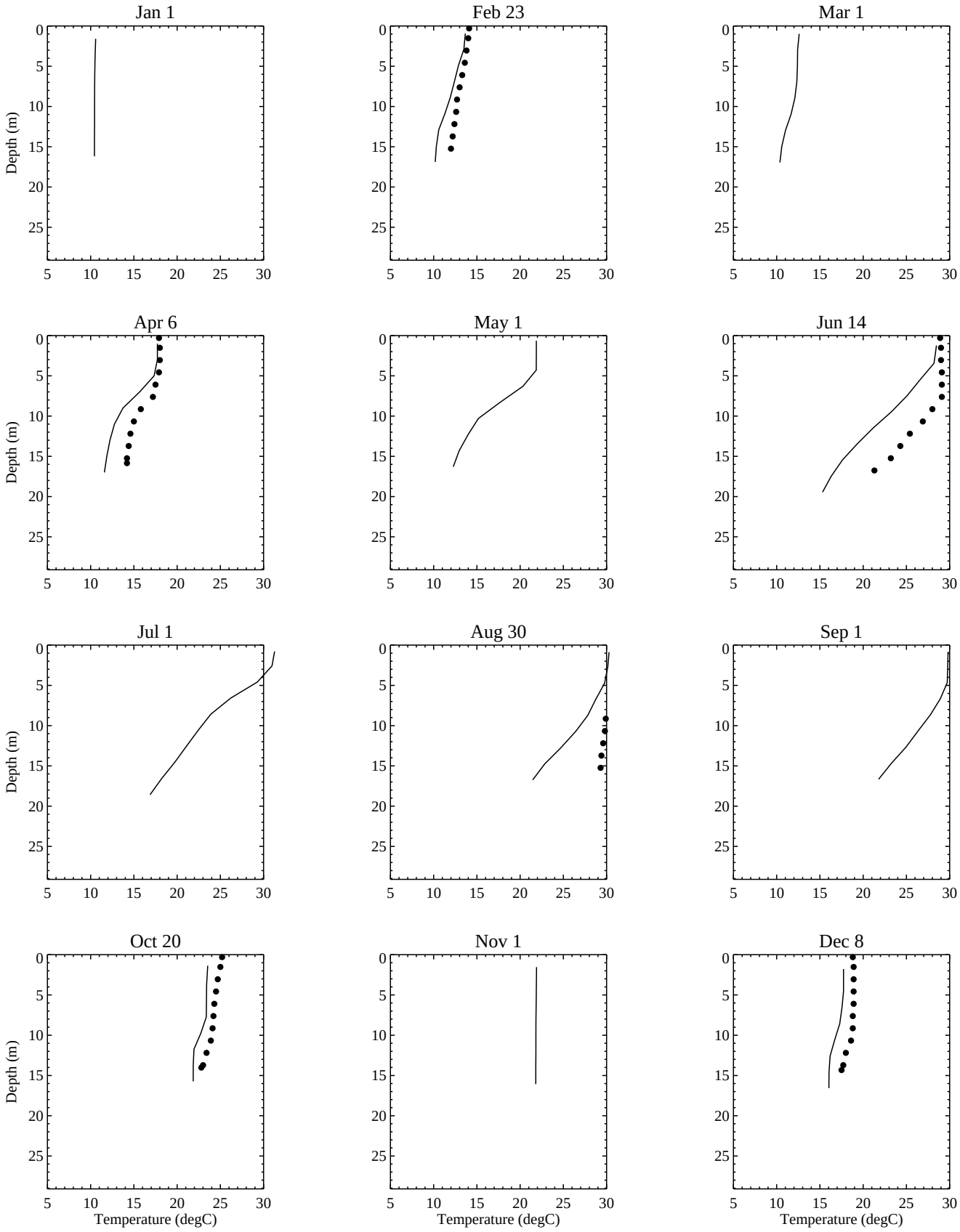

Figure J-4. Vertical profiles of model versus data at Turkey Bend (Segment 28) - Temperature - 1994.

Profiles shown for dates with available data else model results for first day of month shown.

Model Data

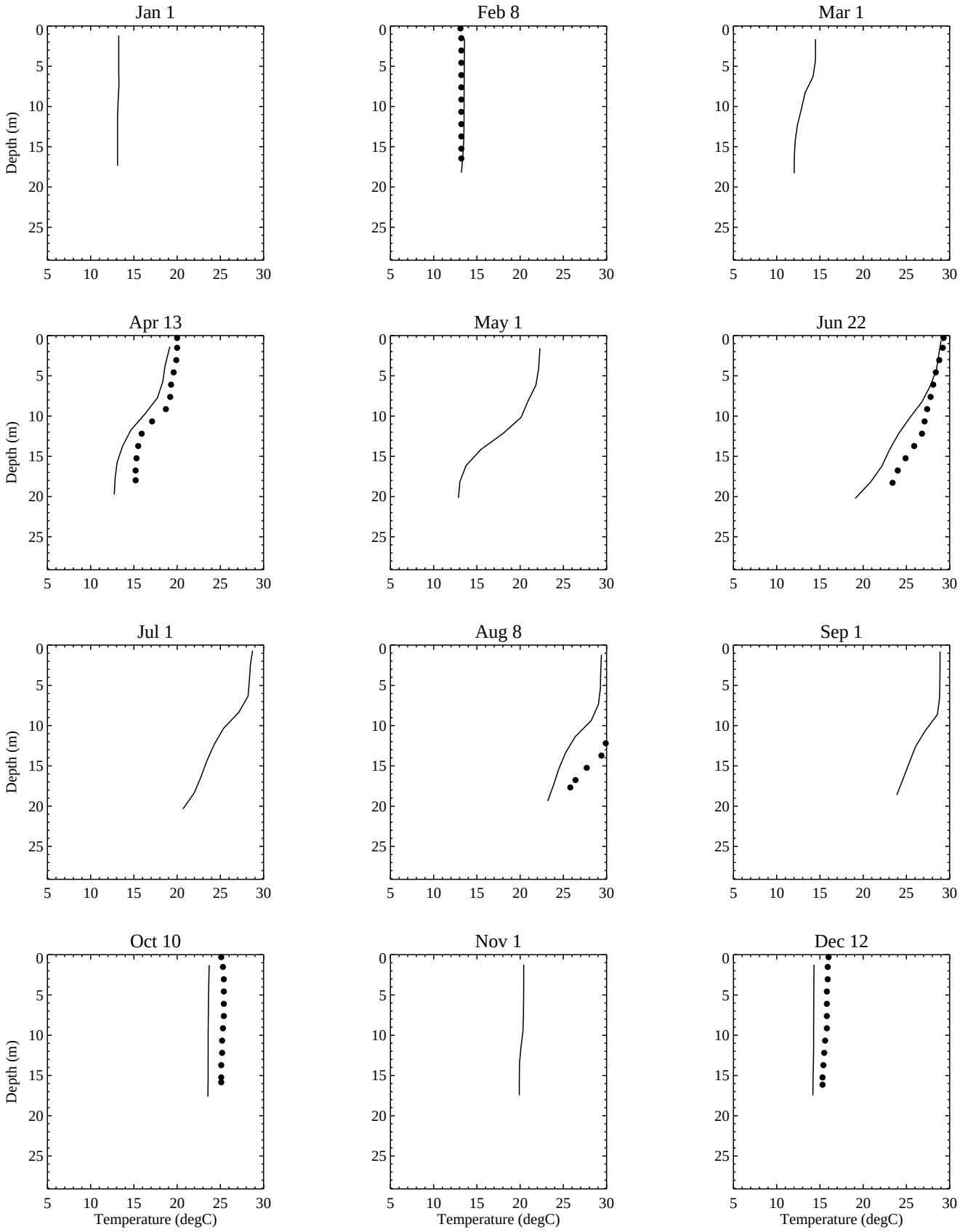

Figure J-4. Vertical profiles of model versus data at Turkey Bend (Segment 28) - Temperature - 1995.

Profiles shown for dates with available data else model results for first day of month shown.

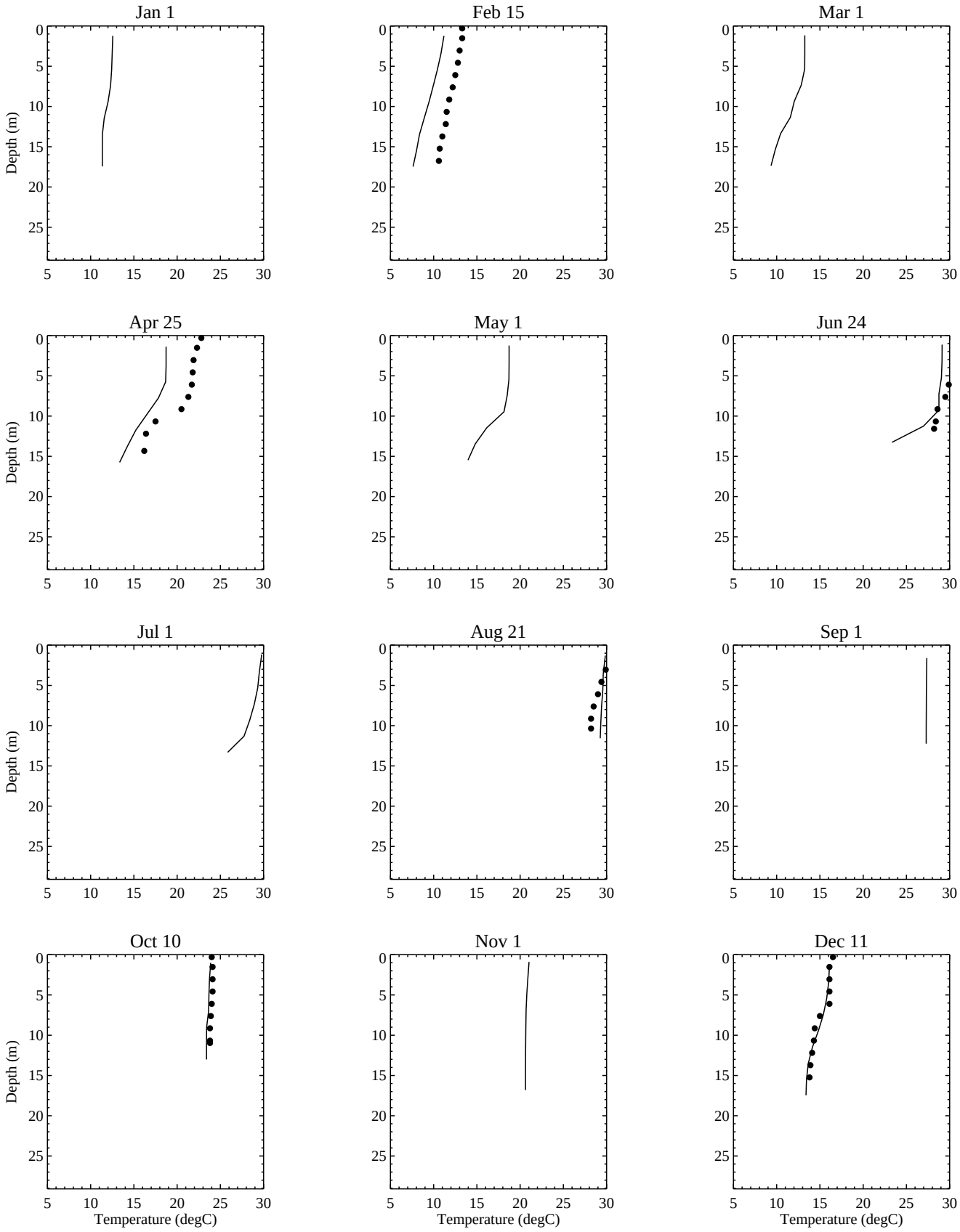

Figure J-4. Vertical profiles of model versus data at Turkey Bend (Segment 28) - Temperature - 1996.

Profiles shown for dates with available data else model results for first day of month shown.

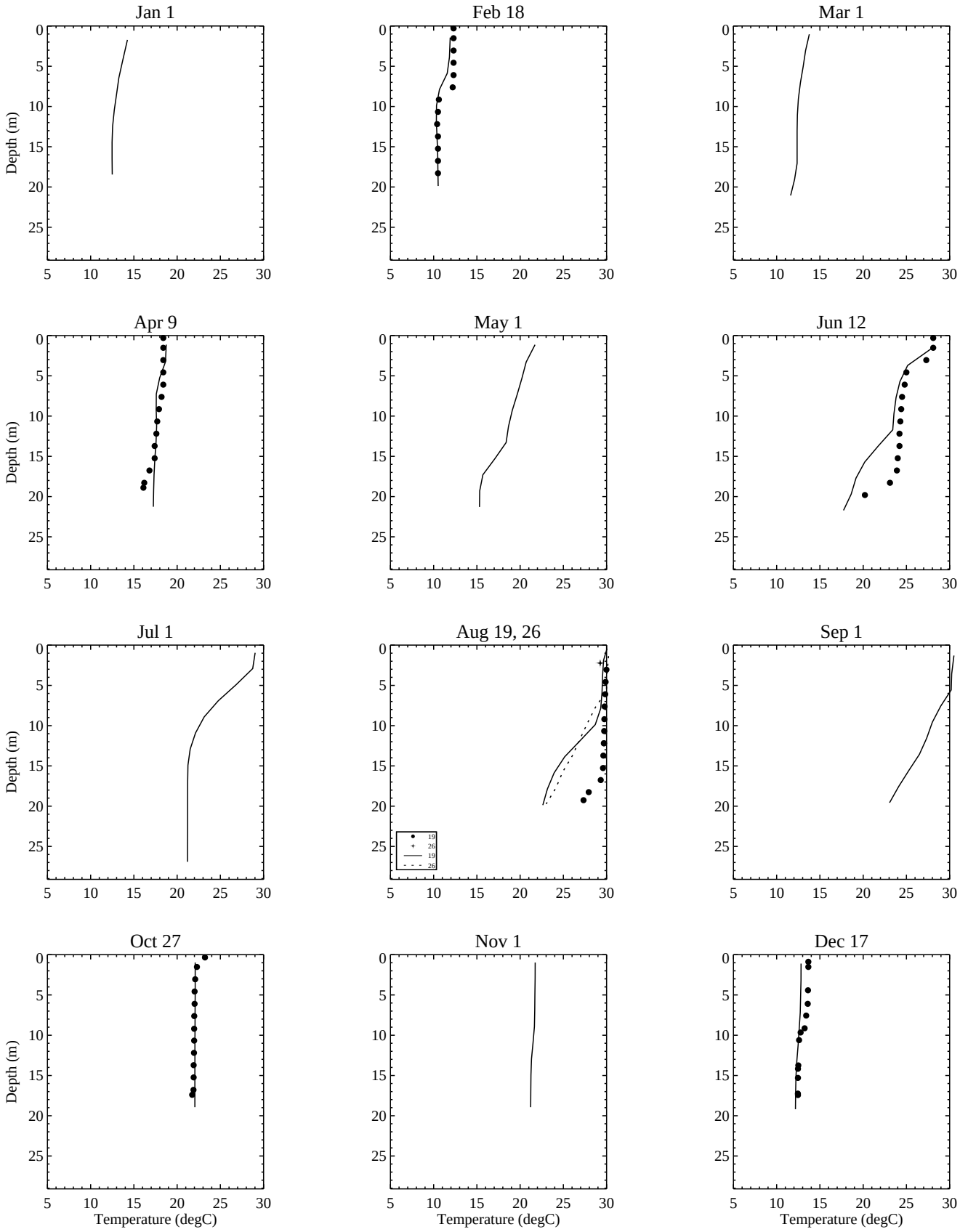

Figure J-4. Vertical profiles of model versus data at Turkey Bend (Segment 28) - Temperature - 1997.

Profiles shown for dates with available data else model results for first day of month shown.

Model Data

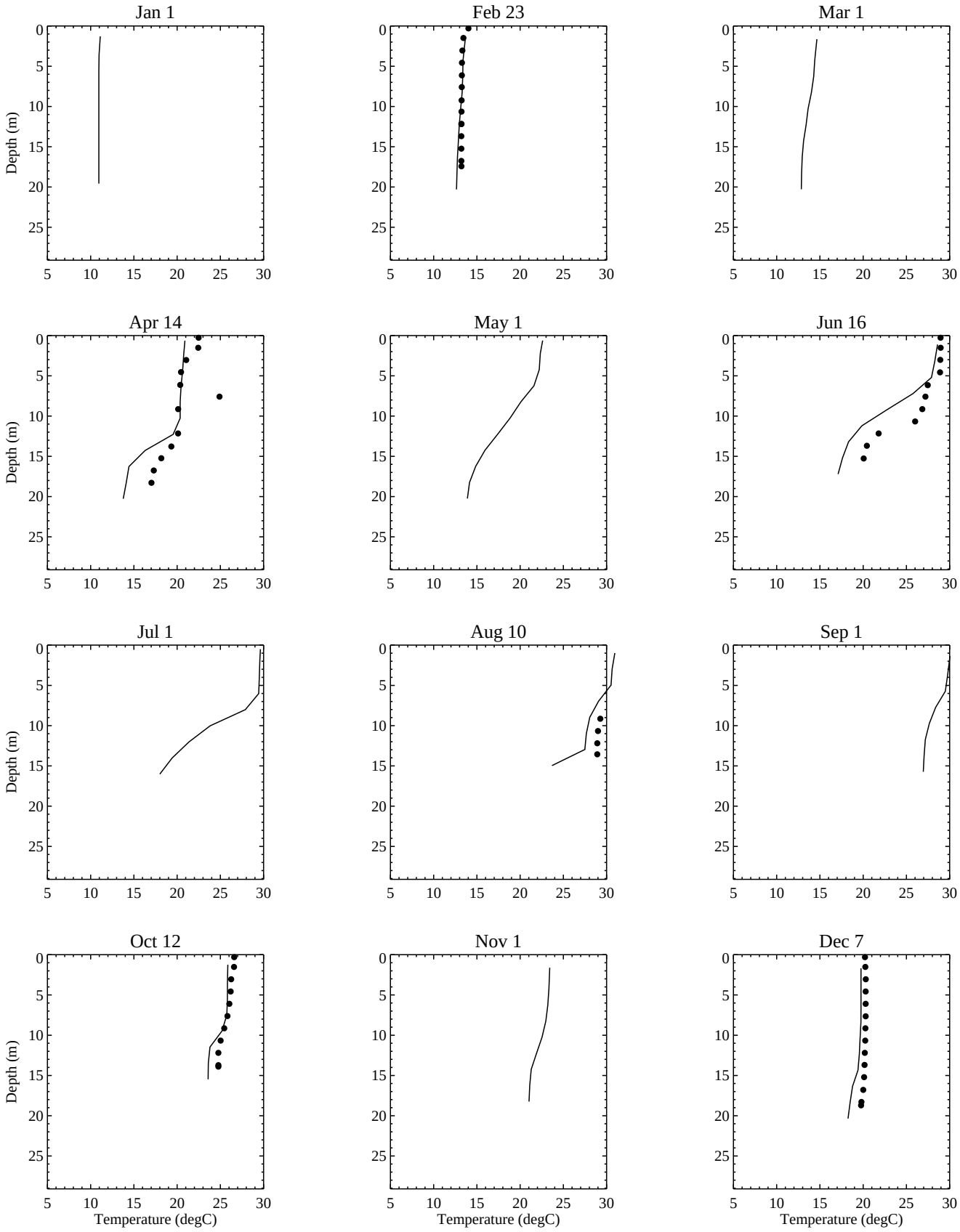

Figure J-4. Vertical profiles of model versus data at Turkey Bend (Segment 28) - Temperature - 1998.

Profiles shown for dates with available data else model results for first day of month shown.

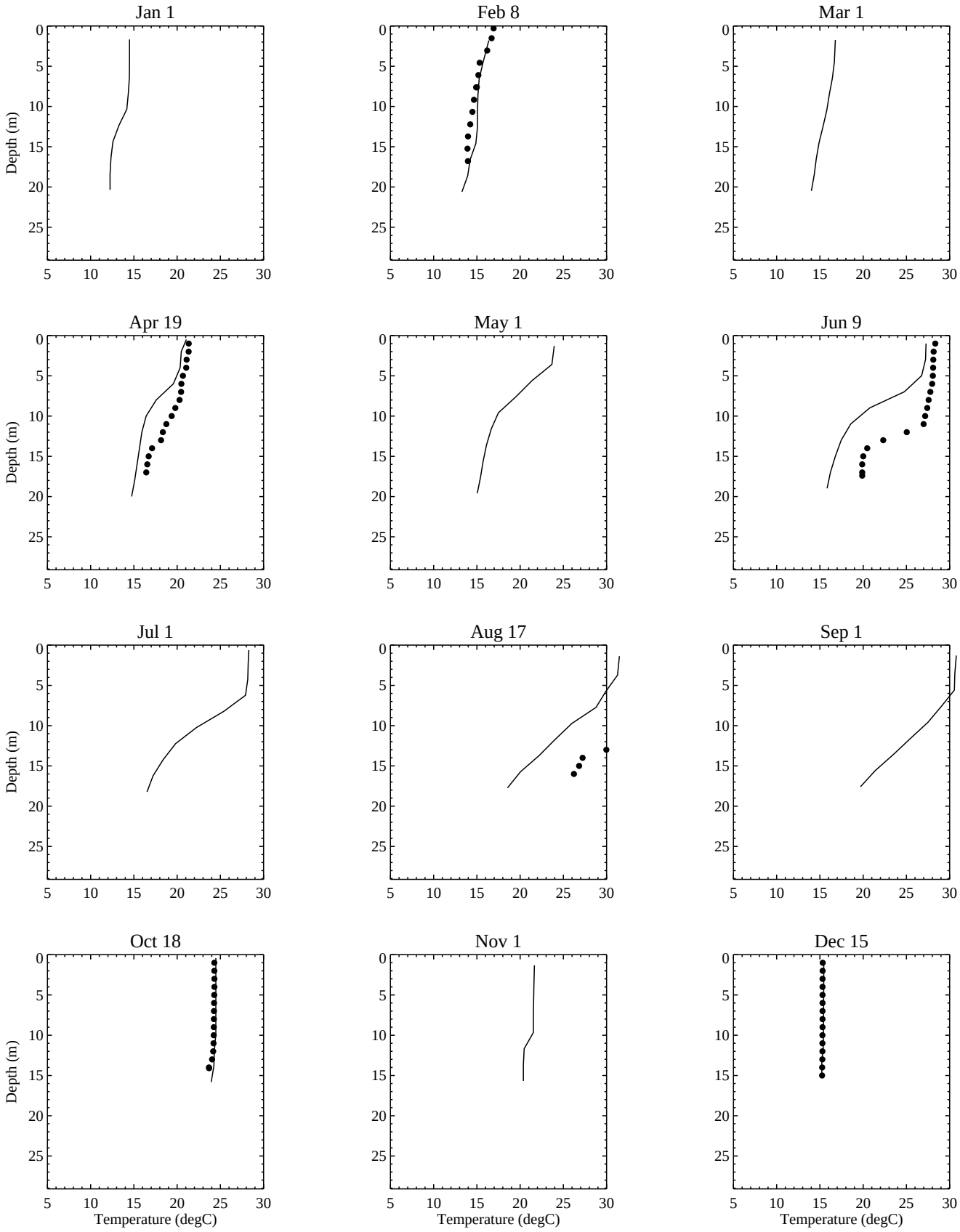

Figure J-4. Vertical profiles of model versus data at Turkey Bend (Segment 28) - Temperature - 1999.

Profiles shown for dates with available data else model results for first day of month shown.

Model Data

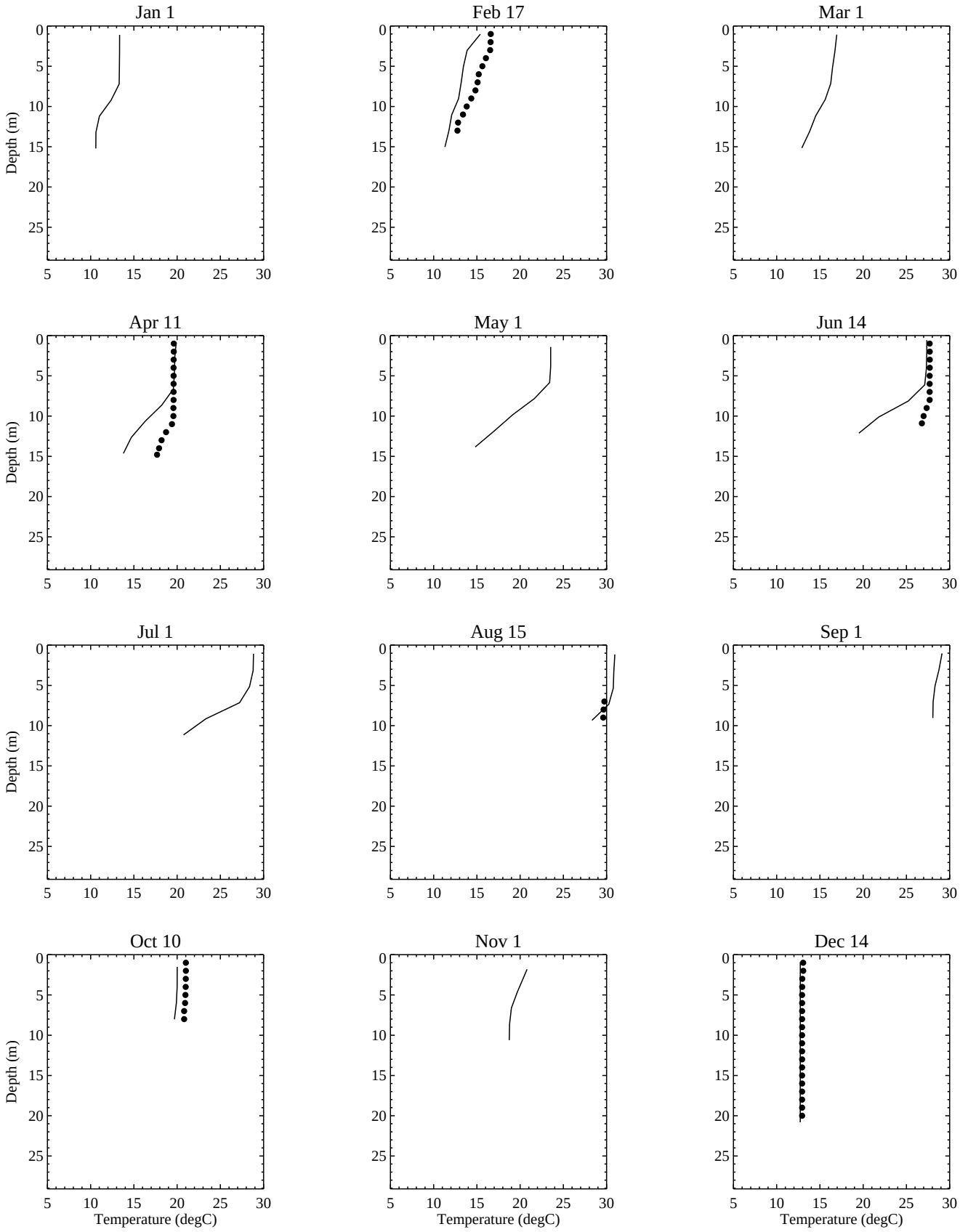

Figure J-4. Vertical profiles of model versus data at Turkey Bend (Segment 28) - Temperature - 2000.

Profiles shown for dates with available data else model results for first day of month shown.

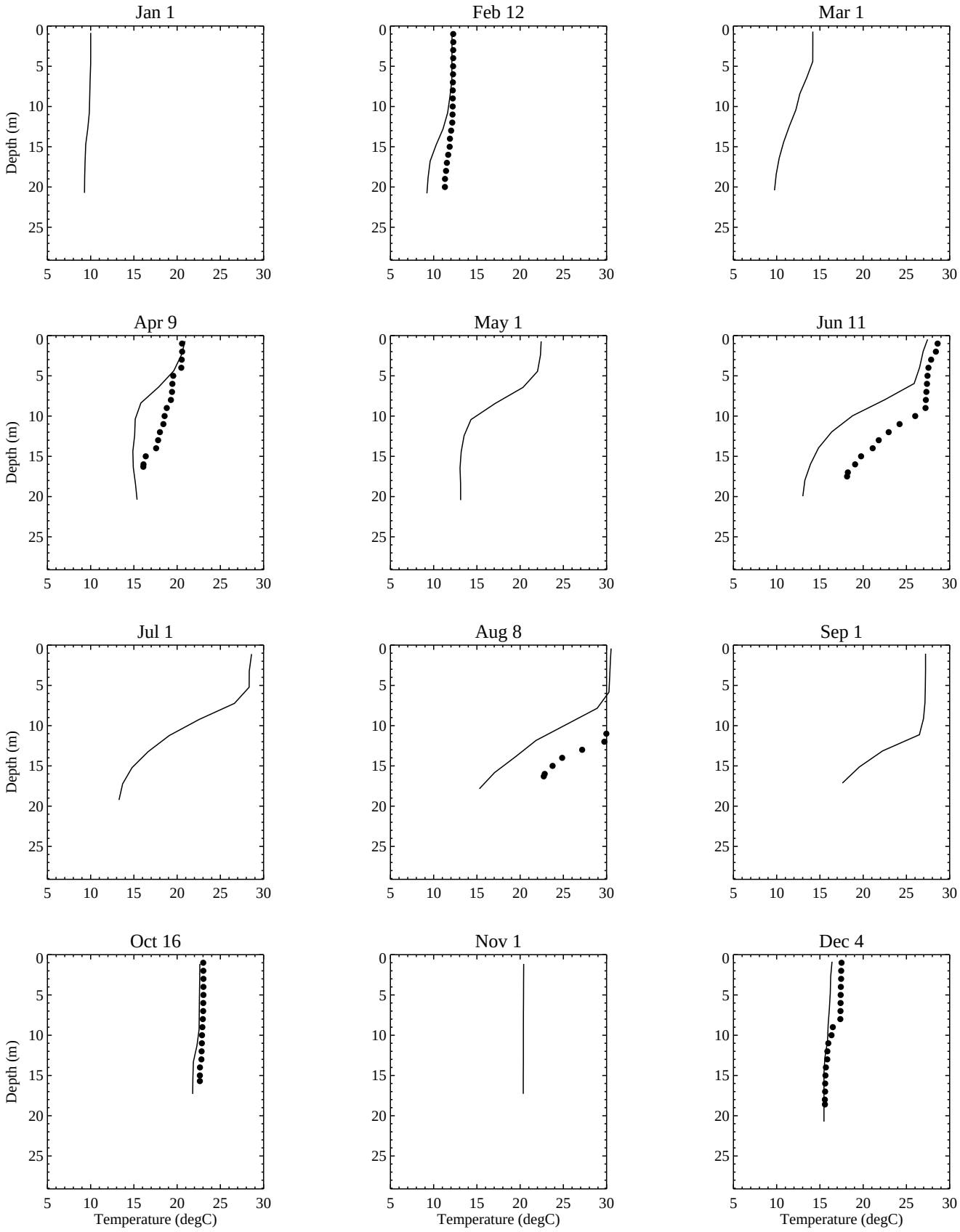

Figure J-4. Vertical profiles of model versus data at Turkey Bend (Segment 28) - Temperature - 2001.

Profiles shown for dates with available data else model results for first day of month shown.

Model Data

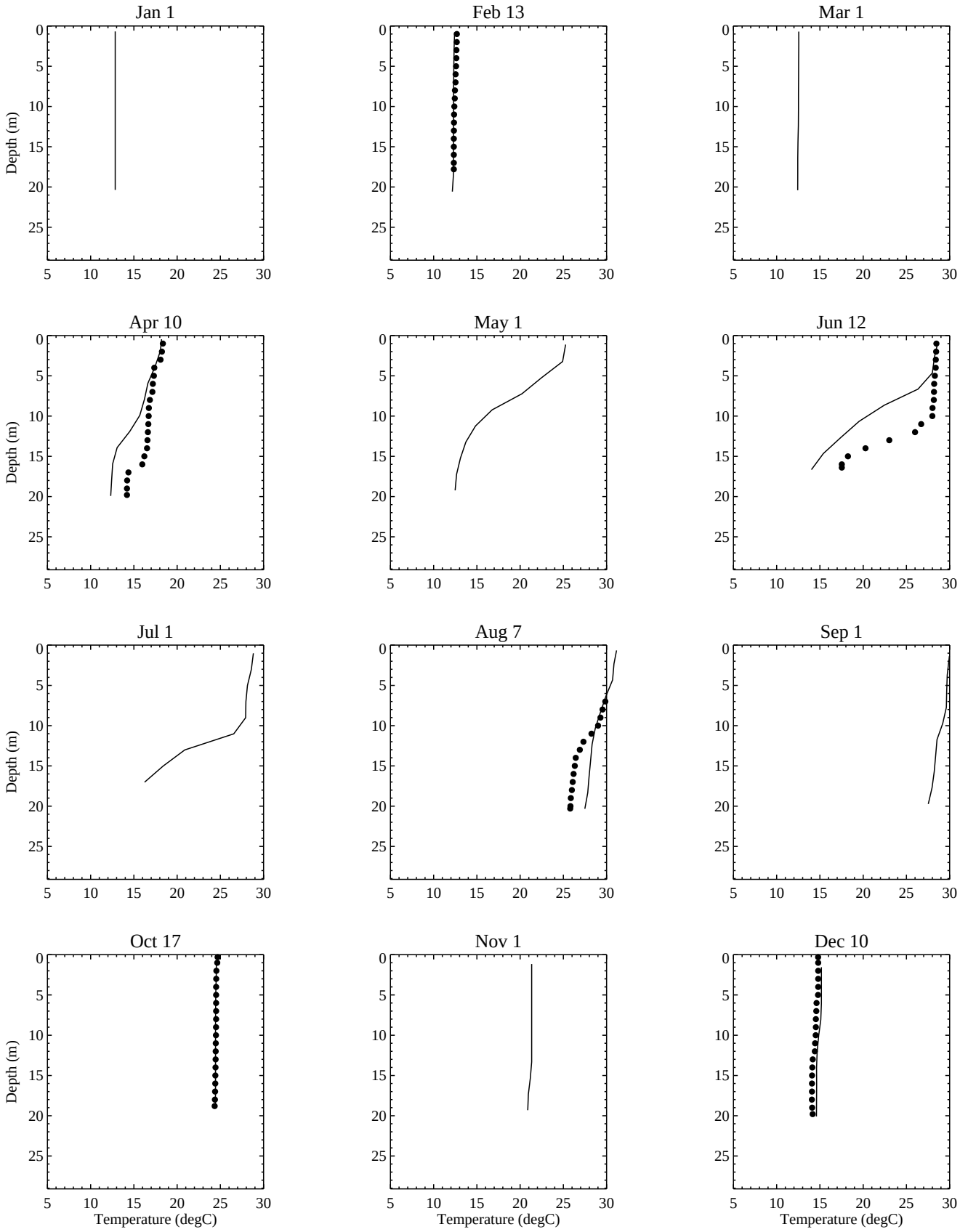

Figure J-4. Vertical profiles of model versus data at Turkey Bend (Segment 28) - Temperature - 2002.

Profiles shown for dates with available data else model results for first day of month shown.

Model Data

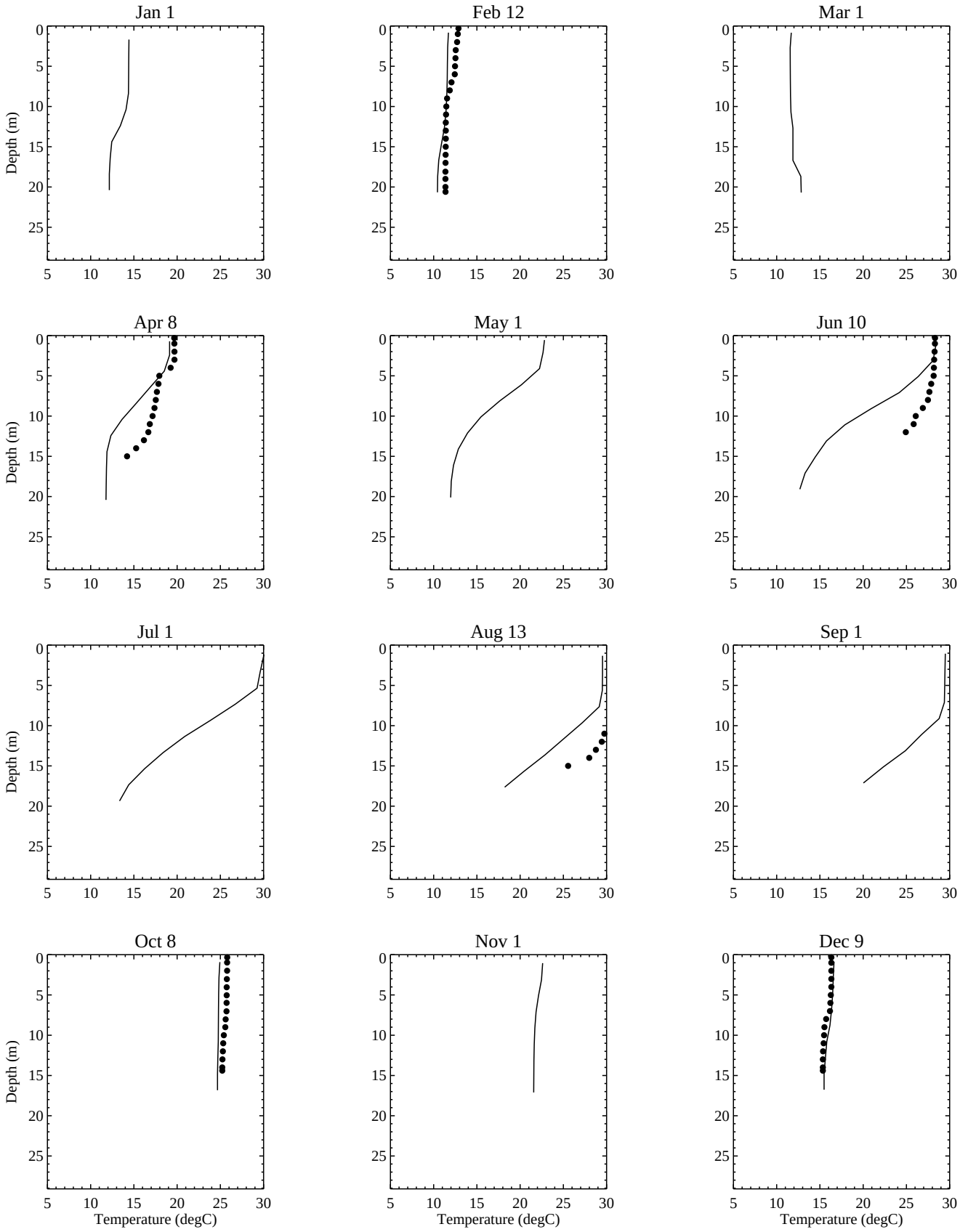

Figure J-4. Vertical profiles of model versus data at Turkey Bend (Segment 28) - Temperature - 2003.

Profiles shown for dates with available data else model results for first day of month shown.

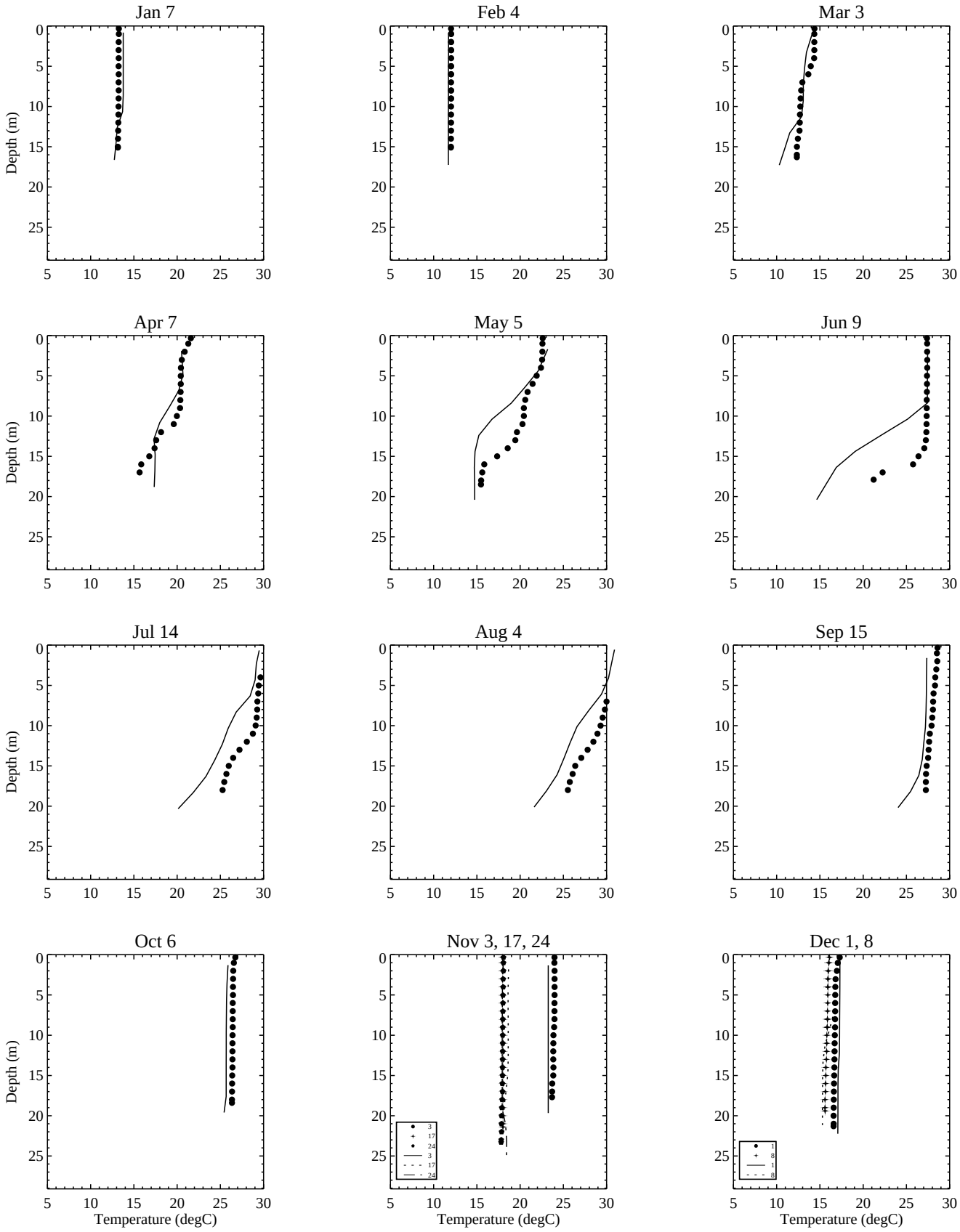

Figure J-4. Vertical profiles of model versus data at Turkey Bend (Segment 28) - Temperature - 2004.

Profiles shown for dates with available data else model results for first day of month shown.

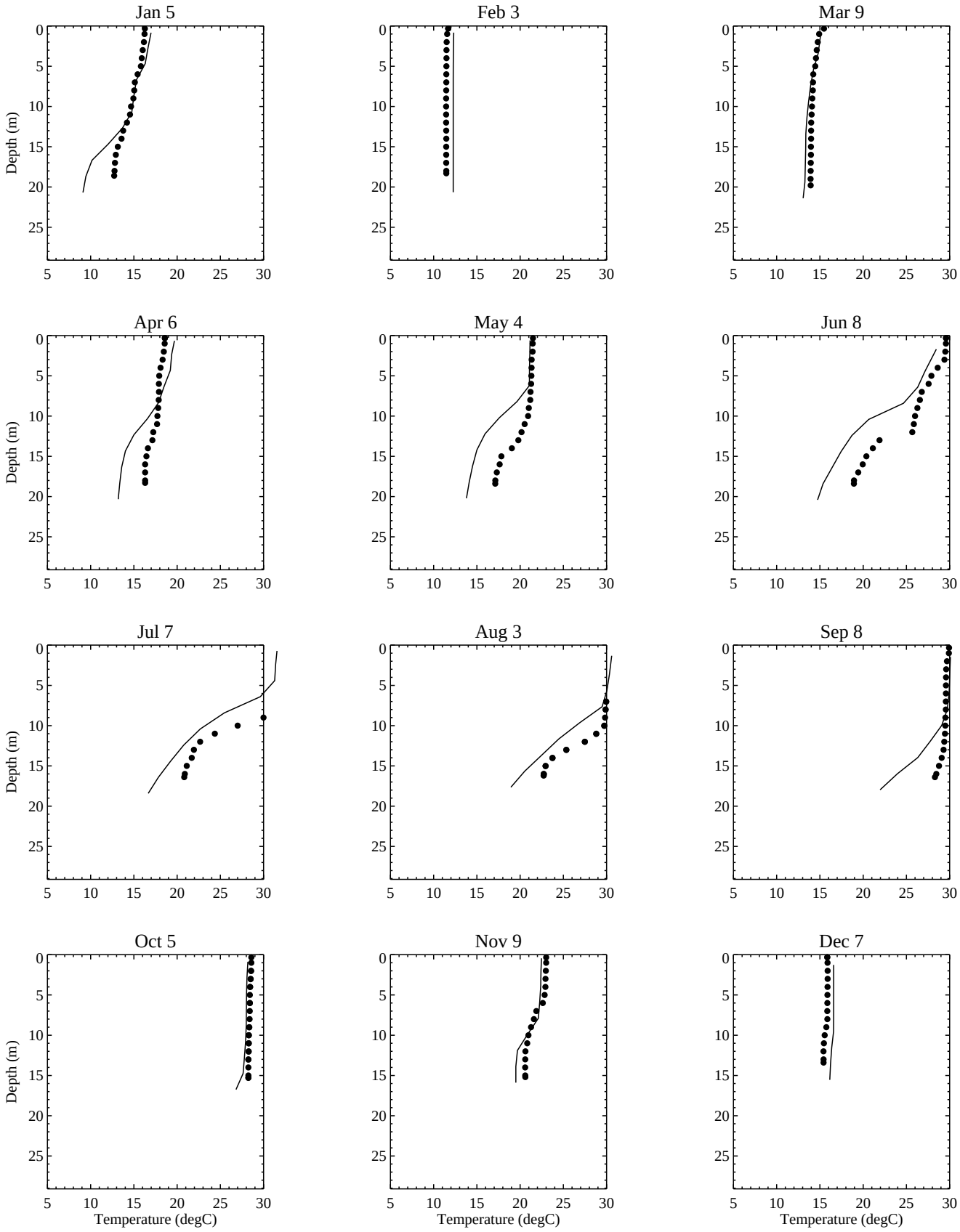

Figure J-4. Vertical profiles of model versus data at Turkey Bend (Segment 28) - Temperature - 2005.

Profiles shown for dates with available data else model results for first day of month shown.

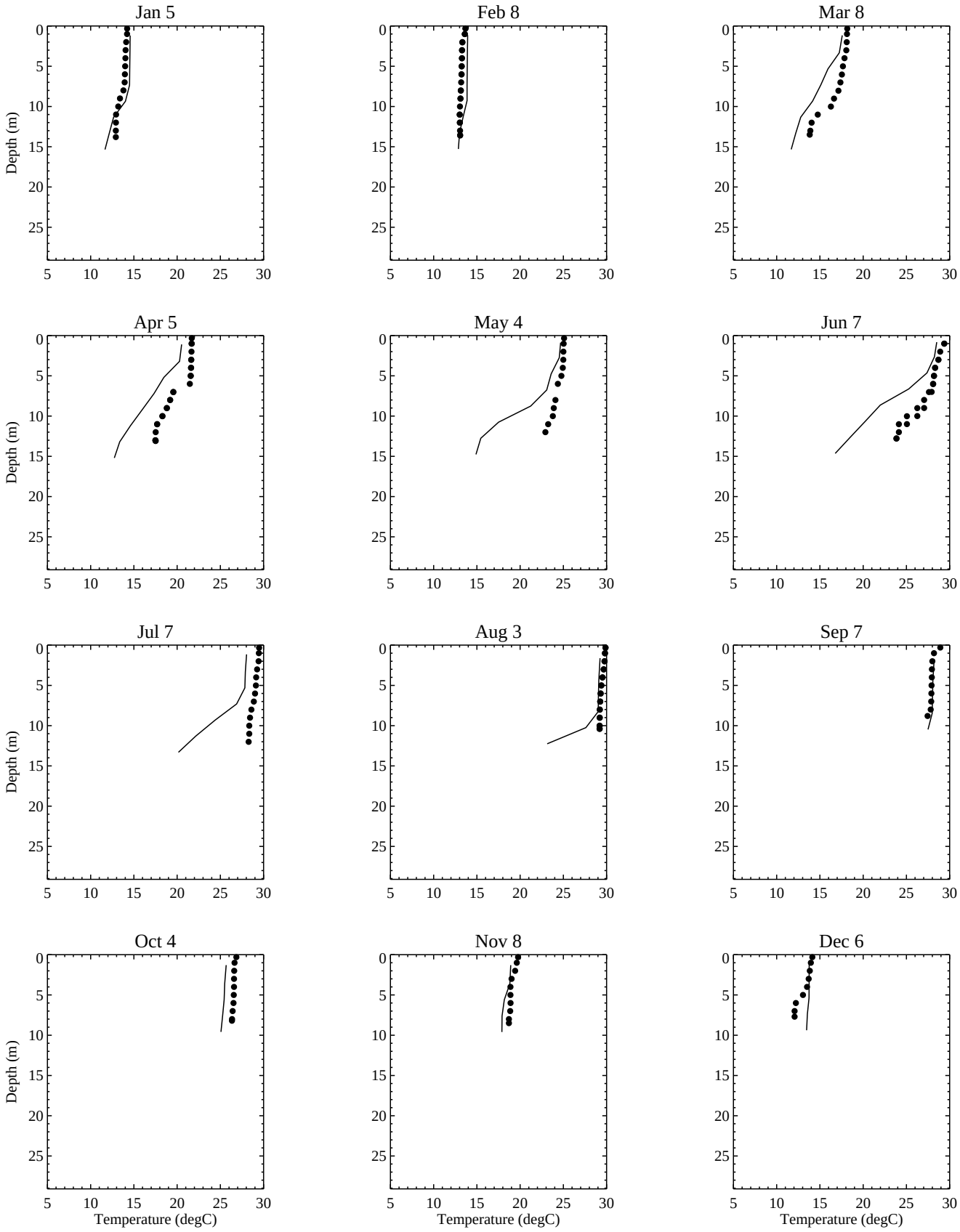

Figure J-4. Vertical profiles of model versus data at Turkey Bend (Segment 28) - Temperature - 2006.

Profiles shown for dates with available data else model results for first day of month shown.

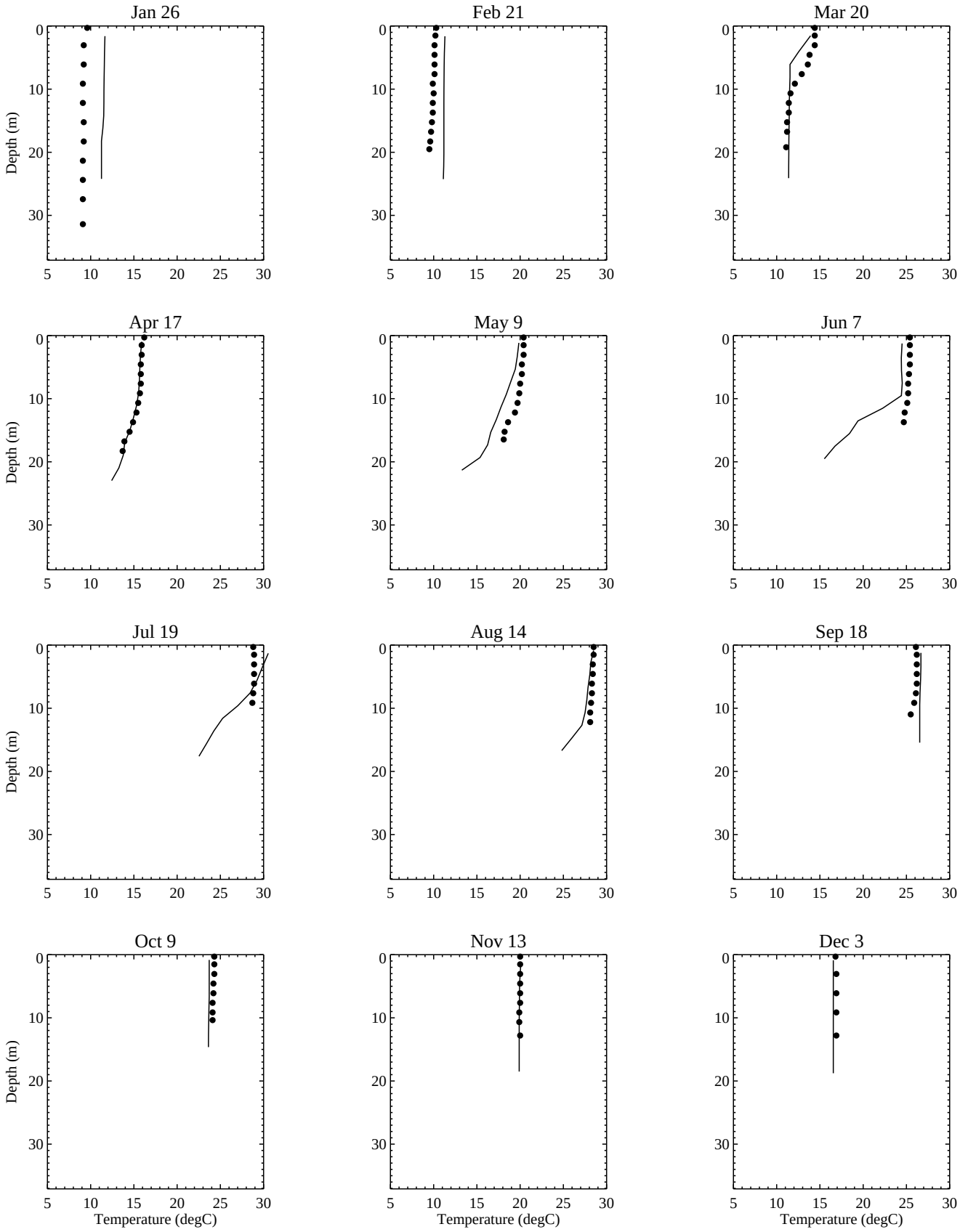

Figure J-5. Vertical profiles of model versus data at Sandy Creek (Segment 161) - Temperature - 1984.

Profiles shown for dates with available data else model results for first day of month shown.

Model Data

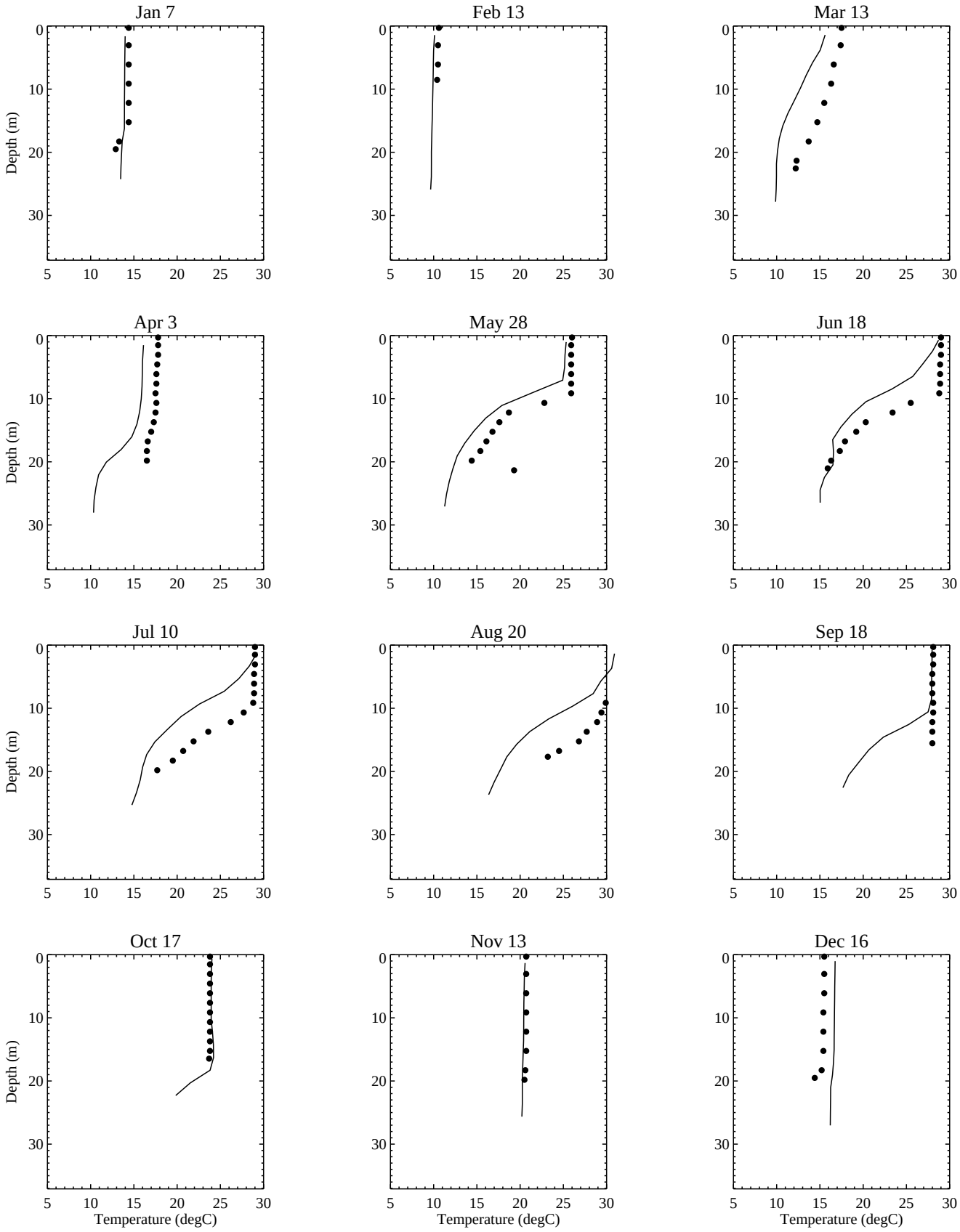

Figure J-5. Vertical profiles of model versus data at Sandy Creek (Segment 161) - Temperature - 1985.

Profiles shown for dates with available data else model results for first day of month shown.

Model Data

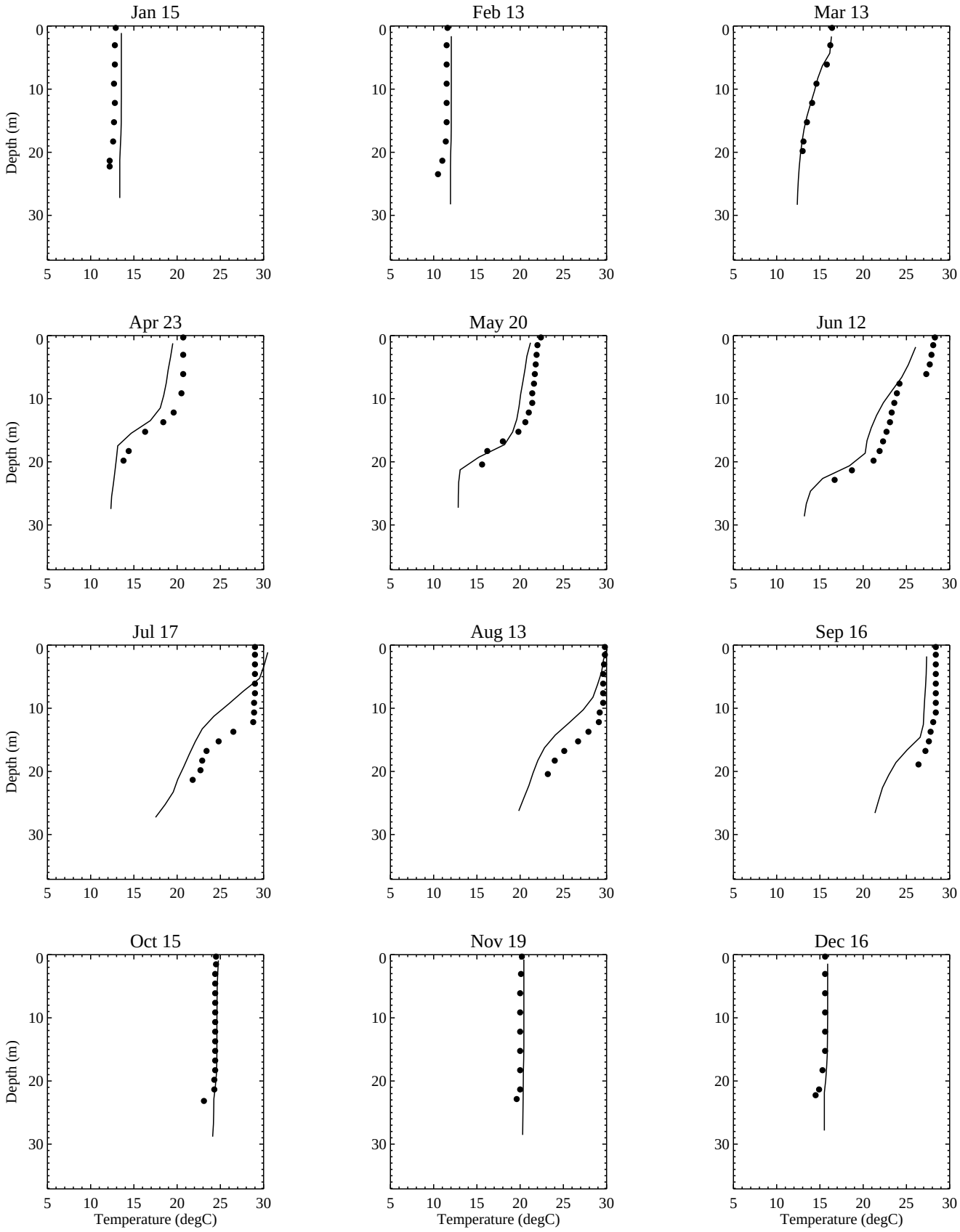

Figure J-5. Vertical profiles of model versus data at Sandy Creek (Segment 161) - Temperature - 1986.

Profiles shown for dates with available data else model results for first day of month shown.

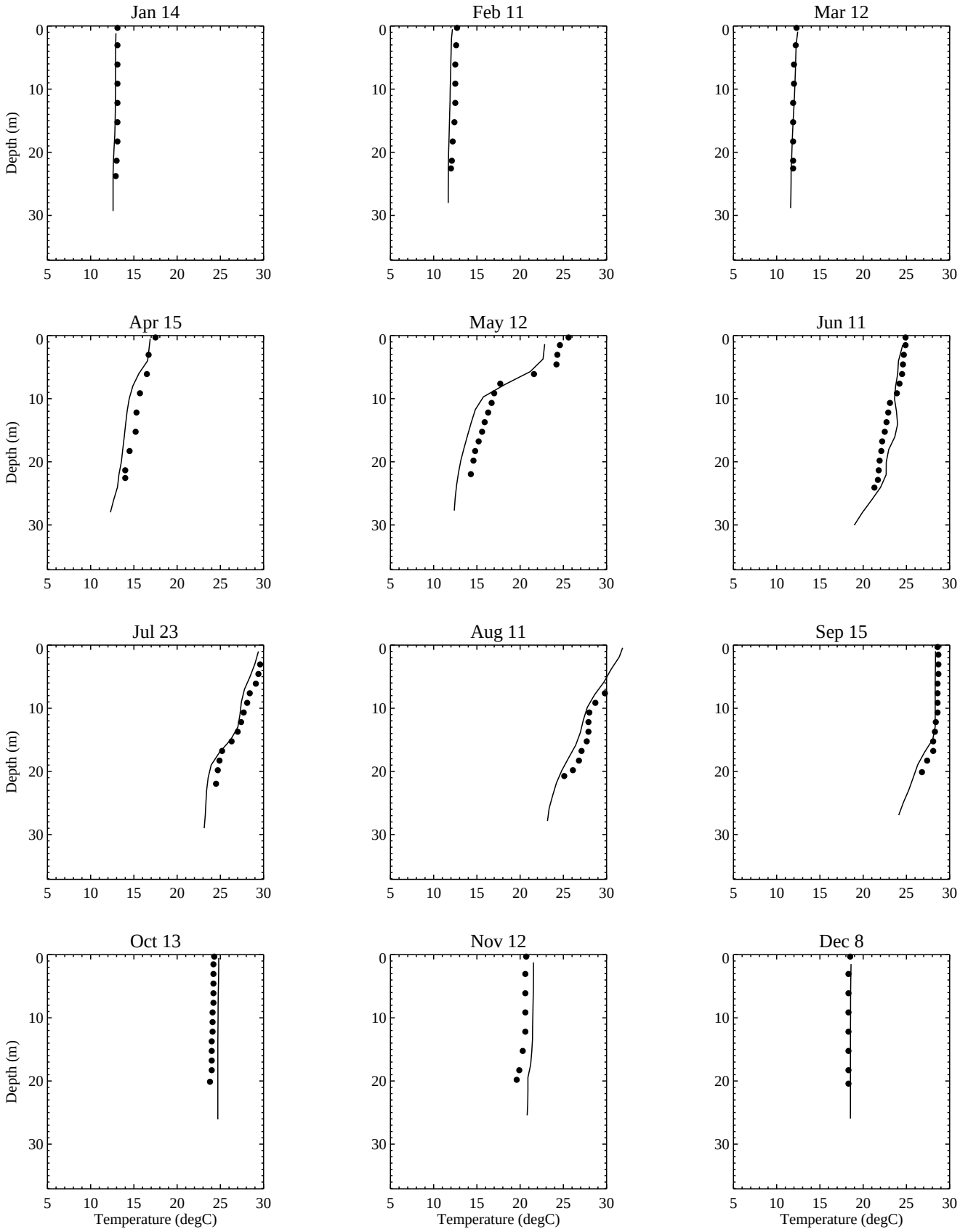

Figure J-5. Vertical profiles of model versus data at Sandy Creek (Segment 161) - Temperature - 1987.

Profiles shown for dates with available data else model results for first day of month shown.

Model Data

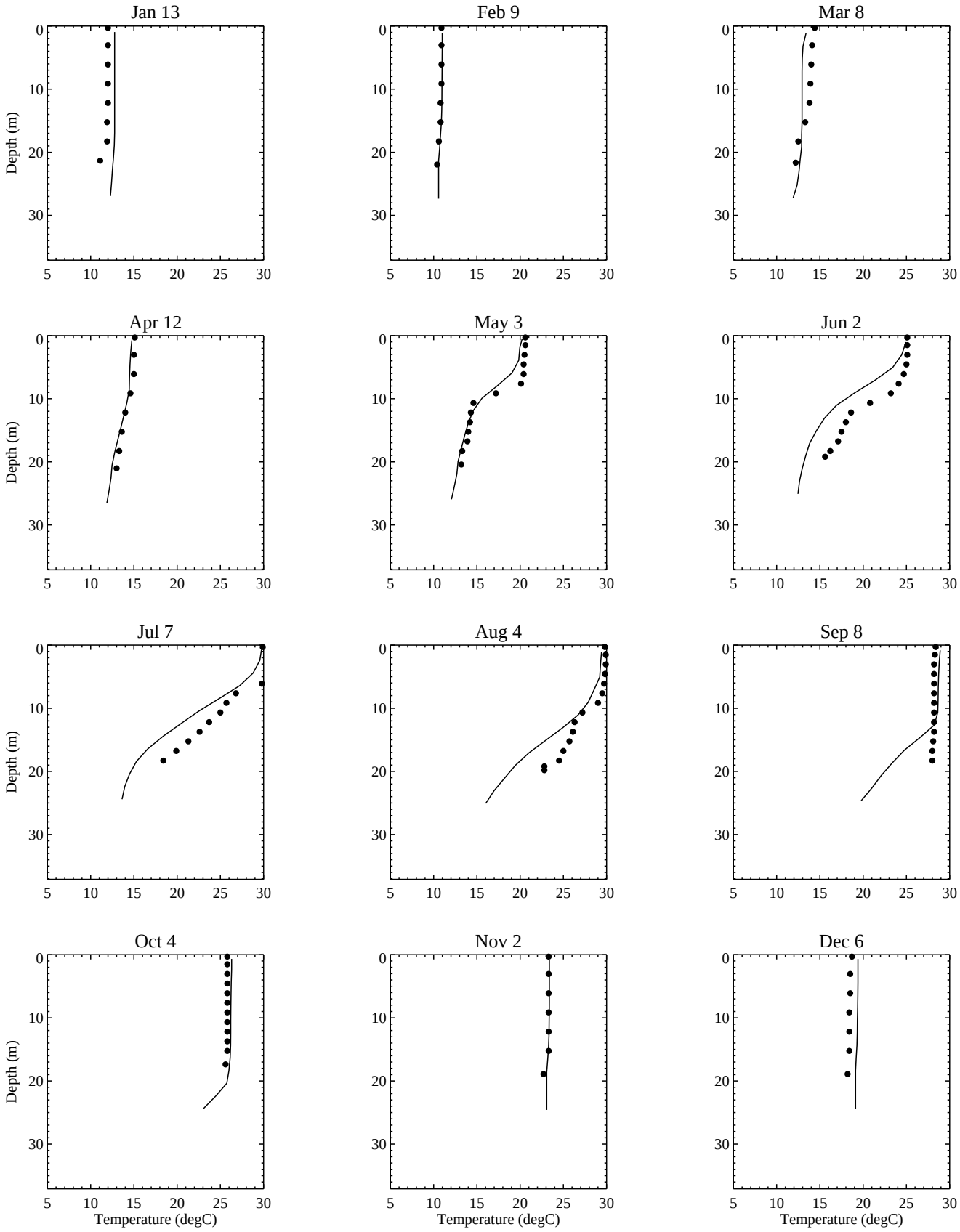

Figure J-5. Vertical profiles of model versus data at Sandy Creek (Segment 161) - Temperature - 1988.

Profiles shown for dates with available data else model results for first day of month shown.

Model Data

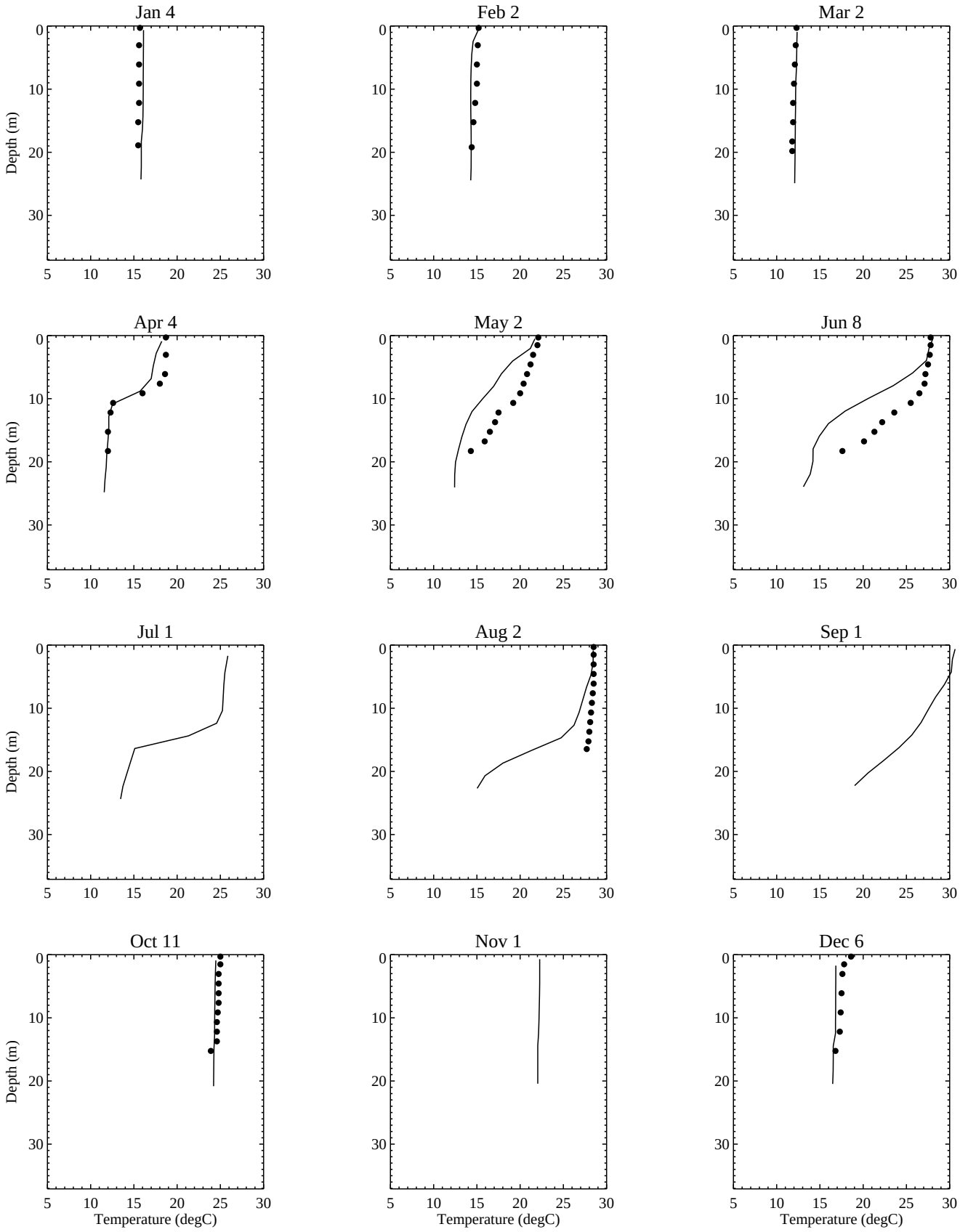

Figure J-5. Vertical profiles of model versus data at Sandy Creek (Segment 161) - Temperature - 1989.

Profiles shown for dates with available data else model results for first day of month shown.

Model Data

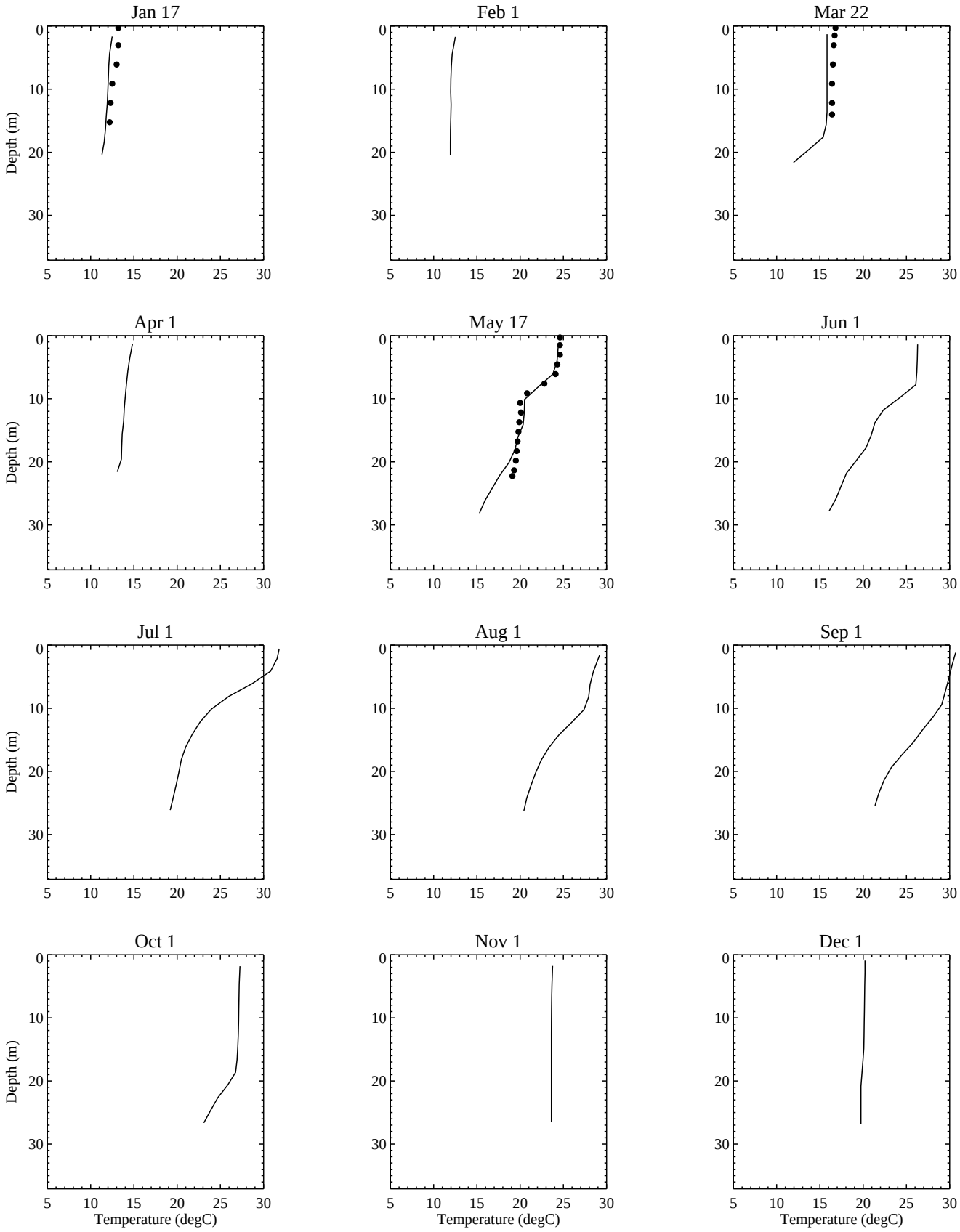

Figure J-5. Vertical profiles of model versus data at Sandy Creek (Segment 161) - Temperature - 1990.

Profiles shown for dates with available data else model results for first day of month shown.

Model ● Data

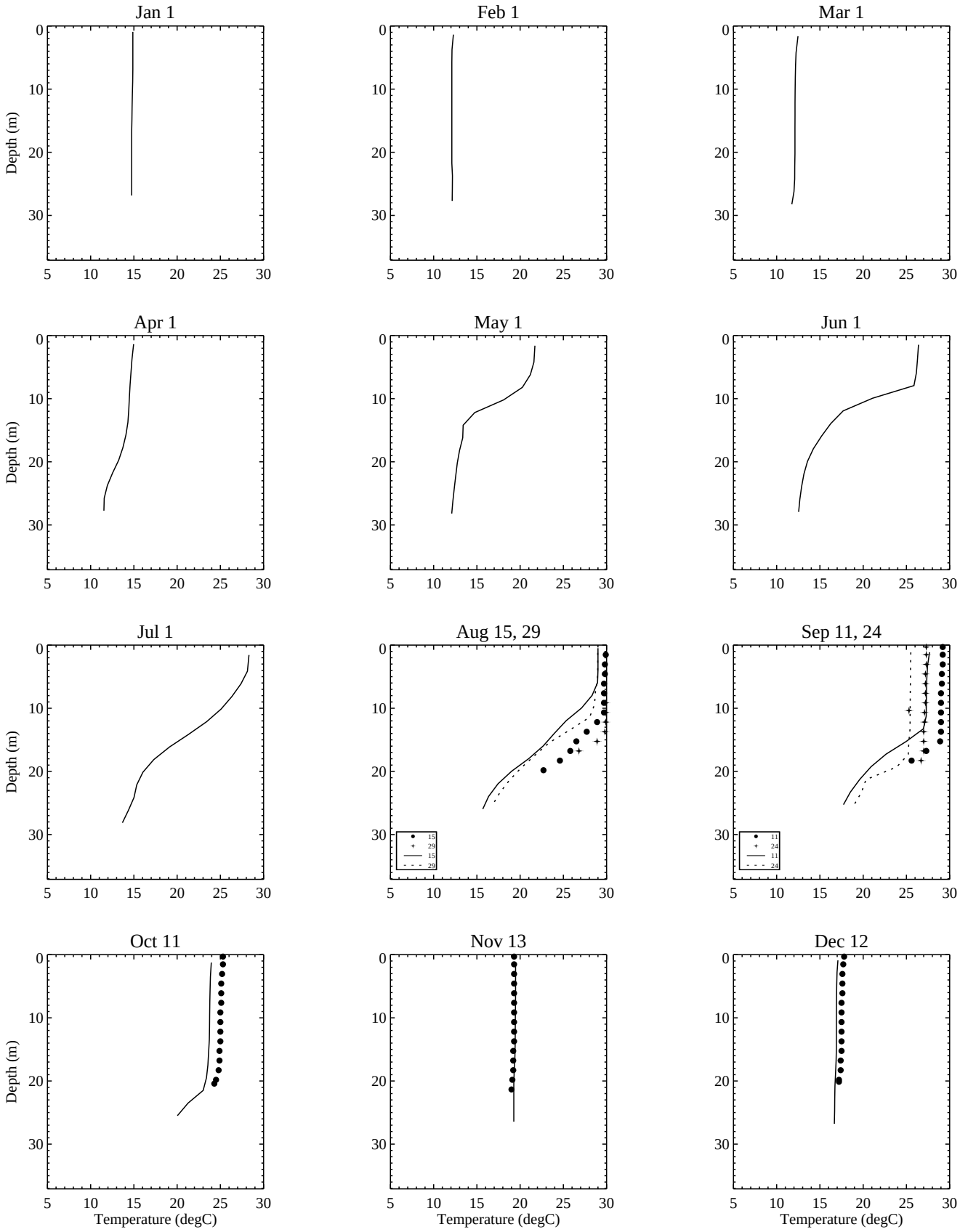

Figure J-5. Vertical profiles of model versus data at Sandy Creek (Segment 161) - Temperature - 1991.

Profiles shown for dates with available data else model results for first day of month shown.

Model Data

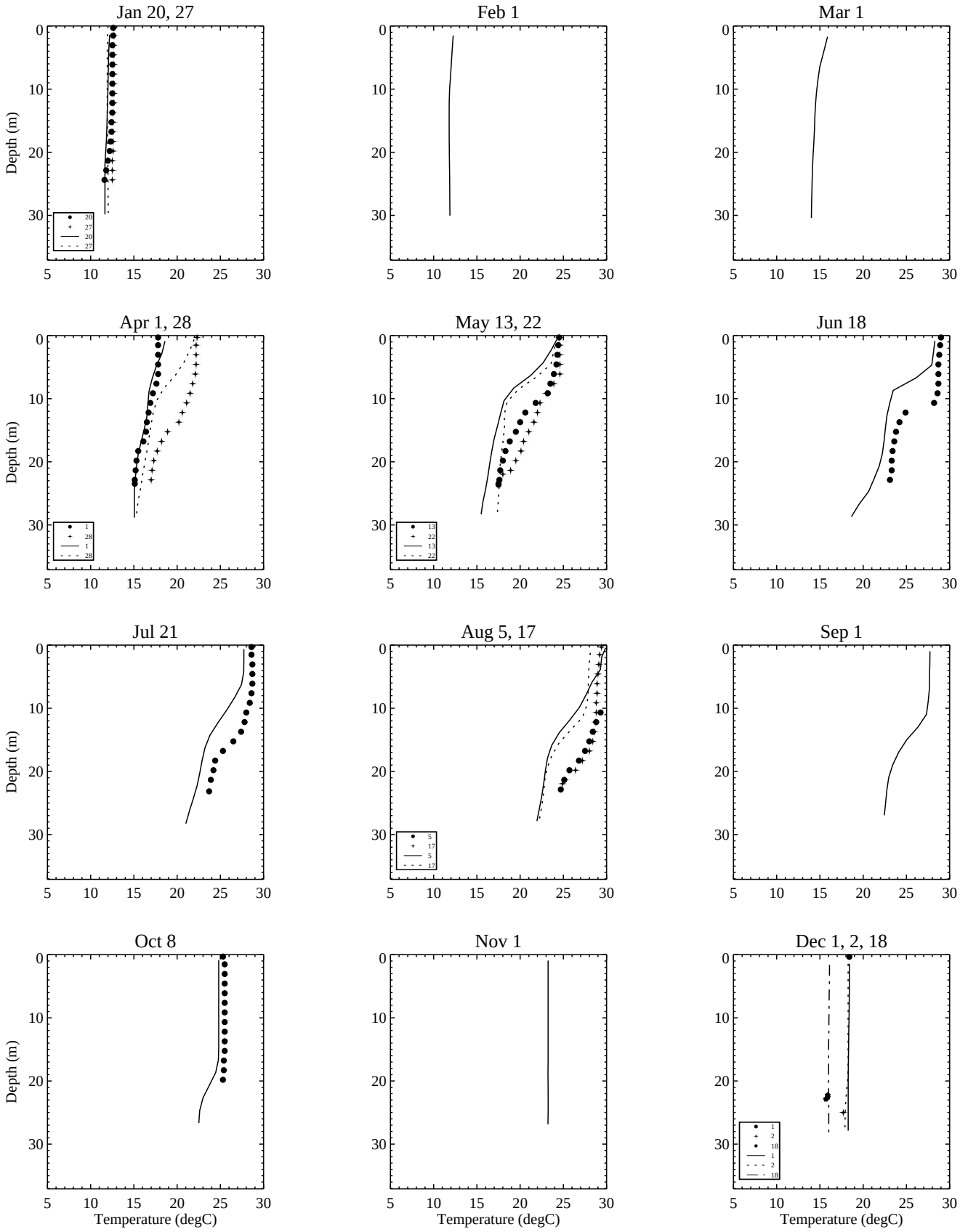

Figure J-5. Vertical profiles of model versus data at Sandy Creek (Segment 161) - Temperature - 1992.

Profiles shown for dates with available data else model results for first day of month shown.

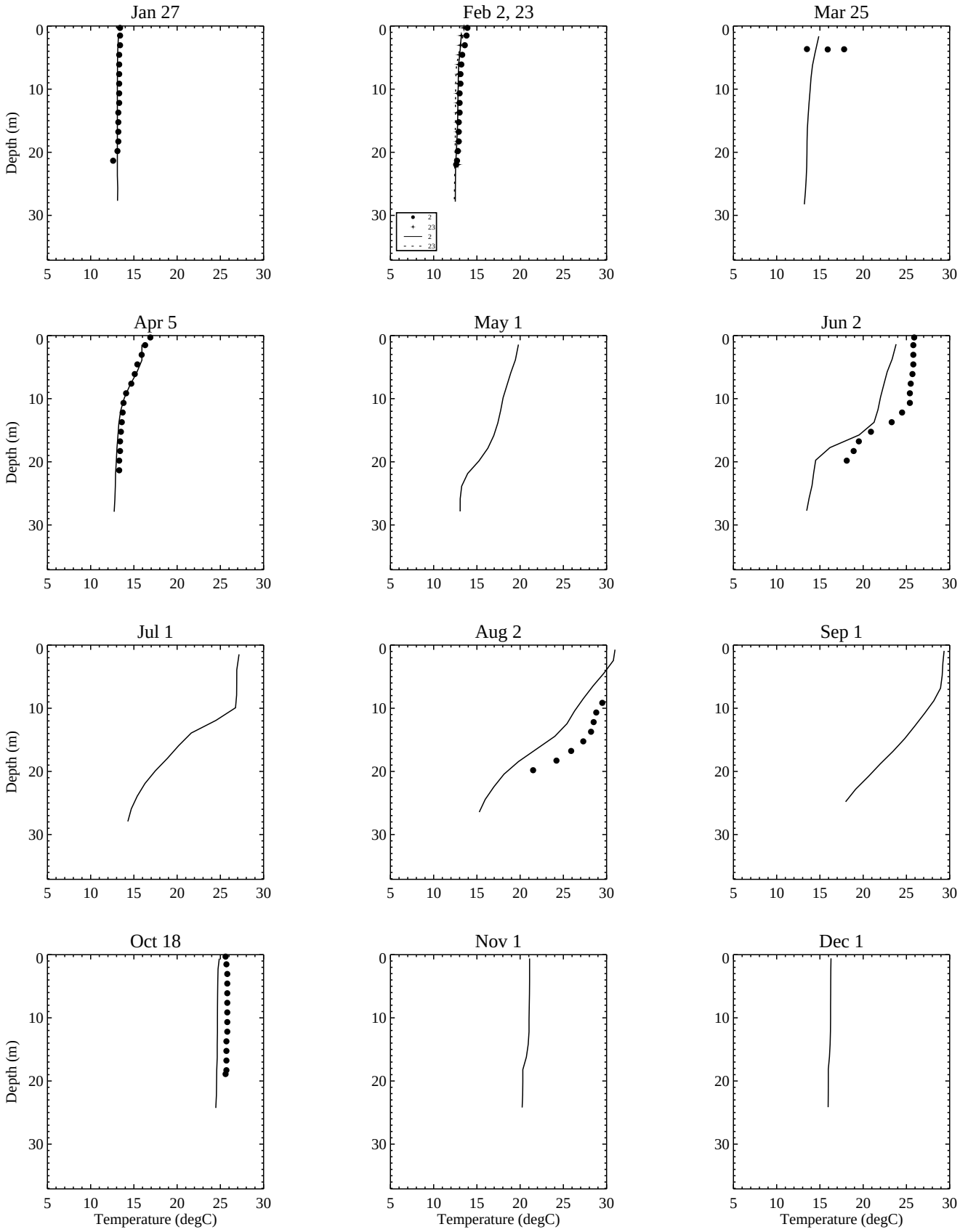

Figure J-5. Vertical profiles of model versus data at Sandy Creek (Segment 161) - Temperature - 1993.

Profiles shown for dates with available data else model results for first day of month shown.

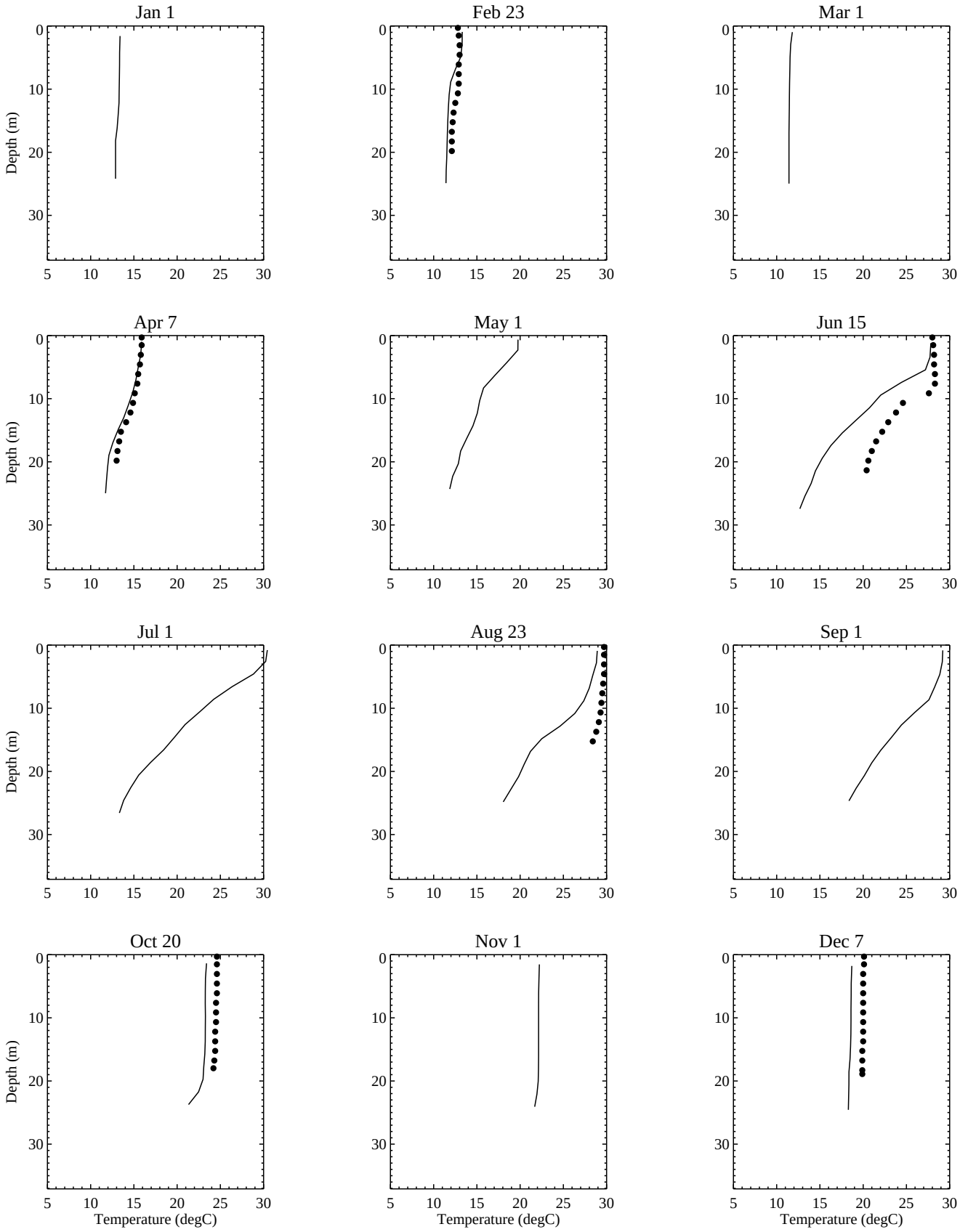

Figure J-5. Vertical profiles of model versus data at Sandy Creek (Segment 161) - Temperature - 1994.

Profiles shown for dates with available data else model results for first day of month shown.

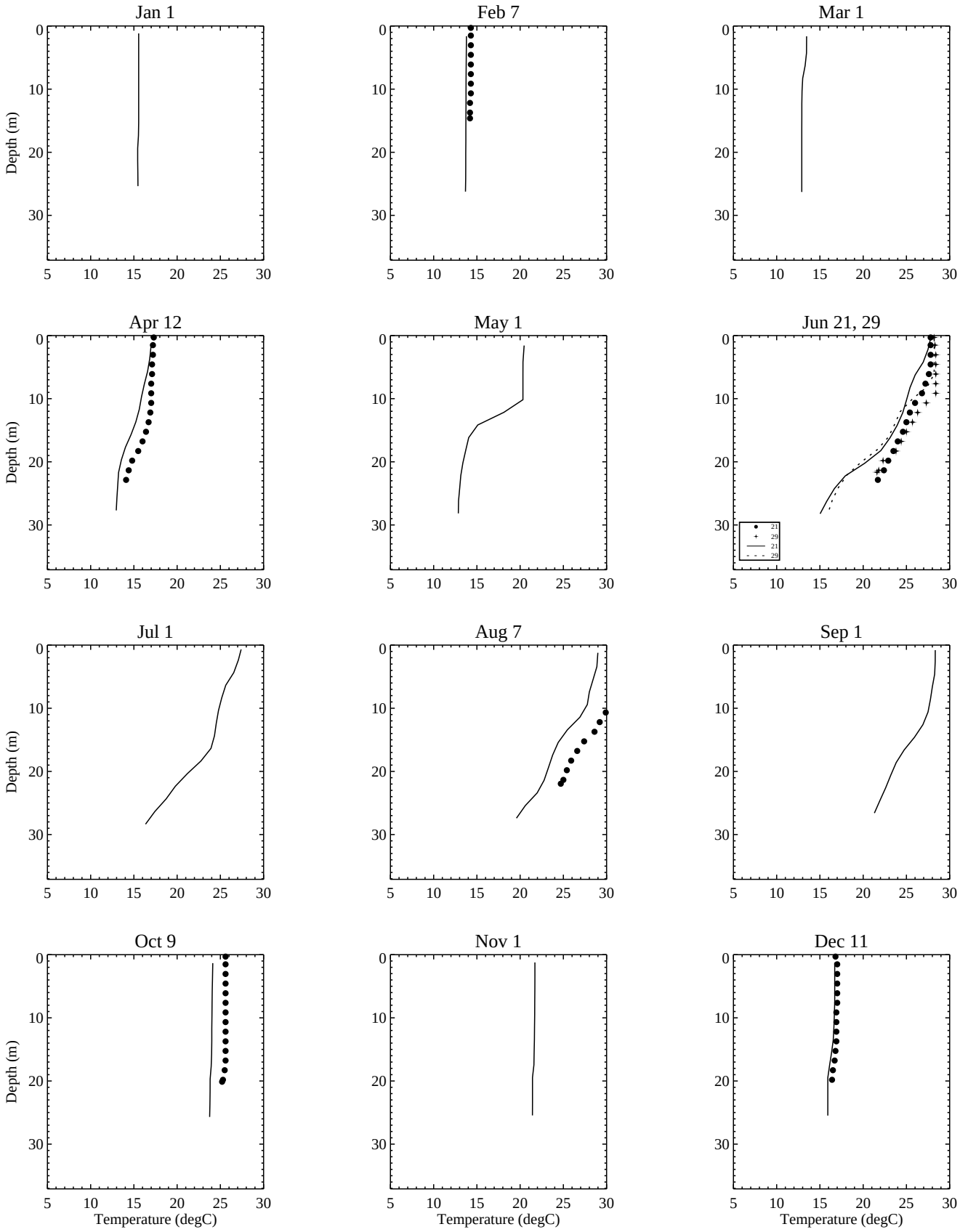

Figure J-5. Vertical profiles of model versus data at Sandy Creek (Segment 161) - Temperature - 1995.

Profiles shown for dates with available data else model results for first day of month shown.

Model Data

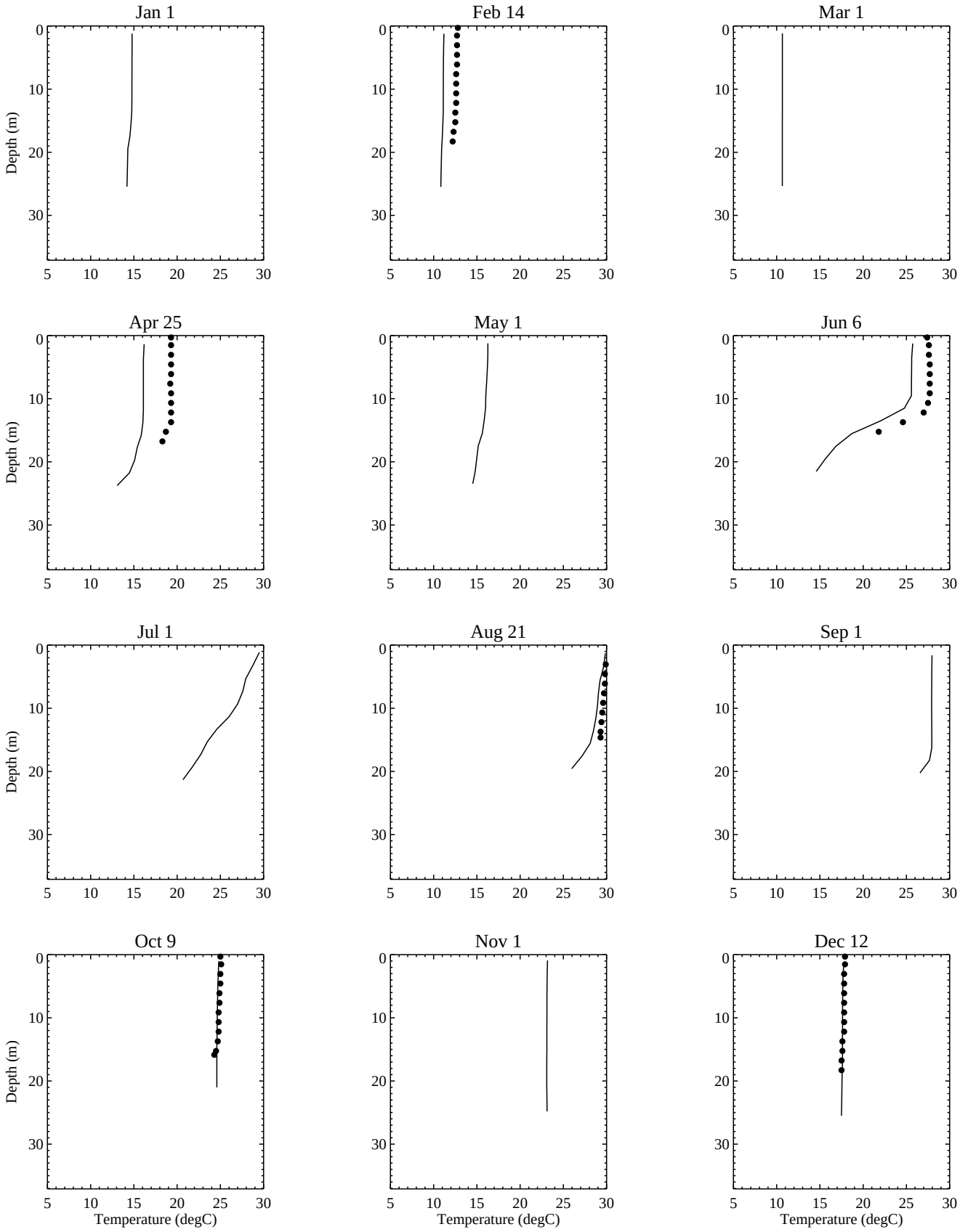

Figure J-5. Vertical profiles of model versus data at Sandy Creek (Segment 161) - Temperature - 1996.

Profiles shown for dates with available data else model results for first day of month shown.

Model Data

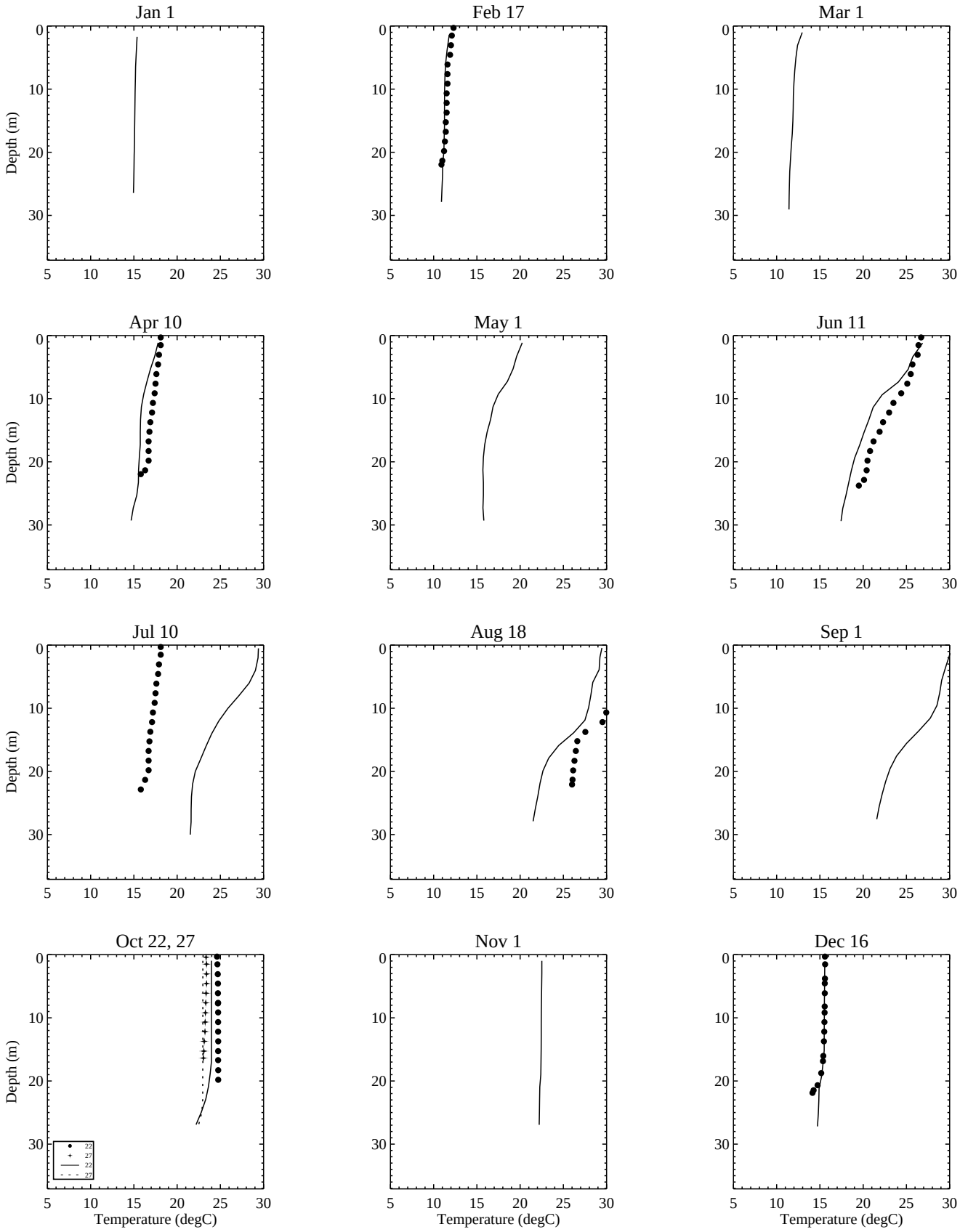

Figure J-5. Vertical profiles of model versus data at Sandy Creek (Segment 161) - Temperature - 1997.

Profiles shown for dates with available data else model results for first day of month shown.

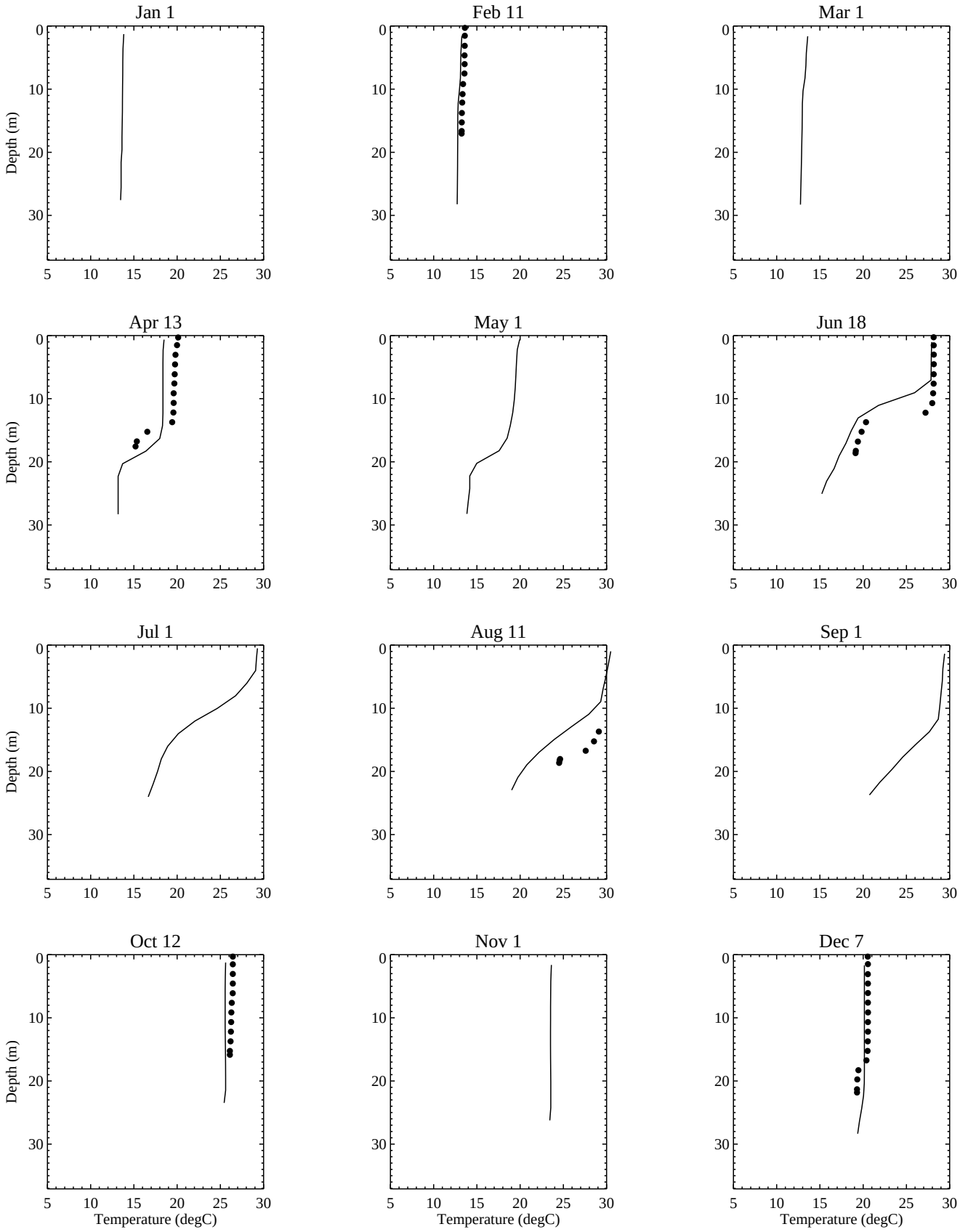

Figure J-5. Vertical profiles of model versus data at Sandy Creek (Segment 161) - Temperature - 1998.

Profiles shown for dates with available data else model results for first day of month shown.

Model Data

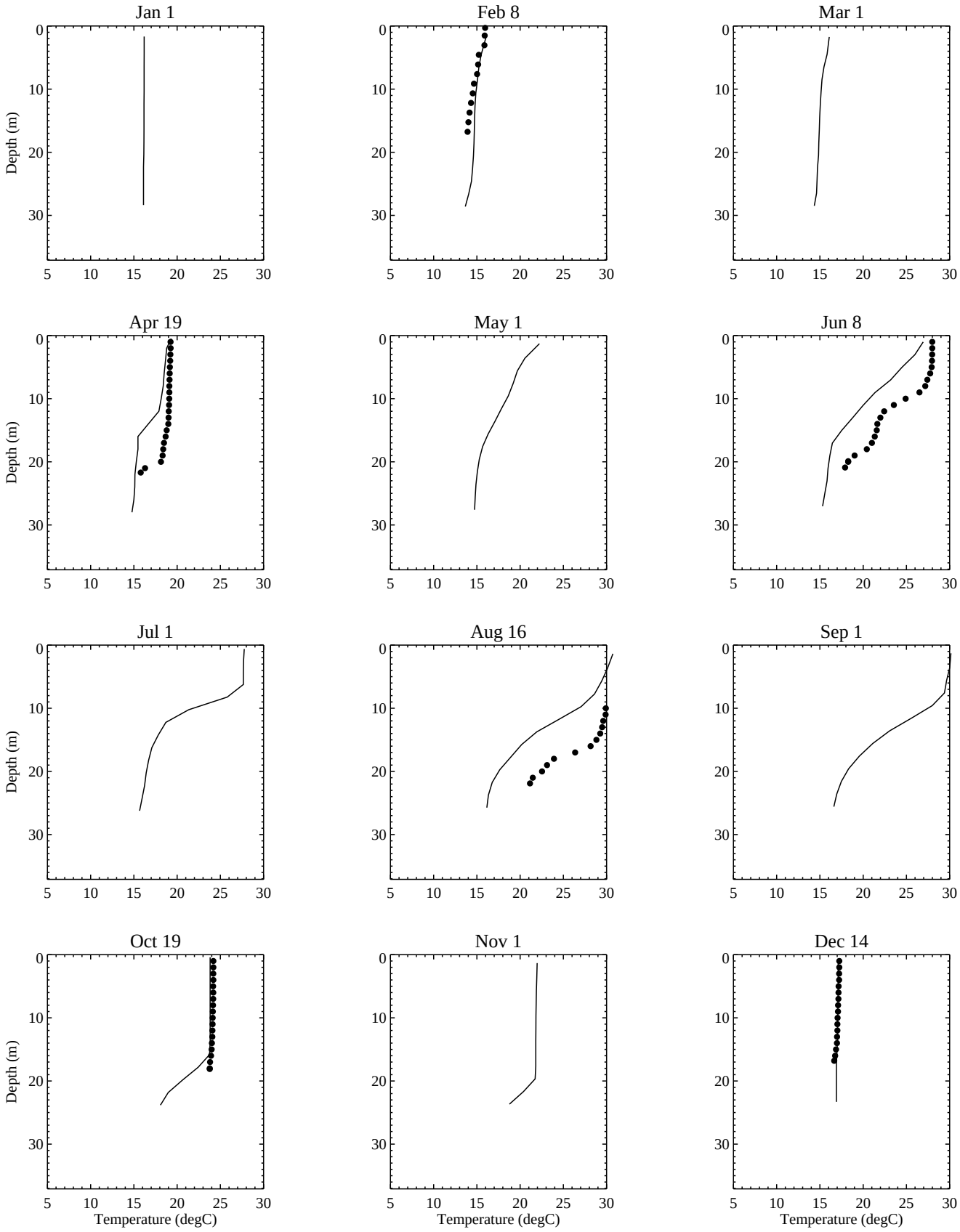

Figure J-5. Vertical profiles of model versus data at Sandy Creek (Segment 161) - Temperature - 1999.

Profiles shown for dates with available data else model results for first day of month shown.

Model Data

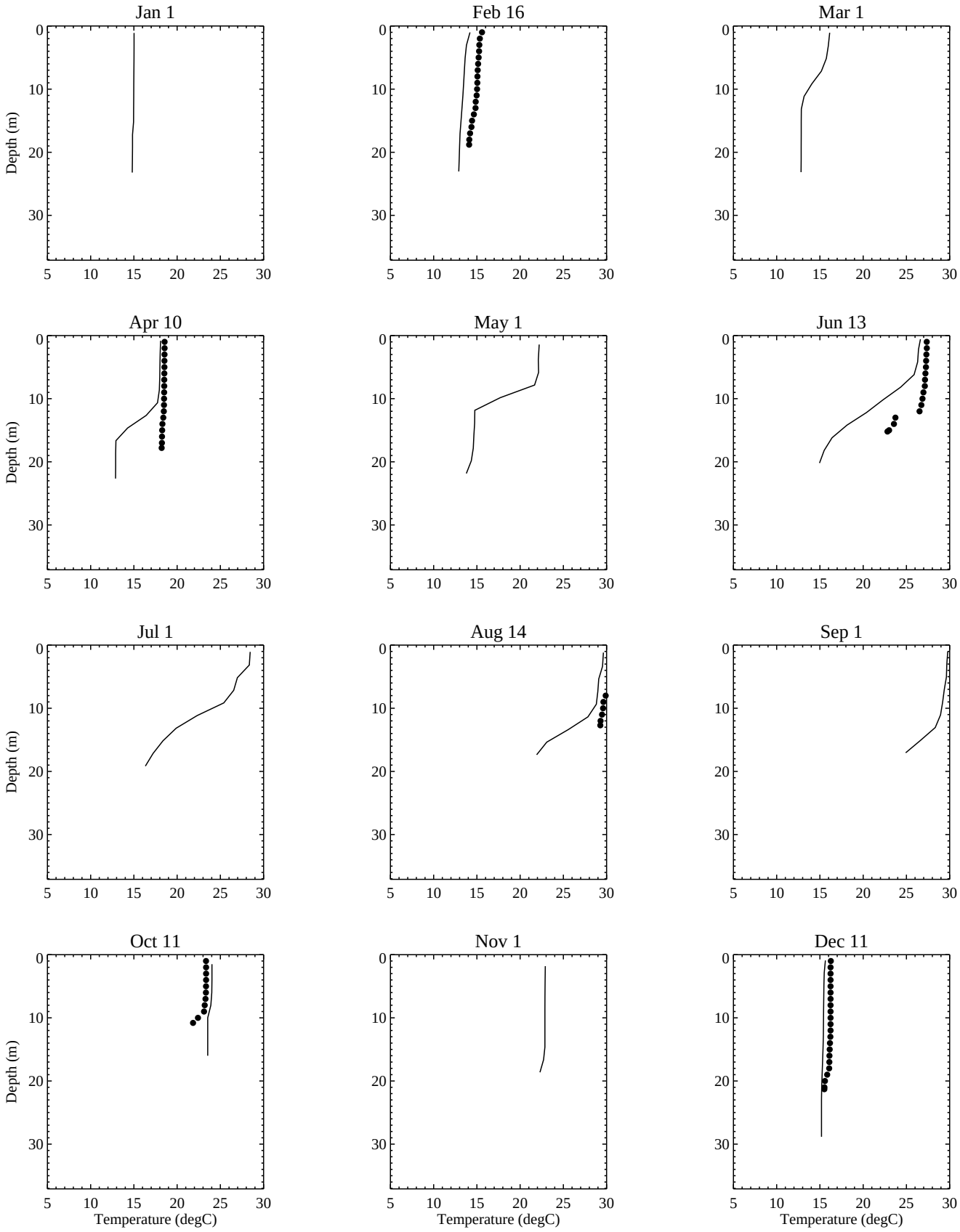

Figure J-5. Vertical profiles of model versus data at Sandy Creek (Segment 161) - Temperature - 2000.

Profiles shown for dates with available data else model results for first day of month shown.

Model Data

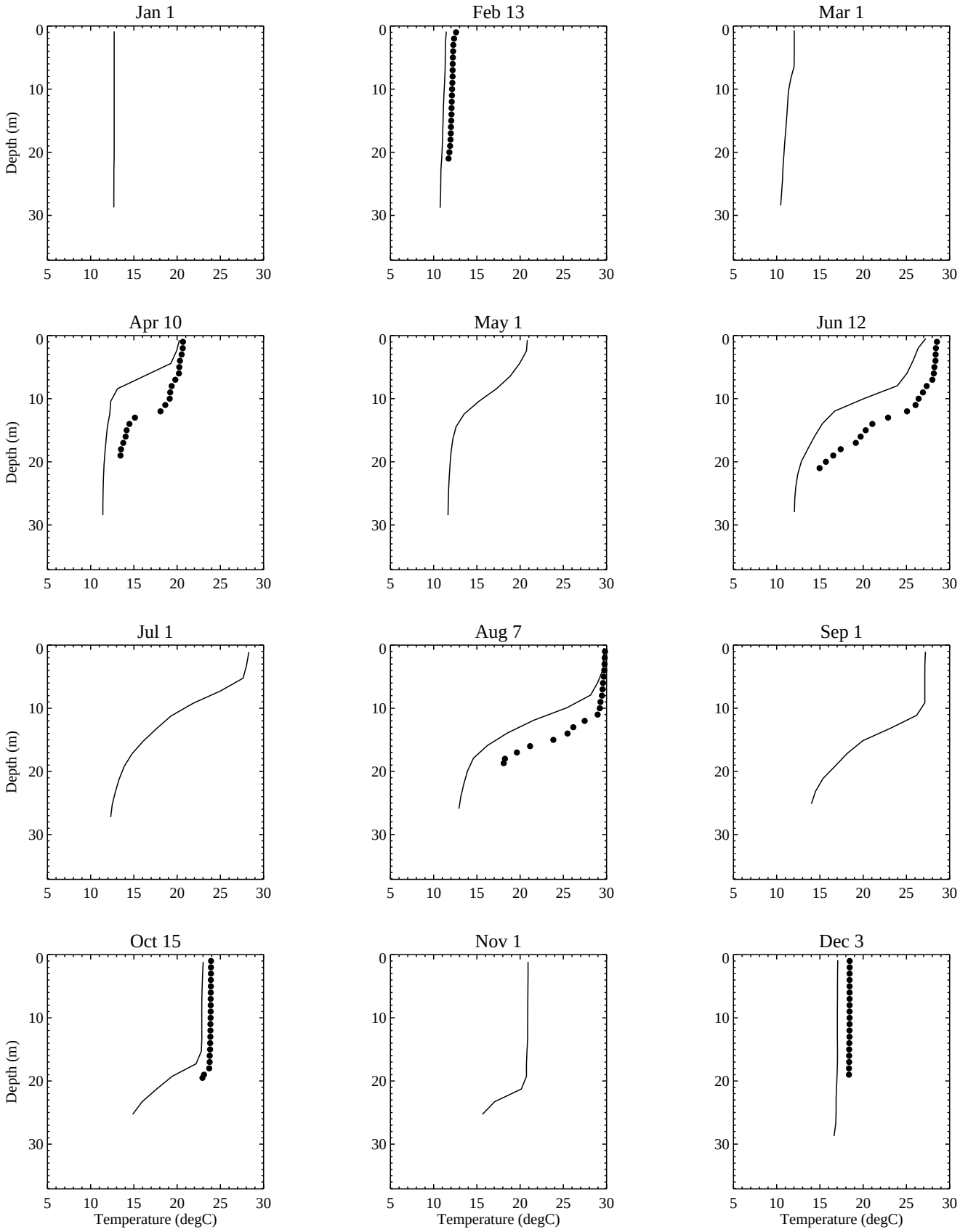

Figure J-5. Vertical profiles of model versus data at Sandy Creek (Segment 161) - Temperature - 2001.

Profiles shown for dates with available data else model results for first day of month shown.

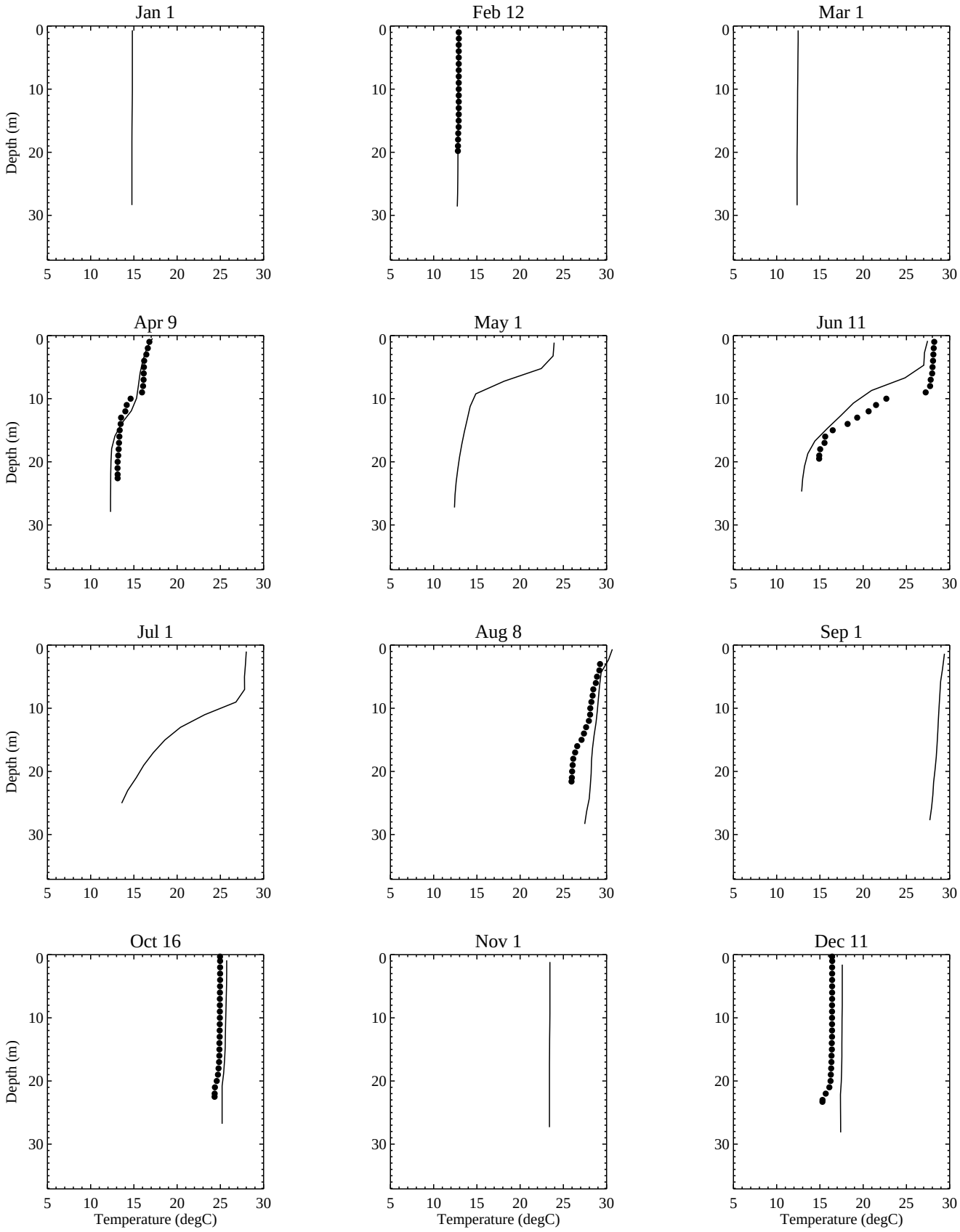

Figure J-5. Vertical profiles of model versus data at Sandy Creek (Segment 161) - Temperature - 2002.

Profiles shown for dates with available data else model results for first day of month shown.

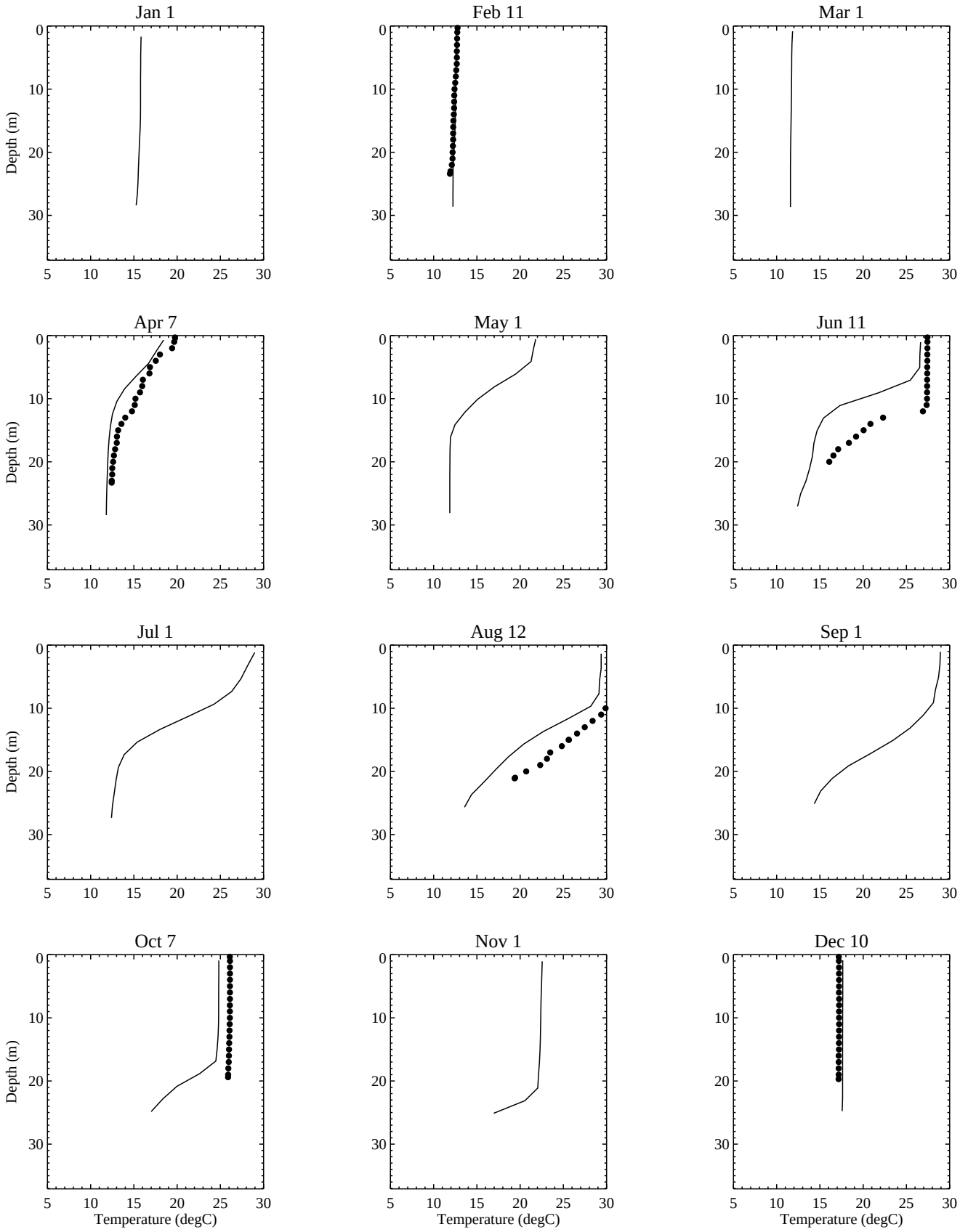

Figure J-5. Vertical profiles of model versus data at Sandy Creek (Segment 161) - Temperature - 2003.

Profiles shown for dates with available data else model results for first day of month shown.

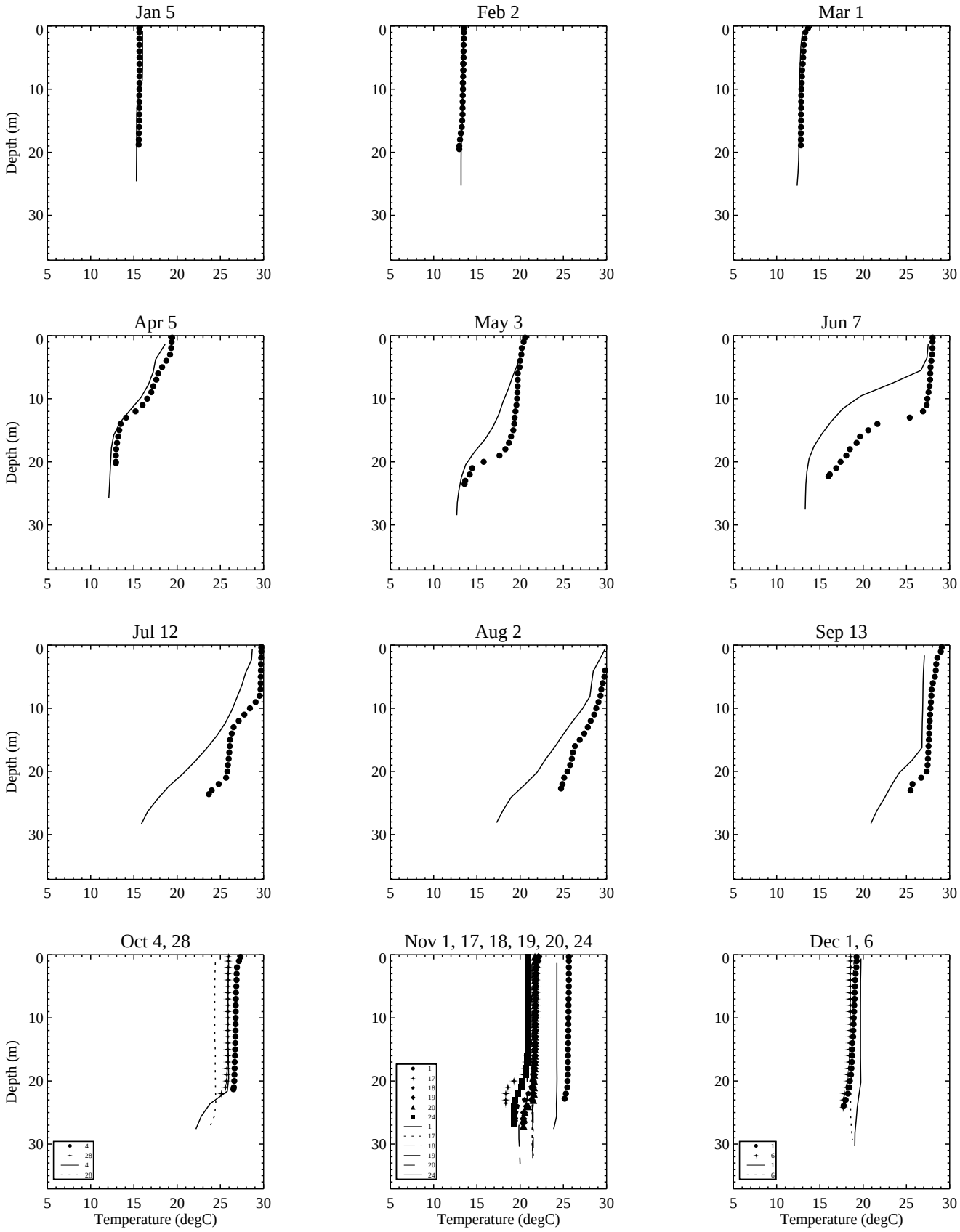

Figure J-5. Vertical profiles of model versus data at Sandy Creek (Segment 161) - Temperature - 2004.

Profiles shown for dates with available data else model results for first day of month shown.

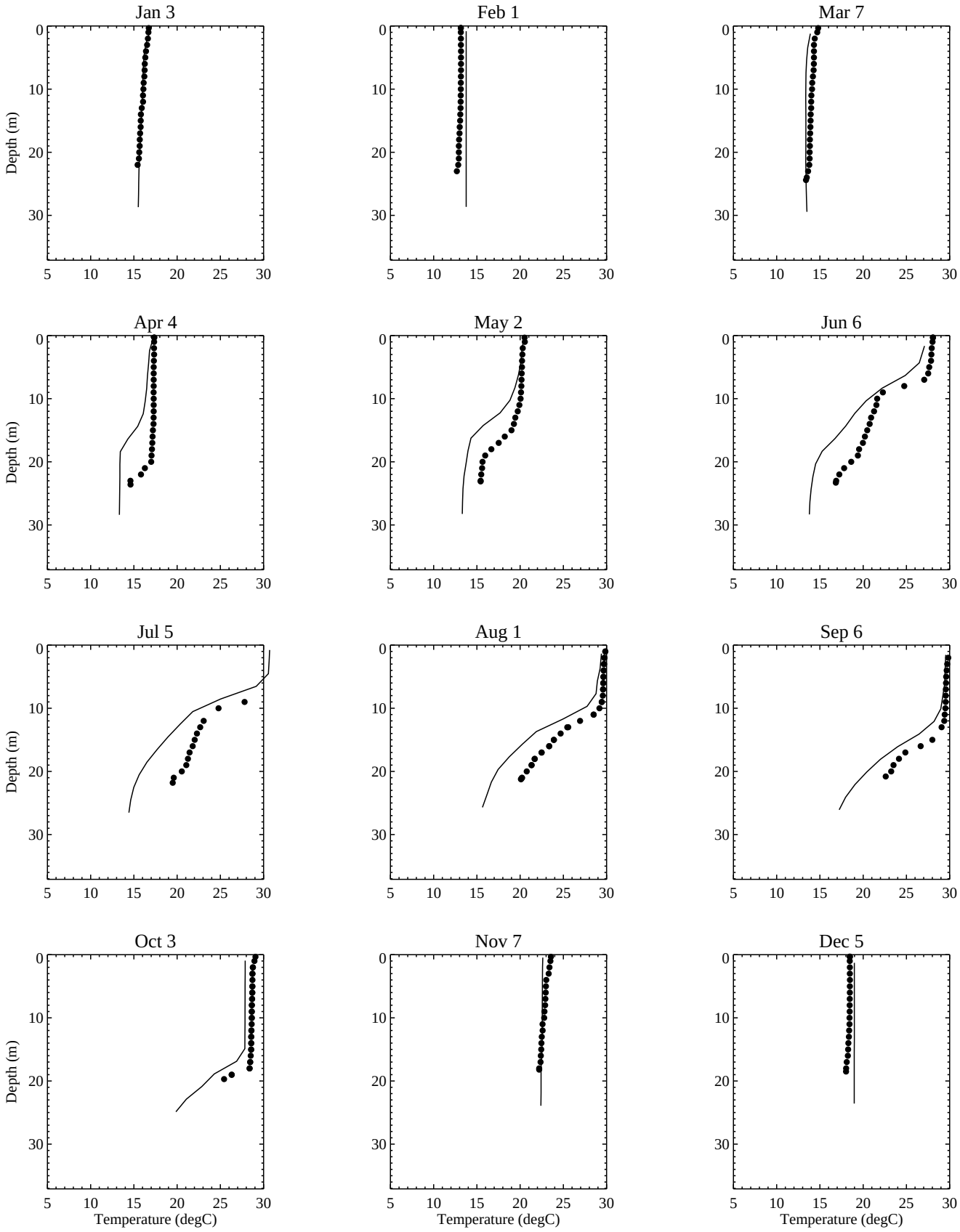

Figure J-5. Vertical profiles of model versus data at Sandy Creek (Segment 161) - Temperature - 2005.

Profiles shown for dates with available data else model results for first day of month shown.

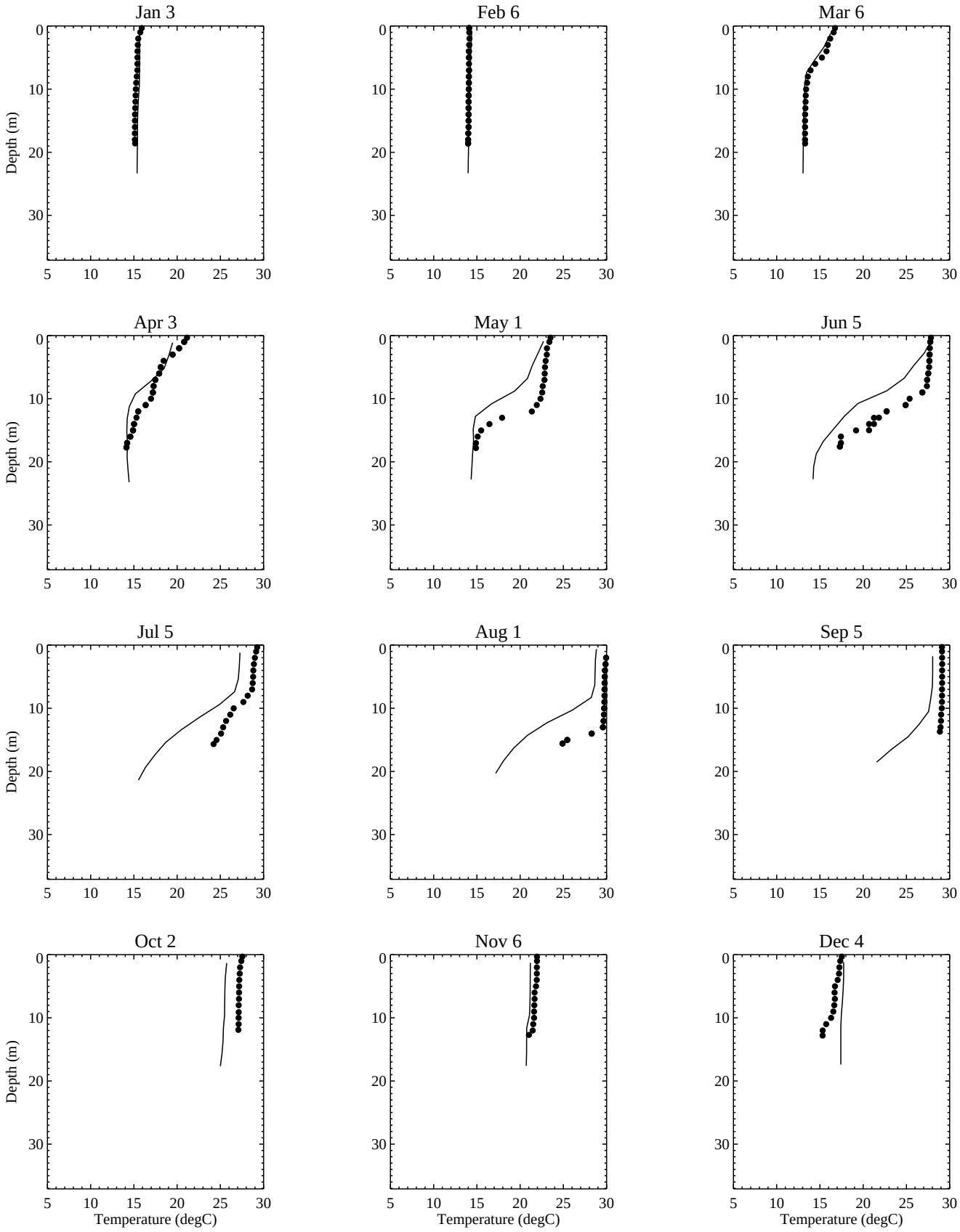

Figure J-5. Vertical profiles of model versus data at Sandy Creek (Segment 161) - Temperature - 2006.

Profiles shown for dates with available data else model results for first day of month shown.

Model Data

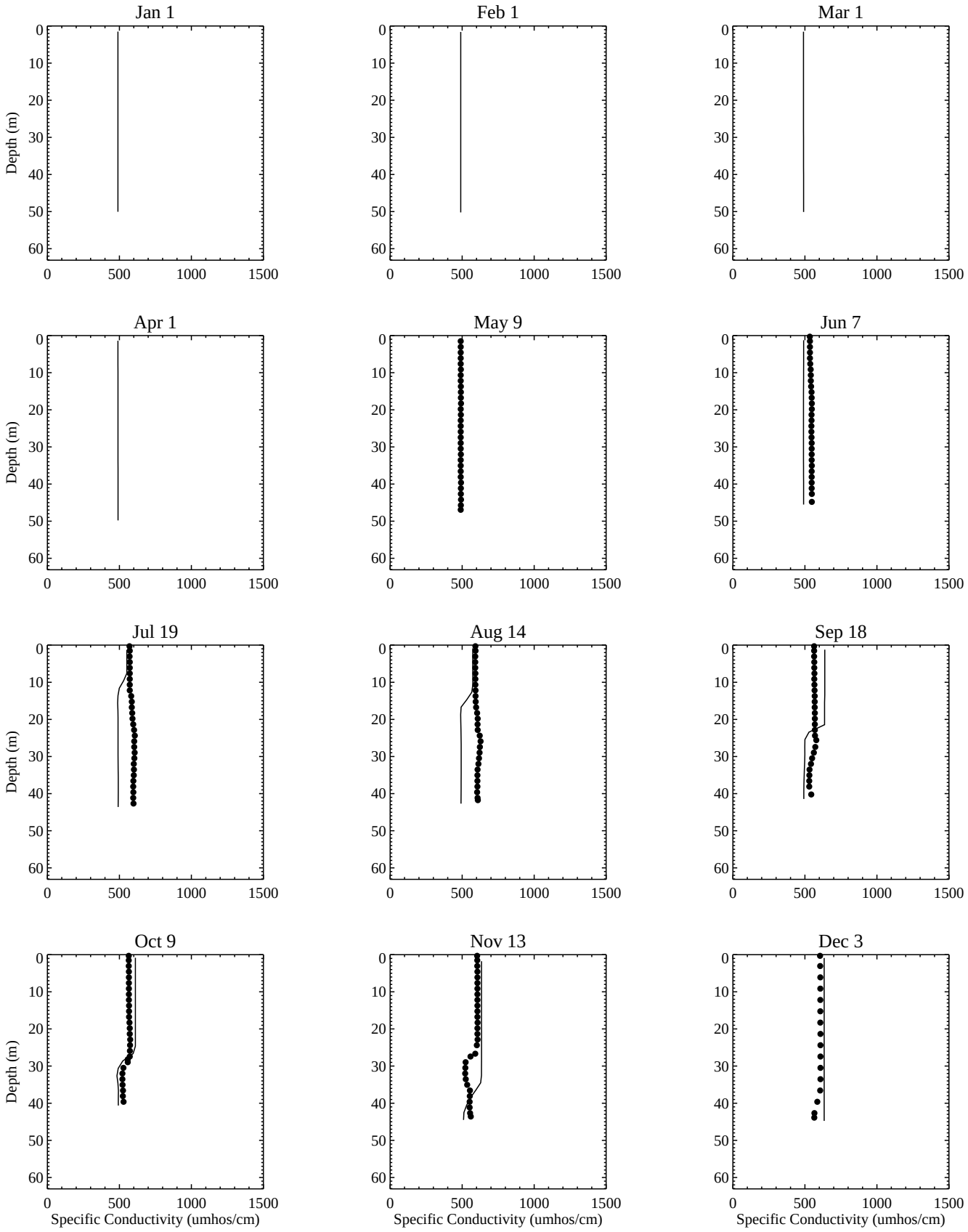

Figure J-6. Vertical profiles of model versus data at Mansfield Dam (Segment 93) - Specific Conductivity - 1984.

Profiles shown for dates with available data else model results for first day of month shown.

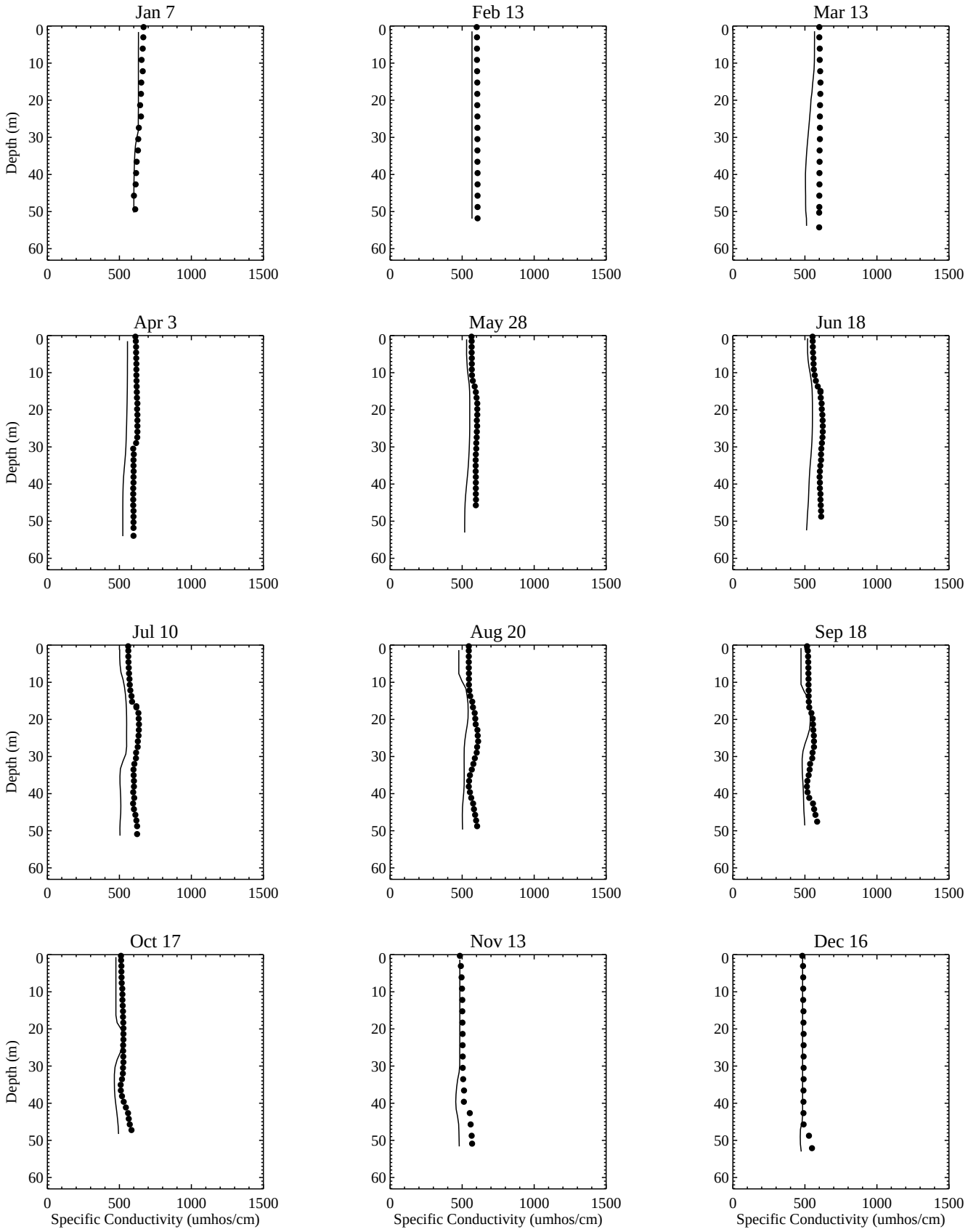

Figure J-6. Vertical profiles of model versus data at Mansfield Dam (Segment 93) - Specific Conductivity - 1985.

Profiles shown for dates with available data else model results for first day of month shown.

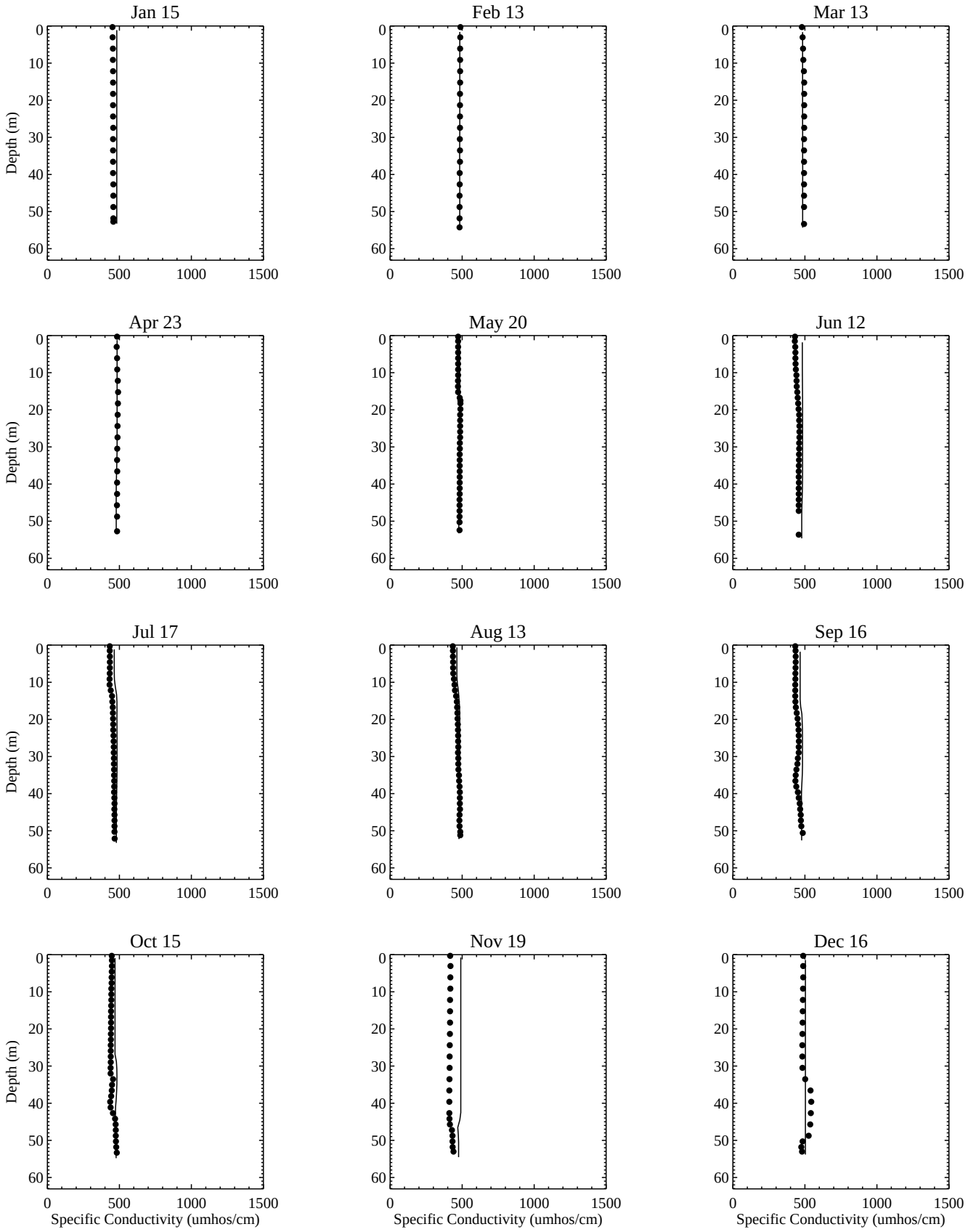

Figure J-6. Vertical profiles of model versus data at Mansfield Dam (Segment 93) - Specific Conductivity - 1986.

Profiles shown for dates with available data else model results for first day of month shown.

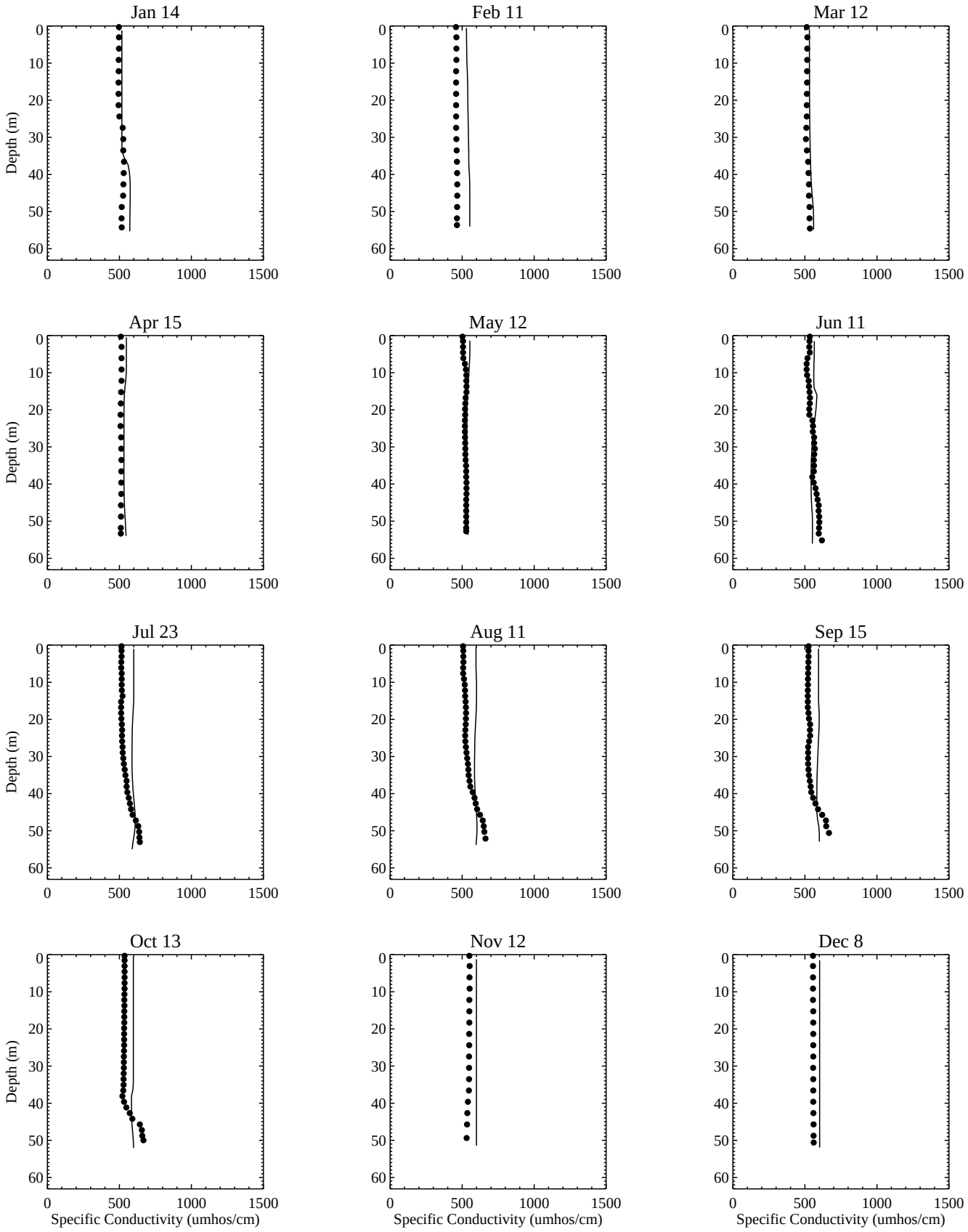

Figure J-6. Vertical profiles of model versus data at Mansfield Dam (Segment 93) - Specific Conductivity - 1987.

Profiles shown for dates with available data else model results for first day of month shown.

Model Data

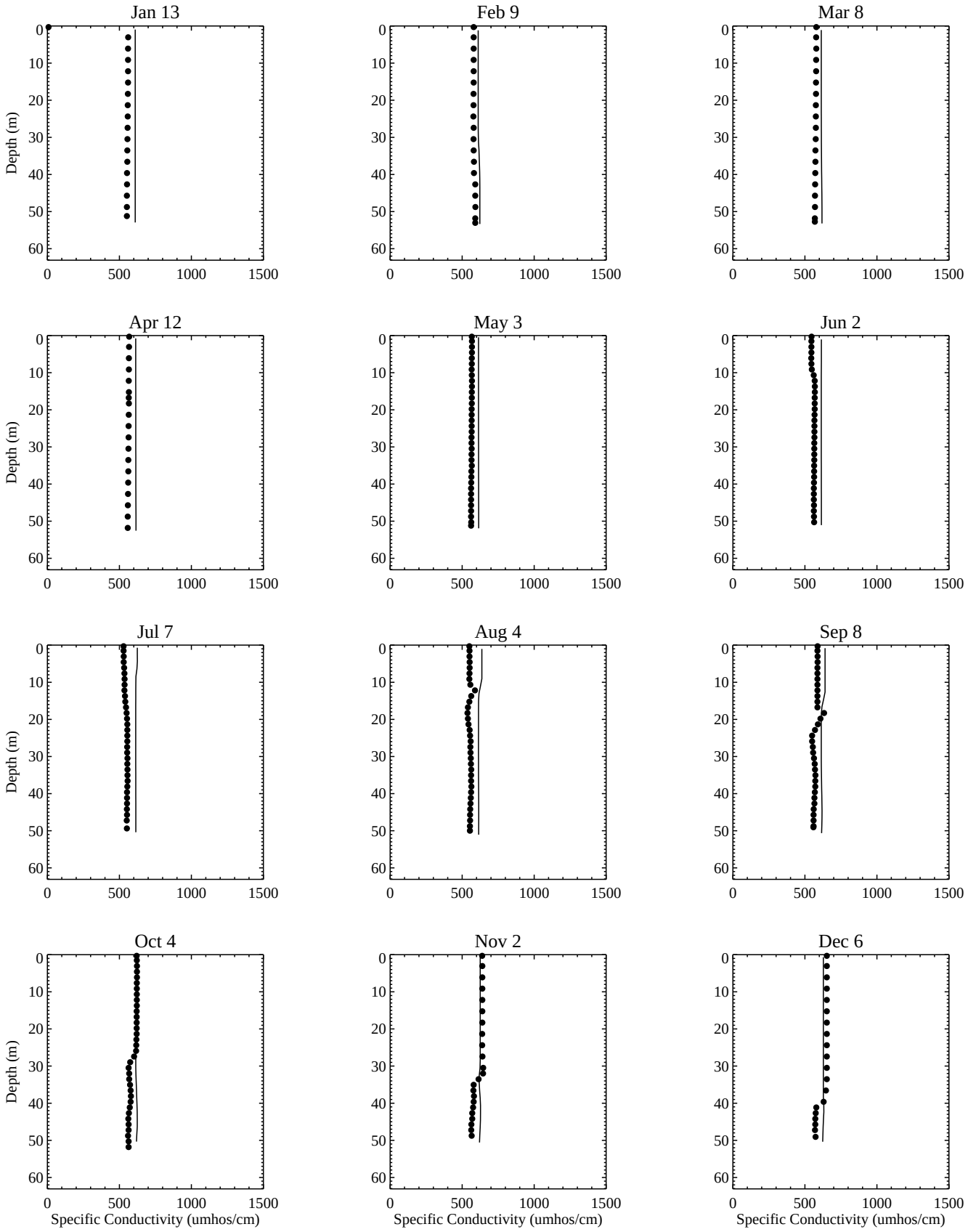

Figure J-6. Vertical profiles of model versus data at Mansfield Dam (Segment 93) - Specific Conductivity - 1988.

Profiles shown for dates with available data else model results for first day of month shown.

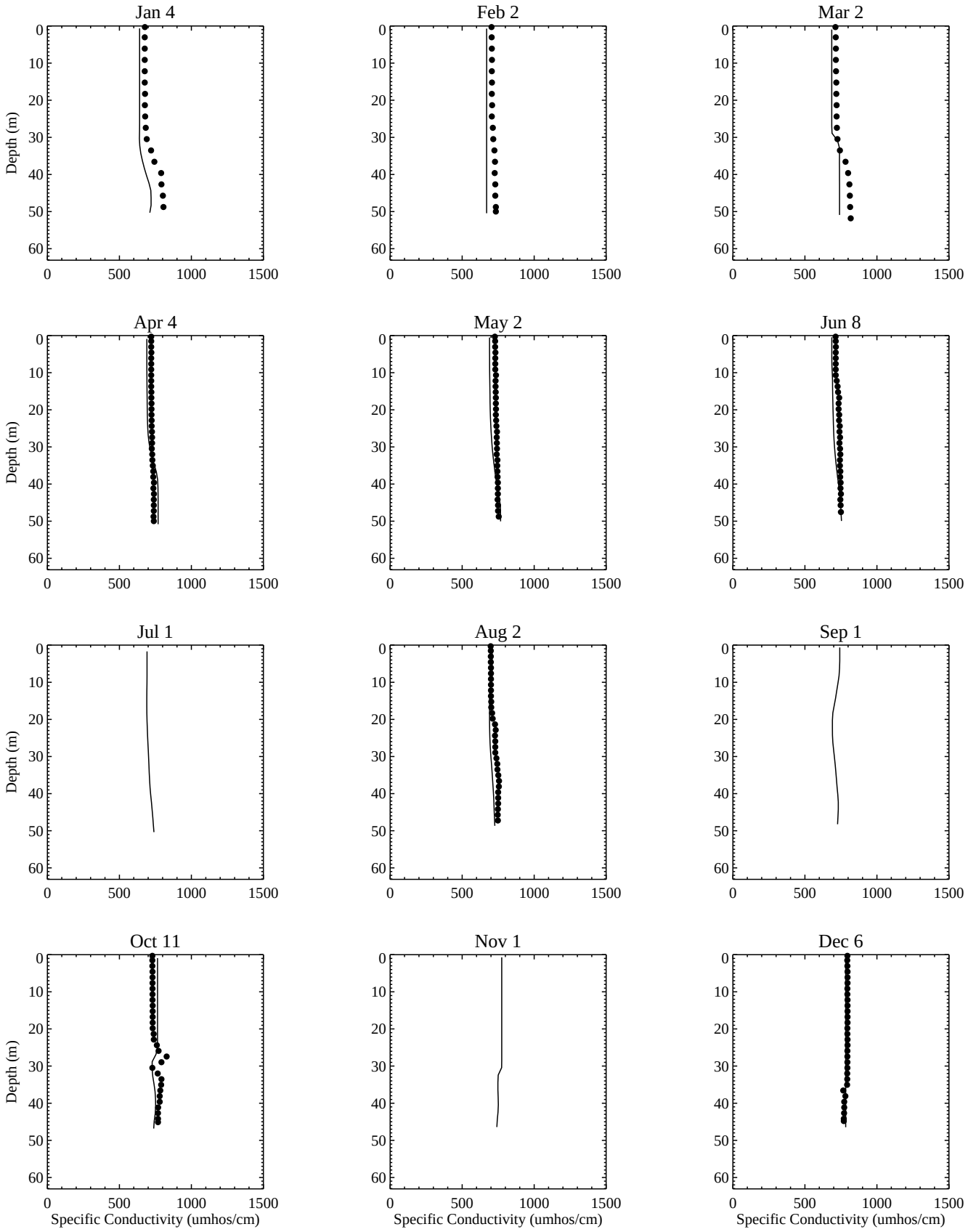

Figure J-6. Vertical profiles of model versus data at Mansfield Dam (Segment 93) - Specific Conductivity - 1989.

Profiles shown for dates with available data else model results for first day of month shown.

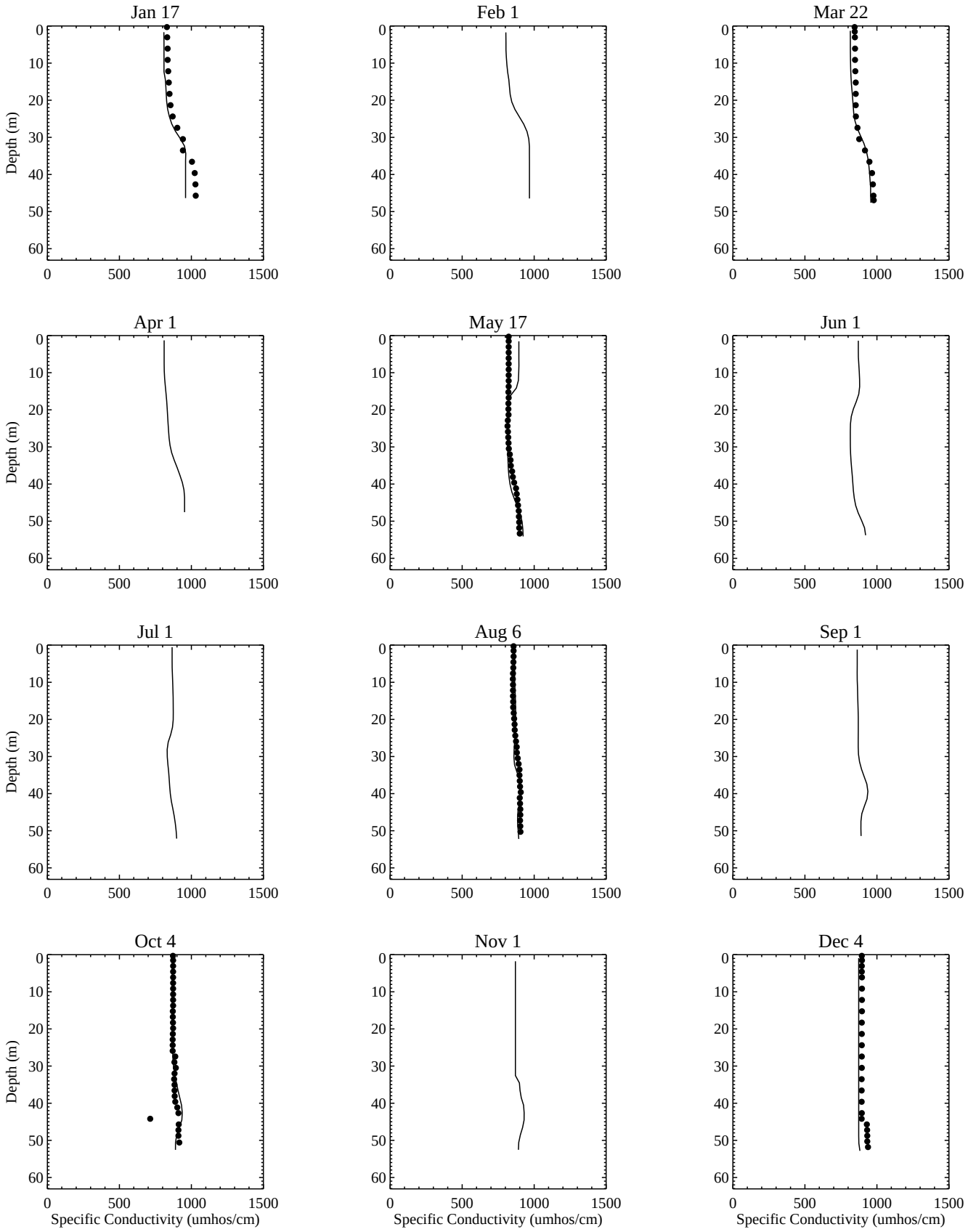

Figure J-6. Vertical profiles of model versus data at Mansfield Dam (Segment 93) - Specific Conductivity - 1990.

Profiles shown for dates with available data else model results for first day of month shown.

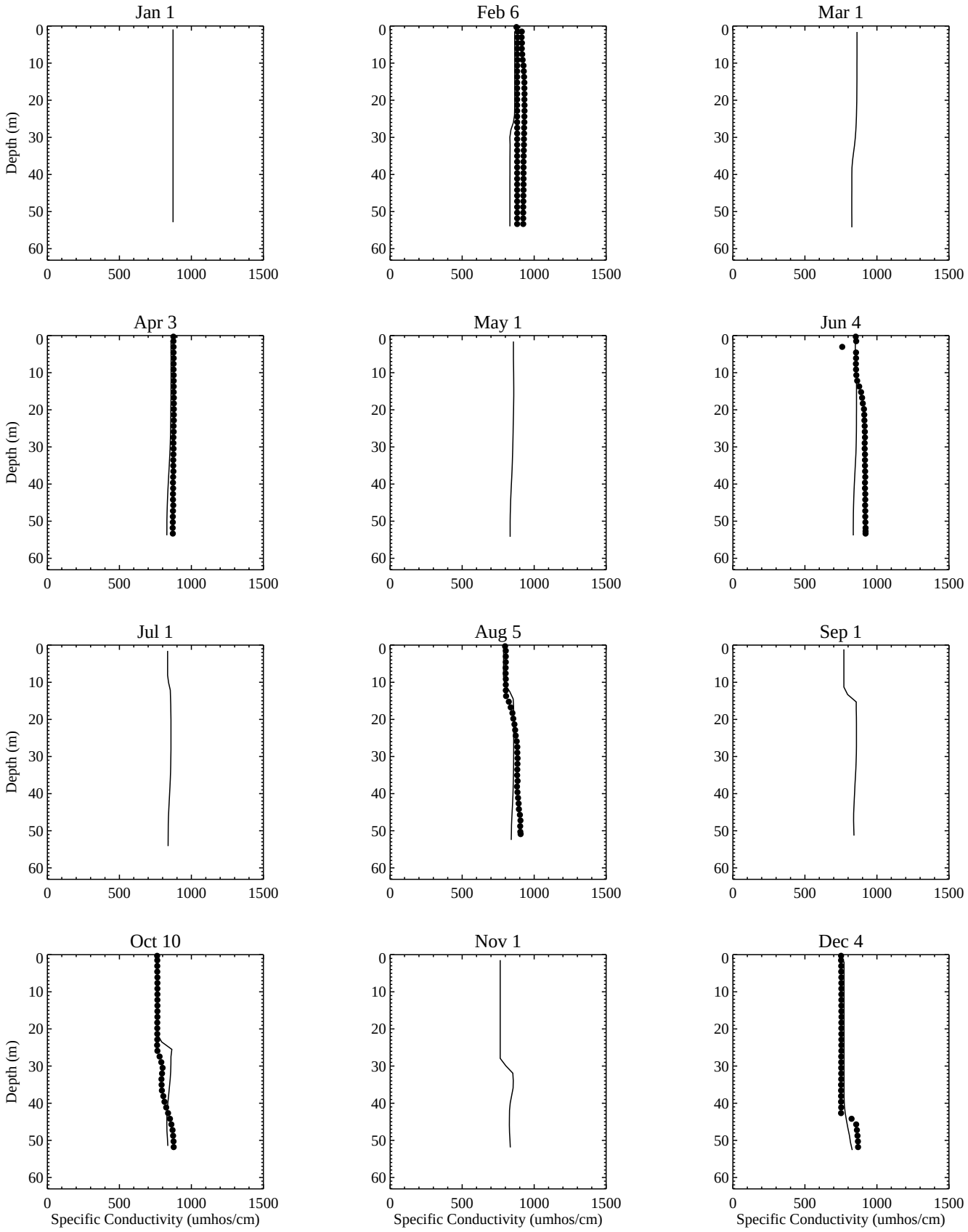

Figure J-6. Vertical profiles of model versus data at Mansfield Dam (Segment 93) - Specific Conductivity - 1991.

Profiles shown for dates with available data else model results for first day of month shown.

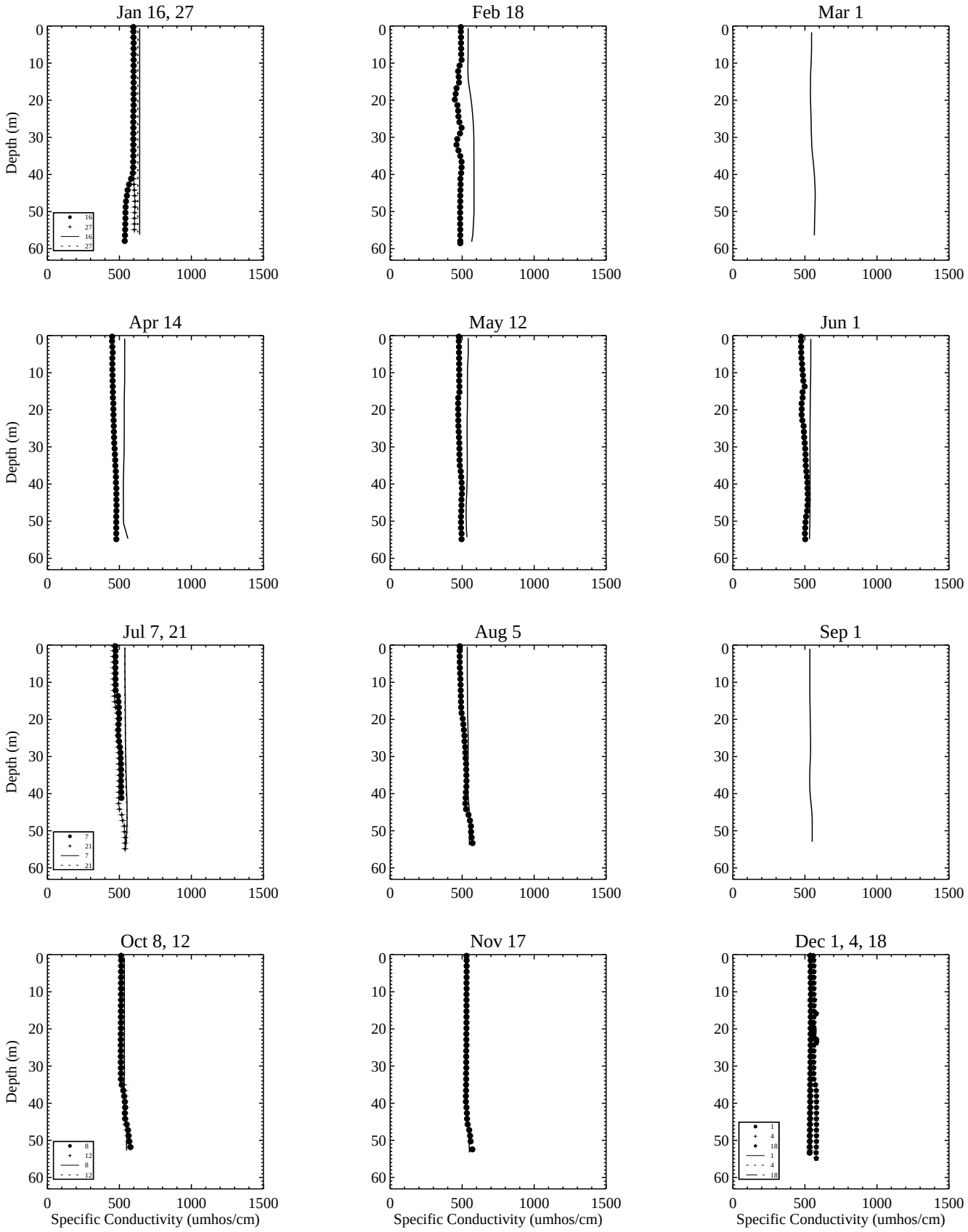

Figure J-6. Vertical profiles of model versus data at Mansfield Dam (Segment 93) - Specific Conductivity - 1992.

Profiles shown for dates with available data else model results for first day of month shown.

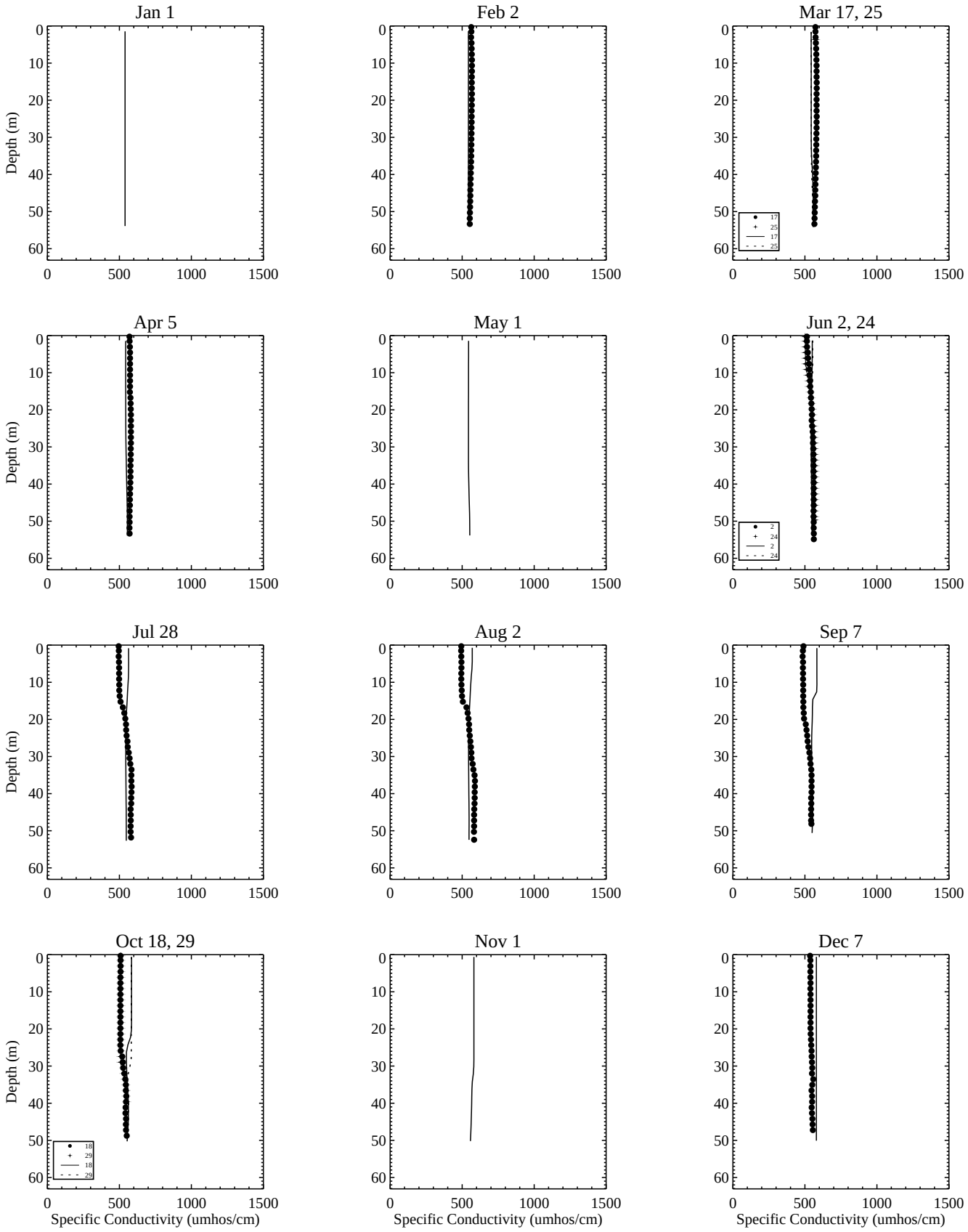

Figure J-6. Vertical profiles of model versus data at Mansfield Dam (Segment 93) - Specific Conductivity - 1993.

Profiles shown for dates with available data else model results for first day of month shown.

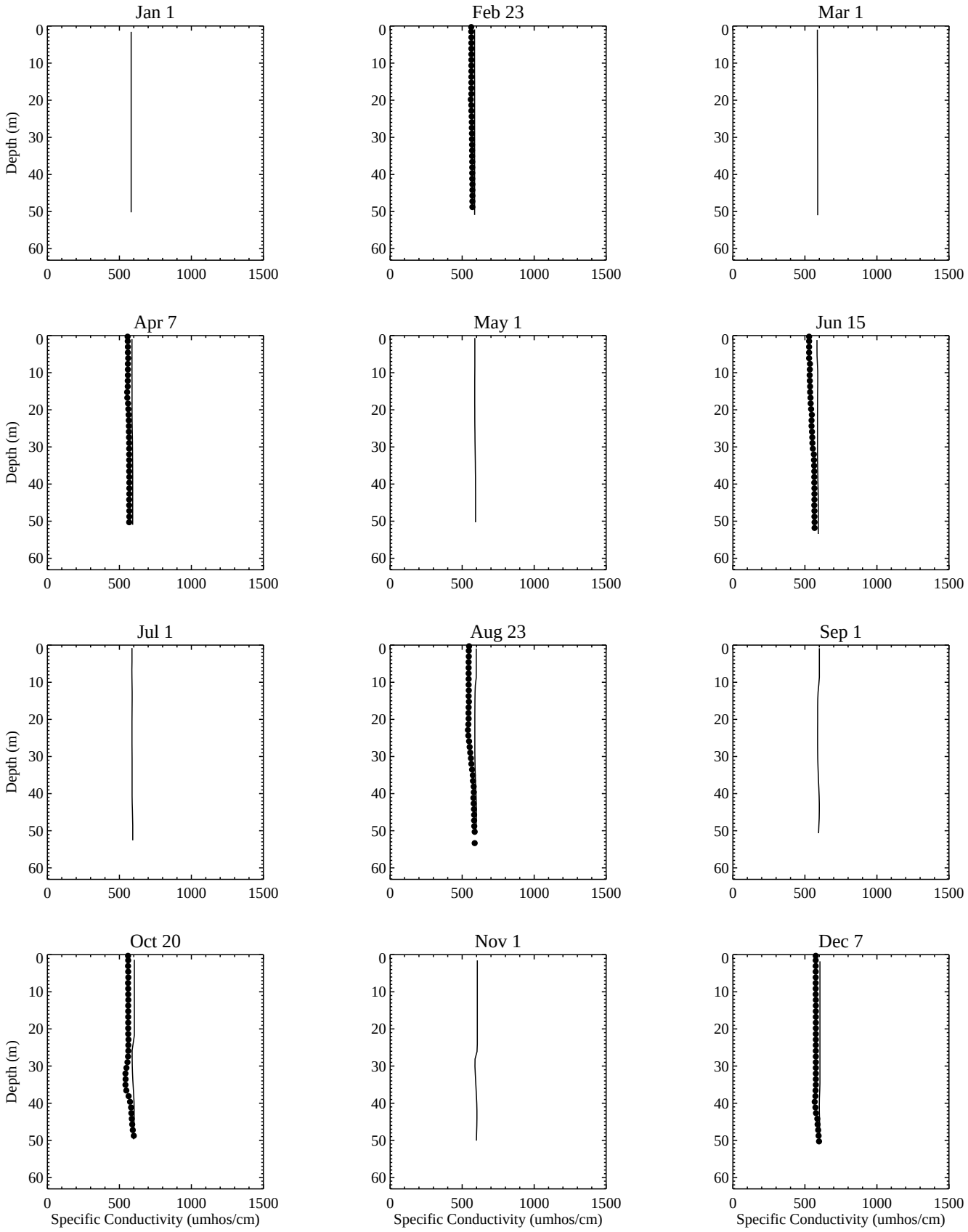

Figure J-6. Vertical profiles of model versus data at Mansfield Dam (Segment 93) - Specific Conductivity - 1994.

Profiles shown for dates with available data else model results for first day of month shown.

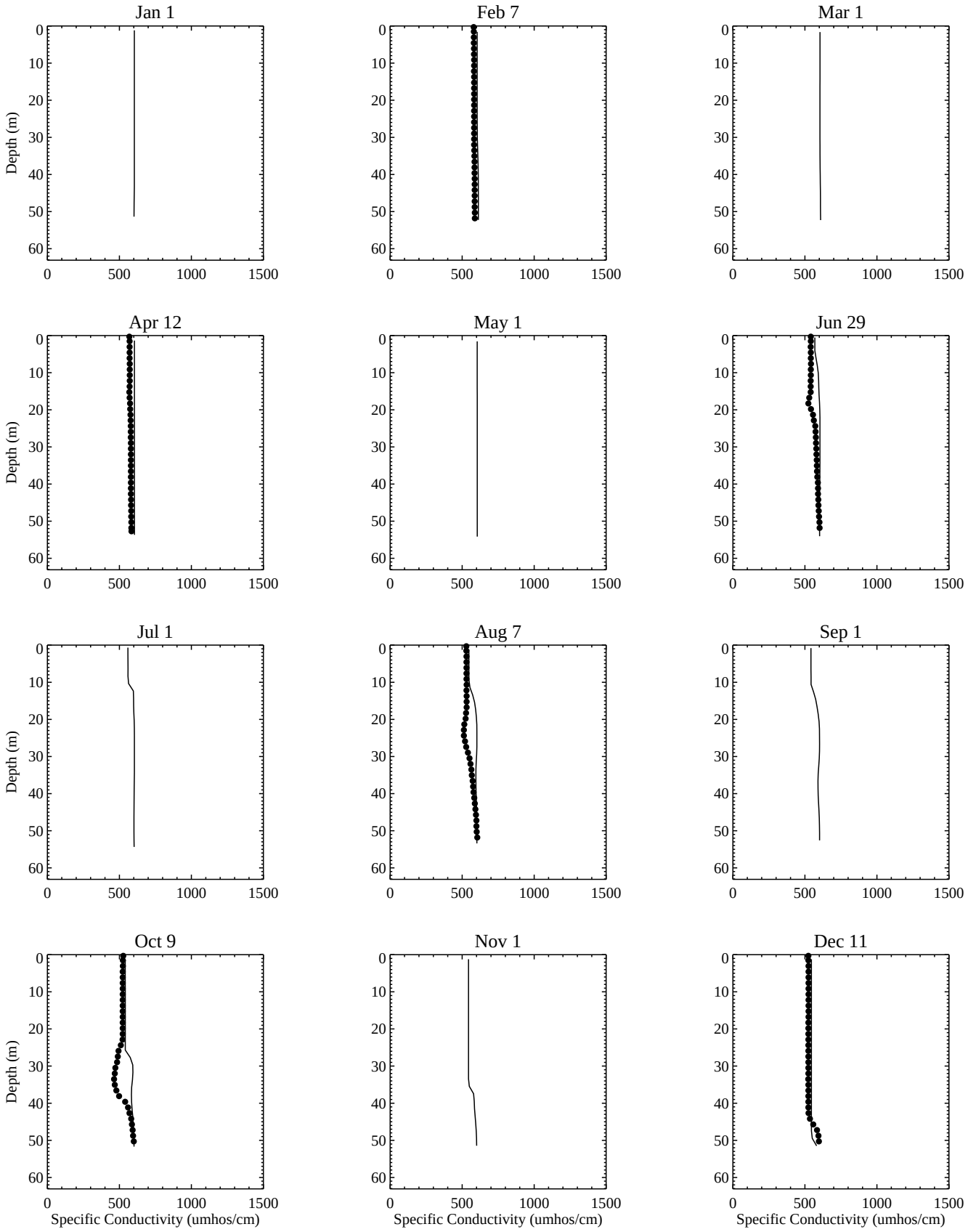

Figure J-6. Vertical profiles of model versus data at Mansfield Dam (Segment 93) - Specific Conductivity - 1995.

Profiles shown for dates with available data else model results for first day of month shown.

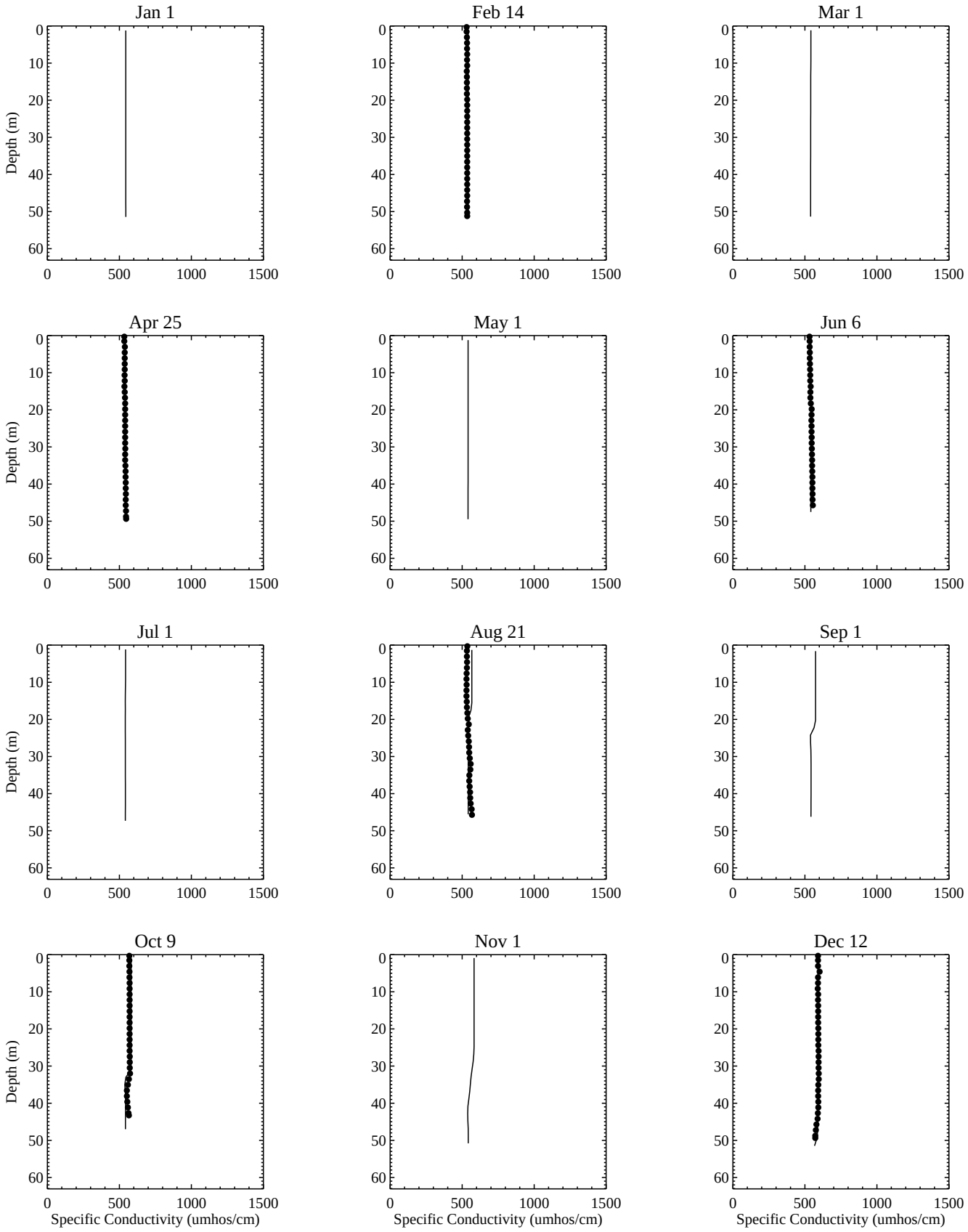

Figure J-6. Vertical profiles of model versus data at Mansfield Dam (Segment 93) - Specific Conductivity - 1996.

Profiles shown for dates with available data else model results for first day of month shown.

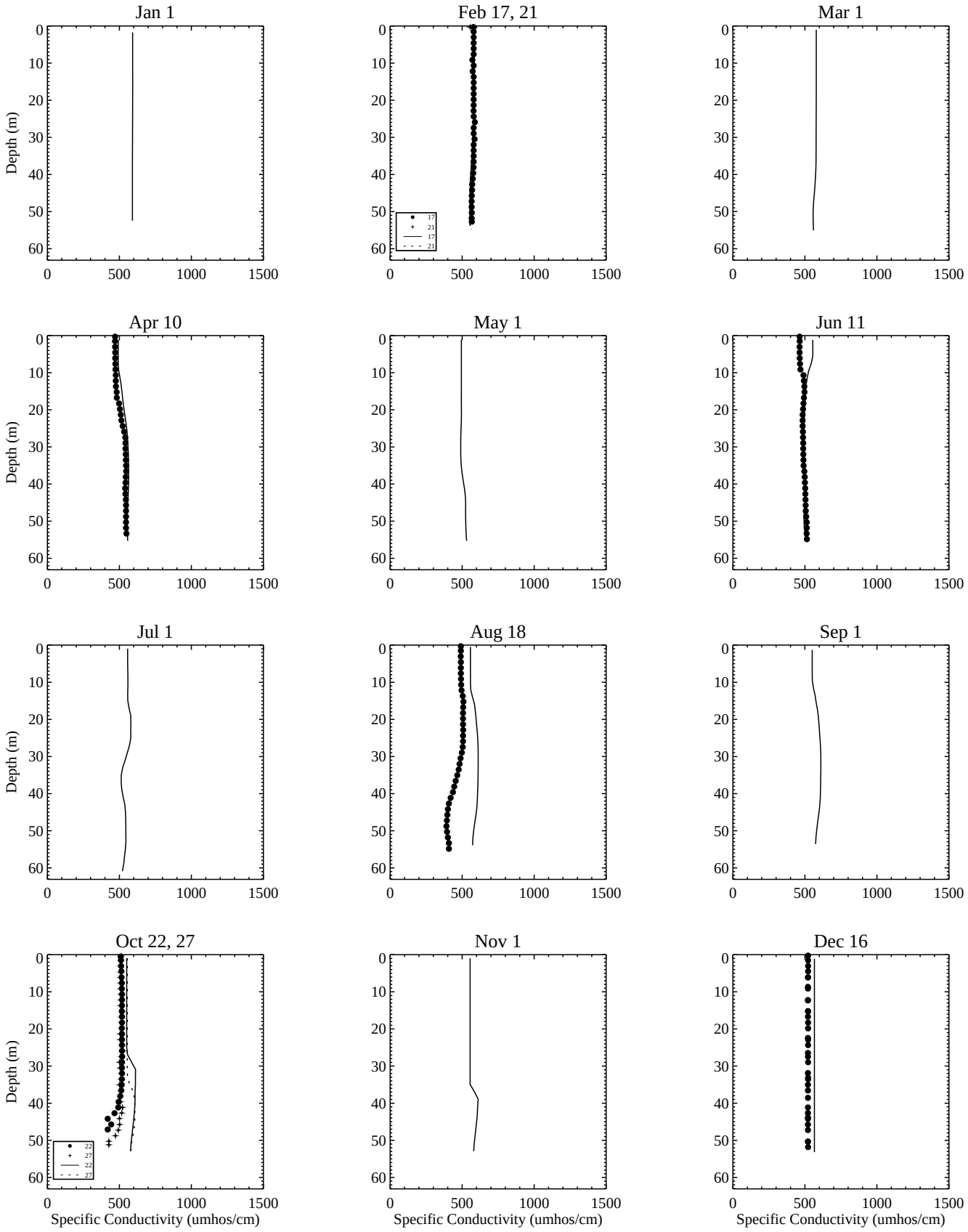

Figure J-6. Vertical profiles of model versus data at Mansfield Dam (Segment 93) - Specific Conductivity - 1997.

Profiles shown for dates with available data else model results for first day of month shown.

Model Data

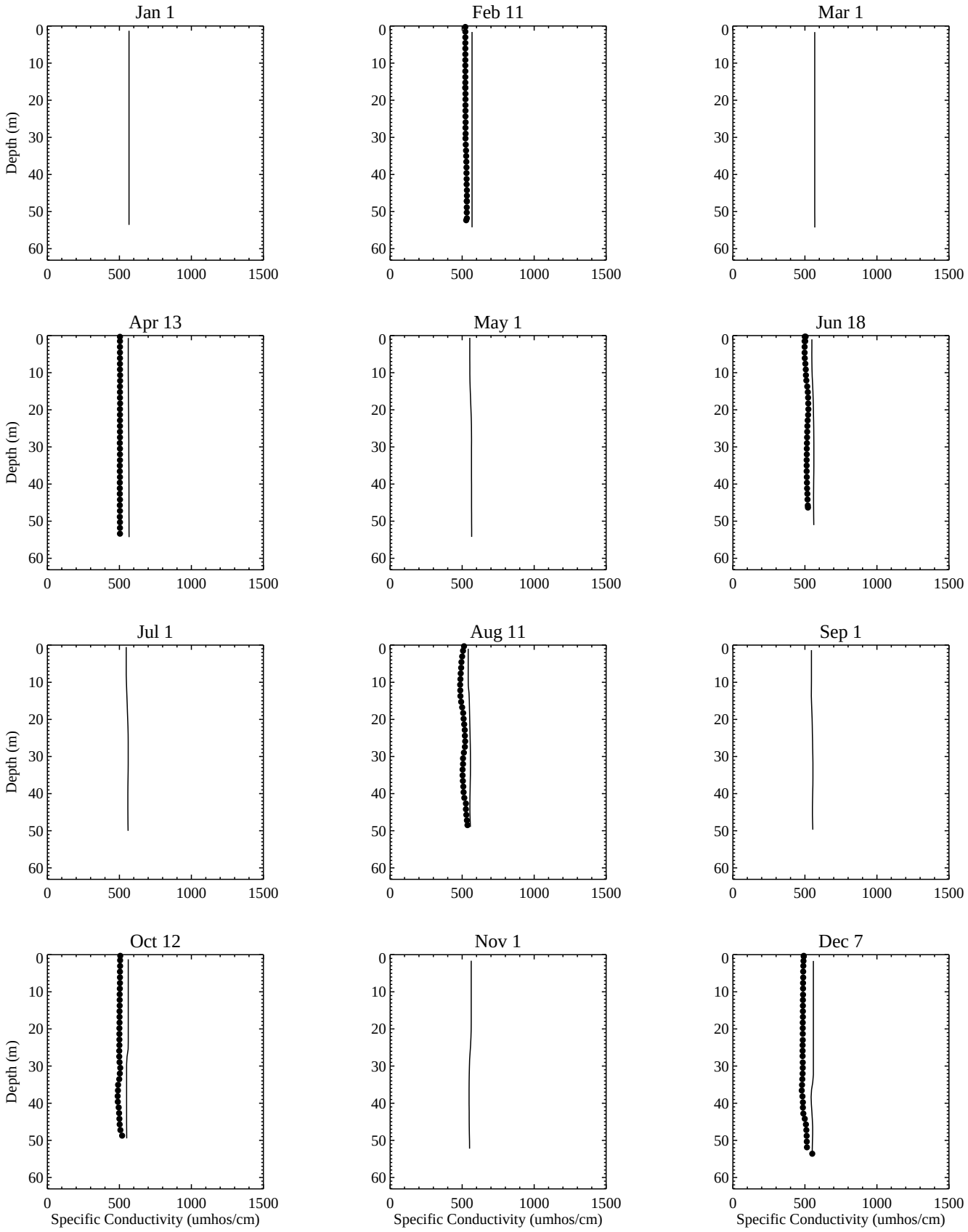

Figure J-6. Vertical profiles of model versus data at Mansfield Dam (Segment 93) - Specific Conductivity - 1998.

Profiles shown for dates with available data else model results for first day of month shown.

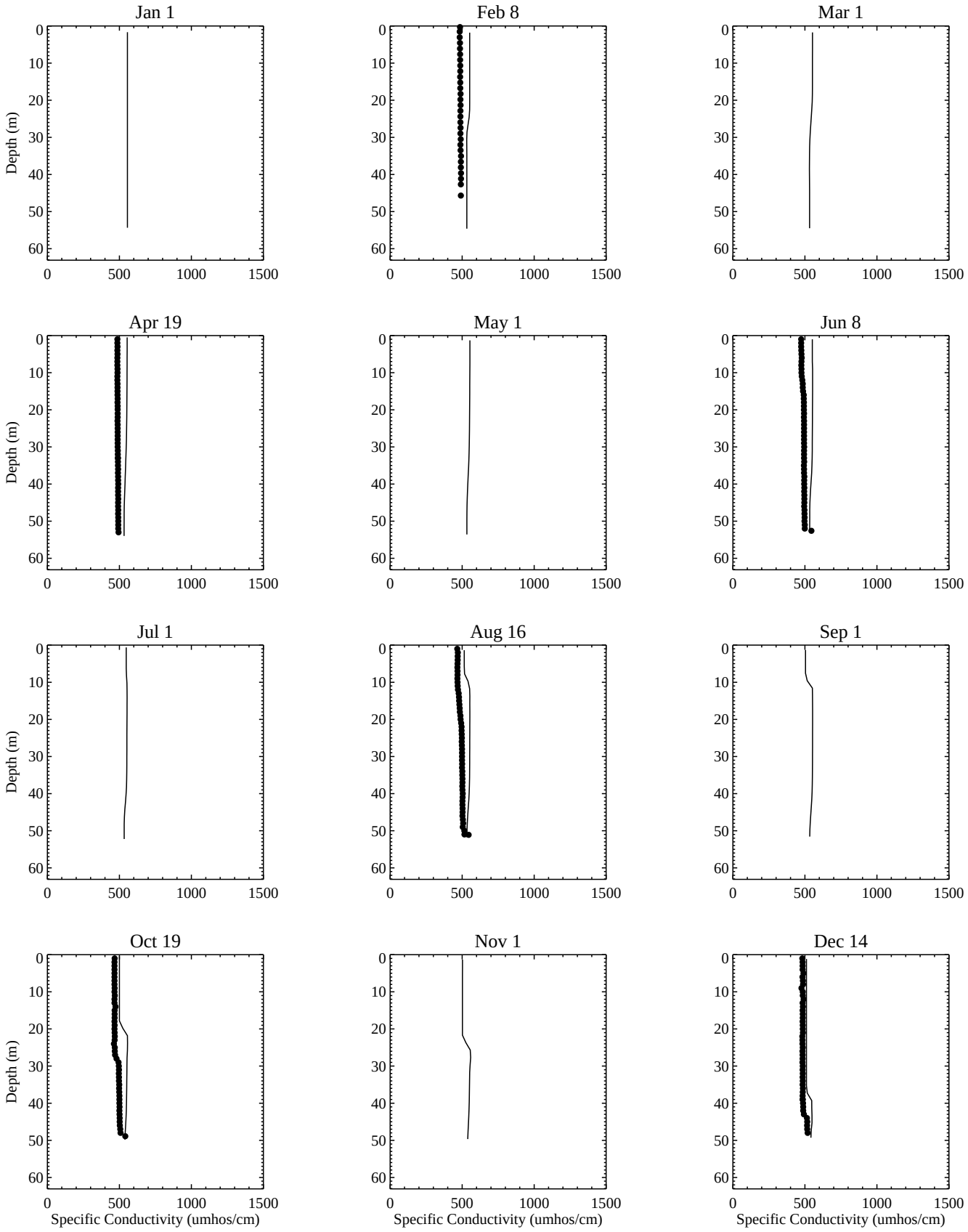

Figure J-6. Vertical profiles of model versus data at Mansfield Dam (Segment 93) - Specific Conductivity - 1999.

Profiles shown for dates with available data else model results for first day of month shown.

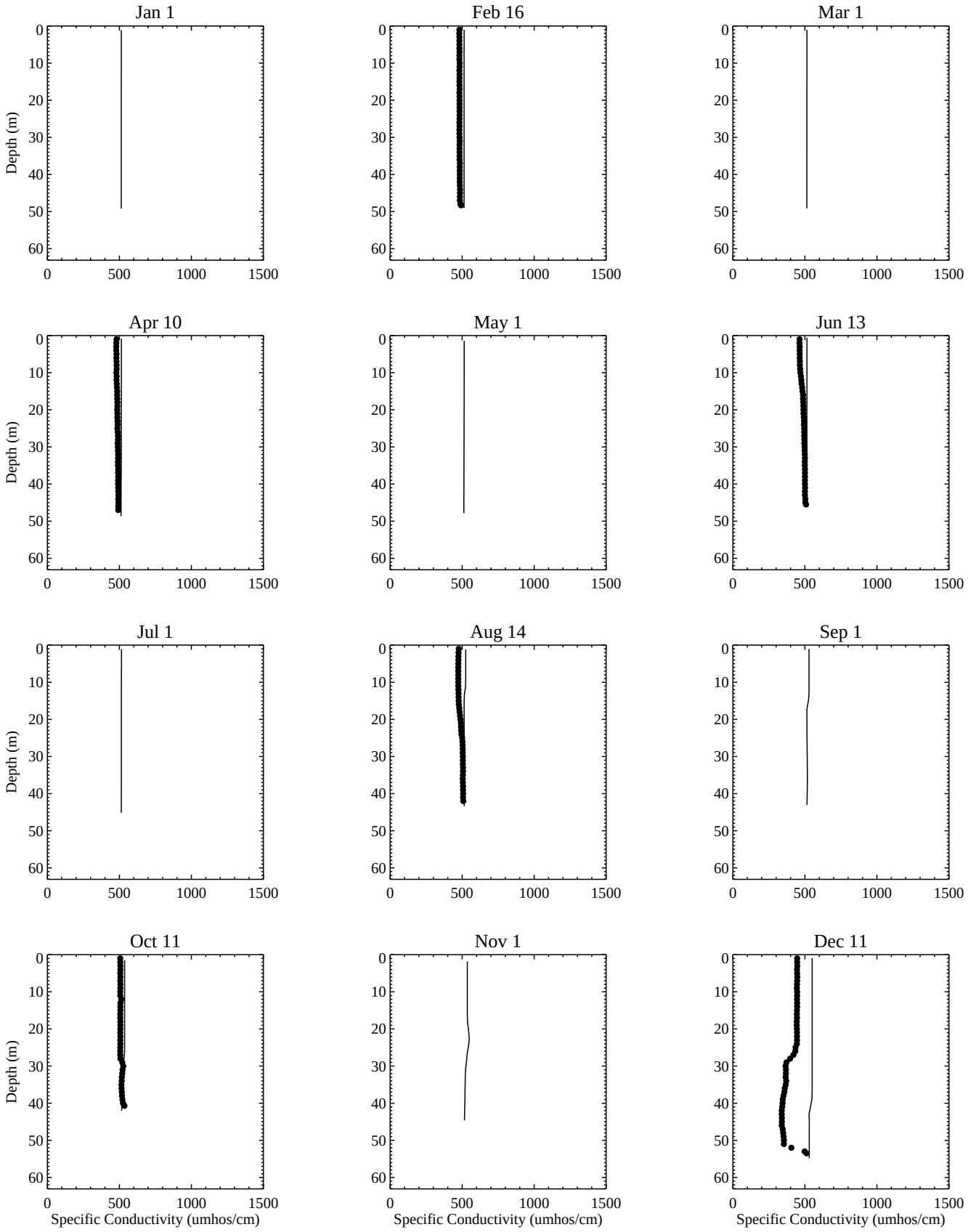

Figure J-6. Vertical profiles of model versus data at Mansfield Dam (Segment 93) - Specific Conductivity - 2000.

Profiles shown for dates with available data else model results for first day of month shown.

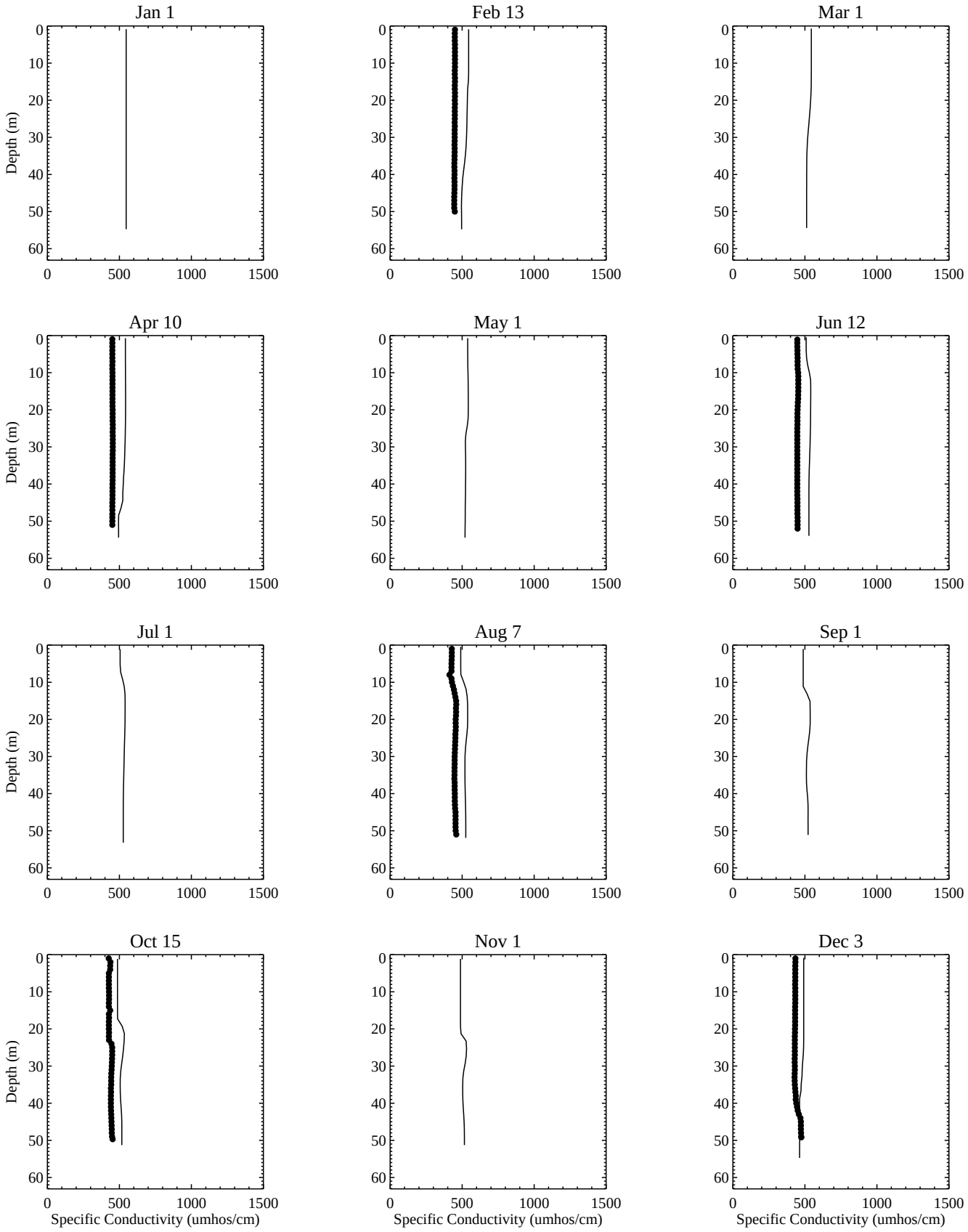

Figure J-6. Vertical profiles of model versus data at Mansfield Dam (Segment 93) - Specific Conductivity - 2001.

Profiles shown for dates with available data else model results for first day of month shown.

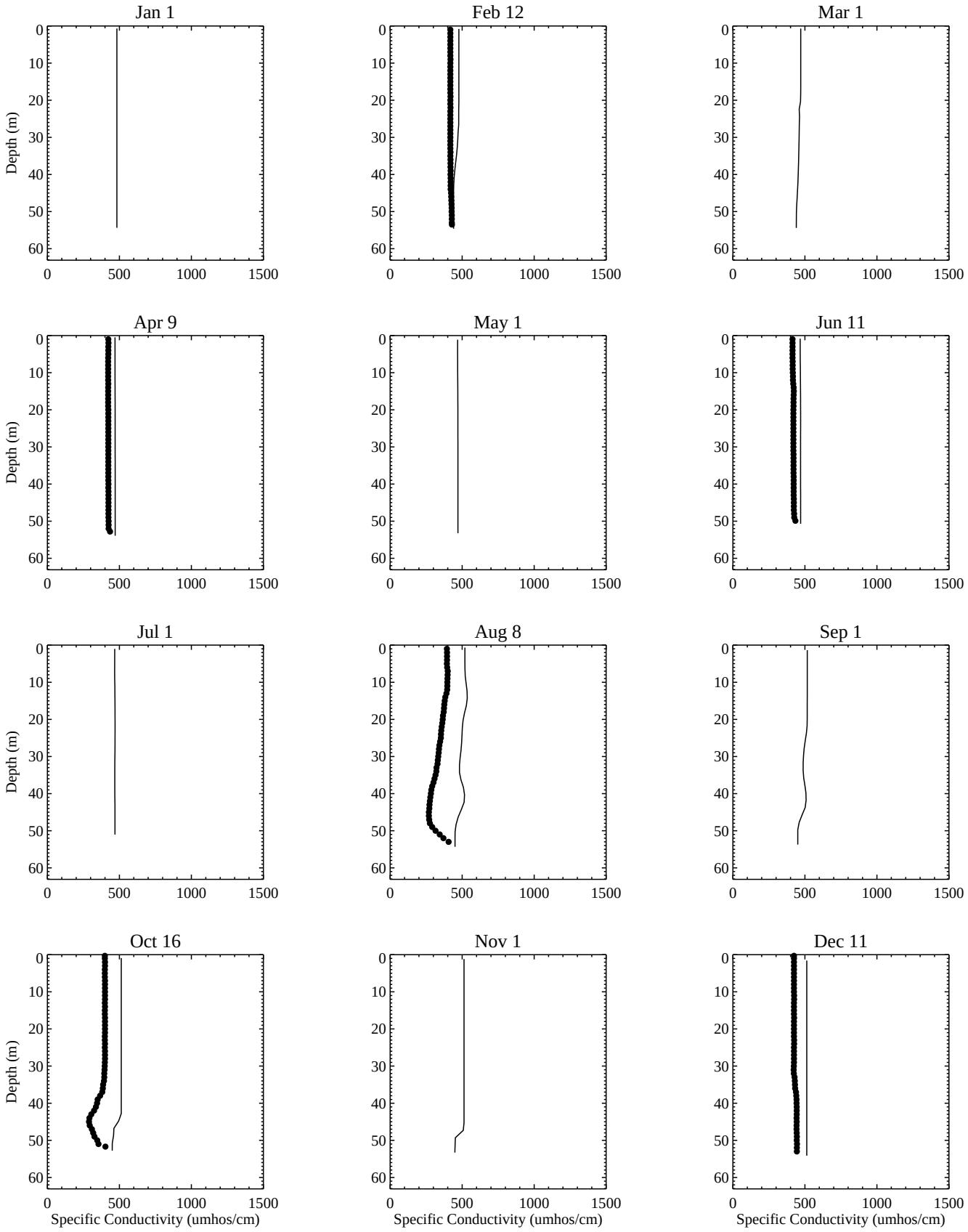

Figure J-6. Vertical profiles of model versus data at Mansfield Dam (Segment 93) - Specific Conductivity - 2002.

Profiles shown for dates with available data else model results for first day of month shown.

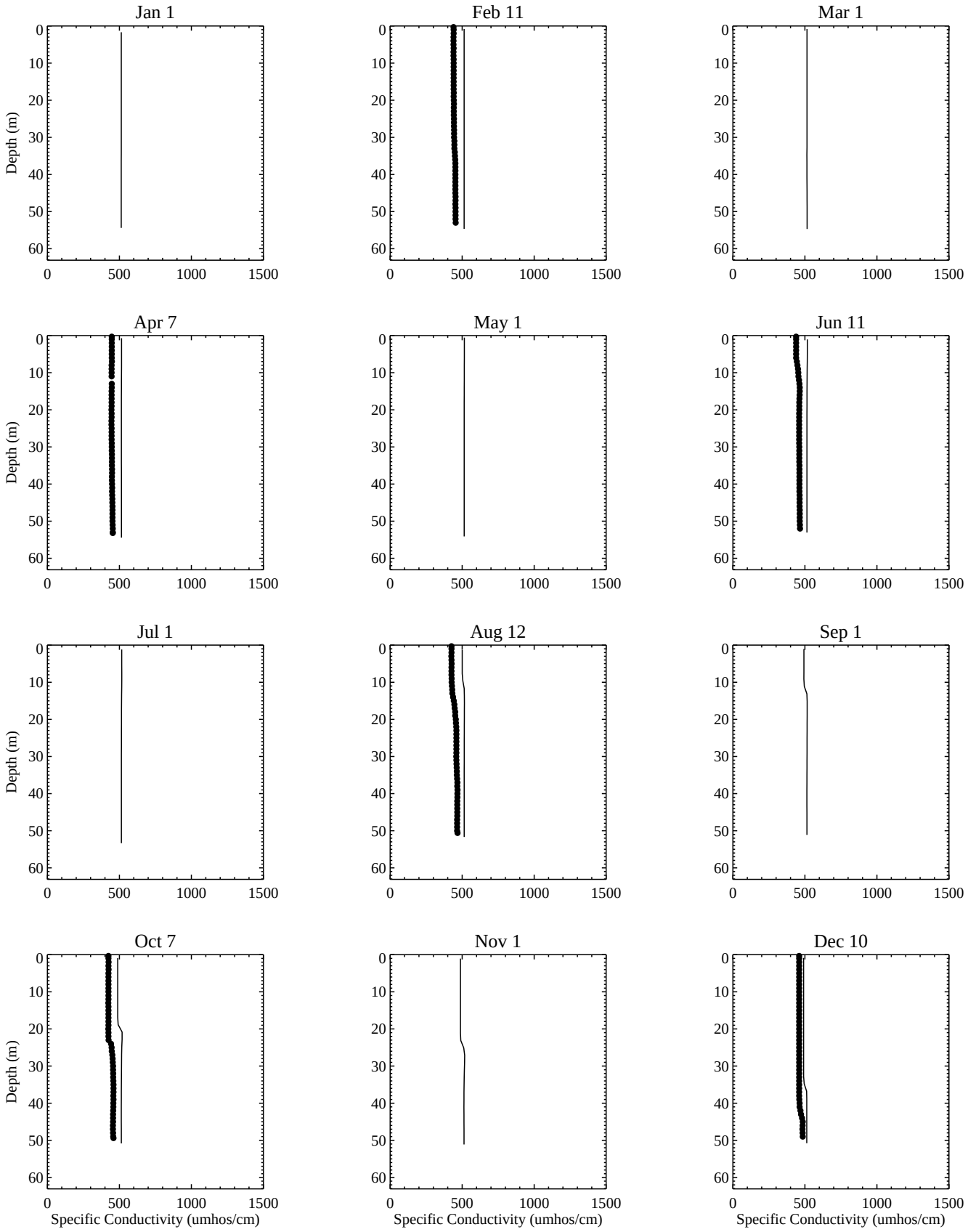

Figure J-6. Vertical profiles of model versus data at Mansfield Dam (Segment 93) - Specific Conductivity - 2003.

Profiles shown for dates with available data else model results for first day of month shown.

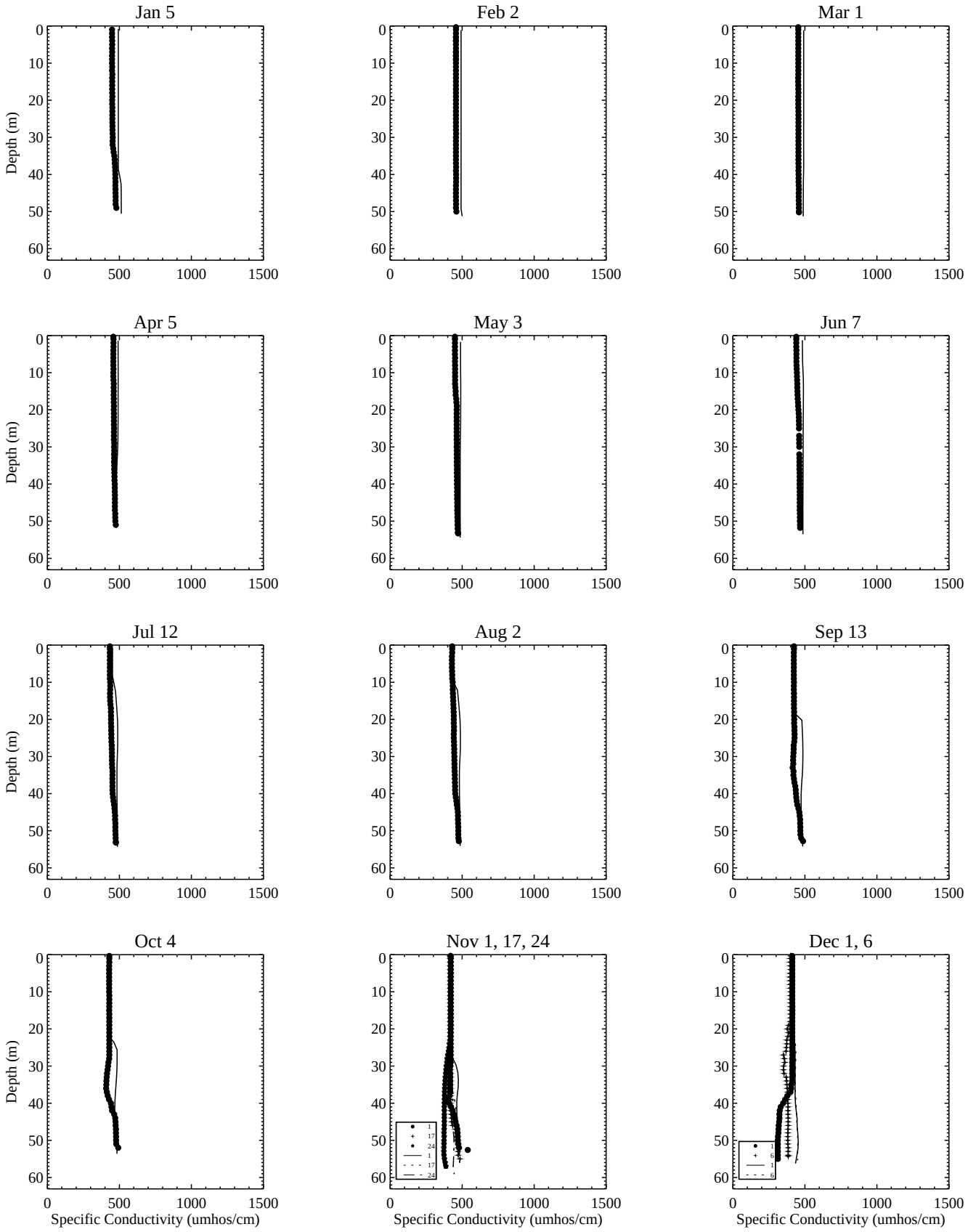

Figure J-6. Vertical profiles of model versus data at Mansfield Dam (Segment 93) - Specific Conductivity - 2004.

Profiles shown for dates with available data else model results for first day of month shown.

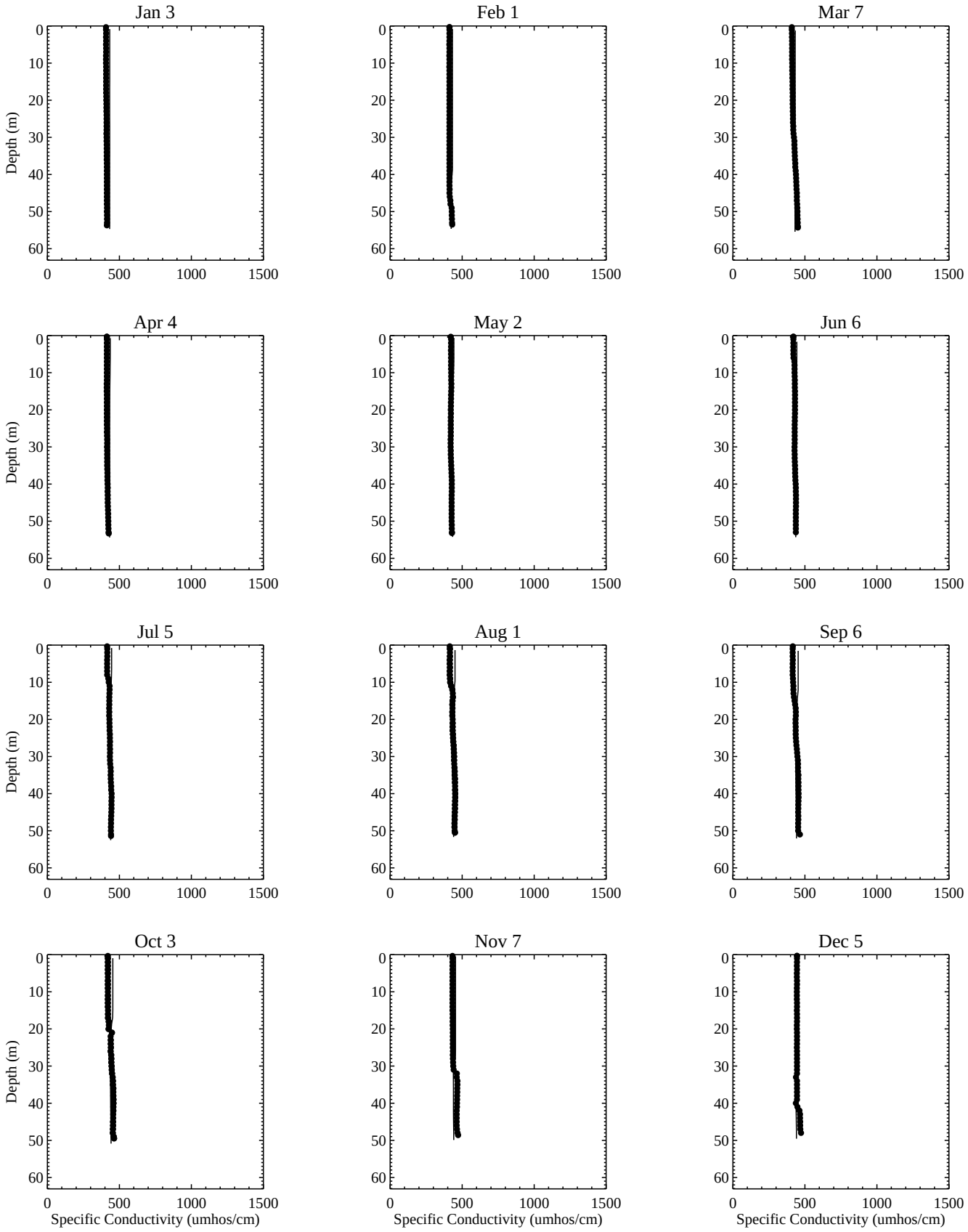

Figure J-6. Vertical profiles of model versus data at Mansfield Dam (Segment 93) - Specific Conductivity - 2005.

Profiles shown for dates with available data else model results for first day of month shown.

Model Data

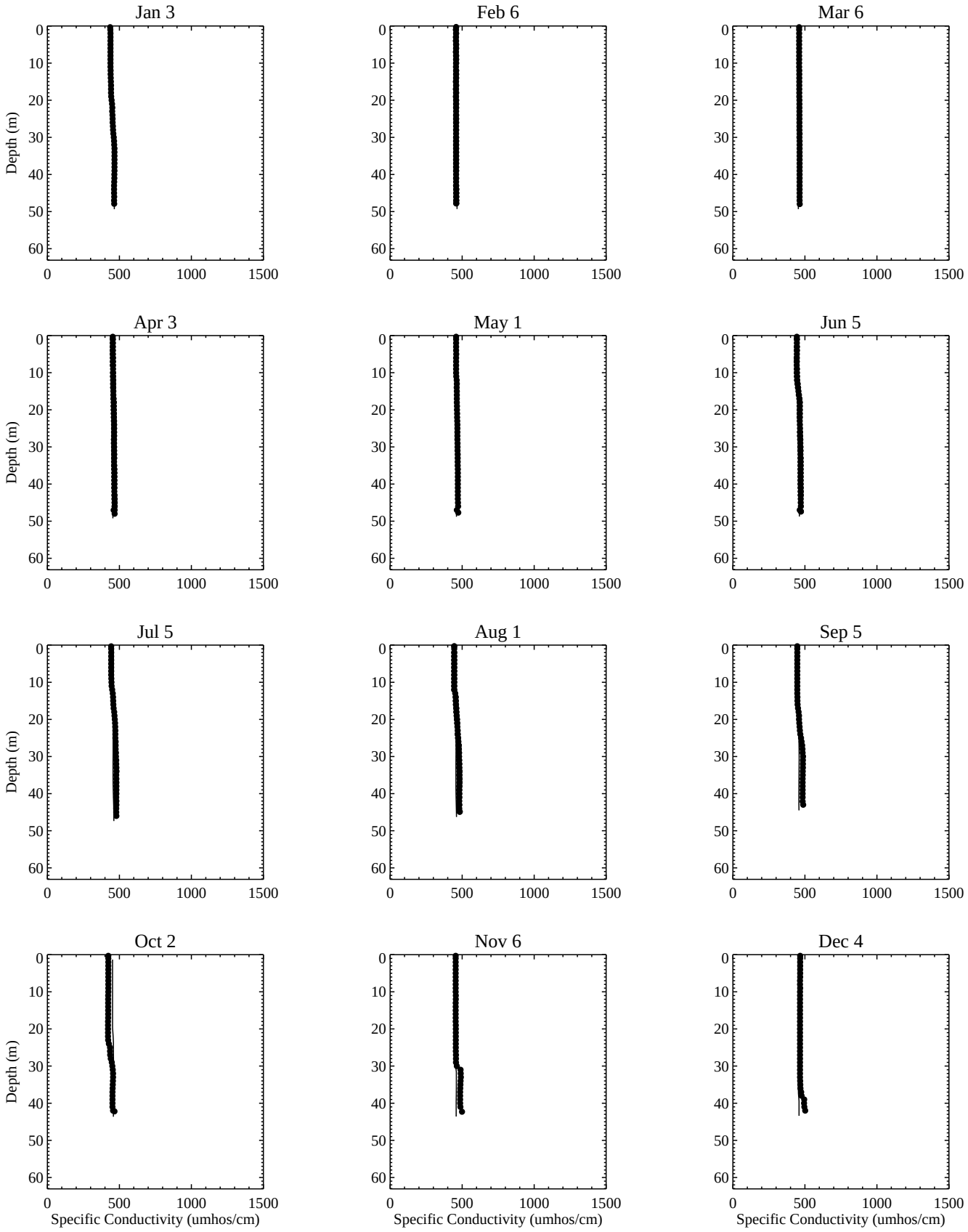

Figure J-6. Vertical profiles of model versus data at Mansfield Dam (Segment 93) - Specific Conductivity - 2006.

Profiles shown for dates with available data else model results for first day of month shown.

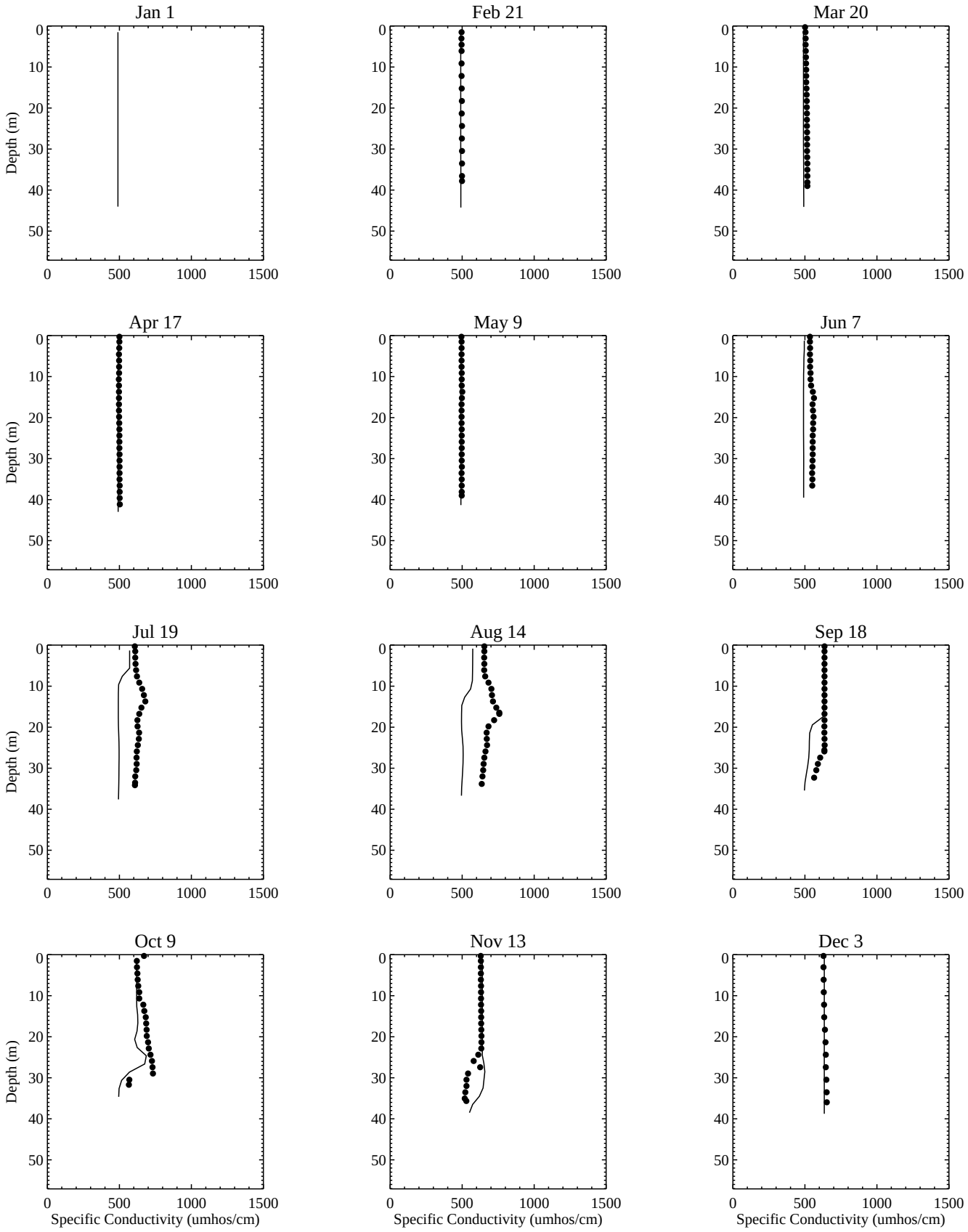

Figure J-7. Vertical profiles of model versus data at Arkansas Bend (Segment 78) - Specific Conductivity - 1984.

Profiles shown for dates with available data else model results for first day of month shown.

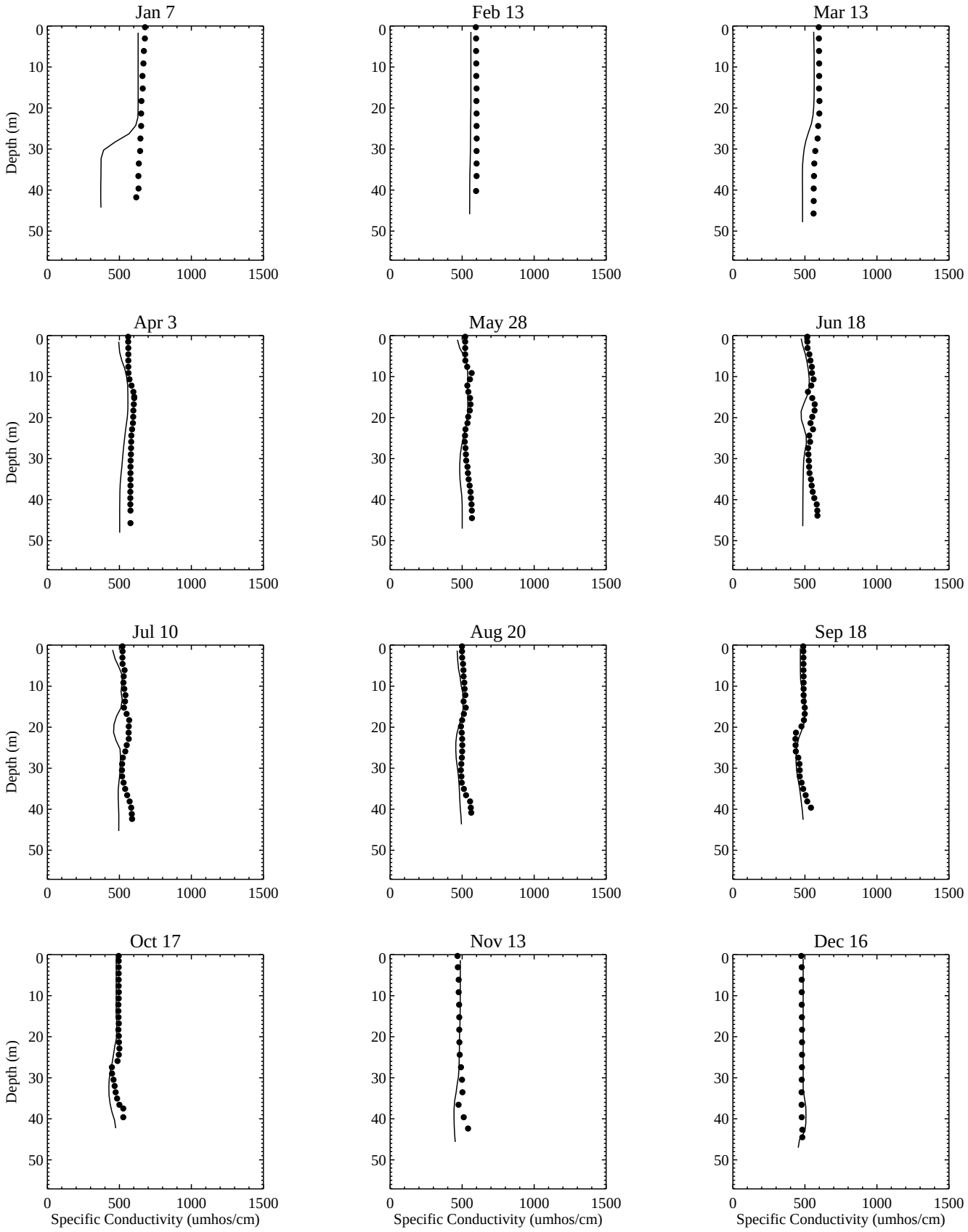

Figure J-7. Vertical profiles of model versus data at Arkansas Bend (Segment 78) - Specific Conductivity - 1985.

Profiles shown for dates with available data else model results for first day of month shown.

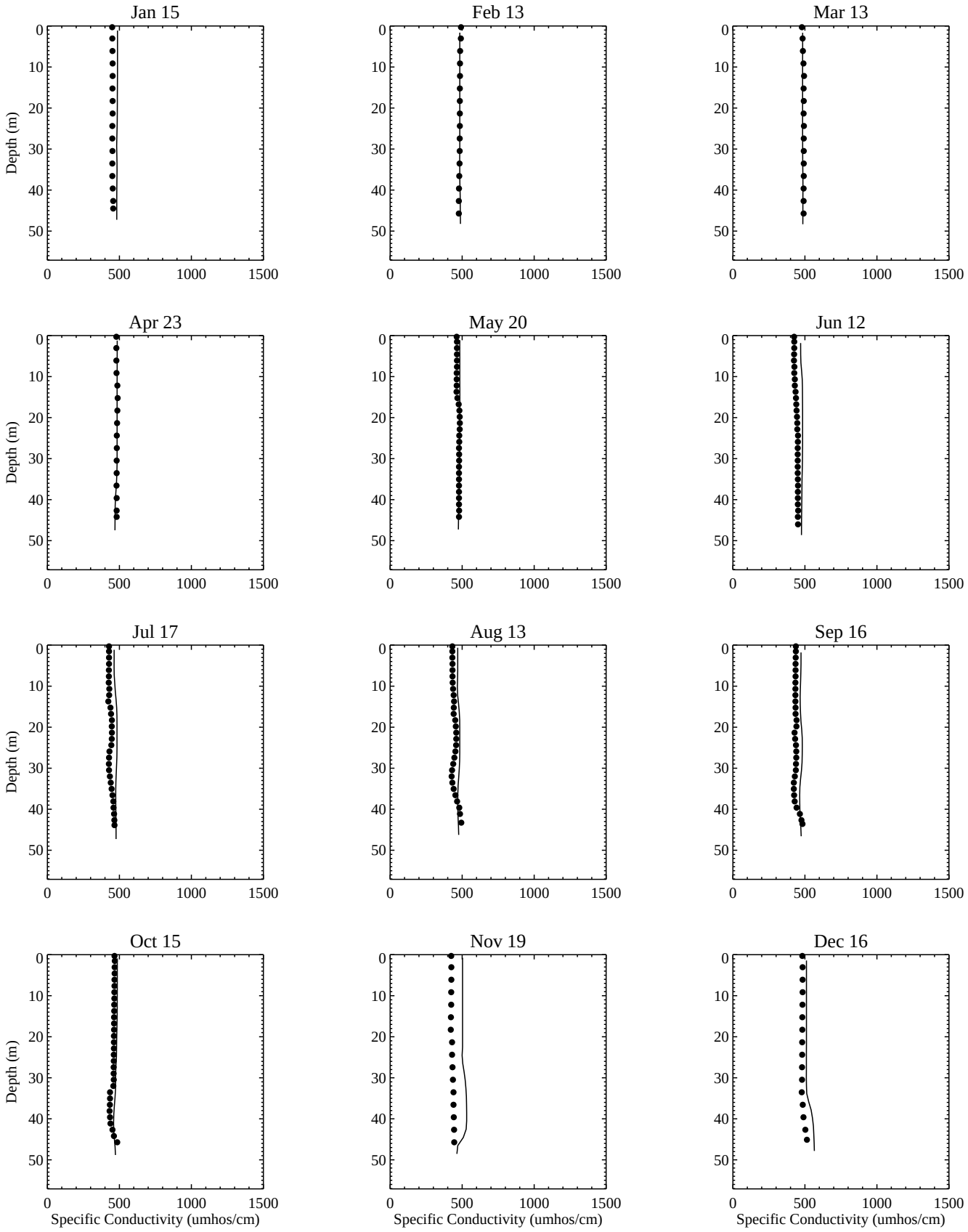

Figure J-7. Vertical profiles of model versus data at Arkansas Bend (Segment 78) - Specific Conductivity - 1986.

Profiles shown for dates with available data else model results for first day of month shown.

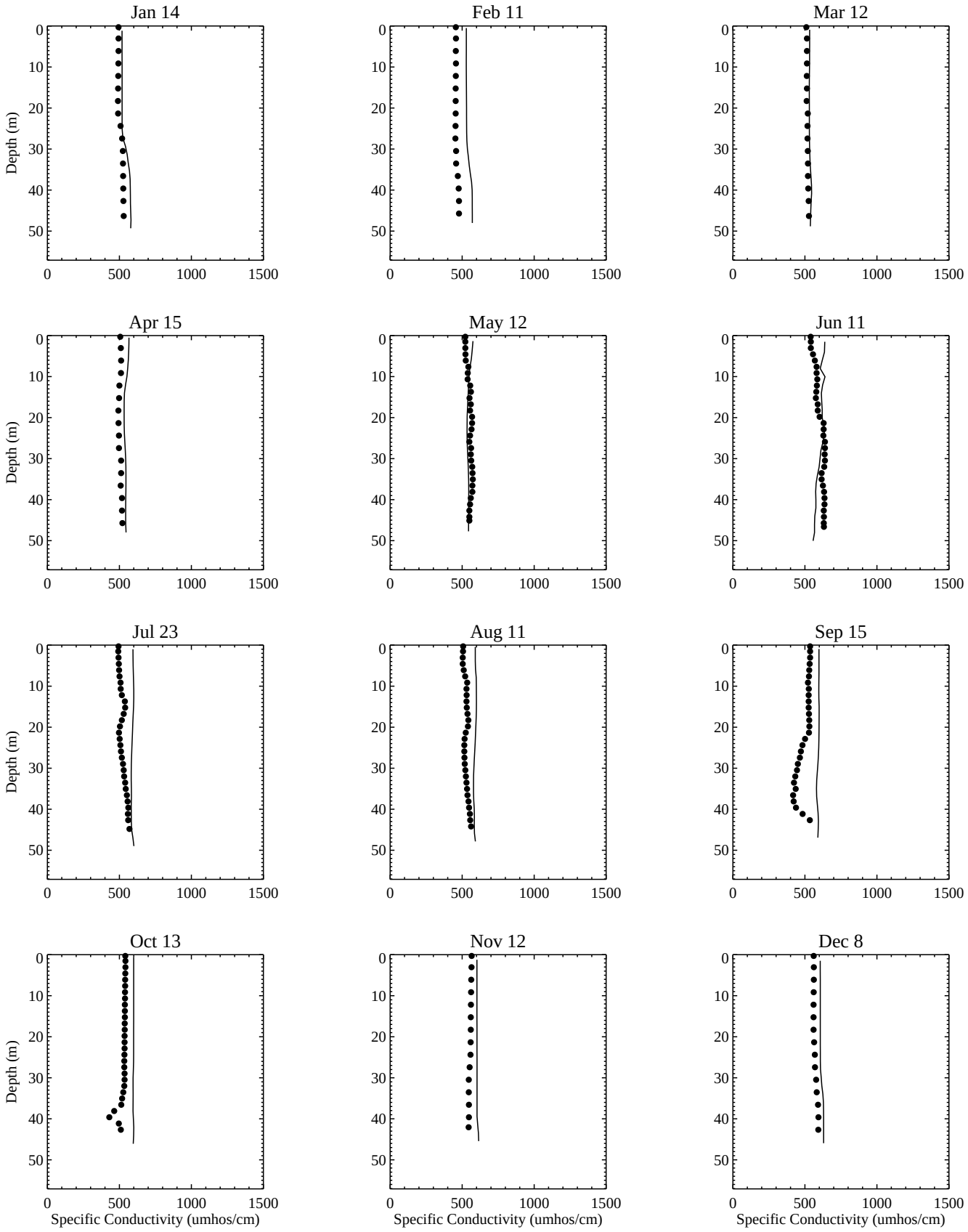

Figure J-7. Vertical profiles of model versus data at Arkansas Bend (Segment 78) - Specific Conductivity - 1987.

Profiles shown for dates with available data else model results for first day of month shown.

Model Data

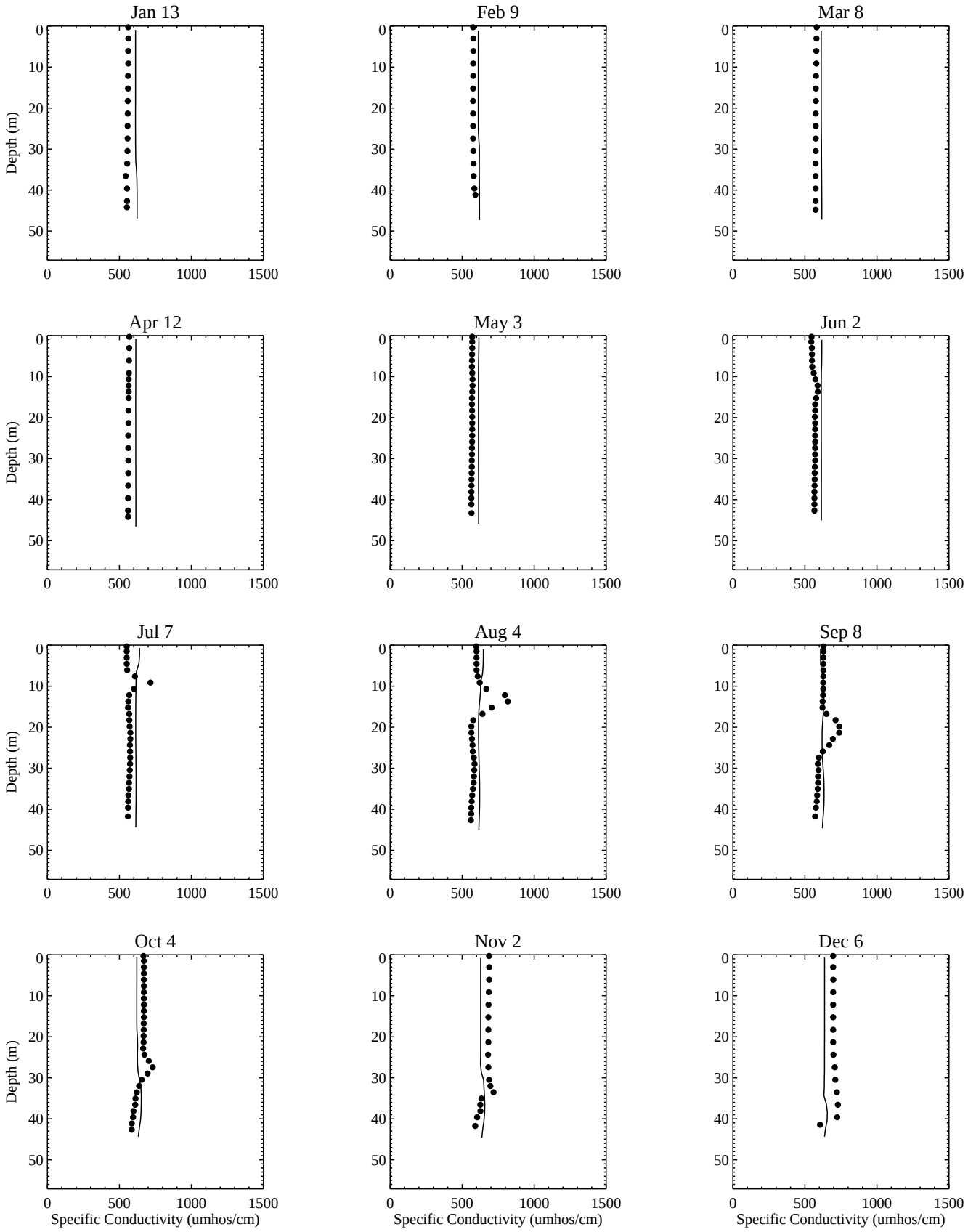

Figure J-7. Vertical profiles of model versus data at Arkansas Bend (Segment 78) - Specific Conductivity - 1988.

Profiles shown for dates with available data else model results for first day of month shown.

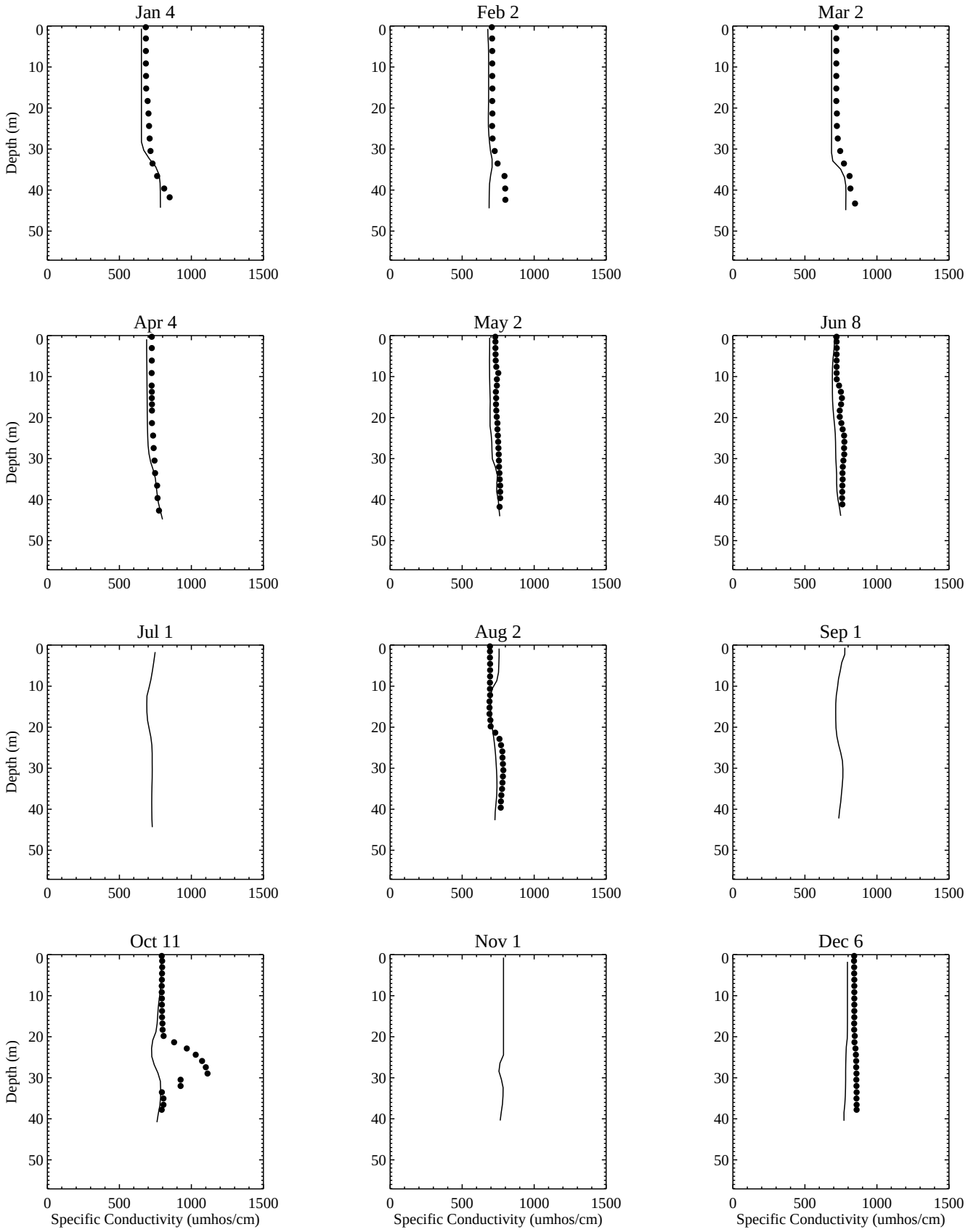

Figure J-7. Vertical profiles of model versus data at Arkansas Bend (Segment 78) - Specific Conductivity - 1989.

Profiles shown for dates with available data else model results for first day of month shown.

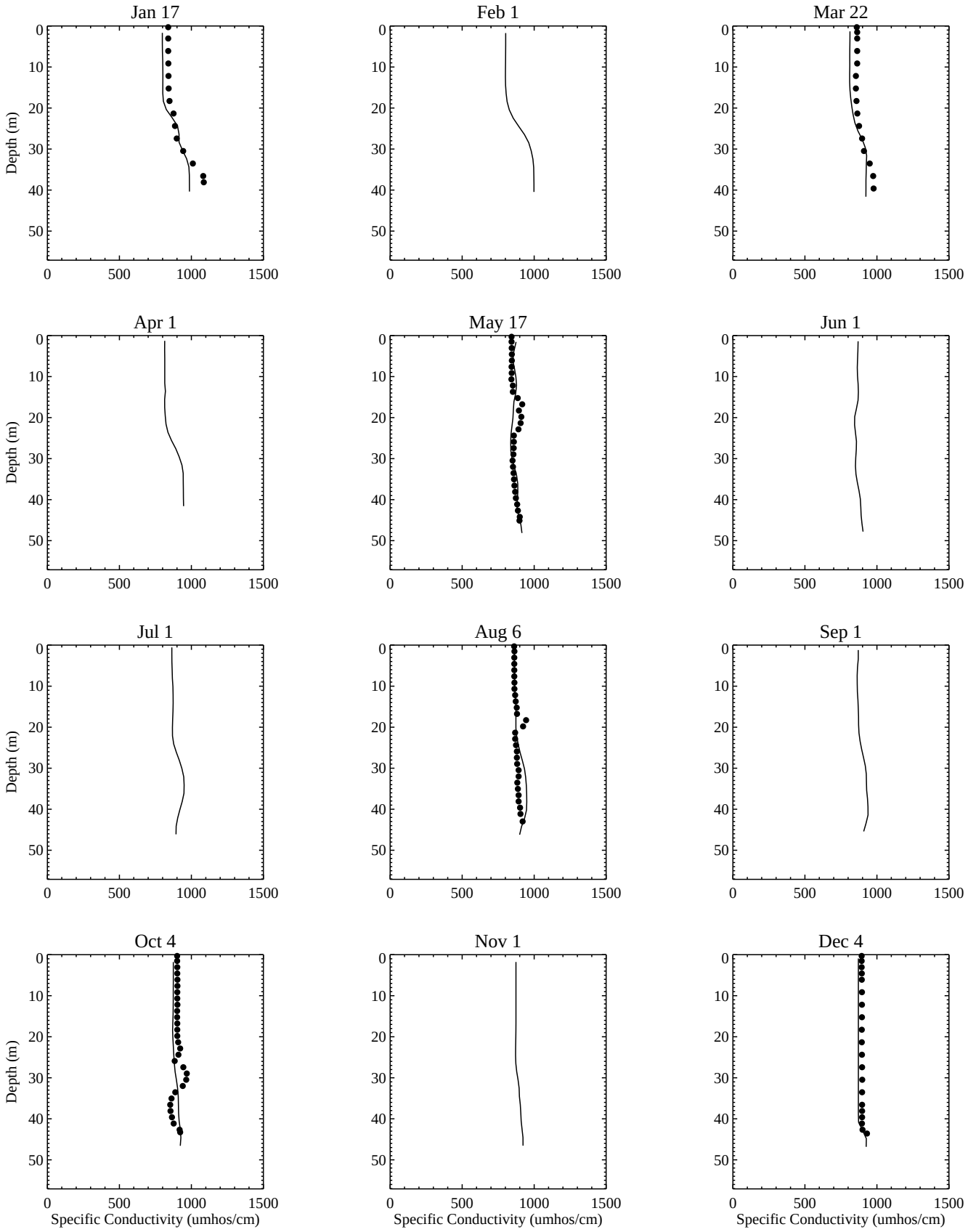

Figure J-7. Vertical profiles of model versus data at Arkansas Bend (Segment 78) - Specific Conductivity - 1990.

Profiles shown for dates with available data else model results for first day of month shown.

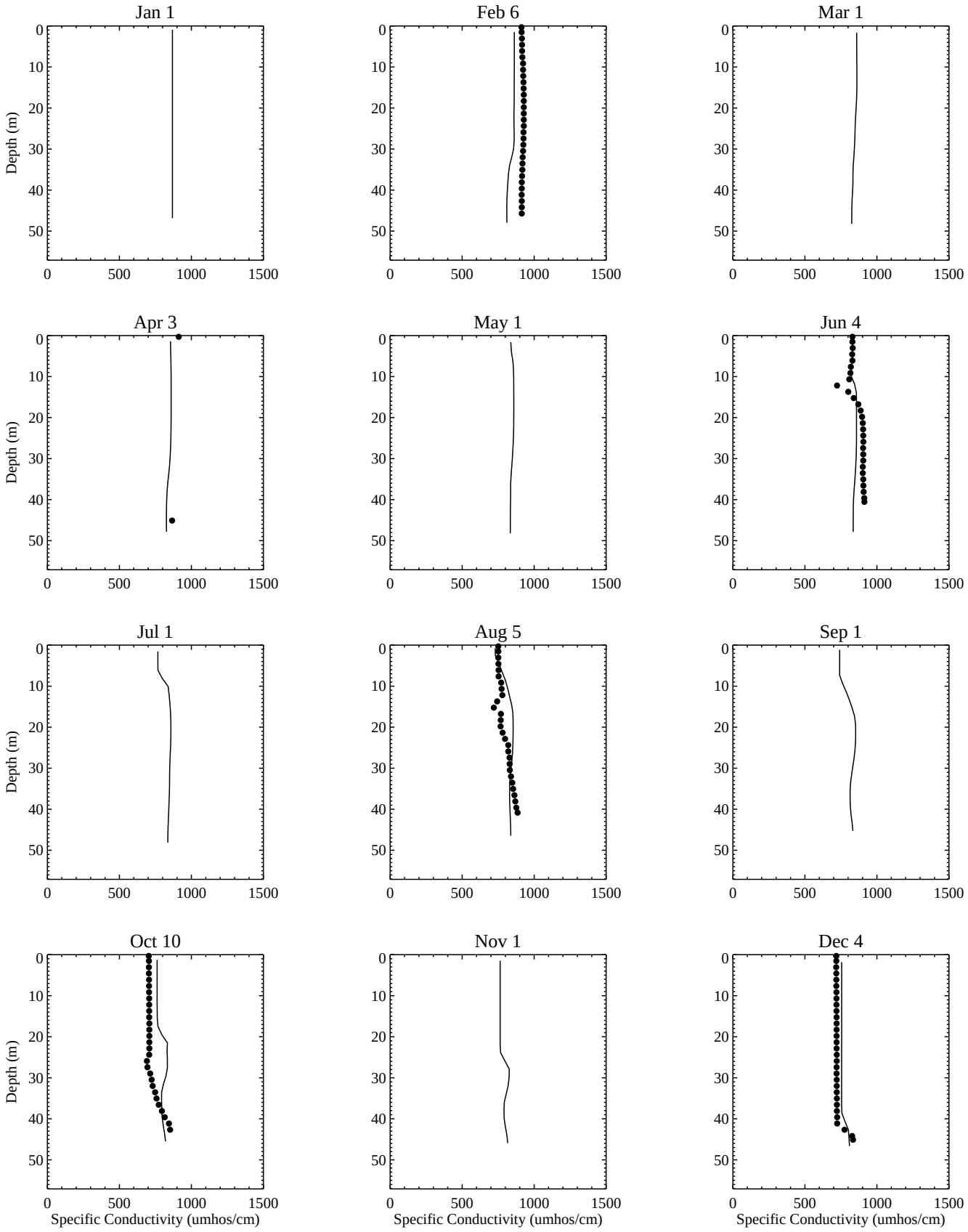

Figure J-7. Vertical profiles of model versus data at Arkansas Bend (Segment 78) - Specific Conductivity - 1991.

Profiles shown for dates with available data else model results for first day of month shown.

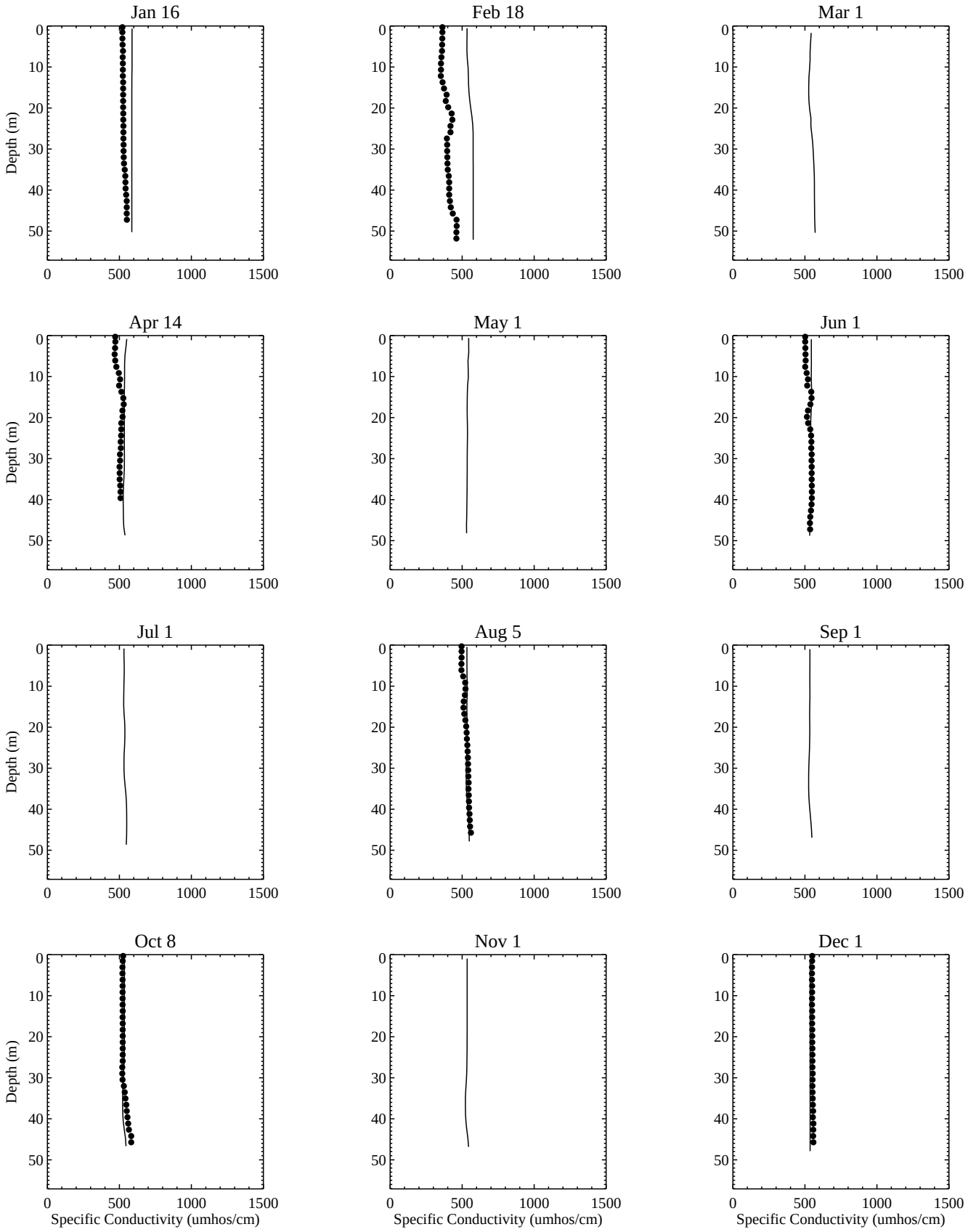

Figure J-7. Vertical profiles of model versus data at Arkansas Bend (Segment 78) - Specific Conductivity - 1992.

Profiles shown for dates with available data else model results for first day of month shown.

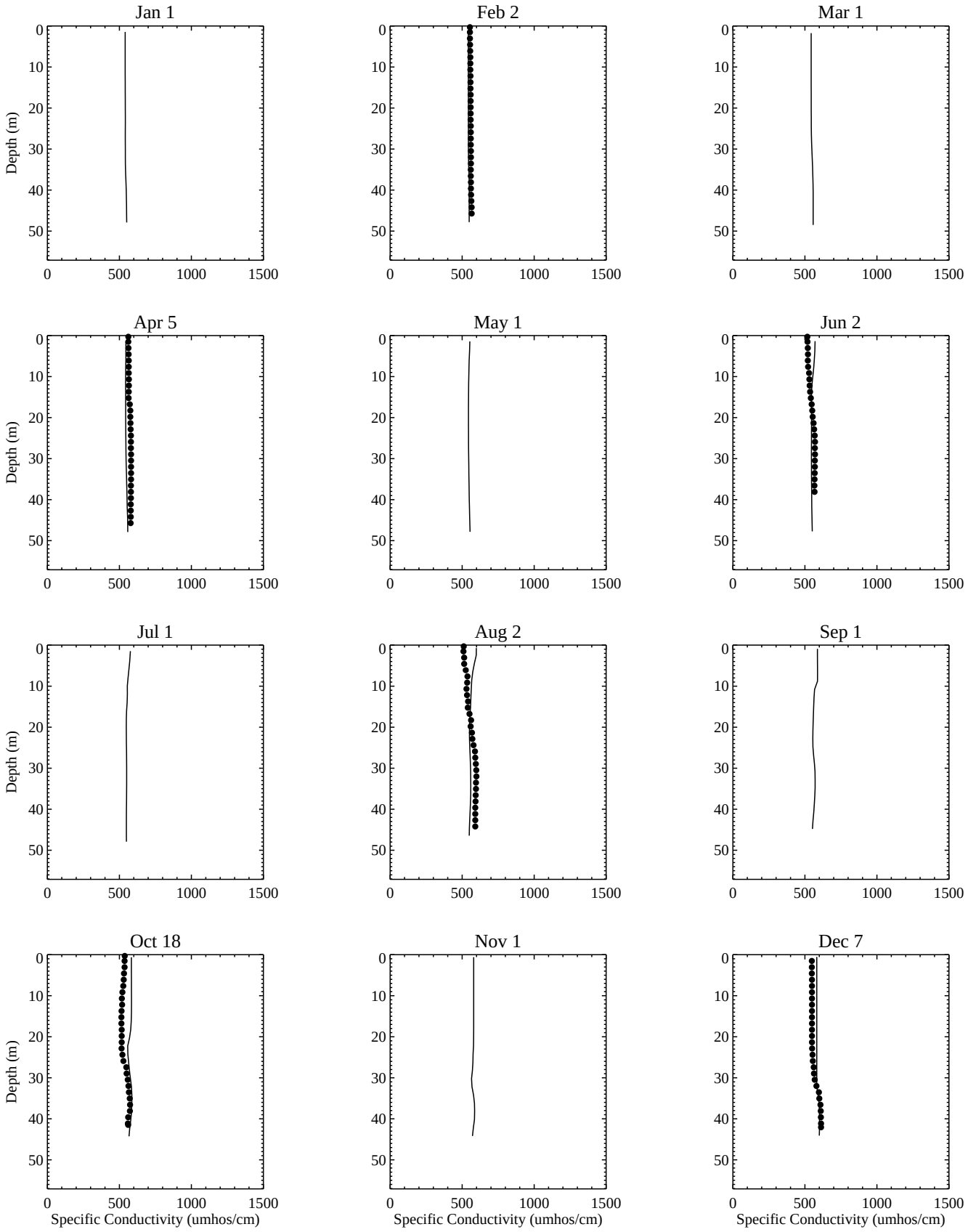

Figure J-7. Vertical profiles of model versus data at Arkansas Bend (Segment 78) - Specific Conductivity - 1993.

Profiles shown for dates with available data else model results for first day of month shown.

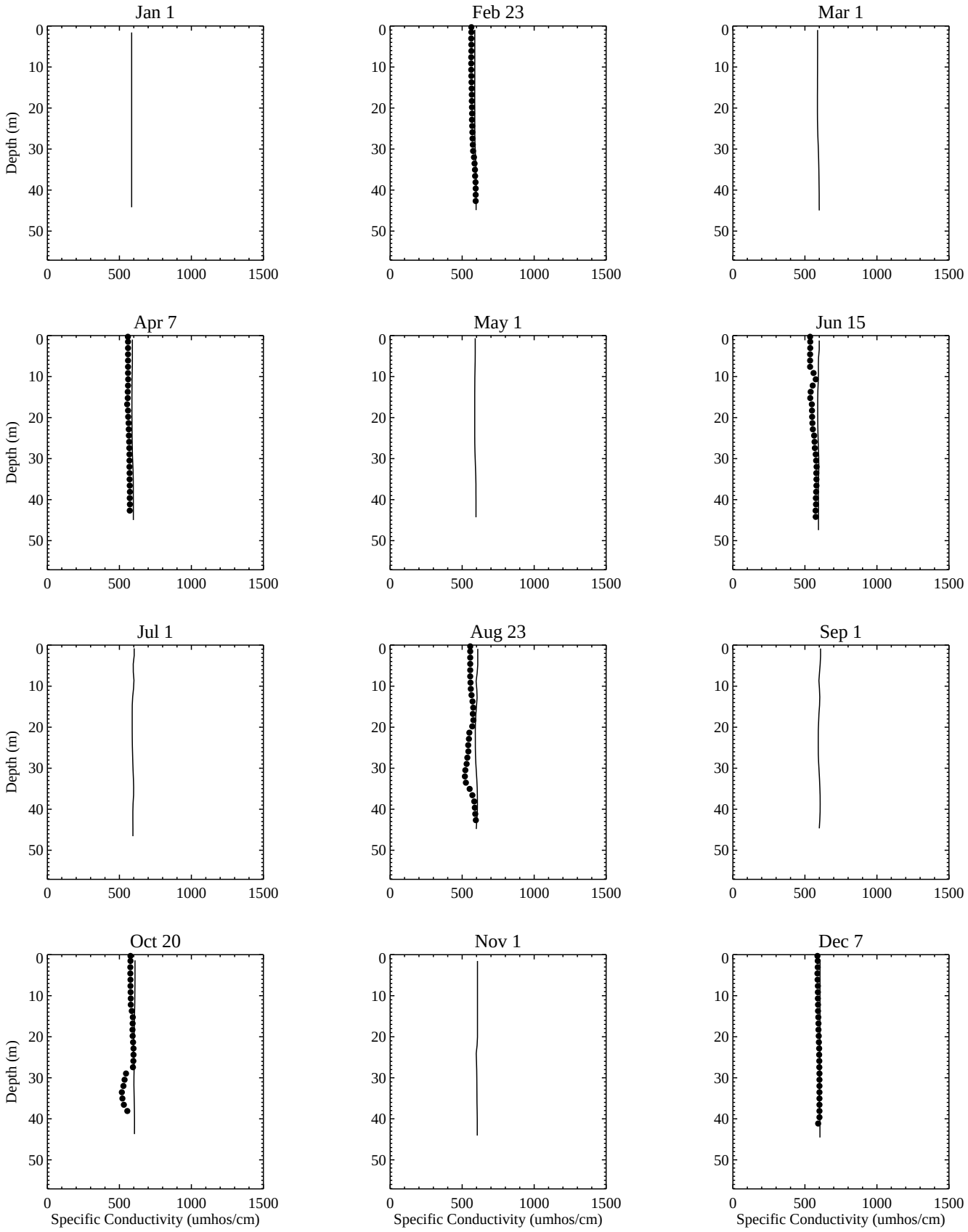

Figure J-7. Vertical profiles of model versus data at Arkansas Bend (Segment 78) - Specific Conductivity - 1994.

Profiles shown for dates with available data else model results for first day of month shown.

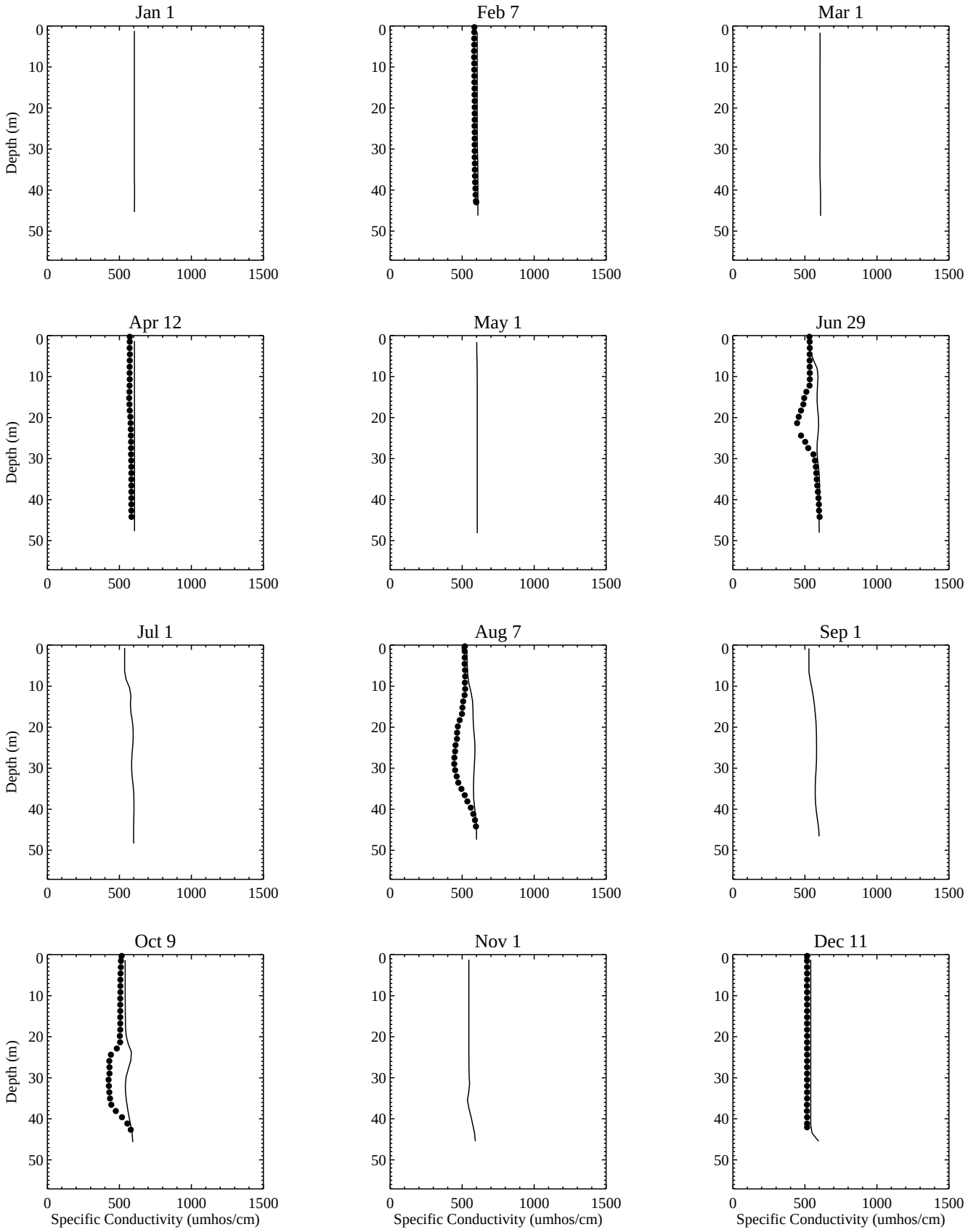

Figure J-7. Vertical profiles of model versus data at Arkansas Bend (Segment 78) - Specific Conductivity - 1995.

Profiles shown for dates with available data else model results for first day of month shown.

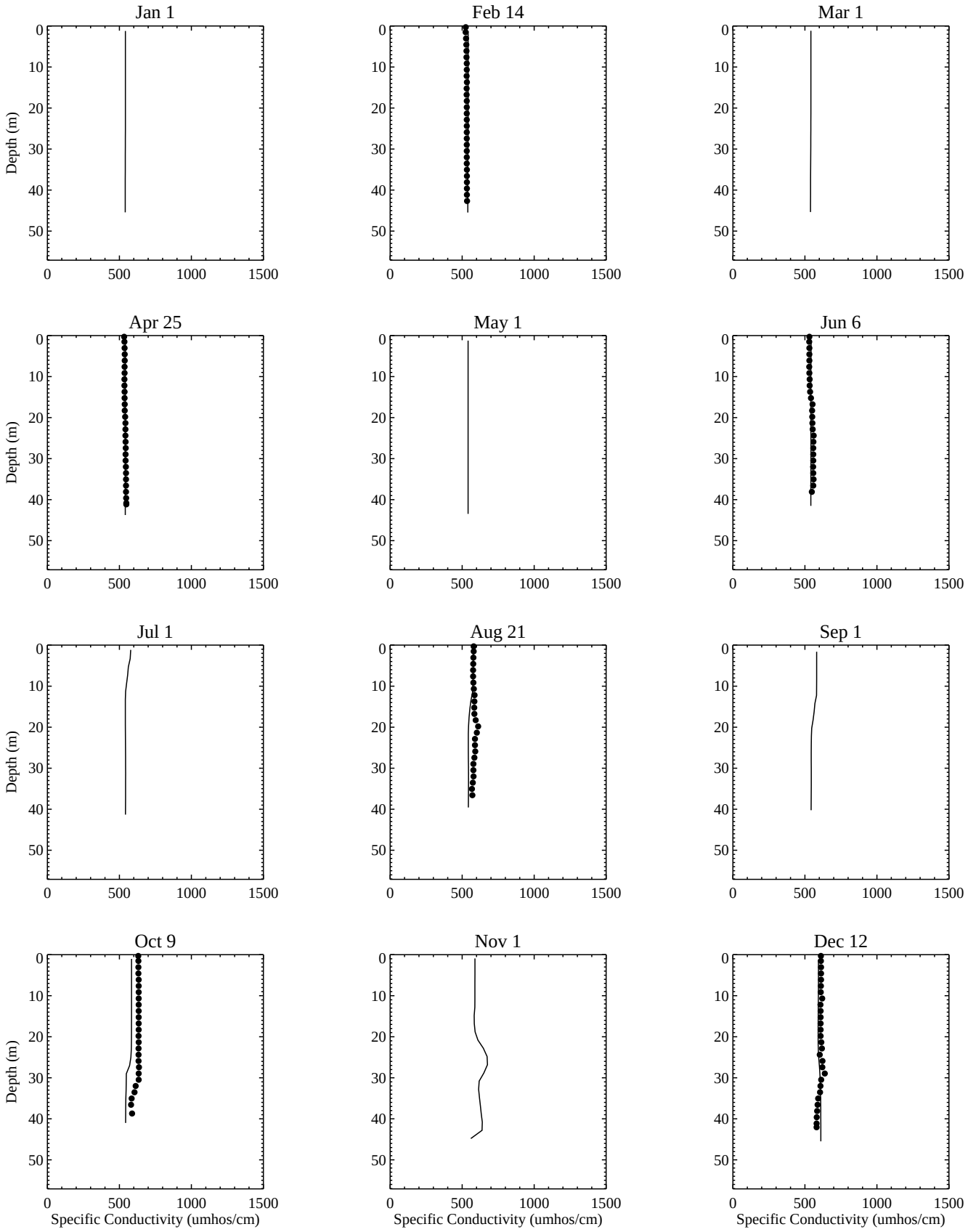

Figure J-7. Vertical profiles of model versus data at Arkansas Bend (Segment 78) - Specific Conductivity - 1996.

Profiles shown for dates with available data else model results for first day of month shown.

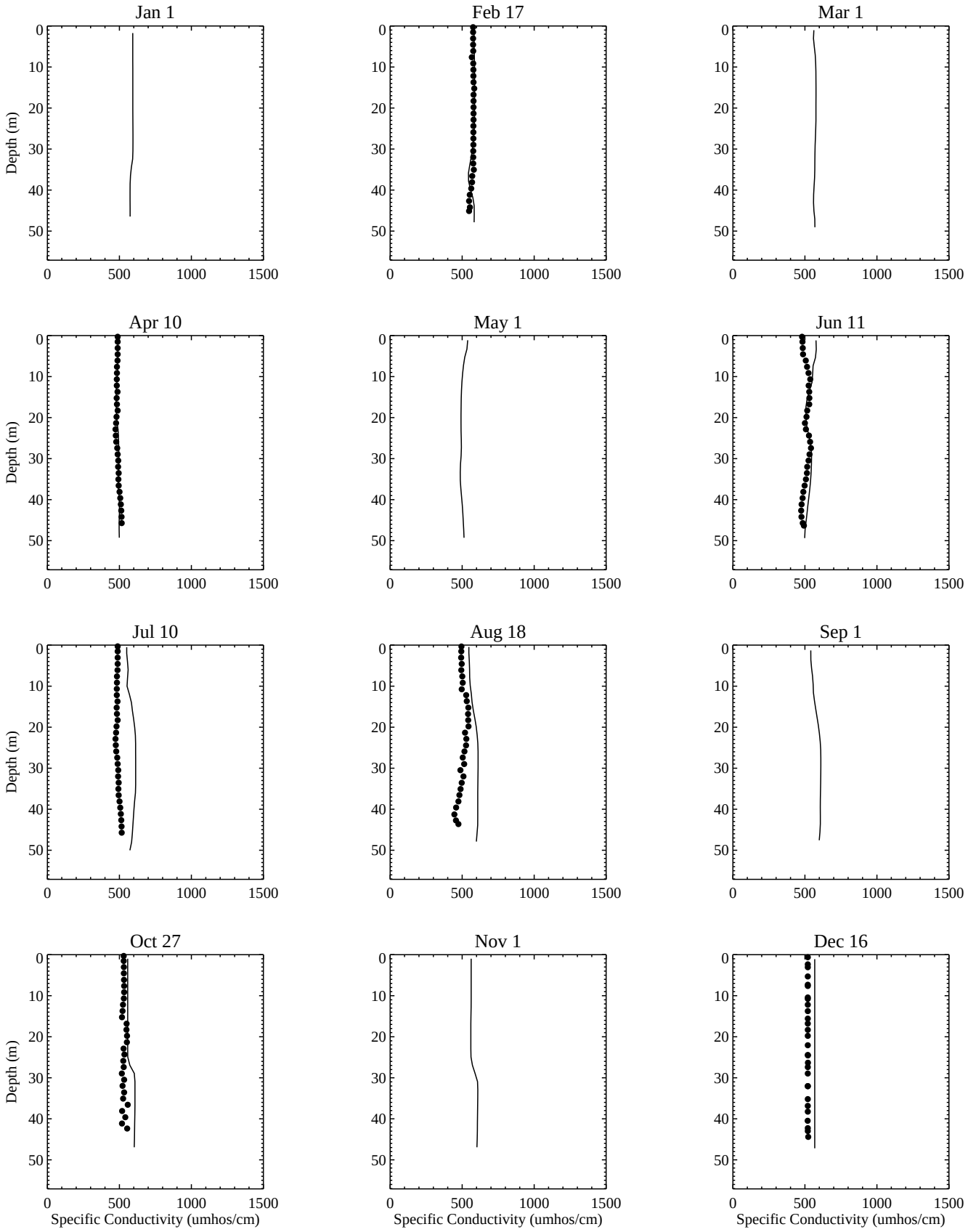

Figure J-7. Vertical profiles of model versus data at Arkansas Bend (Segment 78) - Specific Conductivity - 1997.

Profiles shown for dates with available data else model results for first day of month shown.

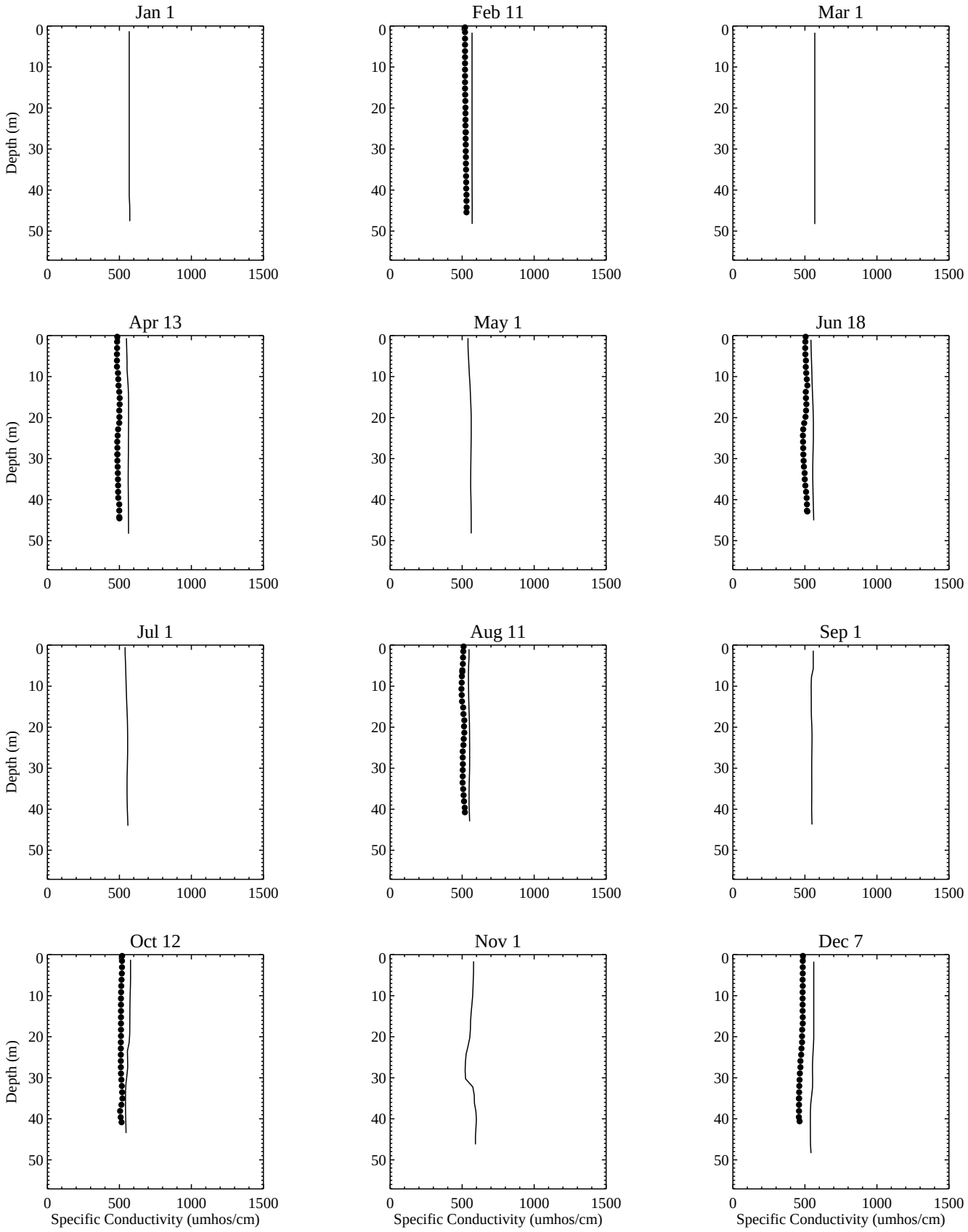

Figure J-7. Vertical profiles of model versus data at Arkansas Bend (Segment 78) - Specific Conductivity - 1998.

Profiles shown for dates with available data else model results for first day of month shown.

Model ● Data

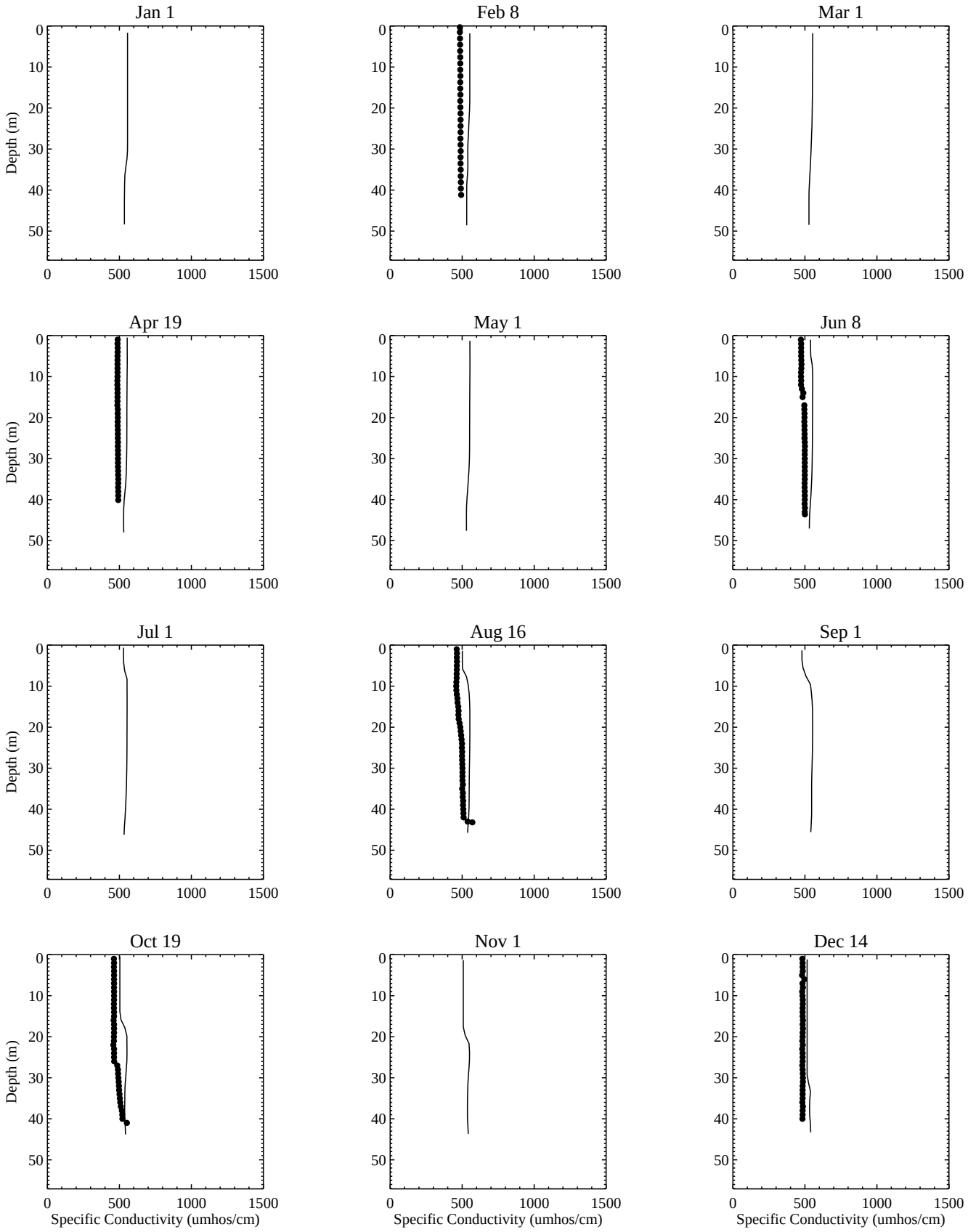

Figure J-7. Vertical profiles of model versus data at Arkansas Bend (Segment 78) - Specific Conductivity - 1999.

Profiles shown for dates with available data else model results for first day of month shown.

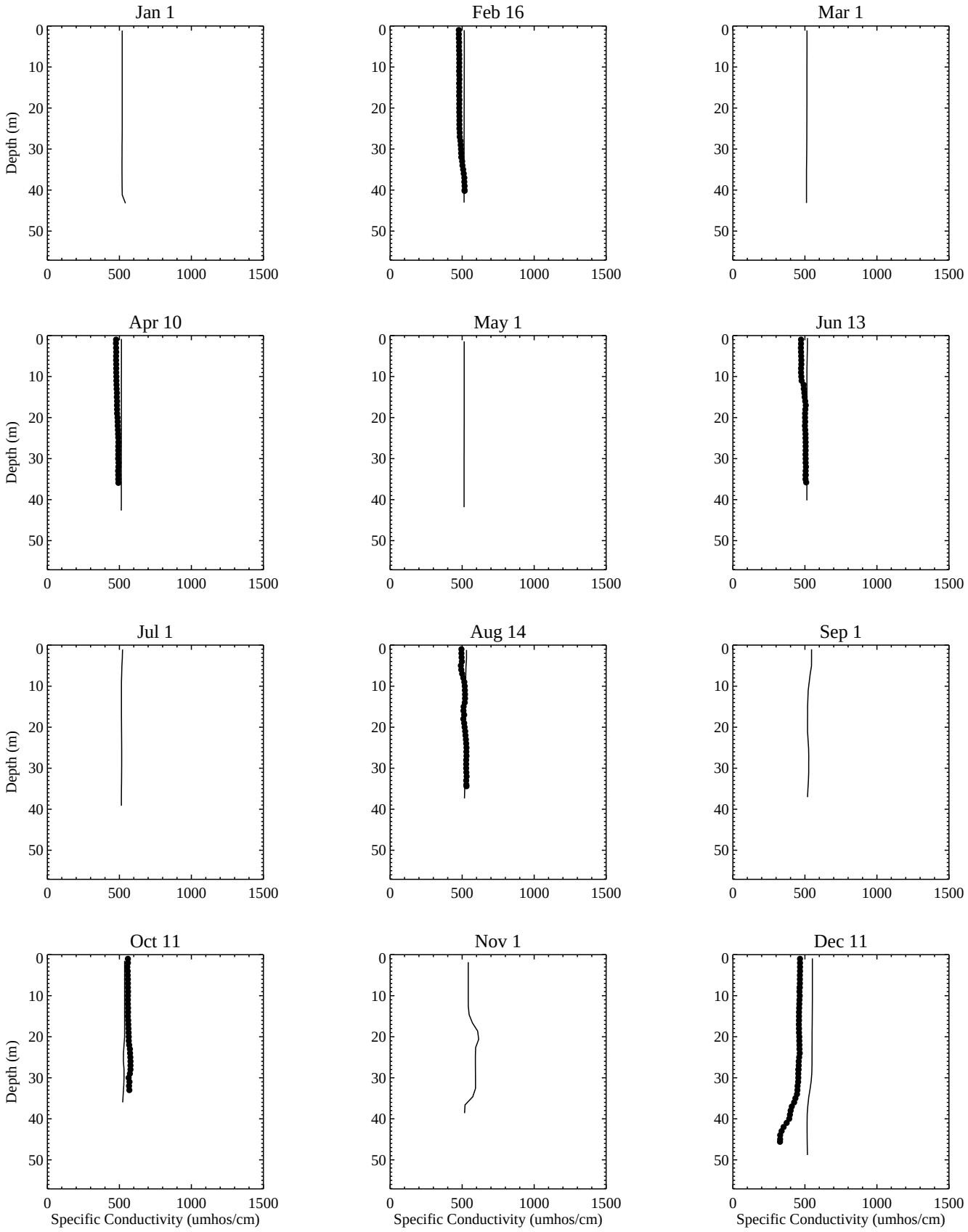

Figure J-7. Vertical profiles of model versus data at Arkansas Bend (Segment 78) - Specific Conductivity - 2000.

Profiles shown for dates with available data else model results for first day of month shown.

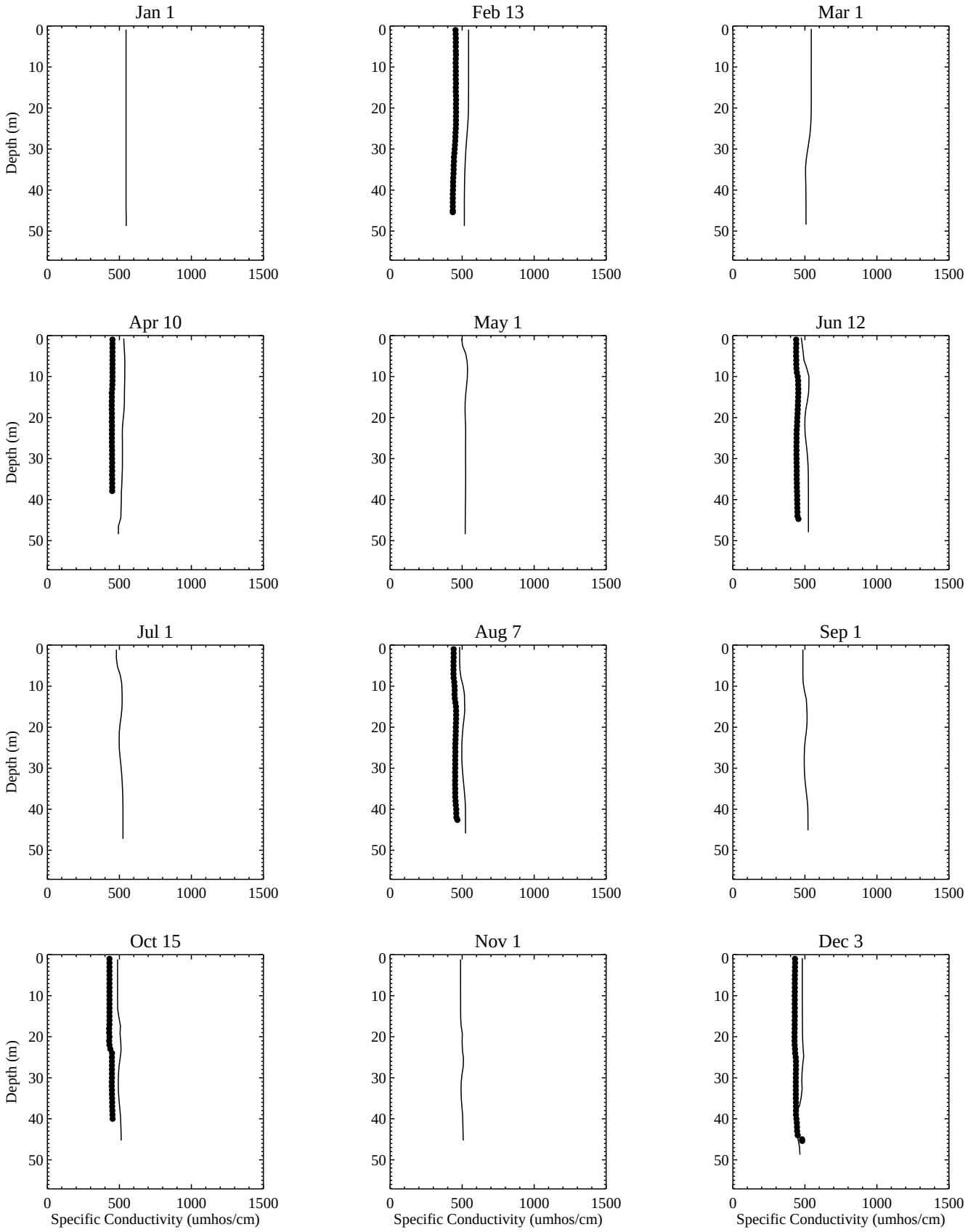

Figure J-7. Vertical profiles of model versus data at Arkansas Bend (Segment 78) - Specific Conductivity - 2001.

Profiles shown for dates with available data else model results for first day of month shown.

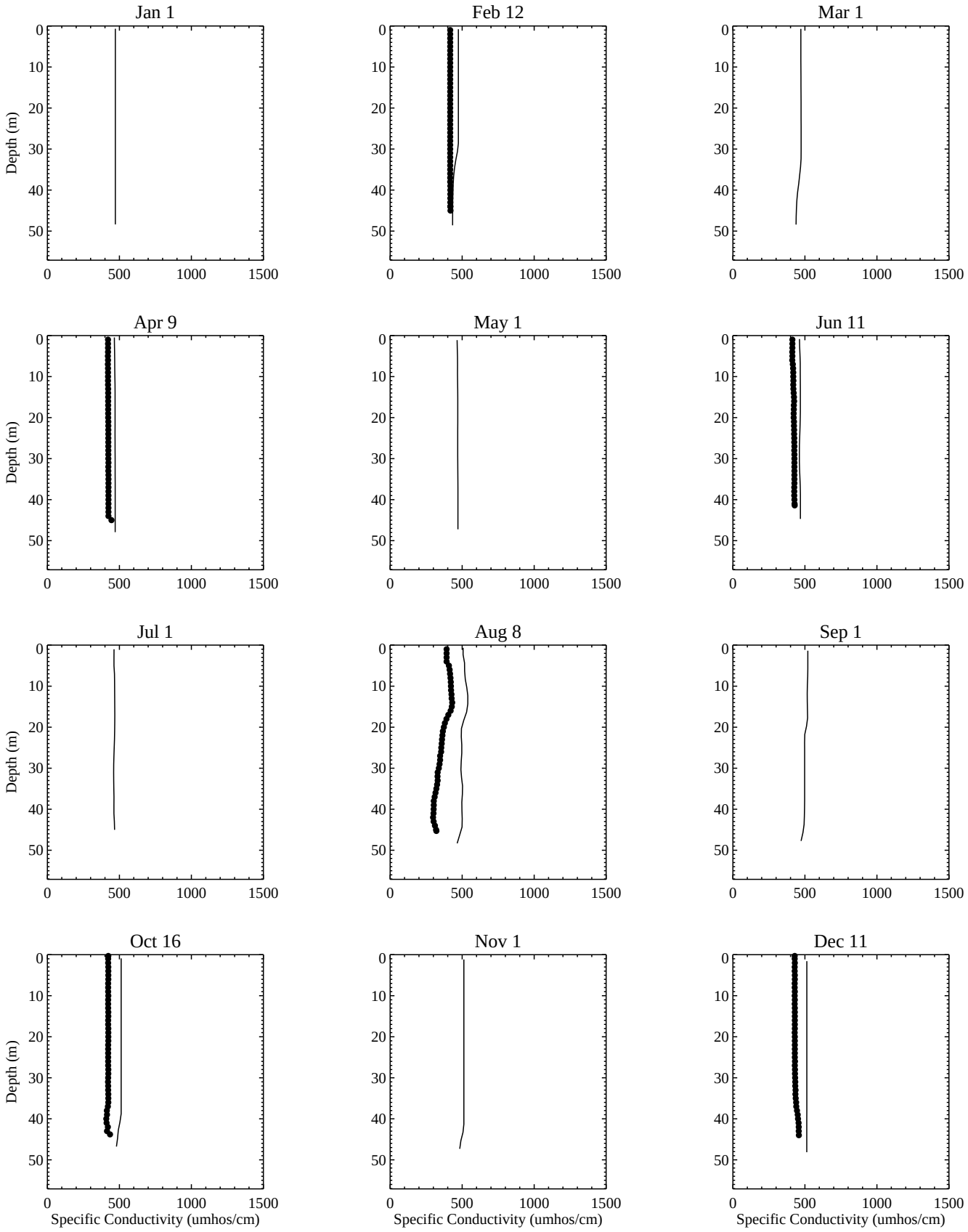

Figure J-7. Vertical profiles of model versus data at Arkansas Bend (Segment 78) - Specific Conductivity - 2002.

Profiles shown for dates with available data else model results for first day of month shown.

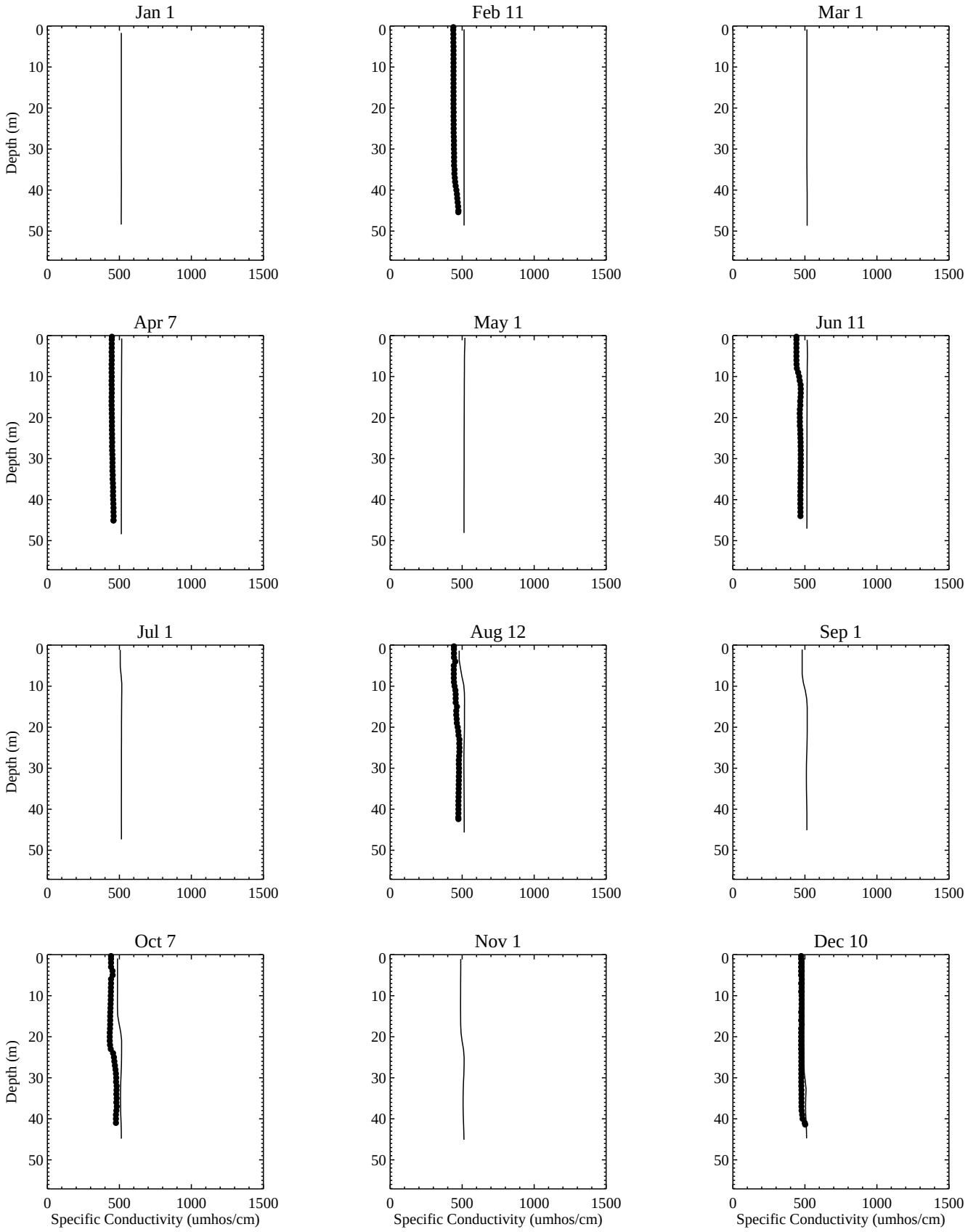

Figure J-7. Vertical profiles of model versus data at Arkansas Bend (Segment 78) - Specific Conductivity - 2003.

Profiles shown for dates with available data else model results for first day of month shown.

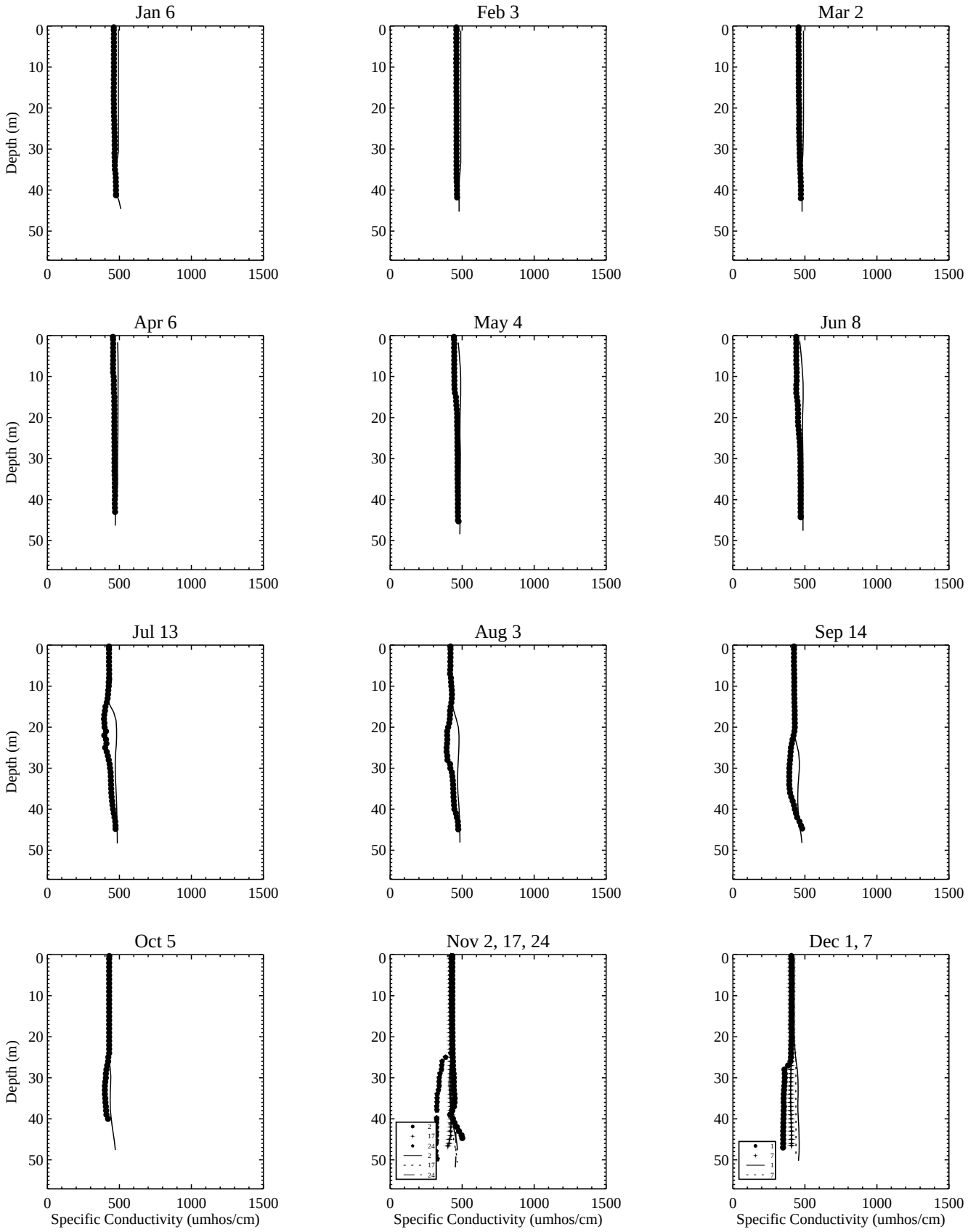

Figure J-7. Vertical profiles of model versus data at Arkansas Bend (Segment 78) - Specific Conductivity - 2004.

Profiles shown for dates with available data else model results for first day of month shown.

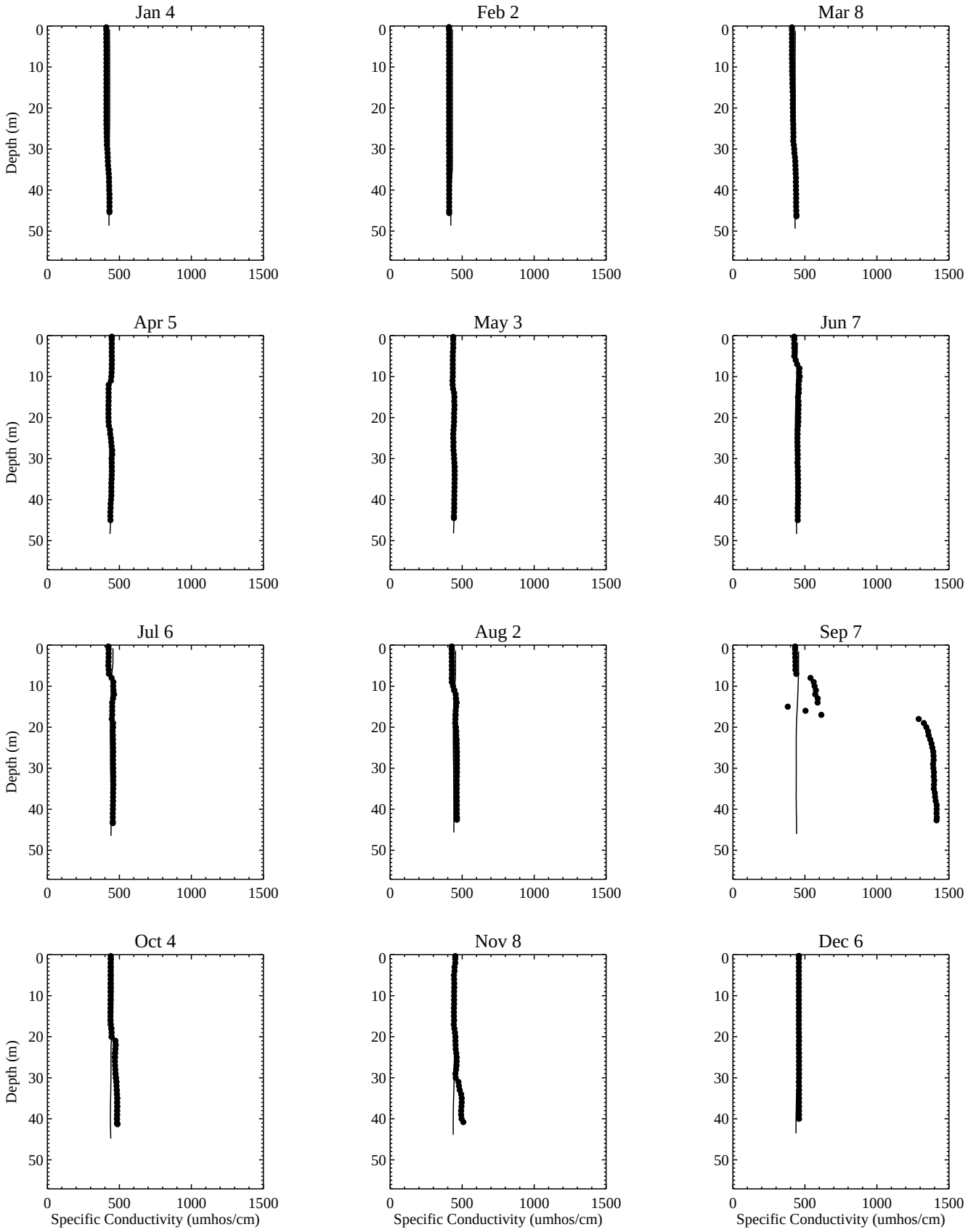

Figure J-7. Vertical profiles of model versus data at Arkansas Bend (Segment 78) - Specific Conductivity - 2005.

Profiles shown for dates with available data else model results for first day of month shown.

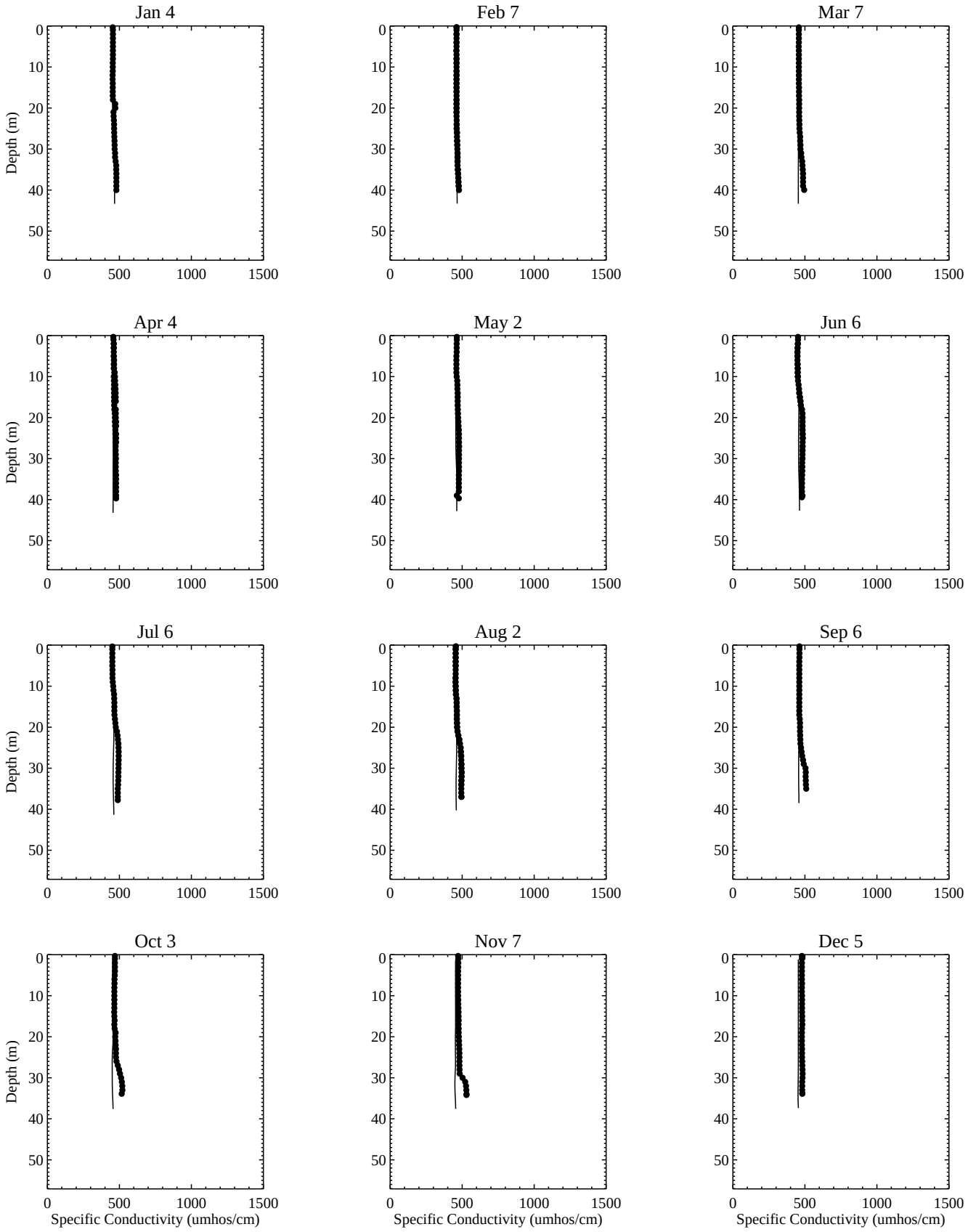

Figure J-7. Vertical profiles of model versus data at Arkansas Bend (Segment 78) - Specific Conductivity - 2006.

Profiles shown for dates with available data else model results for first day of month shown.

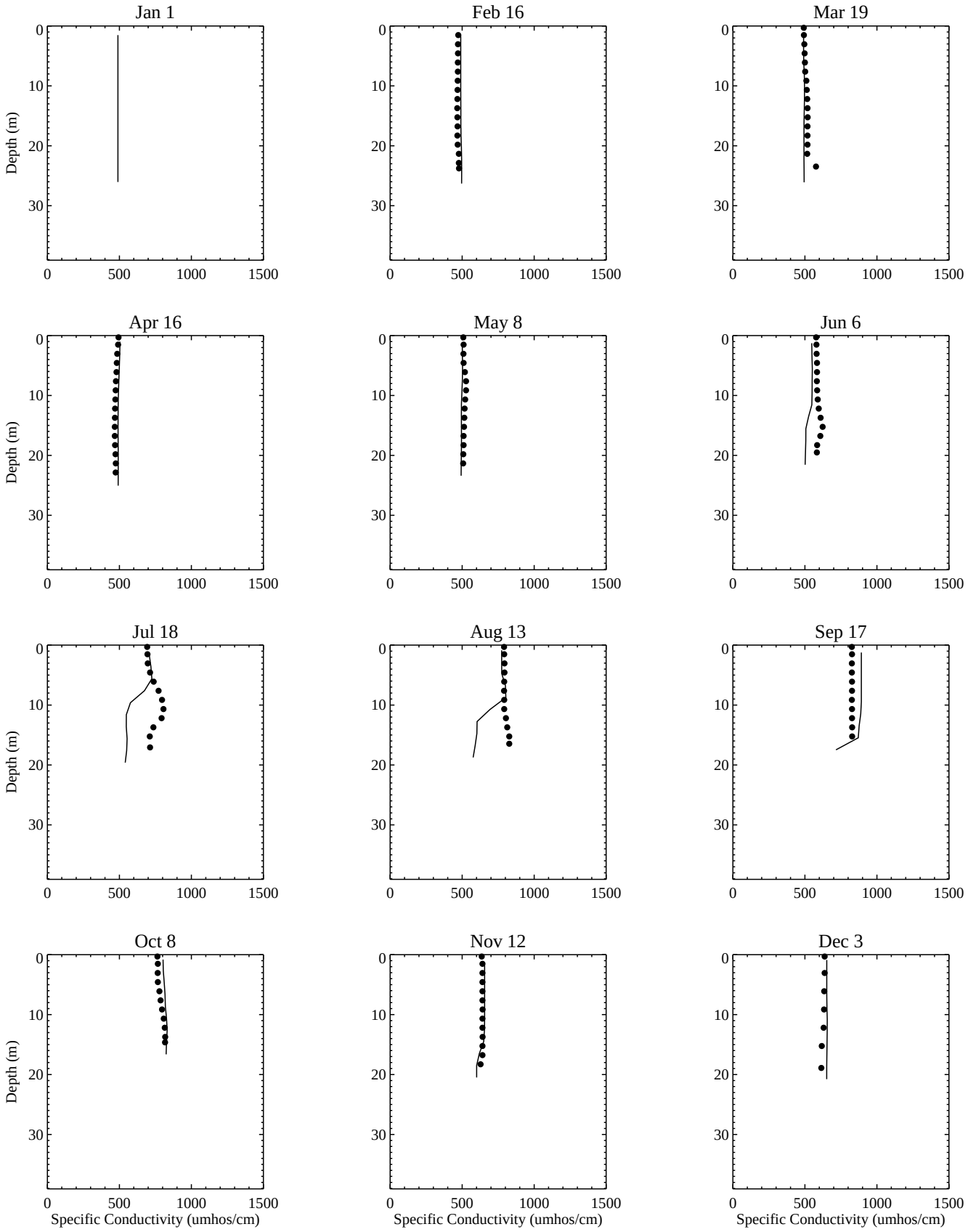

Figure J-8. Vertical profiles of model versus data at Pace Bend (Segment 48) - Specific Conductivity - 1984.

Profiles shown for dates with available data else model results for first day of month shown.

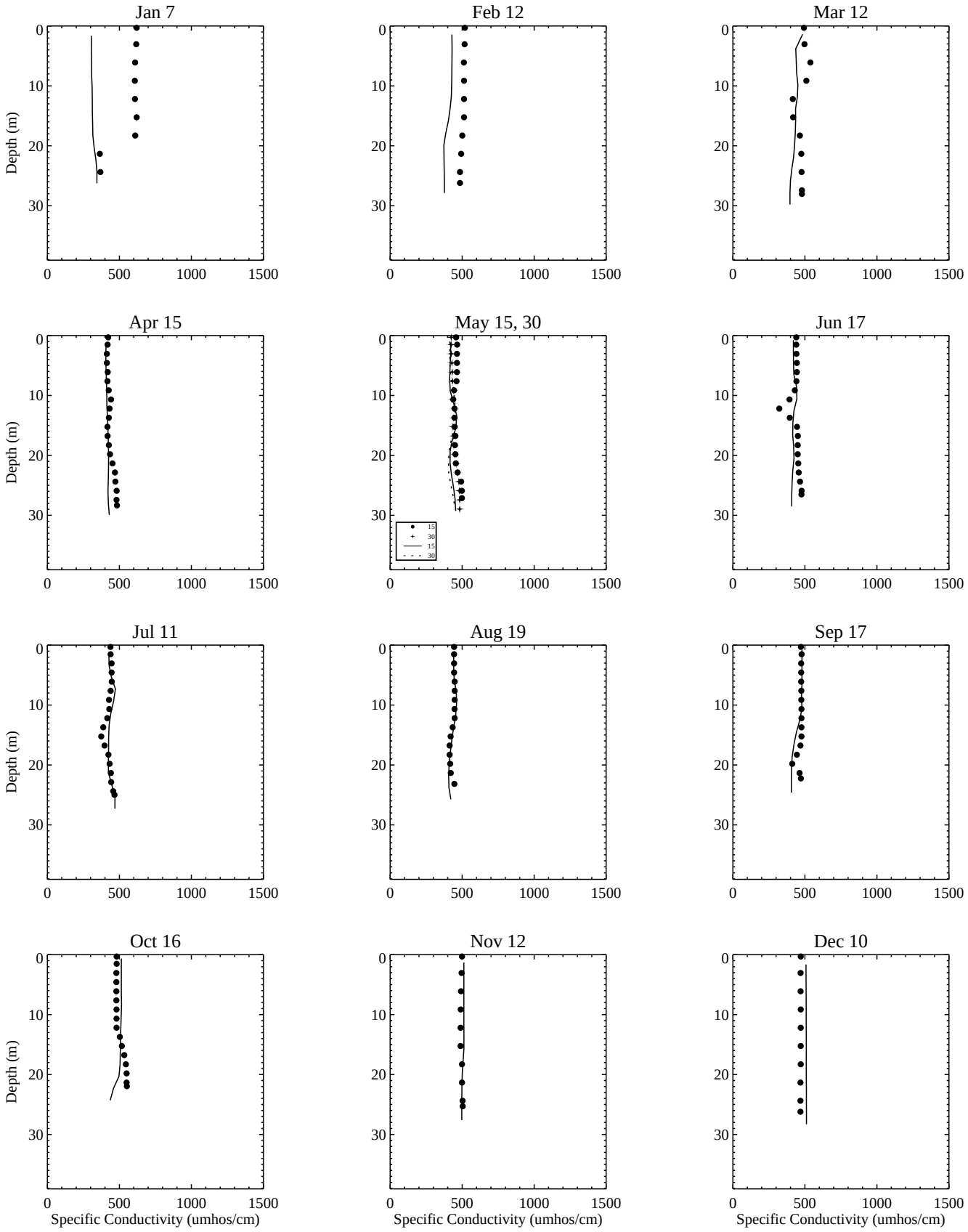

Figure J-8. Vertical profiles of model versus data at Pace Bend (Segment 48) - Specific Conductivity - 1985.

Profiles shown for dates with available data else model results for first day of month shown.

Model Data

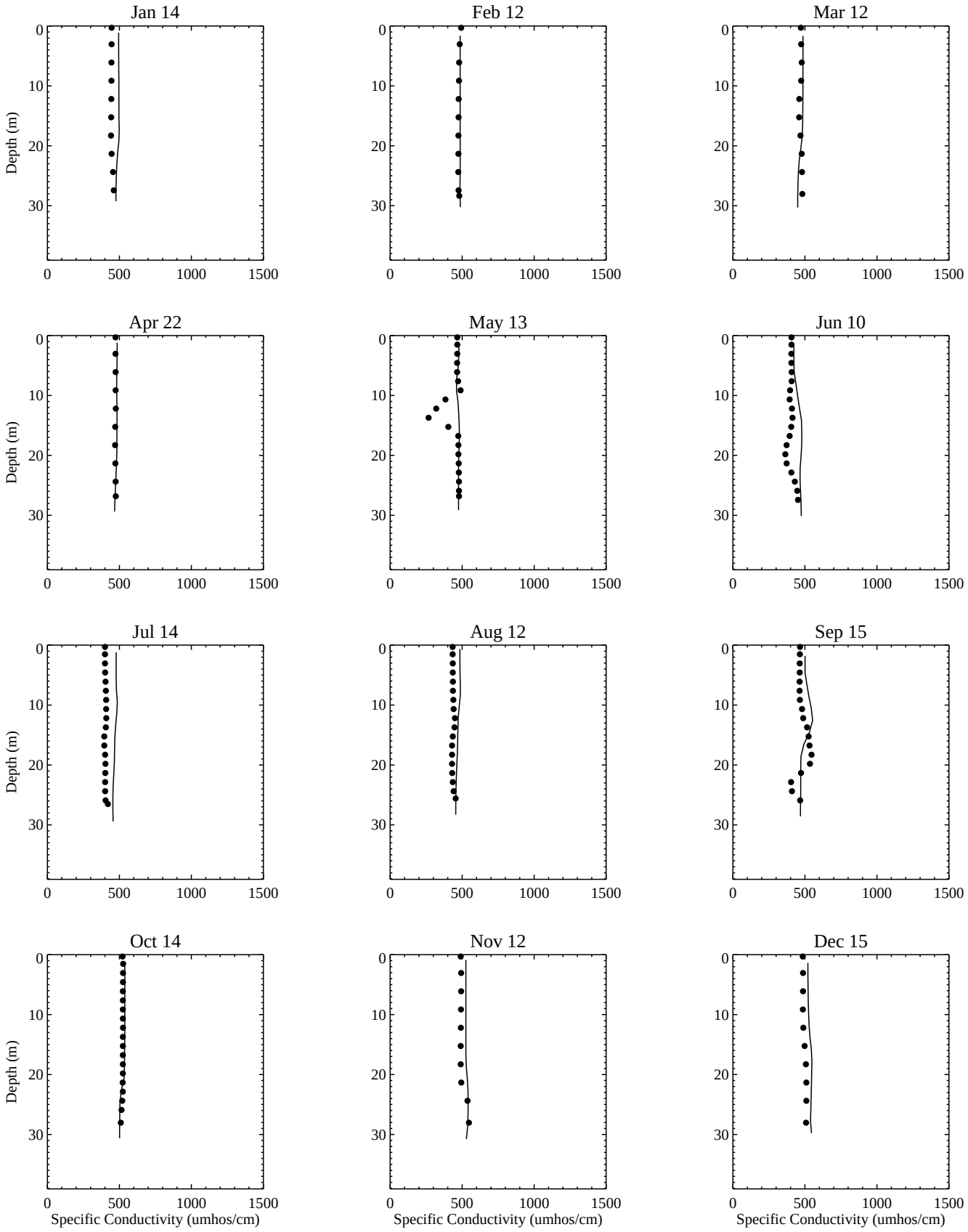

Figure J-8. Vertical profiles of model versus data at Pace Bend (Segment 48) - Specific Conductivity - 1986.

Profiles shown for dates with available data else model results for first day of month shown.

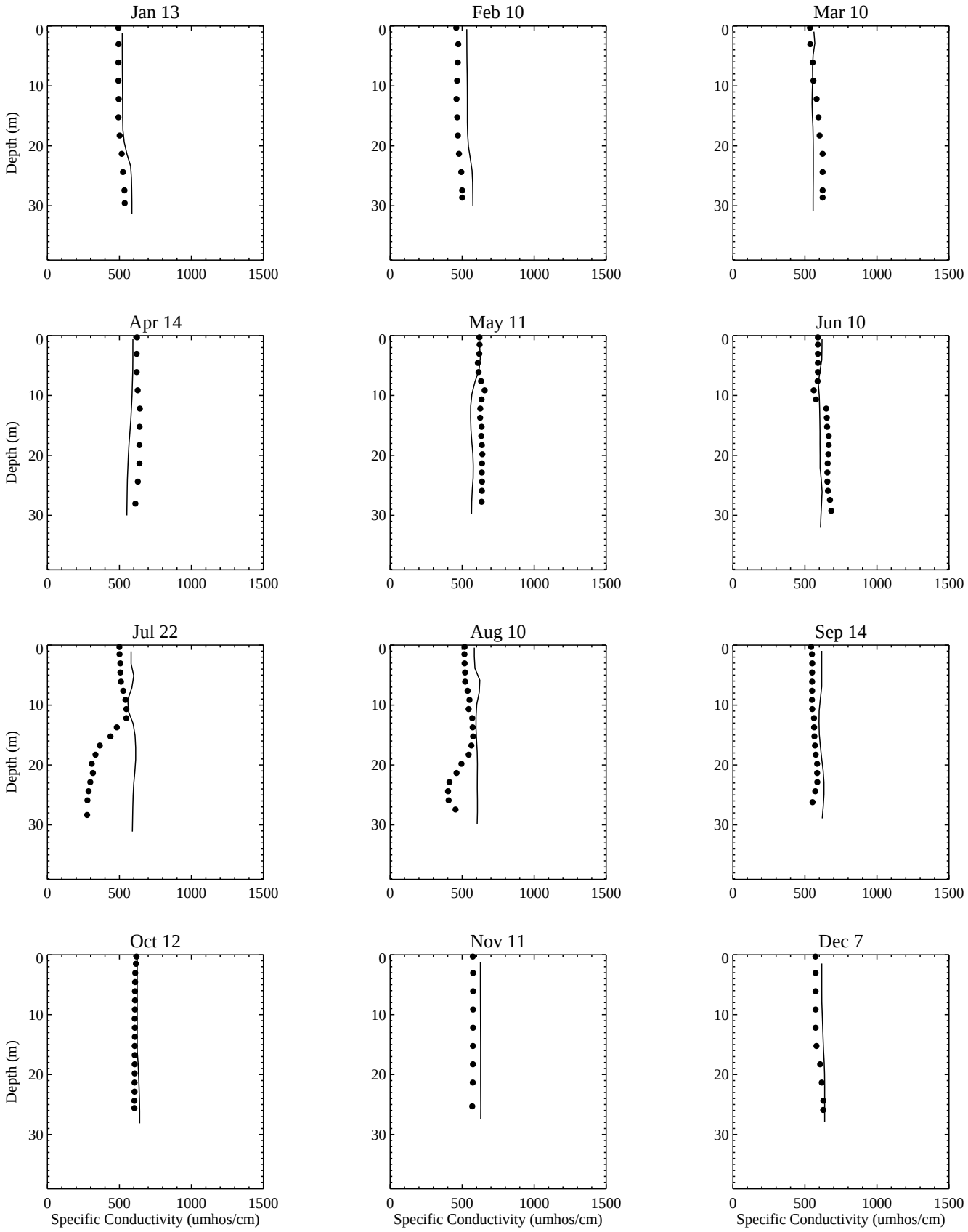

Figure J-8. Vertical profiles of model versus data at Pace Bend (Segment 48) - Specific Conductivity - 1987.

Profiles shown for dates with available data else model results for first day of month shown.

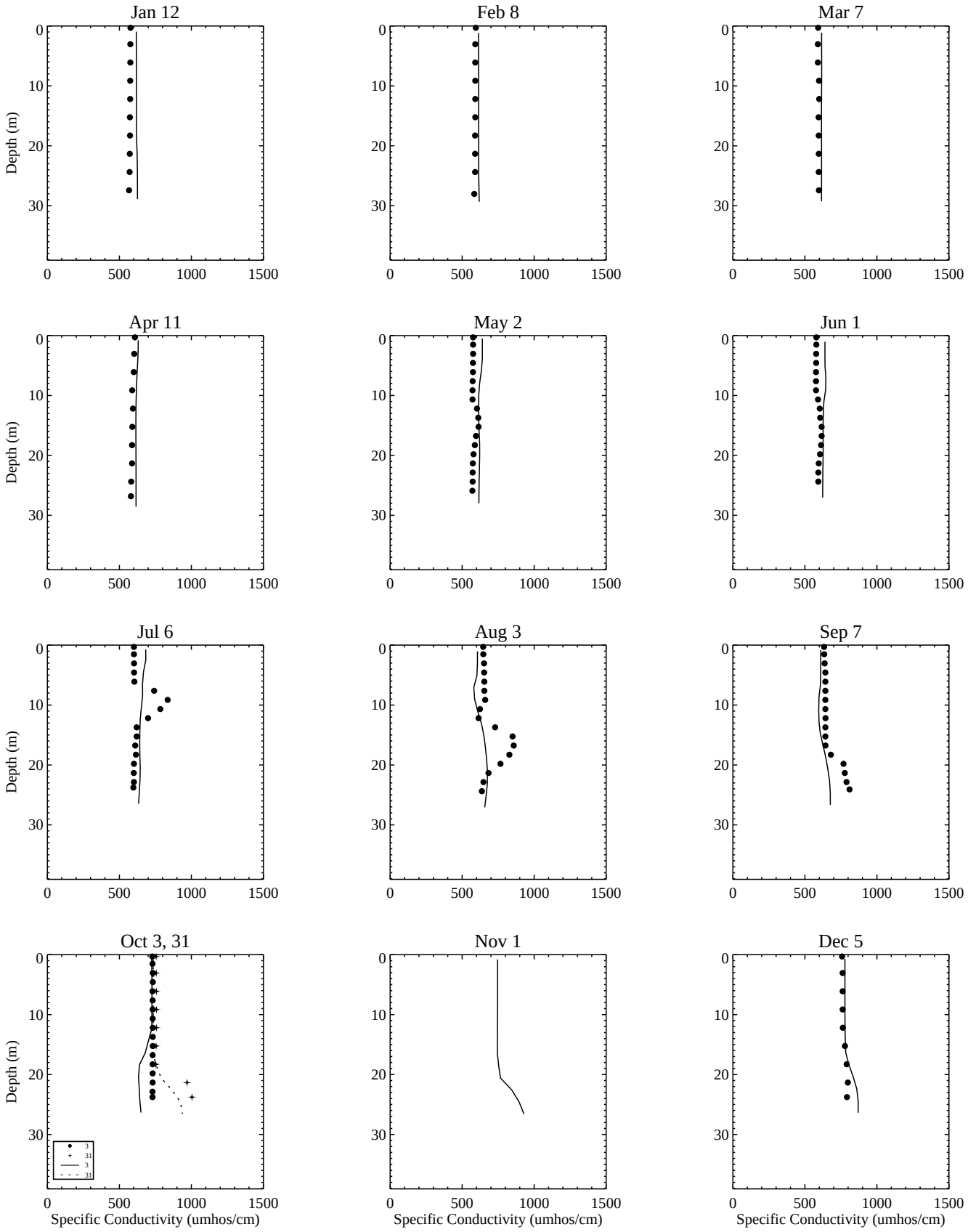

Figure J-8. Vertical profiles of model versus data at Pace Bend (Segment 48) - Specific Conductivity - 1988.

Profiles shown for dates with available data else model results for first day of month shown.

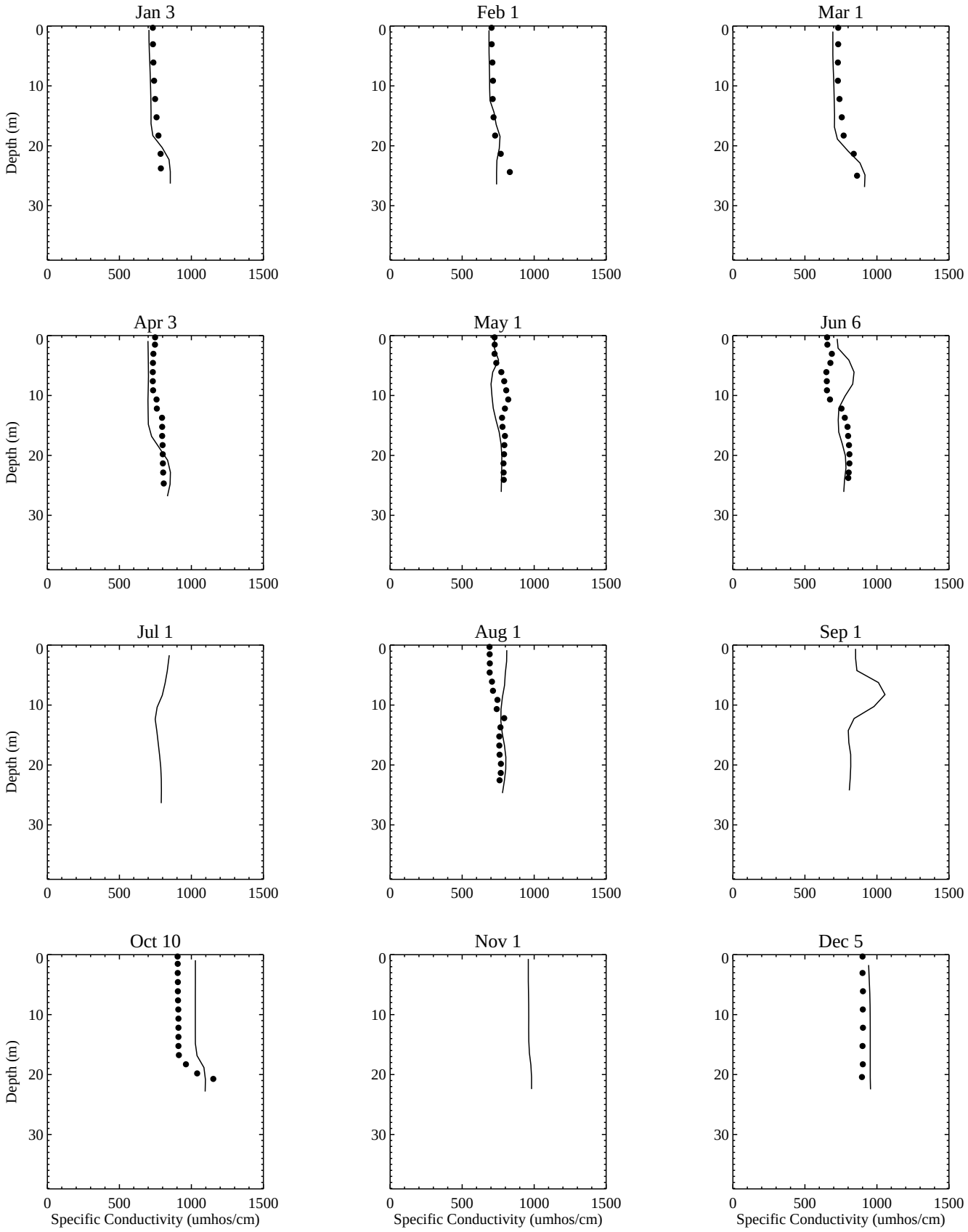

Figure J-8. Vertical profiles of model versus data at Pace Bend (Segment 48) - Specific Conductivity - 1989.

Profiles shown for dates with available data else model results for first day of month shown.

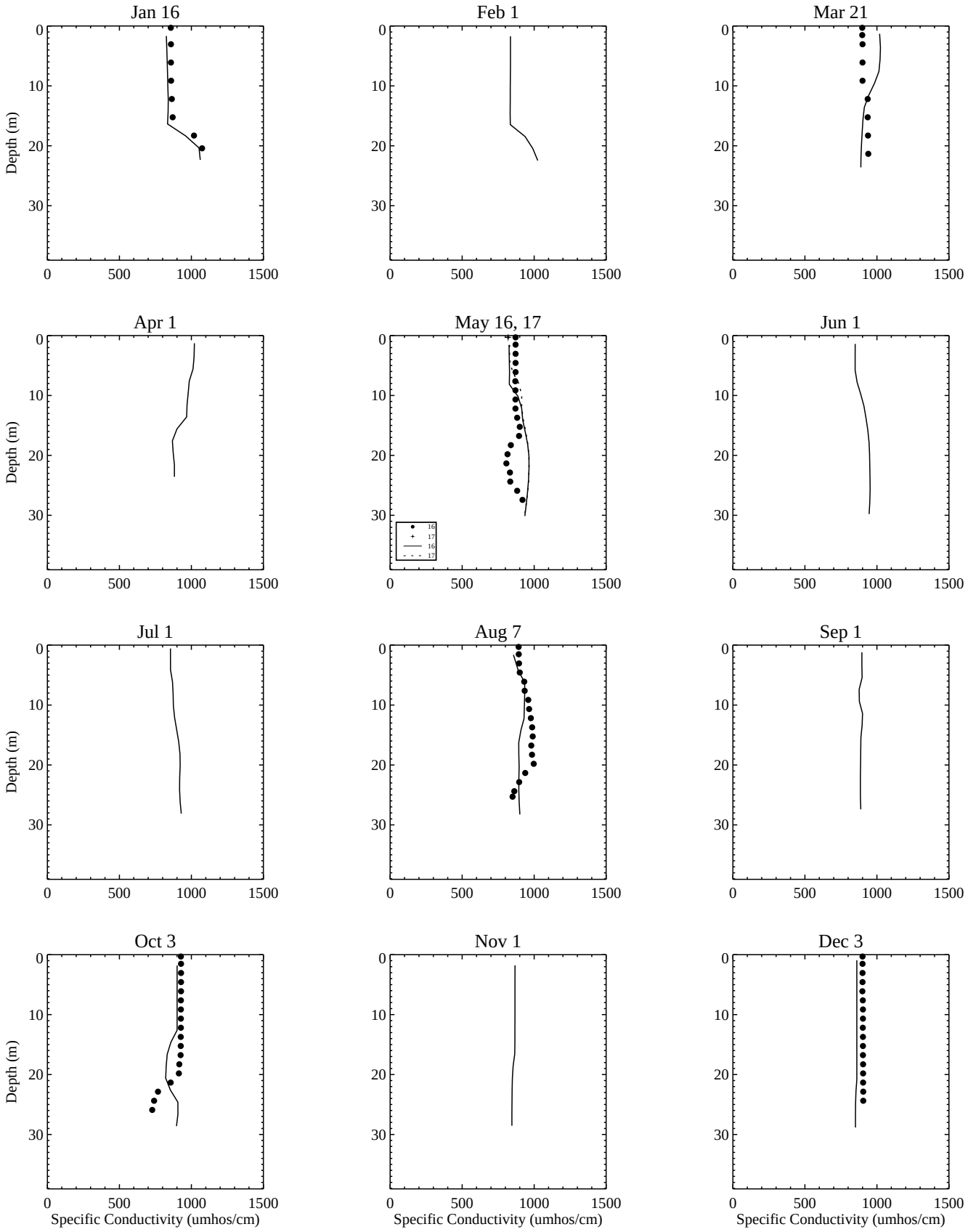

Figure J-8. Vertical profiles of model versus data at Pace Bend (Segment 48) - Specific Conductivity - 1990.

Profiles shown for dates with available data else model results for first day of month shown.

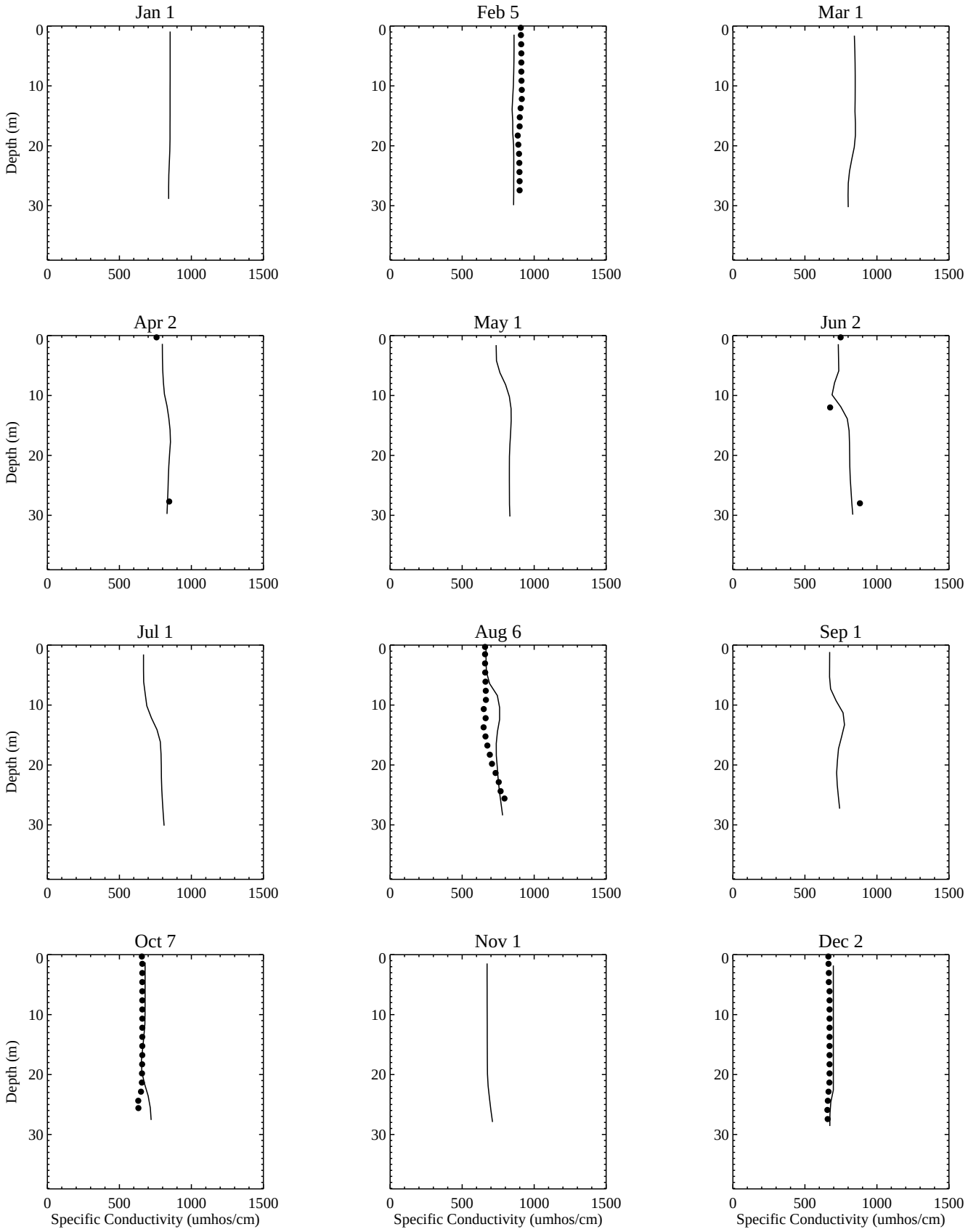

Figure J-8. Vertical profiles of model versus data at Pace Bend (Segment 48) - Specific Conductivity - 1991.

Profiles shown for dates with available data else model results for first day of month shown.

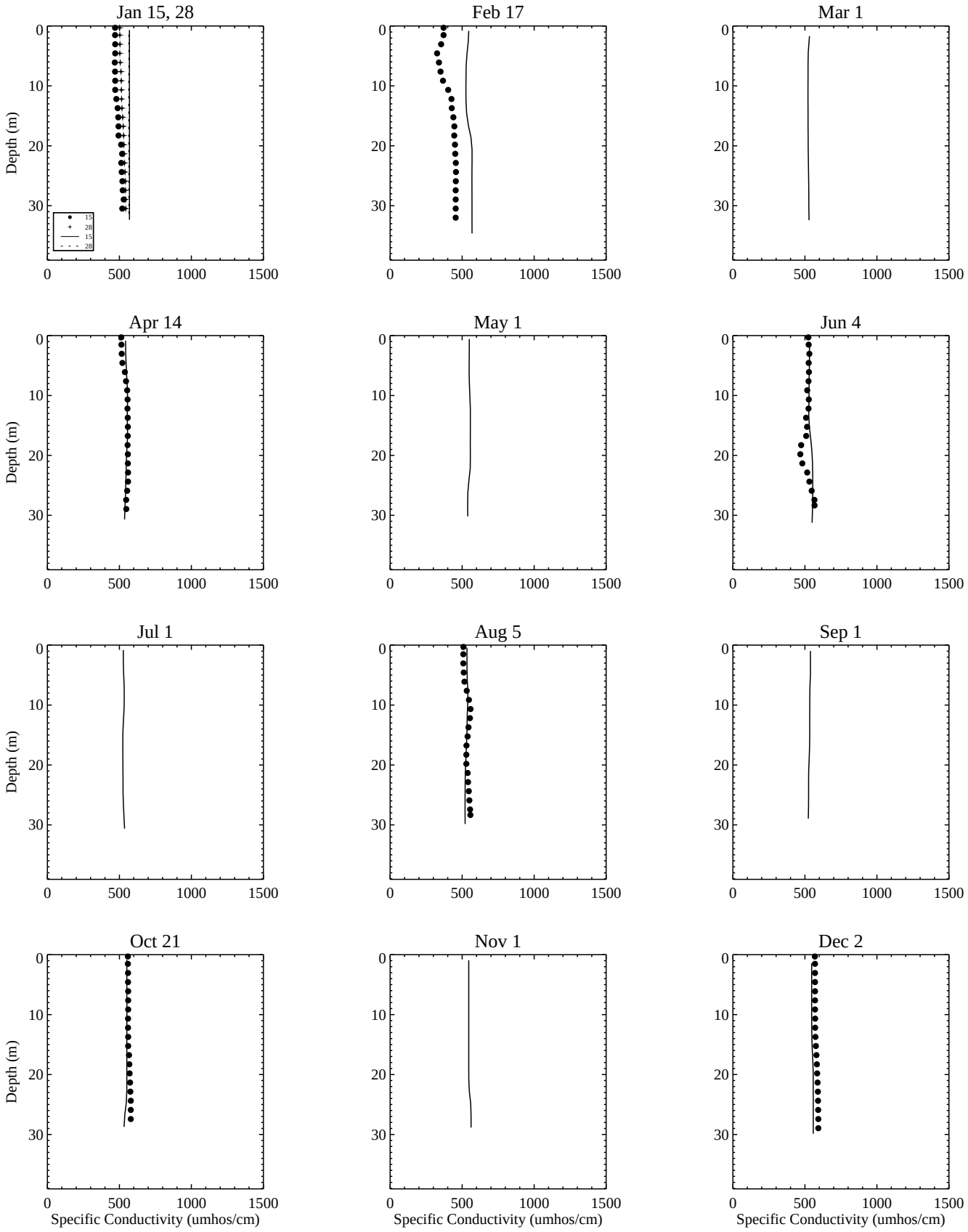

Figure J-8. Vertical profiles of model versus data at Pace Bend (Segment 48) - Specific Conductivity - 1992.

Profiles shown for dates with available data else model results for first day of month shown.

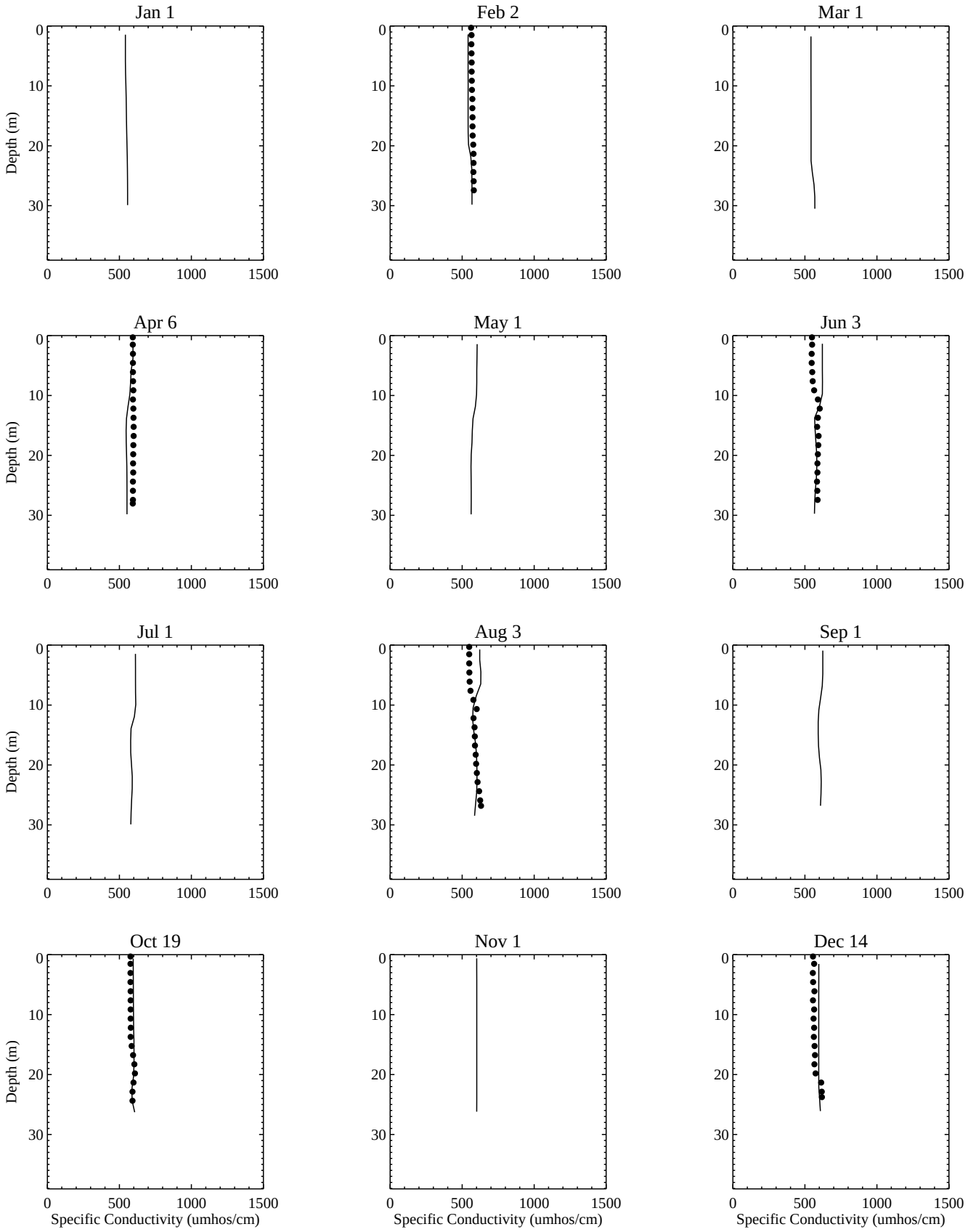

Figure J-8. Vertical profiles of model versus data at Pace Bend (Segment 48) - Specific Conductivity - 1993.

Profiles shown for dates with available data else model results for first day of month shown.

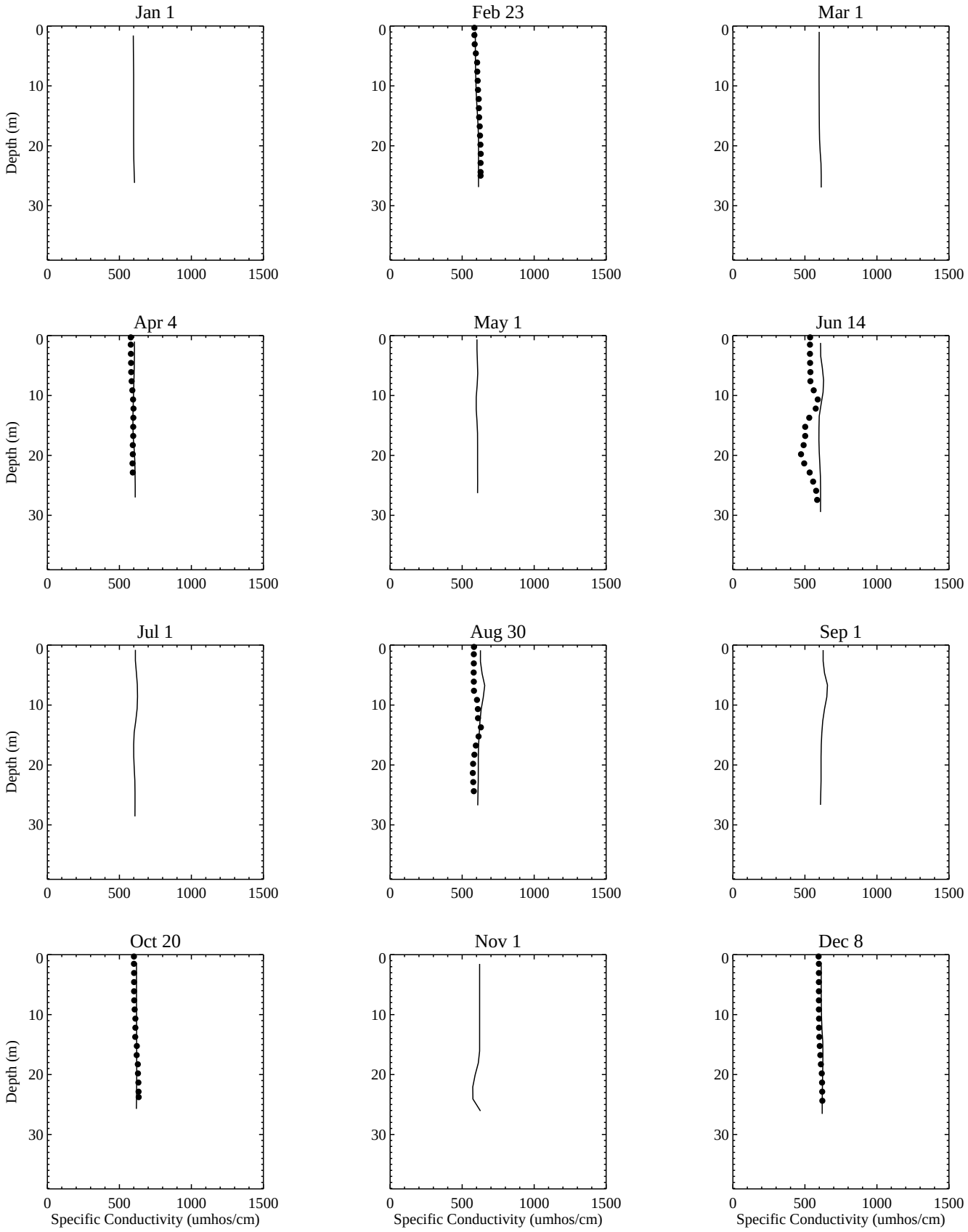

Figure J-8. Vertical profiles of model versus data at Pace Bend (Segment 48) - Specific Conductivity - 1994.

Profiles shown for dates with available data else model results for first day of month shown.

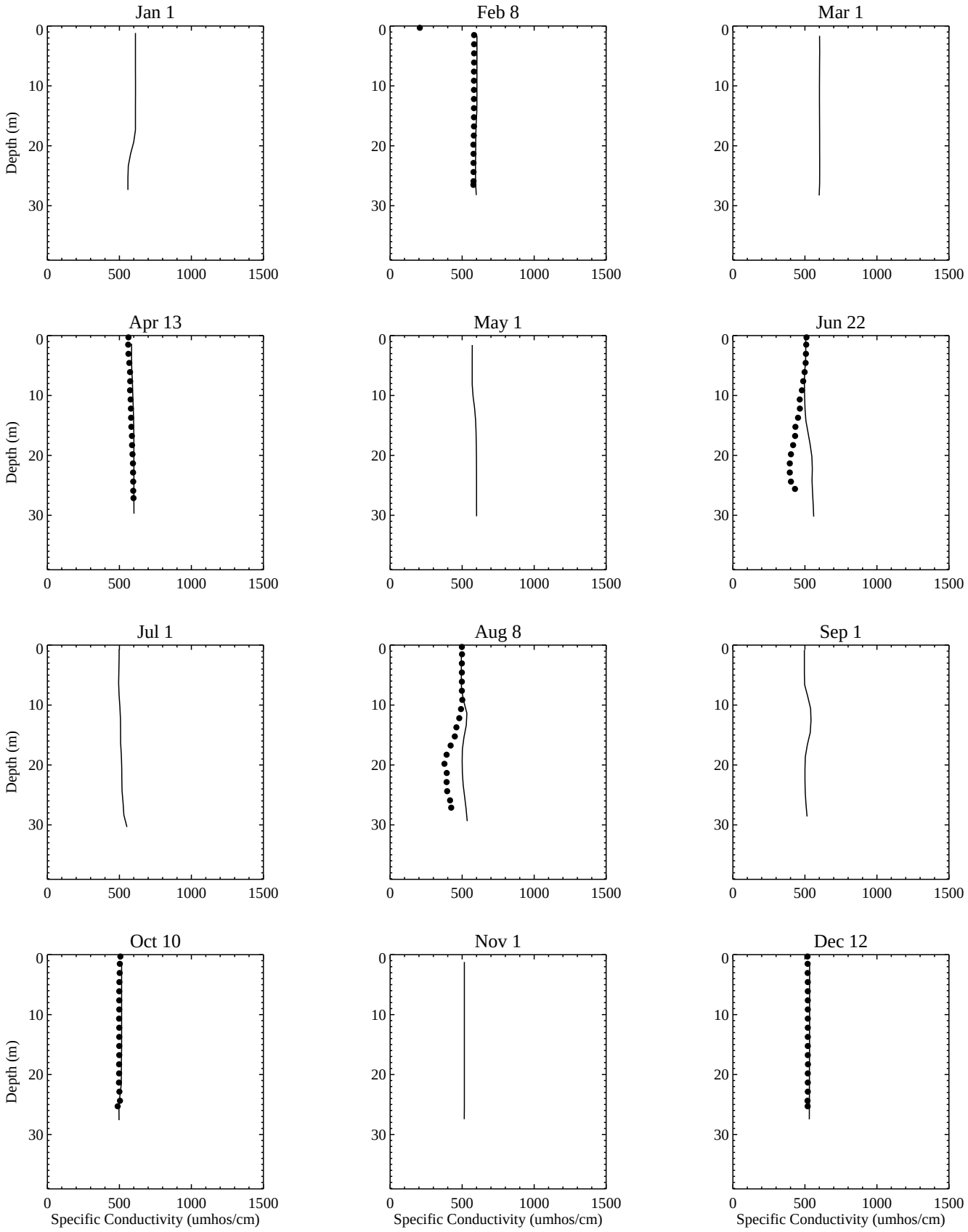

Figure J-8. Vertical profiles of model versus data at Pace Bend (Segment 48) - Specific Conductivity - 1995.

Profiles shown for dates with available data else model results for first day of month shown.

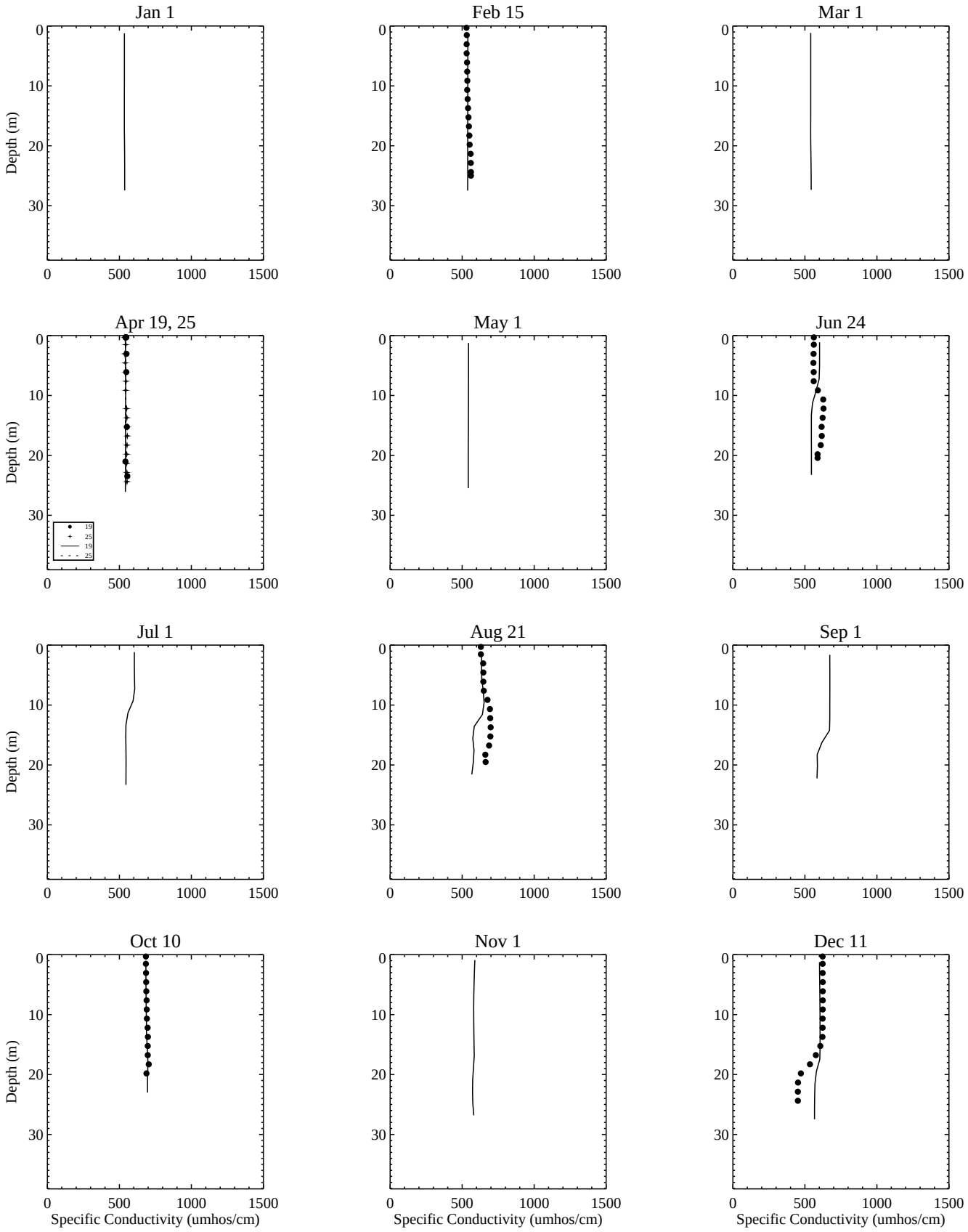

Figure J-8. Vertical profiles of model versus data at Pace Bend (Segment 48) - Specific Conductivity - 1996.

Profiles shown for dates with available data else model results for first day of month shown.

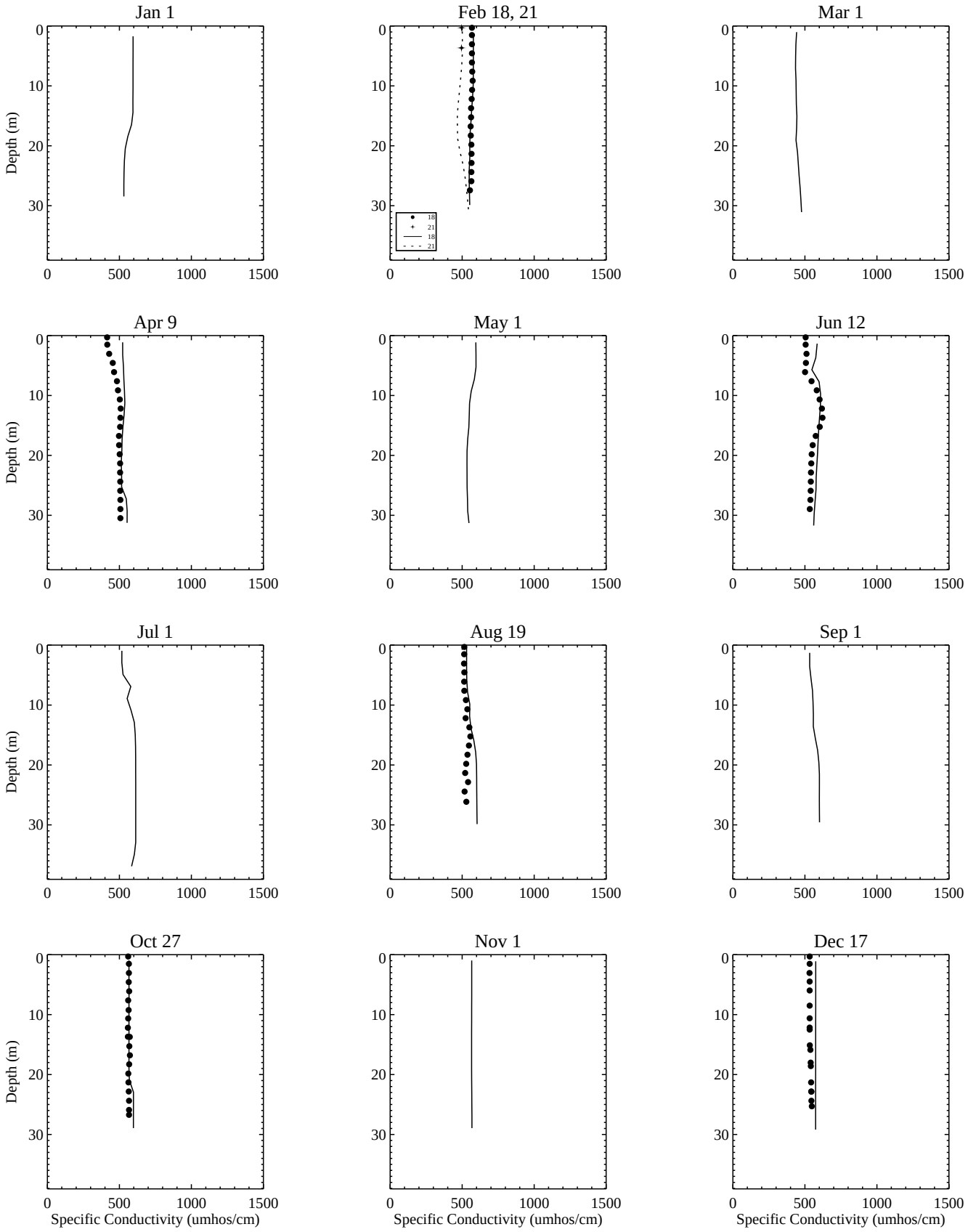

Figure J-8. Vertical profiles of model versus data at Pace Bend (Segment 48) - Specific Conductivity - 1997.

Profiles shown for dates with available data else model results for first day of month shown.

Model ● Data

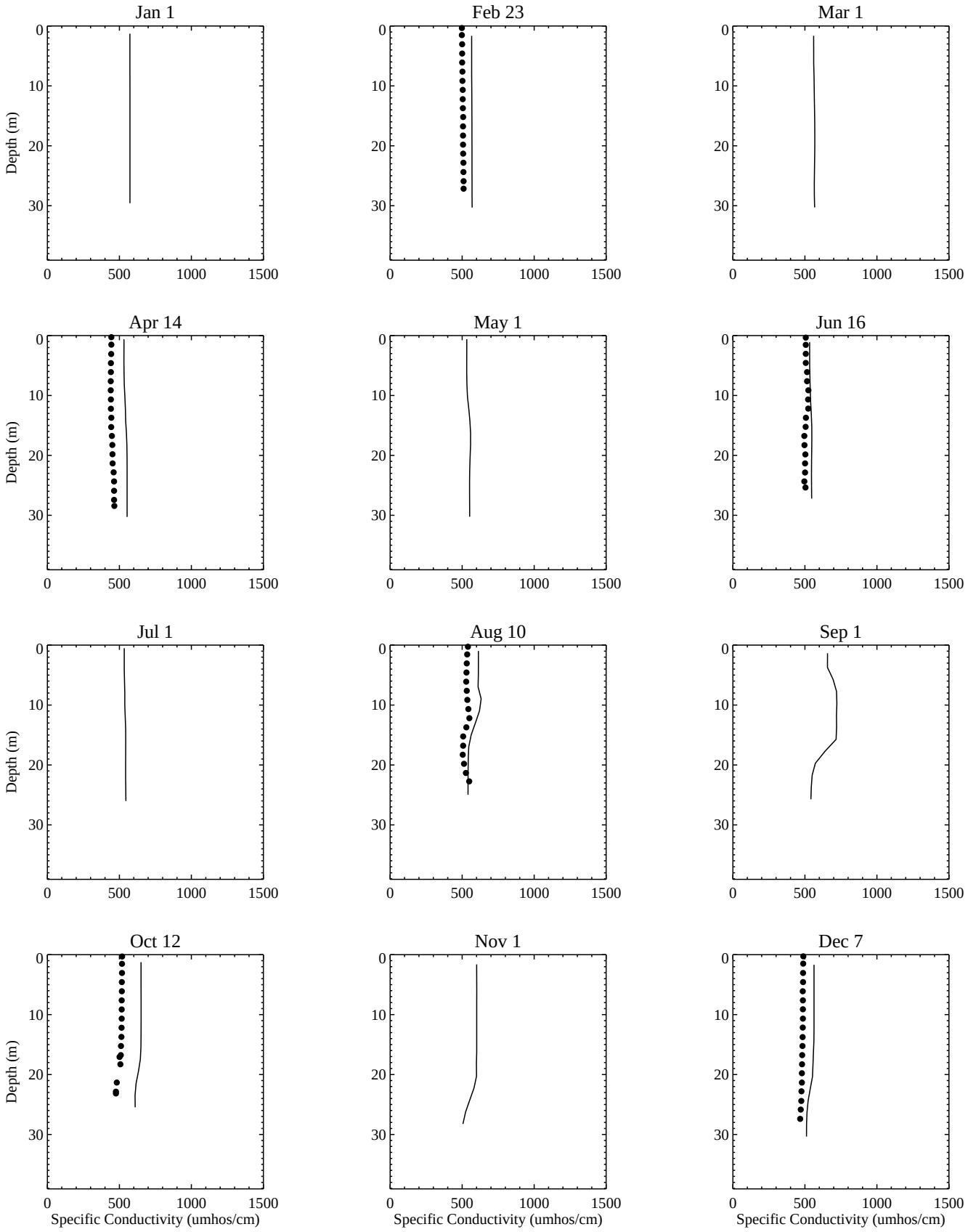

Figure J-8. Vertical profiles of model versus data at Pace Bend (Segment 48) - Specific Conductivity - 1998.

Profiles shown for dates with available data else model results for first day of month shown.

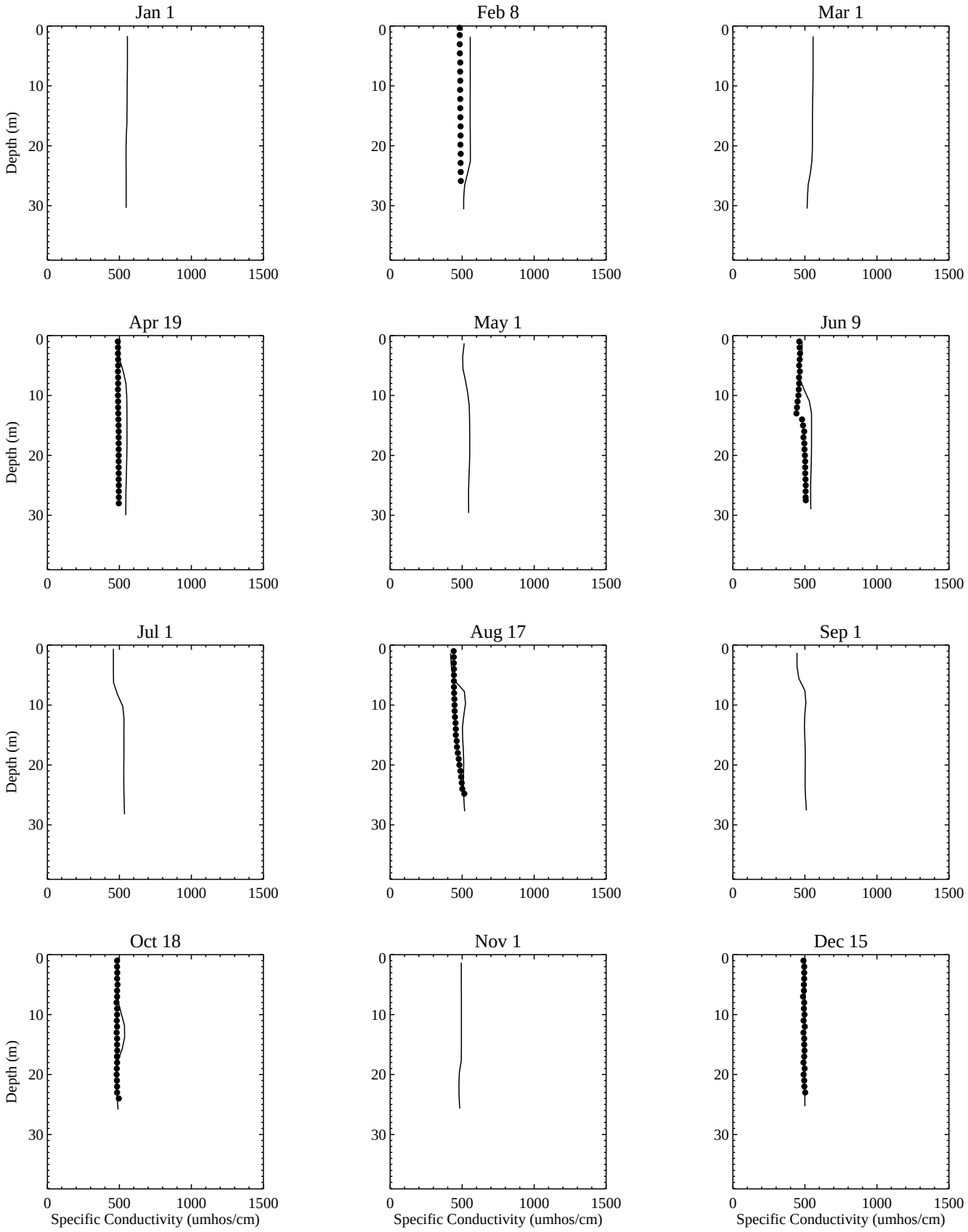

Figure J-8. Vertical profiles of model versus data at Pace Bend (Segment 48) - Specific Conductivity - 1999.

Profiles shown for dates with available data else model results for first day of month shown.

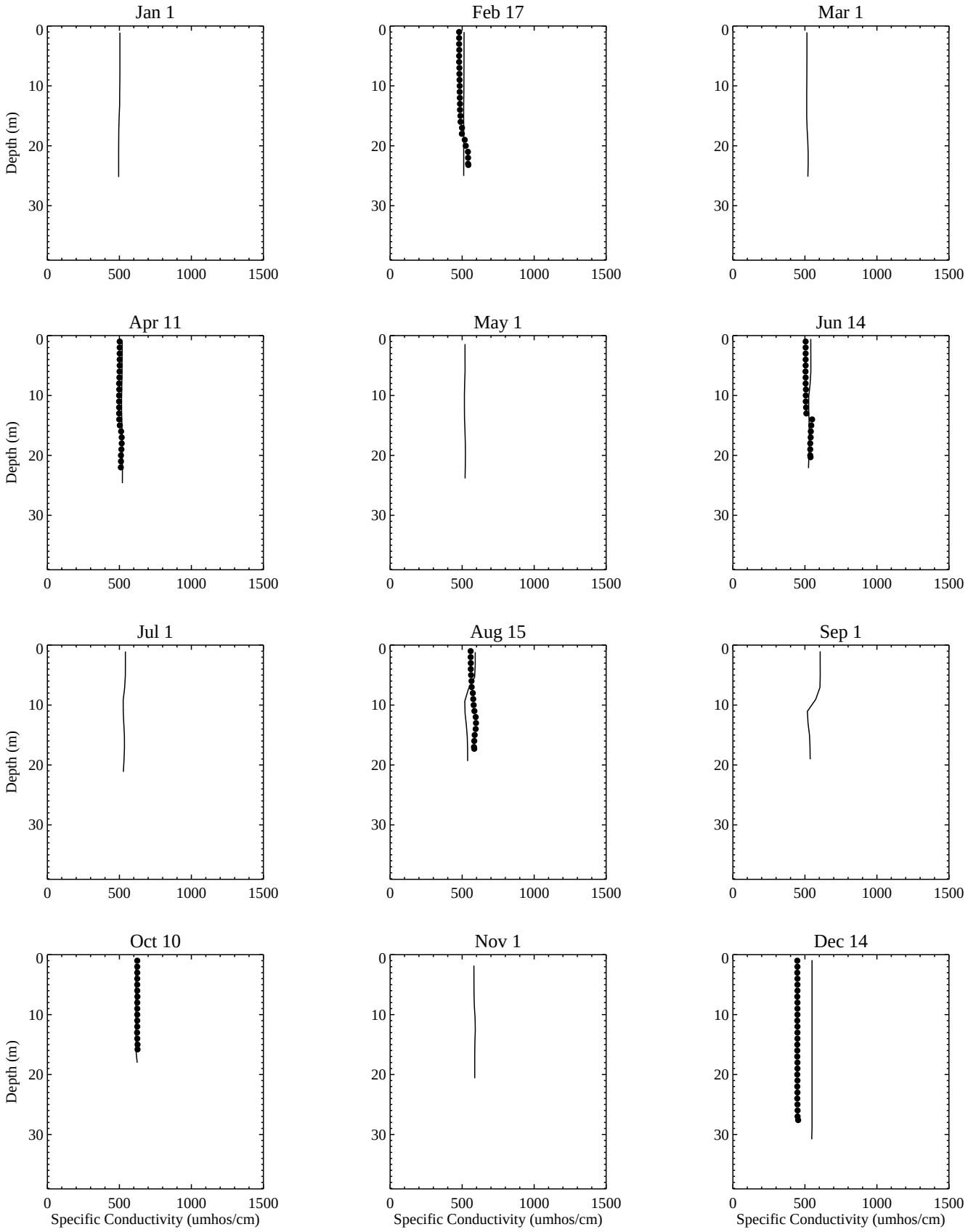

Figure J-8. Vertical profiles of model versus data at Pace Bend (Segment 48) - Specific Conductivity - 2000.

Profiles shown for dates with available data else model results for first day of month shown.

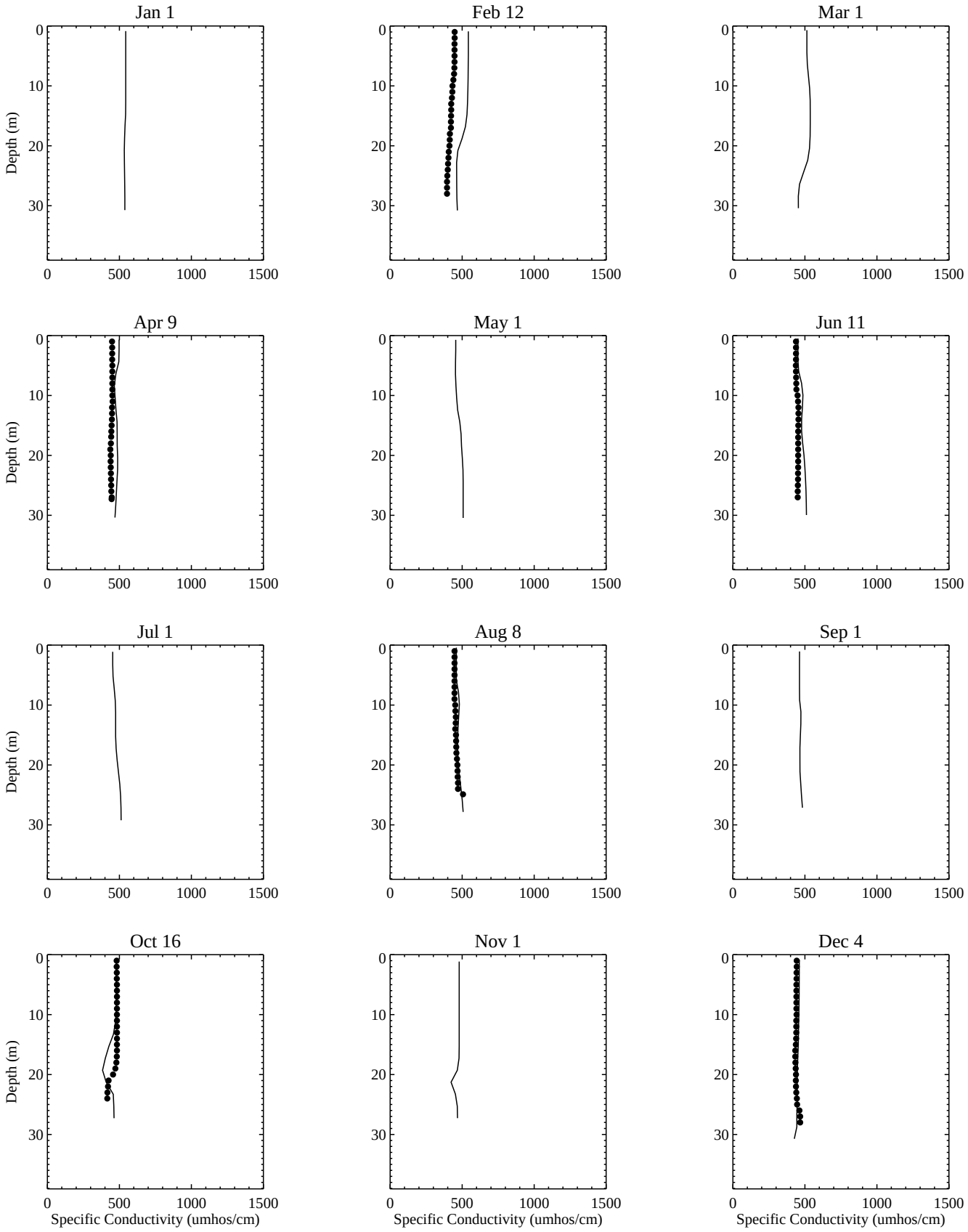

Figure J-8. Vertical profiles of model versus data at Pace Bend (Segment 48) - Specific Conductivity - 2001.

Profiles shown for dates with available data else model results for first day of month shown.

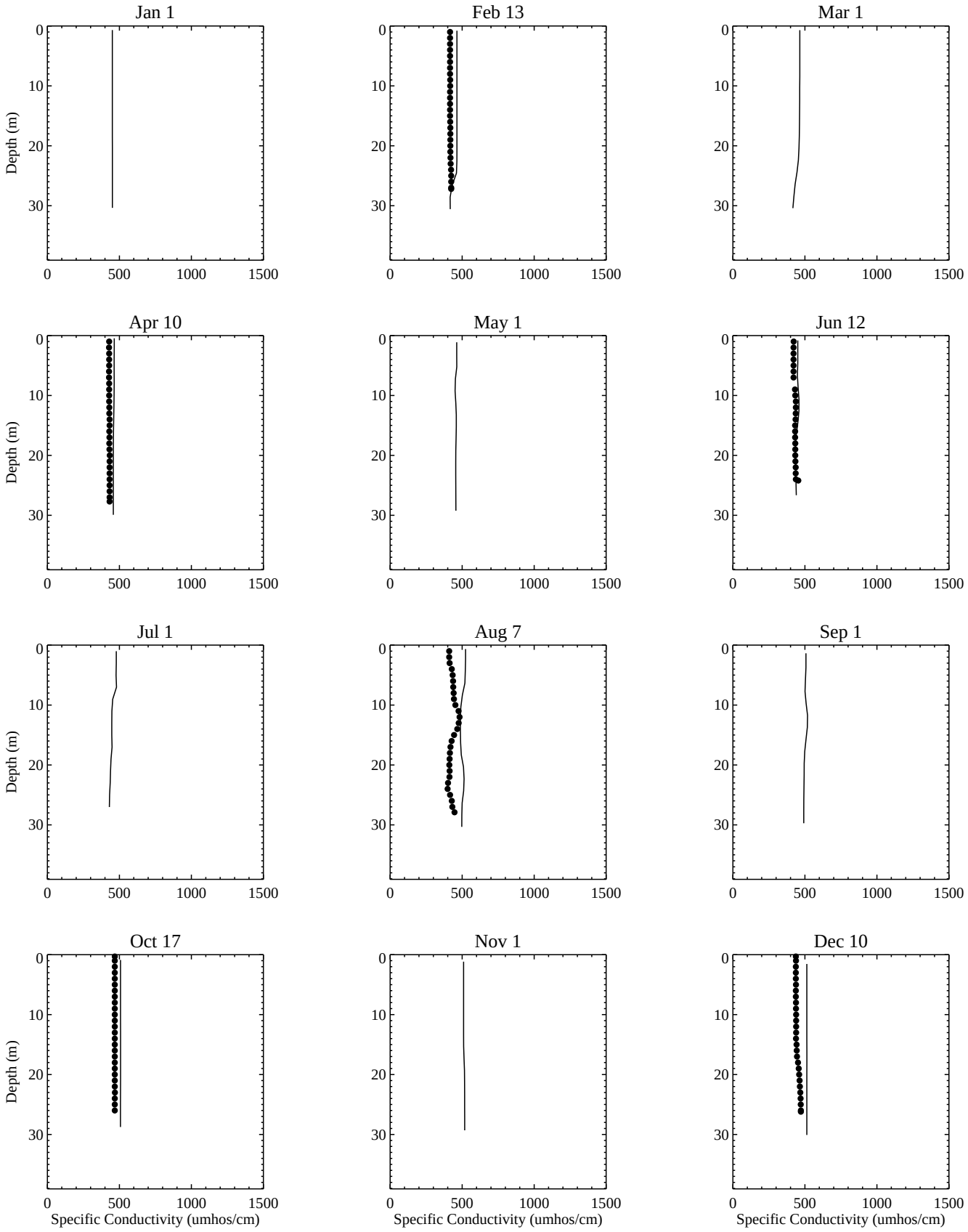

Figure J-8. Vertical profiles of model versus data at Pace Bend (Segment 48) - Specific Conductivity - 2002.

Profiles shown for dates with available data else model results for first day of month shown.

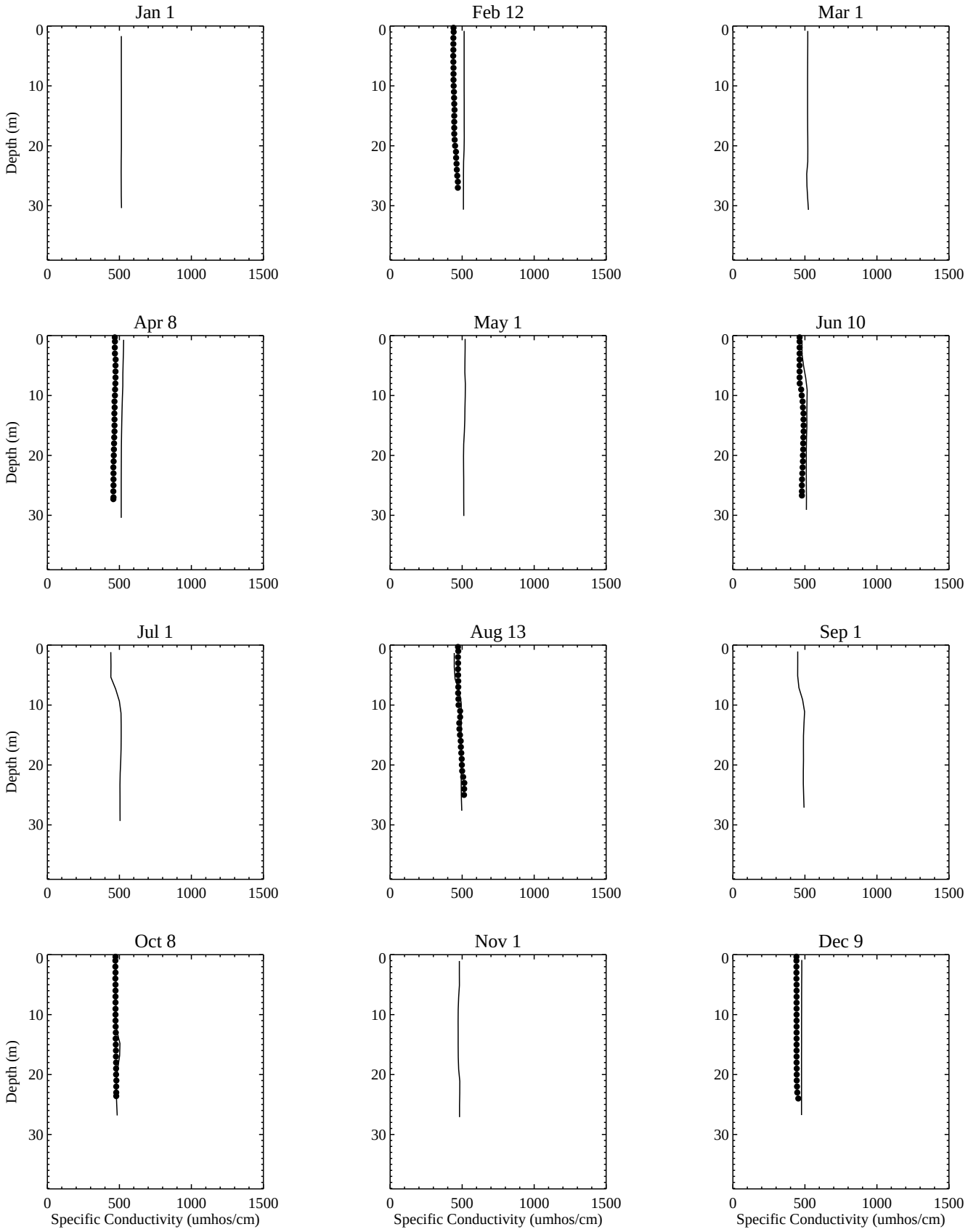

Figure J-8. Vertical profiles of model versus data at Pace Bend (Segment 48) - Specific Conductivity - 2003.

Profiles shown for dates with available data else model results for first day of month shown.

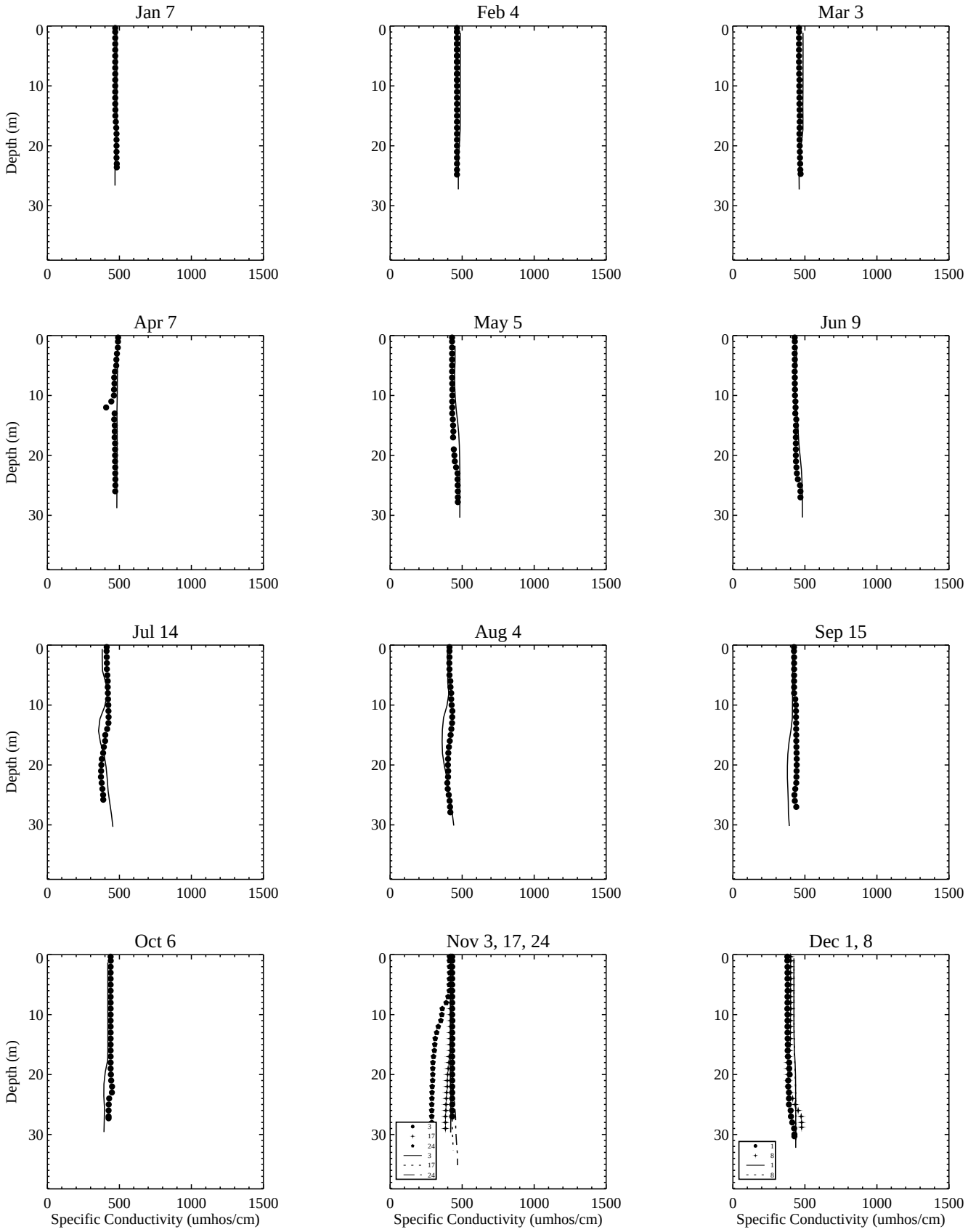

Figure J-8. Vertical profiles of model versus data at Pace Bend (Segment 48) - Specific Conductivity - 2004.

Profiles shown for dates with available data else model results for first day of month shown.

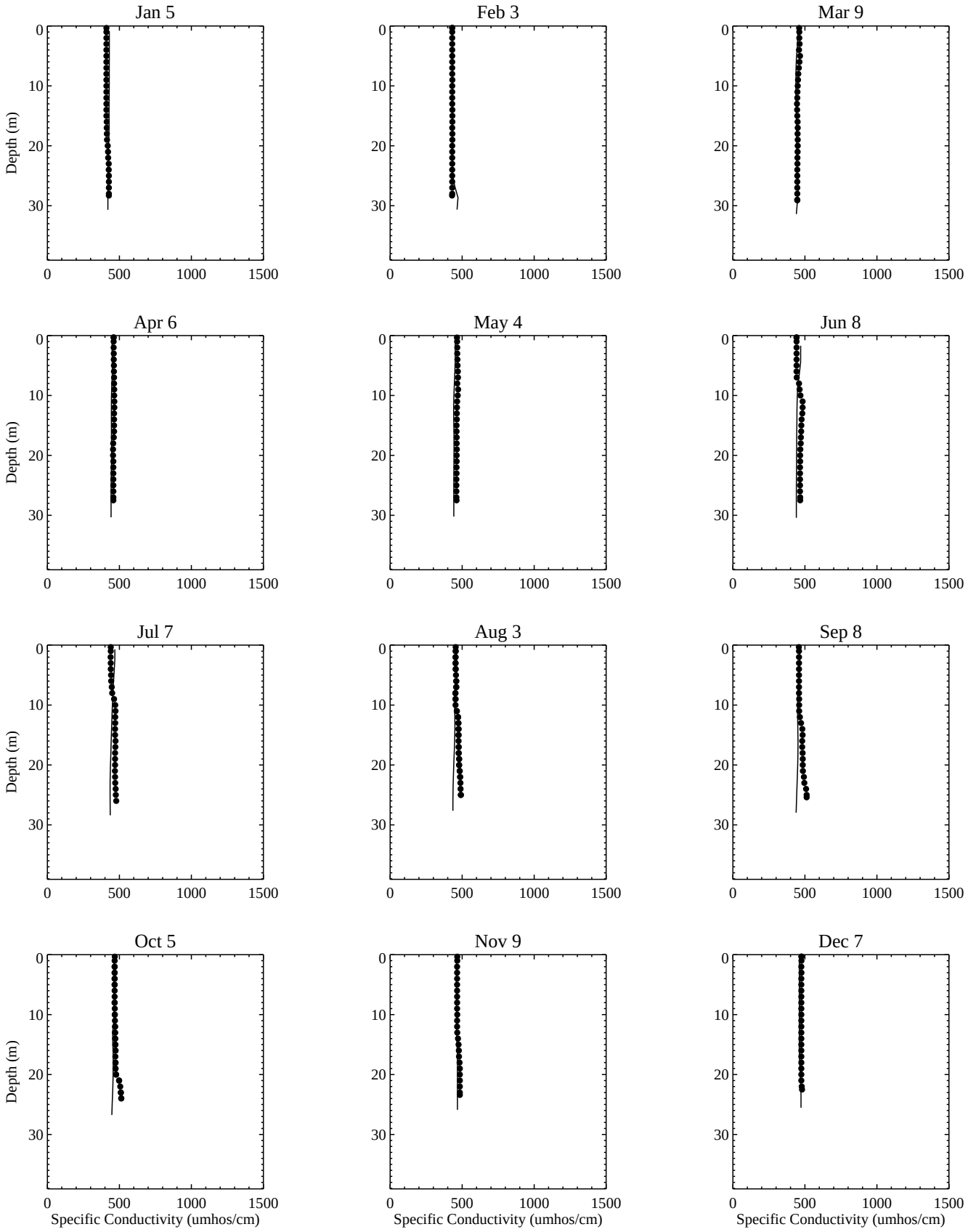

Figure J-8. Vertical profiles of model versus data at Pace Bend (Segment 48) - Specific Conductivity - 2005.

Profiles shown for dates with available data else model results for first day of month shown.

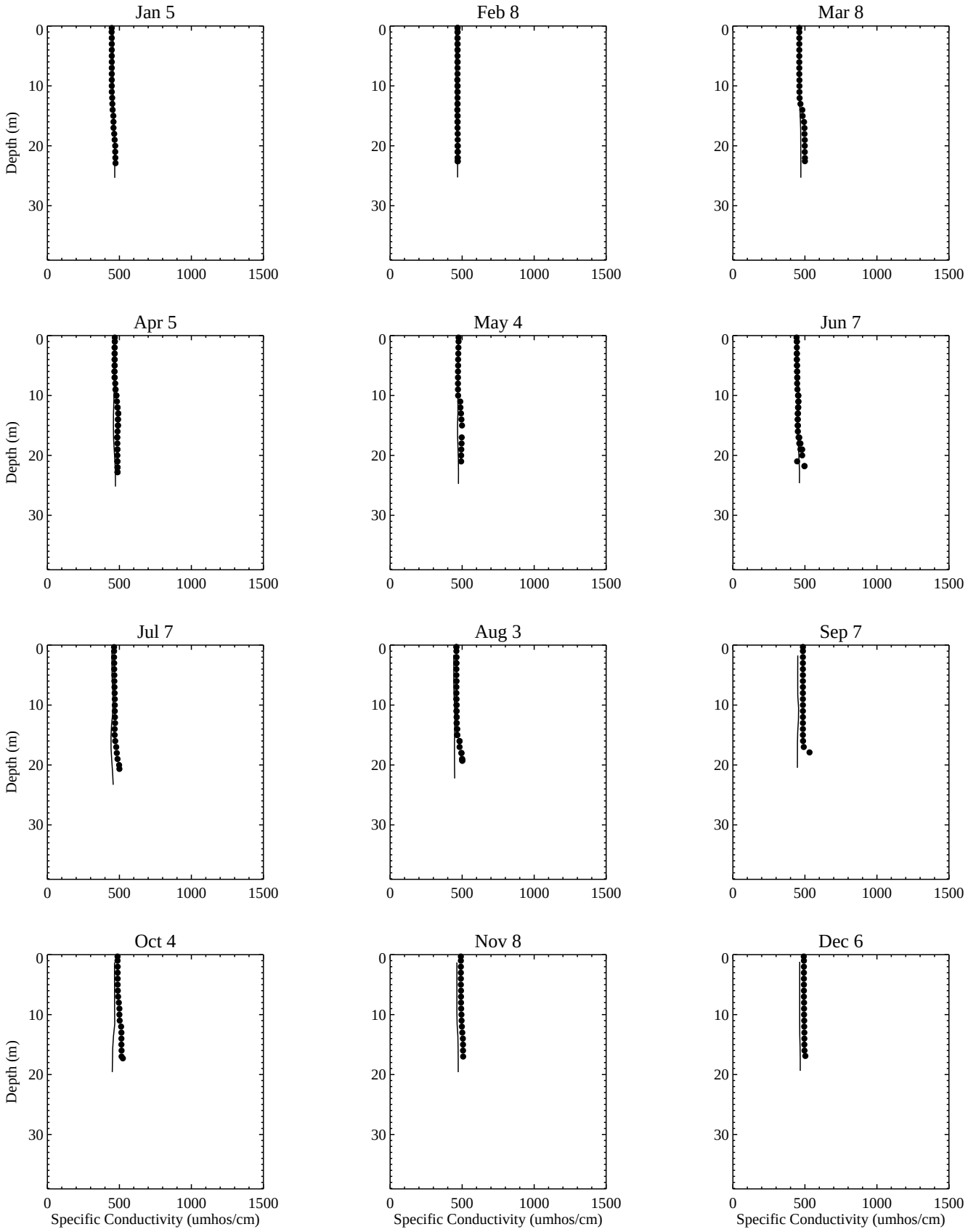

Figure J-8. Vertical profiles of model versus data at Pace Bend (Segment 48) - Specific Conductivity - 2006.

Profiles shown for dates with available data else model results for first day of month shown.

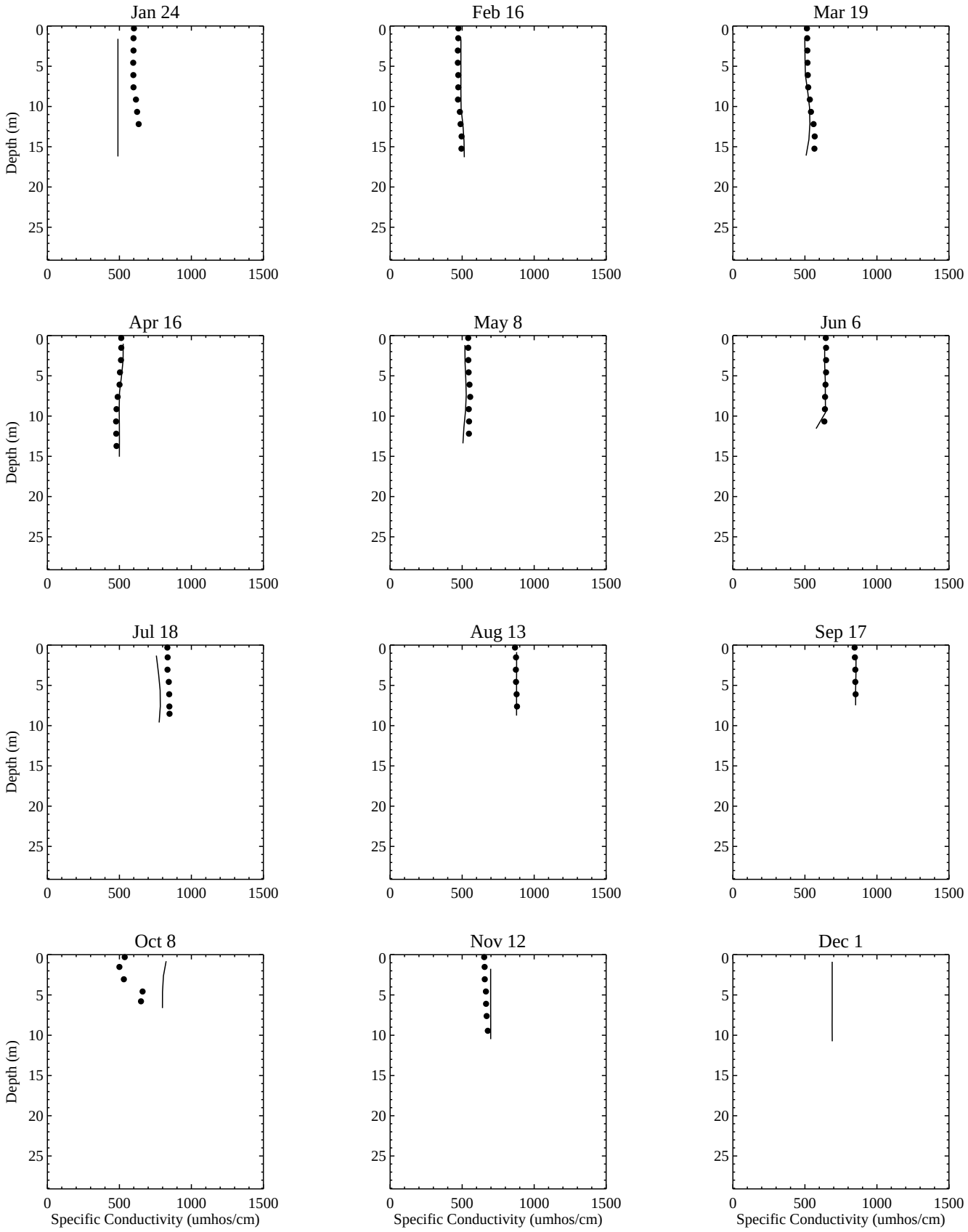

Figure J-9. Vertical profiles of model versus data at Turkey Bend (Segment 28) - Specific Conductivity - 1984.

Profiles shown for dates with available data else model results for first day of month shown.

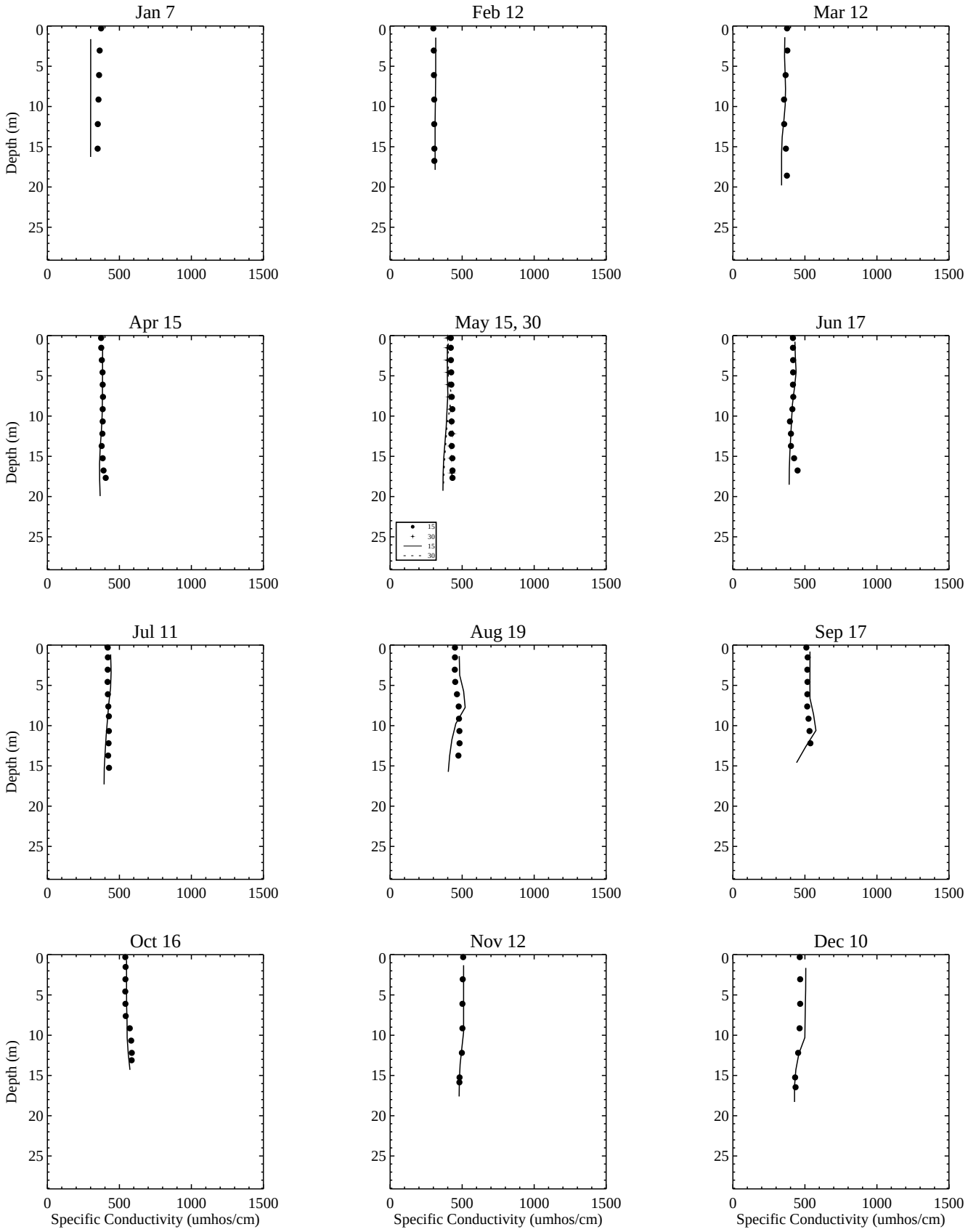

Figure J-9. Vertical profiles of model versus data at Turkey Bend (Segment 28) - Specific Conductivity - 1985.

Profiles shown for dates with available data else model results for first day of month shown.

Model Data

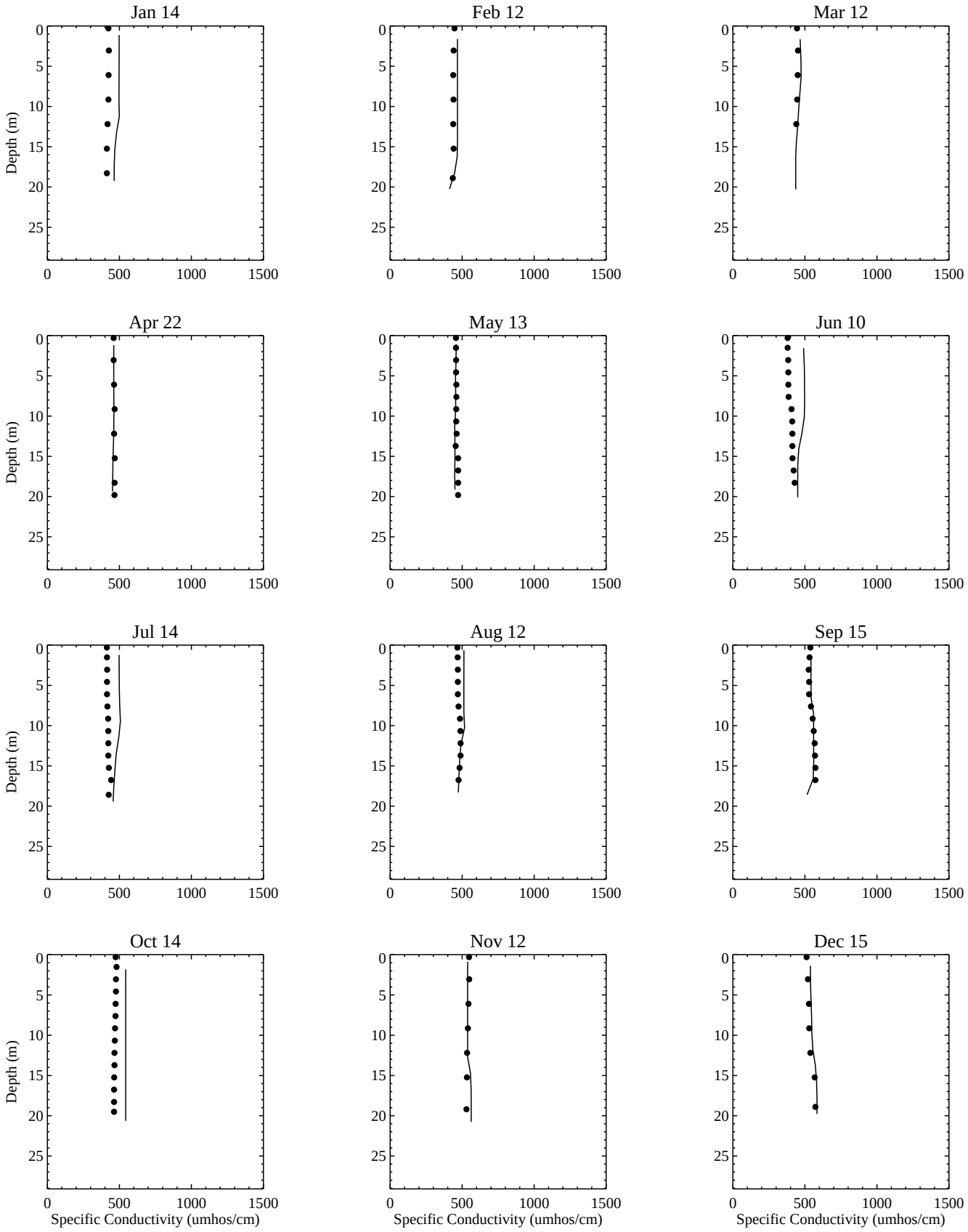

Figure J-9. Vertical profiles of model versus data at Turkey Bend (Segment 28) - Specific Conductivity - 1986.

Profiles shown for dates with available data else model results for first day of month shown.

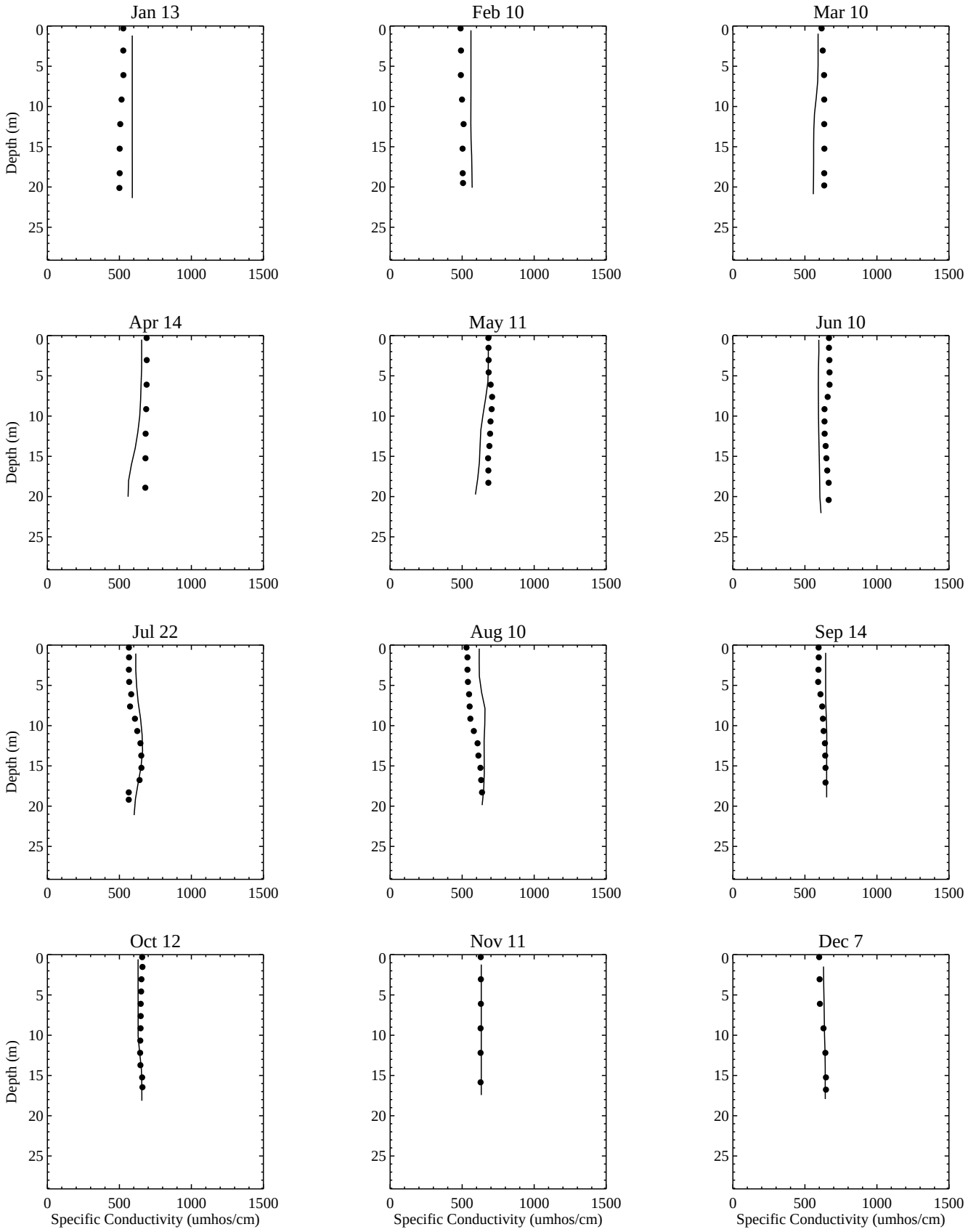

Figure J-9. Vertical profiles of model versus data at Turkey Bend (Segment 28) - Specific Conductivity - 1987.

Profiles shown for dates with available data else model results for first day of month shown.

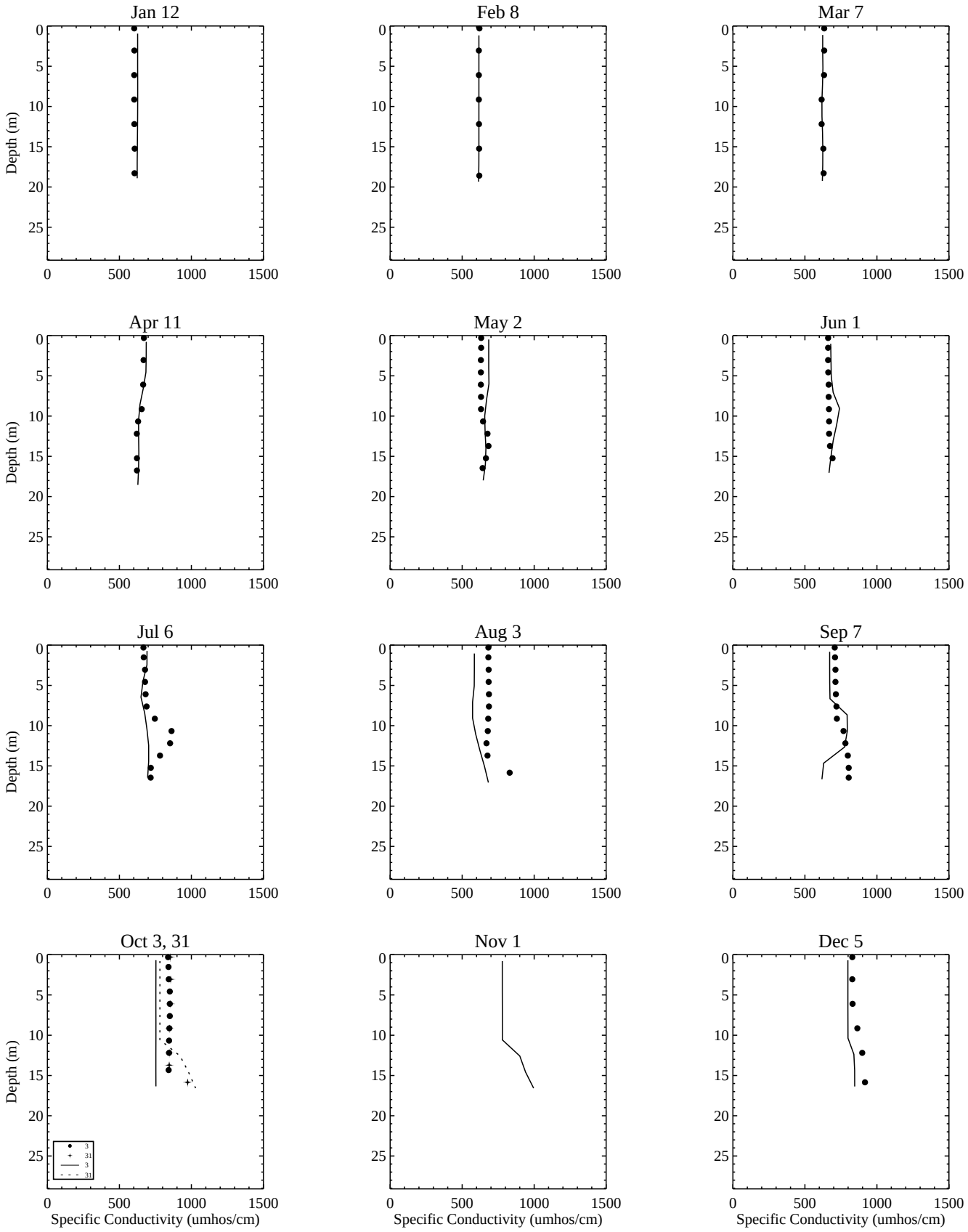

Figure J-9. Vertical profiles of model versus data at Turkey Bend (Segment 28) - Specific Conductivity - 1988.

Profiles shown for dates with available data else model results for first day of month shown.

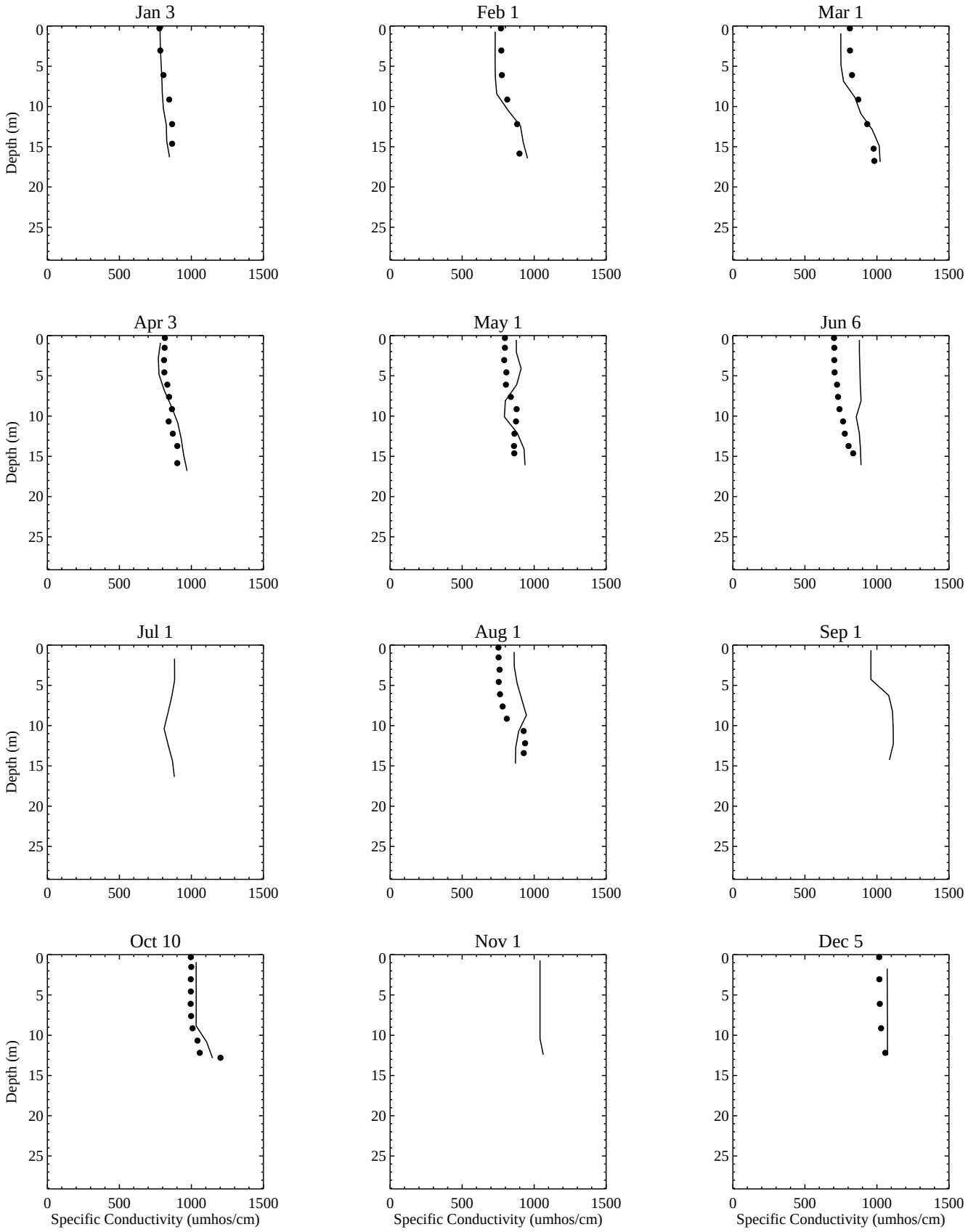

Figure J-9. Vertical profiles of model versus data at Turkey Bend (Segment 28) - Specific Conductivity - 1989.

Profiles shown for dates with available data else model results for first day of month shown.

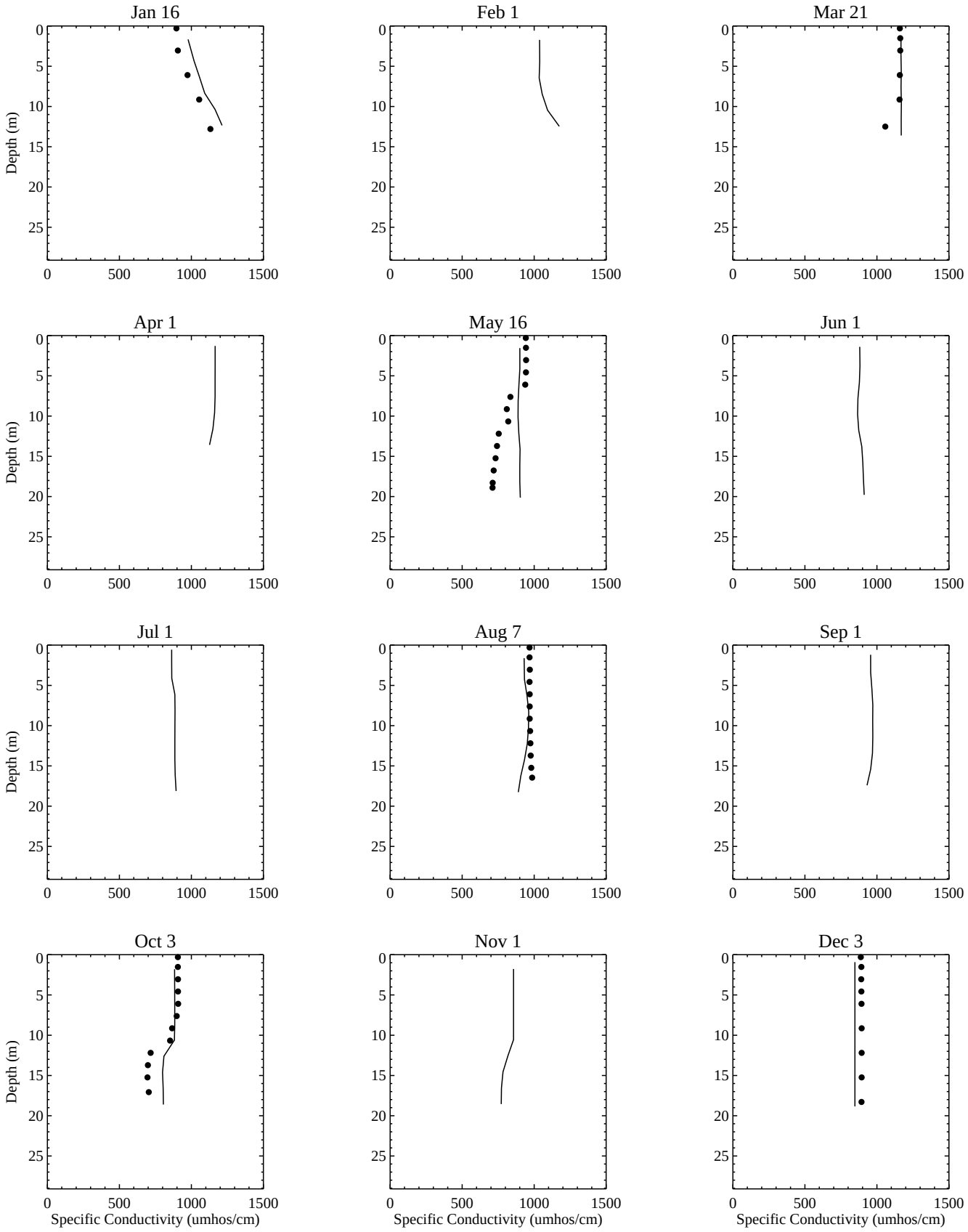

Figure J-9. Vertical profiles of model versus data at Turkey Bend (Segment 28) - Specific Conductivity - 1990.

Profiles shown for dates with available data else model results for first day of month shown.

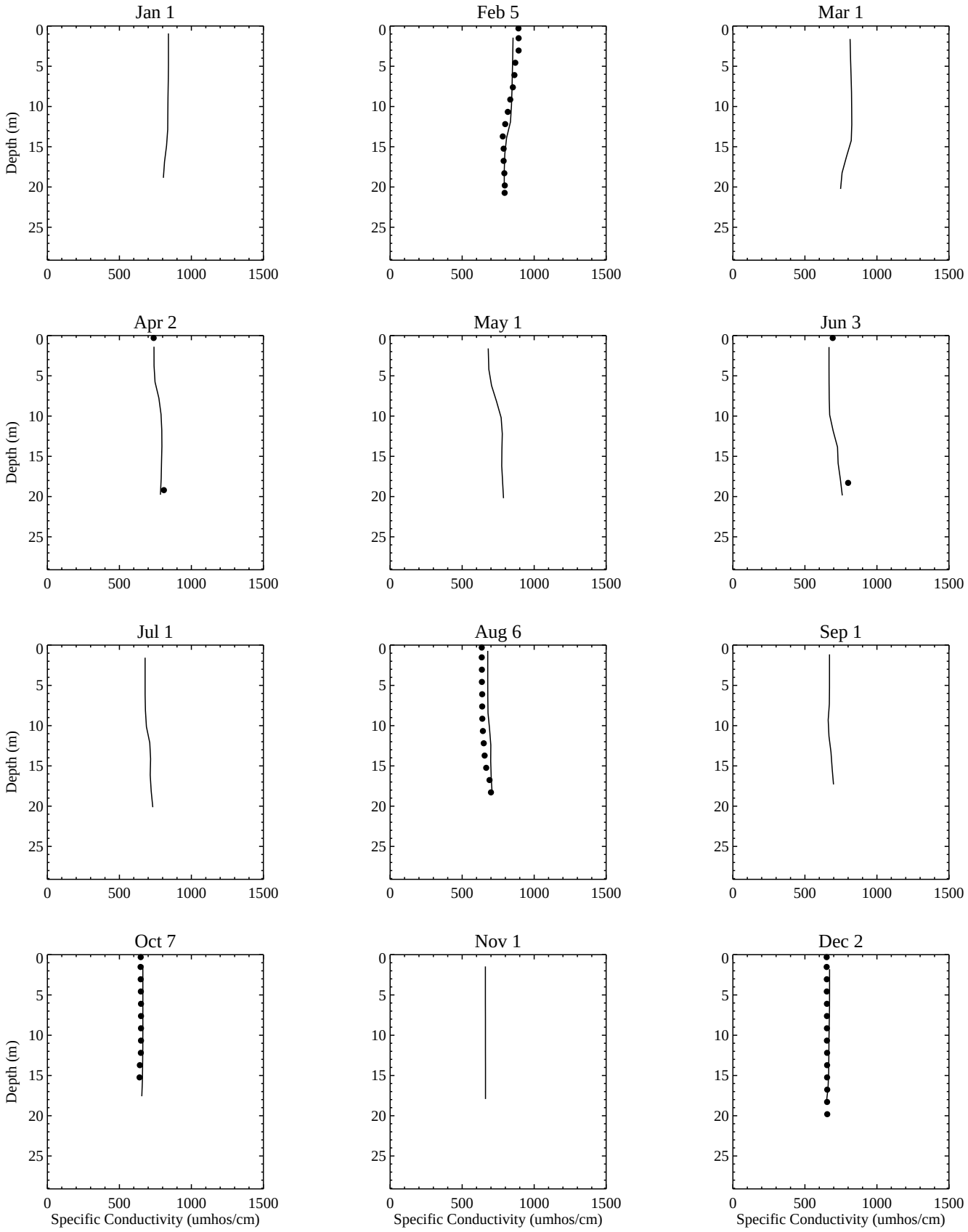

Figure J-9. Vertical profiles of model versus data at Turkey Bend (Segment 28) - Specific Conductivity - 1991.

Profiles shown for dates with available data else model results for first day of month shown.

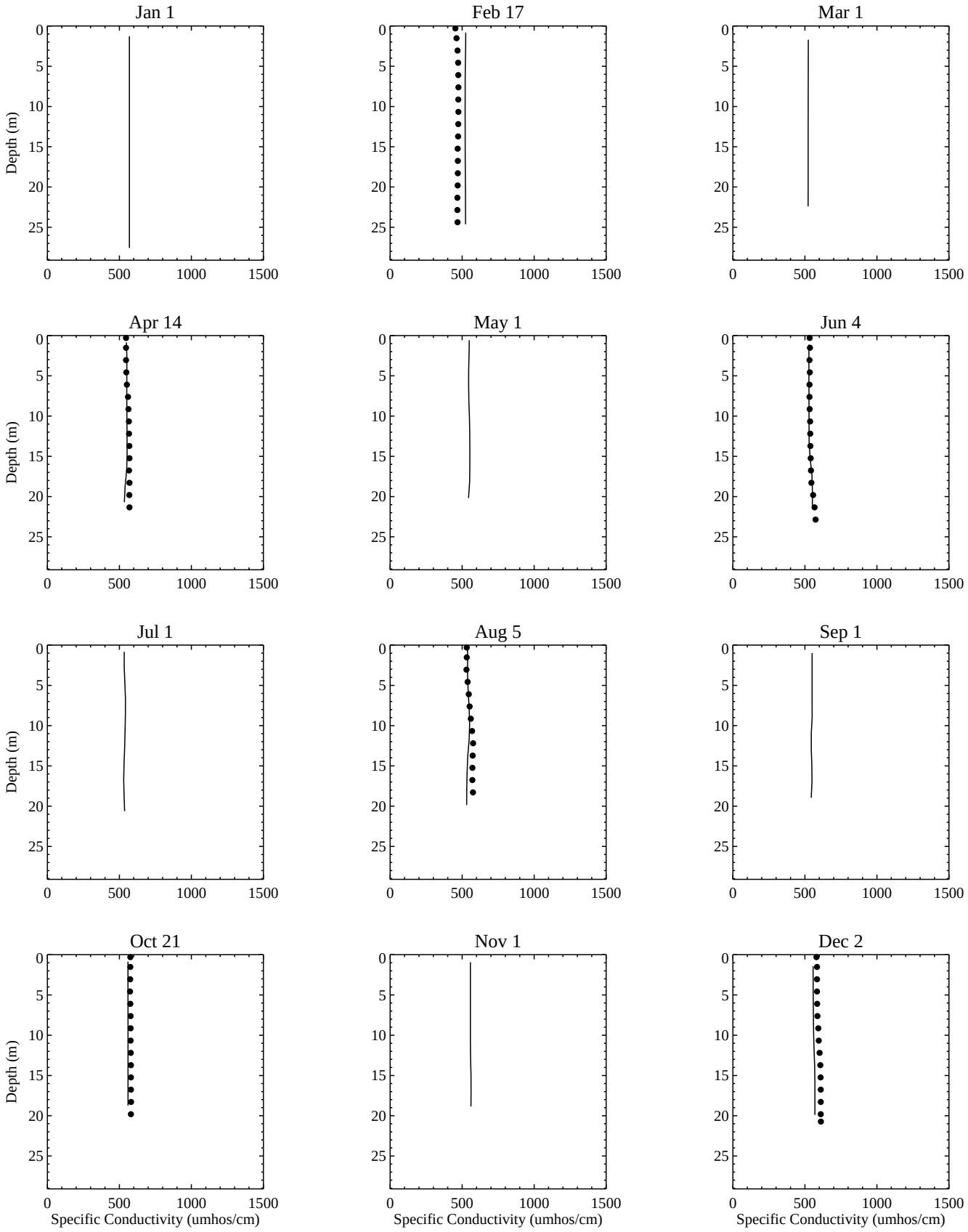

Figure J-9. Vertical profiles of model versus data at Turkey Bend (Segment 28) - Specific Conductivity - 1992.

Profiles shown for dates with available data else model results for first day of month shown.

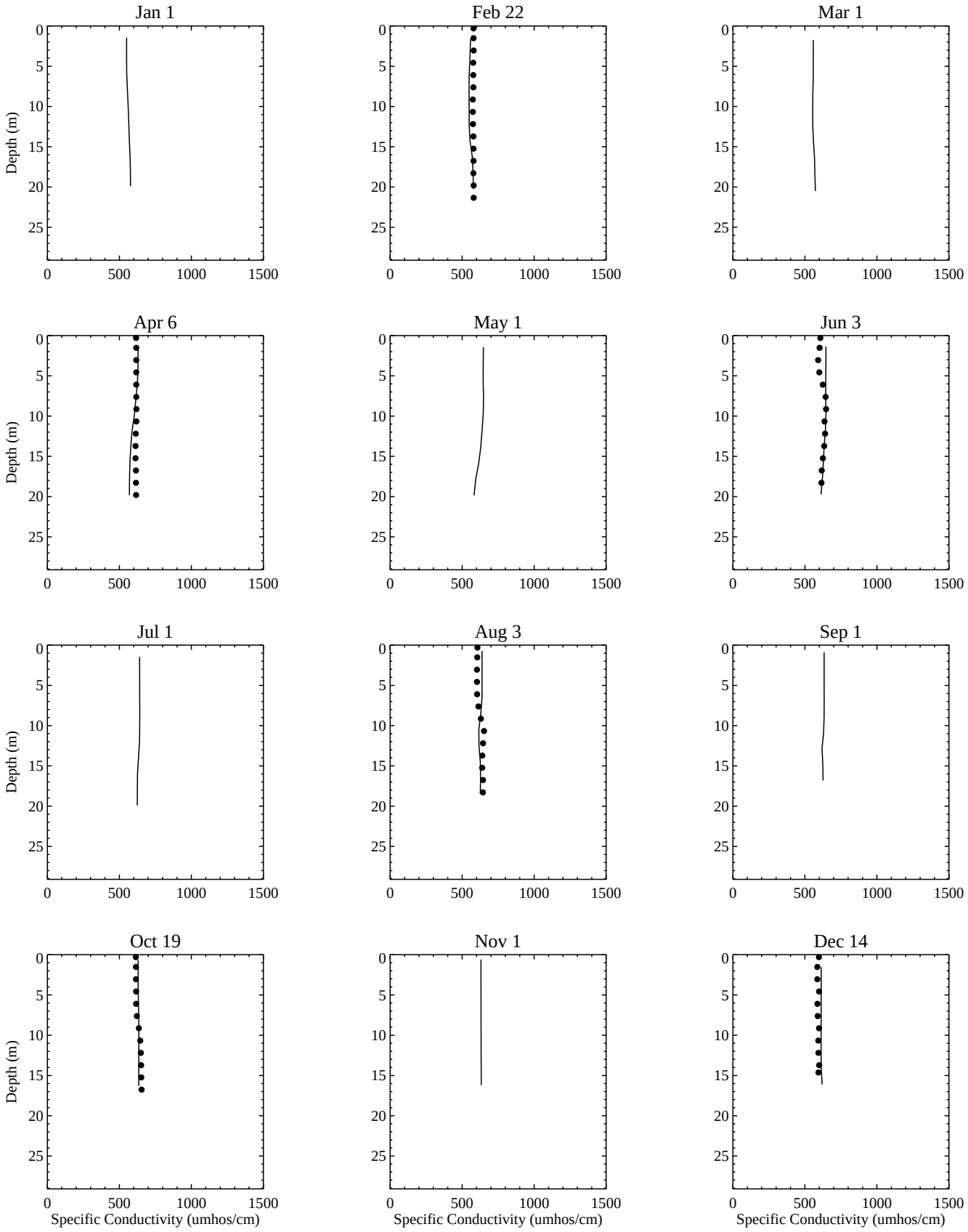

Figure J-9. Vertical profiles of model versus data at Turkey Bend (Segment 28) - Specific Conductivity - 1993.

Profiles shown for dates with available data else model results for first day of month shown.

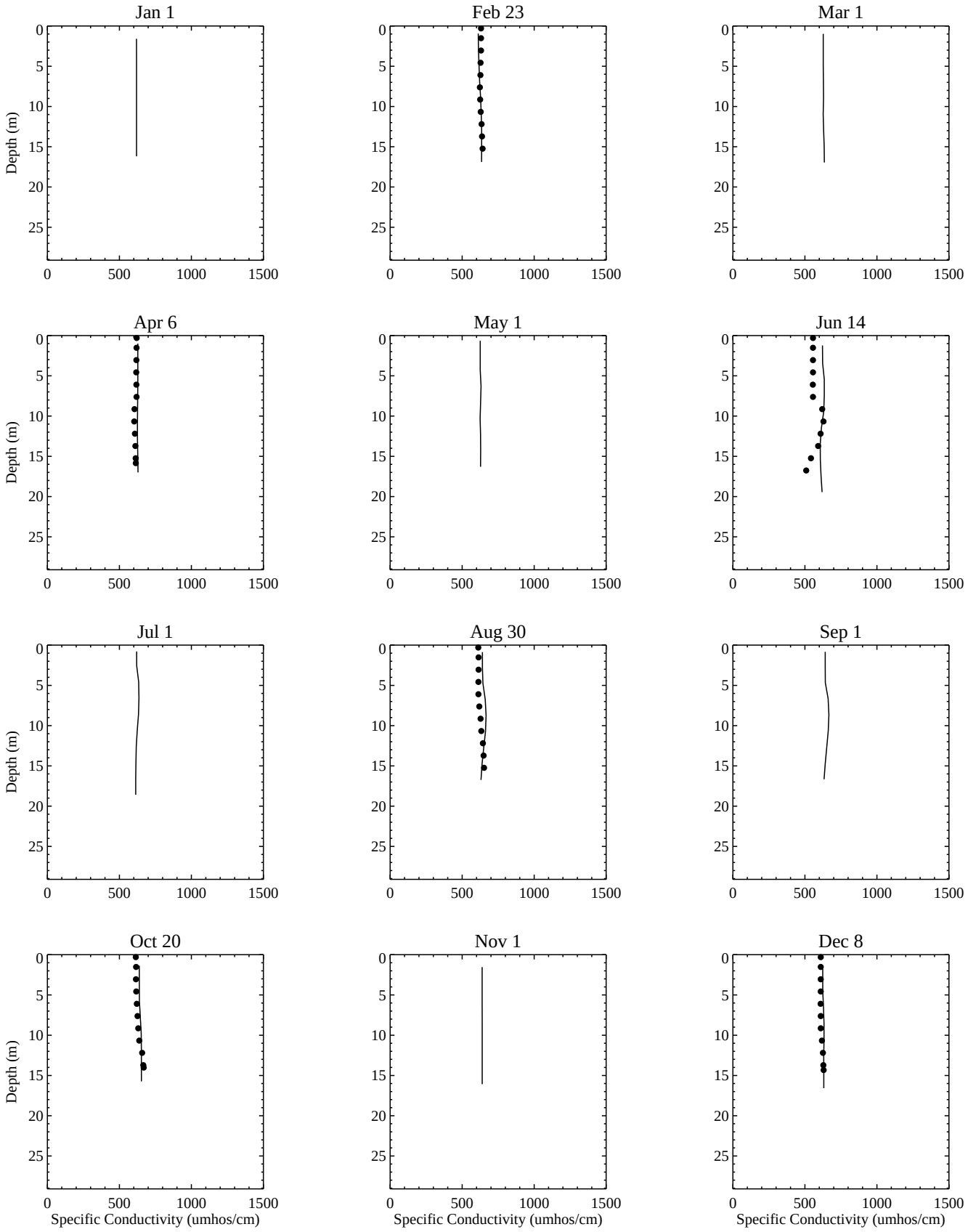

Figure J-9. Vertical profiles of model versus data at Turkey Bend (Segment 28) - Specific Conductivity - 1994.

Profiles shown for dates with available data else model results for first day of month shown.

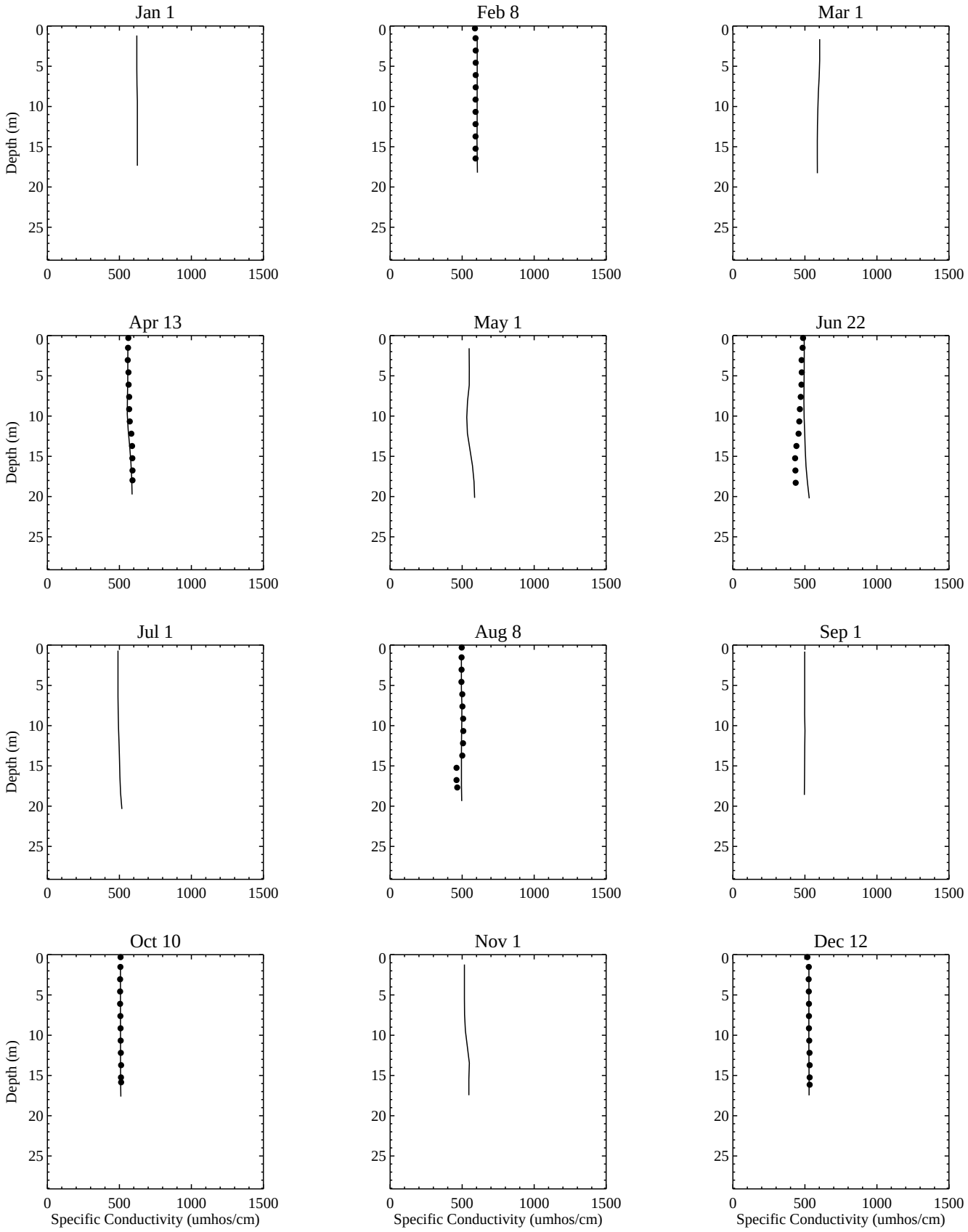

Figure J-9. Vertical profiles of model versus data at Turkey Bend (Segment 28) - Specific Conductivity - 1995.

Profiles shown for dates with available data else model results for first day of month shown.

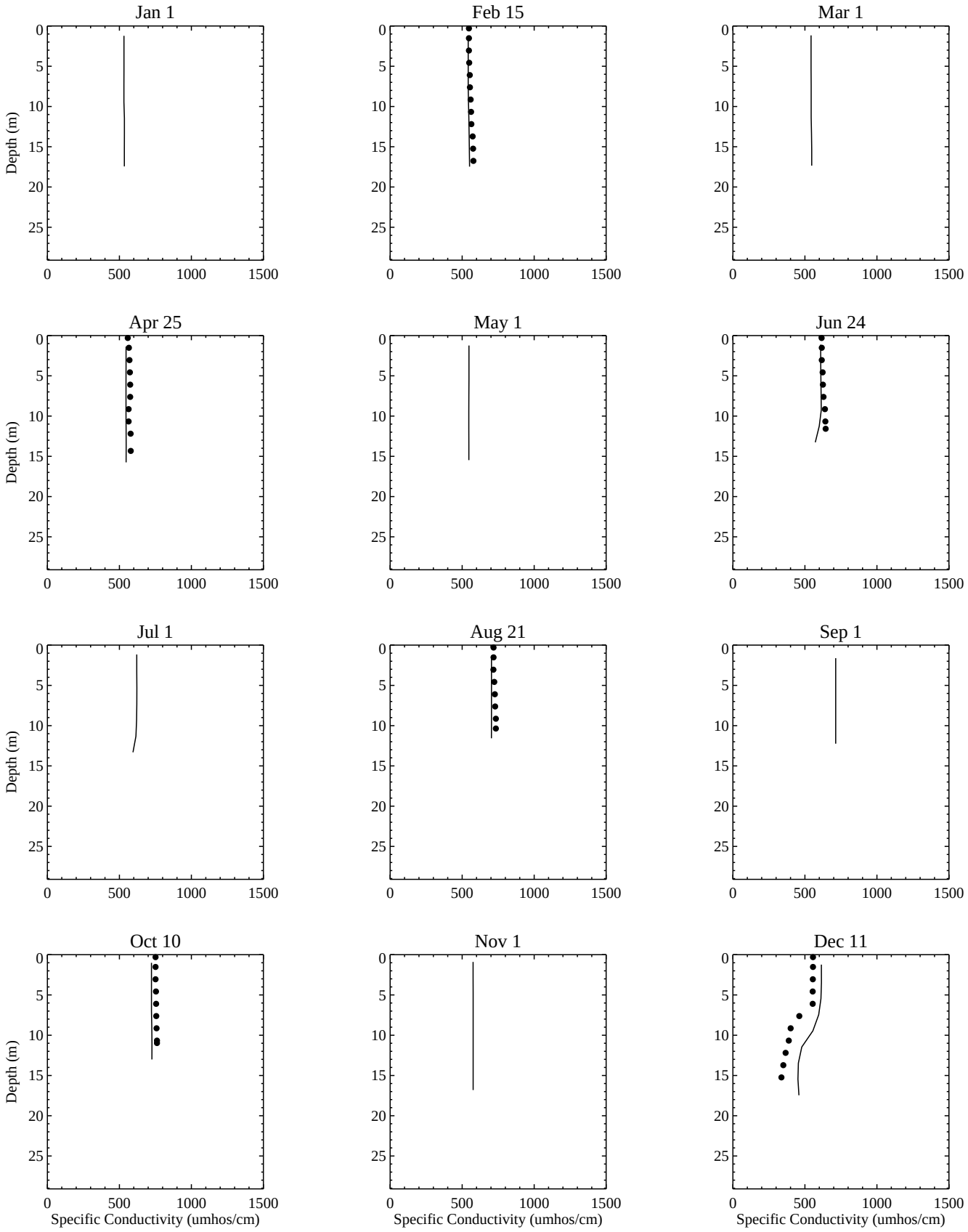

Figure J-9. Vertical profiles of model versus data at Turkey Bend (Segment 28) - Specific Conductivity - 1996.

Profiles shown for dates with available data else model results for first day of month shown.

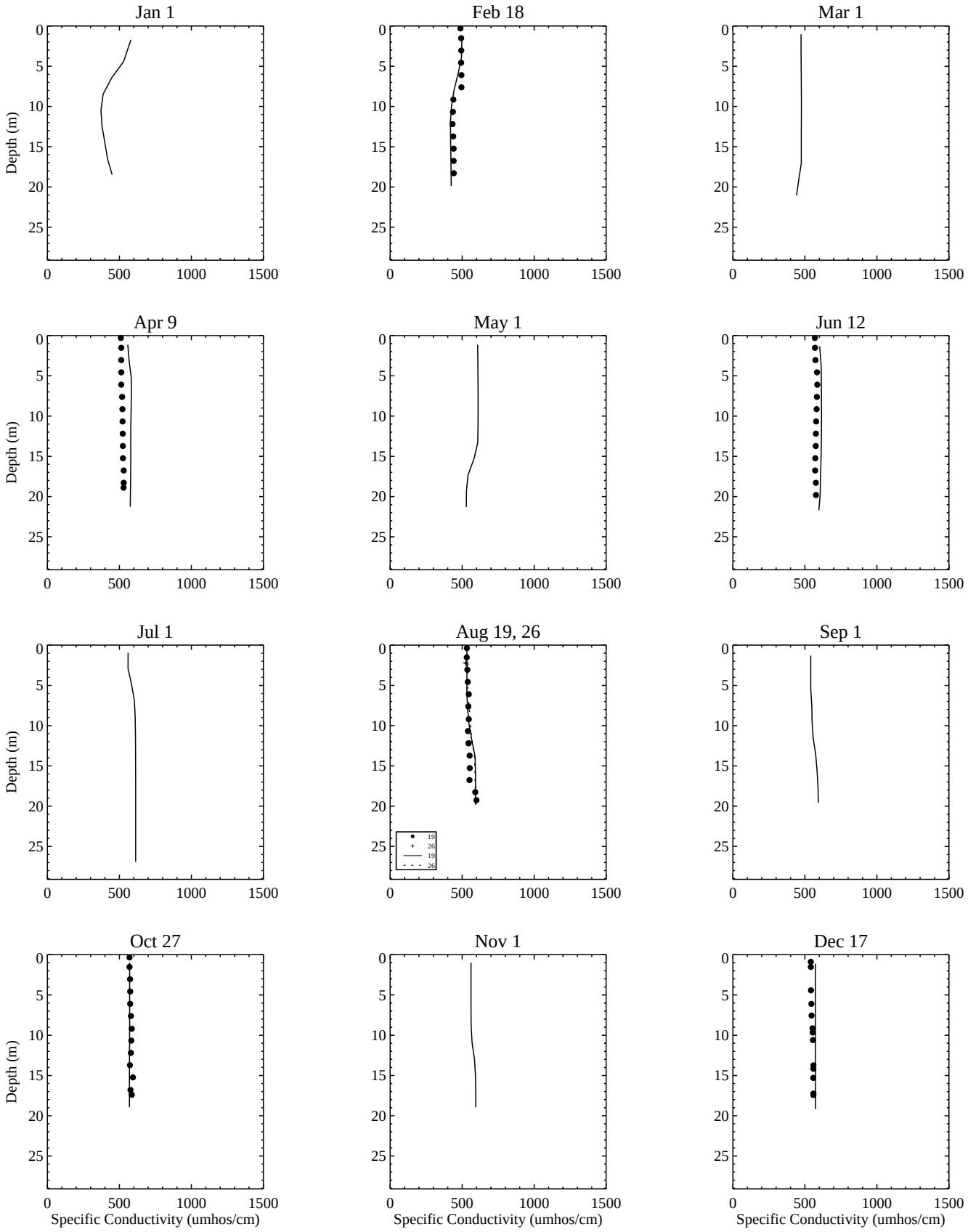

Figure J-9. Vertical profiles of model versus data at Turkey Bend (Segment 28) - Specific Conductivity - 1997.

Profiles shown for dates with available data else model results for first day of month shown.

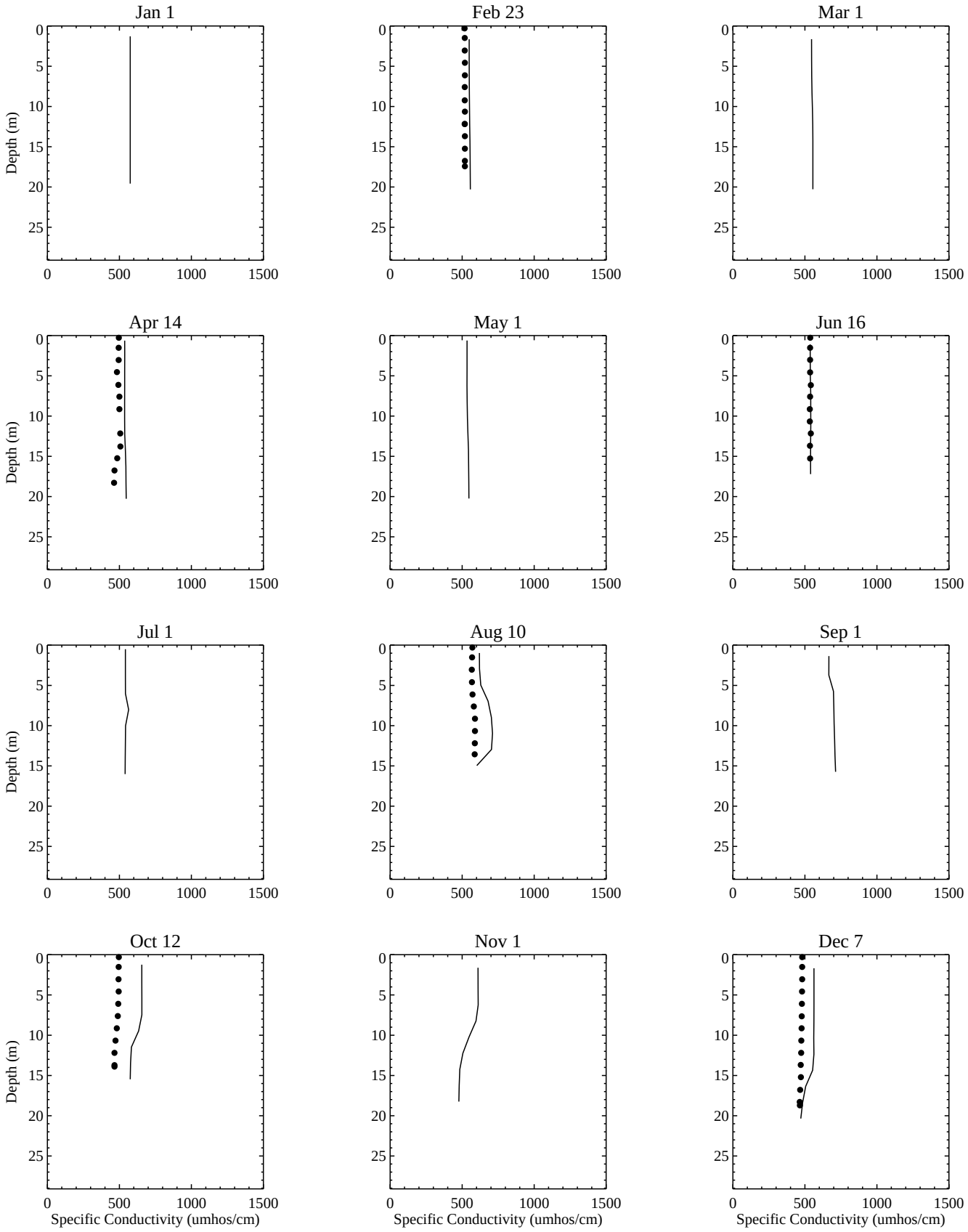

Figure J-9. Vertical profiles of model versus data at Turkey Bend (Segment 28) - Specific Conductivity - 1998.

Profiles shown for dates with available data else model results for first day of month shown.

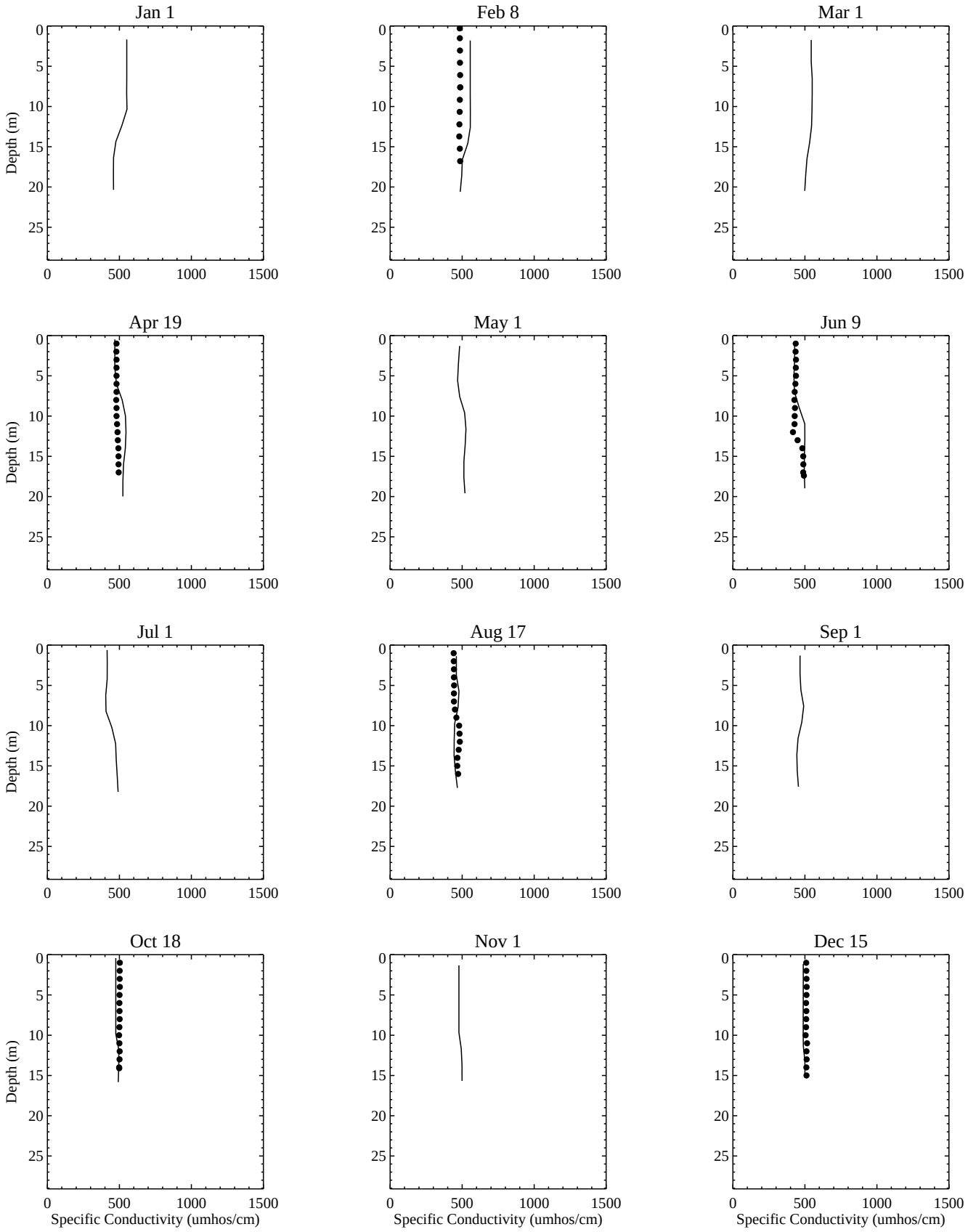

Figure J-9. Vertical profiles of model versus data at Turkey Bend (Segment 28) - Specific Conductivity - 1999.

Profiles shown for dates with available data else model results for first day of month shown.

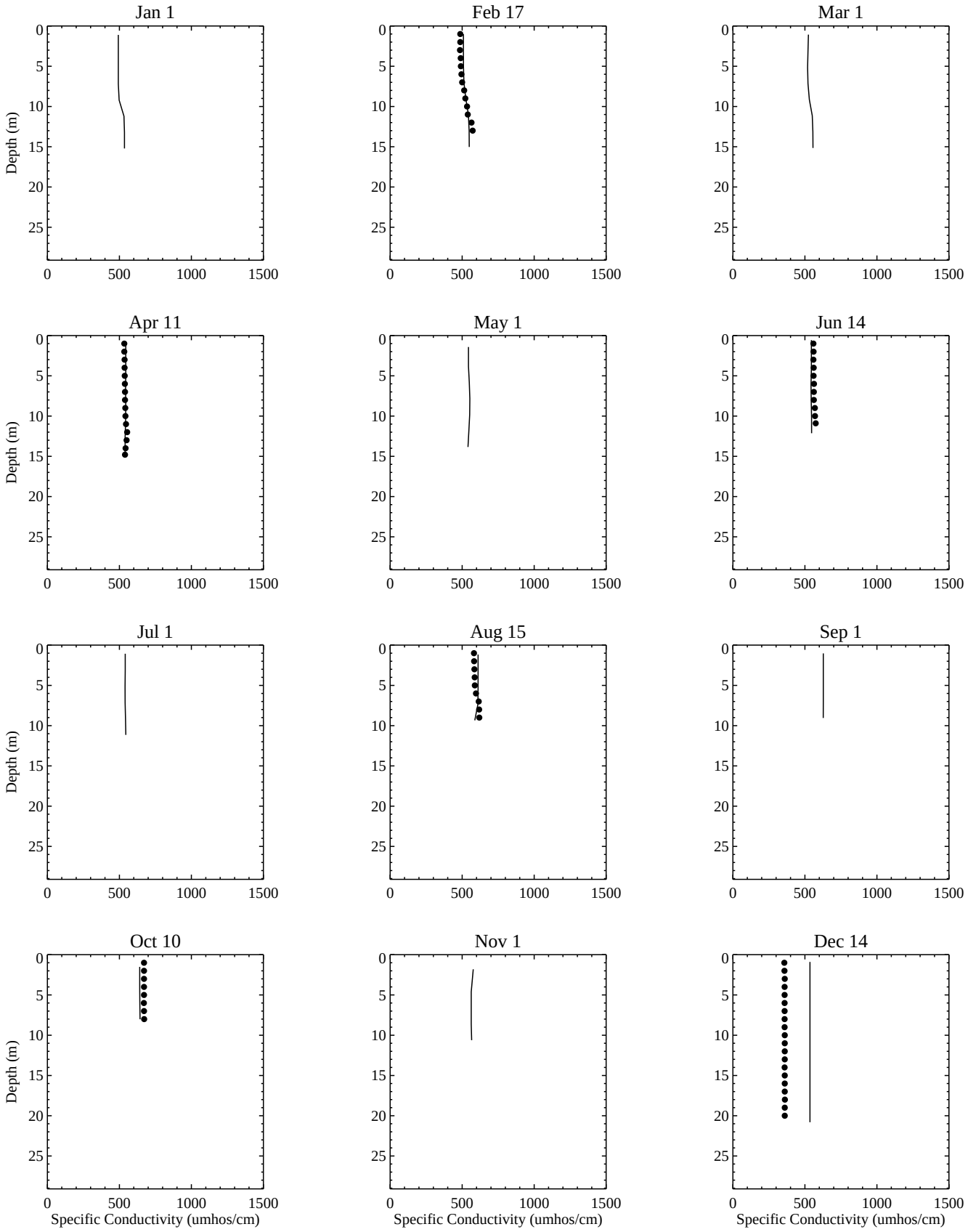

Figure J-9. Vertical profiles of model versus data at Turkey Bend (Segment 28) - Specific Conductivity - 2000.

Profiles shown for dates with available data else model results for first day of month shown.

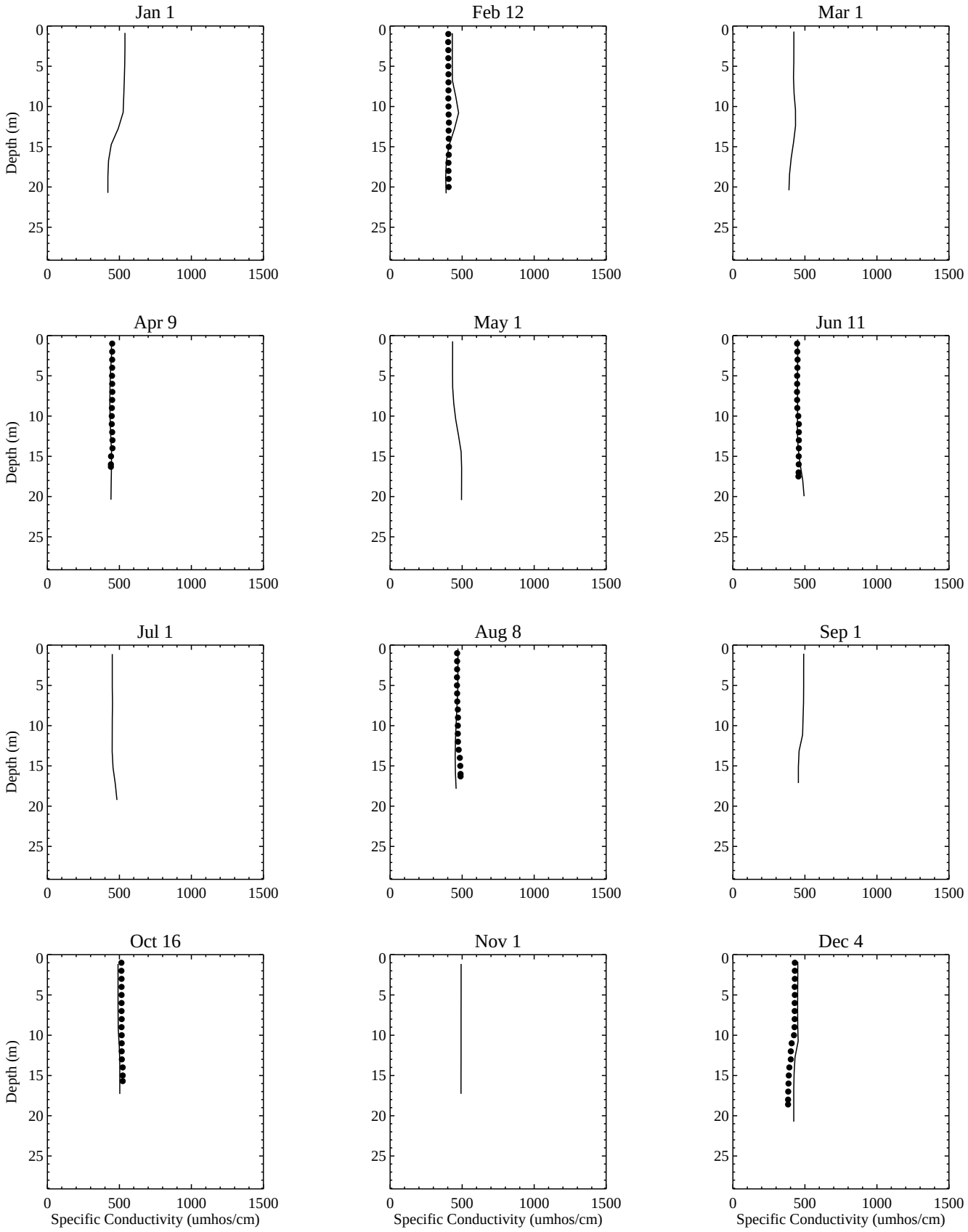

Figure J-9. Vertical profiles of model versus data at Turkey Bend (Segment 28) - Specific Conductivity - 2001.

Profiles shown for dates with available data else model results for first day of month shown.

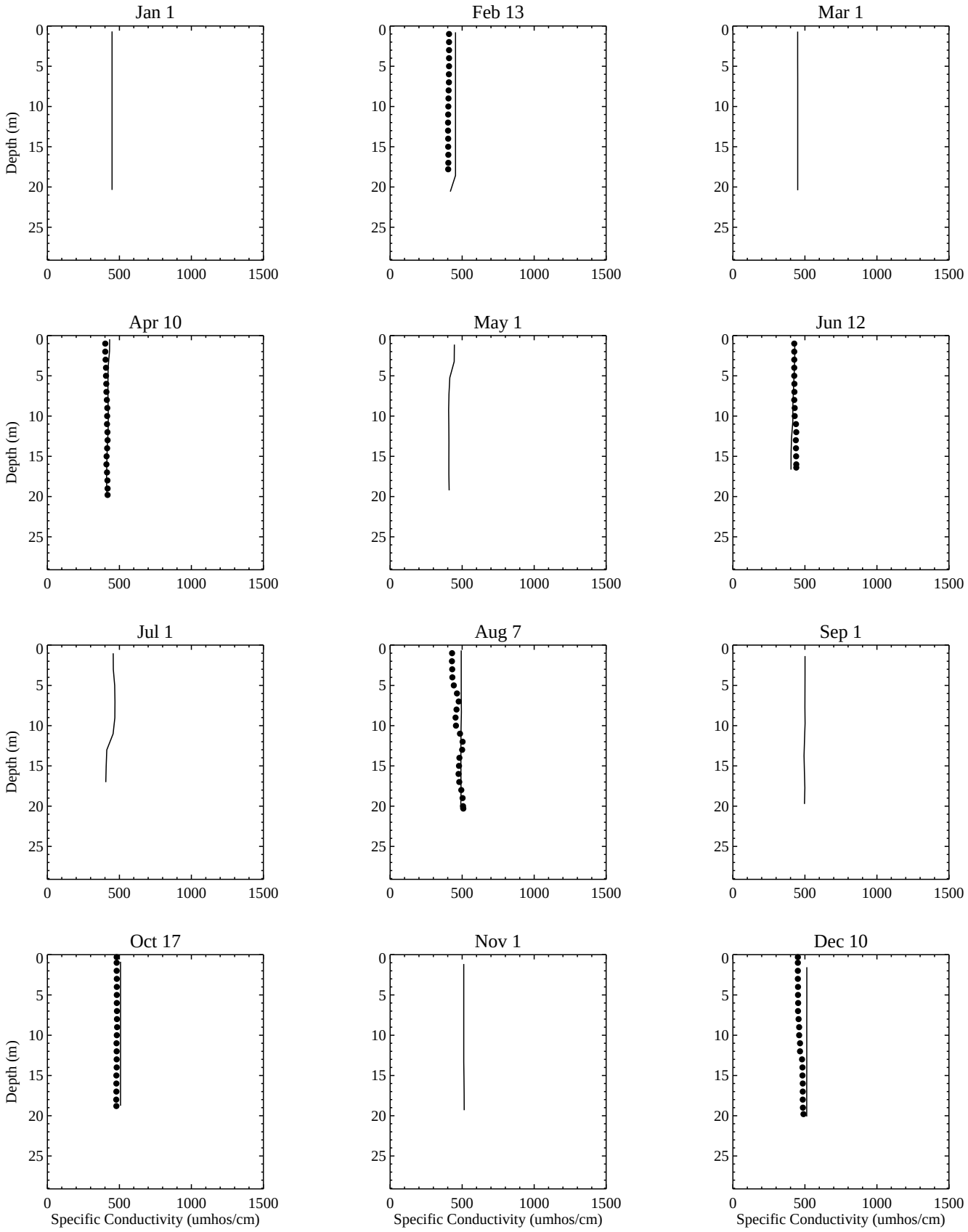

Figure J-9. Vertical profiles of model versus data at Turkey Bend (Segment 28) - Specific Conductivity - 2002.

Profiles shown for dates with available data else model results for first day of month shown.

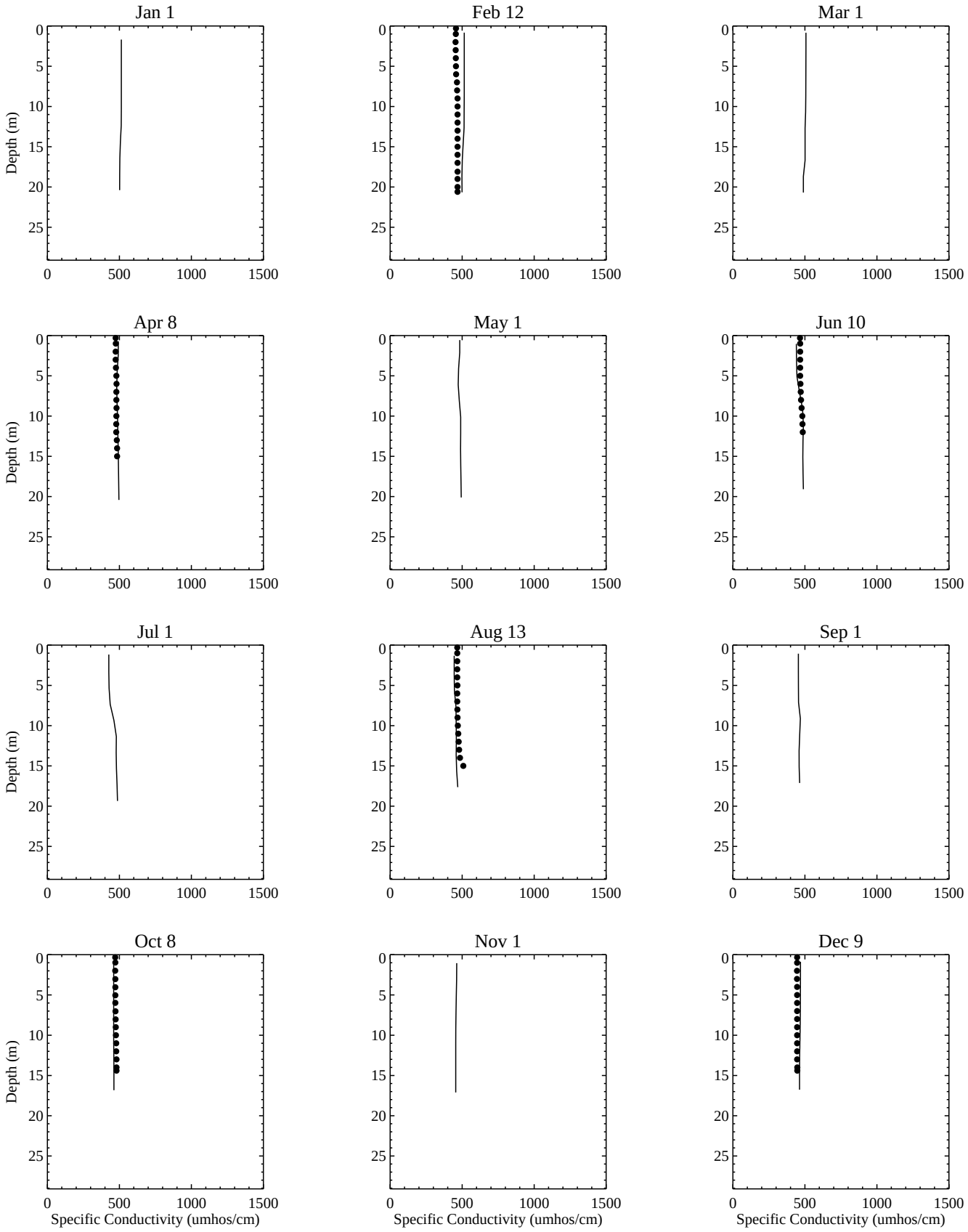

Figure J-9. Vertical profiles of model versus data at Turkey Bend (Segment 28) - Specific Conductivity - 2003.

Profiles shown for dates with available data else model results for first day of month shown.

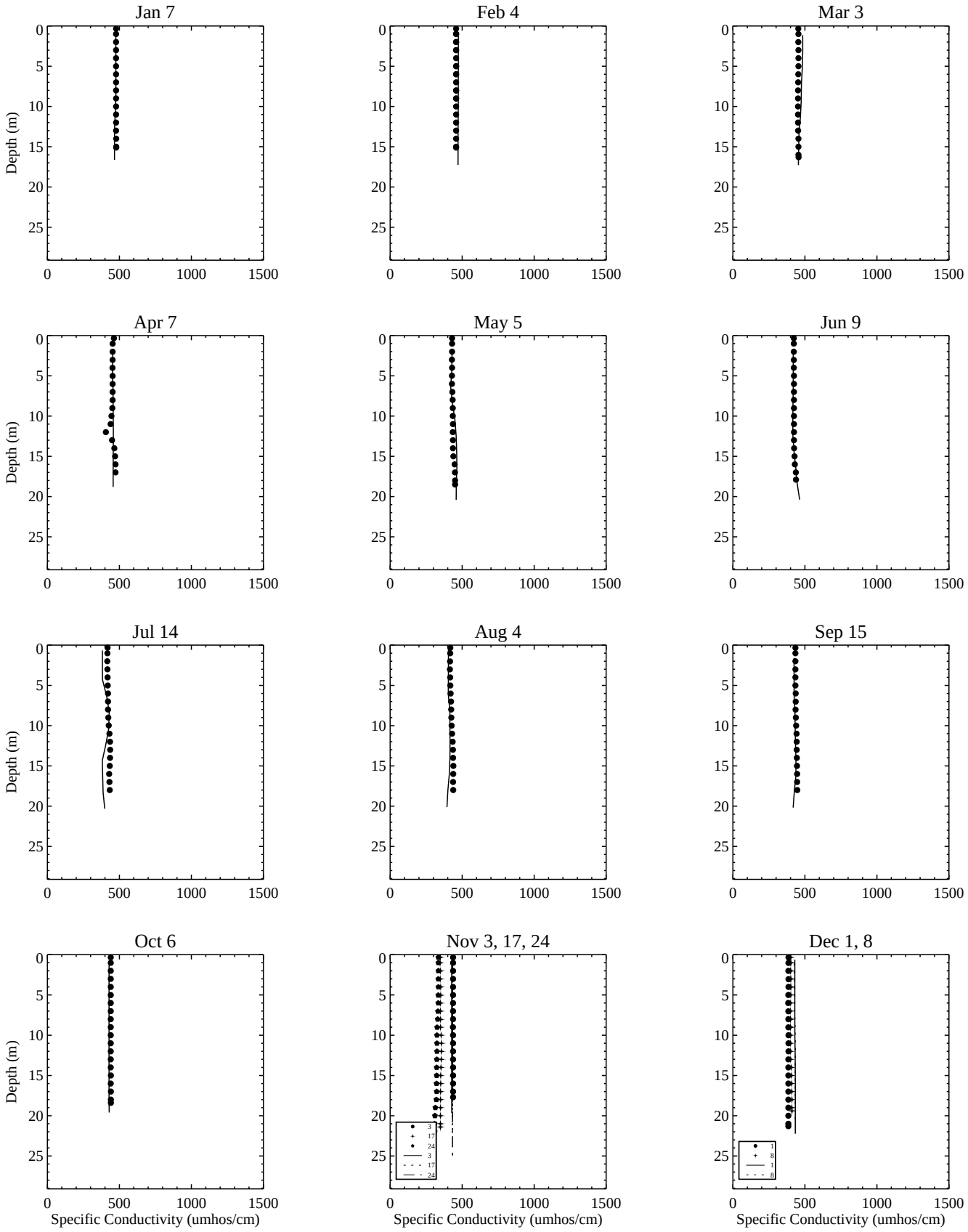

Figure J-9. Vertical profiles of model versus data at Turkey Bend (Segment 28) - Specific Conductivity - 2004.

Profiles shown for dates with available data else model results for first day of month shown.

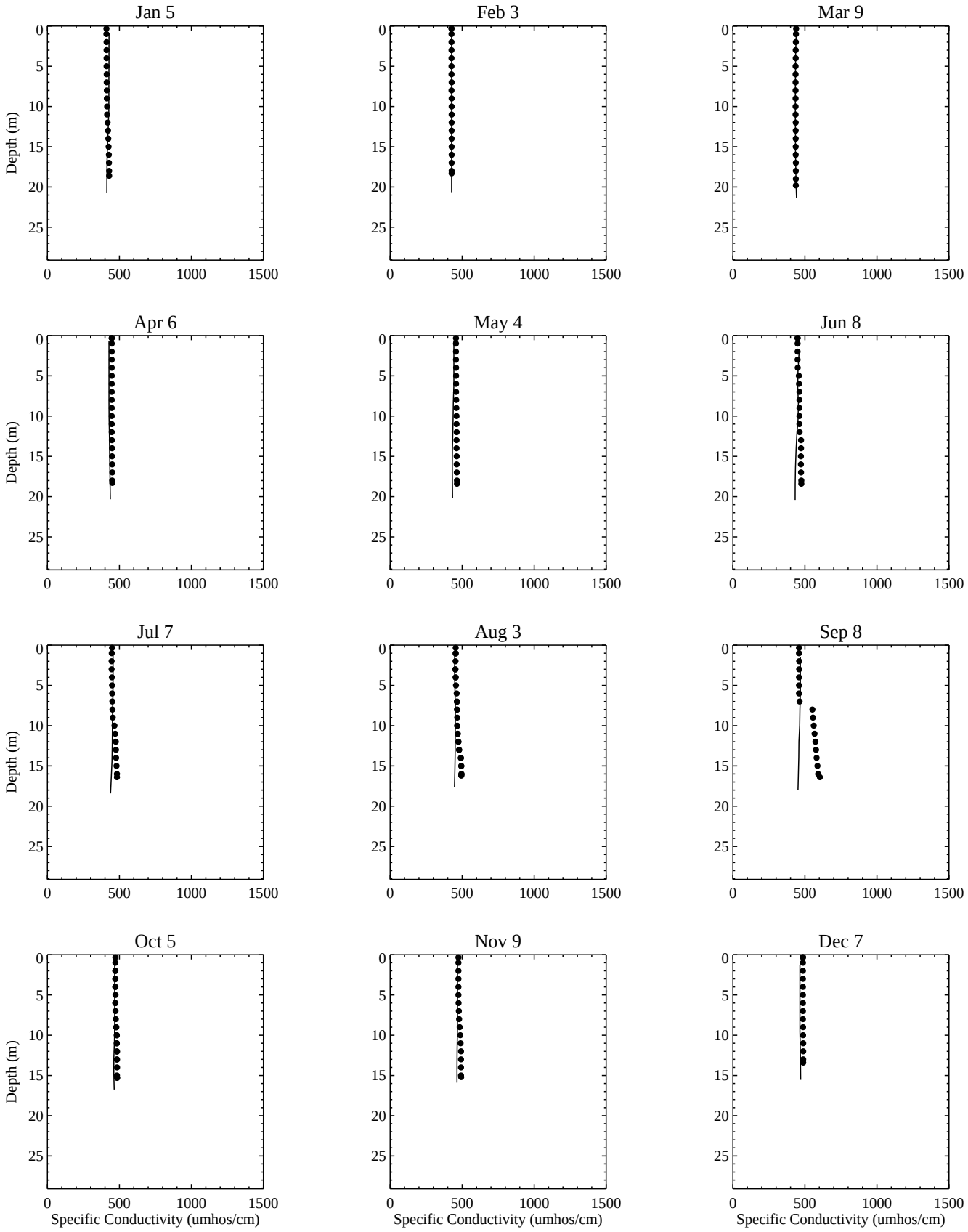

Figure J-9. Vertical profiles of model versus data at Turkey Bend (Segment 28) - Specific Conductivity - 2005.

Profiles shown for dates with available data else model results for first day of month shown.

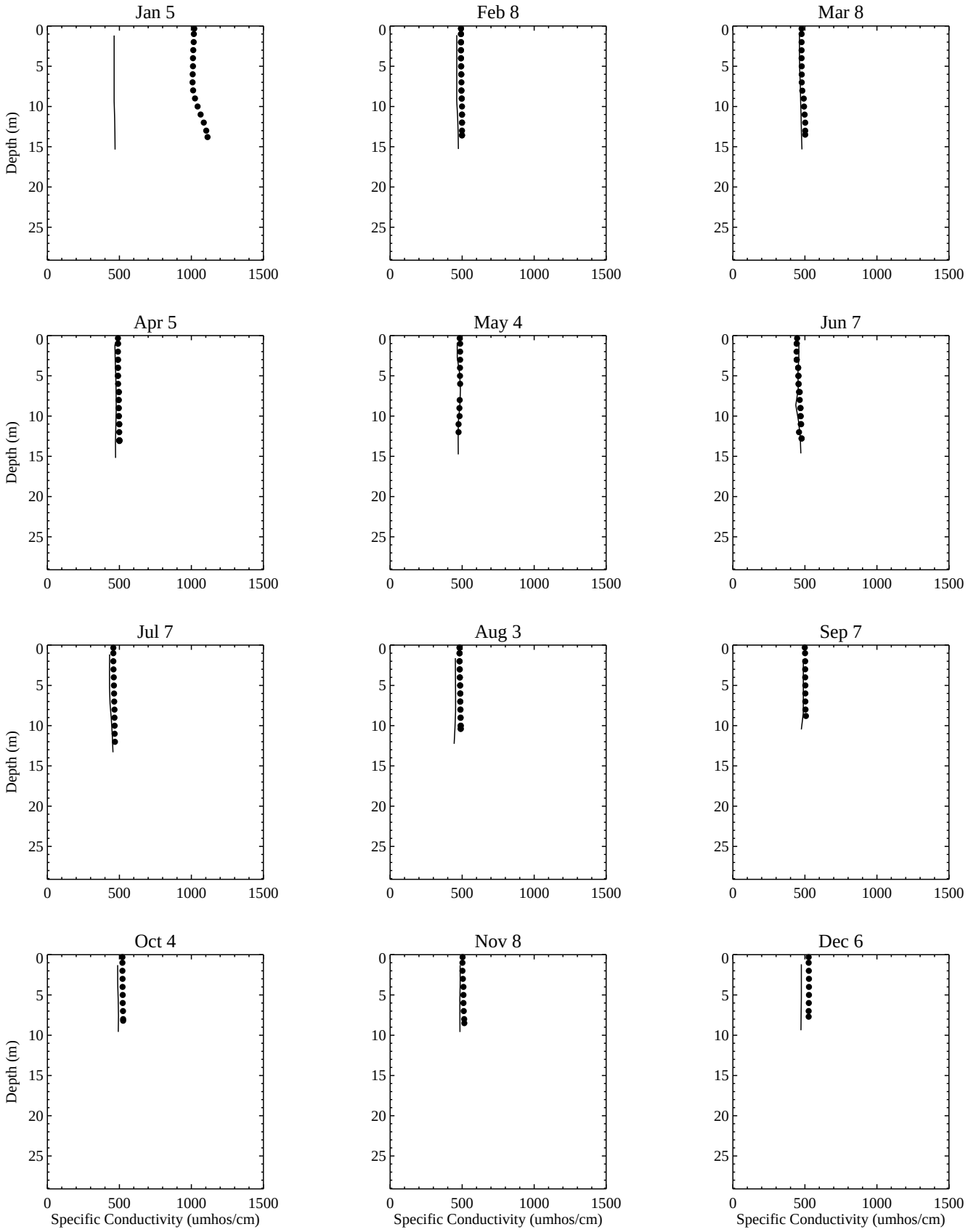

Figure J-9. Vertical profiles of model versus data at Turkey Bend (Segment 28) - Specific Conductivity - 2006.

Profiles shown for dates with available data else model results for first day of month shown.

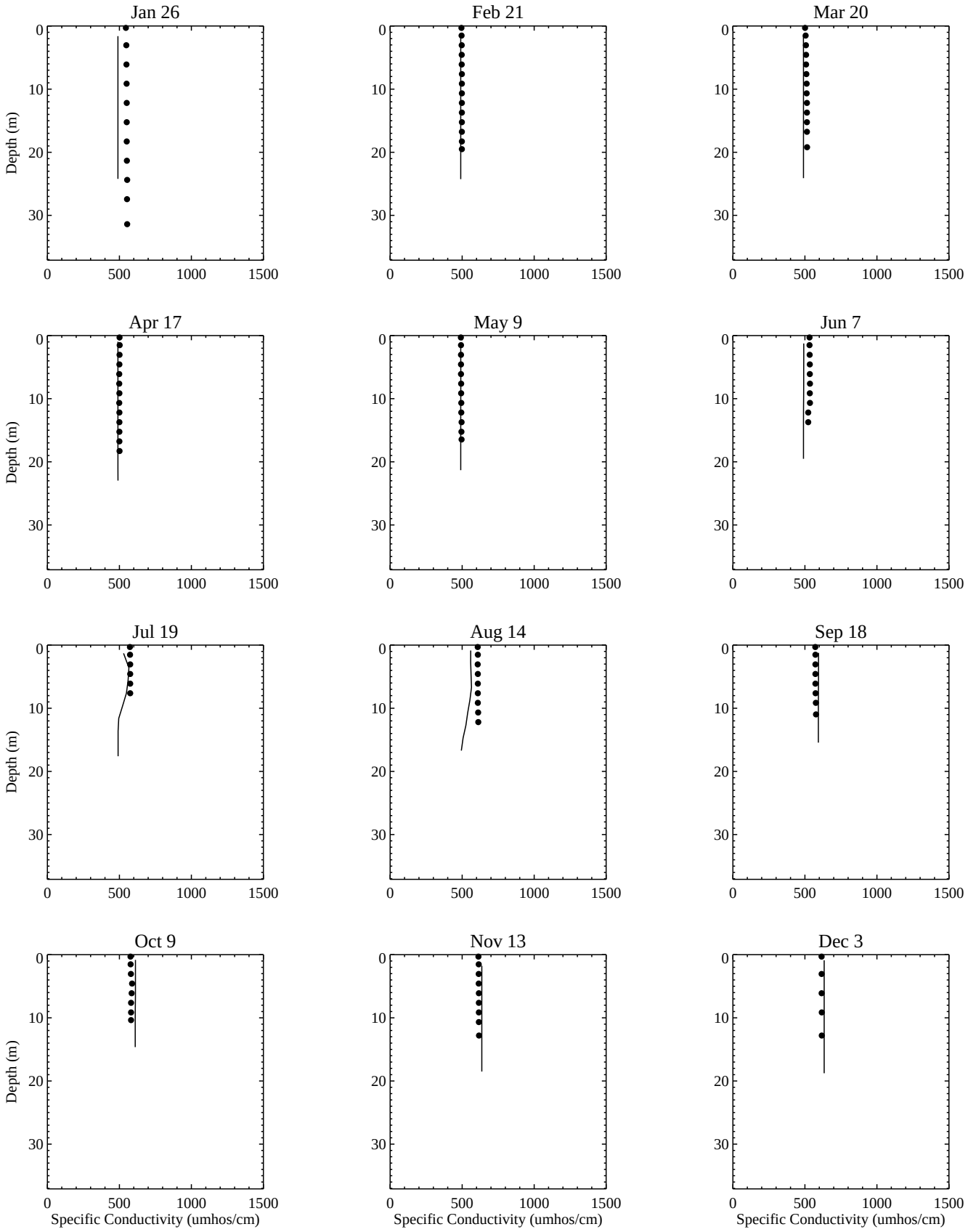

Figure J-10. Vertical profiles of model versus data at Sandy Creek (Segment 161) - Specific Conductivity - 1984.

Profiles shown for dates with available data else model results for first day of month shown.

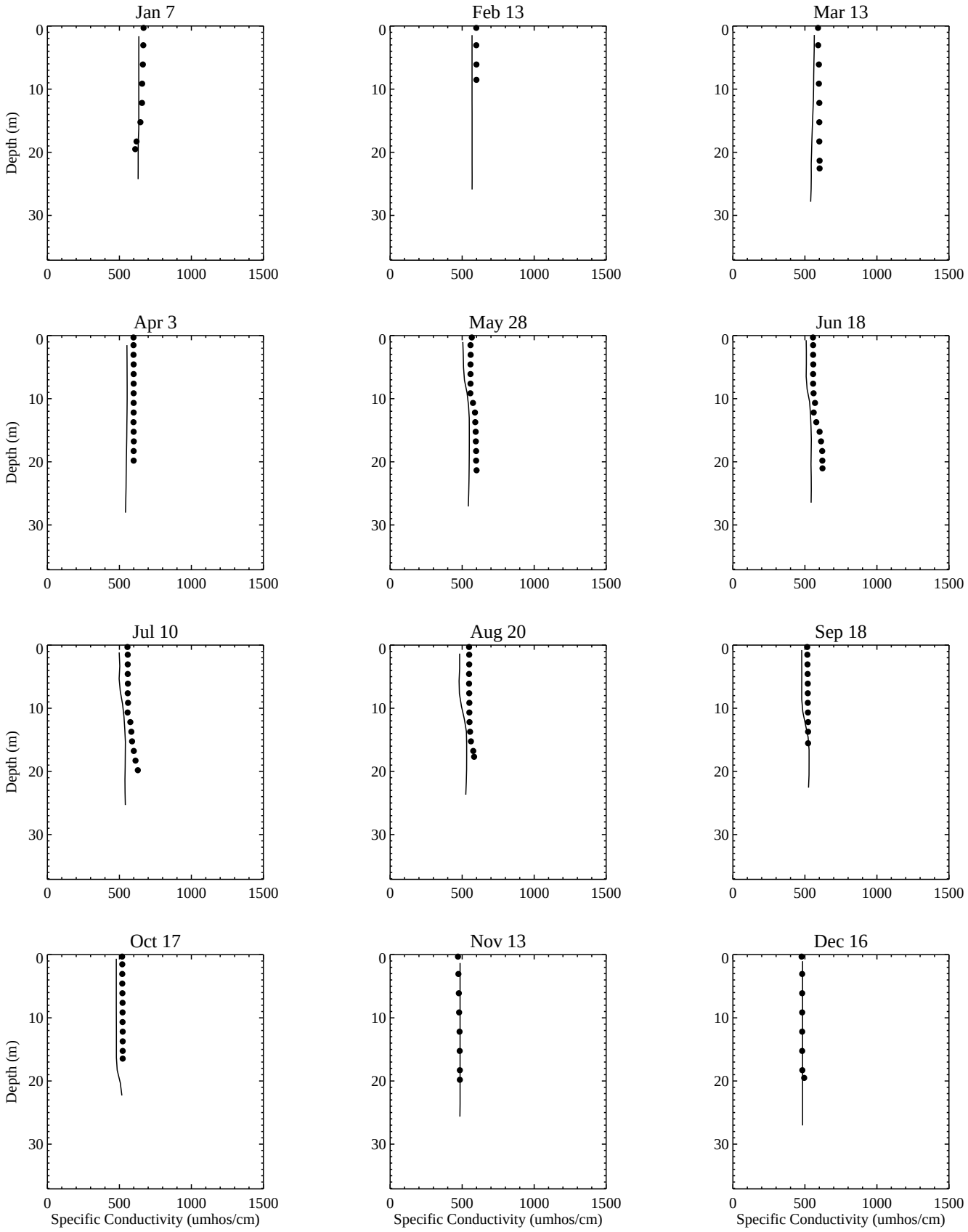

Figure J-10. Vertical profiles of model versus data at Sandy Creek (Segment 161) - Specific Conductivity - 1985.

Profiles shown for dates with available data else model results for first day of month shown.

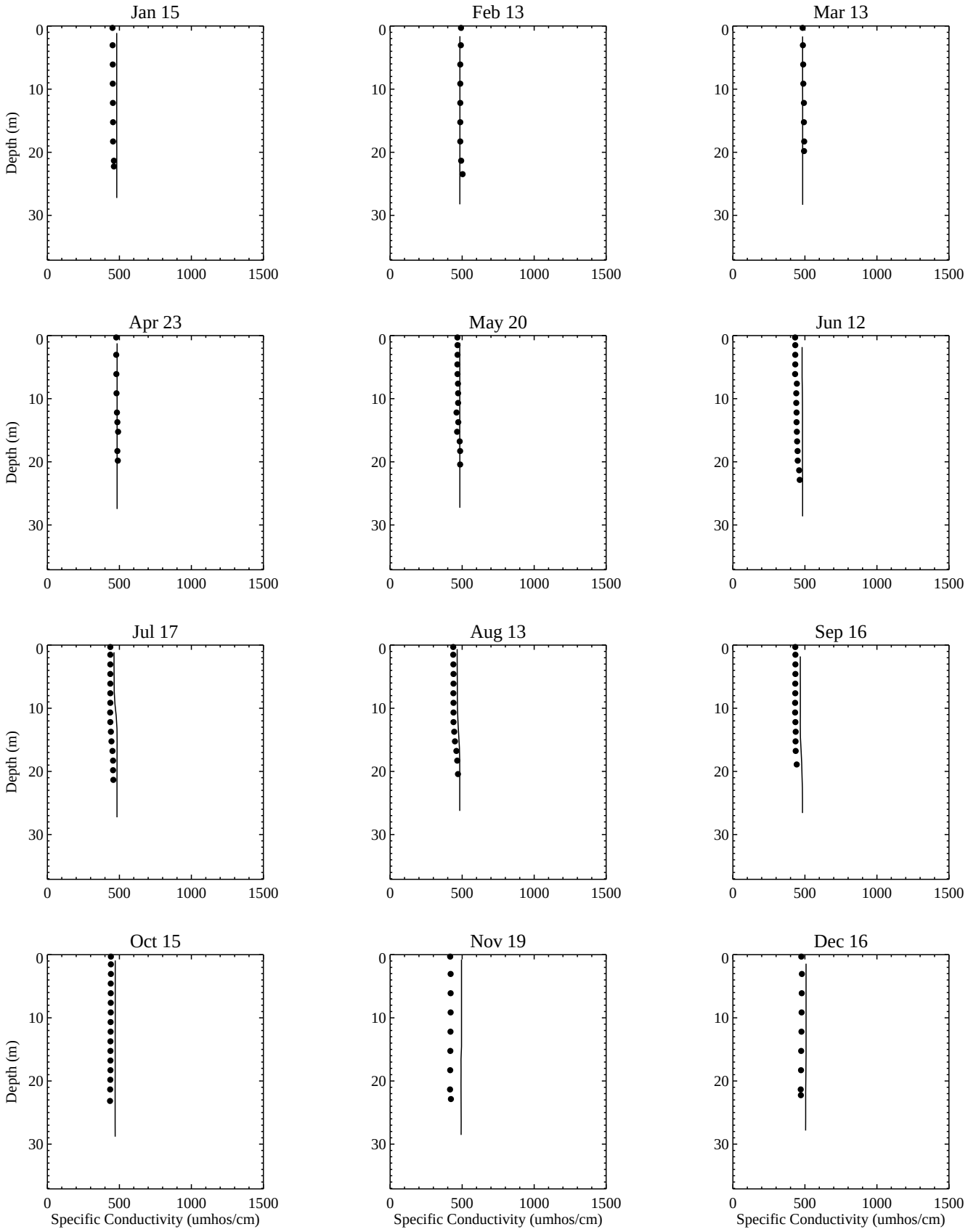

Figure J-10. Vertical profiles of model versus data at Sandy Creek (Segment 161) - Specific Conductivity - 1986.

Profiles shown for dates with available data else model results for first day of month shown.

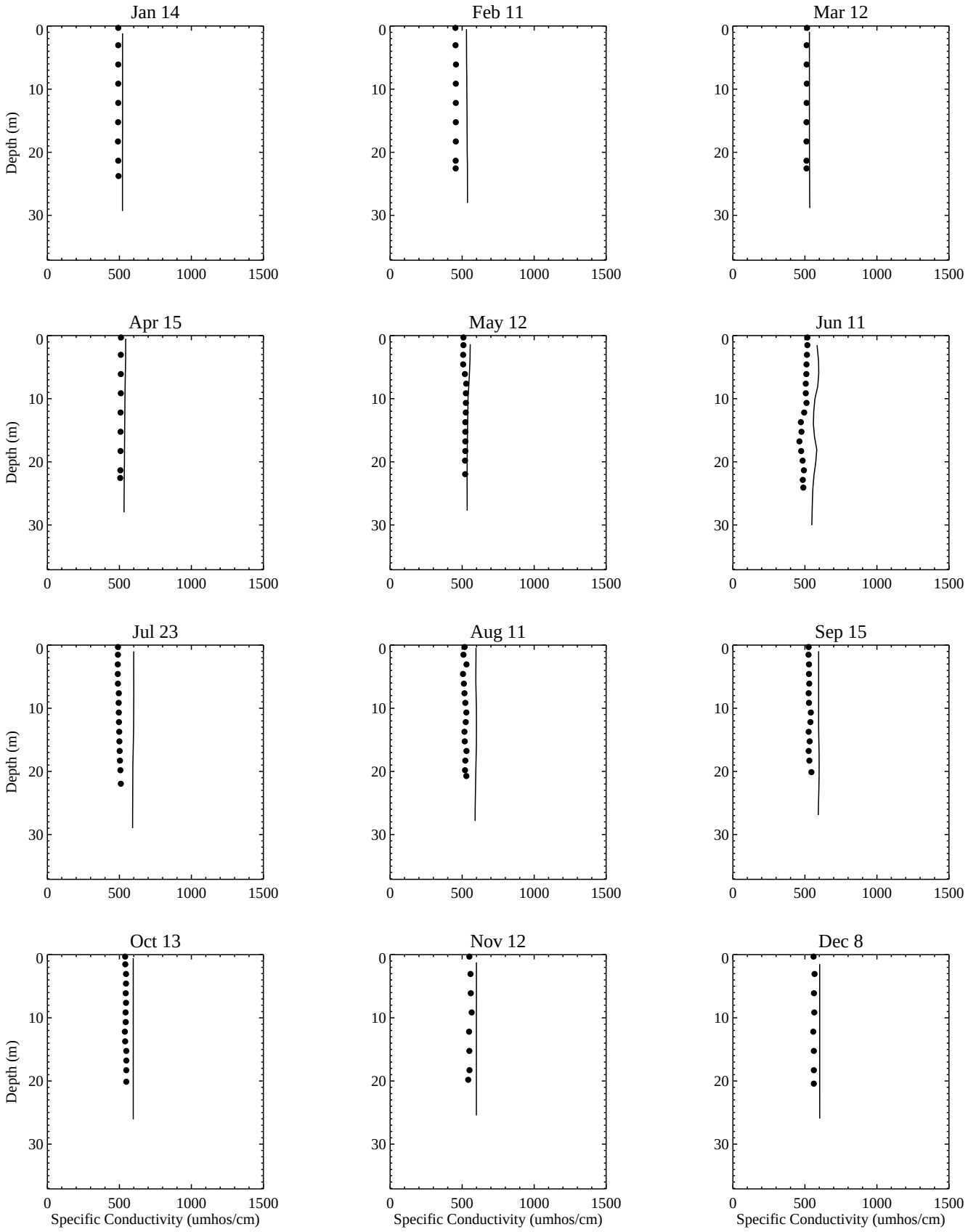

Figure J-10. Vertical profiles of model versus data at Sandy Creek (Segment 161) - Specific Conductivity - 1987.

Profiles shown for dates with available data else model results for first day of month shown.

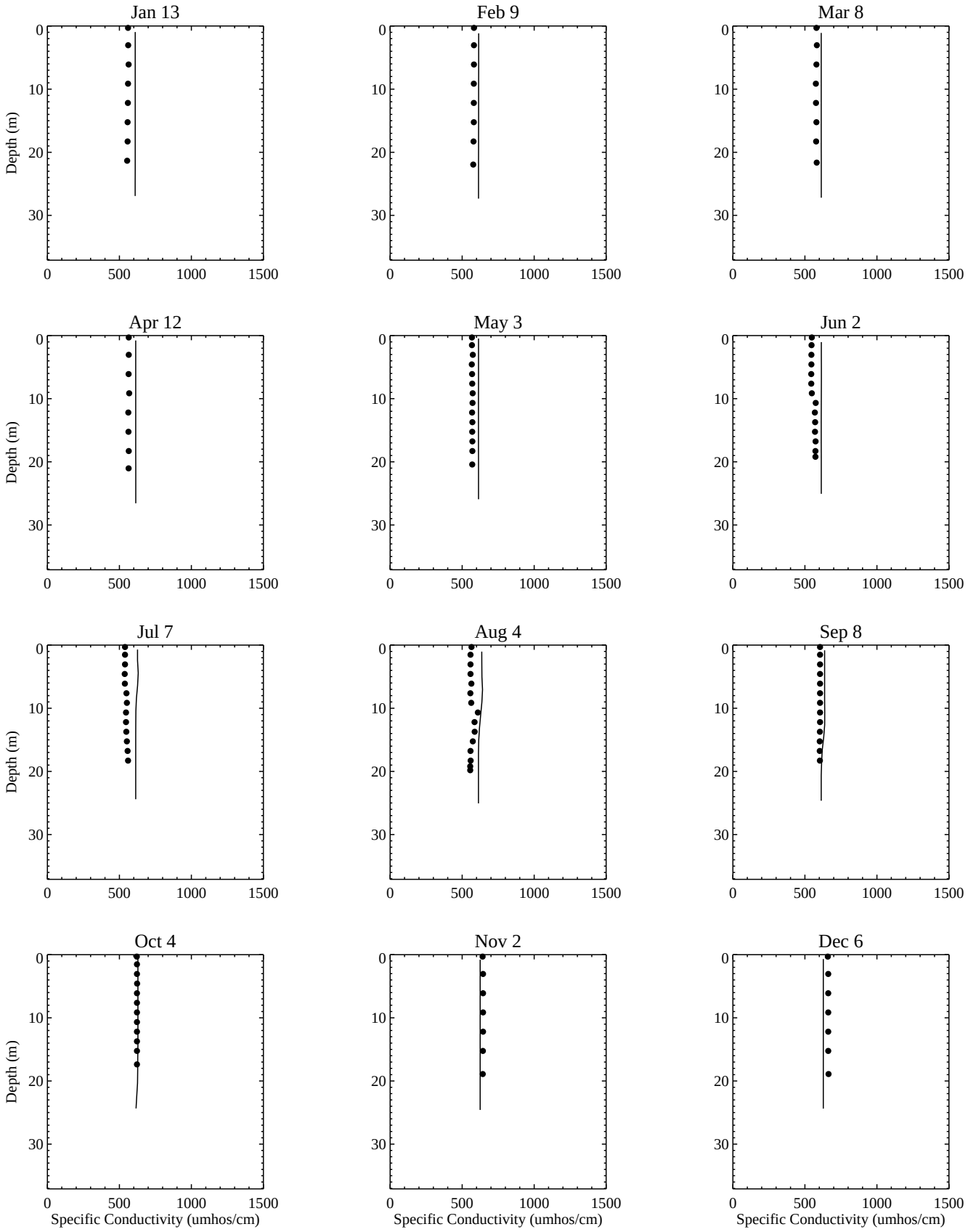

Figure J-10. Vertical profiles of model versus data at Sandy Creek (Segment 161) - Specific Conductivity - 1988.

Profiles shown for dates with available data else model results for first day of month shown.

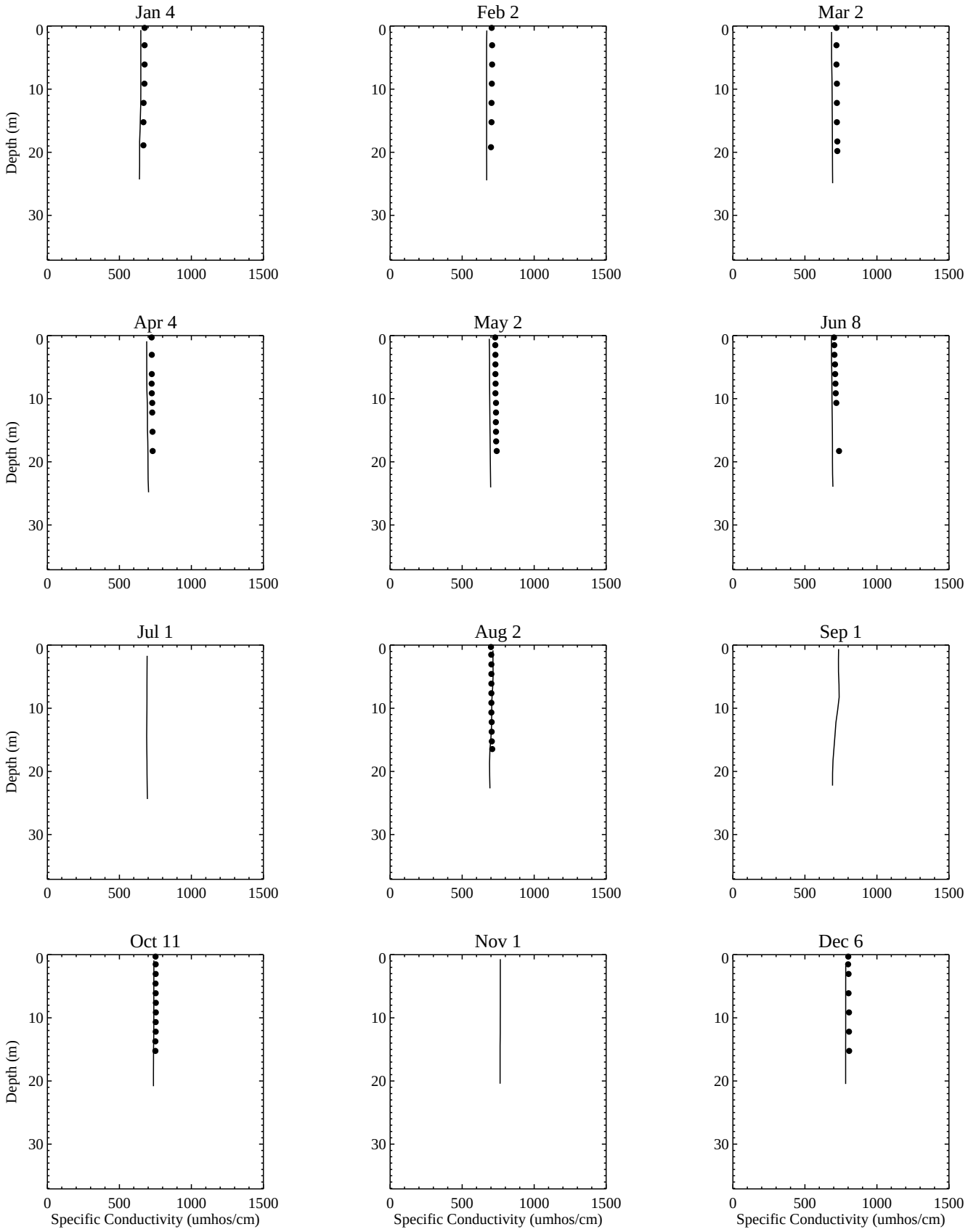

Figure J-10. Vertical profiles of model versus data at Sandy Creek (Segment 161) - Specific Conductivity - 1989.

Profiles shown for dates with available data else model results for first day of month shown.

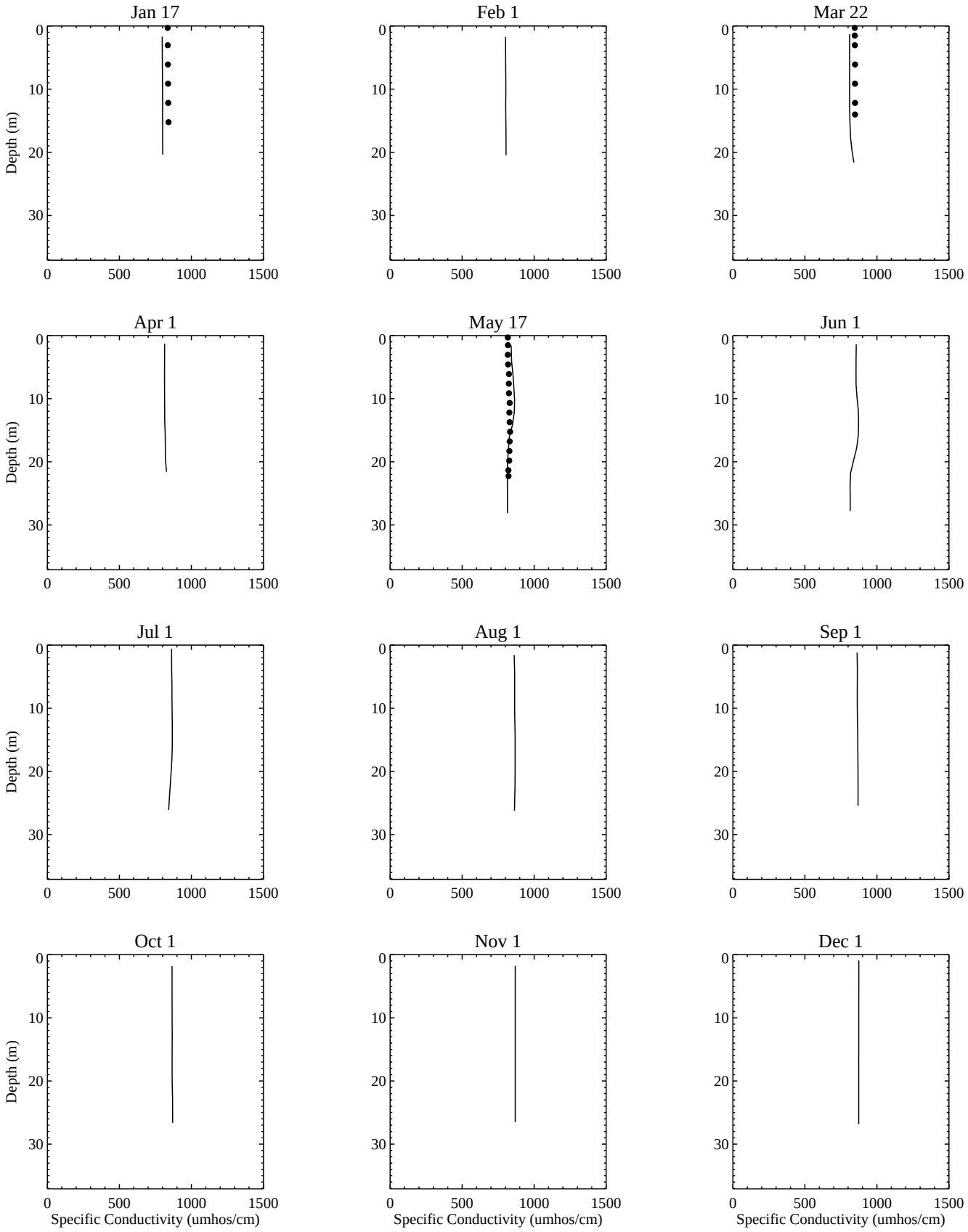

Figure J-10. Vertical profiles of model versus data at Sandy Creek (Segment 161) - Specific Conductivity - 1990.

Profiles shown for dates with available data else model results for first day of month shown.

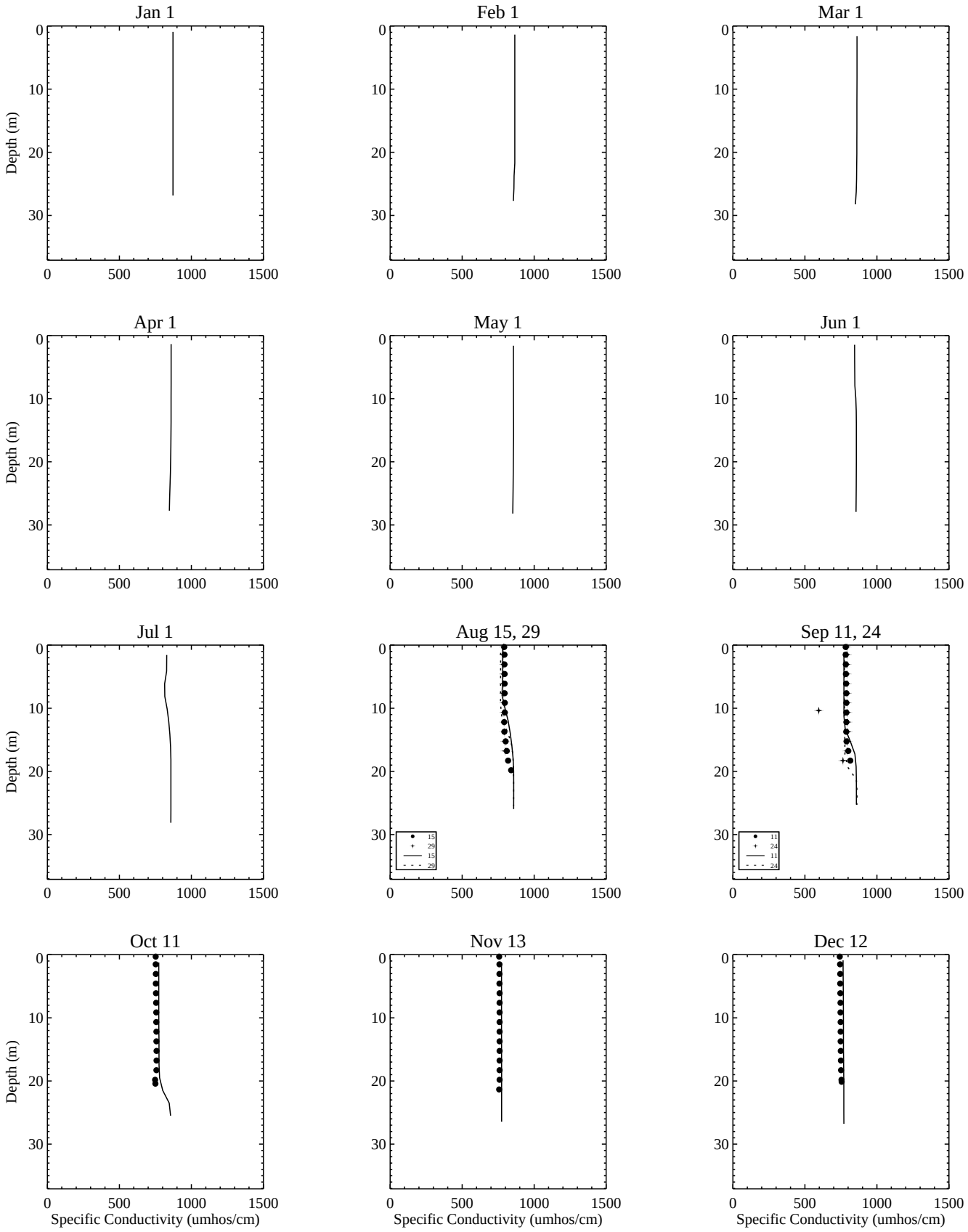

Figure J-10. Vertical profiles of model versus data at Sandy Creek (Segment 161) - Specific Conductivity - 1991.

Profiles shown for dates with available data else model results for first day of month shown.

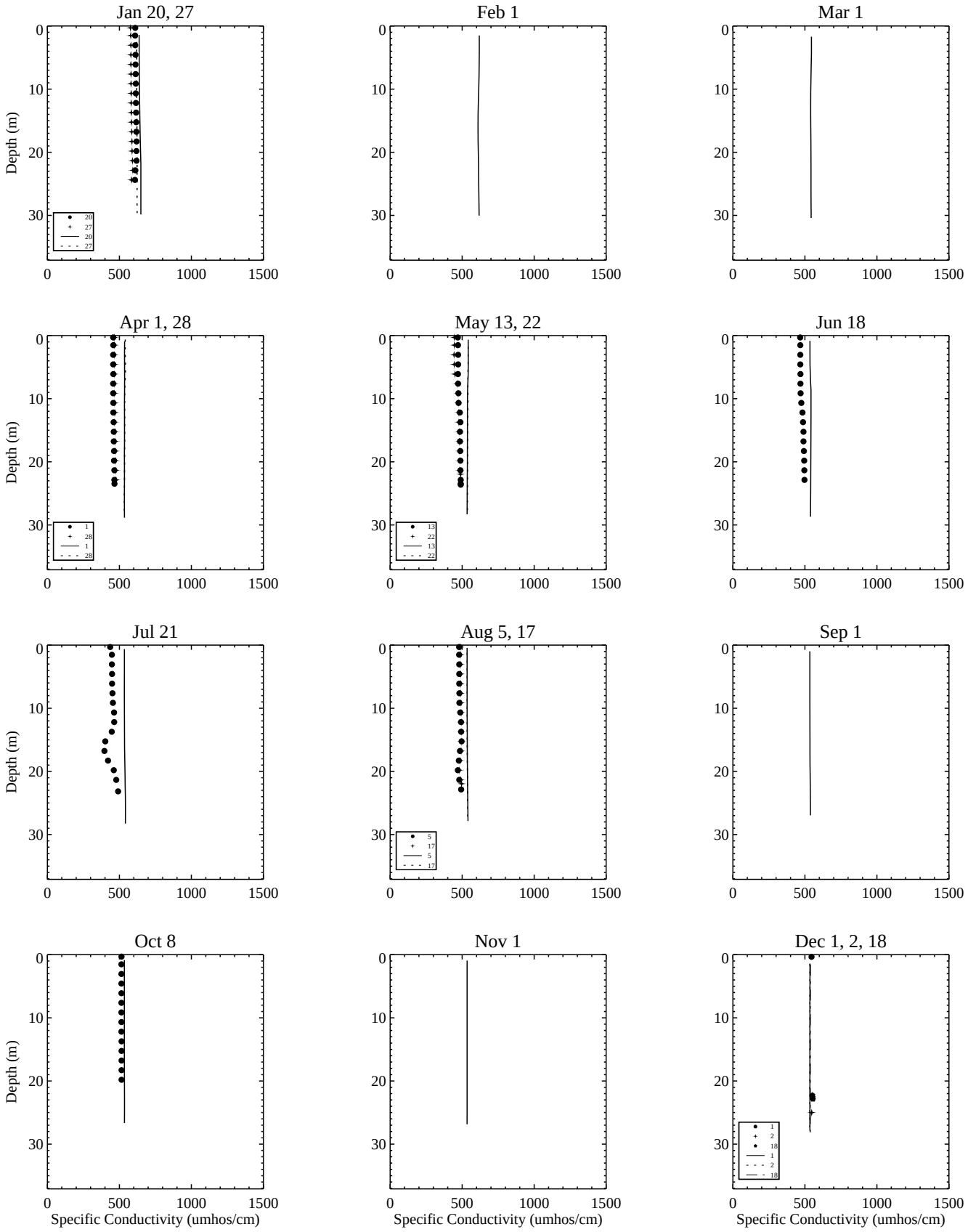

Figure J-10. Vertical profiles of model versus data at Sandy Creek (Segment 161) - Specific Conductivity - 1992.

Profiles shown for dates with available data else model results for first day of month shown.

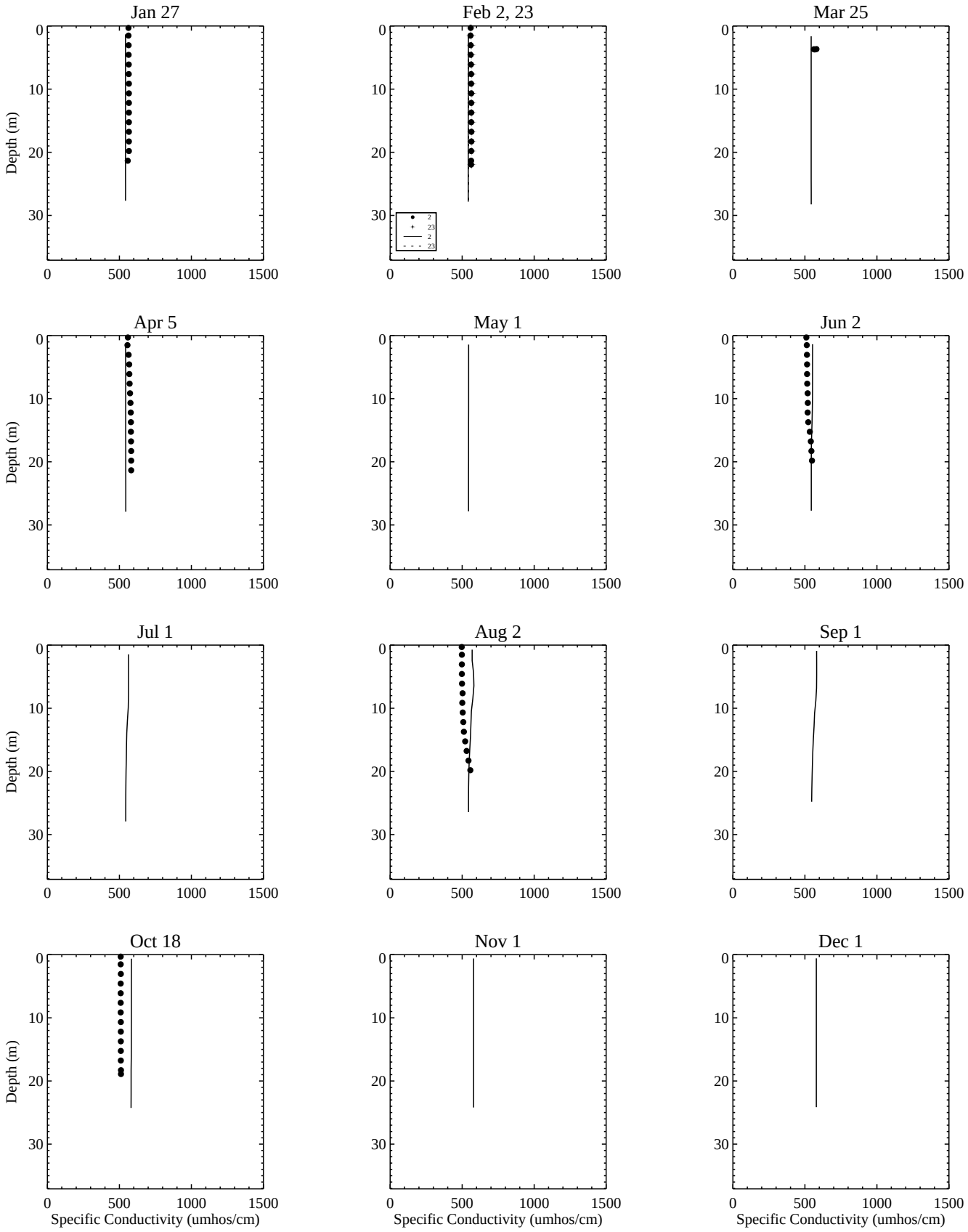

Figure J-10. Vertical profiles of model versus data at Sandy Creek (Segment 161) - Specific Conductivity - 1993.

Profiles shown for dates with available data else model results for first day of month shown.

Model Data

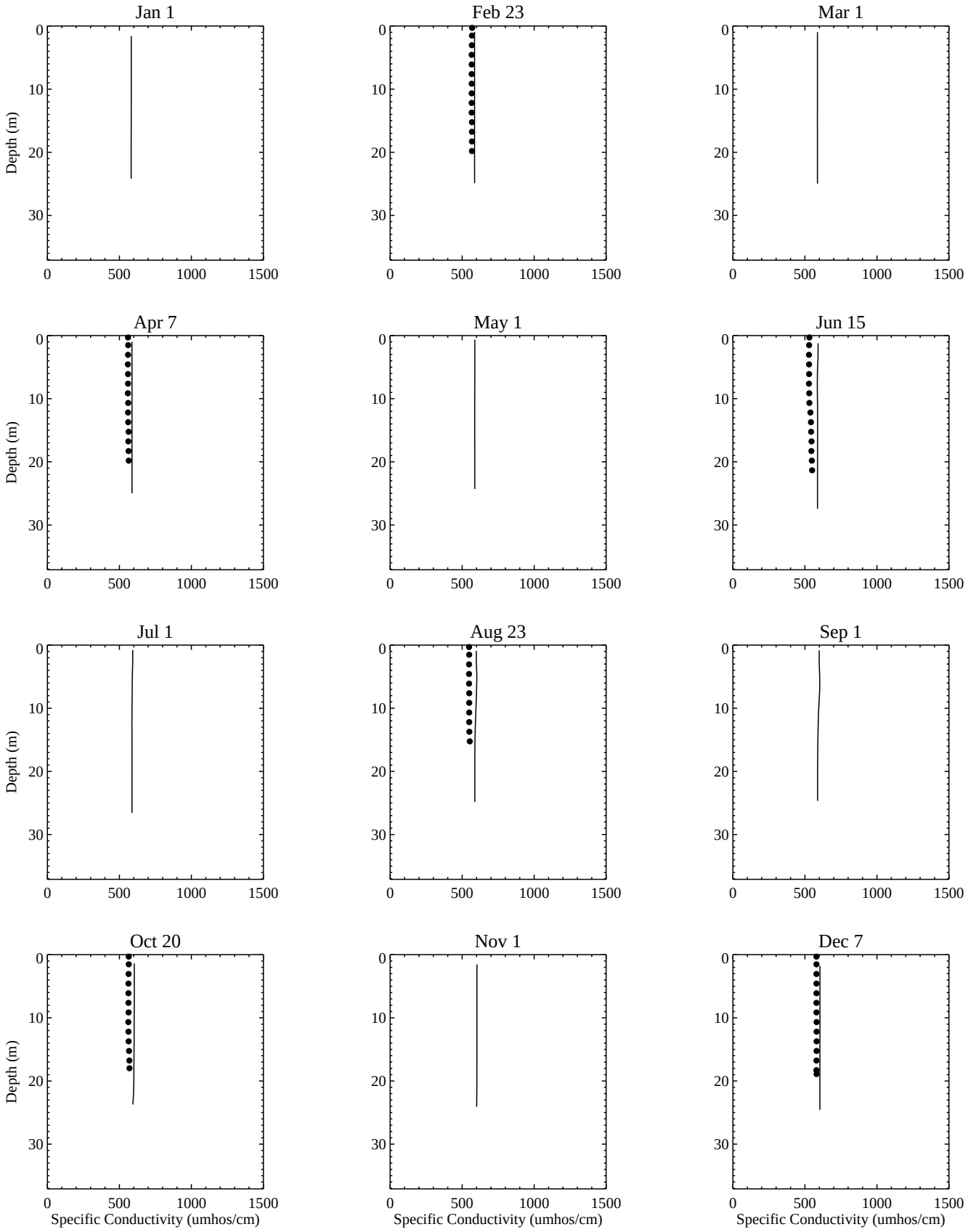

Figure J-10. Vertical profiles of model versus data at Sandy Creek (Segment 161) - Specific Conductivity - 1994.

Profiles shown for dates with available data else model results for first day of month shown.

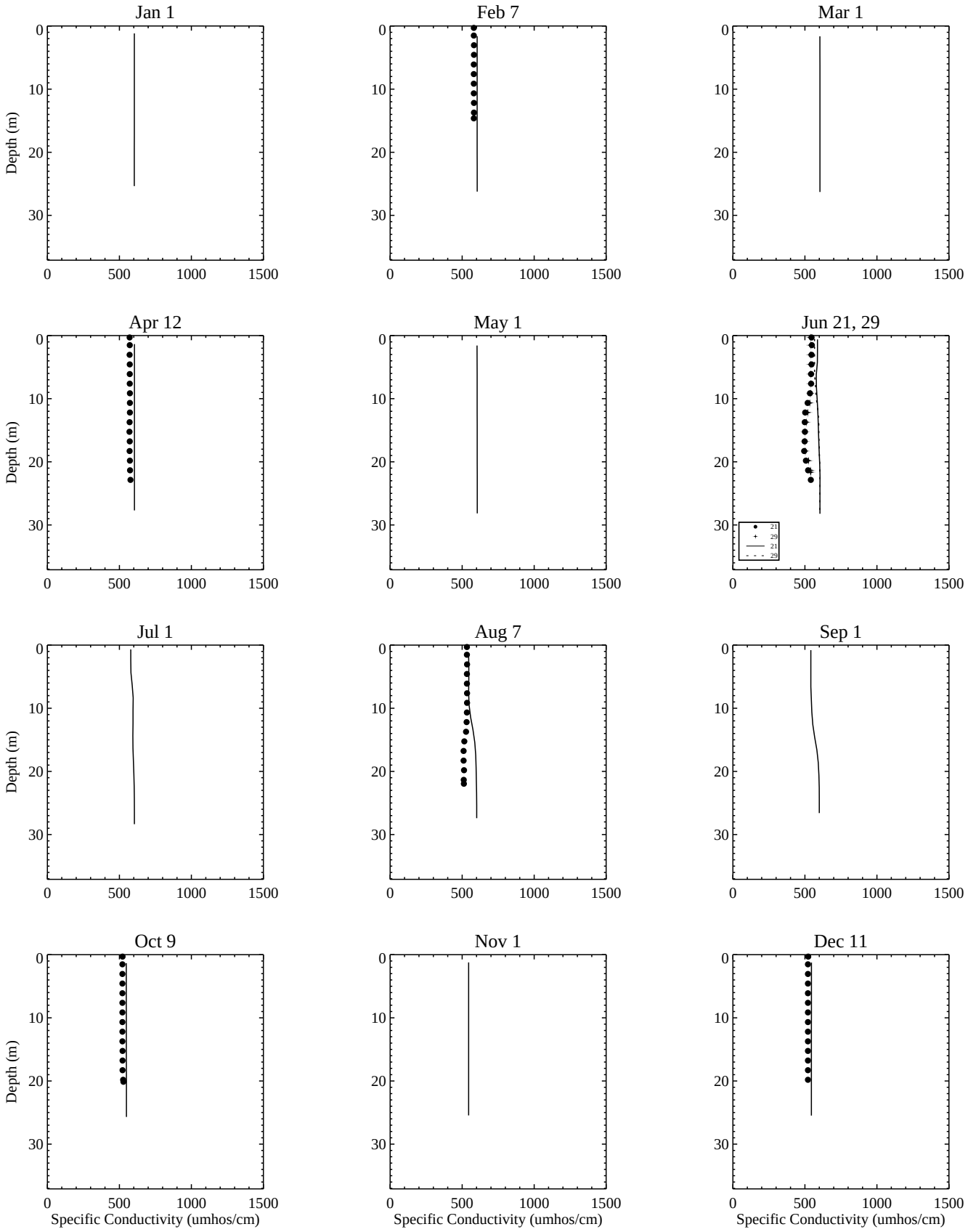

Figure J-10. Vertical profiles of model versus data at Sandy Creek (Segment 161) - Specific Conductivity - 1995.

Profiles shown for dates with available data else model results for first day of month shown.

Model Data

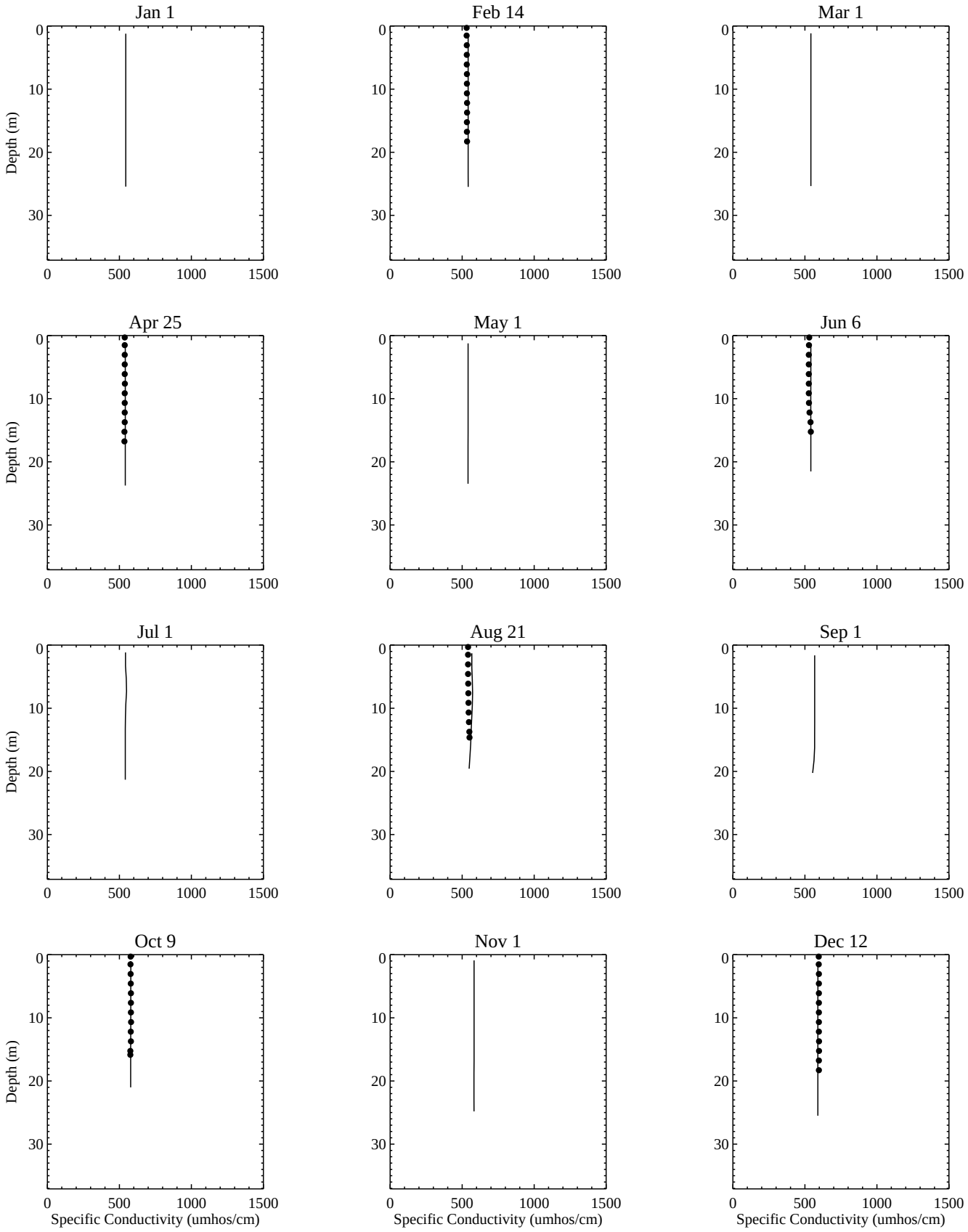

Figure J-10. Vertical profiles of model versus data at Sandy Creek (Segment 161) - Specific Conductivity - 1996.

Profiles shown for dates with available data else model results for first day of month shown.

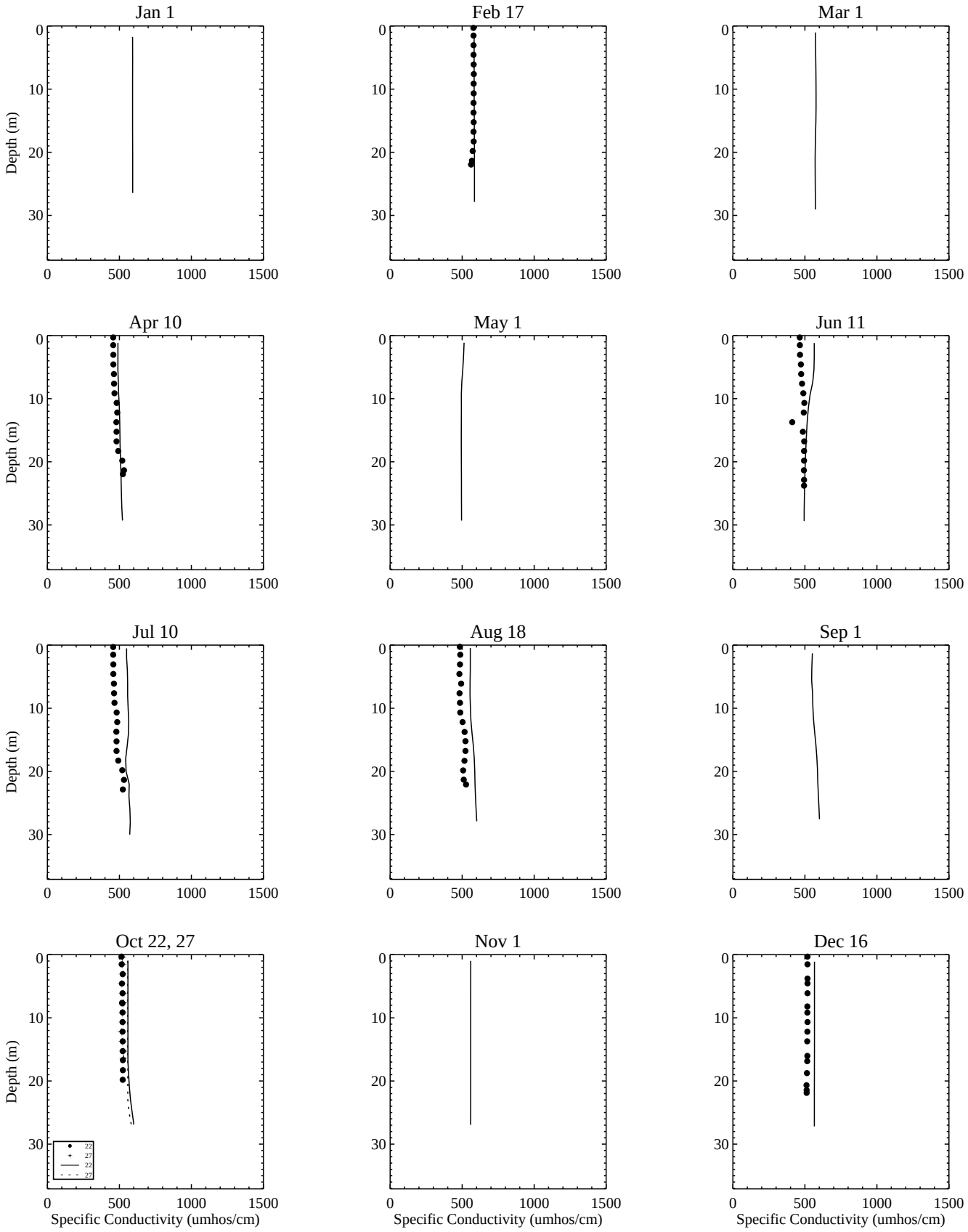

Figure J-10. Vertical profiles of model versus data at Sandy Creek (Segment 161) - Specific Conductivity - 1997.

Profiles shown for dates with available data else model results for first day of month shown.

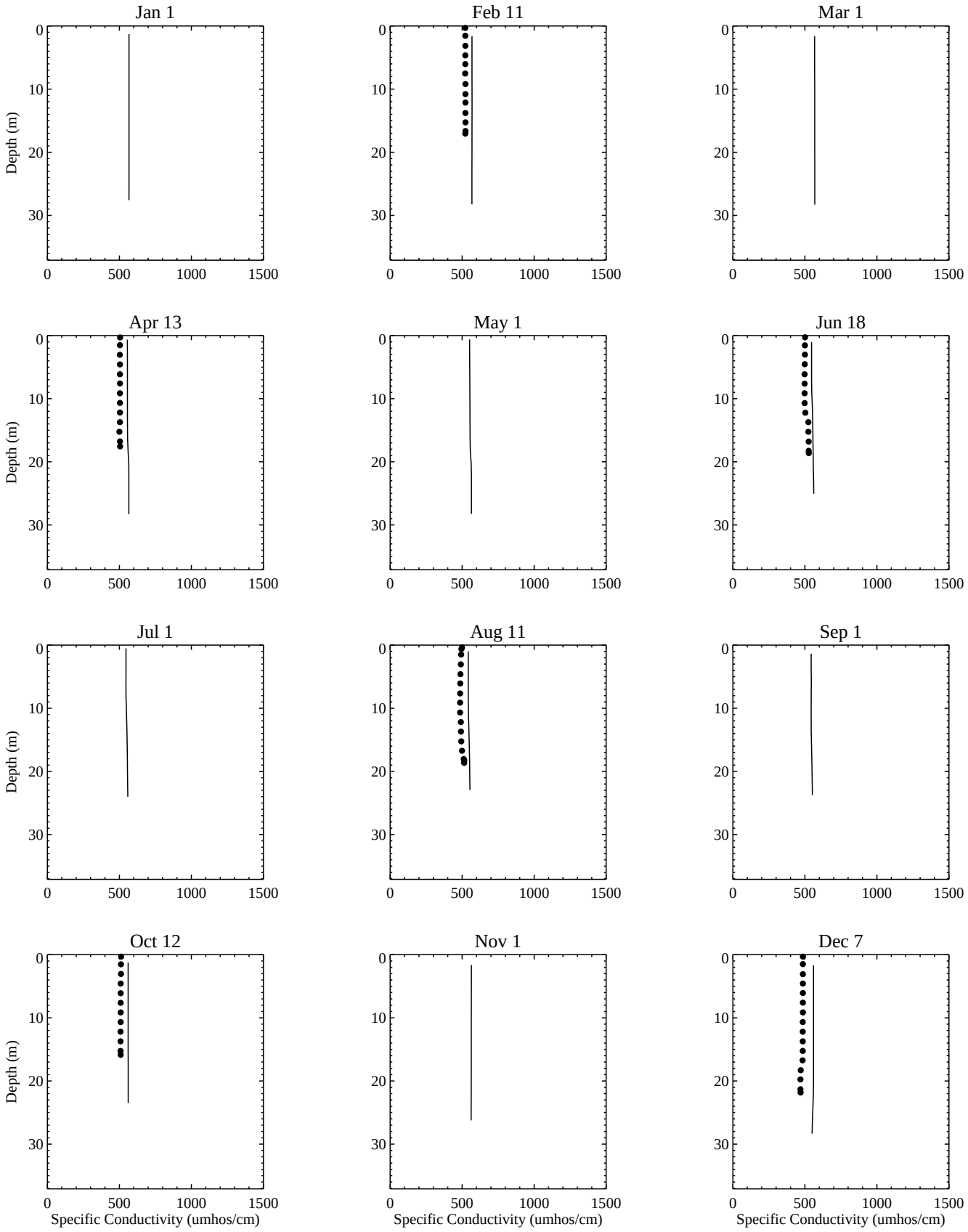

Figure J-10. Vertical profiles of model versus data at Sandy Creek (Segment 161) - Specific Conductivity - 1998.

Profiles shown for dates with available data else model results for first day of month shown.

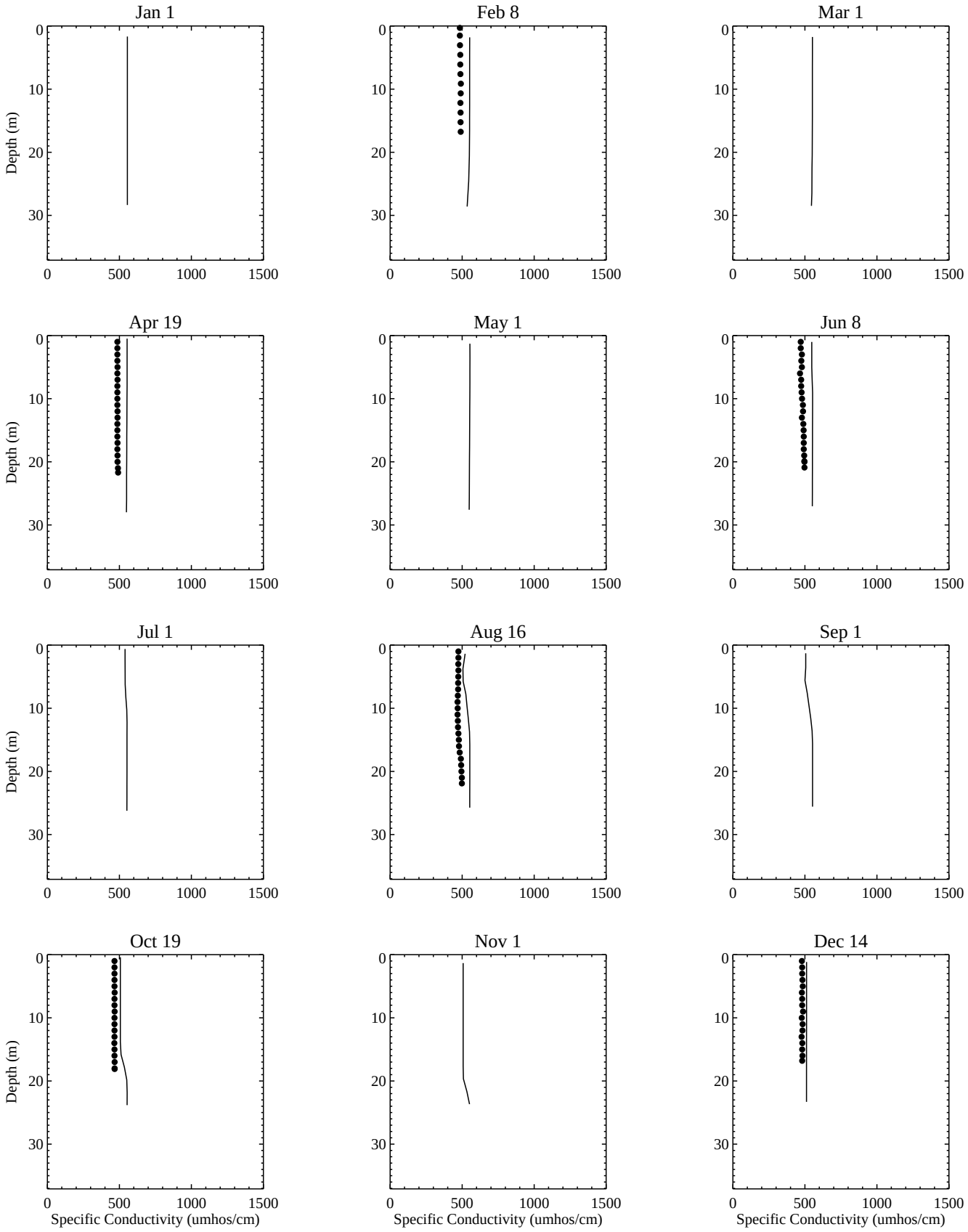

Figure J-10. Vertical profiles of model versus data at Sandy Creek (Segment 161) - Specific Conductivity - 1999.

Profiles shown for dates with available data else model results for first day of month shown.

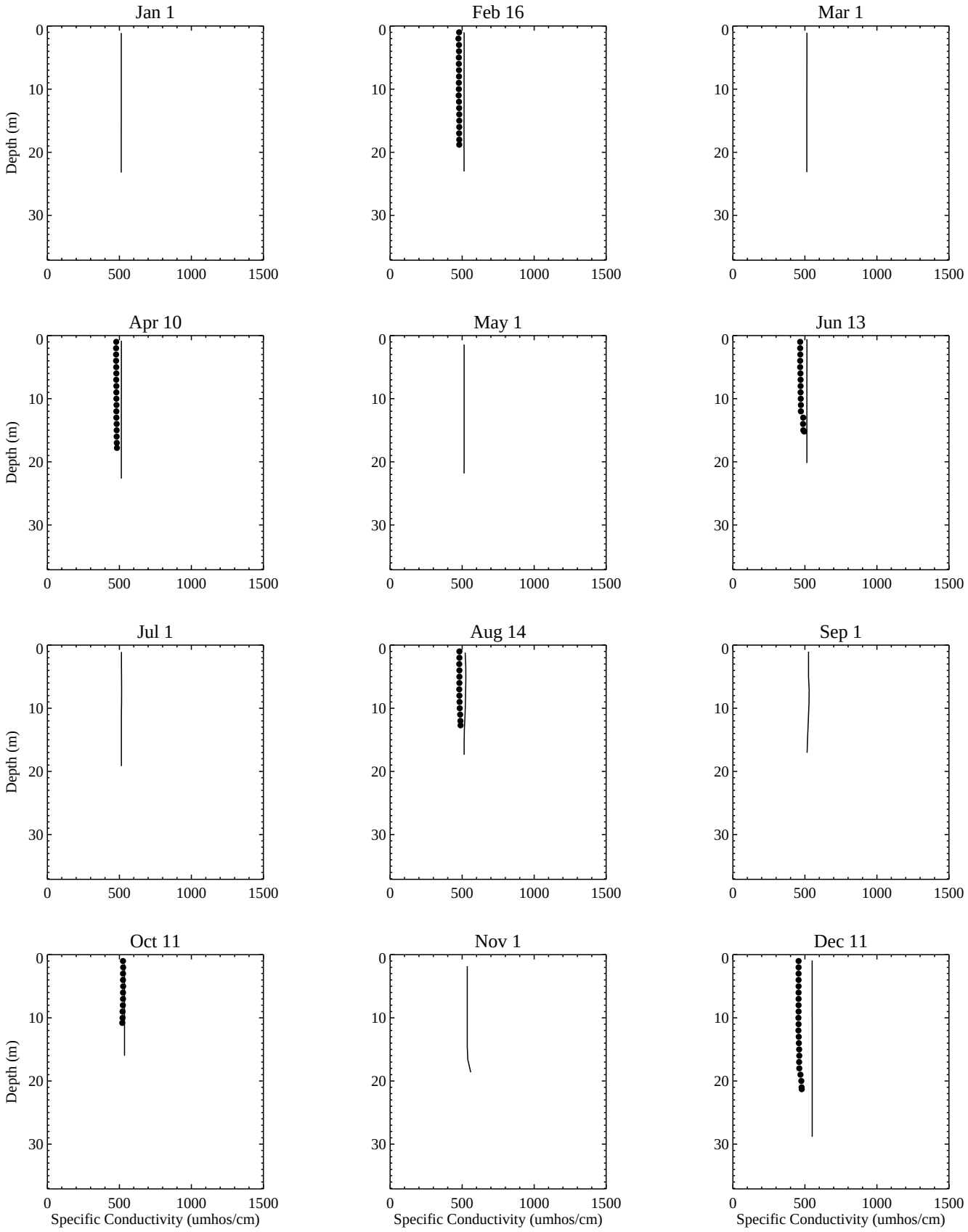

Figure J-10. Vertical profiles of model versus data at Sandy Creek (Segment 161) - Specific Conductivity - 2000.

Profiles shown for dates with available data else model results for first day of month shown.

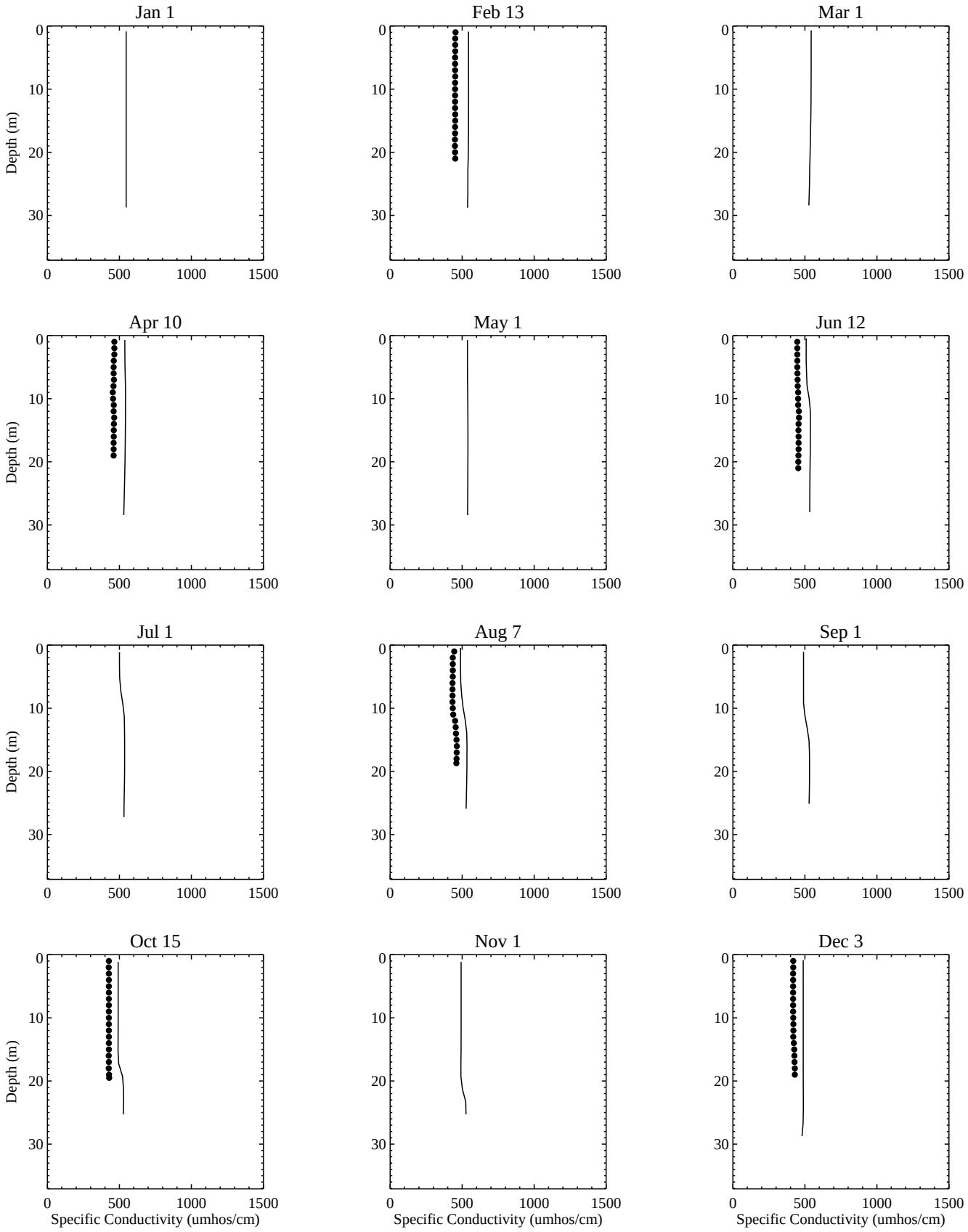

Figure J-10. Vertical profiles of model versus data at Sandy Creek (Segment 161) - Specific Conductivity - 2001.

Profiles shown for dates with available data else model results for first day of month shown.

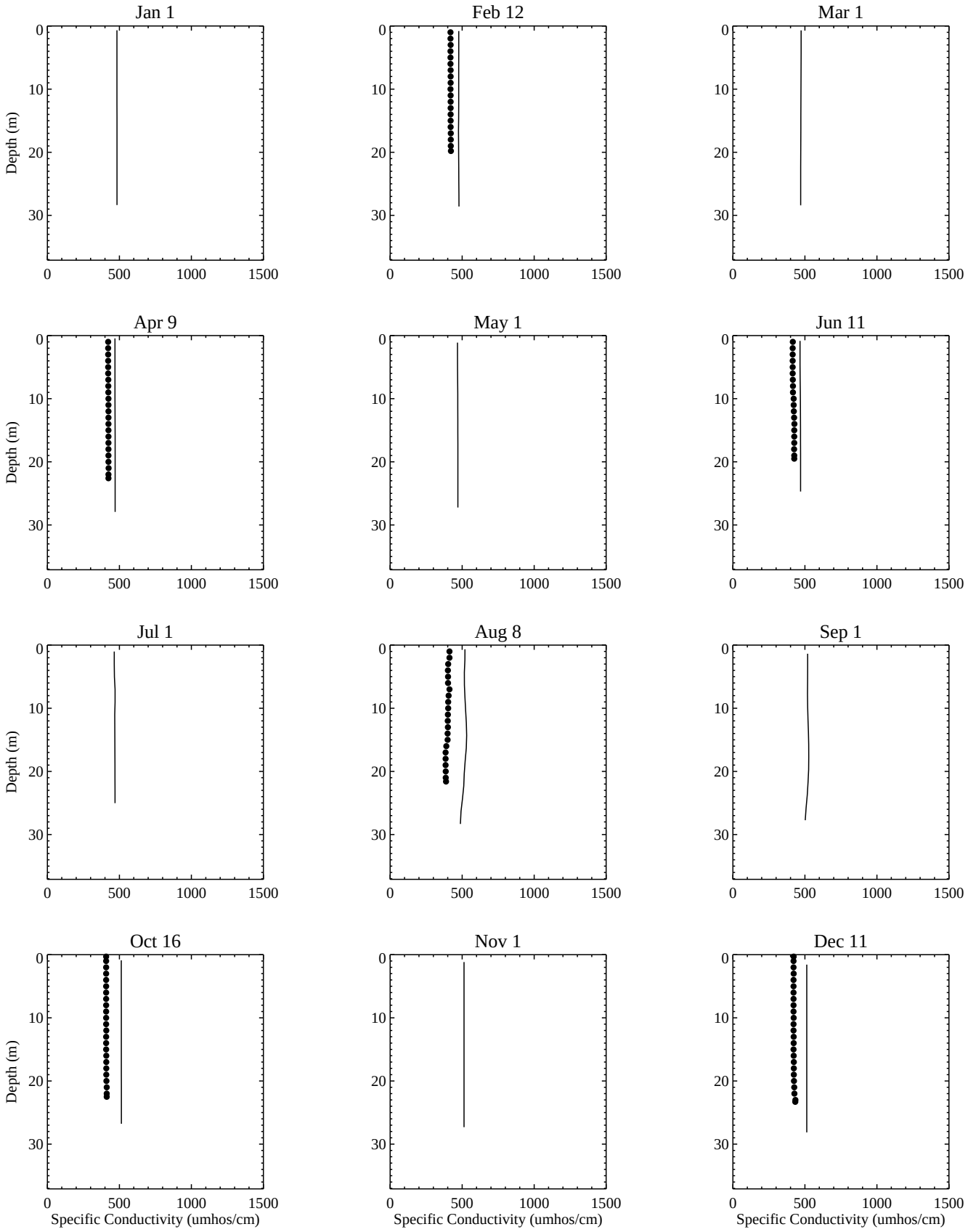

Figure J-10. Vertical profiles of model versus data at Sandy Creek (Segment 161) - Specific Conductivity - 2002.

Profiles shown for dates with available data else model results for first day of month shown.

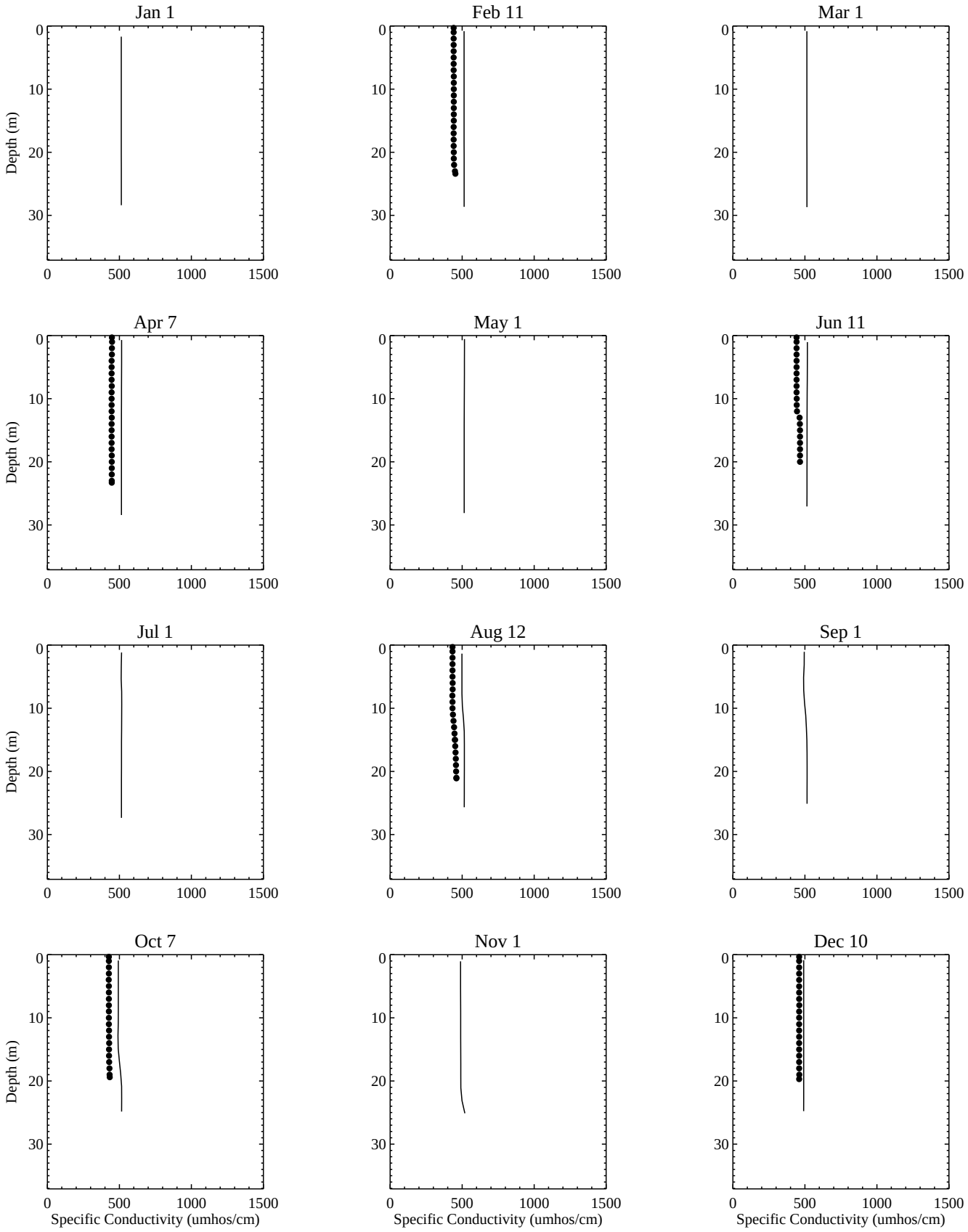

Figure J-10. Vertical profiles of model versus data at Sandy Creek (Segment 161) - Specific Conductivity - 2003.

Profiles shown for dates with available data else model results for first day of month shown.

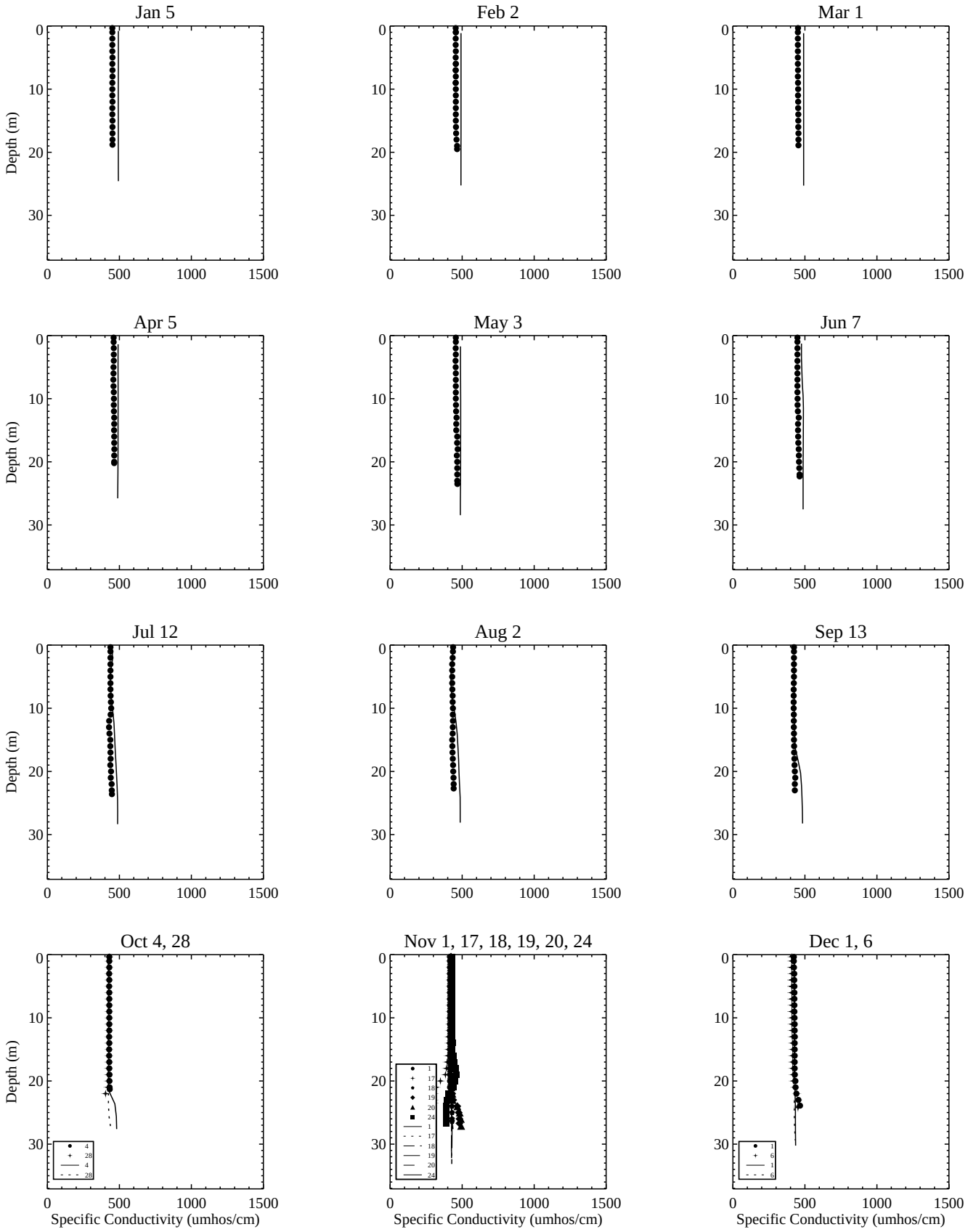

Figure J-10. Vertical profiles of model versus data at Sandy Creek (Segment 161) - Specific Conductivity - 2004.

Profiles shown for dates with available data else model results for first day of month shown.

Model Data

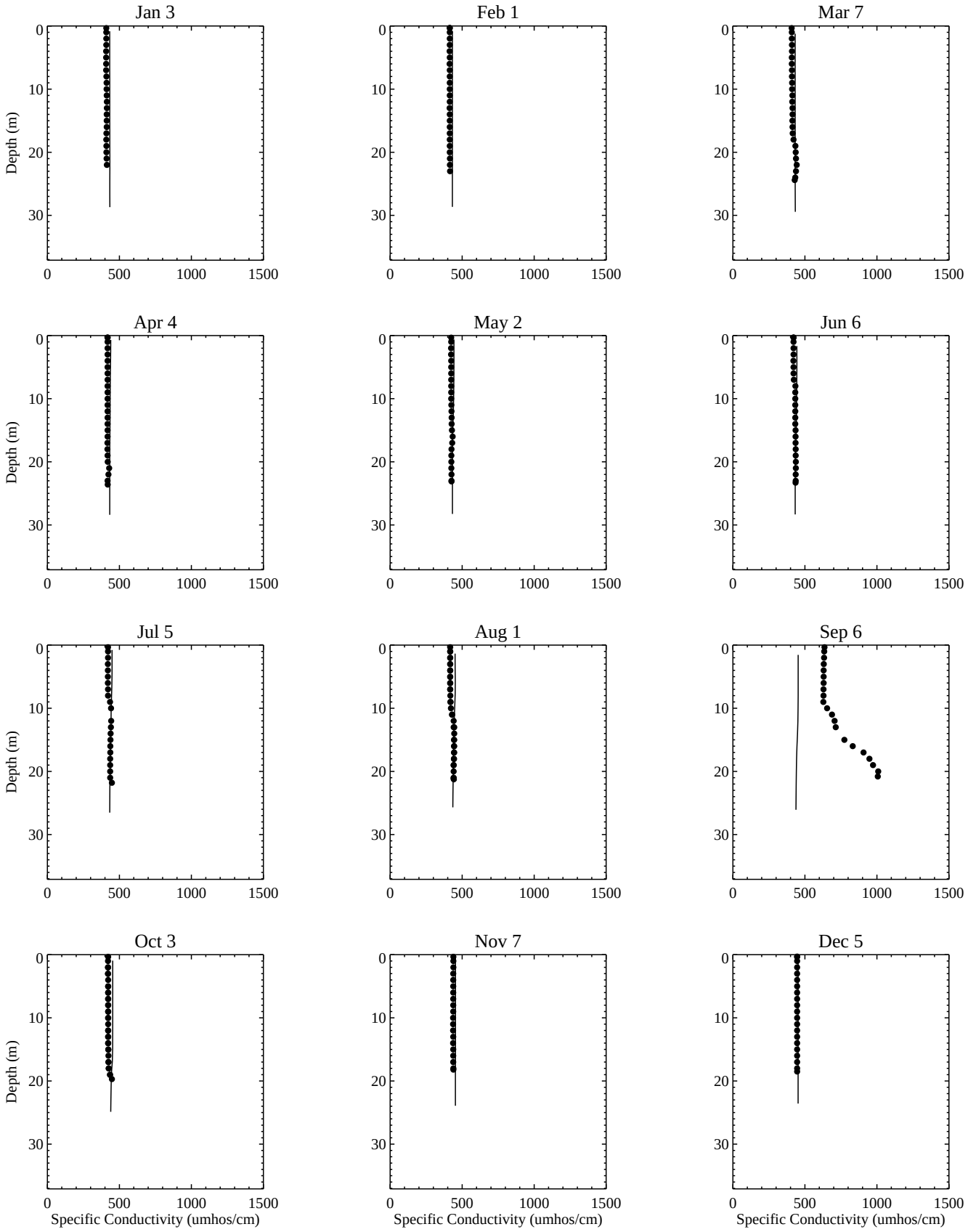

Figure J-10. Vertical profiles of model versus data at Sandy Creek (Segment 161) - Specific Conductivity - 2005.

Profiles shown for dates with available data else model results for first day of month shown.

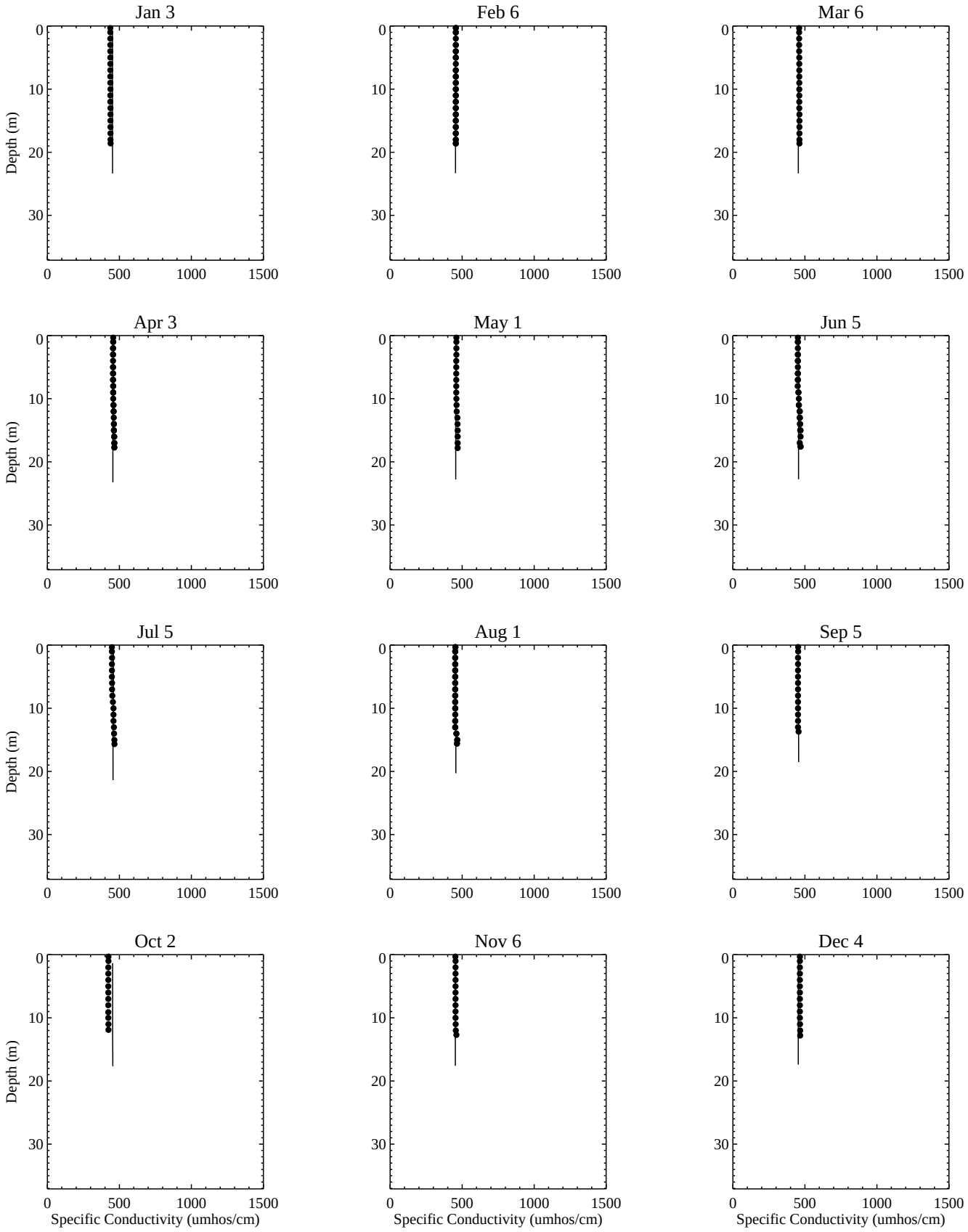

Figure J-10. Vertical profiles of model versus data at Sandy Creek (Segment 161) - Specific Conductivity - 2006.

Profiles shown for dates with available data else model results for first day of month shown.

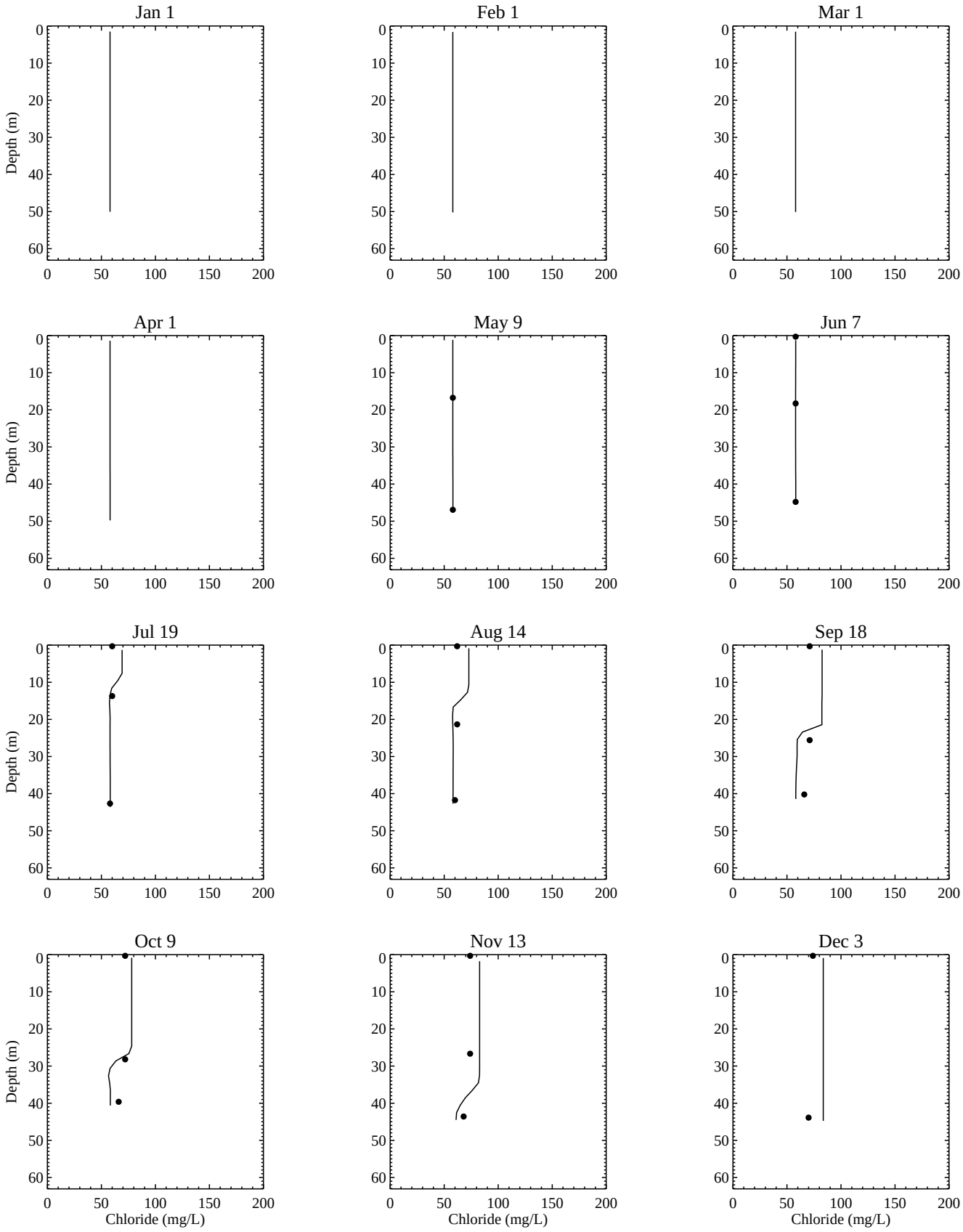

Figure J-11. Vertical profiles of model versus data at Mansfield Dam (Segment 93) - Chloride - 1984.

Profiles shown for dates with available data else model results for first day of month shown.

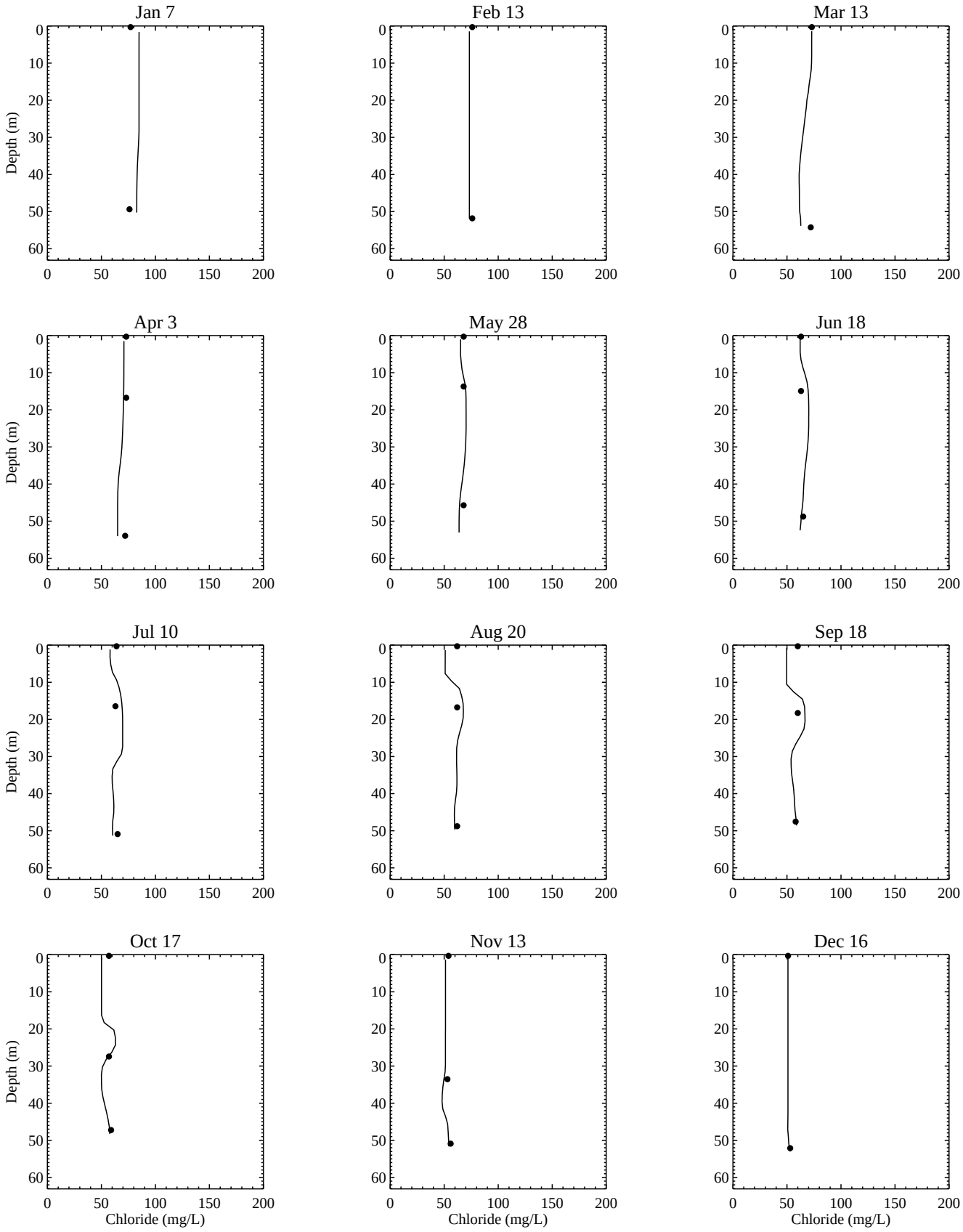

Figure J-11. Vertical profiles of model versus data at Mansfield Dam (Segment 93) - Chloride - 1985.

Profiles shown for dates with available data else model results for first day of month shown.

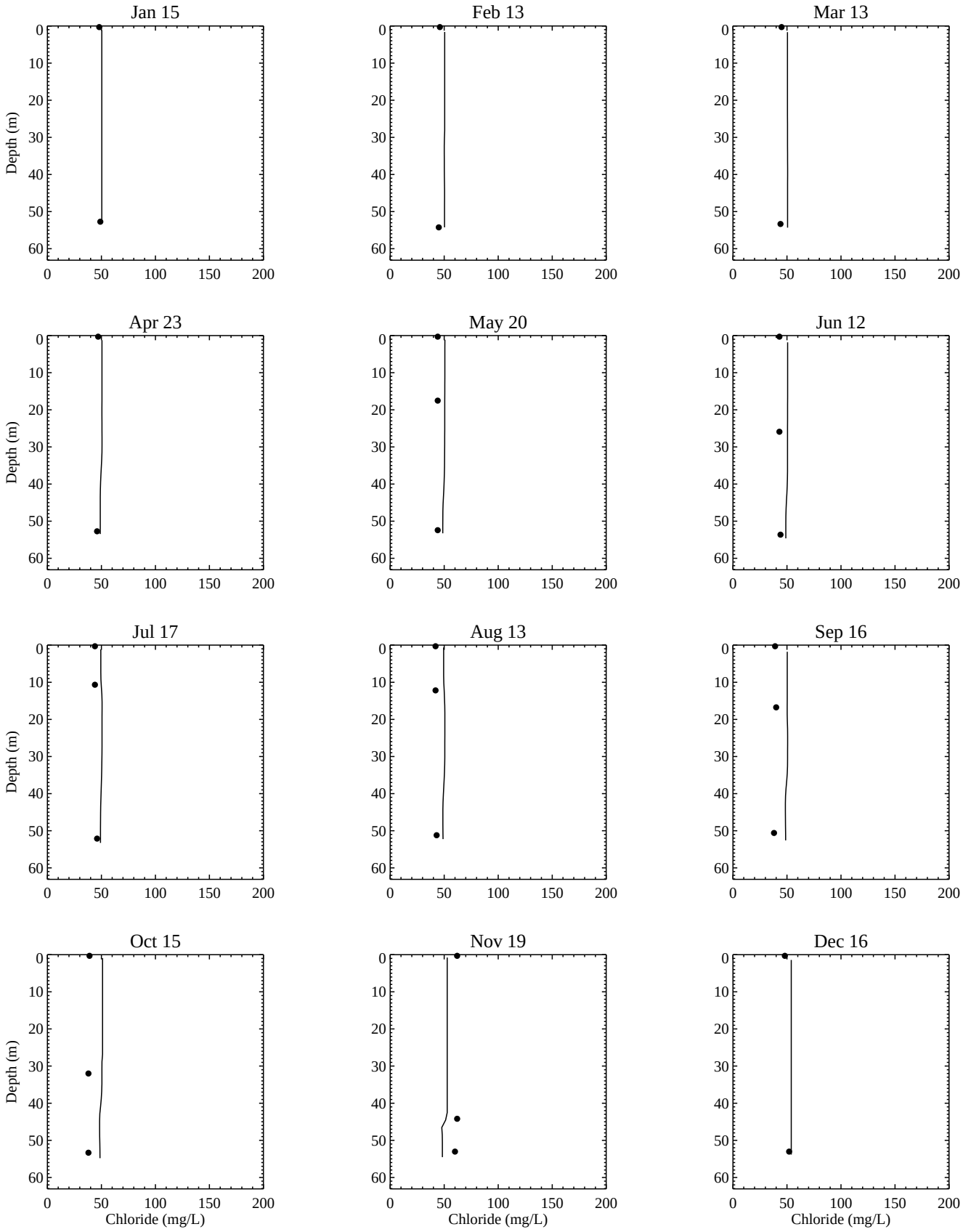

Figure J-11. Vertical profiles of model versus data at Mansfield Dam (Segment 93) - Chloride - 1986.

Profiles shown for dates with available data else model results for first day of month shown.

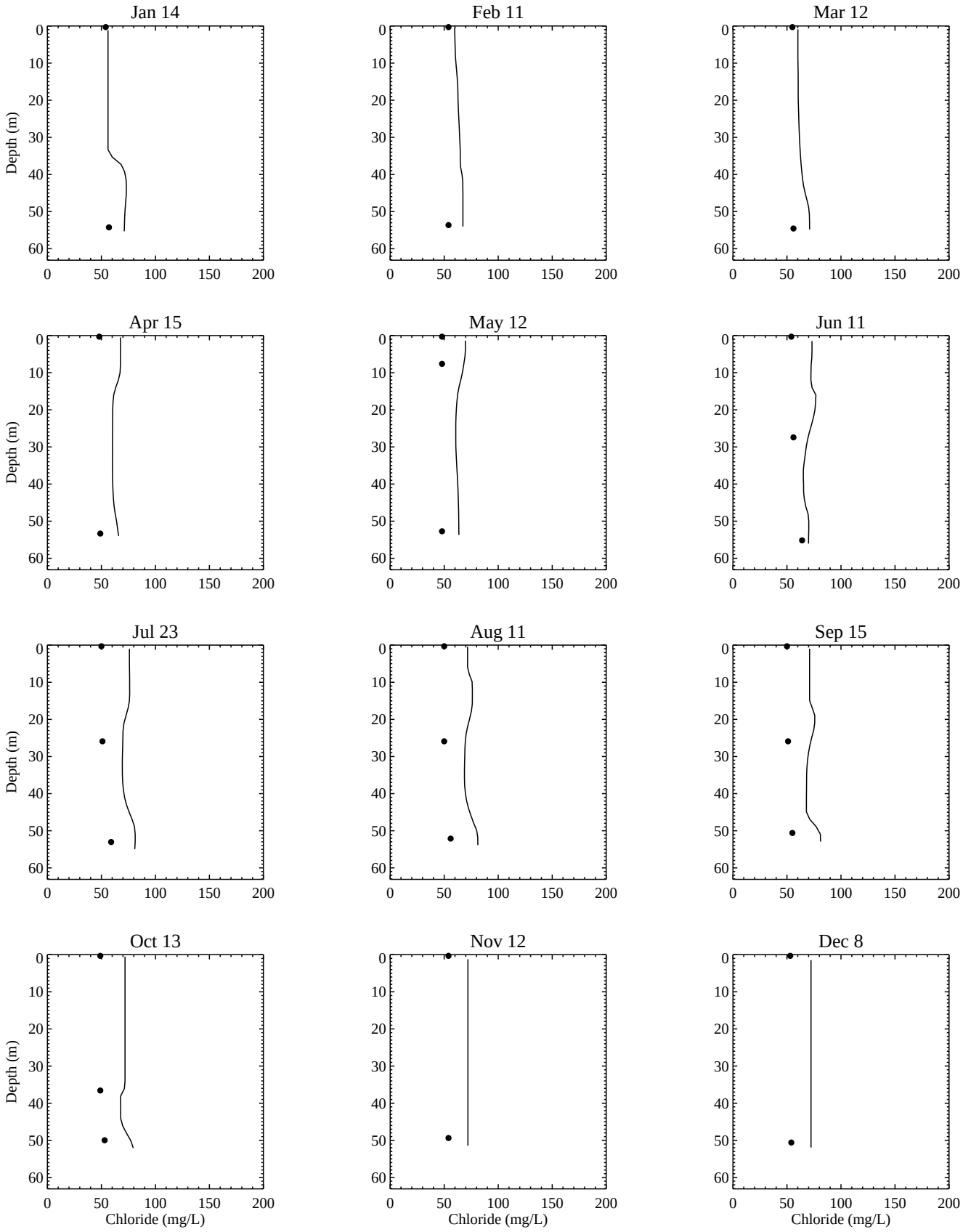

Figure J-11. Vertical profiles of model versus data at Mansfield Dam (Segment 93) - Chloride - 1987.

Profiles shown for dates with available data else model results for first day of month shown.

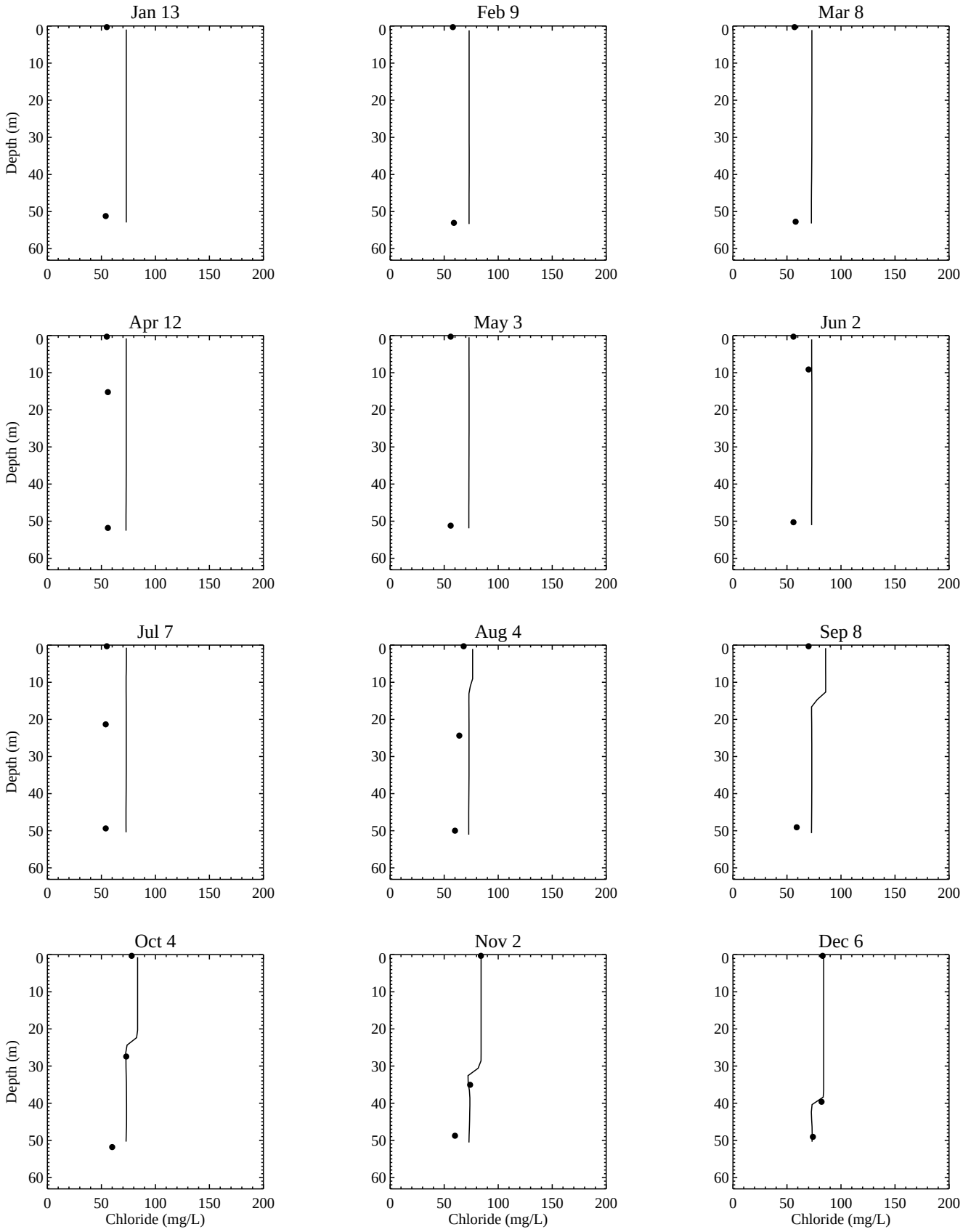

Figure J-11. Vertical profiles of model versus data at Mansfield Dam (Segment 93) - Chloride - 1988.

Profiles shown for dates with available data else model results for first day of month shown.

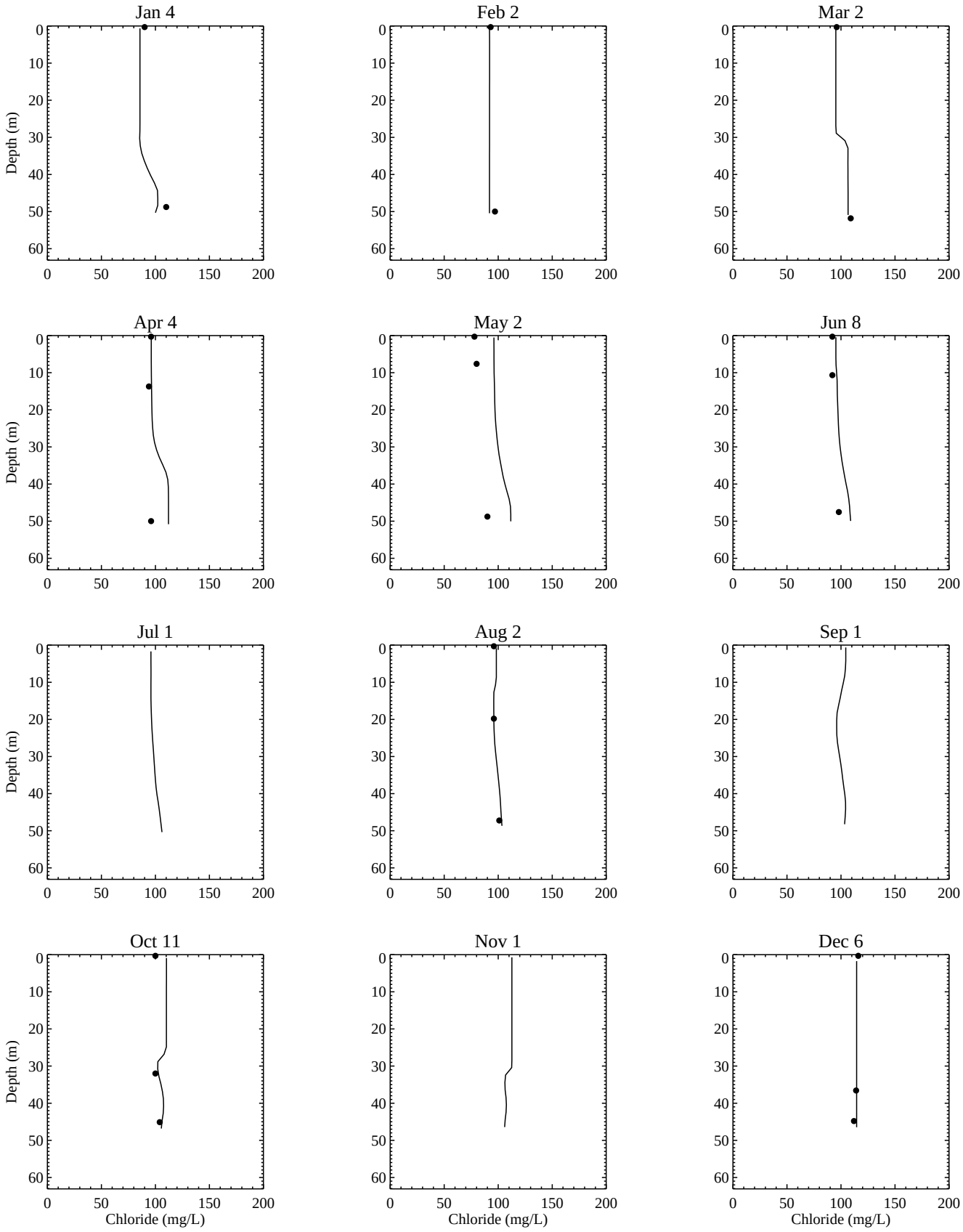

Figure J-11. Vertical profiles of model versus data at Mansfield Dam (Segment 93) - Chloride - 1989.

Profiles shown for dates with available data else model results for first day of month shown.

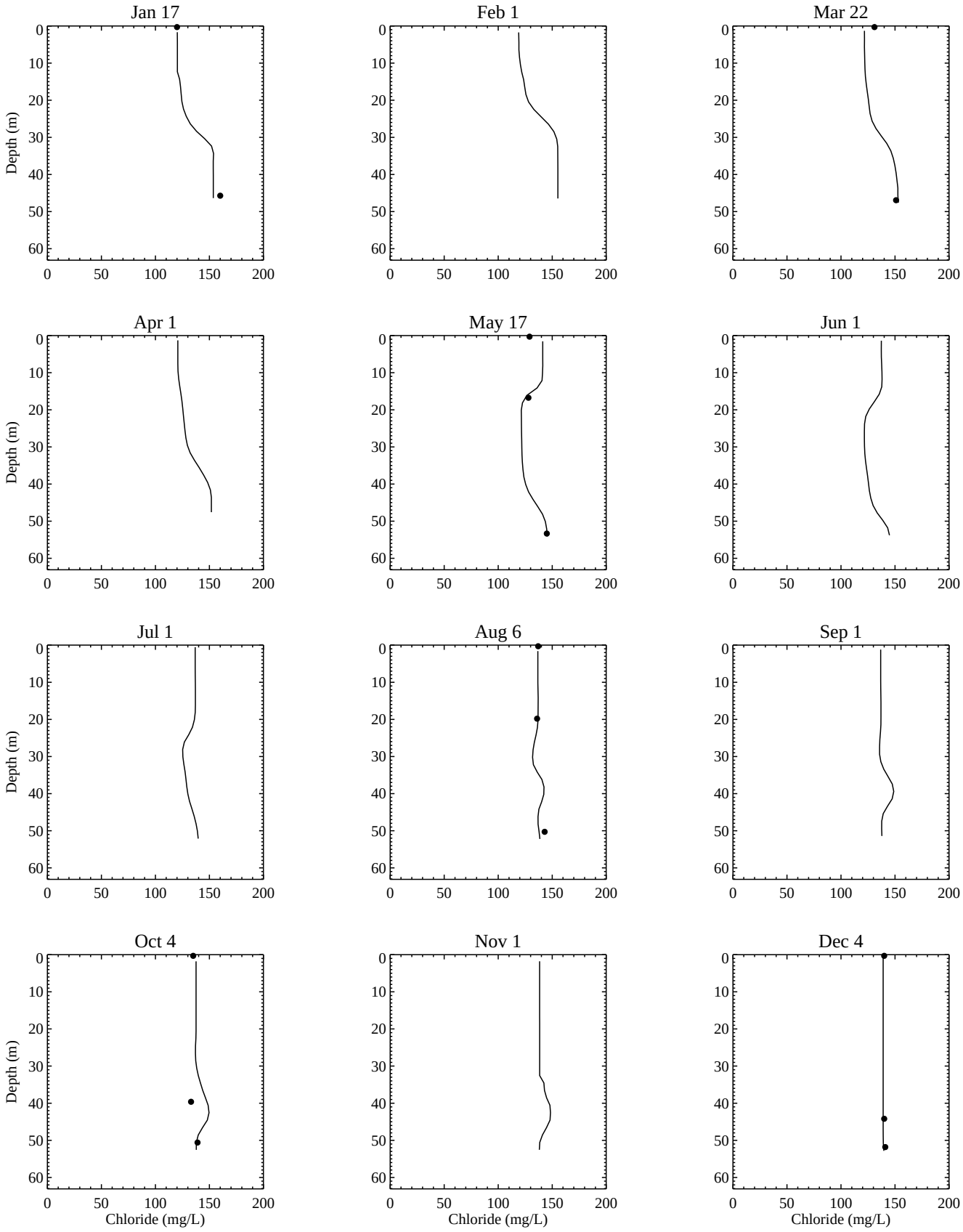

Figure J-11. Vertical profiles of model versus data at Mansfield Dam (Segment 93) - Chloride - 1990.

Profiles shown for dates with available data else model results for first day of month shown.

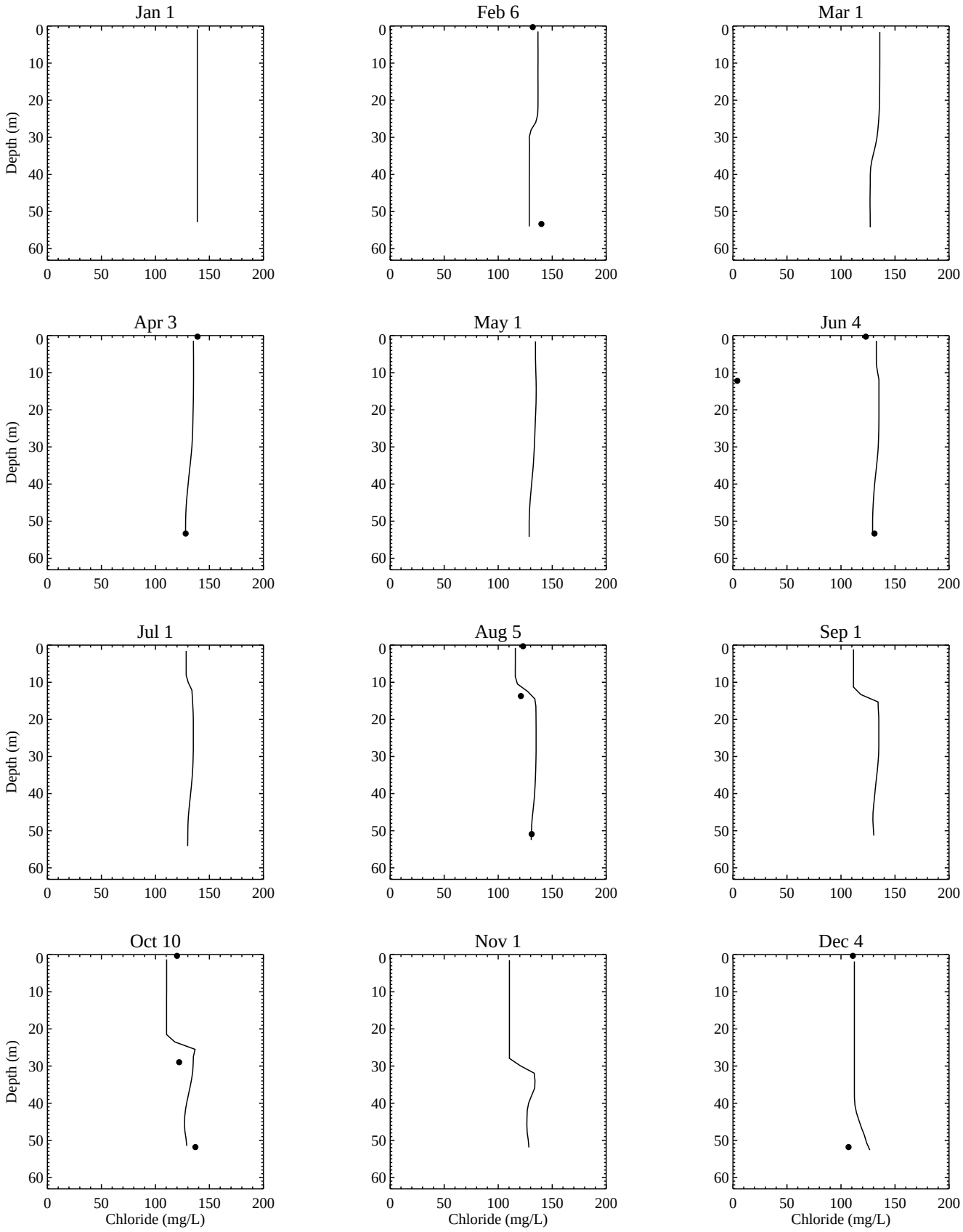

Figure J-11. Vertical profiles of model versus data at Mansfield Dam (Segment 93) - Chloride - 1991.

Profiles shown for dates with available data else model results for first day of month shown.

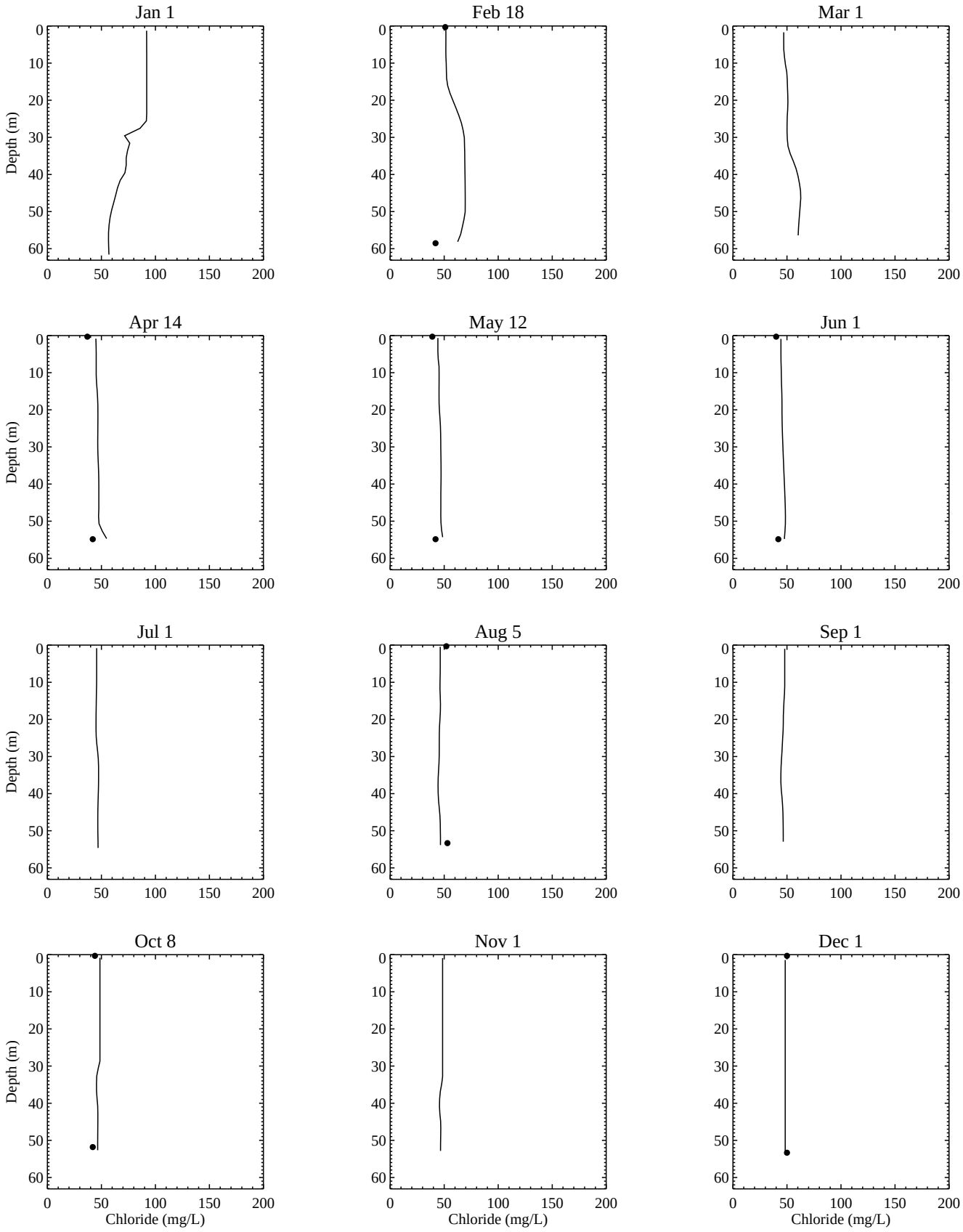

Figure J-11. Vertical profiles of model versus data at Mansfield Dam (Segment 93) - Chloride - 1992.

Profiles shown for dates with available data else model results for first day of month shown.

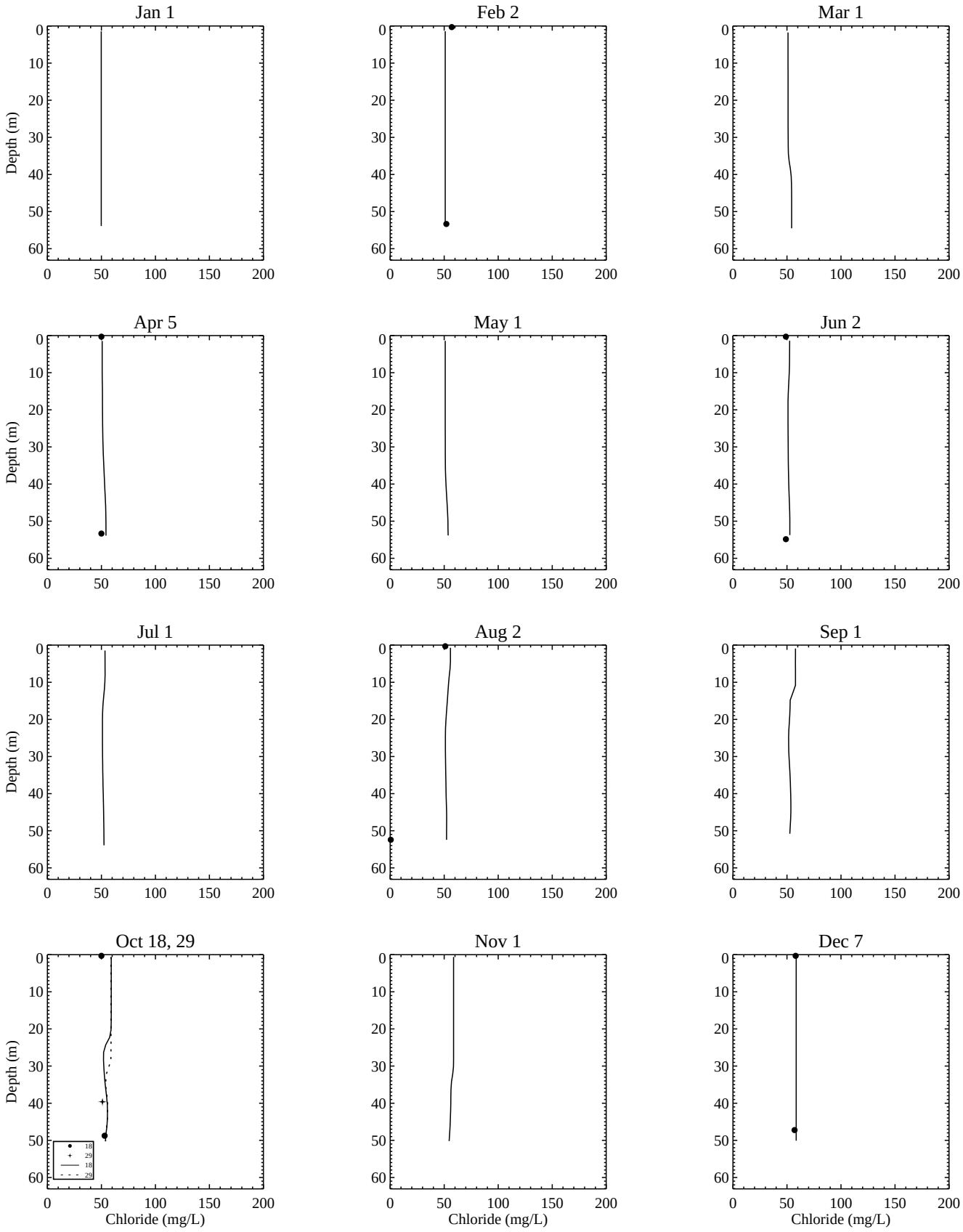

Figure J-11. Vertical profiles of model versus data at Mansfield Dam (Segment 93) - Chloride - 1993.

Profiles shown for dates with available data else model results for first day of month shown.

Model Data

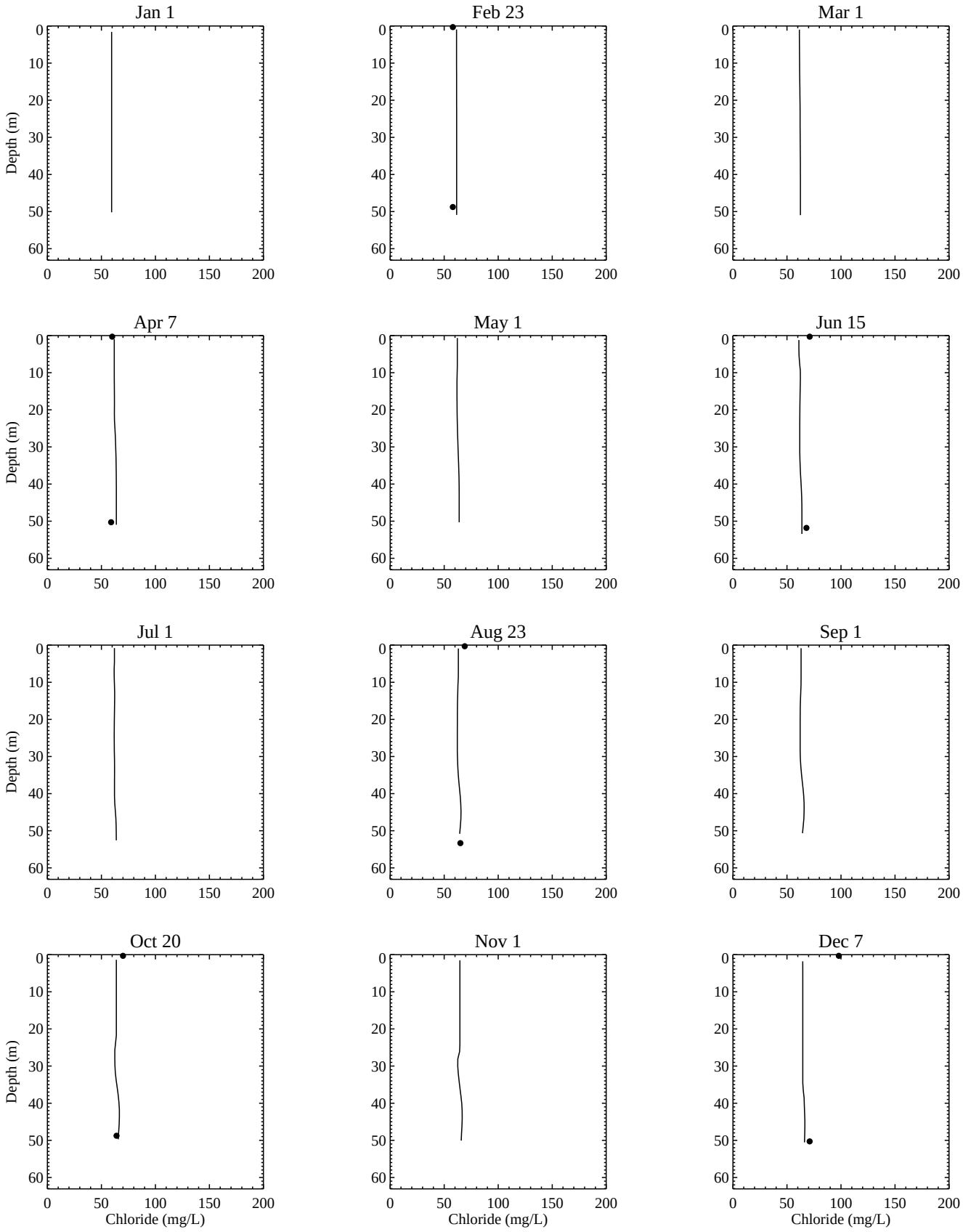

Figure J-11. Vertical profiles of model versus data at Mansfield Dam (Segment 93) - Chloride - 1994.

Profiles shown for dates with available data else model results for first day of month shown.

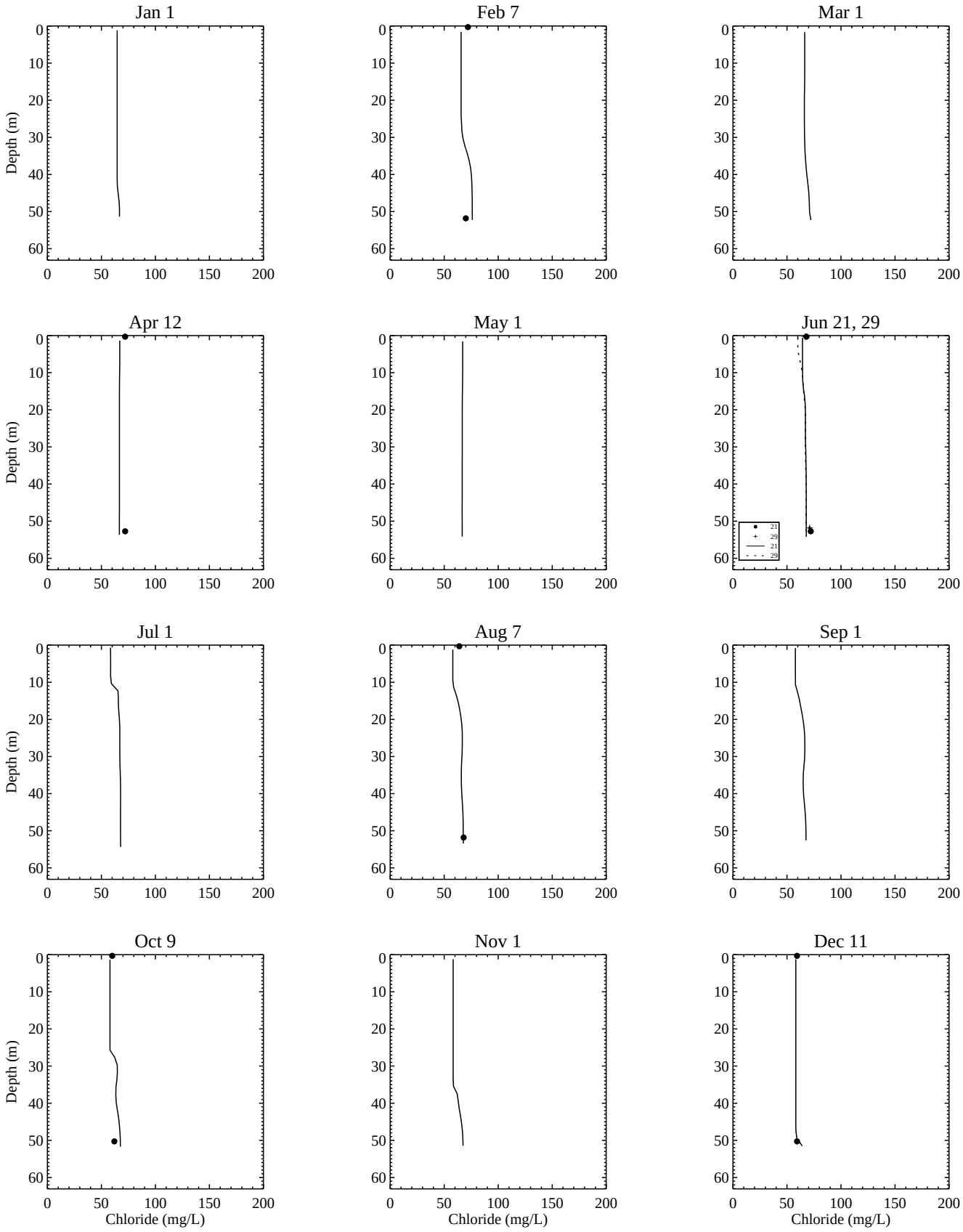

Figure J-11. Vertical profiles of model versus data at Mansfield Dam (Segment 93) - Chloride - 1995.

Profiles shown for dates with available data else model results for first day of month shown.

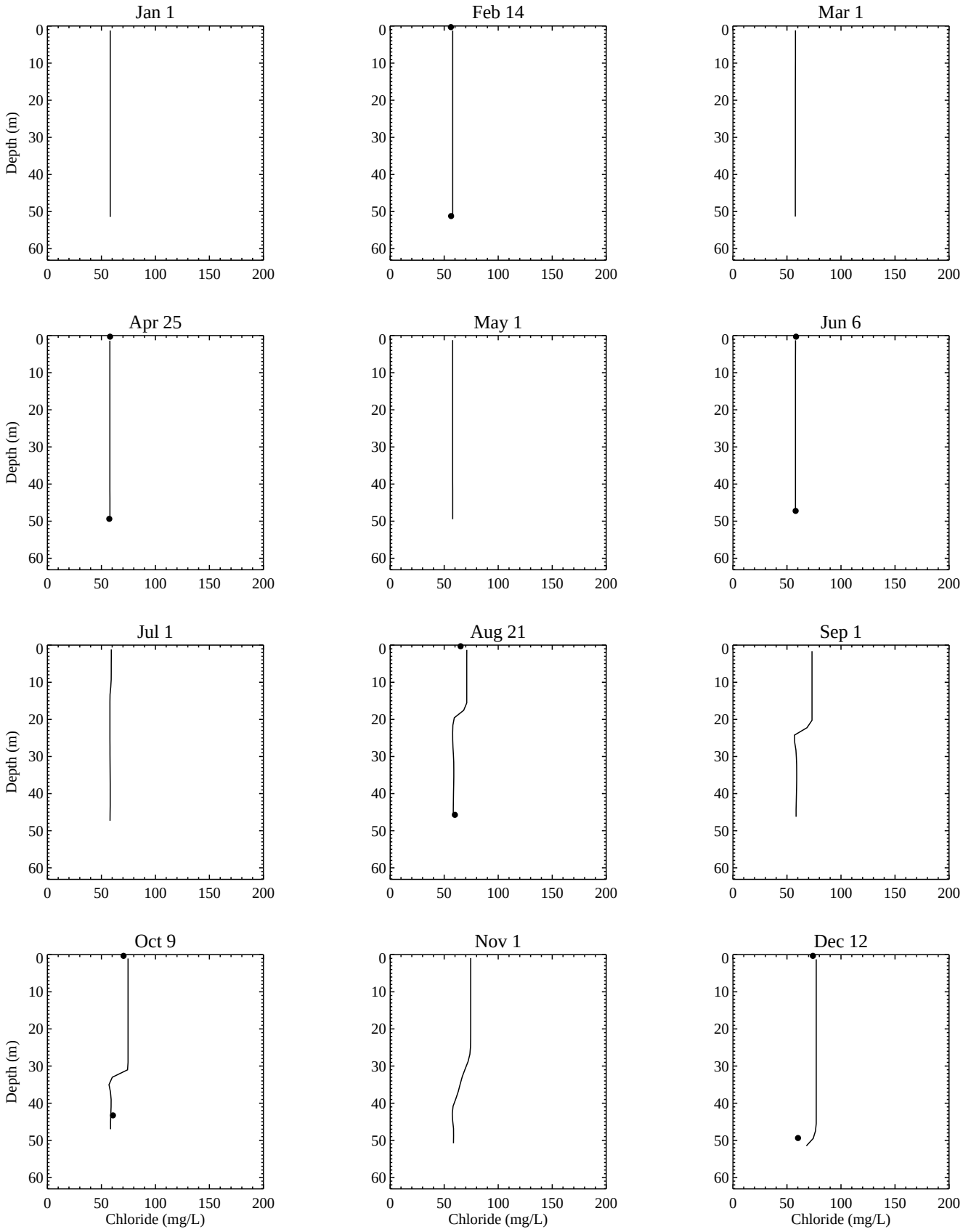

Figure J-11. Vertical profiles of model versus data at Mansfield Dam (Segment 93) - Chloride - 1996.

Profiles shown for dates with available data else model results for first day of month shown.

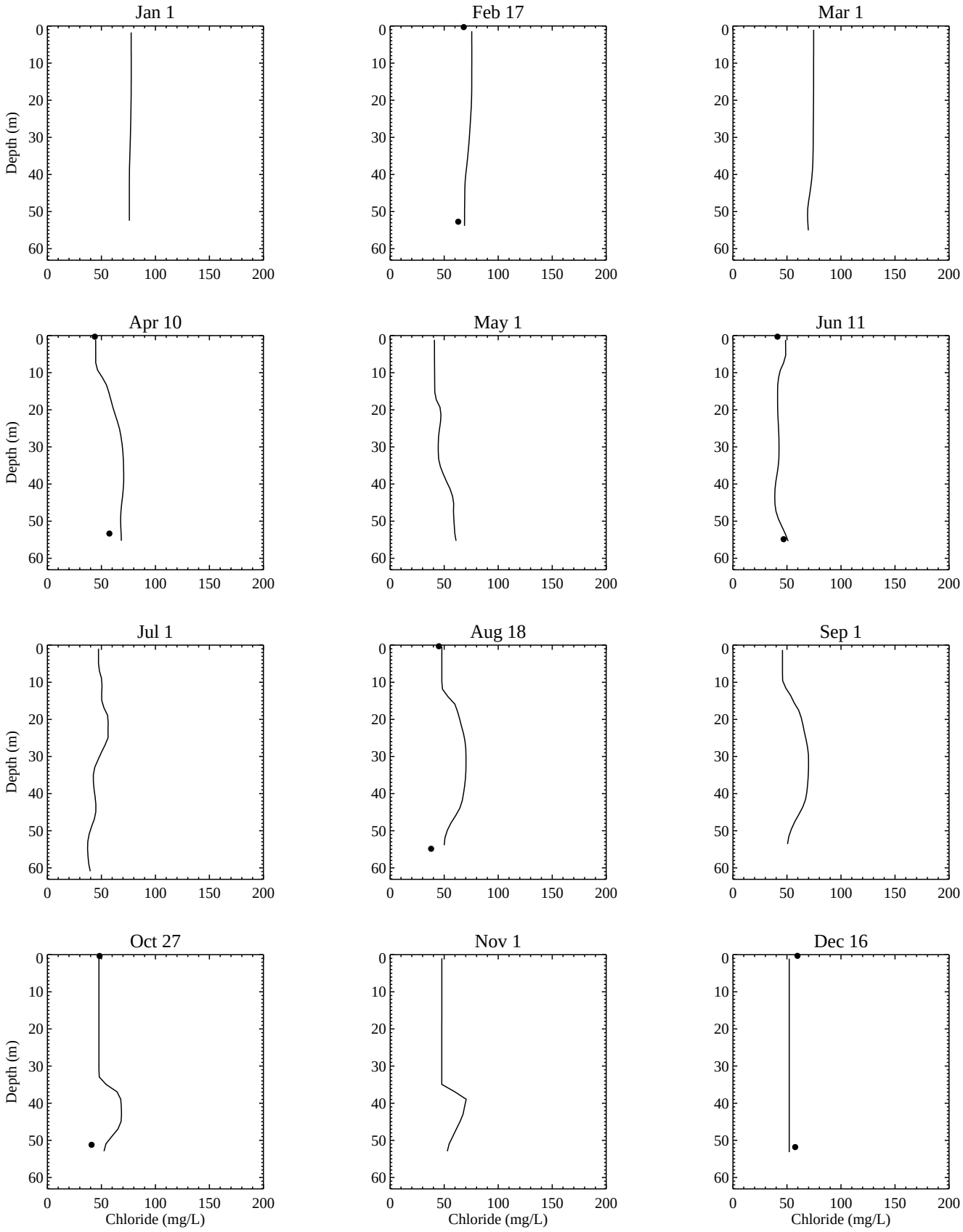

Figure J-11. Vertical profiles of model versus data at Mansfield Dam (Segment 93) - Chloride - 1997.

Profiles shown for dates with available data else model results for first day of month shown.

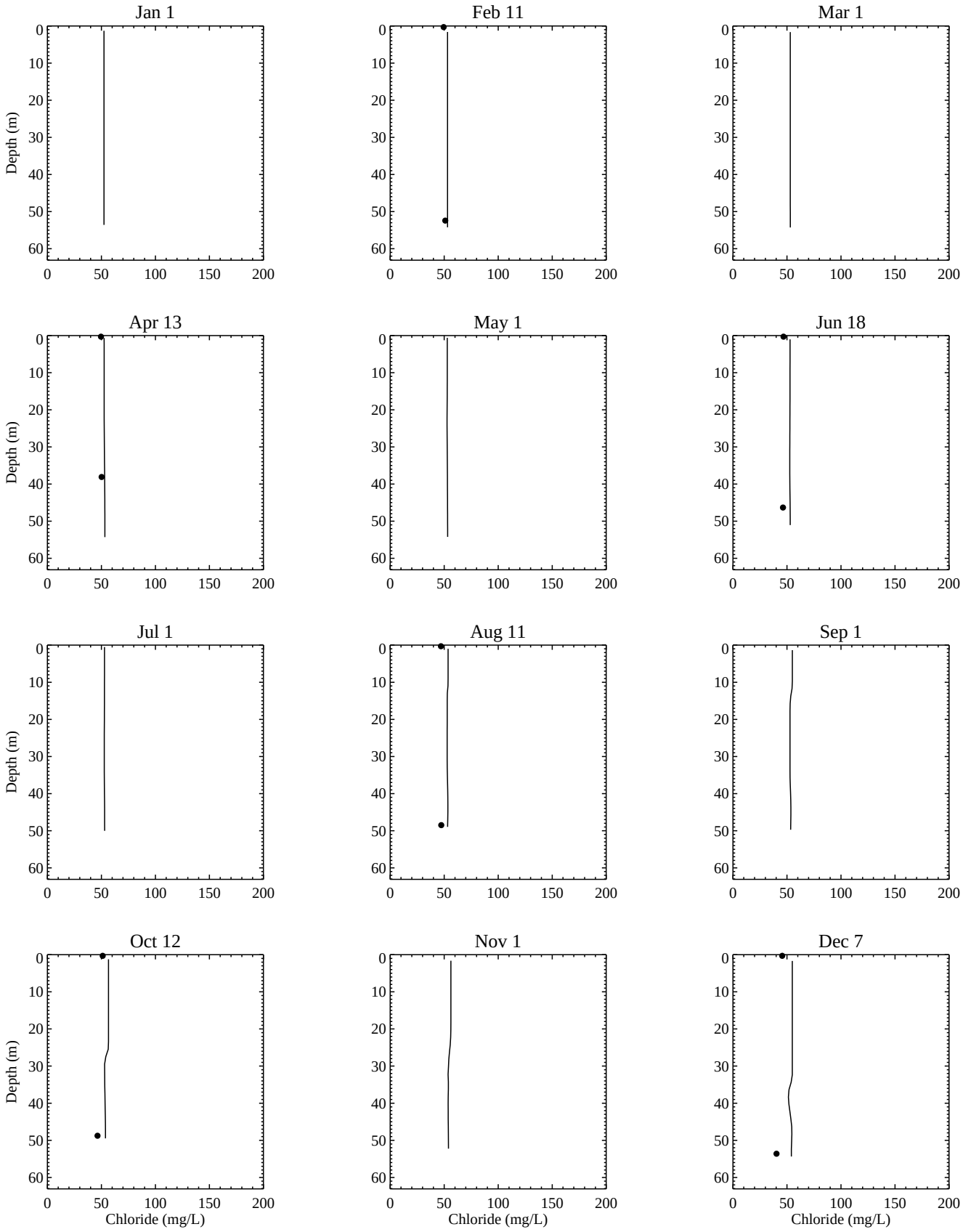

Figure J-11. Vertical profiles of model versus data at Mansfield Dam (Segment 93) - Chloride - 1998.

Profiles shown for dates with available data else model results for first day of month shown.

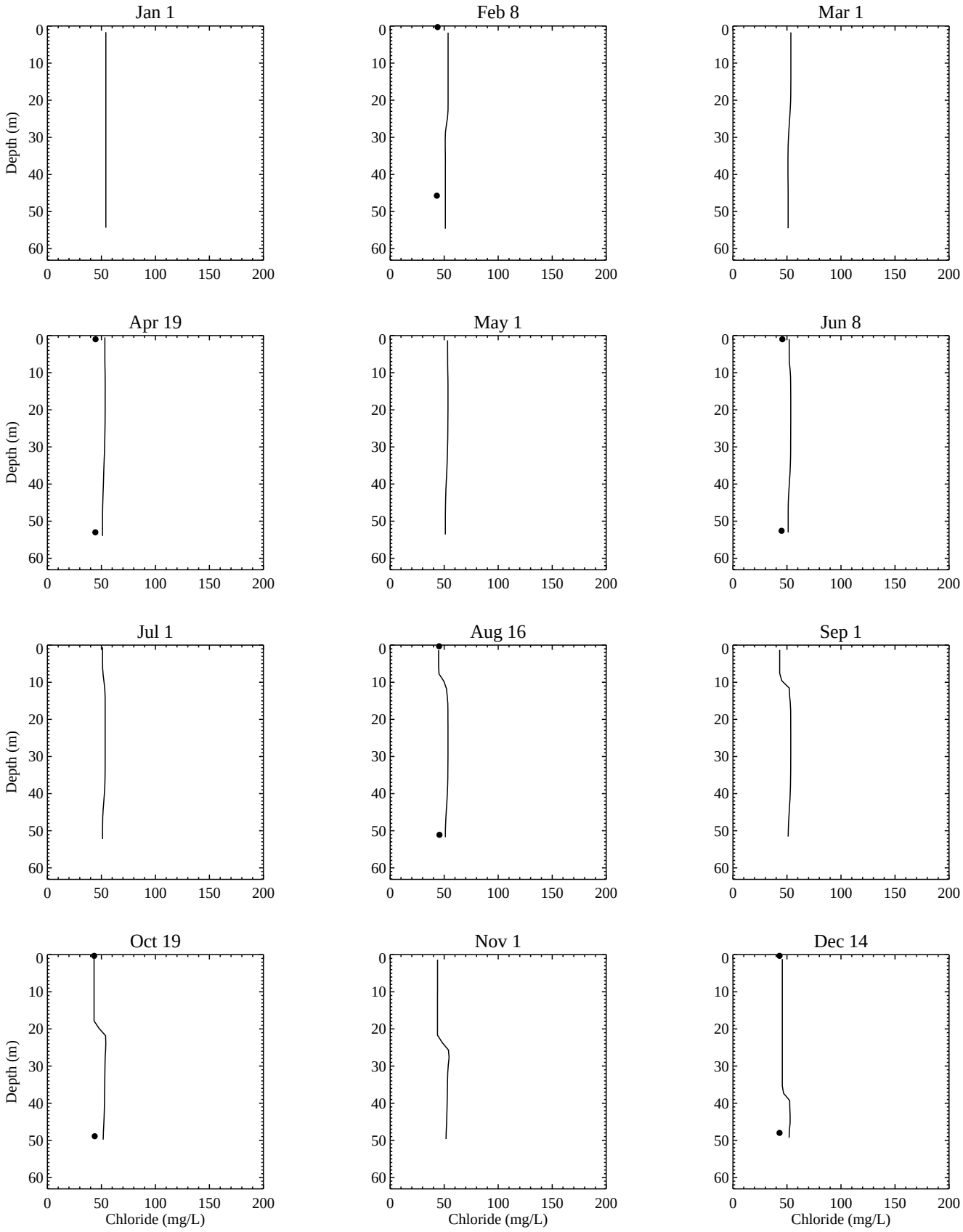

Figure J-11. Vertical profiles of model versus data at Mansfield Dam (Segment 93) - Chloride - 1999.

Profiles shown for dates with available data else model results for first day of month shown.

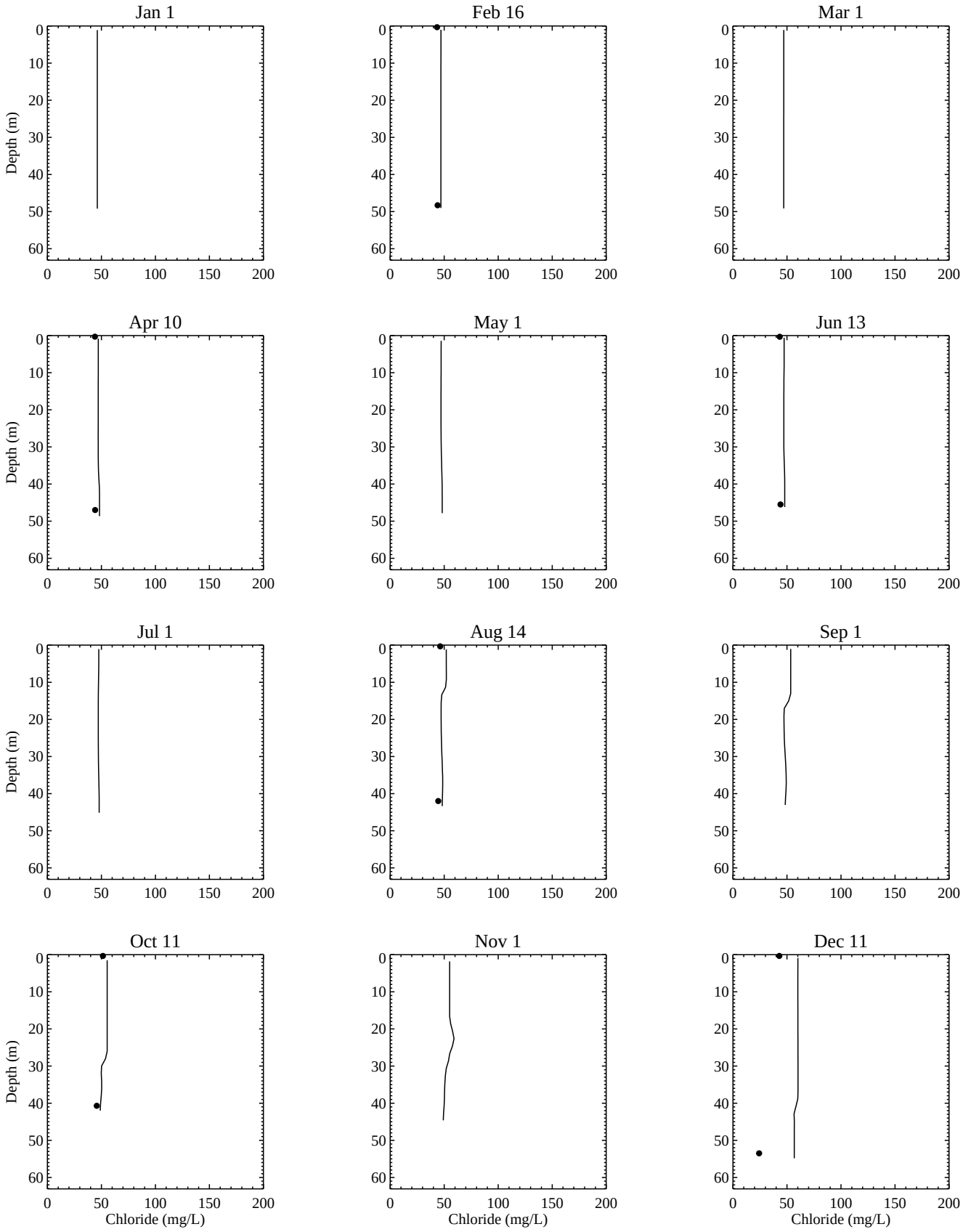

Figure J-11. Vertical profiles of model versus data at Mansfield Dam (Segment 93) - Chloride - 2000.

Profiles shown for dates with available data else model results for first day of month shown.

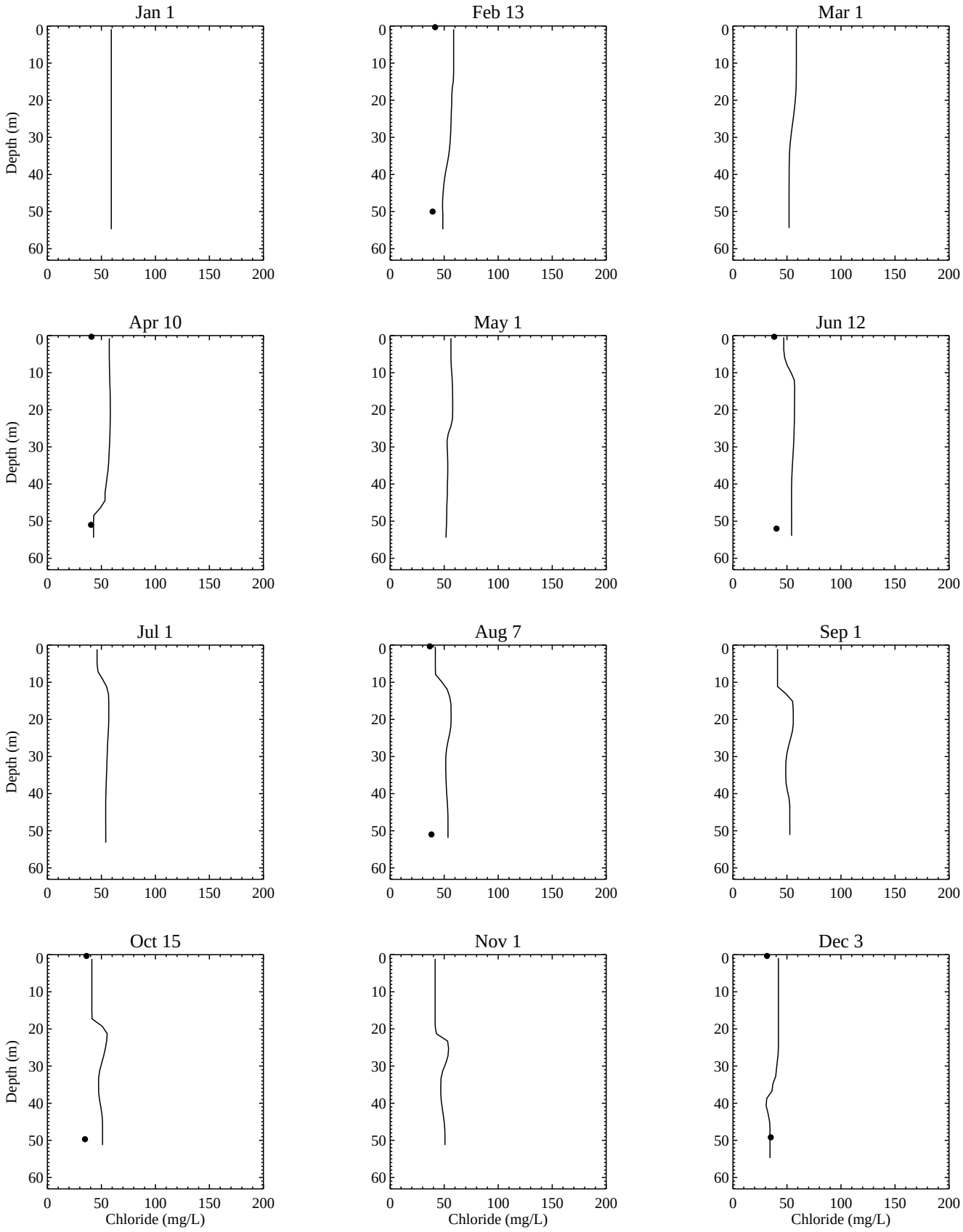

Figure J-11. Vertical profiles of model versus data at Mansfield Dam (Segment 93) - Chloride - 2001.

Profiles shown for dates with available data else model results for first day of month shown.

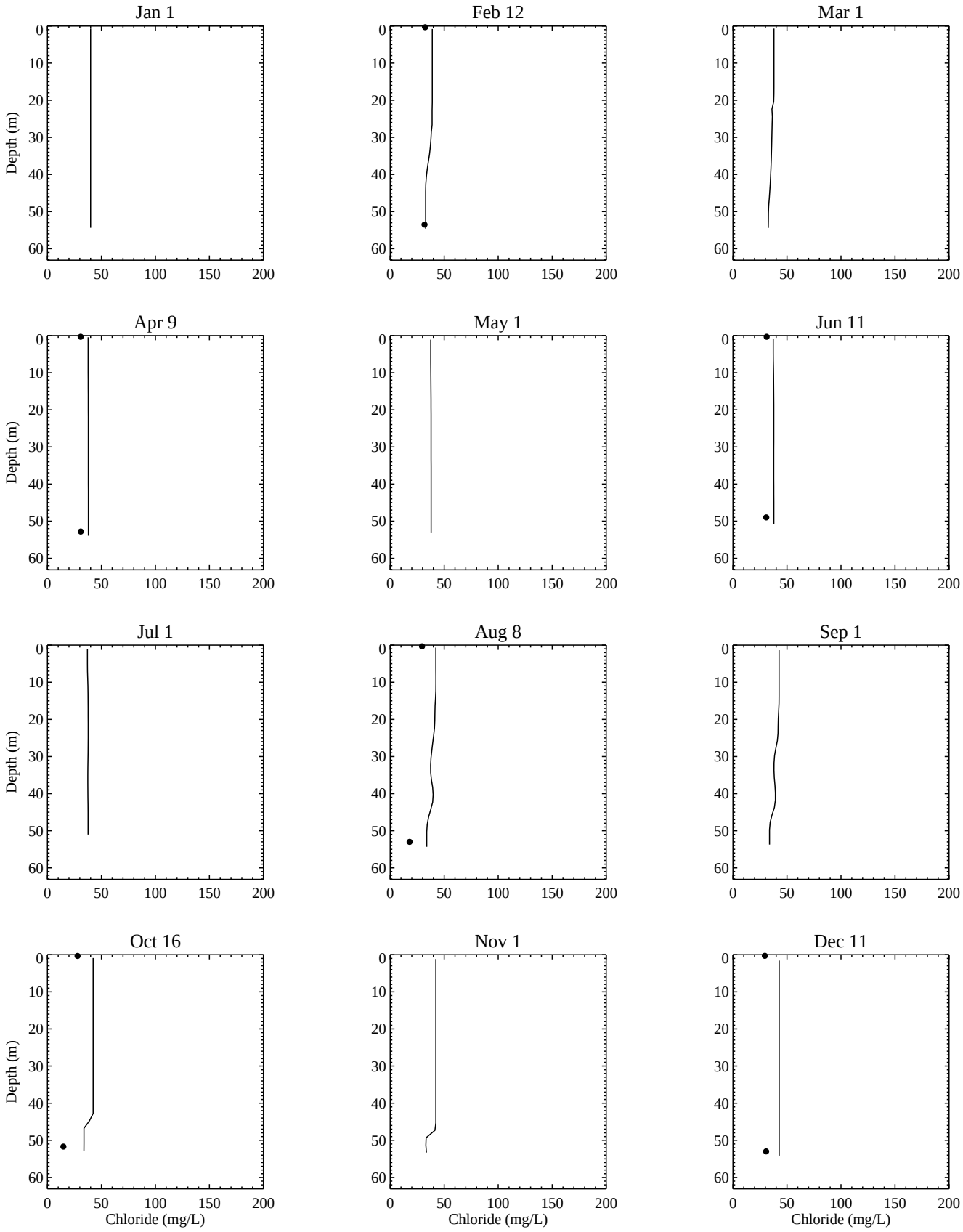

Figure J-11. Vertical profiles of model versus data at Mansfield Dam (Segment 93) - Chloride - 2002.

Profiles shown for dates with available data else model results for first day of month shown.

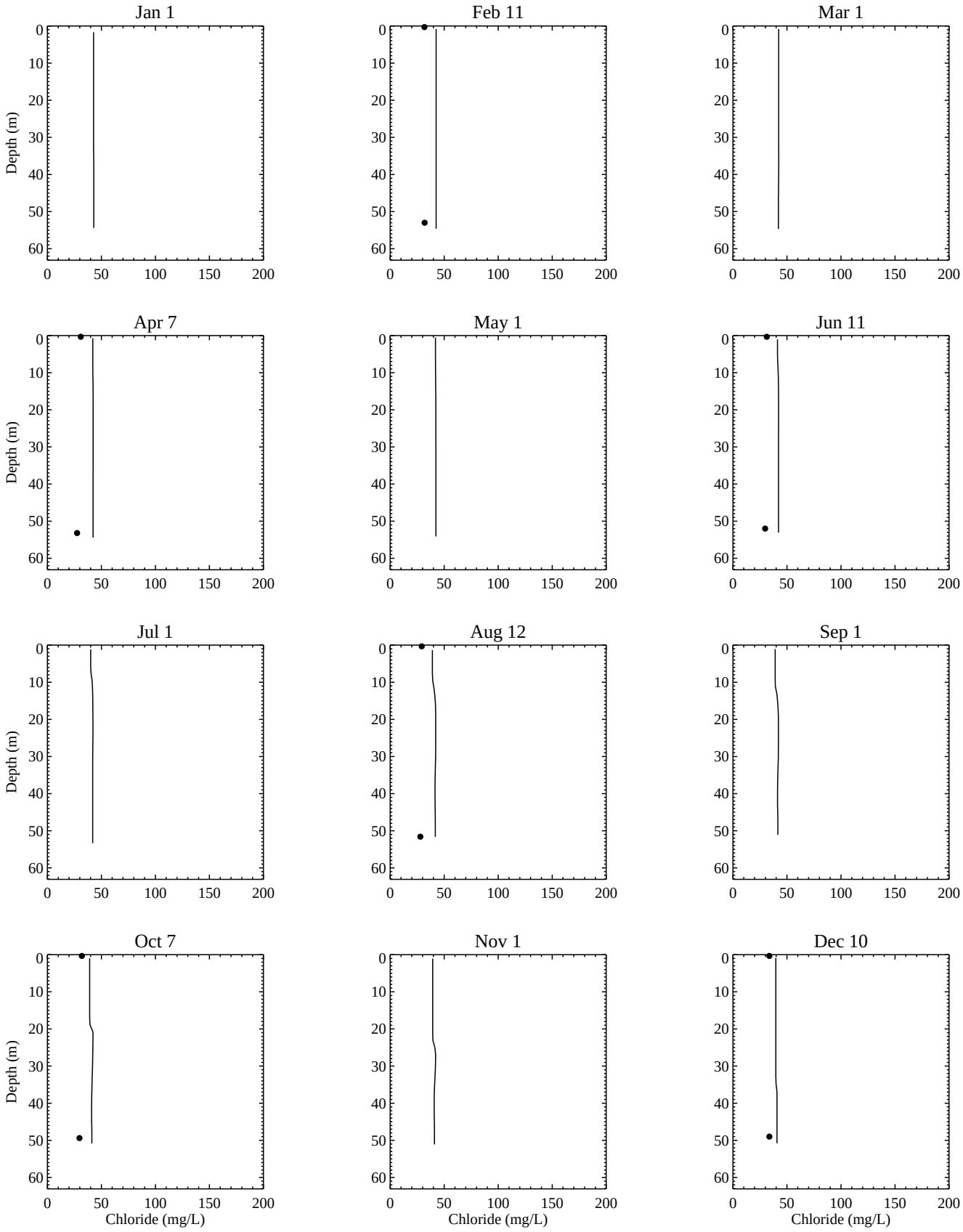

Figure J-11. Vertical profiles of model versus data at Mansfield Dam (Segment 93) - Chloride - 2003.

Profiles shown for dates with available data else model results for first day of month shown.

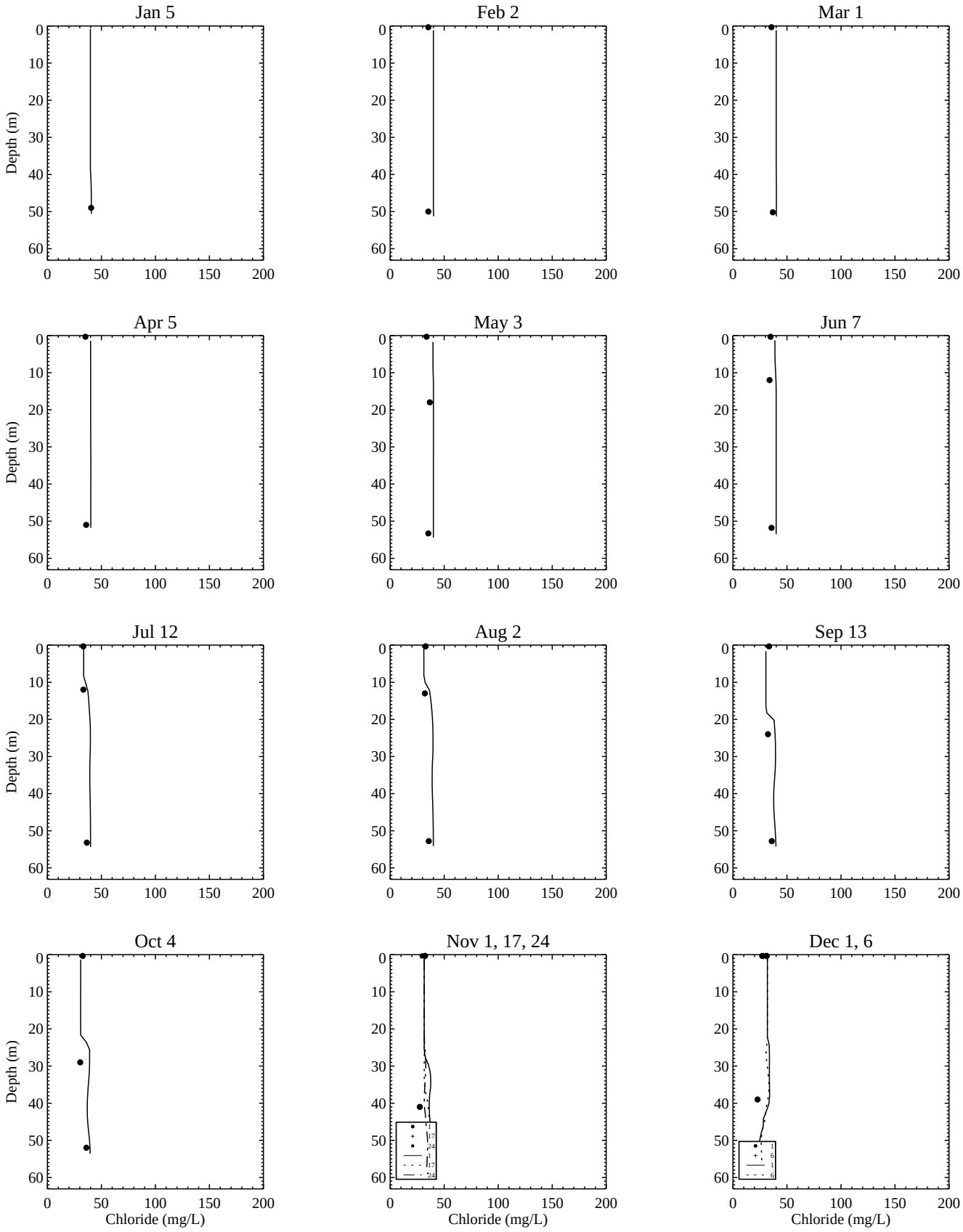

Figure J-11. Vertical profiles of model versus data at Mansfield Dam (Segment 93) - Chloride - 2004.

Profiles shown for dates with available data else model results for first day of month shown.

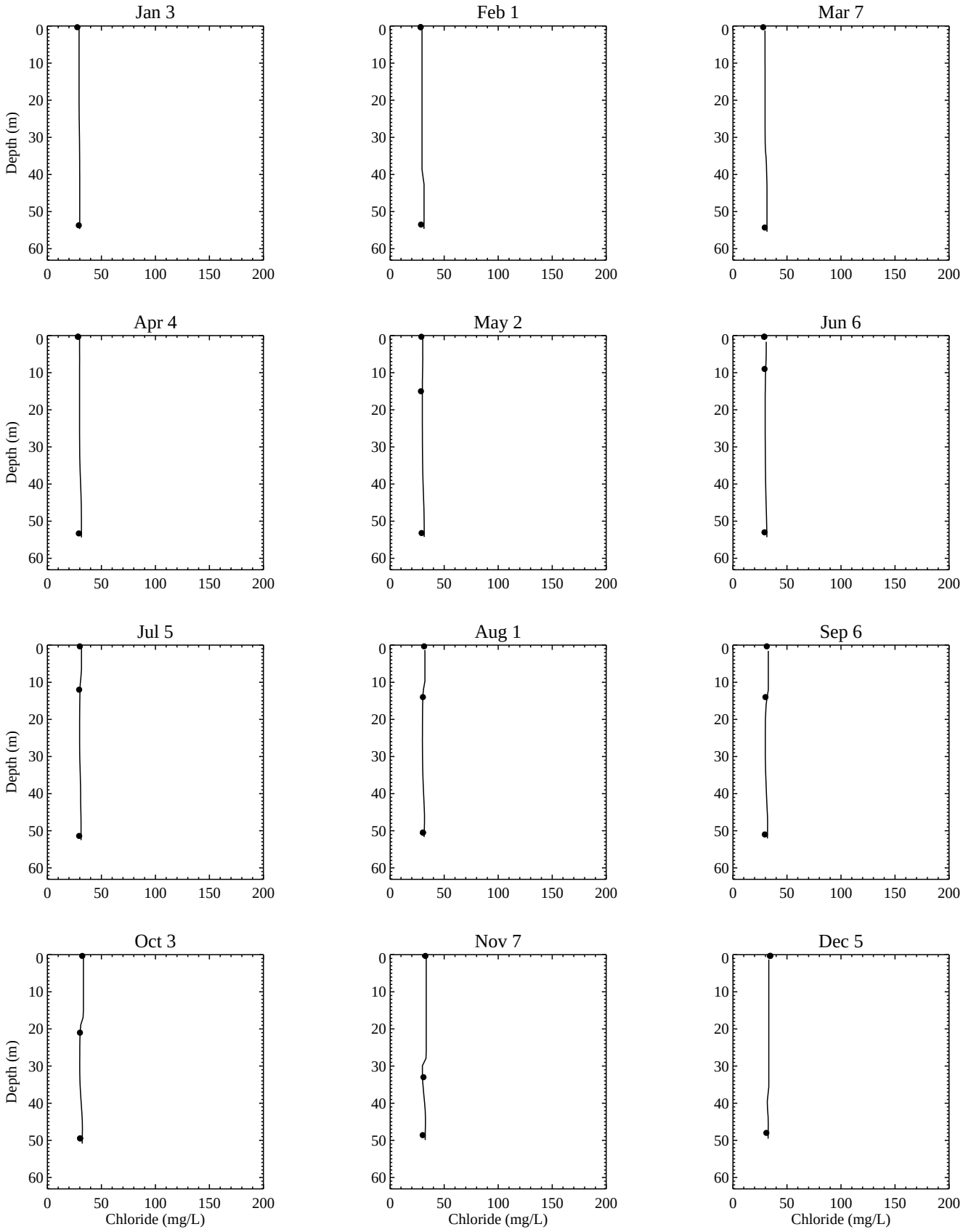

Figure J-11. Vertical profiles of model versus data at Mansfield Dam (Segment 93) - Chloride - 2005.

Profiles shown for dates with available data else model results for first day of month shown.

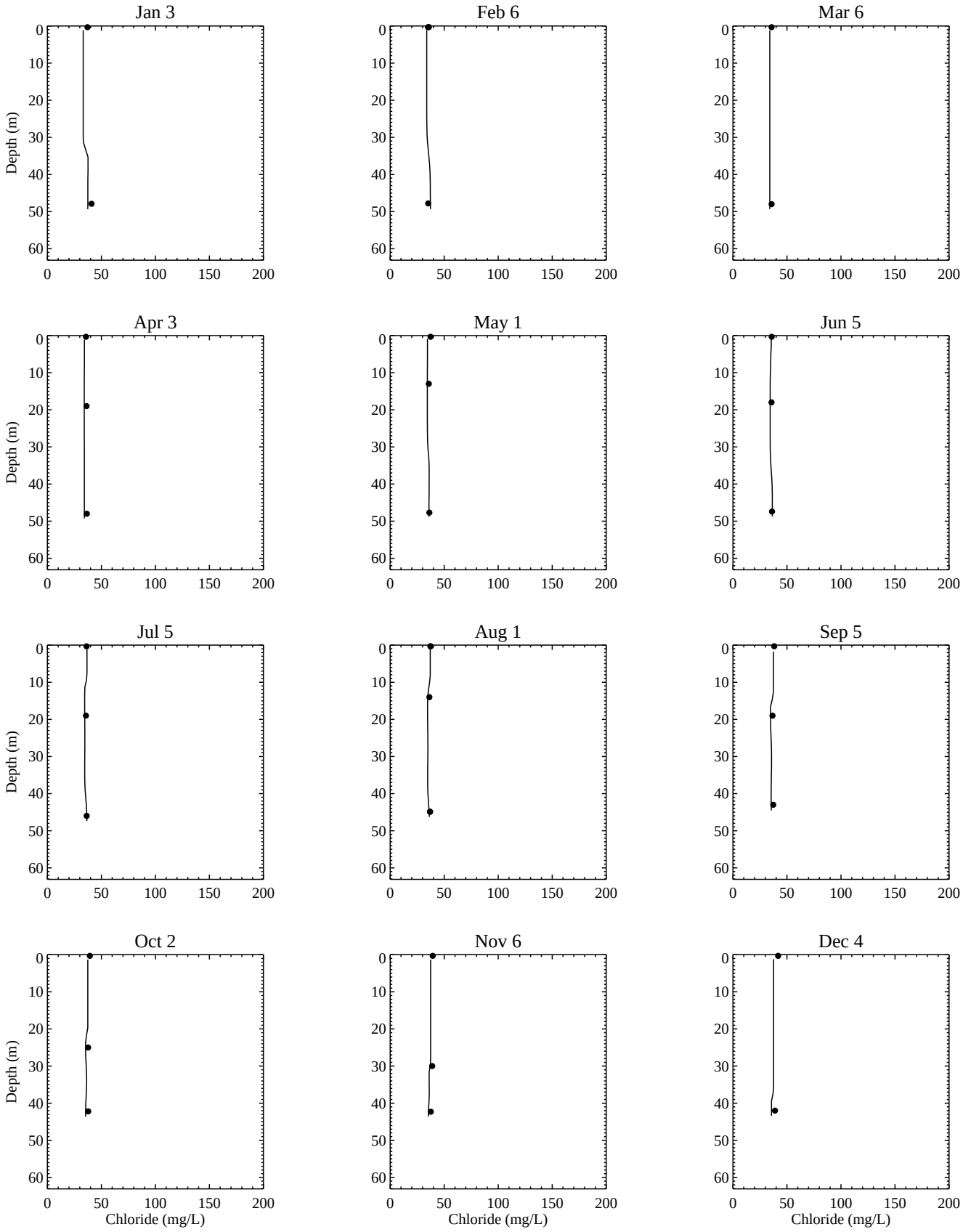

Figure J-11. Vertical profiles of model versus data at Mansfield Dam (Segment 93) - Chloride - 2006.

Profiles shown for dates with available data else model results for first day of month shown.

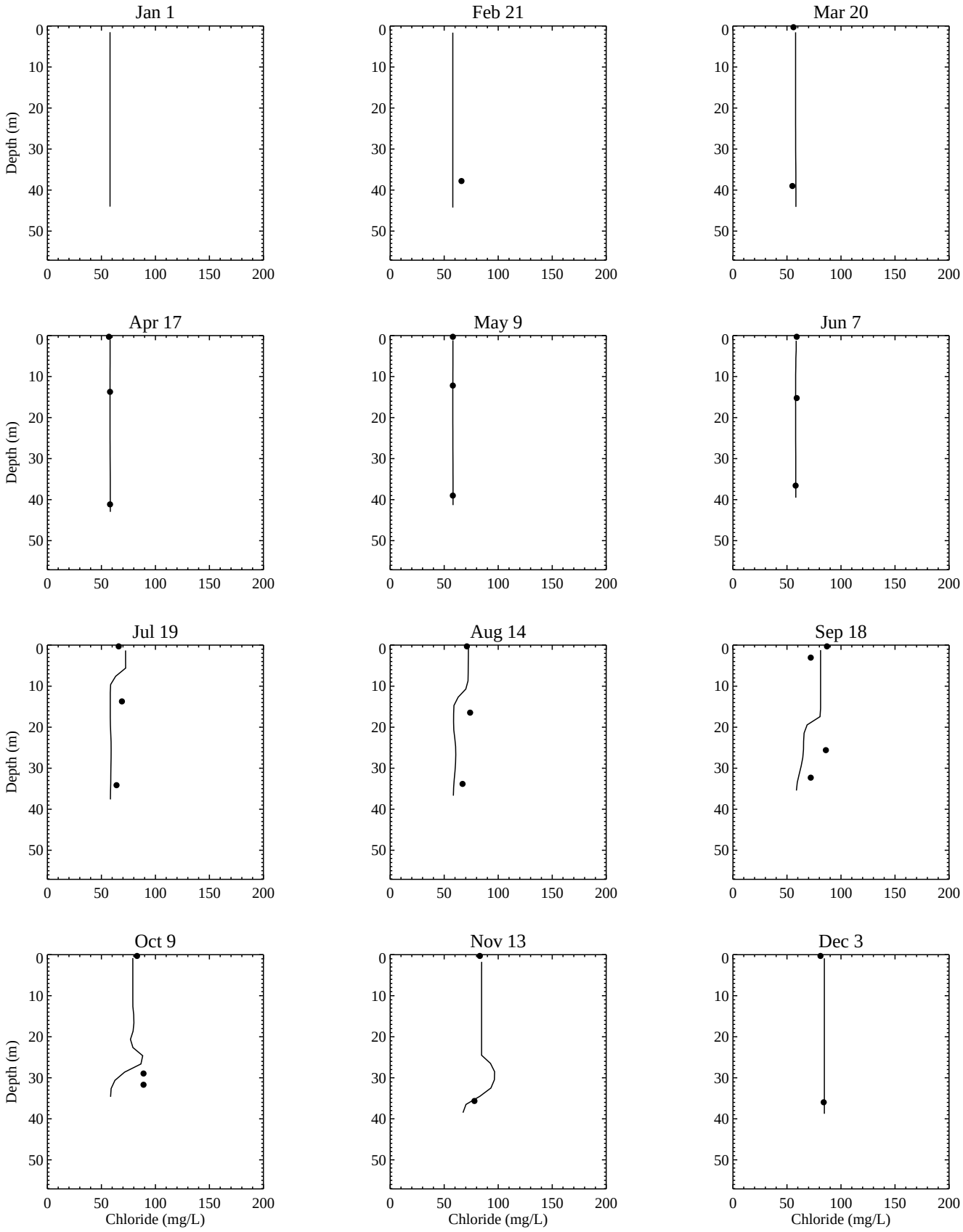

Figure J-12. Vertical profiles of model versus data at Arkansas Bend (Segment 78) - Chloride - 1984.

Profiles shown for dates with available data else model results for first day of month shown.

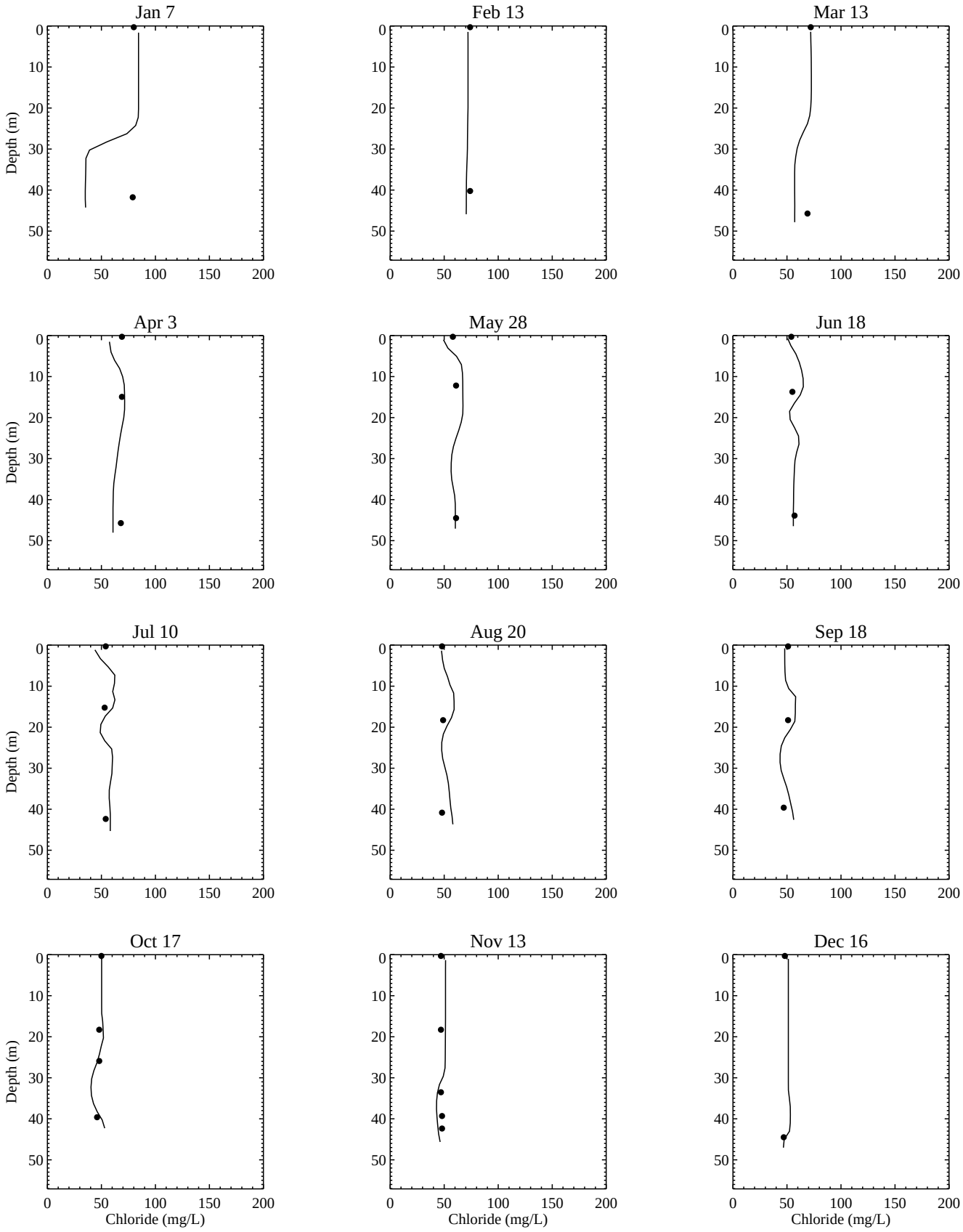

Figure J-12. Vertical profiles of model versus data at Arkansas Bend (Segment 78) - Chloride - 1985.

Profiles shown for dates with available data else model results for first day of month shown.

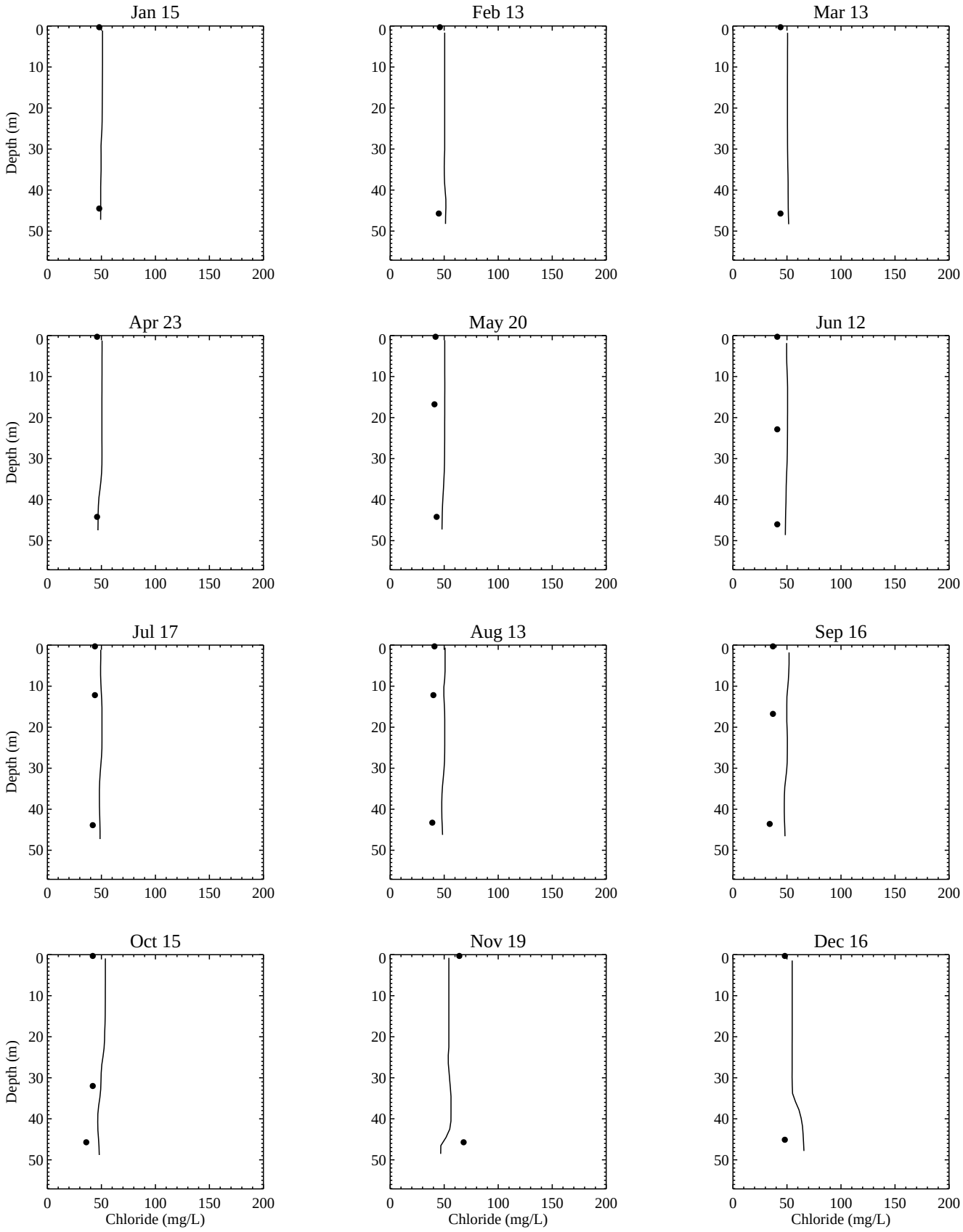

Figure J-12. Vertical profiles of model versus data at Arkansas Bend (Segment 78) - Chloride - 1986.

Profiles shown for dates with available data else model results for first day of month shown.

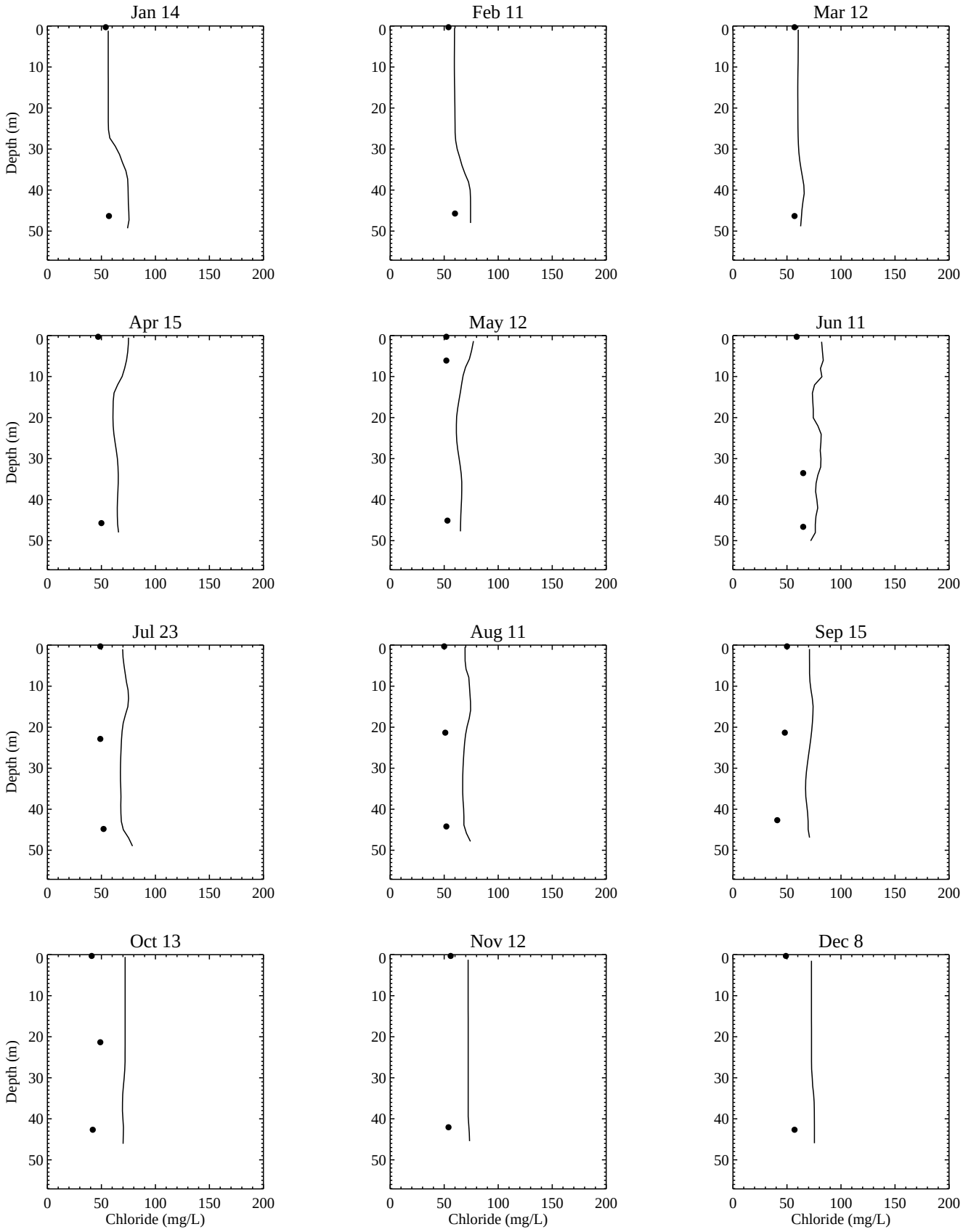

Figure J-12. Vertical profiles of model versus data at Arkansas Bend (Segment 78) - Chloride - 1987.

Profiles shown for dates with available data else model results for first day of month shown.

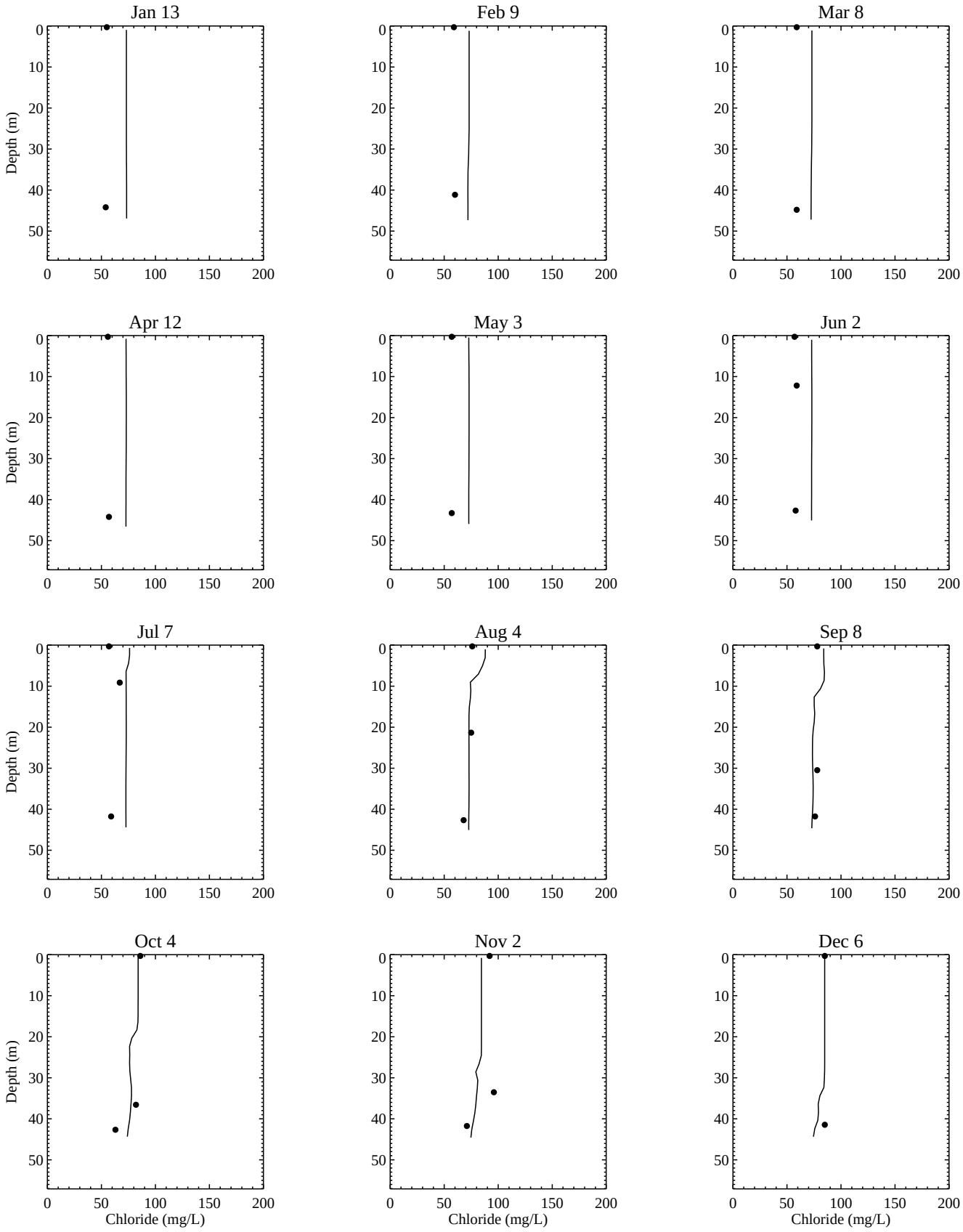

Figure J-12. Vertical profiles of model versus data at Arkansas Bend (Segment 78) - Chloride - 1988.

Profiles shown for dates with available data else model results for first day of month shown.

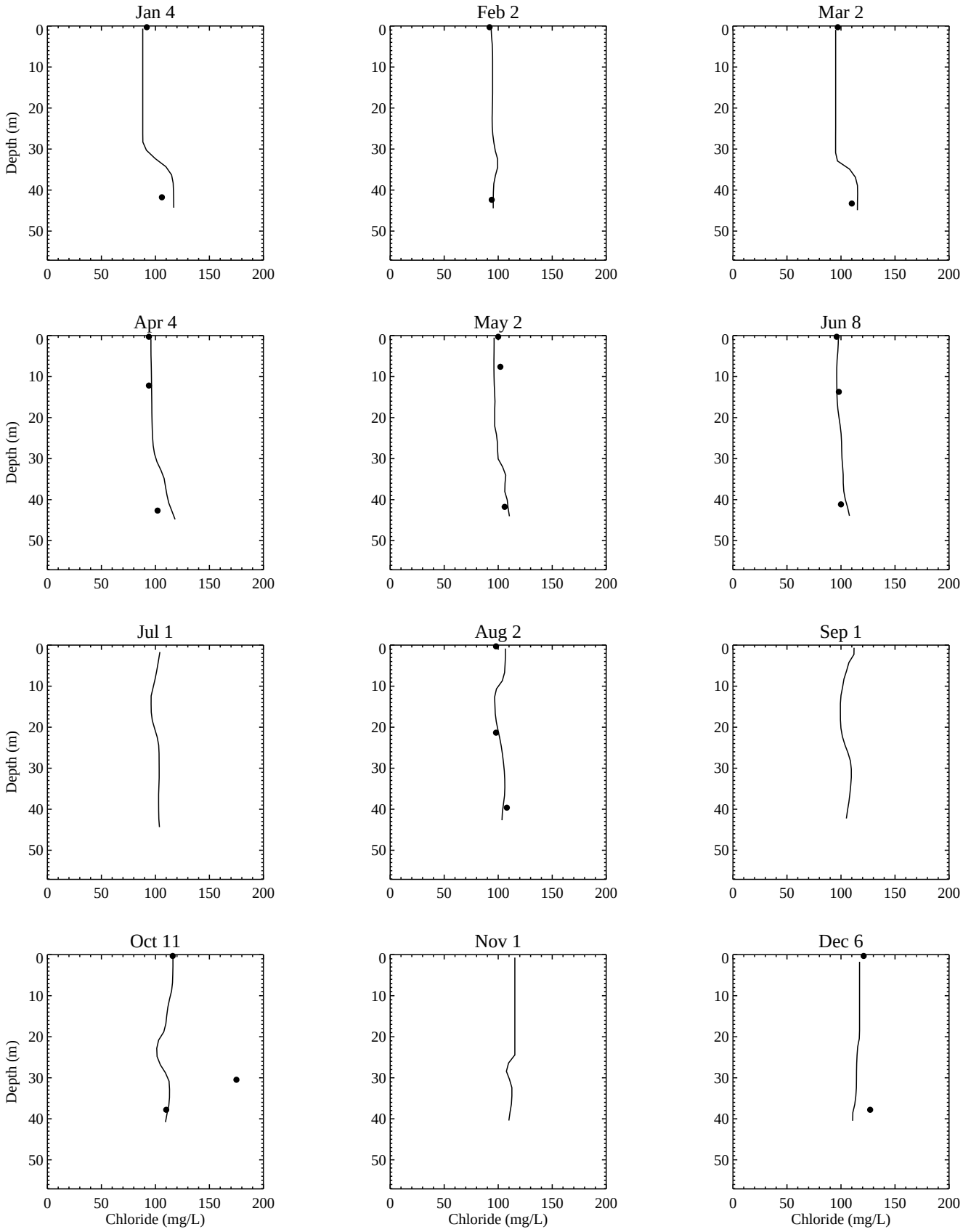

Figure J-12. Vertical profiles of model versus data at Arkansas Bend (Segment 78) - Chloride - 1989.

Profiles shown for dates with available data else model results for first day of month shown.

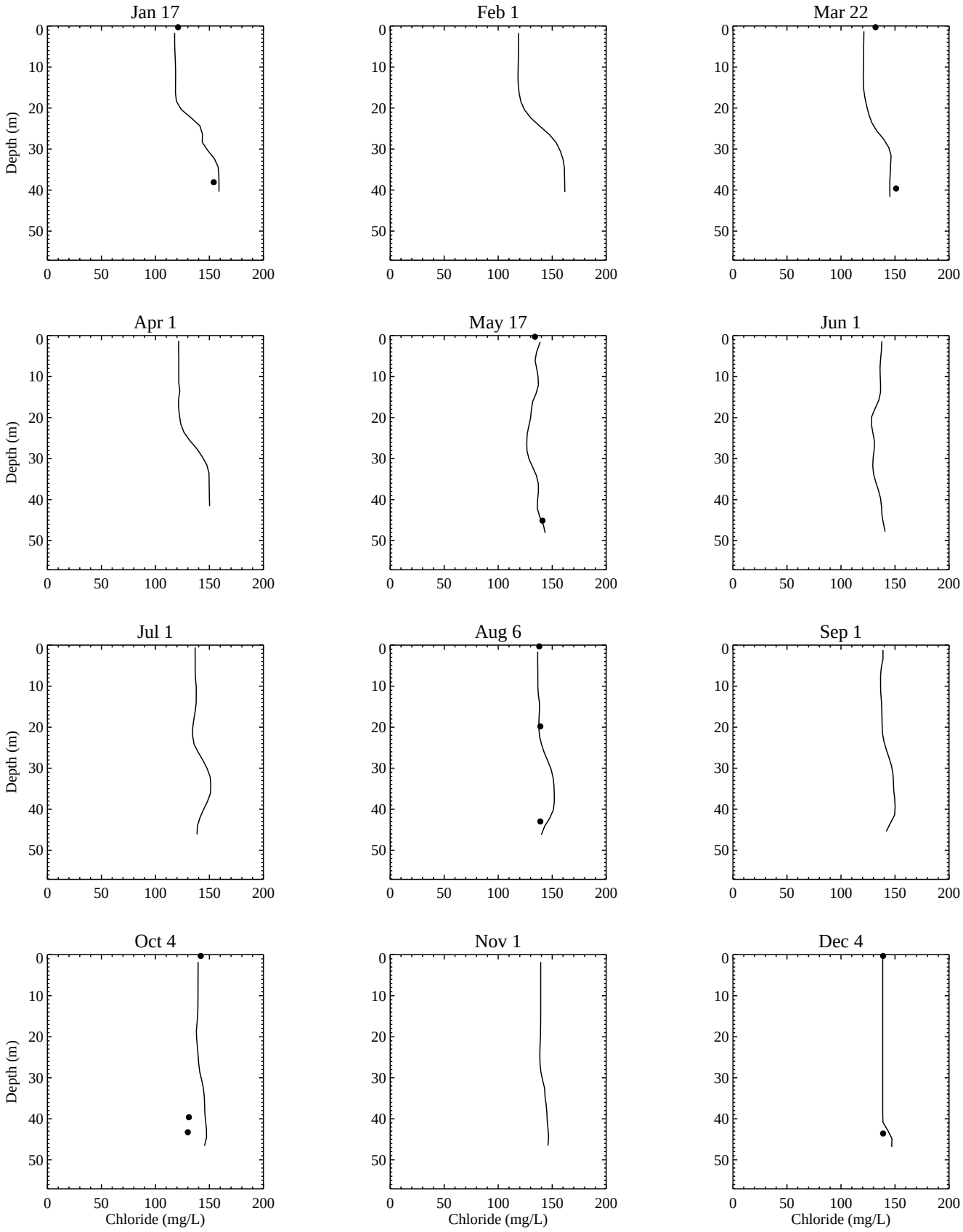

Figure J-12. Vertical profiles of model versus data at Arkansas Bend (Segment 78) - Chloride - 1990.

Profiles shown for dates with available data else model results for first day of month shown.

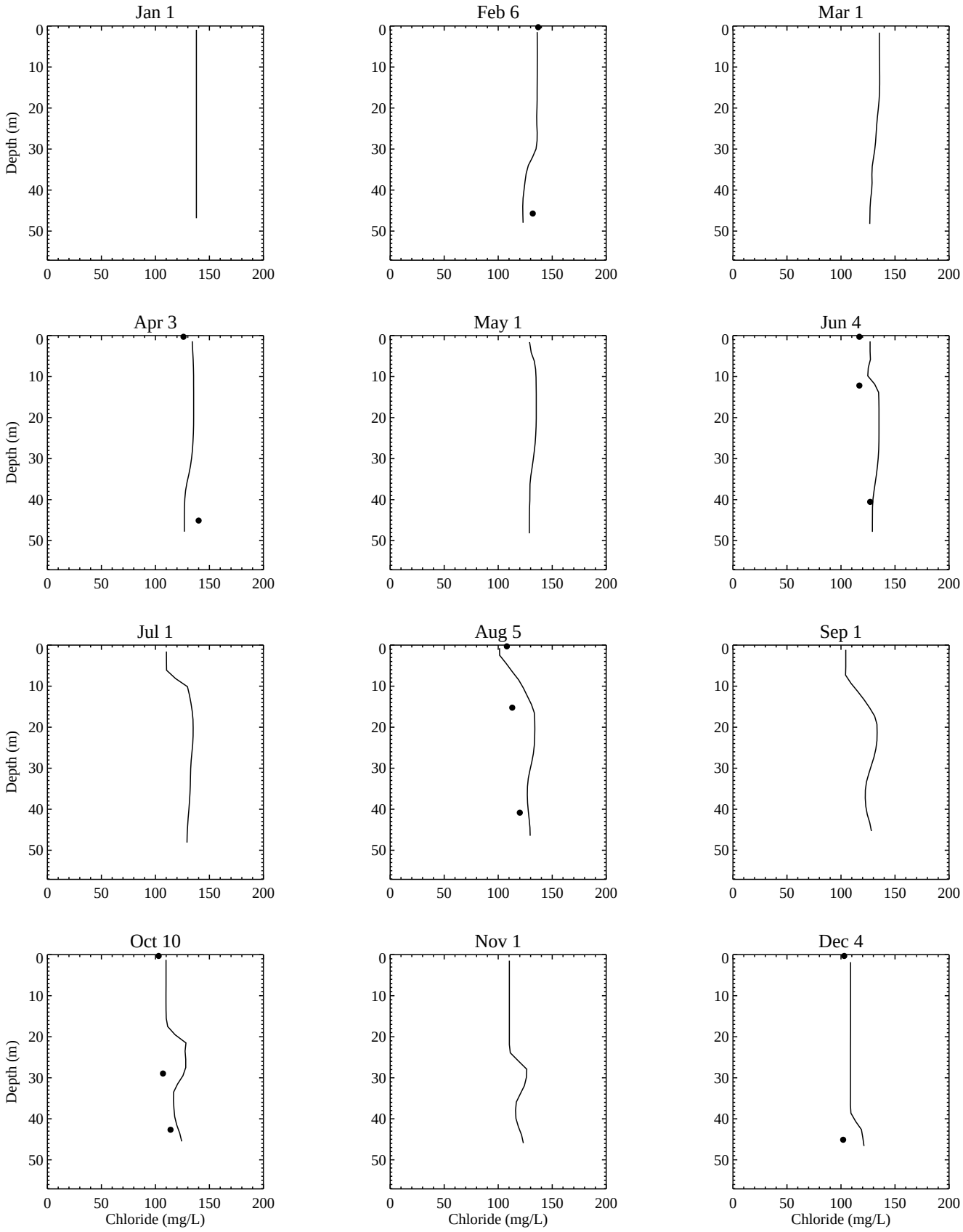

Figure J-12. Vertical profiles of model versus data at Arkansas Bend (Segment 78) - Chloride - 1991.

Profiles shown for dates with available data else model results for first day of month shown.

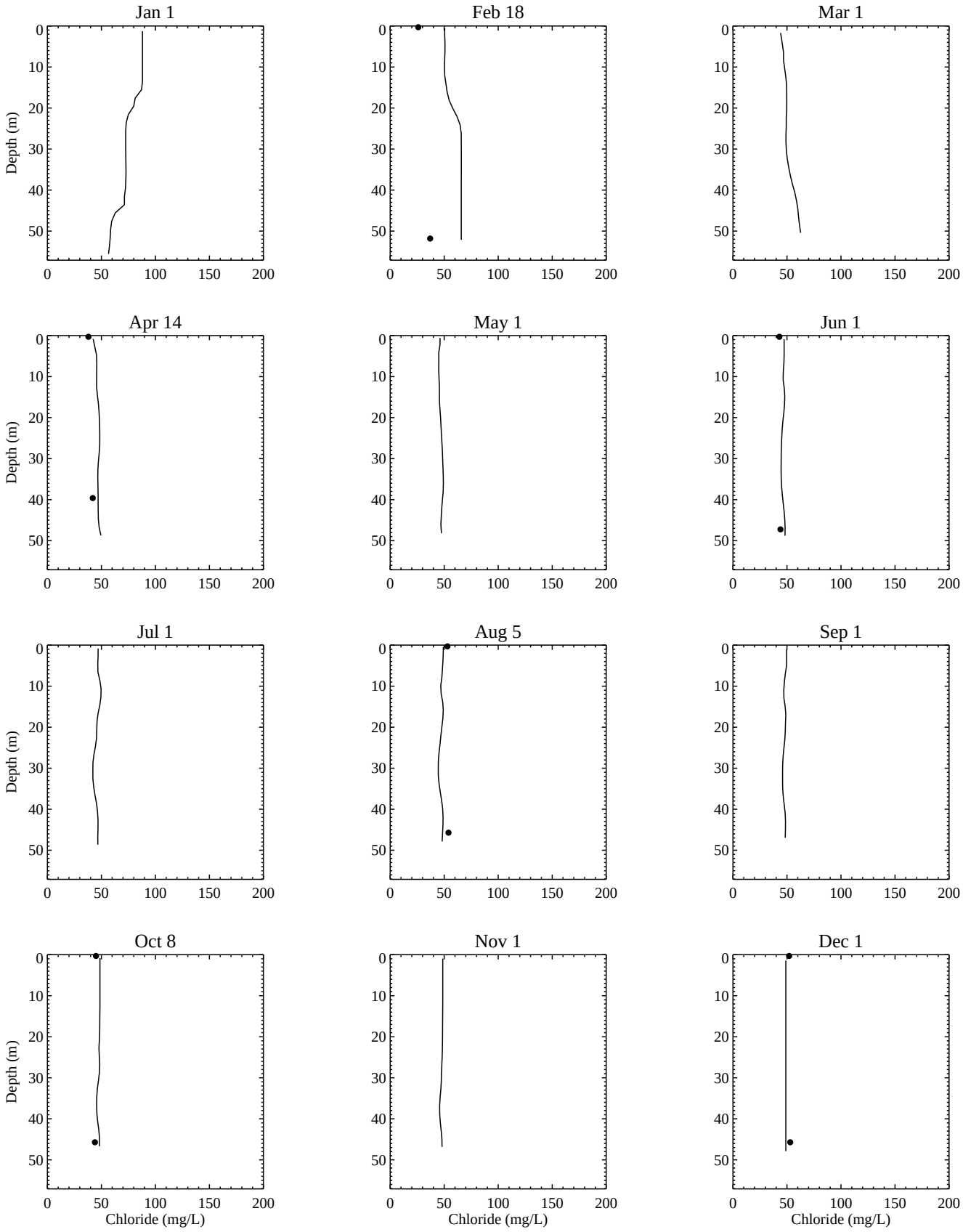

Figure J-12. Vertical profiles of model versus data at Arkansas Bend (Segment 78) - Chloride - 1992.

Profiles shown for dates with available data else model results for first day of month shown.

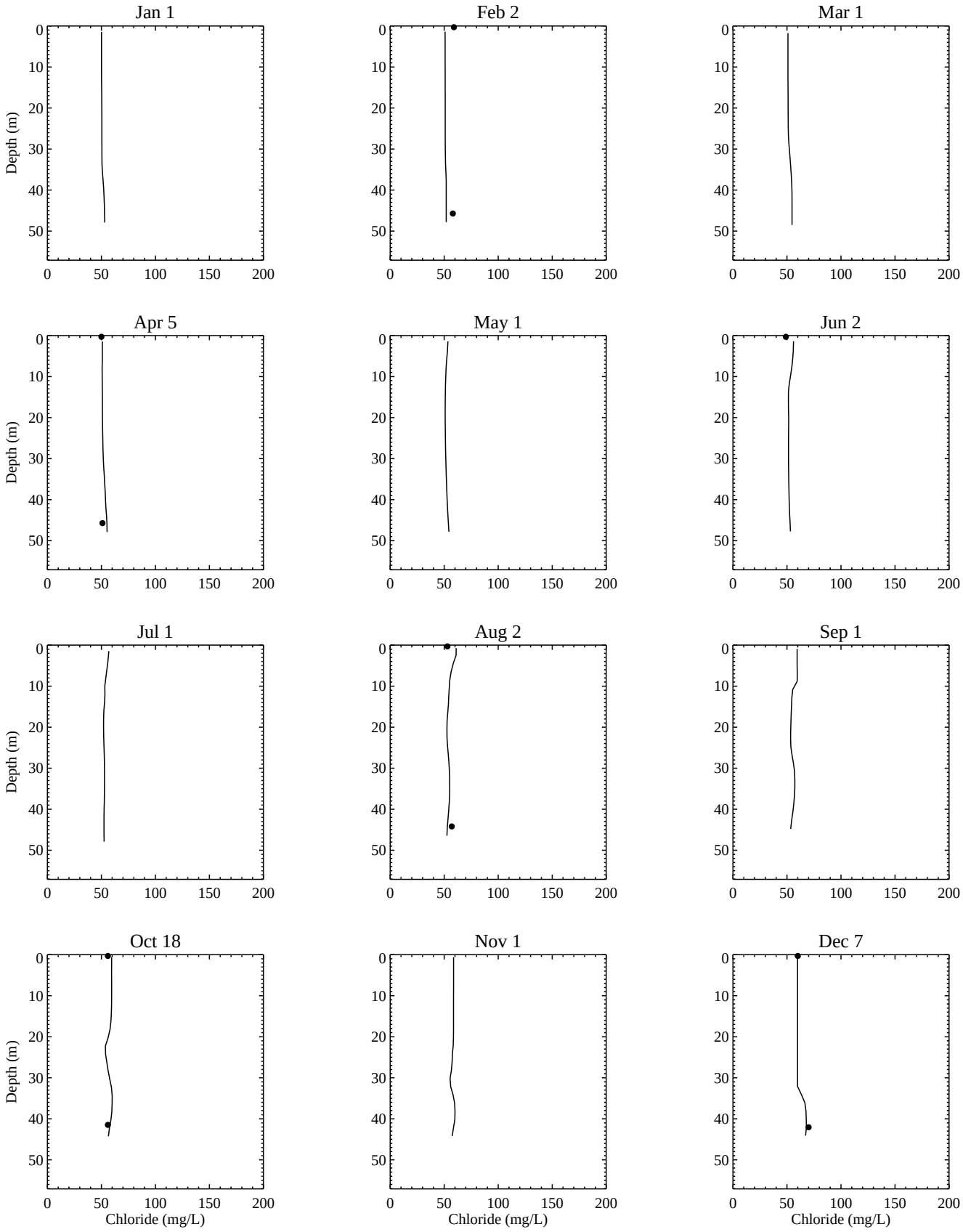

Figure J-12. Vertical profiles of model versus data at Arkansas Bend (Segment 78) - Chloride - 1993.

Profiles shown for dates with available data else model results for first day of month shown.

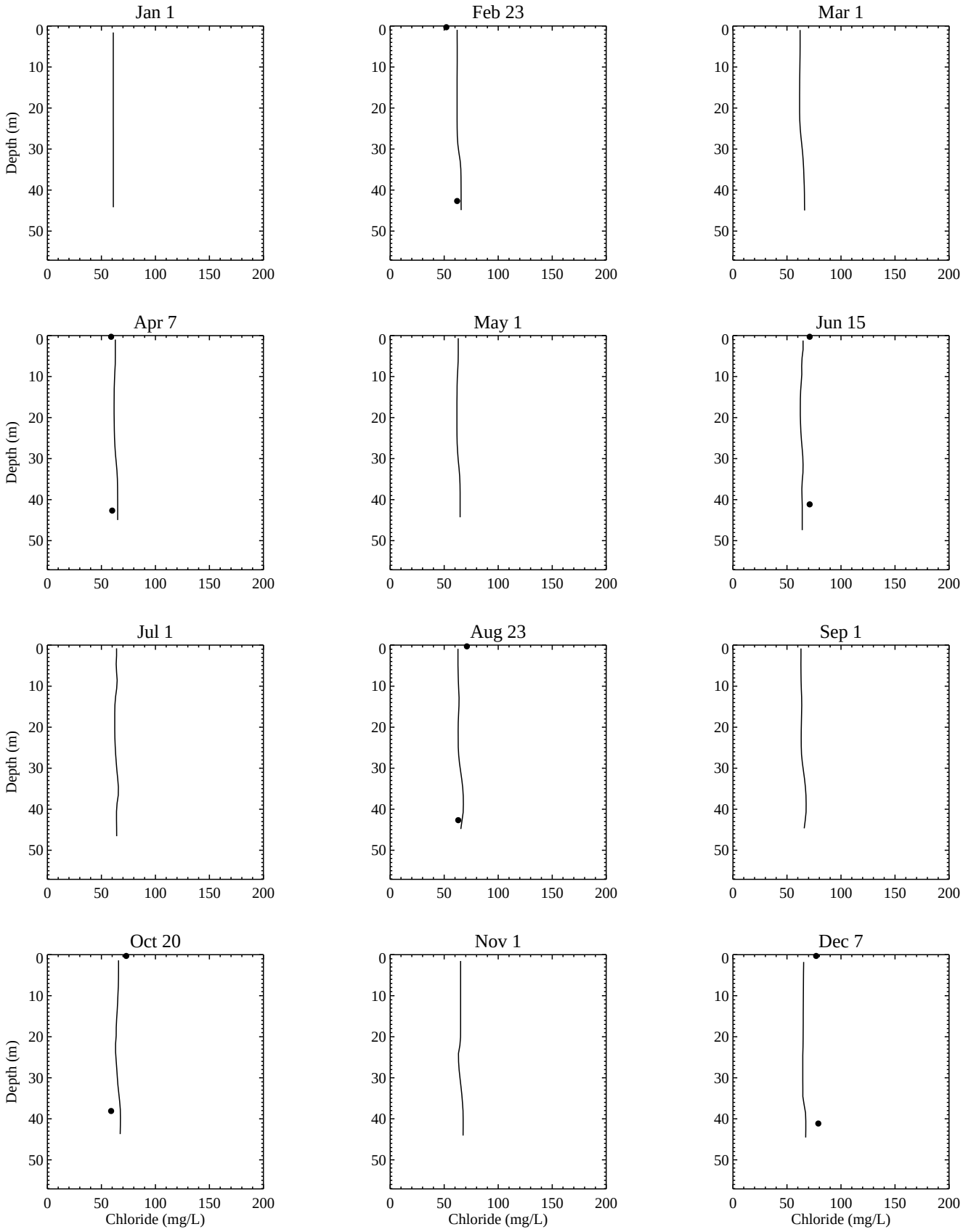

Figure J-12. Vertical profiles of model versus data at Arkansas Bend (Segment 78) - Chloride - 1994.

Profiles shown for dates with available data else model results for first day of month shown.

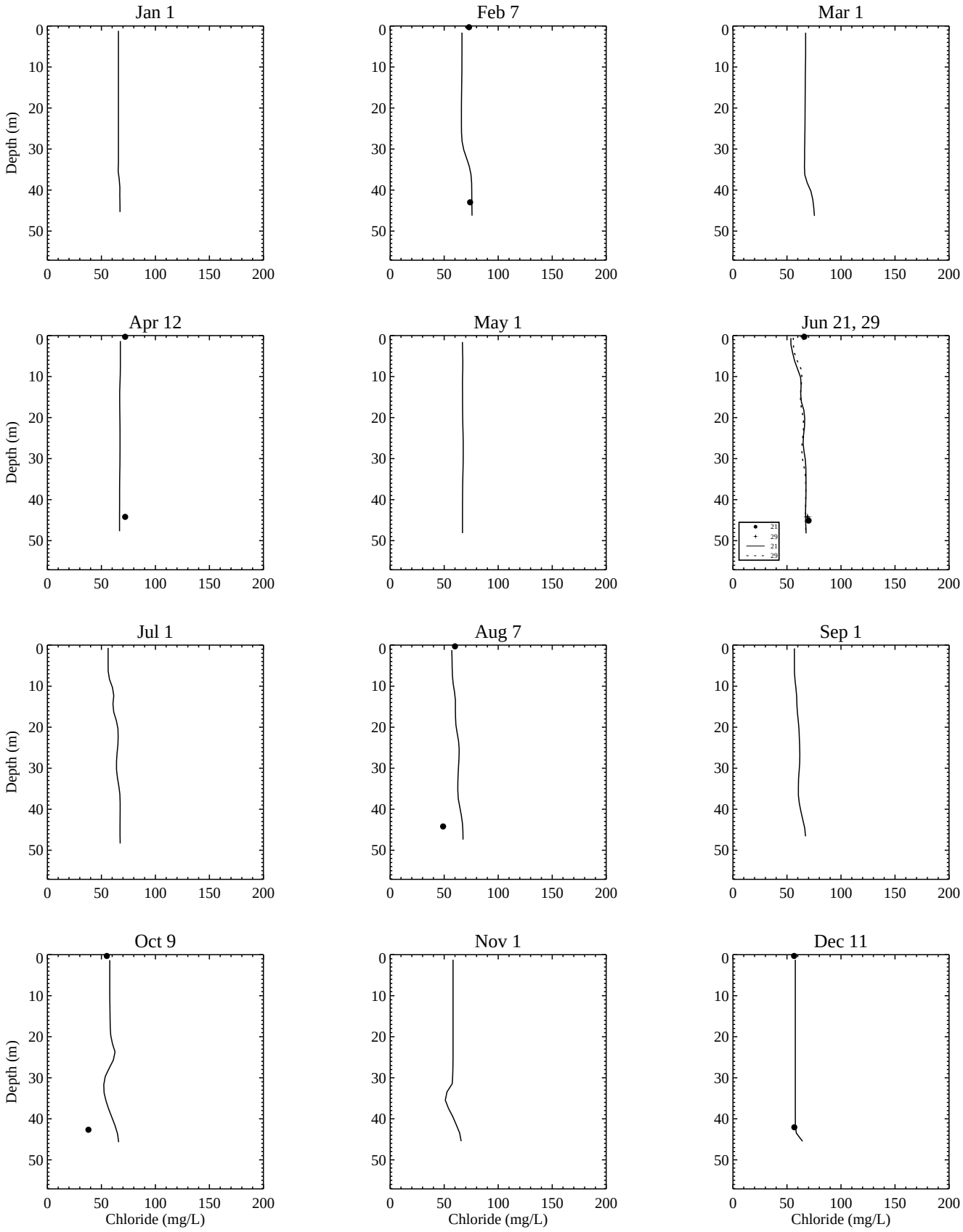

Figure J-12. Vertical profiles of model versus data at Arkansas Bend (Segment 78) - Chloride - 1995.

Profiles shown for dates with available data else model results for first day of month shown.

Model Data

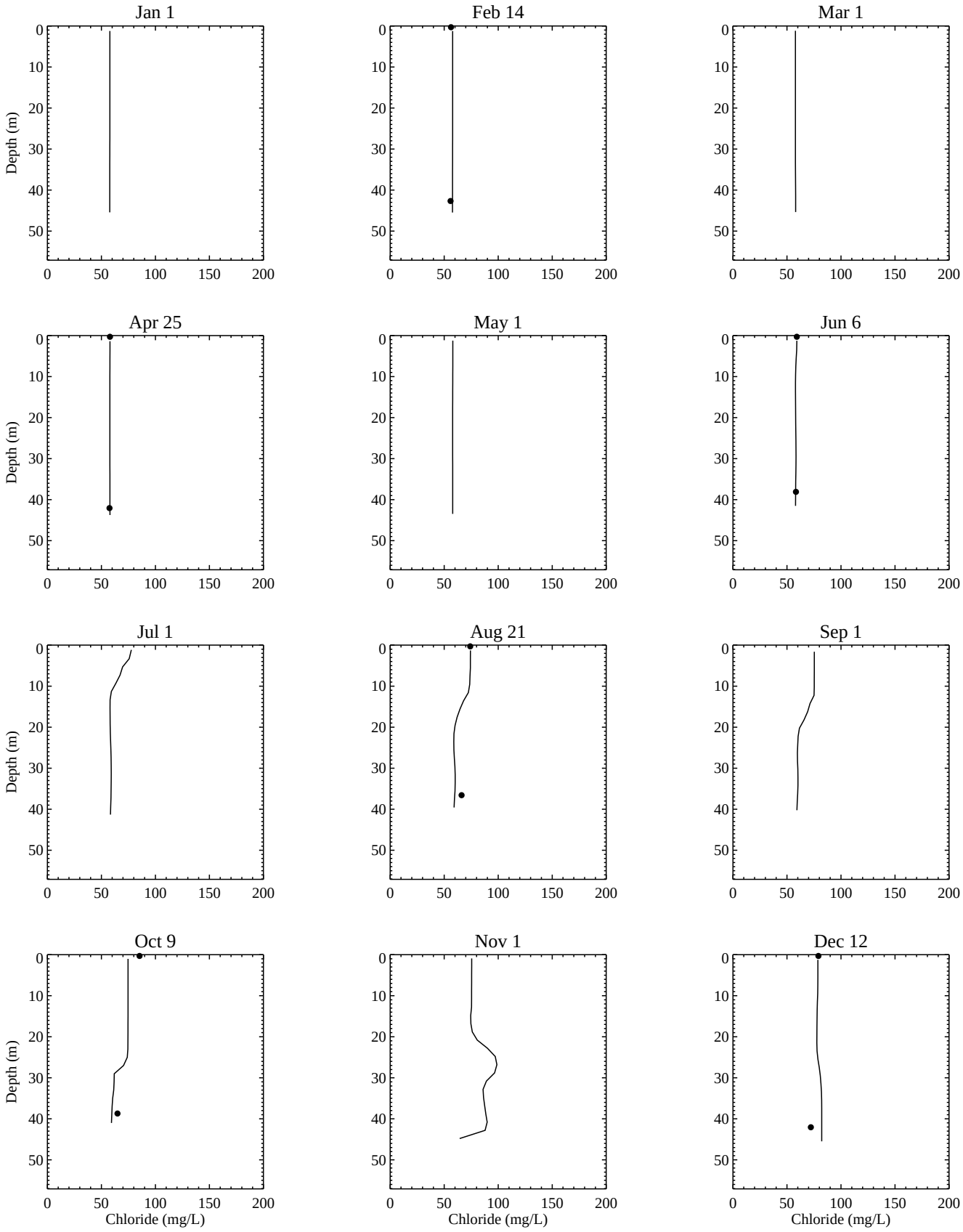

Figure J-12. Vertical profiles of model versus data at Arkansas Bend (Segment 78) - Chloride - 1996.

Profiles shown for dates with available data else model results for first day of month shown.

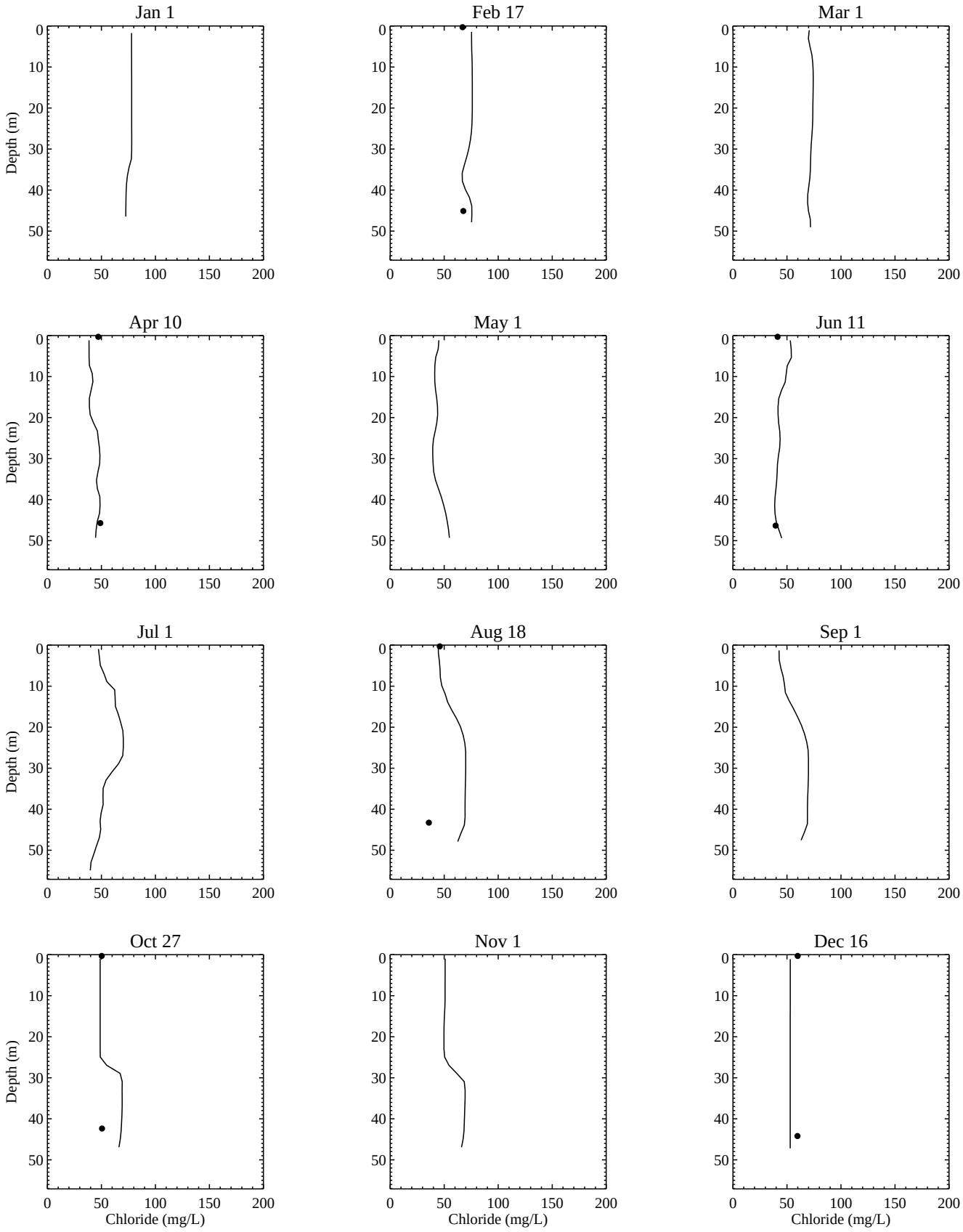

Figure J-12. Vertical profiles of model versus data at Arkansas Bend (Segment 78) - Chloride - 1997.

Profiles shown for dates with available data else model results for first day of month shown.

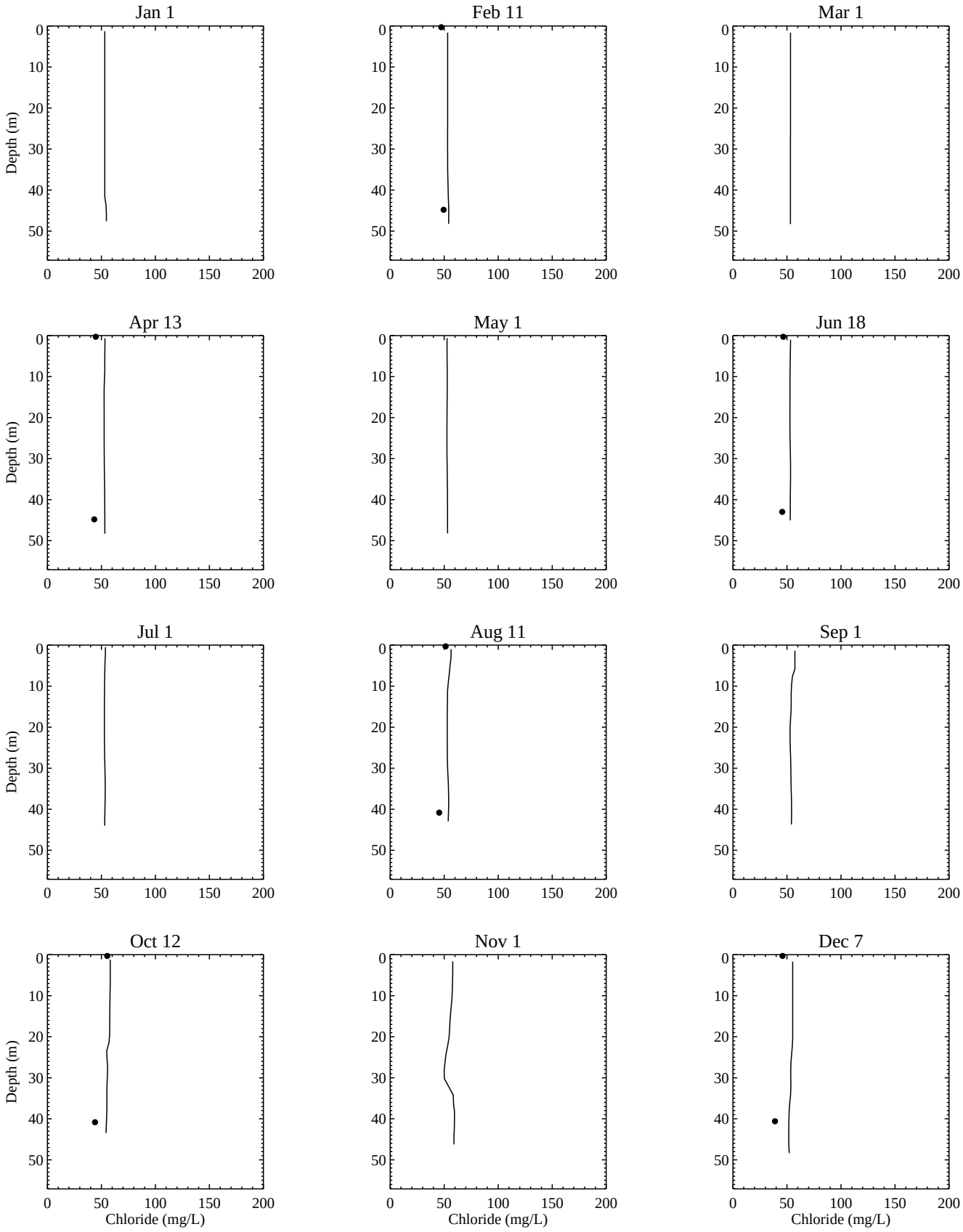

Figure J-12. Vertical profiles of model versus data at Arkansas Bend (Segment 78) - Chloride - 1998.

Profiles shown for dates with available data else model results for first day of month shown.

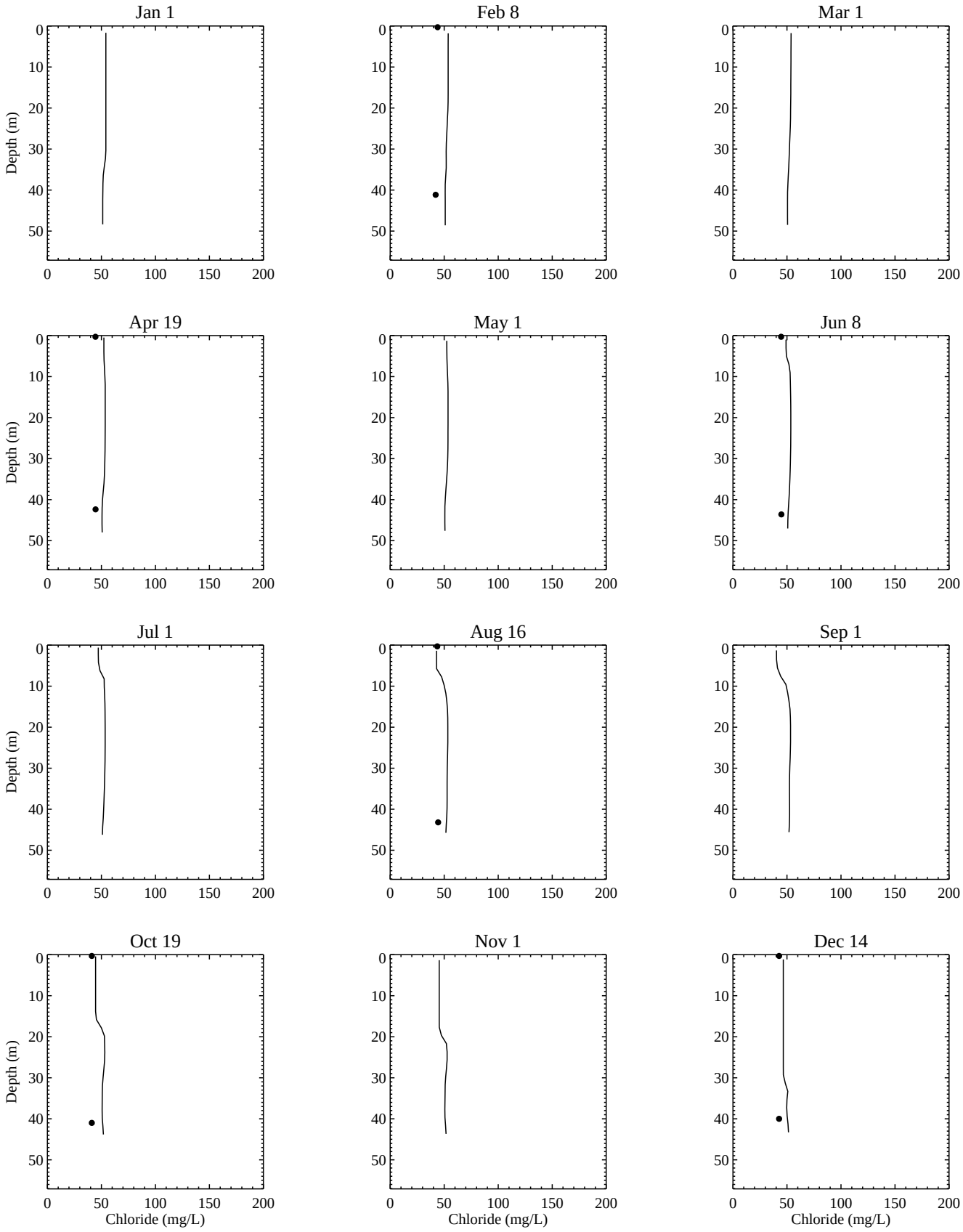

Figure J-12. Vertical profiles of model versus data at Arkansas Bend (Segment 78) - Chloride - 1999.

Profiles shown for dates with available data else model results for first day of month shown.

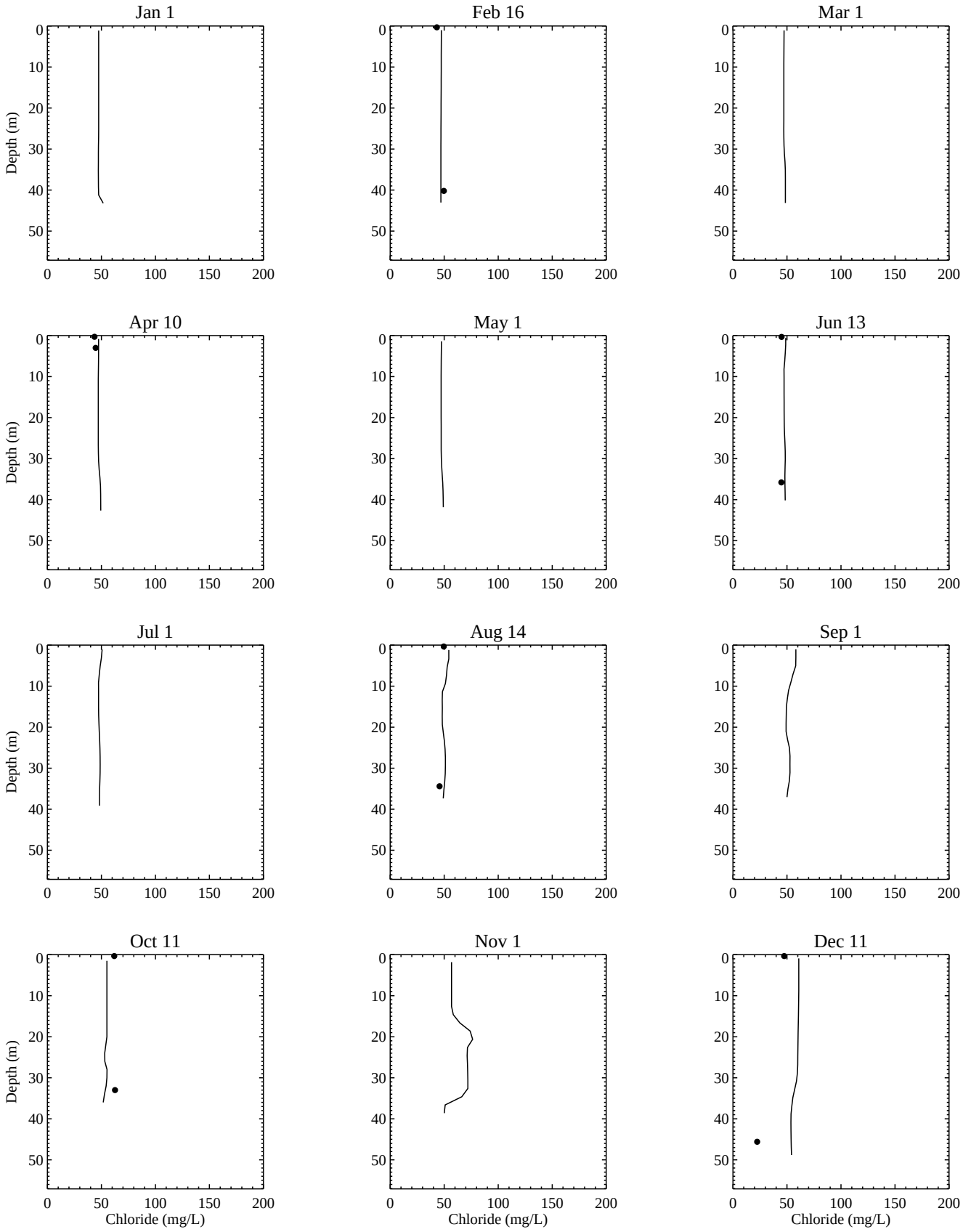

Figure J-12. Vertical profiles of model versus data at Arkansas Bend (Segment 78) - Chloride - 2000.

Profiles shown for dates with available data else model results for first day of month shown.

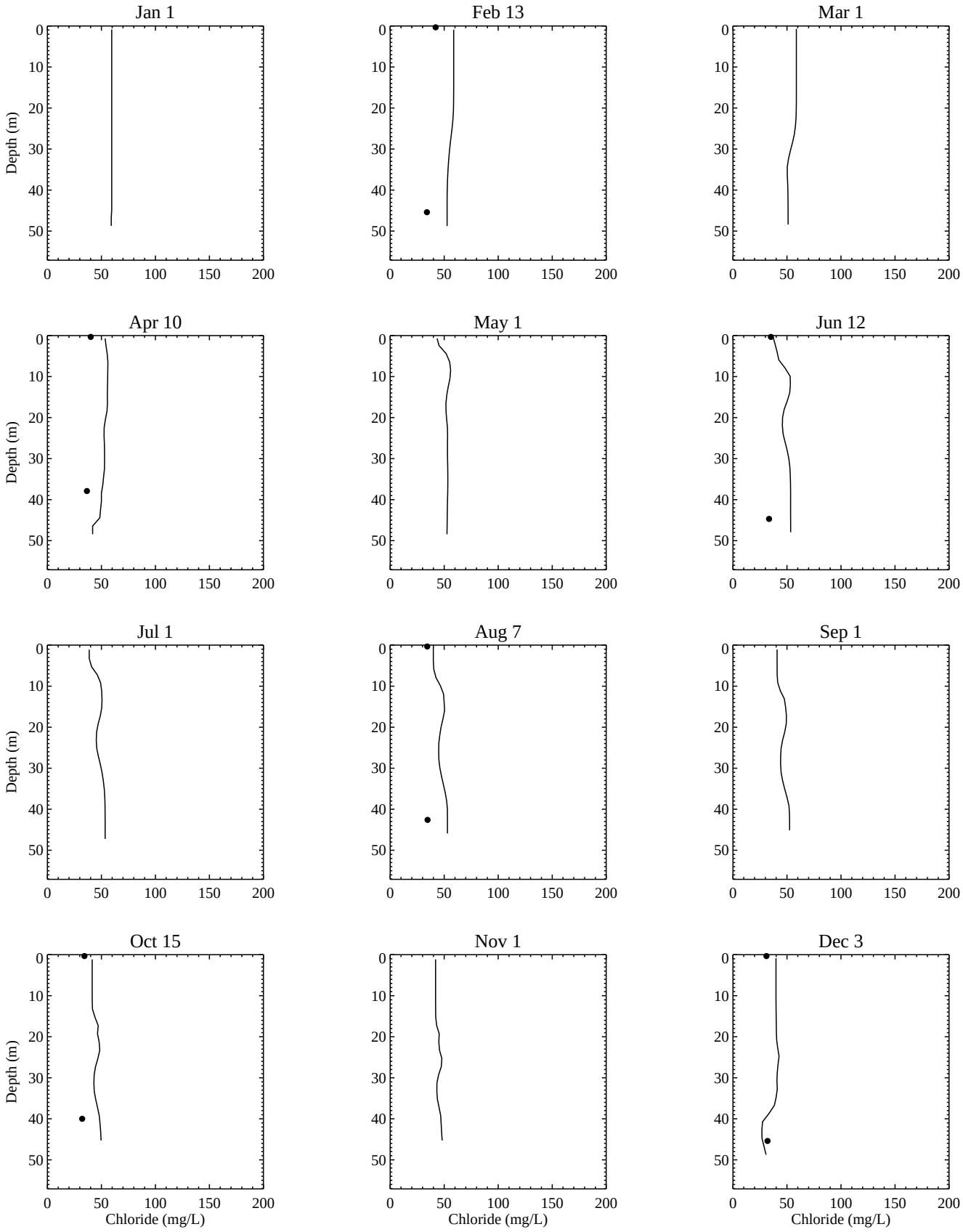

Figure J-12. Vertical profiles of model versus data at Arkansas Bend (Segment 78) - Chloride - 2001.

Profiles shown for dates with available data else model results for first day of month shown.

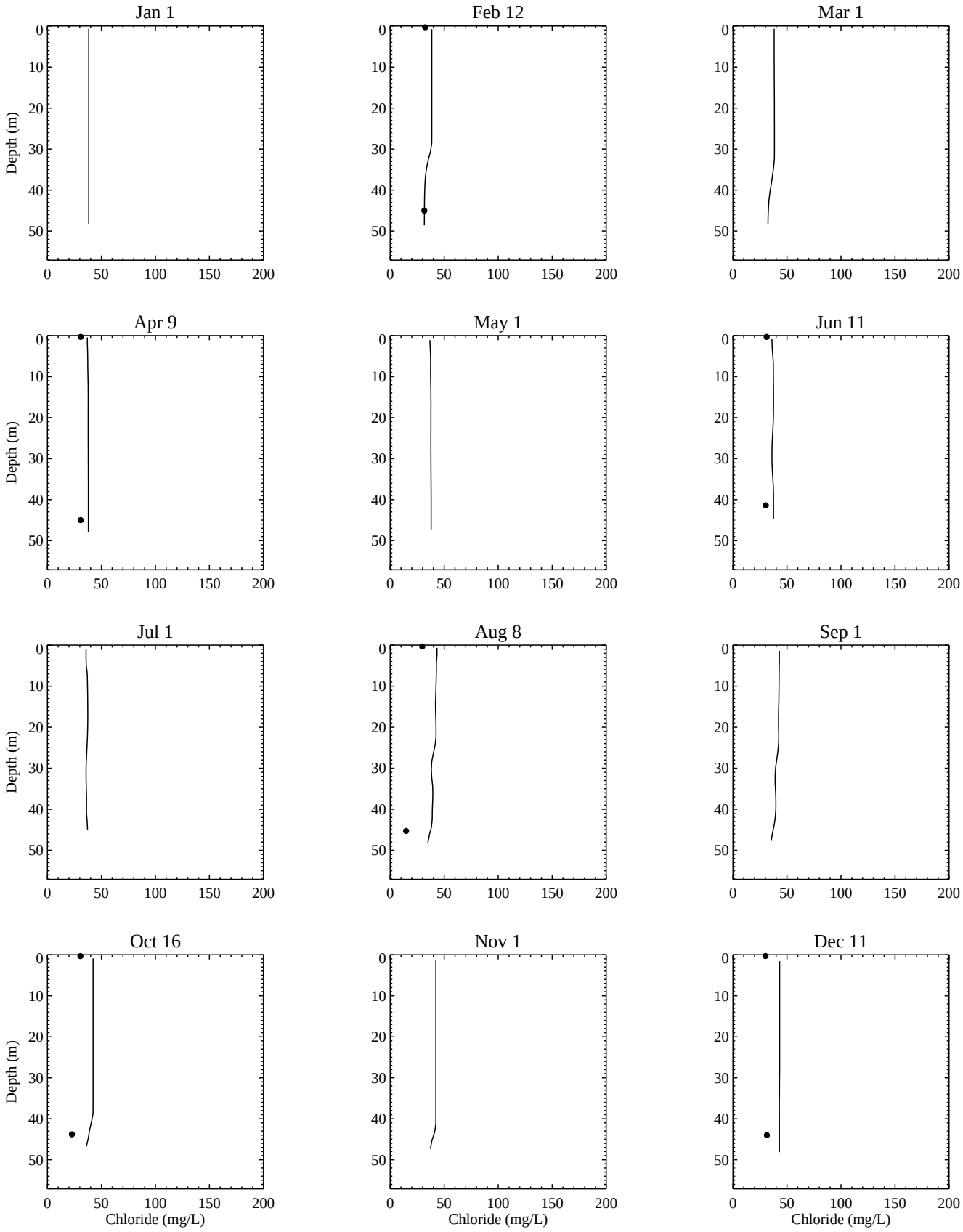

Figure J-12. Vertical profiles of model versus data at Arkansas Bend (Segment 78) - Chloride - 2002.

Profiles shown for dates with available data else model results for first day of month shown.

Model Data

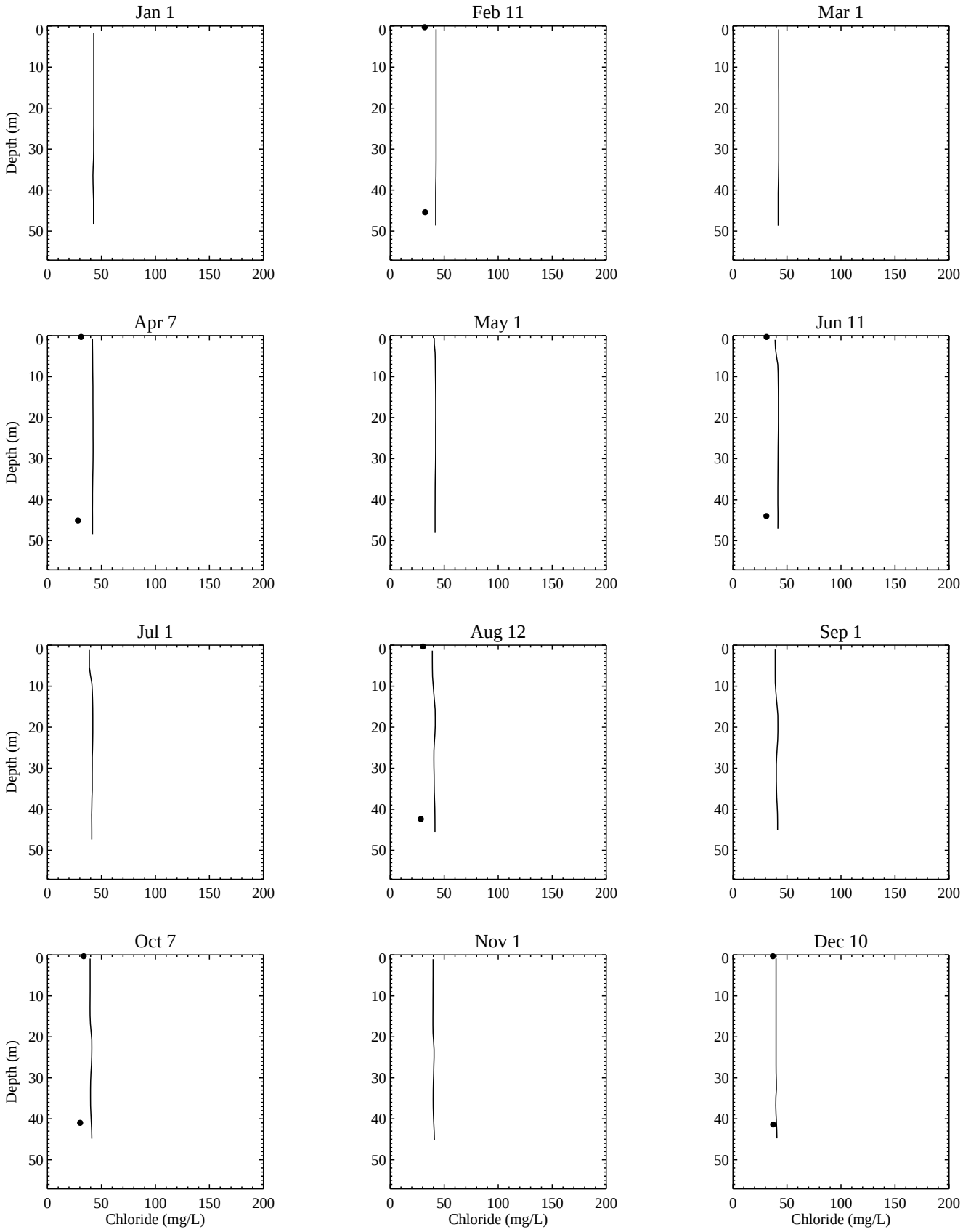

Figure J-12. Vertical profiles of model versus data at Arkansas Bend (Segment 78) - Chloride - 2003.

Profiles shown for dates with available data else model results for first day of month shown.

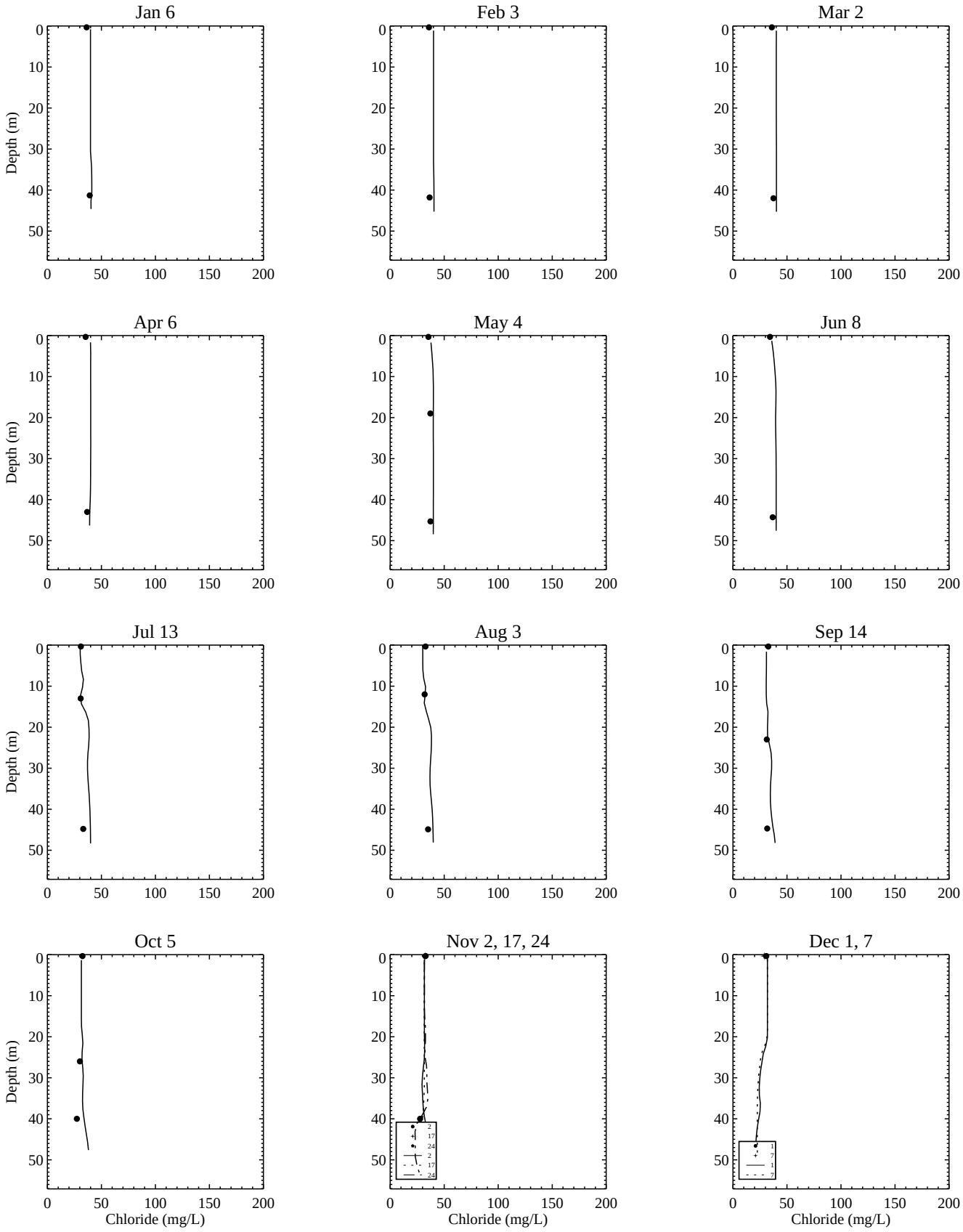

Figure J-12. Vertical profiles of model versus data at Arkansas Bend (Segment 78) - Chloride - 2004.

Profiles shown for dates with available data else model results for first day of month shown.

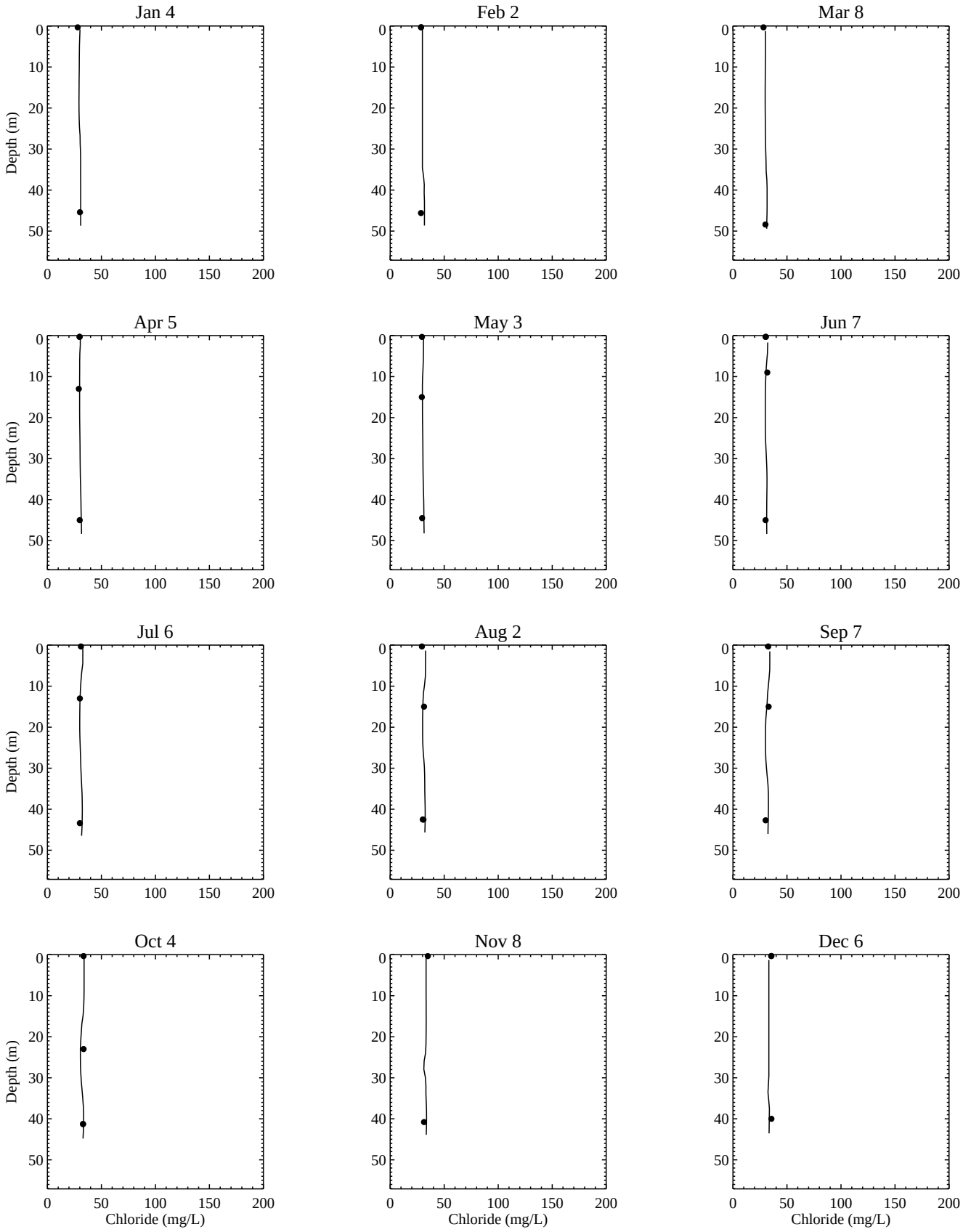

Figure J-12. Vertical profiles of model versus data at Arkansas Bend (Segment 78) - Chloride - 2005.

Profiles shown for dates with available data else model results for first day of month shown.

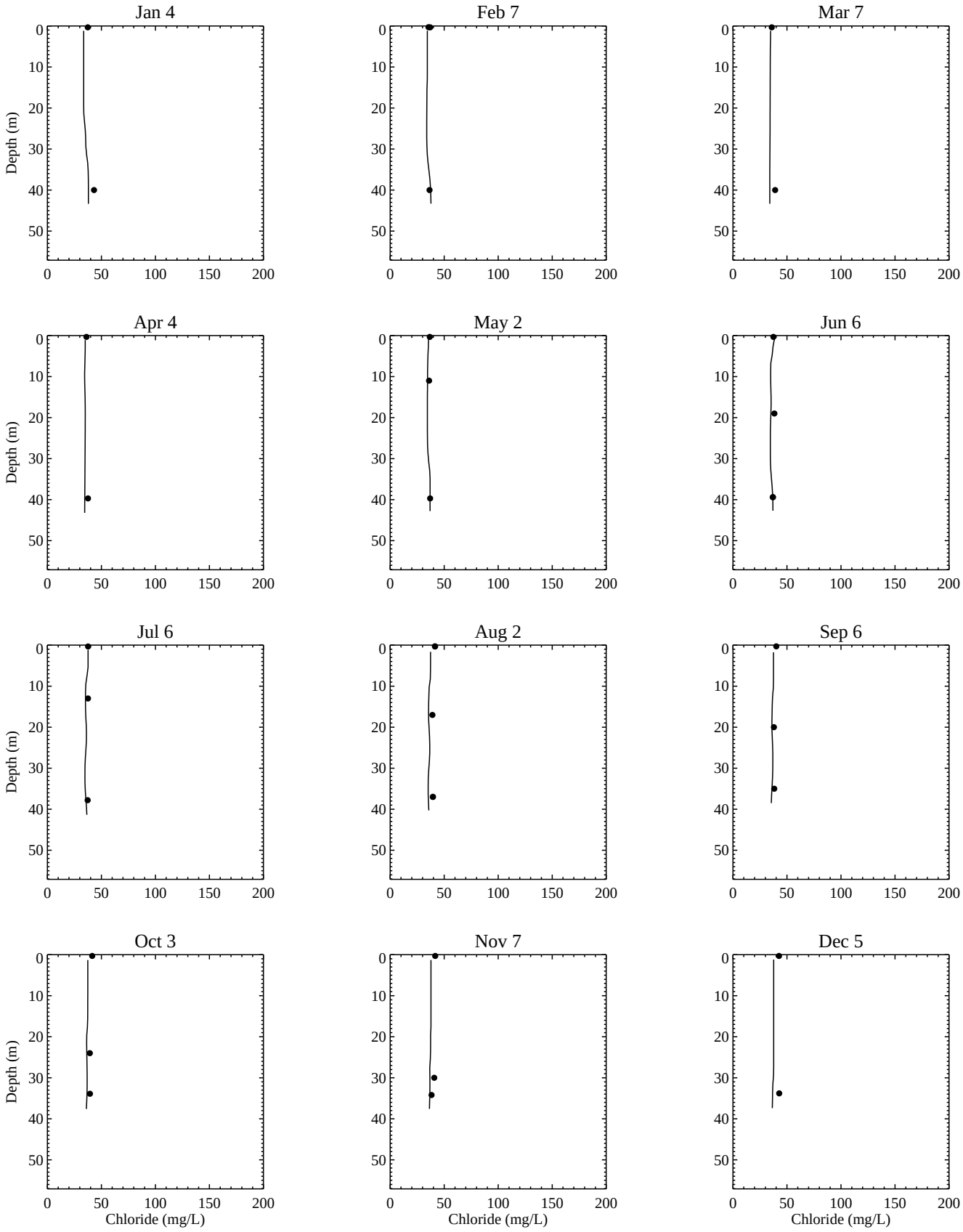

Figure J-12. Vertical profiles of model versus data at Arkansas Bend (Segment 78) - Chloride - 2006.

Profiles shown for dates with available data else model results for first day of month shown.

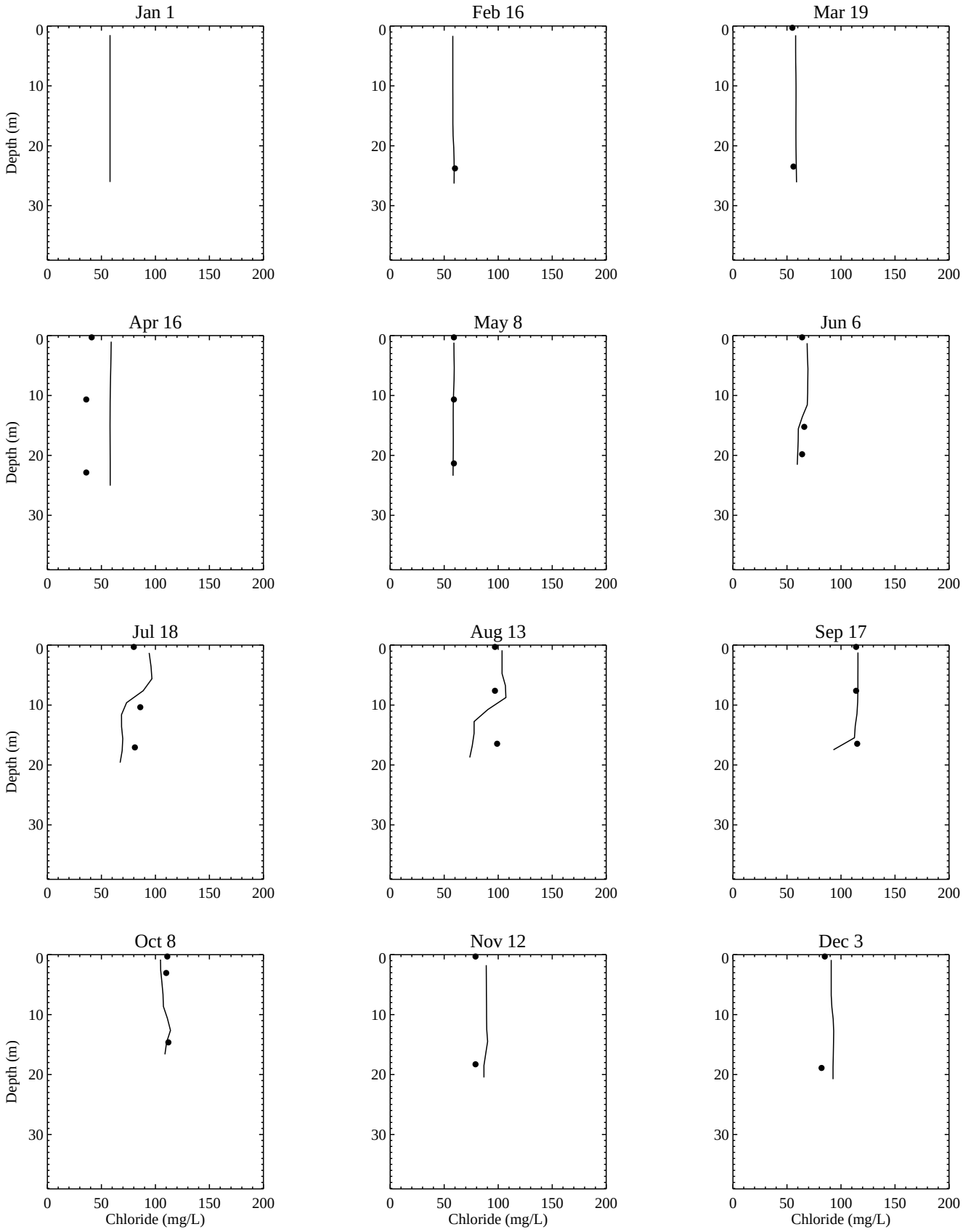

Figure J-13. Vertical profiles of model versus data at Pace Bend (Segment 48) - Chloride - 1984.

Profiles shown for dates with available data else model results for first day of month shown.

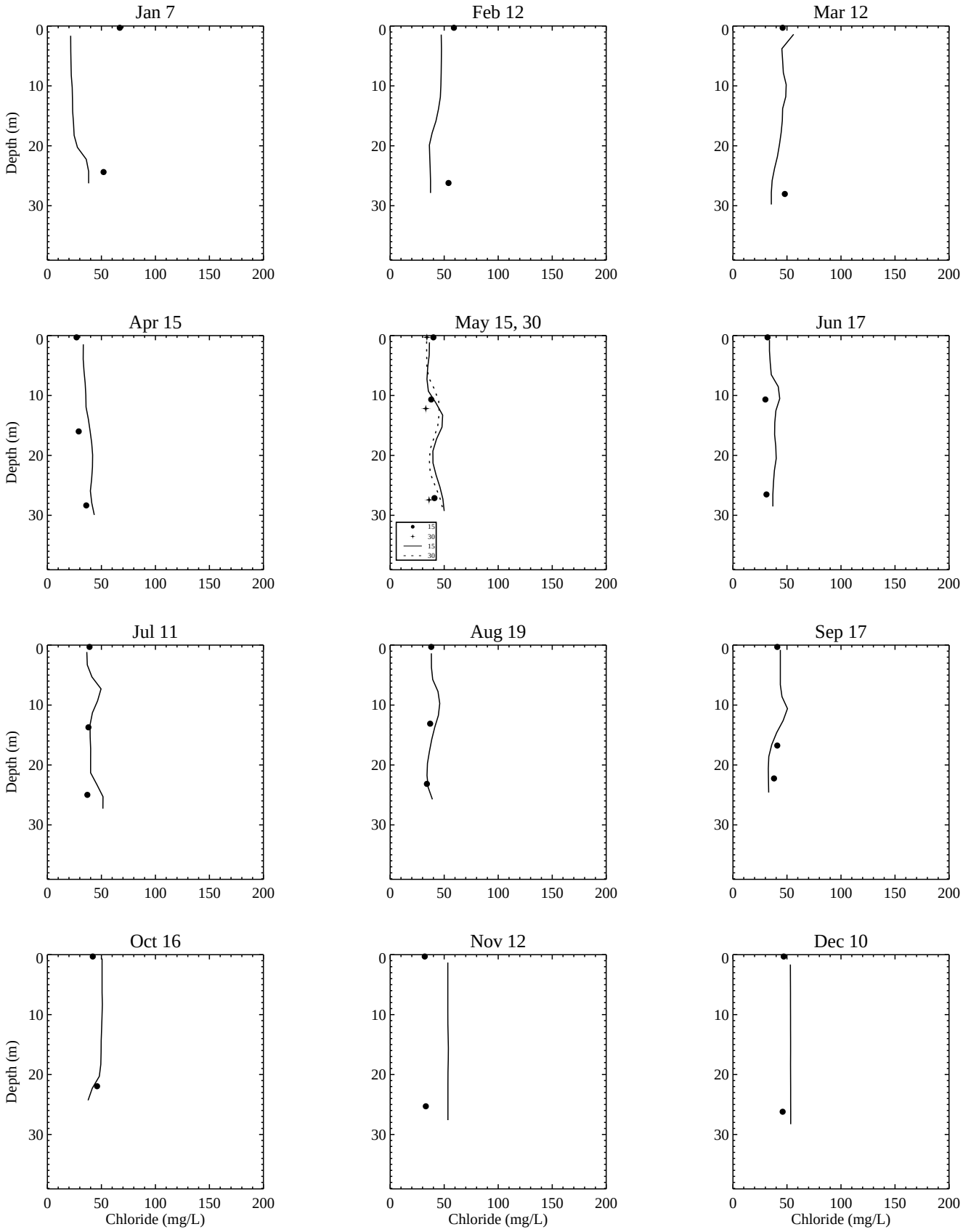

Figure J-13. Vertical profiles of model versus data at Pace Bend (Segment 48) - Chloride - 1985.

Profiles shown for dates with available data else model results for first day of month shown.

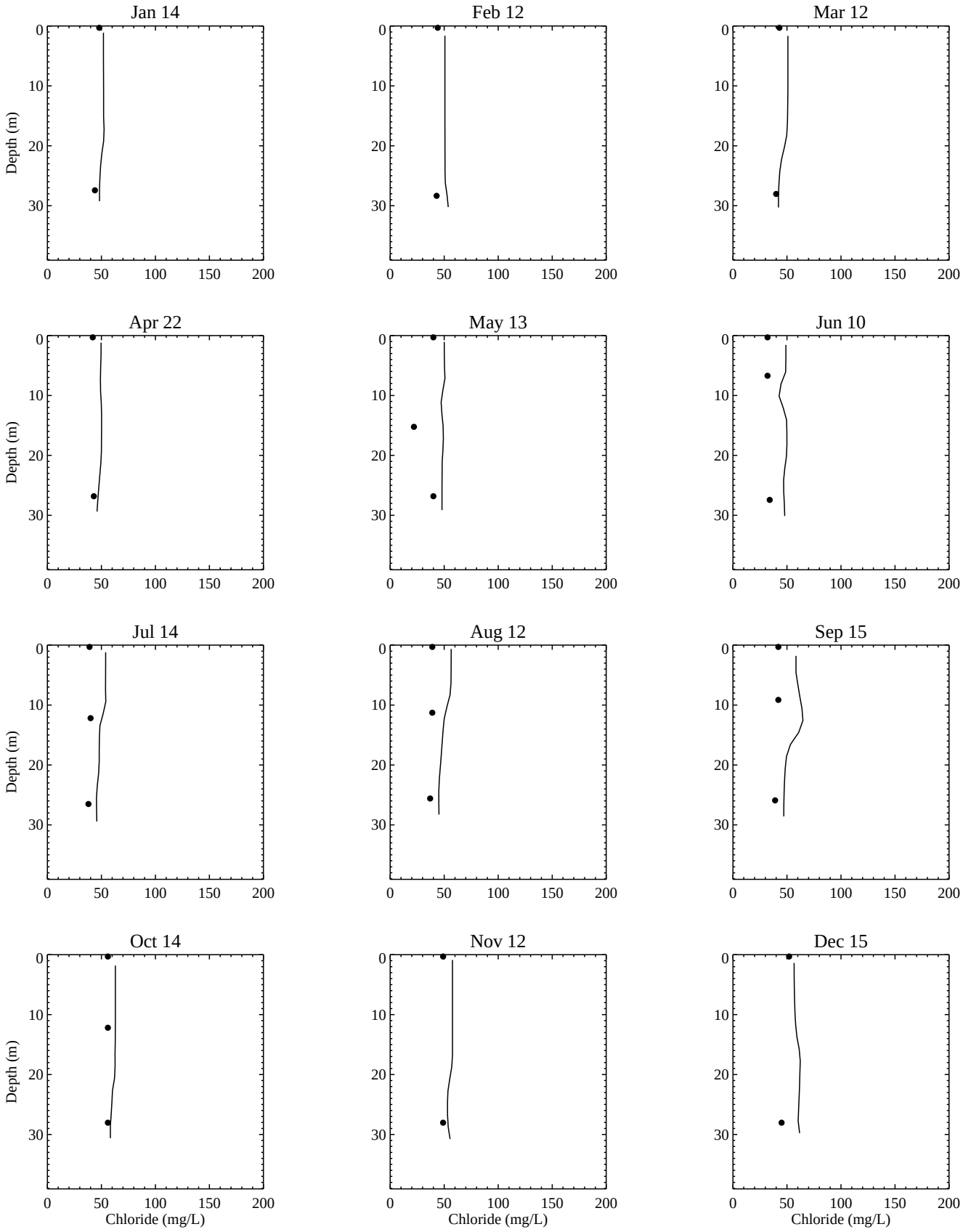

Figure J-13. Vertical profiles of model versus data at Pace Bend (Segment 48) - Chloride - 1986.

Profiles shown for dates with available data else model results for first day of month shown.

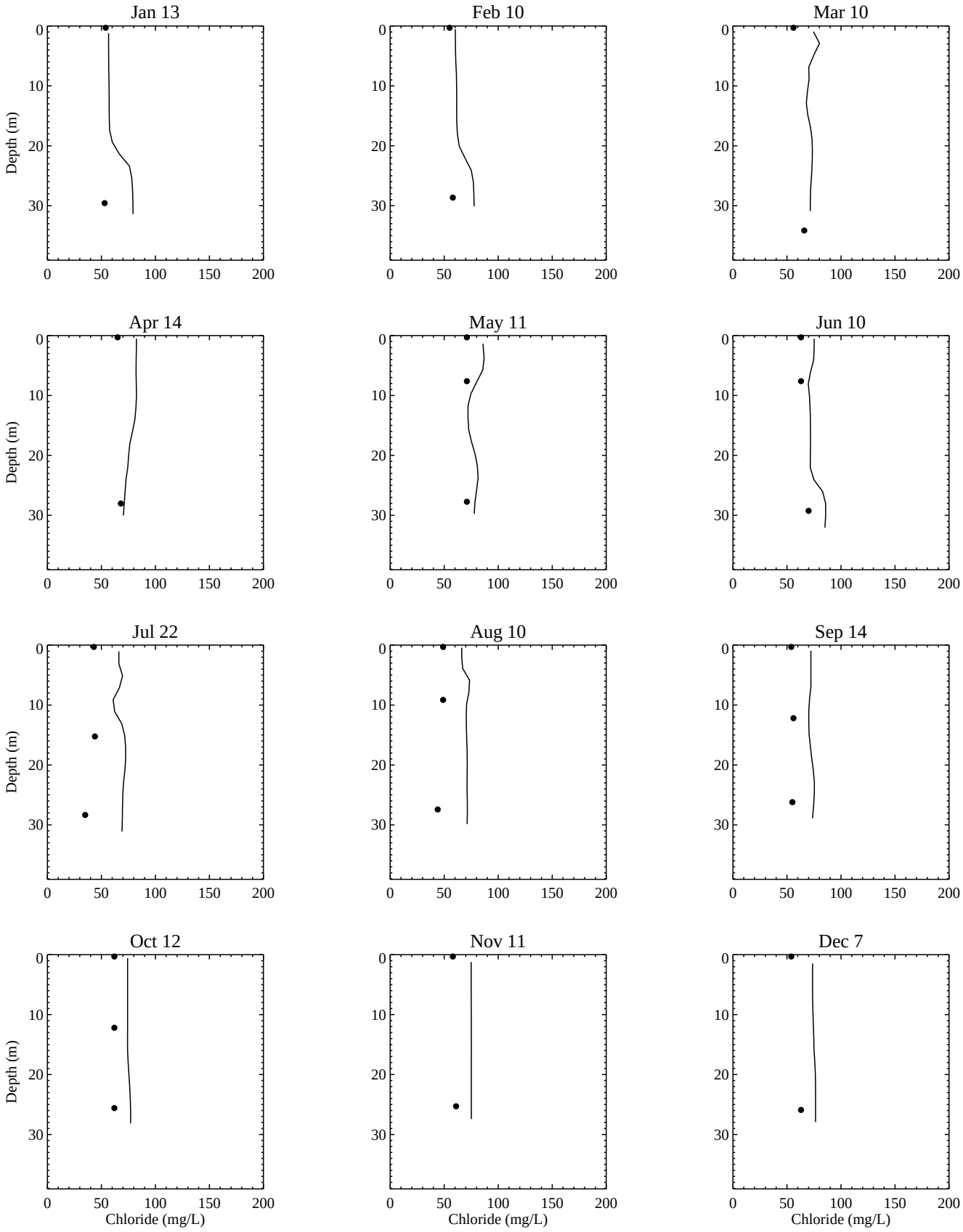

Figure J-13. Vertical profiles of model versus data at Pace Bend (Segment 48) - Chloride - 1987.

Profiles shown for dates with available data else model results for first day of month shown.

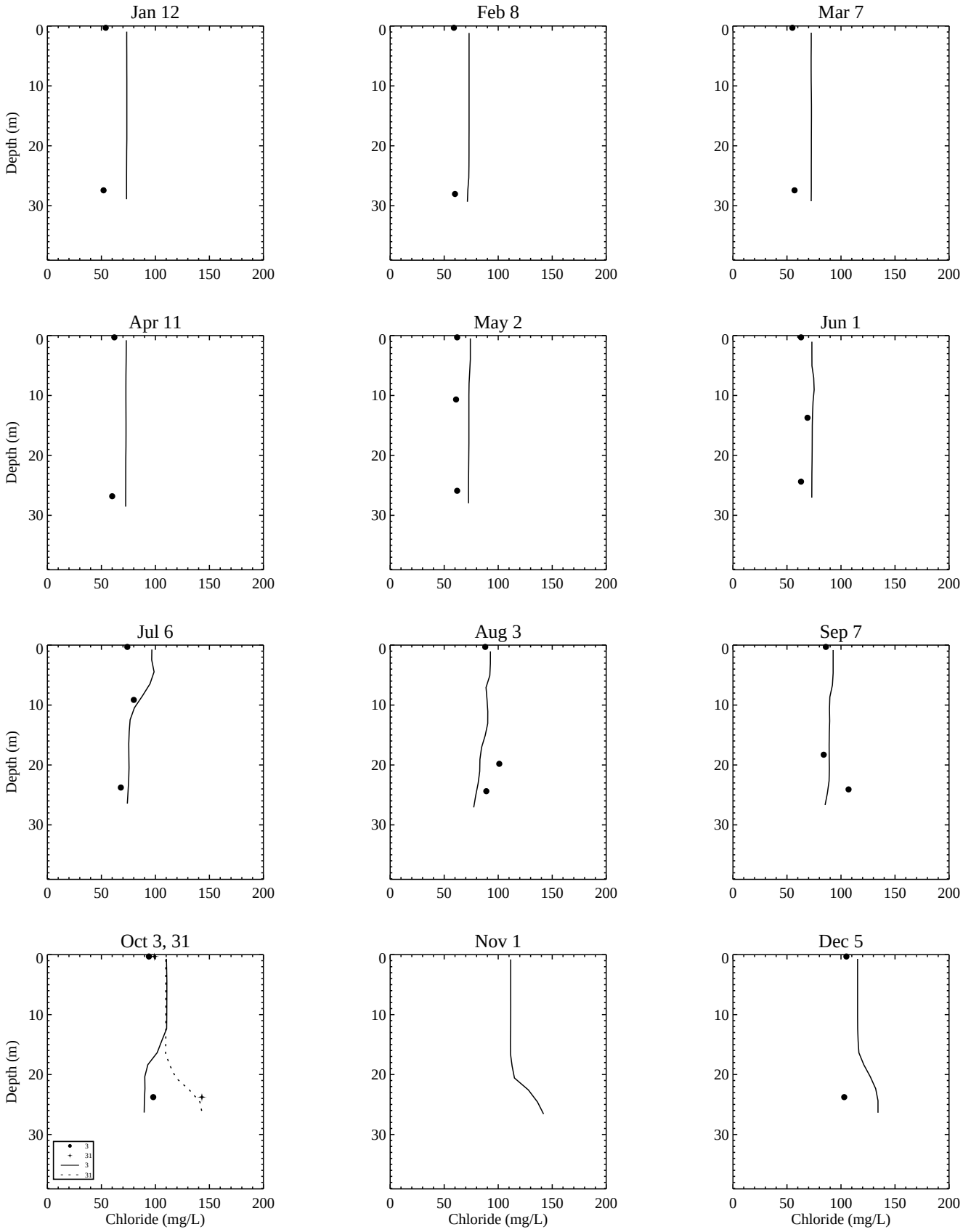

Figure J-13. Vertical profiles of model versus data at Pace Bend (Segment 48) - Chloride - 1988.

Profiles shown for dates with available data else model results for first day of month shown.

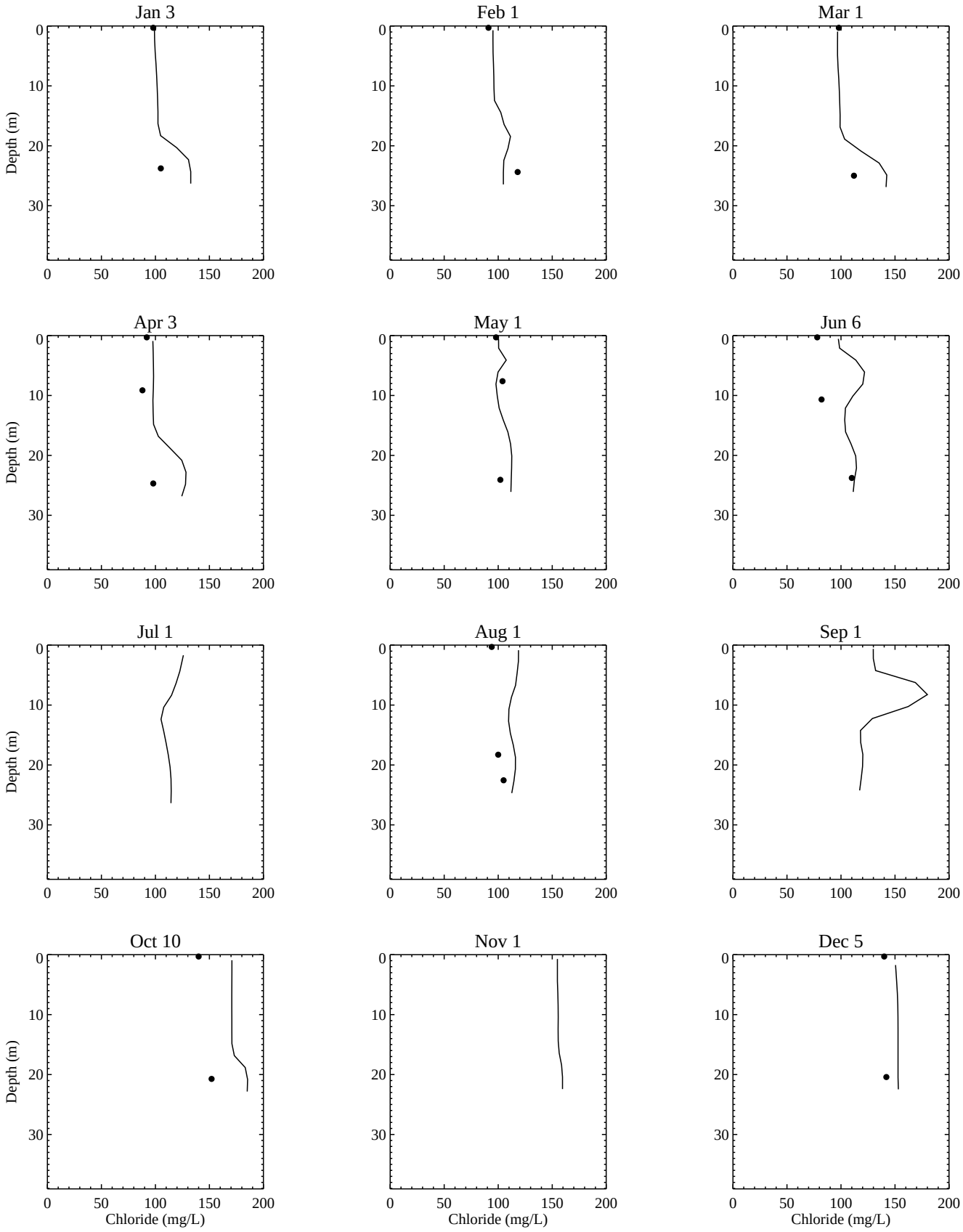

Figure J-13. Vertical profiles of model versus data at Pace Bend (Segment 48) - Chloride - 1989.

Profiles shown for dates with available data else model results for first day of month shown.

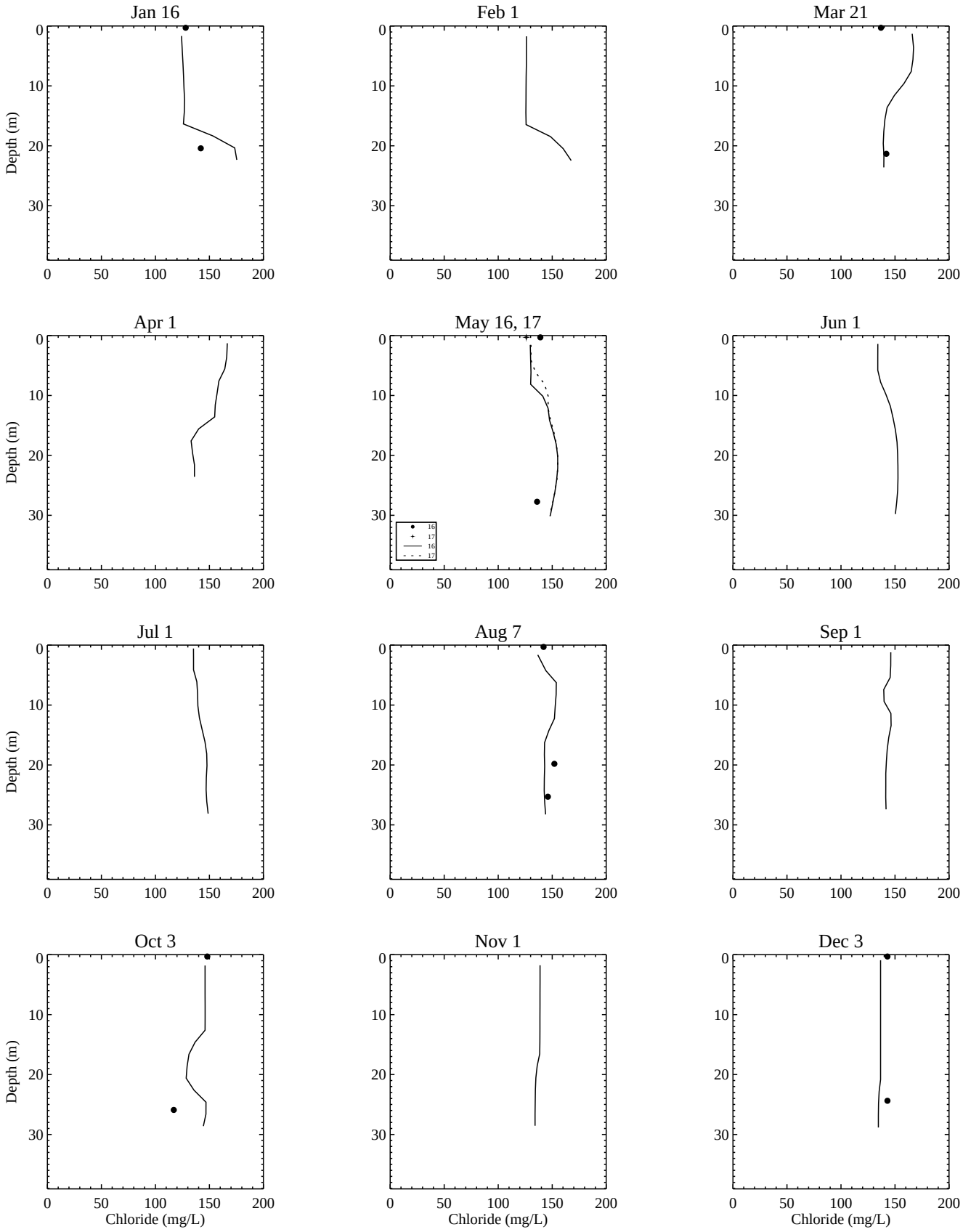

Figure J-13. Vertical profiles of model versus data at Pace Bend (Segment 48) - Chloride - 1990.

Profiles shown for dates with available data else model results for first day of month shown.

Model Data

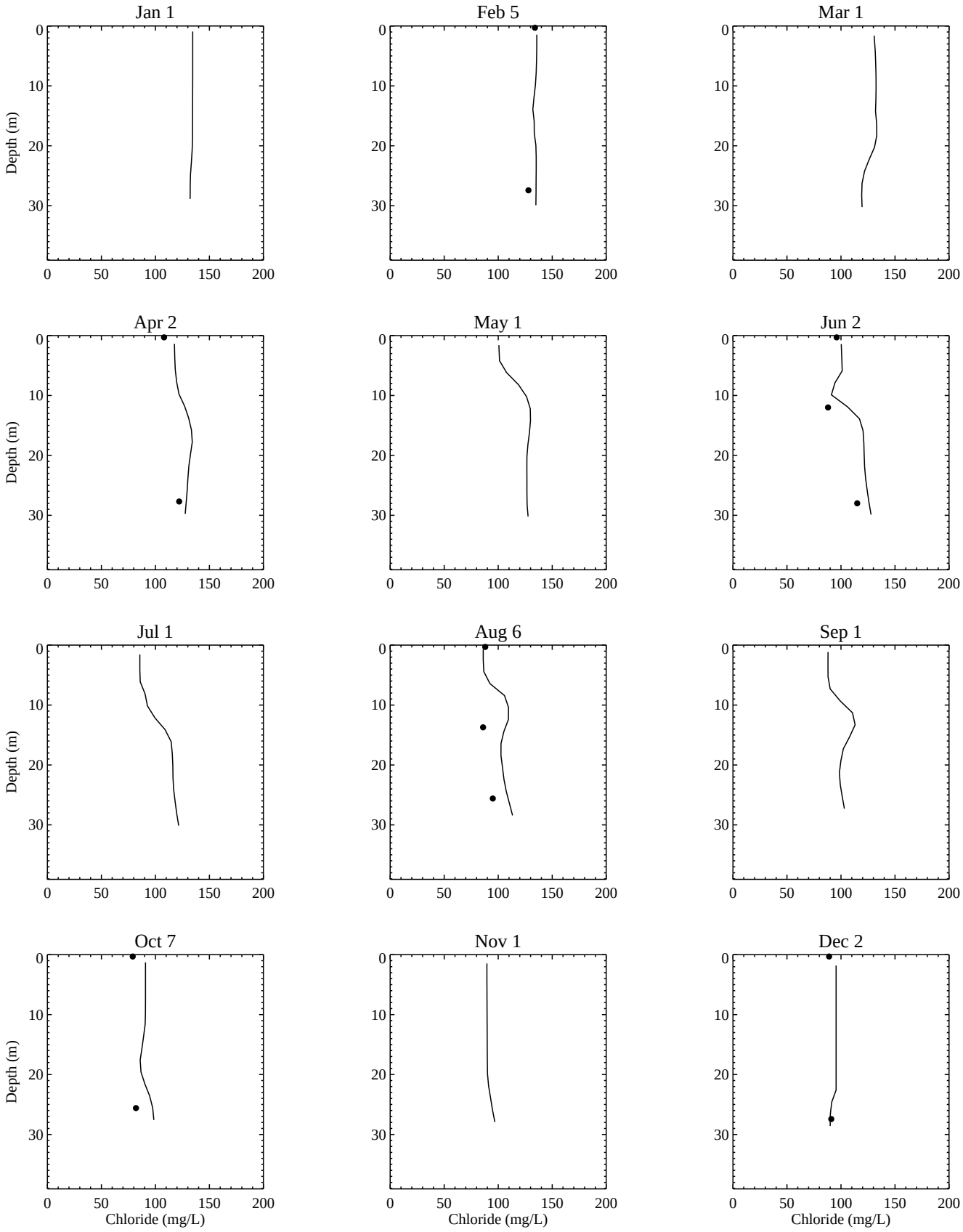

Figure J-13. Vertical profiles of model versus data at Pace Bend (Segment 48) - Chloride - 1991.

Profiles shown for dates with available data else model results for first day of month shown.

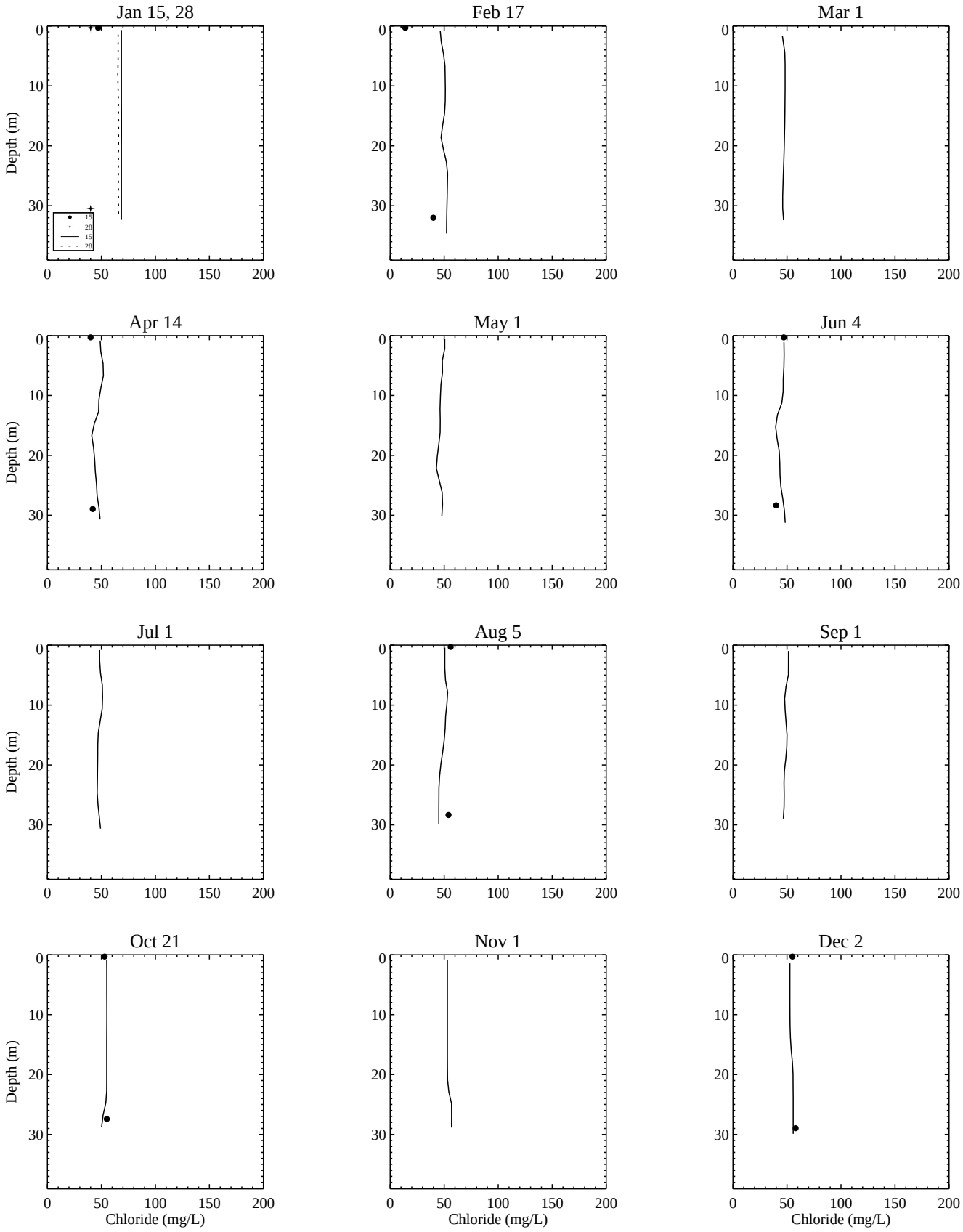

Figure J-13. Vertical profiles of model versus data at Pace Bend (Segment 48) - Chloride - 1992.

Profiles shown for dates with available data else model results for first day of month shown.

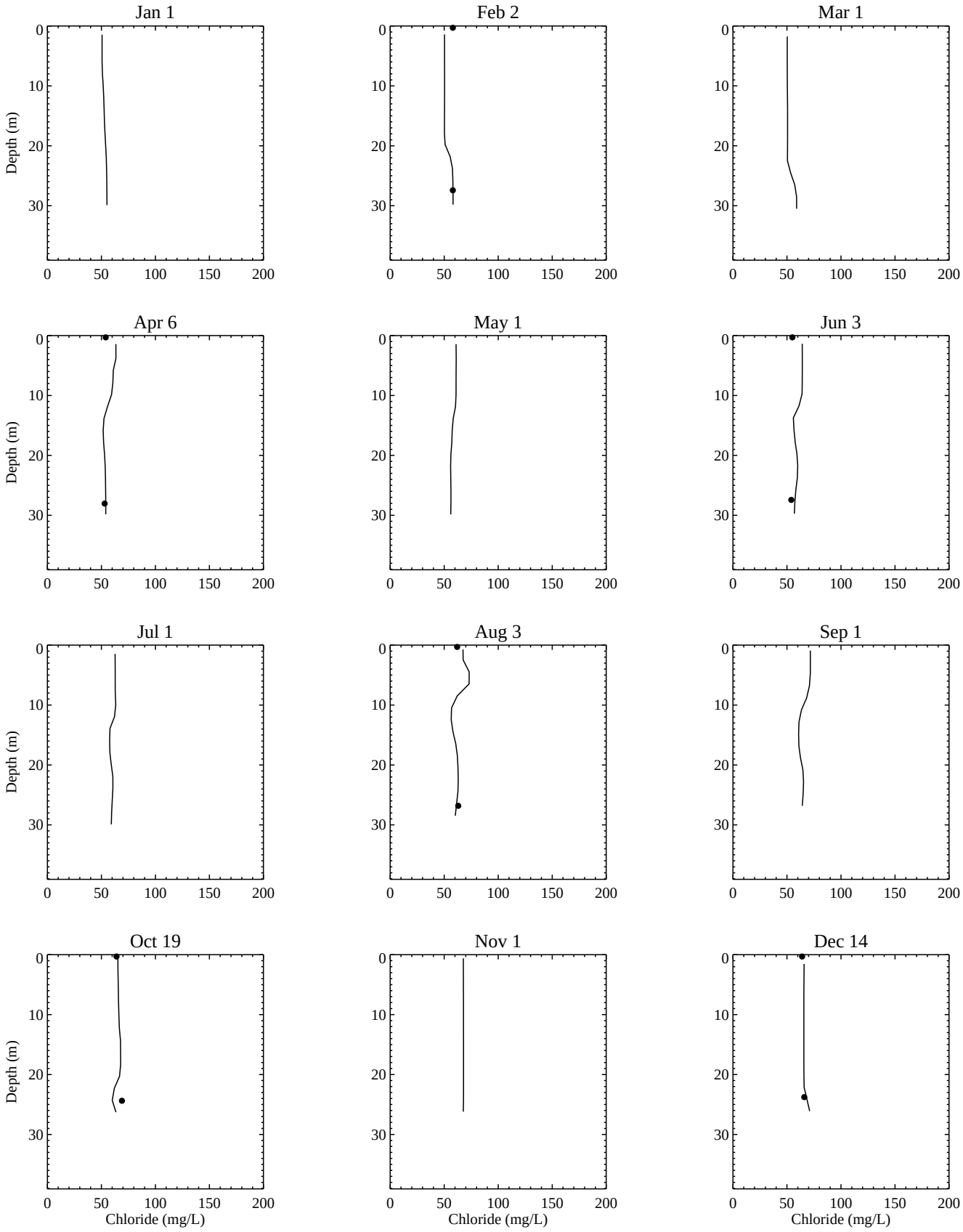

Figure J-13. Vertical profiles of model versus data at Pace Bend (Segment 48) - Chloride - 1993.

Profiles shown for dates with available data else model results for first day of month shown.

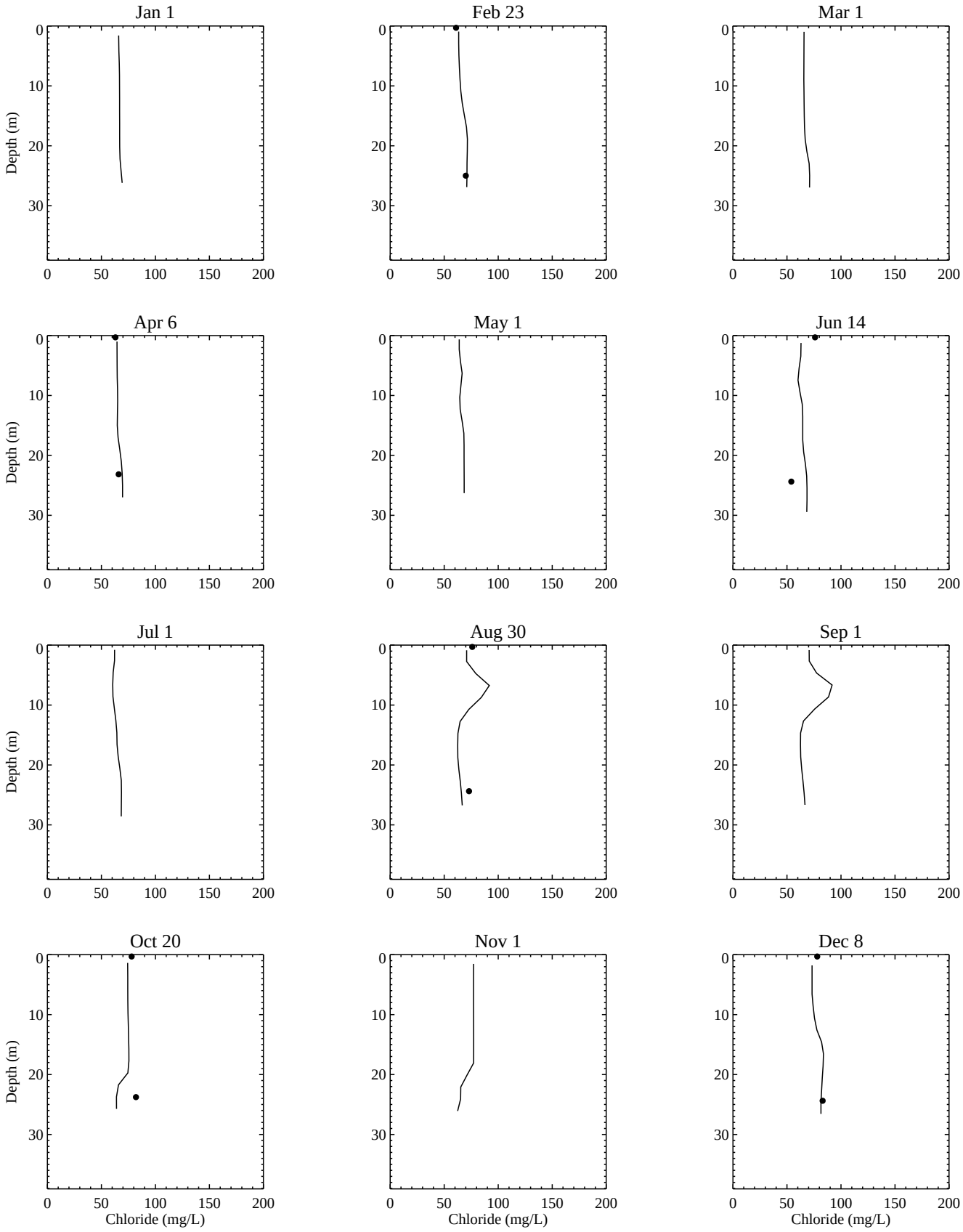

Figure J-13. Vertical profiles of model versus data at Pace Bend (Segment 48) - Chloride - 1994.

Profiles shown for dates with available data else model results for first day of month shown.

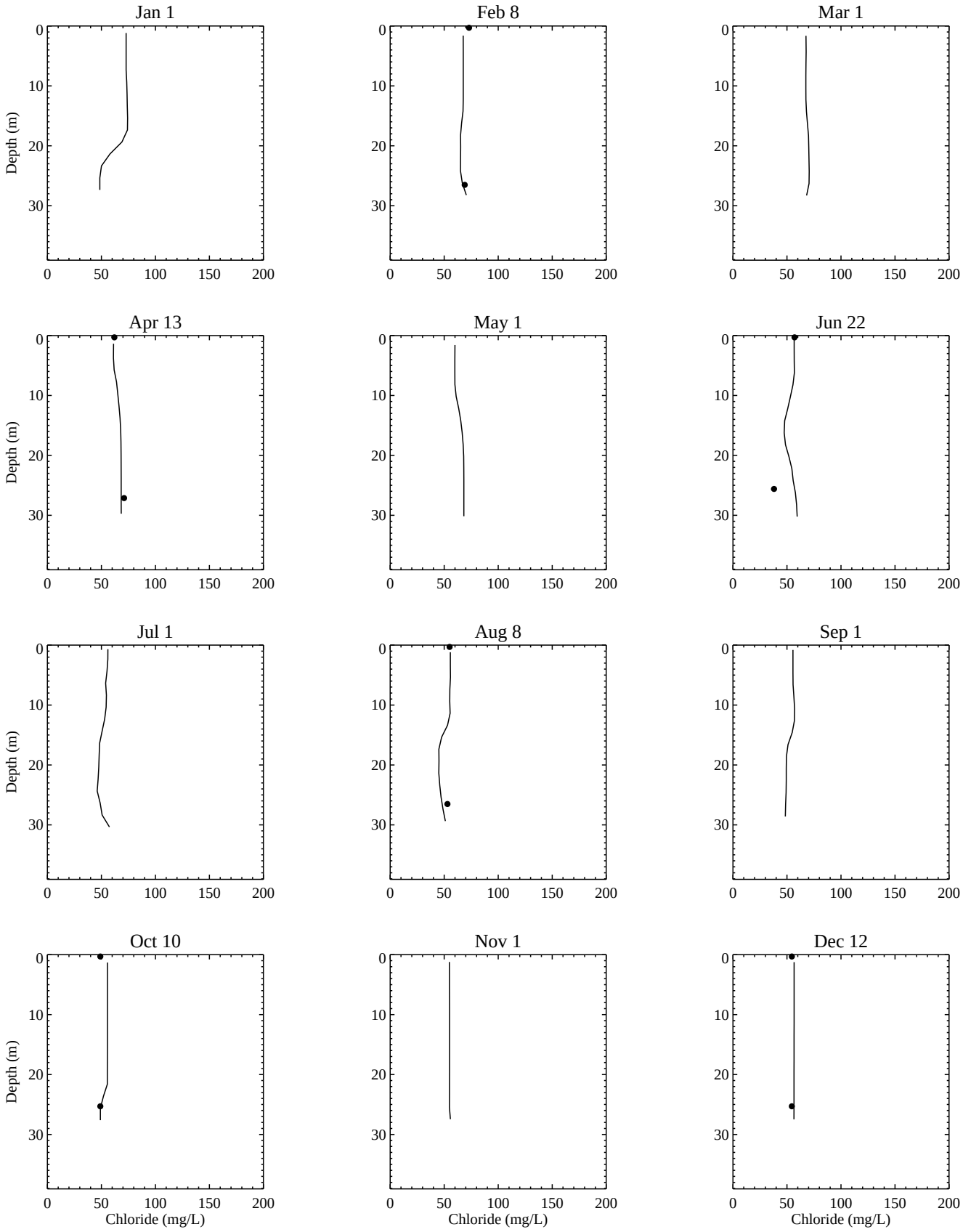

Figure J-13. Vertical profiles of model versus data at Pace Bend (Segment 48) - Chloride - 1995.

Profiles shown for dates with available data else model results for first day of month shown.

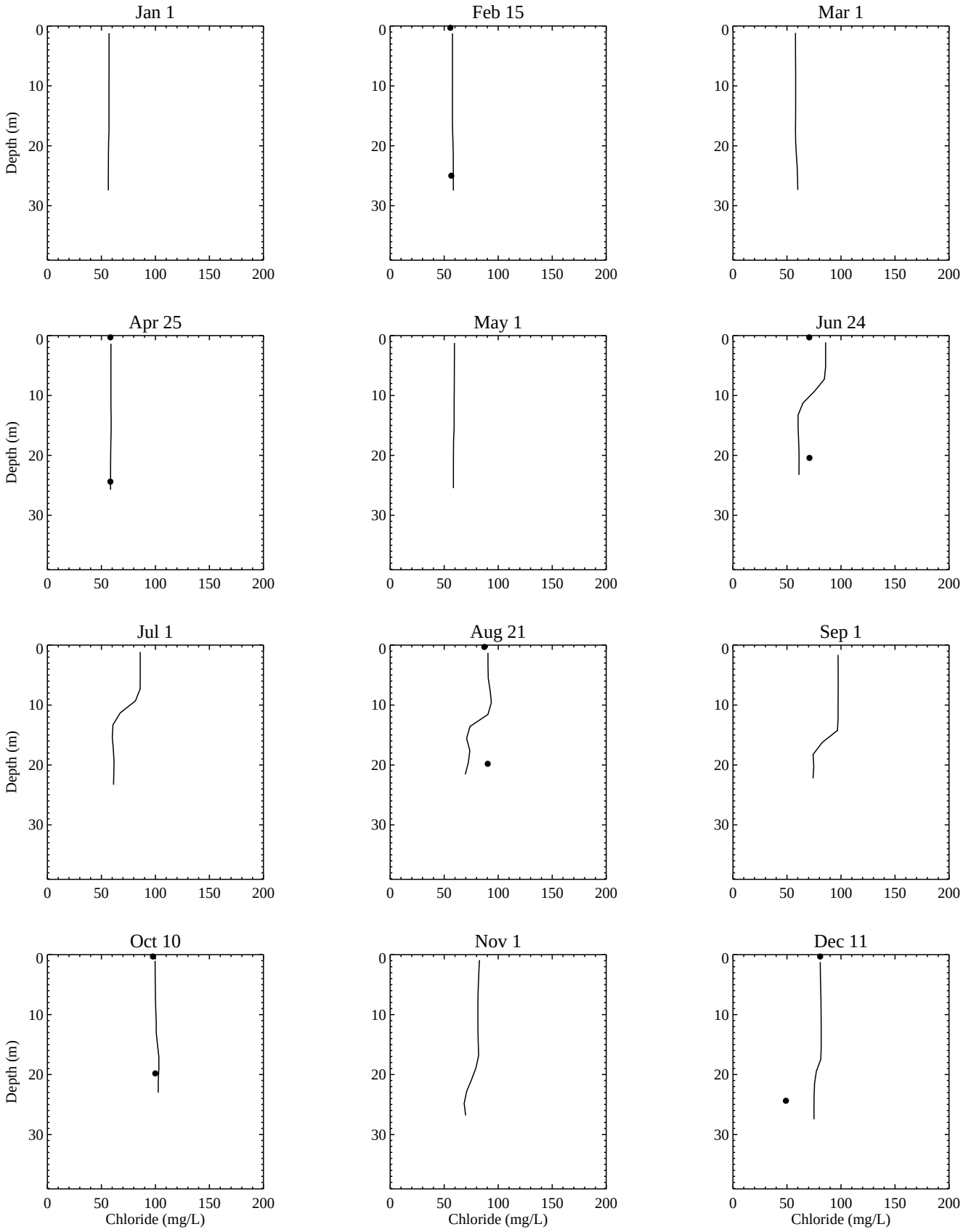

Figure J-13. Vertical profiles of model versus data at Pace Bend (Segment 48) - Chloride - 1996.

Profiles shown for dates with available data else model results for first day of month shown.

Model ● Data

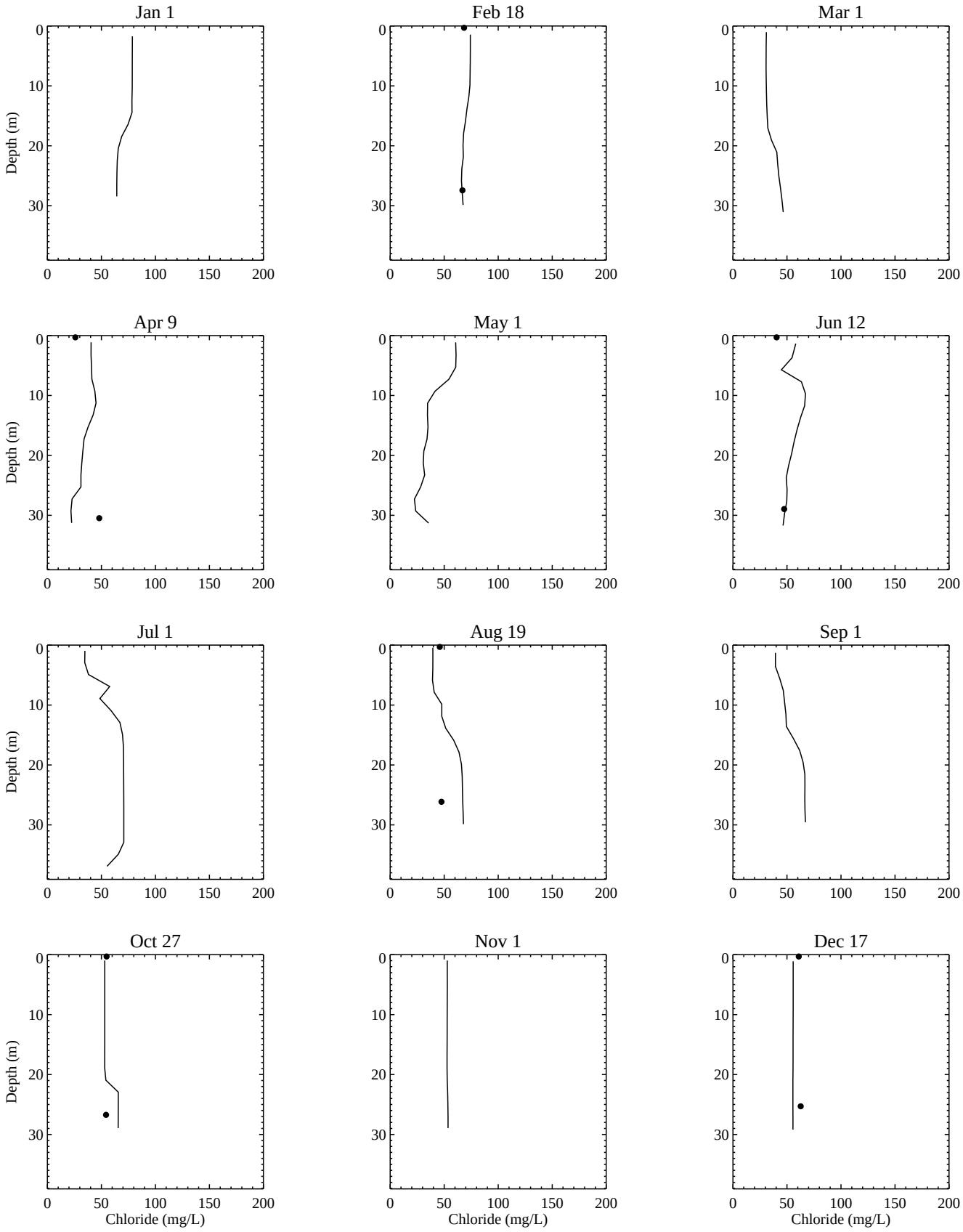

Figure J-13. Vertical profiles of model versus data at Pace Bend (Segment 48) - Chloride - 1997.

Profiles shown for dates with available data else model results for first day of month shown.

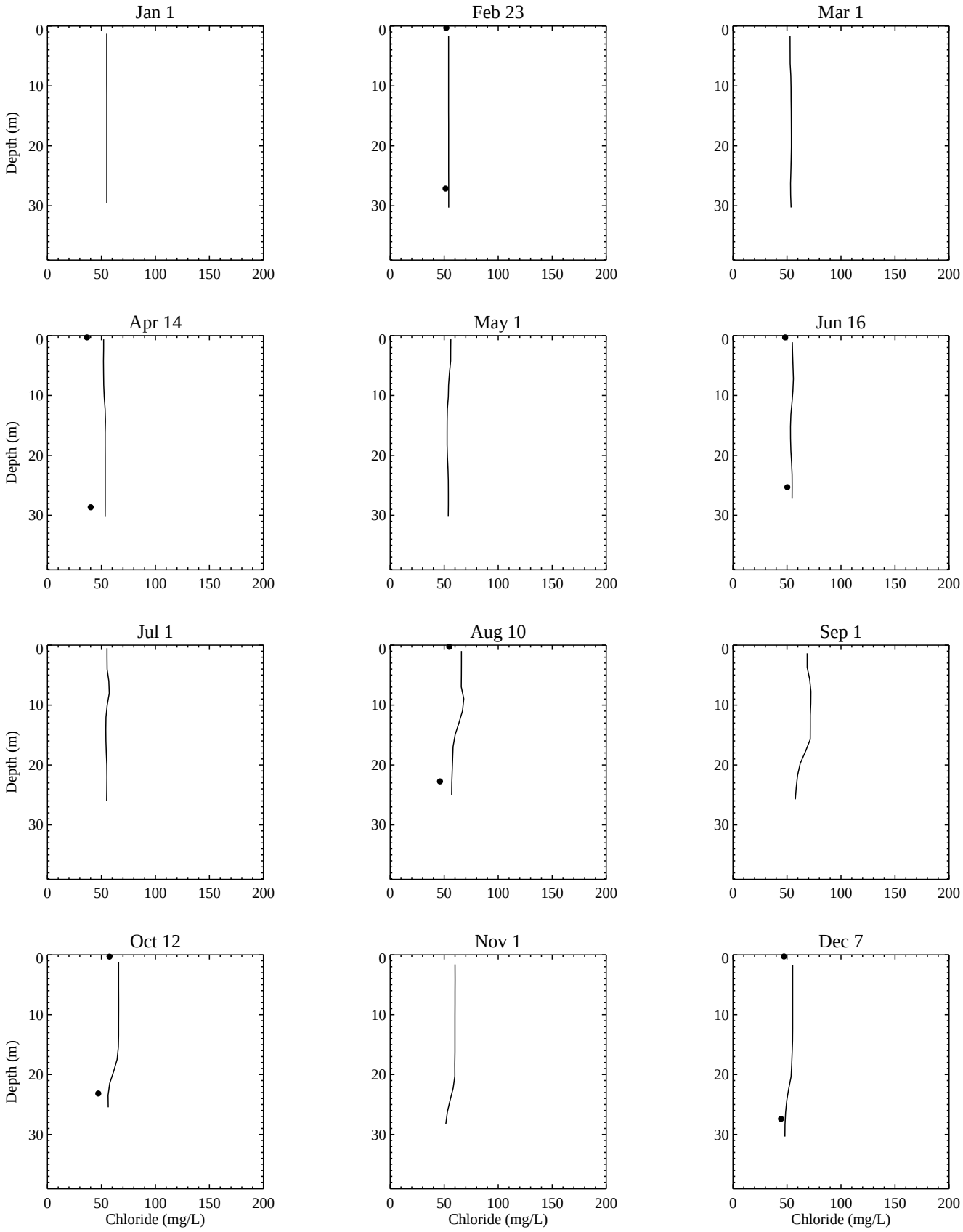

Figure J-13. Vertical profiles of model versus data at Pace Bend (Segment 48) - Chloride - 1998.

Profiles shown for dates with available data else model results for first day of month shown.

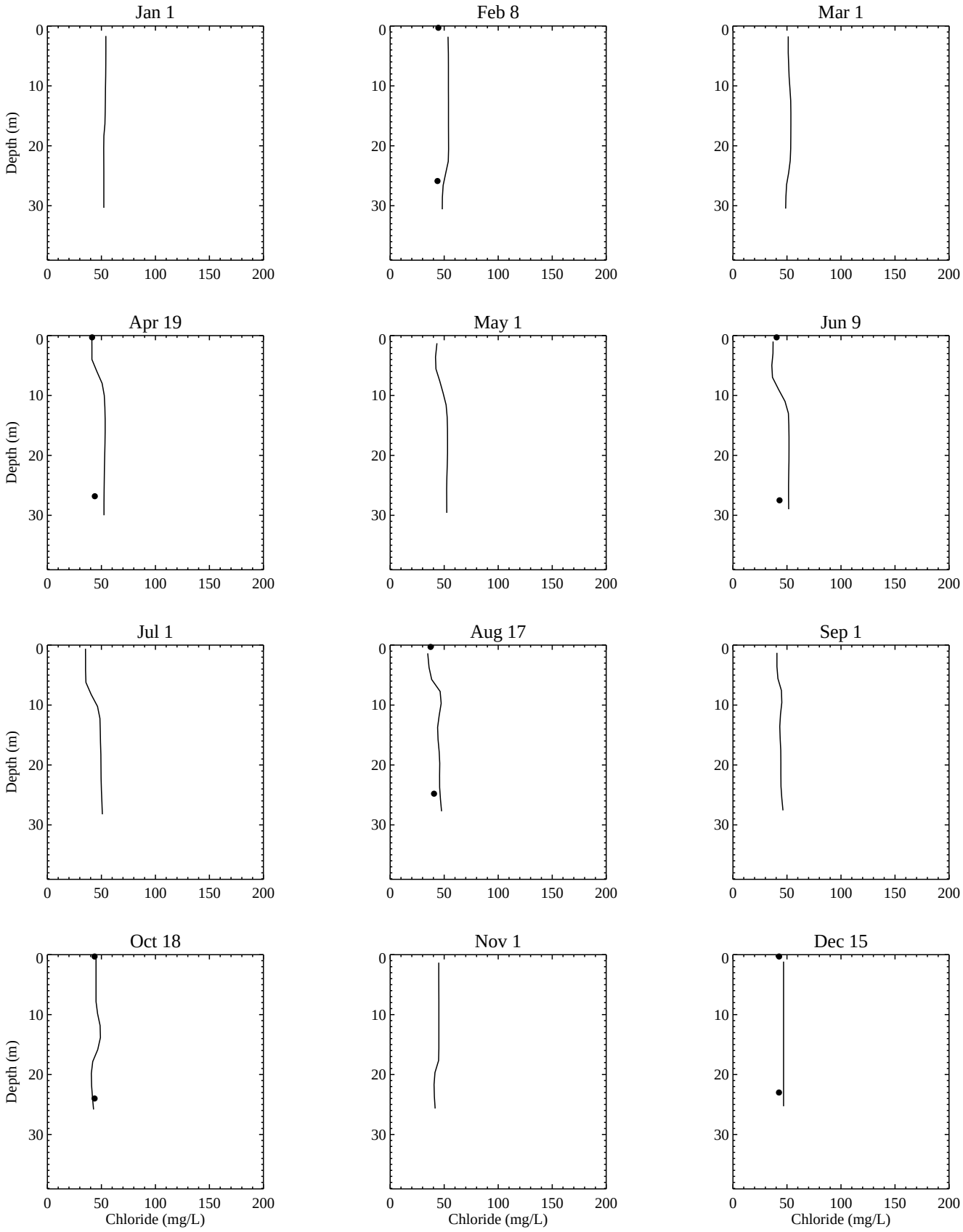

Figure J-13. Vertical profiles of model versus data at Pace Bend (Segment 48) - Chloride - 1999.

Profiles shown for dates with available data else model results for first day of month shown.

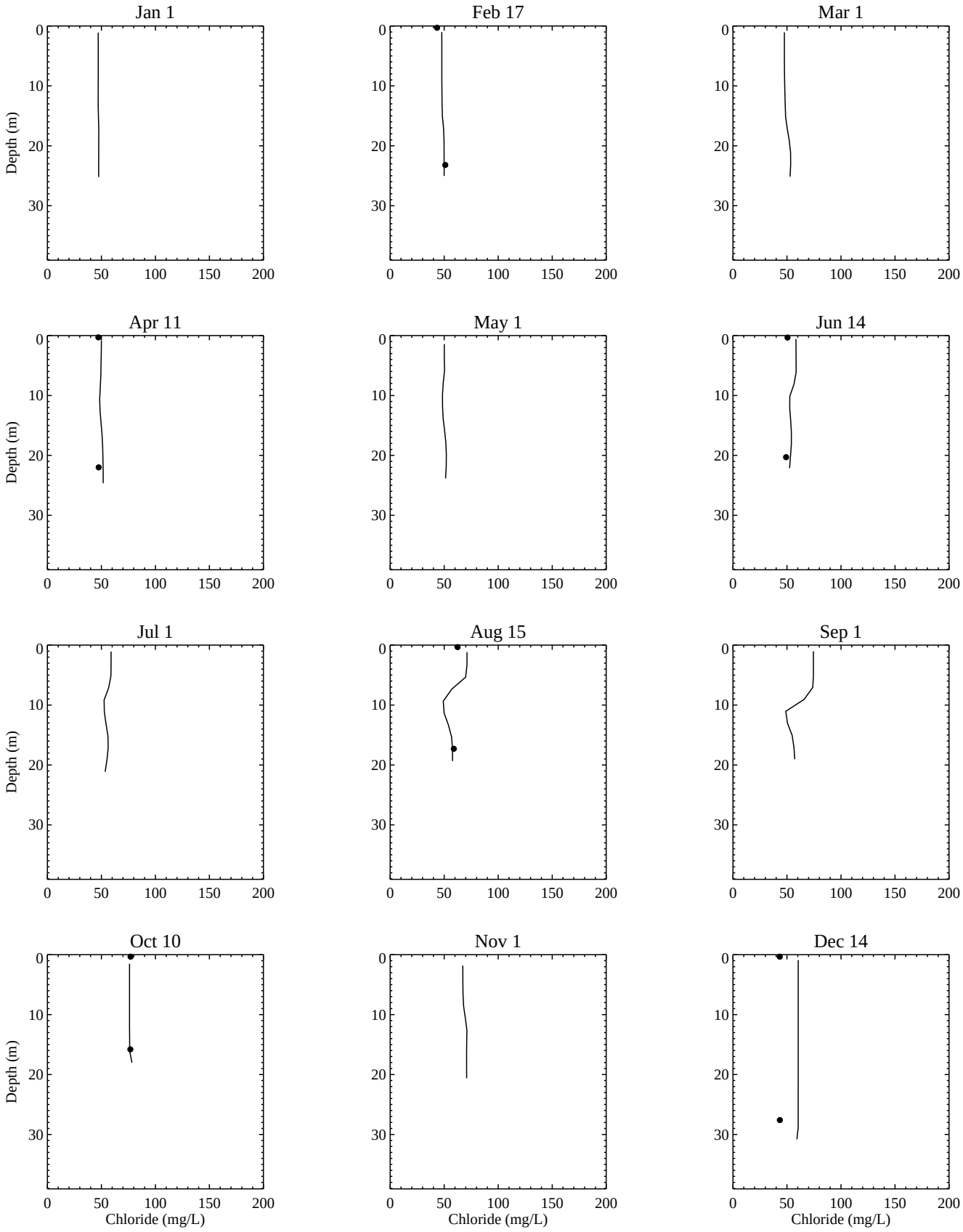

Figure J-13. Vertical profiles of model versus data at Pace Bend (Segment 48) - Chloride - 2000.

Profiles shown for dates with available data else model results for first day of month shown.

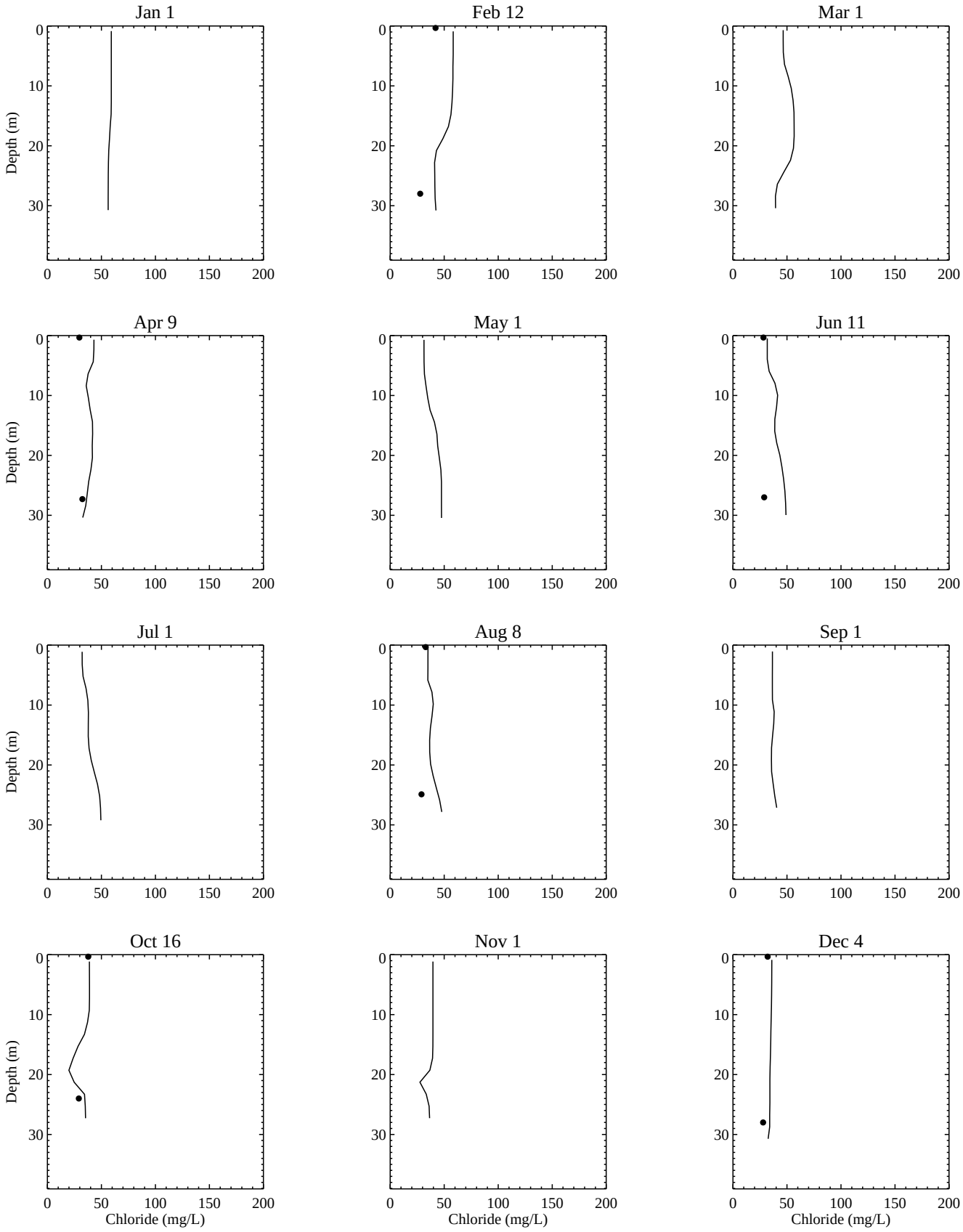

Figure J-13. Vertical profiles of model versus data at Pace Bend (Segment 48) - Chloride - 2001.

Profiles shown for dates with available data else model results for first day of month shown.

Model ● Data

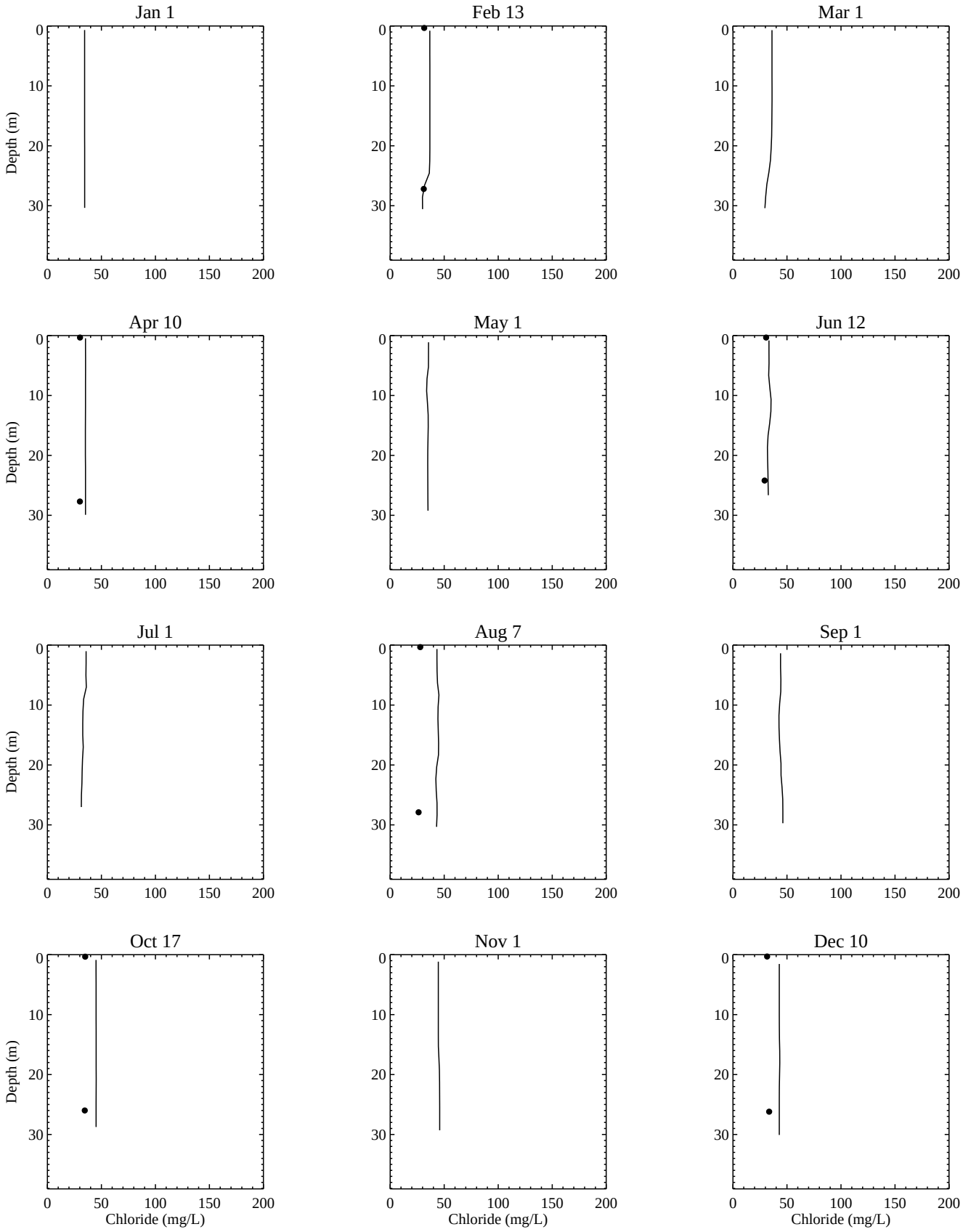

Figure J-13. Vertical profiles of model versus data at Pace Bend (Segment 48) - Chloride - 2002.

Profiles shown for dates with available data else model results for first day of month shown.

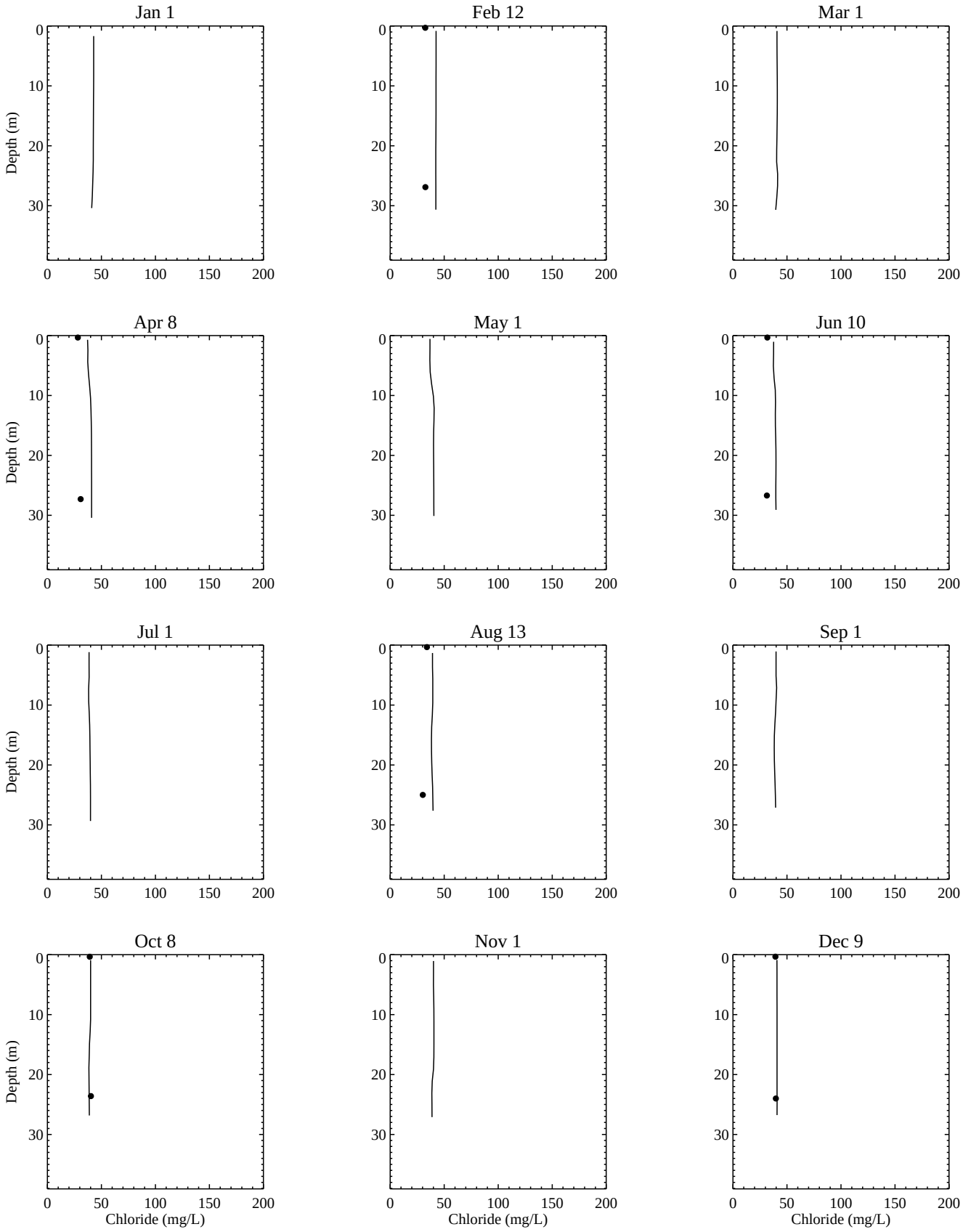

Figure J-13. Vertical profiles of model versus data at Pace Bend (Segment 48) - Chloride - 2003.

Profiles shown for dates with available data else model results for first day of month shown.

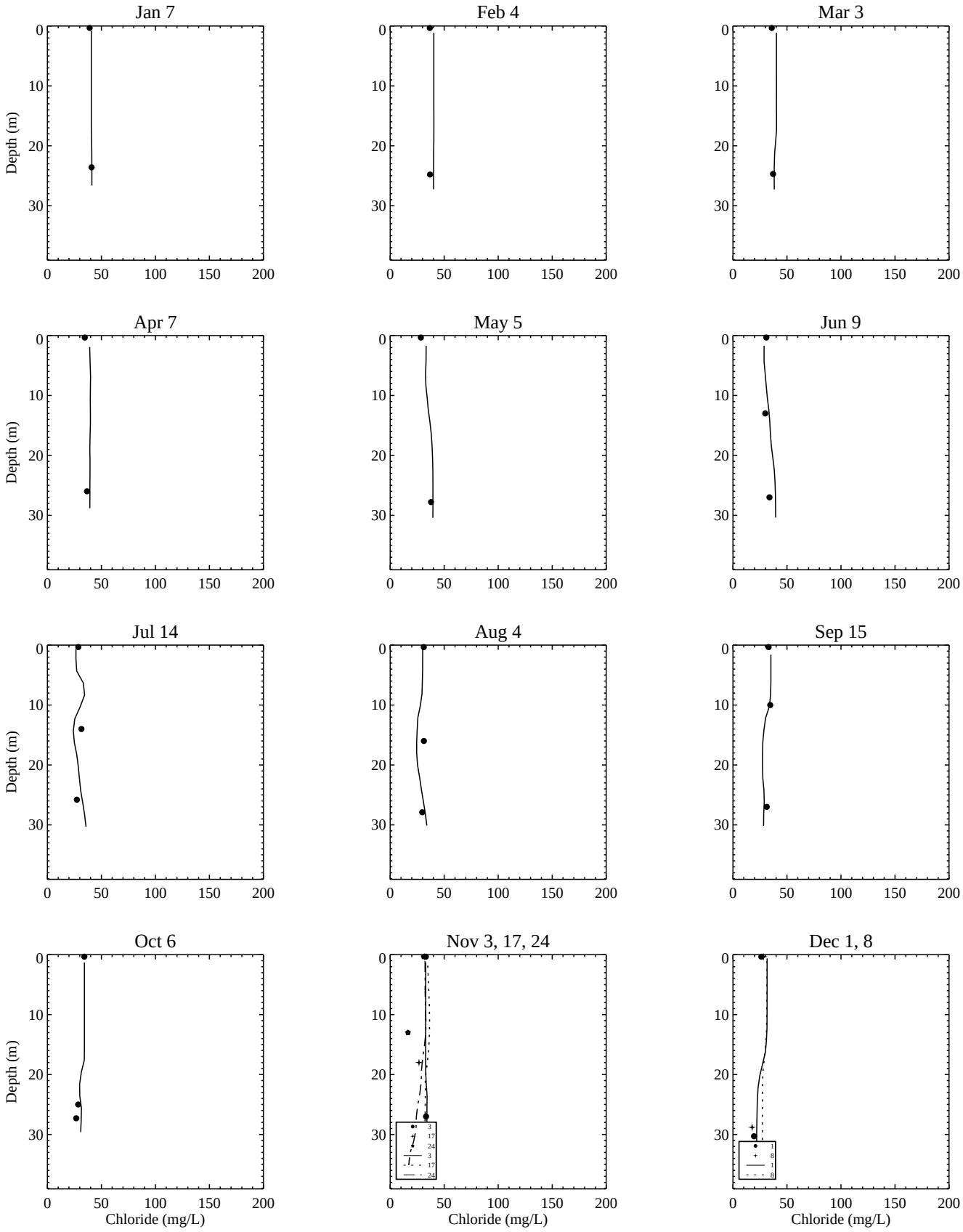

Figure J-13. Vertical profiles of model versus data at Pace Bend (Segment 48) - Chloride - 2004.

Profiles shown for dates with available data else model results for first day of month shown.

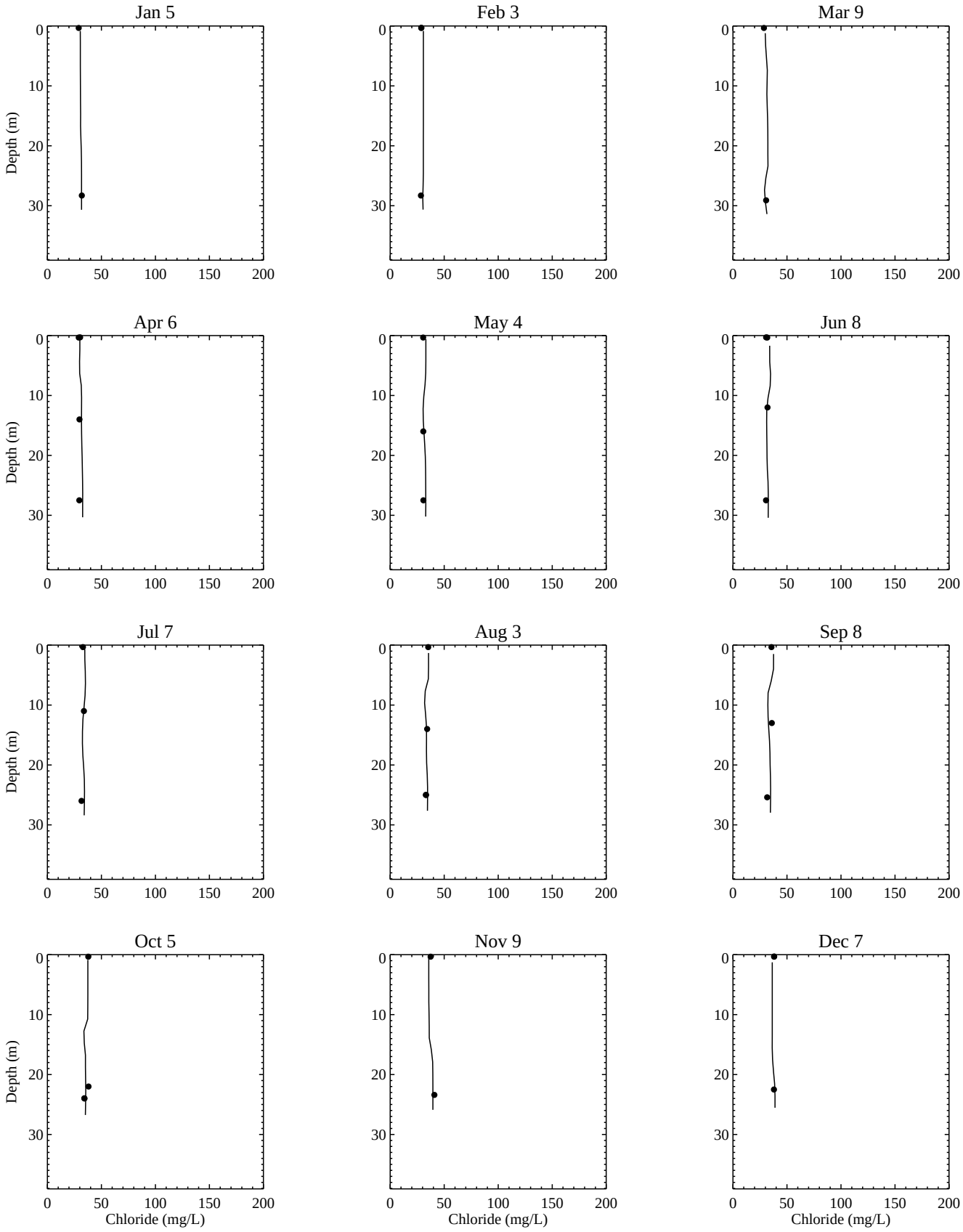

Figure J-13. Vertical profiles of model versus data at Pace Bend (Segment 48) - Chloride - 2005.

Profiles shown for dates with available data else model results for first day of month shown.

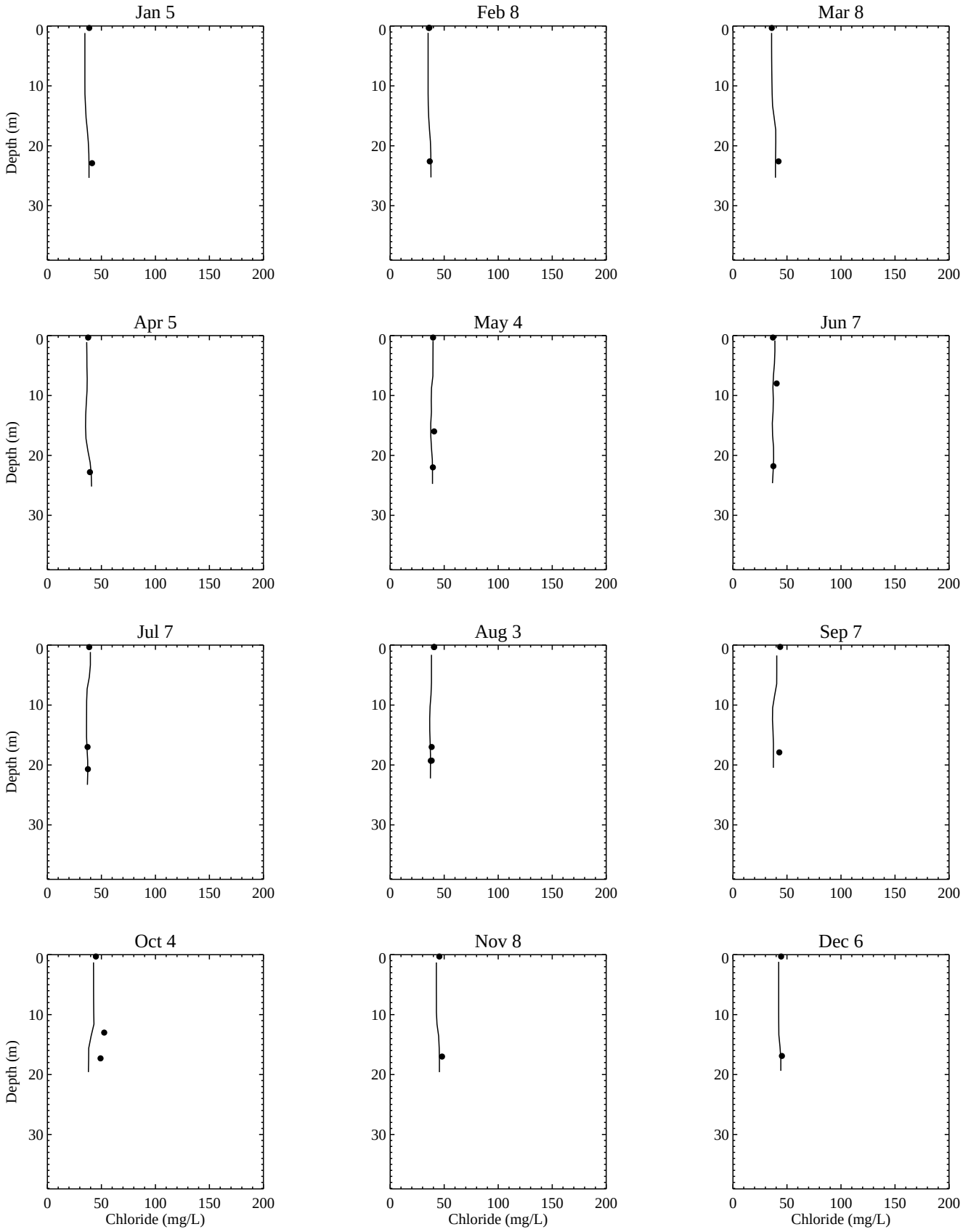

Figure J-13. Vertical profiles of model versus data at Pace Bend (Segment 48) - Chloride - 2006.

Profiles shown for dates with available data else model results for first day of month shown.

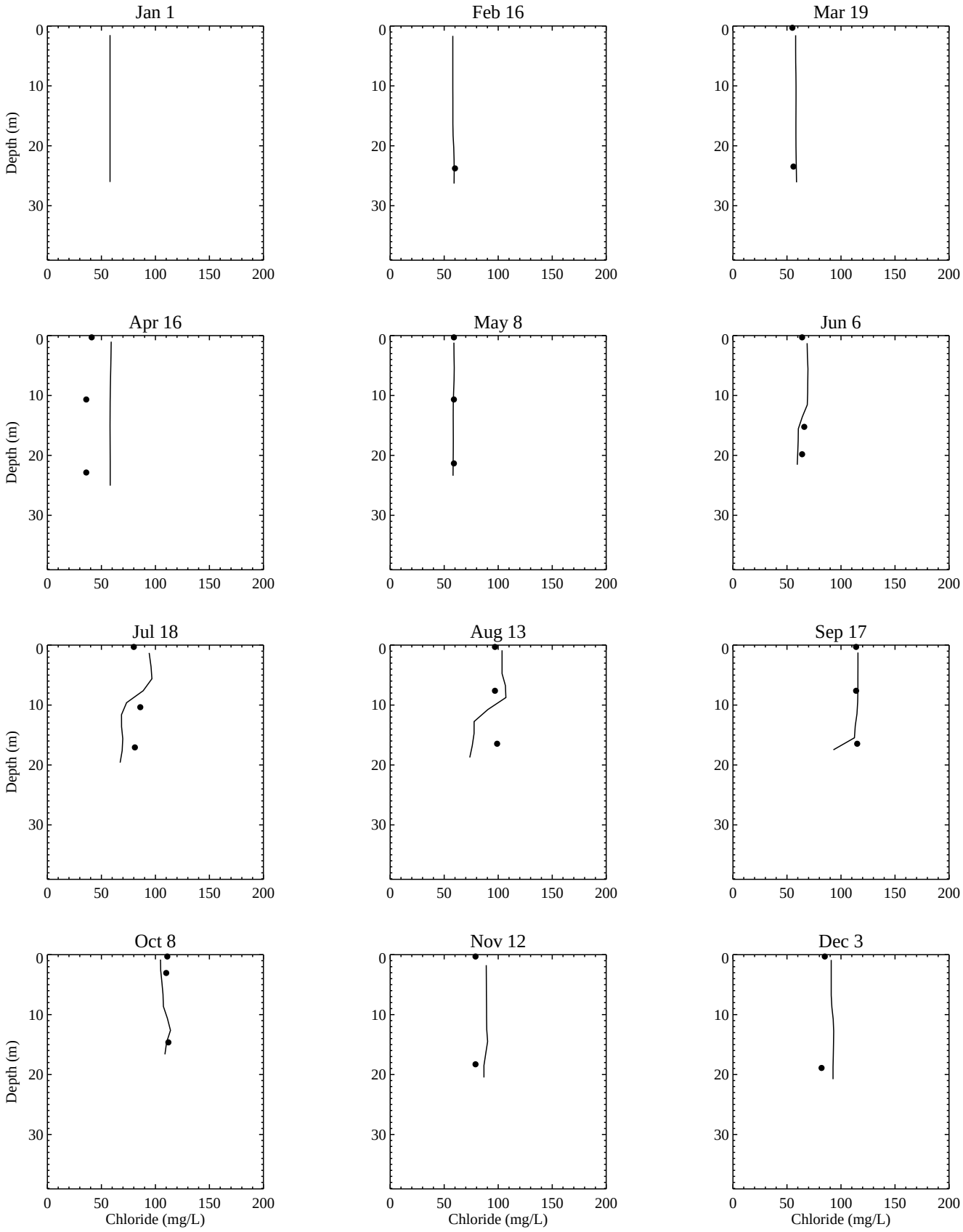

Figure J-13. Vertical profiles of model versus data at Pace Bend (Segment 48) - Chloride - 1984.

Profiles shown for dates with available data else model results for first day of month shown.

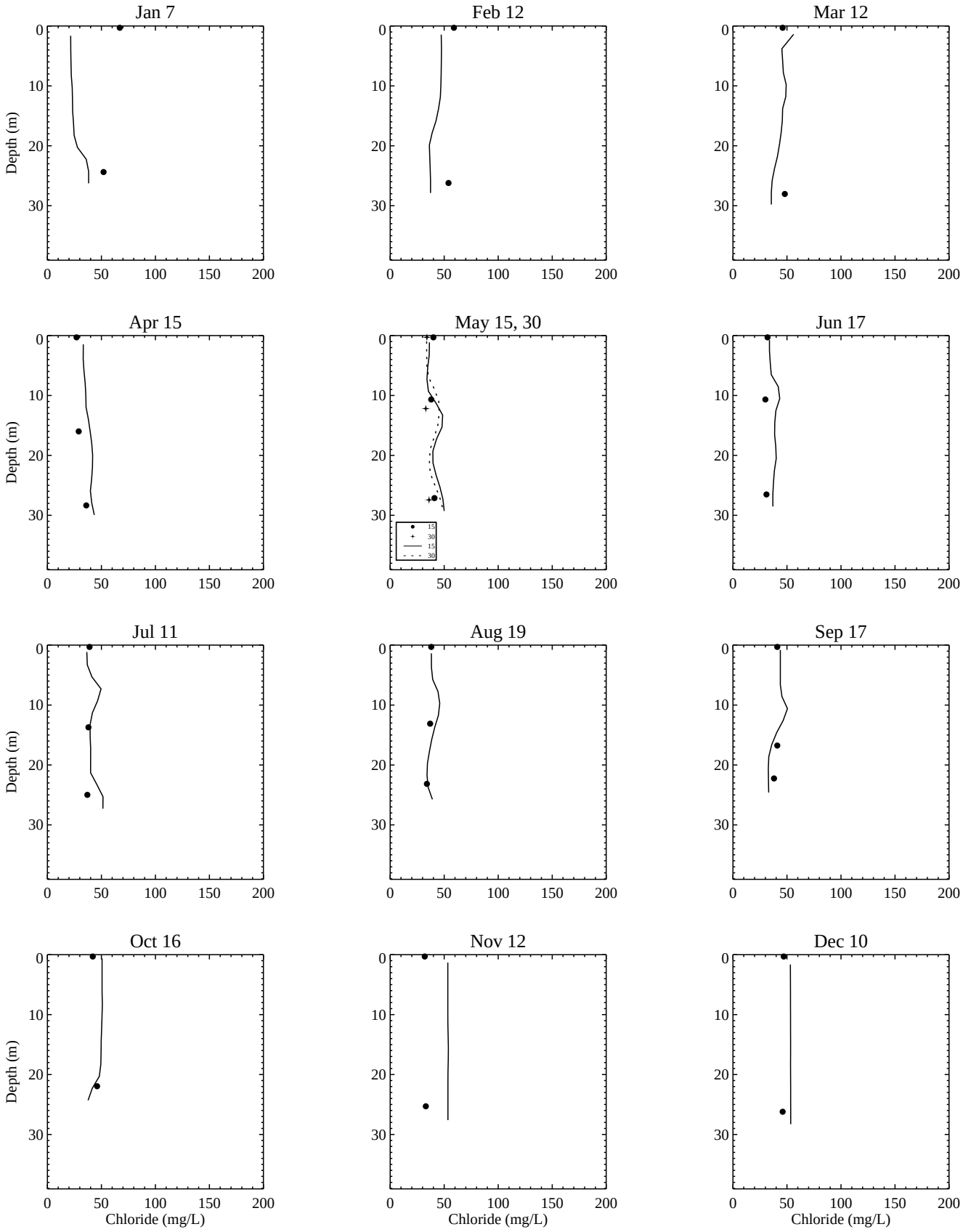

Figure J-13. Vertical profiles of model versus data at Pace Bend (Segment 48) - Chloride - 1985.

Profiles shown for dates with available data else model results for first day of month shown.

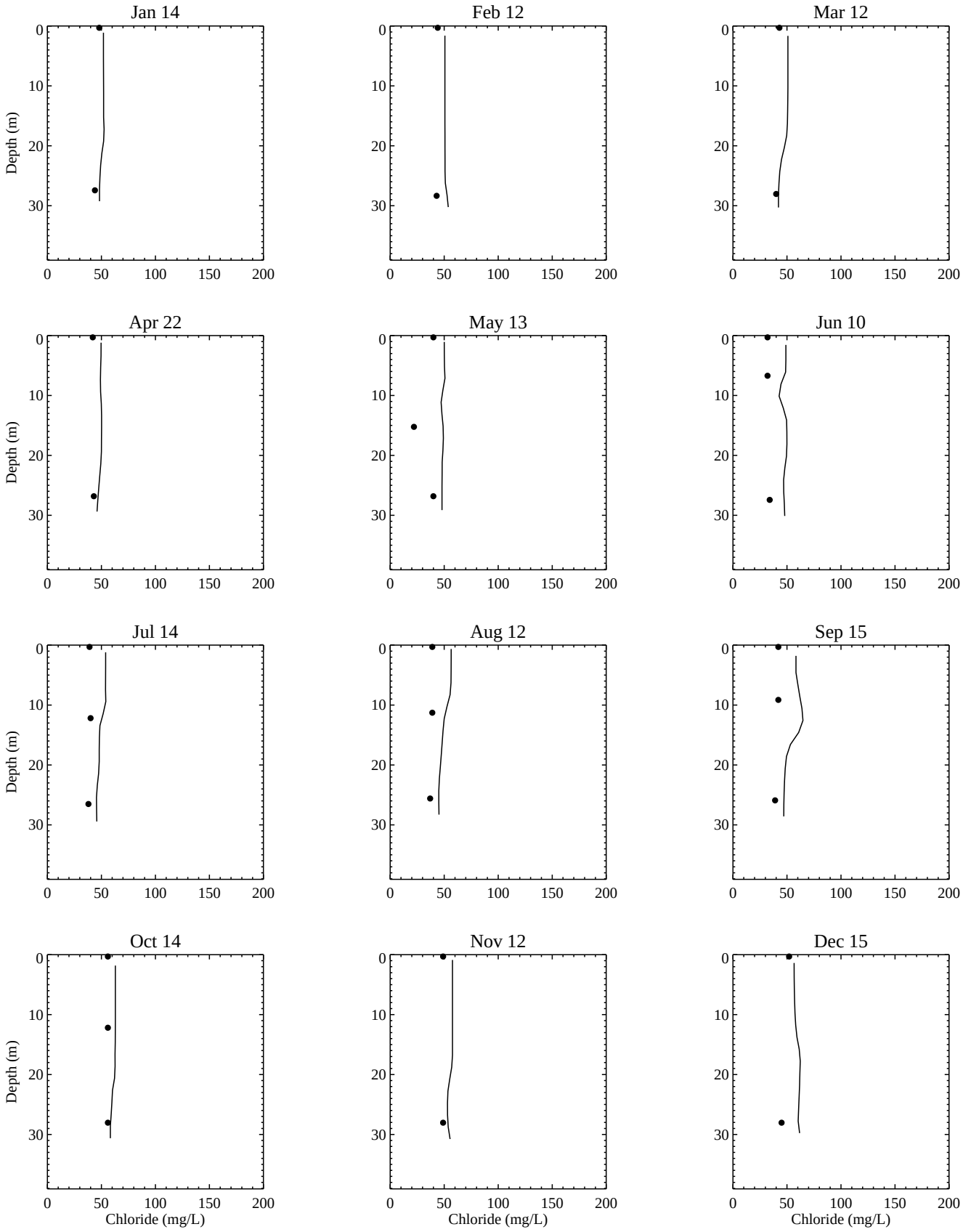

Figure J-13. Vertical profiles of model versus data at Pace Bend (Segment 48) - Chloride - 1986.

Profiles shown for dates with available data else model results for first day of month shown.

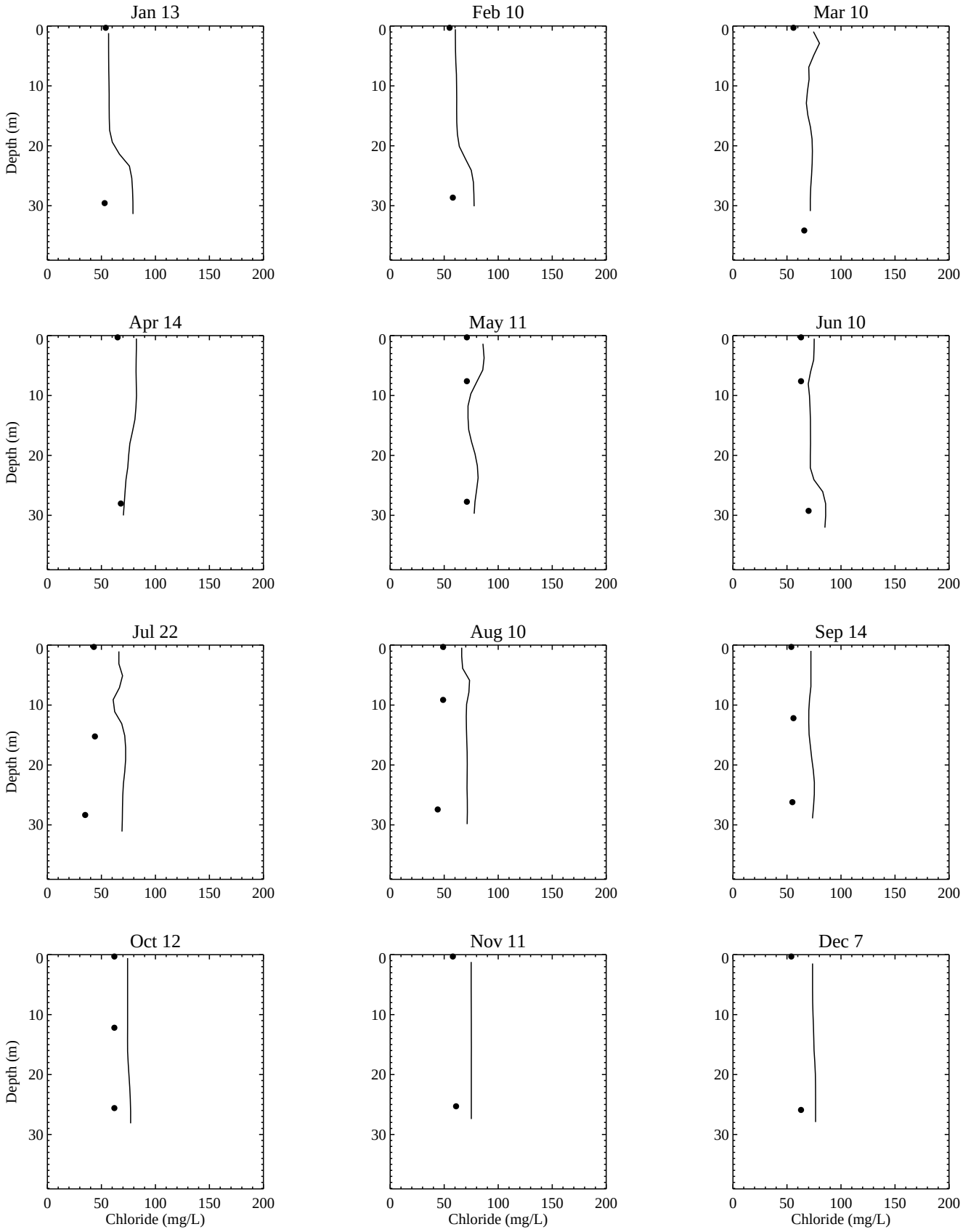

Figure J-13. Vertical profiles of model versus data at Pace Bend (Segment 48) - Chloride - 1987.

Profiles shown for dates with available data else model results for first day of month shown.

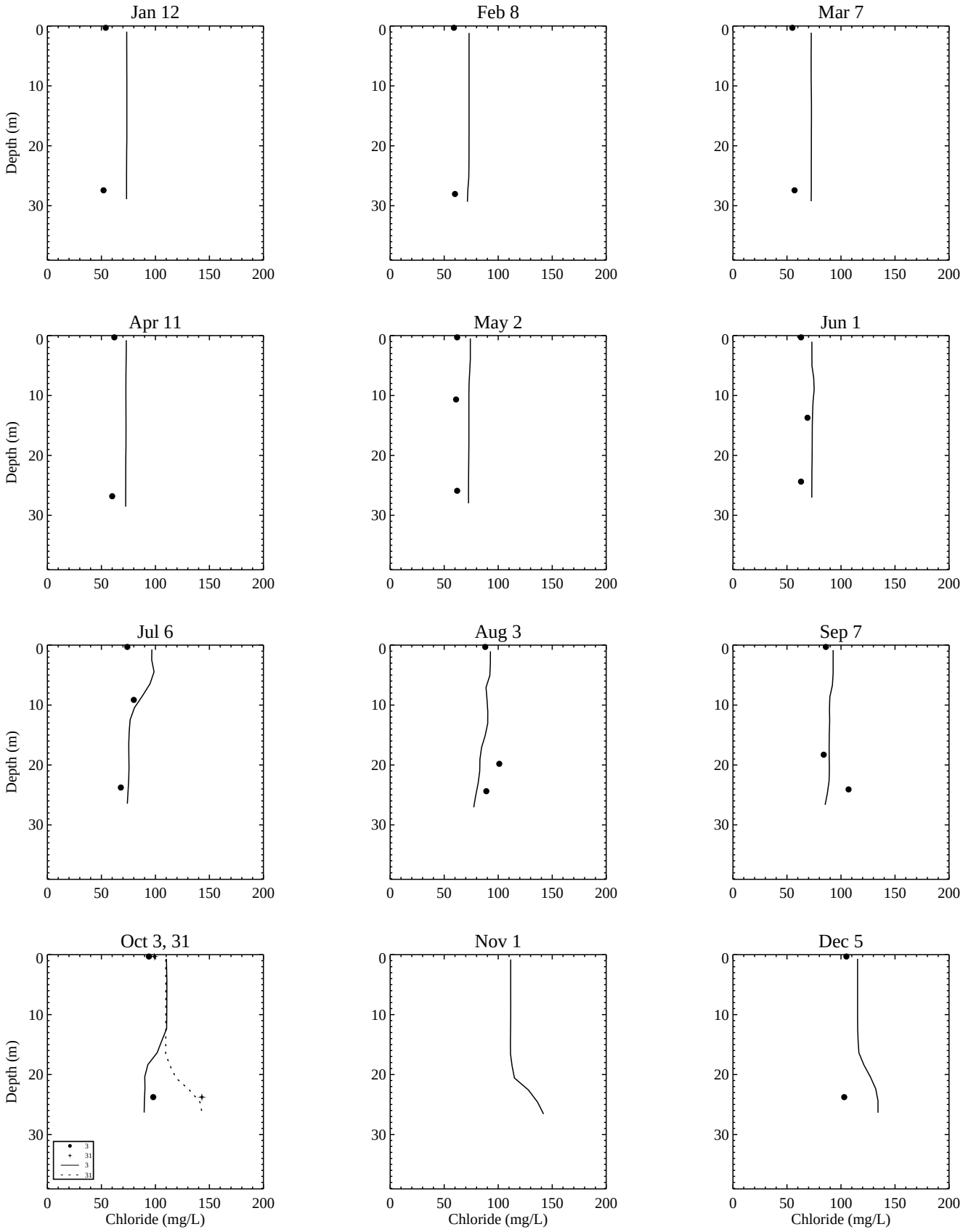

Figure J-13. Vertical profiles of model versus data at Pace Bend (Segment 48) - Chloride - 1988.

Profiles shown for dates with available data else model results for first day of month shown.

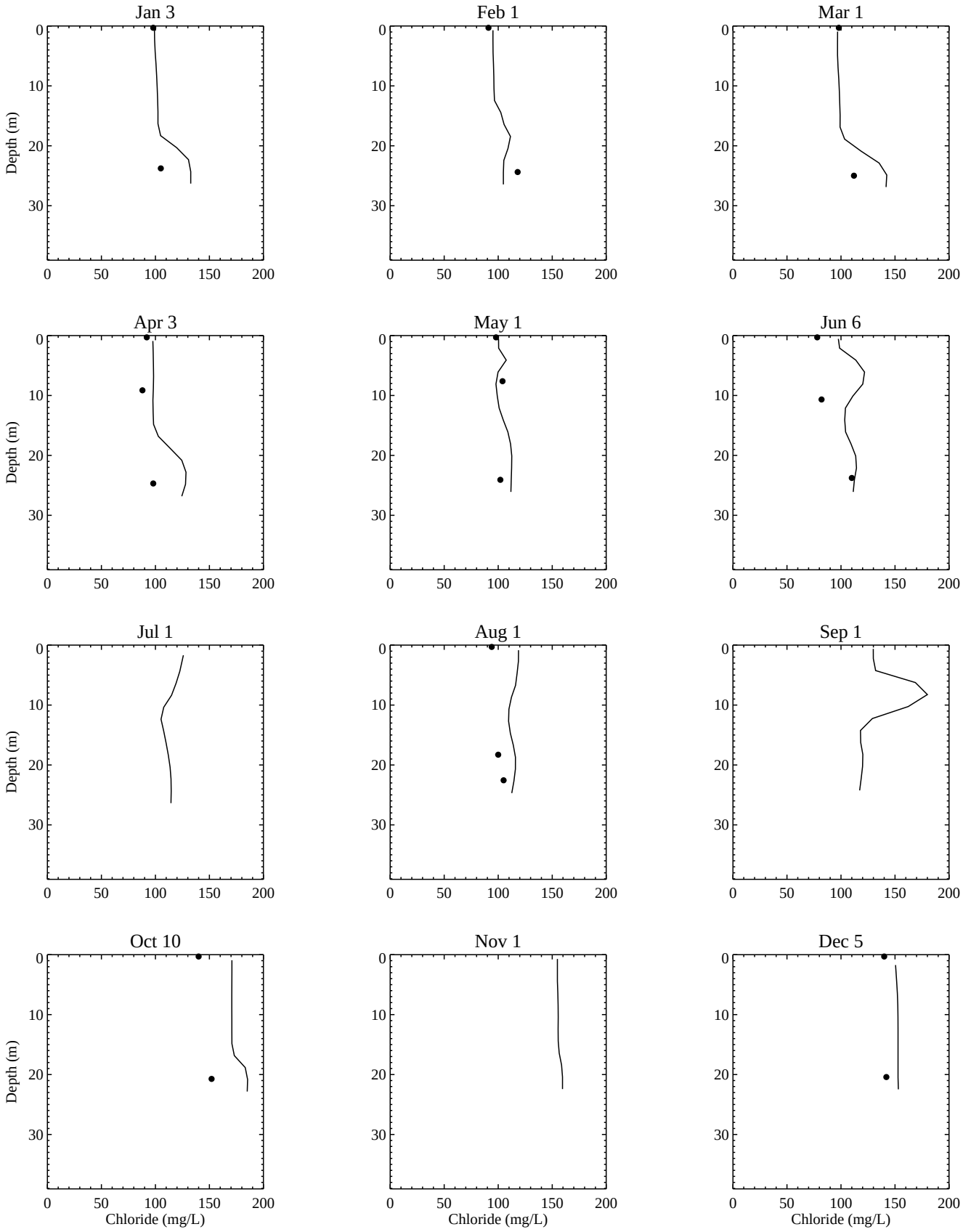

Figure J-13. Vertical profiles of model versus data at Pace Bend (Segment 48) - Chloride - 1989.

Profiles shown for dates with available data else model results for first day of month shown.

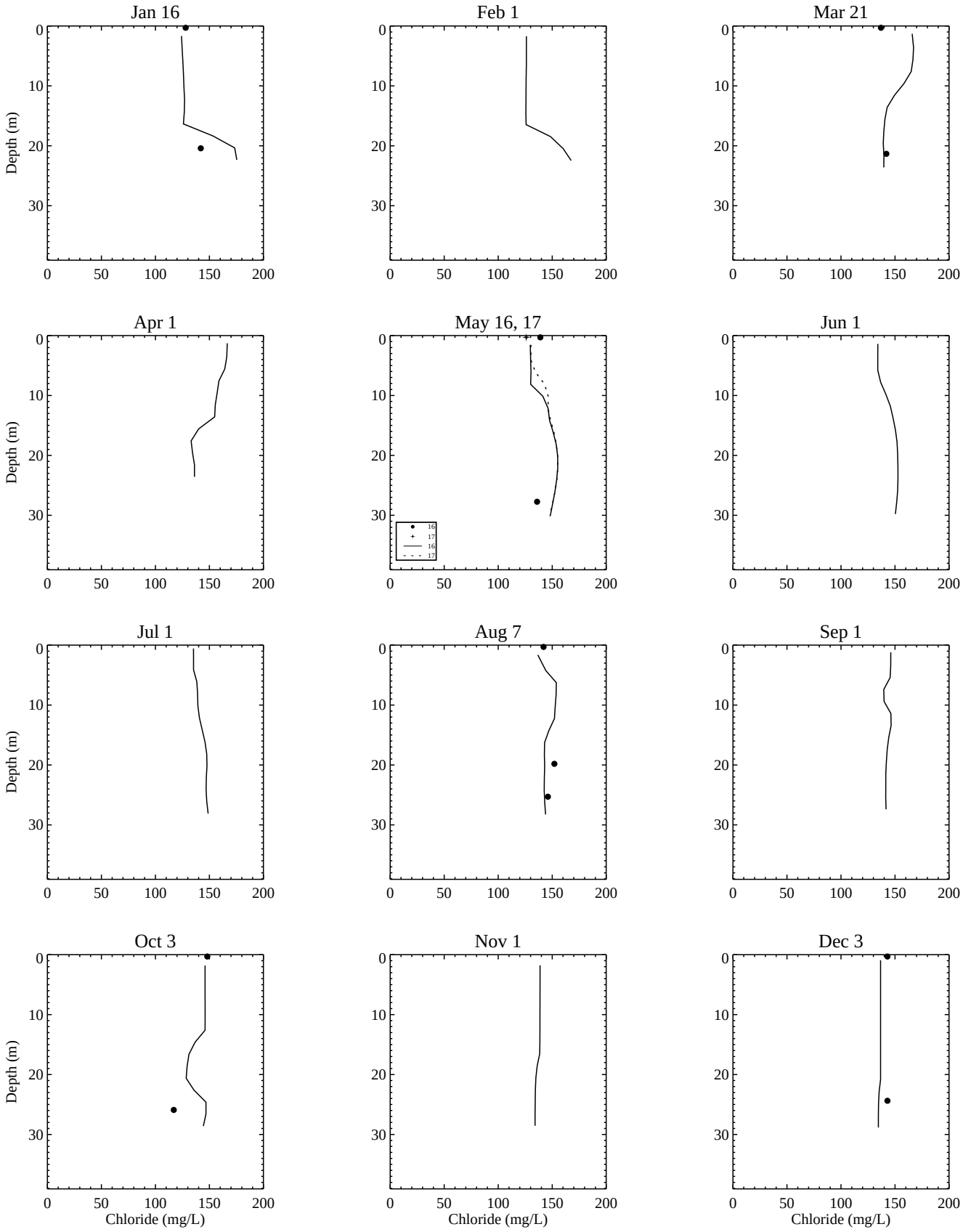

Figure J-13. Vertical profiles of model versus data at Pace Bend (Segment 48) - Chloride - 1990.

Profiles shown for dates with available data else model results for first day of month shown.

Model Data

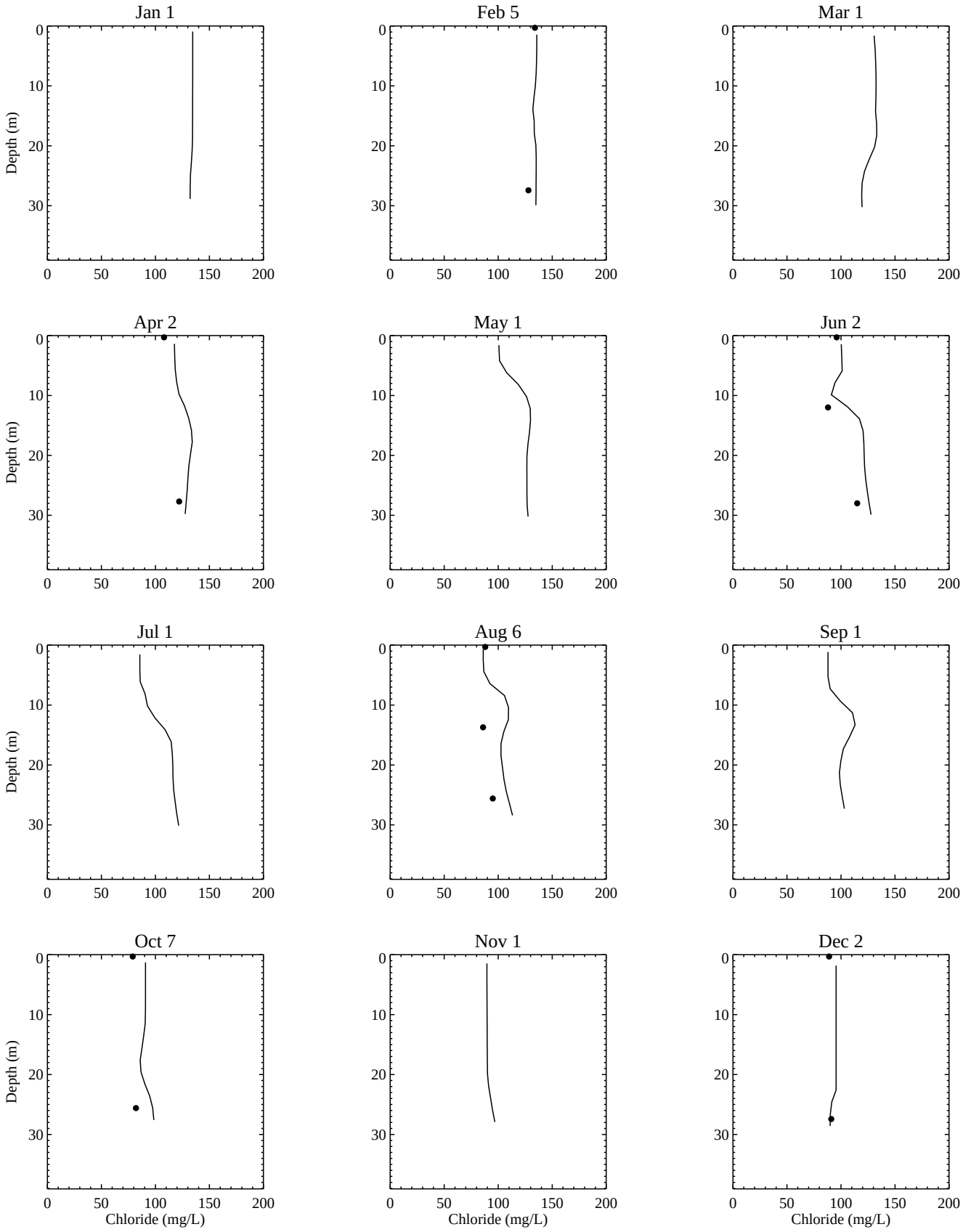

Figure J-13. Vertical profiles of model versus data at Pace Bend (Segment 48) - Chloride - 1991.

Profiles shown for dates with available data else model results for first day of month shown.

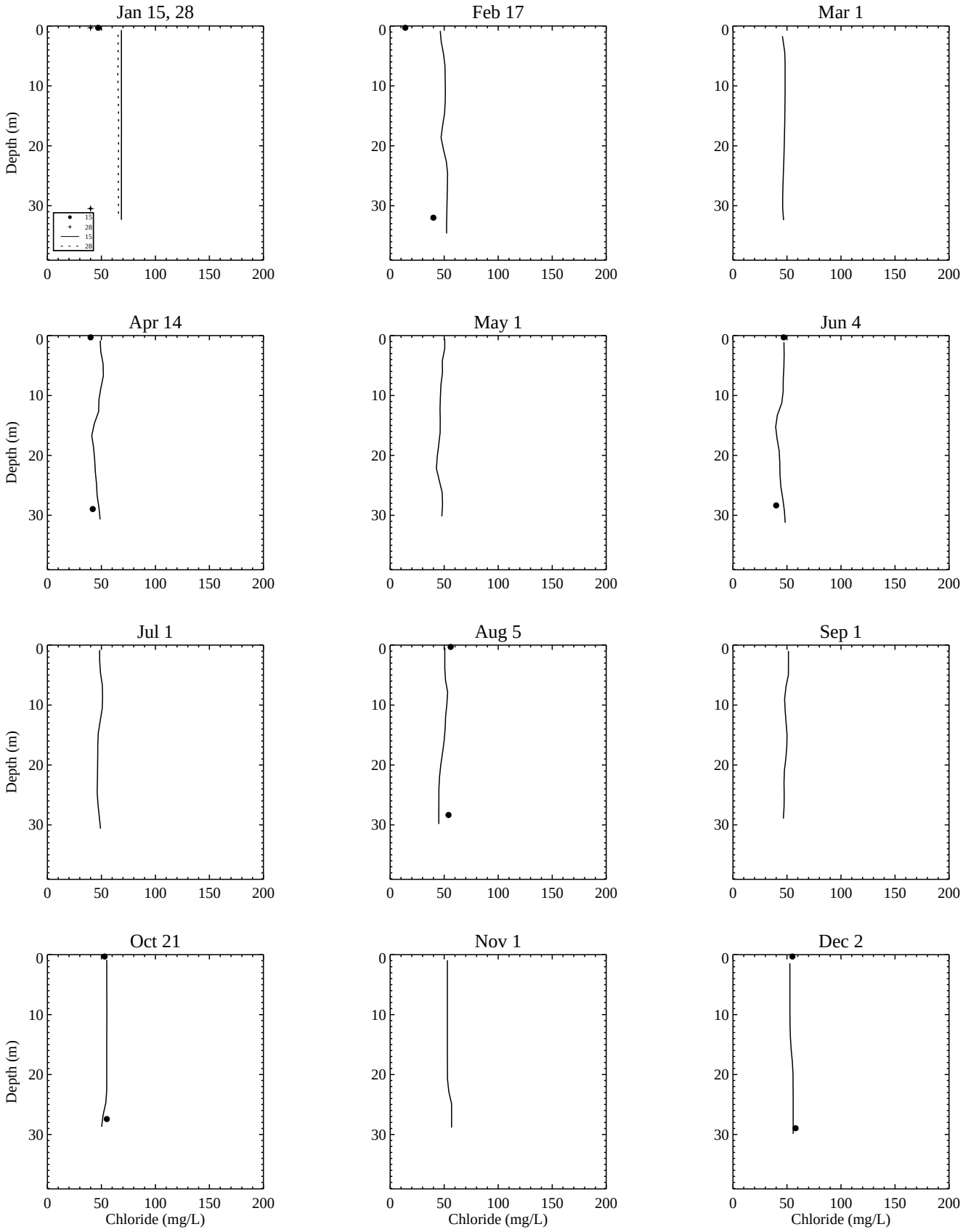

Figure J-13. Vertical profiles of model versus data at Pace Bend (Segment 48) - Chloride - 1992.

Profiles shown for dates with available data else model results for first day of month shown.

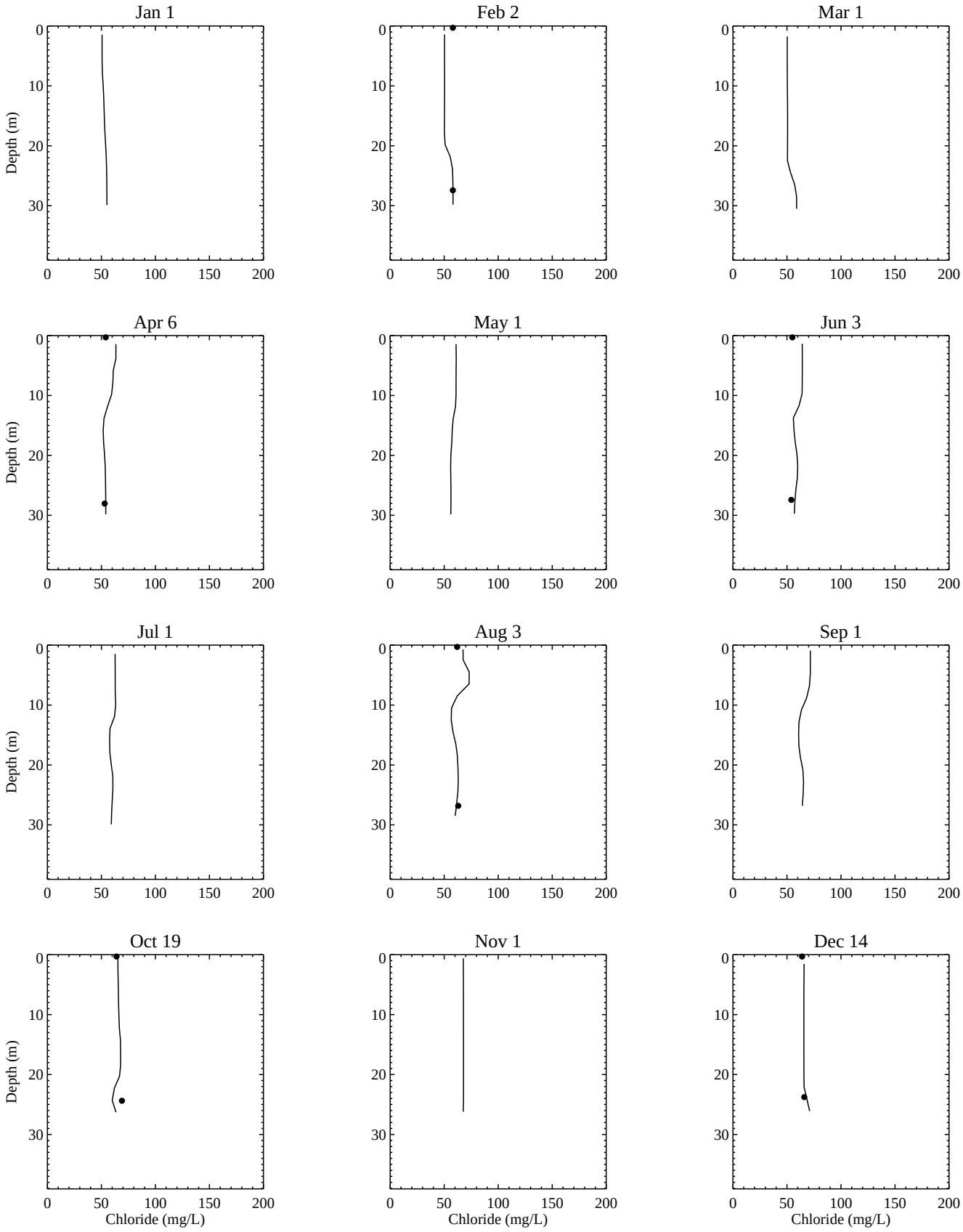

Figure J-13. Vertical profiles of model versus data at Pace Bend (Segment 48) - Chloride - 1993.

Profiles shown for dates with available data else model results for first day of month shown.

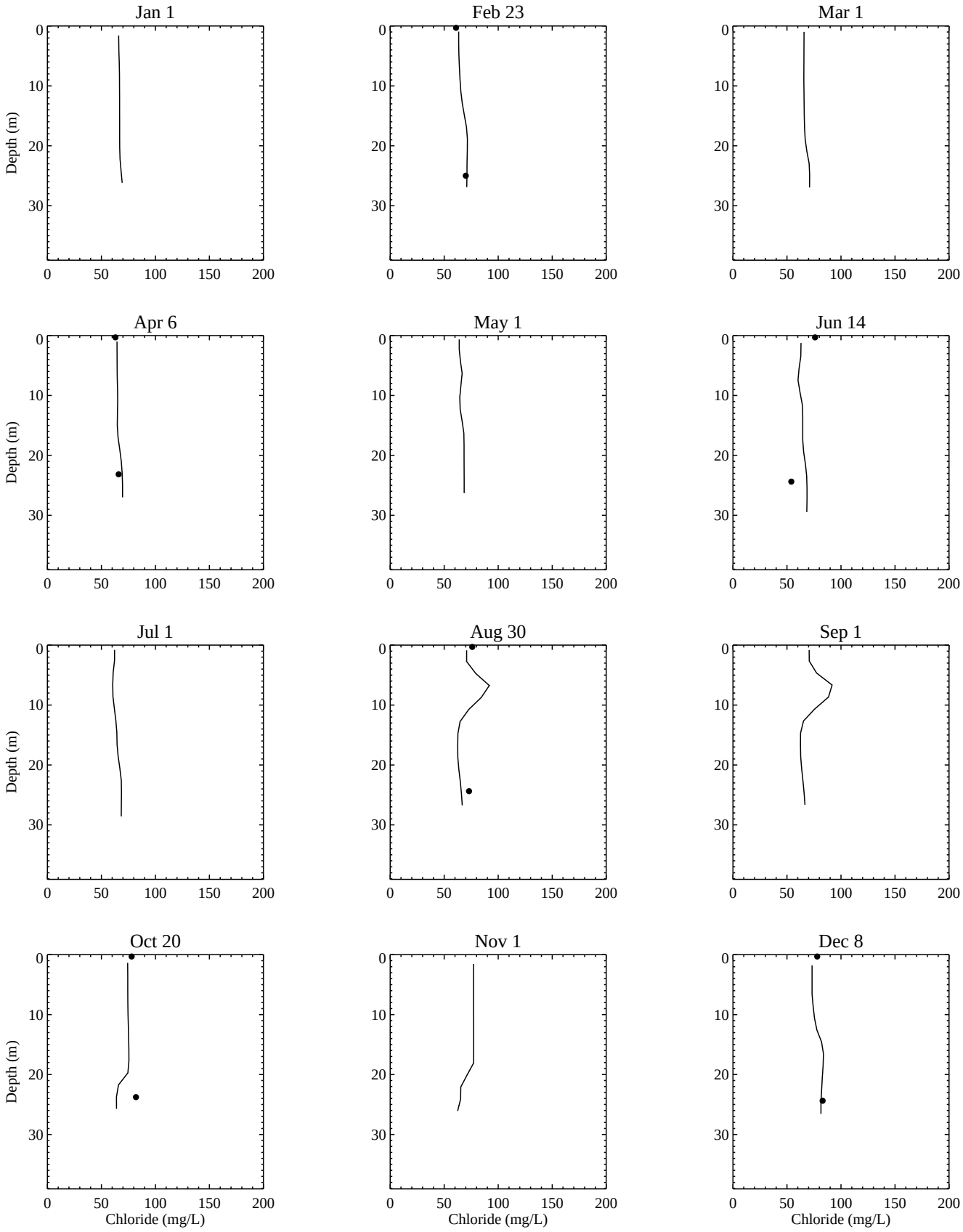

Figure J-13. Vertical profiles of model versus data at Pace Bend (Segment 48) - Chloride - 1994.

Profiles shown for dates with available data else model results for first day of month shown.

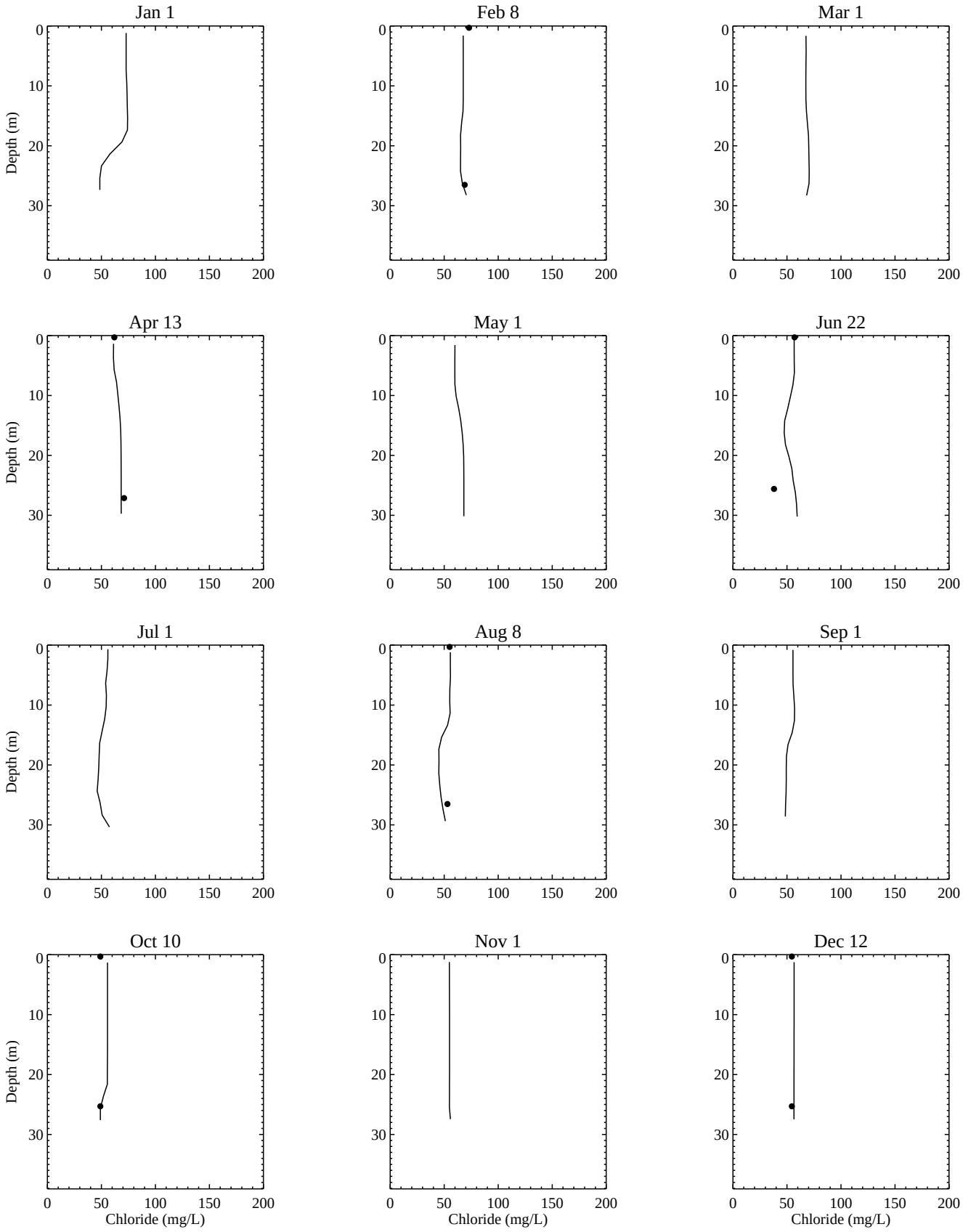

Figure J-13. Vertical profiles of model versus data at Pace Bend (Segment 48) - Chloride - 1995.

Profiles shown for dates with available data else model results for first day of month shown.

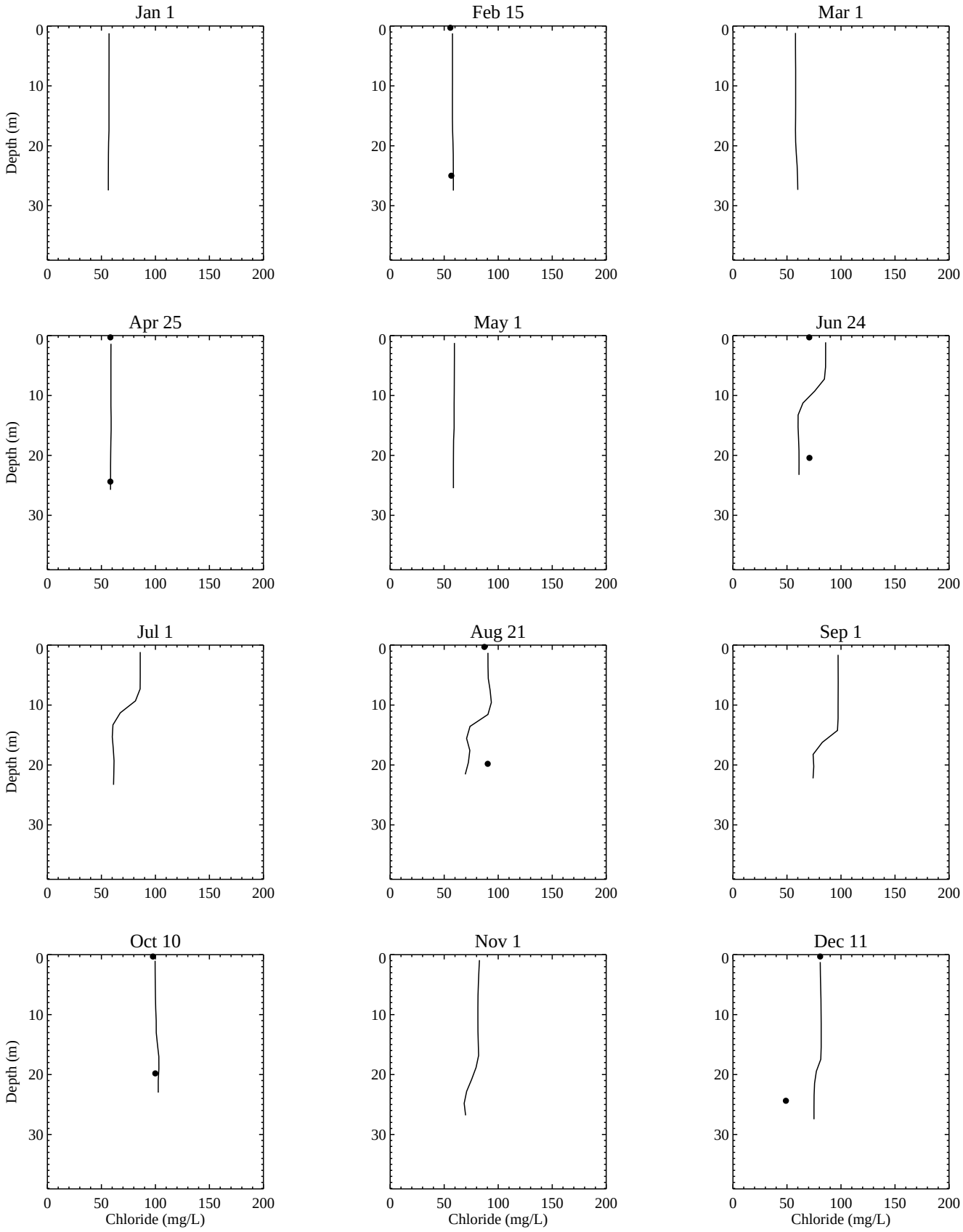

Figure J-13. Vertical profiles of model versus data at Pace Bend (Segment 48) - Chloride - 1996.

Profiles shown for dates with available data else model results for first day of month shown.

Model ● Data

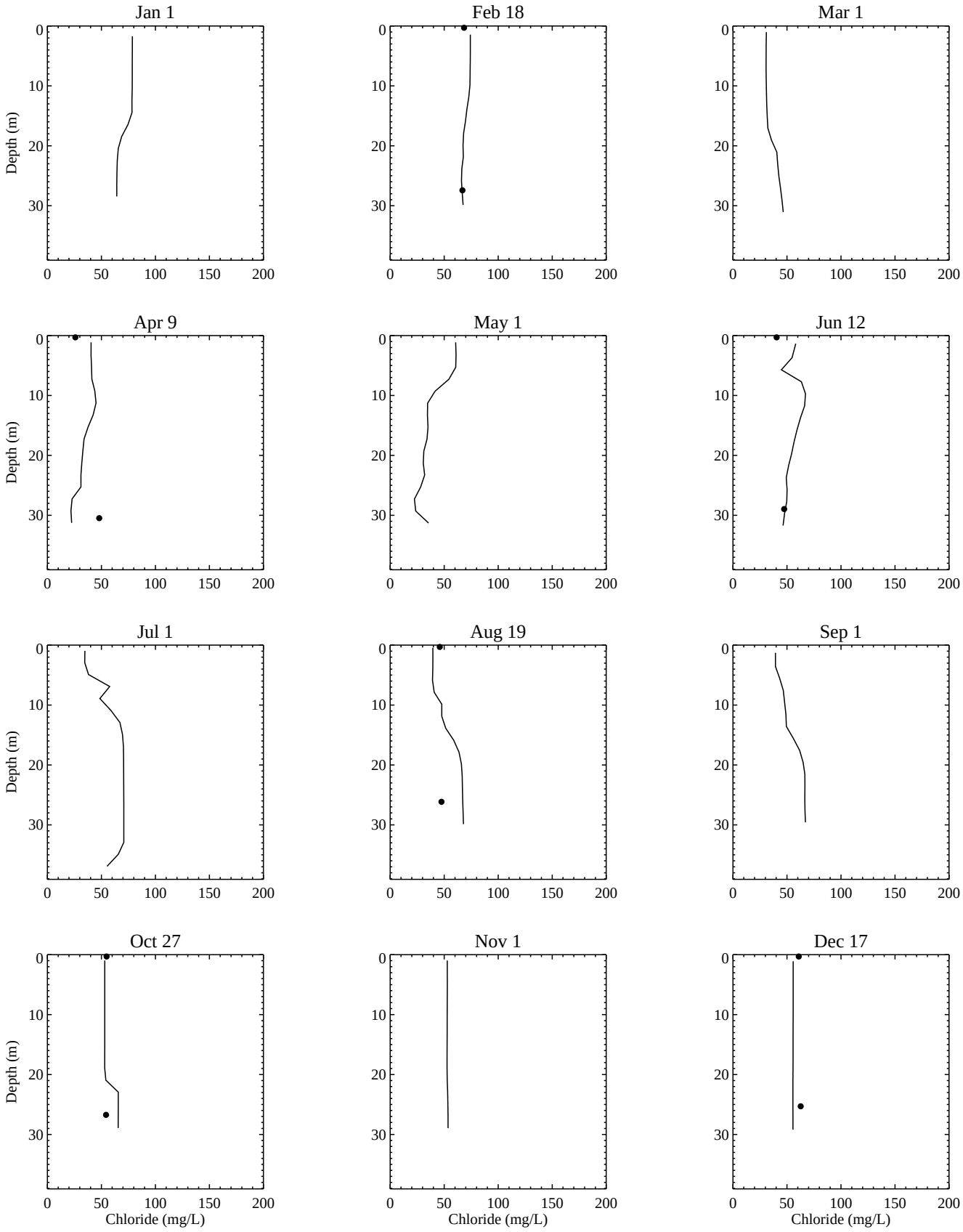

Figure J-13. Vertical profiles of model versus data at Pace Bend (Segment 48) - Chloride - 1997.

Profiles shown for dates with available data else model results for first day of month shown.

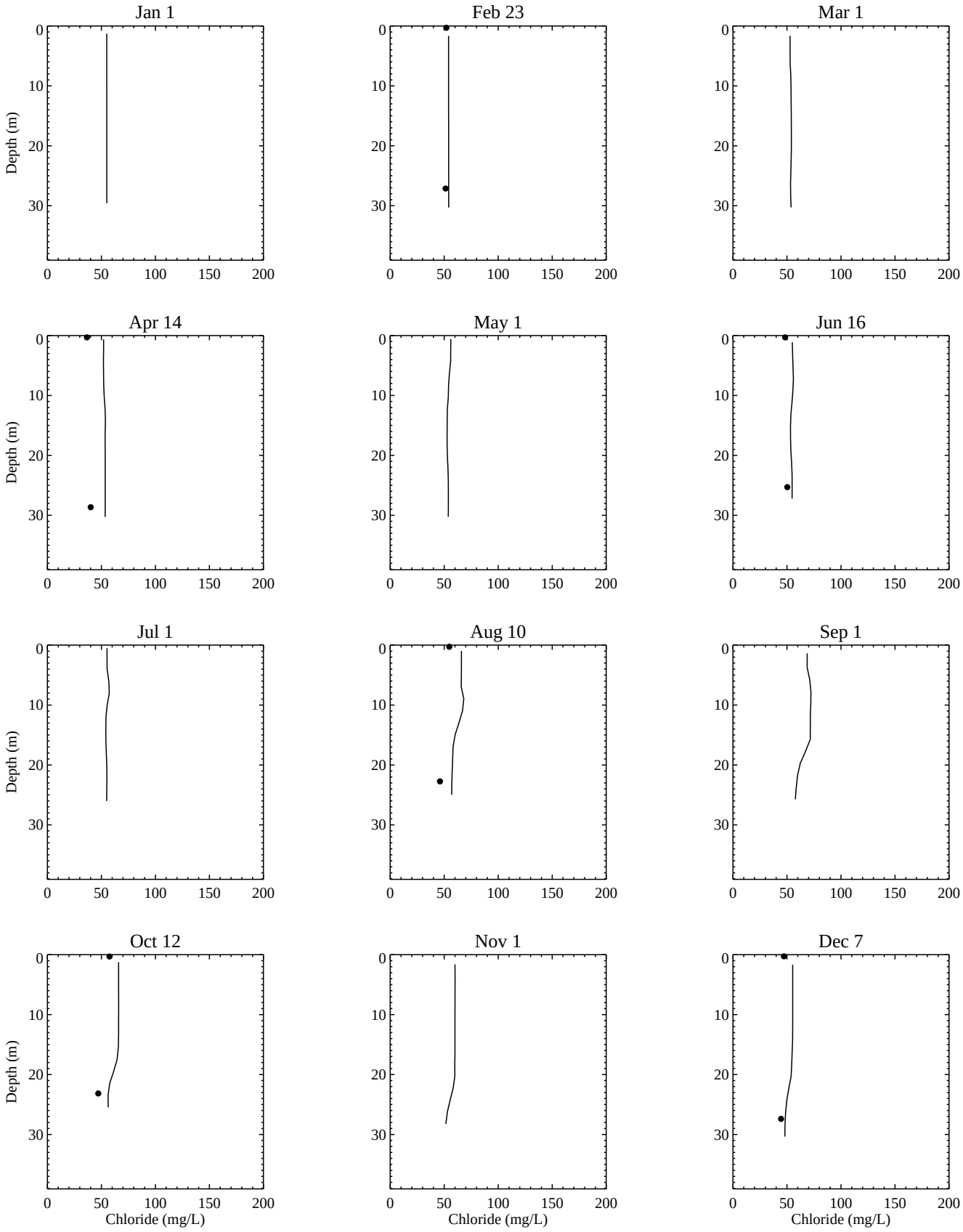

Figure J-13. Vertical profiles of model versus data at Pace Bend (Segment 48) - Chloride - 1998.

Profiles shown for dates with available data else model results for first day of month shown.

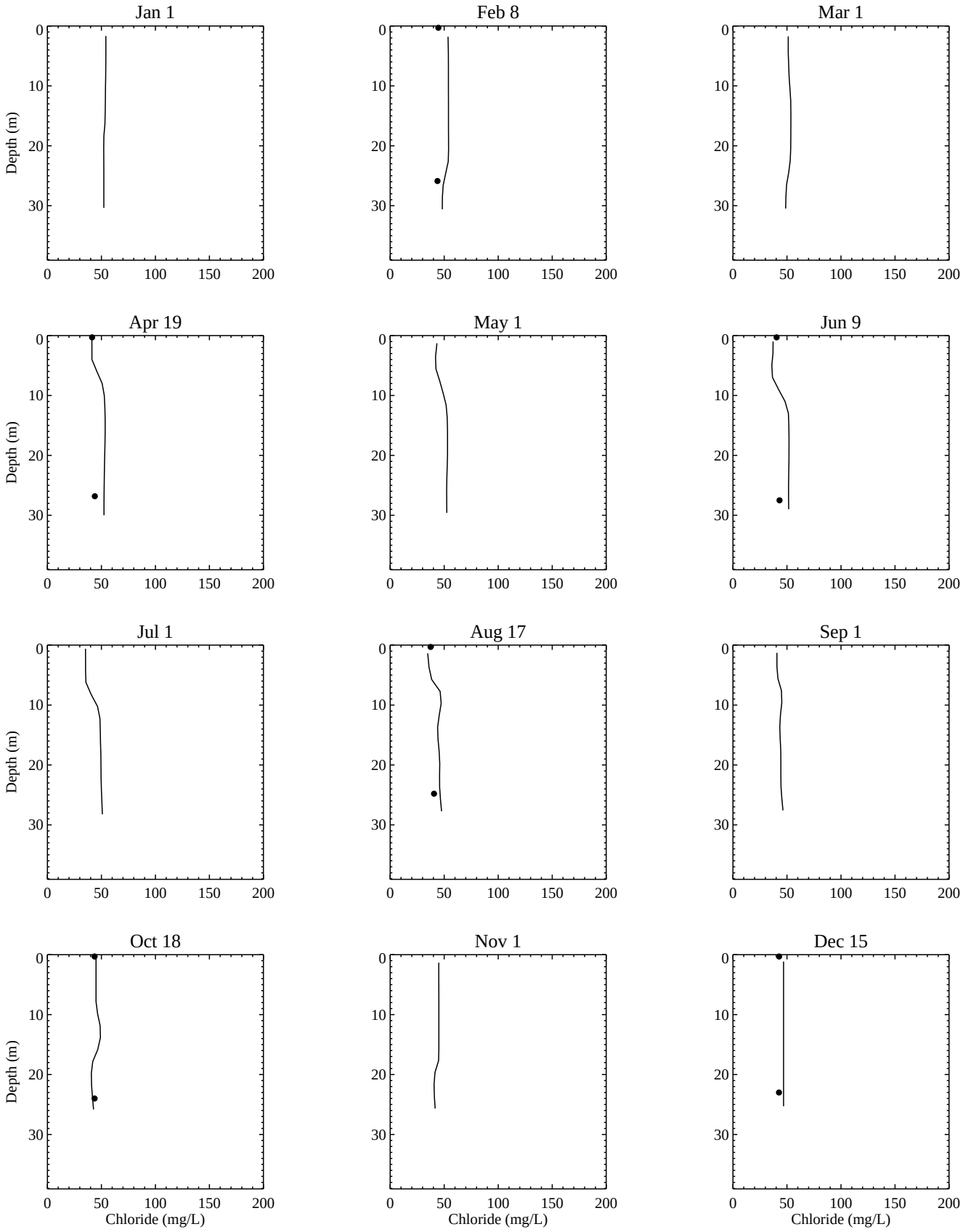

Figure J-13. Vertical profiles of model versus data at Pace Bend (Segment 48) - Chloride - 1999.

Profiles shown for dates with available data else model results for first day of month shown.

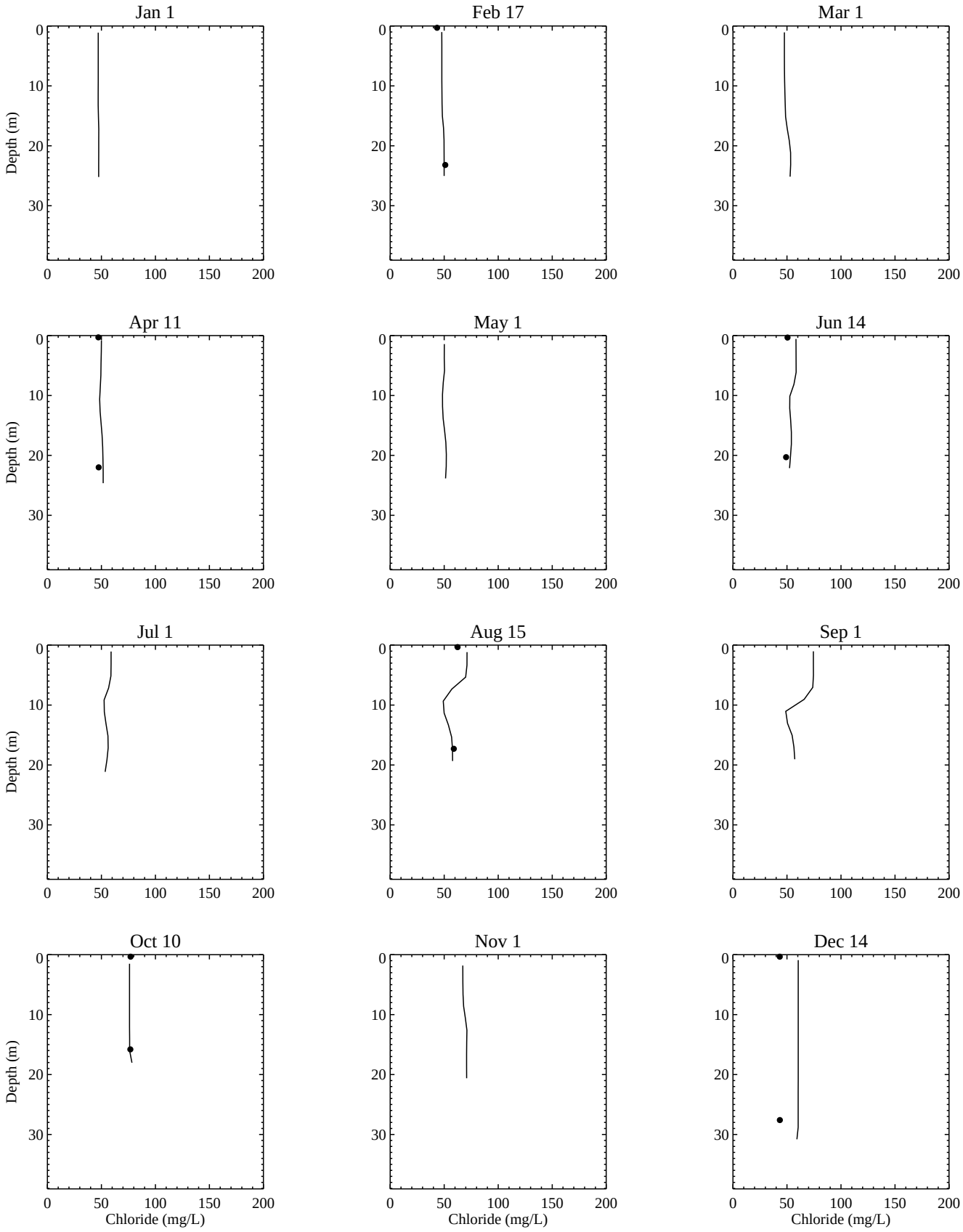

Figure J-13. Vertical profiles of model versus data at Pace Bend (Segment 48) - Chloride - 2000.

Profiles shown for dates with available data else model results for first day of month shown.

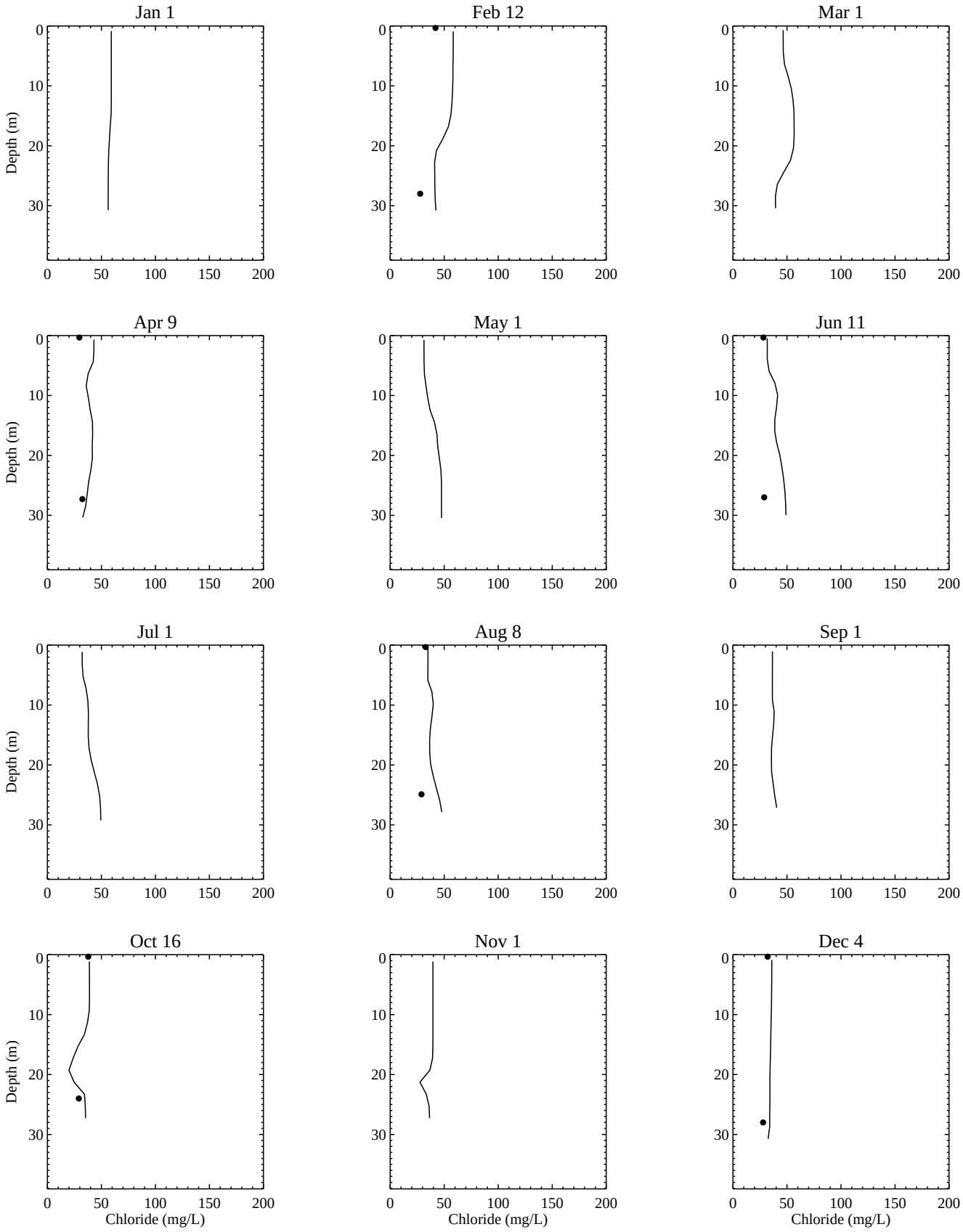

Figure J-13. Vertical profiles of model versus data at Pace Bend (Segment 48) - Chloride - 2001.

Profiles shown for dates with available data else model results for first day of month shown.

Model ● Data

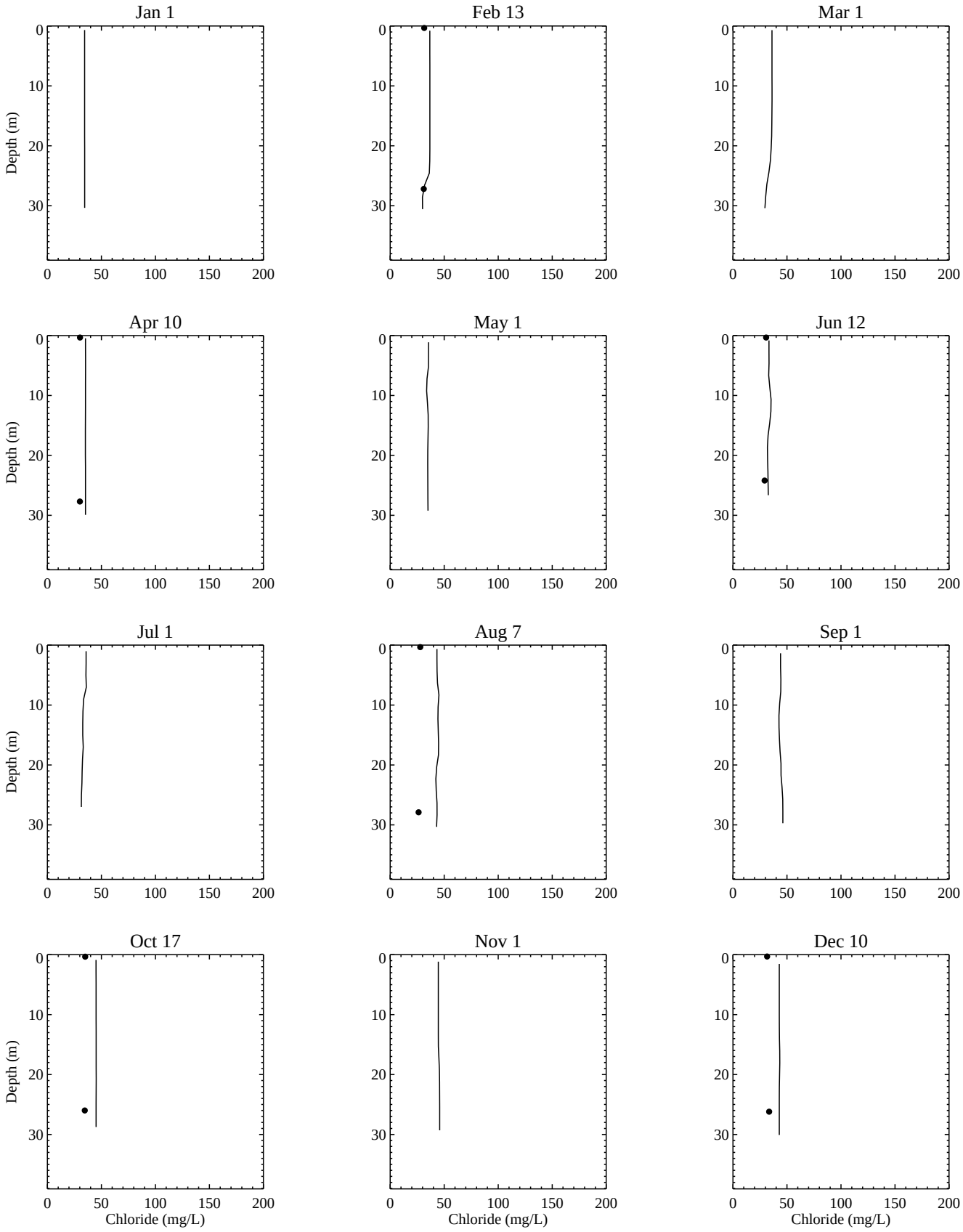

Figure J-13. Vertical profiles of model versus data at Pace Bend (Segment 48) - Chloride - 2002.

Profiles shown for dates with available data else model results for first day of month shown.

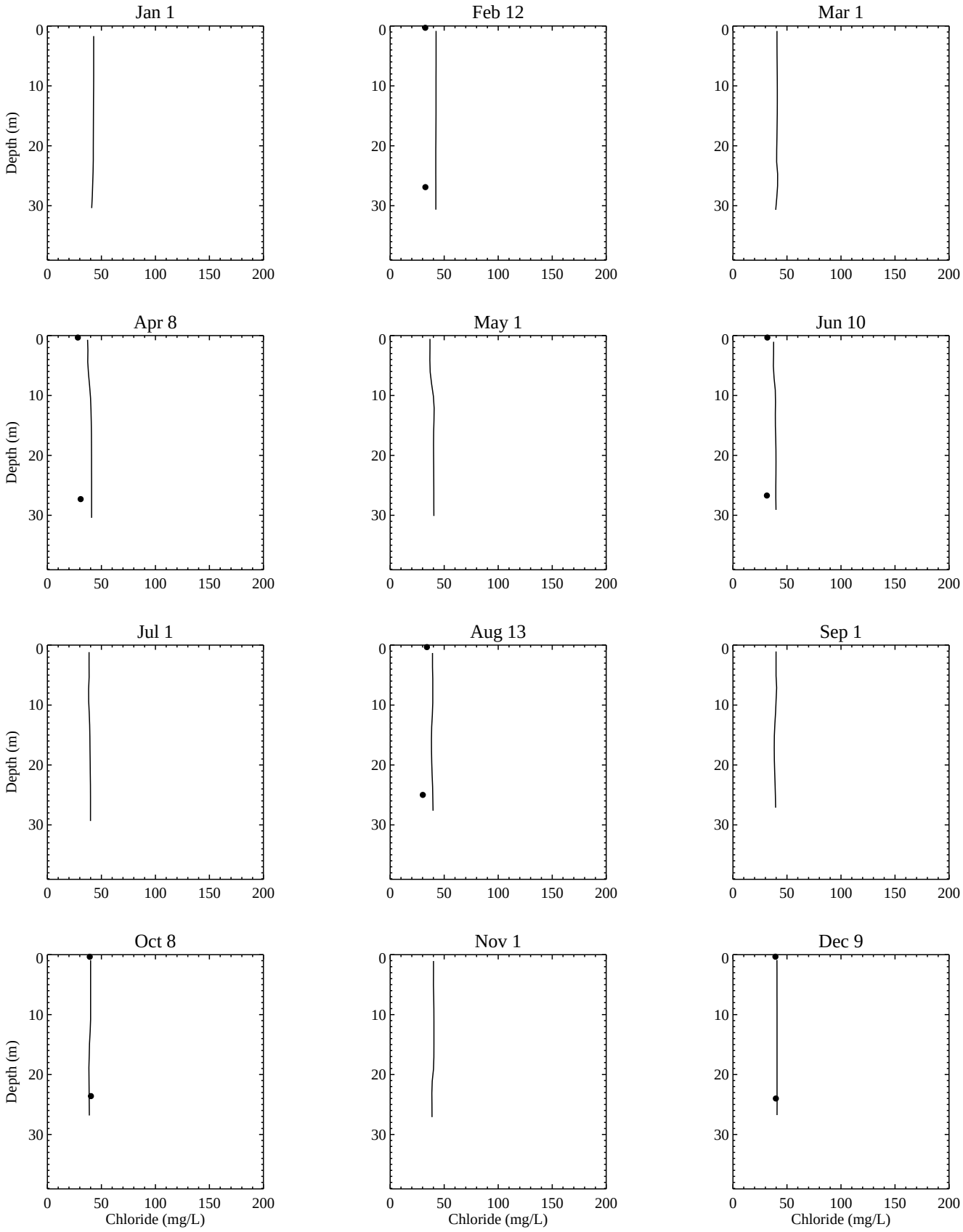

Figure J-13. Vertical profiles of model versus data at Pace Bend (Segment 48) - Chloride - 2003.

Profiles shown for dates with available data else model results for first day of month shown.

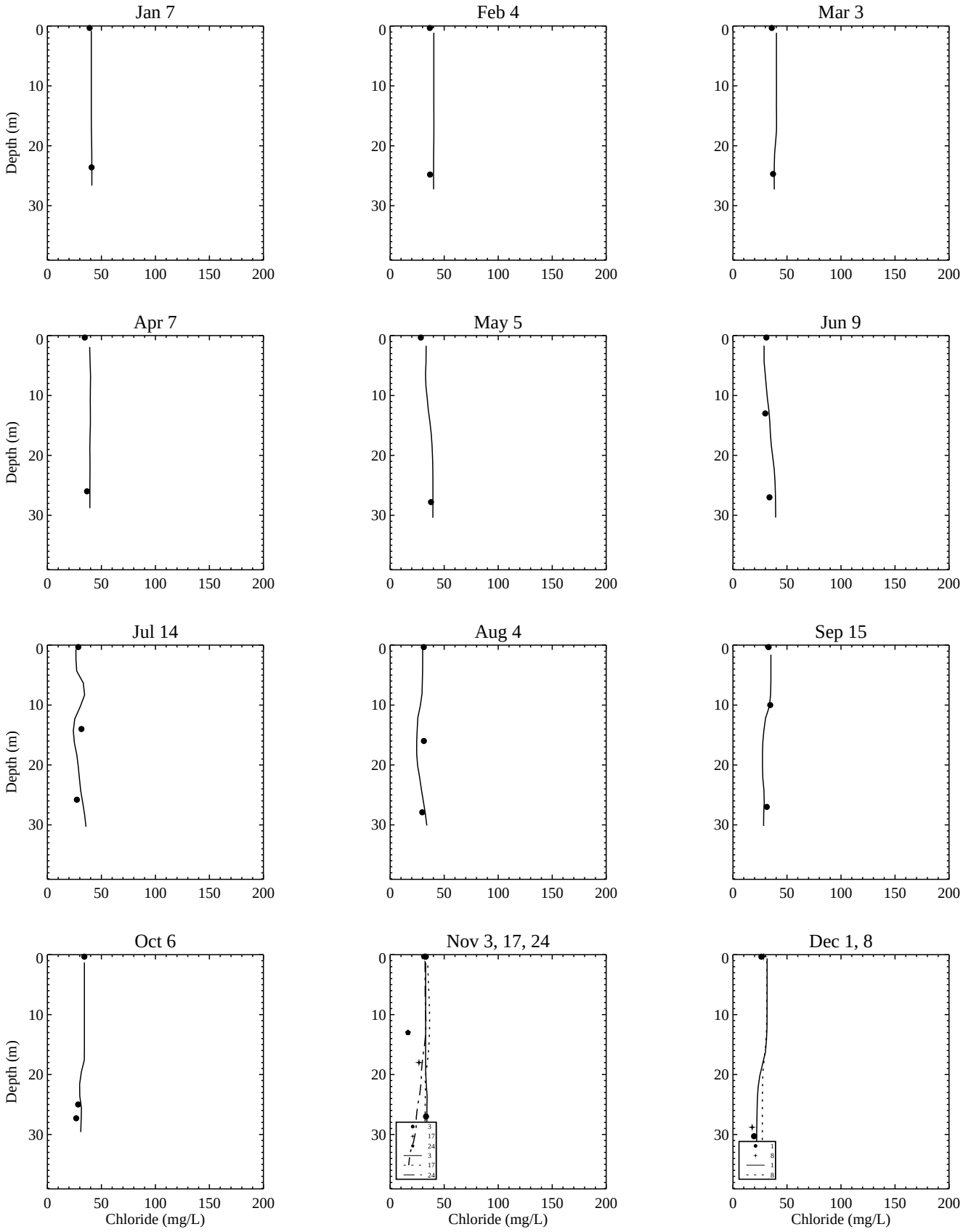

Figure J-13. Vertical profiles of model versus data at Pace Bend (Segment 48) - Chloride - 2004.

Profiles shown for dates with available data else model results for first day of month shown.

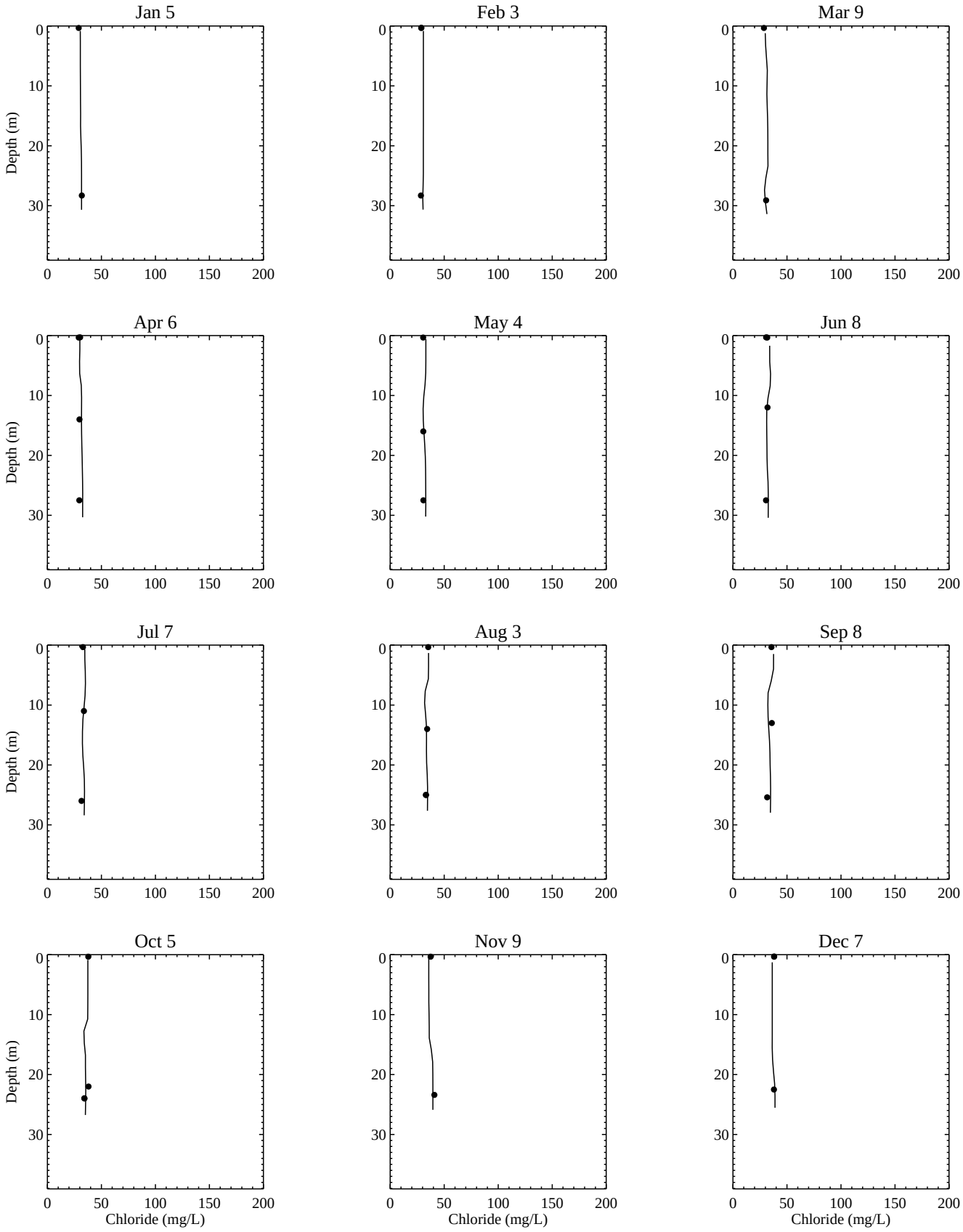

Figure J-13. Vertical profiles of model versus data at Pace Bend (Segment 48) - Chloride - 2005.

Profiles shown for dates with available data else model results for first day of month shown.

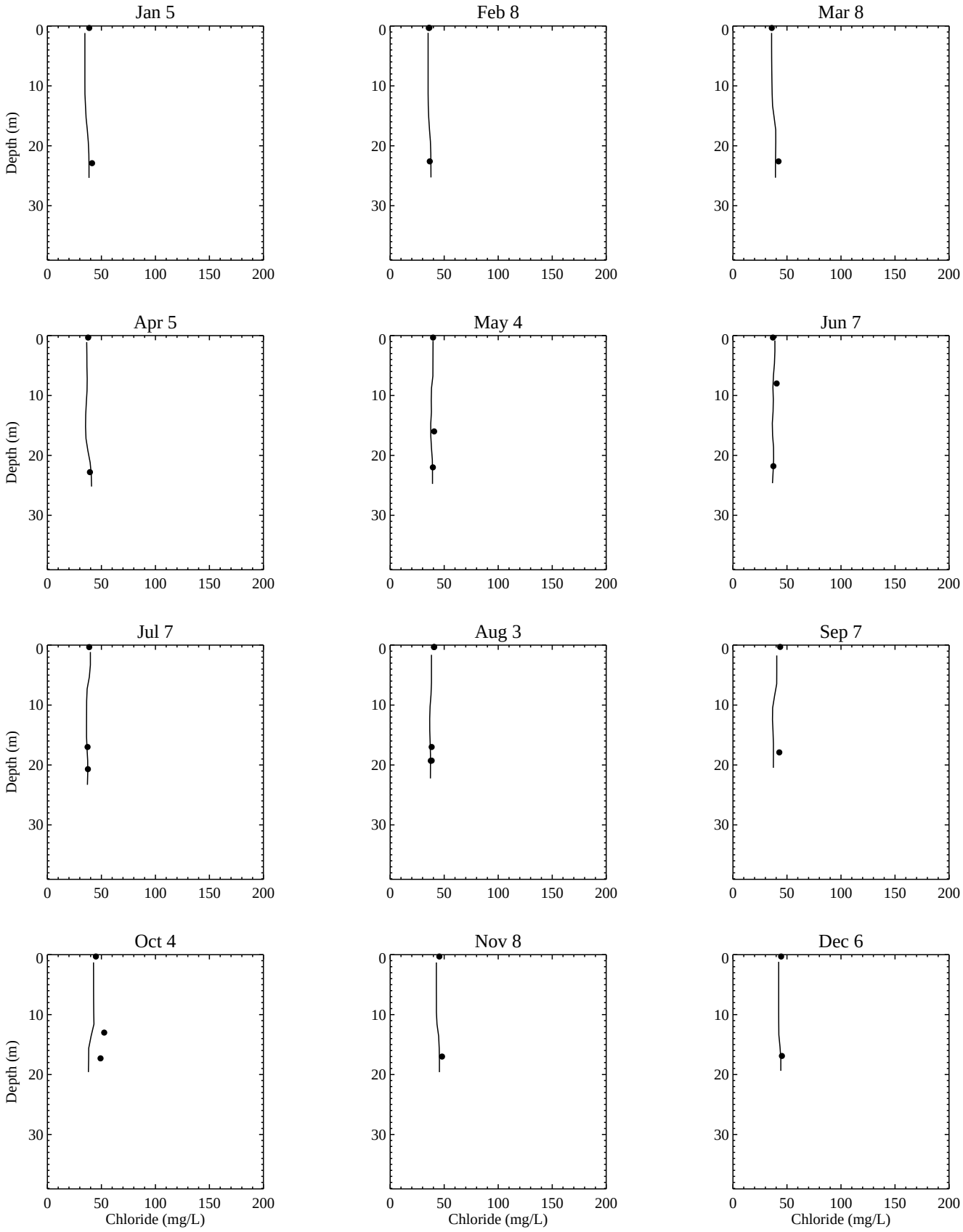

Figure J-13. Vertical profiles of model versus data at Pace Bend (Segment 48) - Chloride - 2006.

Profiles shown for dates with available data else model results for first day of month shown.

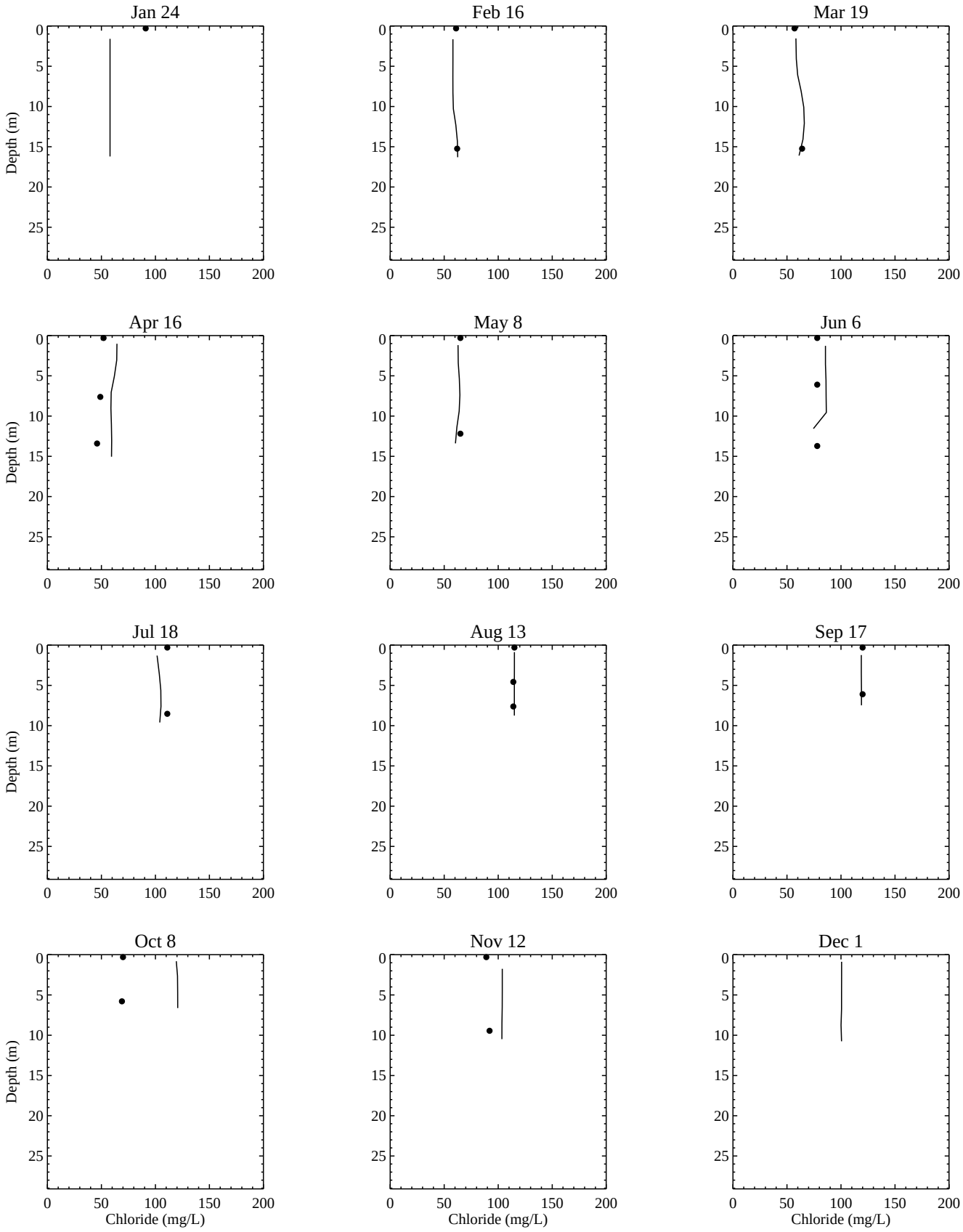

Figure J-14. Vertical profiles of model versus data at Turkey Bend (Segment 28) - Chloride - 1984.

Profiles shown for dates with available data else model results for first day of month shown.

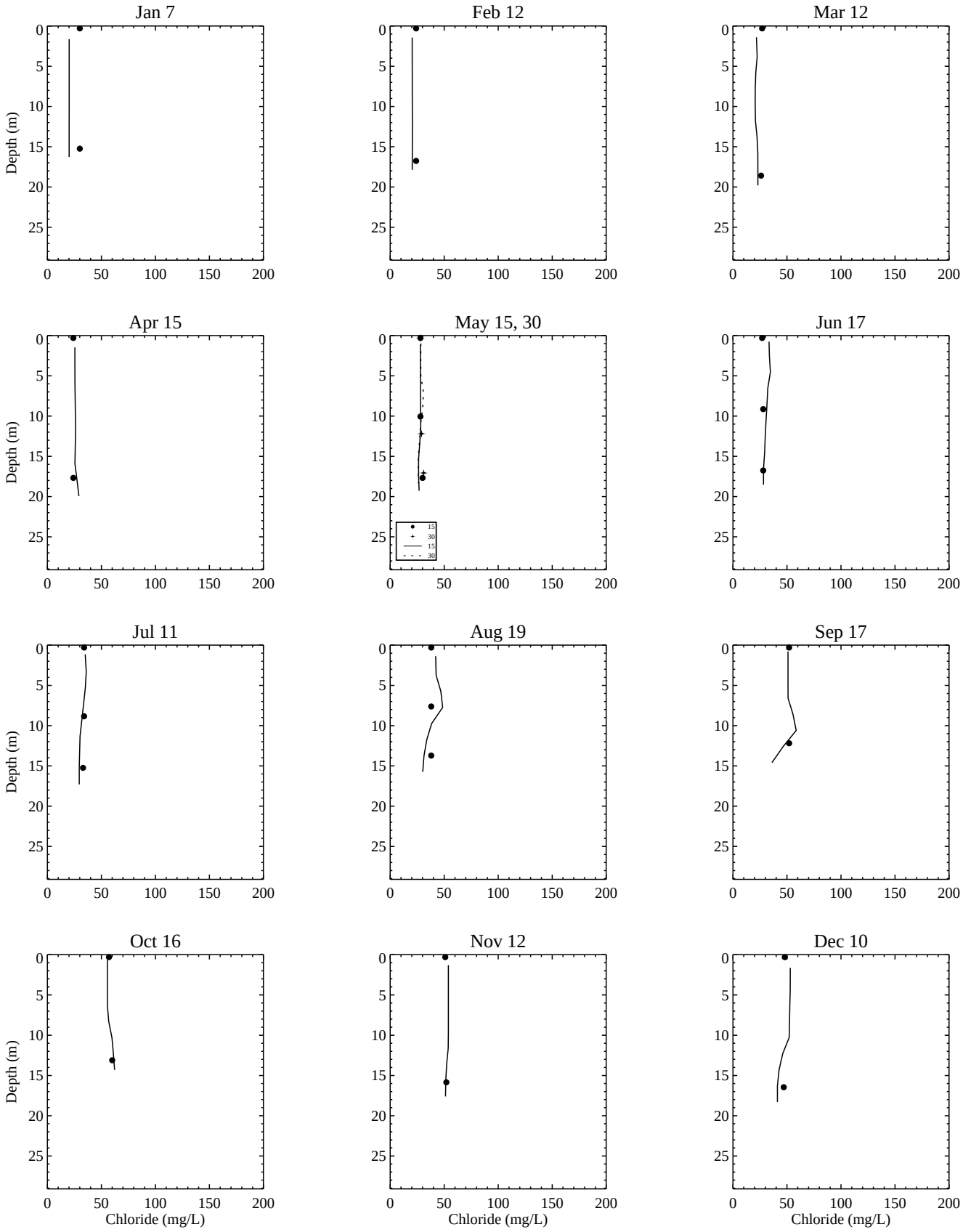

Figure J-14. Vertical profiles of model versus data at Turkey Bend (Segment 28) - Chloride - 1985.

Profiles shown for dates with available data else model results for first day of month shown.

Model Data

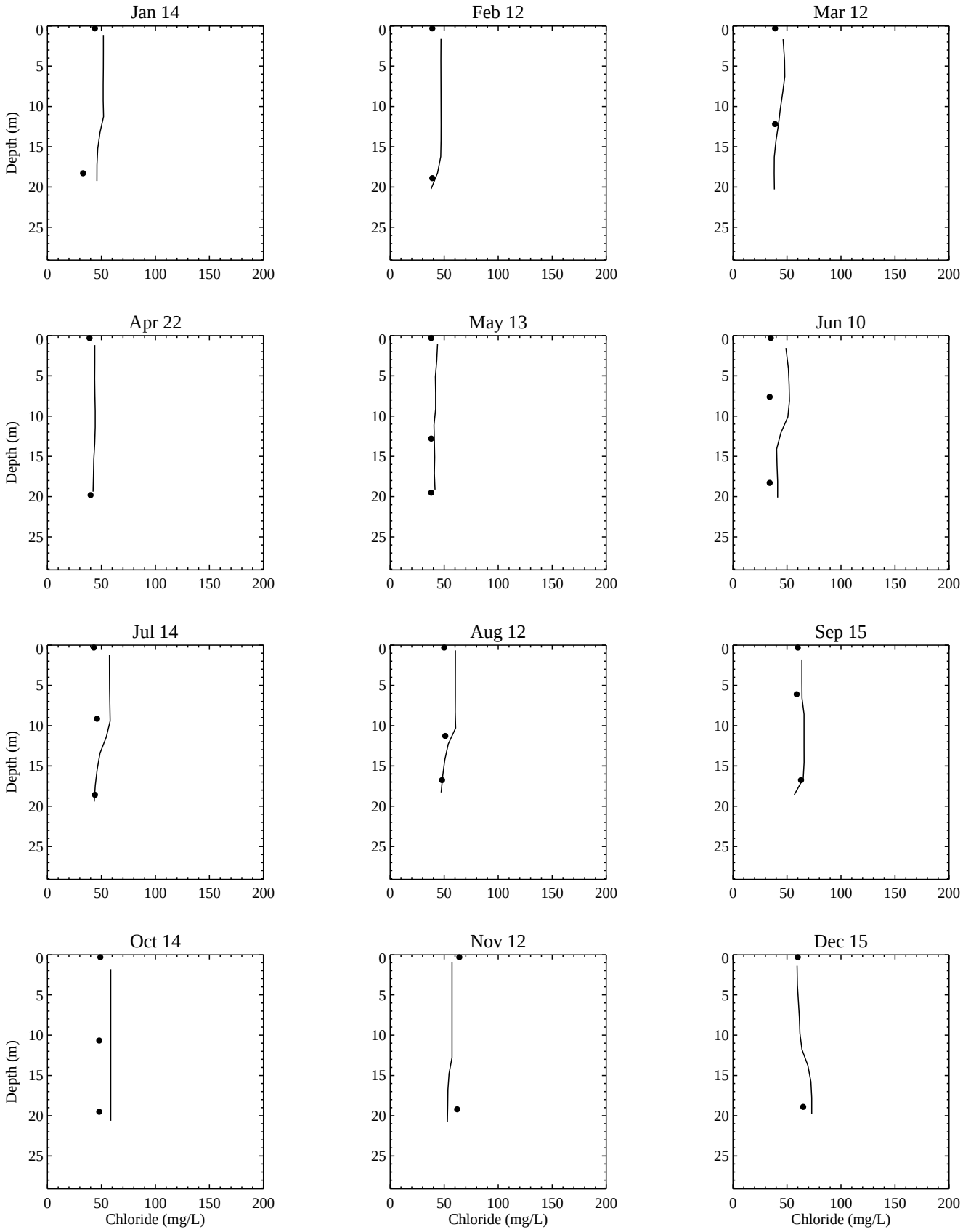

Figure J-14. Vertical profiles of model versus data at Turkey Bend (Segment 28) - Chloride - 1986.

Profiles shown for dates with available data else model results for first day of month shown.

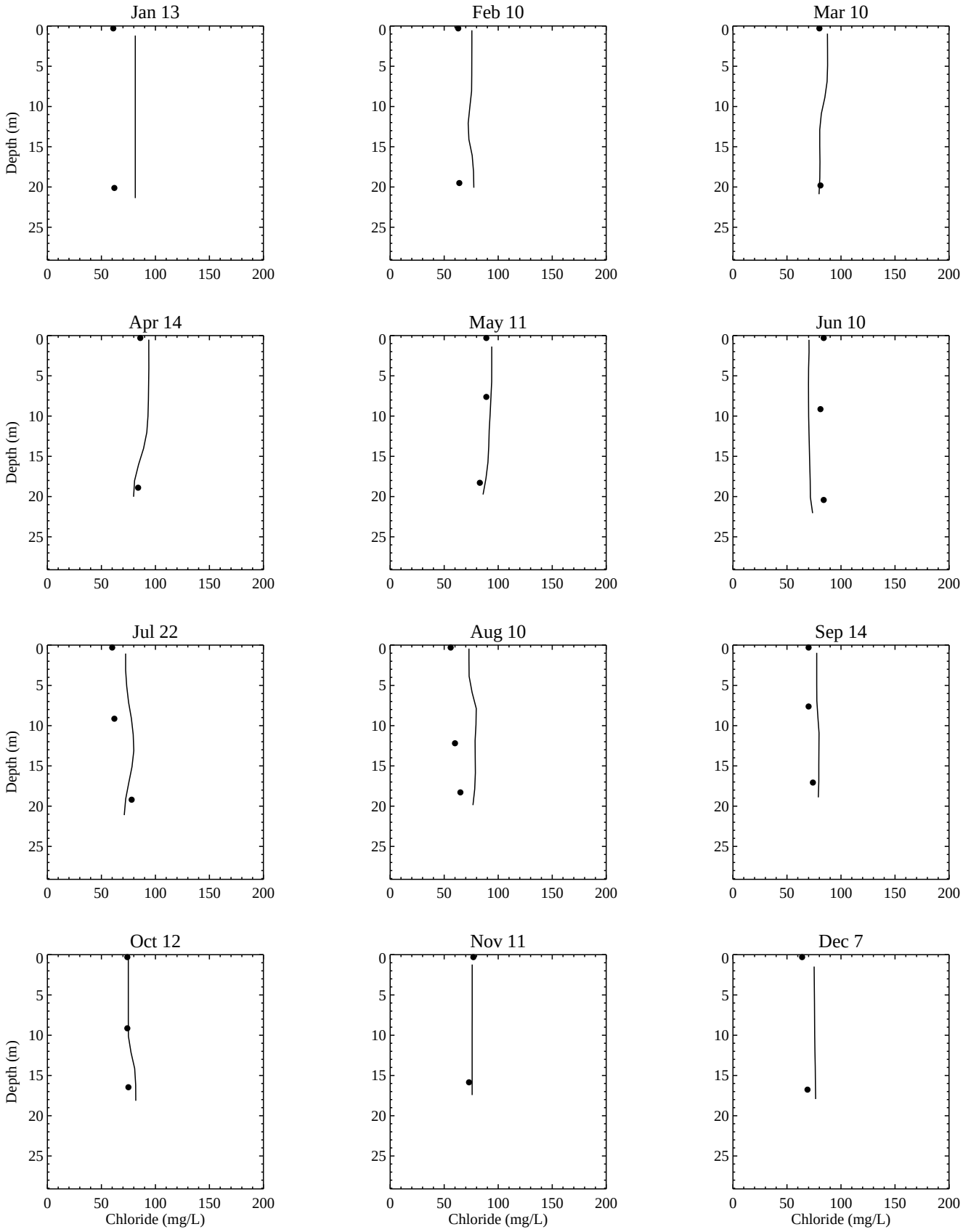

Figure J-14. Vertical profiles of model versus data at Turkey Bend (Segment 28) - Chloride - 1987.

Profiles shown for dates with available data else model results for first day of month shown.

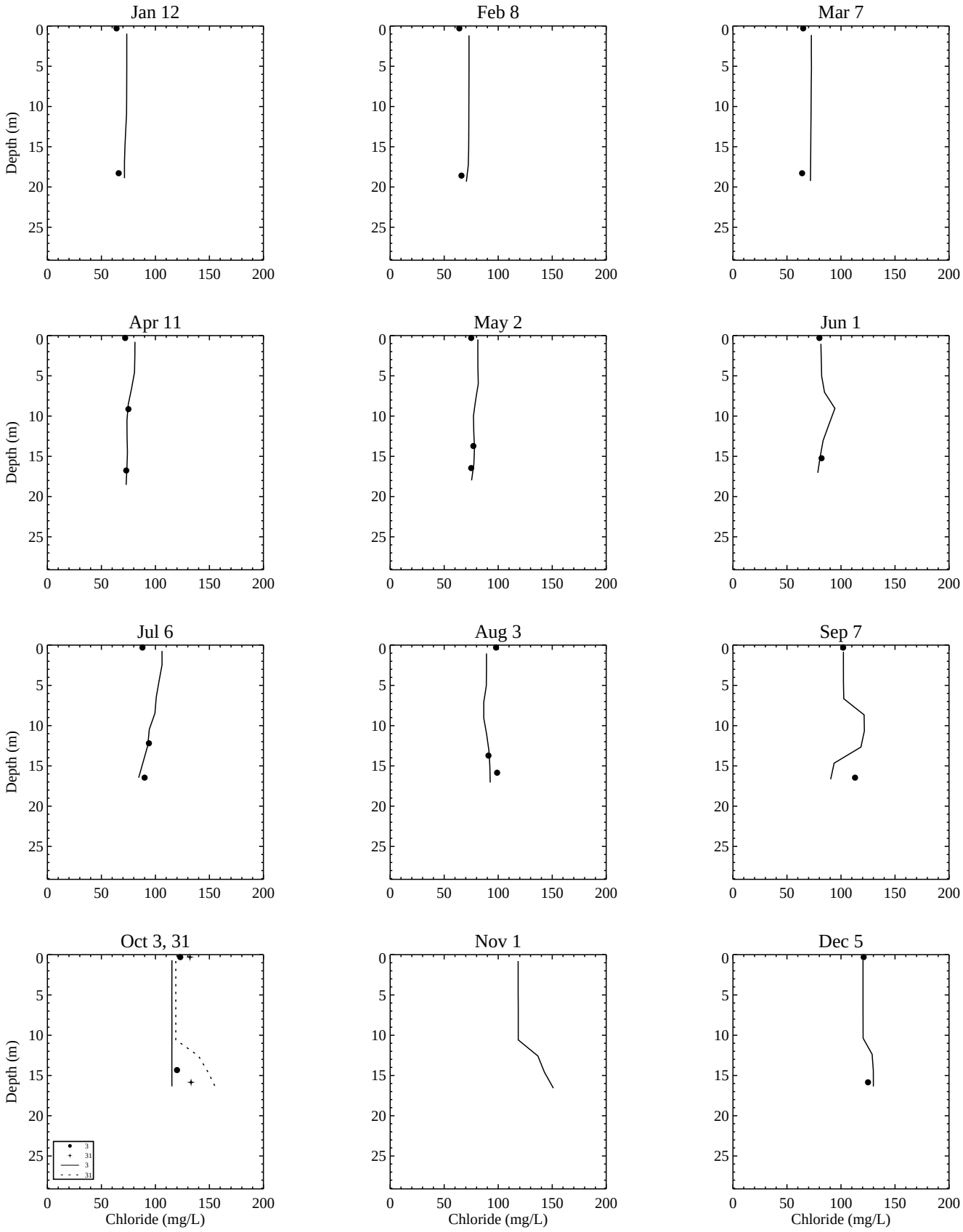

Figure J-14. Vertical profiles of model versus data at Turkey Bend (Segment 28) - Chloride - 1988.

Profiles shown for dates with available data else model results for first day of month shown.

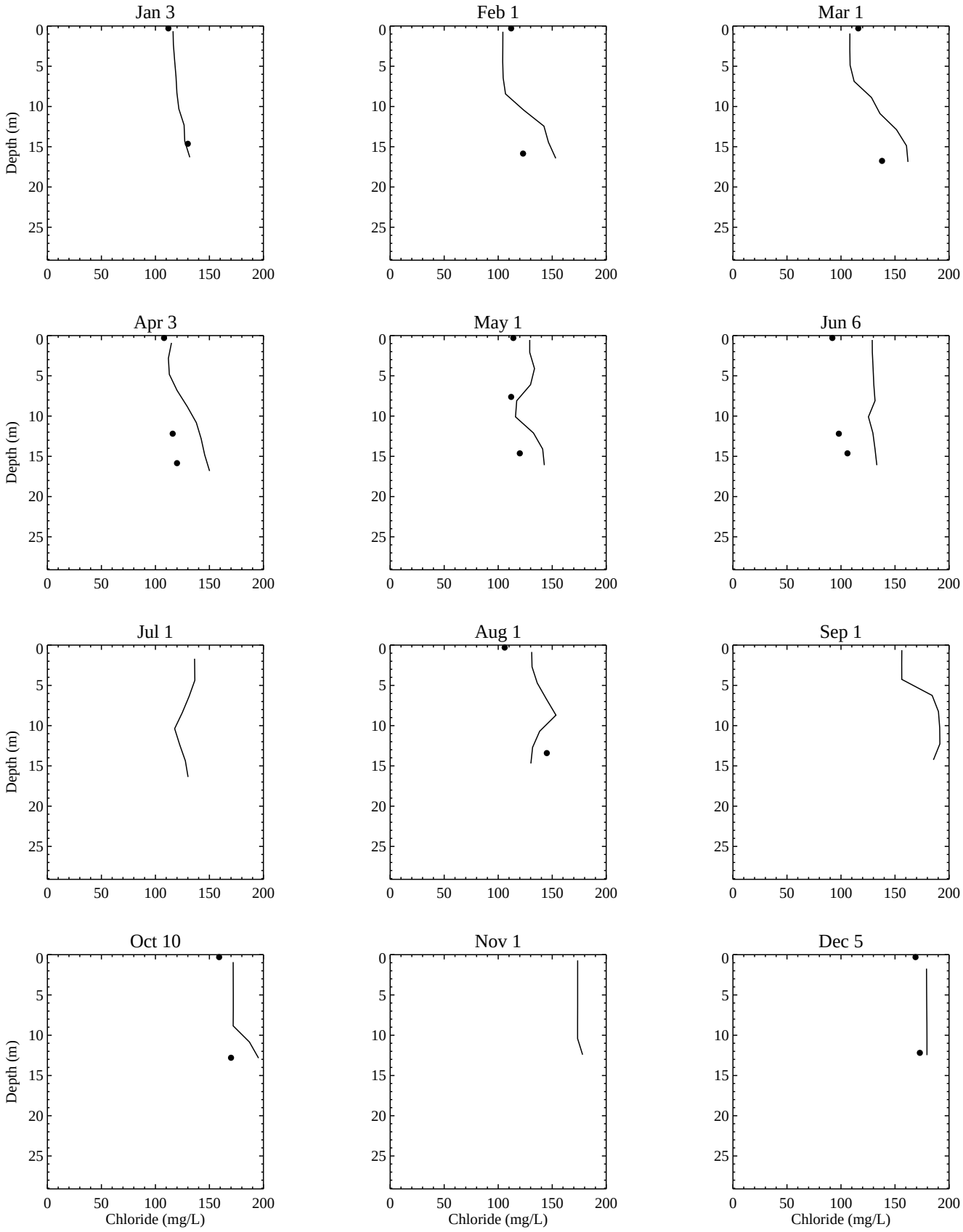

Figure J-14. Vertical profiles of model versus data at Turkey Bend (Segment 28) - Chloride - 1989.

Profiles shown for dates with available data else model results for first day of month shown.

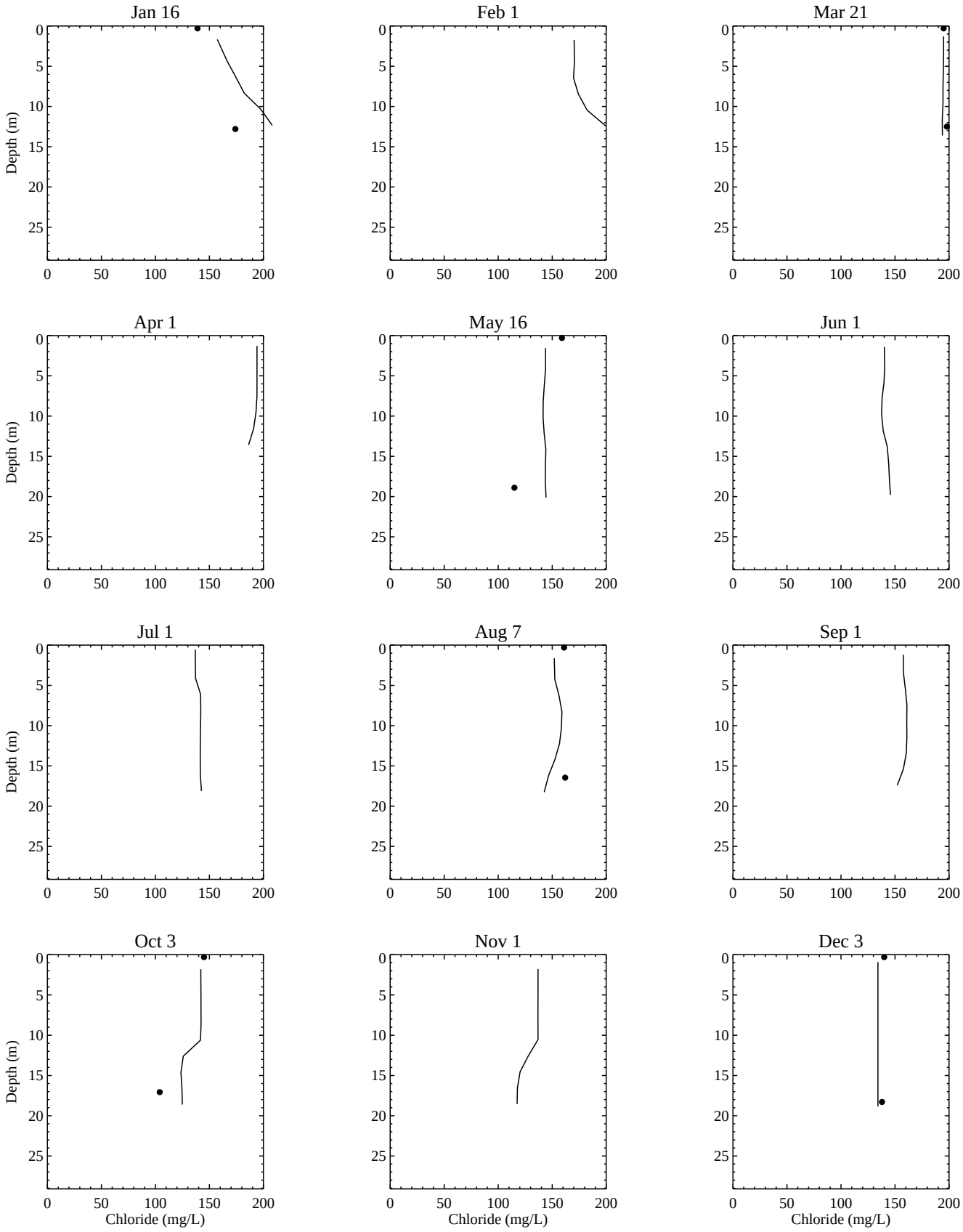

Figure J-14. Vertical profiles of model versus data at Turkey Bend (Segment 28) - Chloride - 1990.

Profiles shown for dates with available data else model results for first day of month shown.

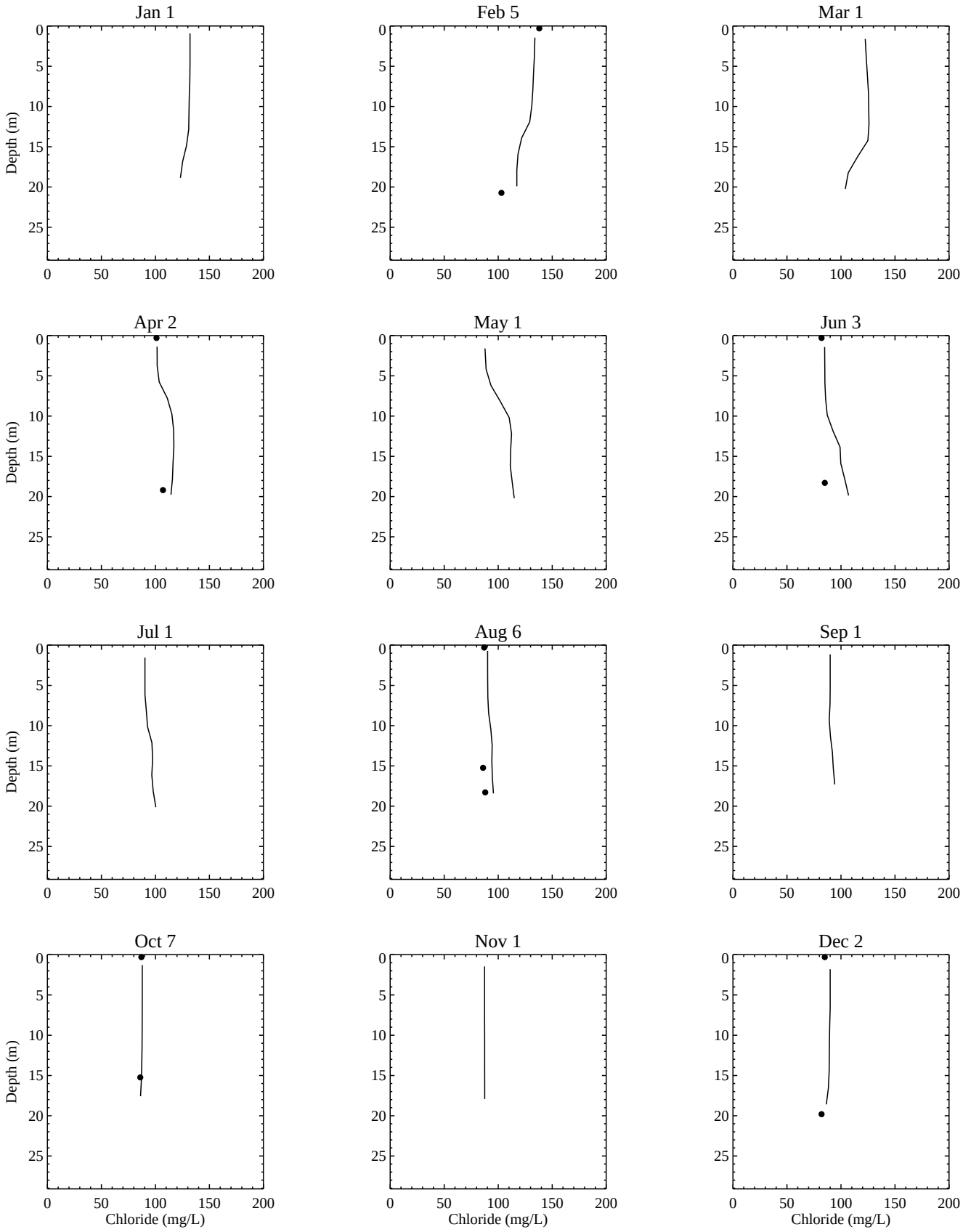

Figure J-14. Vertical profiles of model versus data at Turkey Bend (Segment 28) - Chloride - 1991.

Profiles shown for dates with available data else model results for first day of month shown.

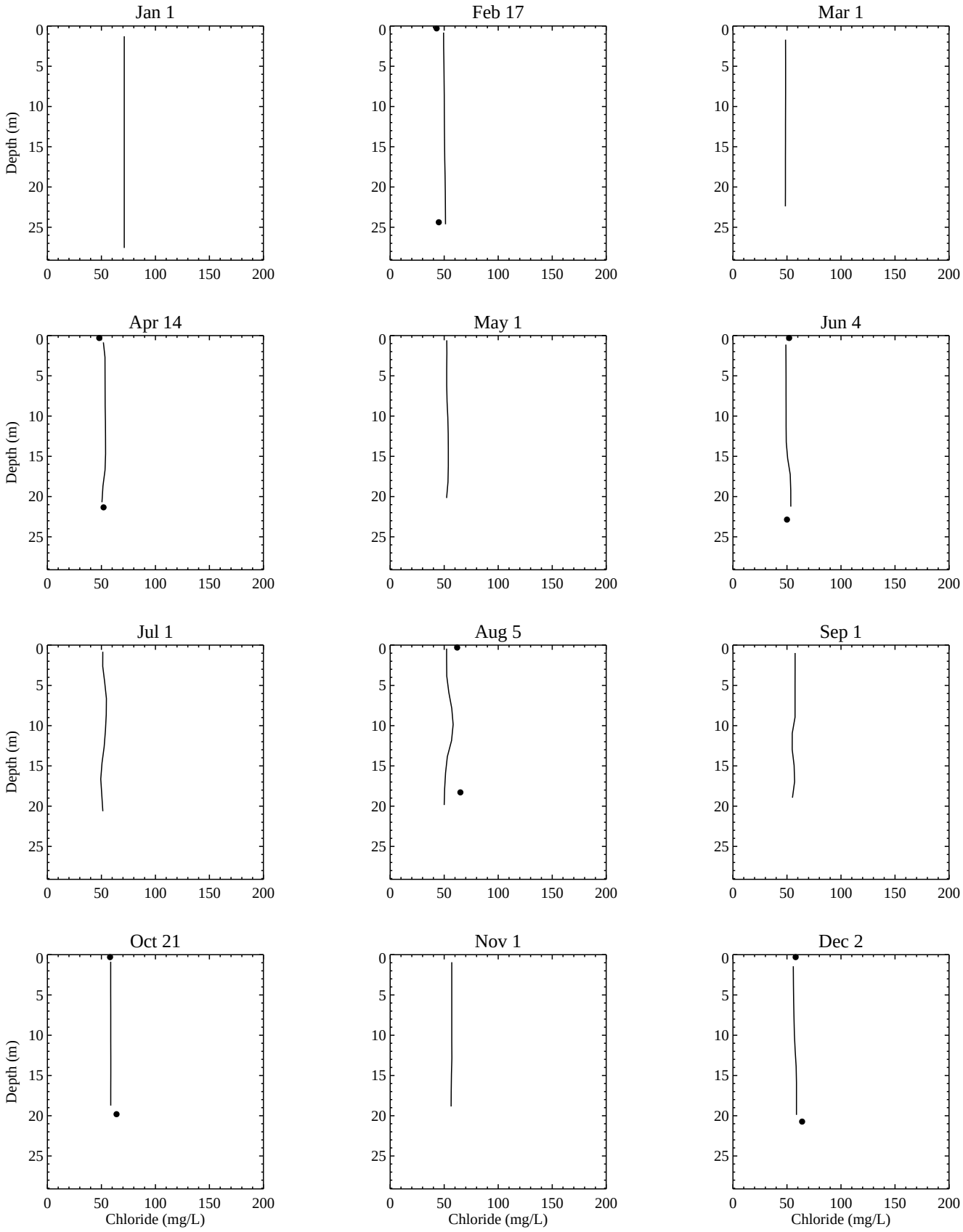

Figure J-14. Vertical profiles of model versus data at Turkey Bend (Segment 28) - Chloride - 1992.

Profiles shown for dates with available data else model results for first day of month shown.

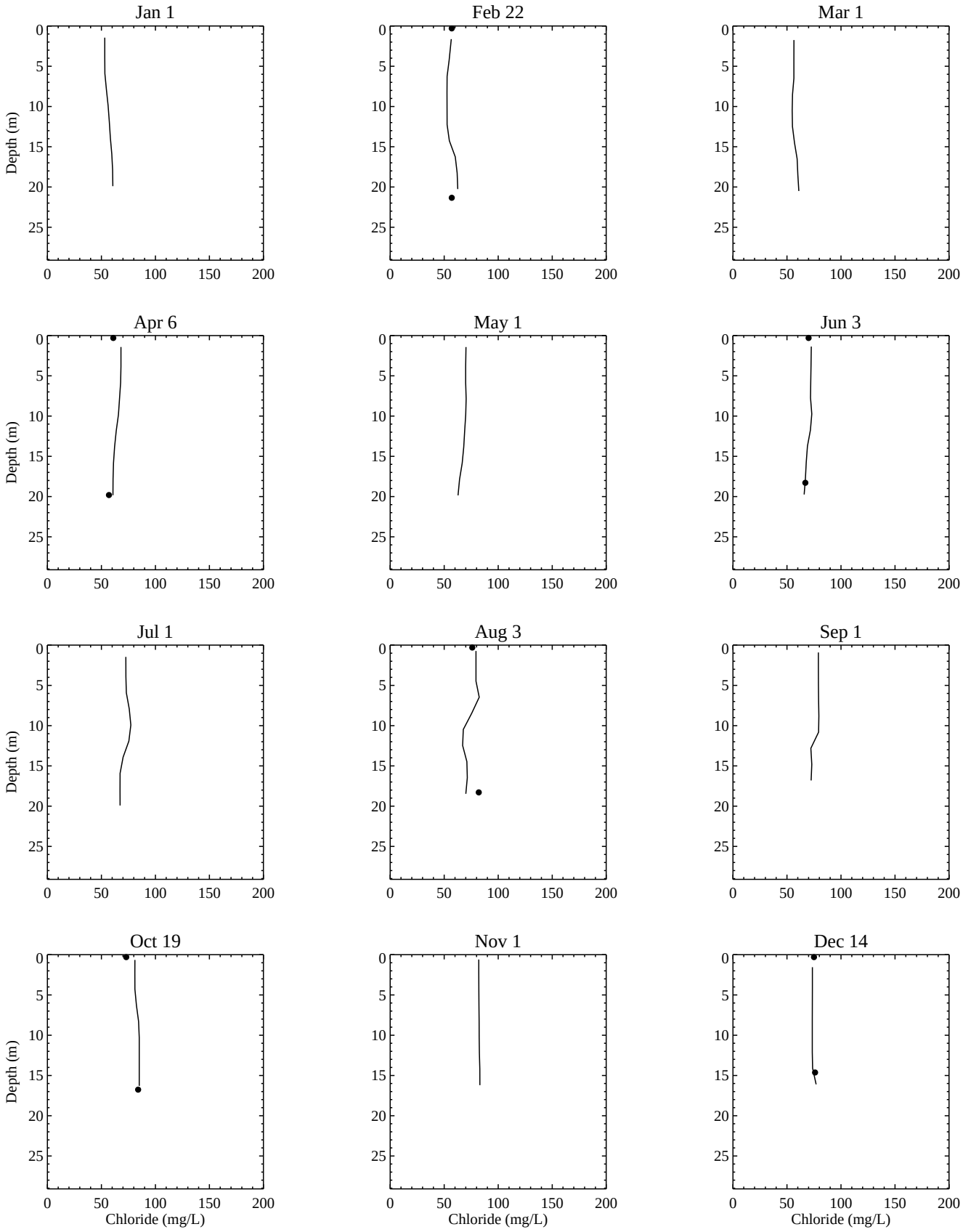

Figure J-14. Vertical profiles of model versus data at Turkey Bend (Segment 28) - Chloride - 1993.

Profiles shown for dates with available data else model results for first day of month shown.

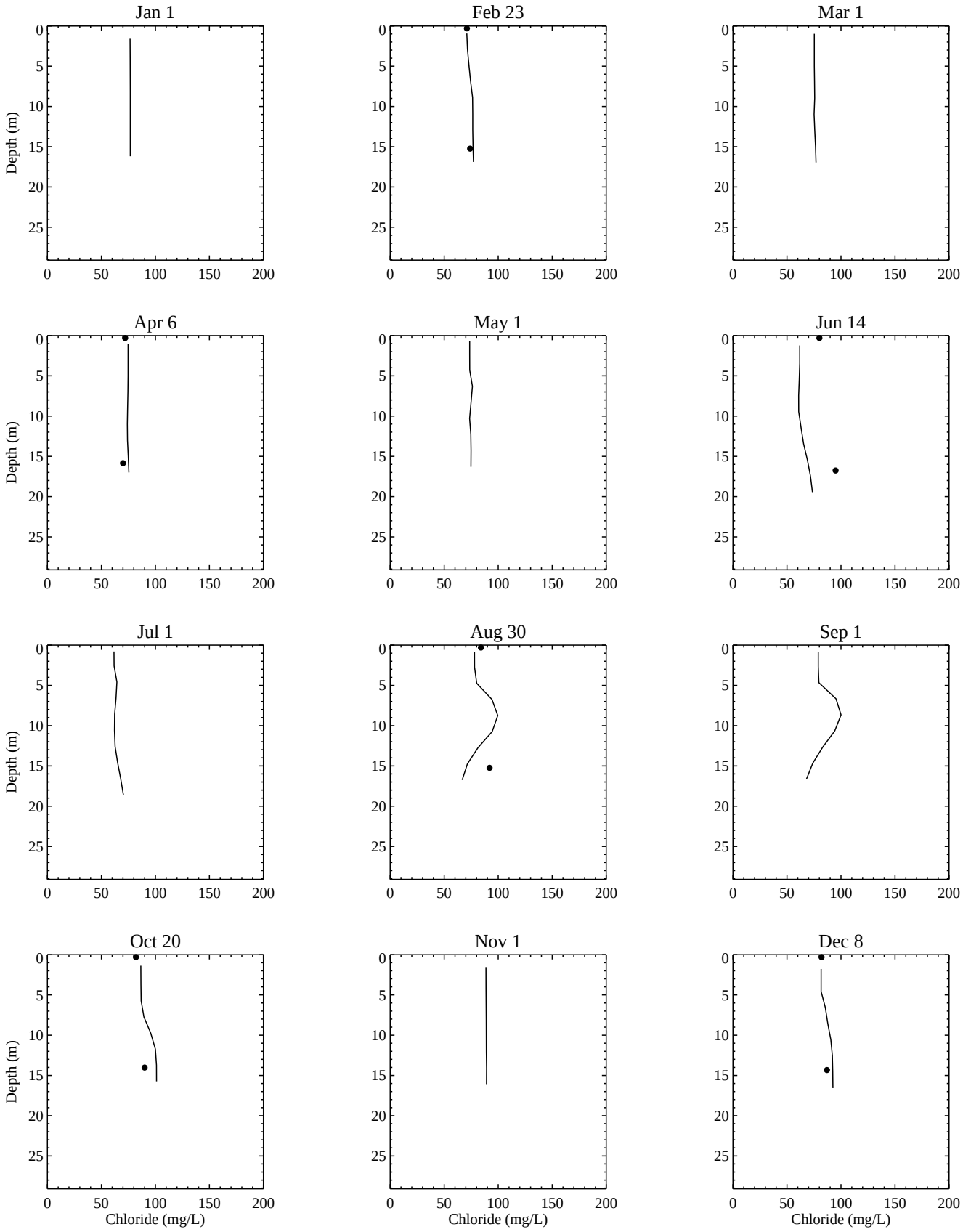

Figure J-14. Vertical profiles of model versus data at Turkey Bend (Segment 28) - Chloride - 1994.

Profiles shown for dates with available data else model results for first day of month shown.

Model Data

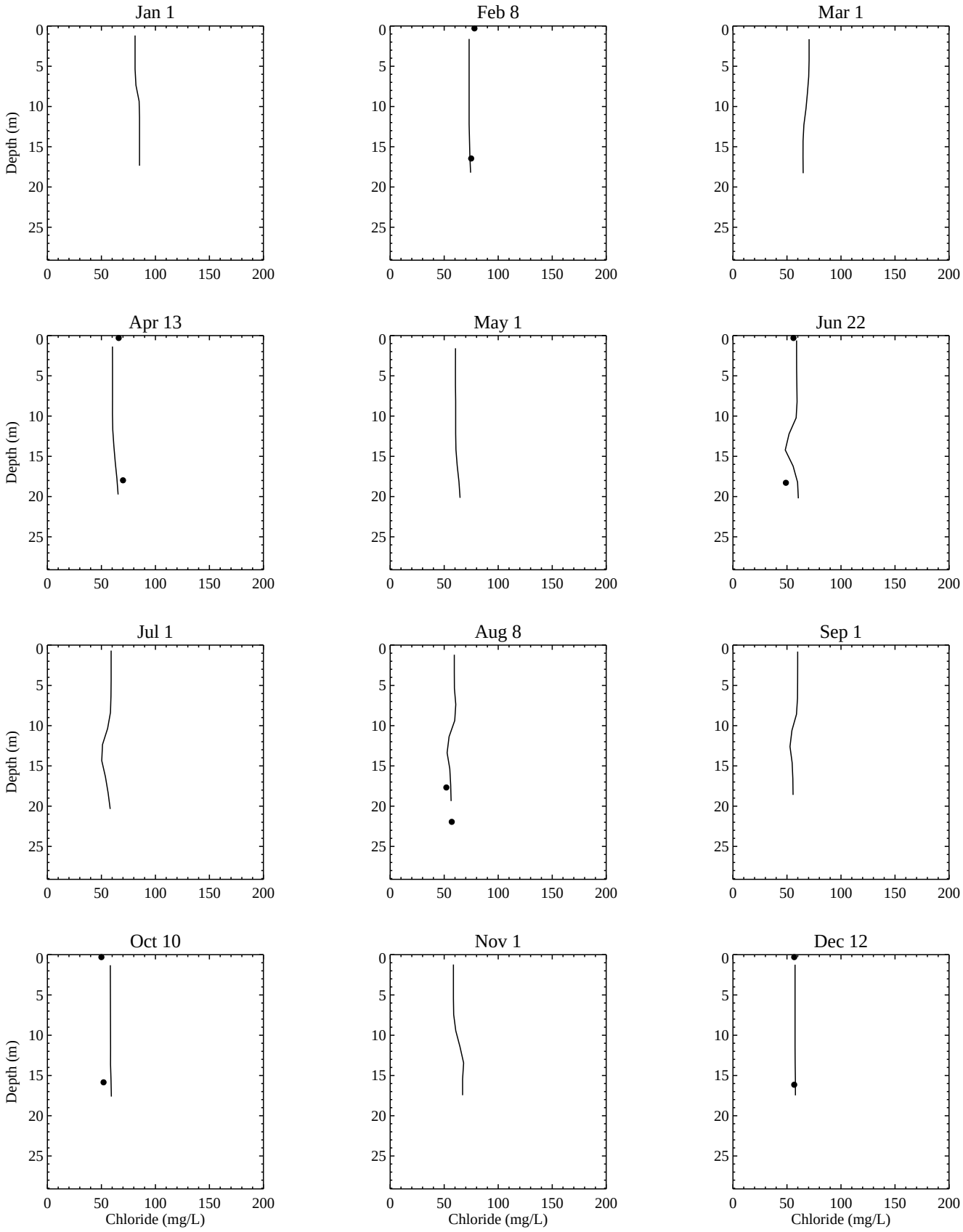

Figure J-14. Vertical profiles of model versus data at Turkey Bend (Segment 28) - Chloride - 1995.

Profiles shown for dates with available data else model results for first day of month shown.

Model Data

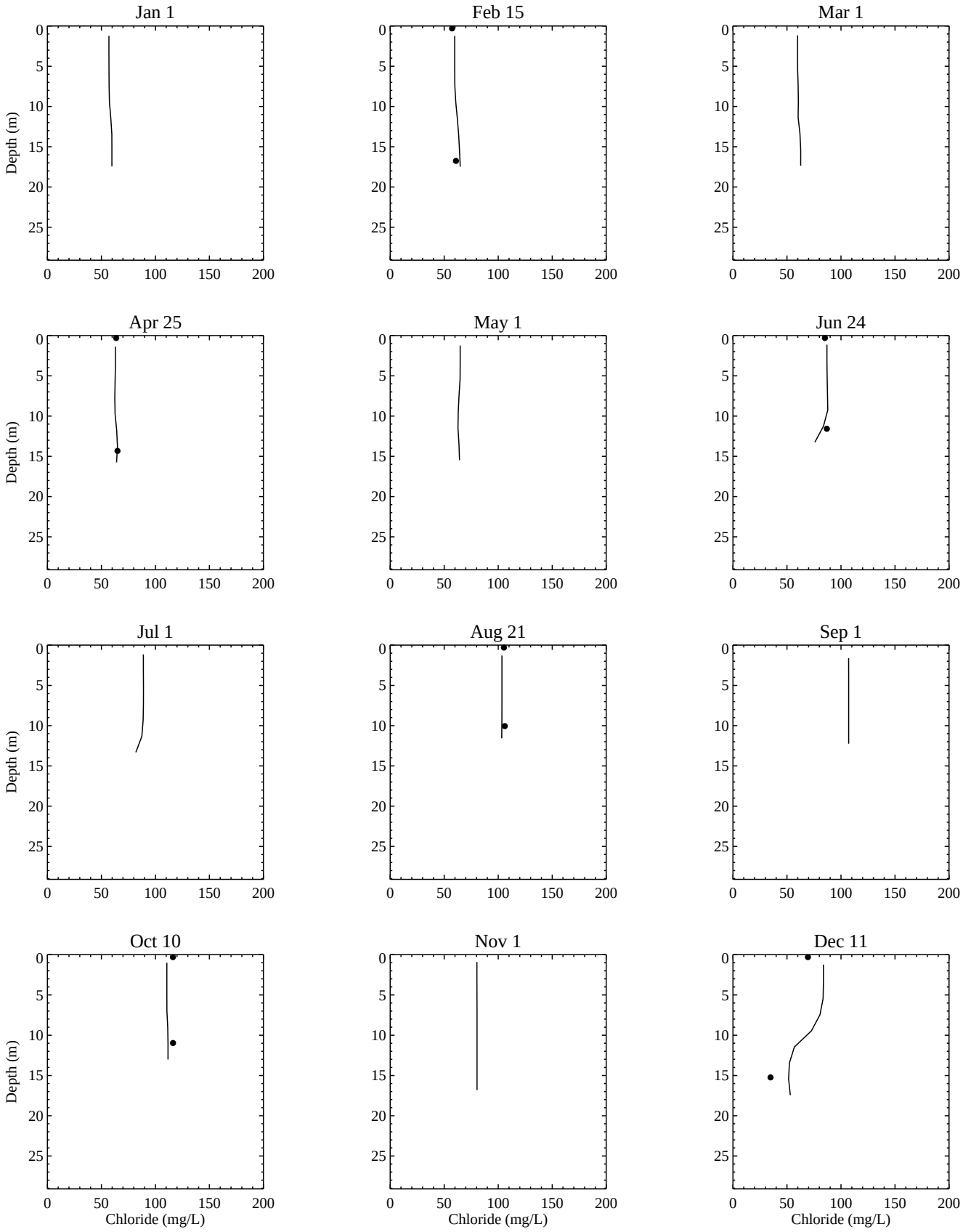

Figure J-14. Vertical profiles of model versus data at Turkey Bend (Segment 28) - Chloride - 1996.

Profiles shown for dates with available data else model results for first day of month shown.

Model Data

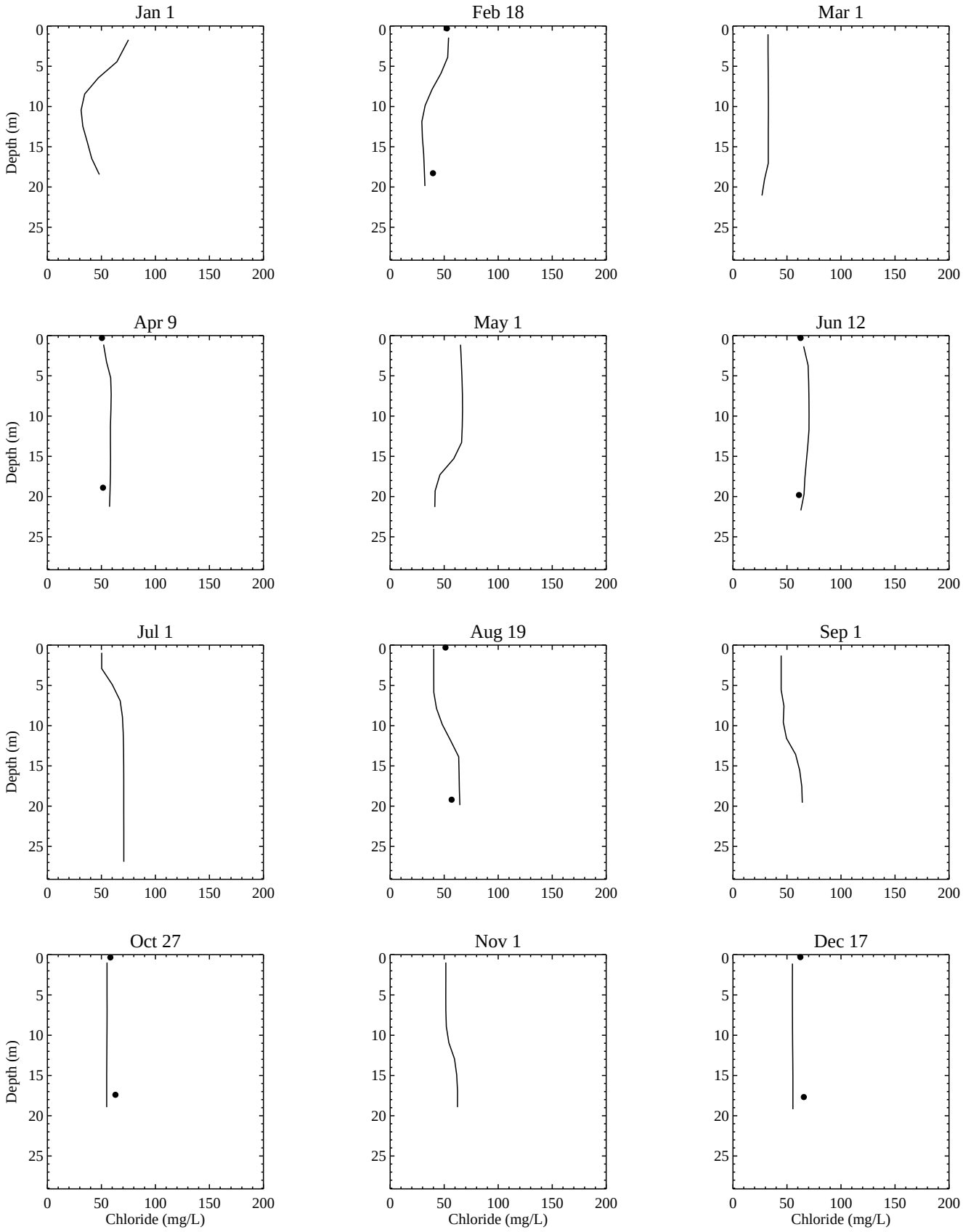

Figure J-14. Vertical profiles of model versus data at Turkey Bend (Segment 28) - Chloride - 1997.

Profiles shown for dates with available data else model results for first day of month shown.

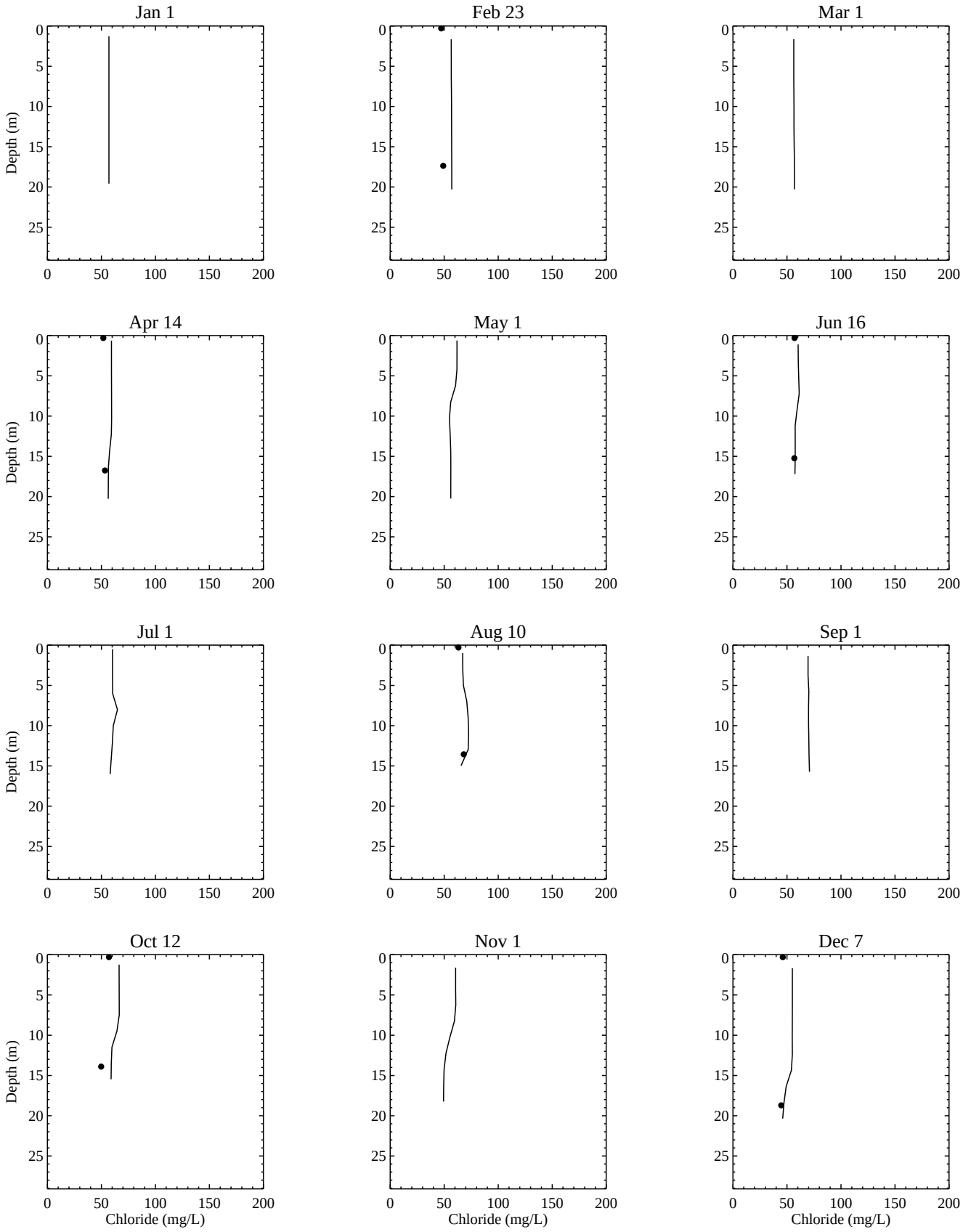

Figure J-14. Vertical profiles of model versus data at Turkey Bend (Segment 28) - Chloride - 1998.

Profiles shown for dates with available data else model results for first day of month shown.

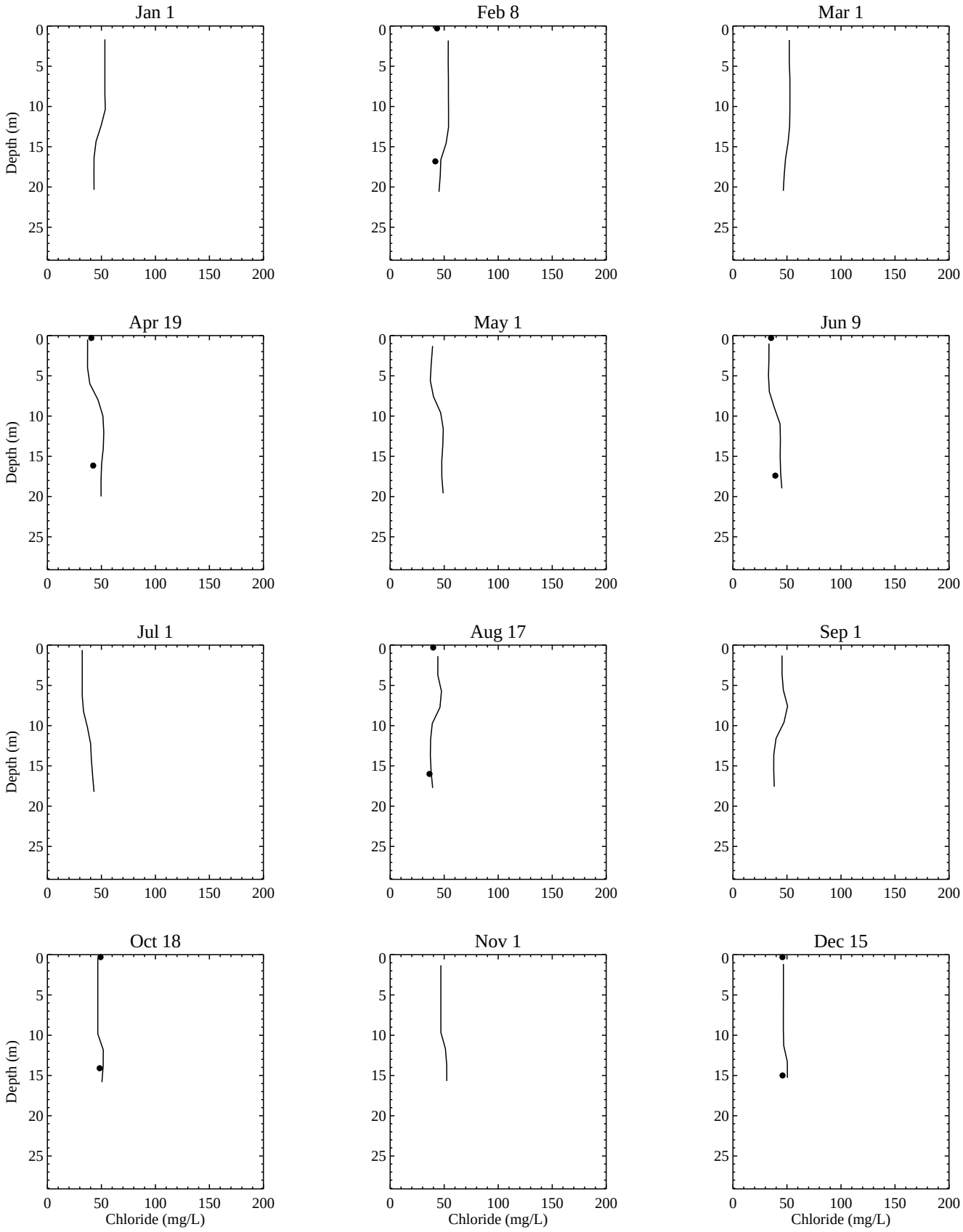

Figure J-14. Vertical profiles of model versus data at Turkey Bend (Segment 28) - Chloride - 1999.

Profiles shown for dates with available data else model results for first day of month shown.

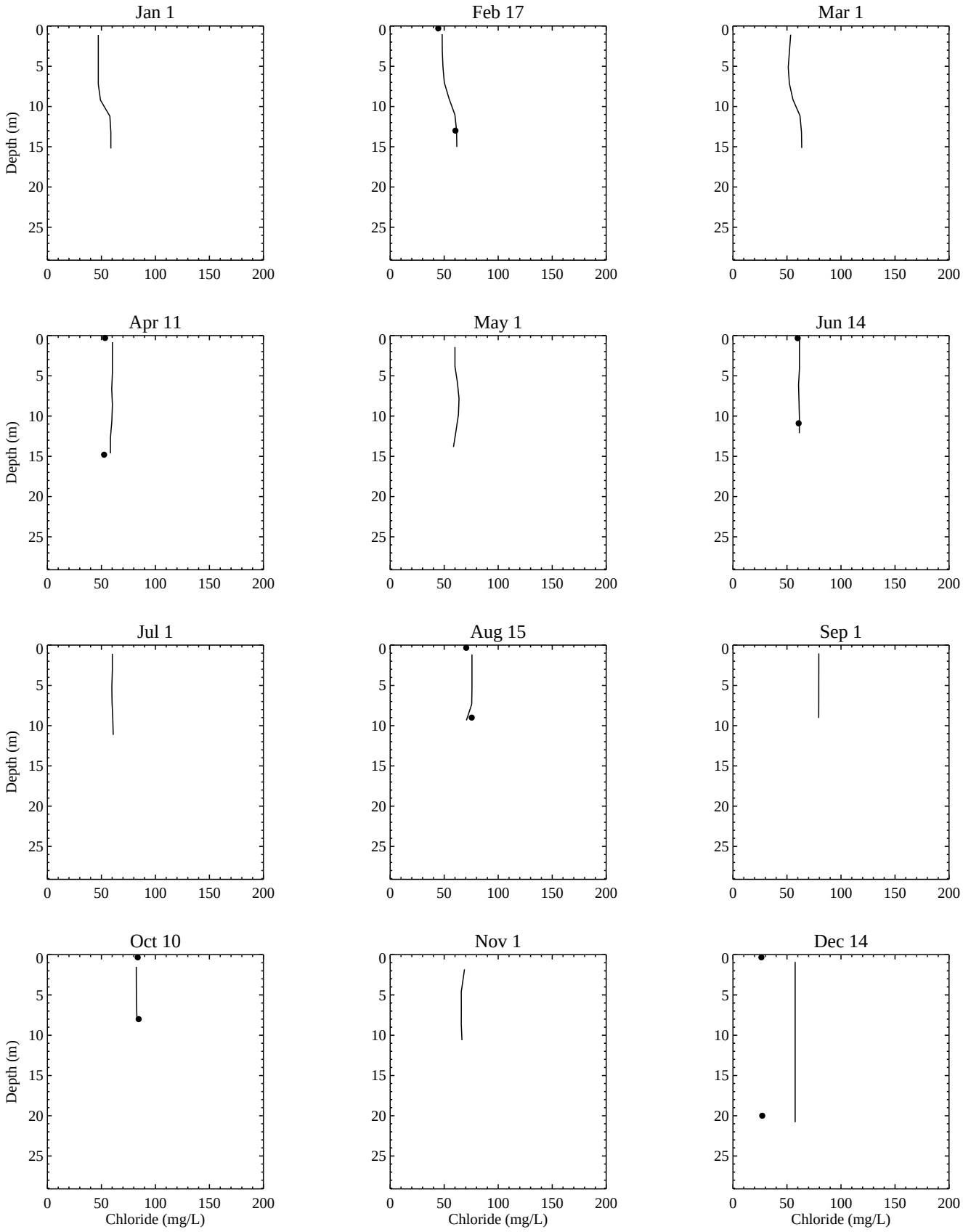

Figure J-14. Vertical profiles of model versus data at Turkey Bend (Segment 28) - Chloride - 2000.

Profiles shown for dates with available data else model results for first day of month shown.

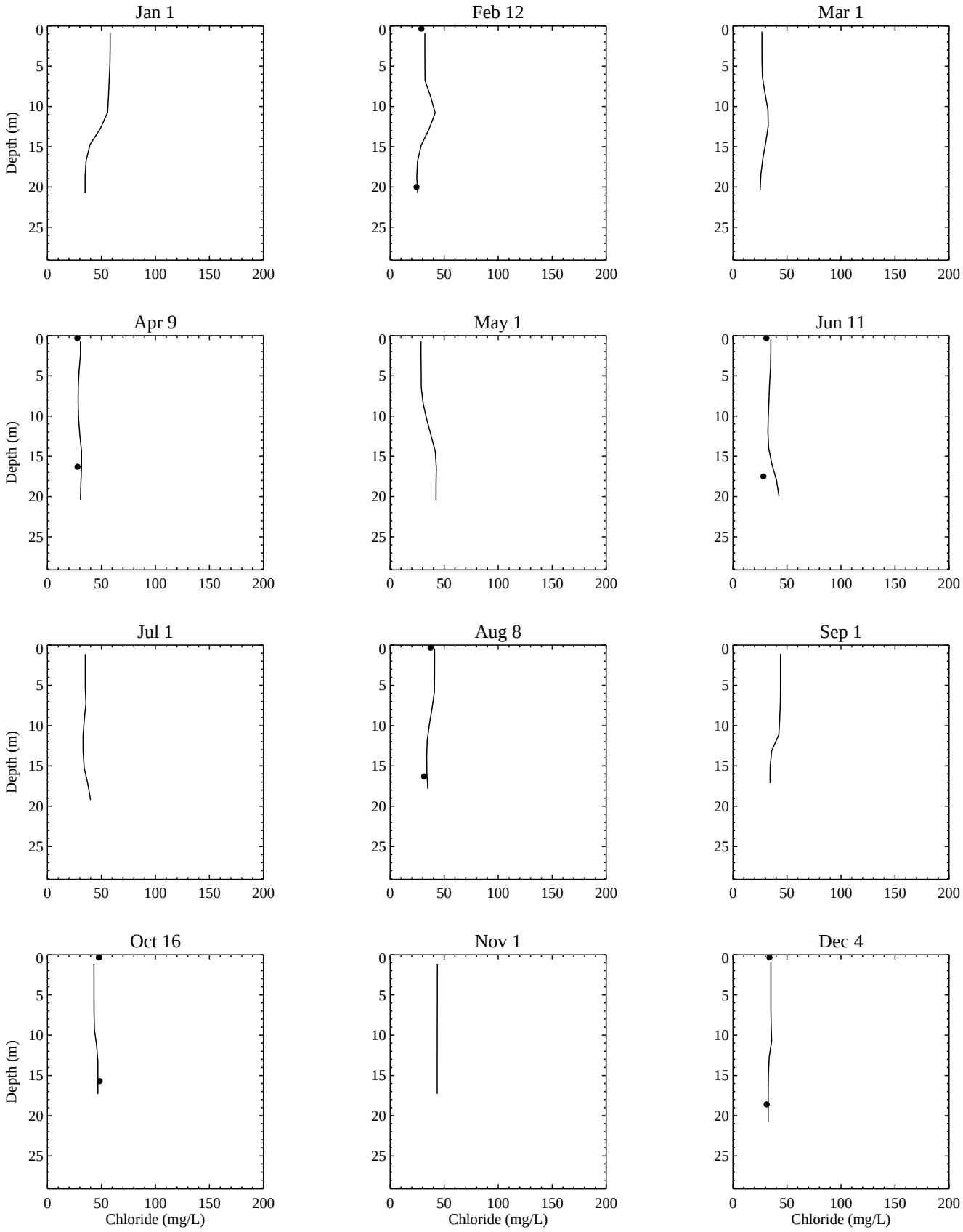

Figure J-14. Vertical profiles of model versus data at Turkey Bend (Segment 28) - Chloride - 2001.

Profiles shown for dates with available data else model results for first day of month shown.

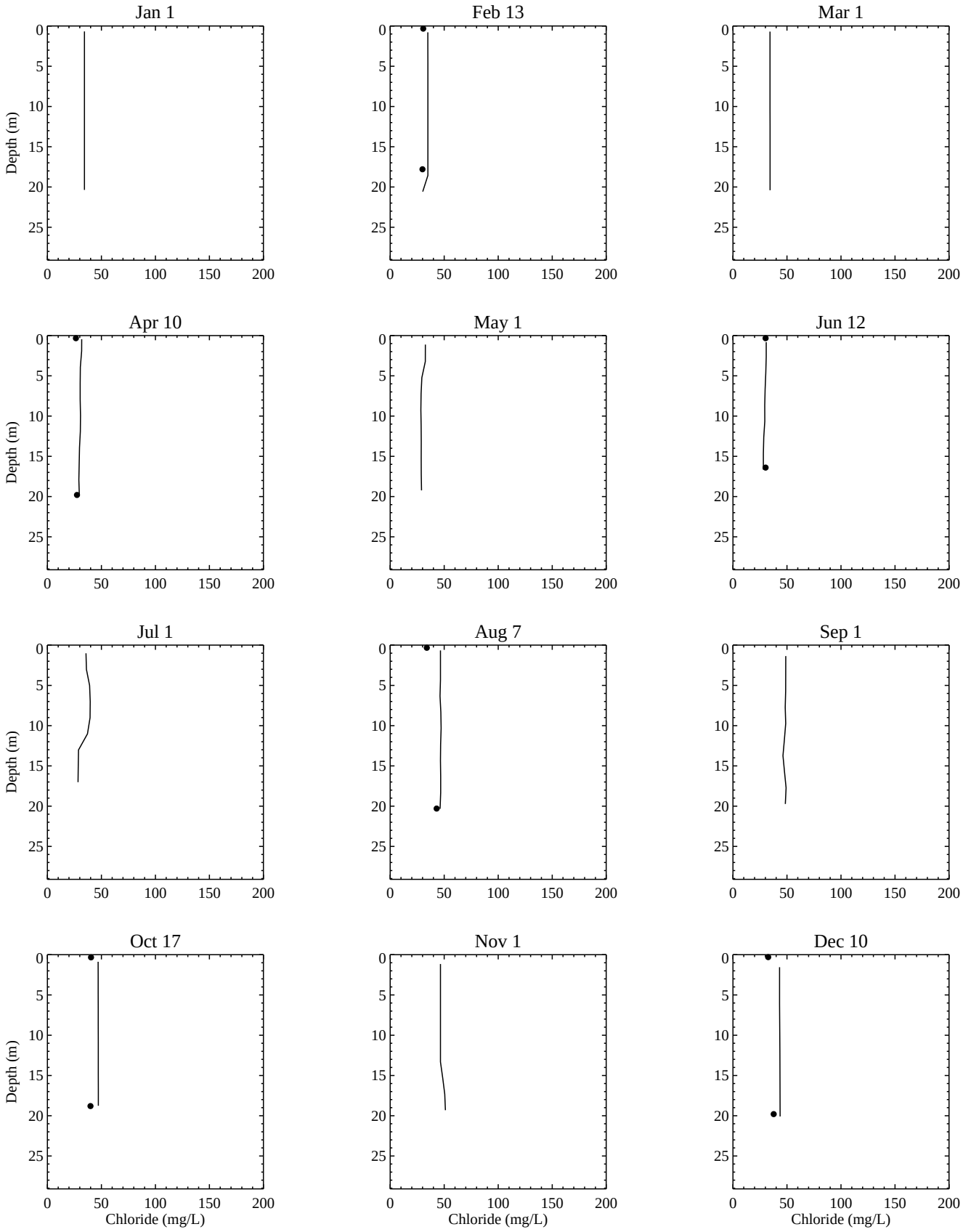

Figure J-14. Vertical profiles of model versus data at Turkey Bend (Segment 28) - Chloride - 2002.

Profiles shown for dates with available data else model results for first day of month shown.

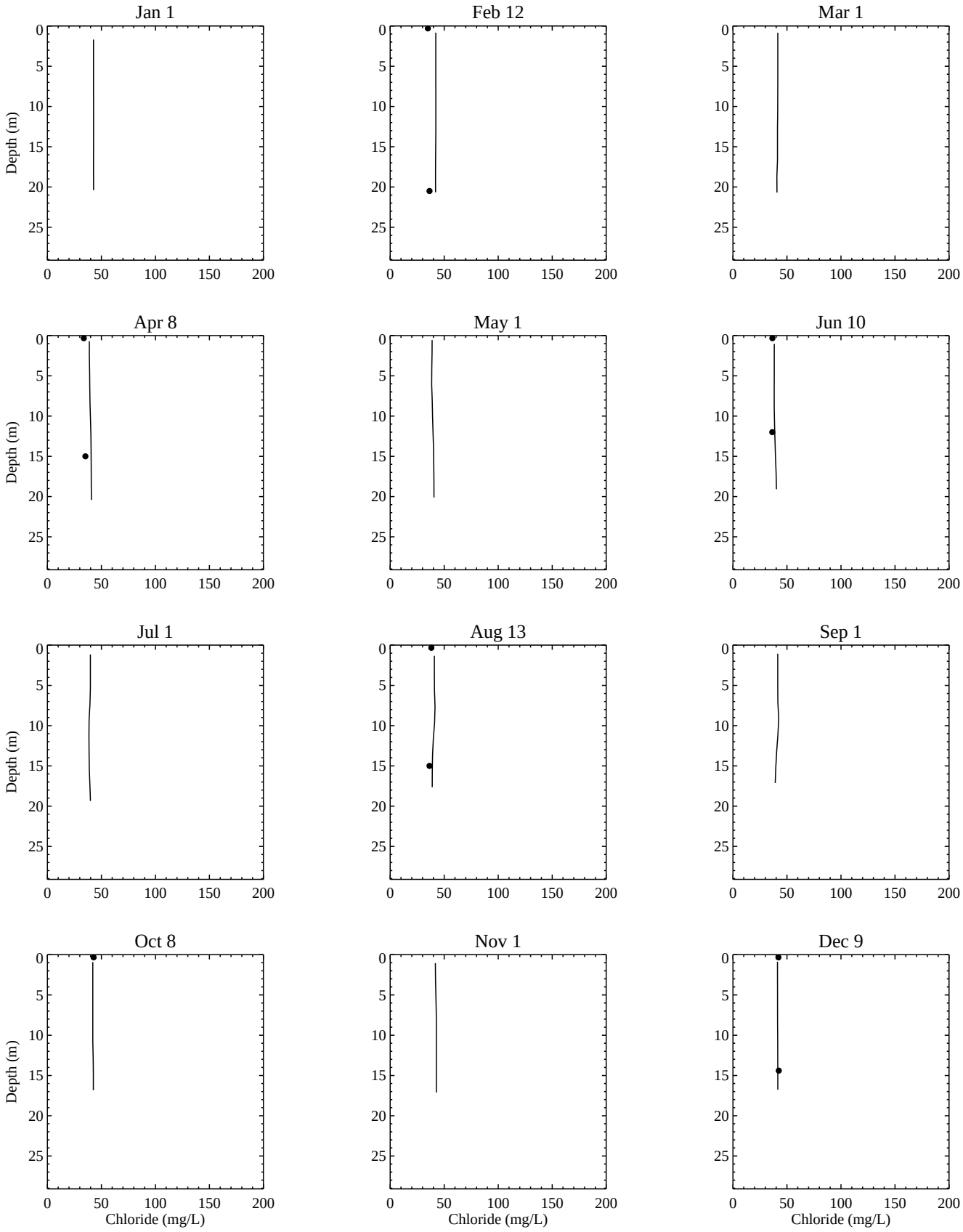

Figure J-14. Vertical profiles of model versus data at Turkey Bend (Segment 28) - Chloride - 2003.

Profiles shown for dates with available data else model results for first day of month shown.

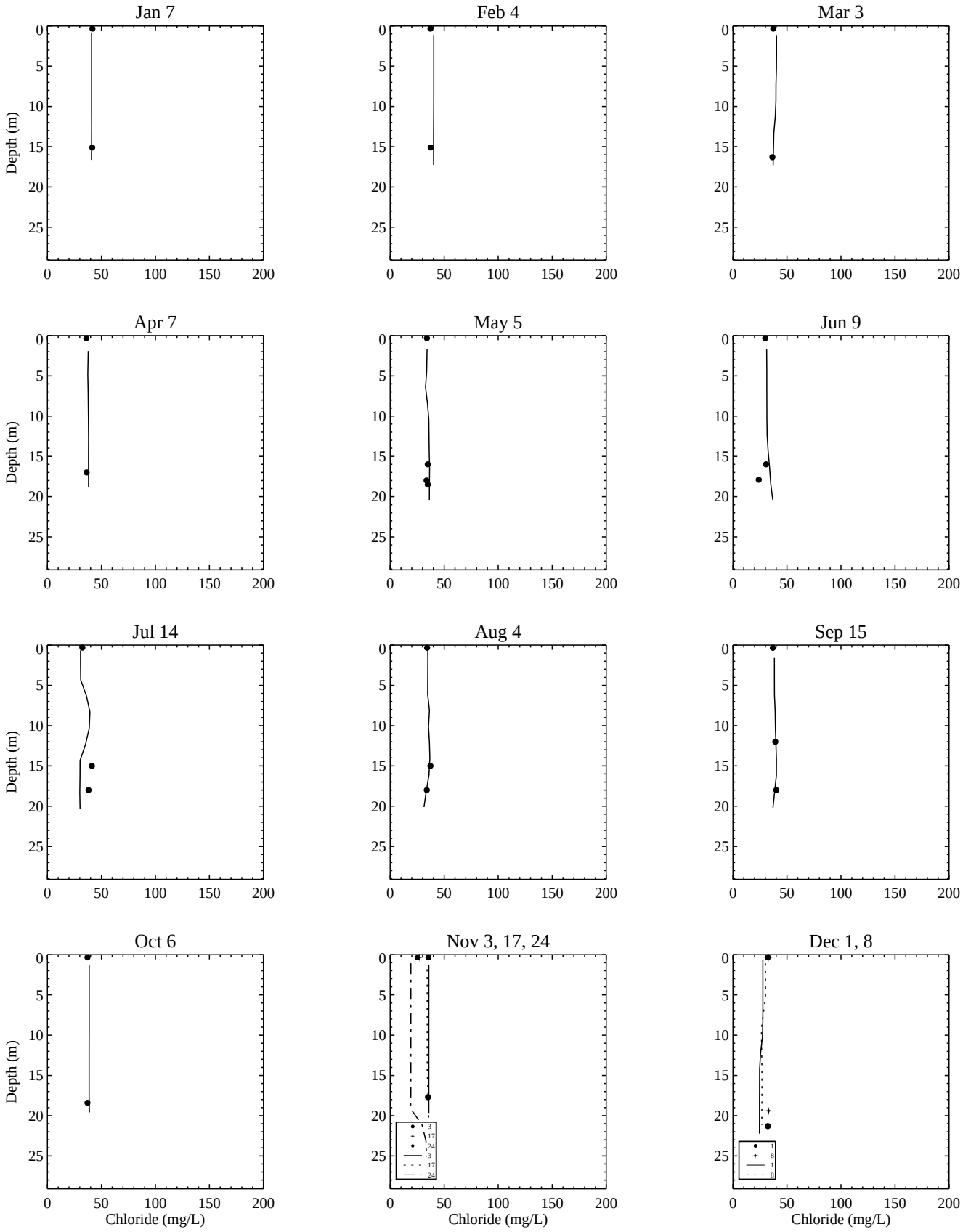

Figure J-14. Vertical profiles of model versus data at Turkey Bend (Segment 28) - Chloride - 2004.

Profiles shown for dates with available data else model results for first day of month shown.

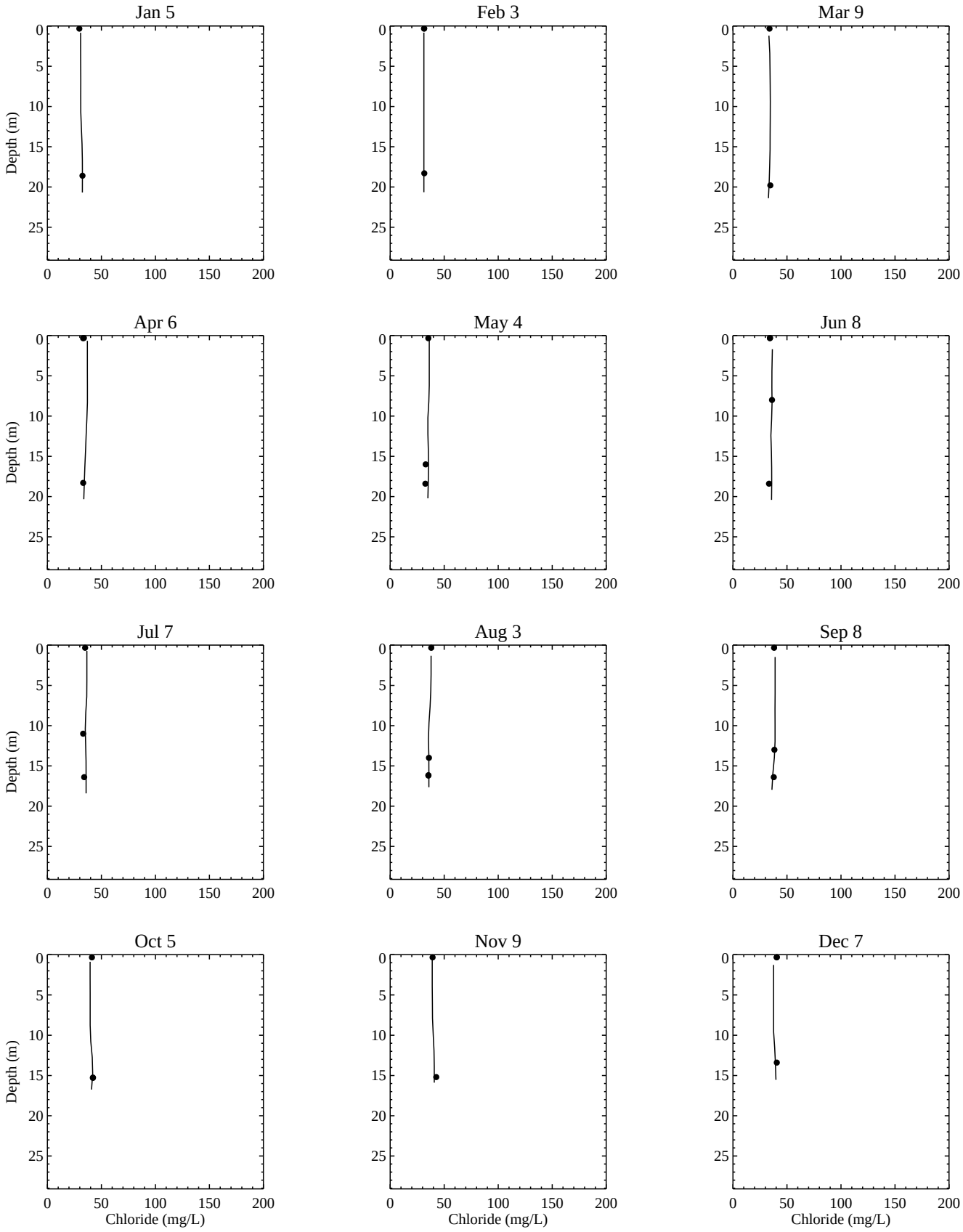

Figure J-14. Vertical profiles of model versus data at Turkey Bend (Segment 28) - Chloride - 2005.

Profiles shown for dates with available data else model results for first day of month shown.

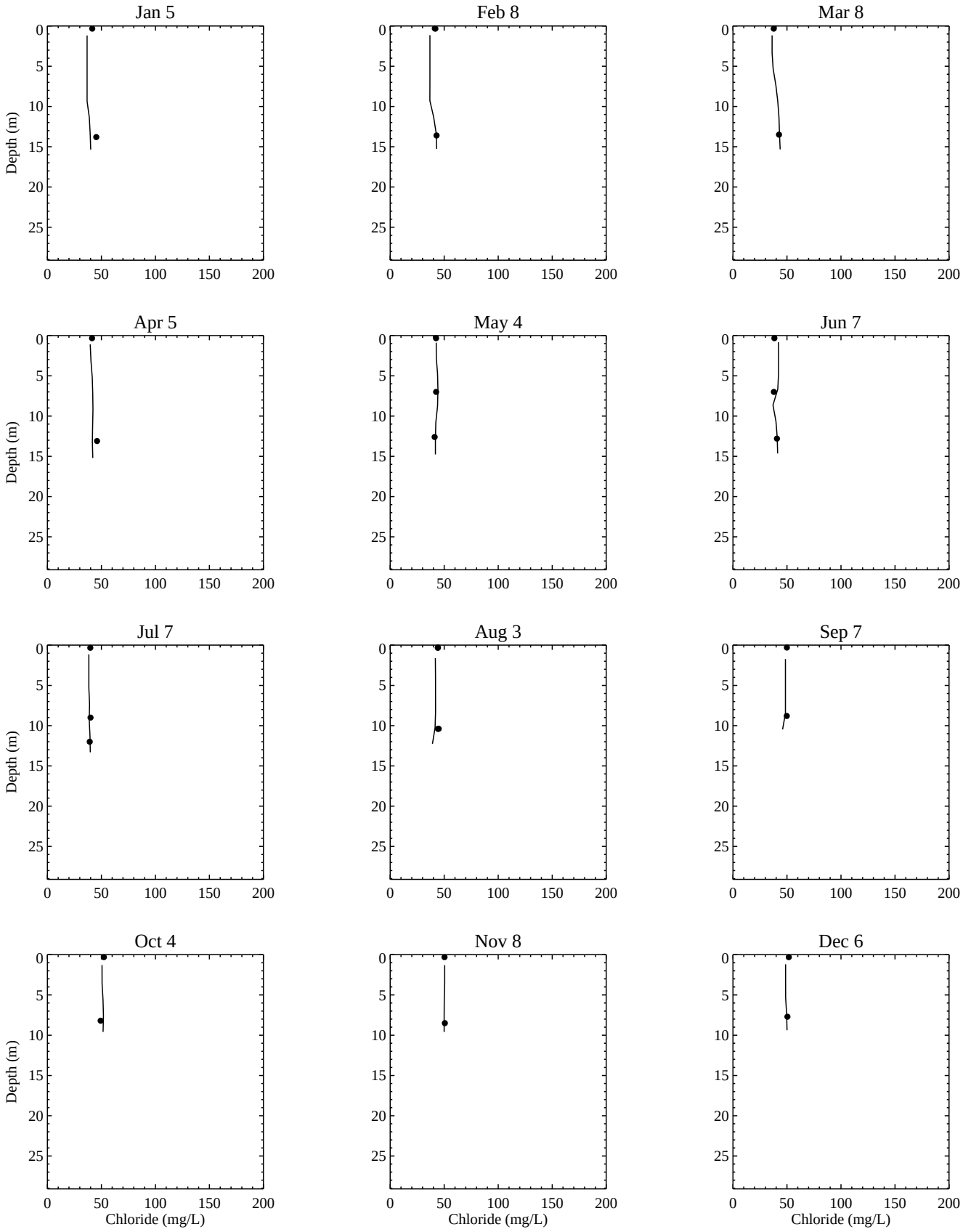

Figure J-14. Vertical profiles of model versus data at Turkey Bend (Segment 28) - Chloride - 2006.

Profiles shown for dates with available data else model results for first day of month shown.

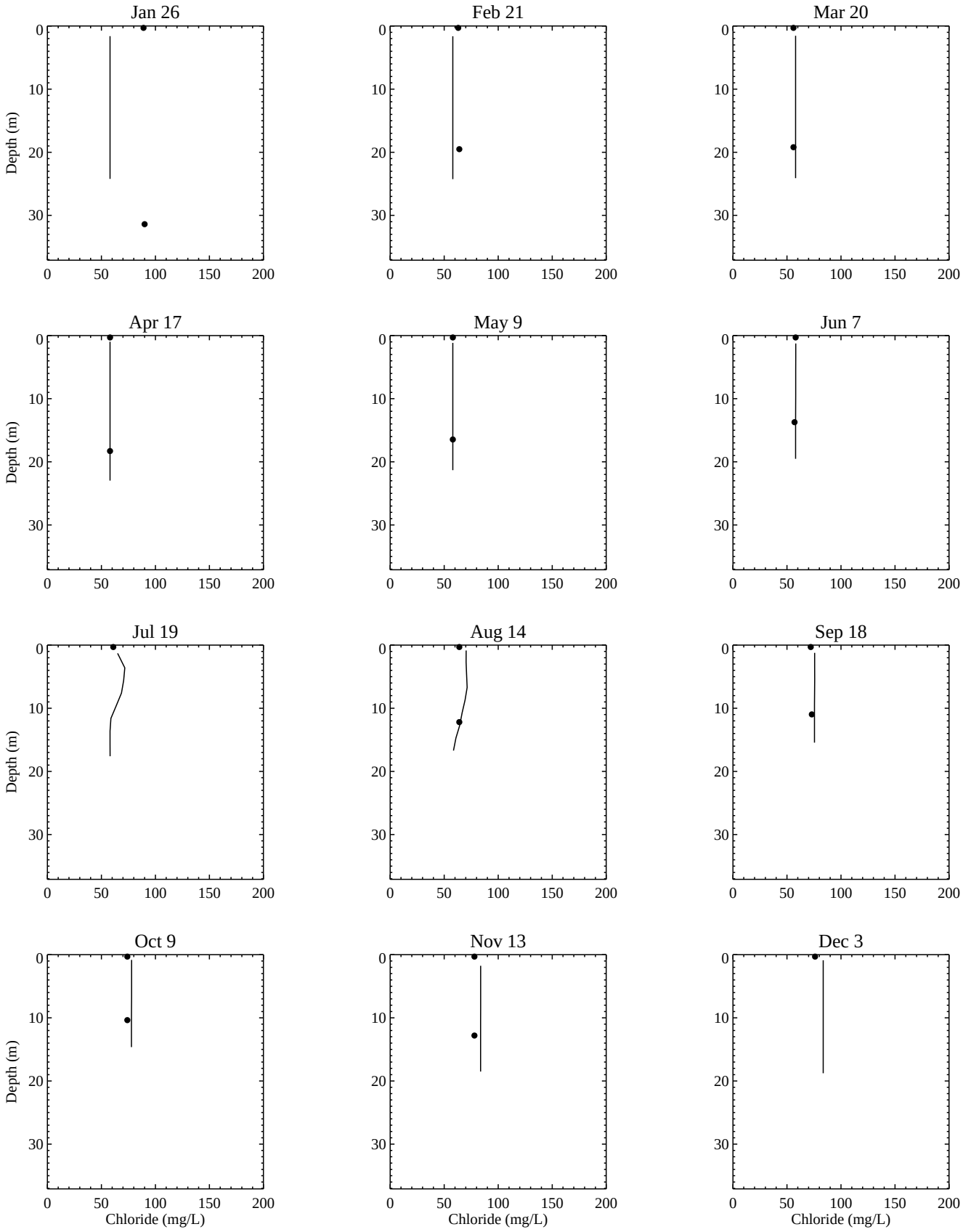

Figure J-15. Vertical profiles of model versus data at Sandy Creek (Segment 161) - Chloride - 1984.

Profiles shown for dates with available data else model results for first day of month shown. Non-detect data shown as open symbols.

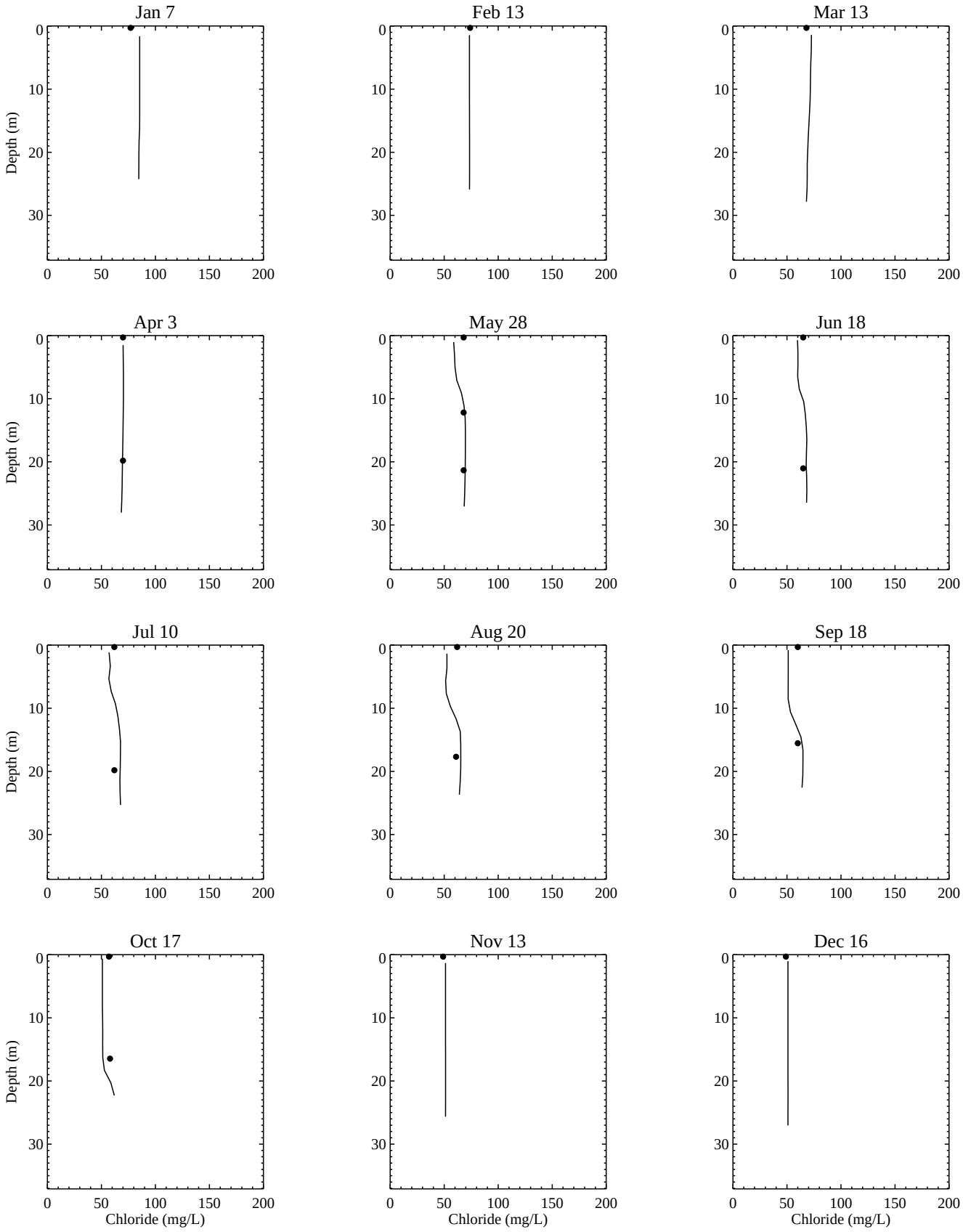

Figure J-15. Vertical profiles of model versus data at Sandy Creek (Segment 161) - Chloride - 1985.

Profiles shown for dates with available data else model results for first day of month shown. Non-detect data shown as open symbols.

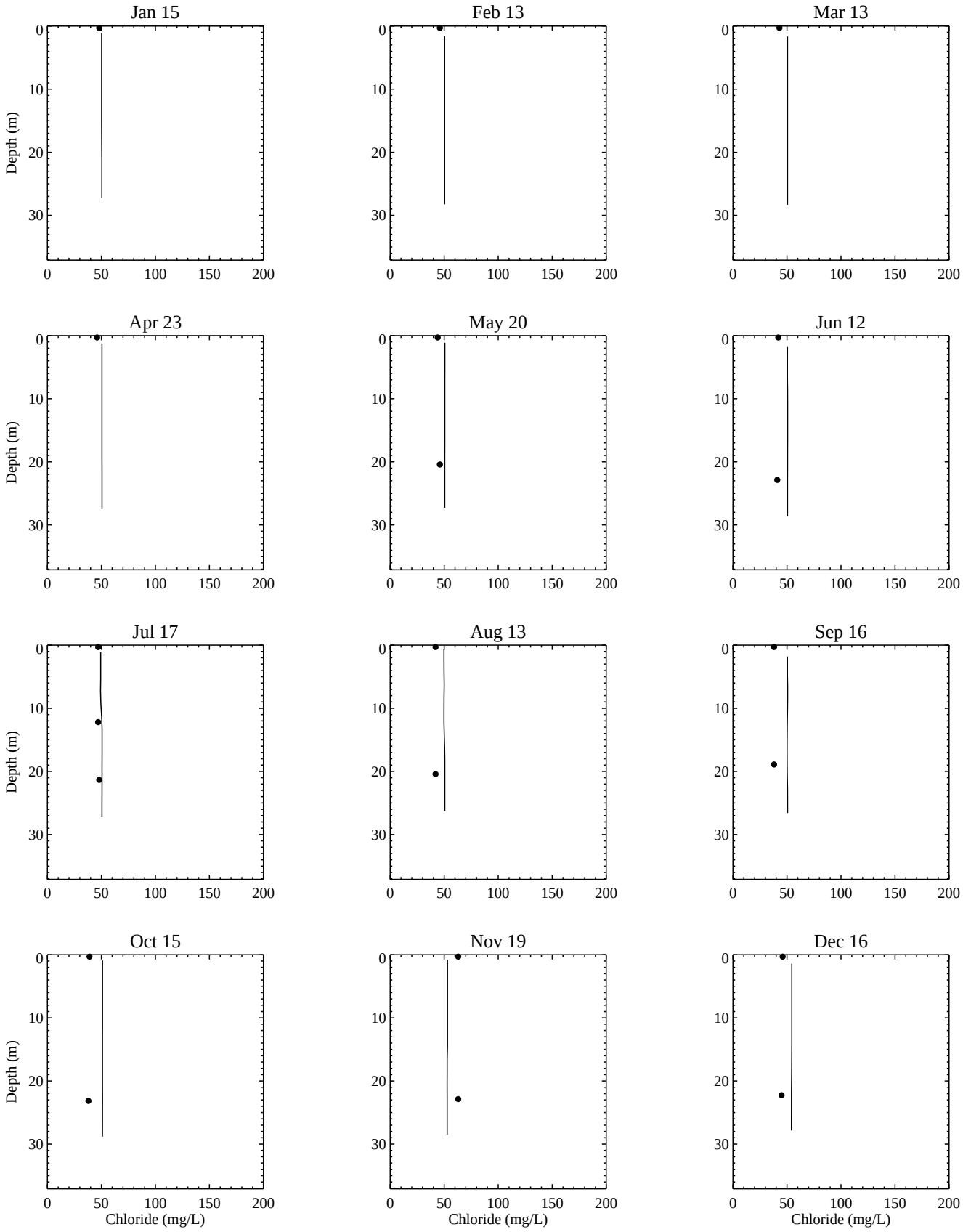

Figure J-15. Vertical profiles of model versus data at Sandy Creek (Segment 161) - Chloride - 1986.

Profiles shown for dates with available data else model results for first day of month shown. Non-detect data shown as open symbols.

Model Data

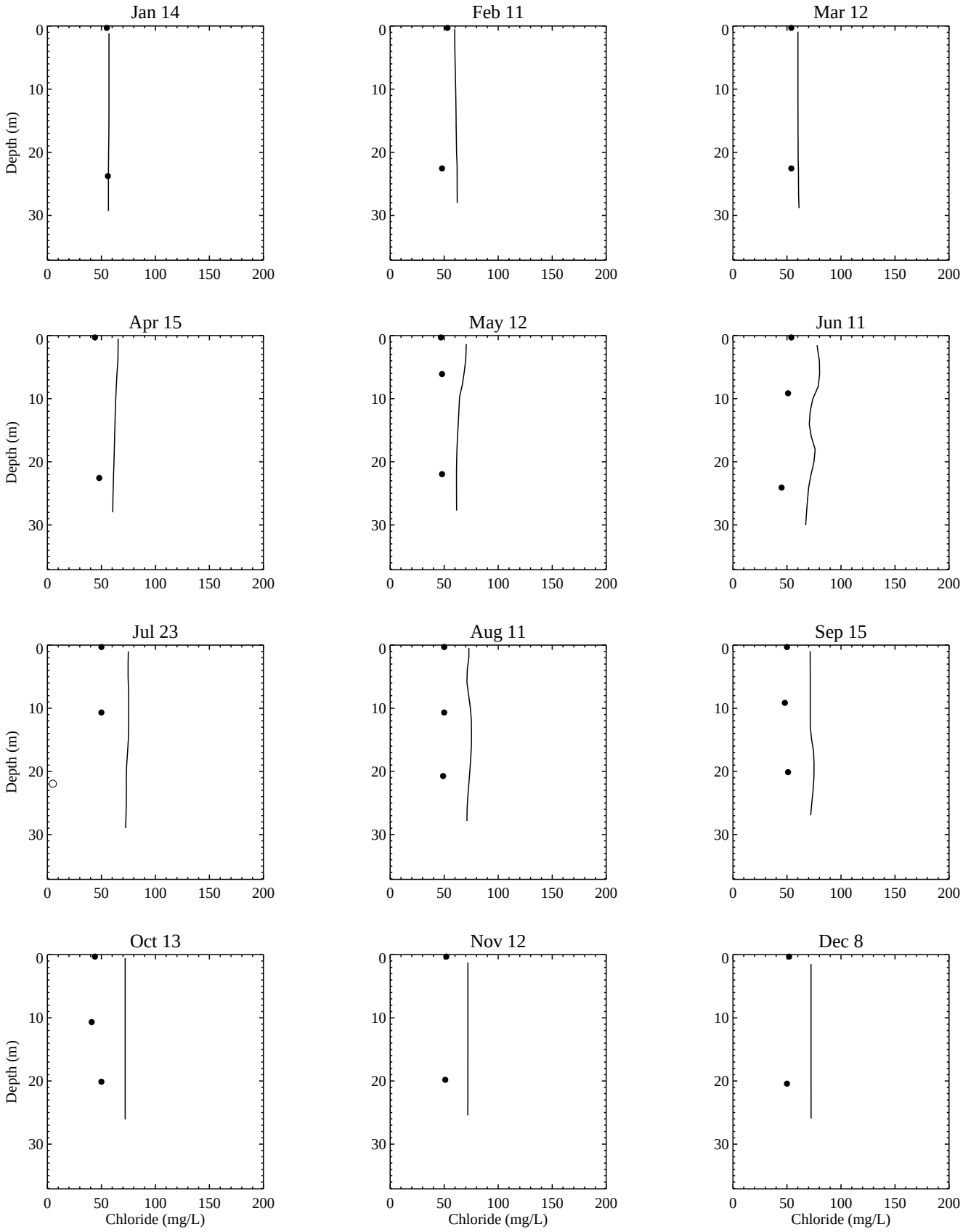

Figure J-15. Vertical profiles of model versus data at Sandy Creek (Segment 161) - Chloride - 1987.

Profiles shown for dates with available data else model results for first day of month shown. Non-detect data shown as open symbols.

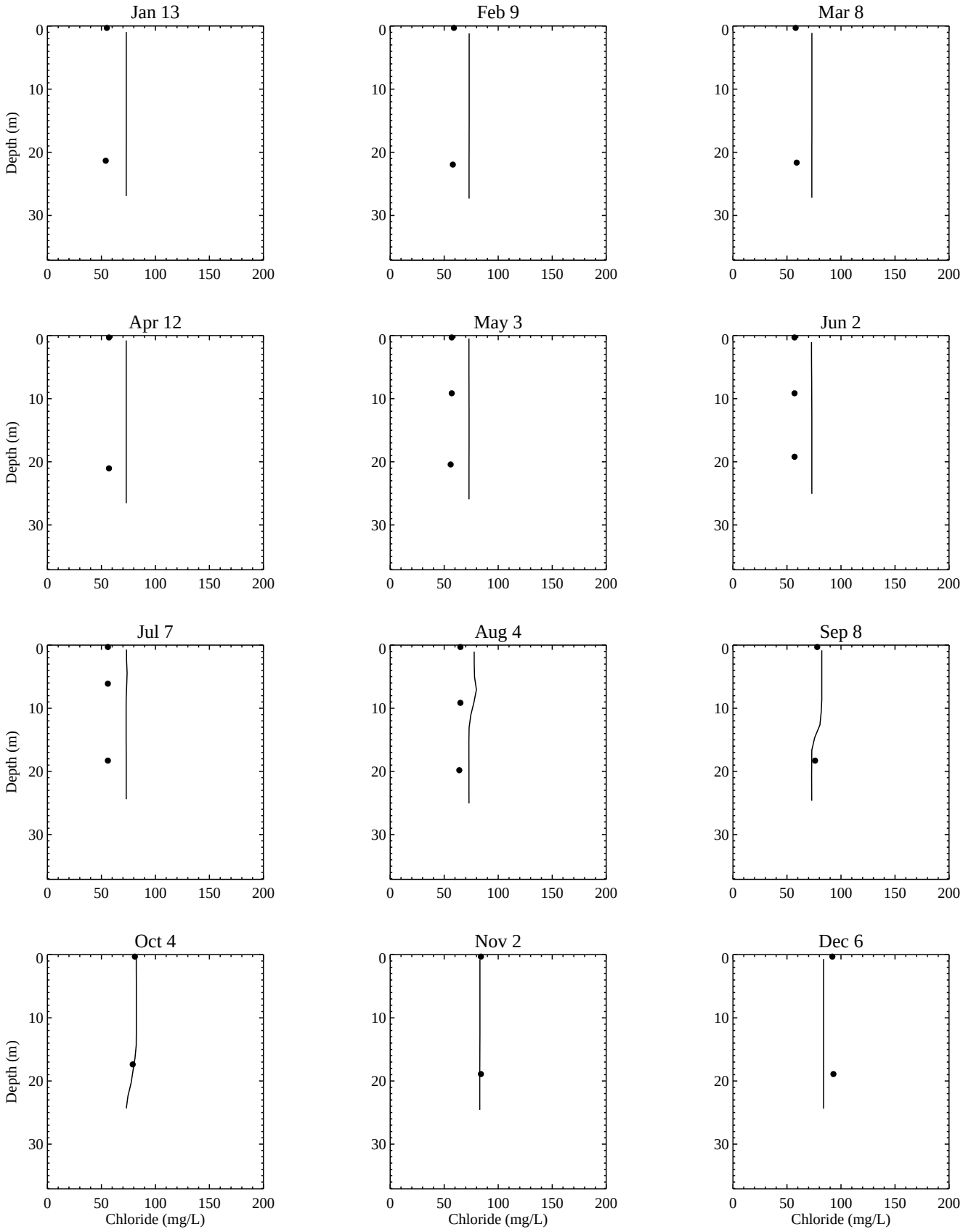

Figure J-15. Vertical profiles of model versus data at Sandy Creek (Segment 161) - Chloride - 1988.

Profiles shown for dates with available data else model results for first day of month shown. Non-detect data shown as open symbols.

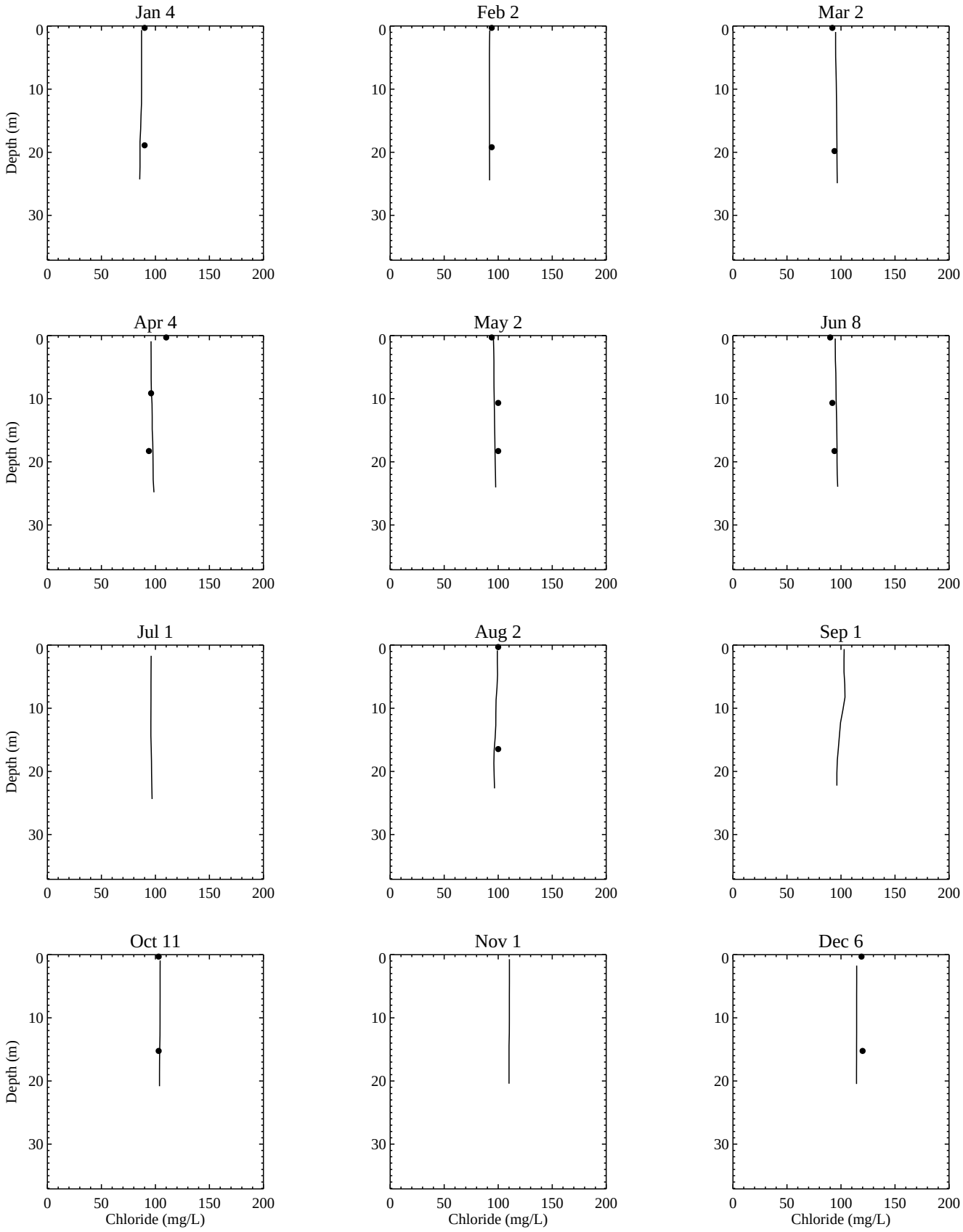

Figure J-15. Vertical profiles of model versus data at Sandy Creek (Segment 161) - Chloride - 1989.

Profiles shown for dates with available data else model results for first day of month shown. Non-detect data shown as open symbols.

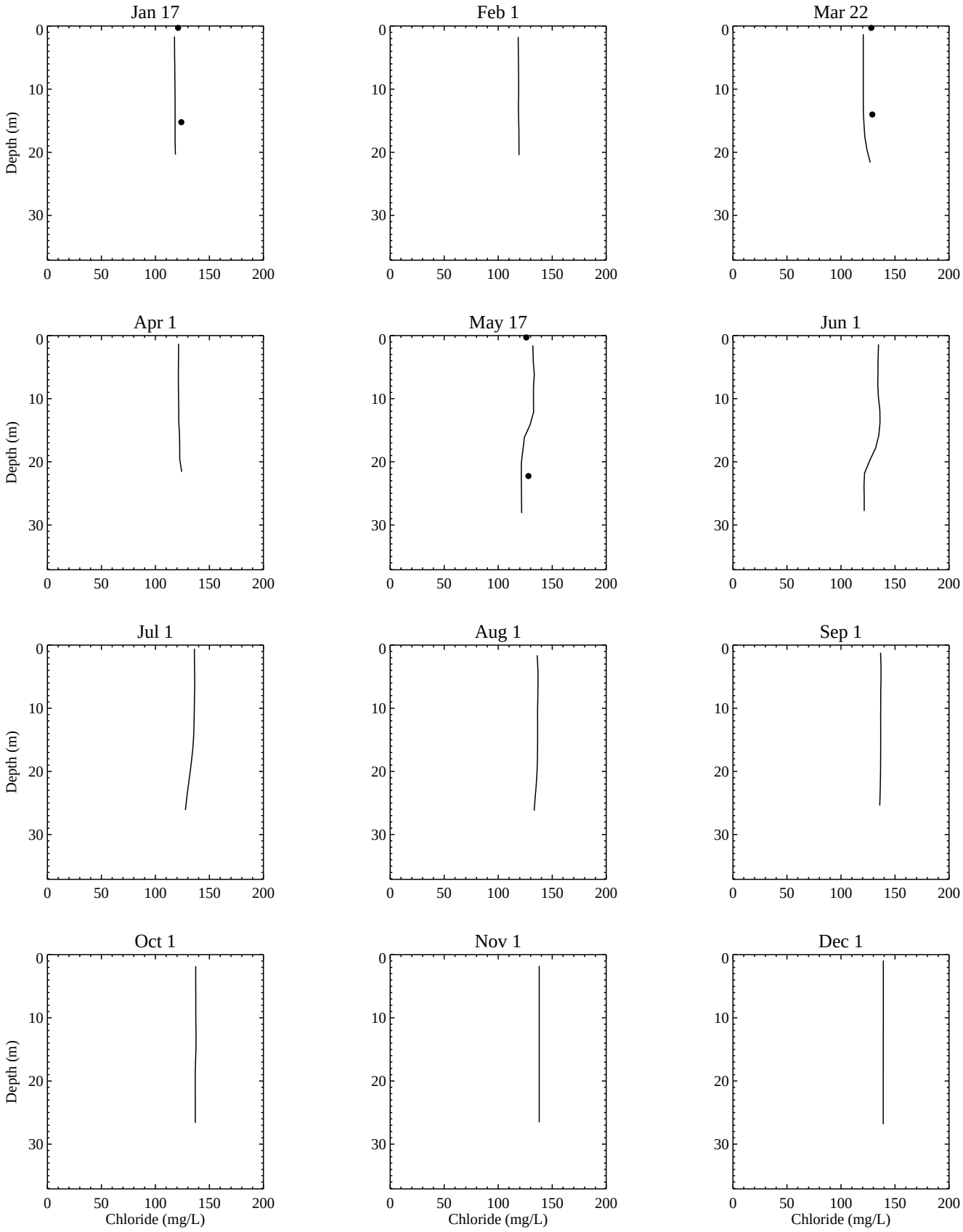

Figure J-15. Vertical profiles of model versus data at Sandy Creek (Segment 161) - Chloride - 1990.

Profiles shown for dates with available data else model results for first day of month shown. Non-detect data shown as open symbols.

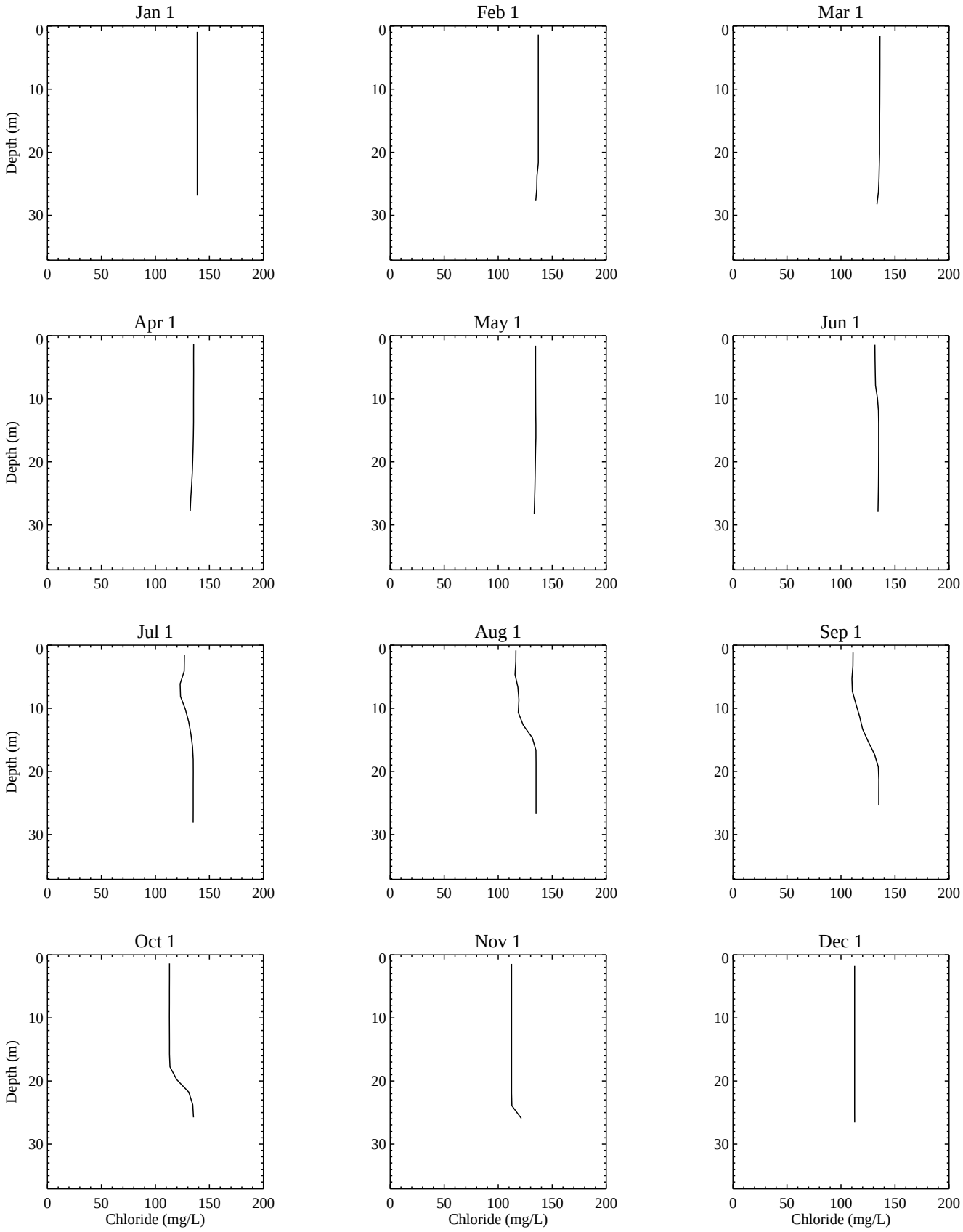

Figure J-15. Vertical profiles of model versus data at Sandy Creek (Segment 161) - Chloride - 1991.

Profiles shown for dates with available data else model results for first day of month shown. Non-detect data shown as open symbols.

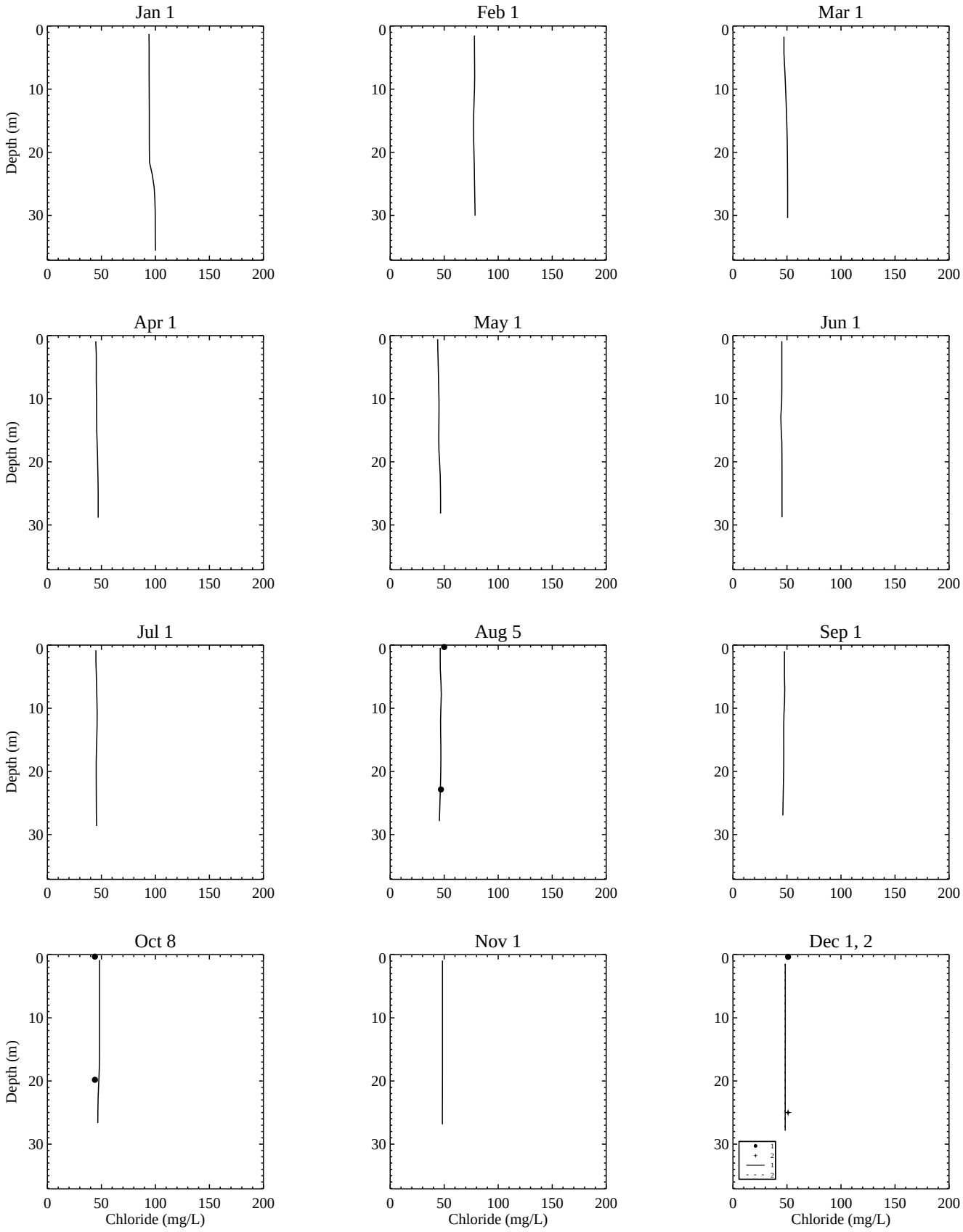

Figure J-15. Vertical profiles of model versus data at Sandy Creek (Segment 161) - Chloride - 1992.

Profiles shown for dates with available data else model results for first day of month shown. Non-detect data shown as open symbols.

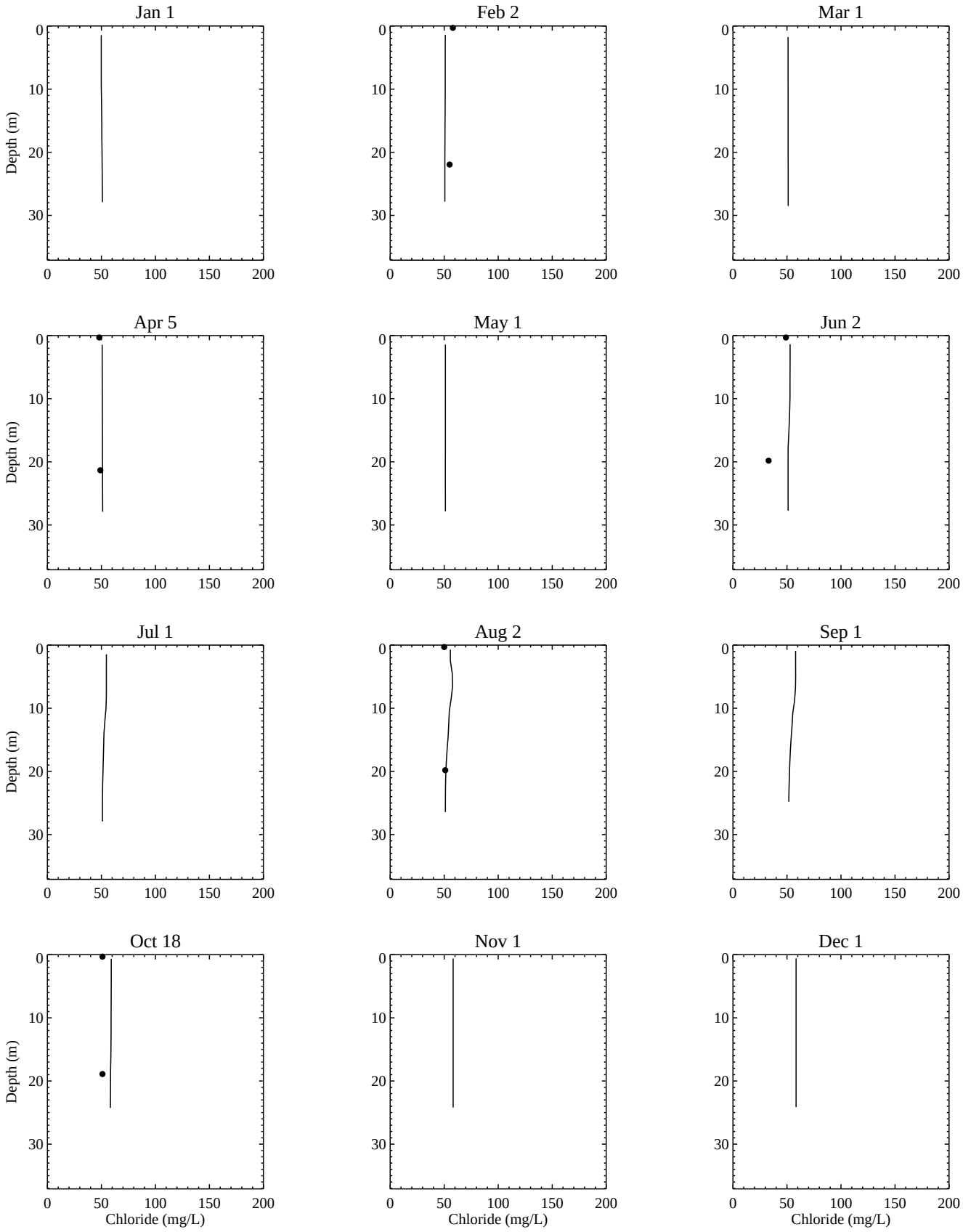

Figure J-15. Vertical profiles of model versus data at Sandy Creek (Segment 161) - Chloride - 1993.

Profiles shown for dates with available data else model results for first day of month shown. Non-detect data shown as open symbols.

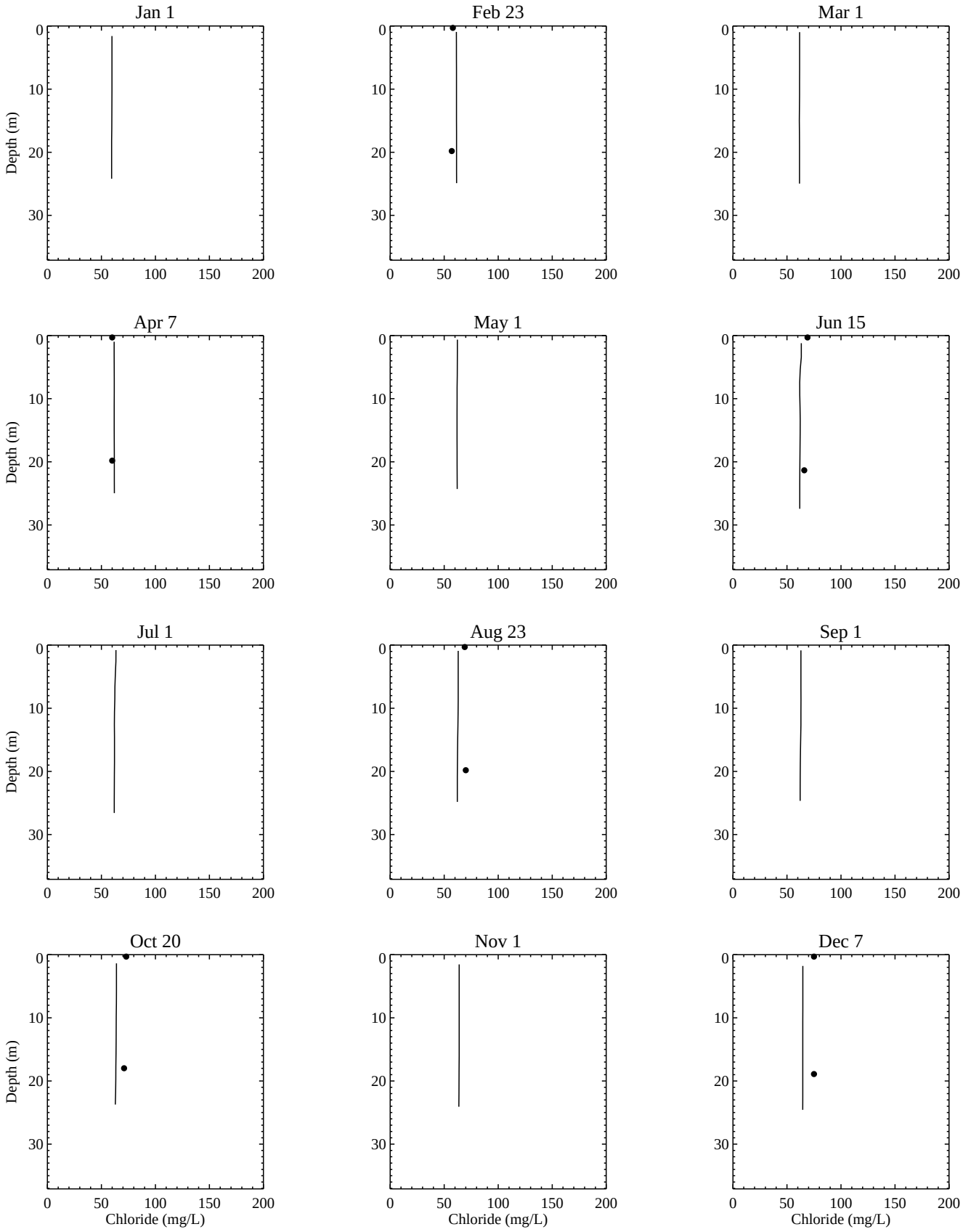

Figure J-15. Vertical profiles of model versus data at Sandy Creek (Segment 161) - Chloride - 1994.

Profiles shown for dates with available data else model results for first day of month shown. Non-detect data shown as open symbols.

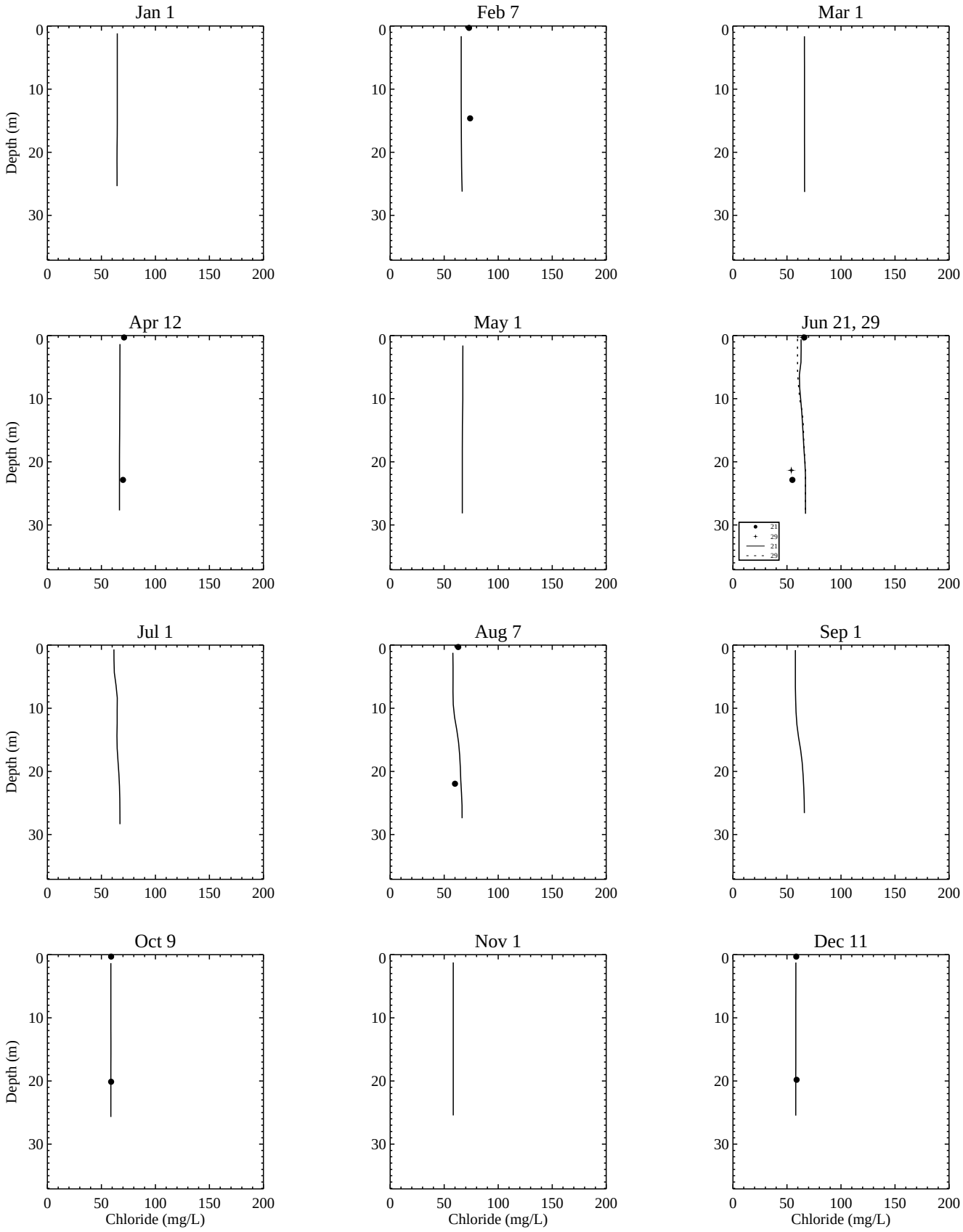

Figure J-15. Vertical profiles of model versus data at Sandy Creek (Segment 161) - Chloride - 1995.

Profiles shown for dates with available data else model results for first day of month shown. Non-detect data shown as open symbols.

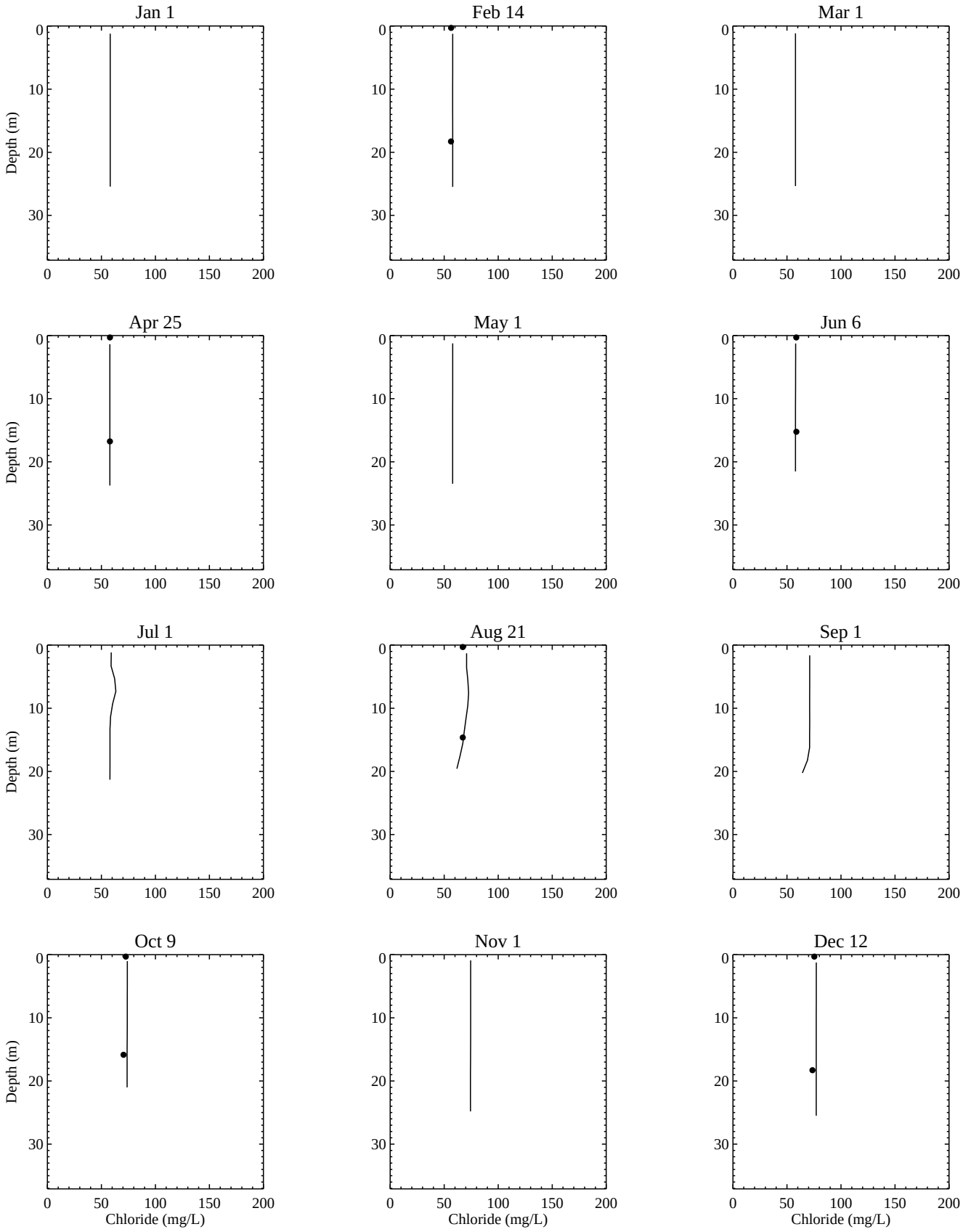

Figure J-15. Vertical profiles of model versus data at Sandy Creek (Segment 161) - Chloride - 1996.

Profiles shown for dates with available data else model results for first day of month shown. Non-detect data shown as open symbols.

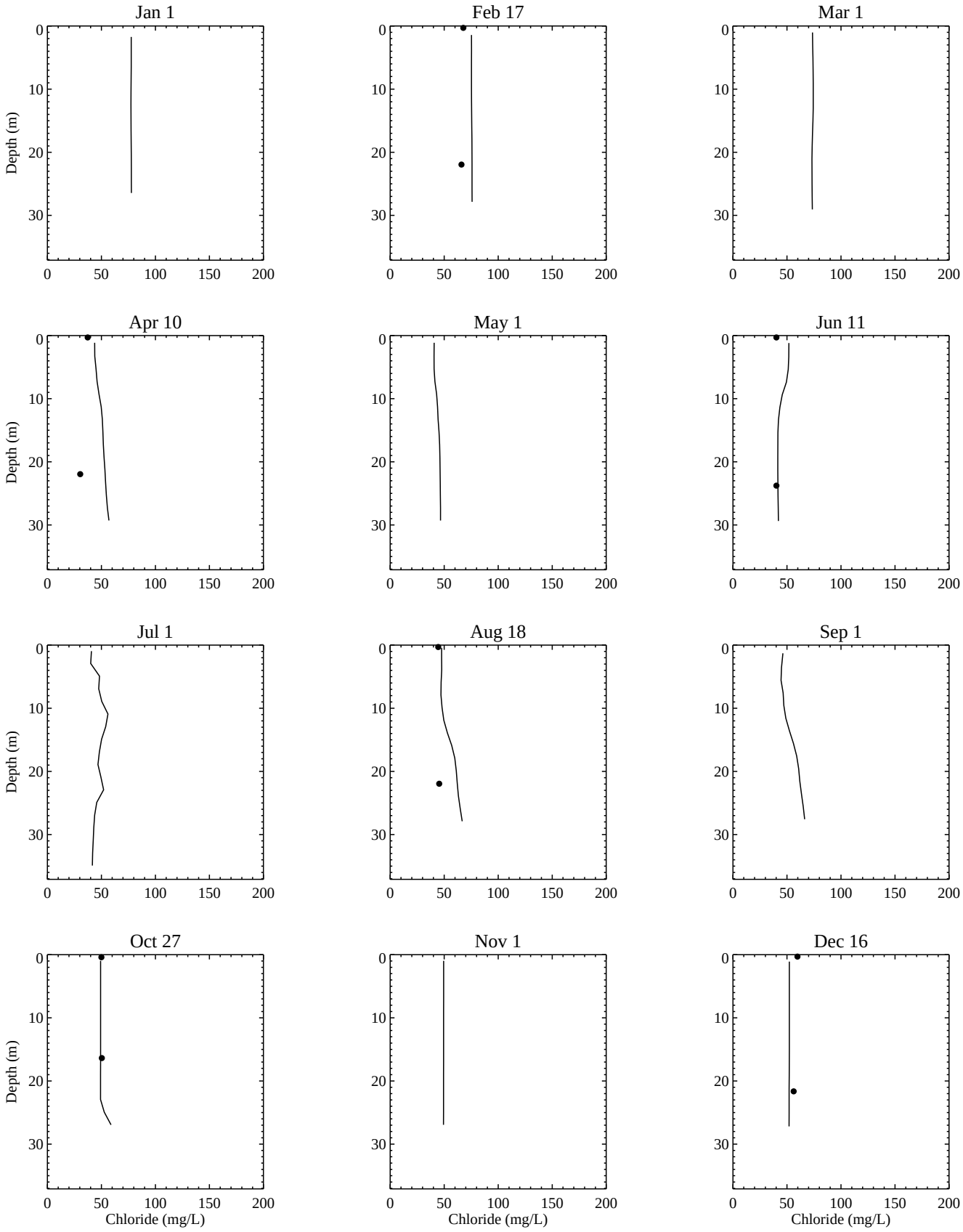

Figure J-15. Vertical profiles of model versus data at Sandy Creek (Segment 161) - Chloride - 1997.

Profiles shown for dates with available data else model results for first day of month shown. Non-detect data shown as open symbols.

Model Data

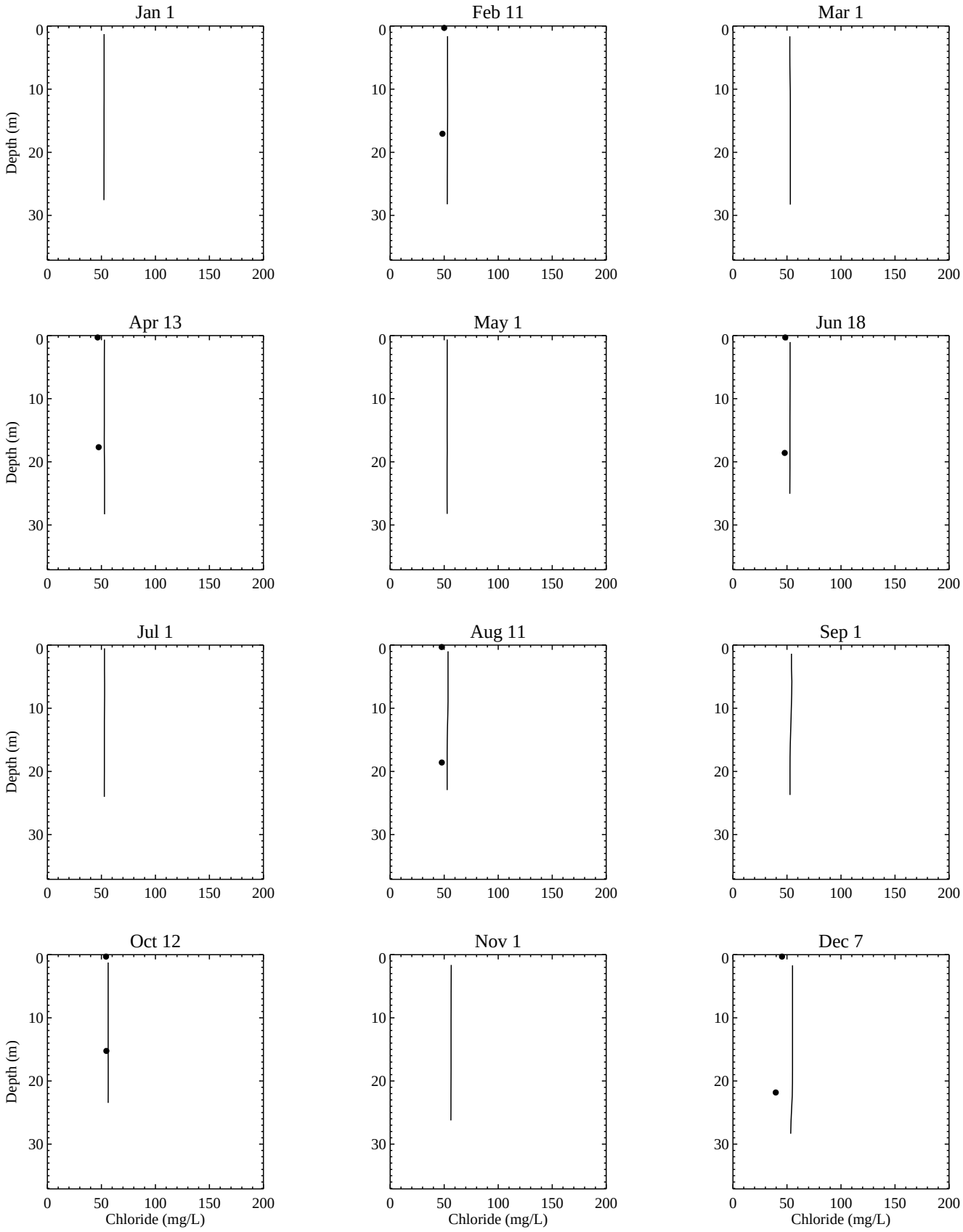

Figure J-15. Vertical profiles of model versus data at Sandy Creek (Segment 161) - Chloride - 1998.

Profiles shown for dates with available data else model results for first day of month shown. Non-detect data shown as open symbols.

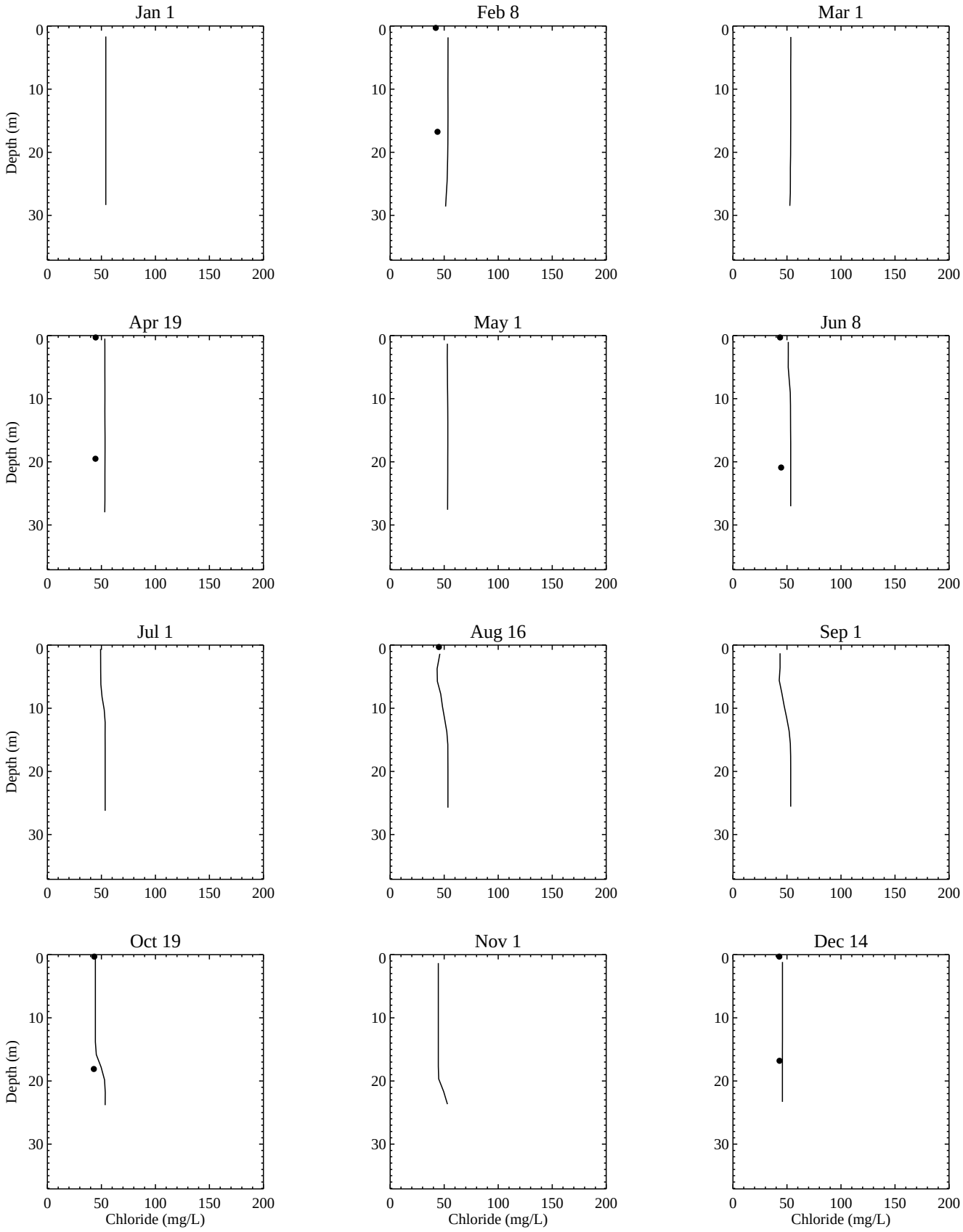

Figure J-15. Vertical profiles of model versus data at Sandy Creek (Segment 161) - Chloride - 1999.

Profiles shown for dates with available data else model results for first day of month shown. Non-detect data shown as open symbols.

Model Data

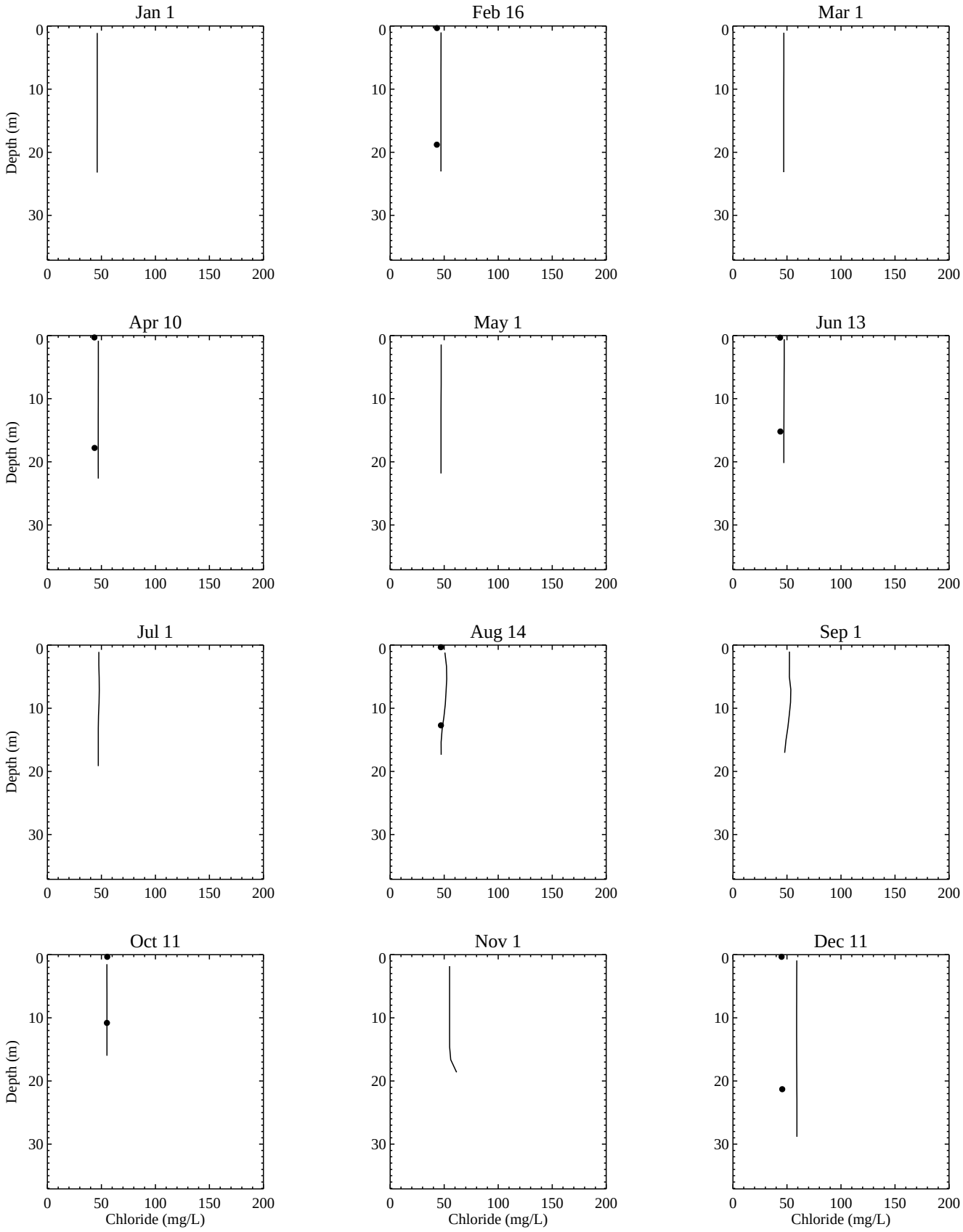

Figure J-15. Vertical profiles of model versus data at Sandy Creek (Segment 161) - Chloride - 2000.

Profiles shown for dates with available data else model results for first day of month shown. Non-detect data shown as open symbols.

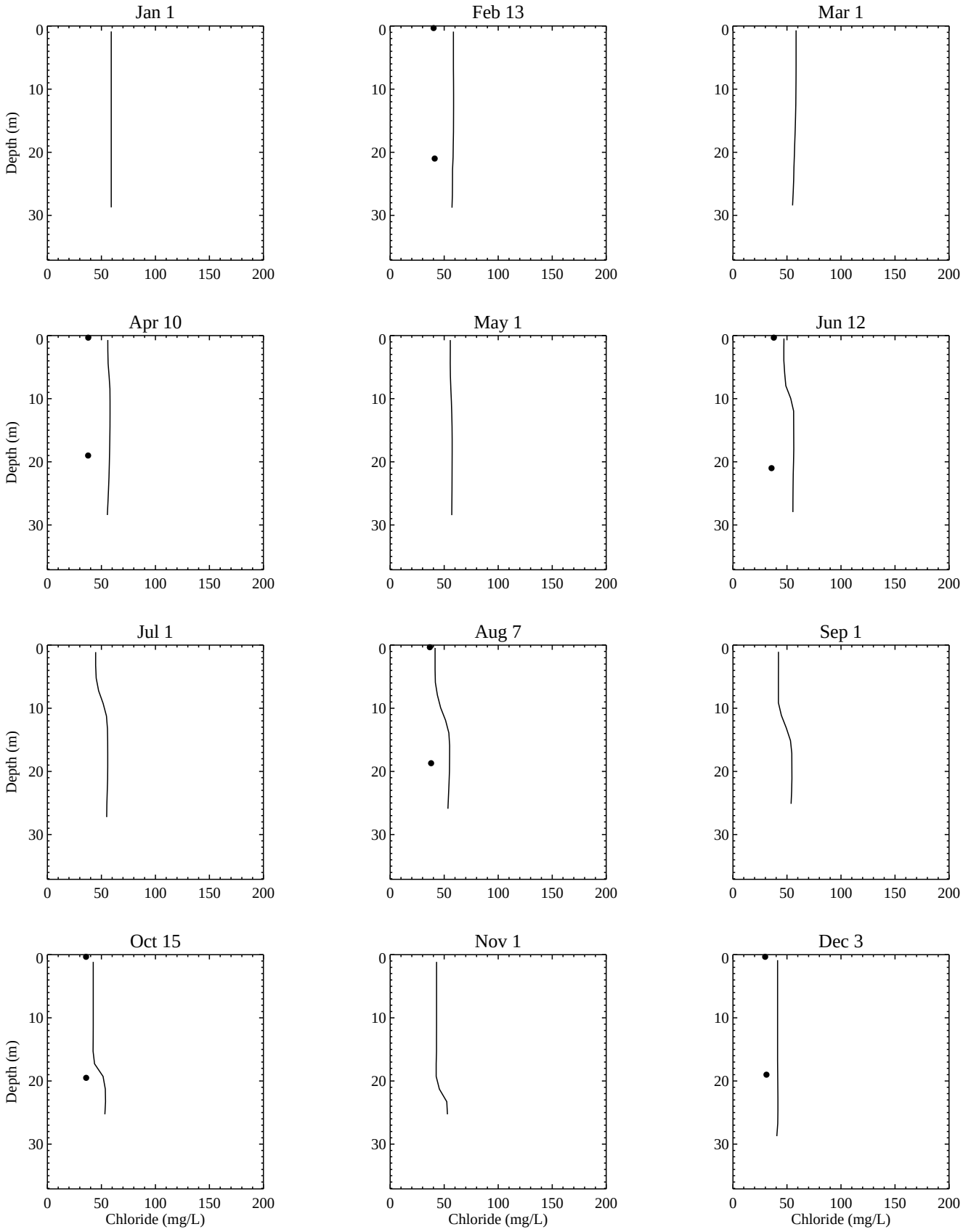

Figure J-15. Vertical profiles of model versus data at Sandy Creek (Segment 161) - Chloride - 2001.

Profiles shown for dates with available data else model results for first day of month shown. Non-detect data shown as open symbols.

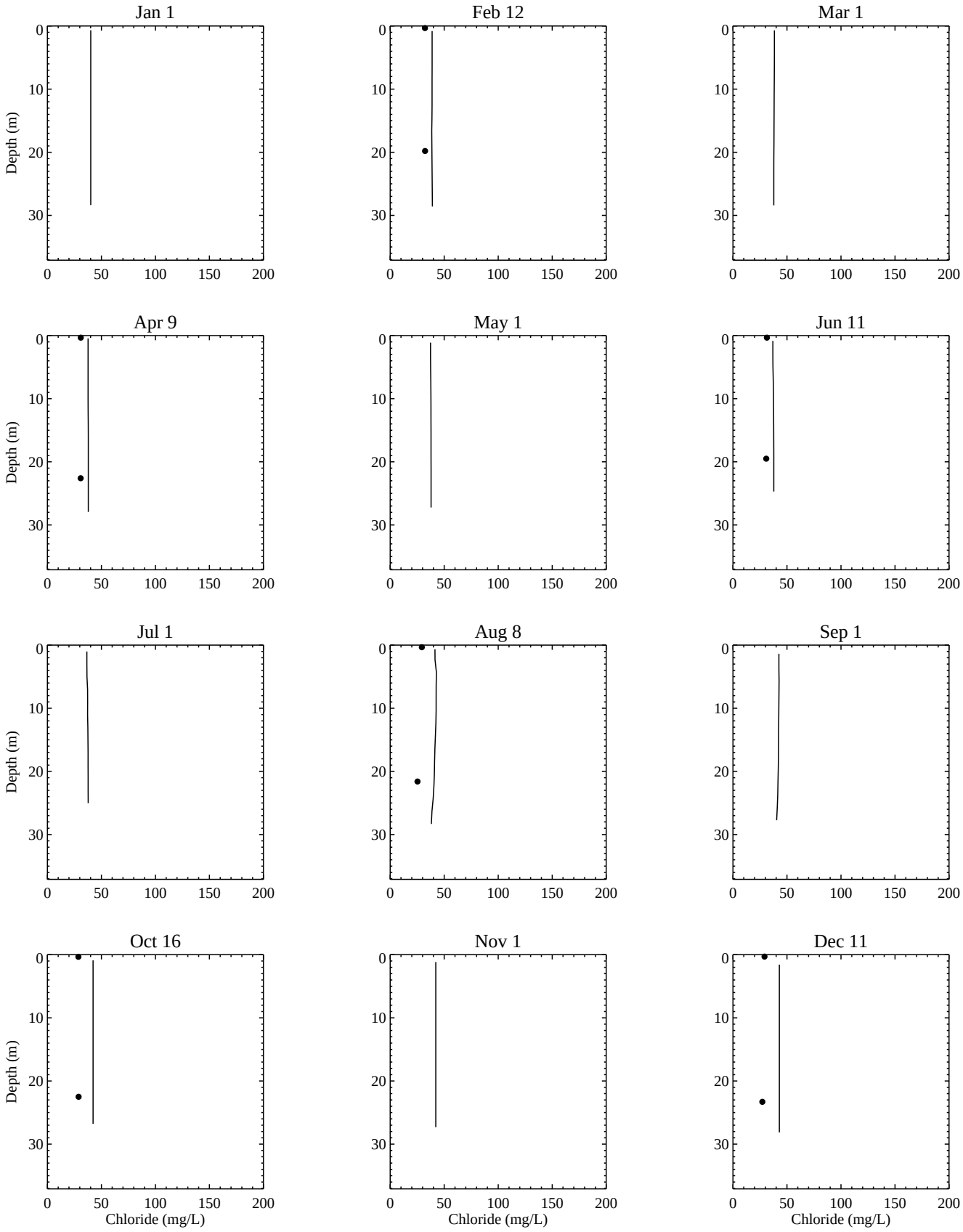

Figure J-15. Vertical profiles of model versus data at Sandy Creek (Segment 161) - Chloride - 2002.

Profiles shown for dates with available data else model results for first day of month shown. Non-detect data shown as open symbols.

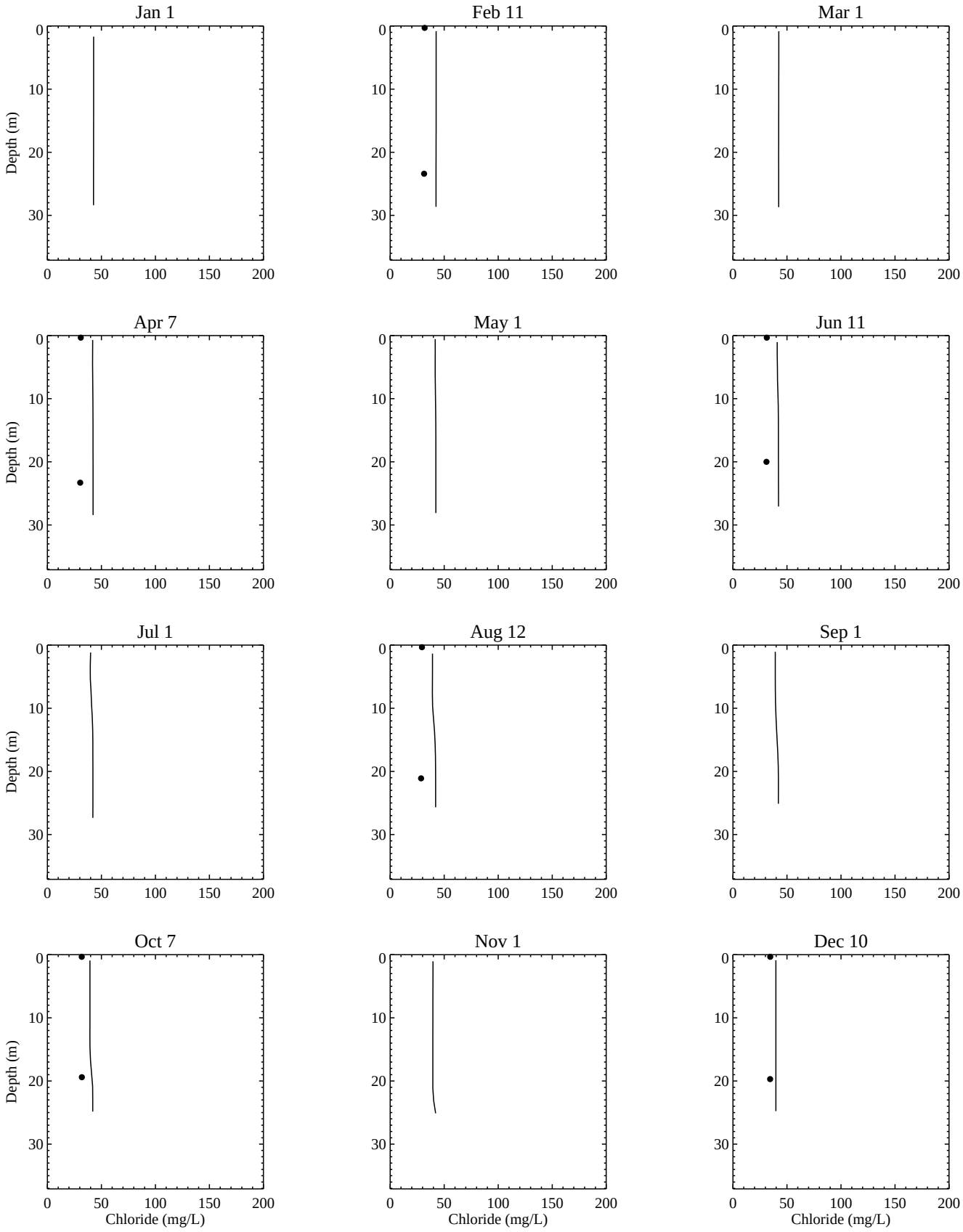

Figure J-15. Vertical profiles of model versus data at Sandy Creek (Segment 161) - Chloride - 2003.

Profiles shown for dates with available data else model results for first day of month shown. Non-detect data shown as open symbols.

Model Data

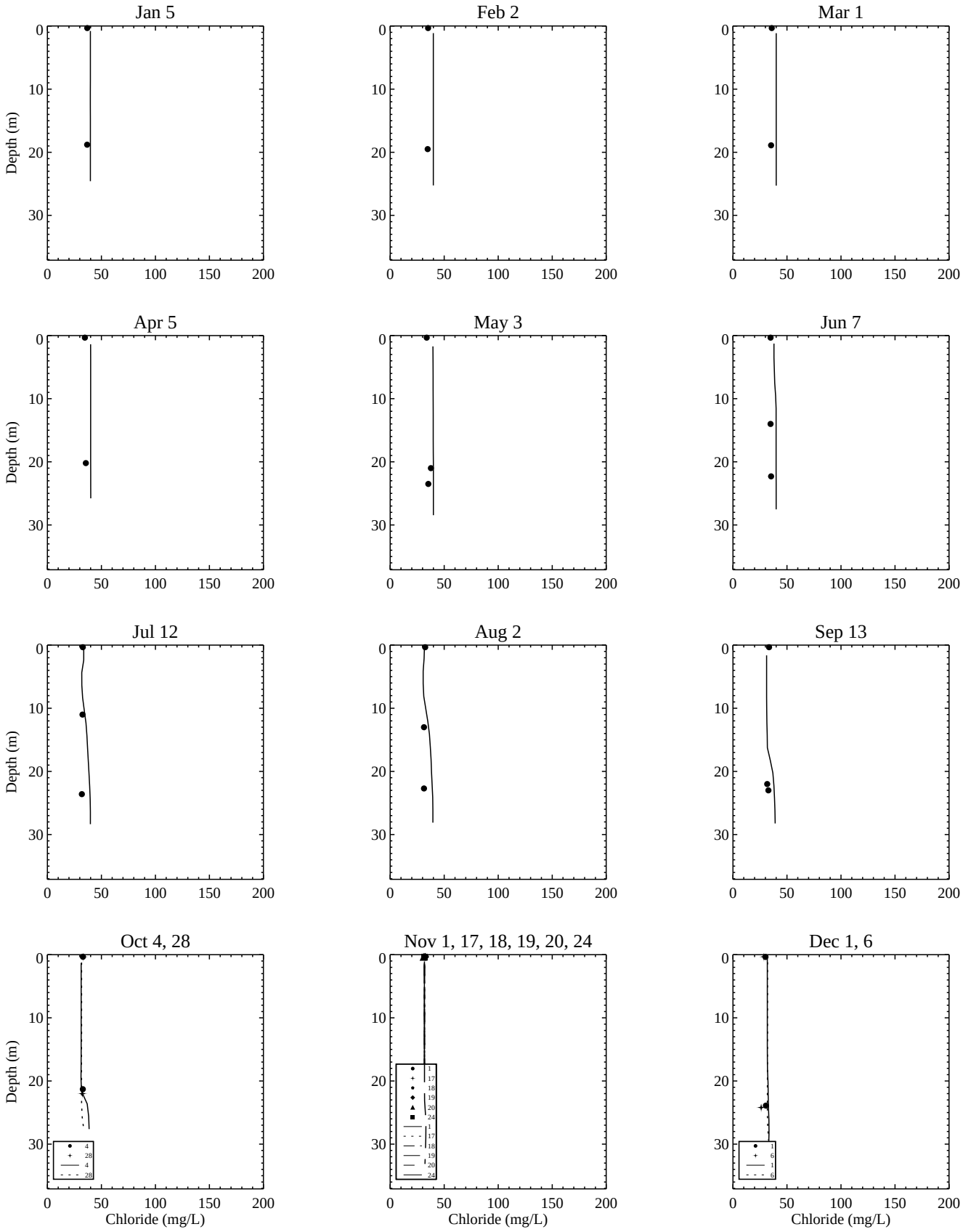

Figure J-15. Vertical profiles of model versus data at Sandy Creek (Segment 161) - Chloride - 2004.

Profiles shown for dates with available data else model results for first day of month shown. Non-detect data shown as open symbols.

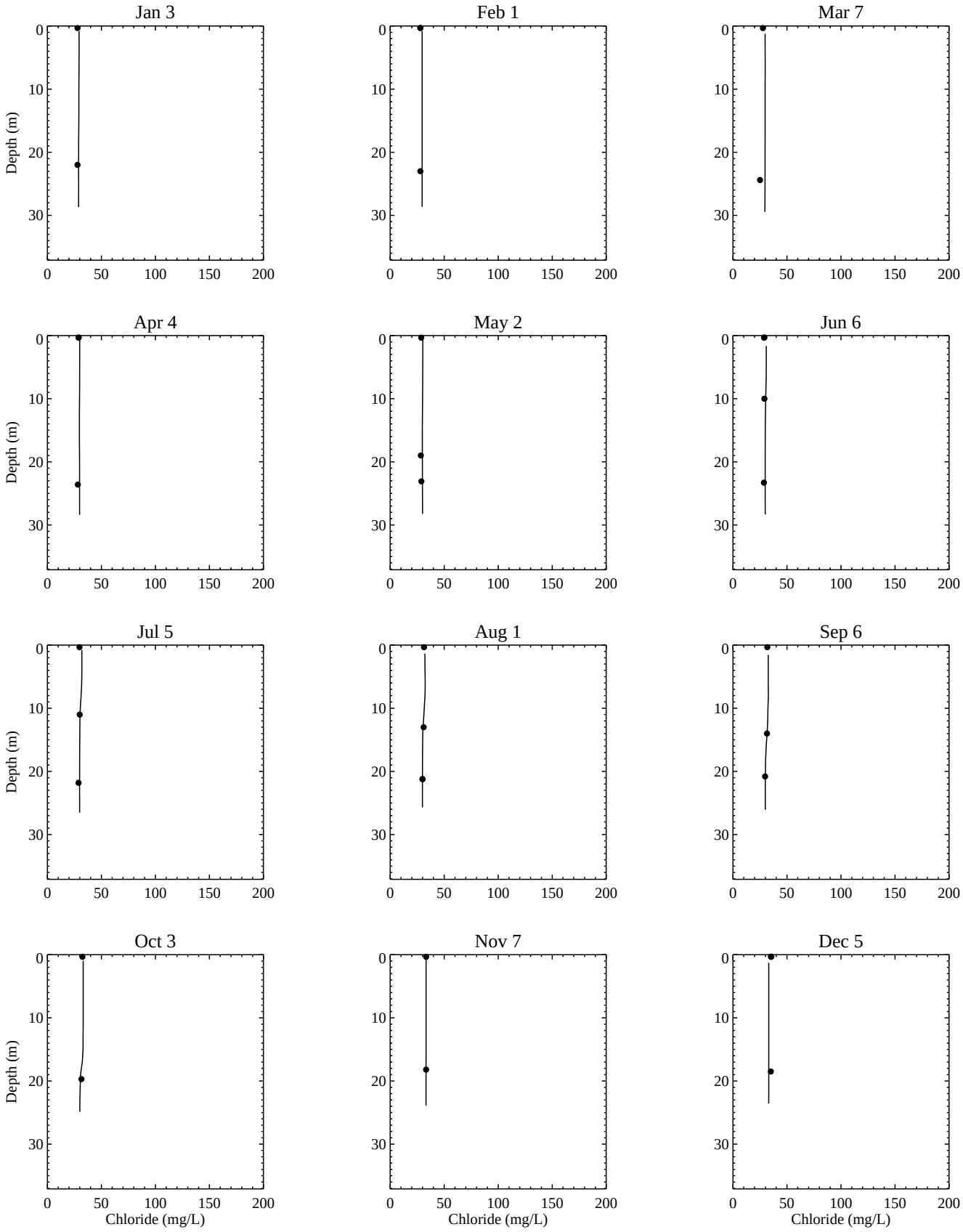

Figure J-15. Vertical profiles of model versus data at Sandy Creek (Segment 161) - Chloride - 2005.

Profiles shown for dates with available data else model results for first day of month shown. Non-detect data shown as open symbols.

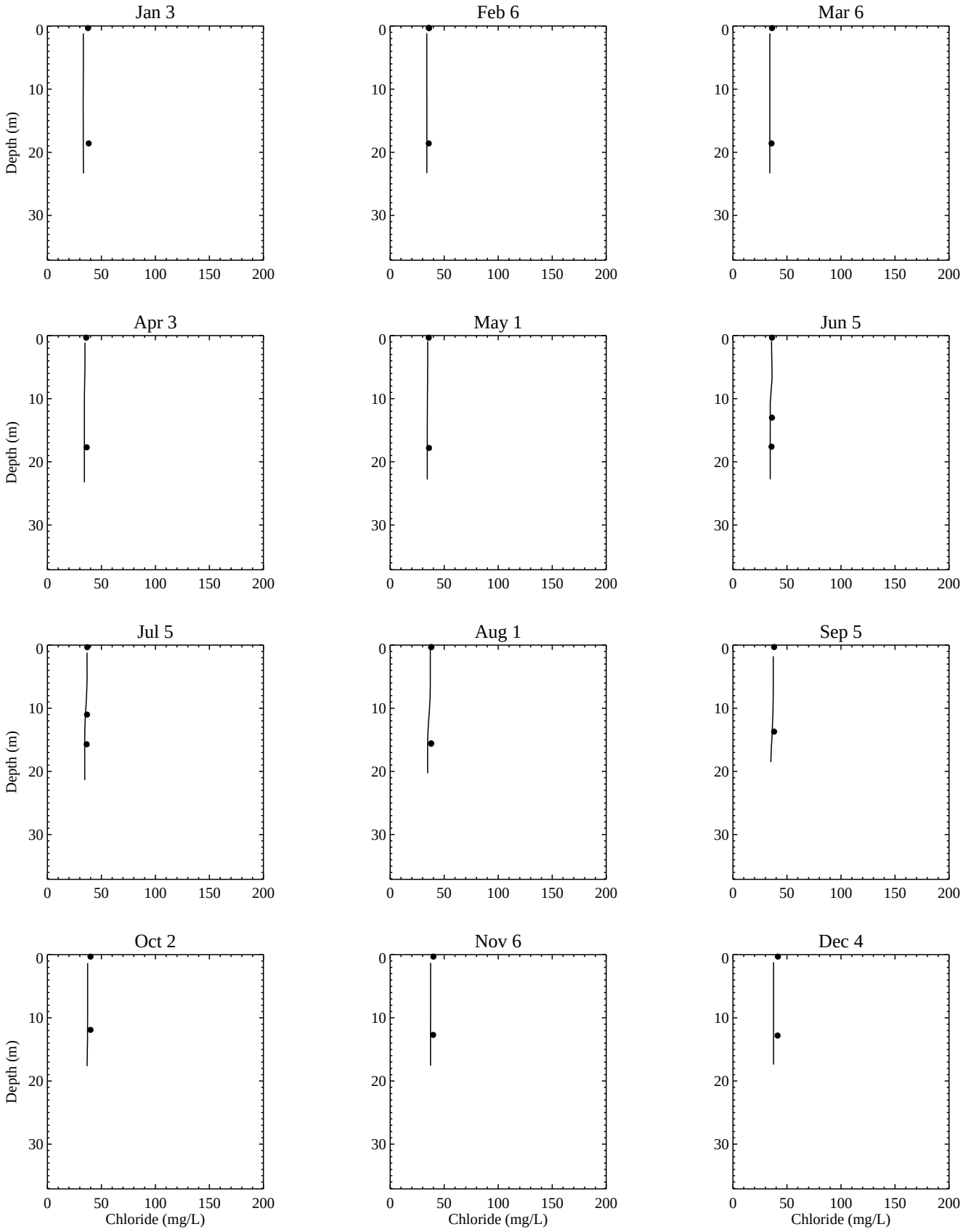

Figure J-15. Vertical profiles of model versus data at Sandy Creek (Segment 161) - Chloride - 2006.

Profiles shown for dates with available data else model results for first day of month shown. Non-detect data shown as open symbols.

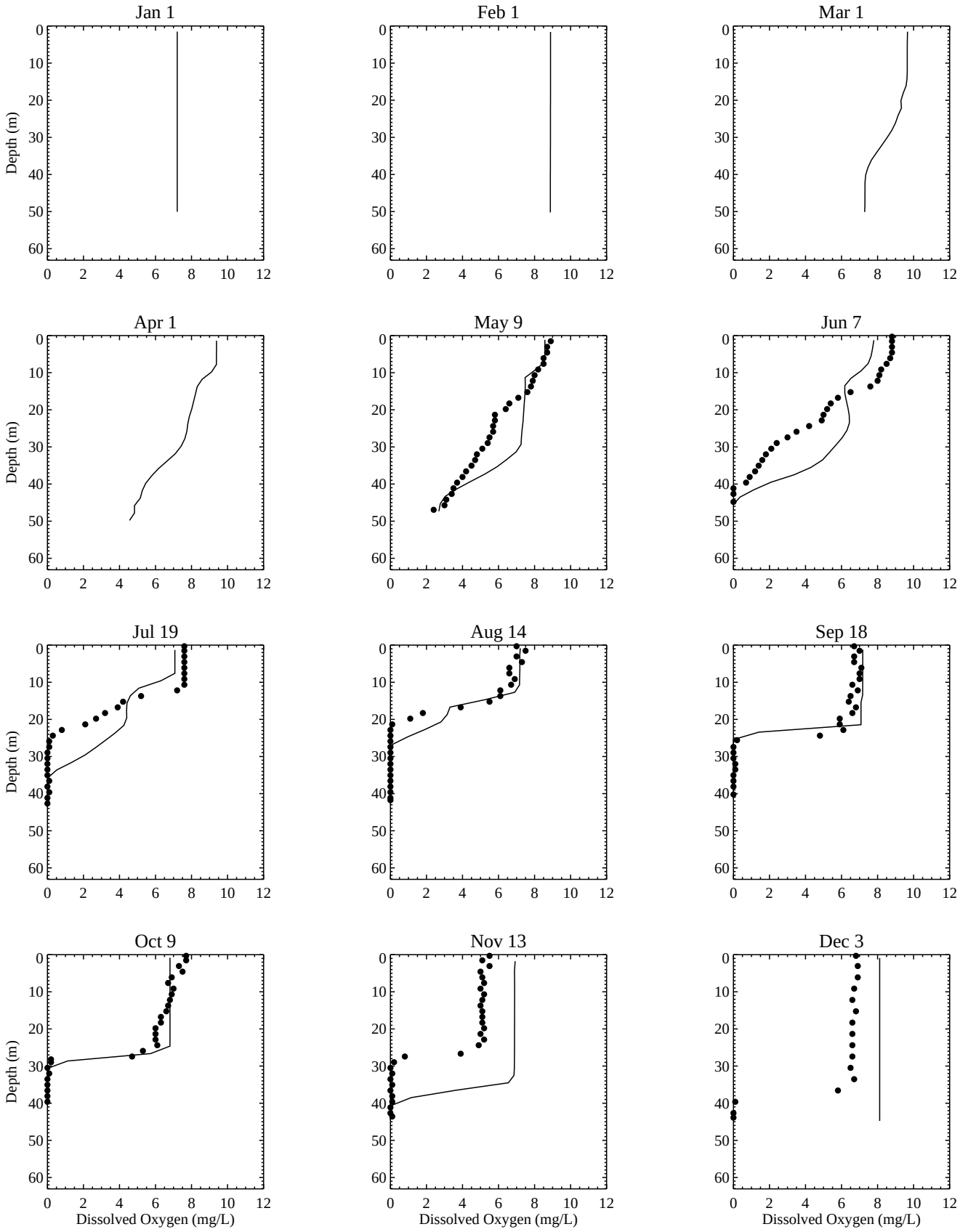

Figure J-16. Vertical profiles of model versus data at Mansfield Dam (Segment 93) - Dissolved Oxygen - 1984.

Profiles shown for dates with available data else model results for first day of month shown.

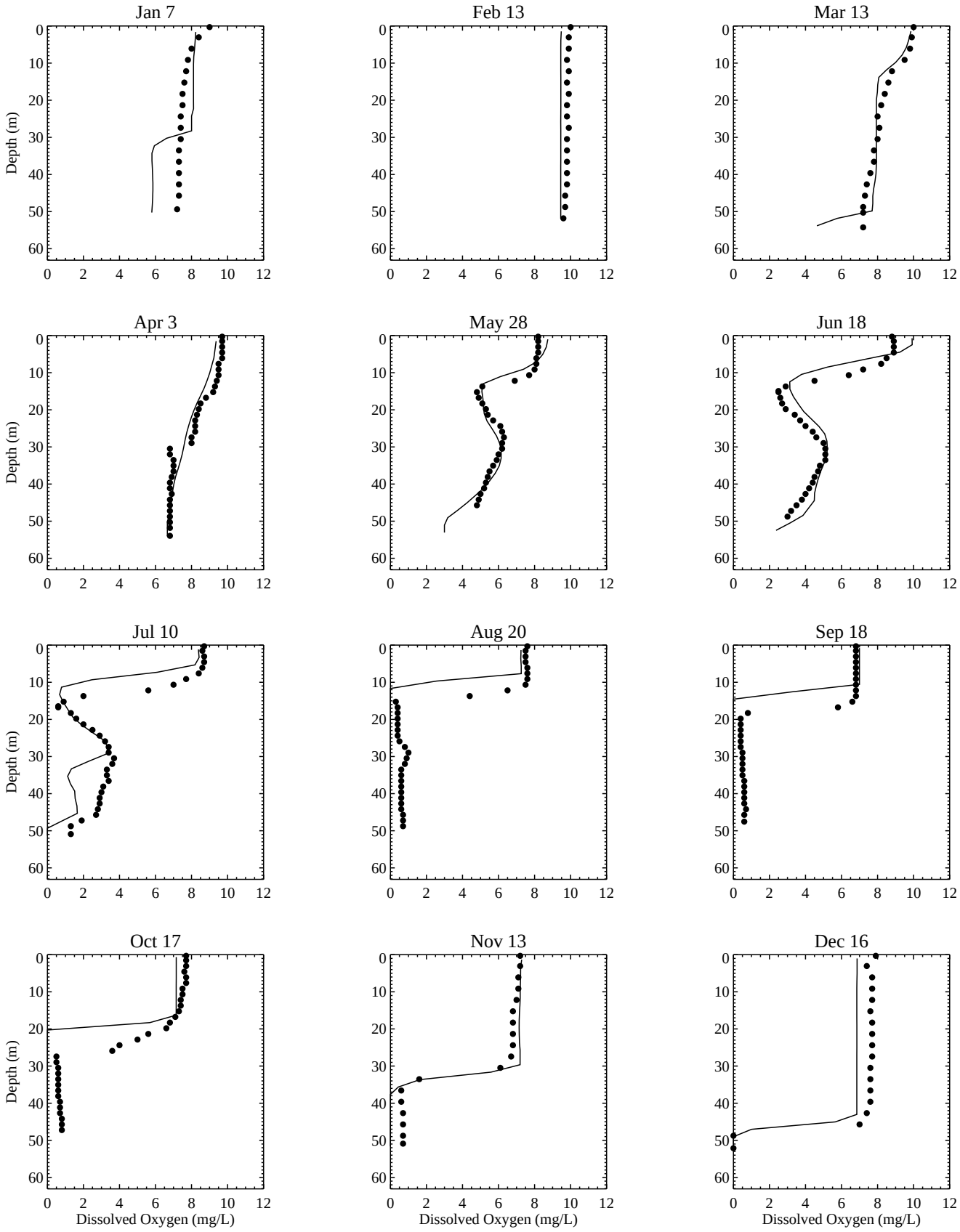

Figure J-16. Vertical profiles of model versus data at Mansfield Dam (Segment 93) - Dissolved Oxygen - 1985.

Profiles shown for dates with available data else model results for first day of month shown.

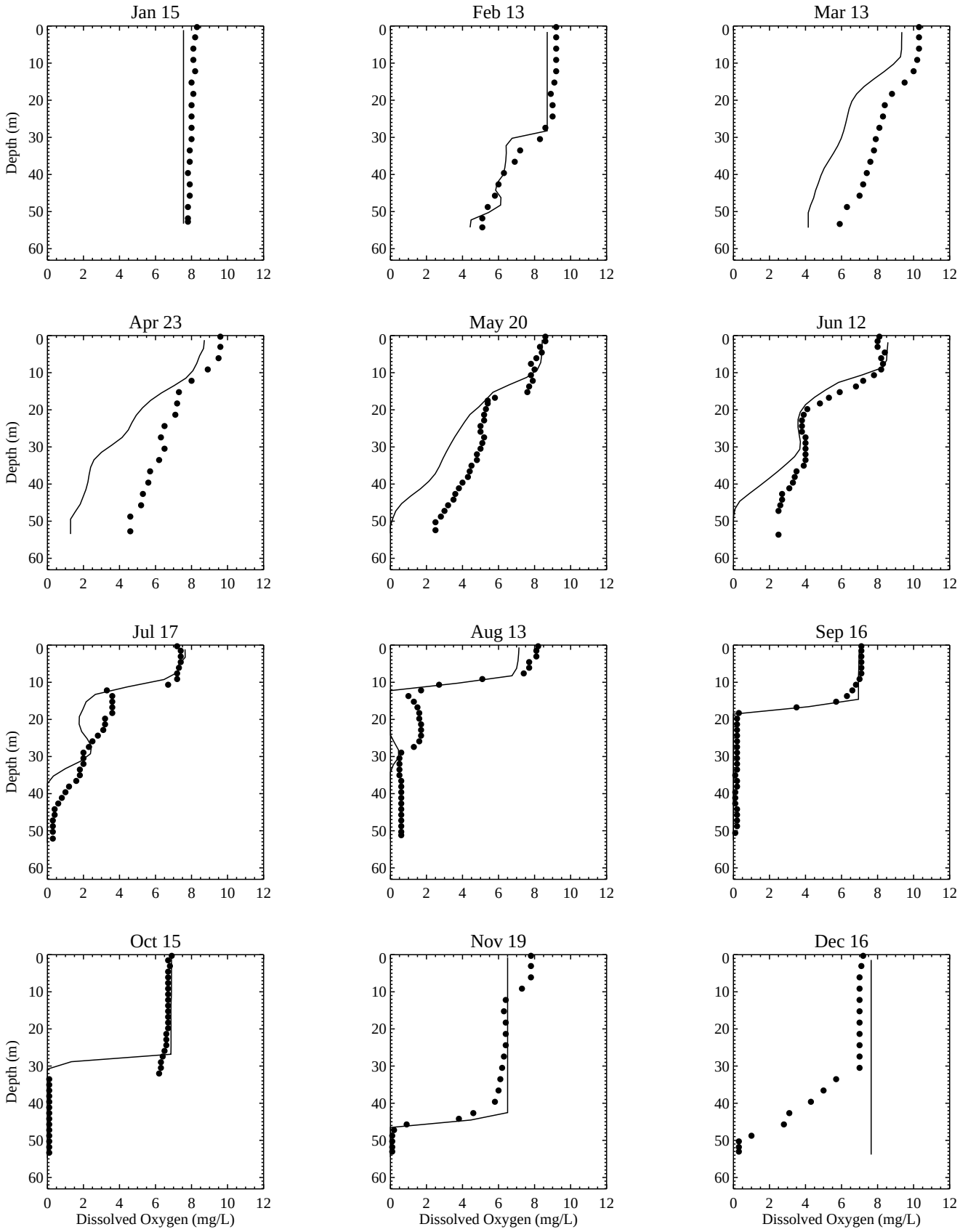

Figure J-16. Vertical profiles of model versus data at Mansfield Dam (Segment 93) - Dissolved Oxygen - 1986.

Profiles shown for dates with available data else model results for first day of month shown.

Model Data

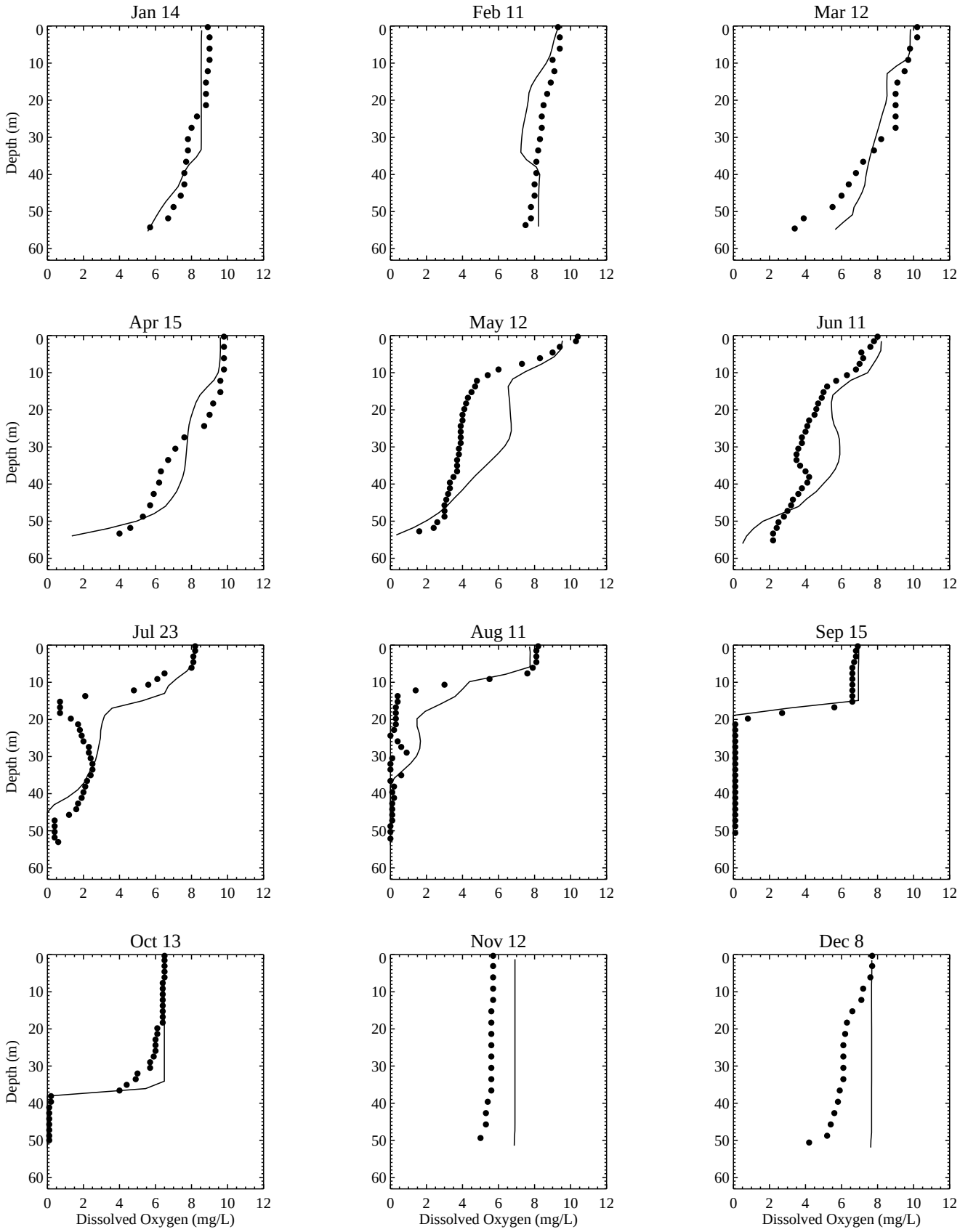

Figure J-16. Vertical profiles of model versus data at Mansfield Dam (Segment 93) - Dissolved Oxygen - 1987.

Profiles shown for dates with available data else model results for first day of month shown.

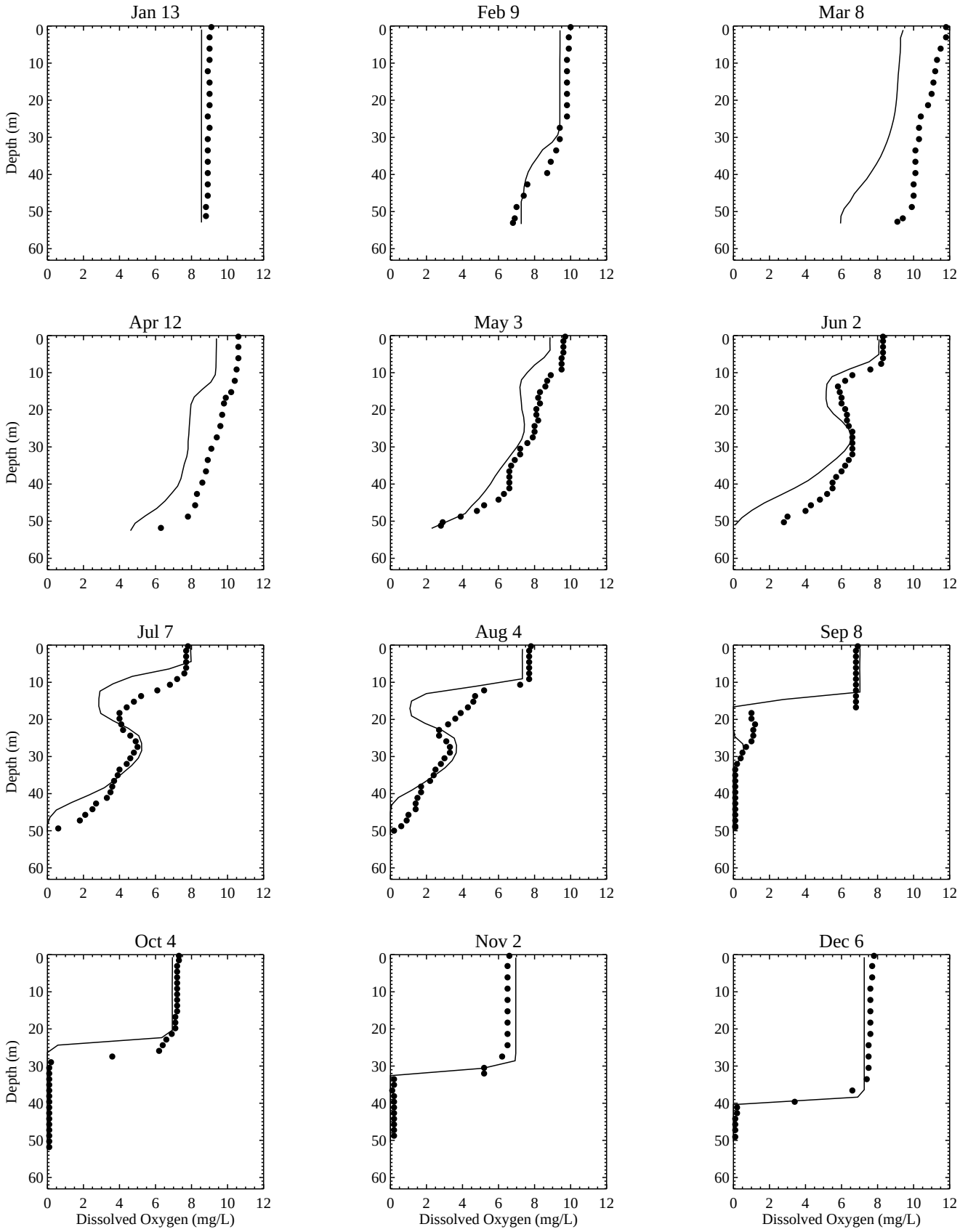

Figure J-16. Vertical profiles of model versus data at Mansfield Dam (Segment 93) - Dissolved Oxygen - 1988.

Profiles shown for dates with available data else model results for first day of month shown.

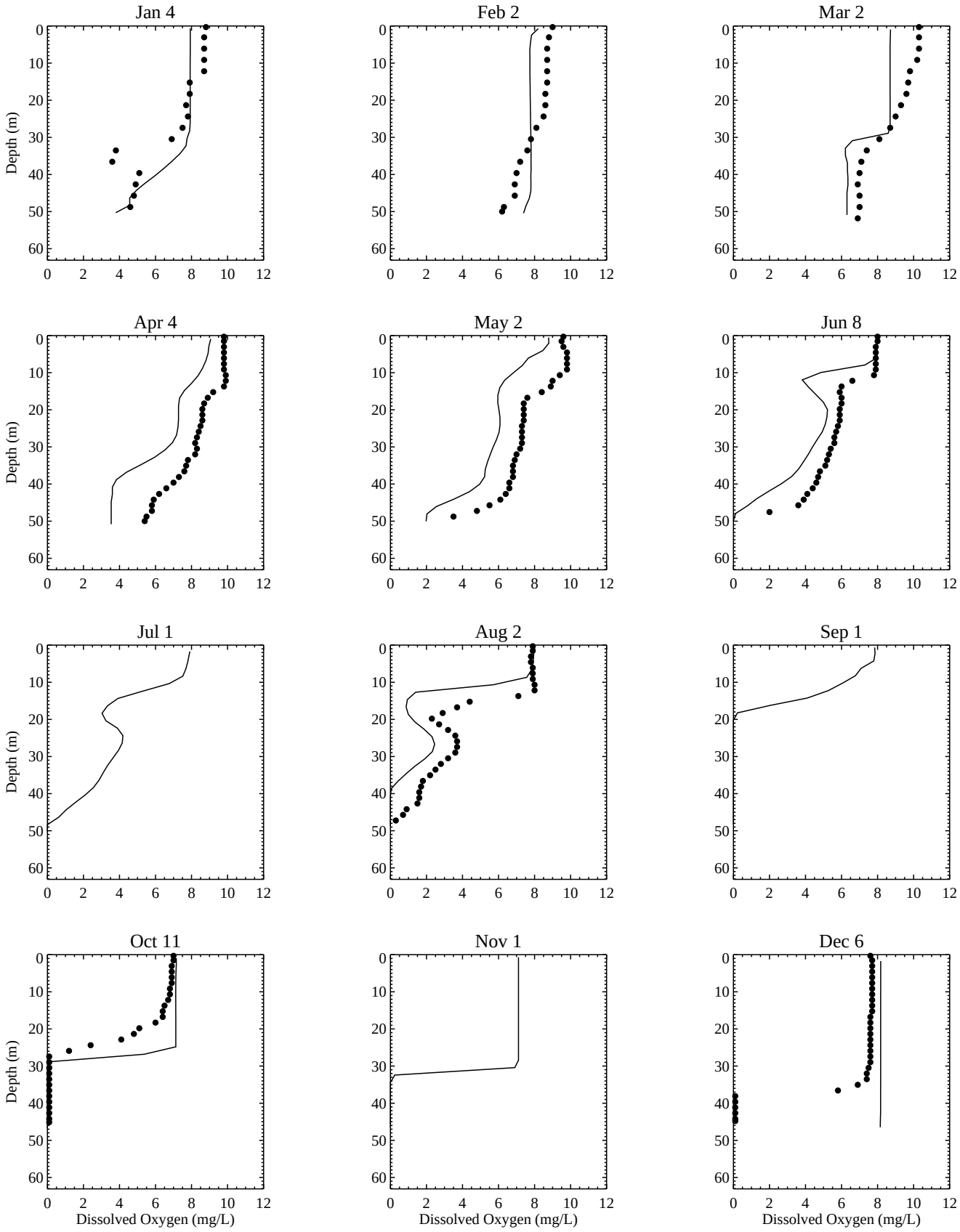

Figure J-16. Vertical profiles of model versus data at Mansfield Dam (Segment 93) - Dissolved Oxygen - 1989.

Profiles shown for dates with available data else model results for first day of month shown.

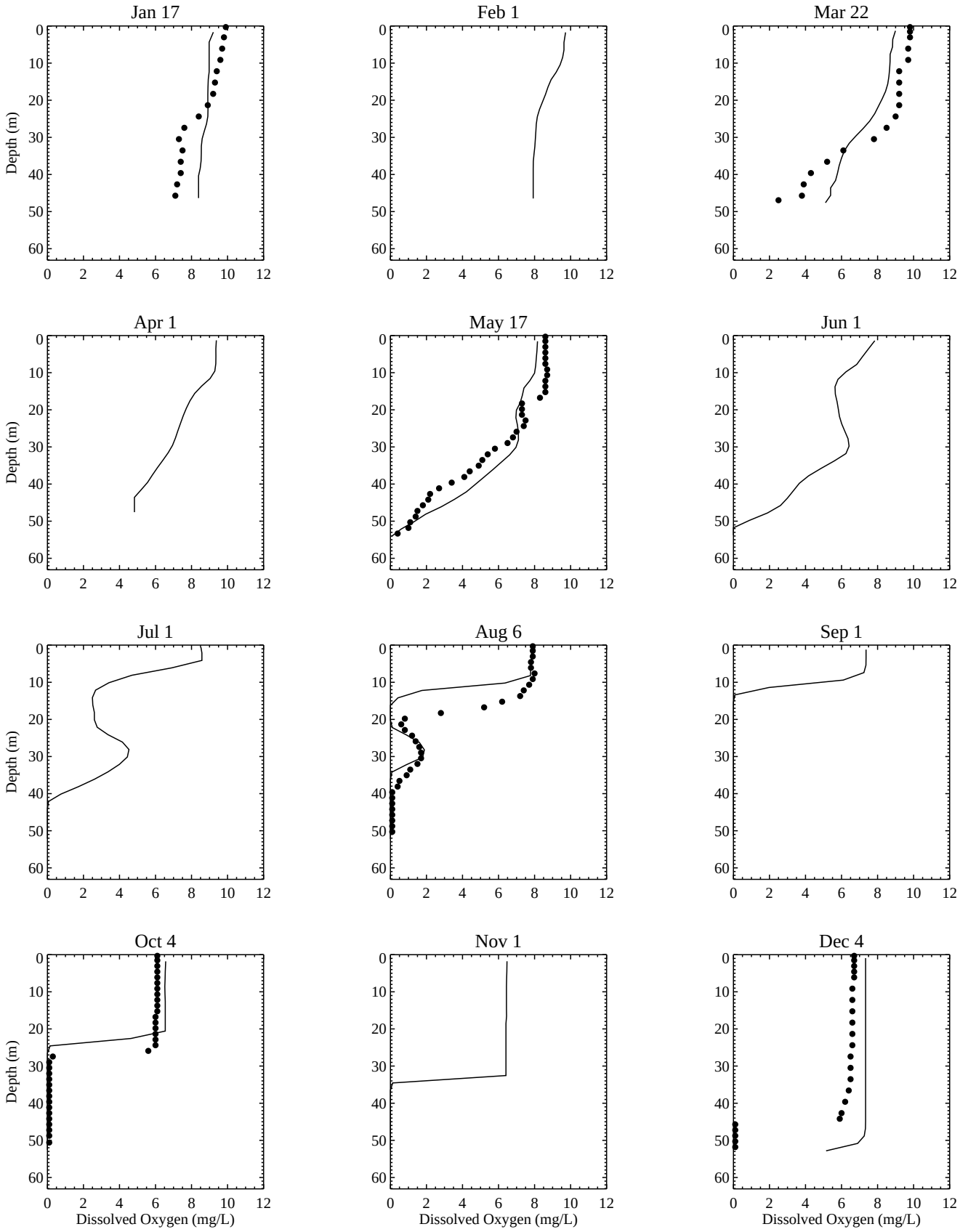

Figure J-16. Vertical profiles of model versus data at Mansfield Dam (Segment 93) - Dissolved Oxygen - 1990.

Profiles shown for dates with available data else model results for first day of month shown.

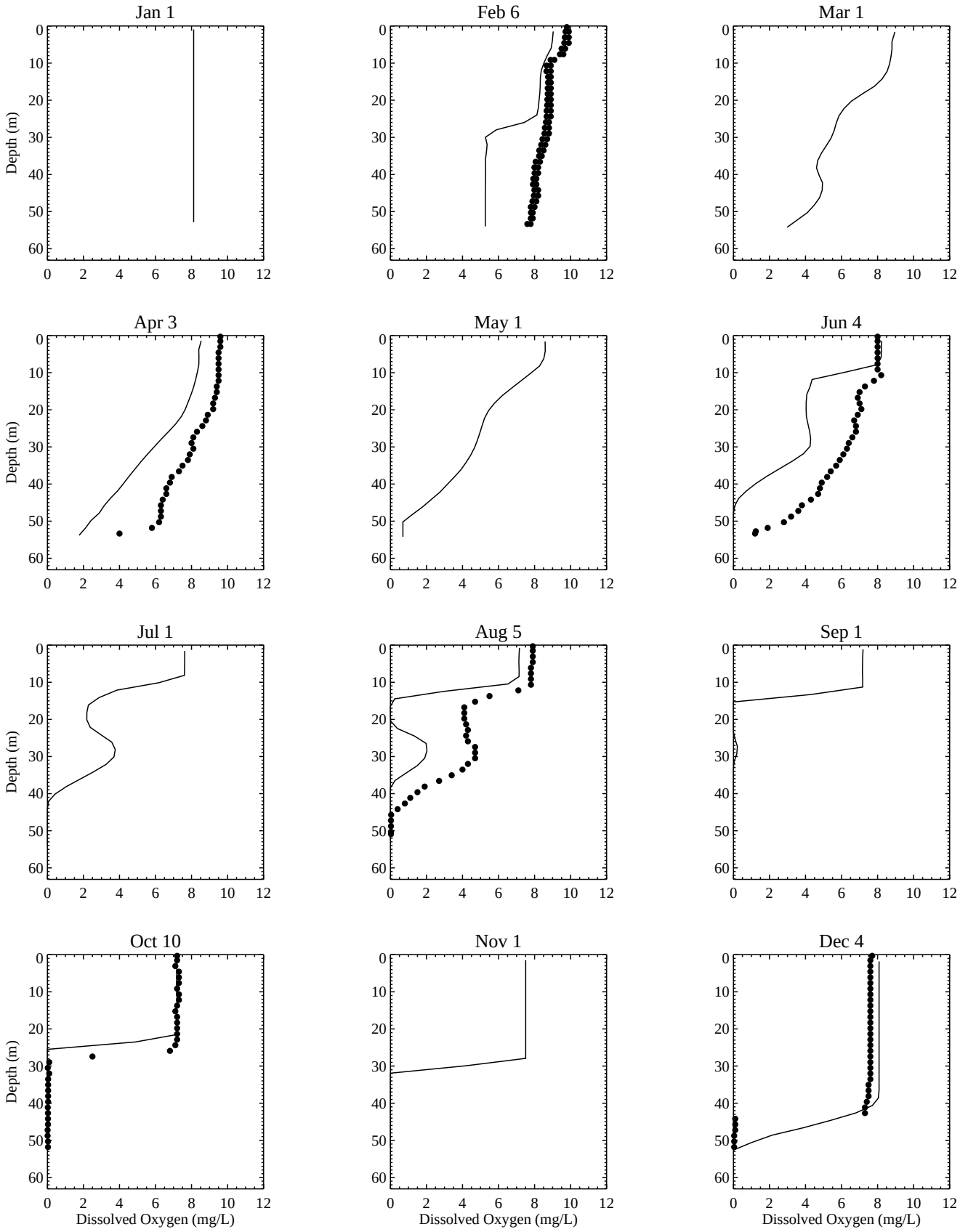

Figure J-16. Vertical profiles of model versus data at Mansfield Dam (Segment 93) - Dissolved Oxygen - 1991.

Profiles shown for dates with available data else model results for first day of month shown.

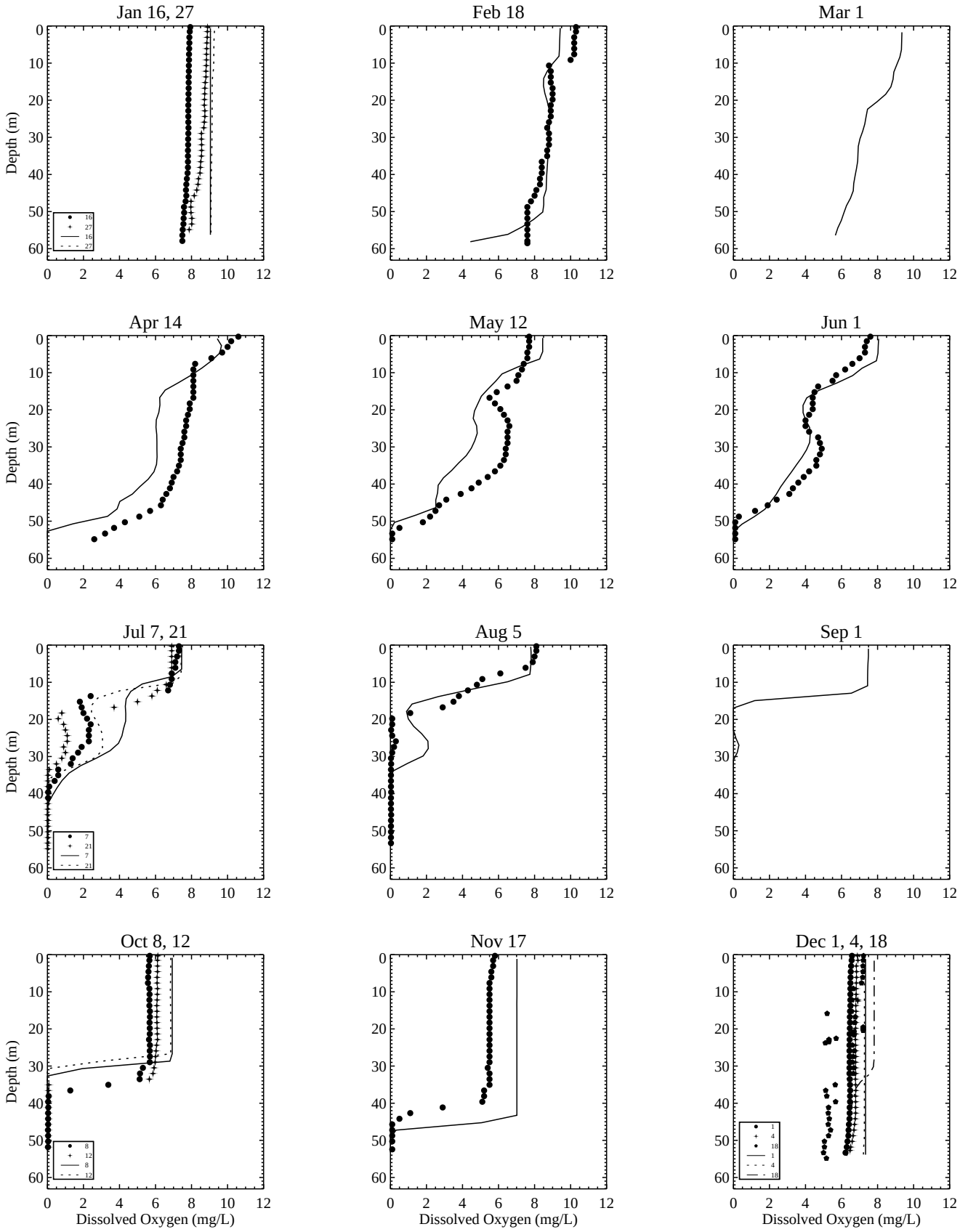

Figure J-16. Vertical profiles of model versus data at Mansfield Dam (Segment 93) - Dissolved Oxygen - 1992.

Profiles shown for dates with available data else model results for first day of month shown.

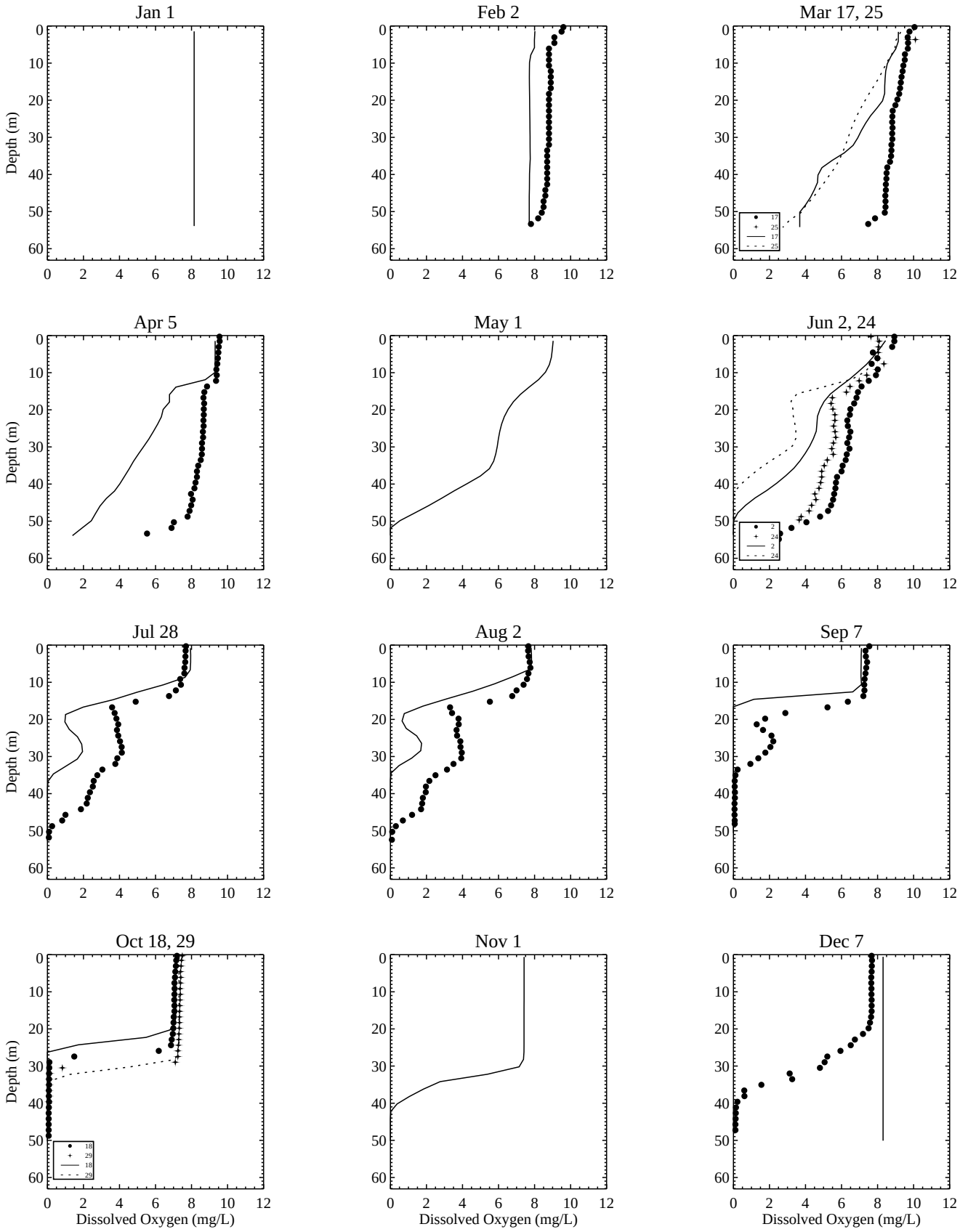

Figure J-16. Vertical profiles of model versus data at Mansfield Dam (Segment 93) - Dissolved Oxygen - 1993.

Profiles shown for dates with available data else model results for first day of month shown.

Model ● Data

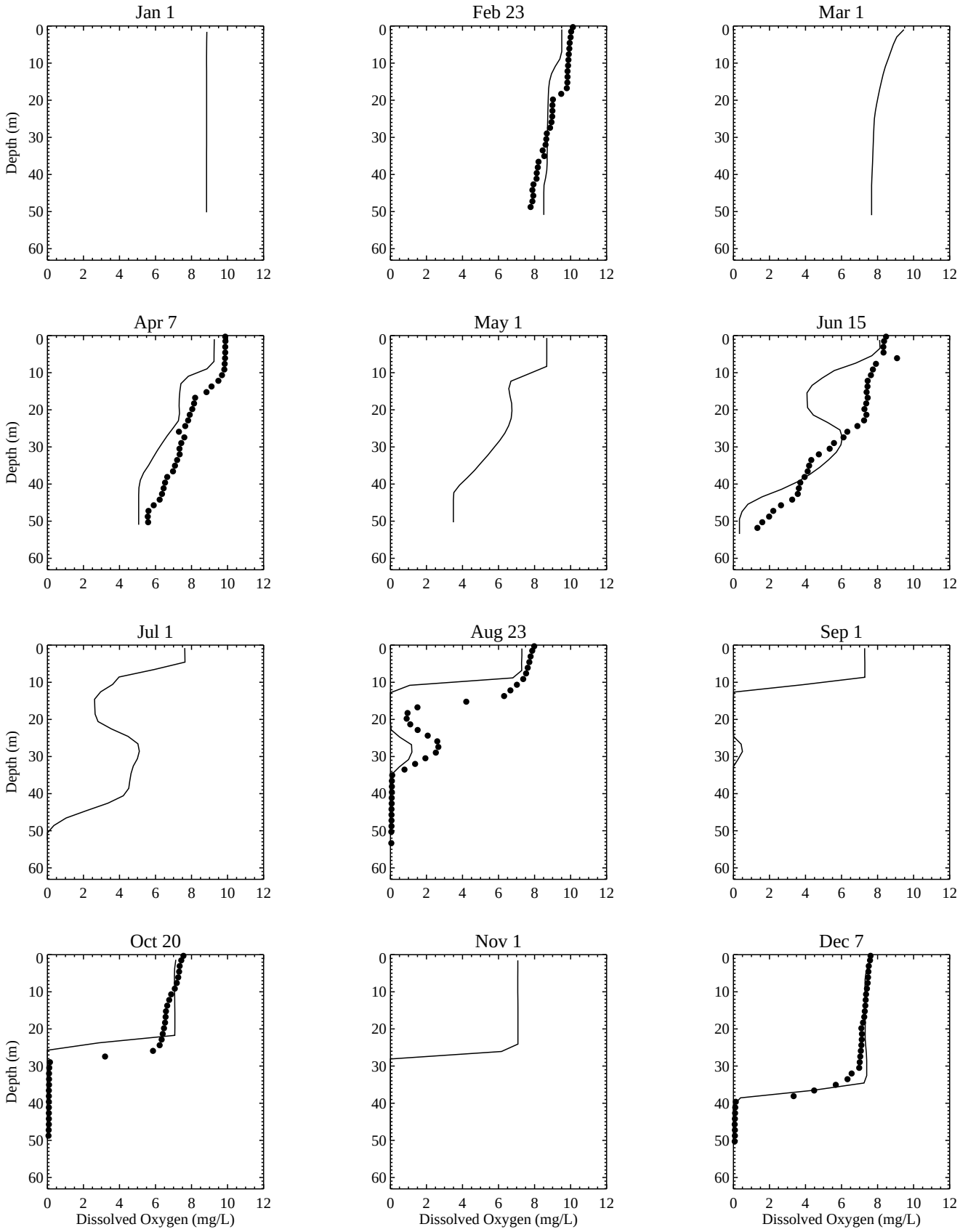

Figure J-16. Vertical profiles of model versus data at Mansfield Dam (Segment 93) - Dissolved Oxygen - 1994.

Profiles shown for dates with available data else model results for first day of month shown.

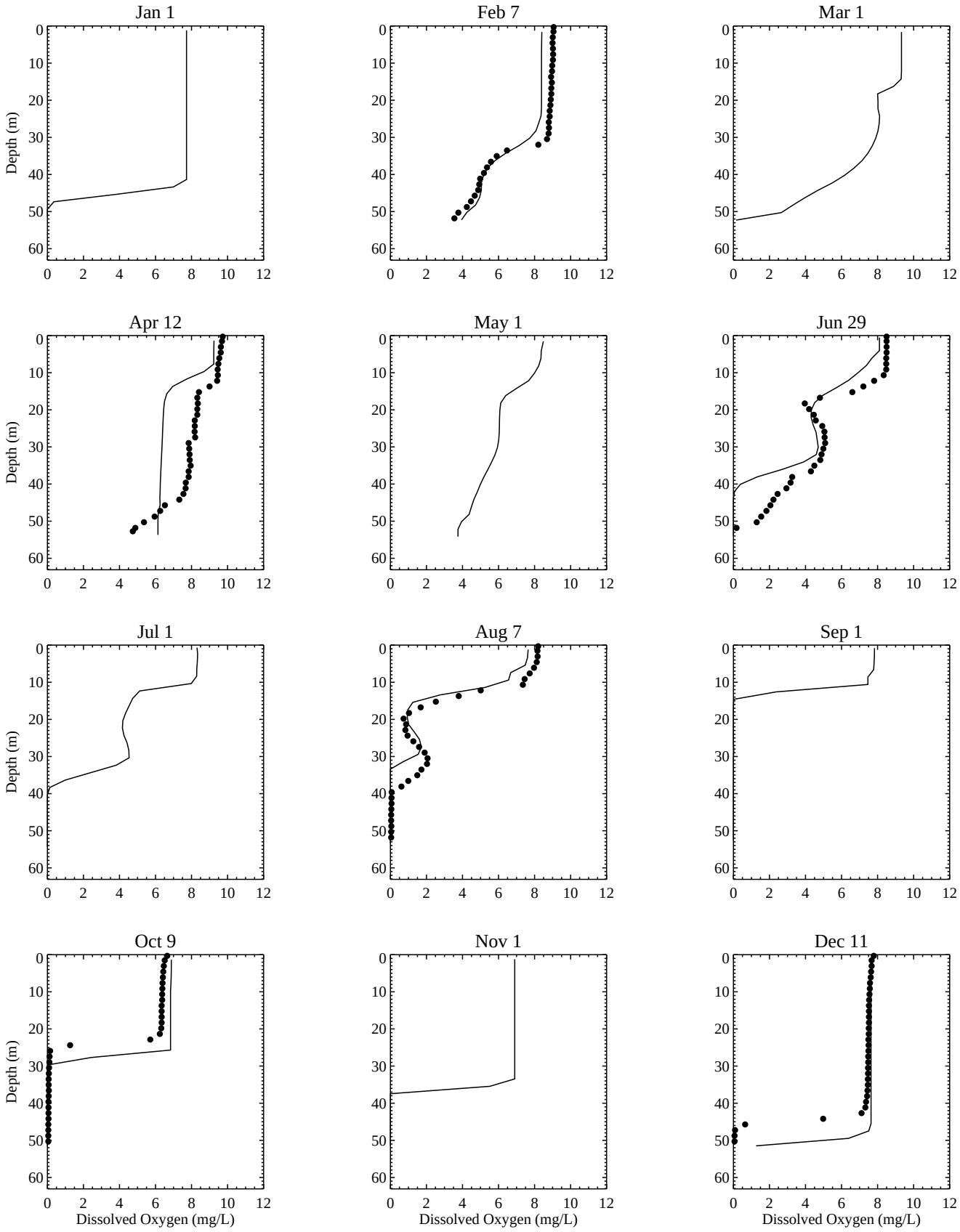

Figure J-16. Vertical profiles of model versus data at Mansfield Dam (Segment 93) - Dissolved Oxygen - 1995.

Profiles shown for dates with available data else model results for first day of month shown.

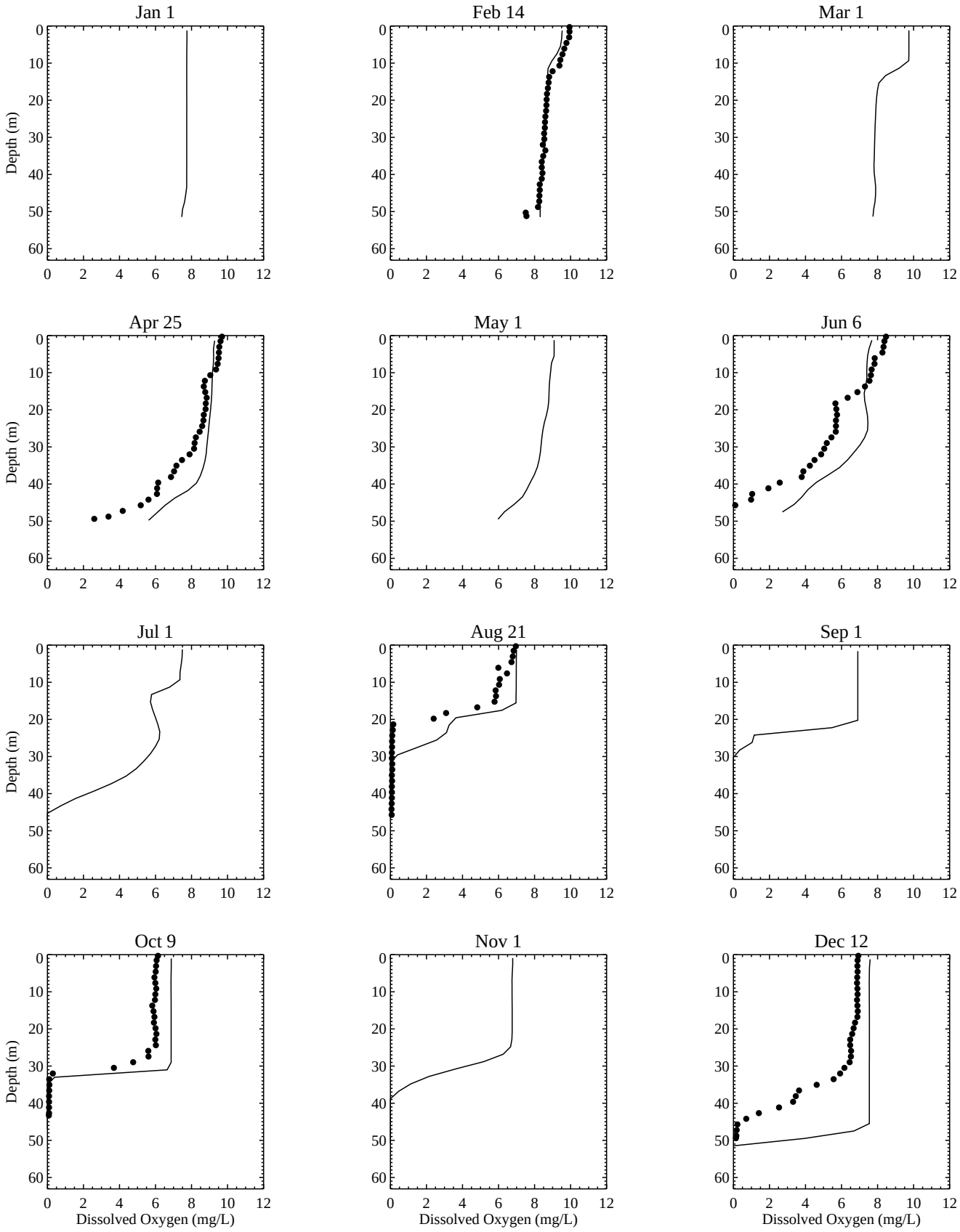

Figure J-16. Vertical profiles of model versus data at Mansfield Dam (Segment 93) - Dissolved Oxygen - 1996.

Profiles shown for dates with available data else model results for first day of month shown.

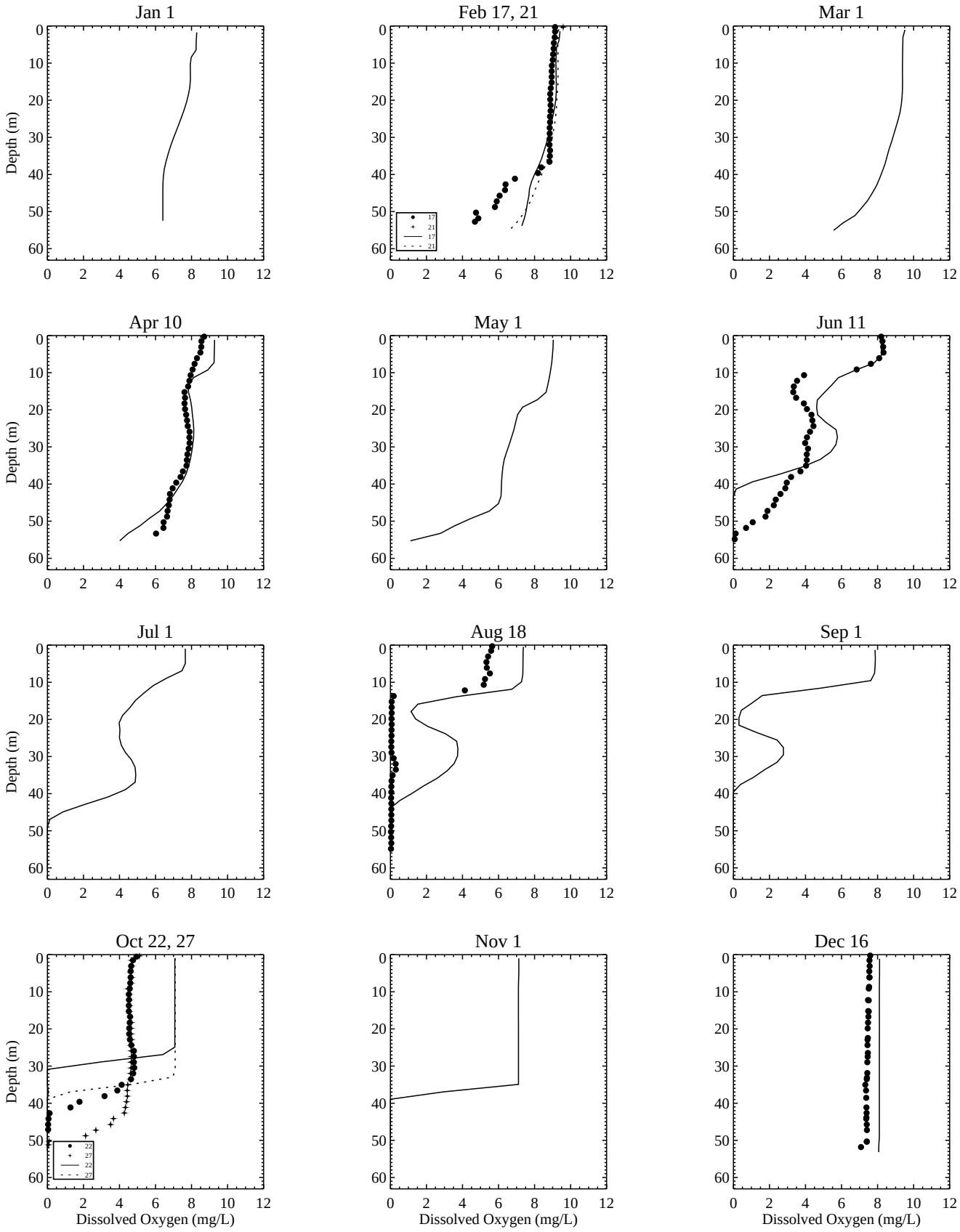

Figure J-16. Vertical profiles of model versus data at Mansfield Dam (Segment 93) - Dissolved Oxygen - 1997.

Profiles shown for dates with available data else model results for first day of month shown.

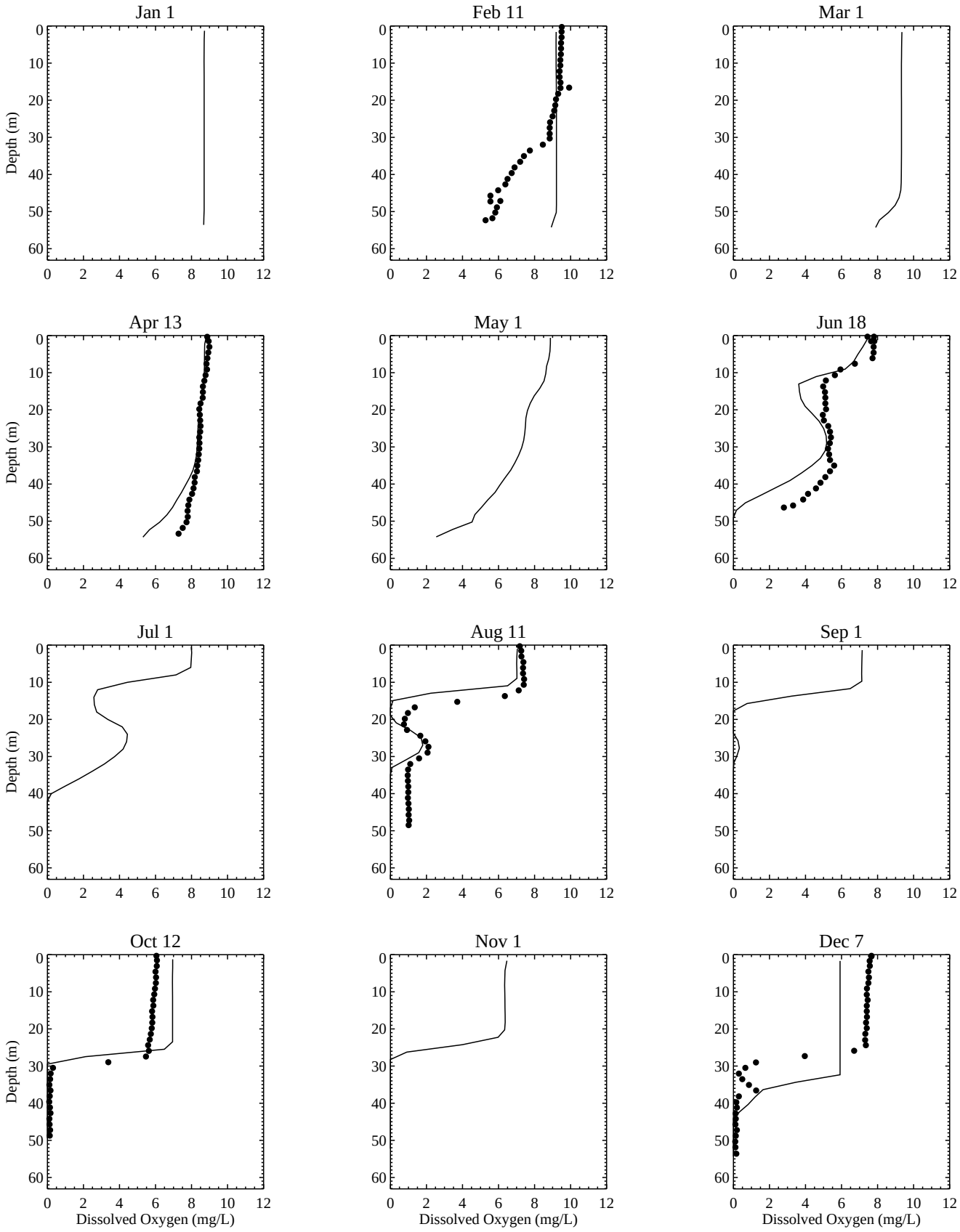

Figure J-16. Vertical profiles of model versus data at Mansfield Dam (Segment 93) - Dissolved Oxygen - 1998.

Profiles shown for dates with available data else model results for first day of month shown.

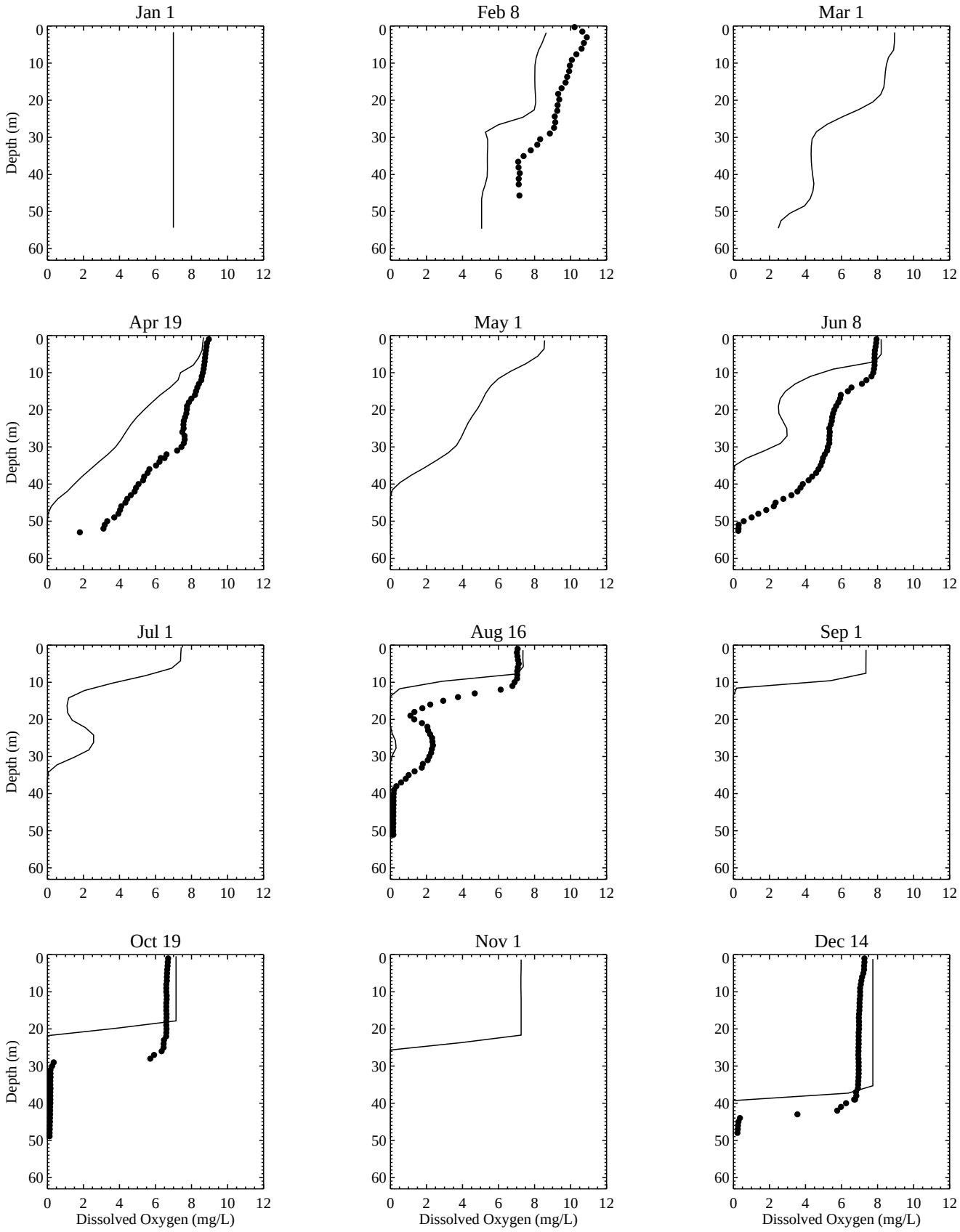

Figure J-16. Vertical profiles of model versus data at Mansfield Dam (Segment 93) - Dissolved Oxygen - 1999.

Profiles shown for dates with available data else model results for first day of month shown.

Model Data

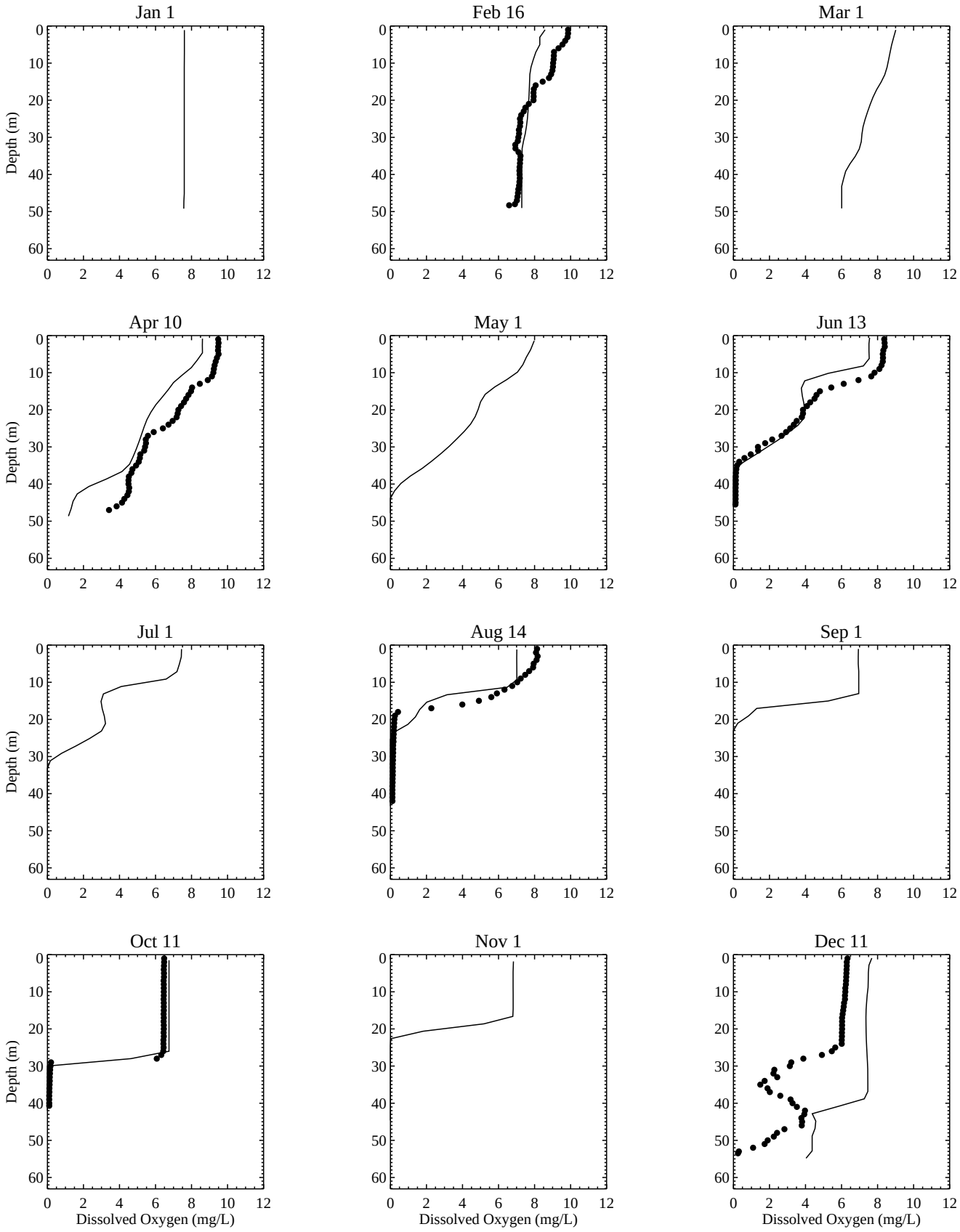

Figure J-16. Vertical profiles of model versus data at Mansfield Dam (Segment 93) - Dissolved Oxygen - 2000.

Profiles shown for dates with available data else model results for first day of month shown.

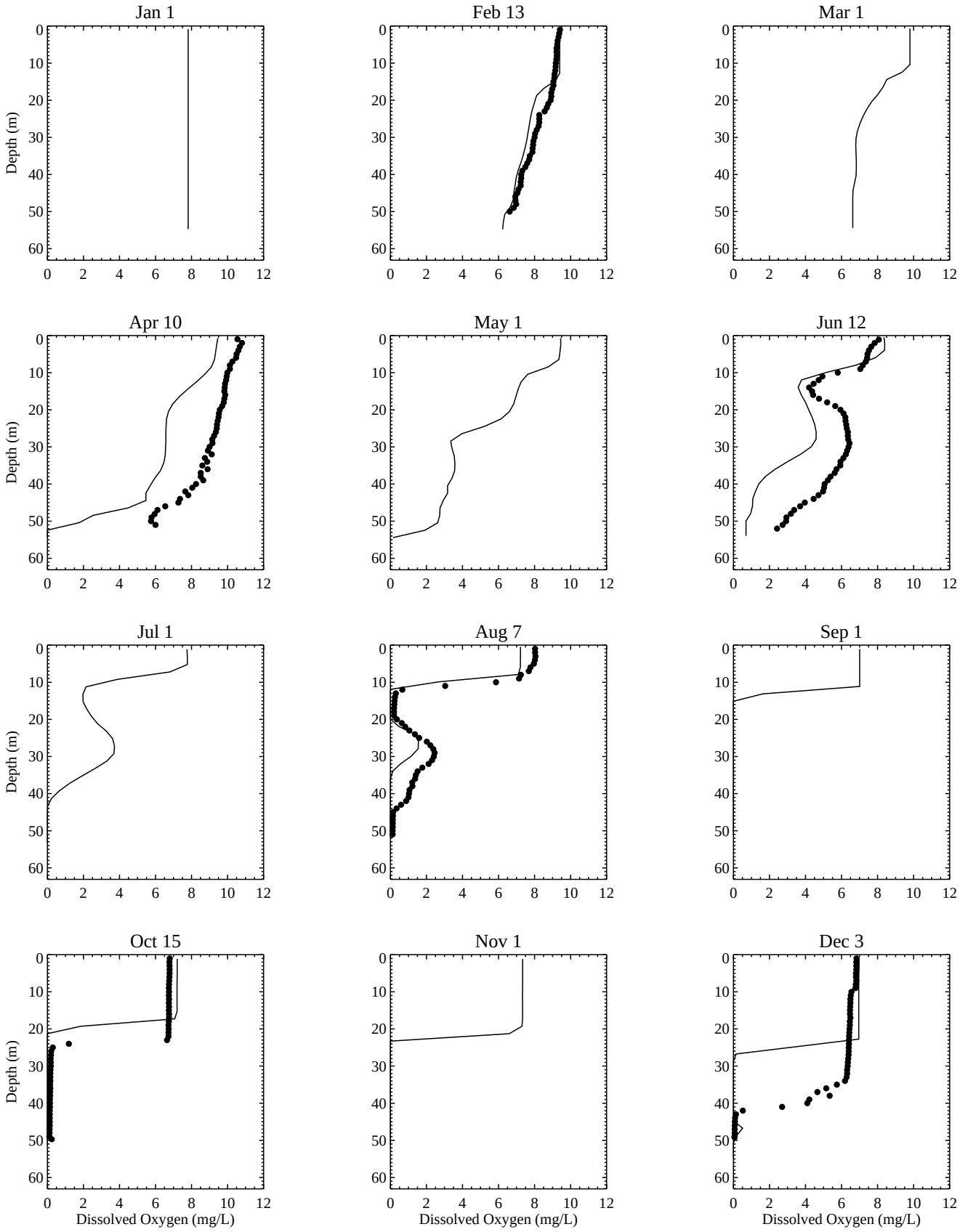

Figure J-16. Vertical profiles of model versus data at Mansfield Dam (Segment 93) - Dissolved Oxygen - 2001.

Profiles shown for dates with available data else model results for first day of month shown.

Model Data

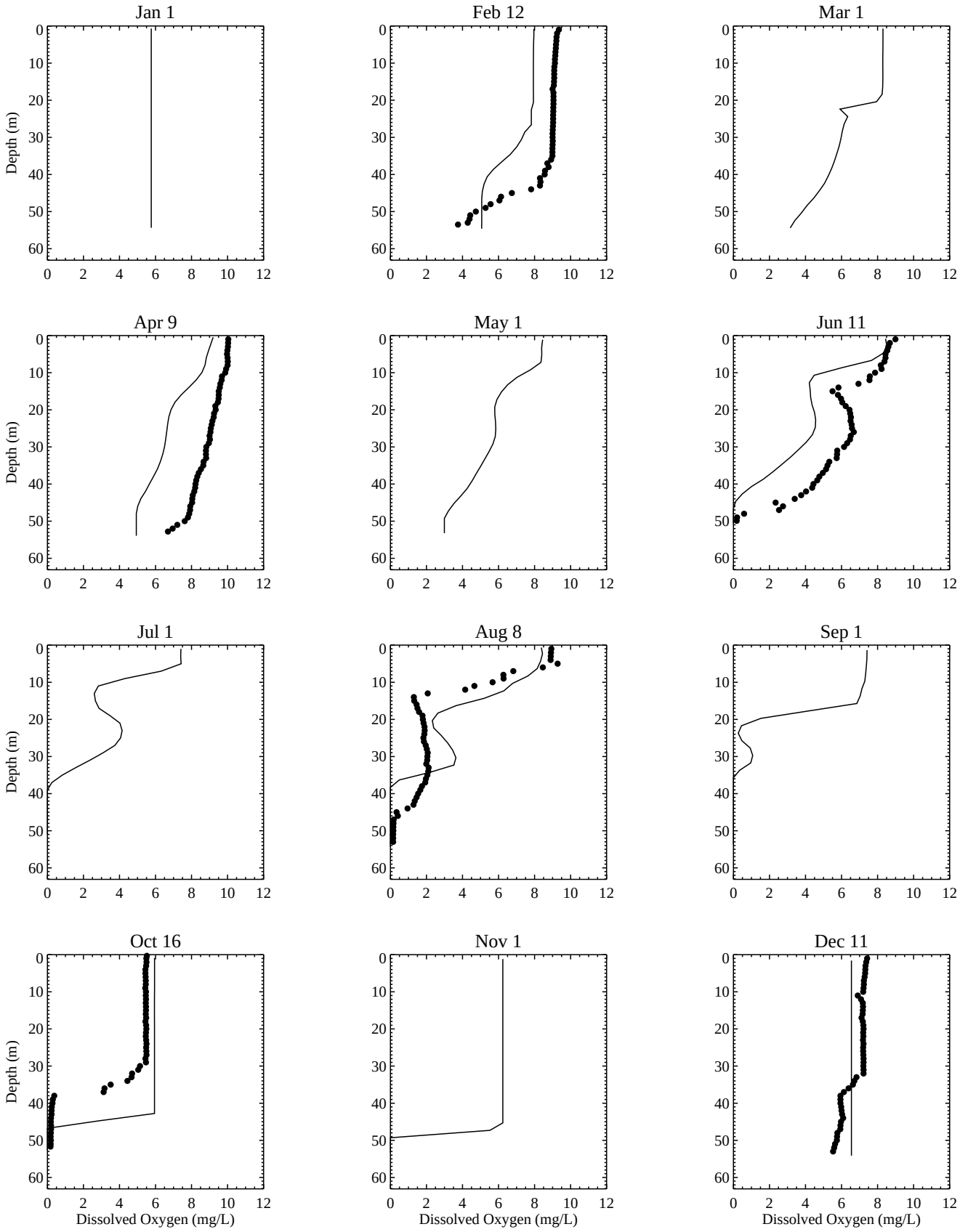

Figure J-16. Vertical profiles of model versus data at Mansfield Dam (Segment 93) - Dissolved Oxygen - 2002.

Profiles shown for dates with available data else model results for first day of month shown.

Model Data

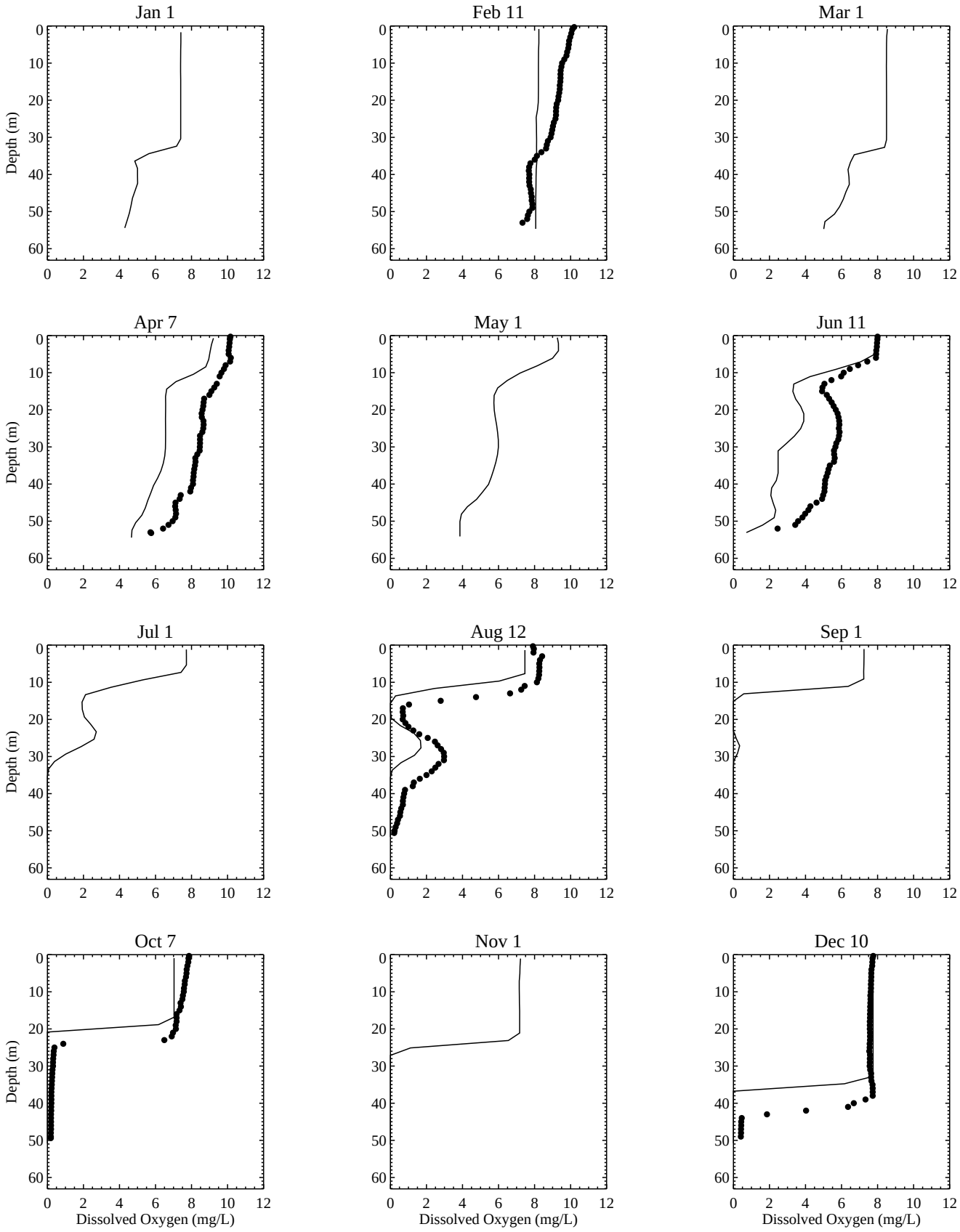

Figure J-16. Vertical profiles of model versus data at Mansfield Dam (Segment 93) - Dissolved Oxygen - 2003.

Profiles shown for dates with available data else model results for first day of month shown.

Model Data

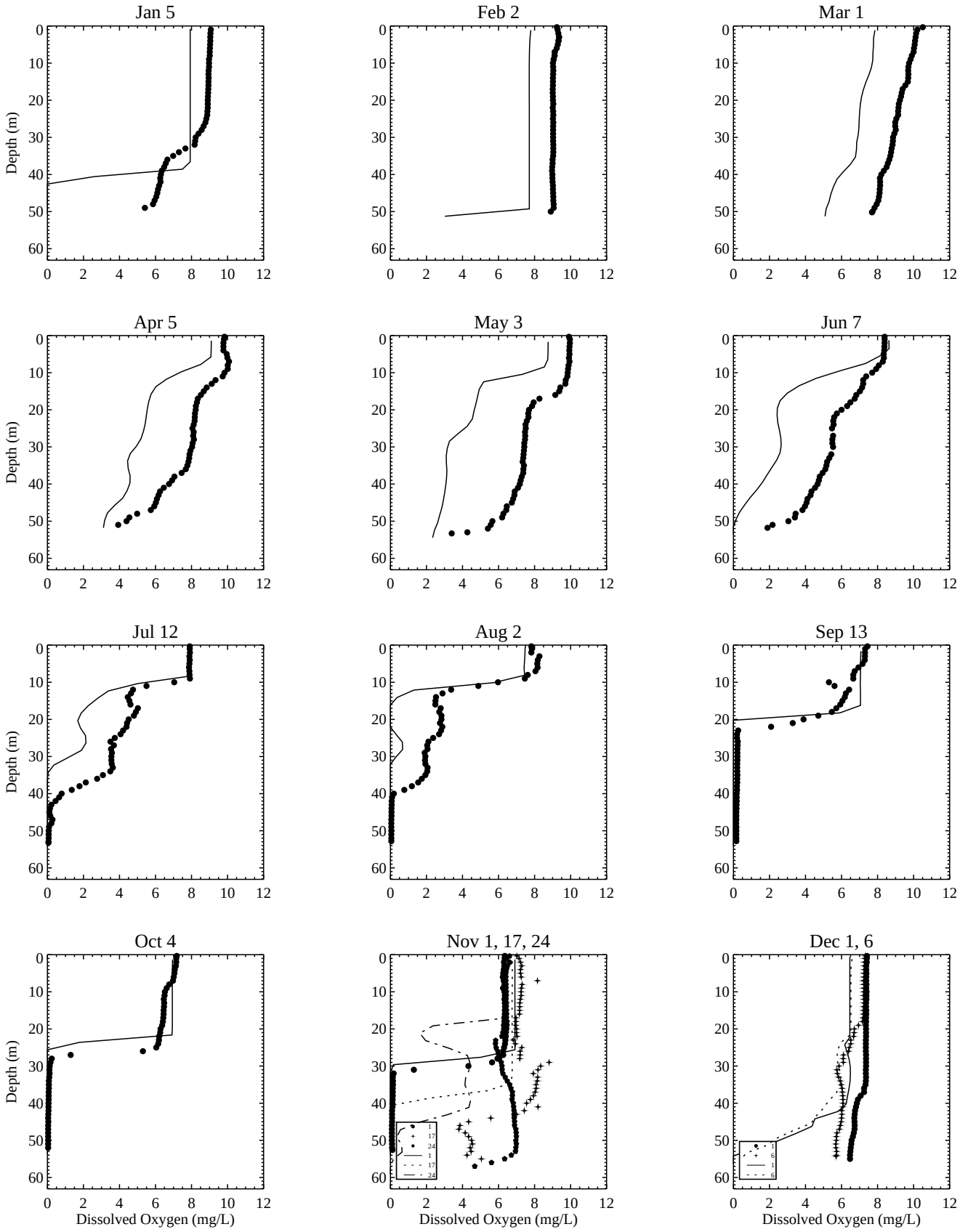

Figure J-16. Vertical profiles of model versus data at Mansfield Dam (Segment 93) - Dissolved Oxygen - 2004.

Profiles shown for dates with available data else model results for first day of month shown.

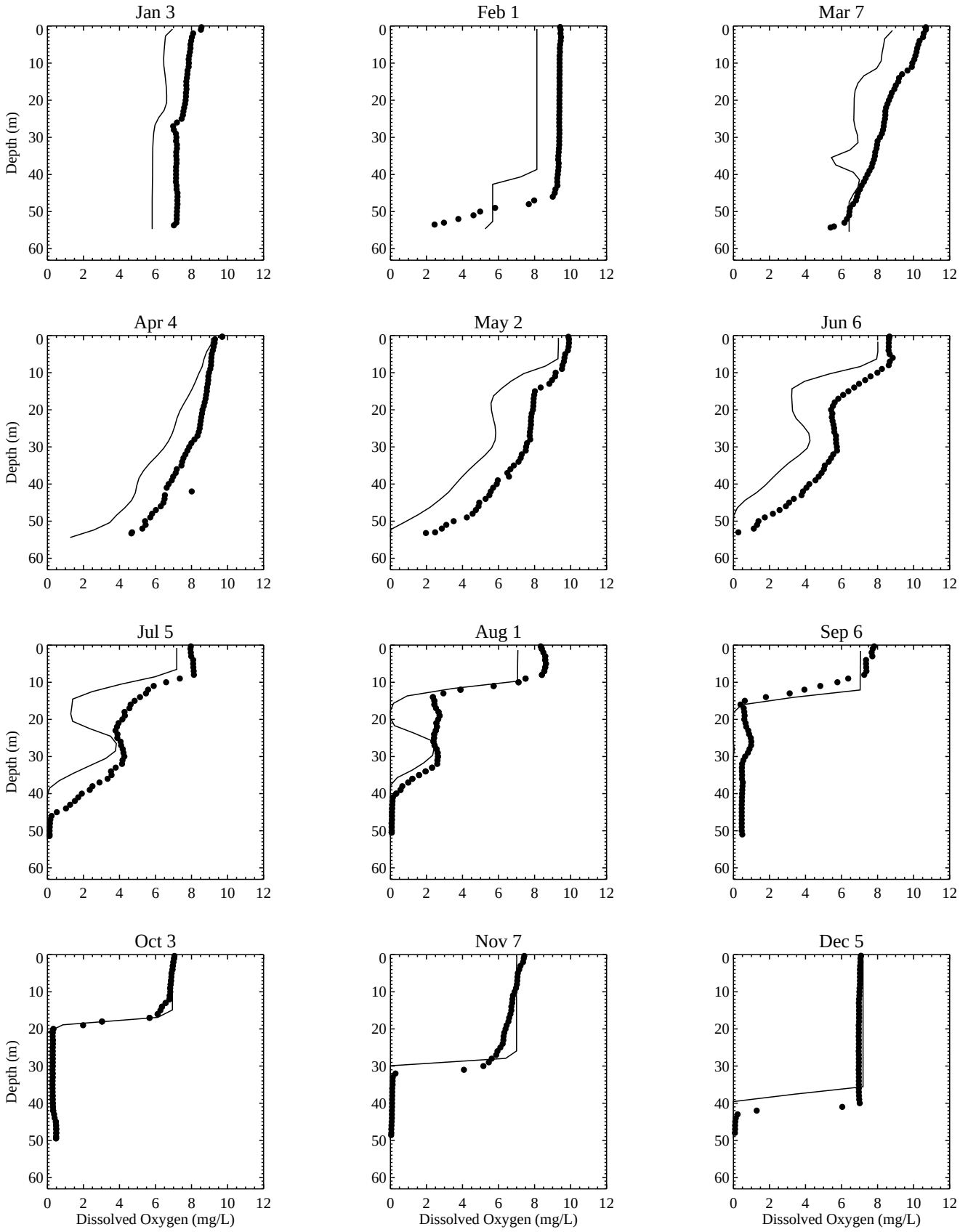

Figure J-16. Vertical profiles of model versus data at Mansfield Dam (Segment 93) - Dissolved Oxygen - 2005.

Profiles shown for dates with available data else model results for first day of month shown.

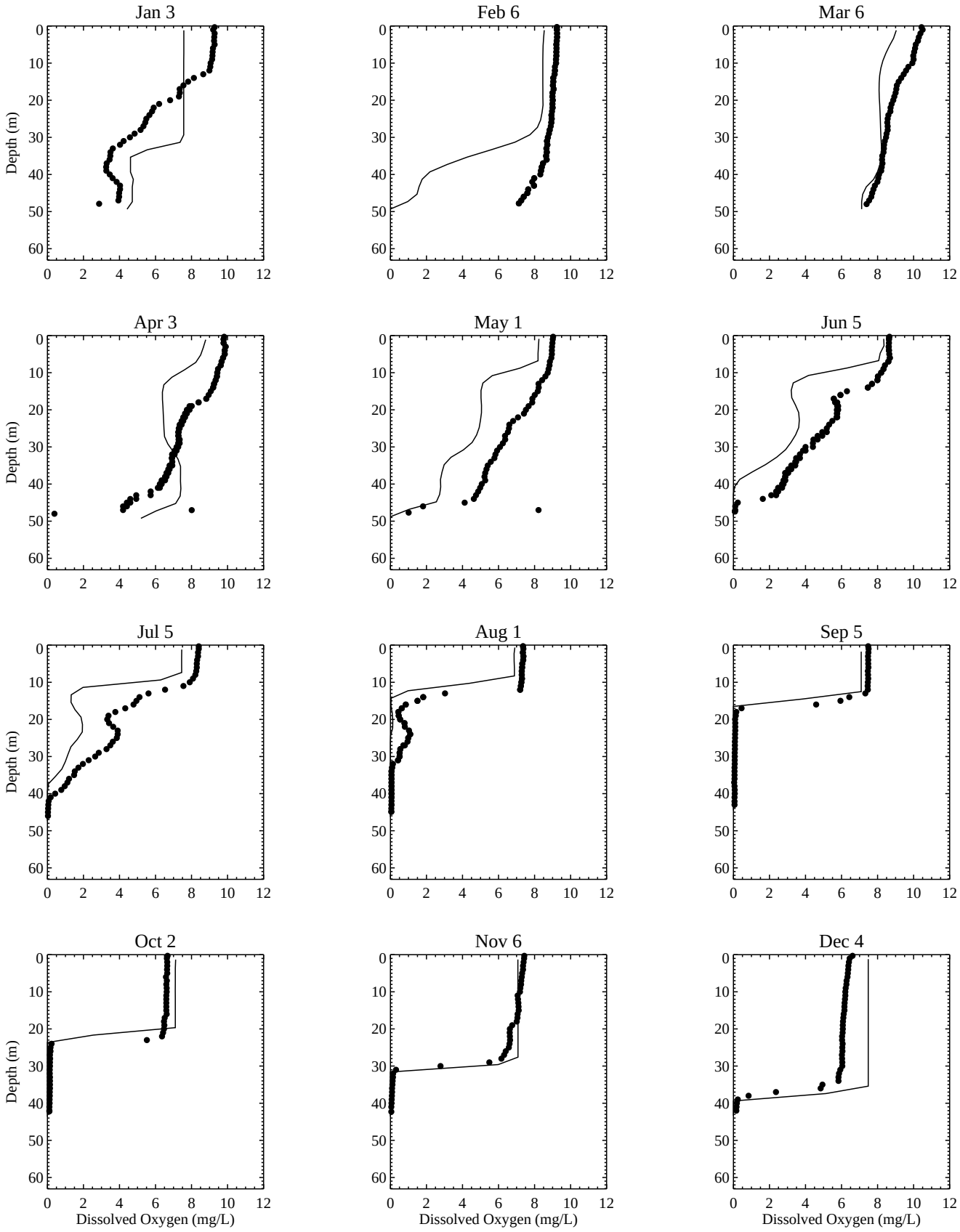

Figure J-16. Vertical profiles of model versus data at Mansfield Dam (Segment 93) - Dissolved Oxygen - 2006.

Profiles shown for dates with available data else model results for first day of month shown.

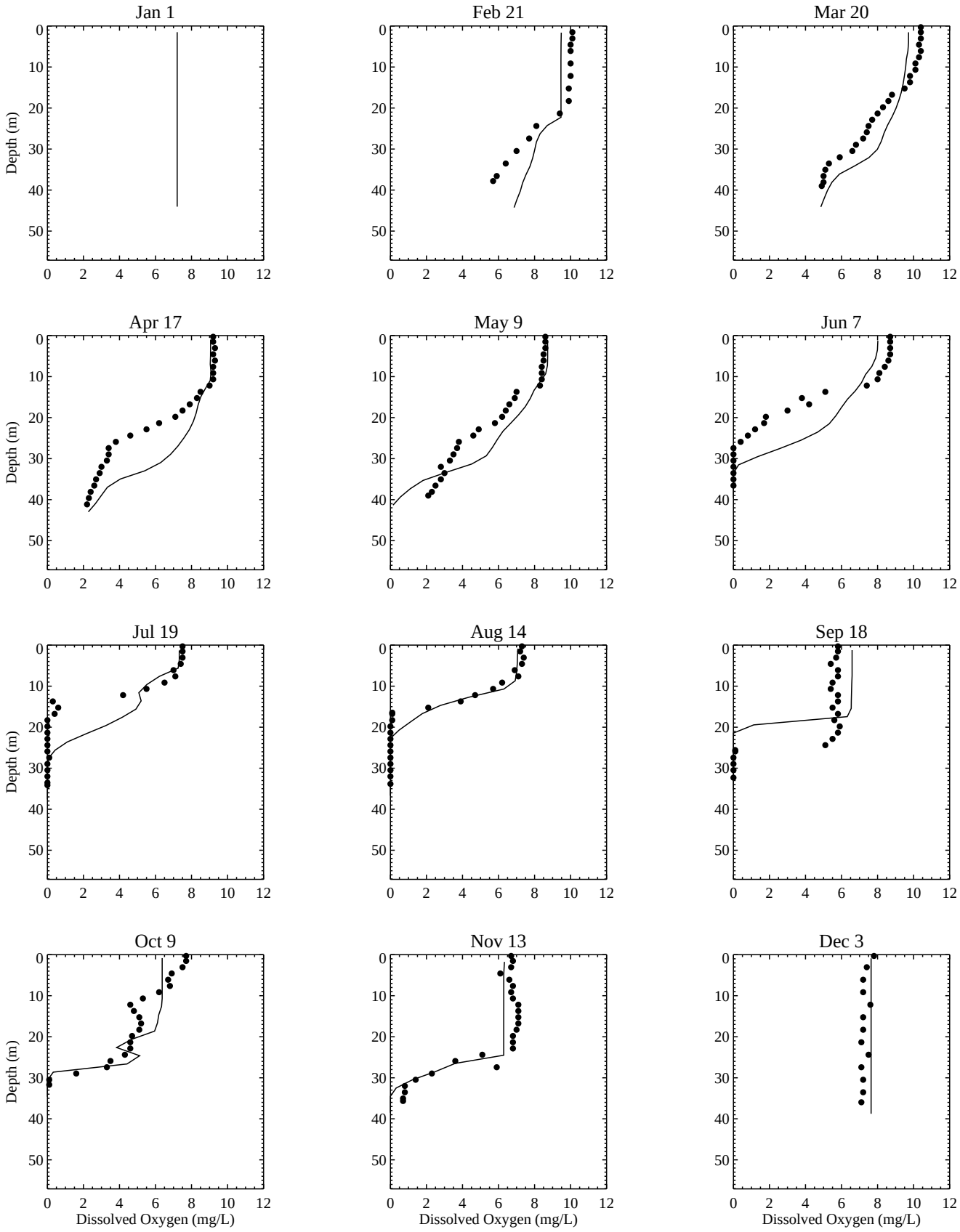

Figure J-17. Vertical profiles of model versus data at Arkansas Bend (Segment 78) - Dissolved Oxygen - 1984.

Profiles shown for dates with available data else model results for first day of month shown.

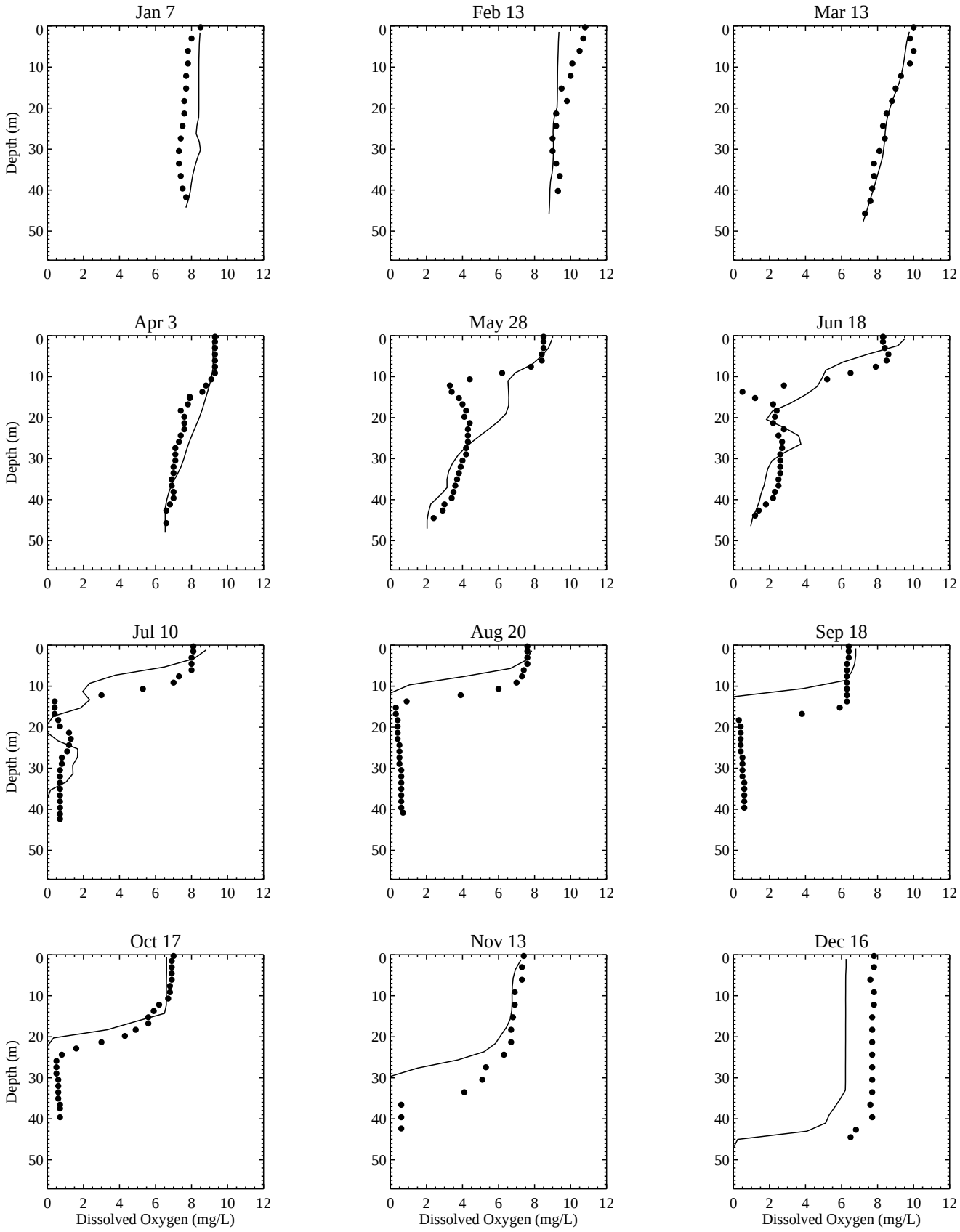

Figure J-17. Vertical profiles of model versus data at Arkansas Bend (Segment 78) - Dissolved Oxygen - 1985.

Profiles shown for dates with available data else model results for first day of month shown.

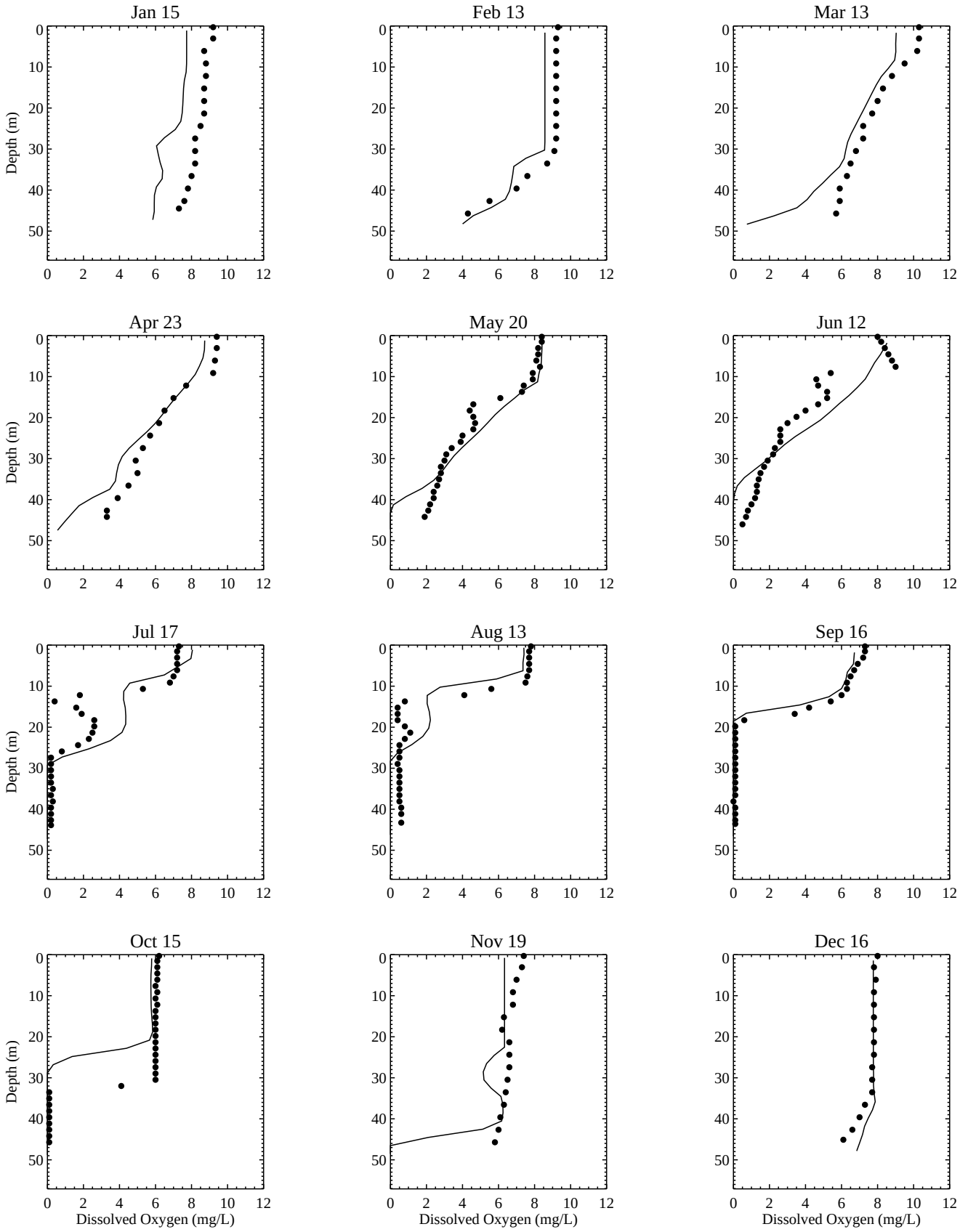

Figure J-17. Vertical profiles of model versus data at Arkansas Bend (Segment 78) - Dissolved Oxygen - 1986.

Profiles shown for dates with available data else model results for first day of month shown.

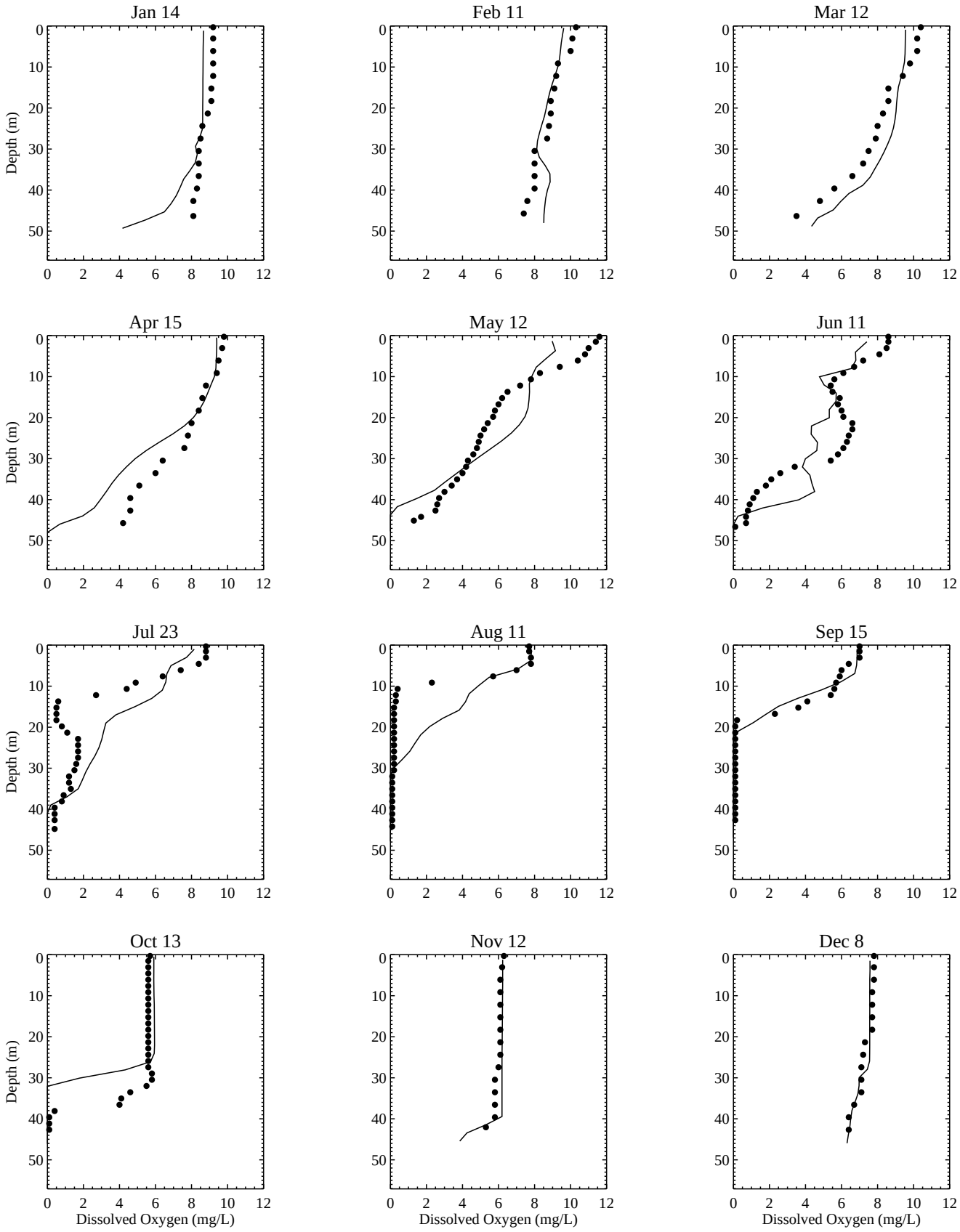

Figure J-17. Vertical profiles of model versus data at Arkansas Bend (Segment 78) - Dissolved Oxygen - 1987.

Profiles shown for dates with available data else model results for first day of month shown.

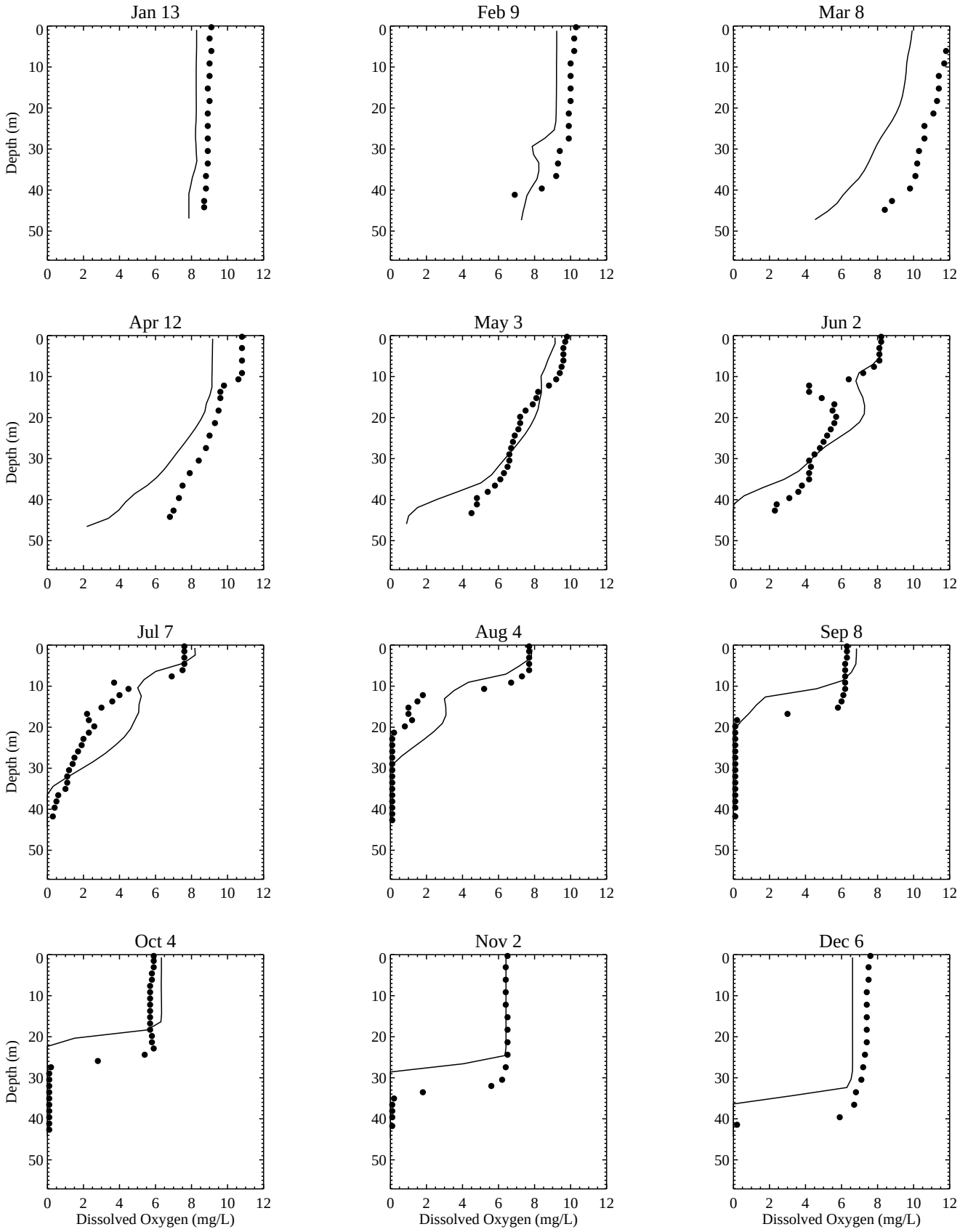

Figure J-17. Vertical profiles of model versus data at Arkansas Bend (Segment 78) - Dissolved Oxygen - 1988.

Profiles shown for dates with available data else model results for first day of month shown.

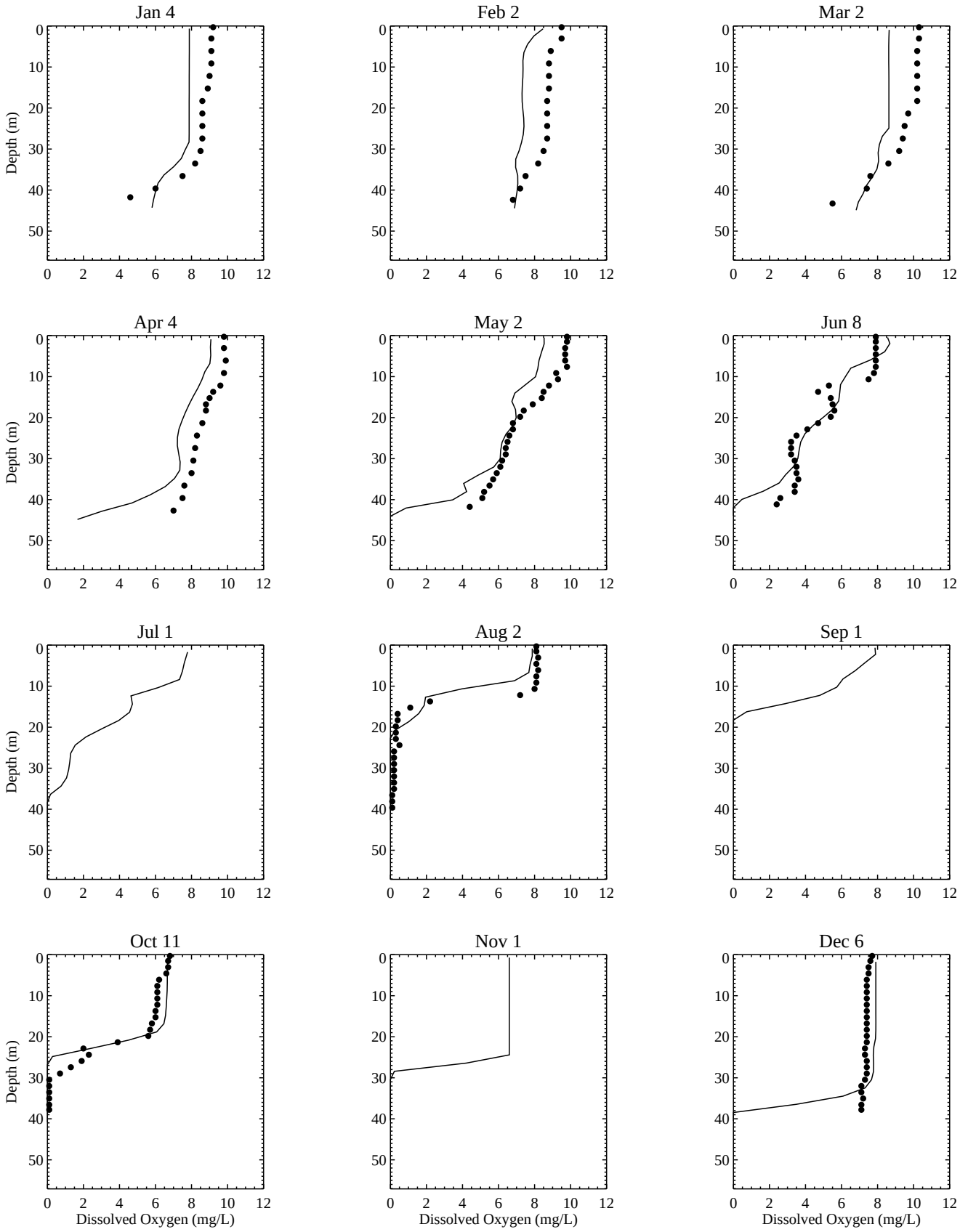

Figure J-17. Vertical profiles of model versus data at Arkansas Bend (Segment 78) - Dissolved Oxygen - 1989.

Profiles shown for dates with available data else model results for first day of month shown.

Model Data

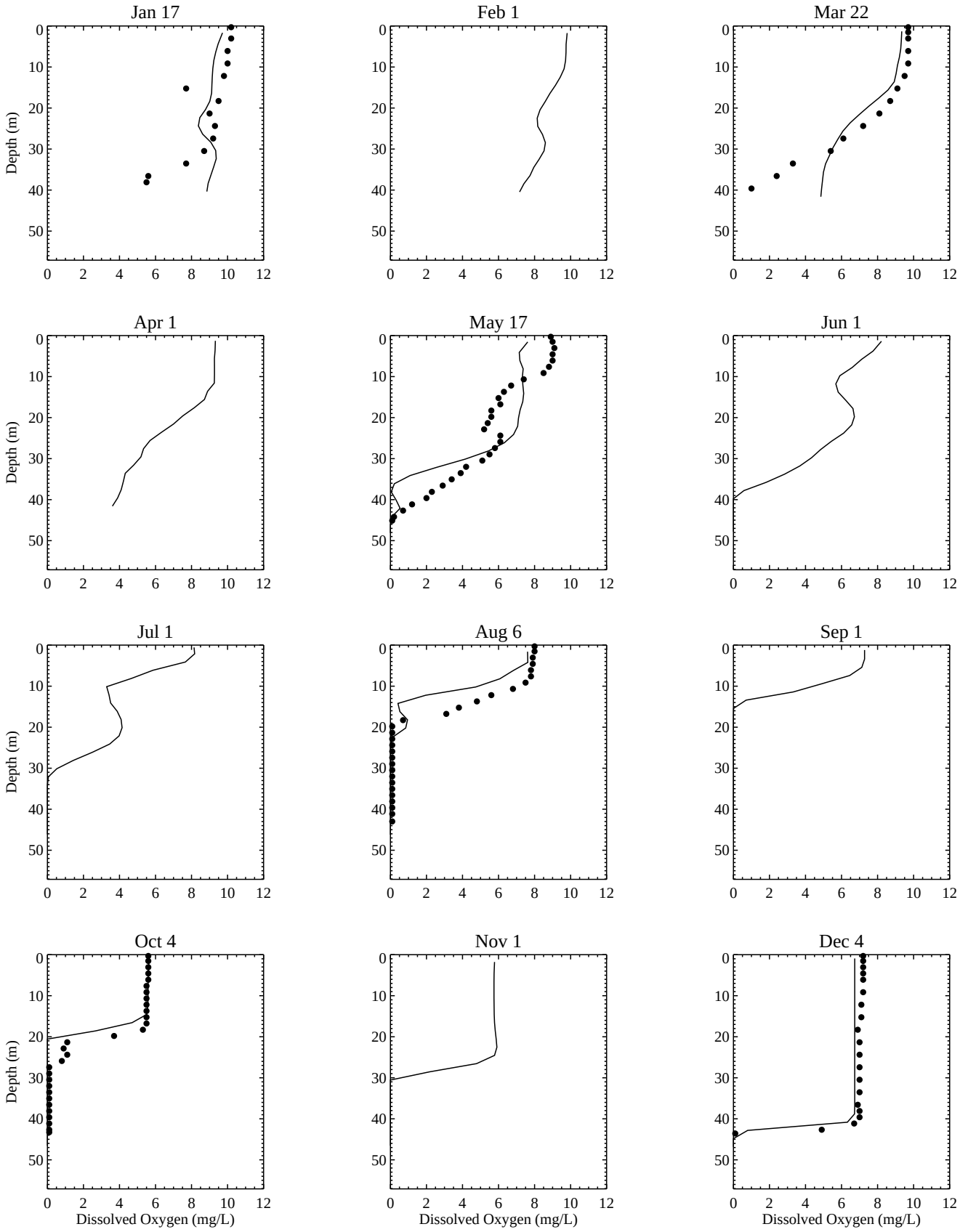

Figure J-17. Vertical profiles of model versus data at Arkansas Bend (Segment 78) - Dissolved Oxygen - 1990.

Profiles shown for dates with available data else model results for first day of month shown.

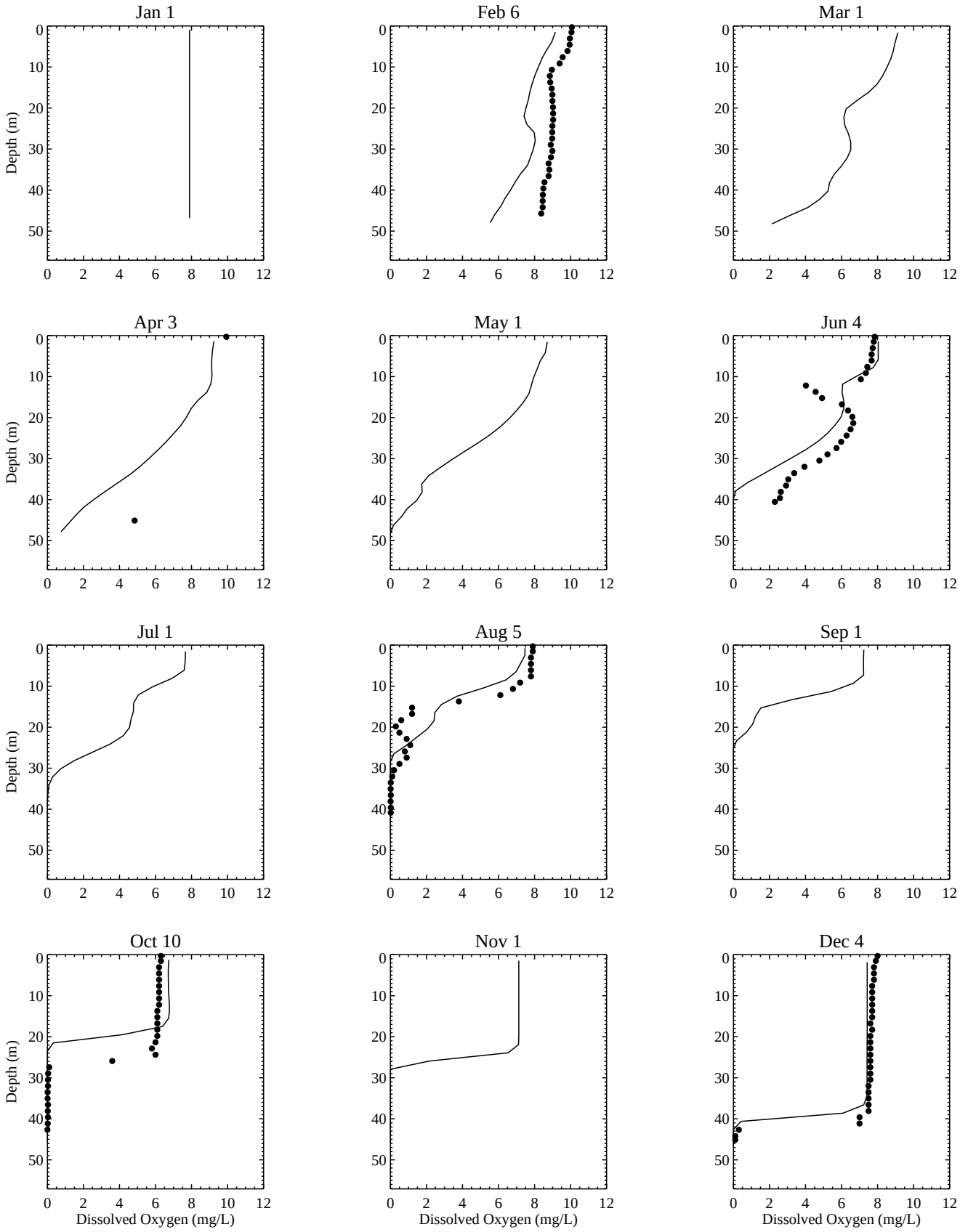

Figure J-17. Vertical profiles of model versus data at Arkansas Bend (Segment 78) - Dissolved Oxygen - 1991.

Profiles shown for dates with available data else model results for first day of month shown.

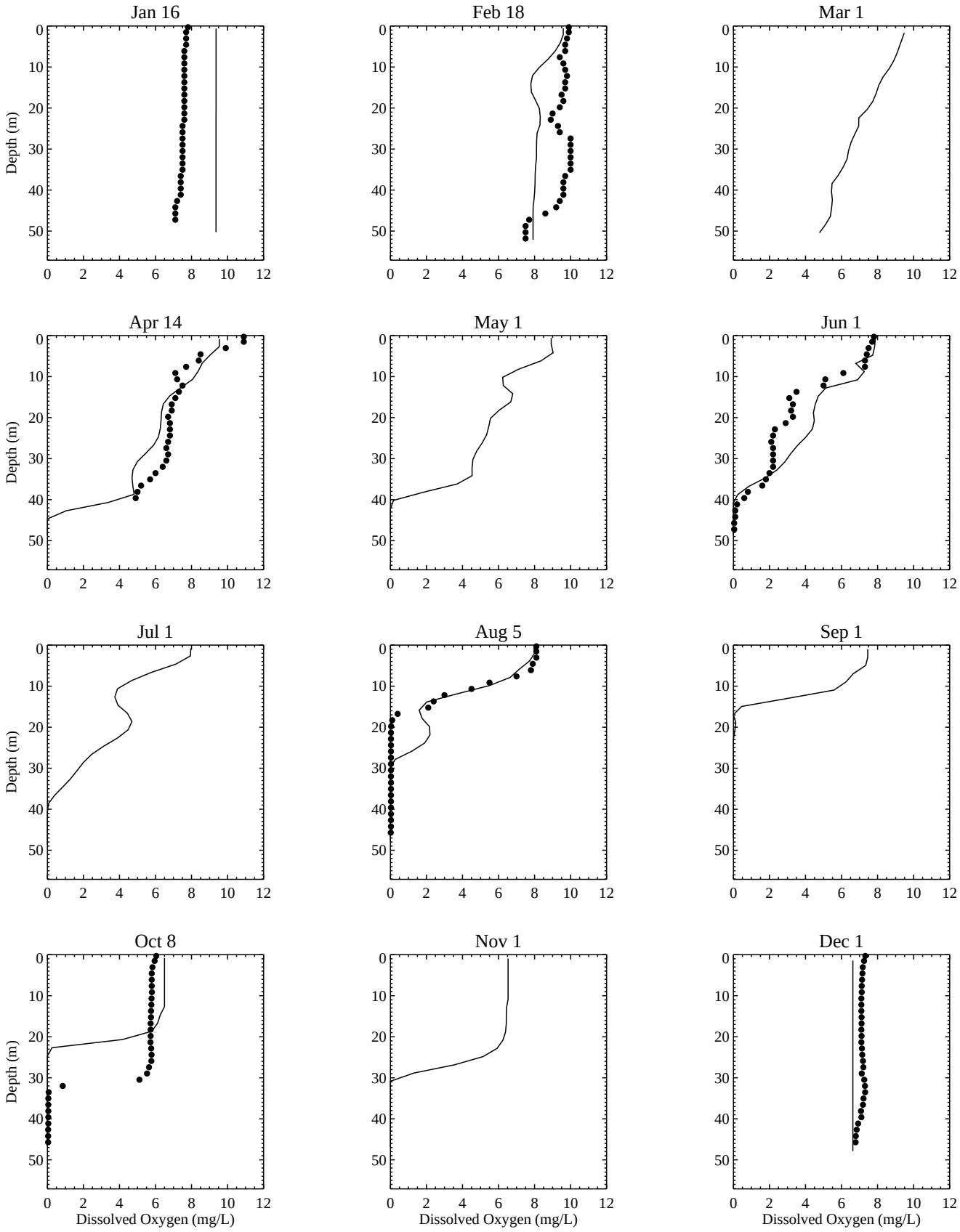

Figure J-17. Vertical profiles of model versus data at Arkansas Bend (Segment 78) - Dissolved Oxygen - 1992.

Profiles shown for dates with available data else model results for first day of month shown.

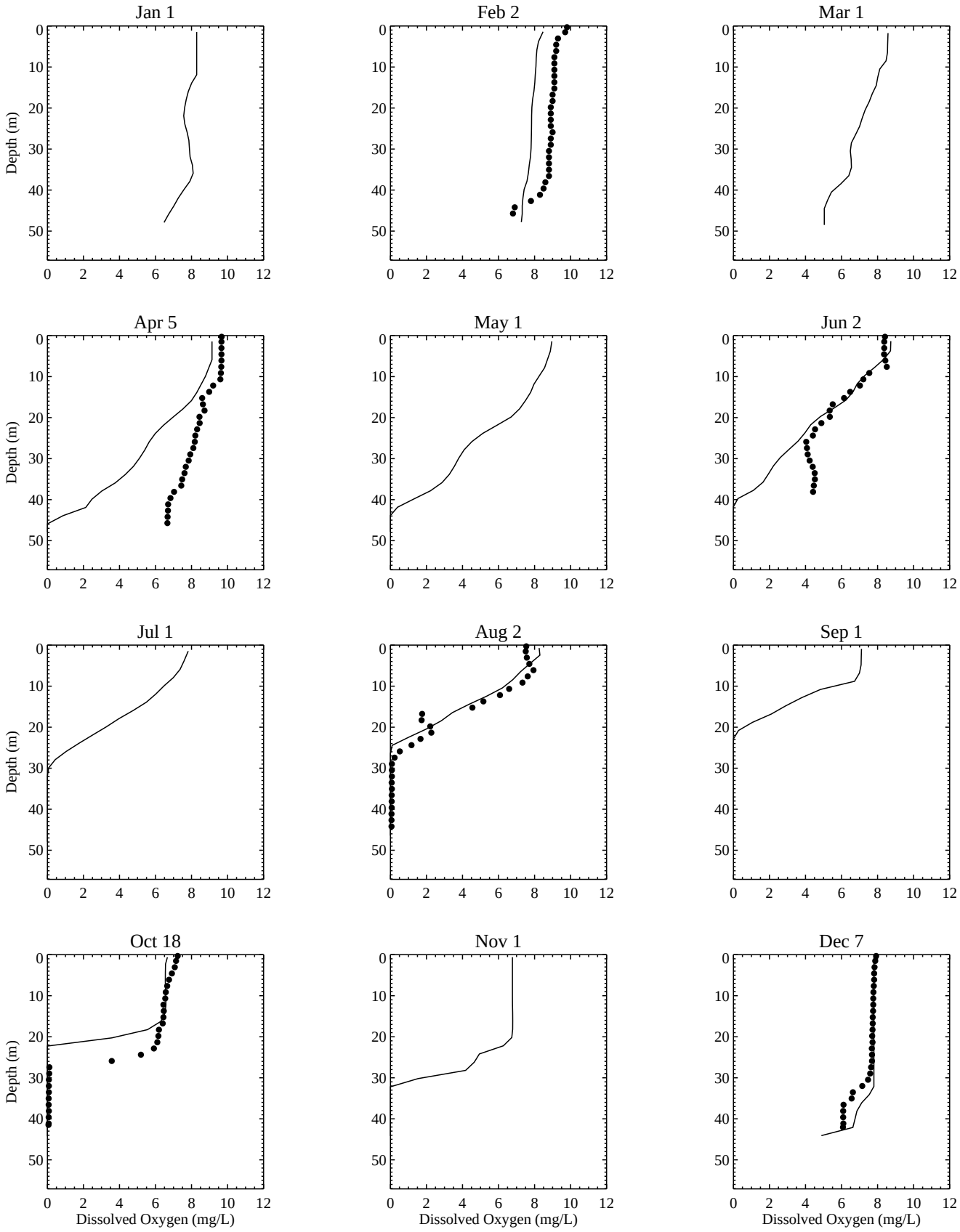

Figure J-17. Vertical profiles of model versus data at Arkansas Bend (Segment 78) - Dissolved Oxygen - 1993.

Profiles shown for dates with available data else model results for first day of month shown.

Model Data

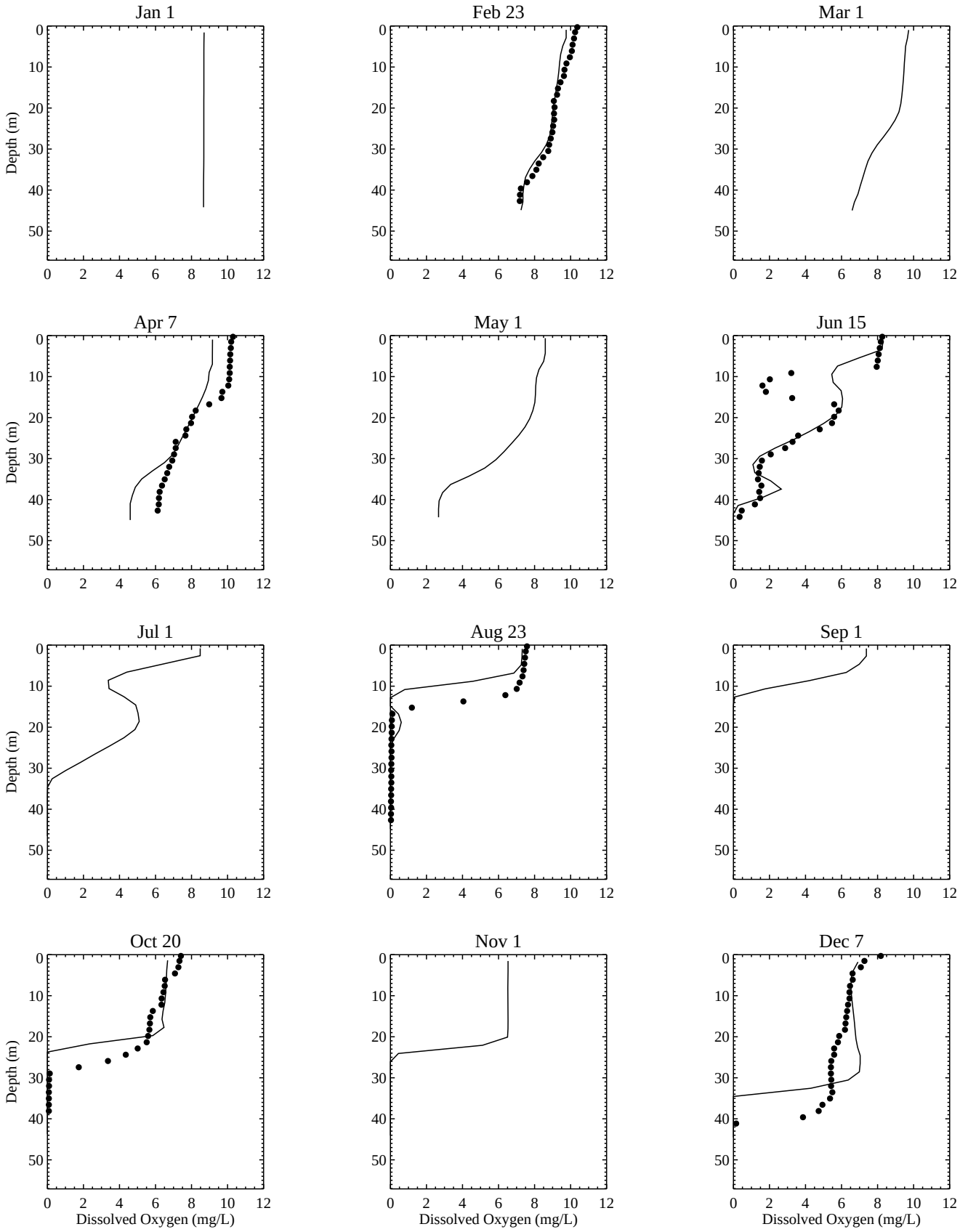

Figure J-17. Vertical profiles of model versus data at Arkansas Bend (Segment 78) - Dissolved Oxygen - 1994.

Profiles shown for dates with available data else model results for first day of month shown.

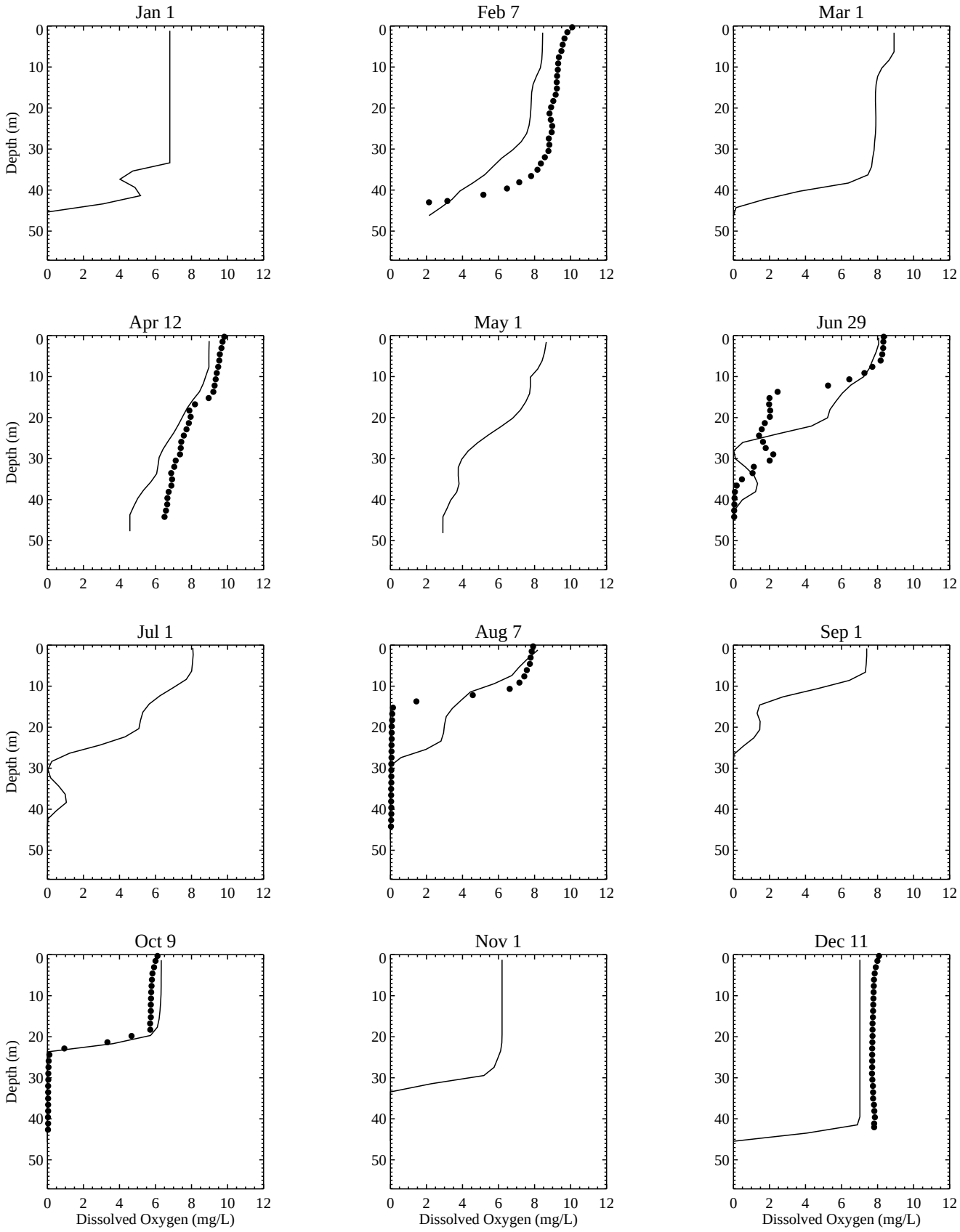

Figure J-17. Vertical profiles of model versus data at Arkansas Bend (Segment 78) - Dissolved Oxygen - 1995.

Profiles shown for dates with available data else model results for first day of month shown.

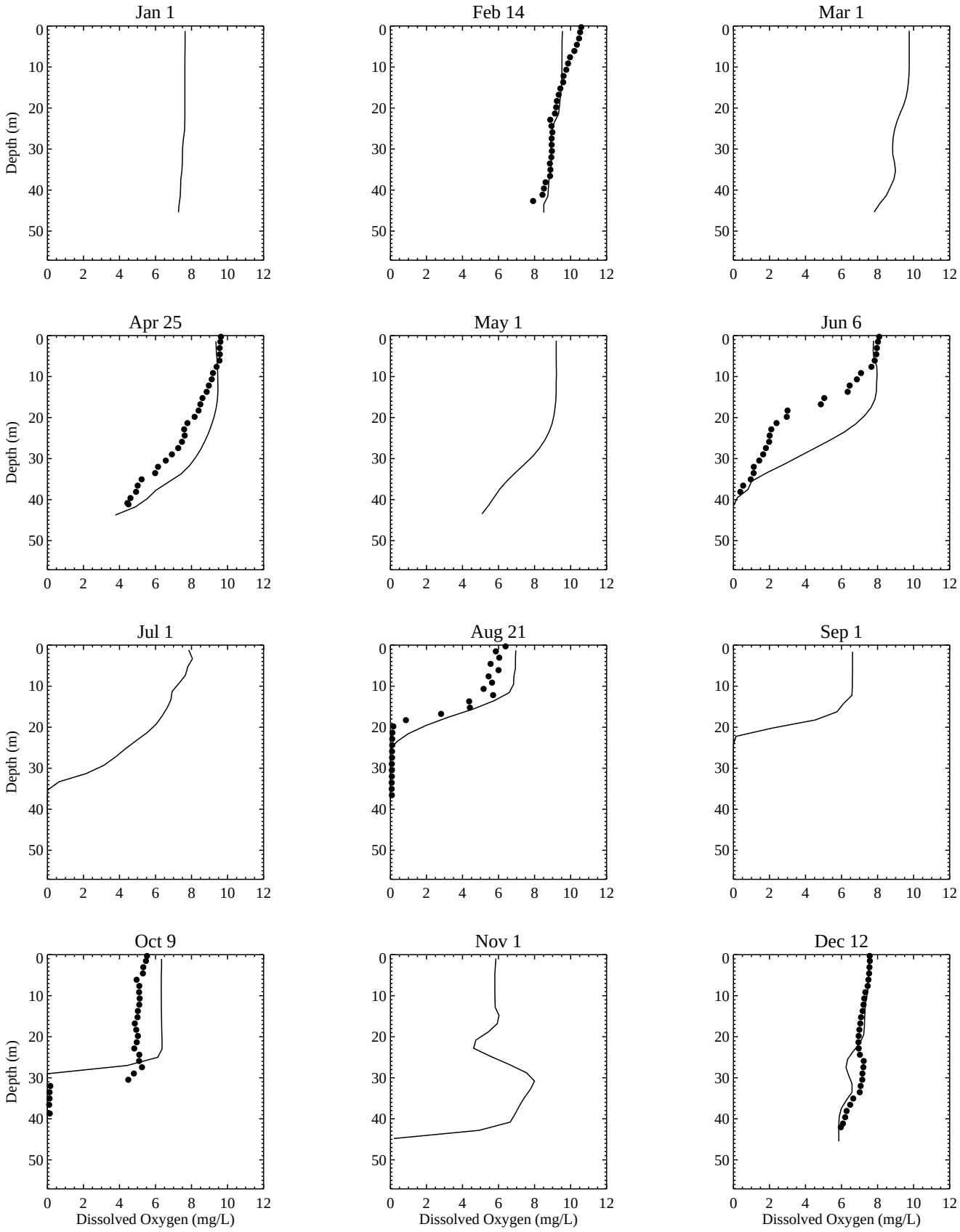

Figure J-17. Vertical profiles of model versus data at Arkansas Bend (Segment 78) - Dissolved Oxygen - 1996.

Profiles shown for dates with available data else model results for first day of month shown.

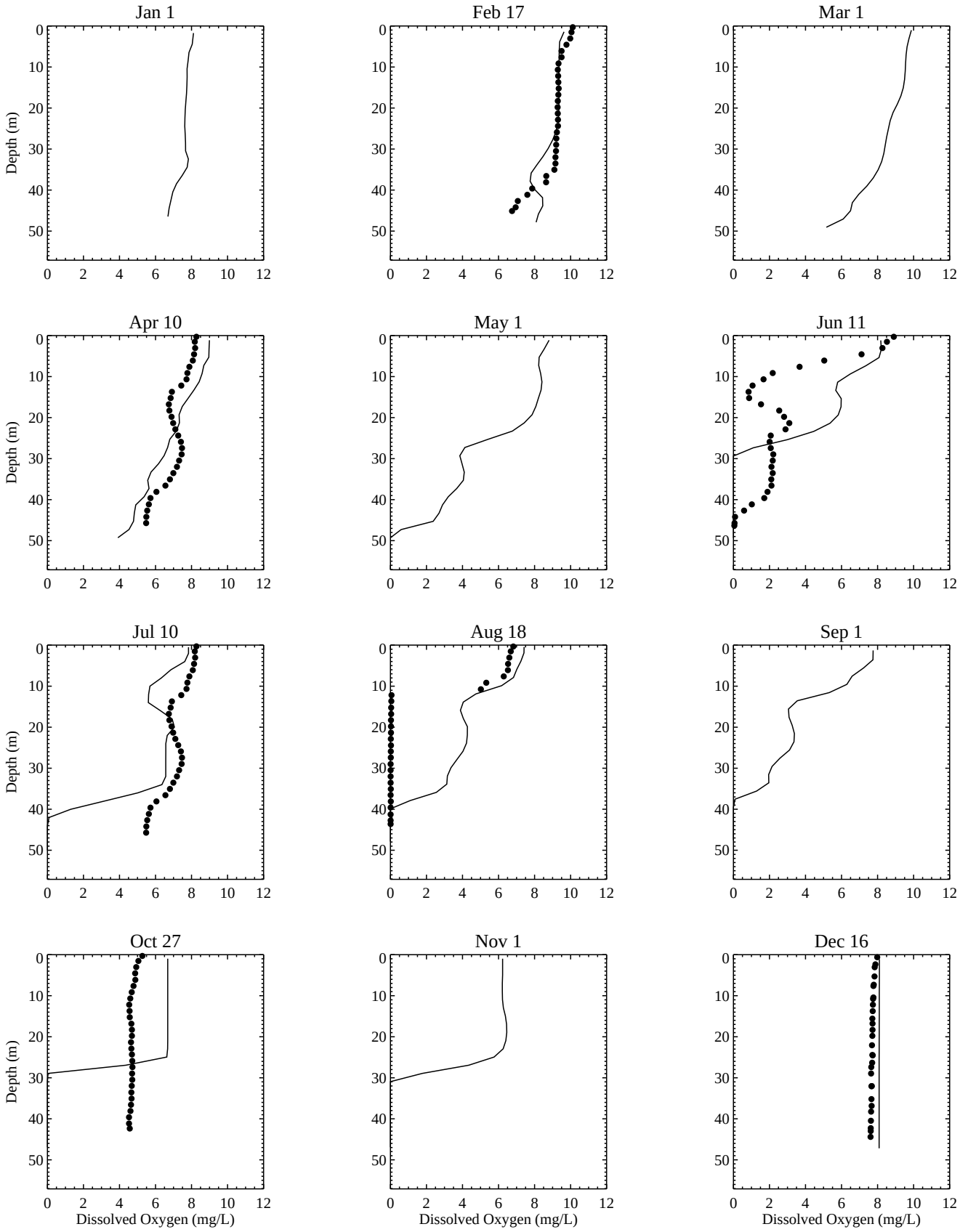

Figure J-17. Vertical profiles of model versus data at Arkansas Bend (Segment 78) - Dissolved Oxygen - 1997.

Profiles shown for dates with available data else model results for first day of month shown.

Model ● Data

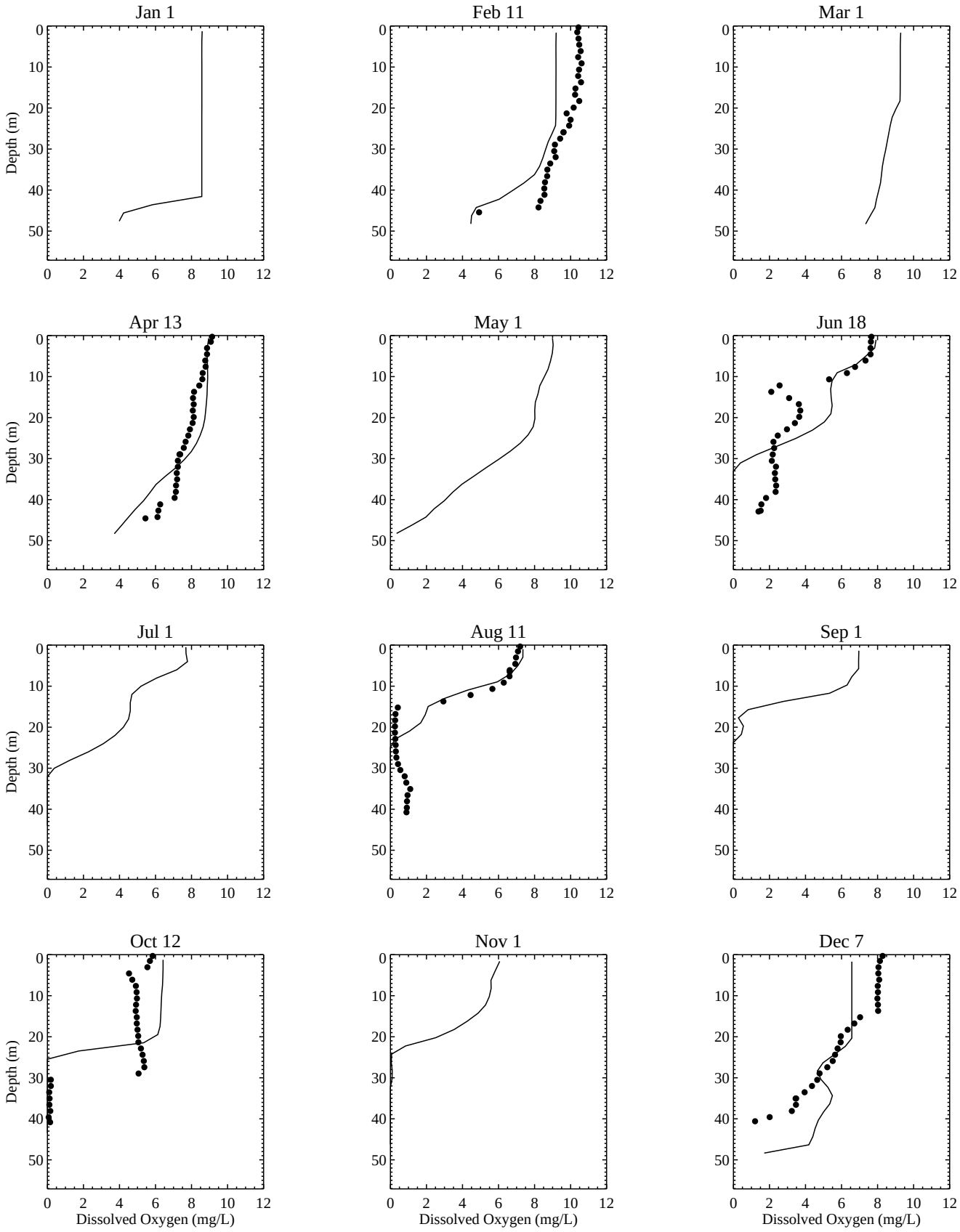

Figure J-17. Vertical profiles of model versus data at Arkansas Bend (Segment 78) - Dissolved Oxygen - 1998.

Profiles shown for dates with available data else model results for first day of month shown.

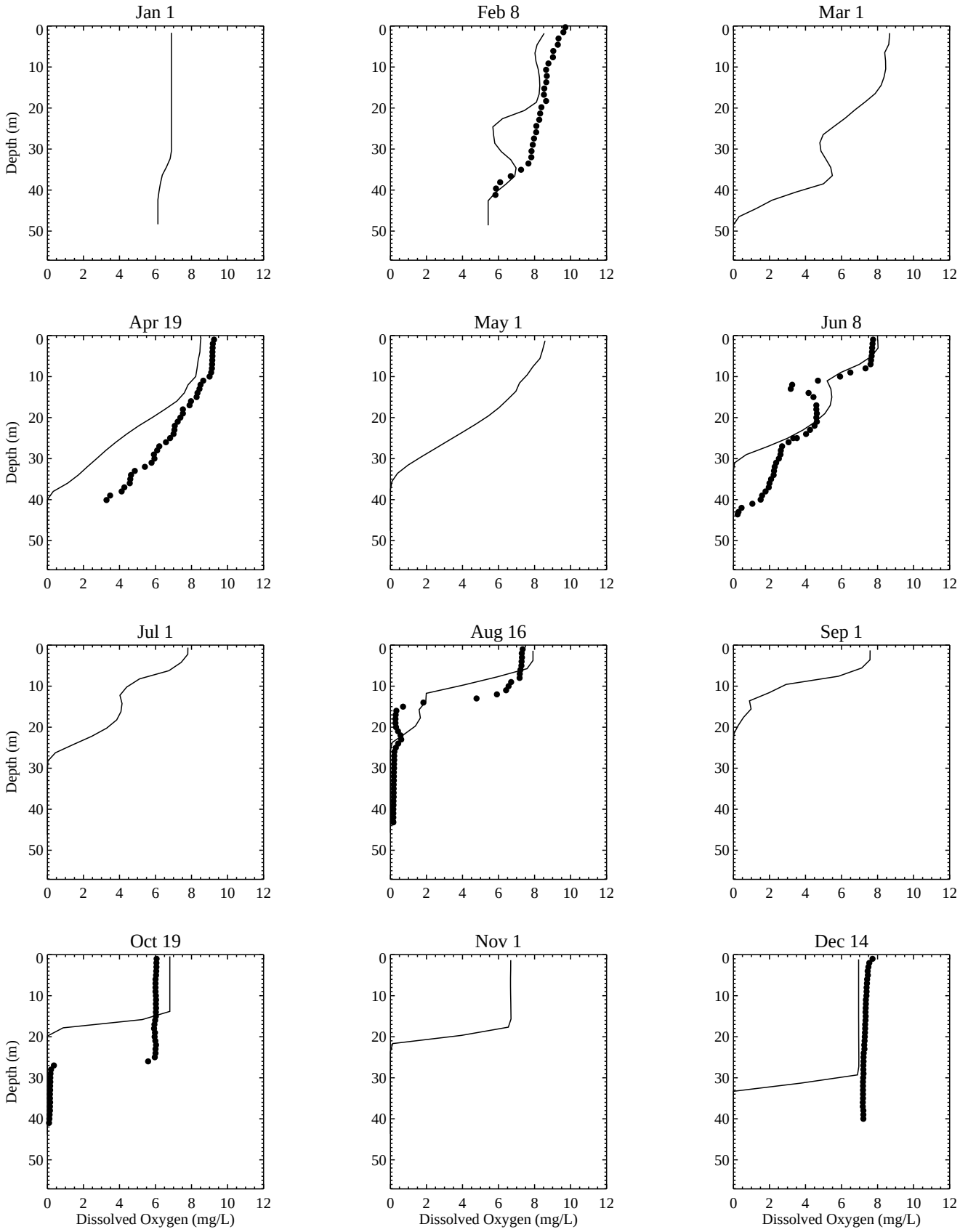

Figure J-17. Vertical profiles of model versus data at Arkansas Bend (Segment 78) - Dissolved Oxygen - 1999.

Profiles shown for dates with available data else model results for first day of month shown.

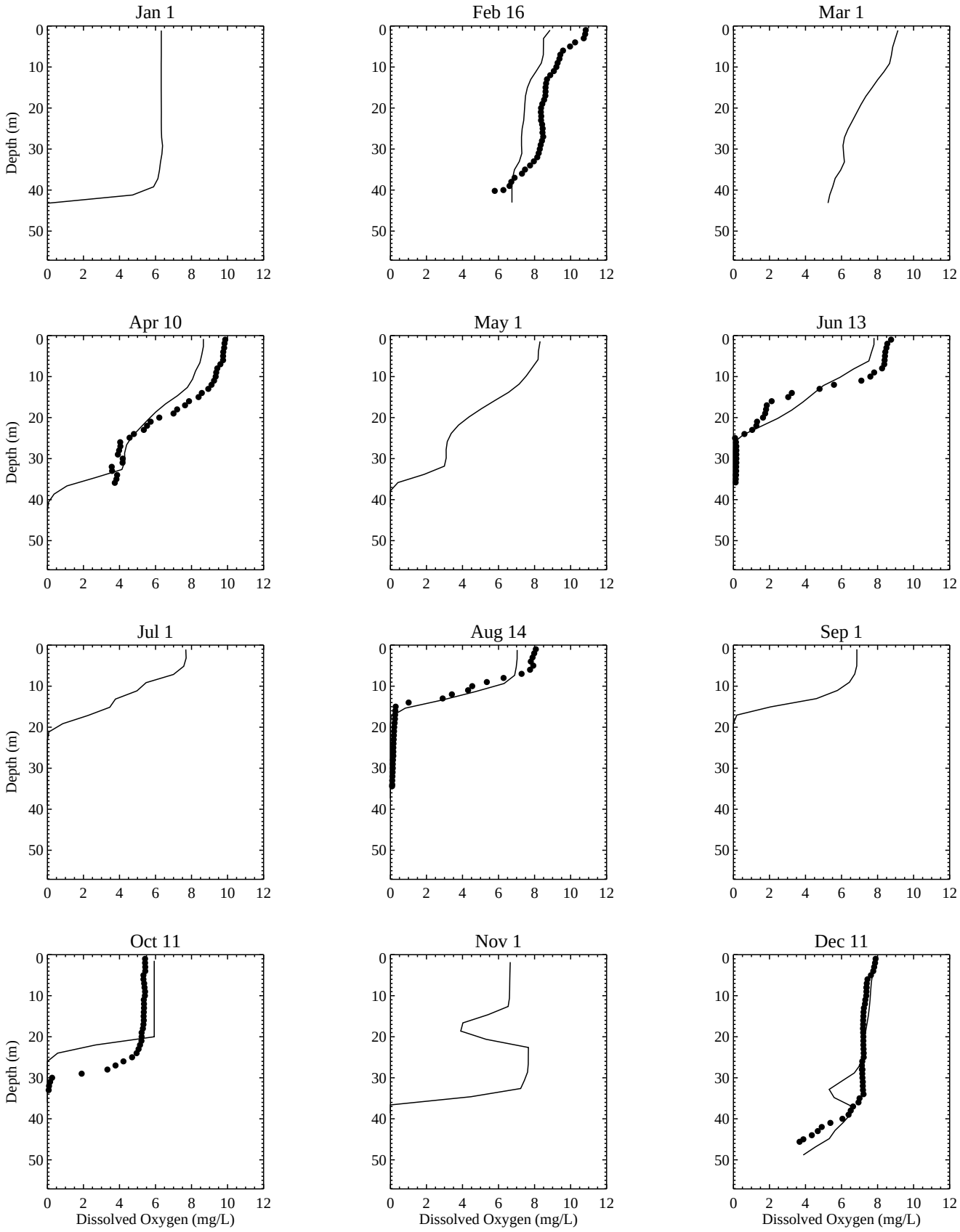

Figure J-17. Vertical profiles of model versus data at Arkansas Bend (Segment 78) - Dissolved Oxygen - 2000.

Profiles shown for dates with available data else model results for first day of month shown.

Model Data

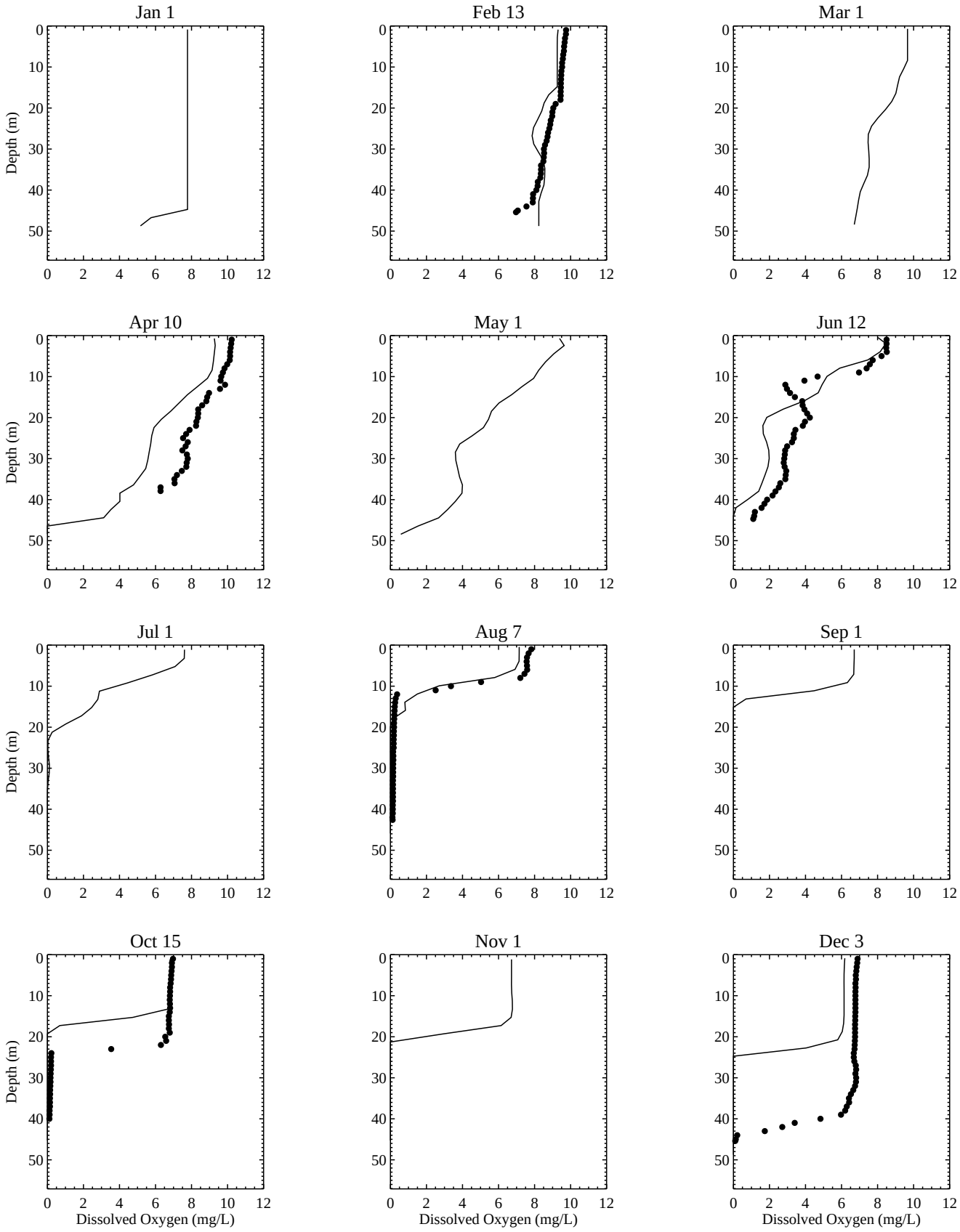

Figure J-17. Vertical profiles of model versus data at Arkansas Bend (Segment 78) - Dissolved Oxygen - 2001.

Profiles shown for dates with available data else model results for first day of month shown.

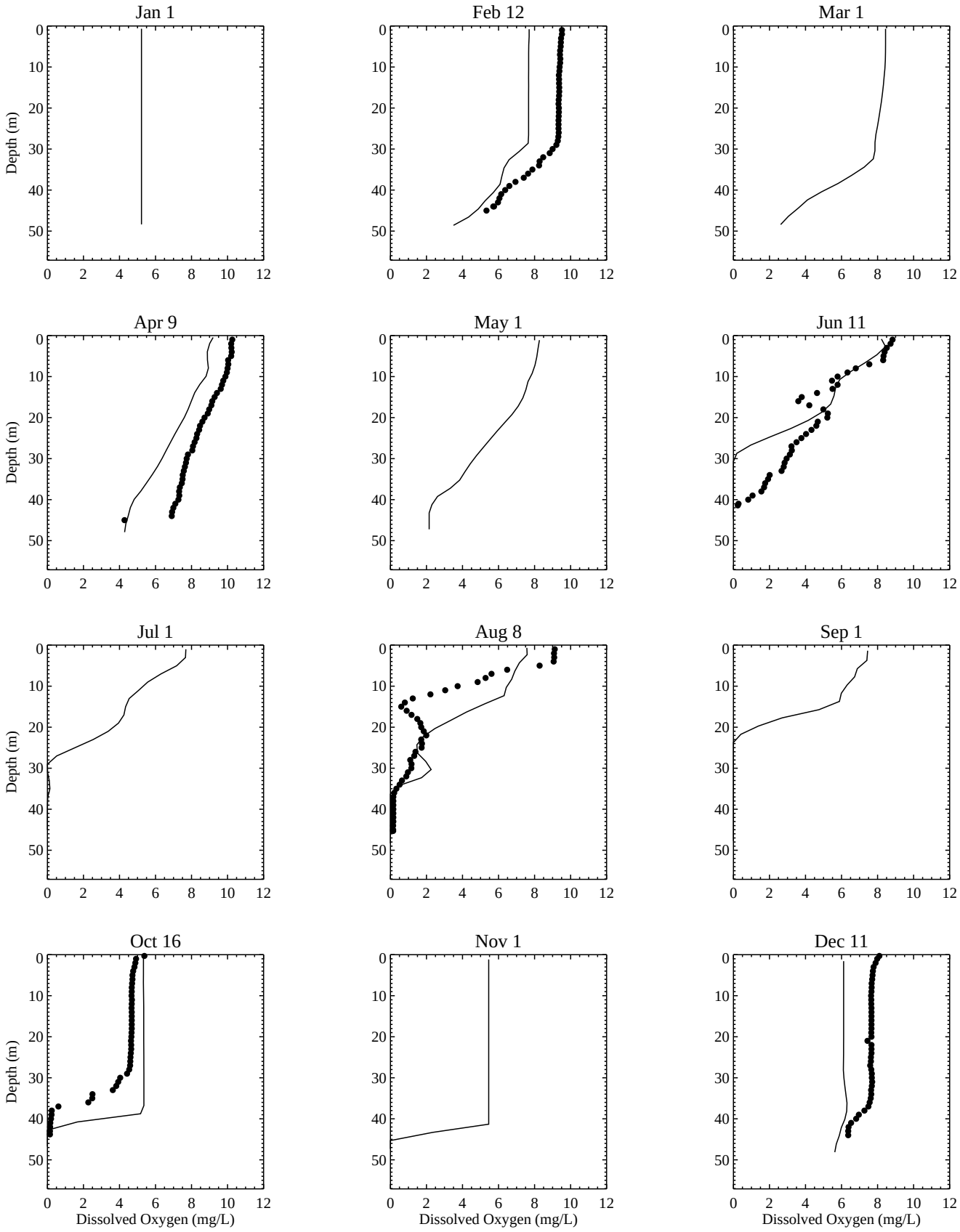

Figure J-17. Vertical profiles of model versus data at Arkansas Bend (Segment 78) - Dissolved Oxygen - 2002.

Profiles shown for dates with available data else model results for first day of month shown.

Model Data

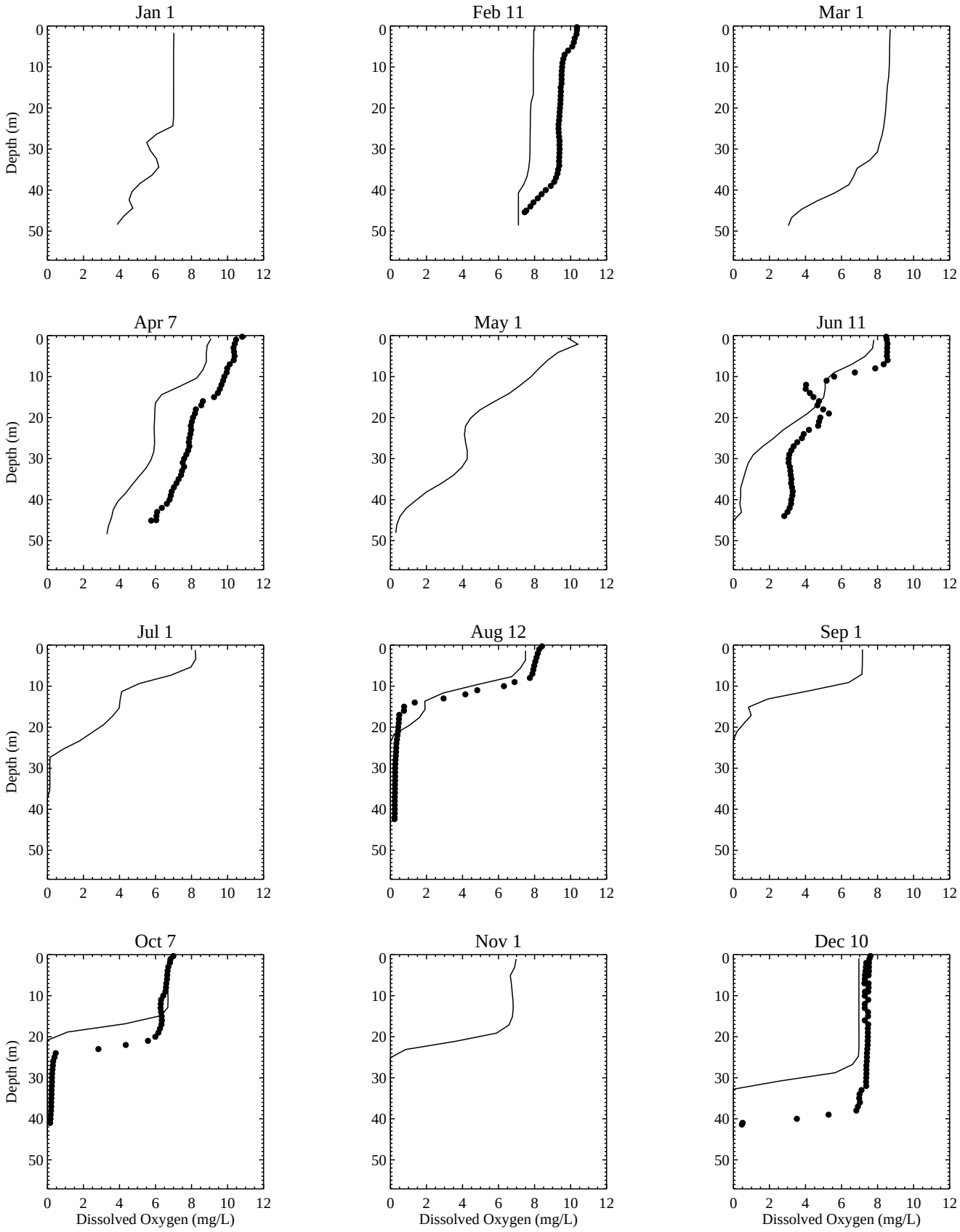

Figure J-17. Vertical profiles of model versus data at Arkansas Bend (Segment 78) - Dissolved Oxygen - 2003.

Profiles shown for dates with available data else model results for first day of month shown.

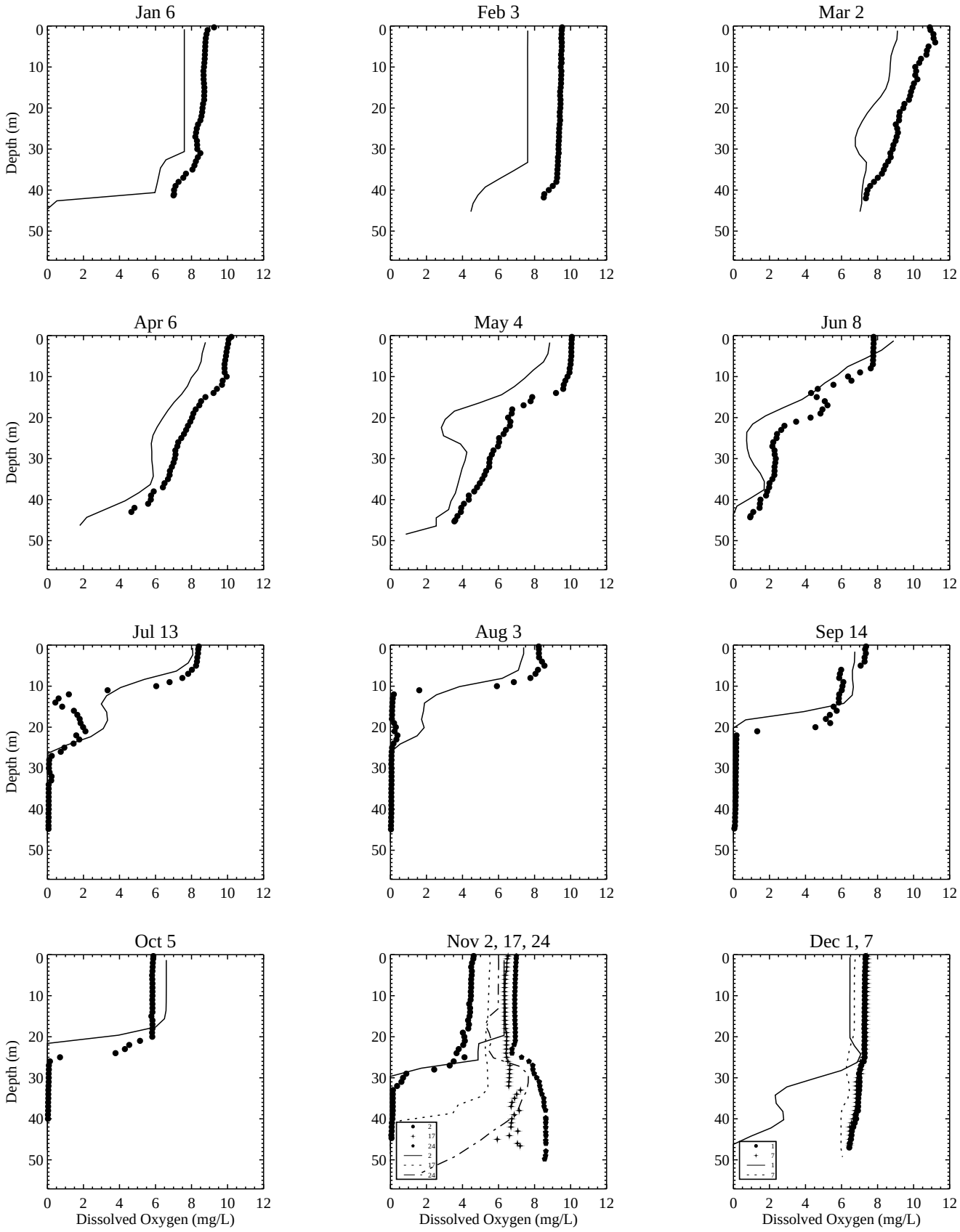

Figure J-17. Vertical profiles of model versus data at Arkansas Bend (Segment 78) - Dissolved Oxygen - 2004.

Profiles shown for dates with available data else model results for first day of month shown.

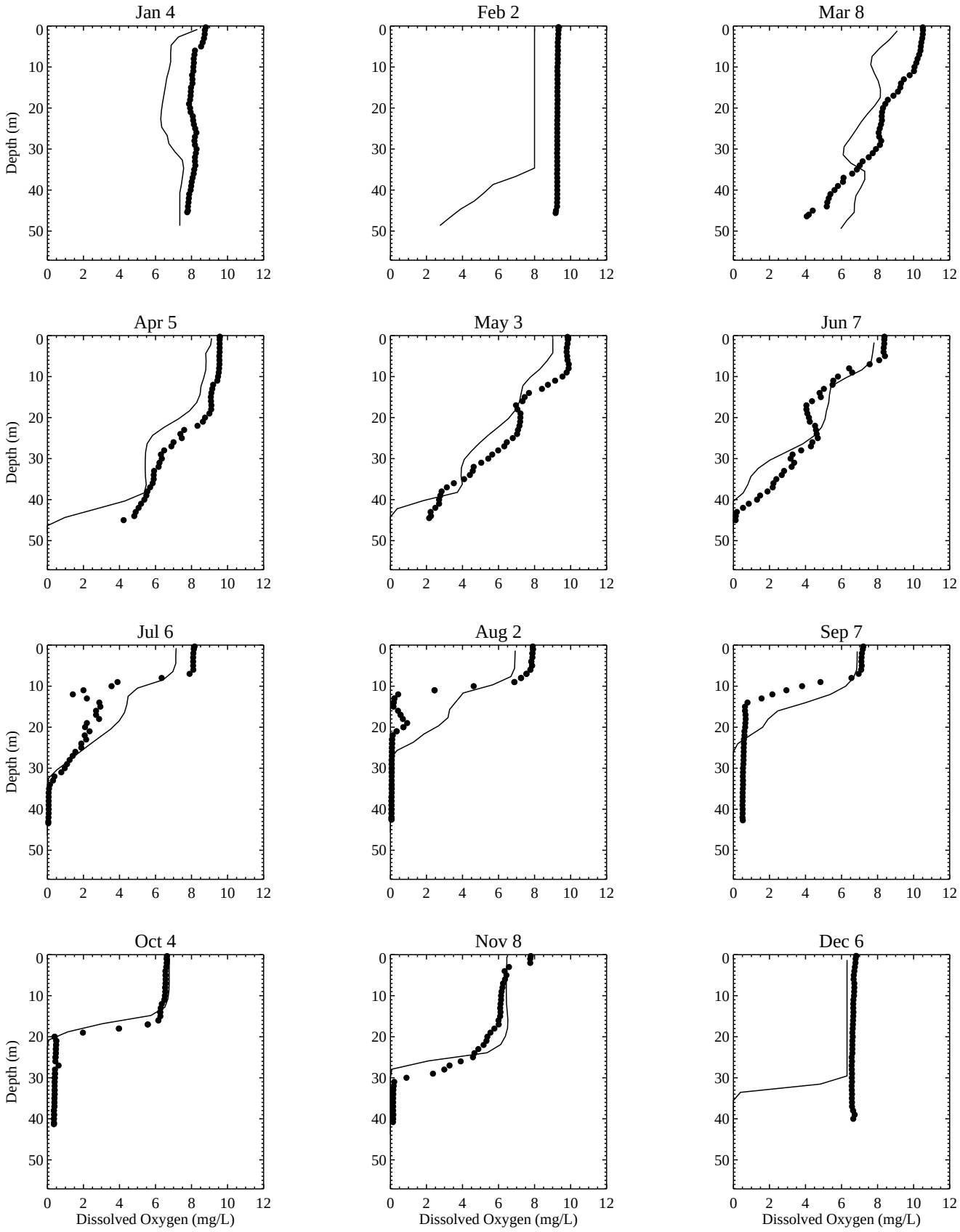

Figure J-17. Vertical profiles of model versus data at Arkansas Bend (Segment 78) - Dissolved Oxygen - 2005.

Profiles shown for dates with available data else model results for first day of month shown.

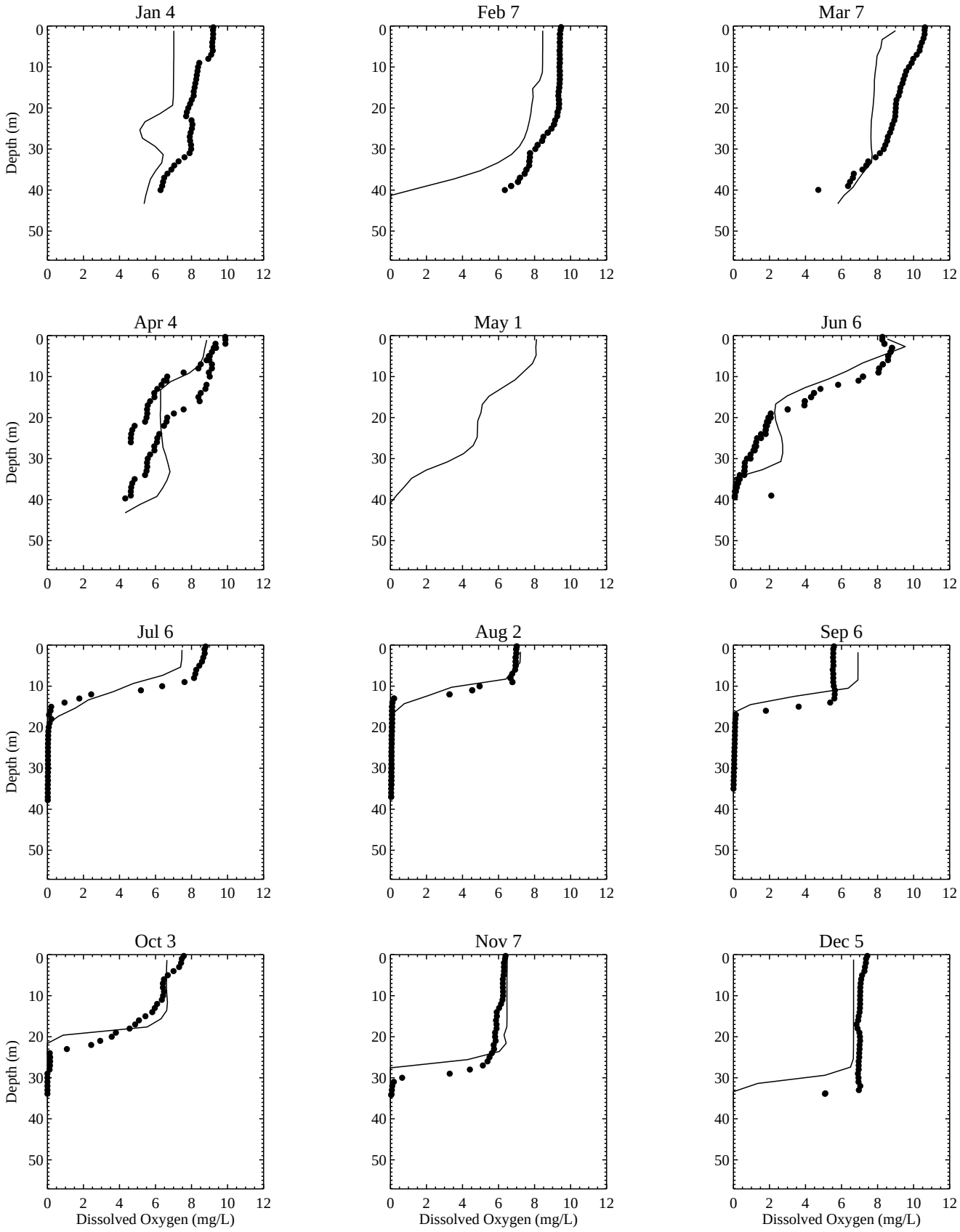

Figure J-17. Vertical profiles of model versus data at Arkansas Bend (Segment 78) - Dissolved Oxygen - 2006.

Profiles shown for dates with available data else model results for first day of month shown.

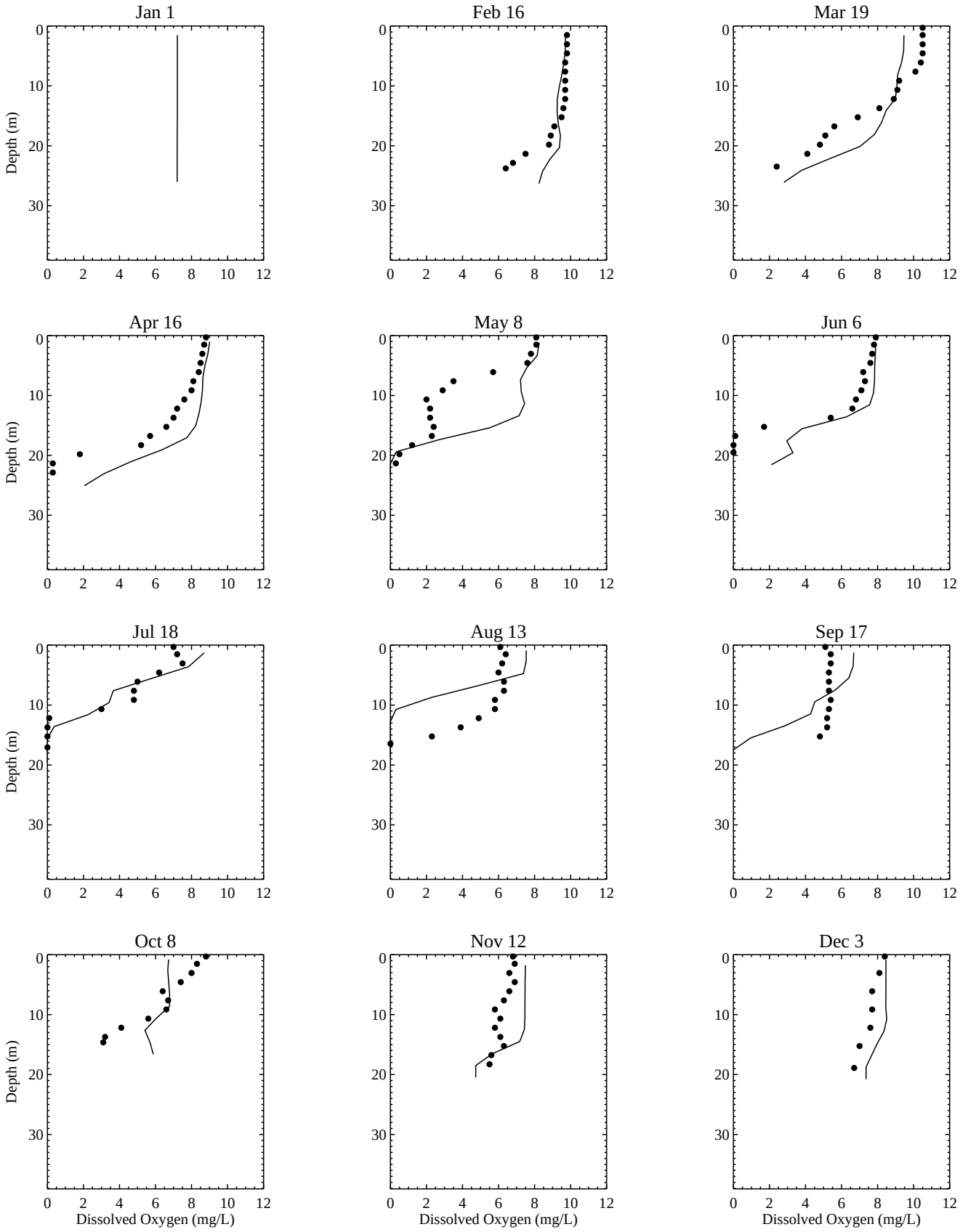

Figure J-18. Vertical profiles of model versus data at Pace Bend (Segment 48) - Dissolved Oxygen - 1984.

Profiles shown for dates with available data else model results for first day of month shown.

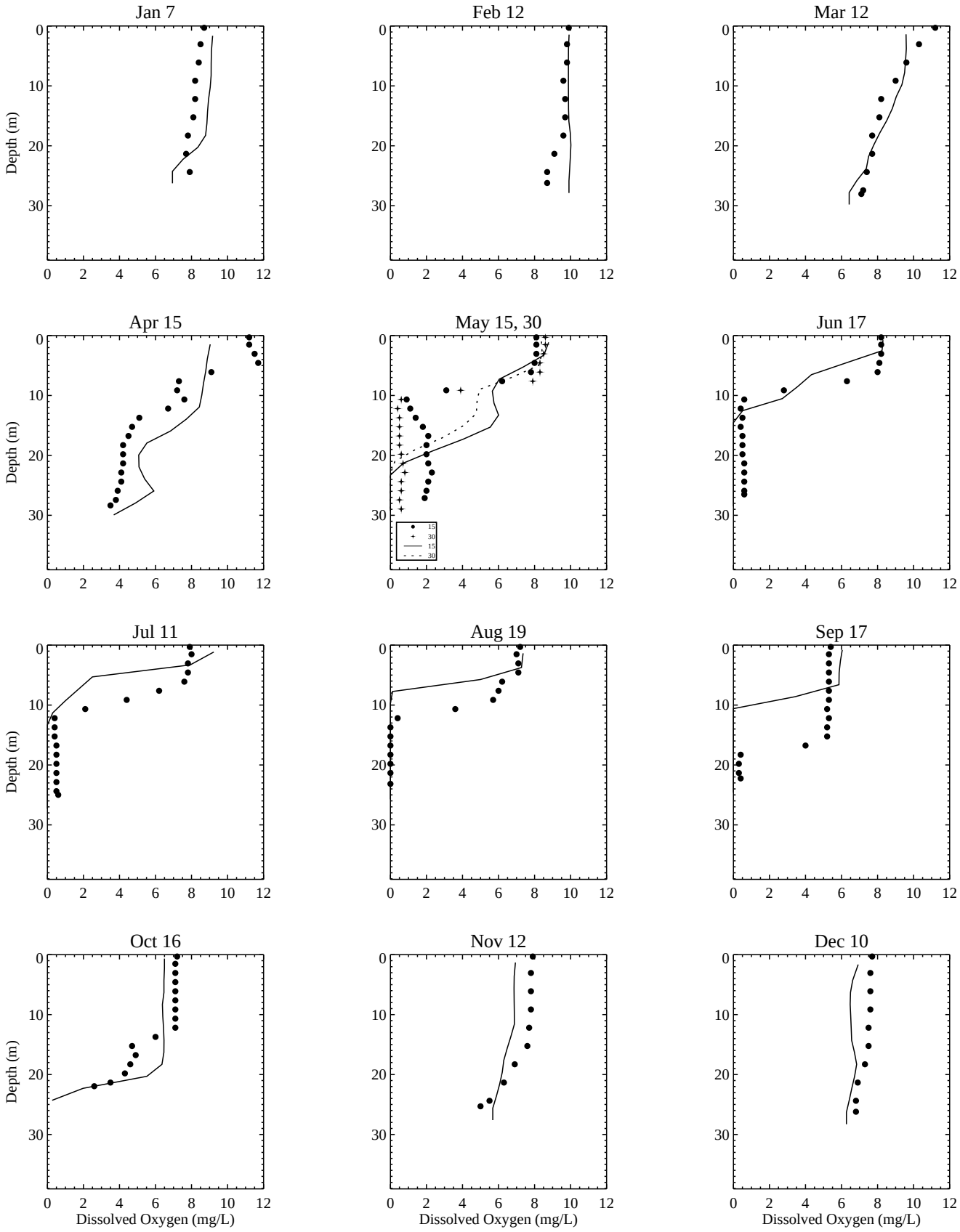

Figure J-18. Vertical profiles of model versus data at Pace Bend (Segment 48) - Dissolved Oxygen - 1985.

Profiles shown for dates with available data else model results for first day of month shown.

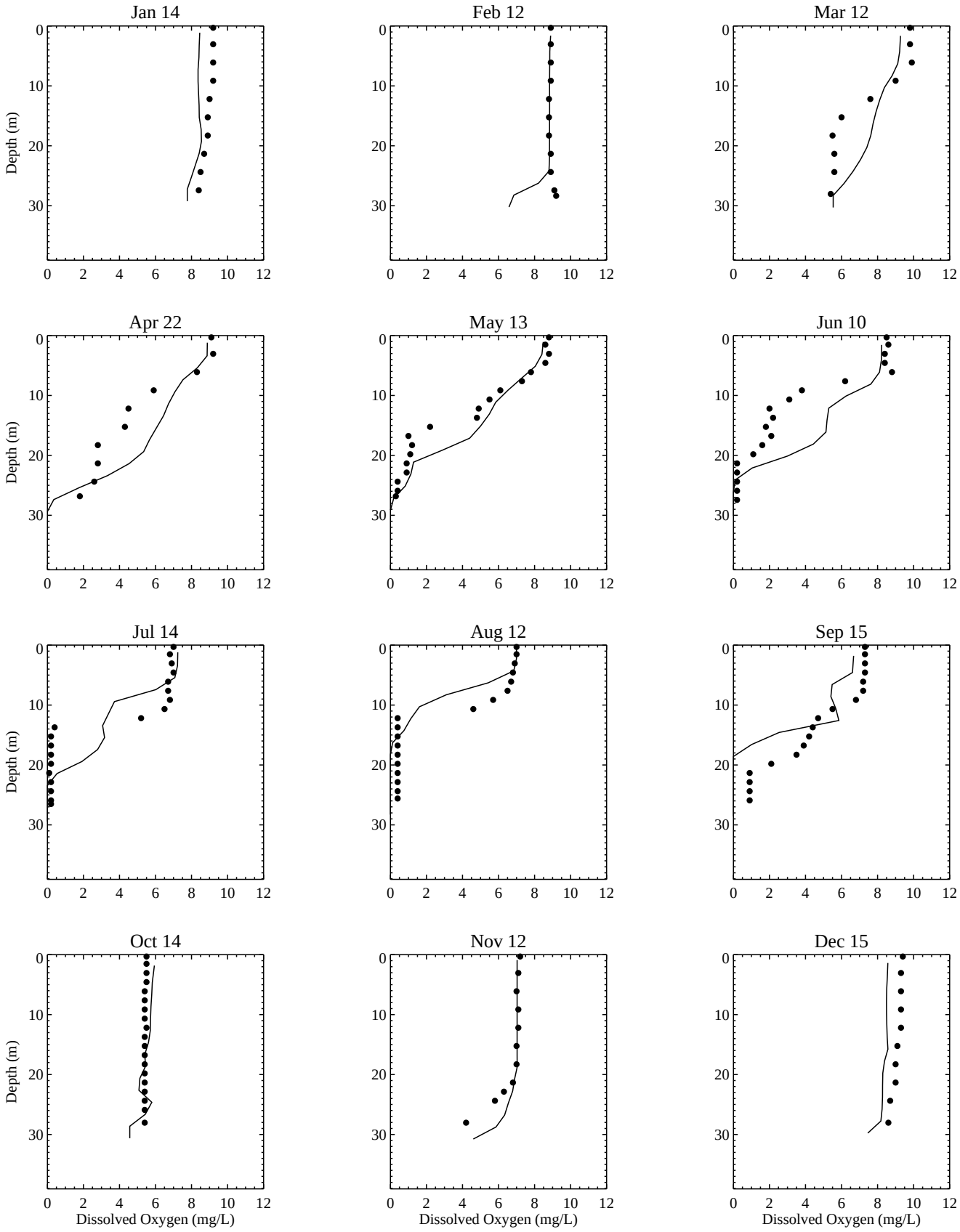

Figure J-18. Vertical profiles of model versus data at Pace Bend (Segment 48) - Dissolved Oxygen - 1986.

Profiles shown for dates with available data else model results for first day of month shown.

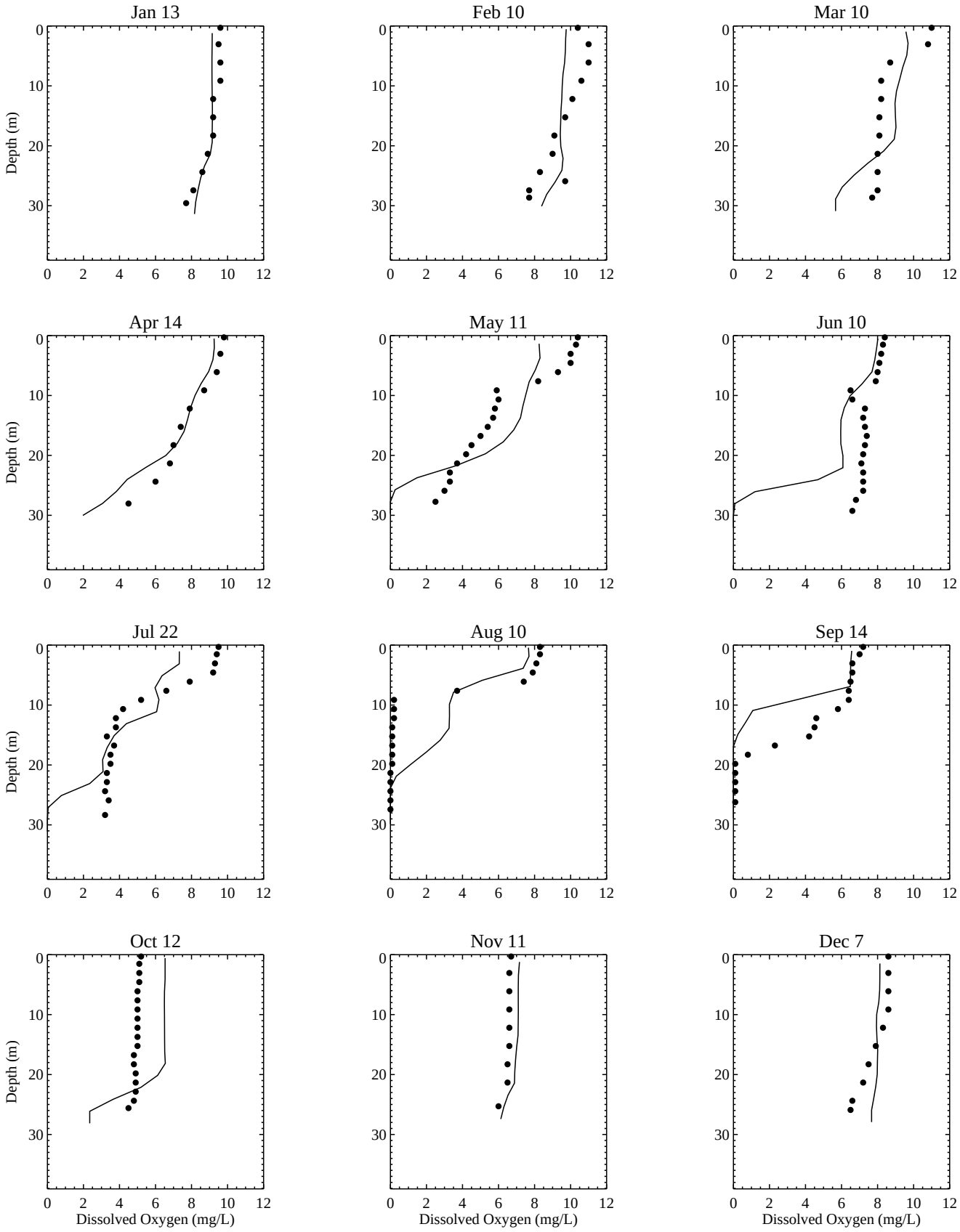

Figure J-18. Vertical profiles of model versus data at Pace Bend (Segment 48) - Dissolved Oxygen - 1987.

Profiles shown for dates with available data else model results for first day of month shown.

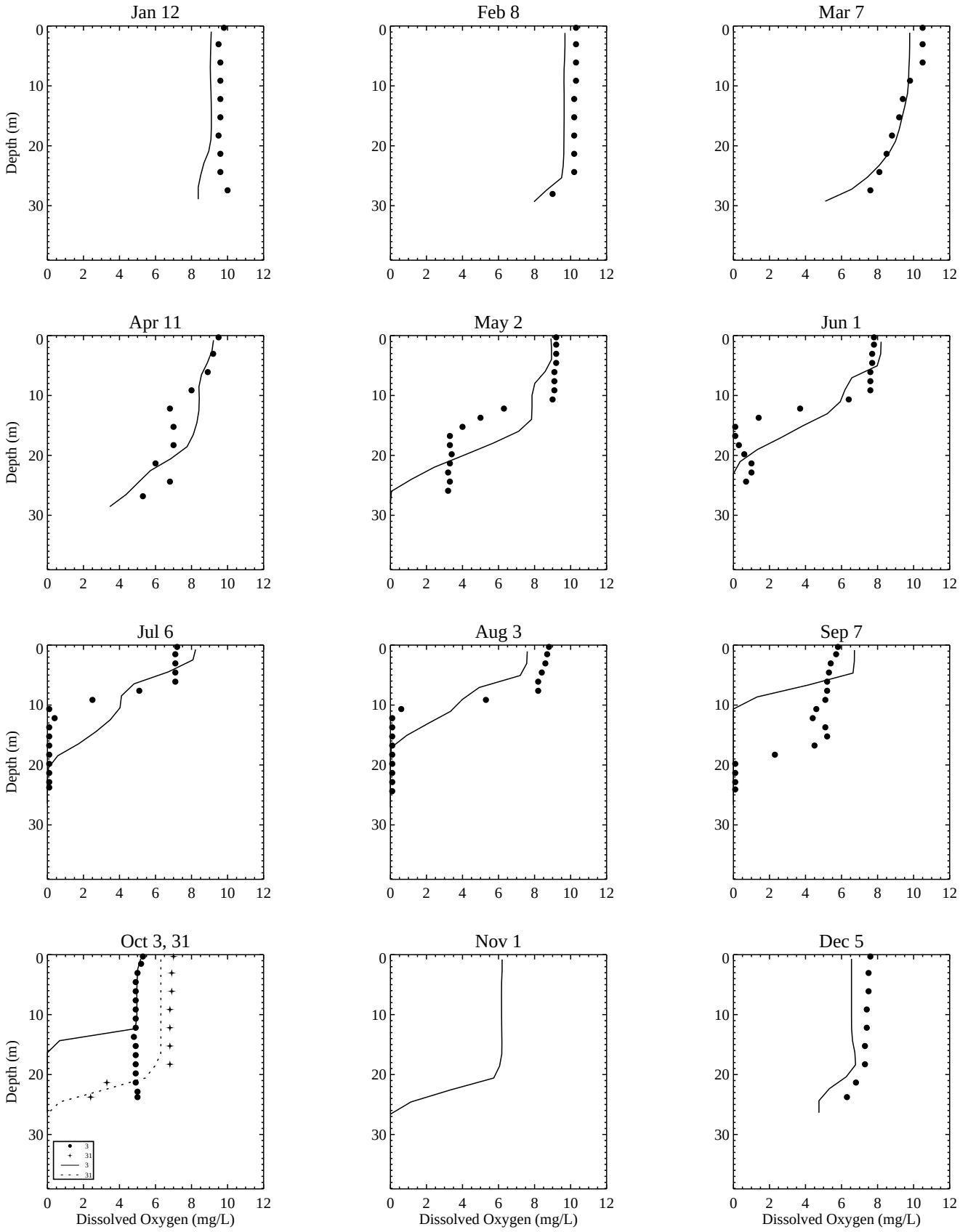

Figure J-18. Vertical profiles of model versus data at Pace Bend (Segment 48) - Dissolved Oxygen - 1988.

Profiles shown for dates with available data else model results for first day of month shown.

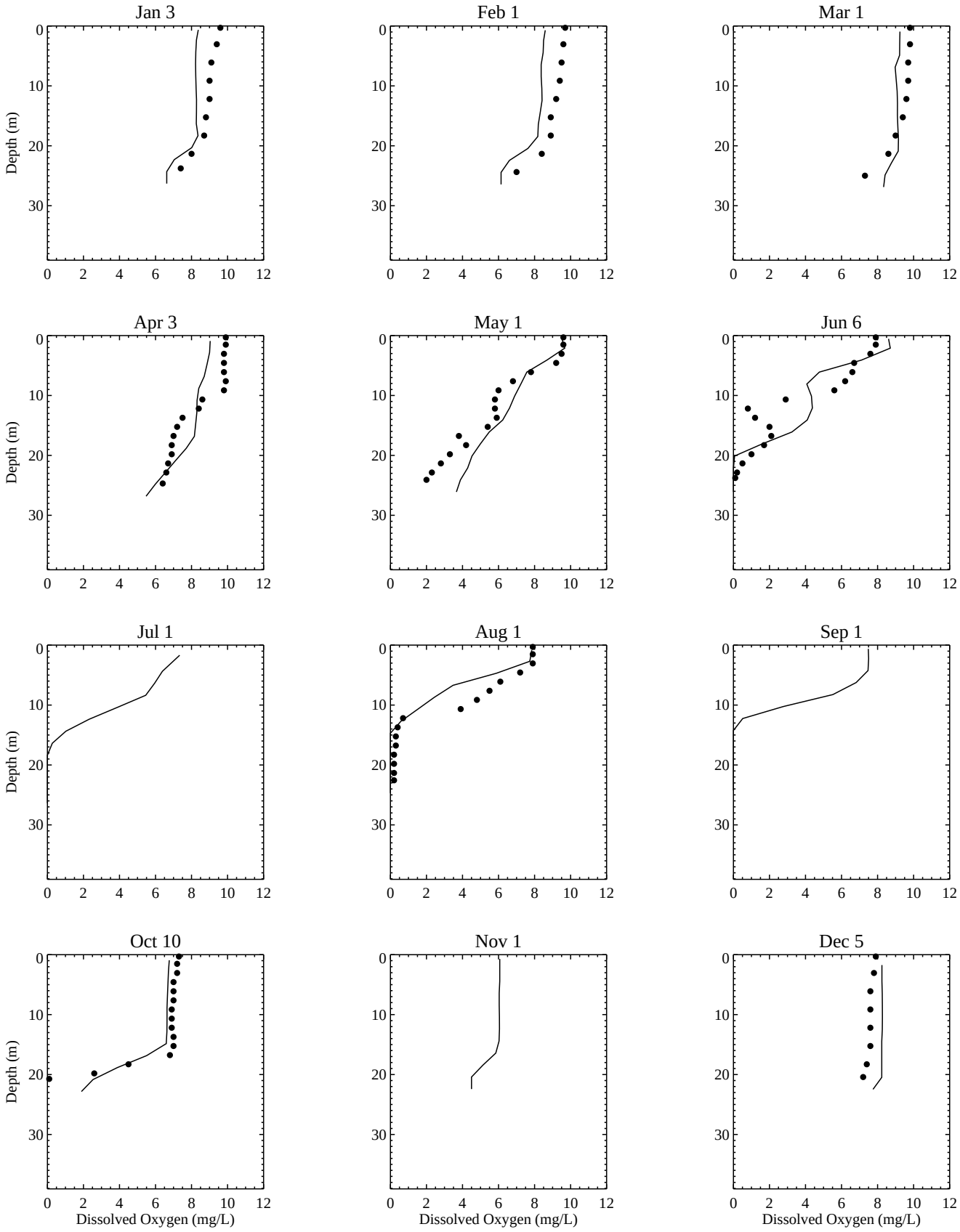

Figure J-18. Vertical profiles of model versus data at Pace Bend (Segment 48) - Dissolved Oxygen - 1989.

Profiles shown for dates with available data else model results for first day of month shown.

Model Data

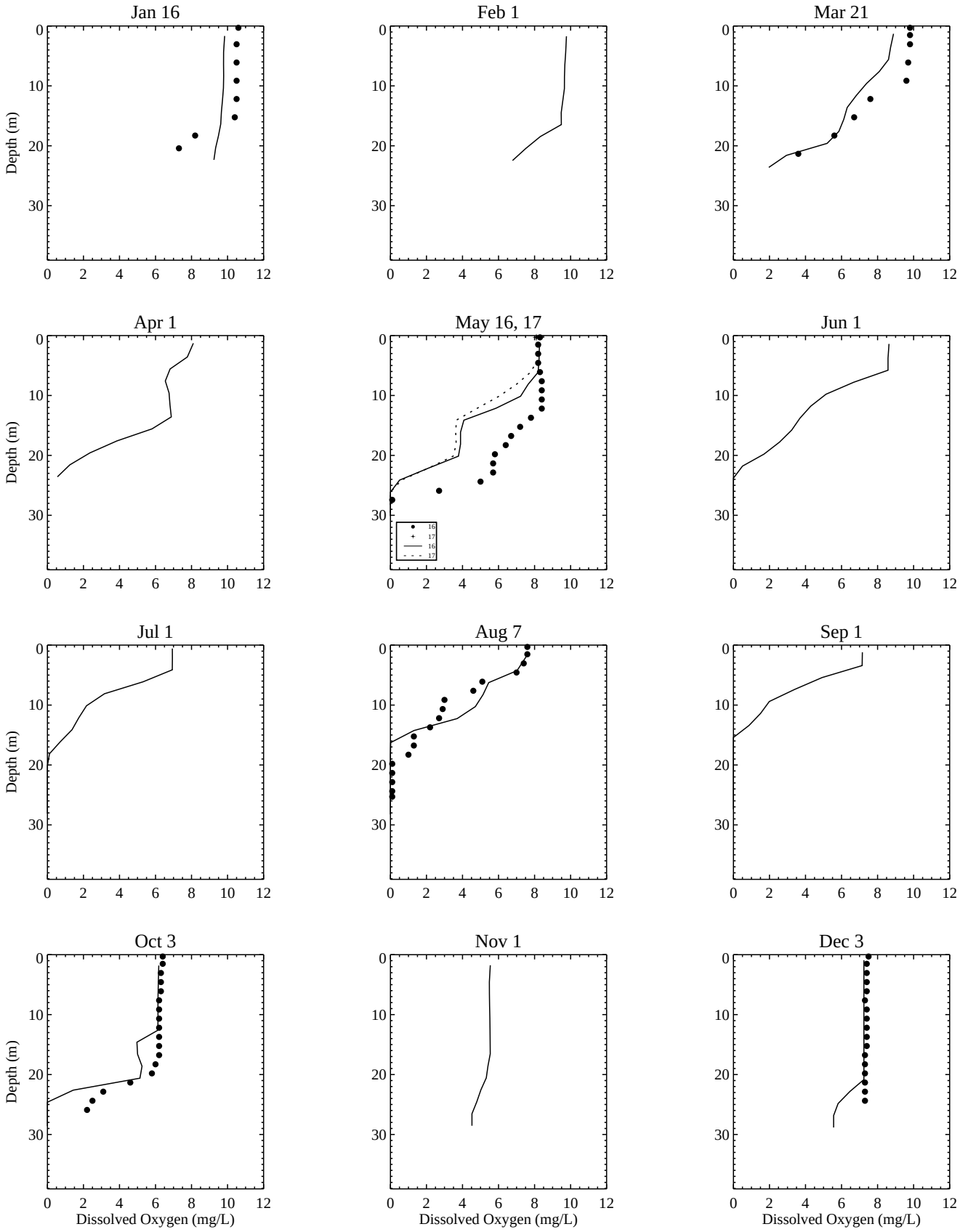

Figure J-18. Vertical profiles of model versus data at Pace Bend (Segment 48) - Dissolved Oxygen - 1990.

Profiles shown for dates with available data else model results for first day of month shown.

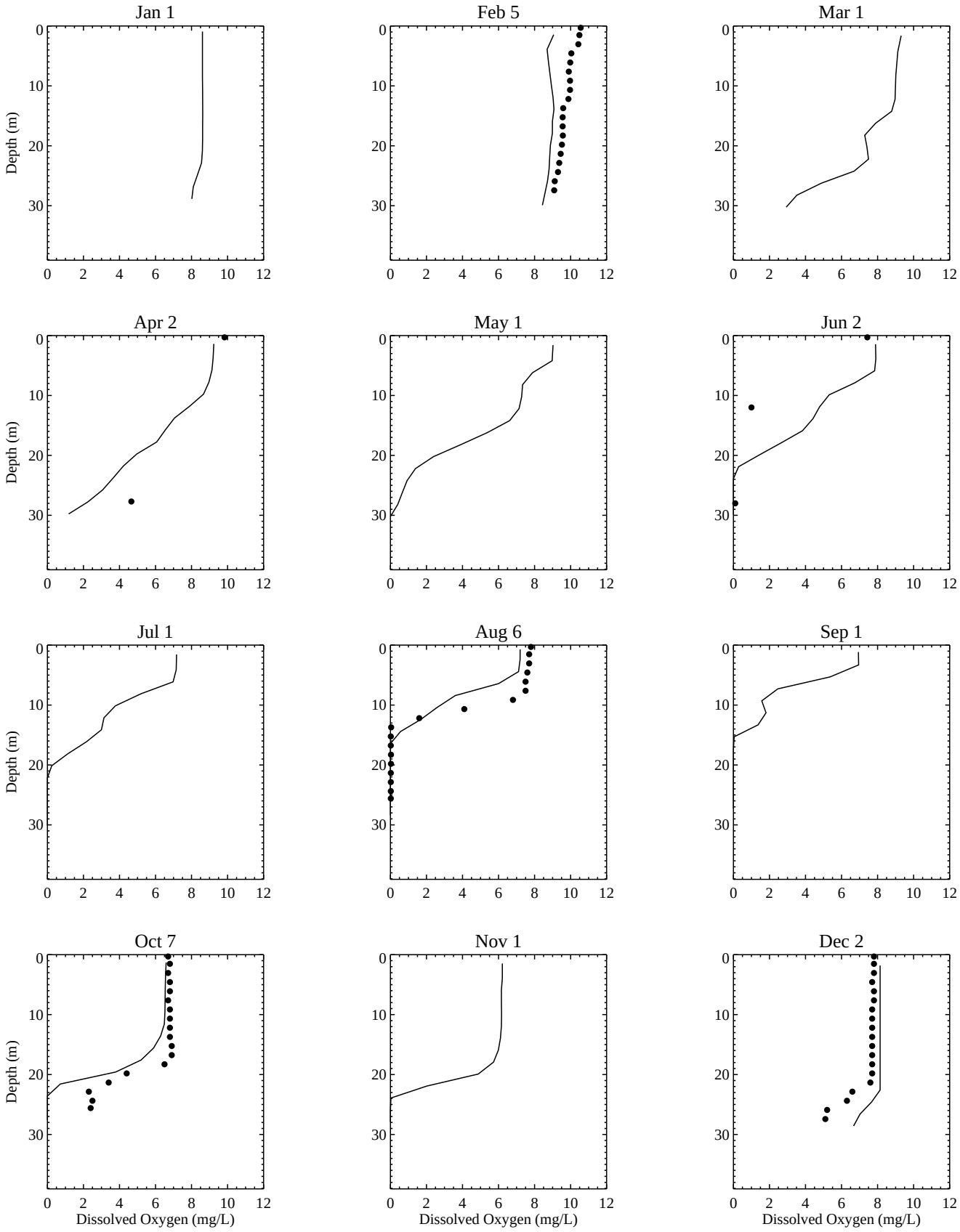

Figure J-18. Vertical profiles of model versus data at Pace Bend (Segment 48) - Dissolved Oxygen - 1991.

Profiles shown for dates with available data else model results for first day of month shown.

Model Data

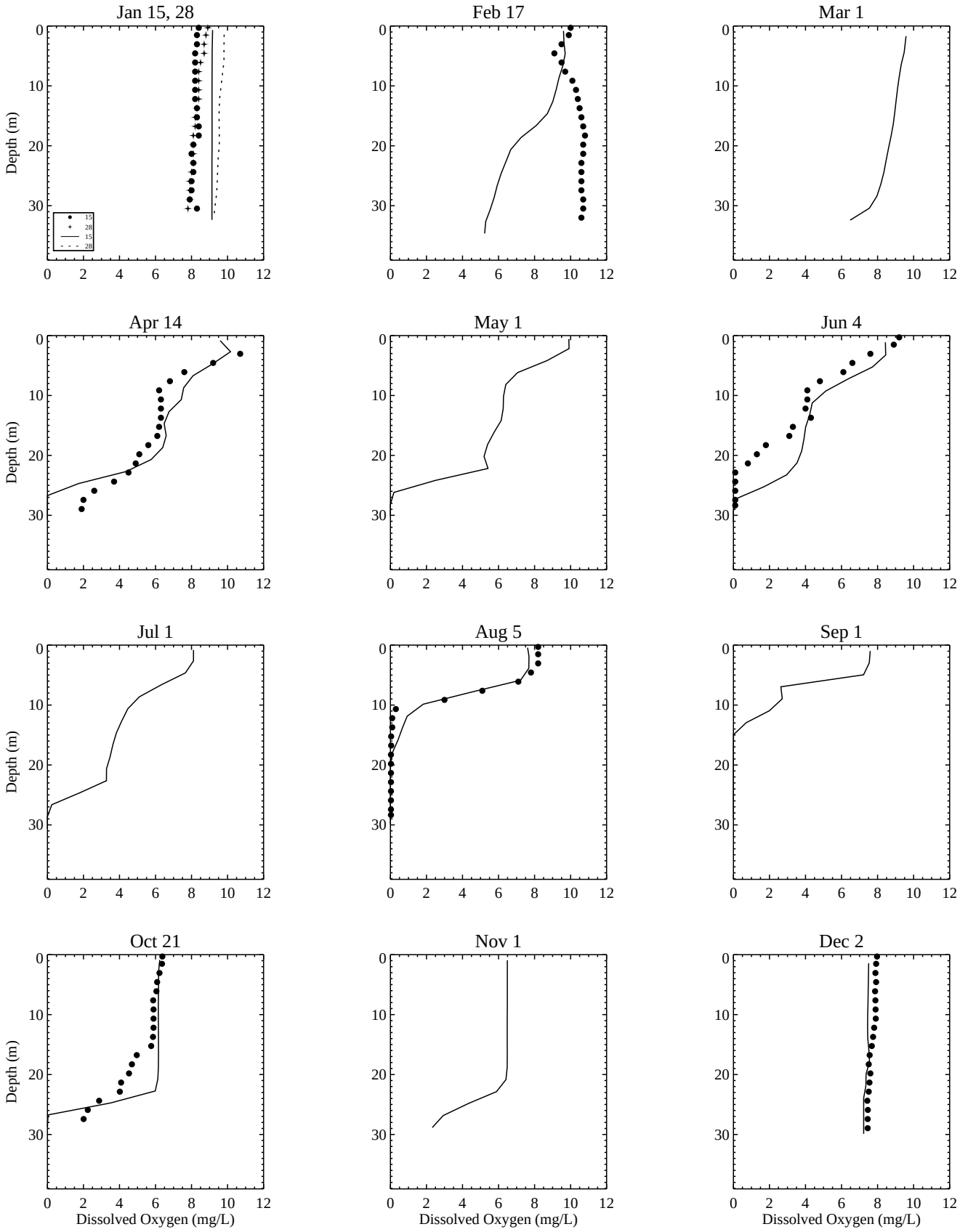

Figure J-18. Vertical profiles of model versus data at Pace Bend (Segment 48) - Dissolved Oxygen - 1992.

Profiles shown for dates with available data else model results for first day of month shown.

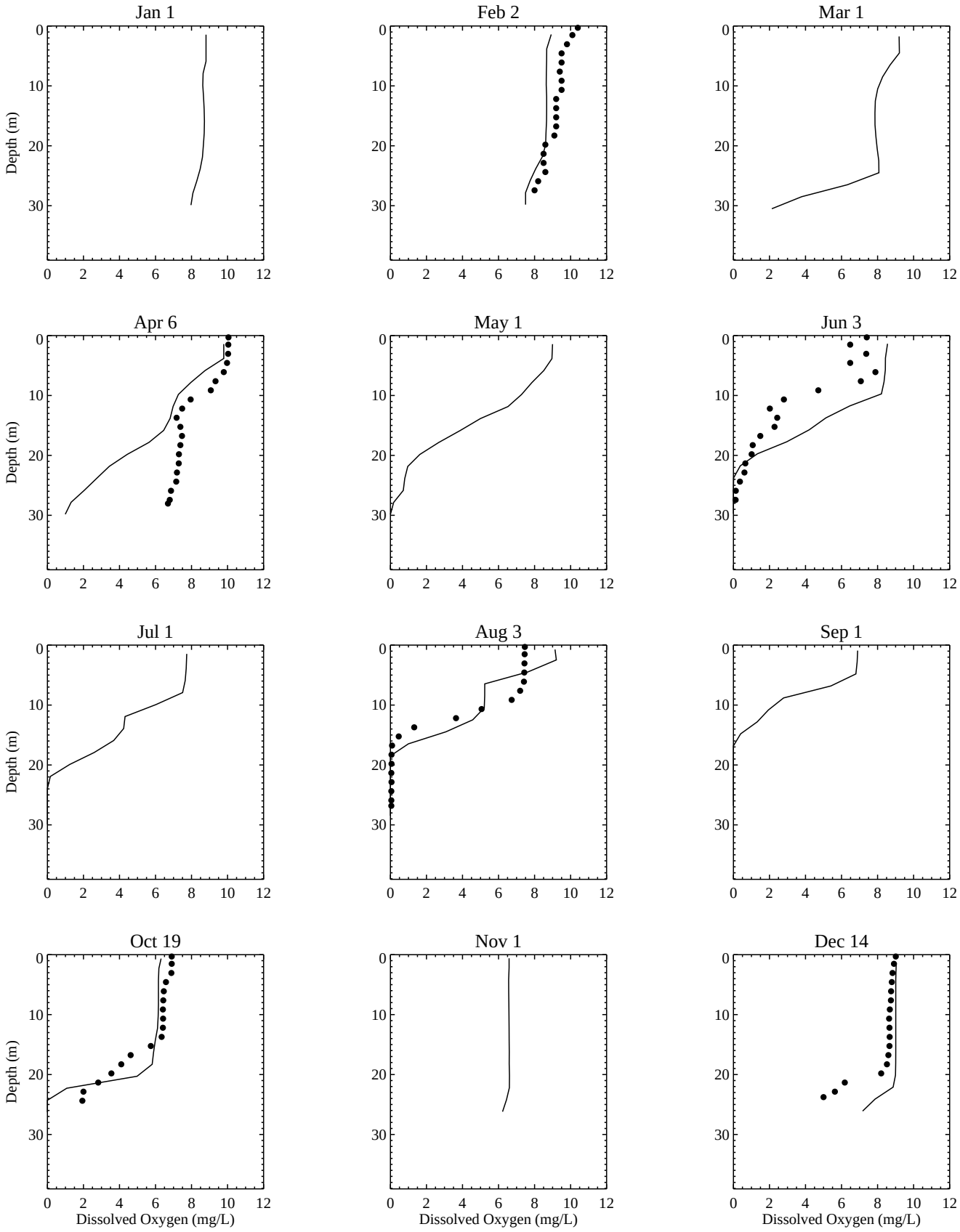

Figure J-18. Vertical profiles of model versus data at Pace Bend (Segment 48) - Dissolved Oxygen - 1993.

Profiles shown for dates with available data else model results for first day of month shown.

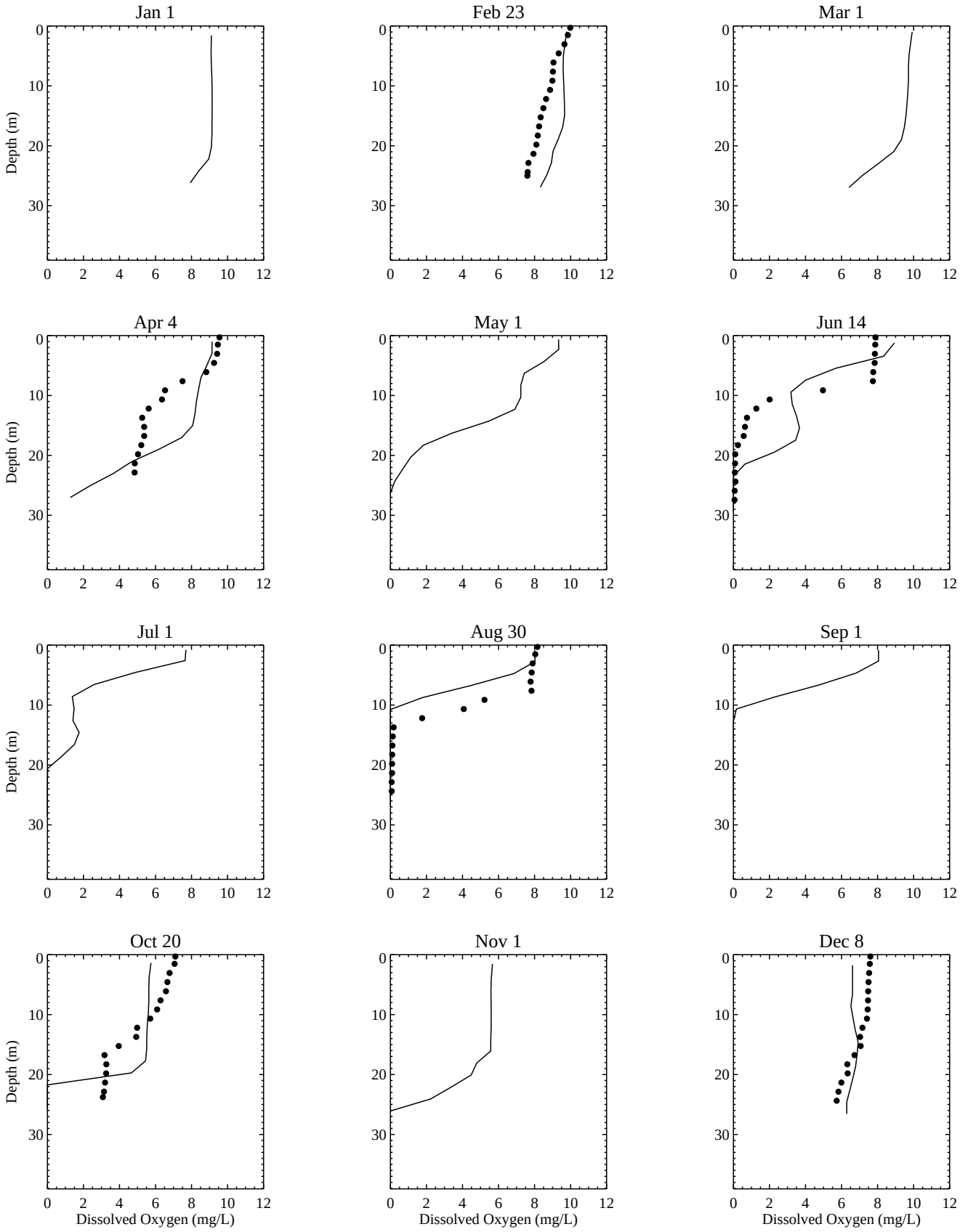

Figure J-18. Vertical profiles of model versus data at Pace Bend (Segment 48) - Dissolved Oxygen - 1994.

Profiles shown for dates with available data else model results for first day of month shown.

Model Data

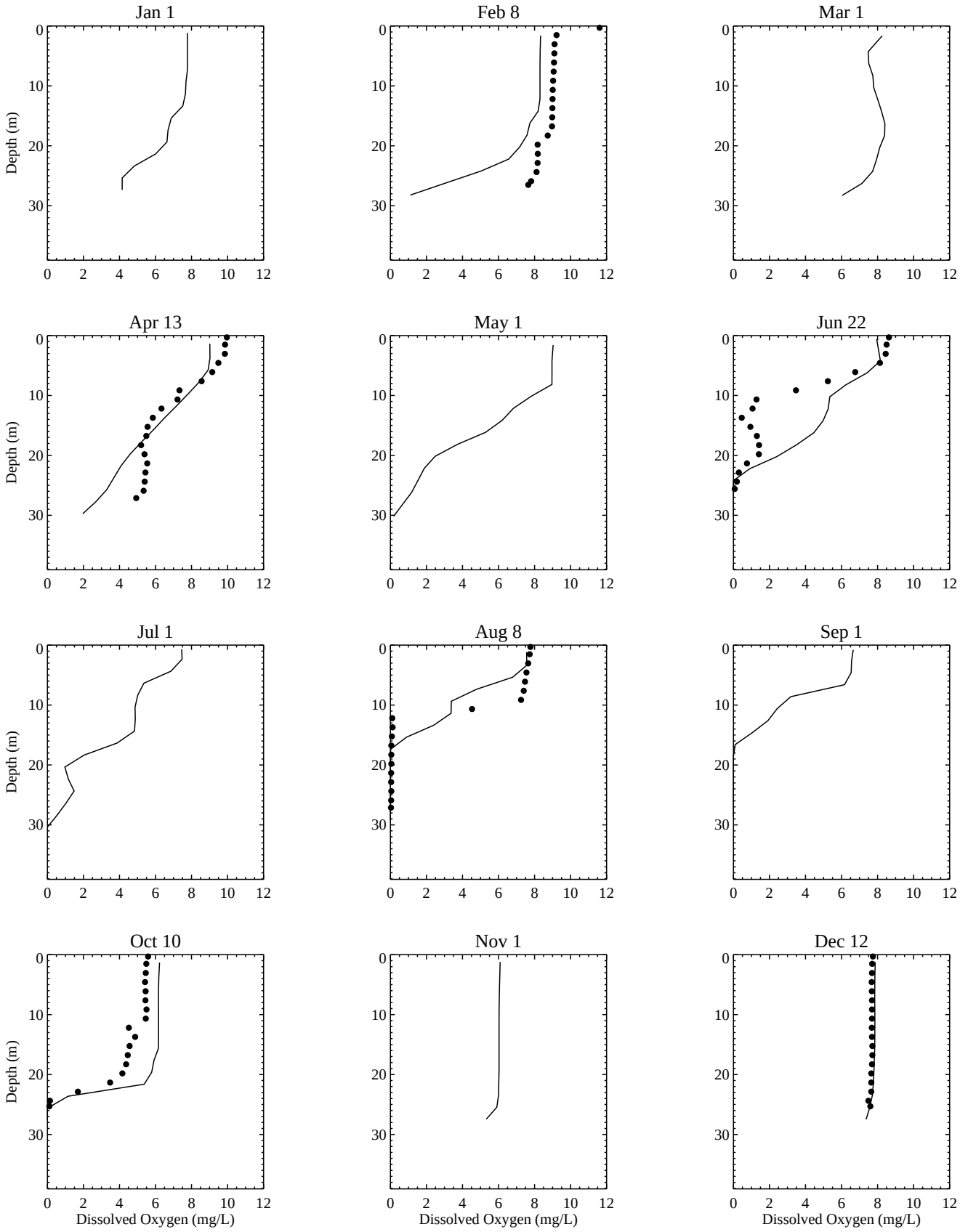

Figure J-18. Vertical profiles of model versus data at Pace Bend (Segment 48) - Dissolved Oxygen - 1995.

Profiles shown for dates with available data else model results for first day of month shown.

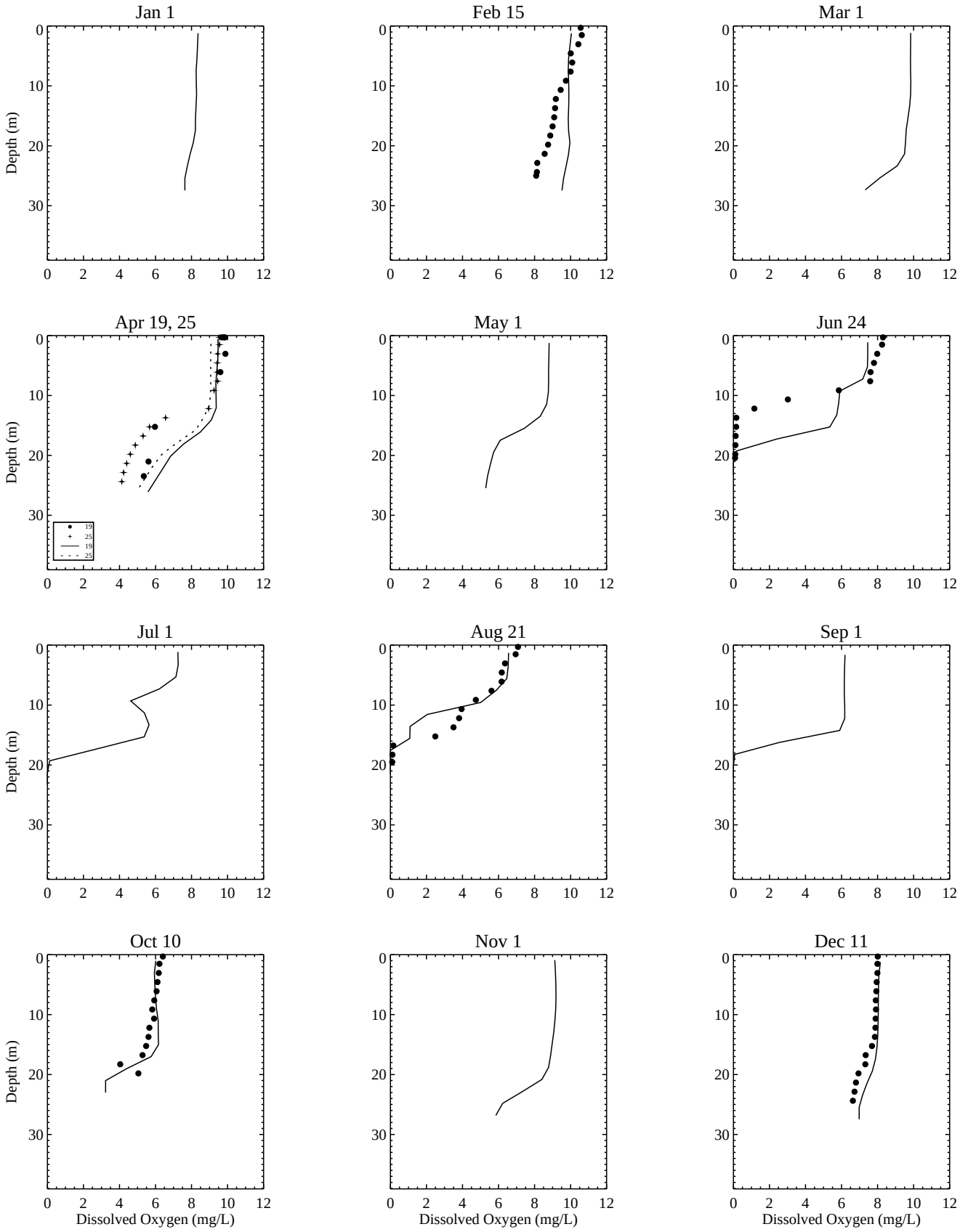

Figure J-18. Vertical profiles of model versus data at Pace Bend (Segment 48) - Dissolved Oxygen - 1996.

Profiles shown for dates with available data else model results for first day of month shown.

Model Data

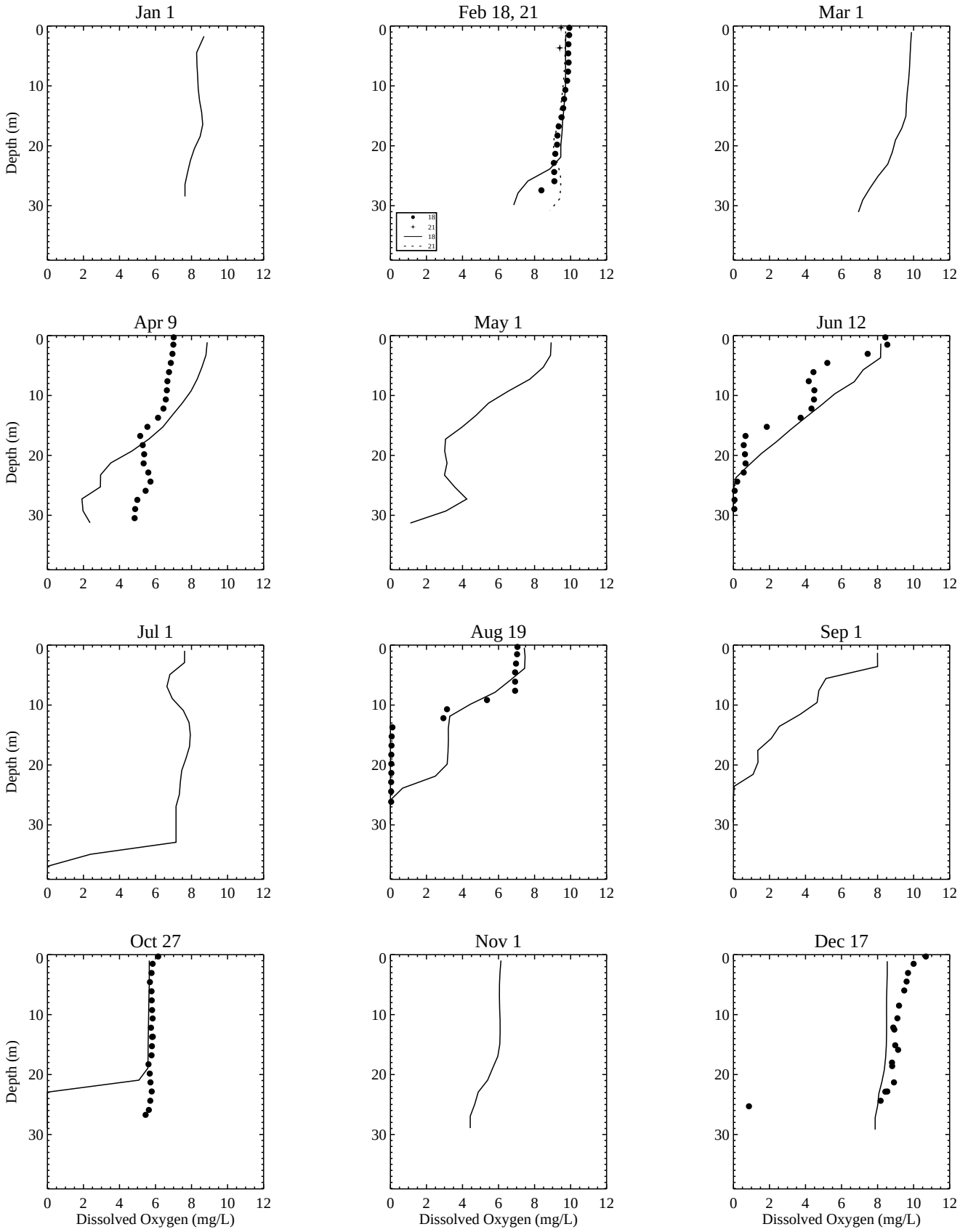

Figure J-18. Vertical profiles of model versus data at Pace Bend (Segment 48) - Dissolved Oxygen - 1997.

Profiles shown for dates with available data else model results for first day of month shown.

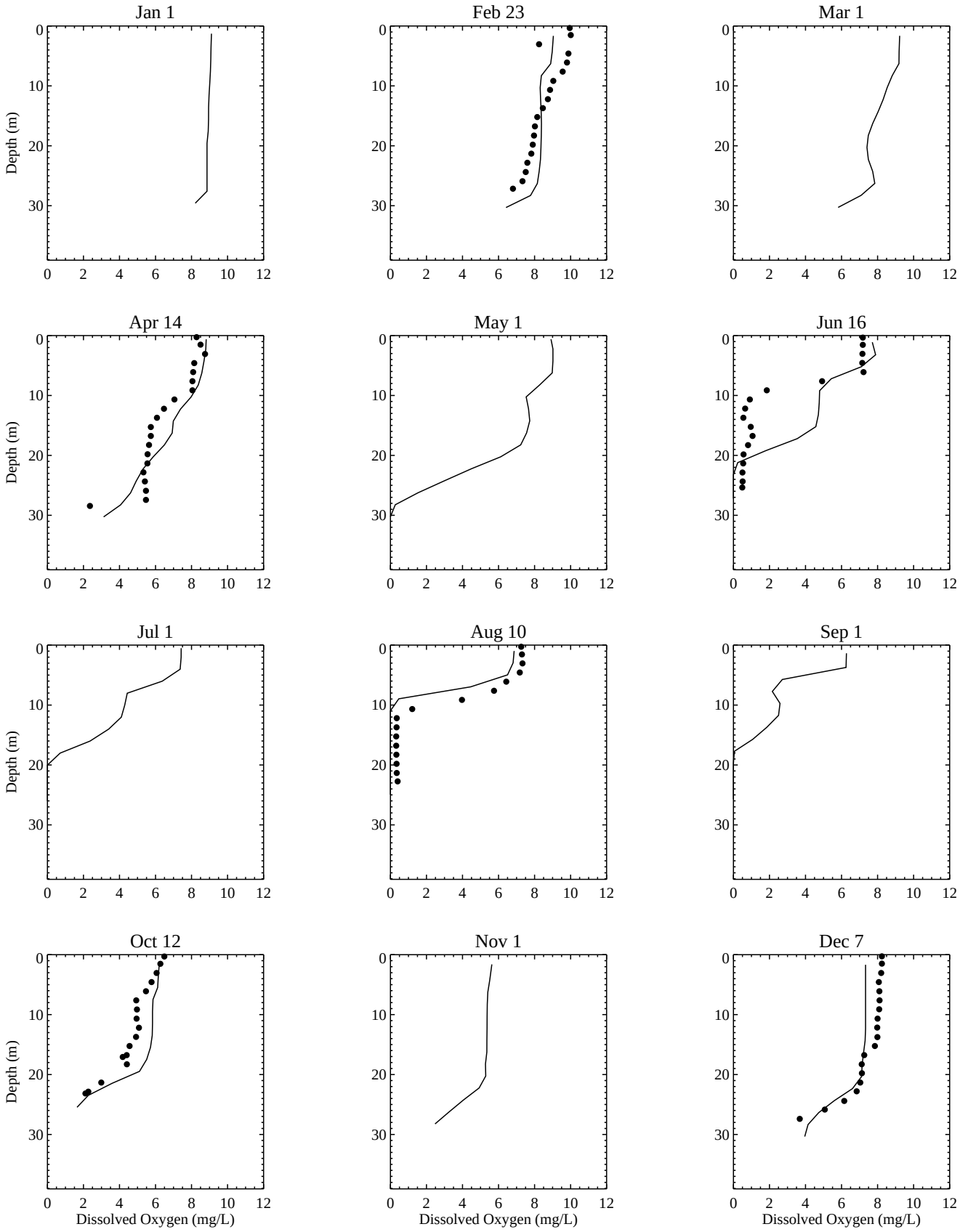

Figure J-18. Vertical profiles of model versus data at Pace Bend (Segment 48) - Dissolved Oxygen - 1998.

Profiles shown for dates with available data else model results for first day of month shown.

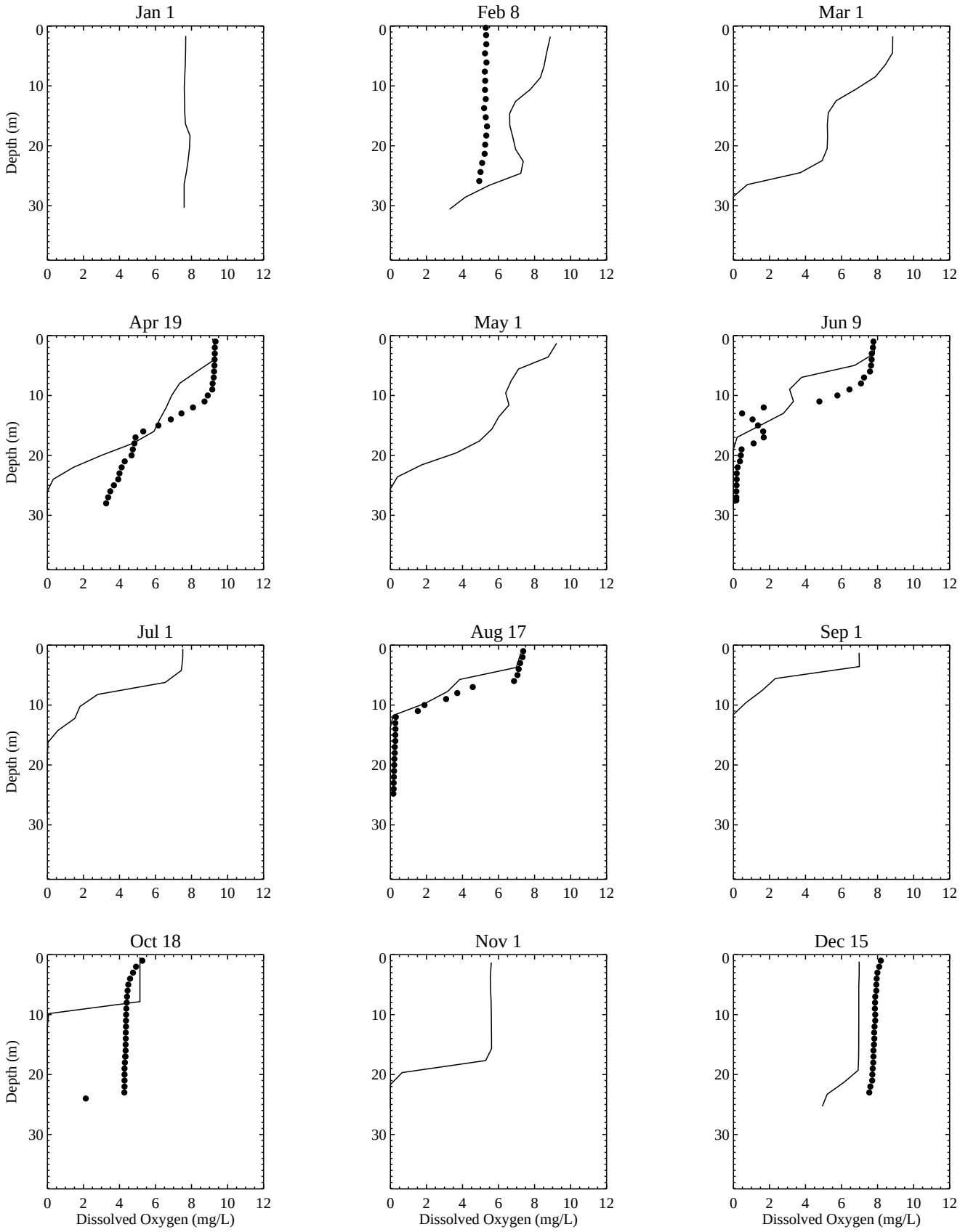

Figure J-18. Vertical profiles of model versus data at Pace Bend (Segment 48) - Dissolved Oxygen - 1999.

Profiles shown for dates with available data else model results for first day of month shown.

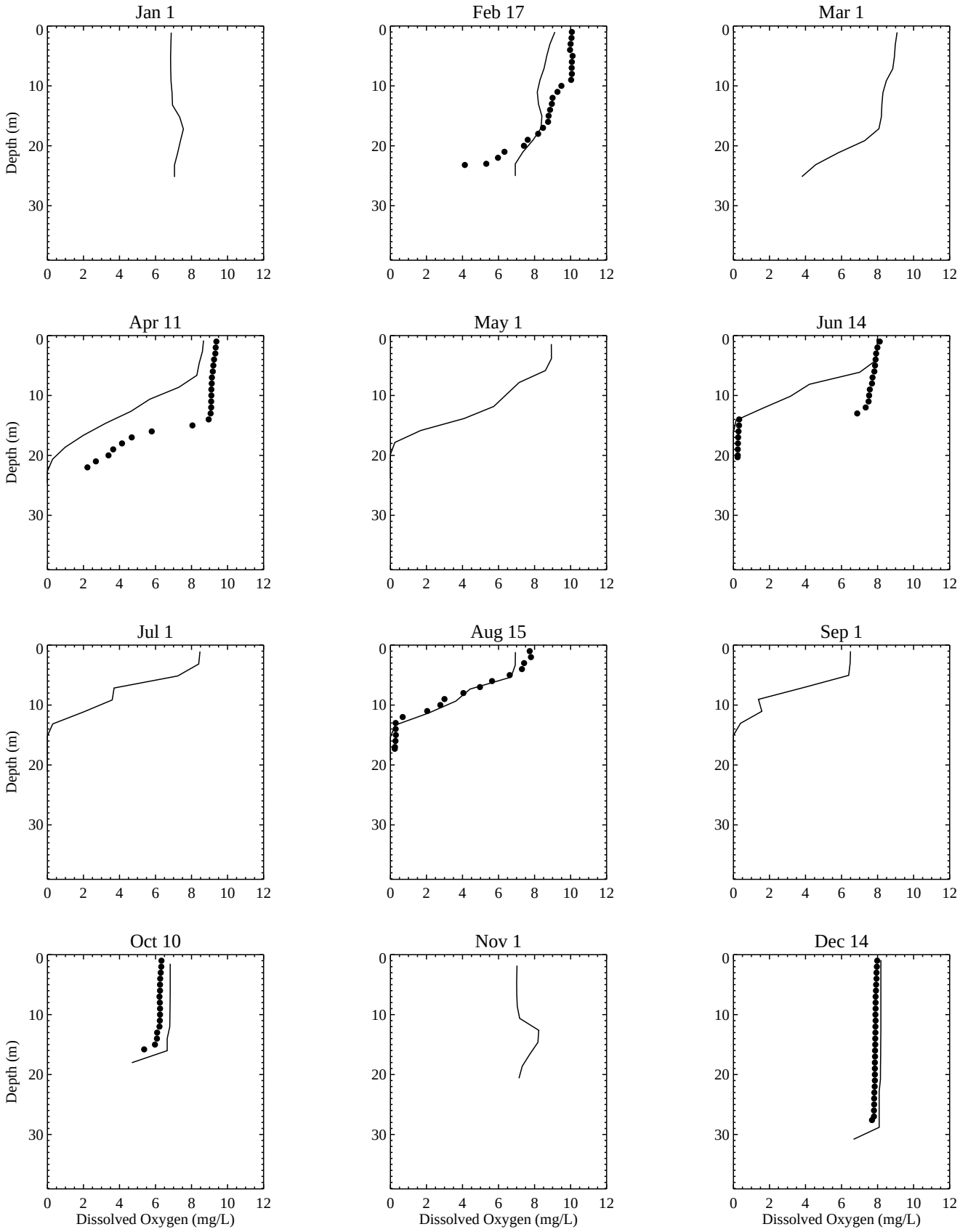

Figure J-18. Vertical profiles of model versus data at Pace Bend (Segment 48) - Dissolved Oxygen - 2000.

Profiles shown for dates with available data else model results for first day of month shown.

Model Data

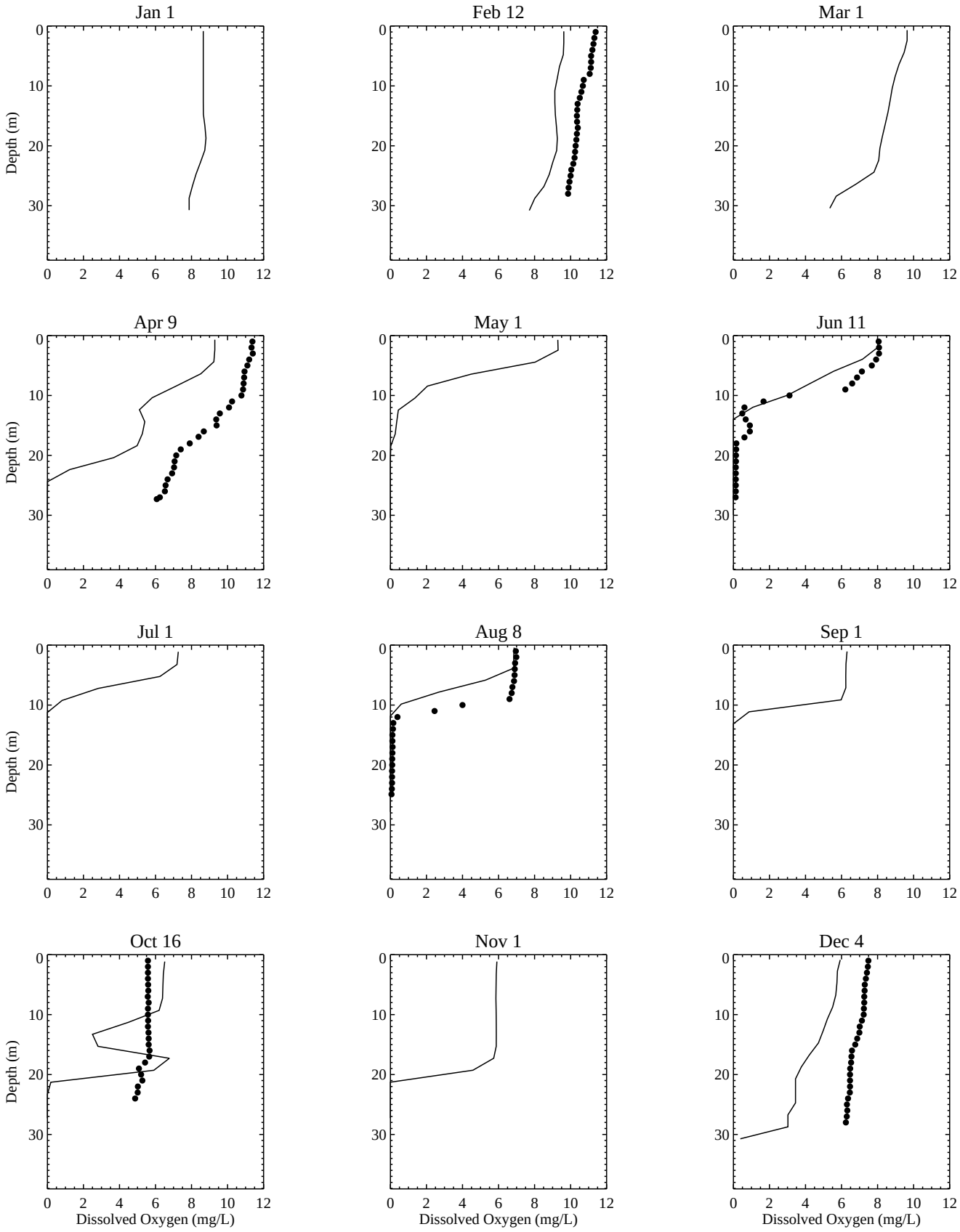

Figure J-18. Vertical profiles of model versus data at Pace Bend (Segment 48) - Dissolved Oxygen - 2001.

Profiles shown for dates with available data else model results for first day of month shown.

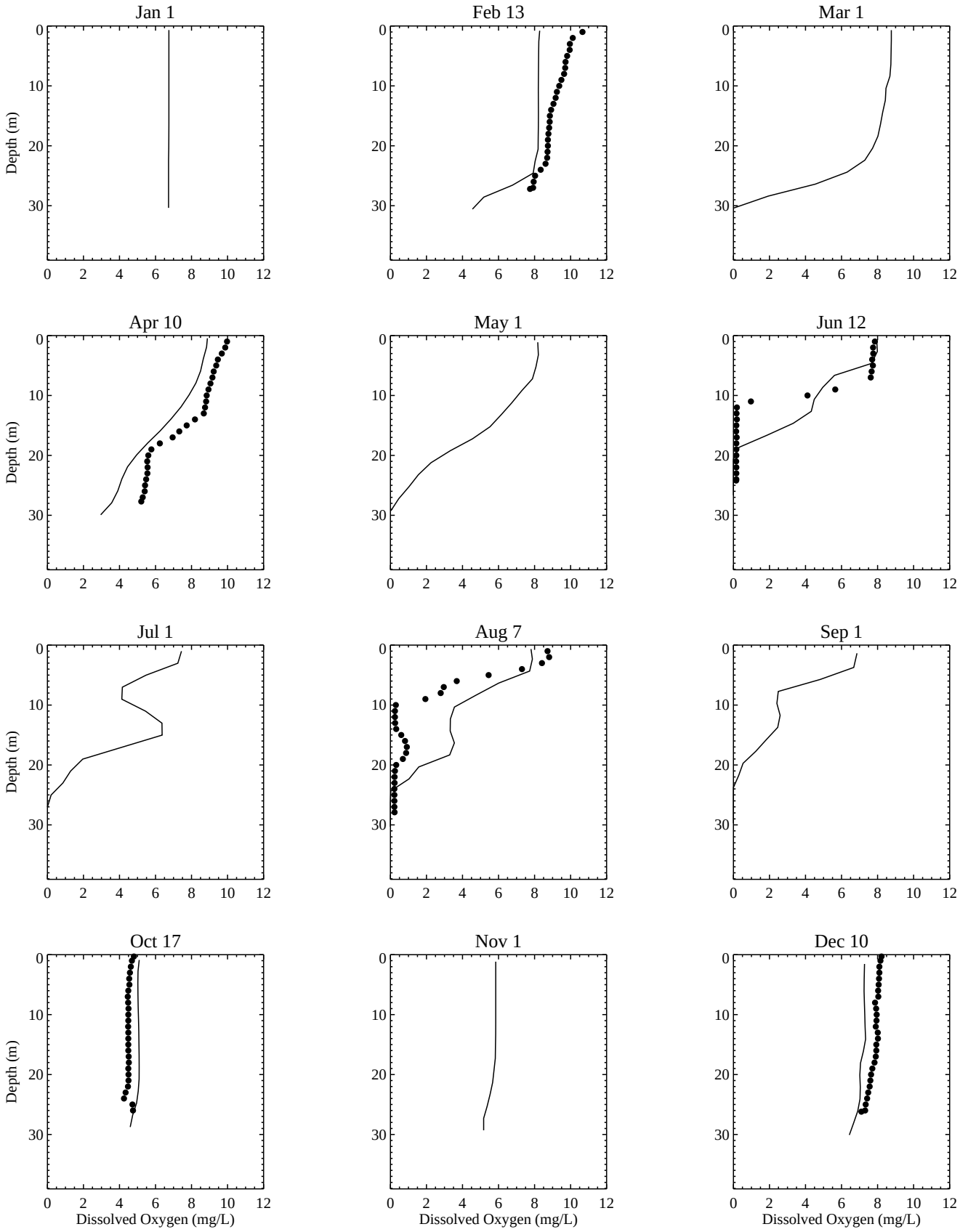

Figure J-18. Vertical profiles of model versus data at Pace Bend (Segment 48) - Dissolved Oxygen - 2002.

Profiles shown for dates with available data else model results for first day of month shown.

Model Data

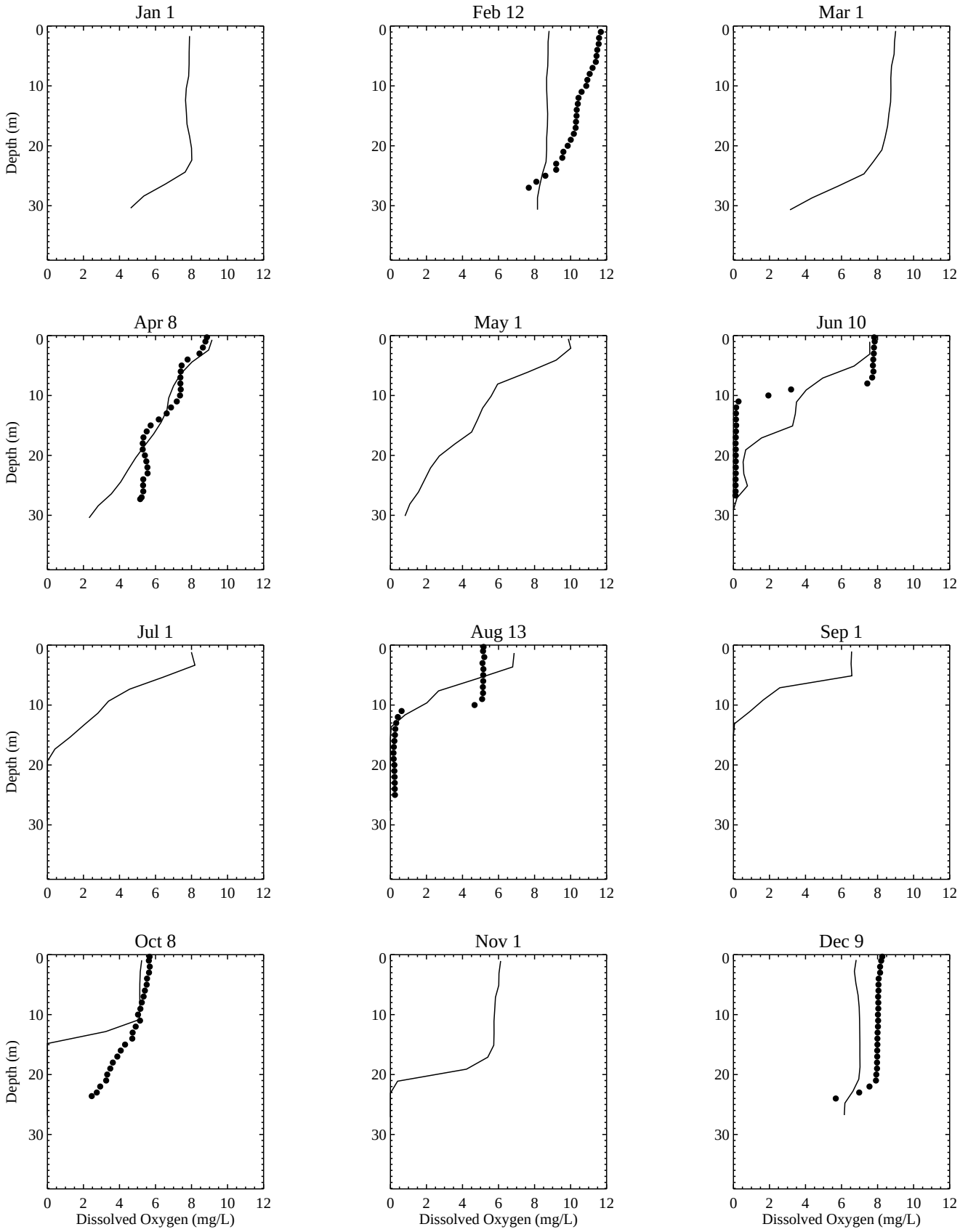

Figure J-18. Vertical profiles of model versus data at Pace Bend (Segment 48) - Dissolved Oxygen - 2003.

Profiles shown for dates with available data else model results for first day of month shown.

Model Data

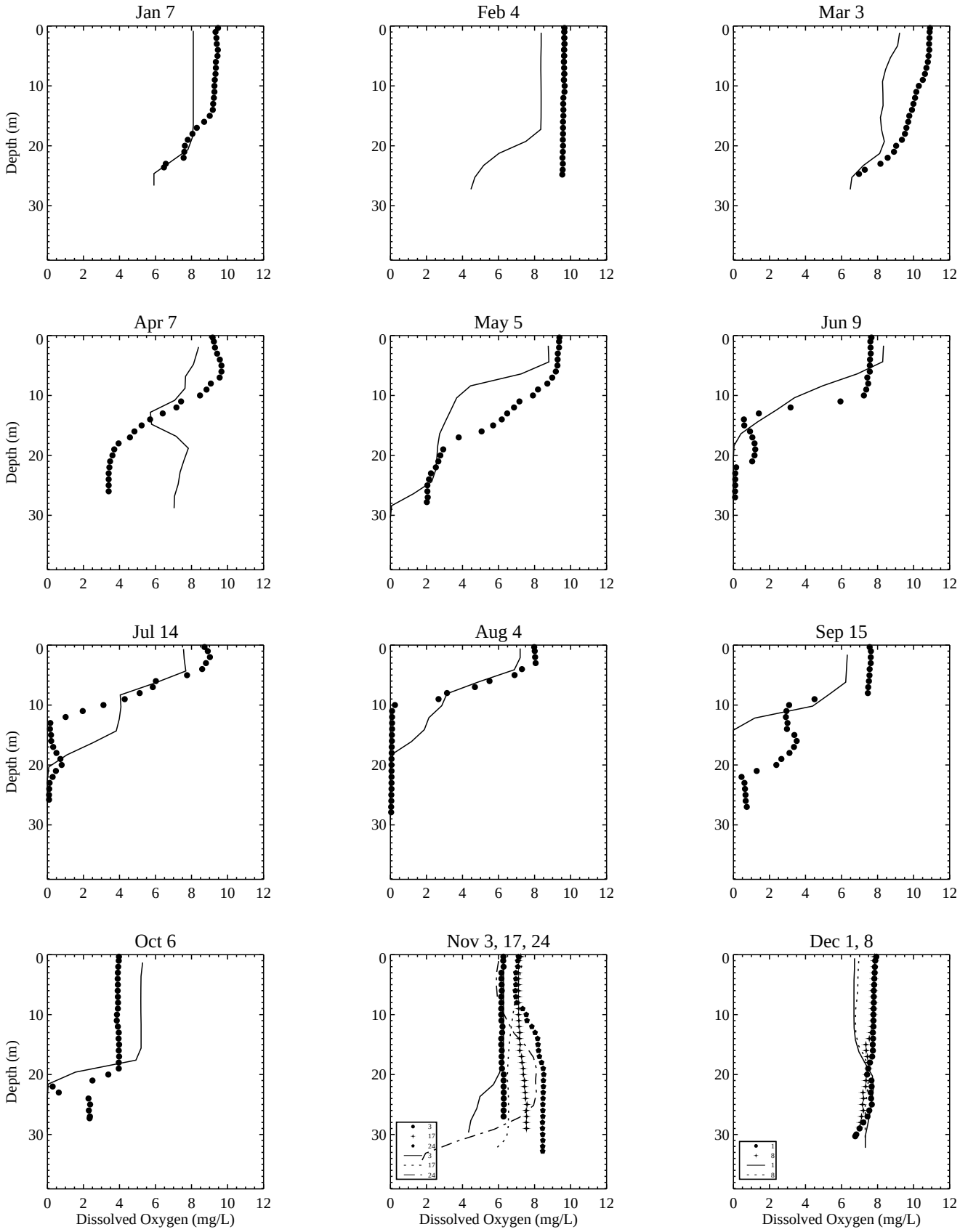

Figure J-18. Vertical profiles of model versus data at Pace Bend (Segment 48) - Dissolved Oxygen - 2004.

Profiles shown for dates with available data else model results for first day of month shown.

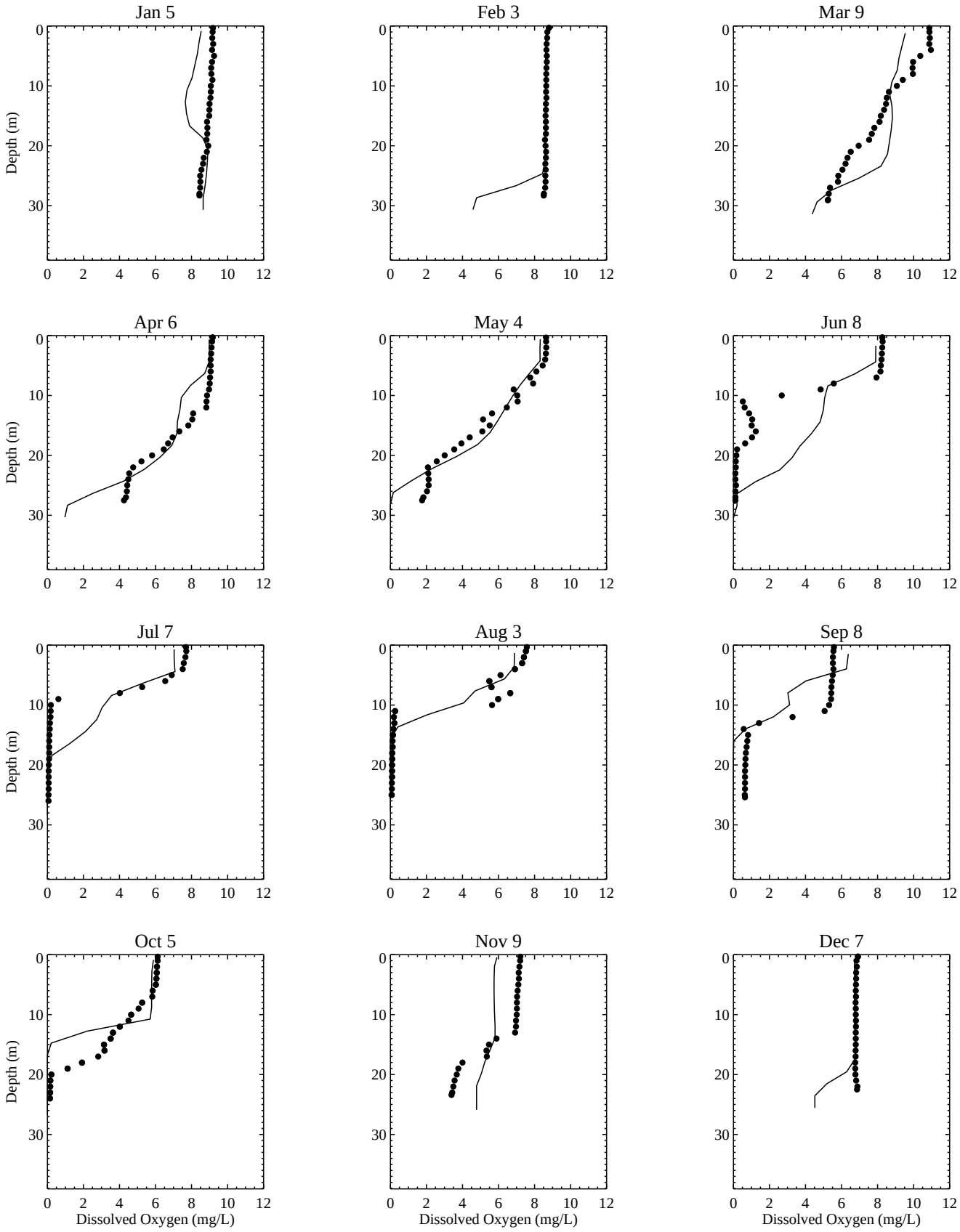

Figure J-18. Vertical profiles of model versus data at Pace Bend (Segment 48) - Dissolved Oxygen - 2005.

Profiles shown for dates with available data else model results for first day of month shown.

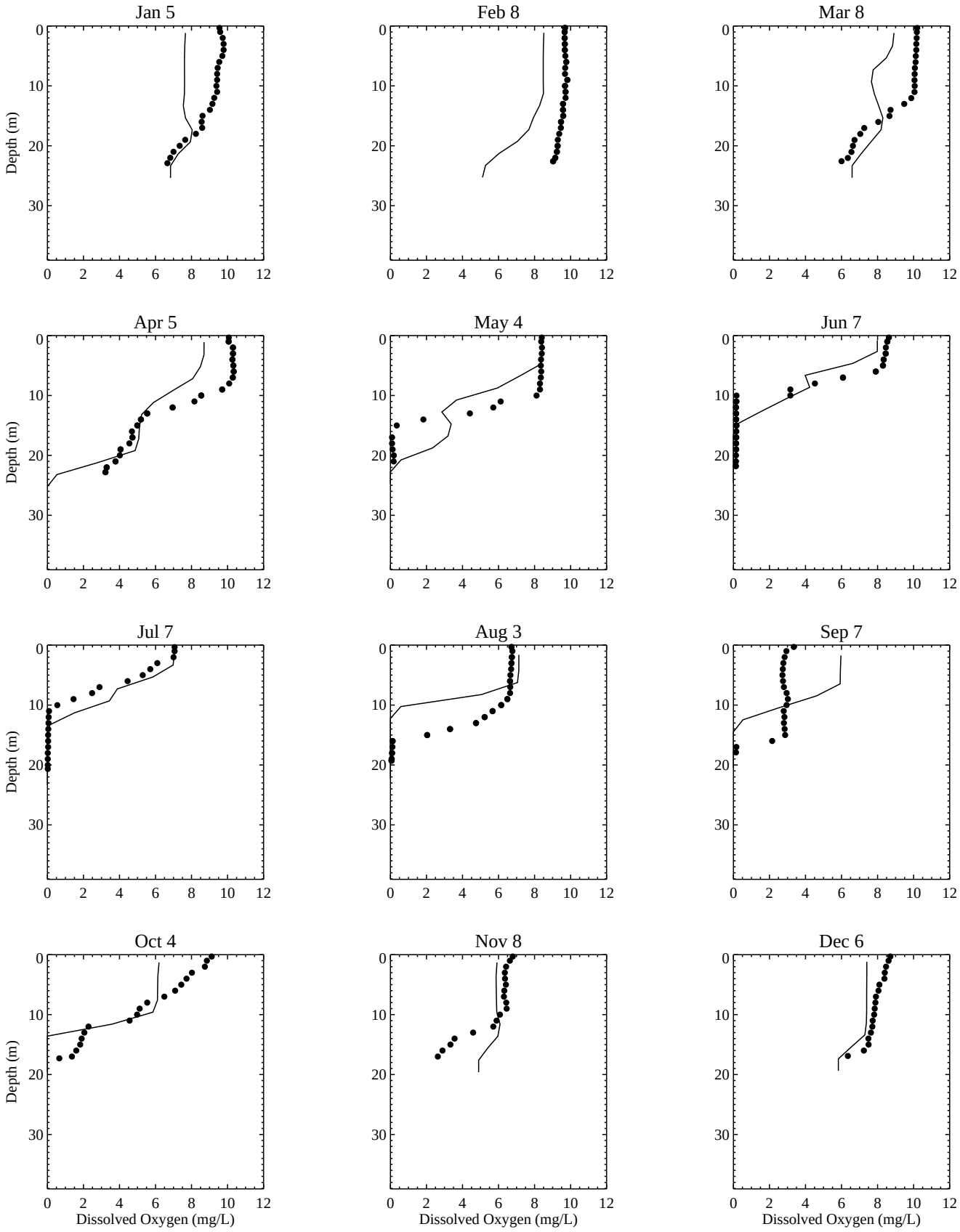

Figure J-18. Vertical profiles of model versus data at Pace Bend (Segment 48) - Dissolved Oxygen - 2006.

Profiles shown for dates with available data else model results for first day of month shown.

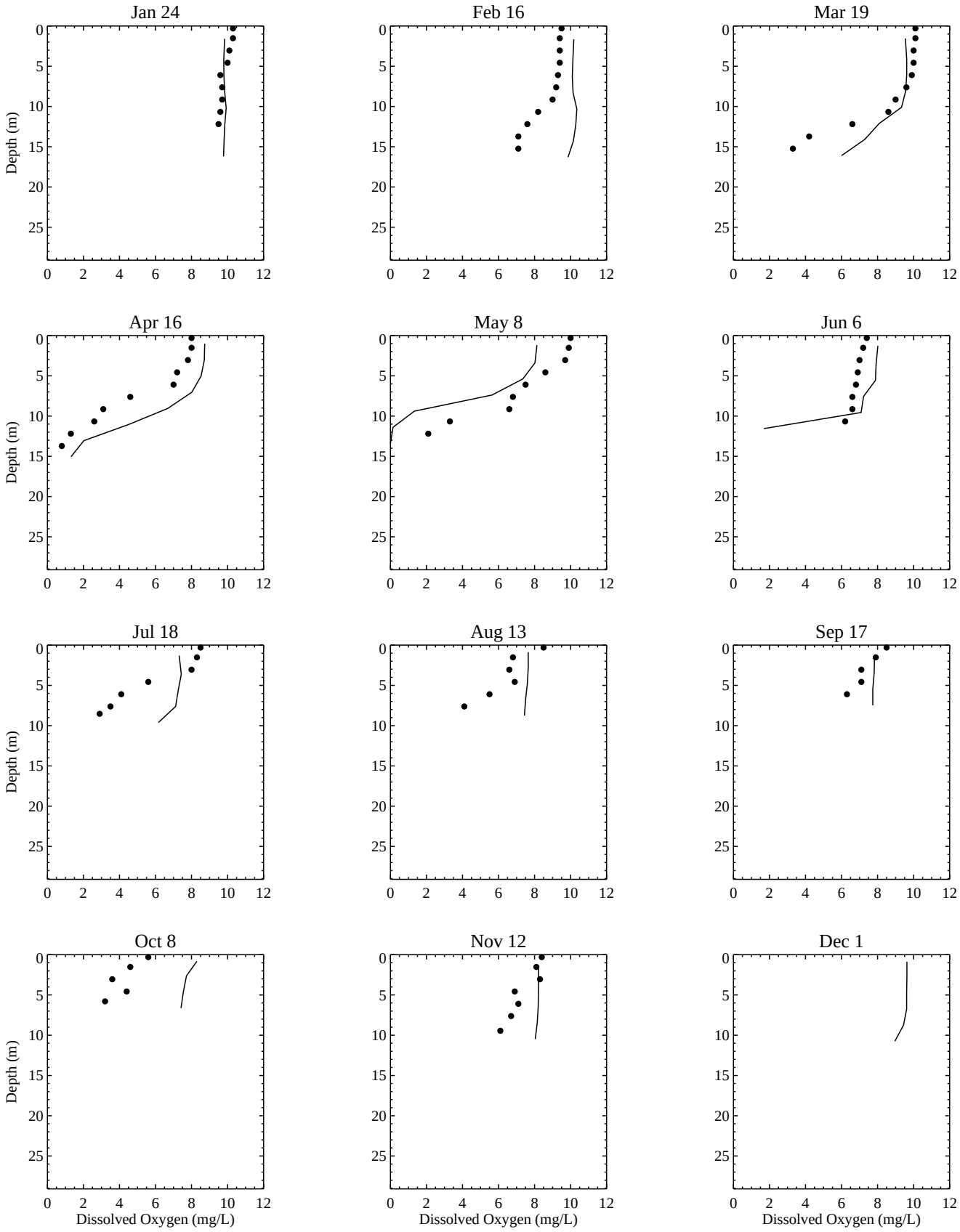

Figure J-19. Vertical profiles of model versus data at Turkey Bend (Segment 28) - Dissolved Oxygen - 1984.

Profiles shown for dates with available data else model results for first day of month shown.

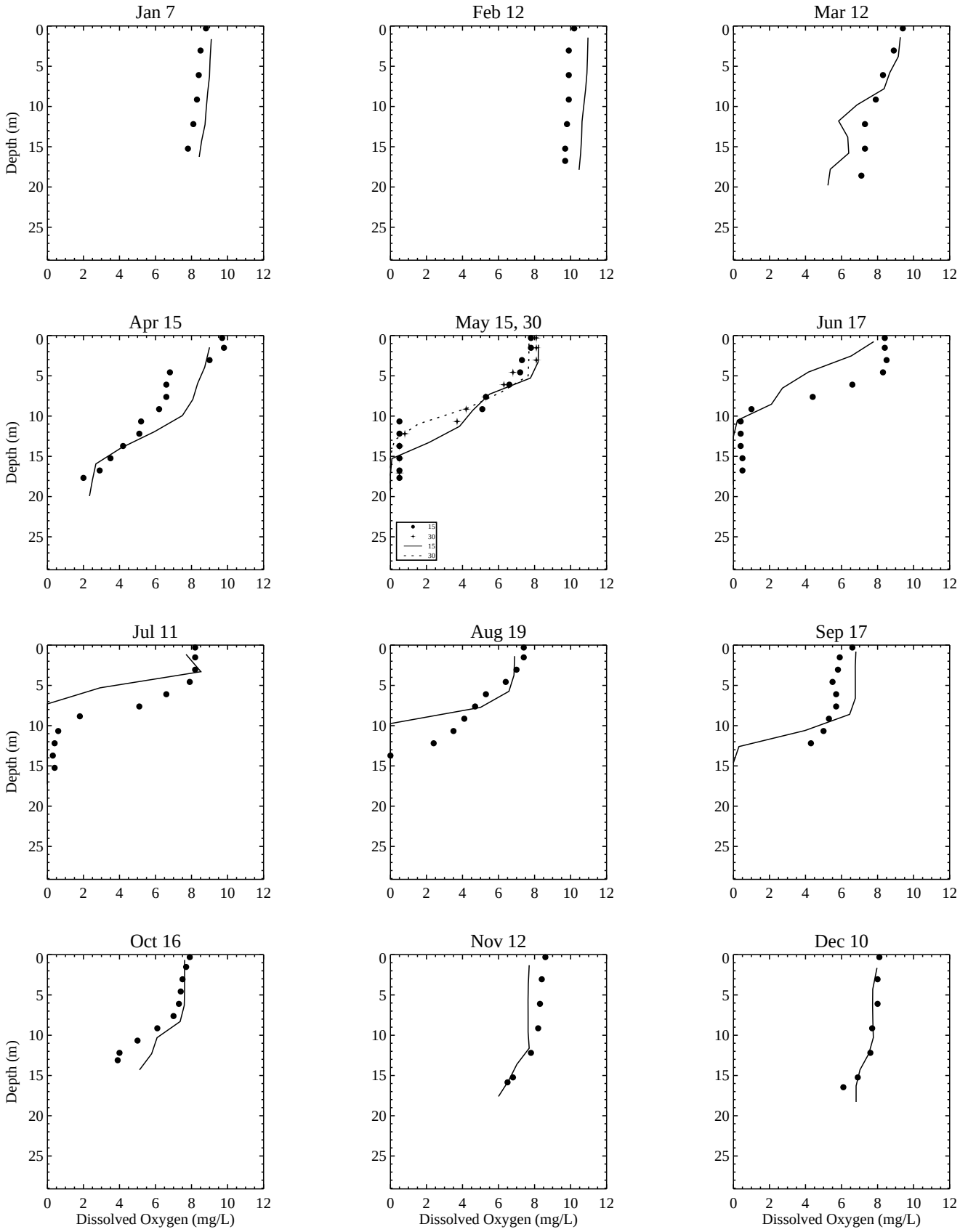

Figure J-19. Vertical profiles of model versus data at Turkey Bend (Segment 28) - Dissolved Oxygen - 1985.

Profiles shown for dates with available data else model results for first day of month shown.

Model Data

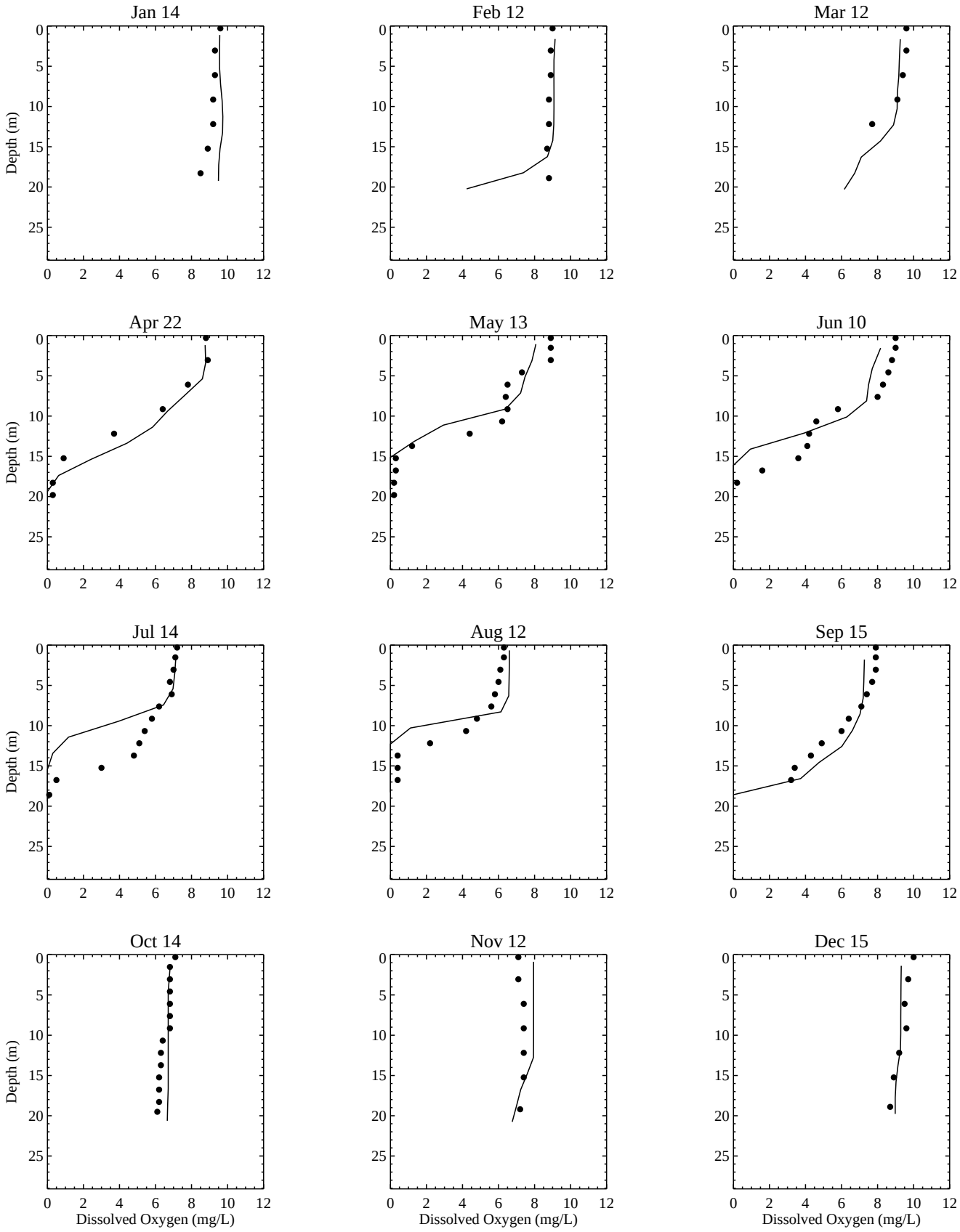

Figure J-19. Vertical profiles of model versus data at Turkey Bend (Segment 28) - Dissolved Oxygen - 1986.

Profiles shown for dates with available data else model results for first day of month shown.

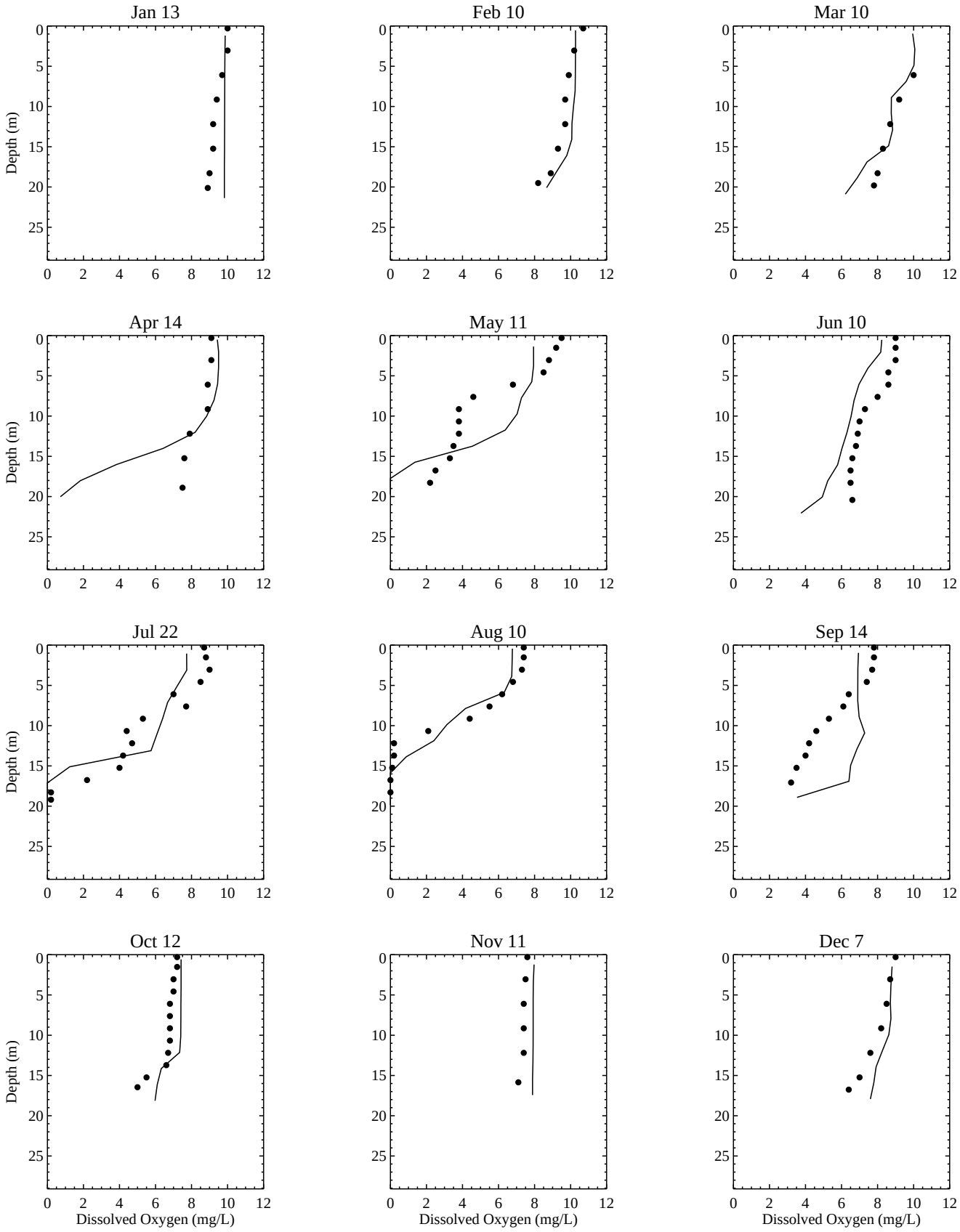

Figure J-19. Vertical profiles of model versus data at Turkey Bend (Segment 28) - Dissolved Oxygen - 1987.

Profiles shown for dates with available data else model results for first day of month shown.

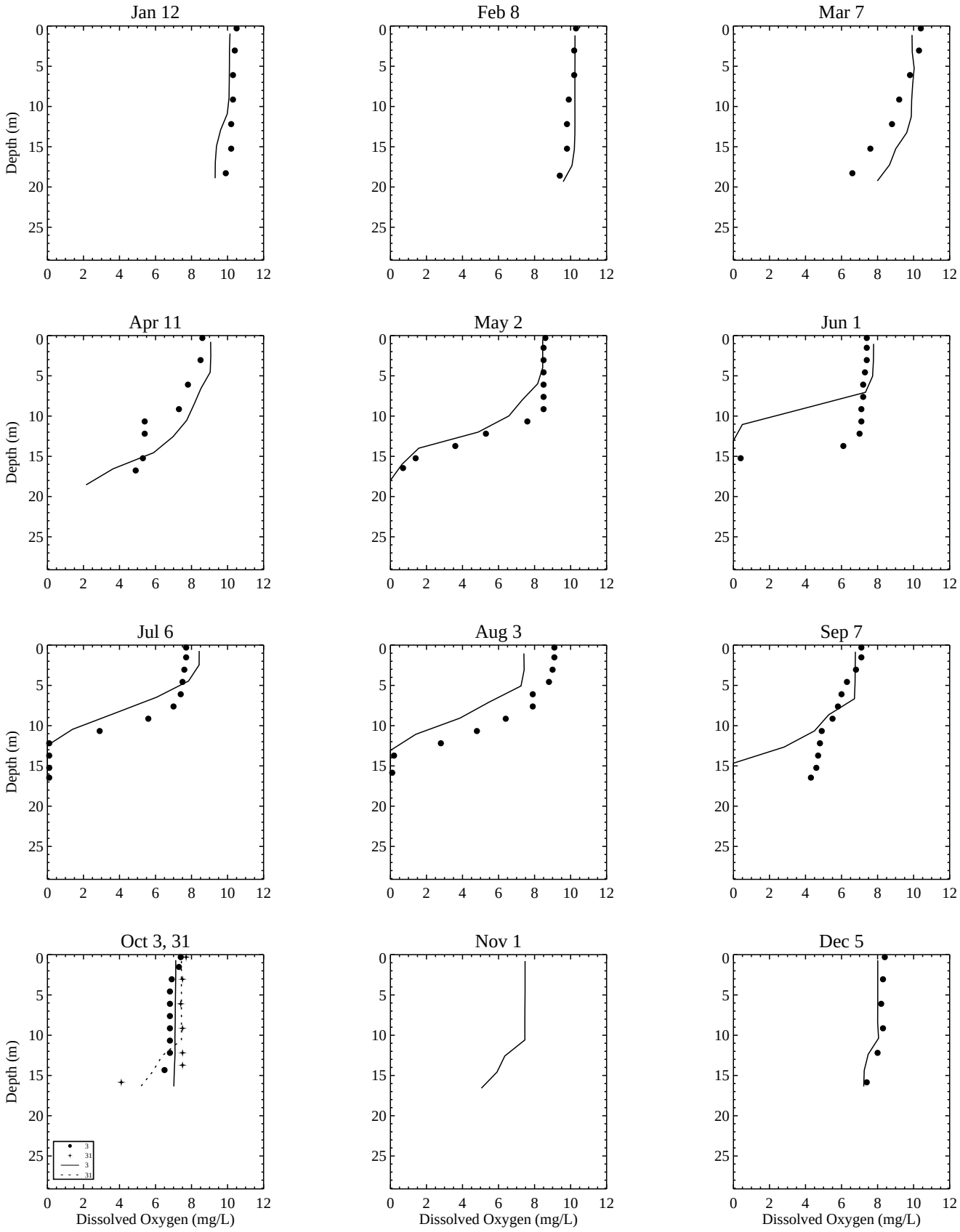

Figure J-19. Vertical profiles of model versus data at Turkey Bend (Segment 28) - Dissolved Oxygen - 1988.

Profiles shown for dates with available data else model results for first day of month shown.

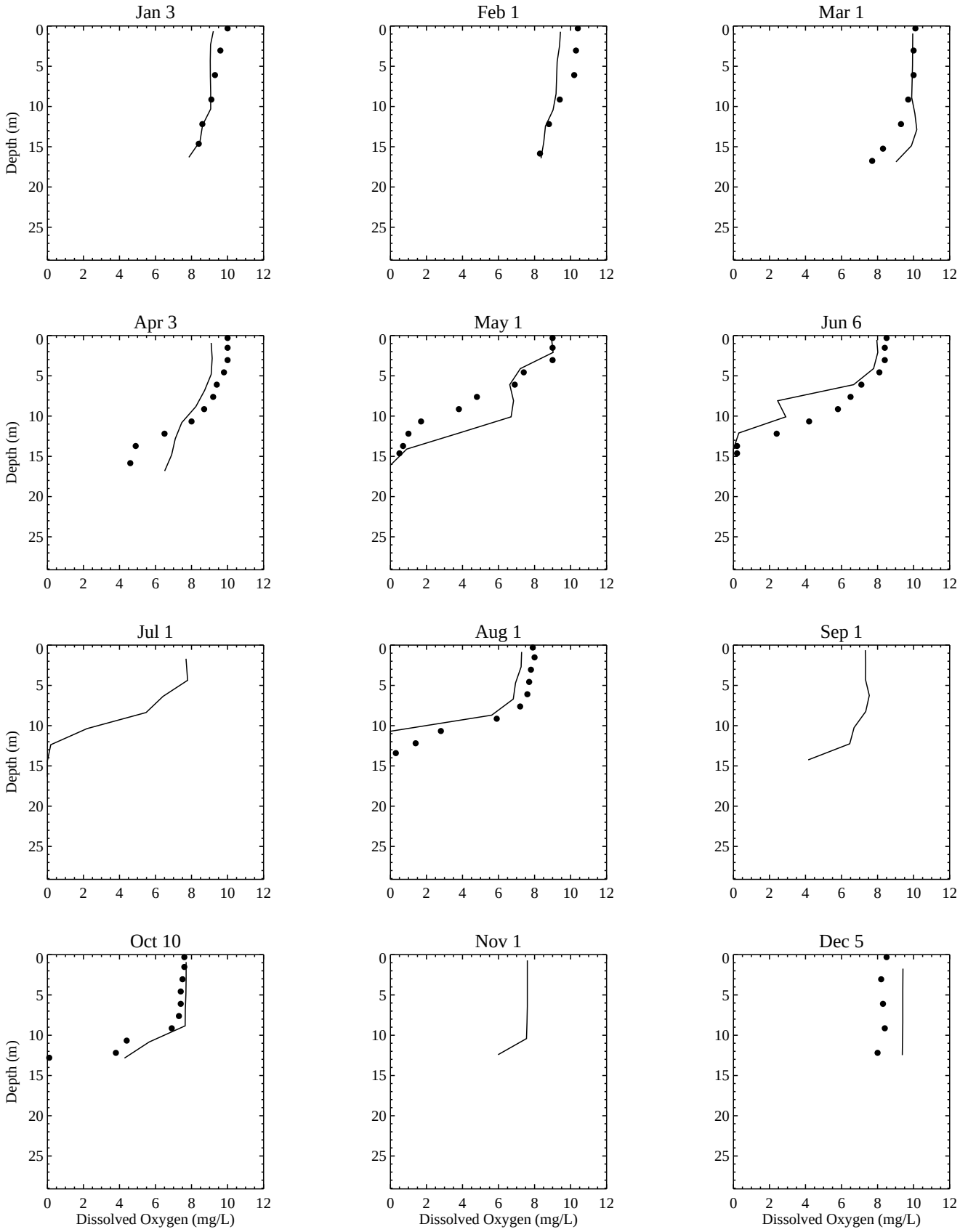

Figure J-19. Vertical profiles of model versus data at Turkey Bend (Segment 28) - Dissolved Oxygen - 1989.

Profiles shown for dates with available data else model results for first day of month shown.

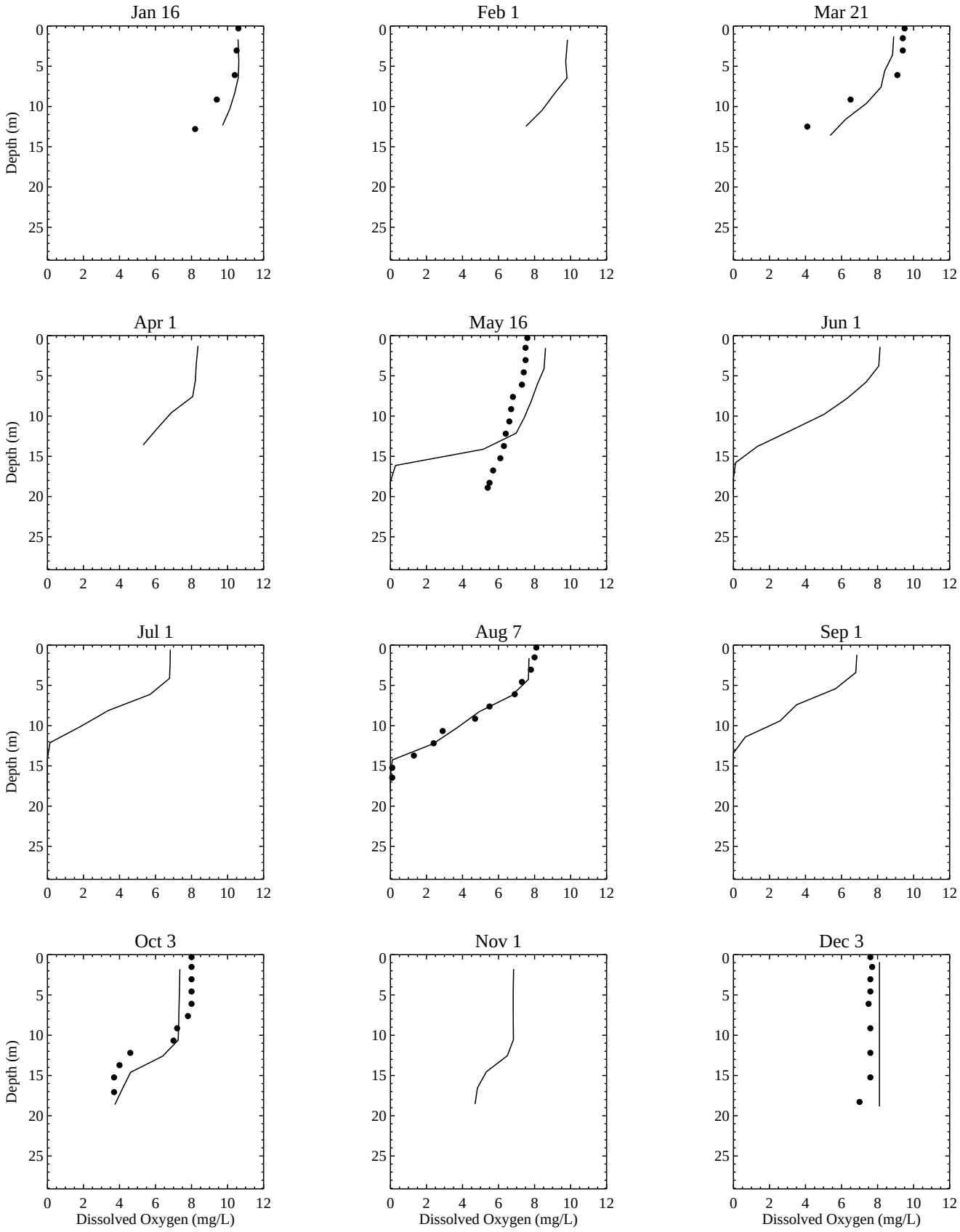

Figure J-19. Vertical profiles of model versus data at Turkey Bend (Segment 28) - Dissolved Oxygen - 1990.

Profiles shown for dates with available data else model results for first day of month shown.

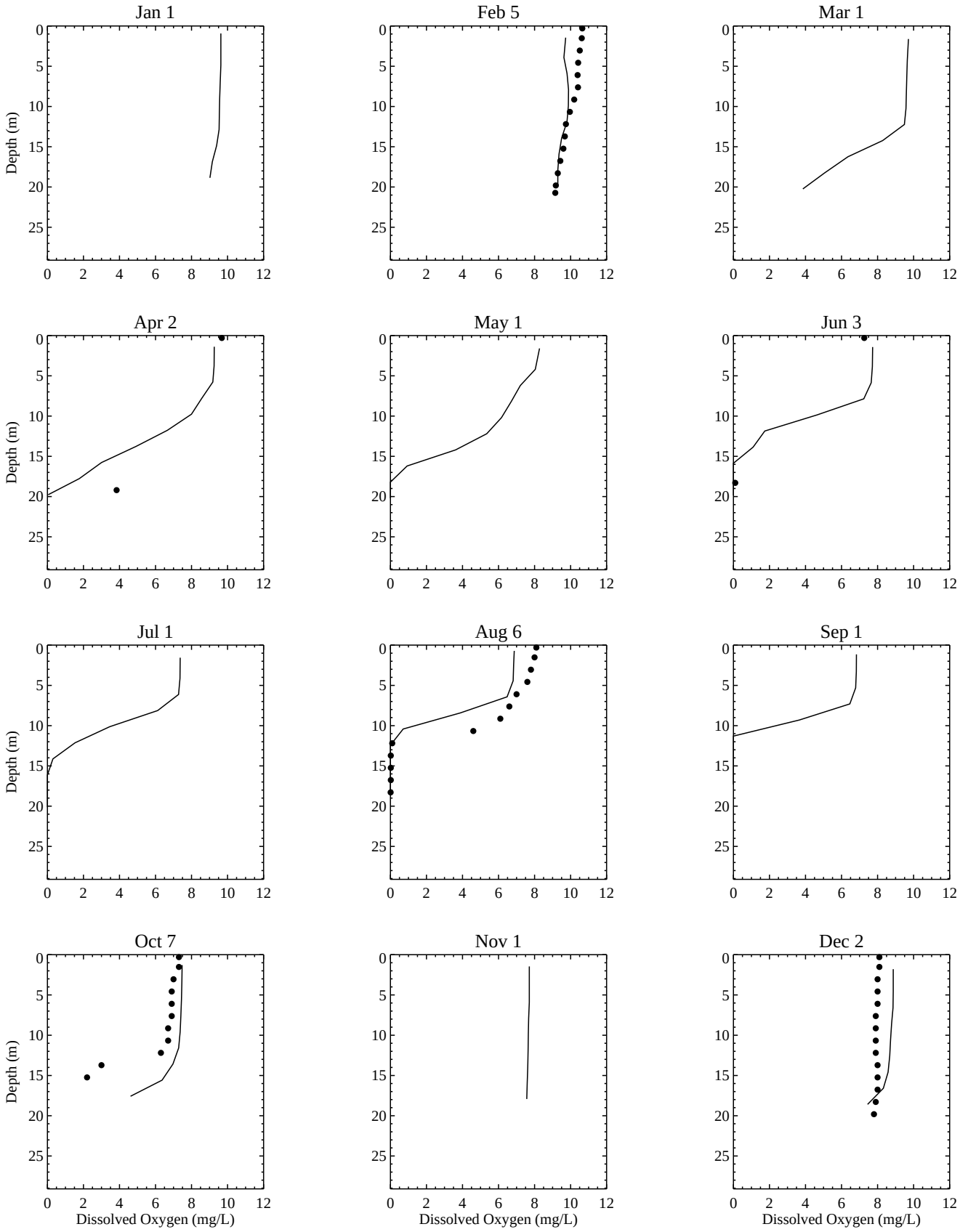

Figure J-19. Vertical profiles of model versus data at Turkey Bend (Segment 28) - Dissolved Oxygen - 1991.

Profiles shown for dates with available data else model results for first day of month shown.

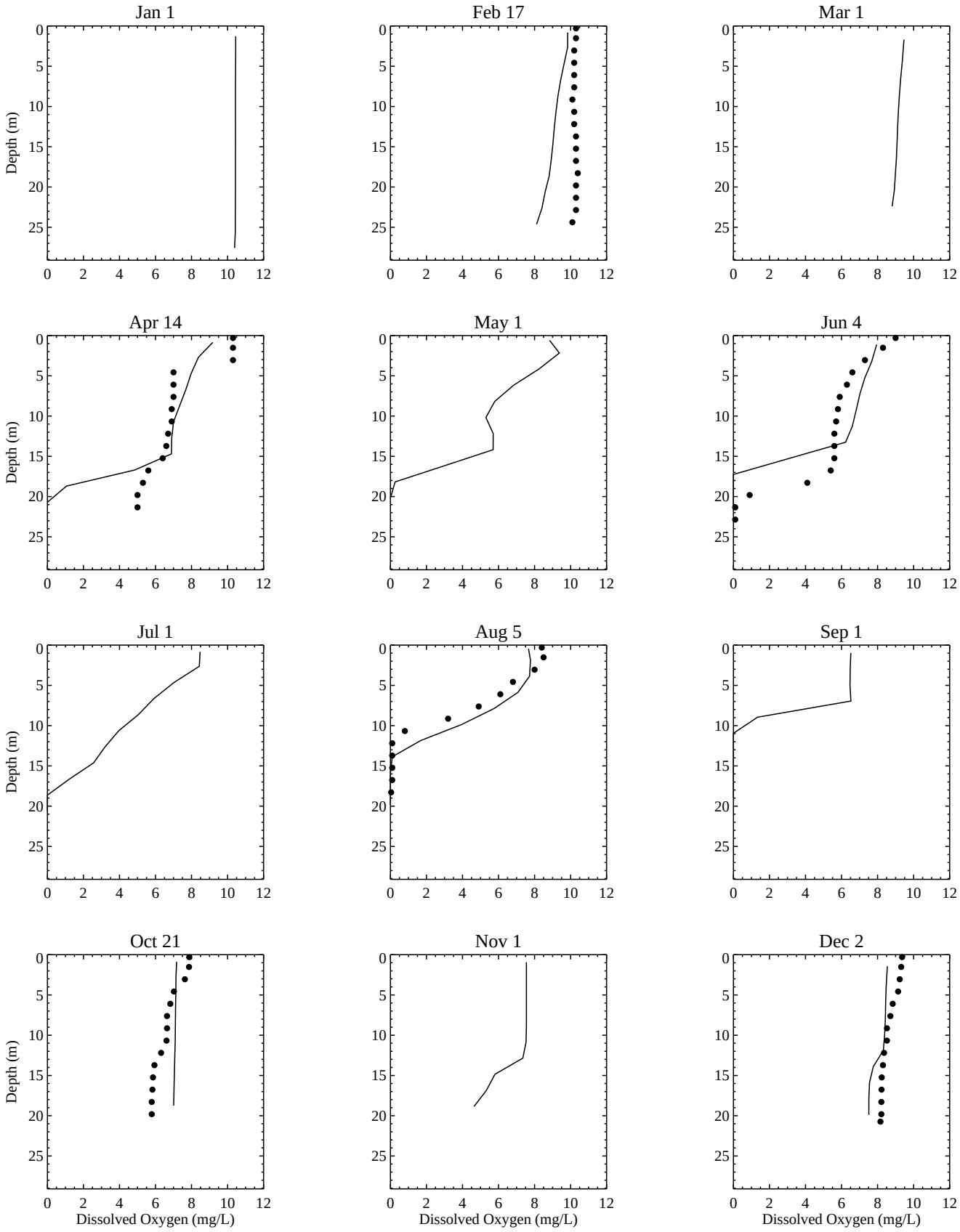

Figure J-19. Vertical profiles of model versus data at Turkey Bend (Segment 28) - Dissolved Oxygen - 1992.

Profiles shown for dates with available data else model results for first day of month shown.

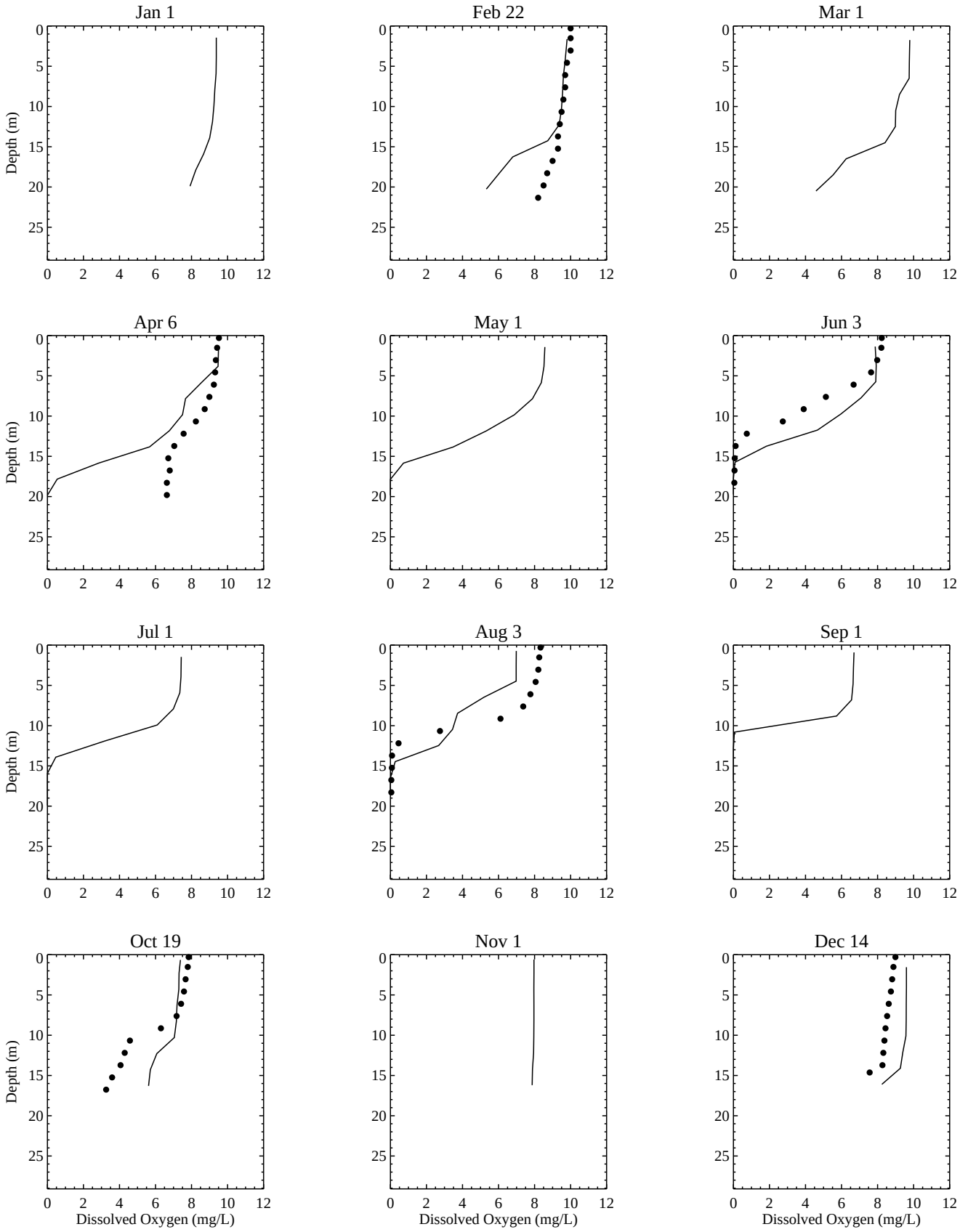

Figure J-19. Vertical profiles of model versus data at Turkey Bend (Segment 28) - Dissolved Oxygen - 1993.

Profiles shown for dates with available data else model results for first day of month shown.

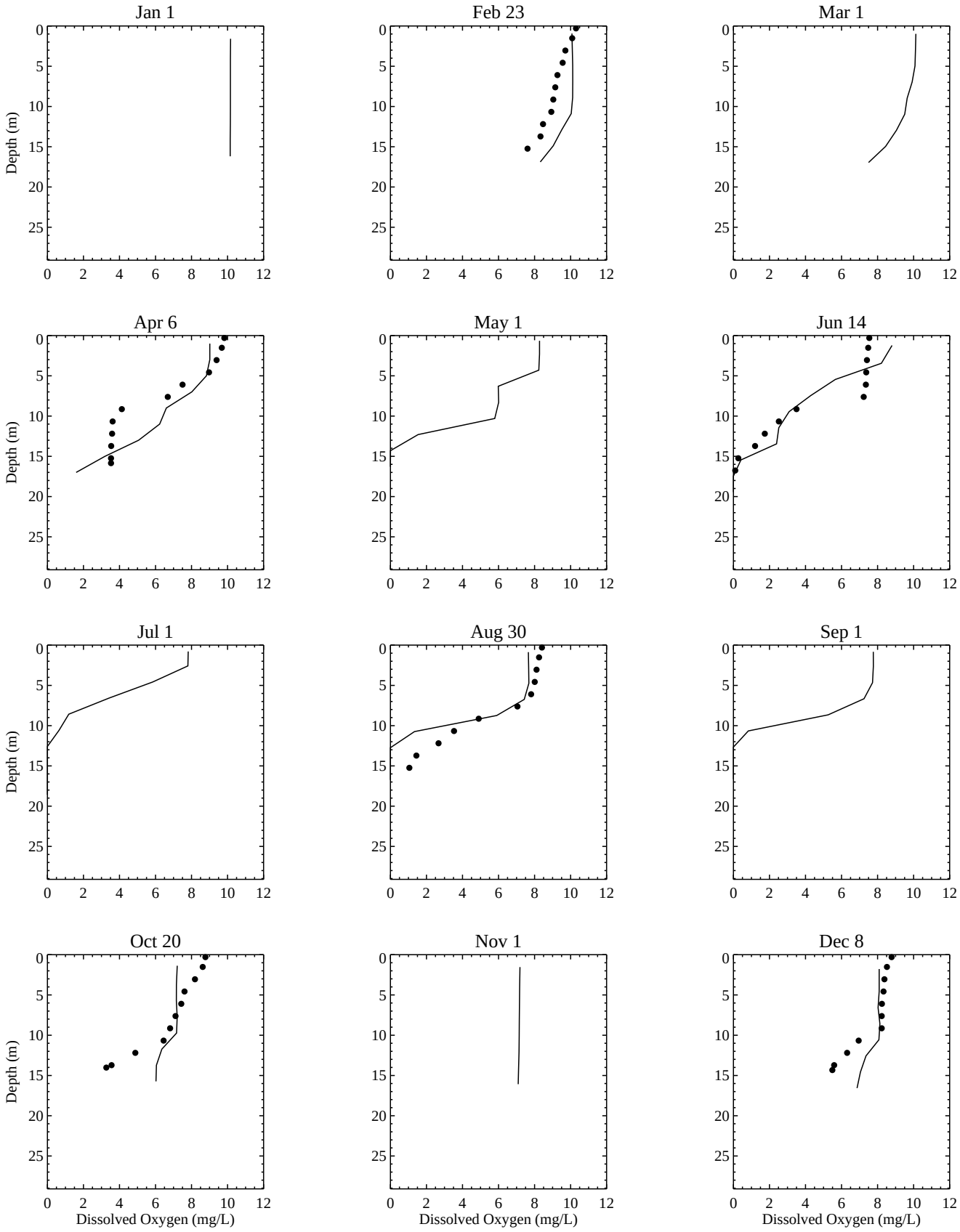

Figure J-19. Vertical profiles of model versus data at Turkey Bend (Segment 28) - Dissolved Oxygen - 1994.

Profiles shown for dates with available data else model results for first day of month shown.

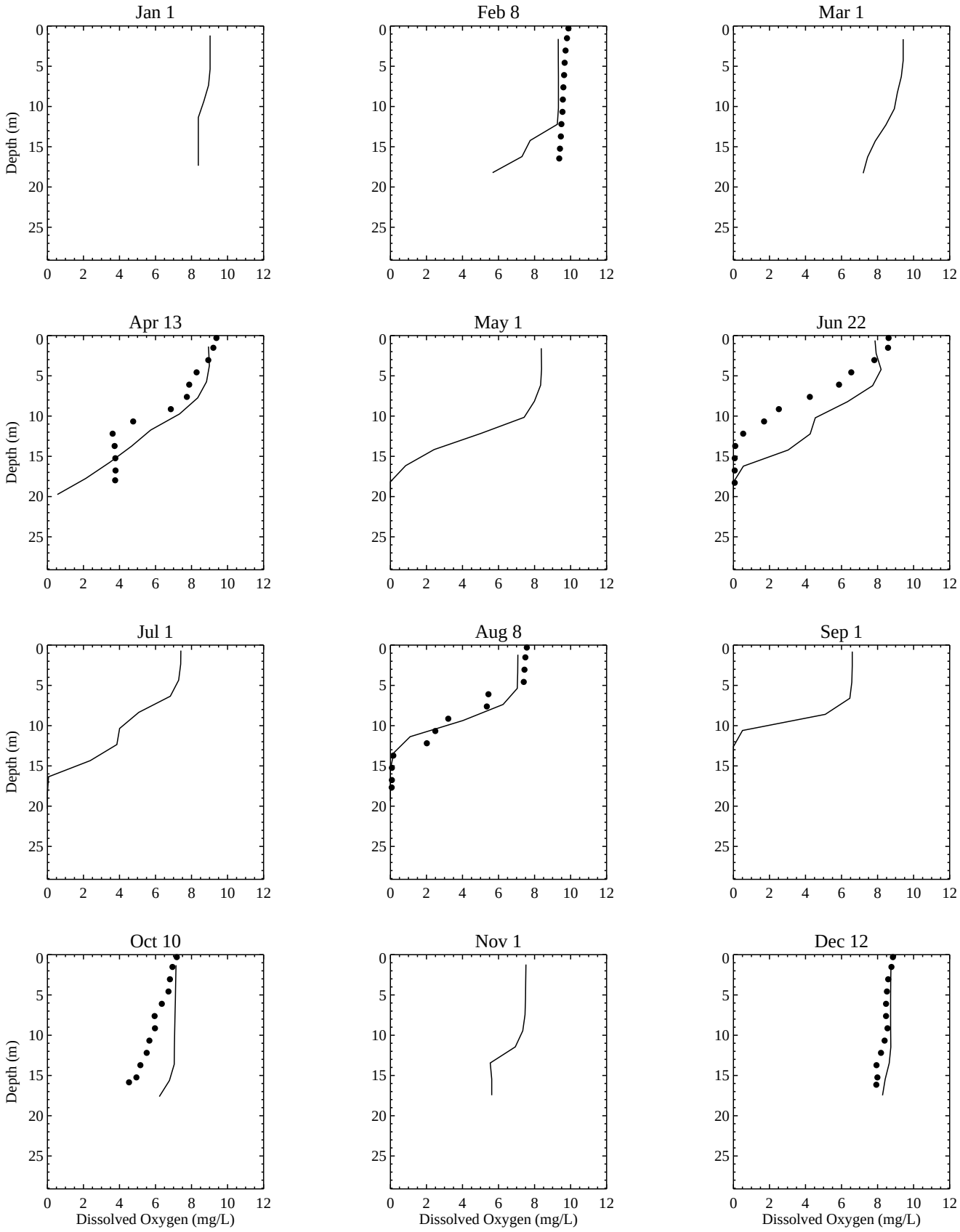

Figure J-19. Vertical profiles of model versus data at Turkey Bend (Segment 28) - Dissolved Oxygen - 1995.

Profiles shown for dates with available data else model results for first day of month shown.

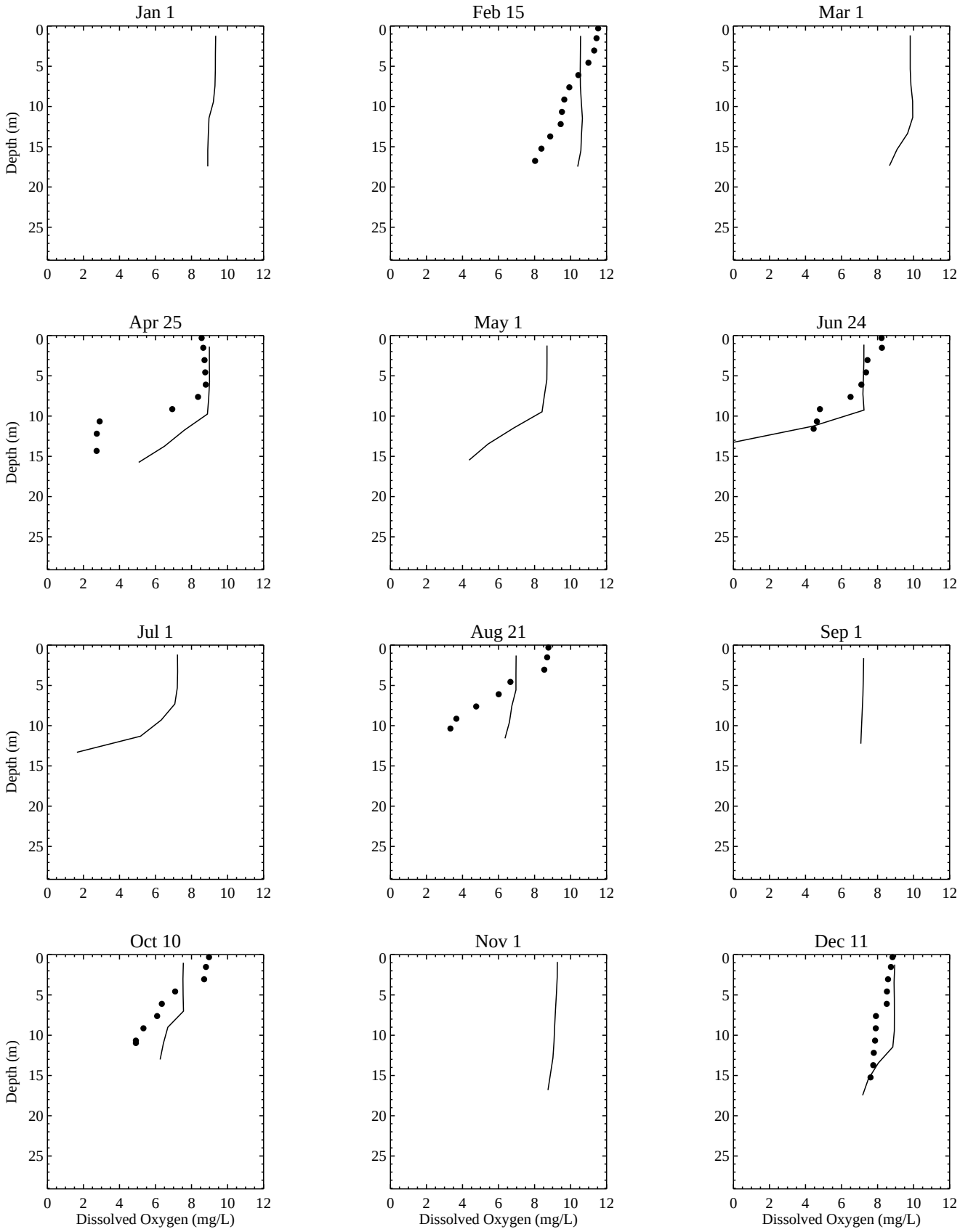

Figure J-19. Vertical profiles of model versus data at Turkey Bend (Segment 28) - Dissolved Oxygen - 1996.

Profiles shown for dates with available data else model results for first day of month shown.

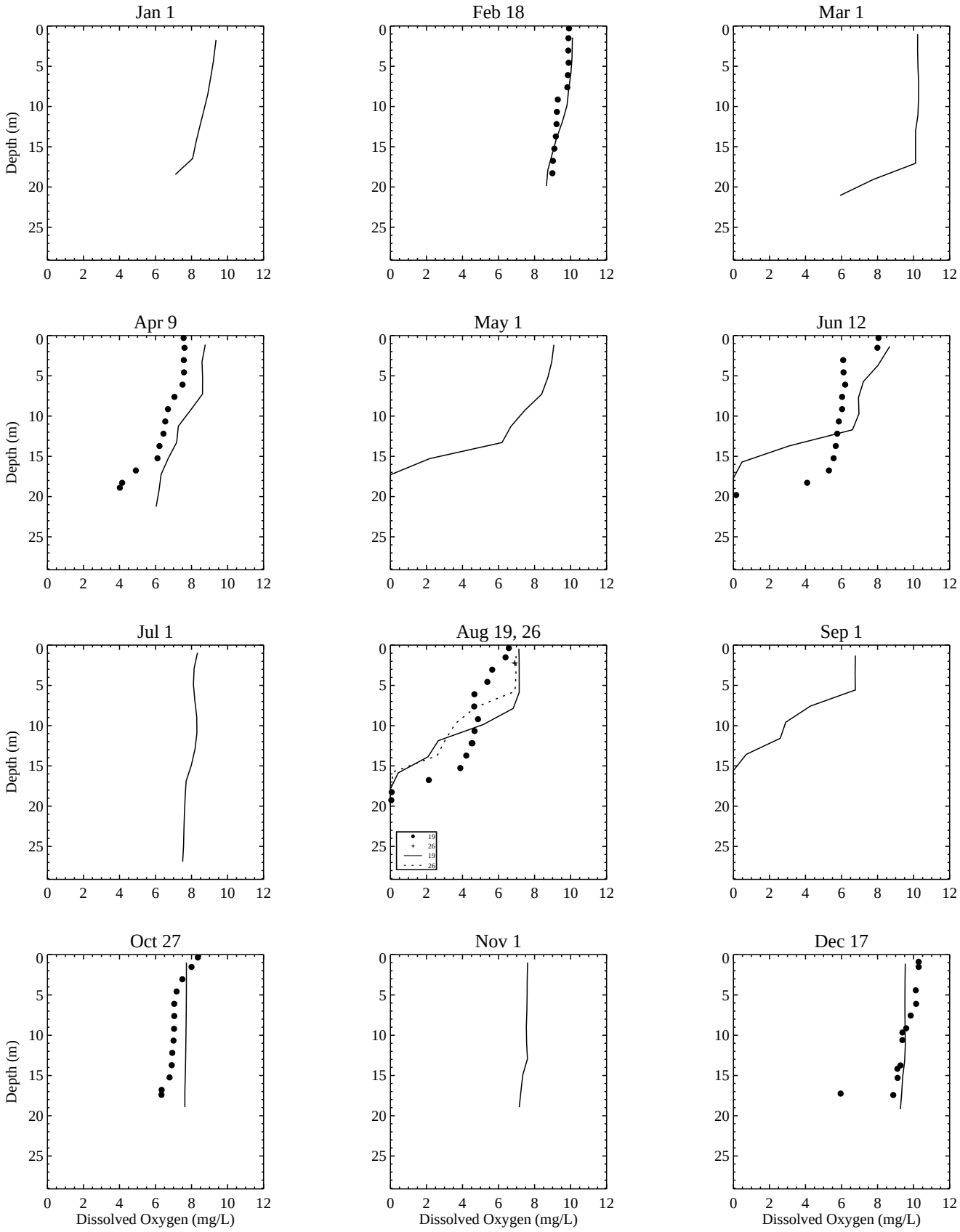

Figure J-19. Vertical profiles of model versus data at Turkey Bend (Segment 28) - Dissolved Oxygen - 1997.

Profiles shown for dates with available data else model results for first day of month shown.

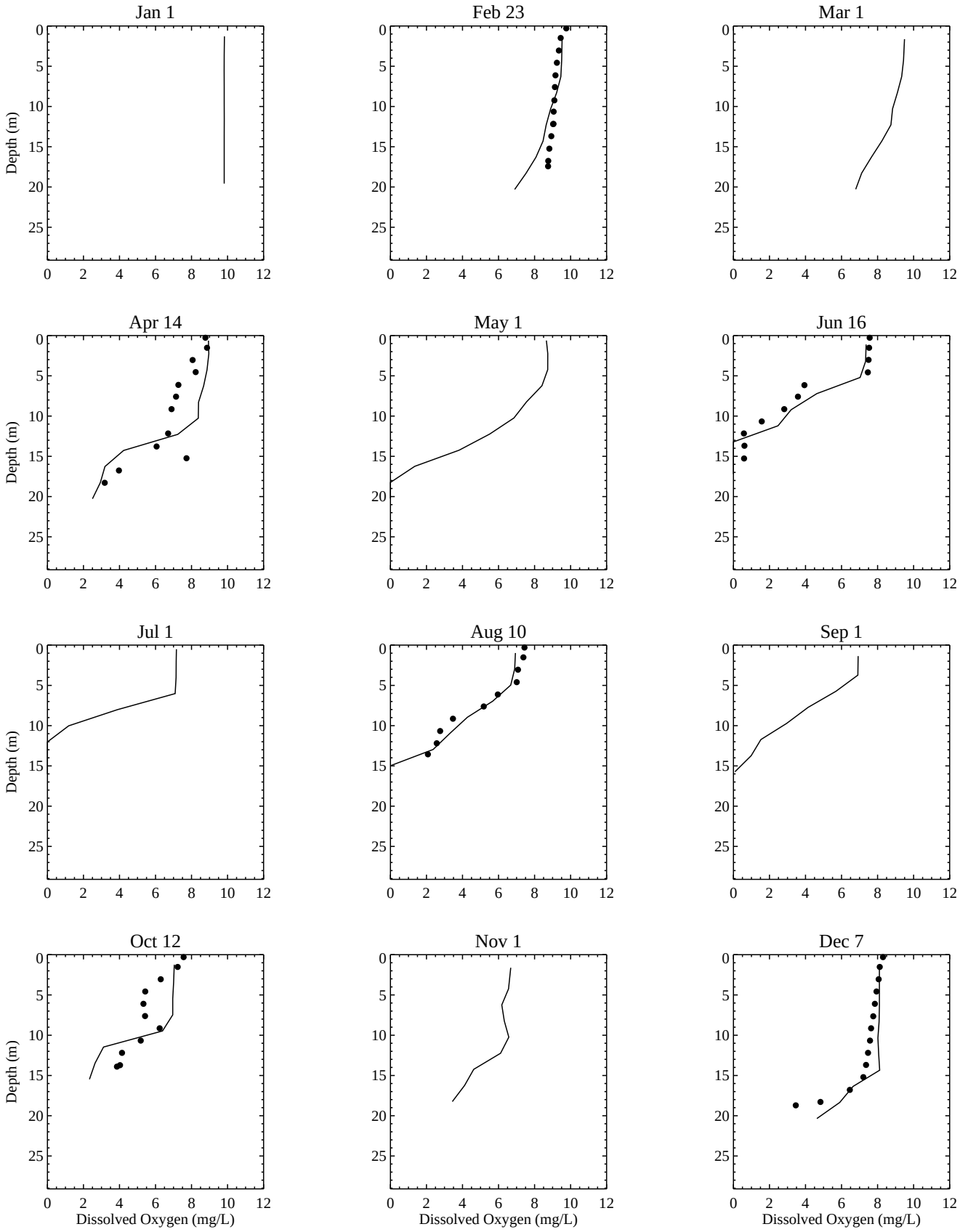

Figure J-19. Vertical profiles of model versus data at Turkey Bend (Segment 28) - Dissolved Oxygen - 1998.

Profiles shown for dates with available data else model results for first day of month shown.

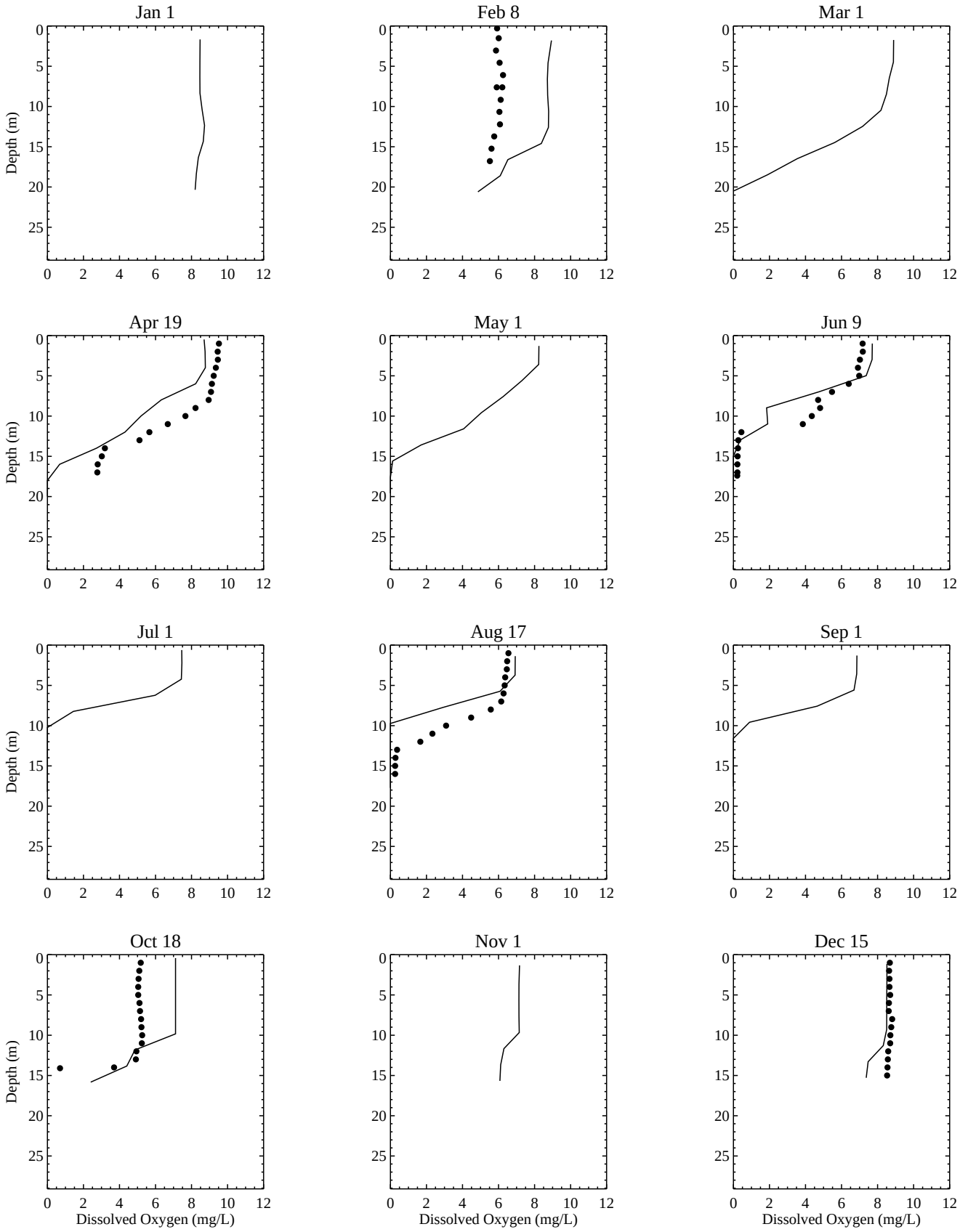

Figure J-19. Vertical profiles of model versus data at Turkey Bend (Segment 28) - Dissolved Oxygen - 1999.

Profiles shown for dates with available data else model results for first day of month shown.

Model Data

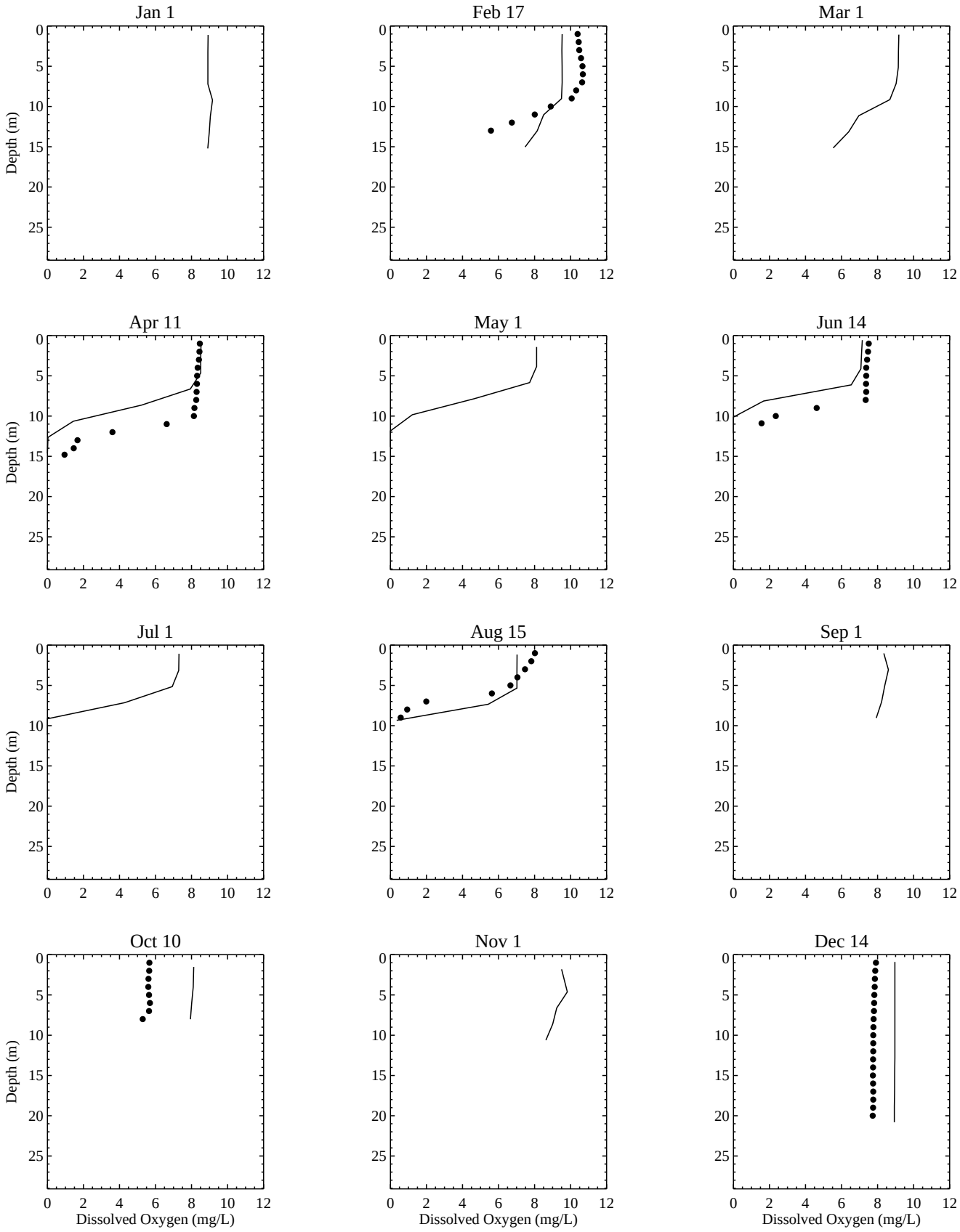

Figure J-19. Vertical profiles of model versus data at Turkey Bend (Segment 28) - Dissolved Oxygen - 2000.

Profiles shown for dates with available data else model results for first day of month shown.

Model Data

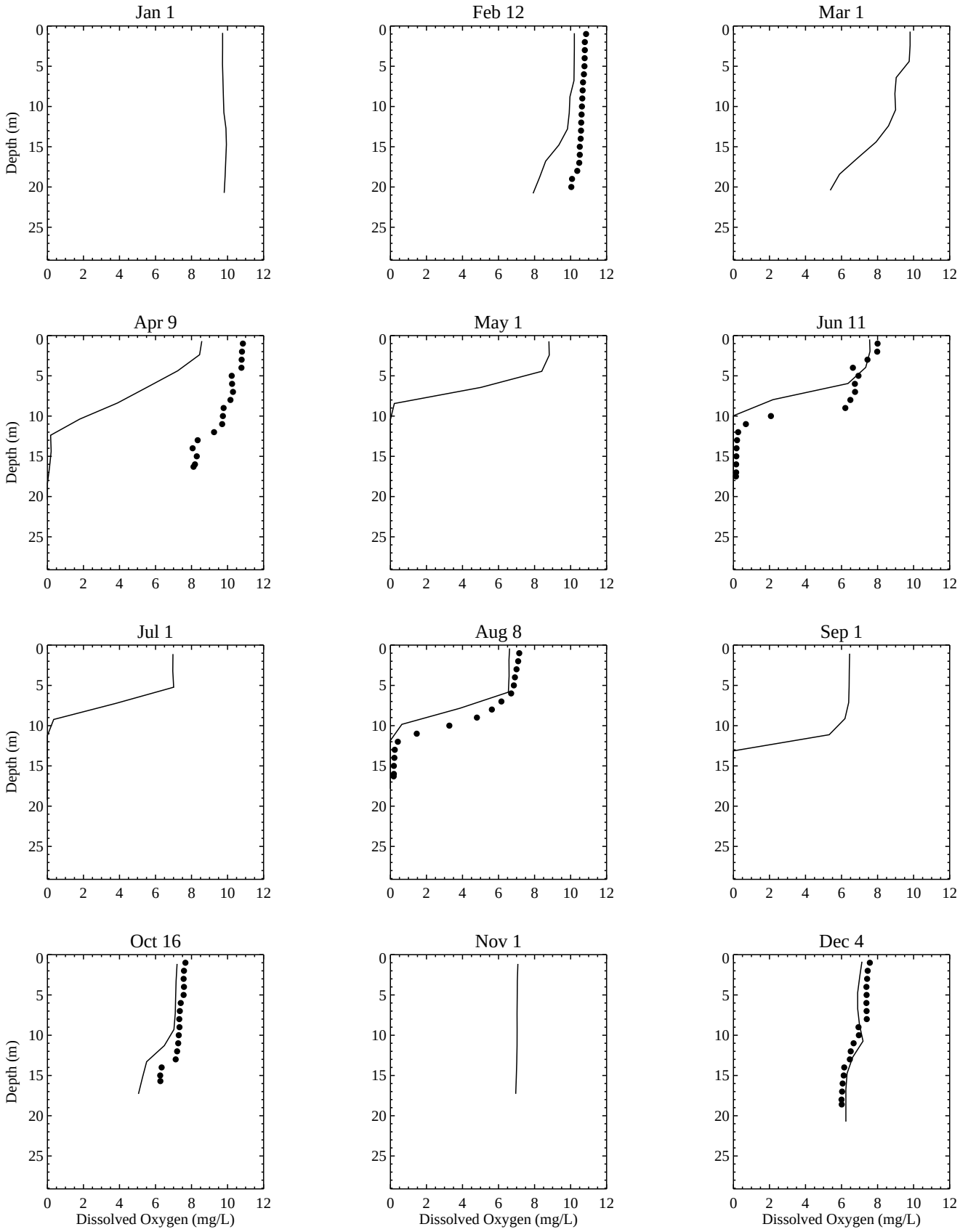

Figure J-19. Vertical profiles of model versus data at Turkey Bend (Segment 28) - Dissolved Oxygen - 2001.

Profiles shown for dates with available data else model results for first day of month shown.

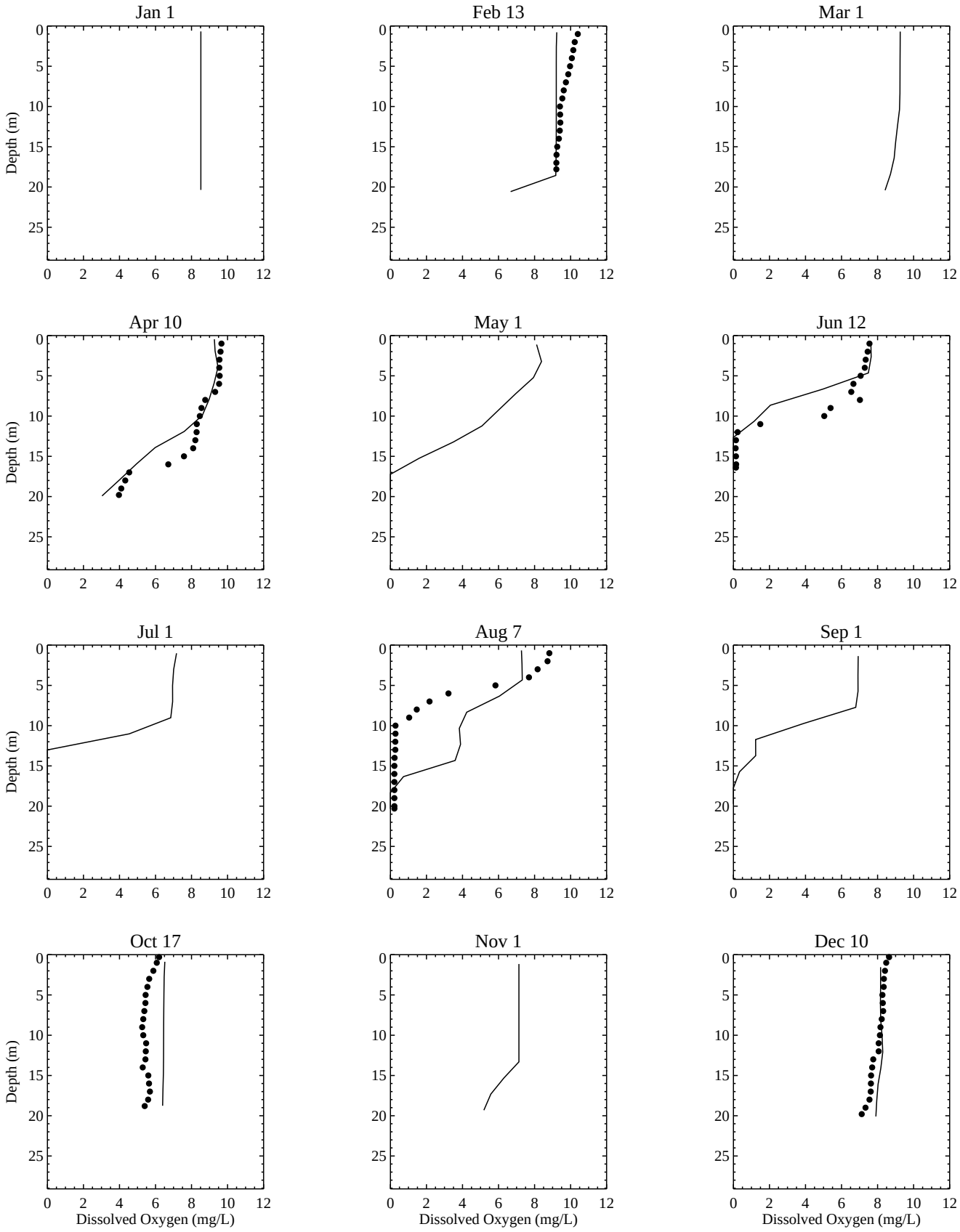

Figure J-19. Vertical profiles of model versus data at Turkey Bend (Segment 28) - Dissolved Oxygen - 2002.

Profiles shown for dates with available data else model results for first day of month shown.

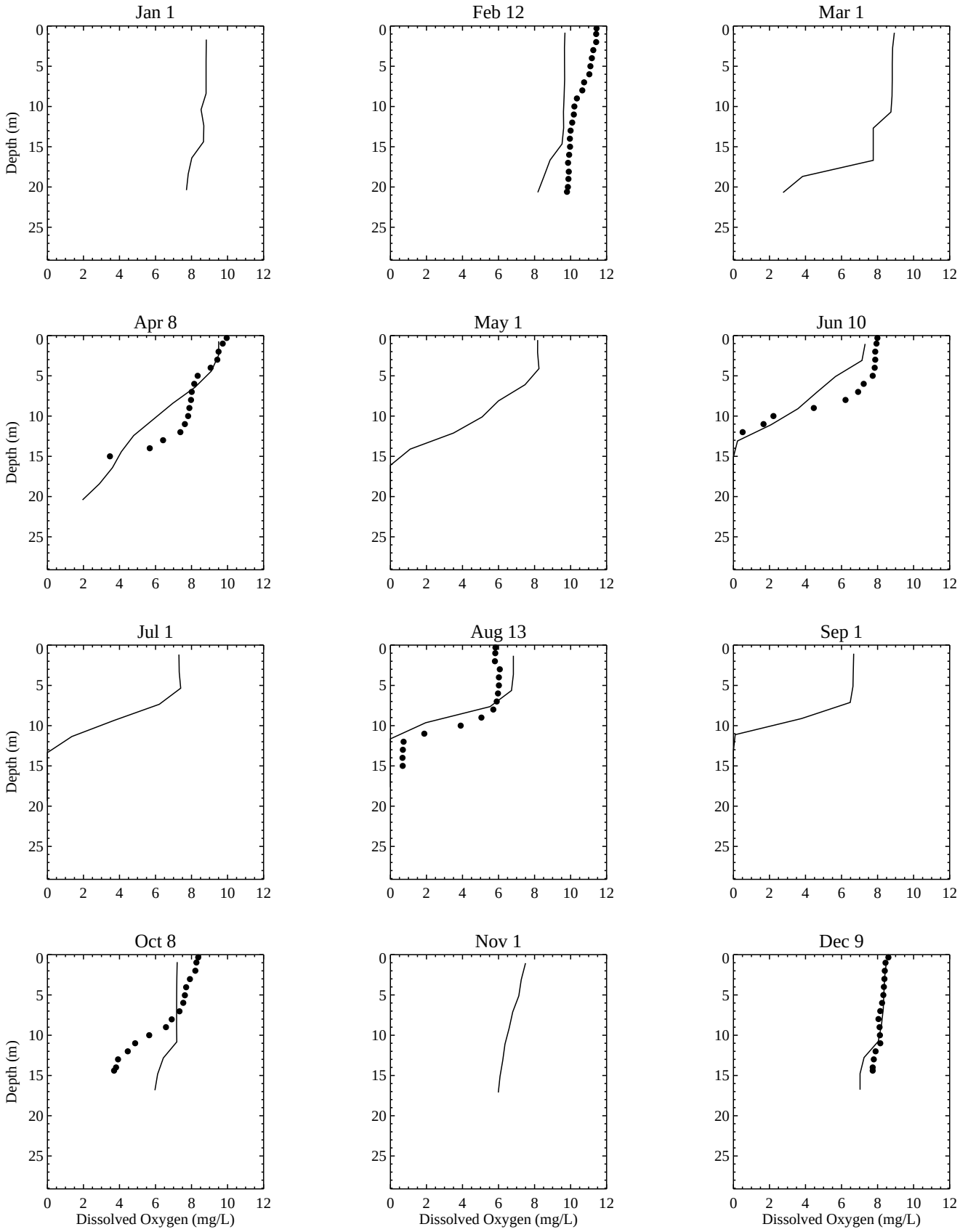

Figure J-19. Vertical profiles of model versus data at Turkey Bend (Segment 28) - Dissolved Oxygen - 2003.

Profiles shown for dates with available data else model results for first day of month shown.

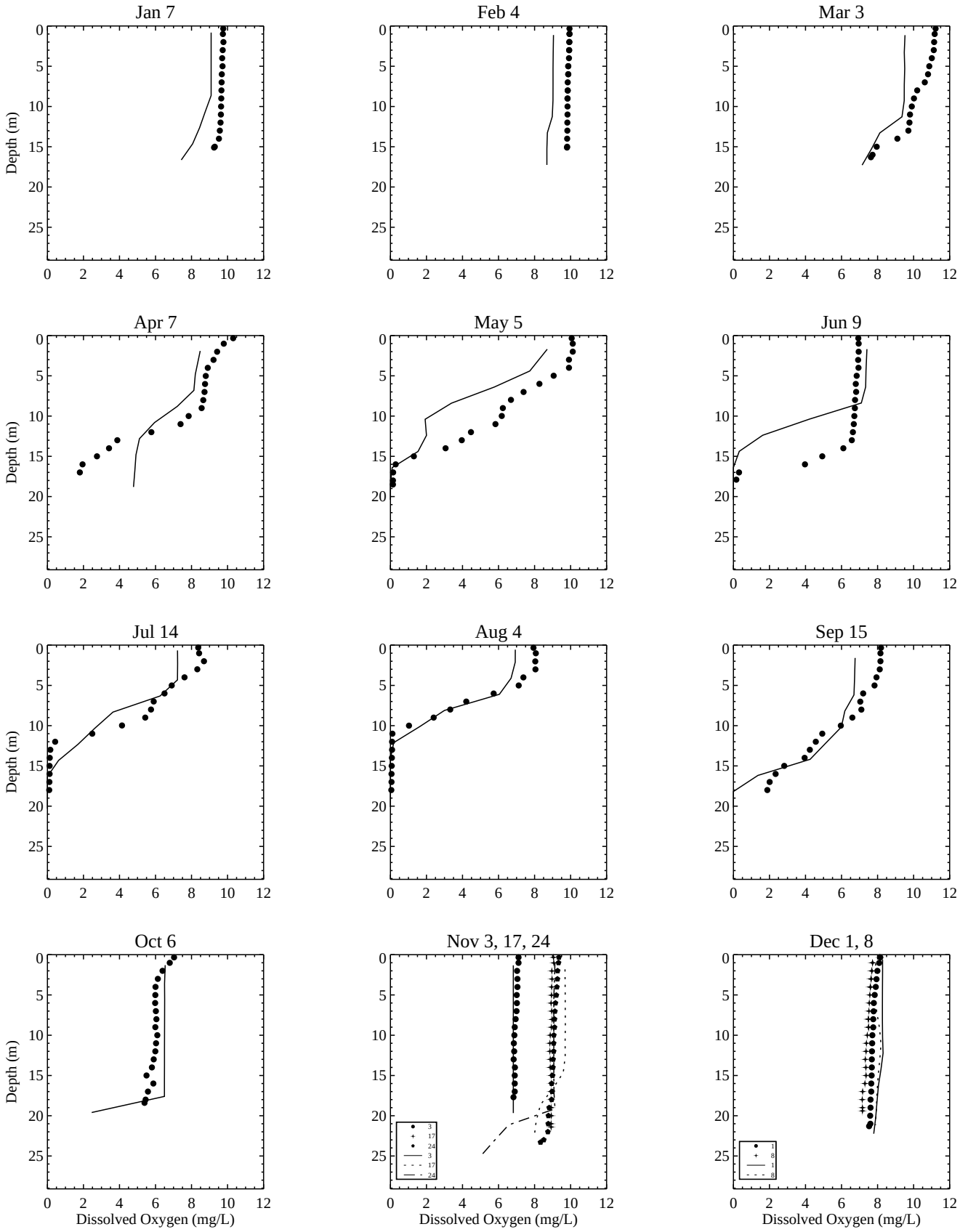

Figure J-19. Vertical profiles of model versus data at Turkey Bend (Segment 28) - Dissolved Oxygen - 2004.

Profiles shown for dates with available data else model results for first day of month shown.

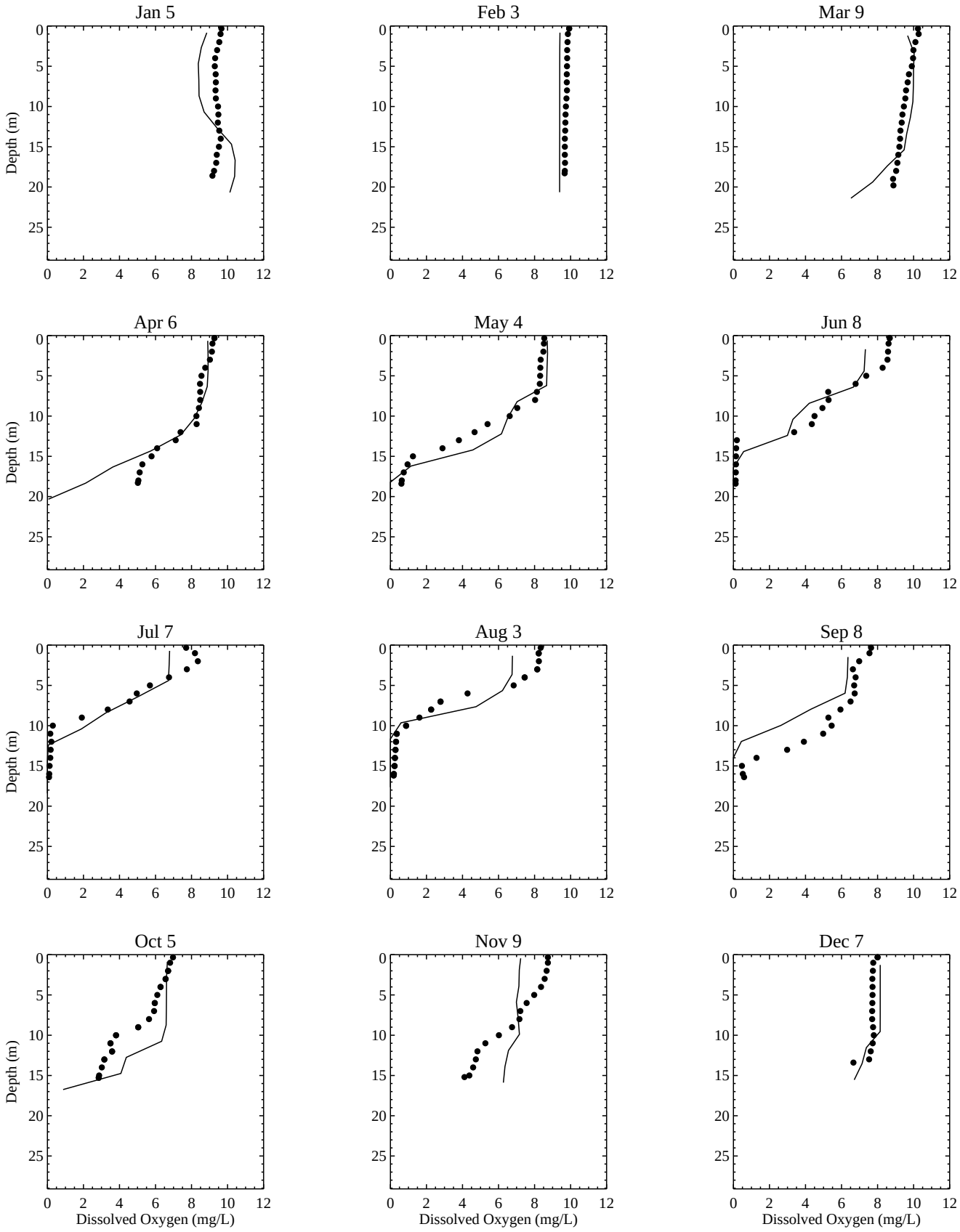

Figure J-19. Vertical profiles of model versus data at Turkey Bend (Segment 28) - Dissolved Oxygen - 2005.

Profiles shown for dates with available data else model results for first day of month shown.

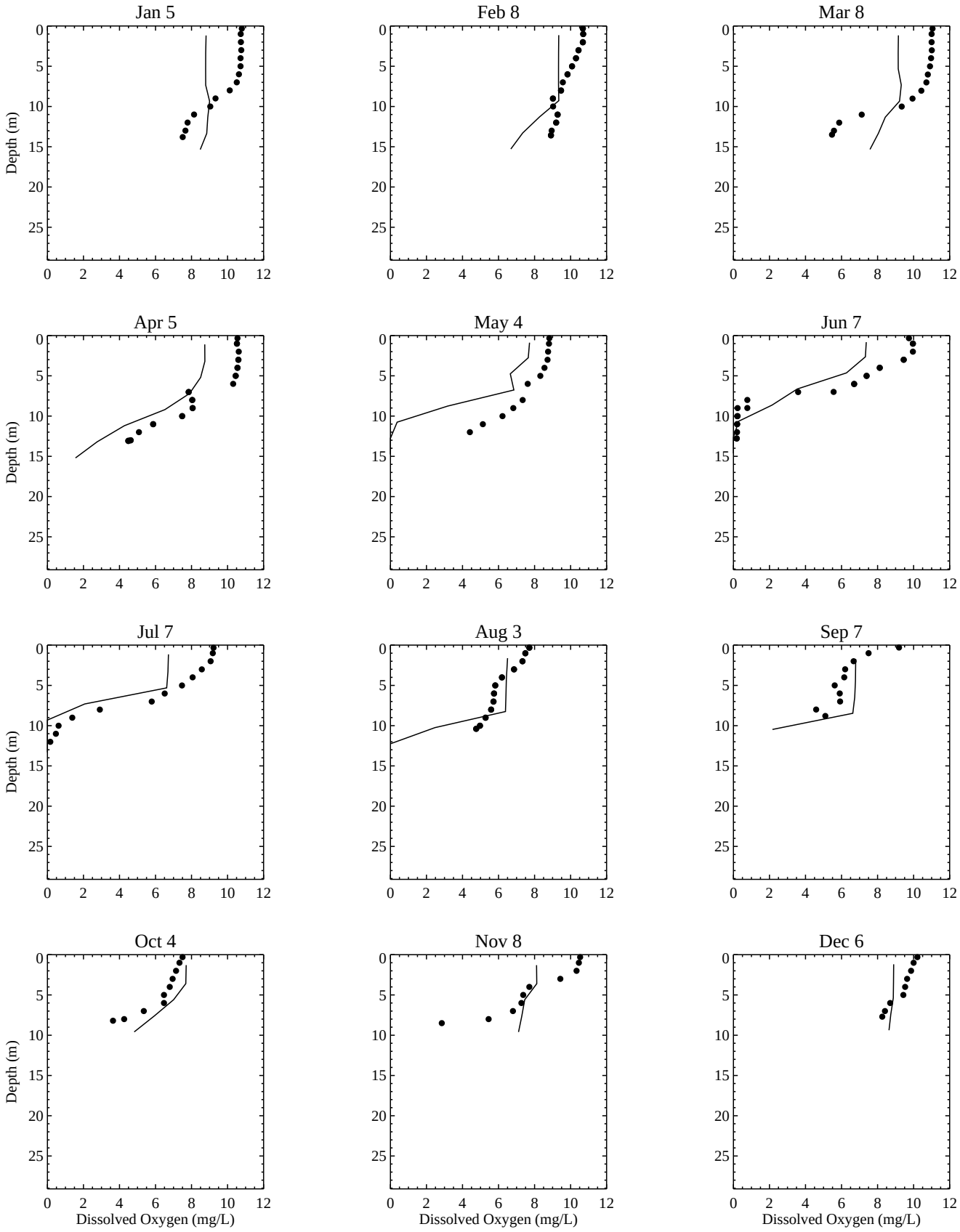

Figure J-19. Vertical profiles of model versus data at Turkey Bend (Segment 28) - Dissolved Oxygen - 2006.

Profiles shown for dates with available data else model results for first day of month shown.

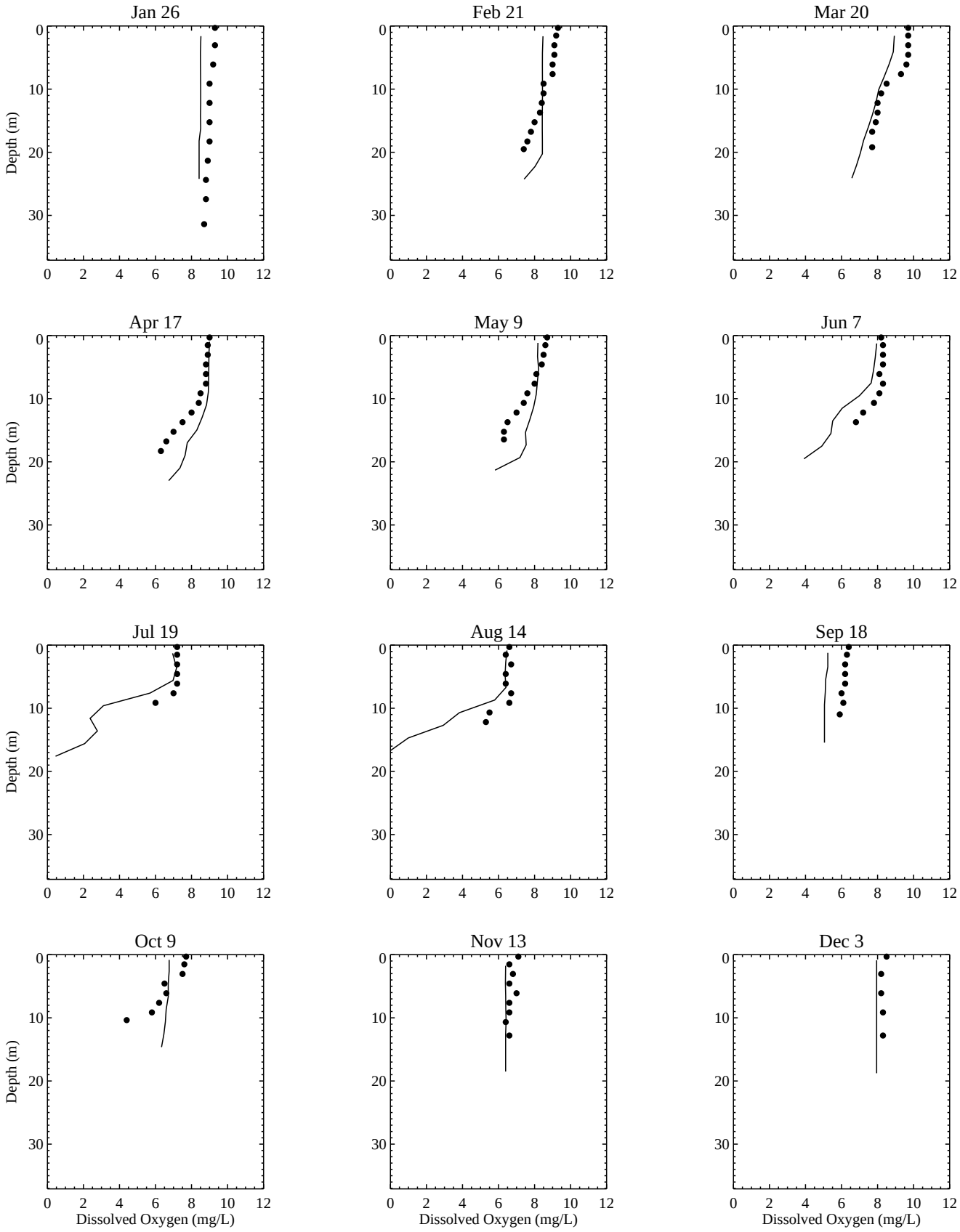

Figure J-20. Vertical profiles of model versus data at Sandy Creek (Segment 161) - Dissolved Oxygen - 1984.

Profiles shown for dates with available data else model results for first day of month shown.

Model Data

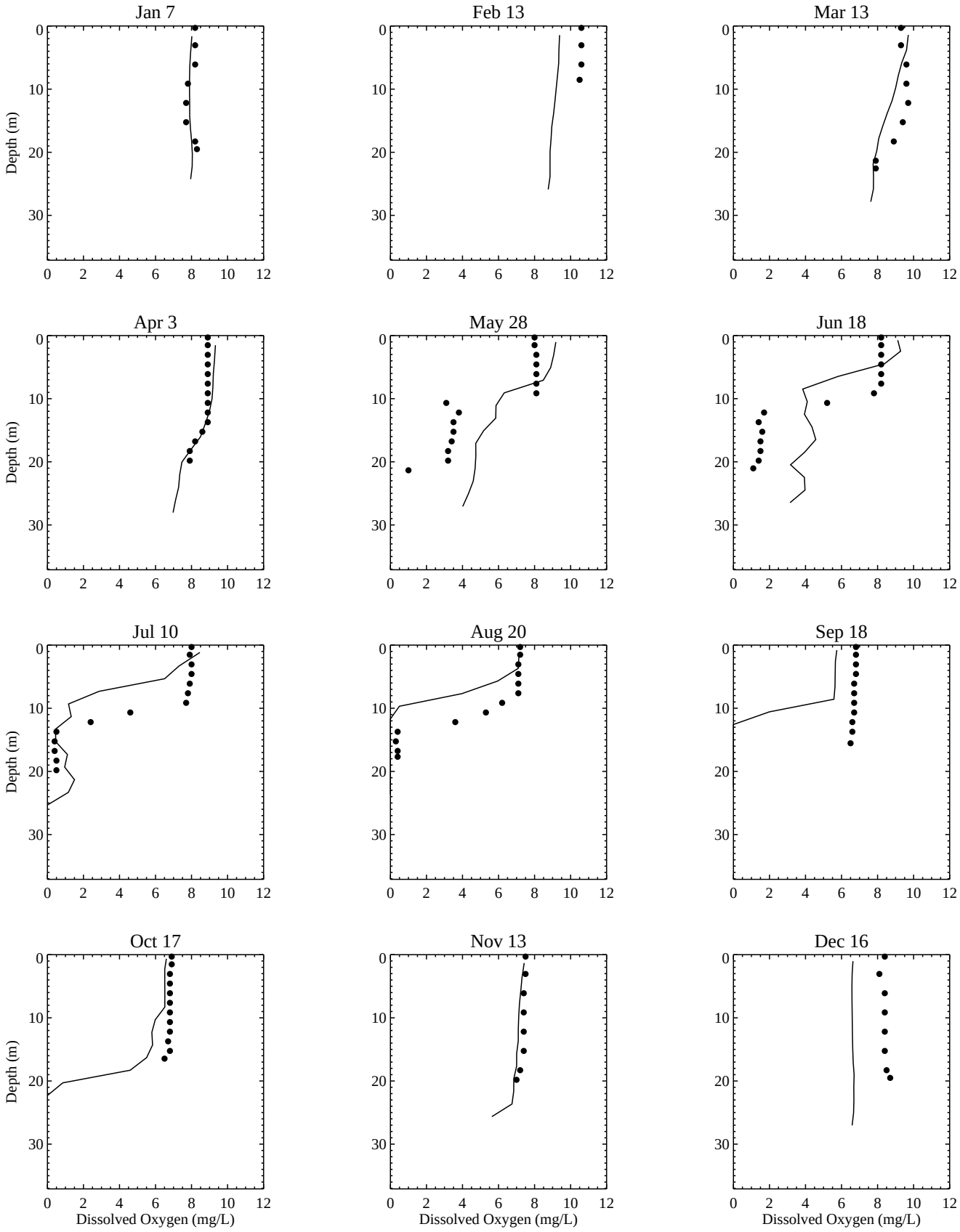

Figure J-20. Vertical profiles of model versus data at Sandy Creek (Segment 161) - Dissolved Oxygen - 1985.

Profiles shown for dates with available data else model results for first day of month shown.

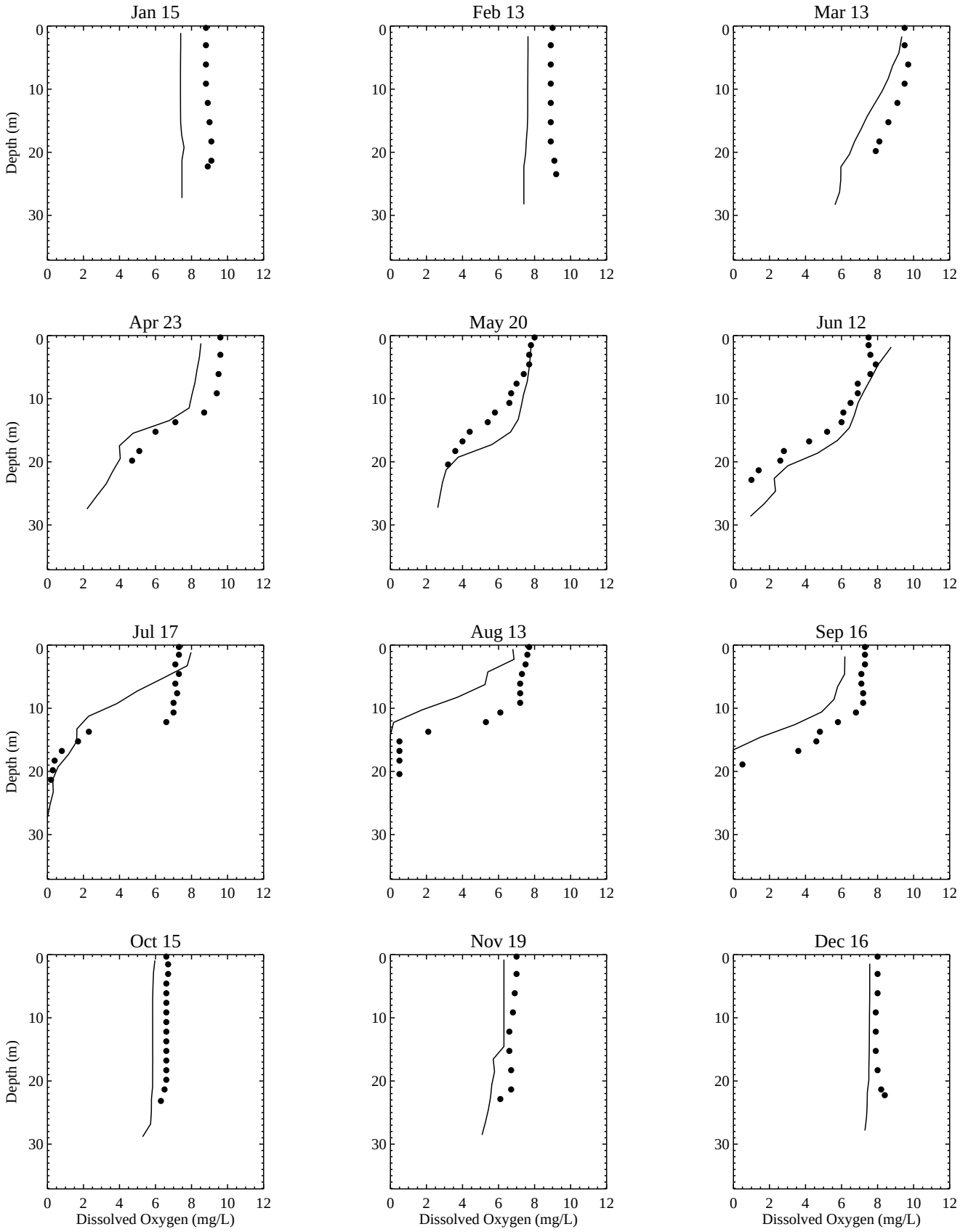

Figure J-20. Vertical profiles of model versus data at Sandy Creek (Segment 161) - Dissolved Oxygen - 1986.

Profiles shown for dates with available data else model results for first day of month shown.

Model Data

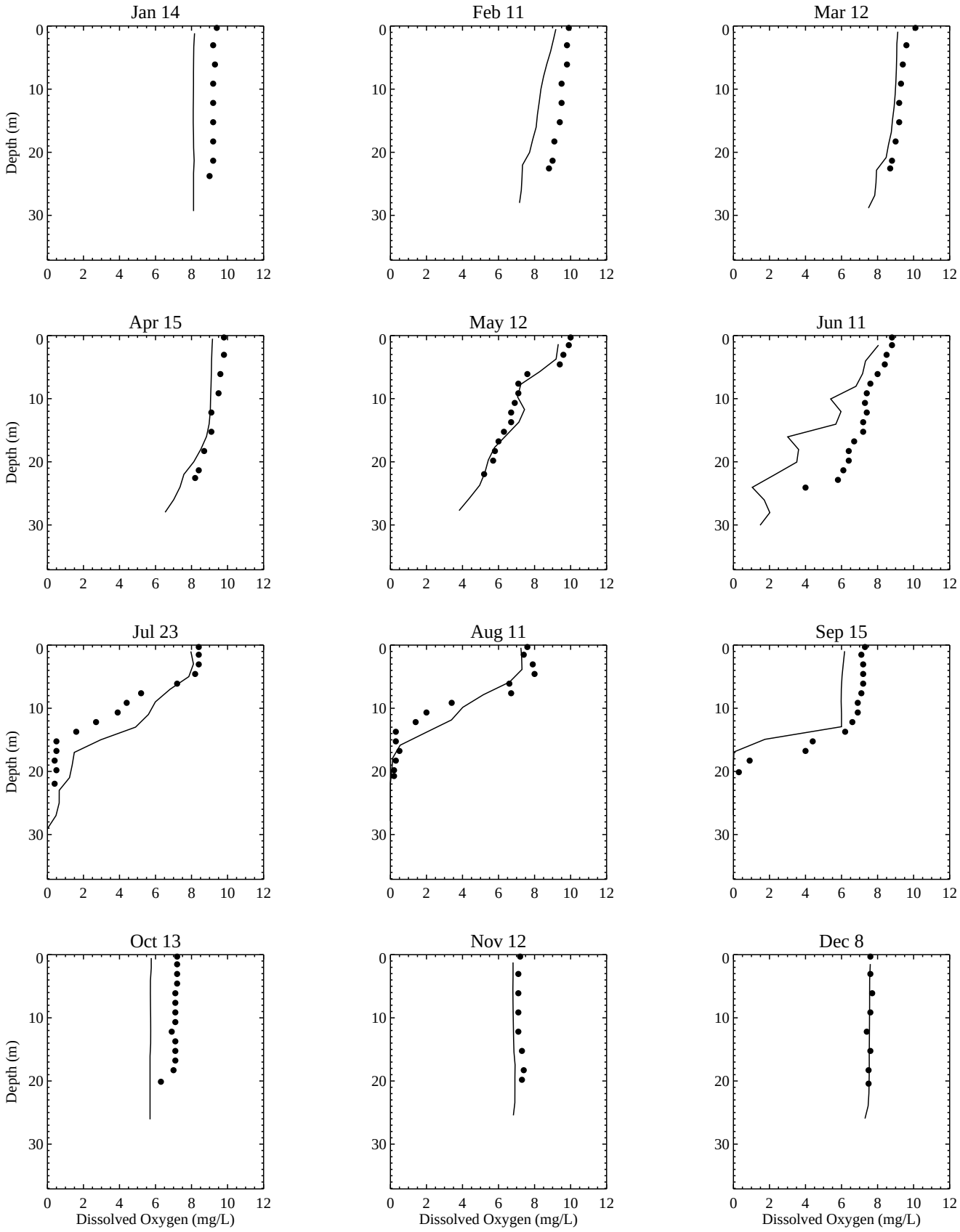

Figure J-20. Vertical profiles of model versus data at Sandy Creek (Segment 161) - Dissolved Oxygen - 1987.

Profiles shown for dates with available data else model results for first day of month shown.

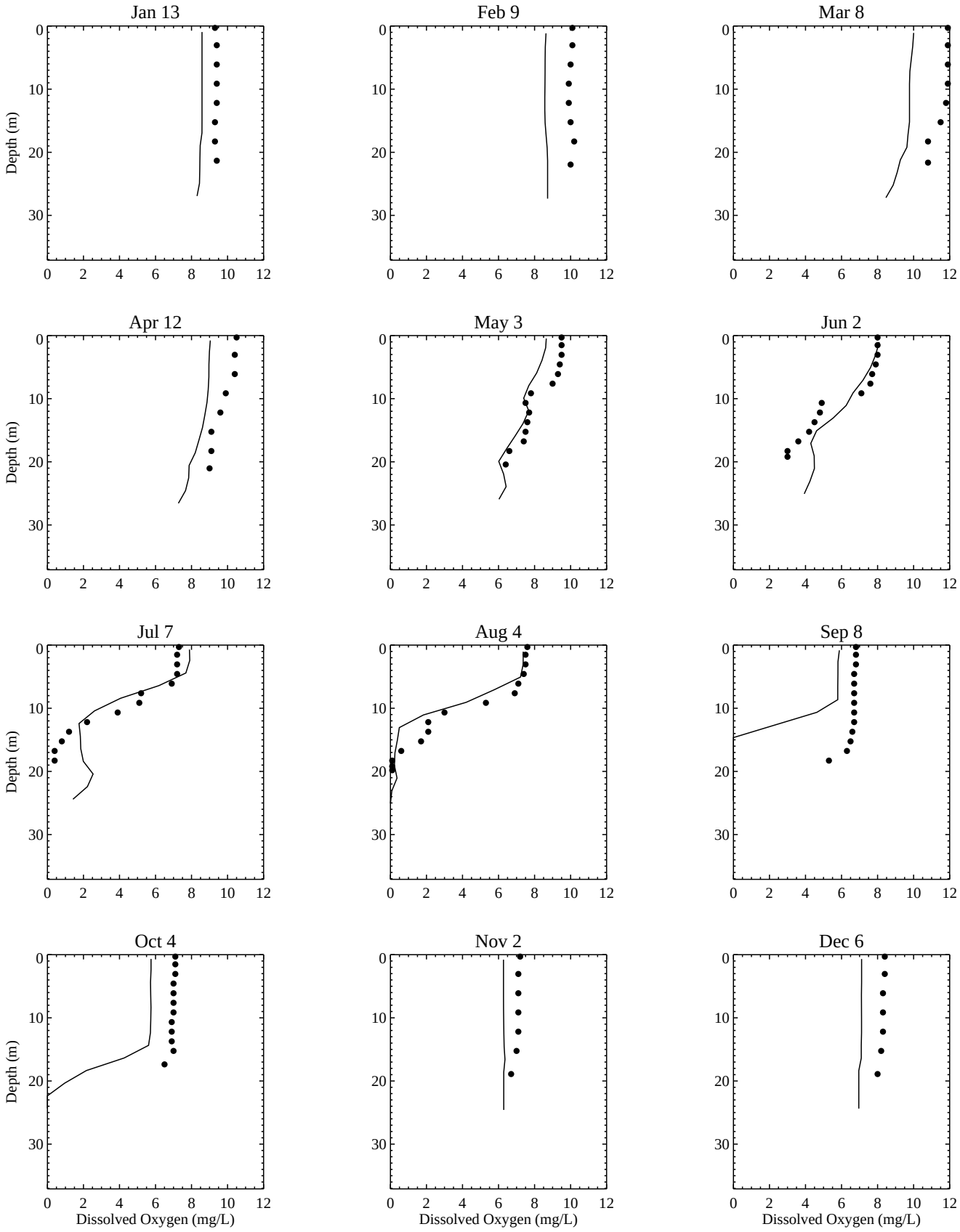

Figure J-20. Vertical profiles of model versus data at Sandy Creek (Segment 161) - Dissolved Oxygen - 1988.

Profiles shown for dates with available data else model results for first day of month shown.

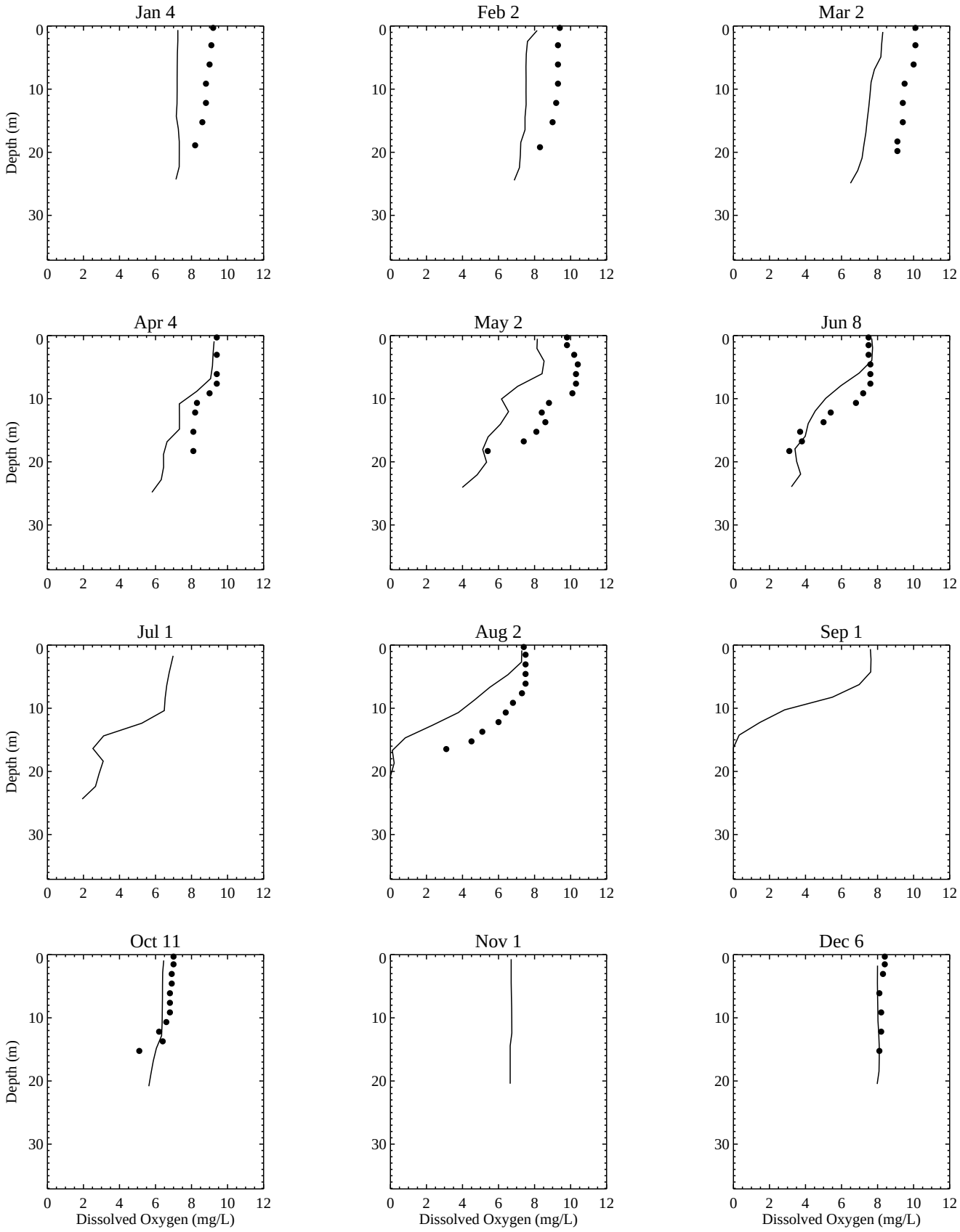

Figure J-20. Vertical profiles of model versus data at Sandy Creek (Segment 161) - Dissolved Oxygen - 1989.

Profiles shown for dates with available data else model results for first day of month shown.

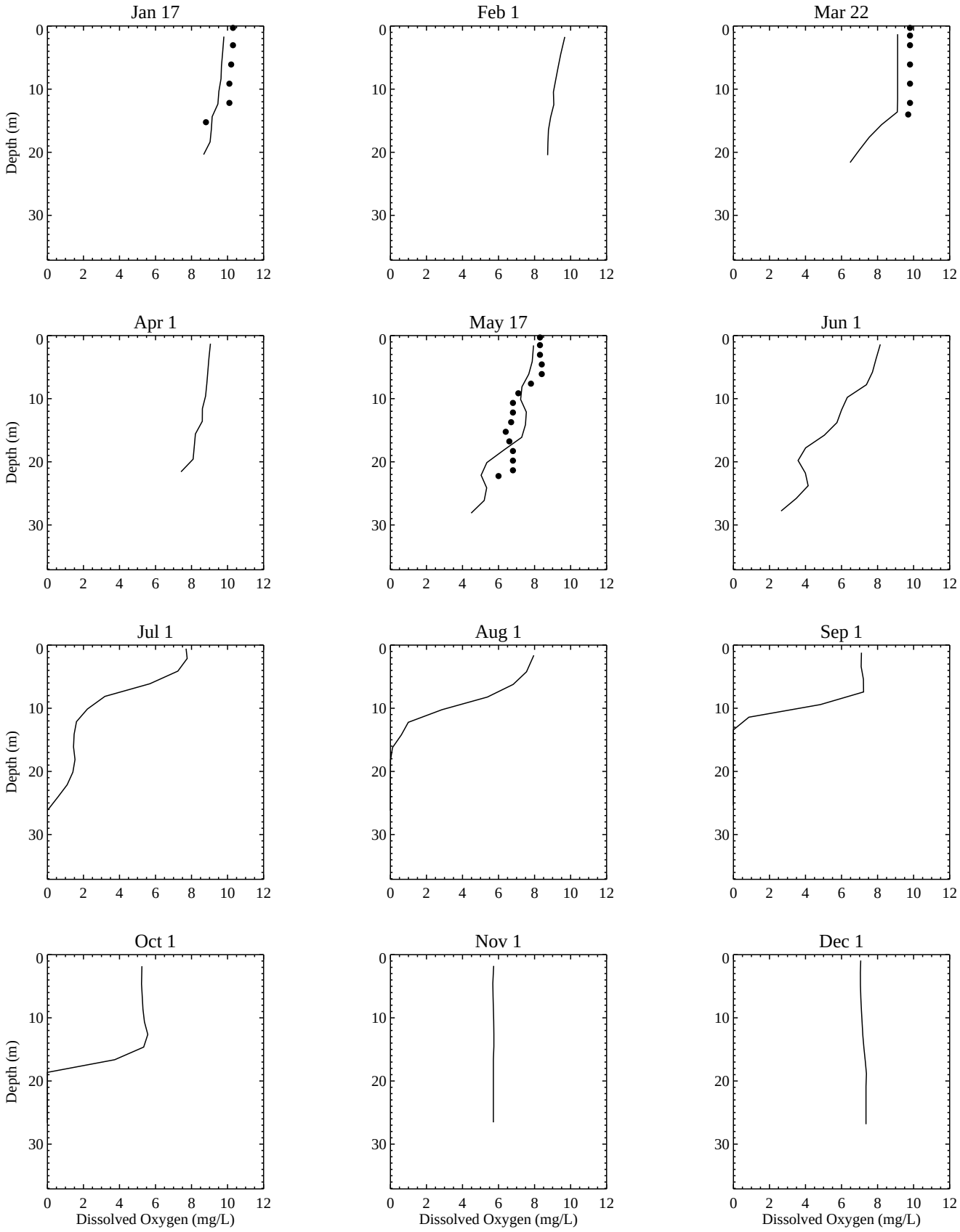

Figure J-20. Vertical profiles of model versus data at Sandy Creek (Segment 161) - Dissolved Oxygen - 1990.

Profiles shown for dates with available data else model results for first day of month shown.

Model ● Data

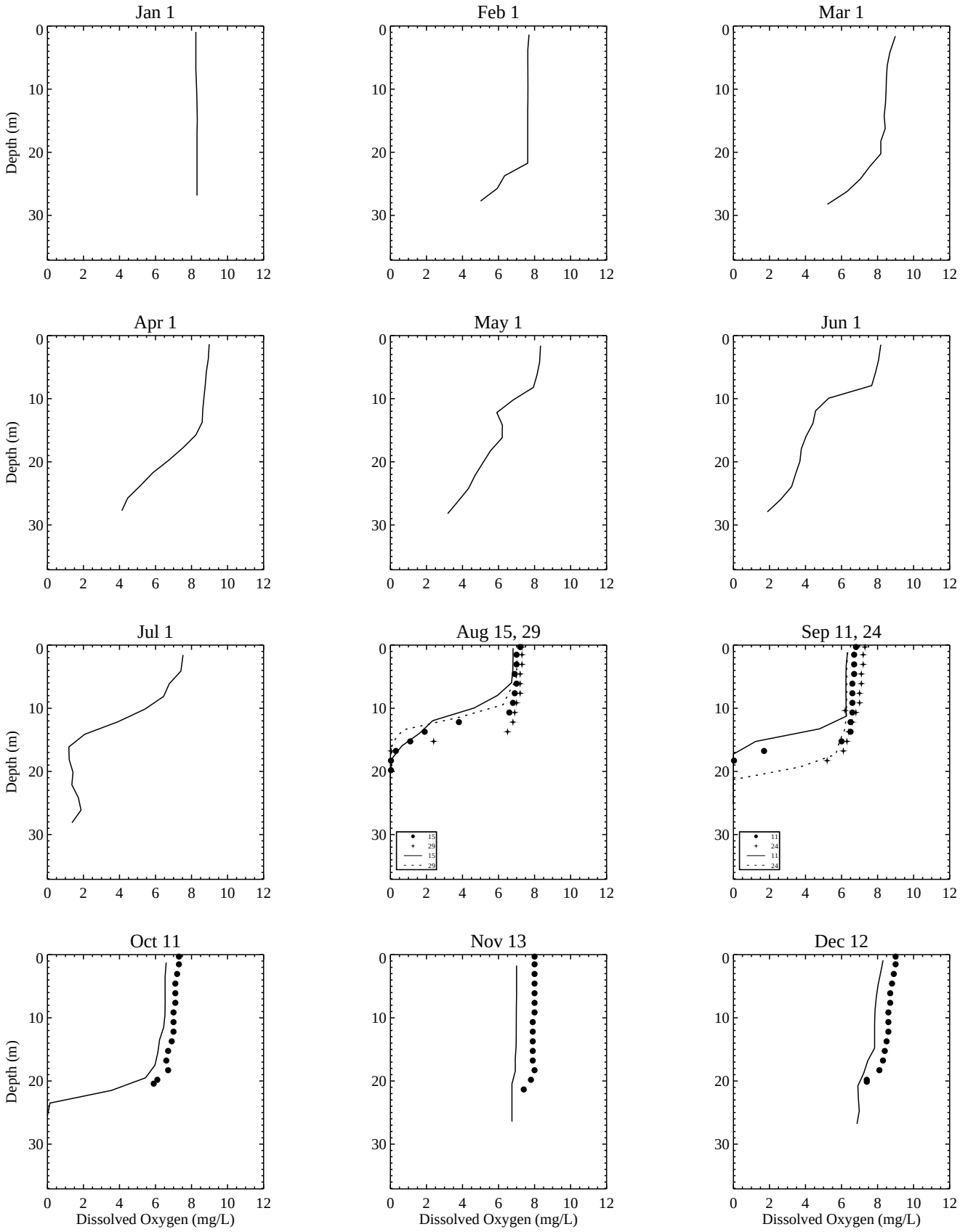

Figure J-20. Vertical profiles of model versus data at Sandy Creek (Segment 161) - Dissolved Oxygen - 1991.

Profiles shown for dates with available data else model results for first day of month shown.

Model Data

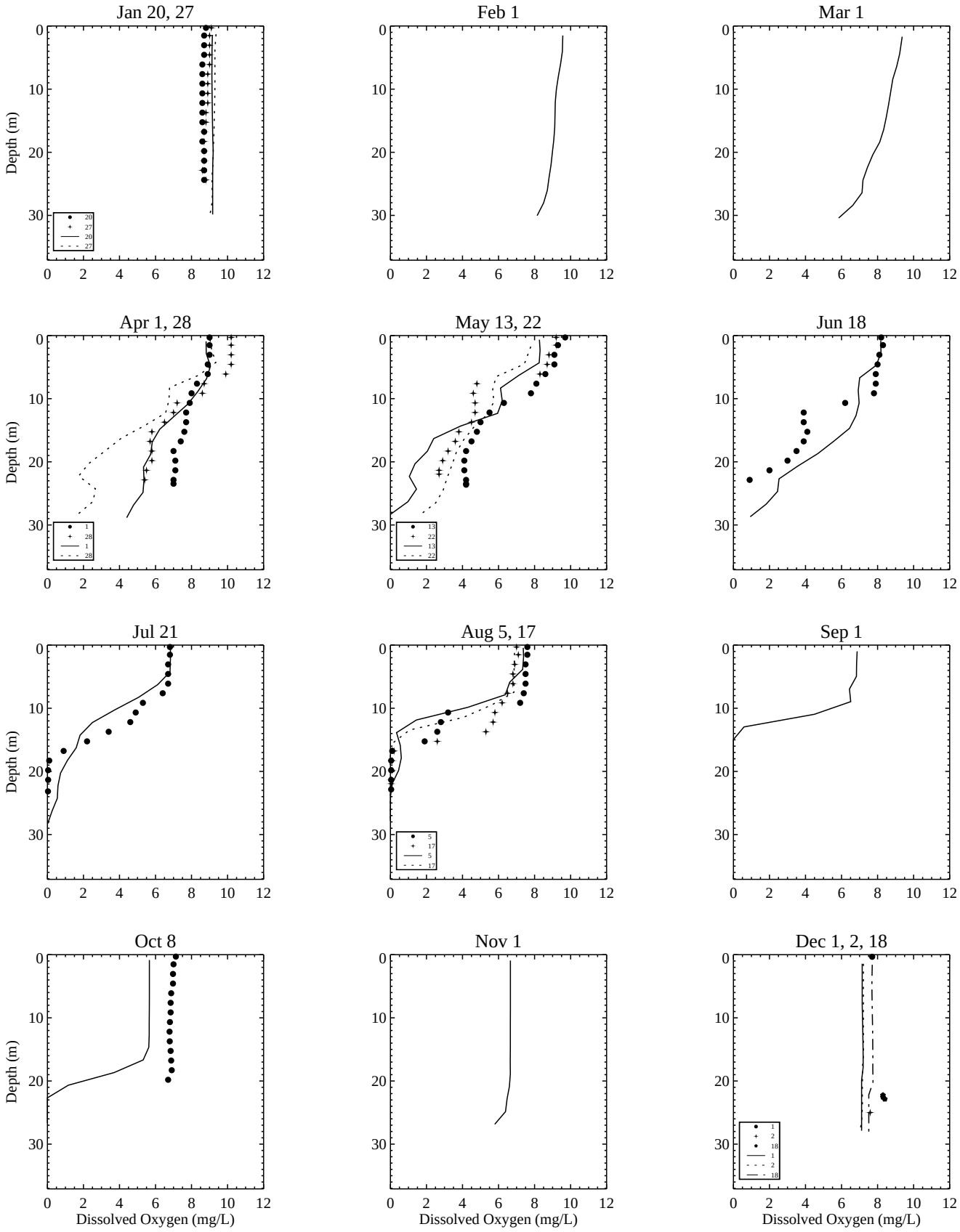

Figure J-20. Vertical profiles of model versus data at Sandy Creek (Segment 161) - Dissolved Oxygen - 1992.

Profiles shown for dates with available data else model results for first day of month shown.

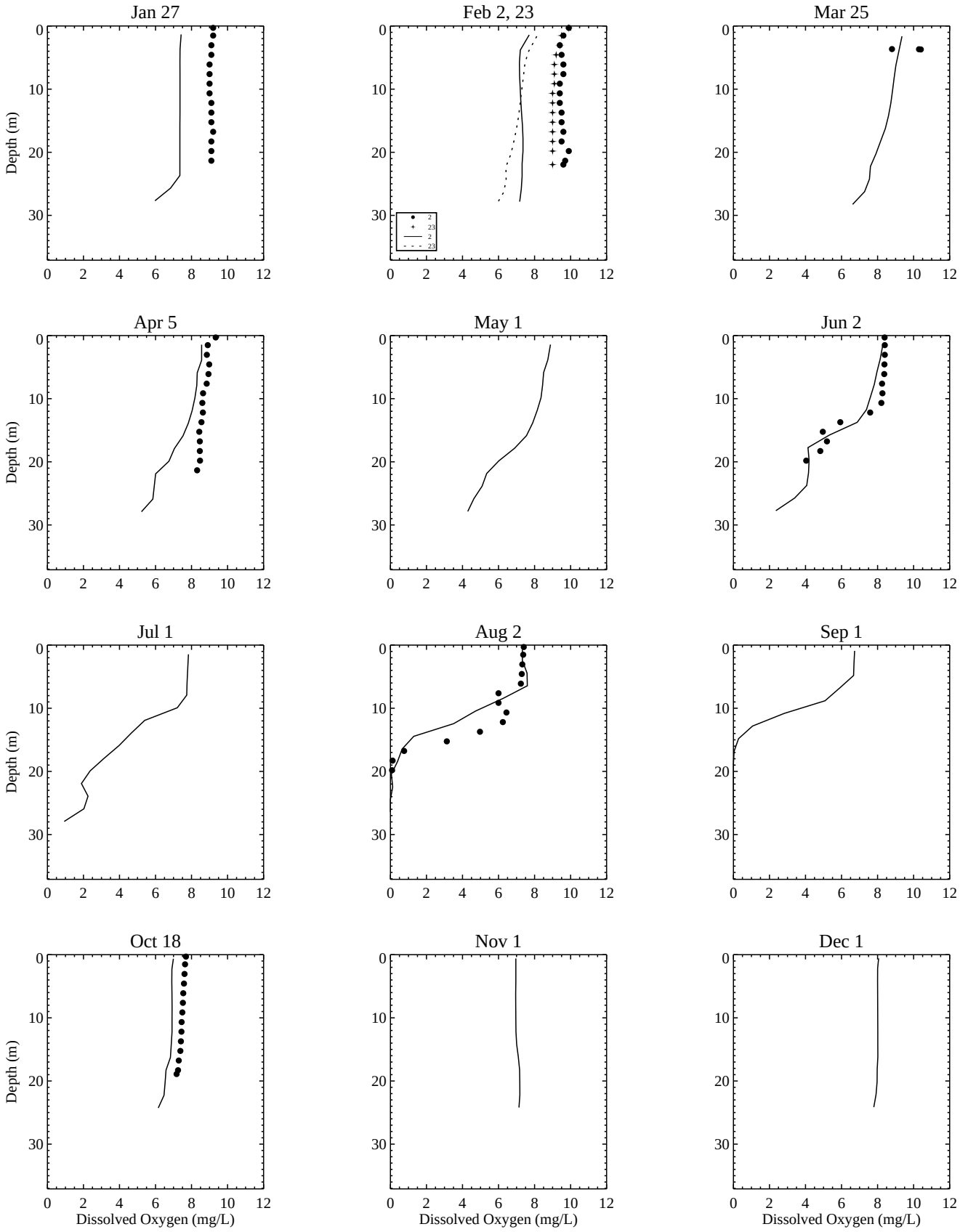

Figure J-20. Vertical profiles of model versus data at Sandy Creek (Segment 161) - Dissolved Oxygen - 1993.

Profiles shown for dates with available data else model results for first day of month shown.

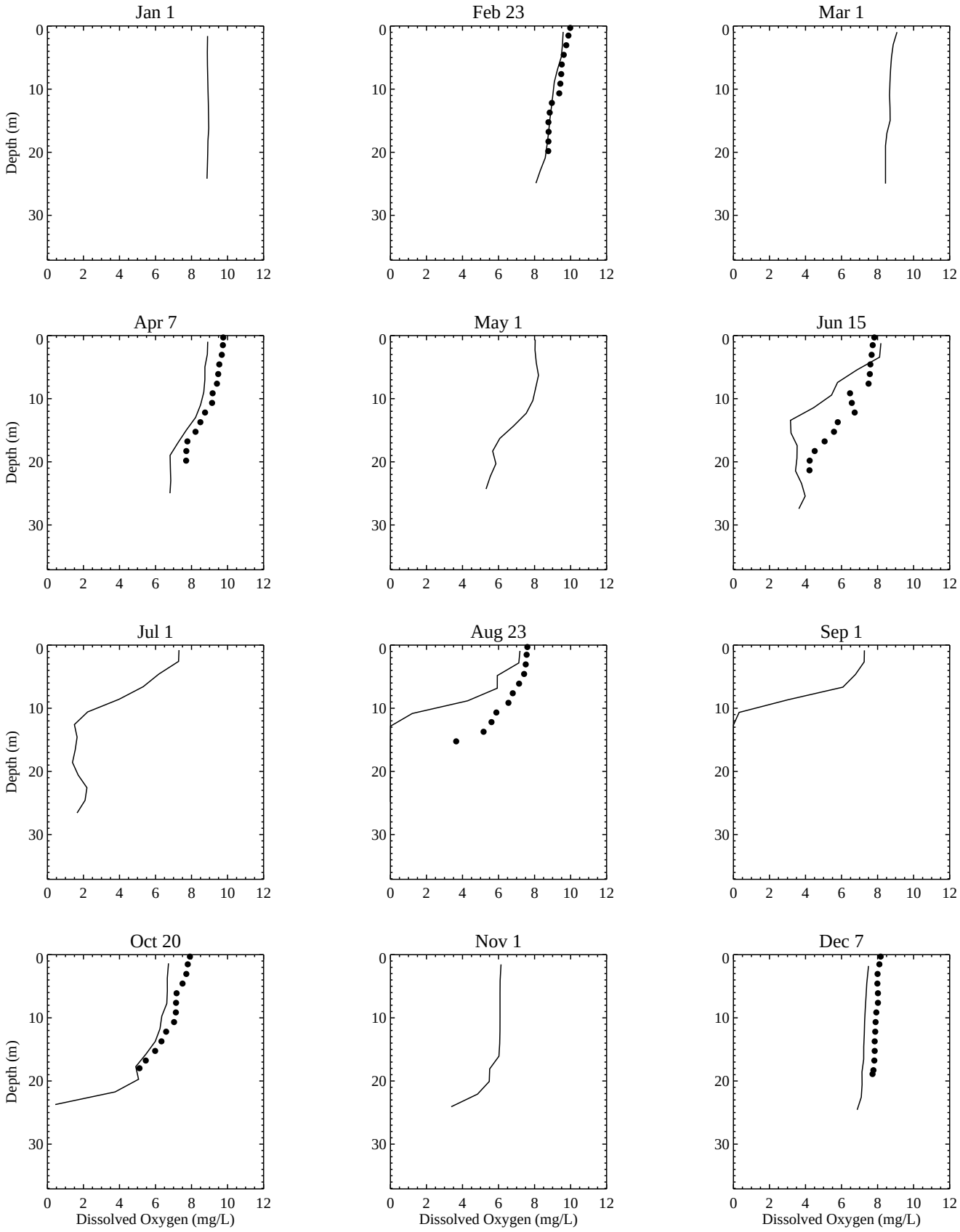

Figure J-20. Vertical profiles of model versus data at Sandy Creek (Segment 161) - Dissolved Oxygen - 1994.

Profiles shown for dates with available data else model results for first day of month shown.

Model ● Data

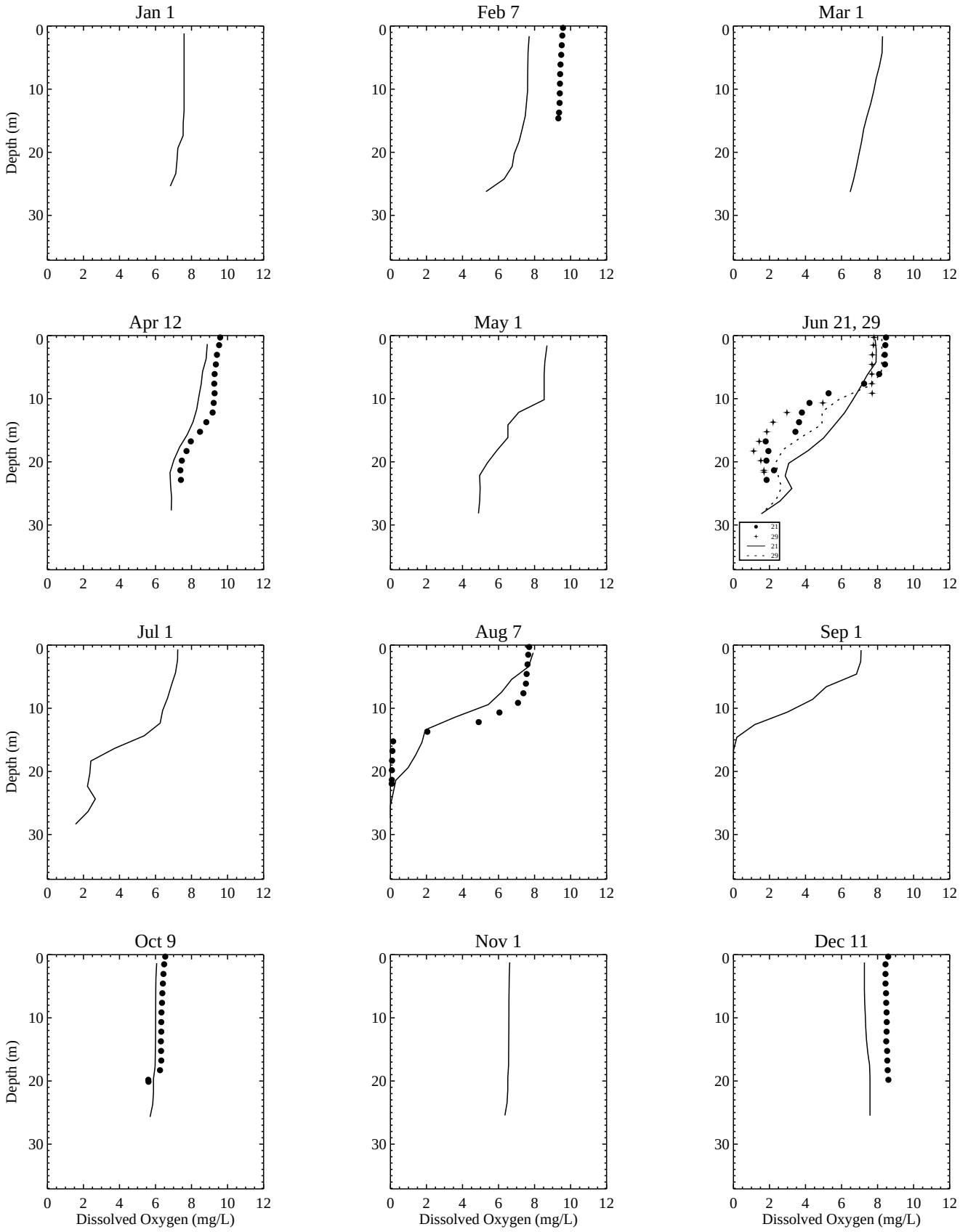

Figure J-20. Vertical profiles of model versus data at Sandy Creek (Segment 161) - Dissolved Oxygen - 1995.

Profiles shown for dates with available data else model results for first day of month shown.

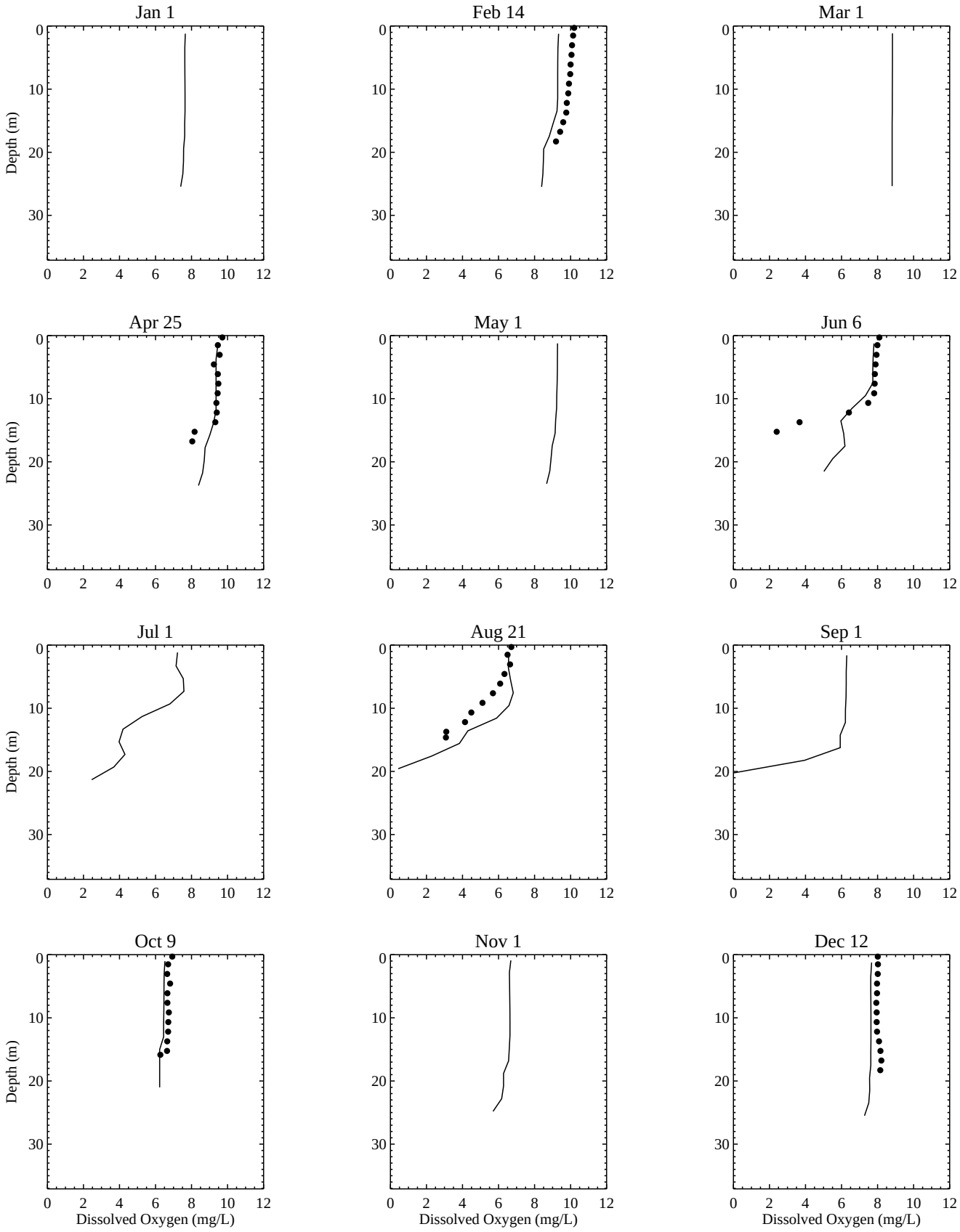

Figure J-20. Vertical profiles of model versus data at Sandy Creek (Segment 161) - Dissolved Oxygen - 1996.

Profiles shown for dates with available data else model results for first day of month shown.

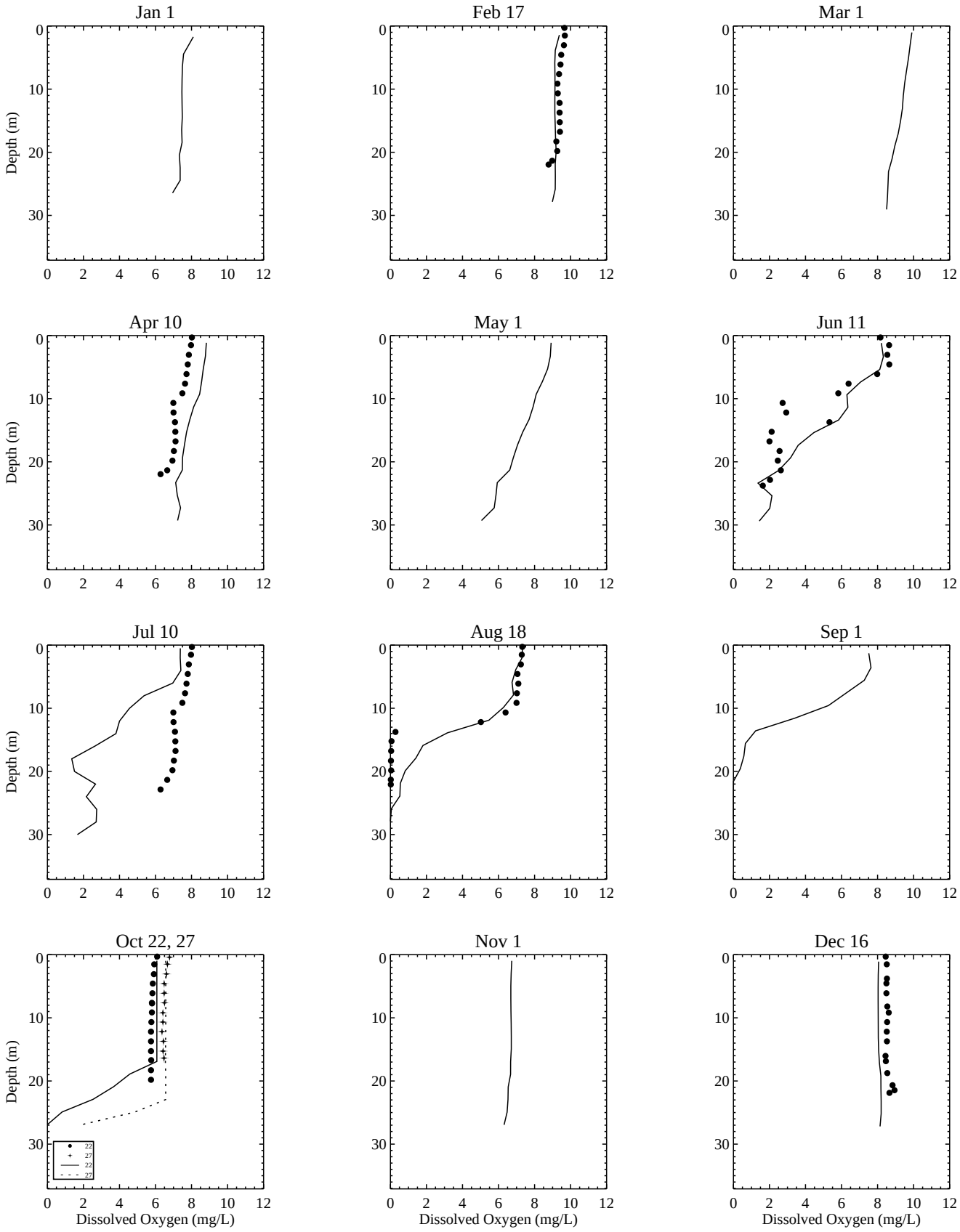

Figure J-20. Vertical profiles of model versus data at Sandy Creek (Segment 161) - Dissolved Oxygen - 1997.

Profiles shown for dates with available data else model results for first day of month shown.

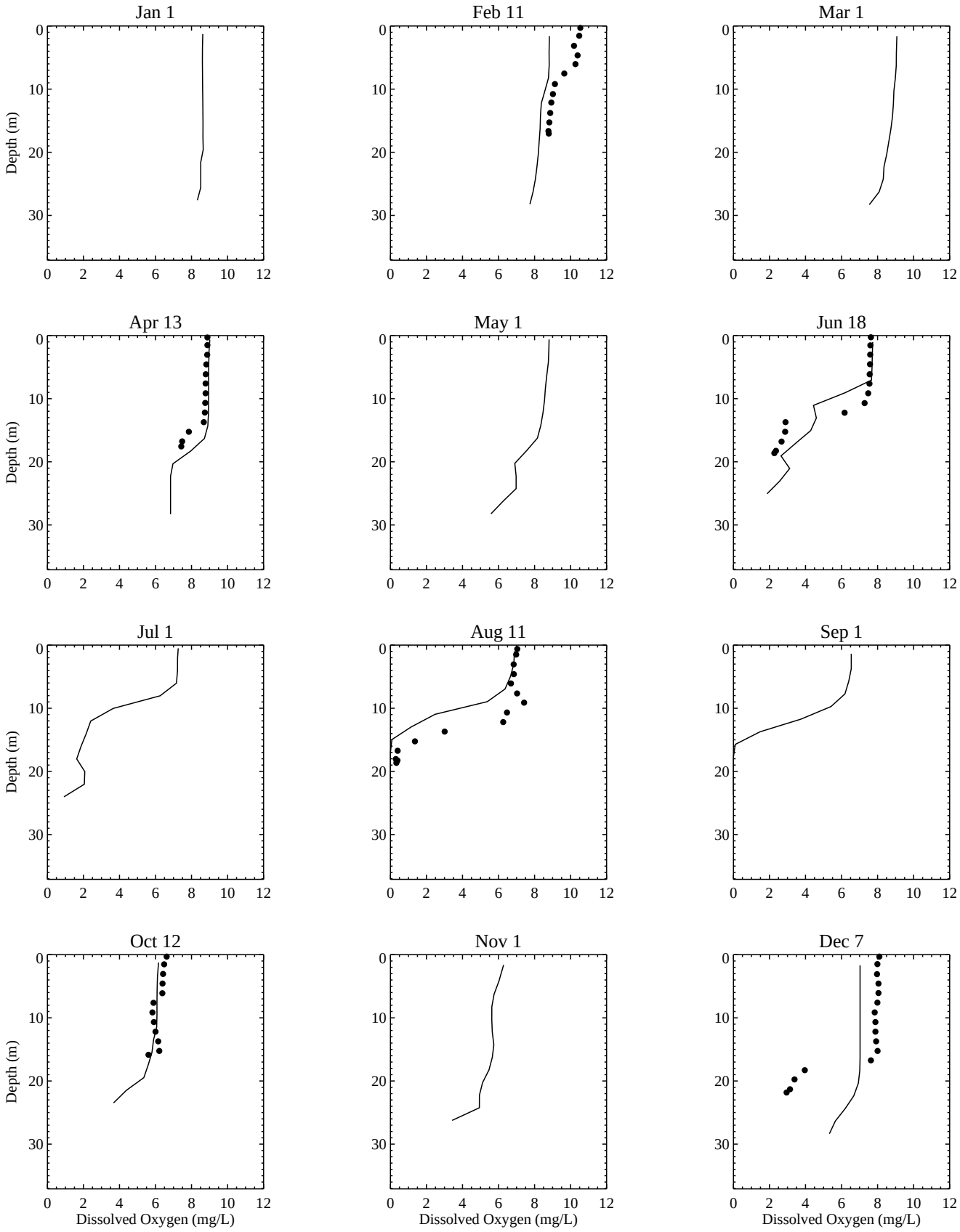

Figure J-20. Vertical profiles of model versus data at Sandy Creek (Segment 161) - Dissolved Oxygen - 1998.

Profiles shown for dates with available data else model results for first day of month shown.

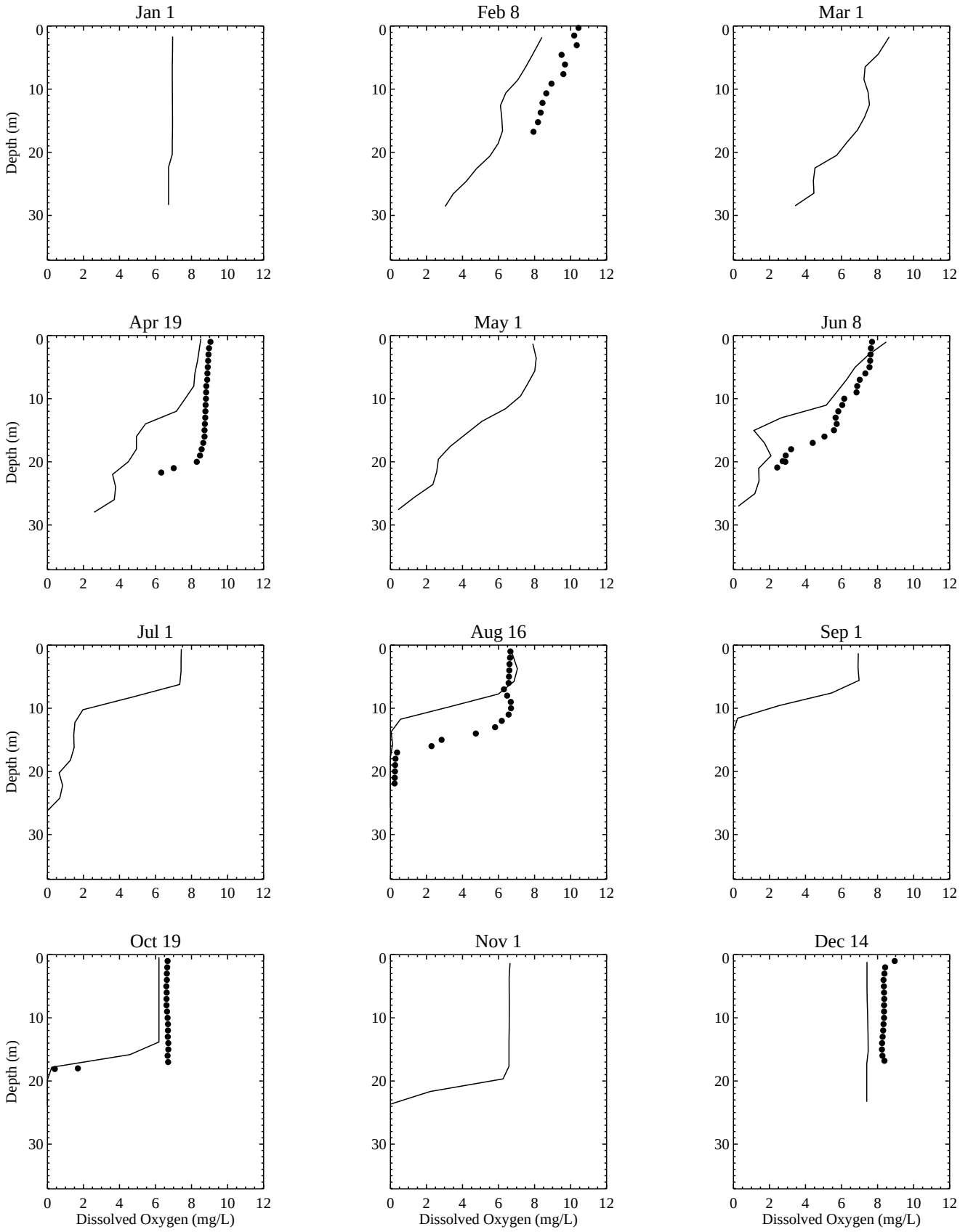

Figure J-20. Vertical profiles of model versus data at Sandy Creek (Segment 161) - Dissolved Oxygen - 1999.

Profiles shown for dates with available data else model results for first day of month shown.

Model Data

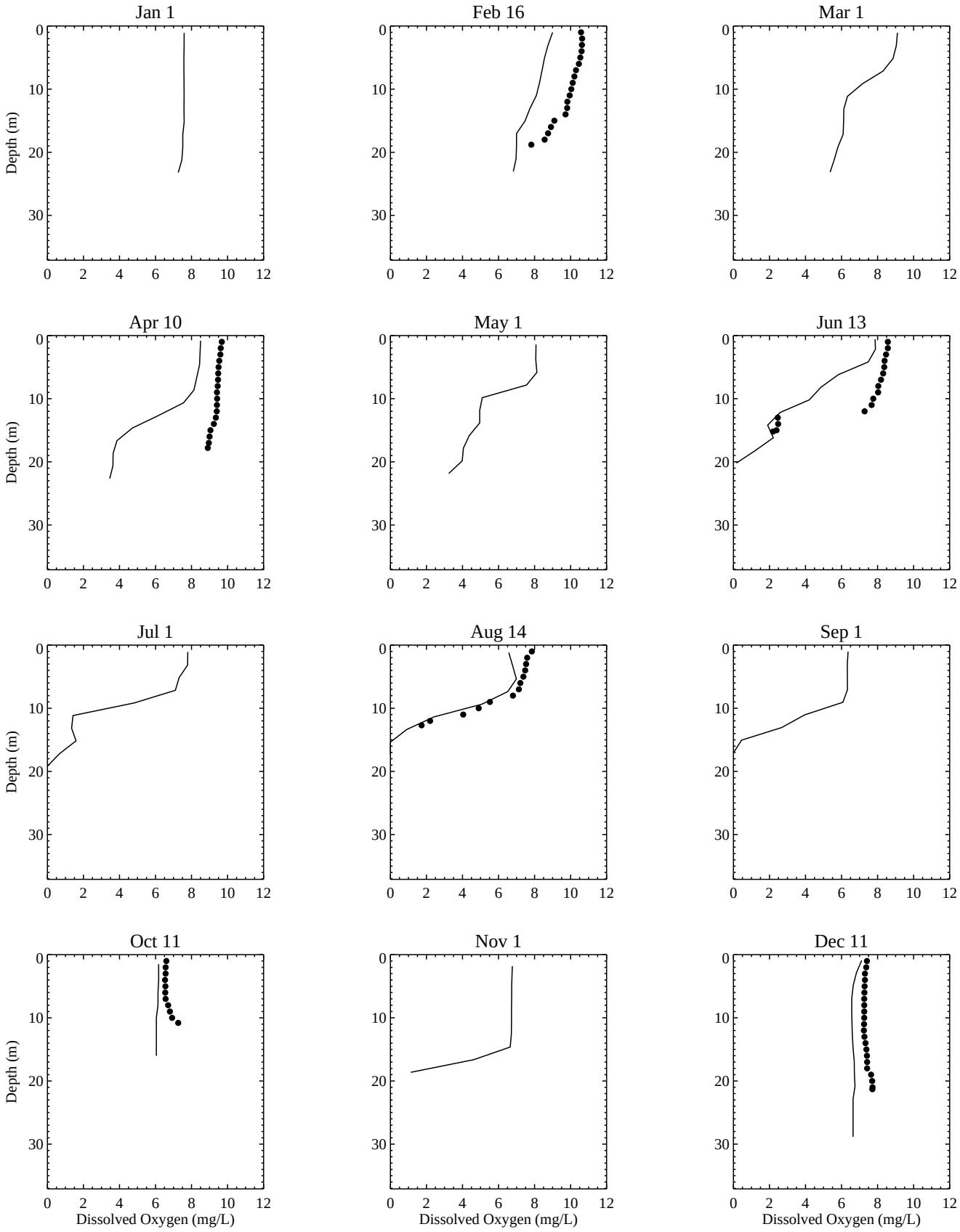

Figure J-20. Vertical profiles of model versus data at Sandy Creek (Segment 161) - Dissolved Oxygen - 2000.

Profiles shown for dates with available data else model results for first day of month shown.

Model Data

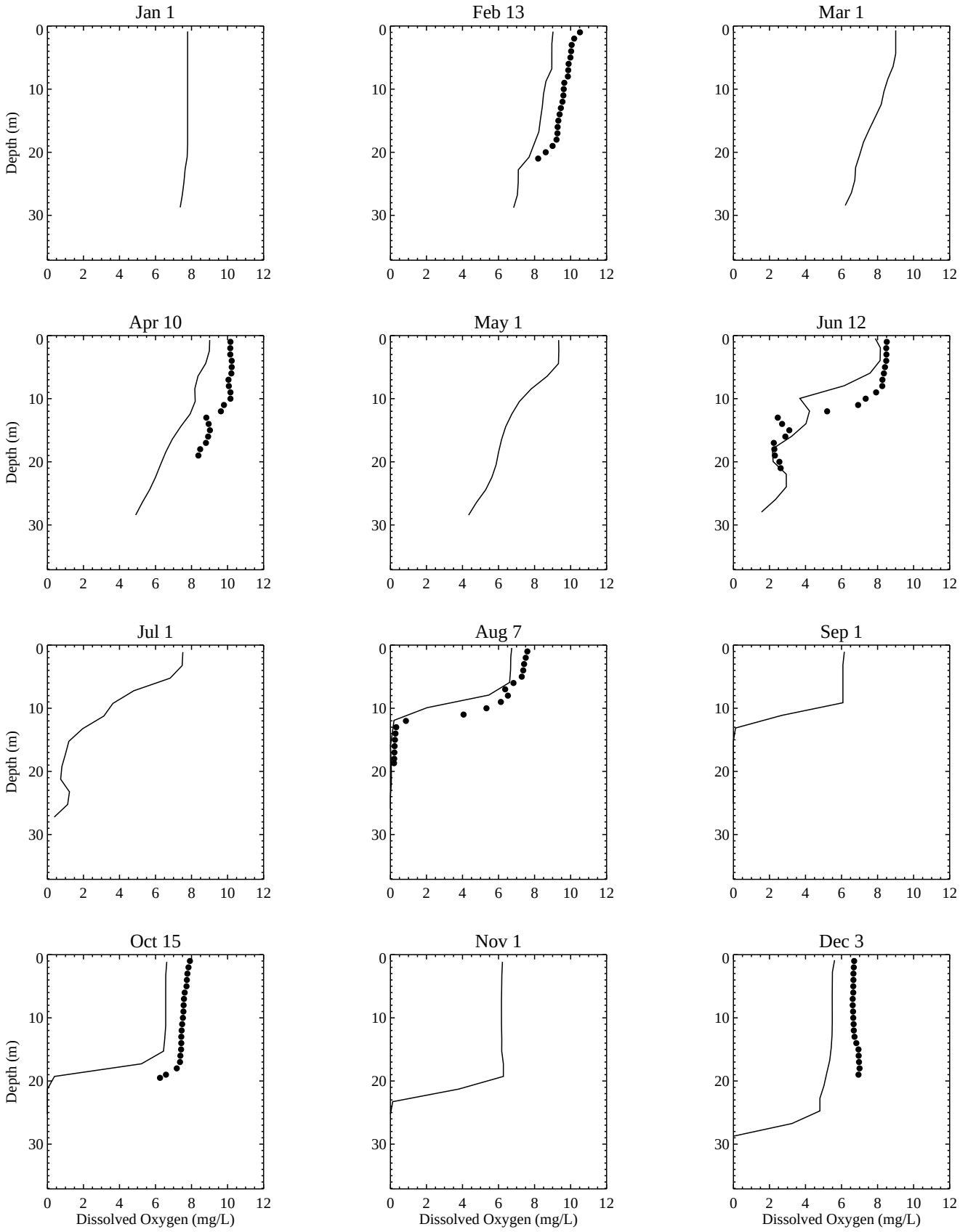

Figure J-20. Vertical profiles of model versus data at Sandy Creek (Segment 161) - Dissolved Oxygen - 2001.

Profiles shown for dates with available data else model results for first day of month shown.

Model Data

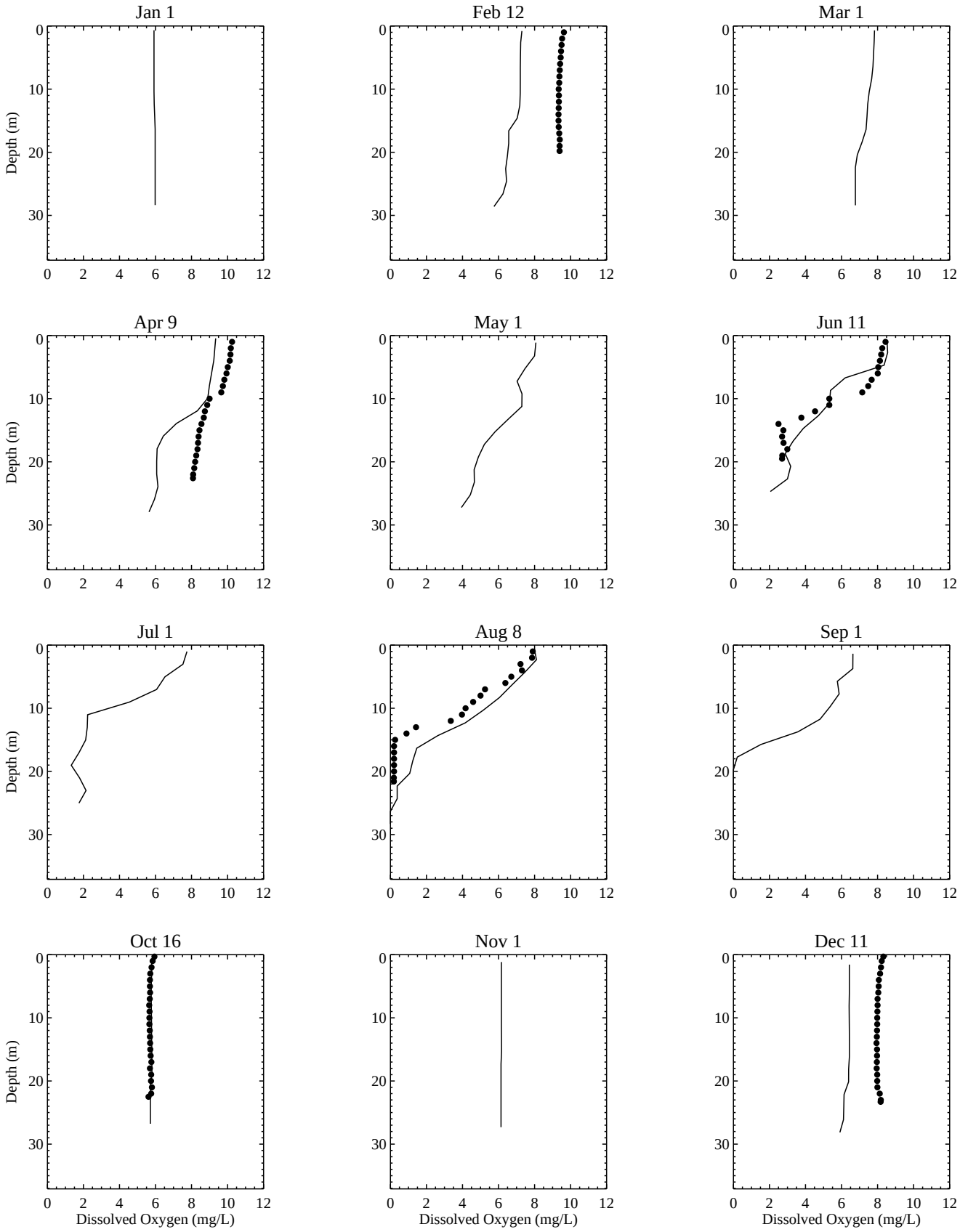

Figure J-20. Vertical profiles of model versus data at Sandy Creek (Segment 161) - Dissolved Oxygen - 2002.

Profiles shown for dates with available data else model results for first day of month shown.

Model Data

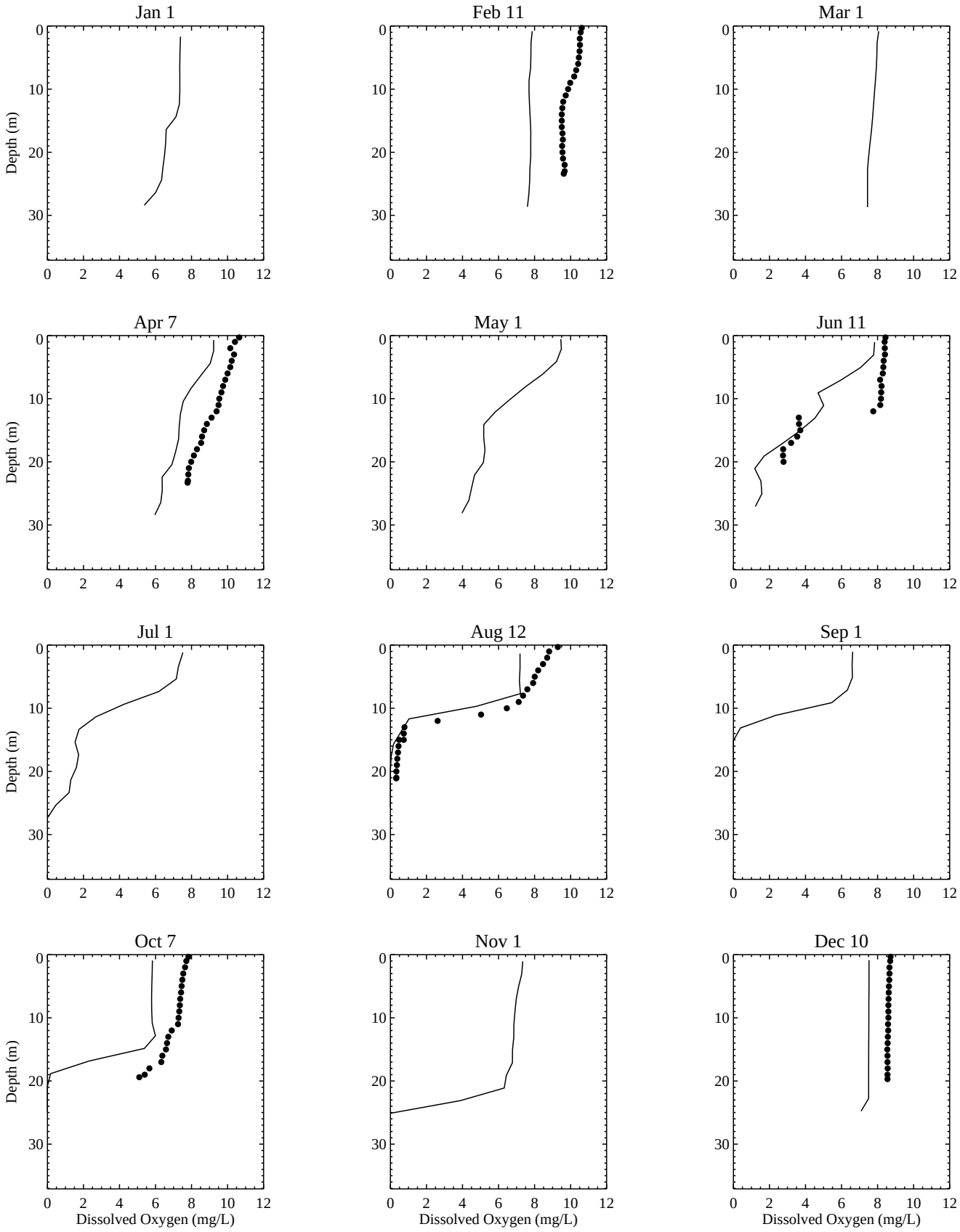

Figure J-20. Vertical profiles of model versus data at Sandy Creek (Segment 161) - Dissolved Oxygen - 2003.

Profiles shown for dates with available data else model results for first day of month shown.

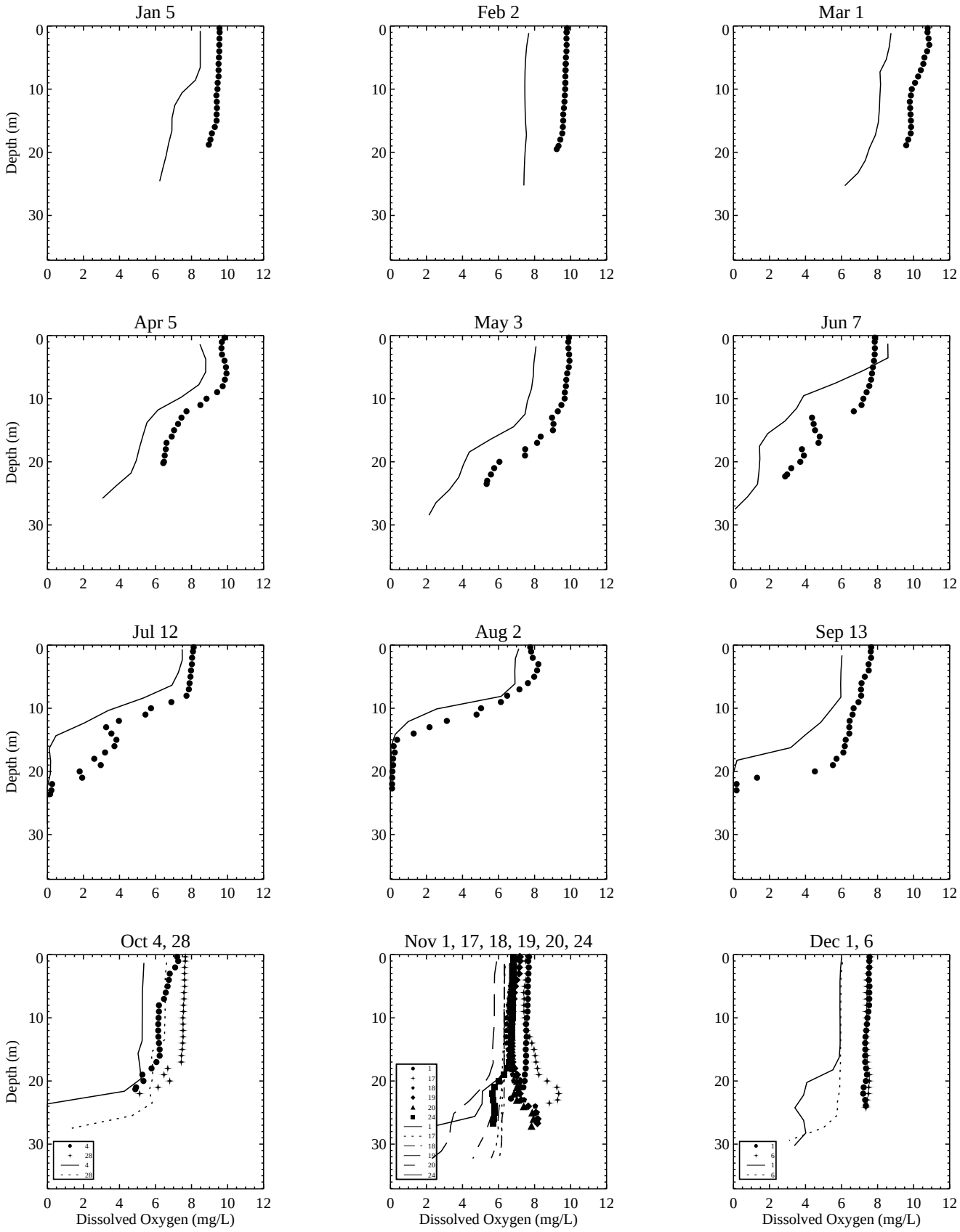

Figure J-20. Vertical profiles of model versus data at Sandy Creek (Segment 161) - Dissolved Oxygen - 2004.

Profiles shown for dates with available data else model results for first day of month shown.

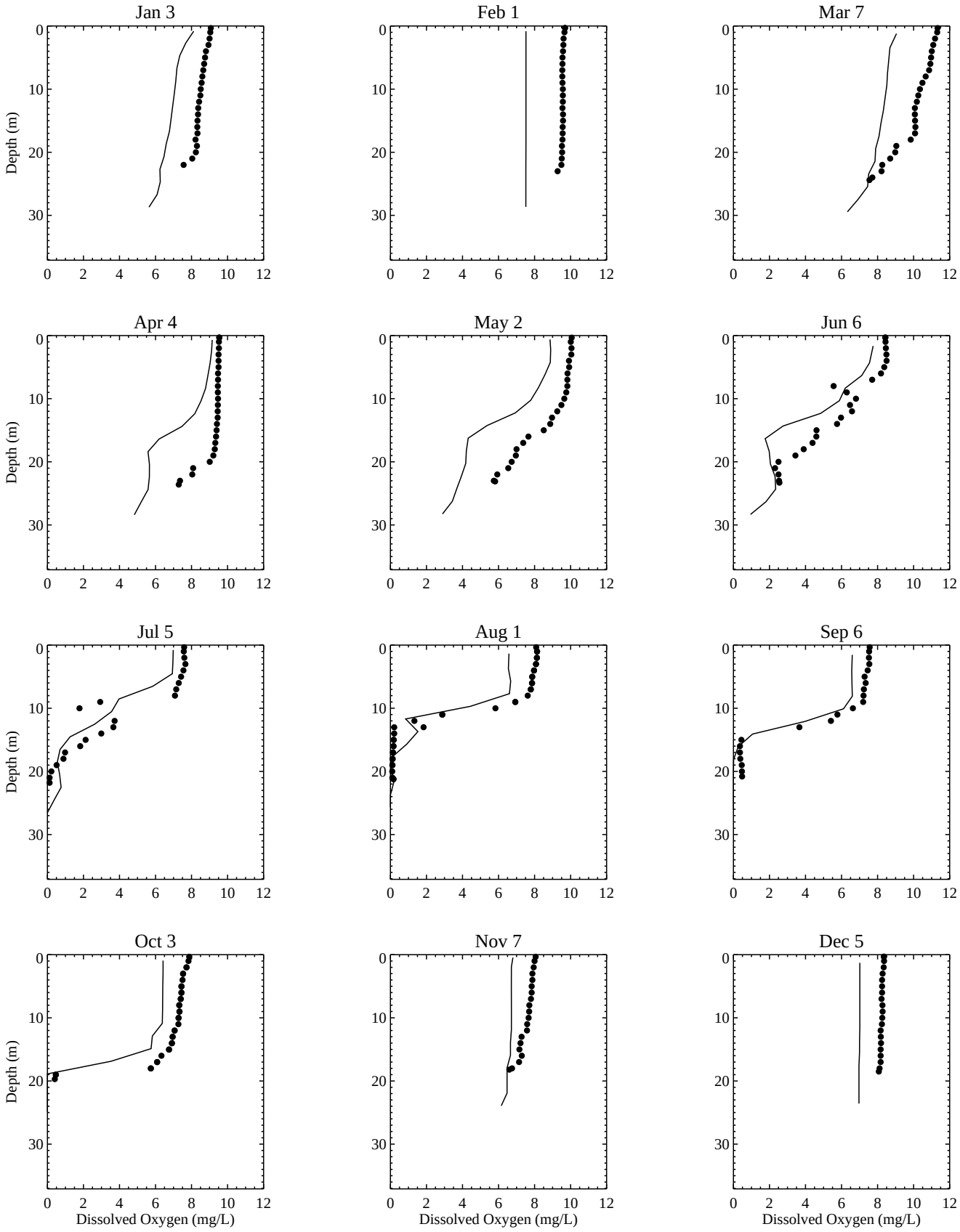

Figure J-20. Vertical profiles of model versus data at Sandy Creek (Segment 161) - Dissolved Oxygen - 2005.

Profiles shown for dates with available data else model results for first day of month shown.

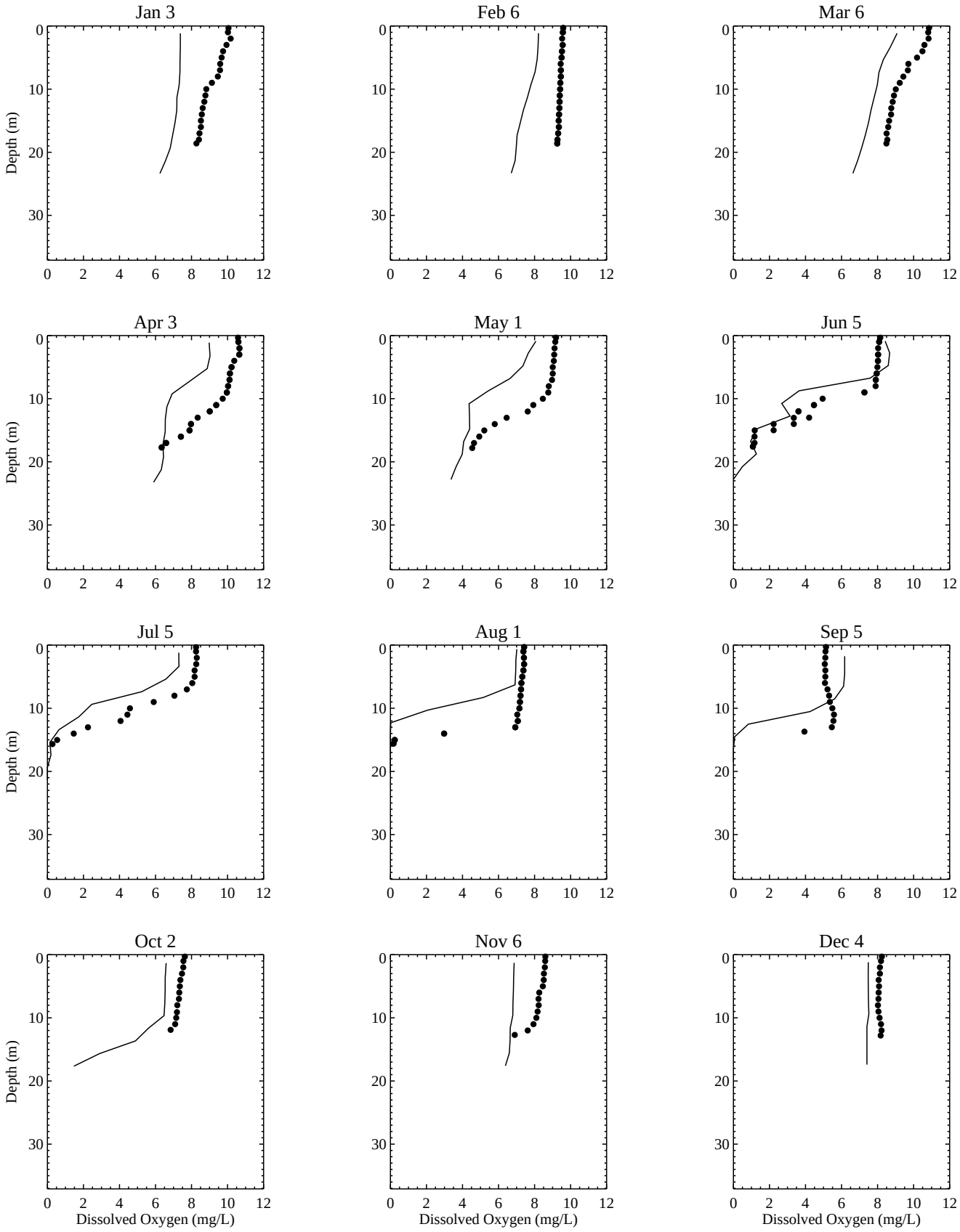

Figure J-20. Vertical profiles of model versus data at Sandy Creek (Segment 161) - Dissolved Oxygen - 2006.

Profiles shown for dates with available data else model results for first day of month shown.

Model Data

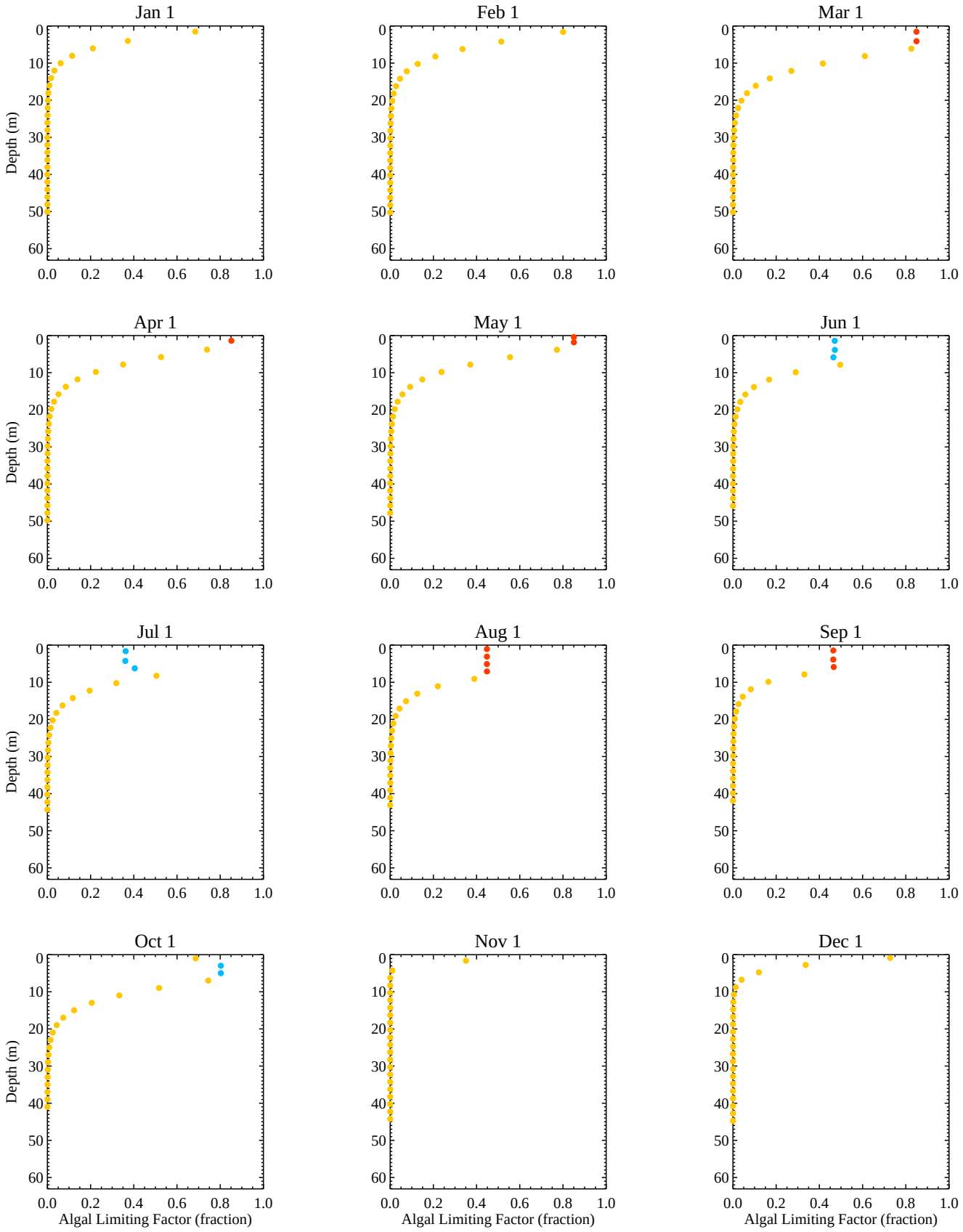

Figure J-21. Vertical profiles of algal limiting factor at Mansfield Dam (Segment 93) during 1984.

Profiles shown for first day of month.

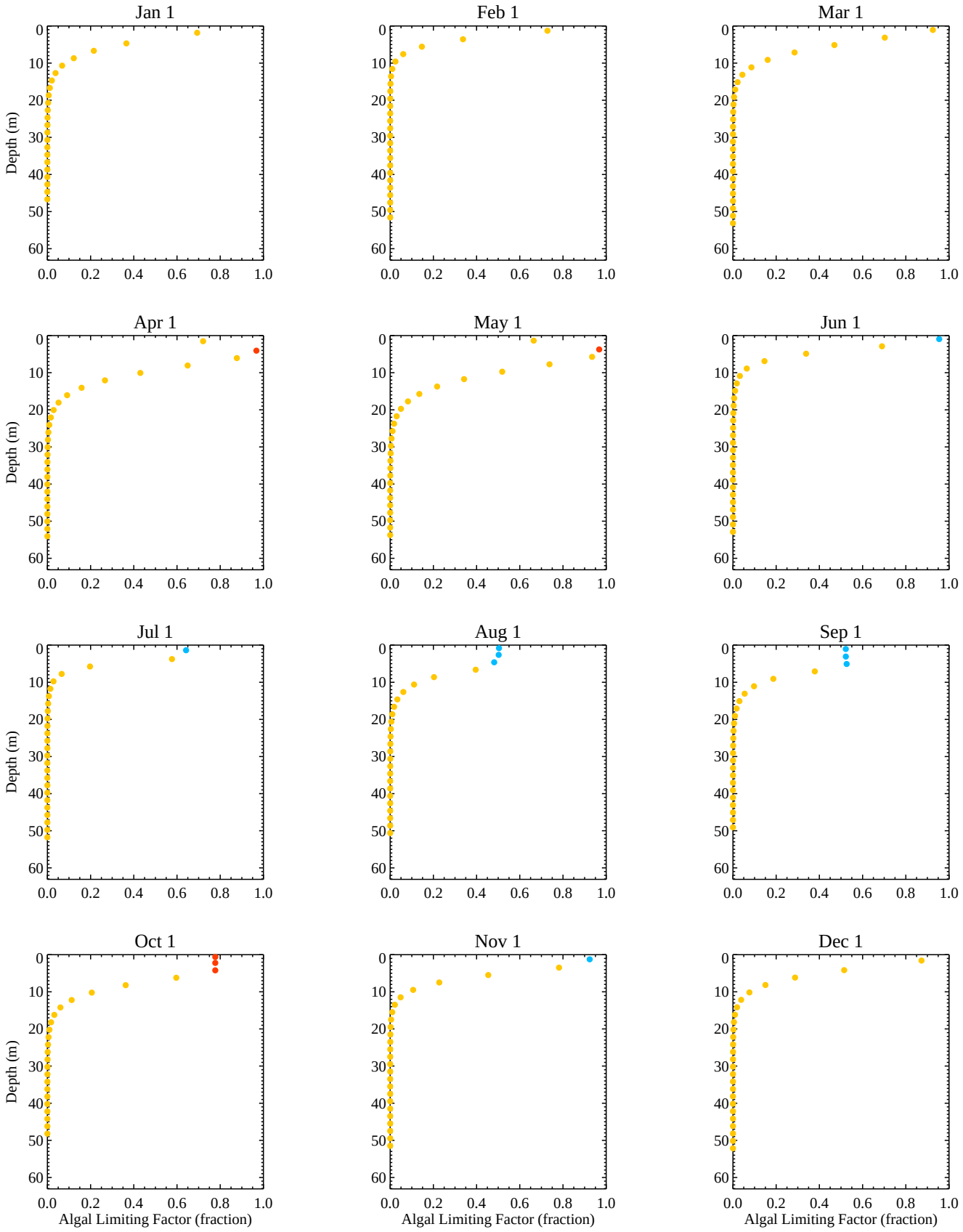

Figure J-21. Vertical profiles of algal limiting factor at Mansfield Dam (Segment 93) during 1985.

Profiles shown for first day of month.

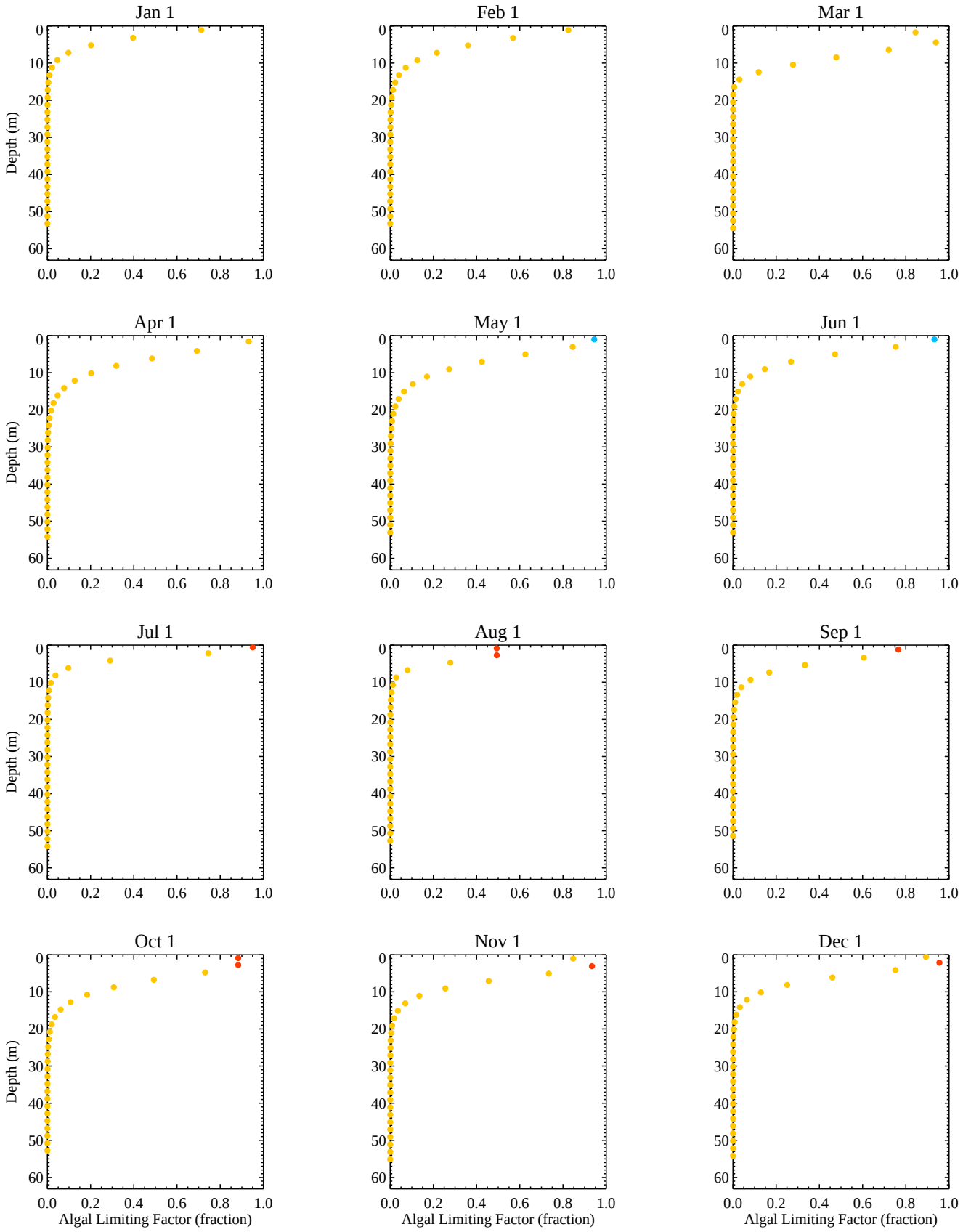

Figure J-21. Vertical profiles of algal limiting factor at Mansfield Dam (Segment 93) during 1986.

Profiles shown for first day of month.

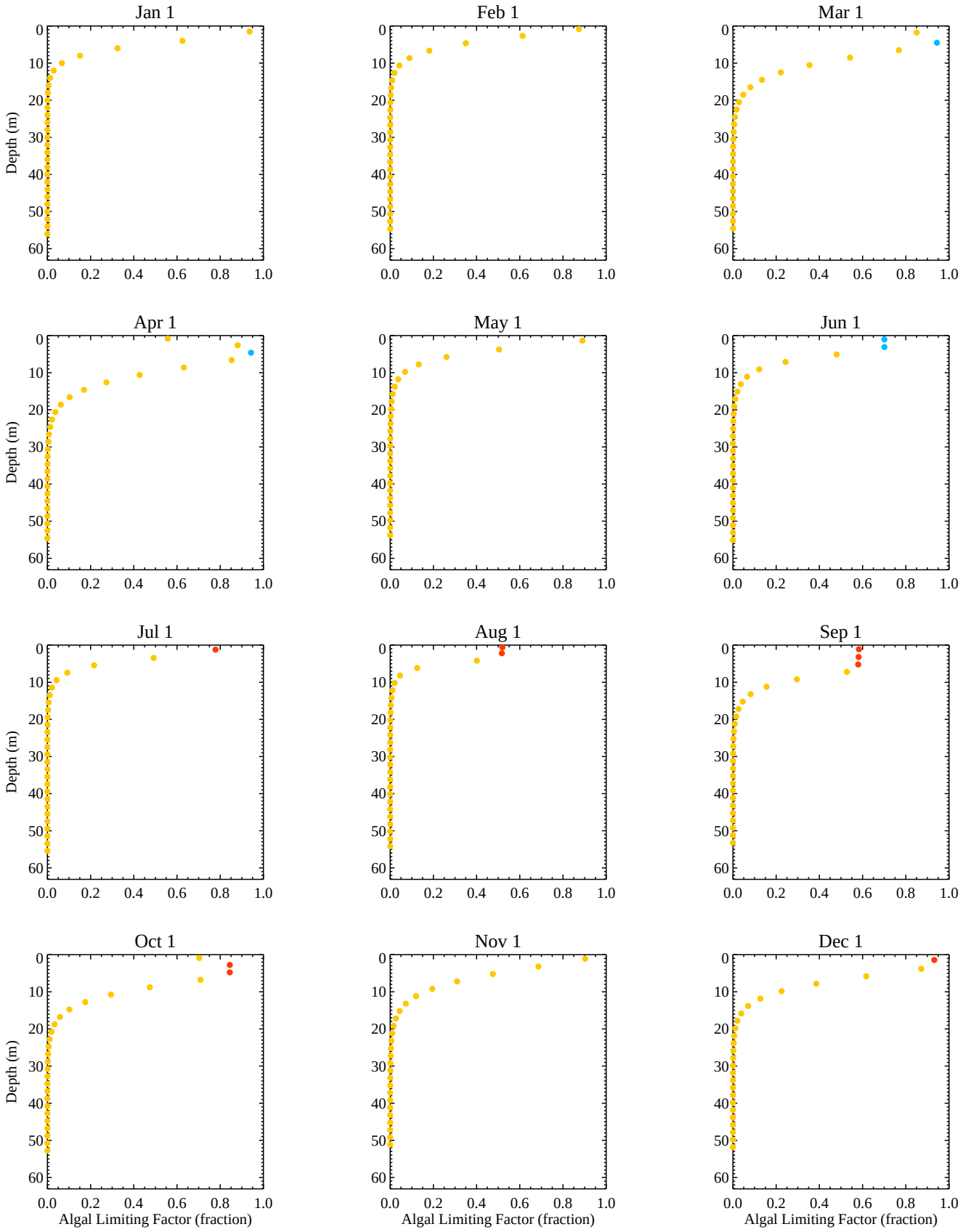

Figure J-21. Vertical profiles of algal limiting factor at Mansfield Dam (Segment 93) during 1987.

Profiles shown for first day of month.

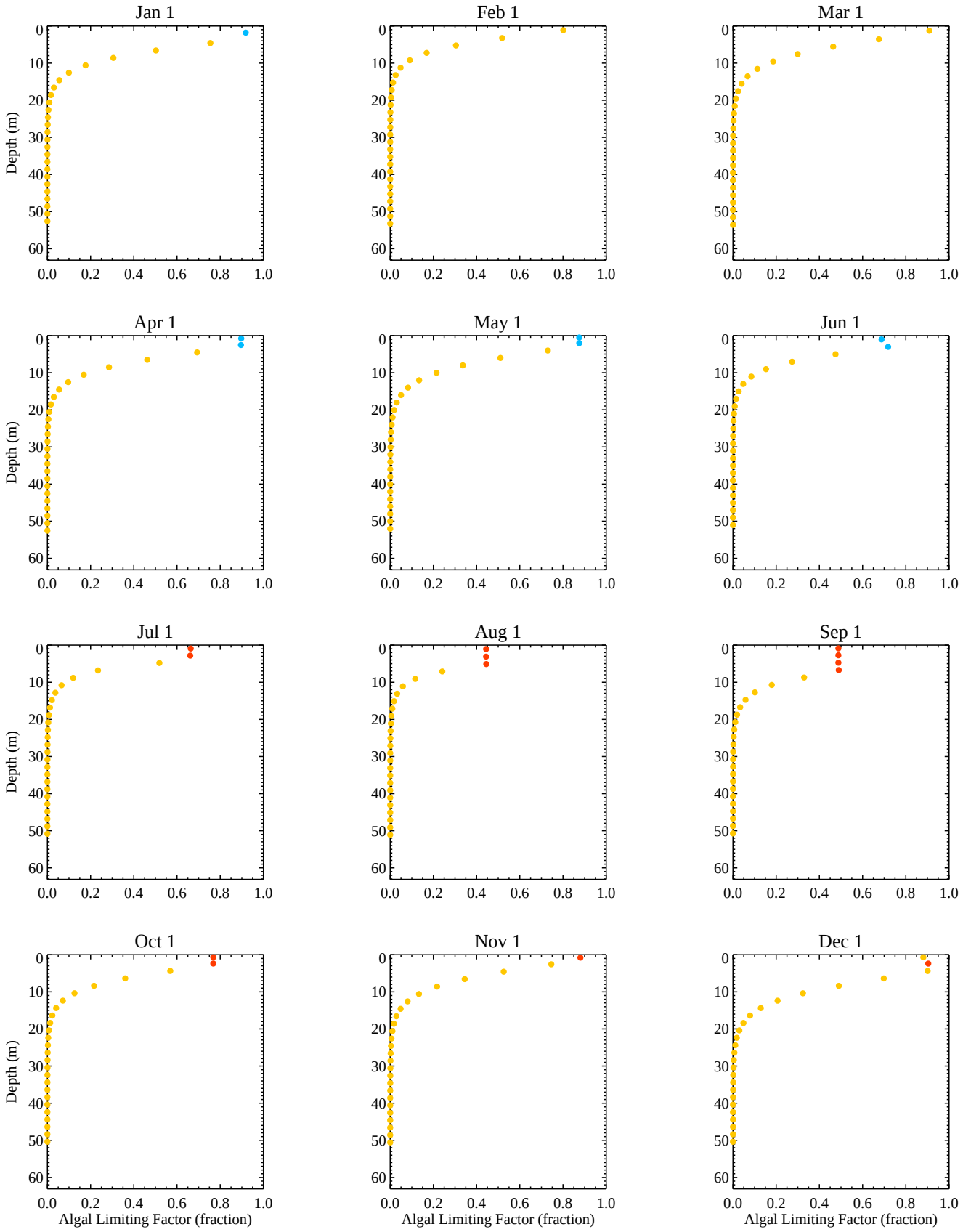

Figure J-21. Vertical profiles of algal limiting factor at Mansfield Dam (Segment 93) during 1988.

Profiles shown for first day of month.

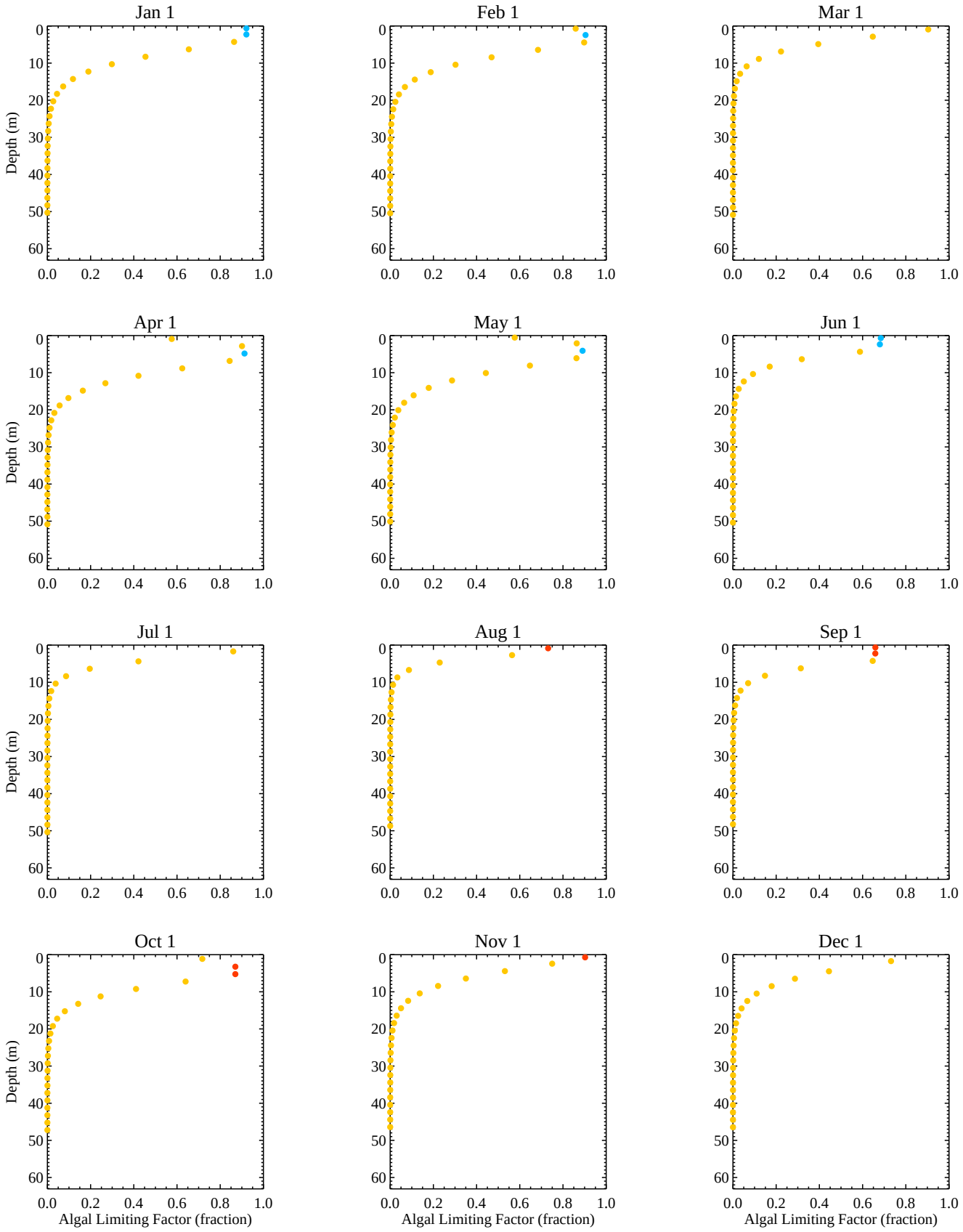

Figure J-21. Vertical profiles of algal limiting factor at Mansfield Dam (Segment 93) during 1989.

Profiles shown for first day of month.

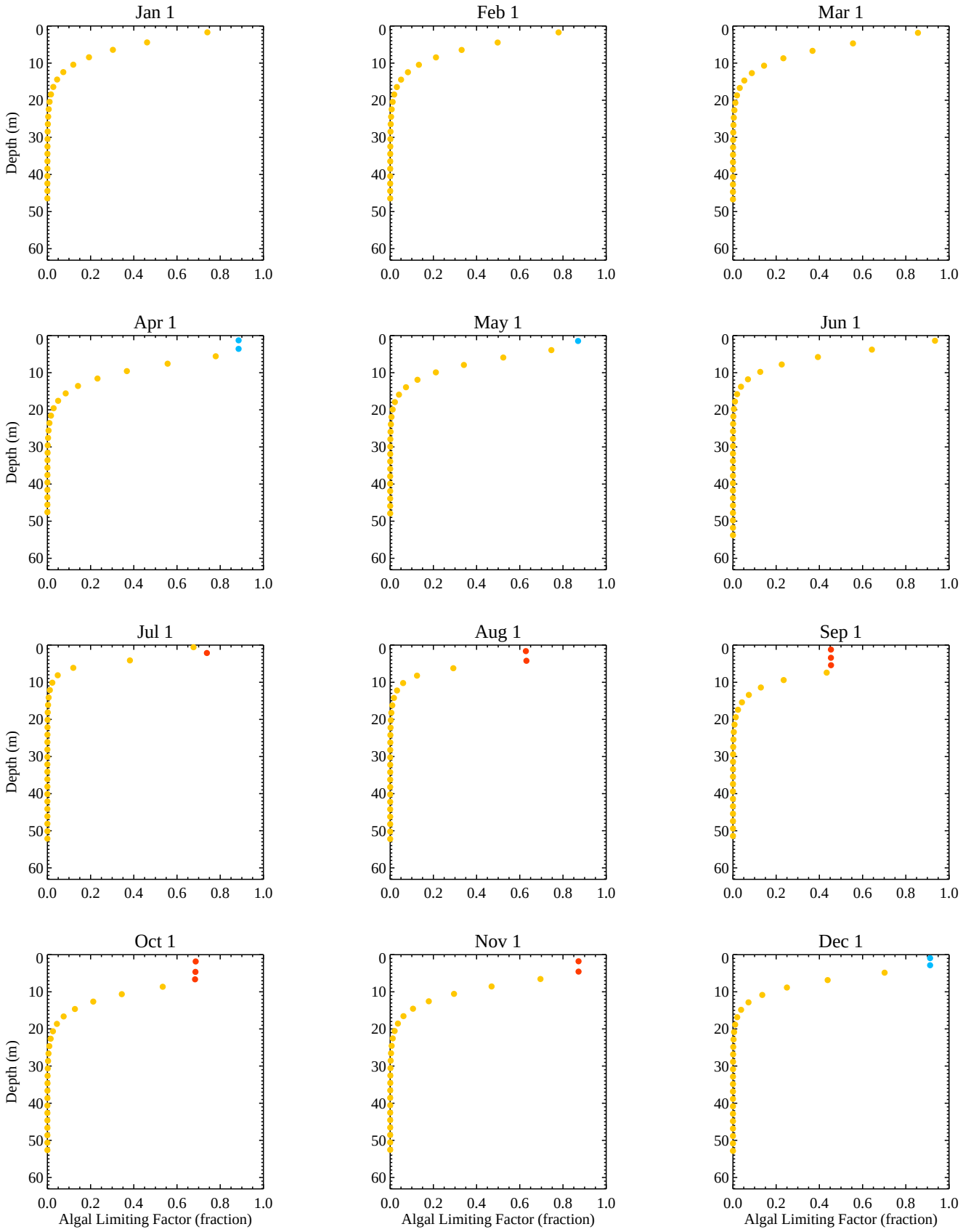

Figure J-21. Vertical profiles of algal limiting factor at Mansfield Dam (Segment 93) during 1990.

Profiles shown for first day of month.

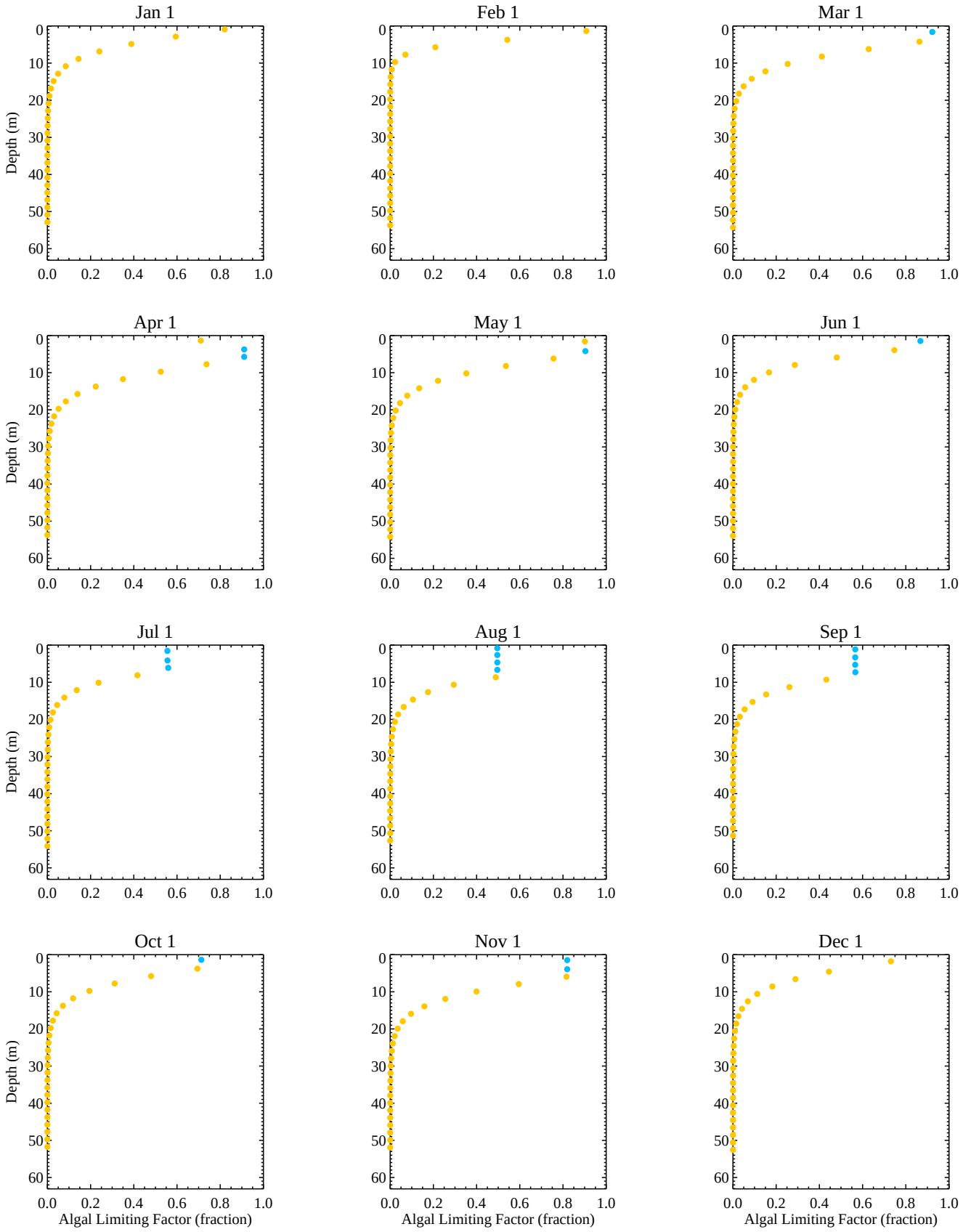

Figure J-21. Vertical profiles of algal limiting factor at Mansfield Dam (Segment 93) during 1991.

Profiles shown for first day of month.

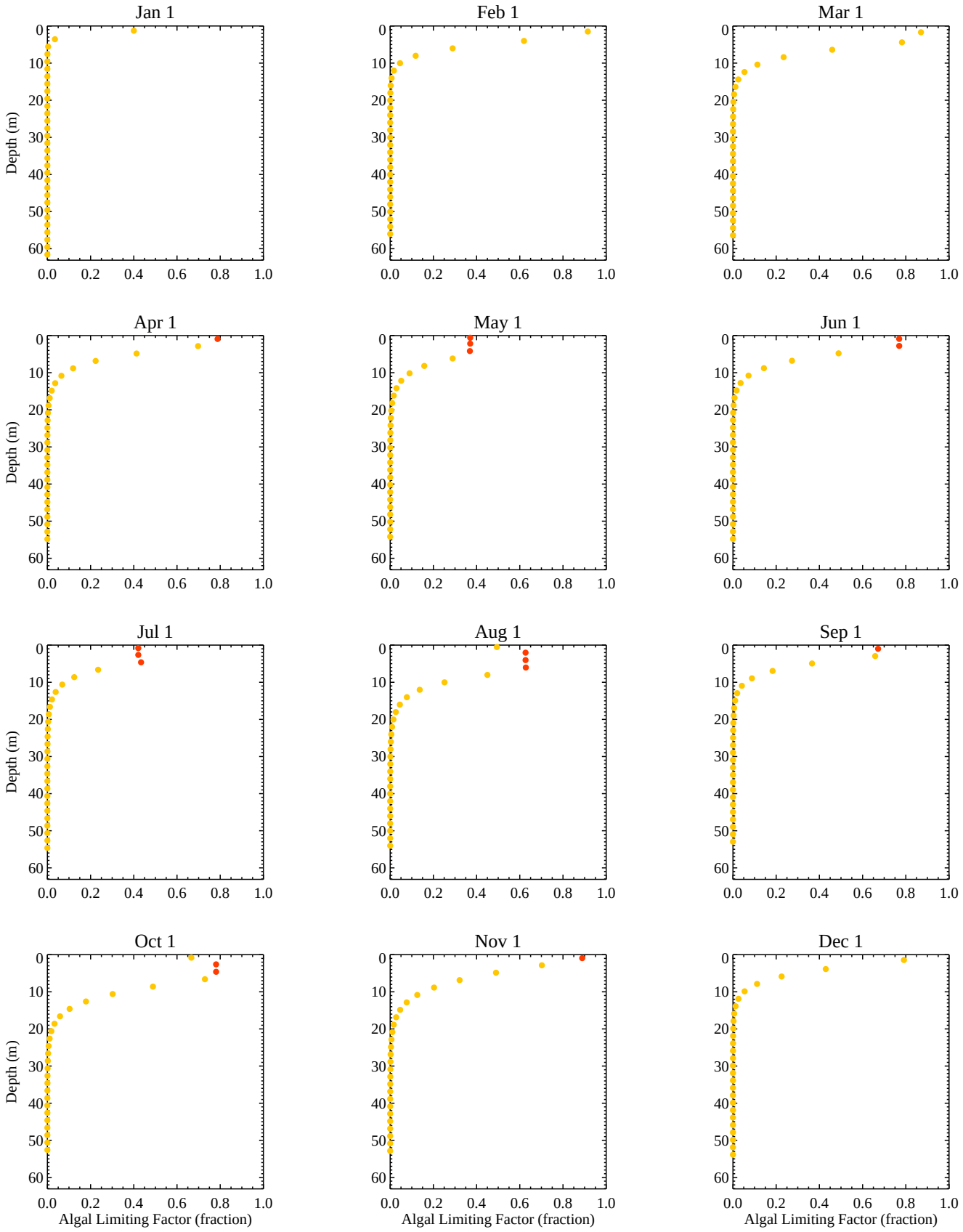

Figure J-21. Vertical profiles of algal limiting factor at Mansfield Dam (Segment 93) during 1992.

Profiles shown for first day of month.

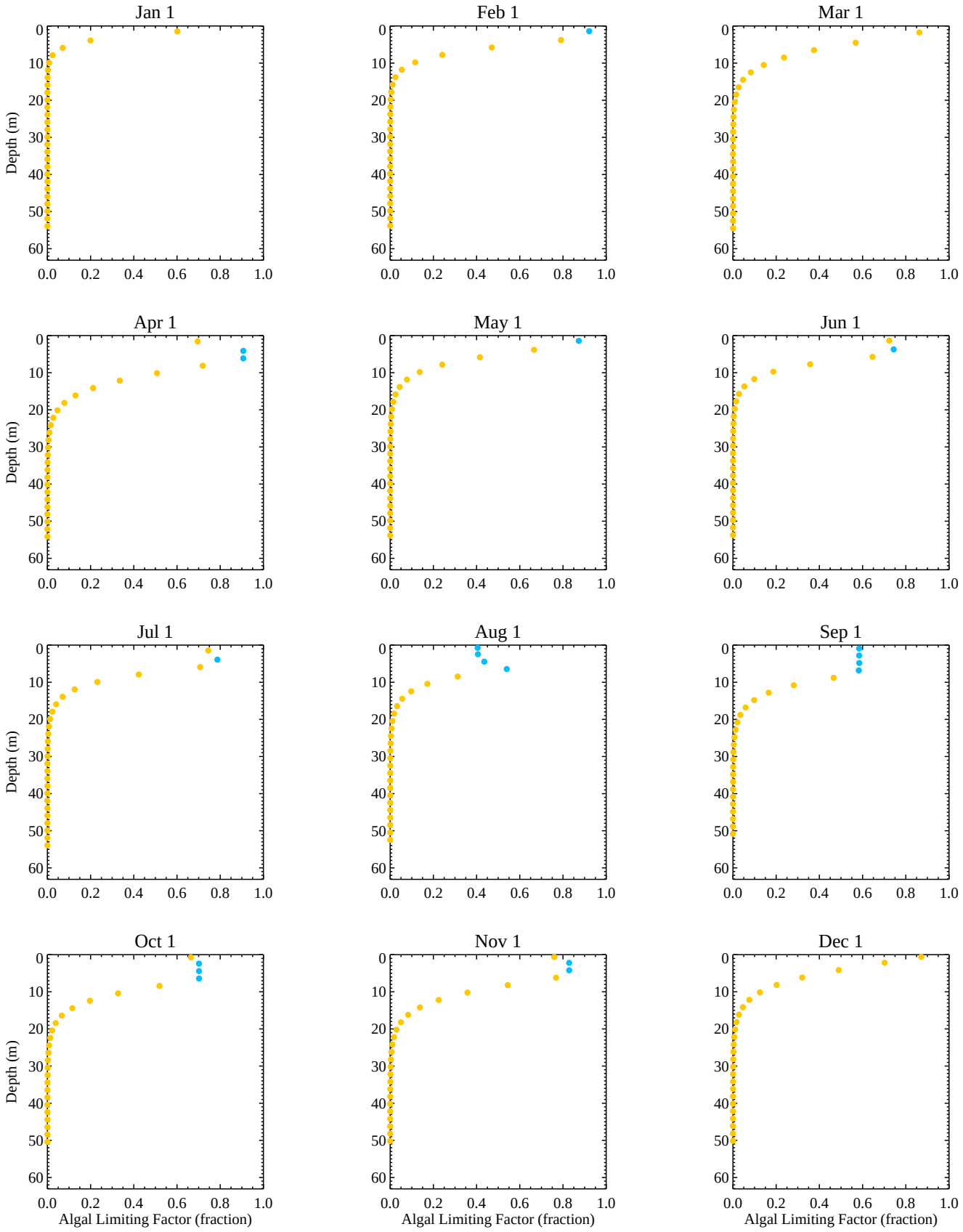

Figure J-21. Vertical profiles of algal limiting factor at Mansfield Dam (Segment 93) during 1993.

Profiles shown for first day of month.

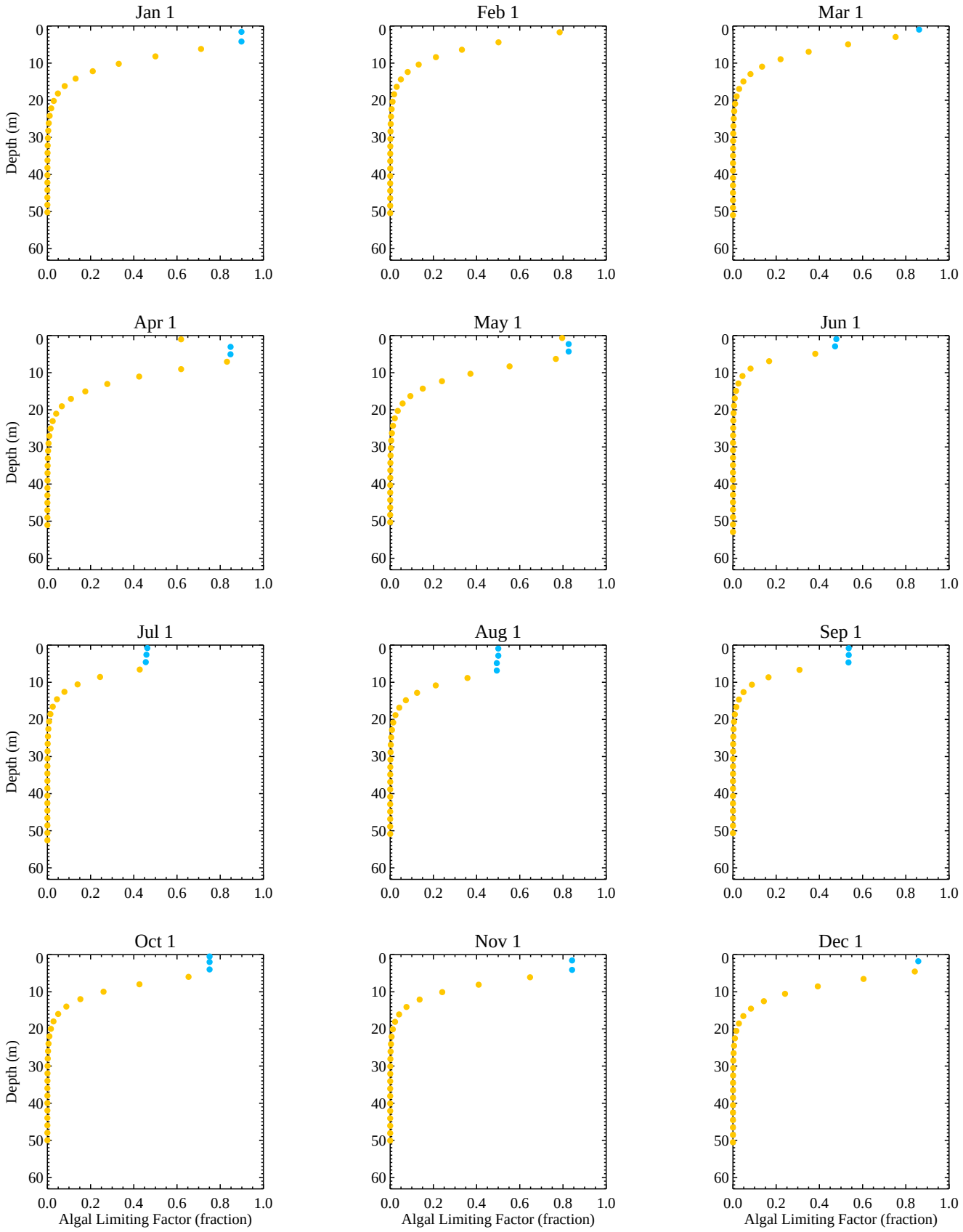

Figure J-21. Vertical profiles of algal limiting factor at Mansfield Dam (Segment 93) during 1994.

Profiles shown for first day of month.

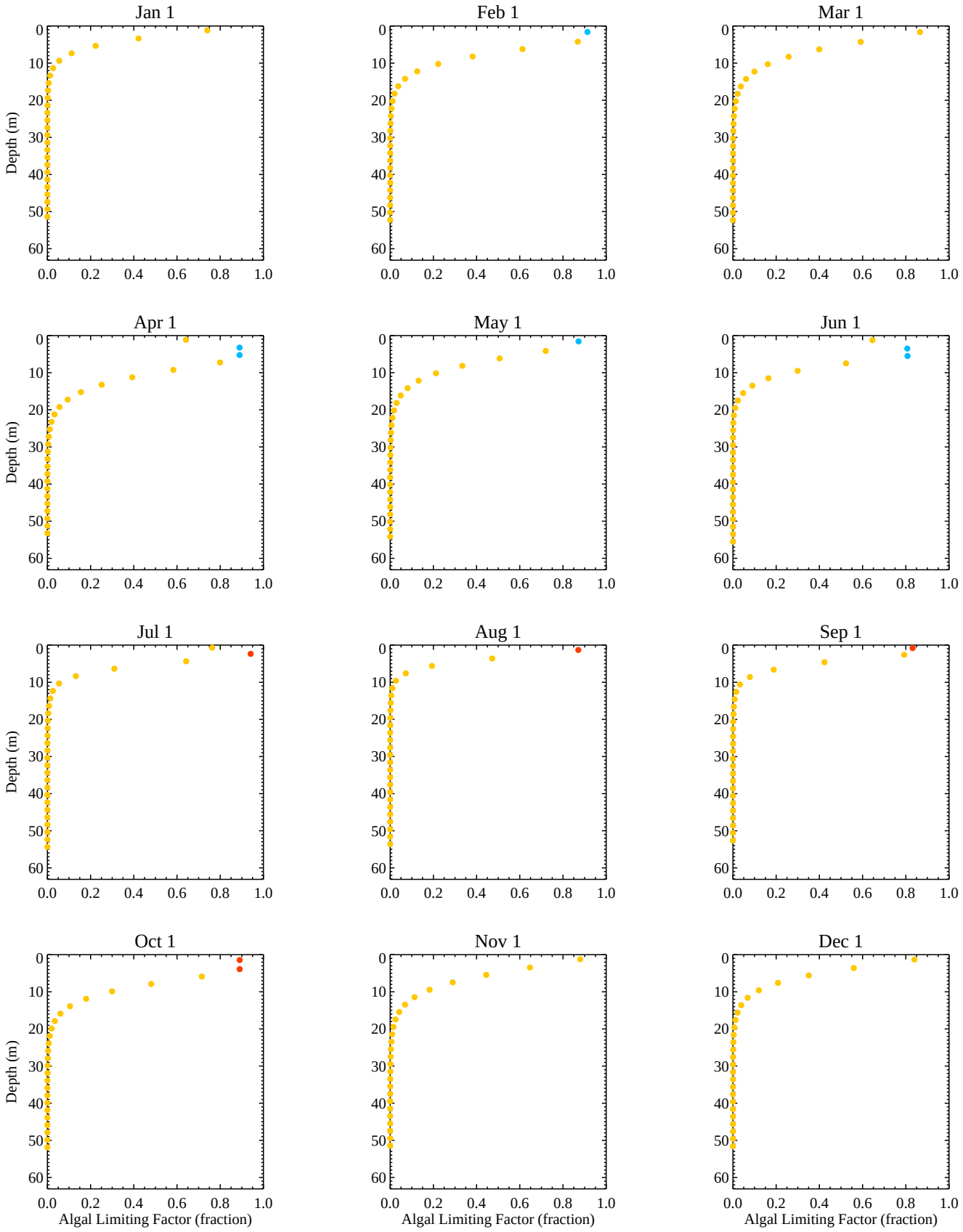

Figure J-21. Vertical profiles of algal limiting factor at Mansfield Dam (Segment 93) during 1995.

Profiles shown for first day of month.

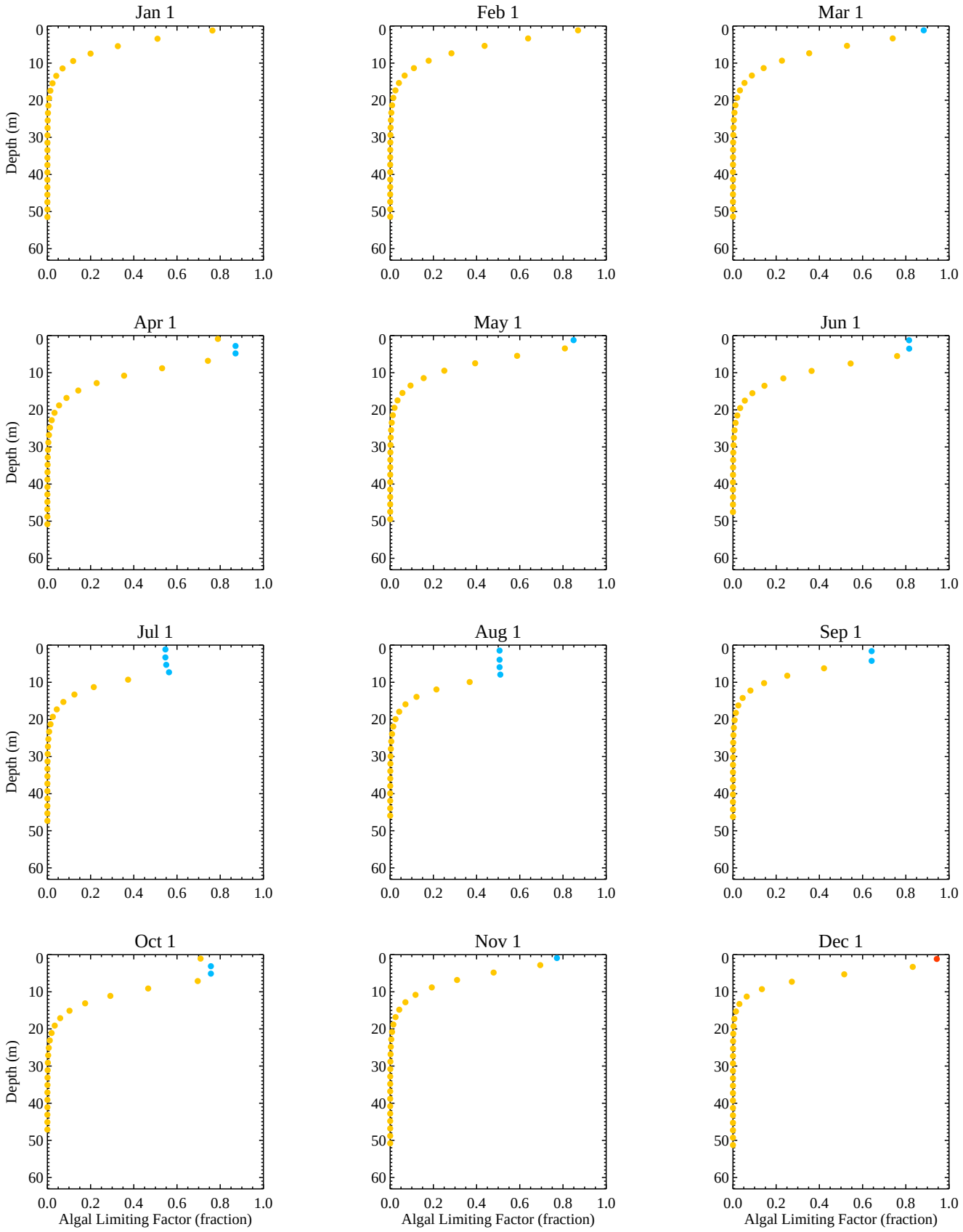

Figure J-21. Vertical profiles of algal limiting factor at Mansfield Dam (Segment 93) during 1996.

Profiles shown for first day of month.

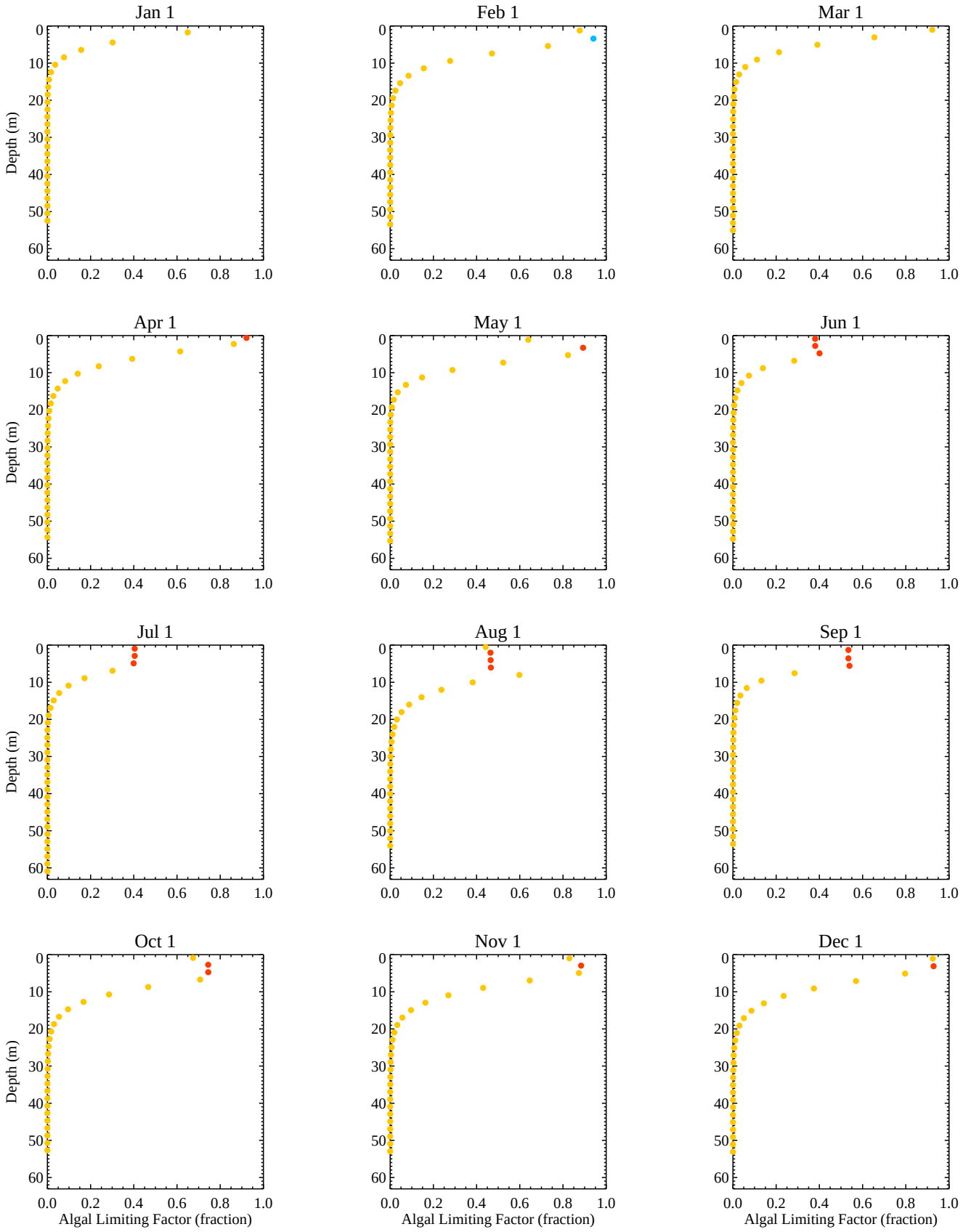

Figure J-21. Vertical profiles of algal limiting factor at Mansfield Dam (Segment 93) during 1997.

Profiles shown for first day of month.

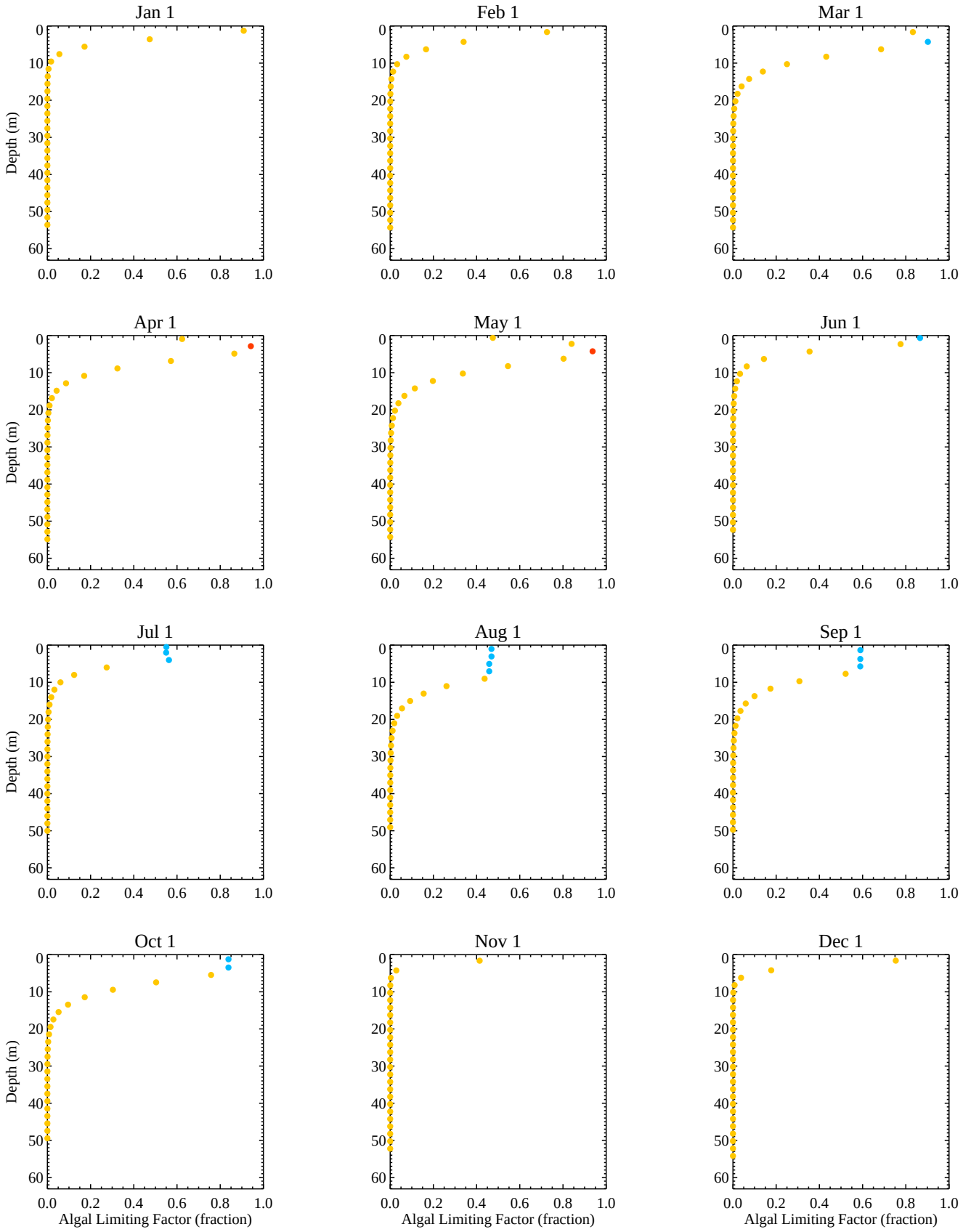

Figure J-21. Vertical profiles of algal limiting factor at Mansfield Dam (Segment 93) during 1998.

Profiles shown for first day of month.

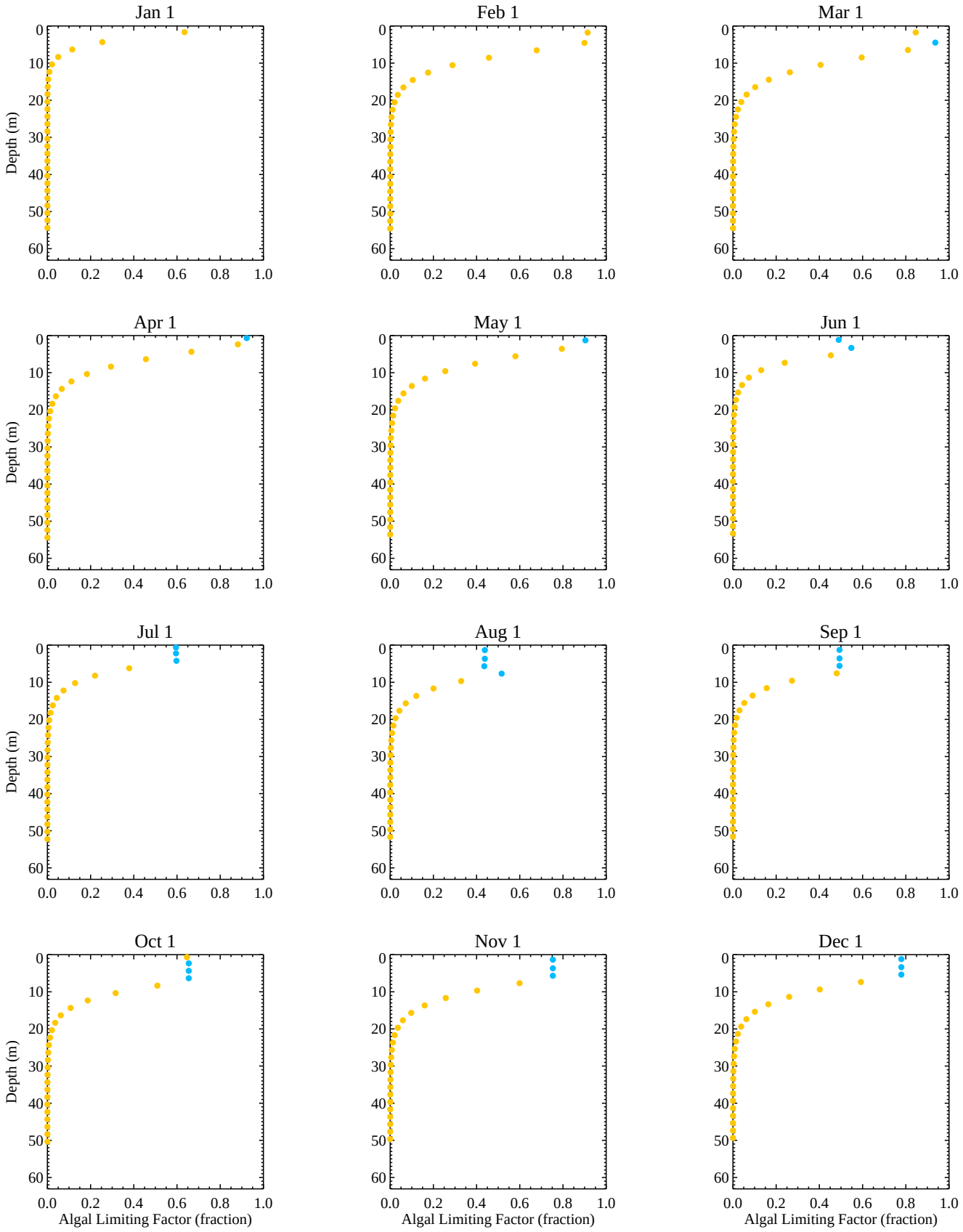

Figure J-21. Vertical profiles of algal limiting factor at Mansfield Dam (Segment 93) during 1999.

Profiles shown for first day of month.

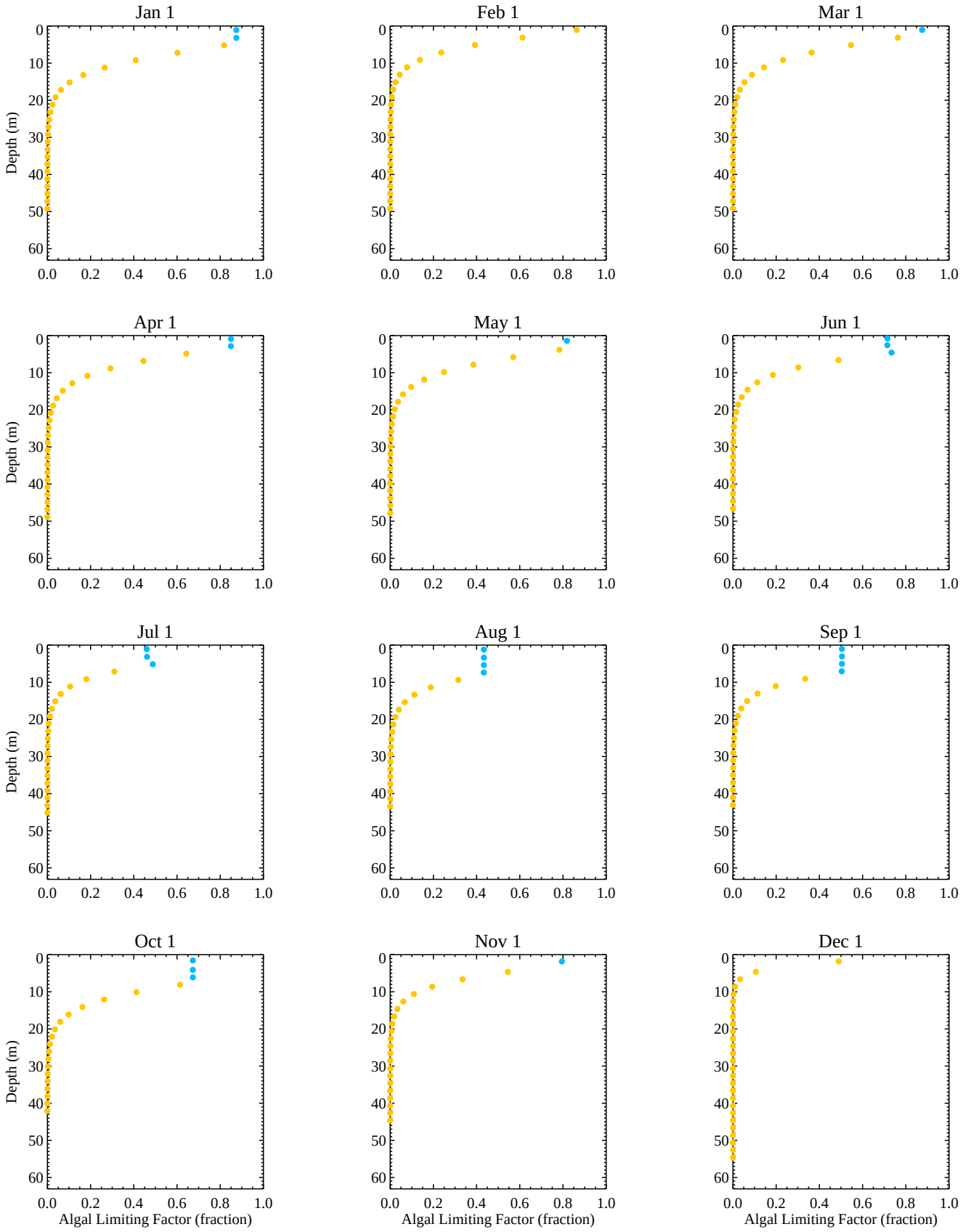

Figure J-21. Vertical profiles of algal limiting factor at Mansfield Dam (Segment 93) during 2000.

Profiles shown for first day of month.

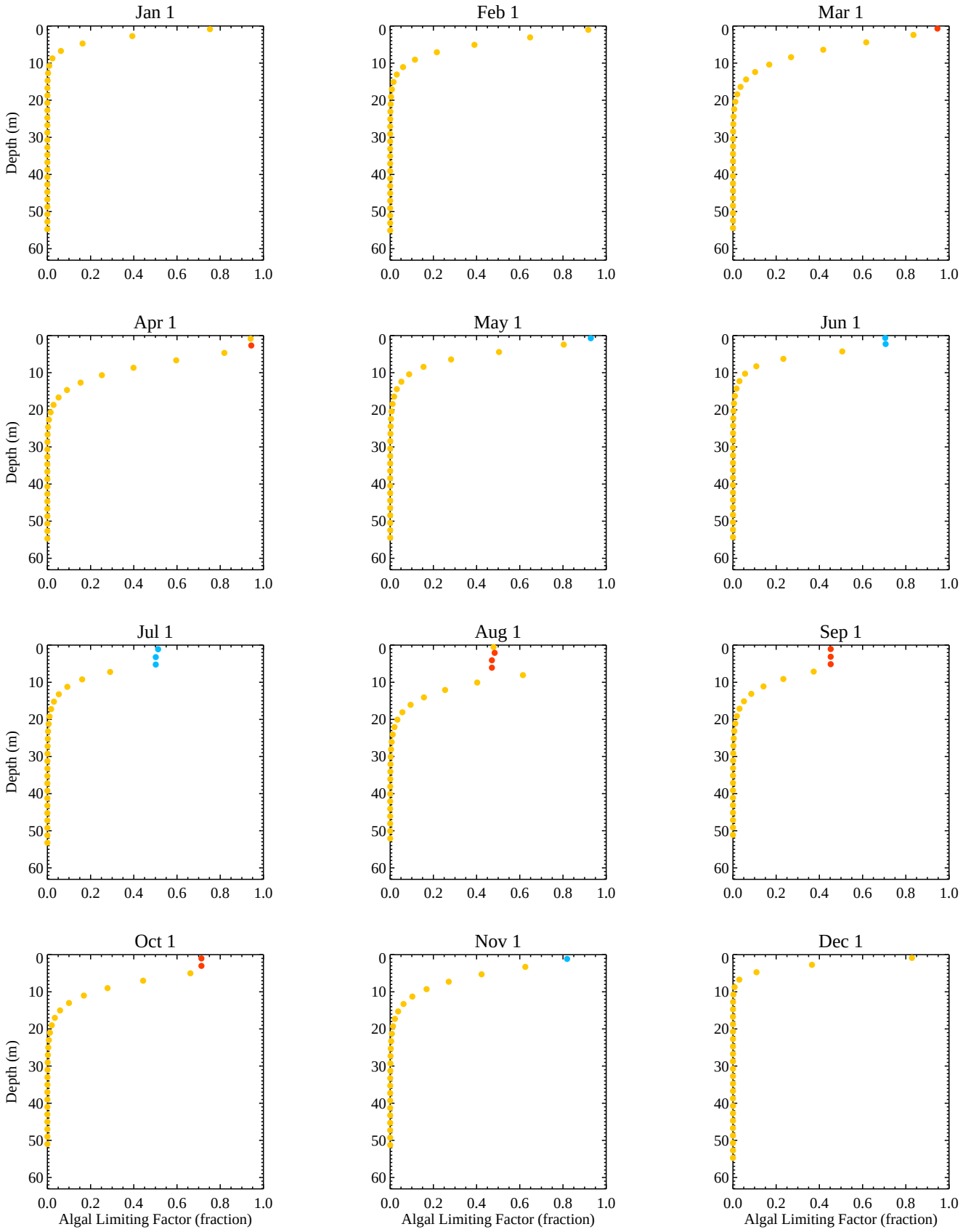

Figure J-21. Vertical profiles of algal limiting factor at Mansfield Dam (Segment 93) during 2001.

Profiles shown for first day of month.

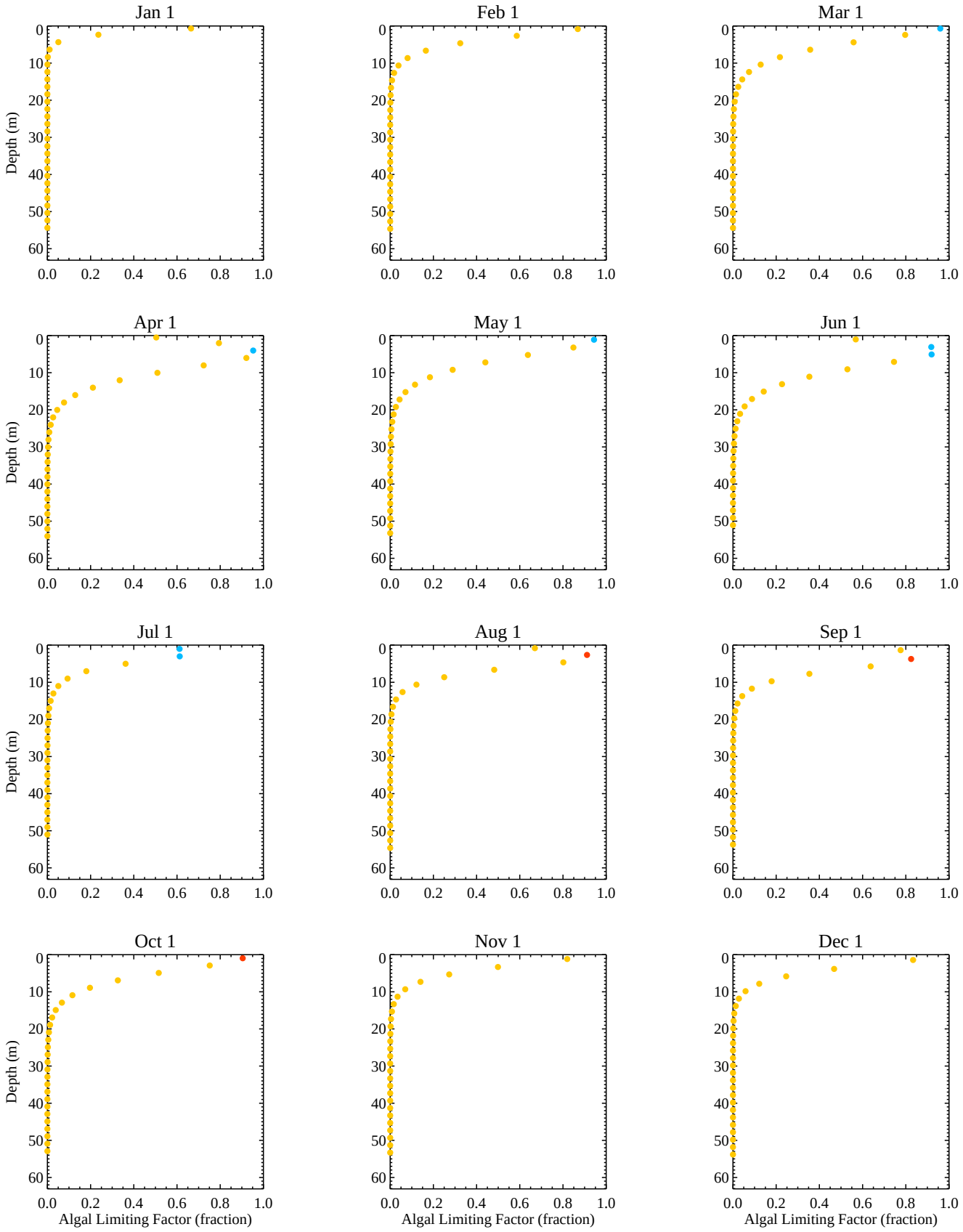

Figure J-21. Vertical profiles of algal limiting factor at Mansfield Dam (Segment 93) during 2002.

Profiles shown for first day of month.

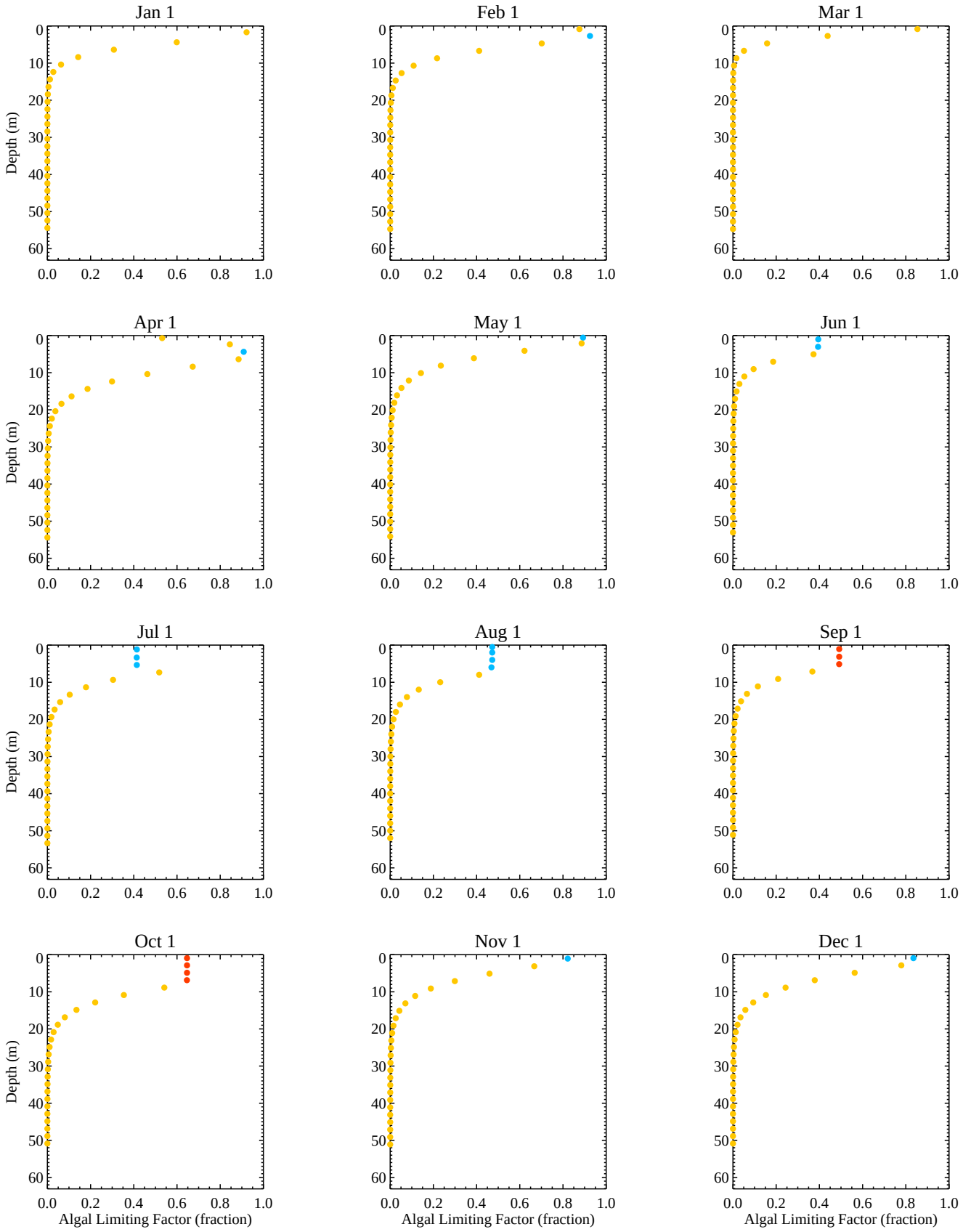

Figure J-21. Vertical profiles of algal limiting factor at Mansfield Dam (Segment 93) during 2003.

Profiles shown for first day of month.

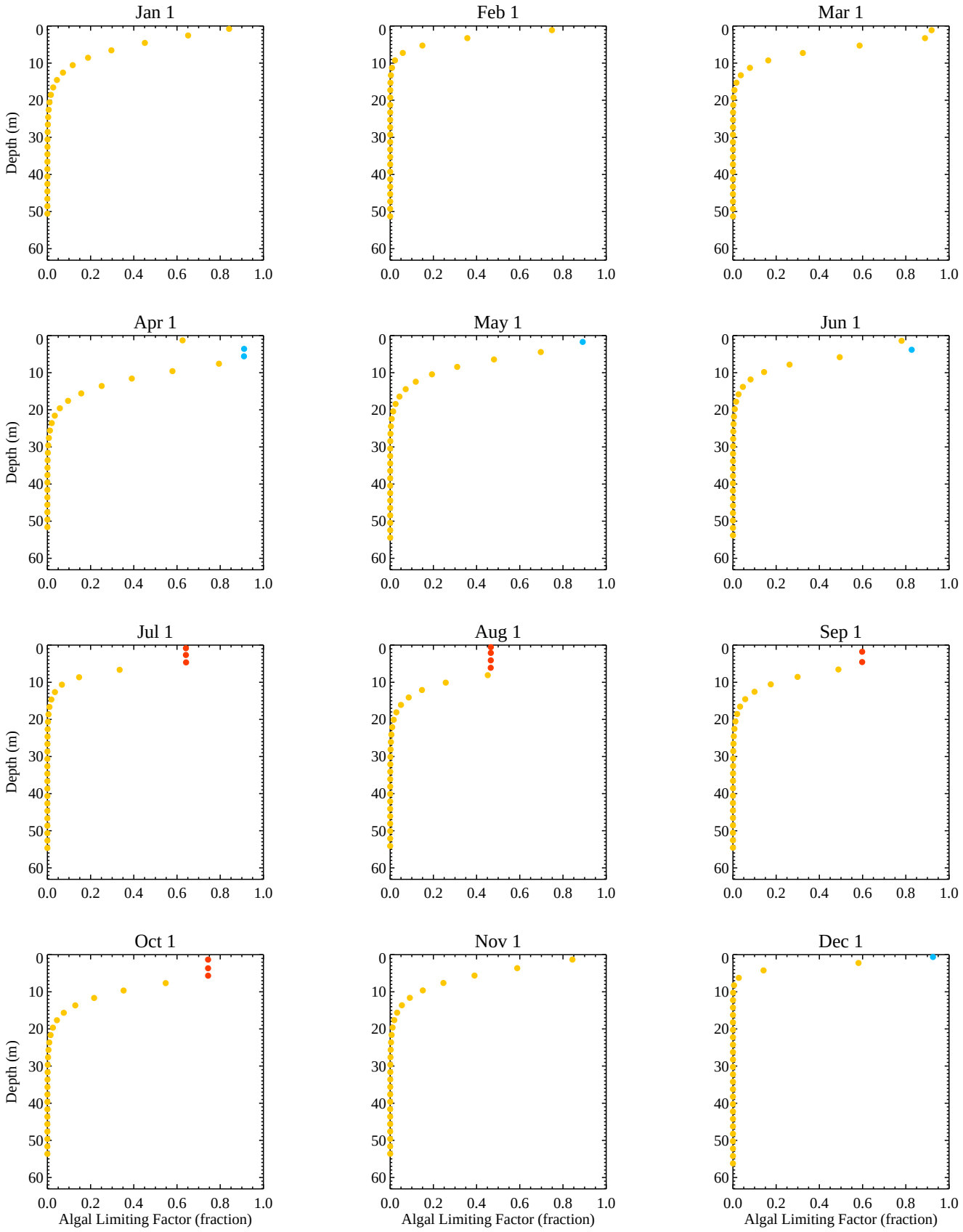

Figure J-21. Vertical profiles of algal limiting factor at Mansfield Dam (Segment 93) during 2004.

Profiles shown for first day of month.

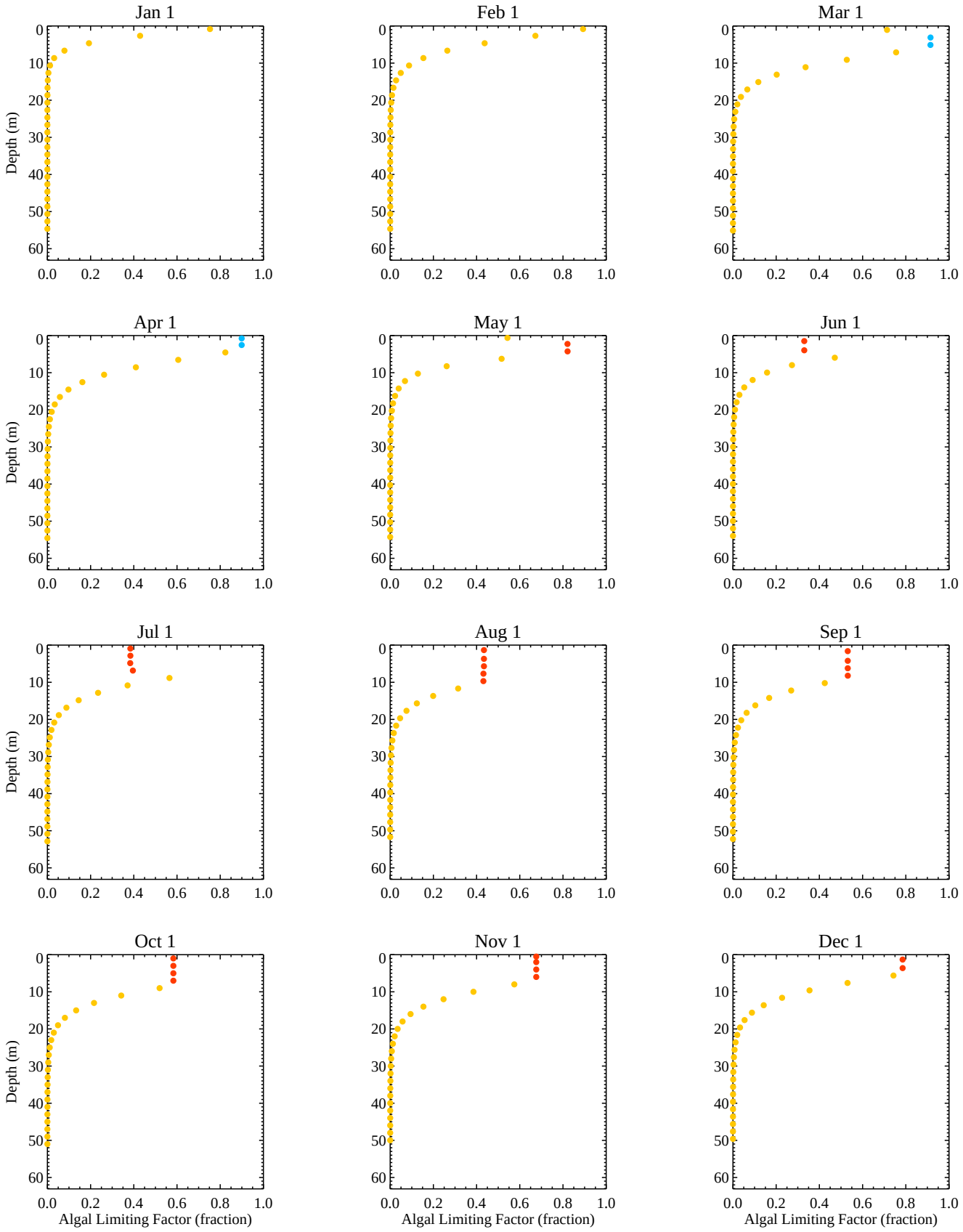

Figure J-21. Vertical profiles of algal limiting factor at Mansfield Dam (Segment 93) during 2005.

Profiles shown for first day of month.

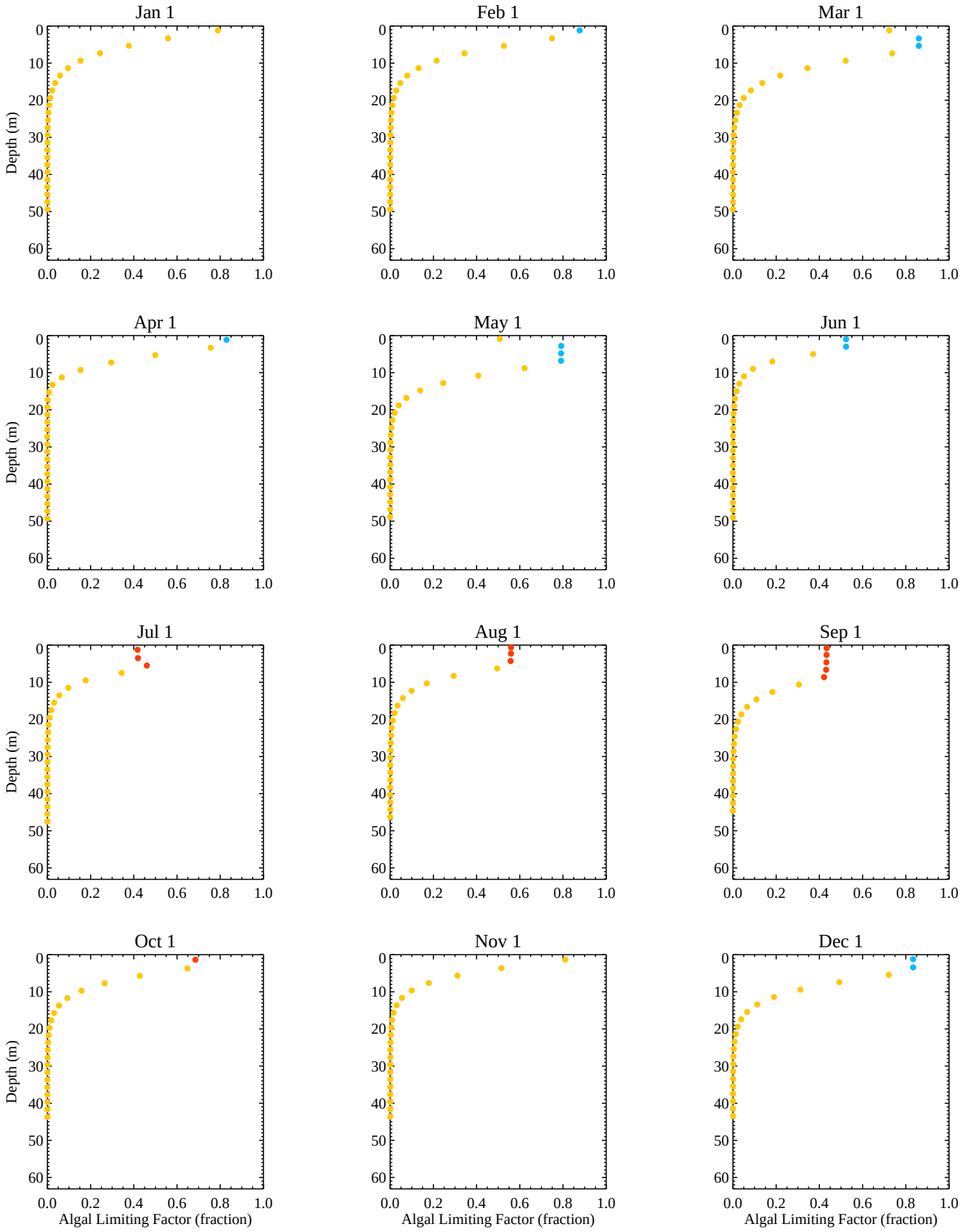

Figure J-21. Vertical profiles of algal limiting factor at Mansfield Dam (Segment 93) during 2006.

Profiles shown for first day of month.

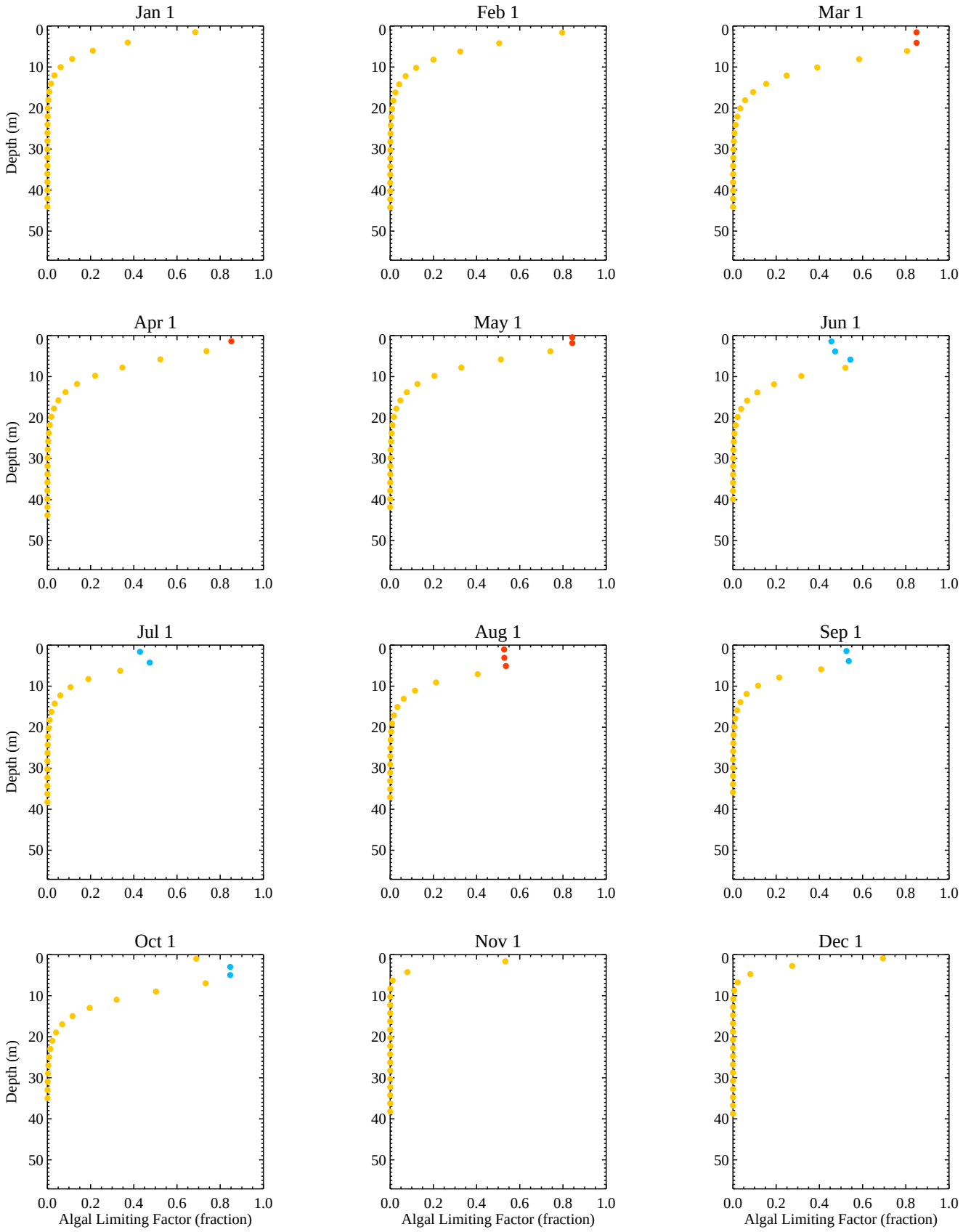

Figure J-22. Vertical profiles of algal limiting factor at Arkansas Bend (Segment 78) during 1984.

Profiles shown for first day of month.

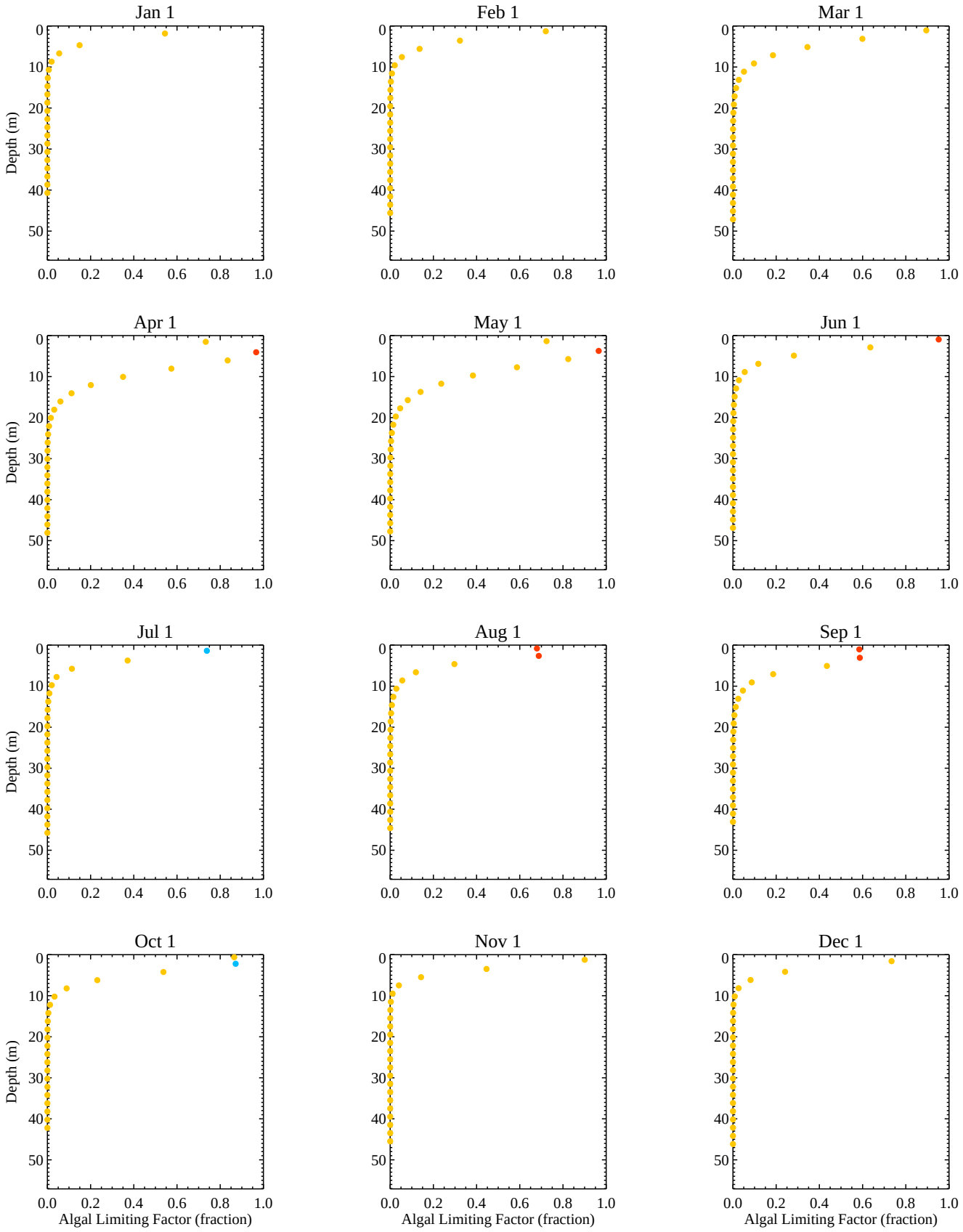

Figure J-22. Vertical profiles of algal limiting factor at Arkansas Bend (Segment 78) during 1985.

Profiles shown for first day of month.

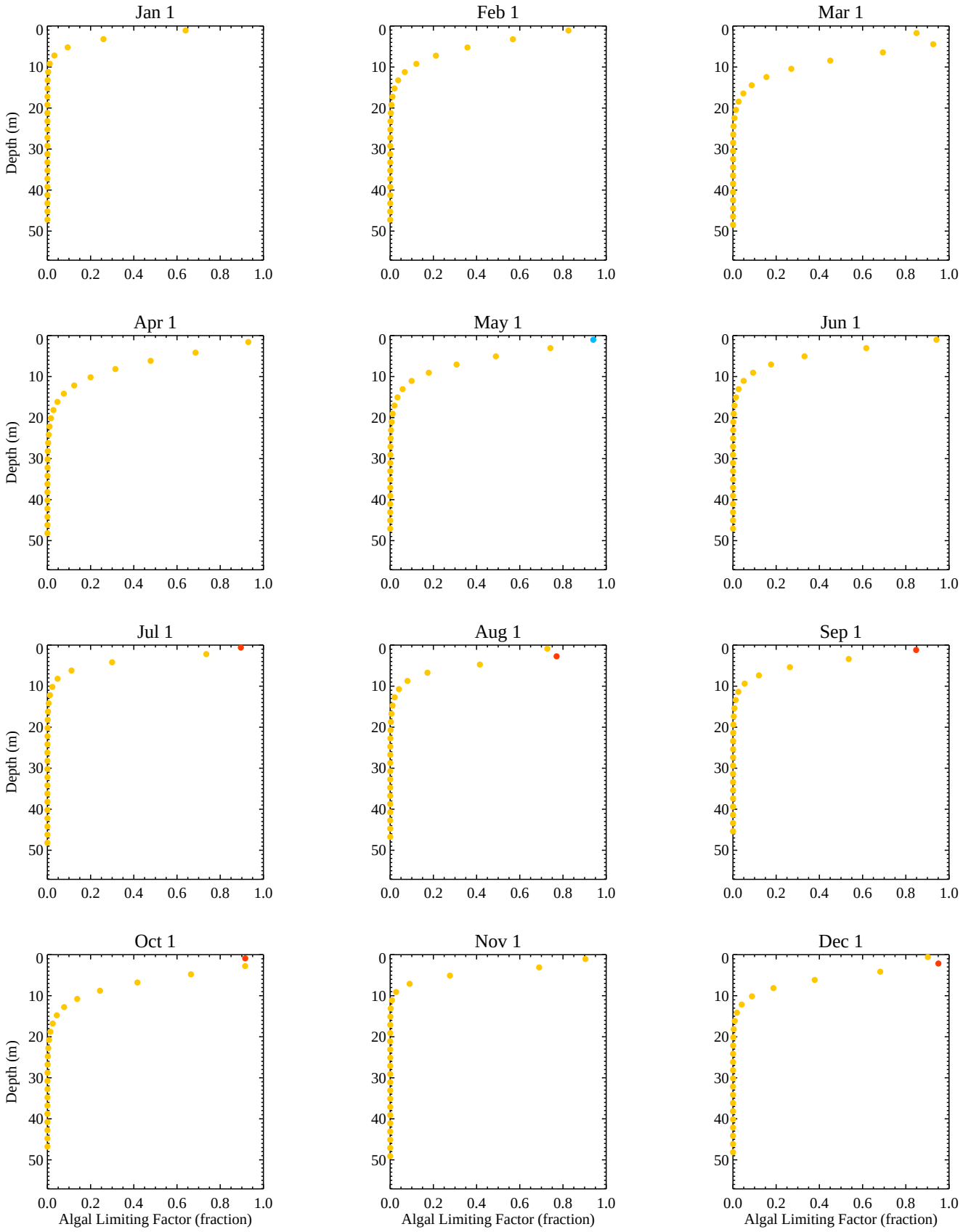

Figure J-22. Vertical profiles of algal limiting factor at Arkansas Bend (Segment 78) during 1986.

Profiles shown for first day of month.

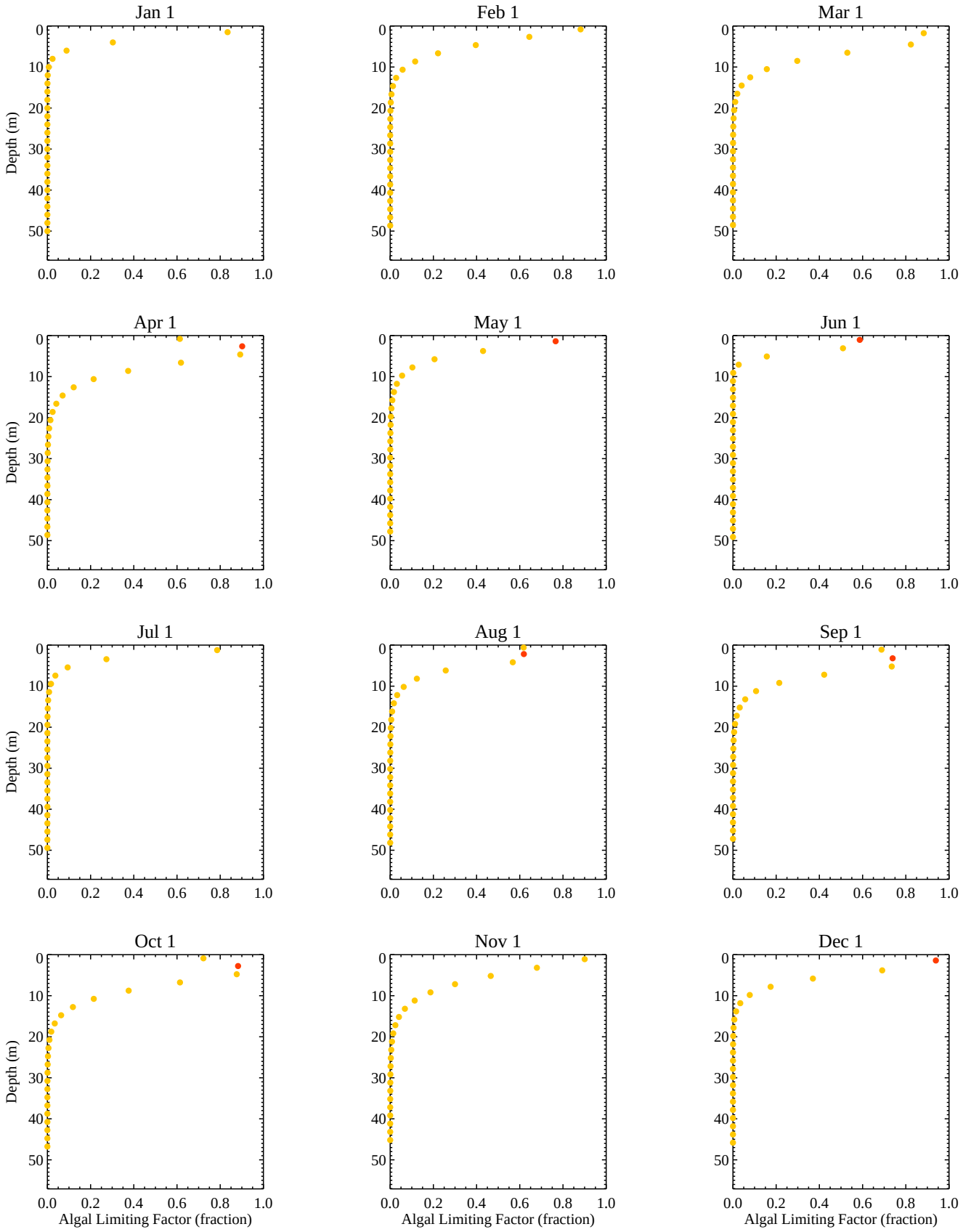

Figure J-22. Vertical profiles of algal limiting factor at Arkansas Bend (Segment 78) during 1987.

Profiles shown for first day of month.

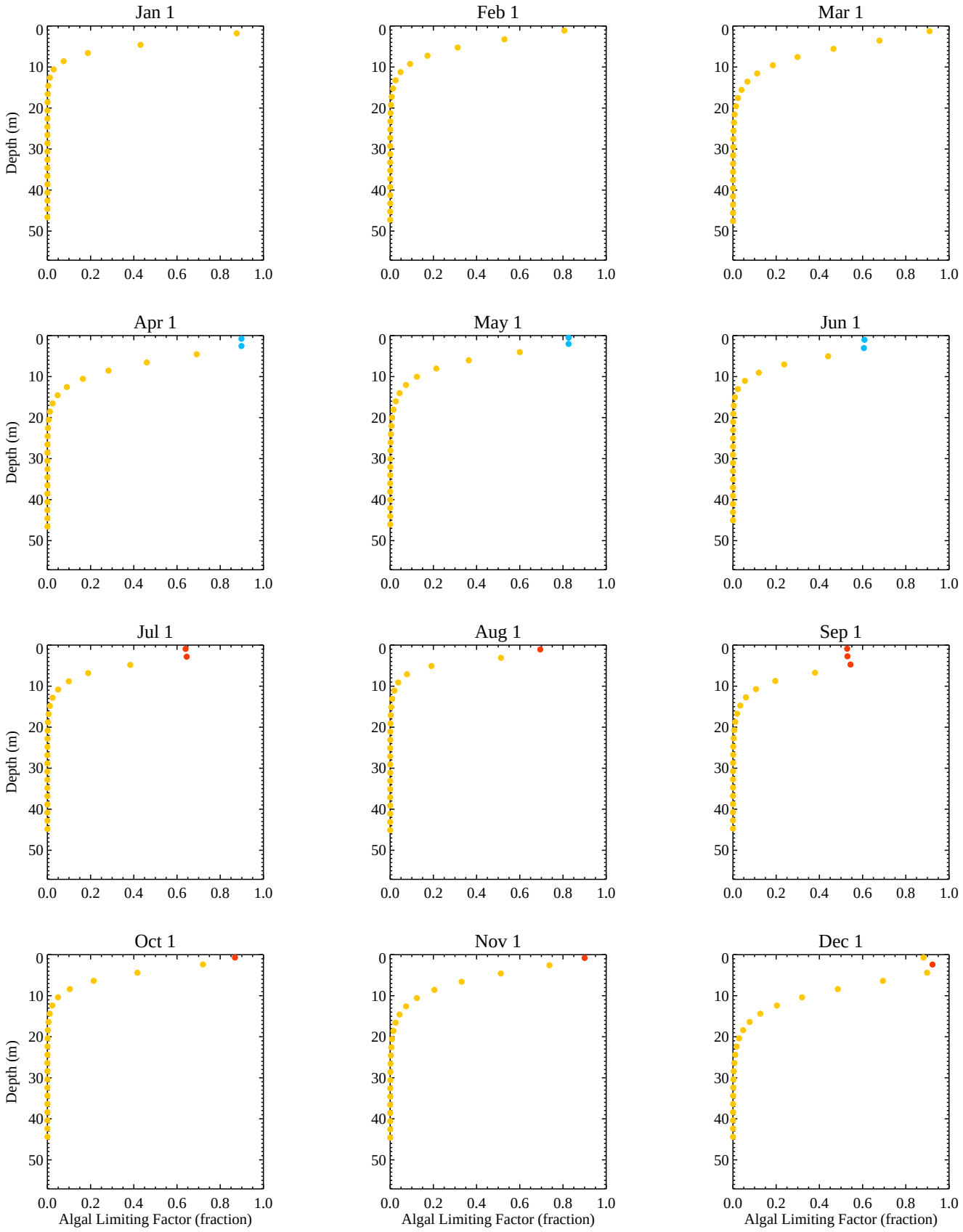

Figure J-22. Vertical profiles of algal limiting factor at Arkansas Bend (Segment 78) during 1988.

Profiles shown for first day of month.

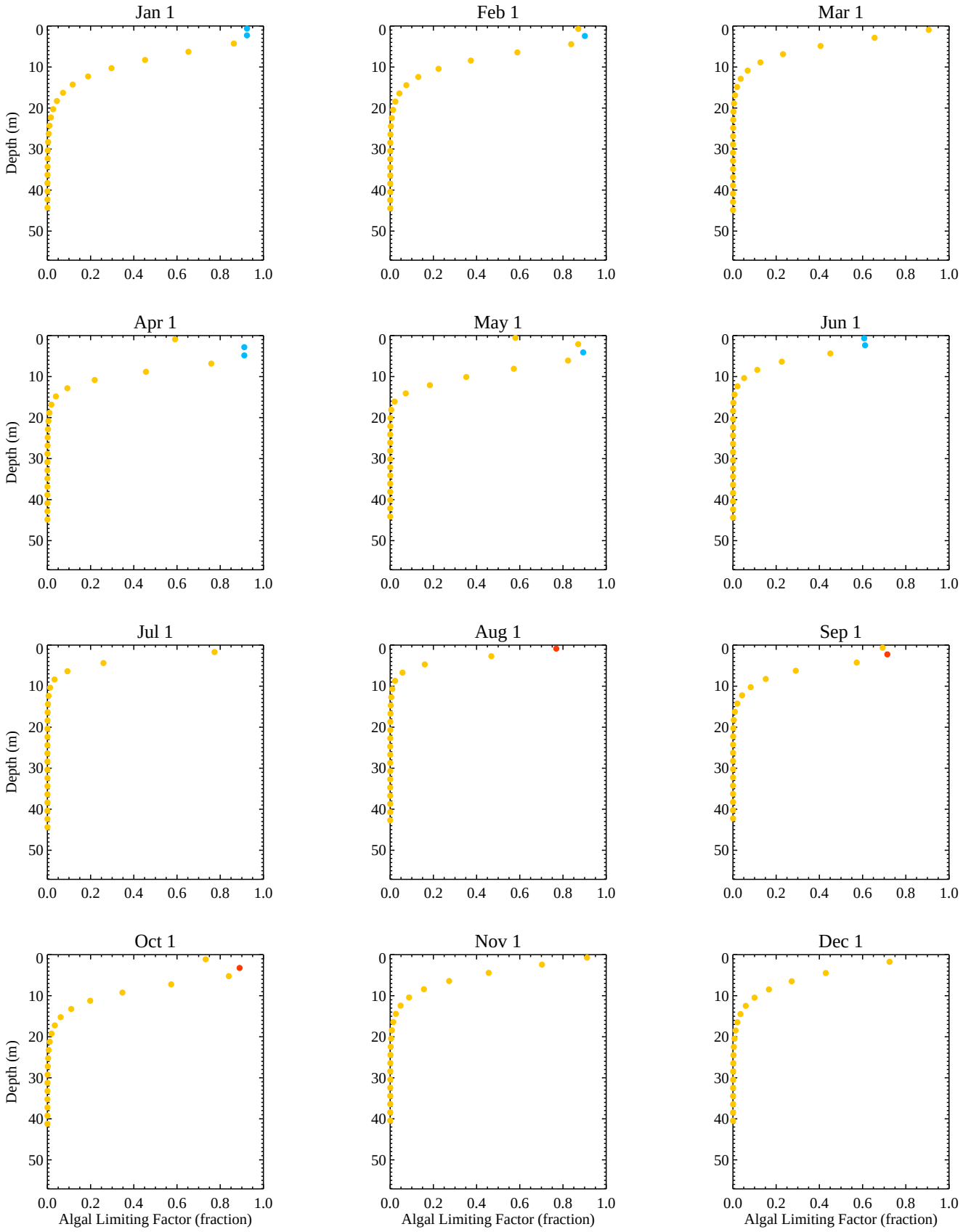

Figure J-22. Vertical profiles of algal limiting factor at Arkansas Bend (Segment 78) during 1989.

Profiles shown for first day of month.

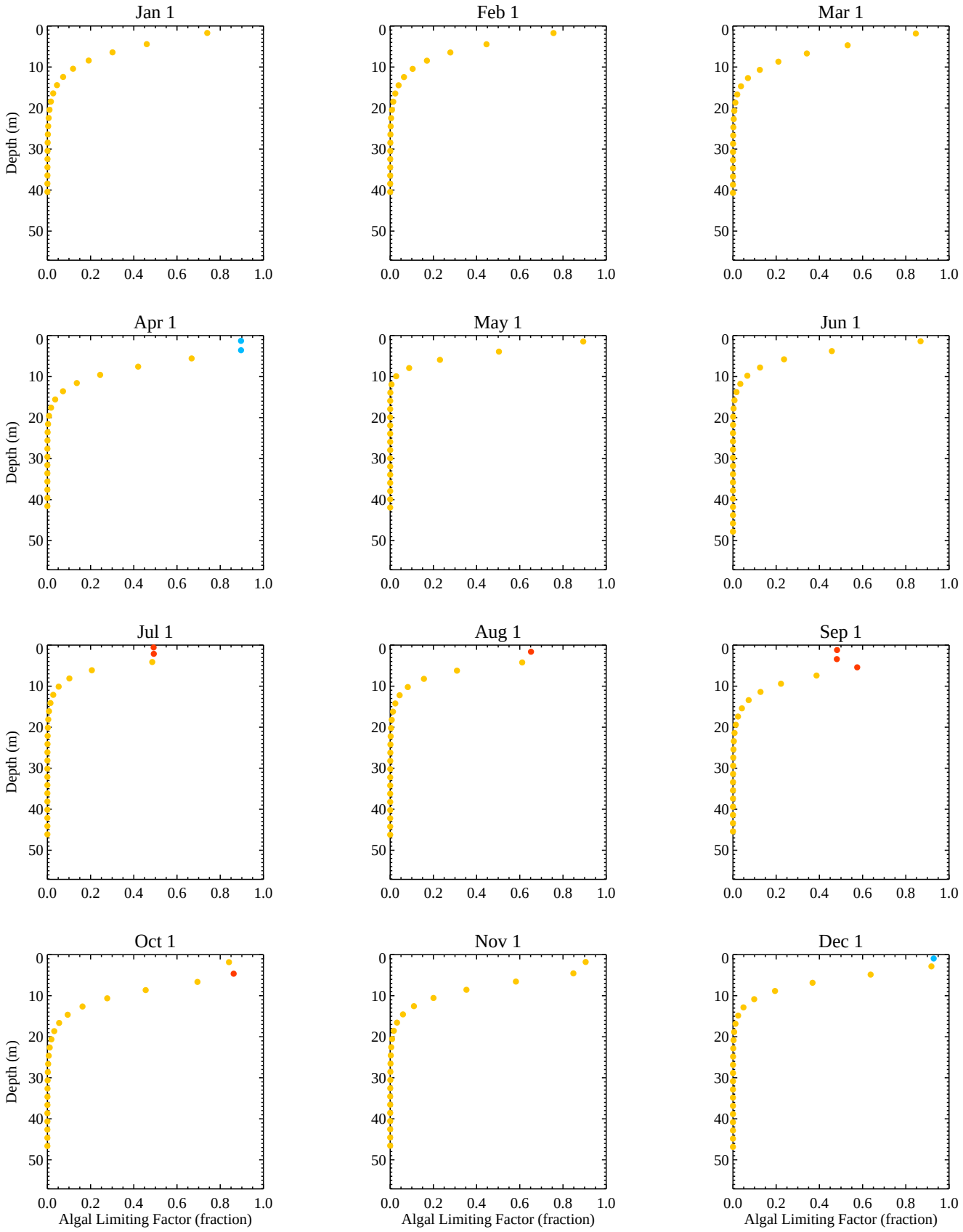

Figure J-22. Vertical profiles of algal limiting factor at Arkansas Bend (Segment 78) during 1990.

Profiles shown for first day of month.

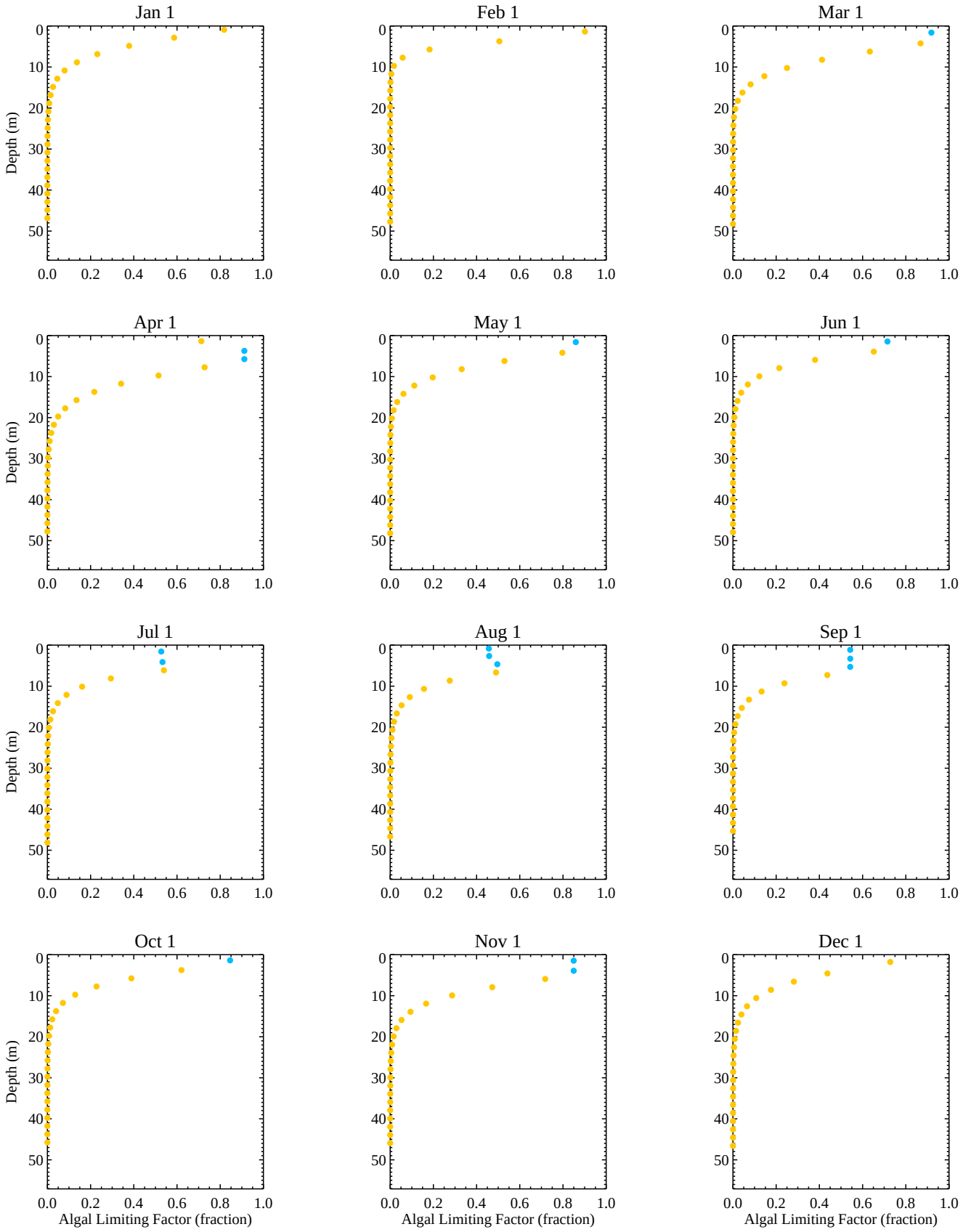

Figure J-22. Vertical profiles of algal limiting factor at Arkansas Bend (Segment 78) during 1991.

Profiles shown for first day of month.

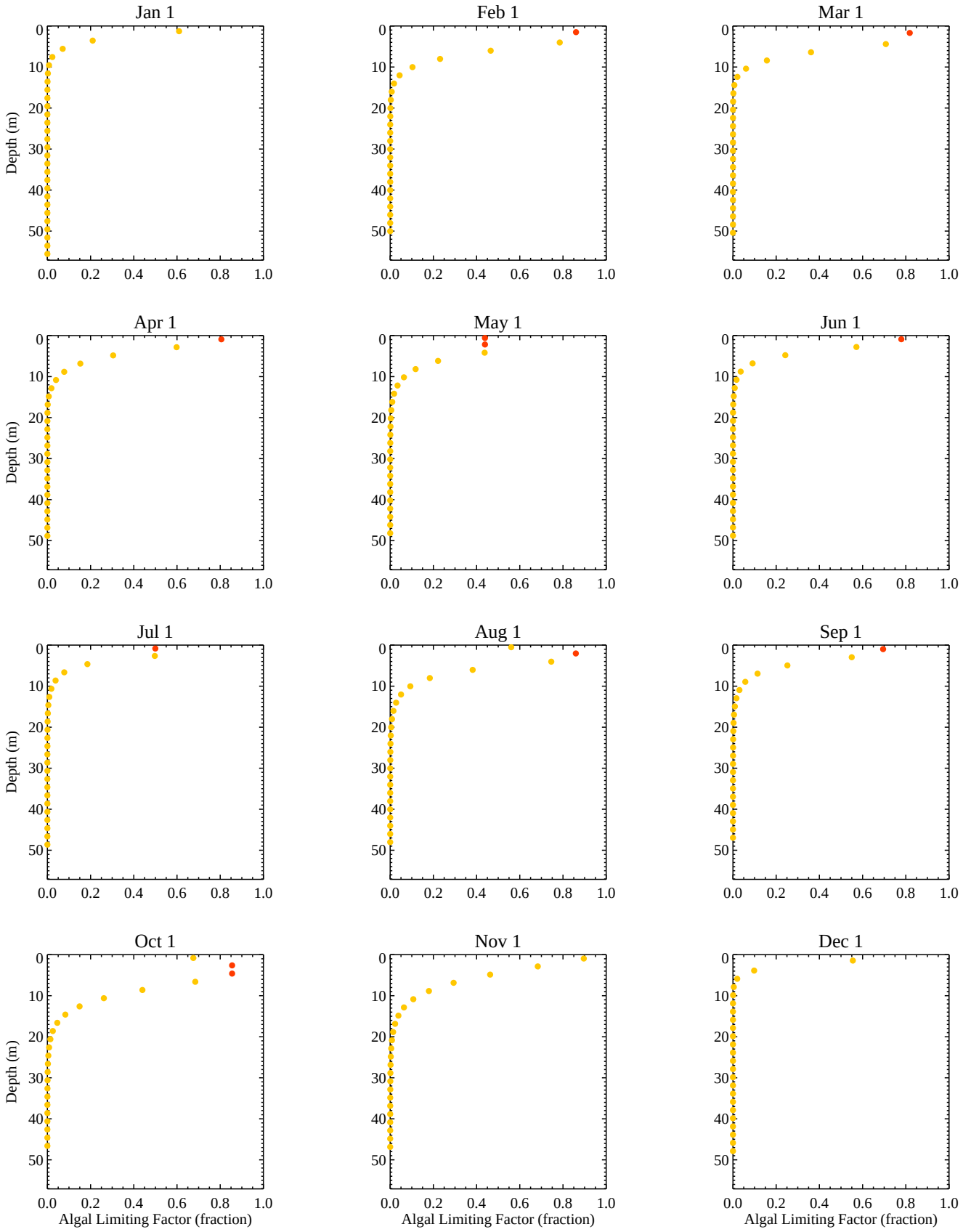

Figure J-22. Vertical profiles of algal limiting factor at Arkansas Bend (Segment 78) during 1992.

Profiles shown for first day of month.

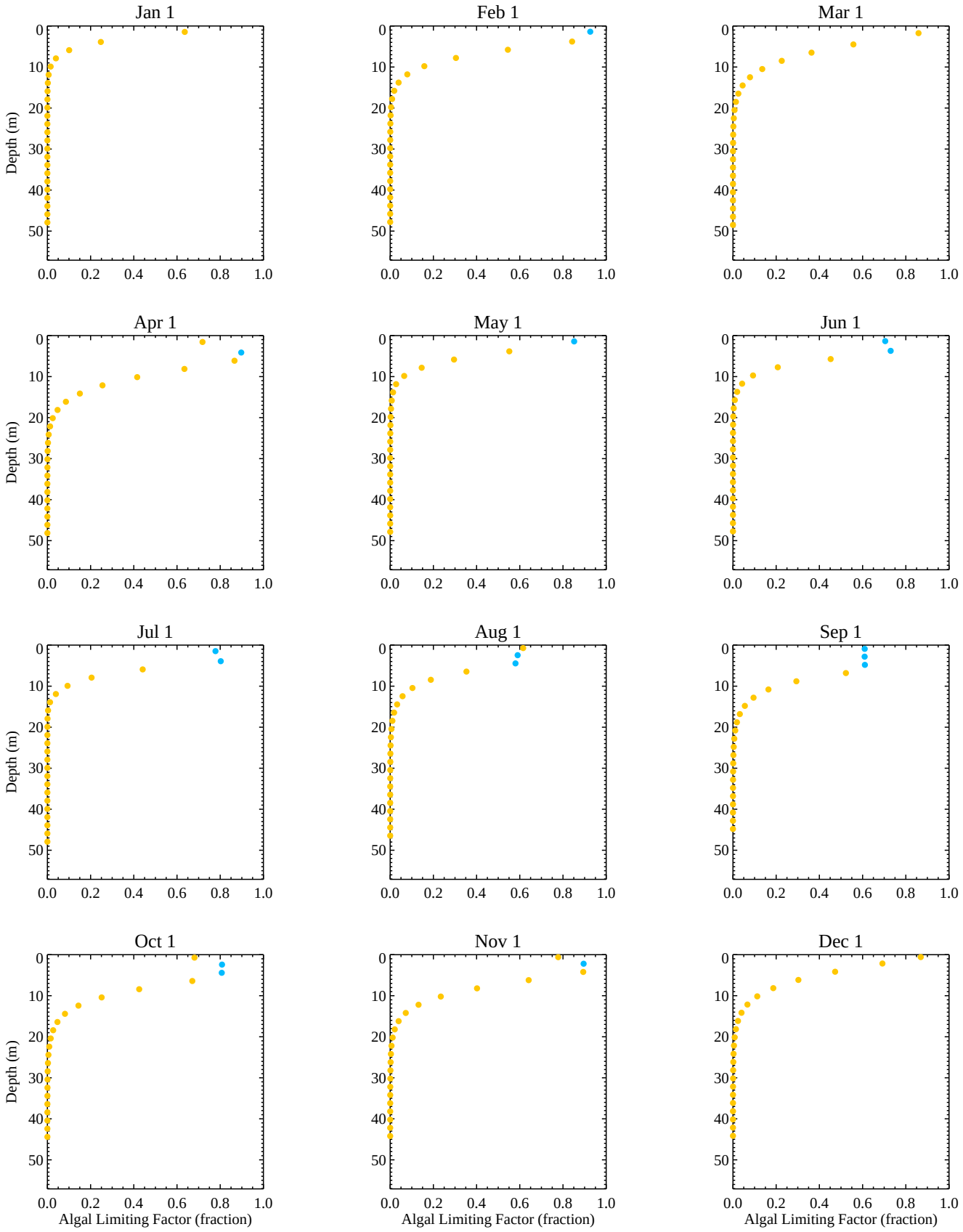

Figure J-22. Vertical profiles of algal limiting factor at Arkansas Bend (Segment 78) during 1993.

Profiles shown for first day of month.

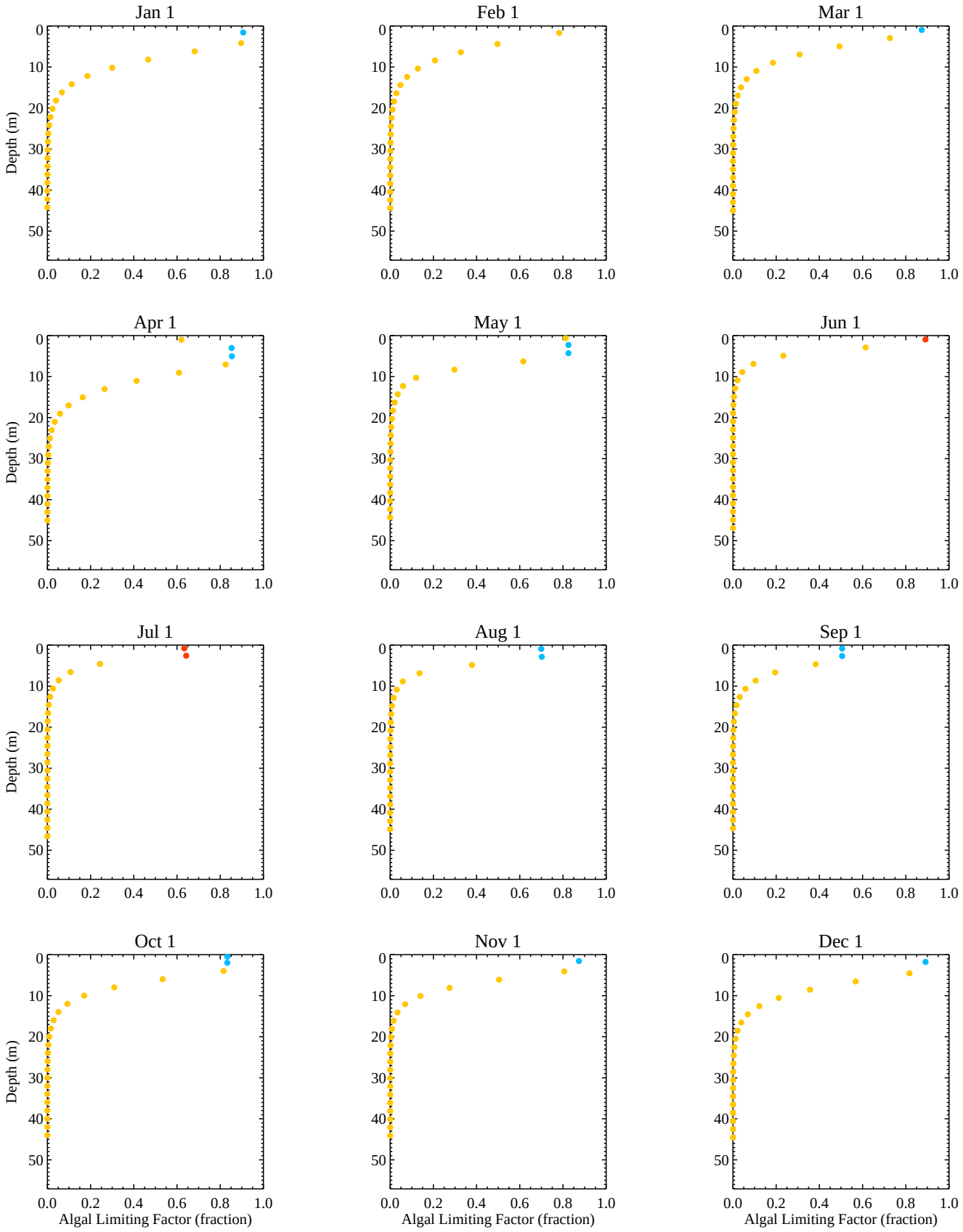

Figure J-22. Vertical profiles of algal limiting factor at Arkansas Bend (Segment 78) during 1994.

Profiles shown for first day of month.

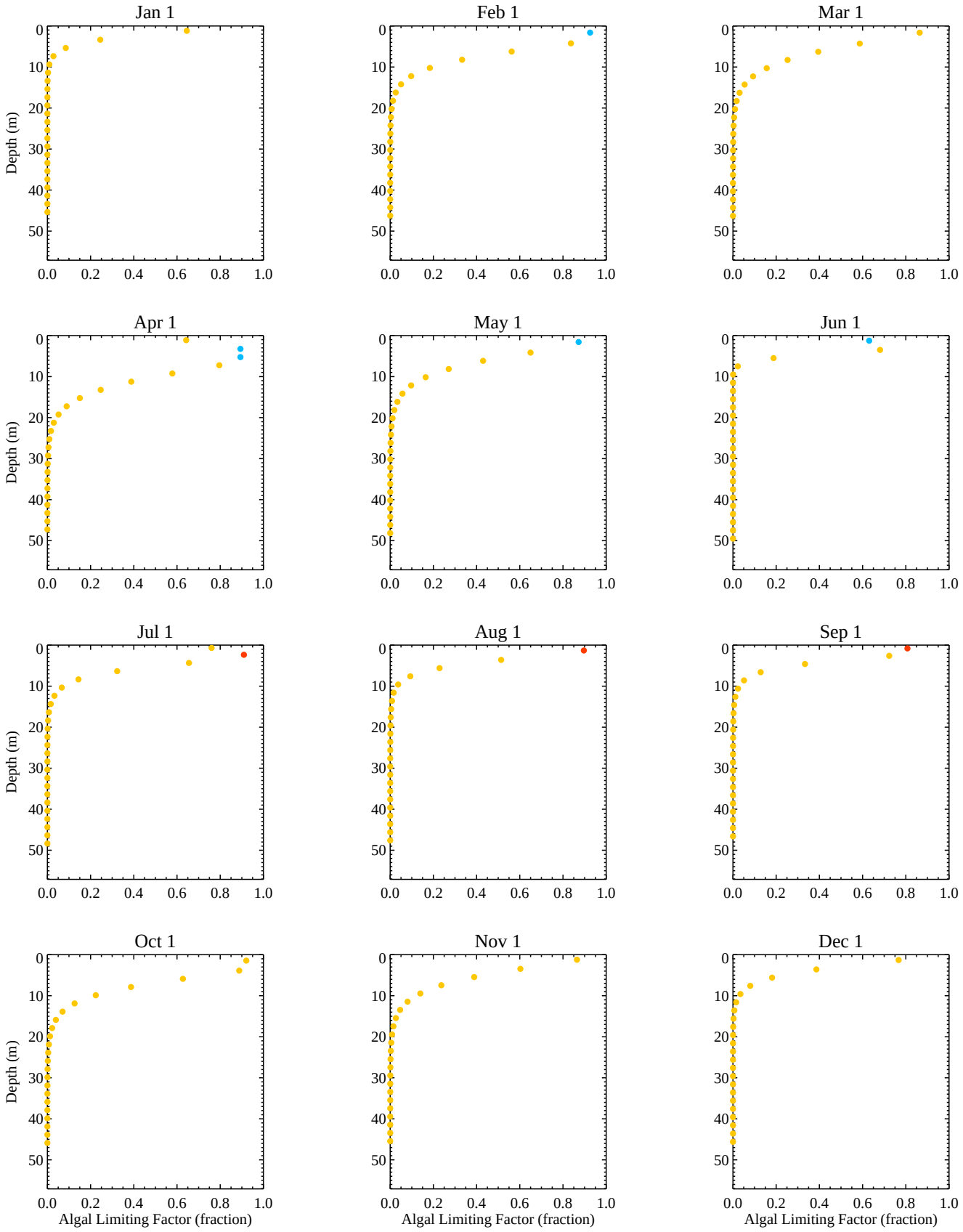

Figure J-22. Vertical profiles of algal limiting factor at Arkansas Bend (Segment 78) during 1995.

Profiles shown for first day of month.

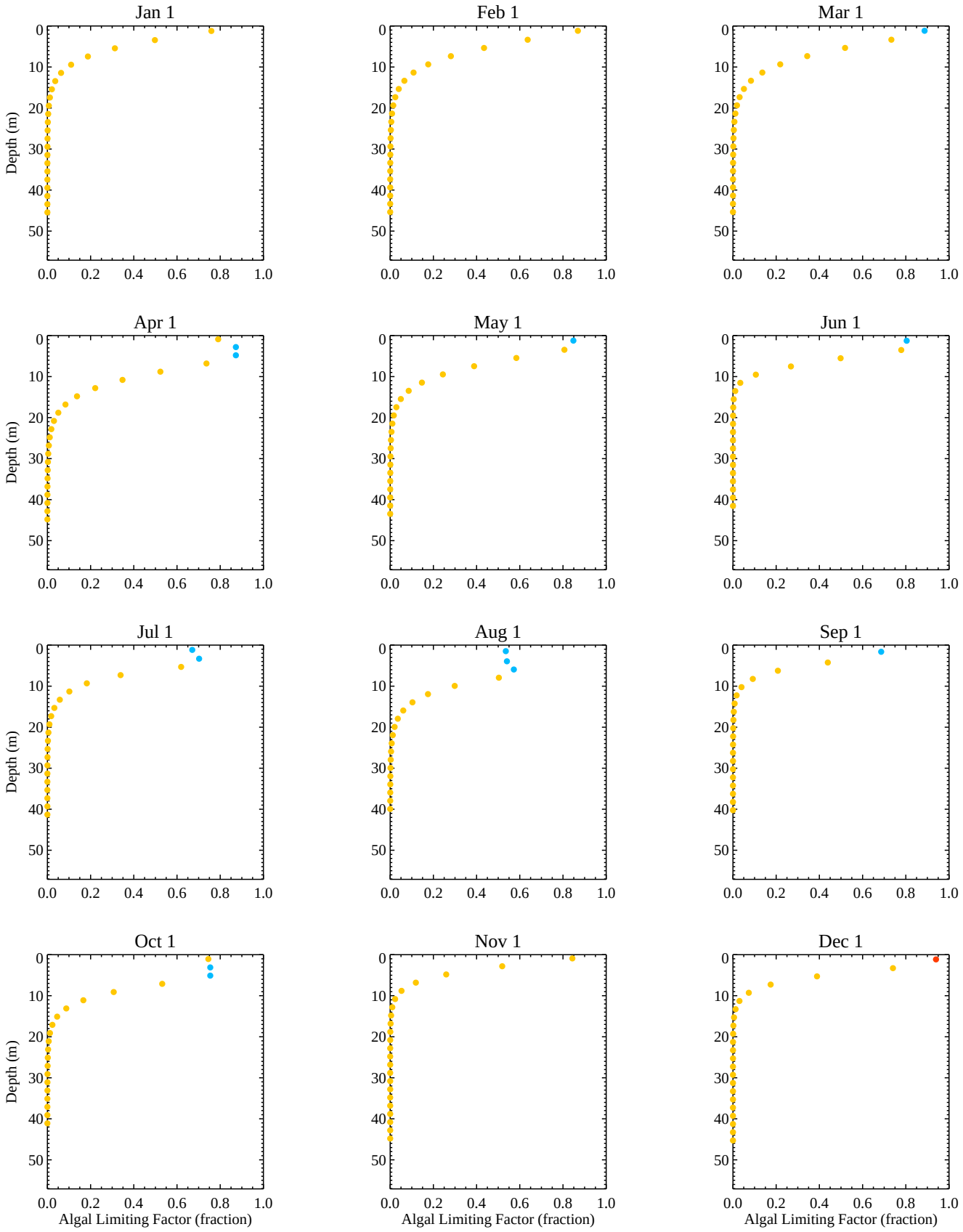

Figure J-22. Vertical profiles of algal limiting factor at Arkansas Bend (Segment 78) during 1996.

Profiles shown for first day of month.

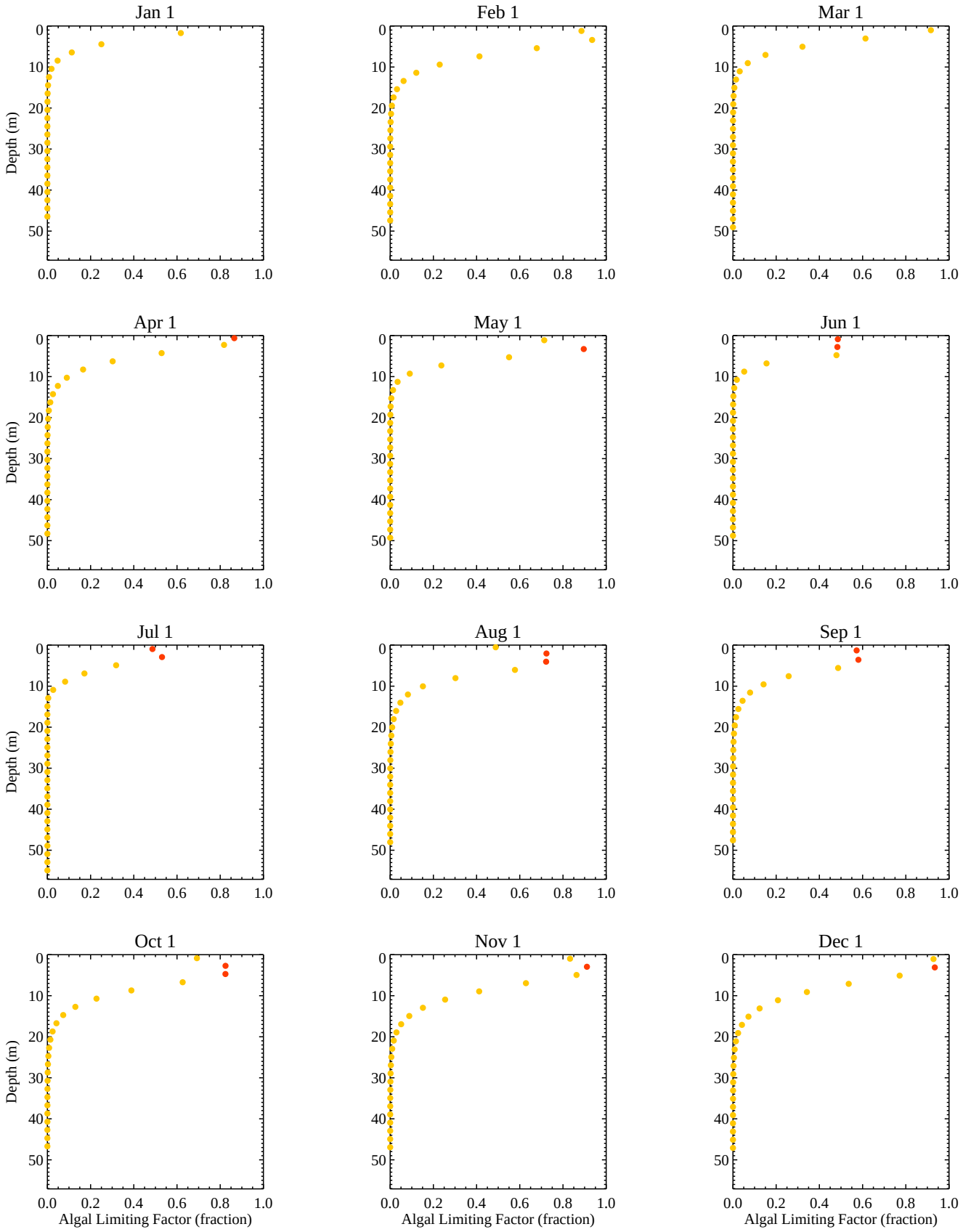

Figure J-22. Vertical profiles of algal limiting factor at Arkansas Bend (Segment 78) during 1997.

Profiles shown for first day of month.

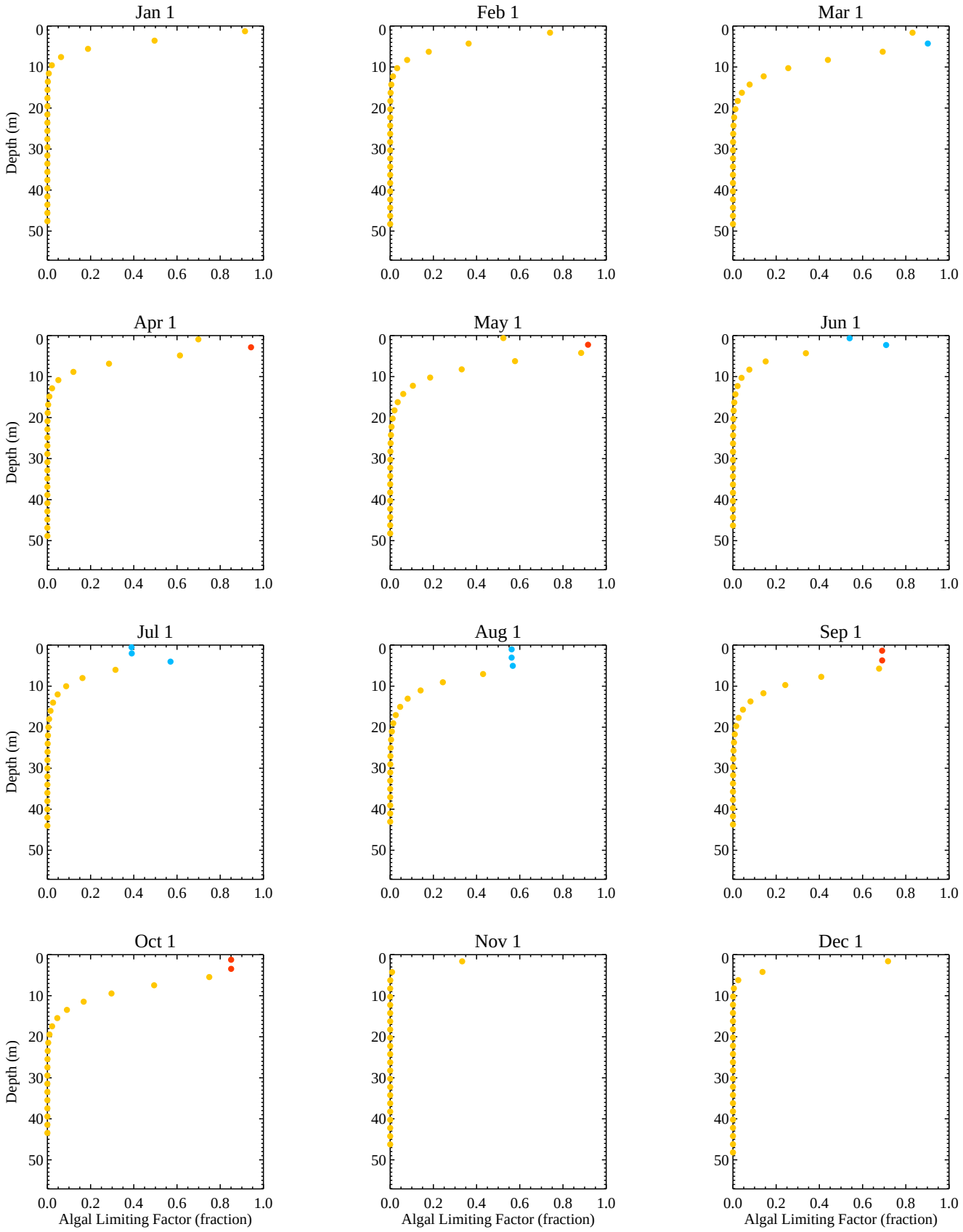

Figure J-22. Vertical profiles of algal limiting factor at Arkansas Bend (Segment 78) during 1998.

Profiles shown for first day of month.

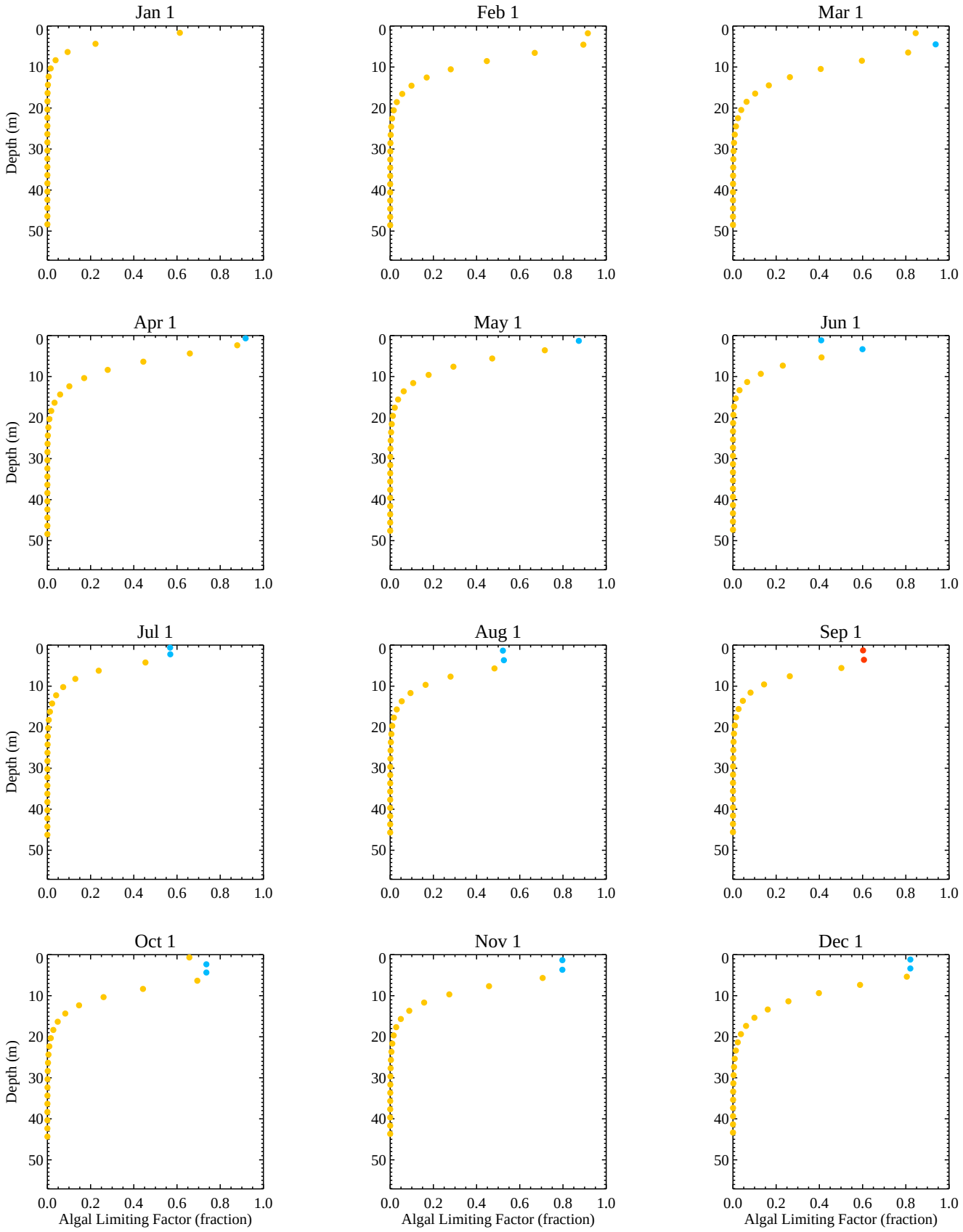

Figure J-22. Vertical profiles of algal limiting factor at Arkansas Bend (Segment 78) during 1999.

Profiles shown for first day of month.

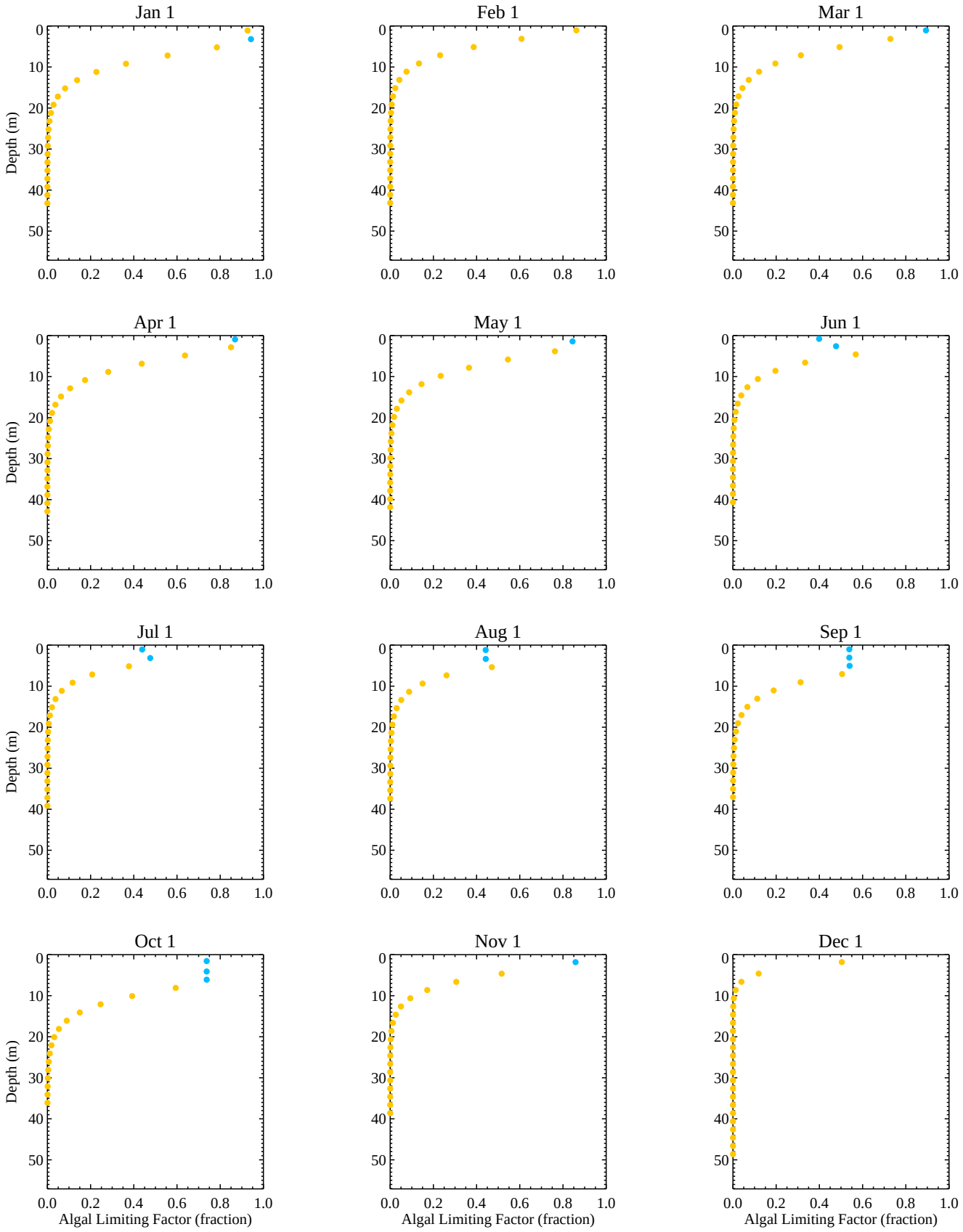

Figure J-22. Vertical profiles of algal limiting factor at Arkansas Bend (Segment 78) during 2000.

Profiles shown for first day of month.

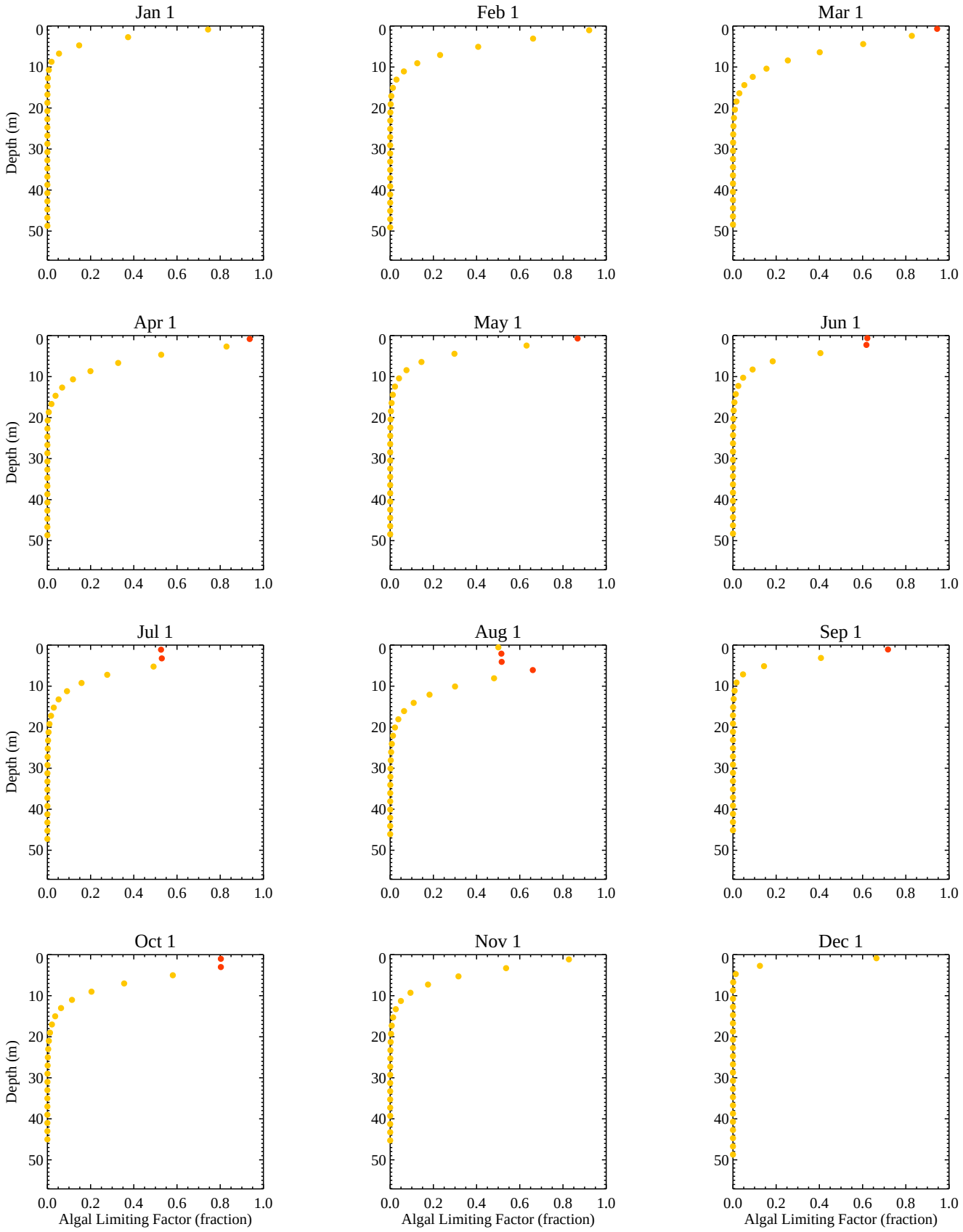

Figure J-22. Vertical profiles of algal limiting factor at Arkansas Bend (Segment 78) during 2001.

Profiles shown for first day of month.

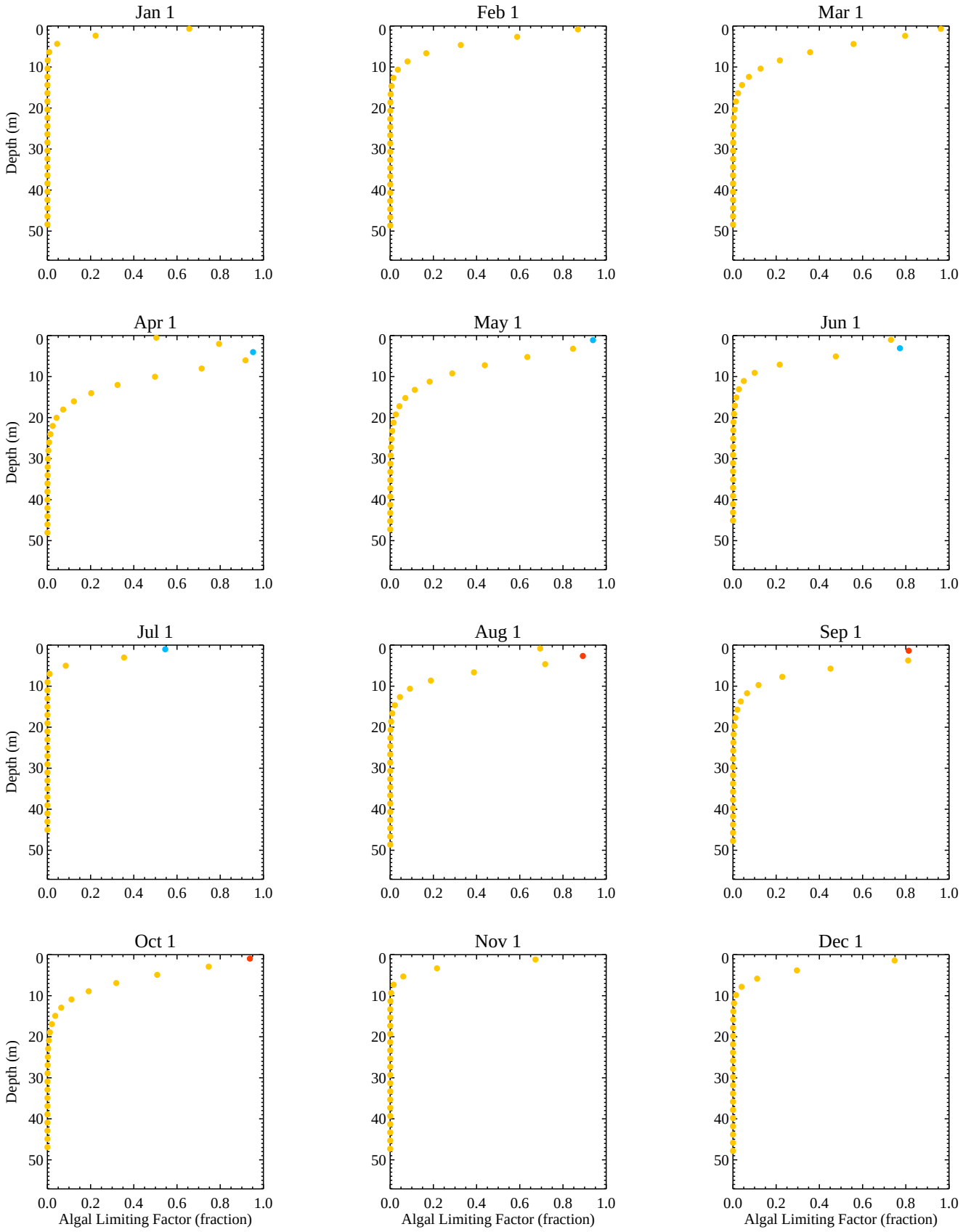

Figure J-22. Vertical profiles of algal limiting factor at Arkansas Bend (Segment 78) during 2002.

Profiles shown for first day of month.

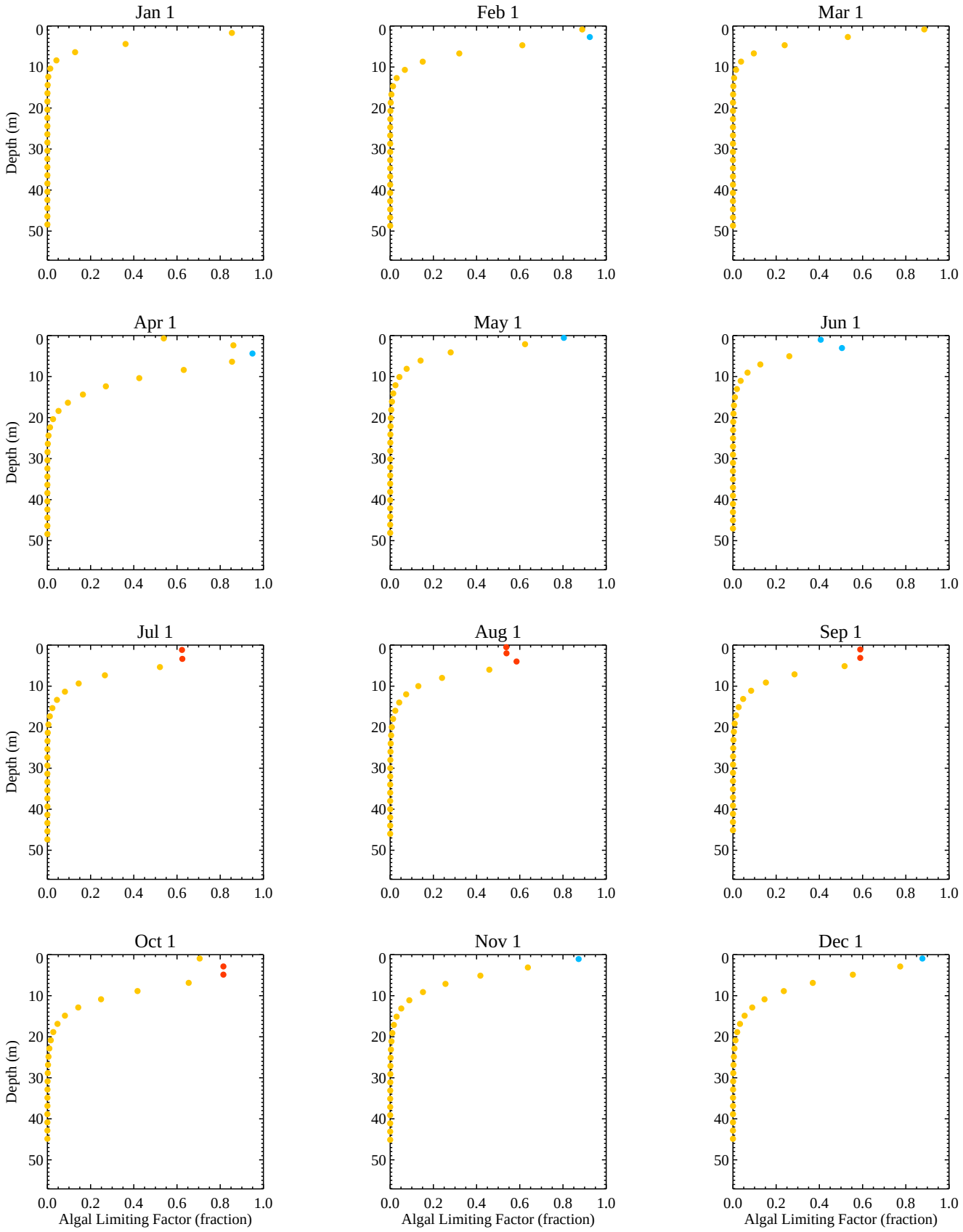

Figure J-22. Vertical profiles of algal limiting factor at Arkansas Bend (Segment 78) during 2003.

Profiles shown for first day of month.

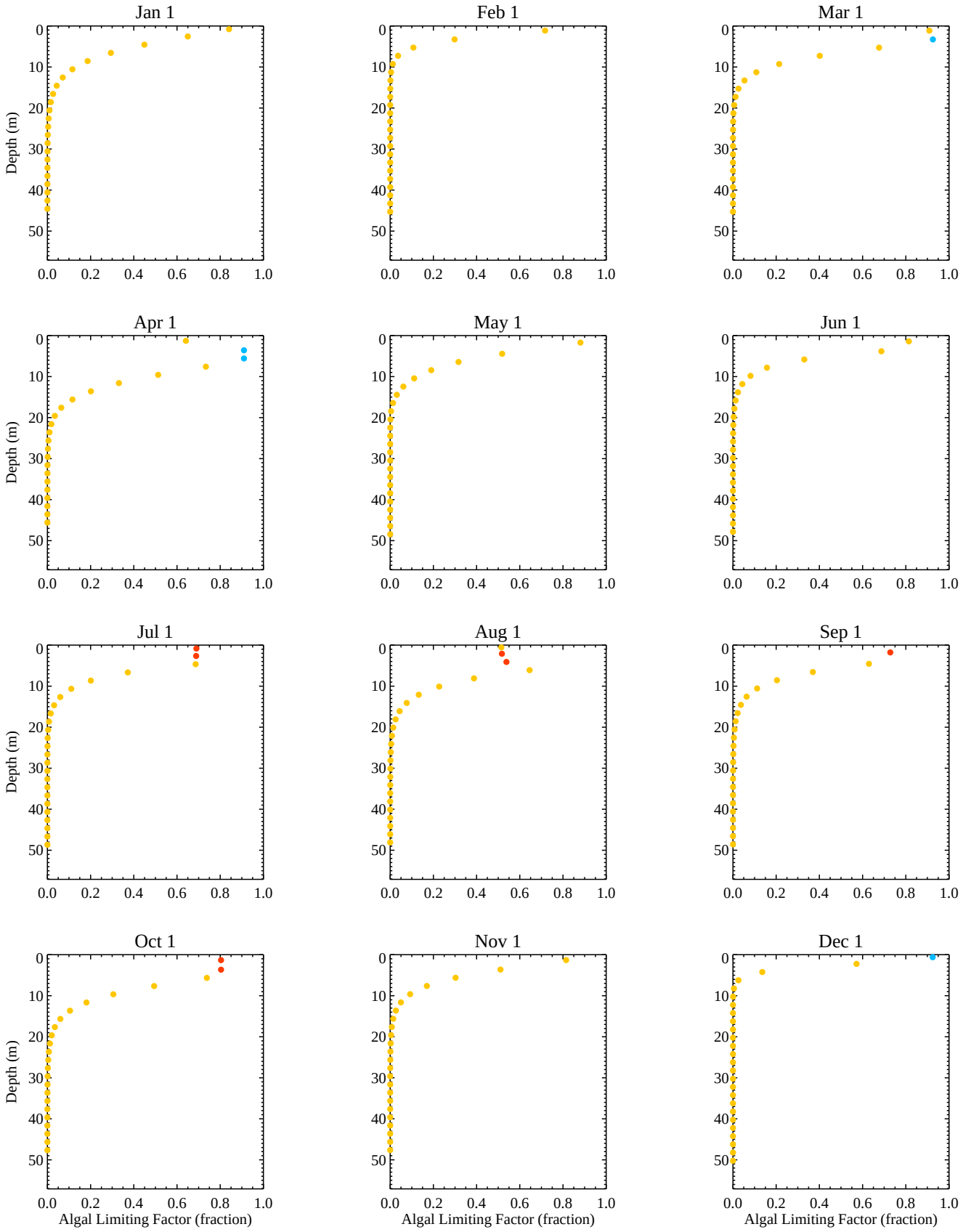

Figure J-22. Vertical profiles of algal limiting factor at Arkansas Bend (Segment 78) during 2004.

Profiles shown for first day of month.

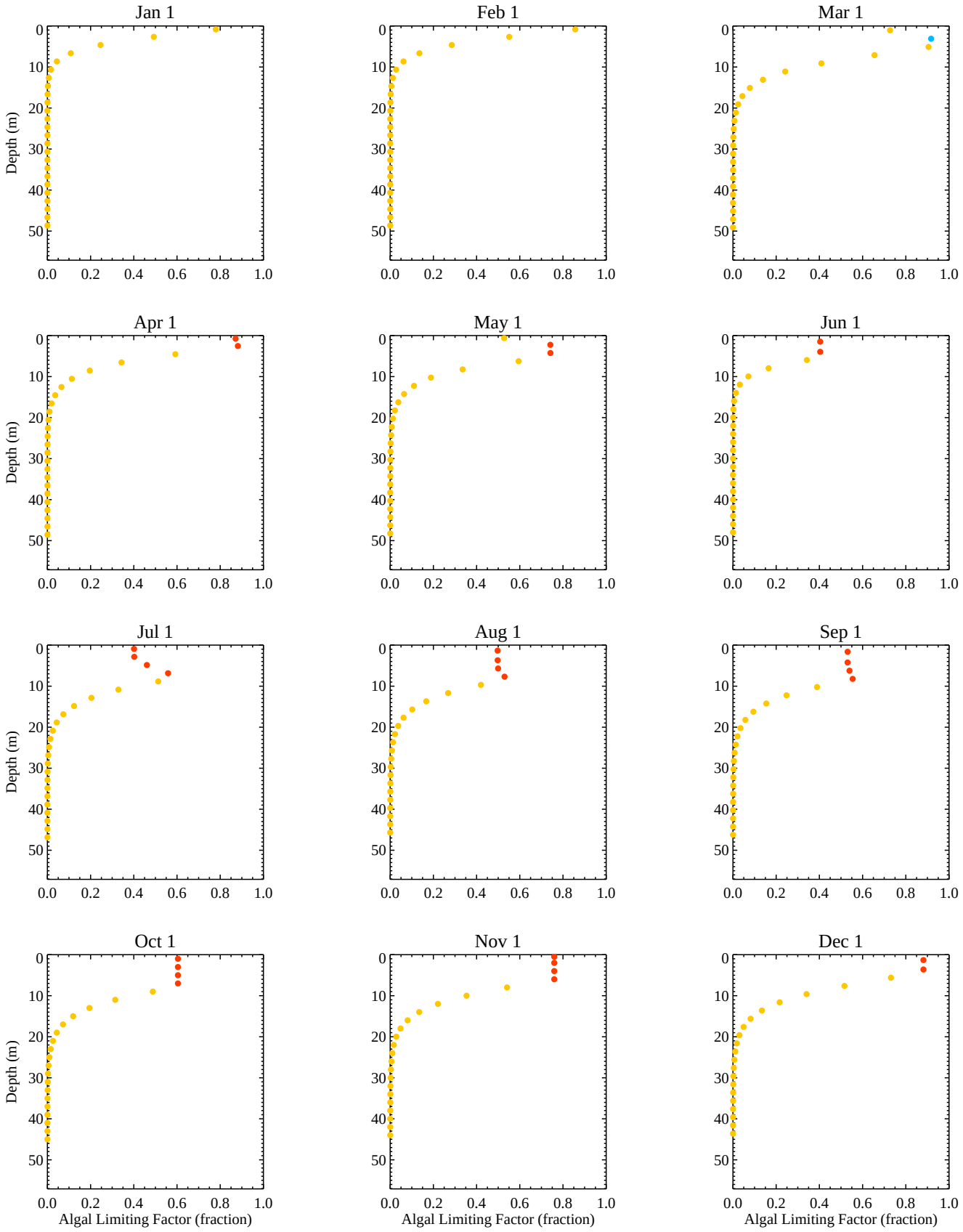

Figure J-22. Vertical profiles of algal limiting factor at Arkansas Bend (Segment 78) during 2005.

Profiles shown for first day of month.

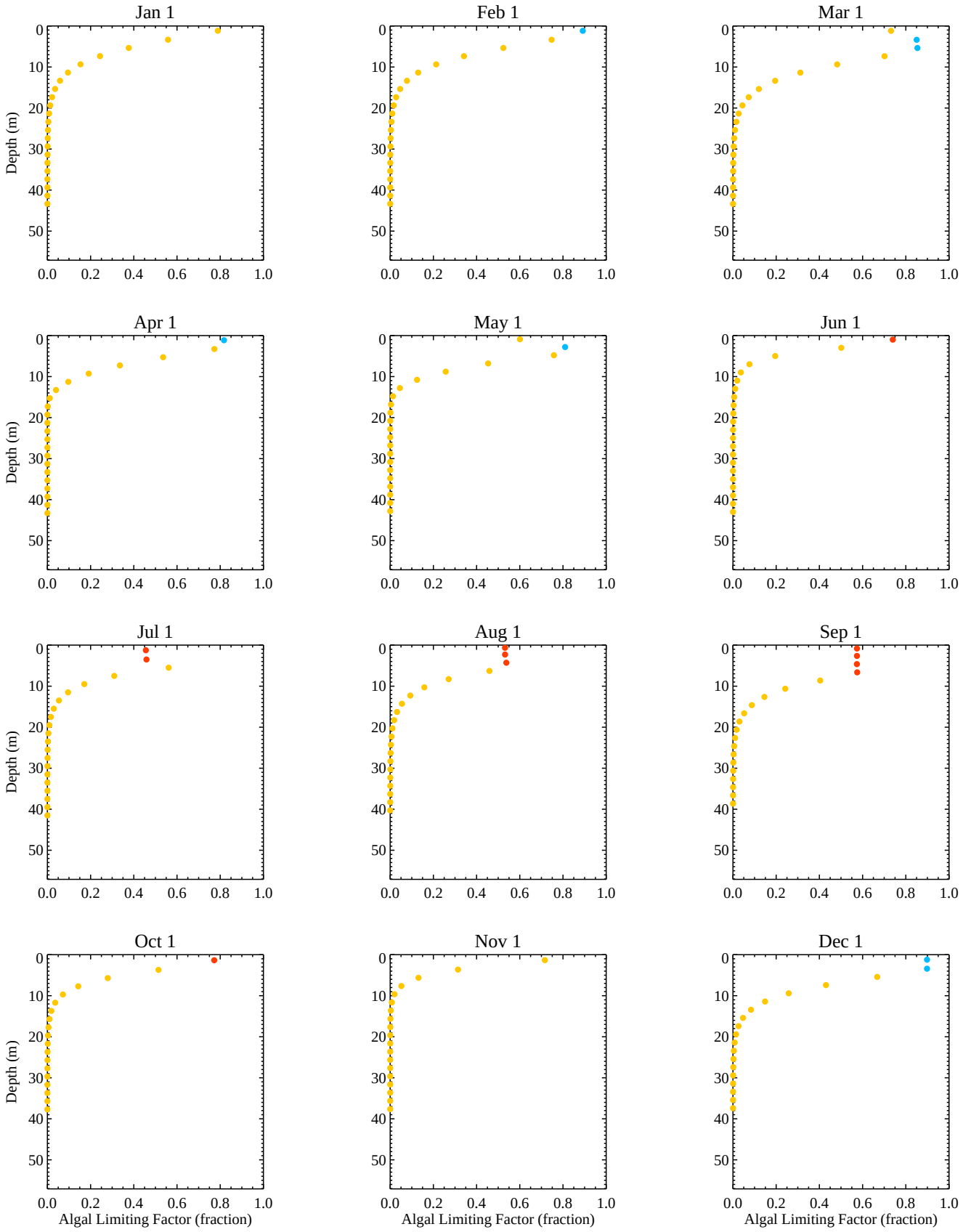

Figure J-22. Vertical profiles of algal limiting factor at Arkansas Bend (Segment 78) during 2006.

Profiles shown for first day of month.

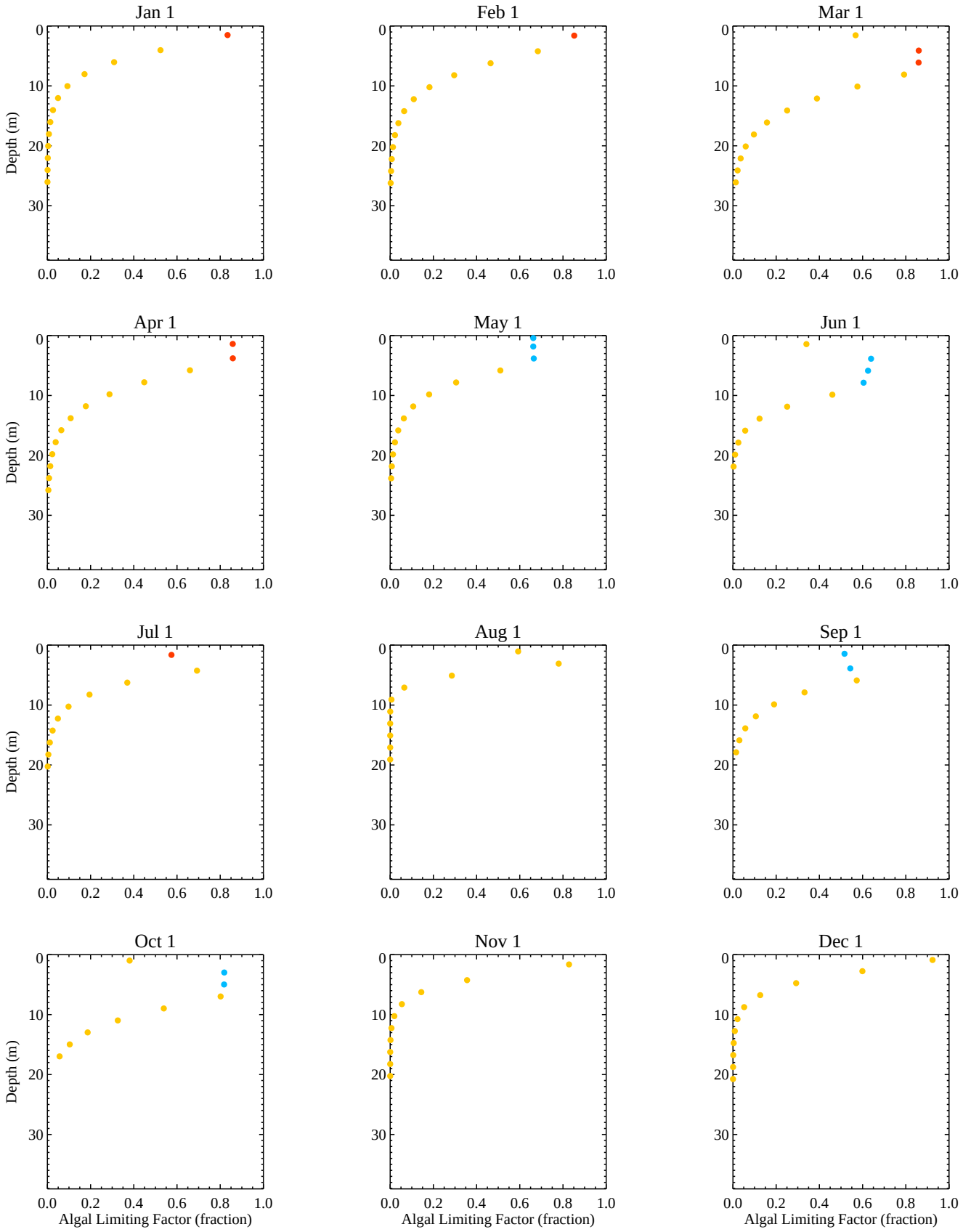

Figure J-23. Vertical profiles of algal limiting factor at Pace Bend (Segment 48) during 1984.

Profiles shown for first day of month.

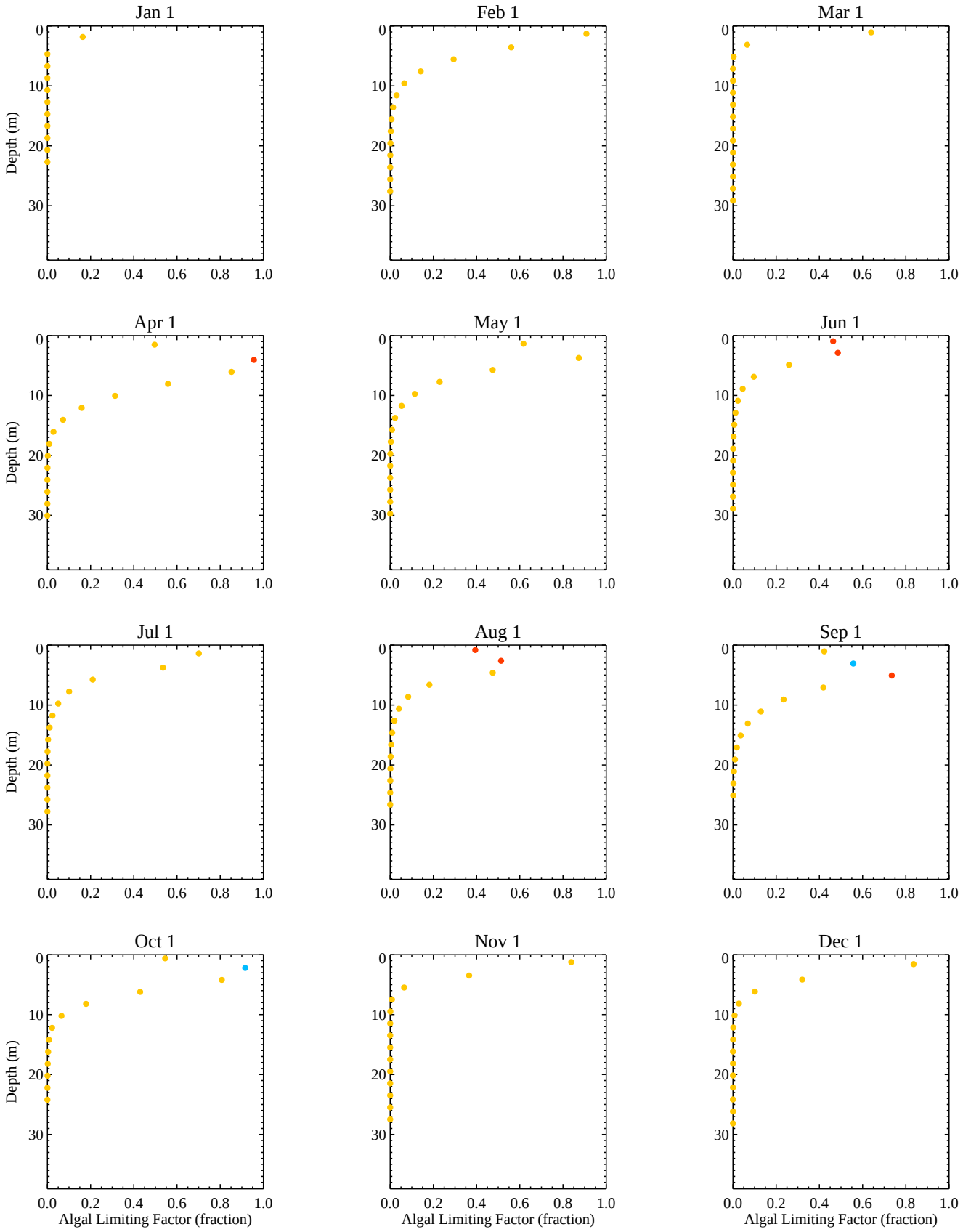

Figure J-23. Vertical profiles of algal limiting factor at Pace Bend (Segment 48) during 1985.

Profiles shown for first day of month.

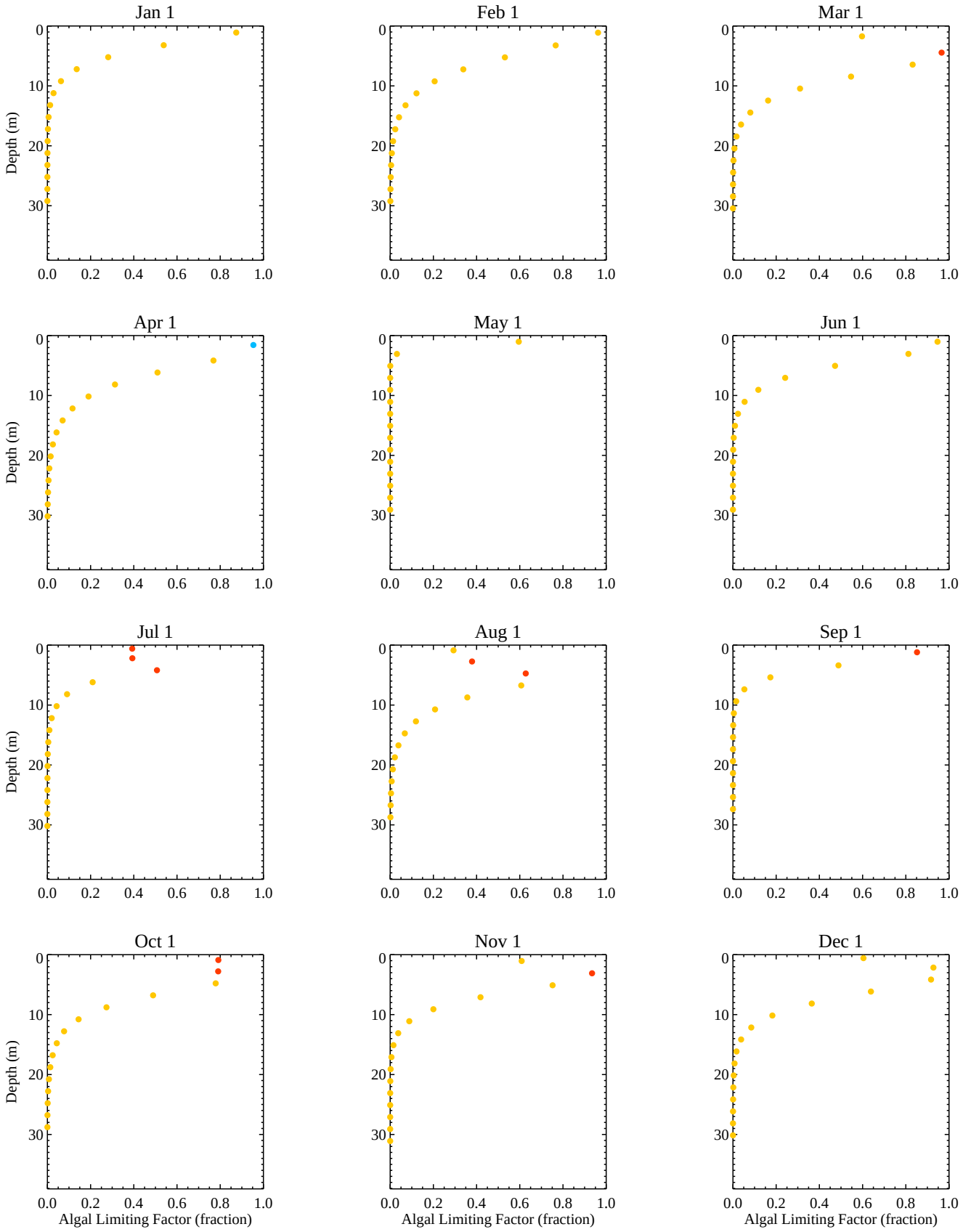

Figure J-23. Vertical profiles of algal limiting factor at Pace Bend (Segment 48) during 1986.

Profiles shown for first day of month.

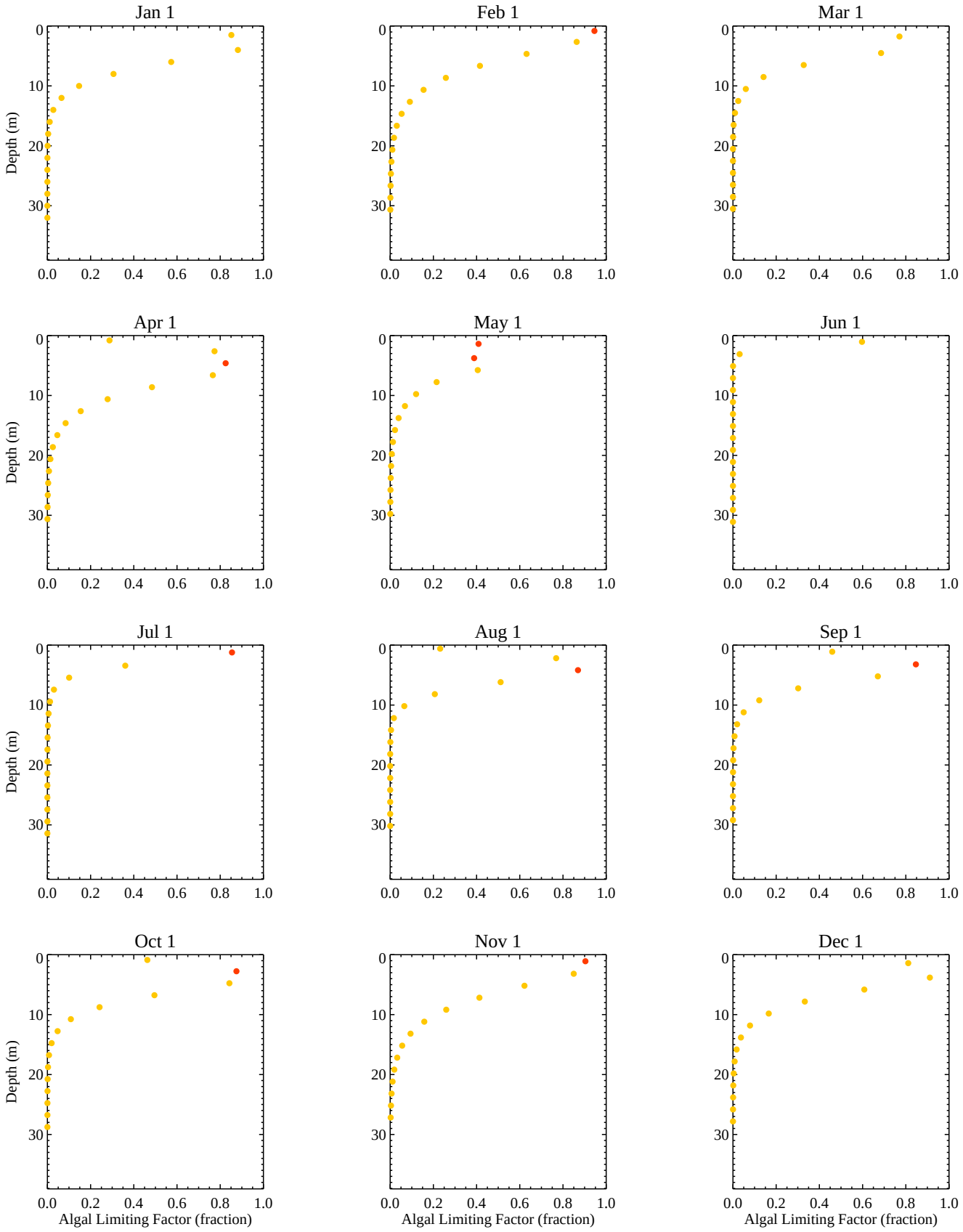

Figure J-23. Vertical profiles of algal limiting factor at Pace Bend (Segment 48) during 1987.

Profiles shown for first day of month.

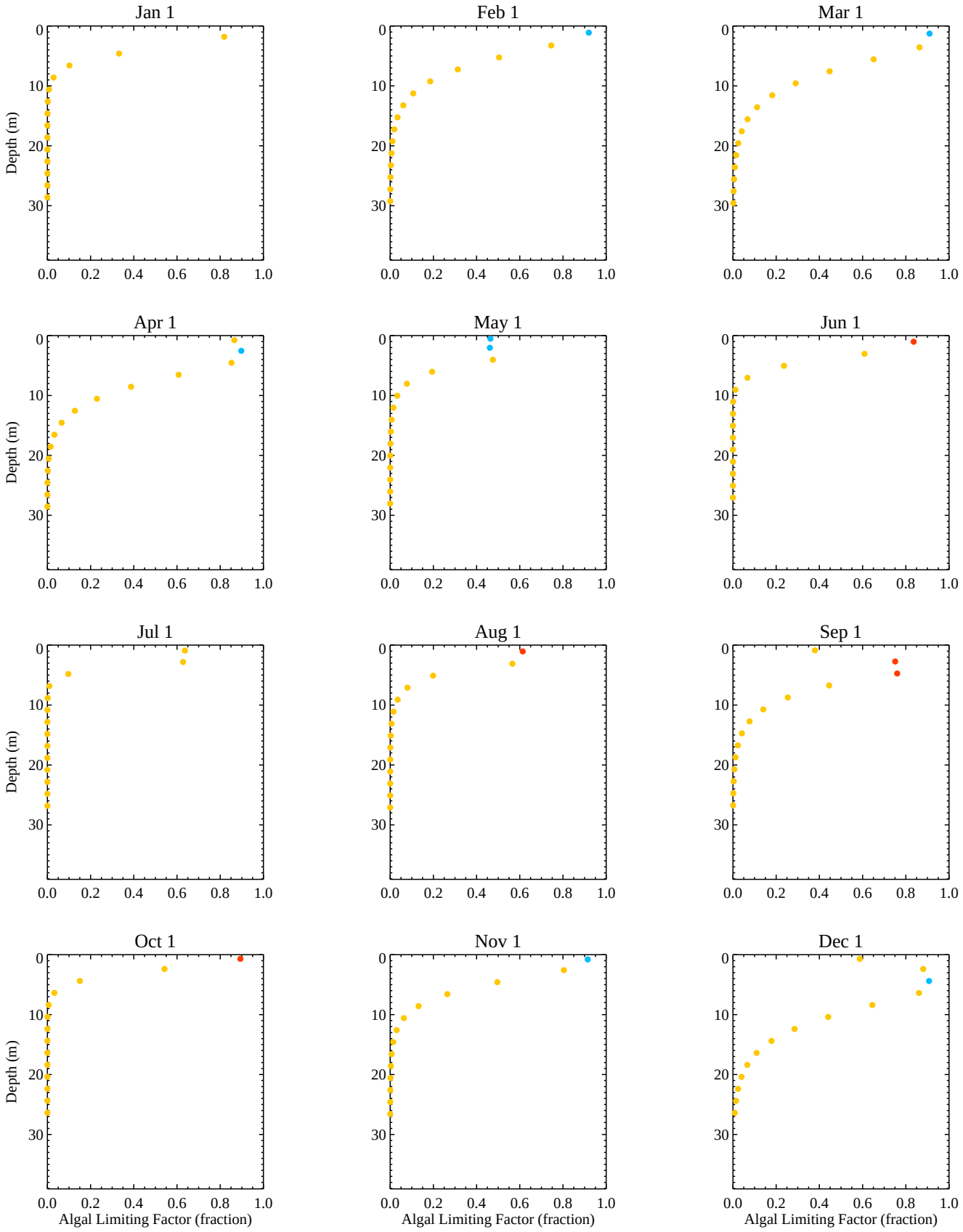

Figure J-23. Vertical profiles of algal limiting factor at Pace Bend (Segment 48) during 1988.

Profiles shown for first day of month.

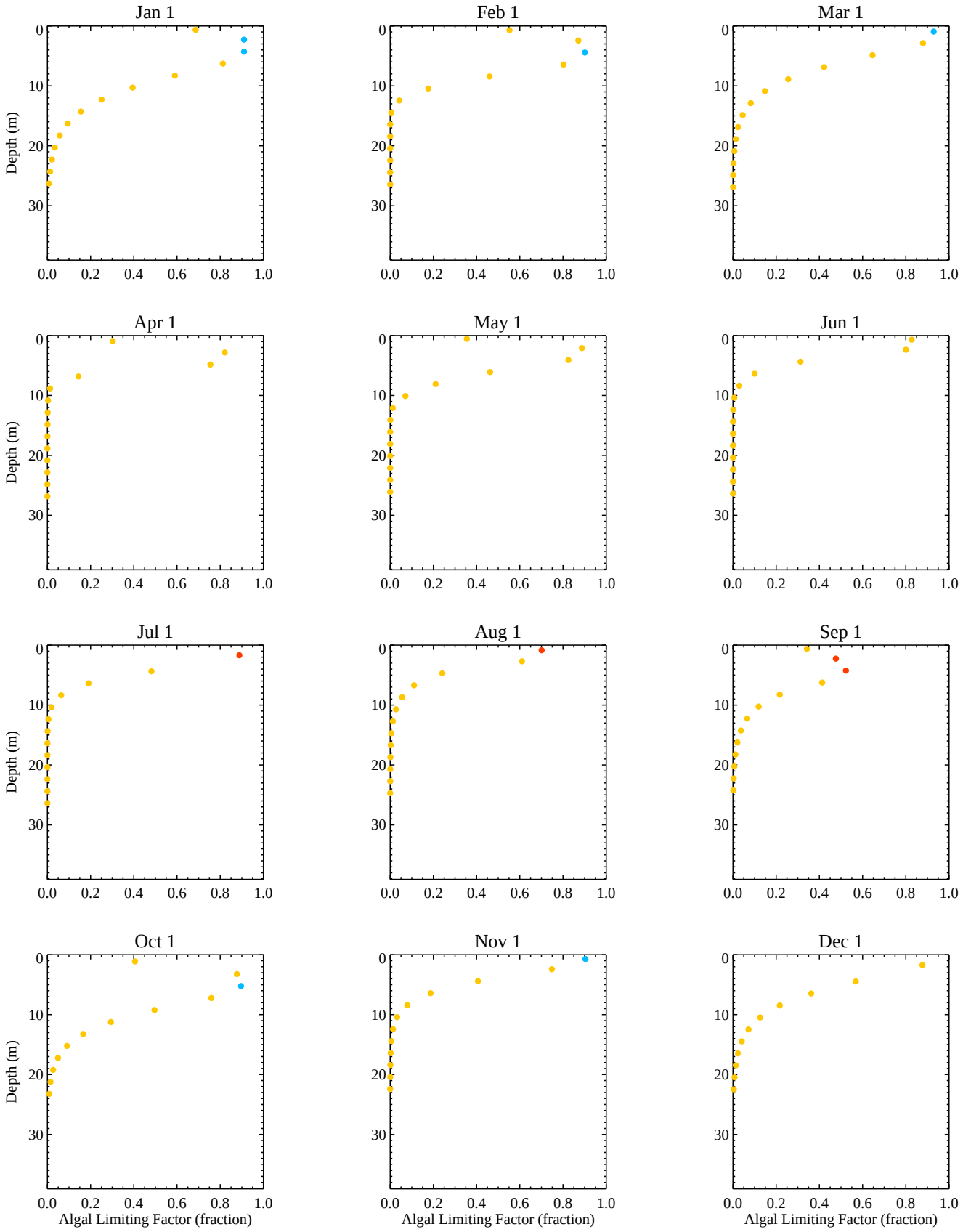

Figure J-23. Vertical profiles of algal limiting factor at Pace Bend (Segment 48) during 1989.

Profiles shown for first day of month.

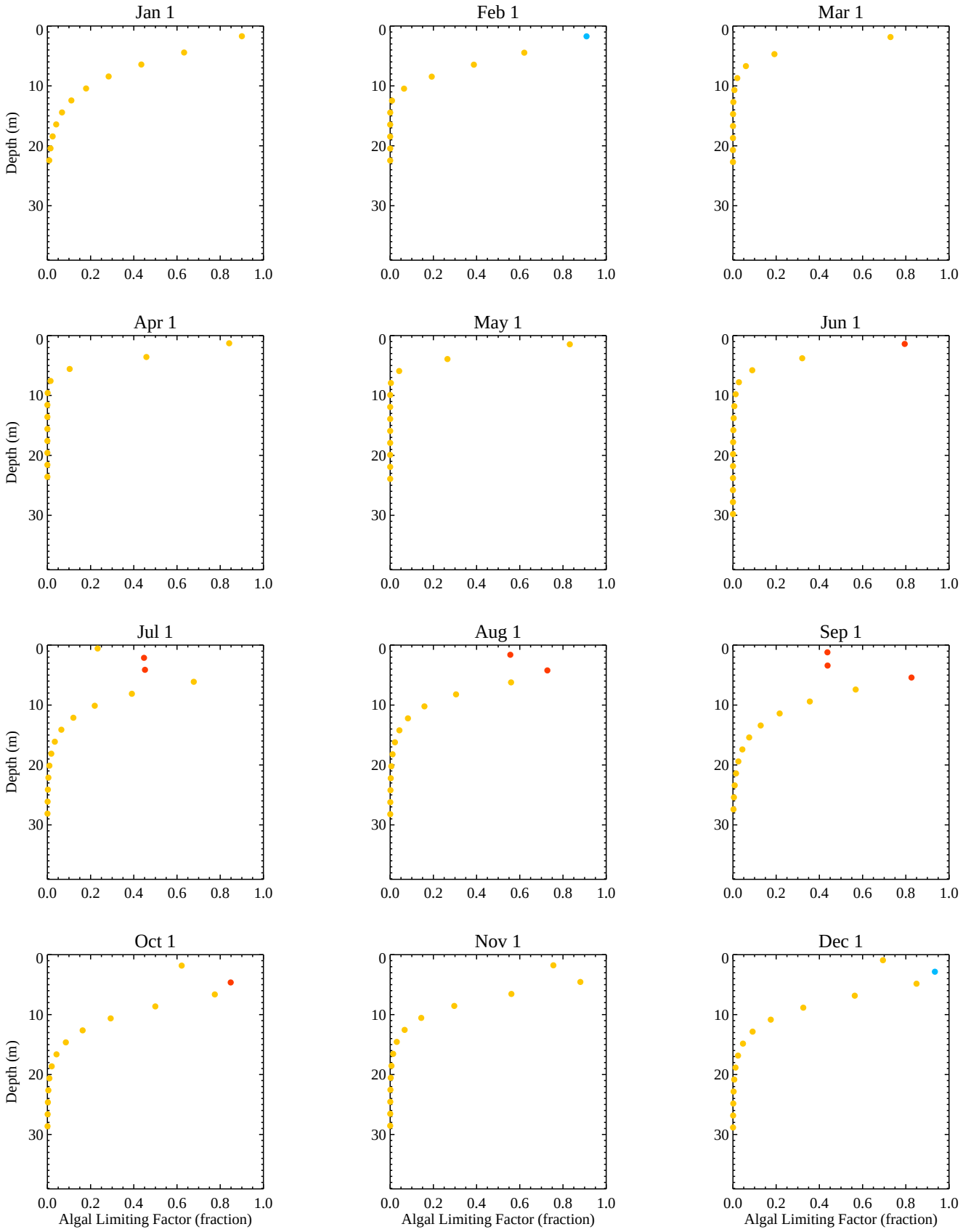

Figure J-23. Vertical profiles of algal limiting factor at Pace Bend (Segment 48) during 1990.

Profiles shown for first day of month.

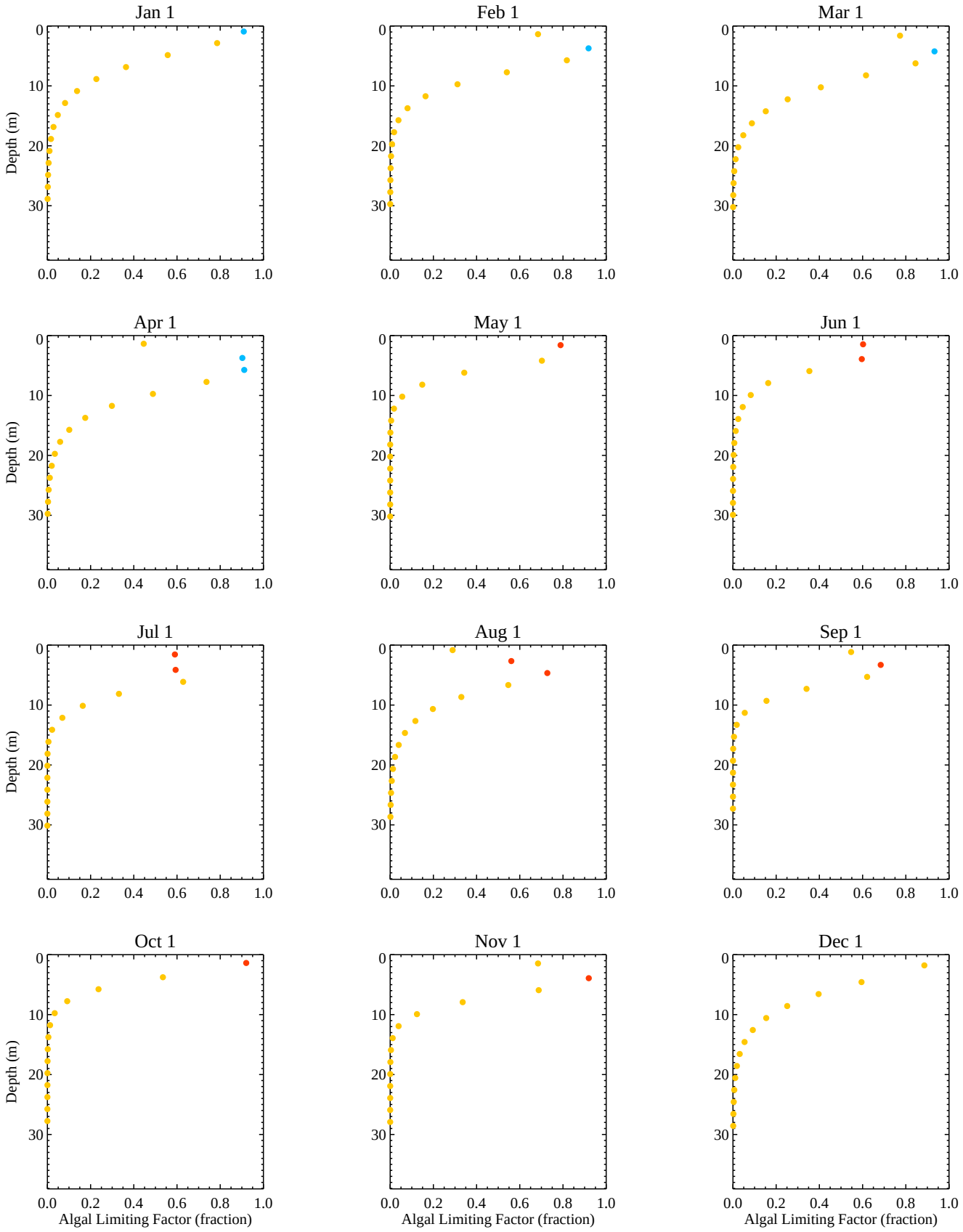

Figure J-23. Vertical profiles of algal limiting factor at Pace Bend (Segment 48) during 1991.

Profiles shown for first day of month.

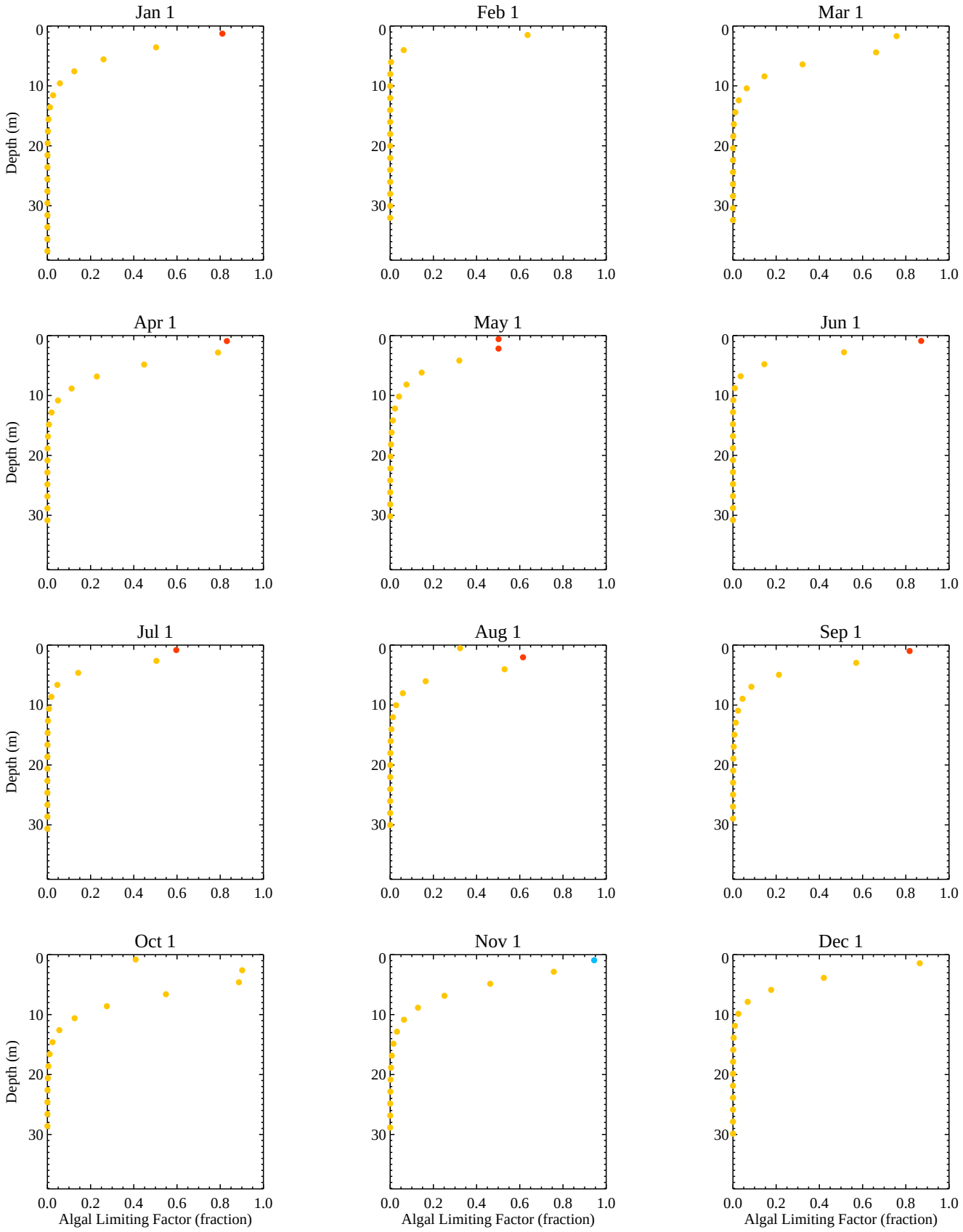

Figure J-23. Vertical profiles of algal limiting factor at Pace Bend (Segment 48) during 1992.

Profiles shown for first day of month.

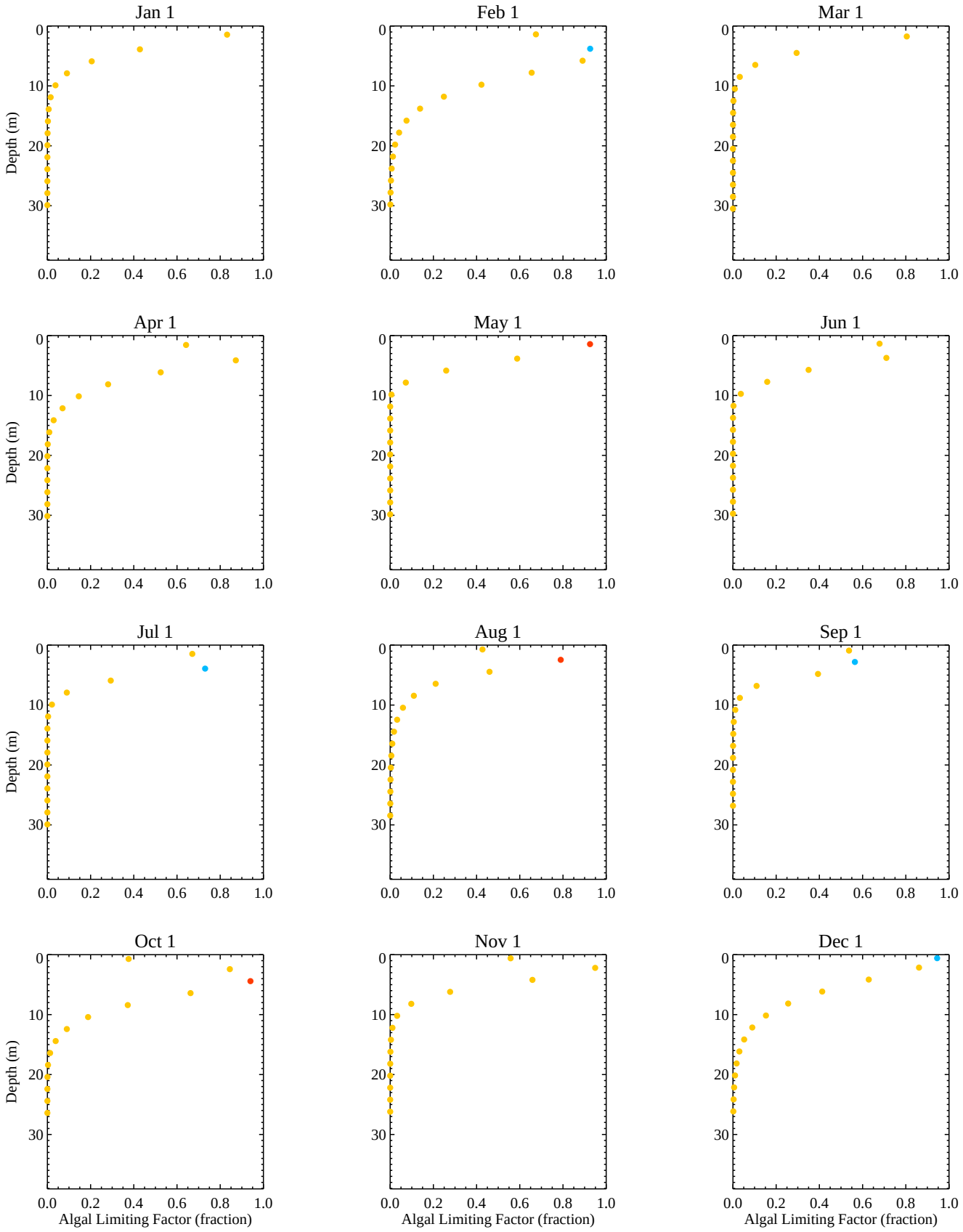

Figure J-23. Vertical profiles of algal limiting factor at Pace Bend (Segment 48) during 1993.

Profiles shown for first day of month.

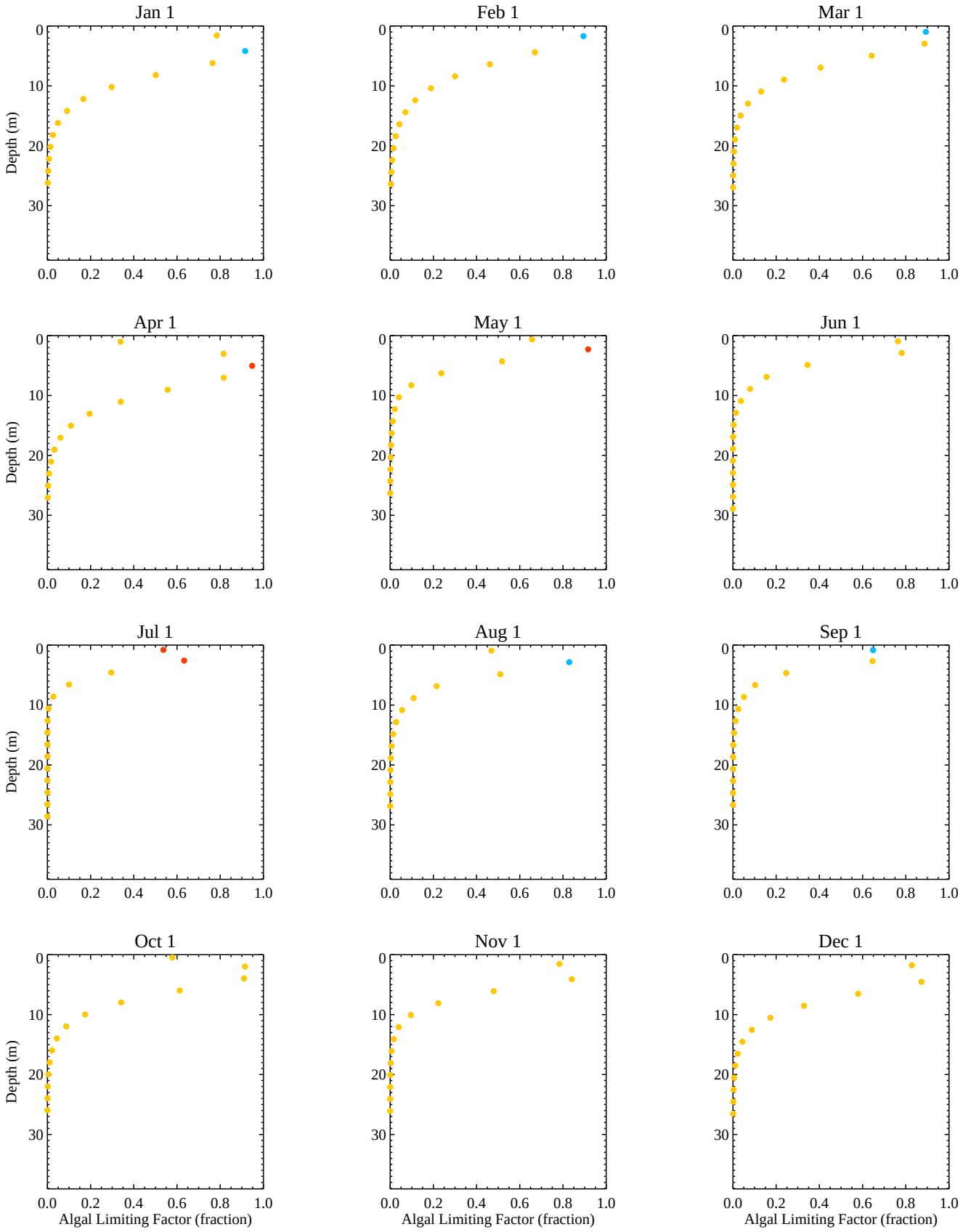

Figure J-23. Vertical profiles of algal limiting factor at Pace Bend (Segment 48) during 1994.

Profiles shown for first day of month.

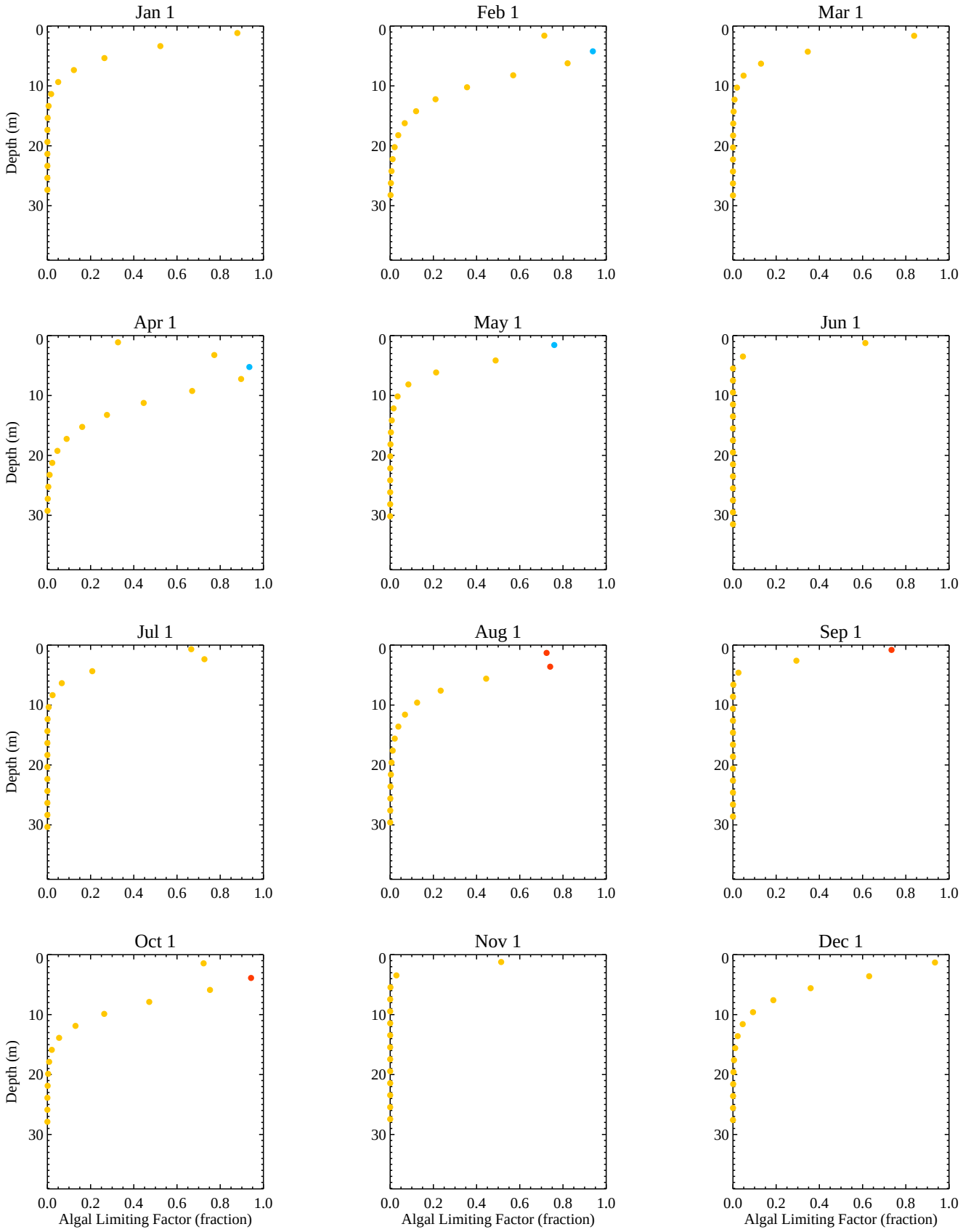

Figure J-23. Vertical profiles of algal limiting factor at Pace Bend (Segment 48) during 1995.

Profiles shown for first day of month.

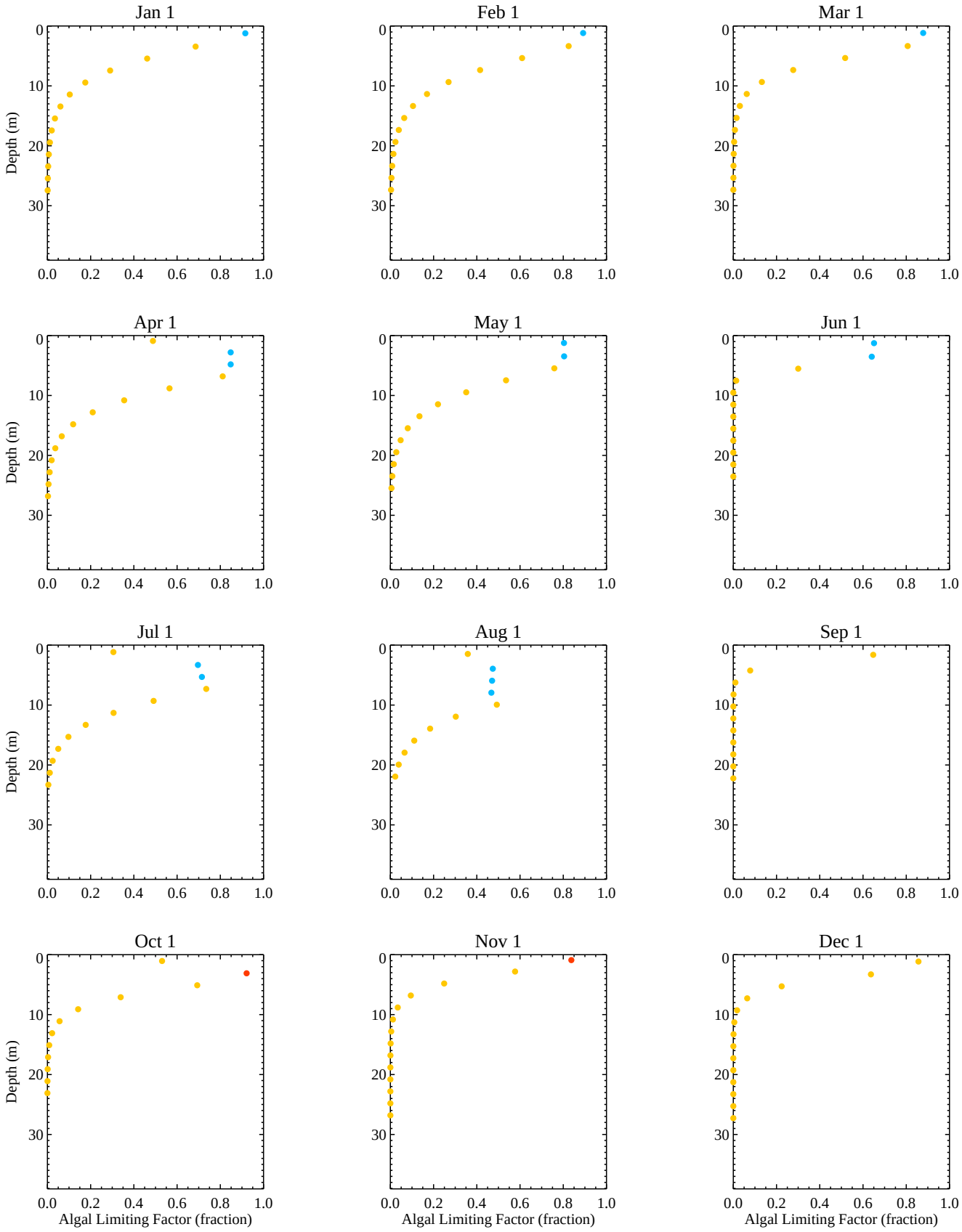

Figure J-23. Vertical profiles of algal limiting factor at Pace Bend (Segment 48) during 1996.

Profiles shown for first day of month.

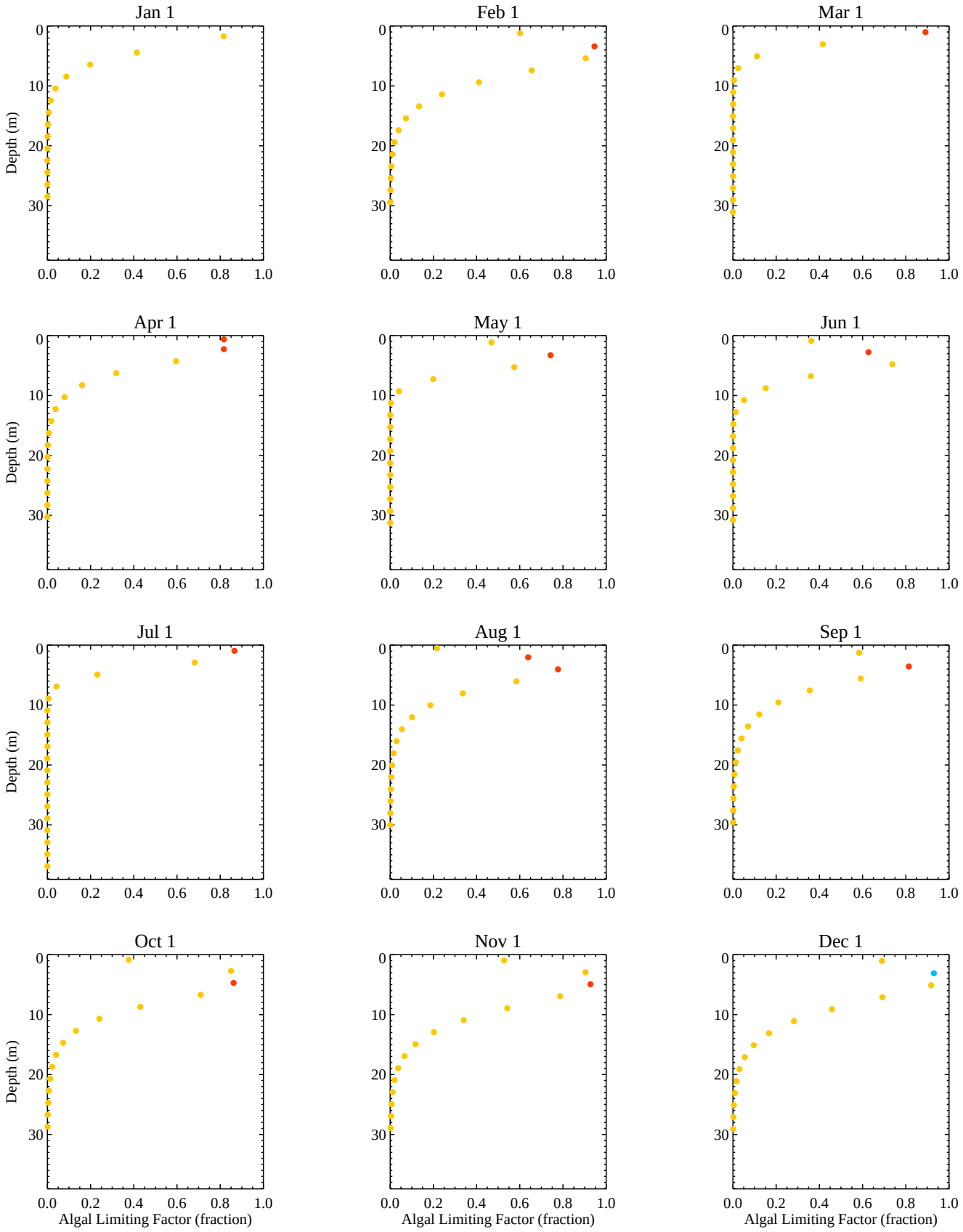

Figure J-23. Vertical profiles of algal limiting factor at Pace Bend (Segment 48) during 1997.

Profiles shown for first day of month.

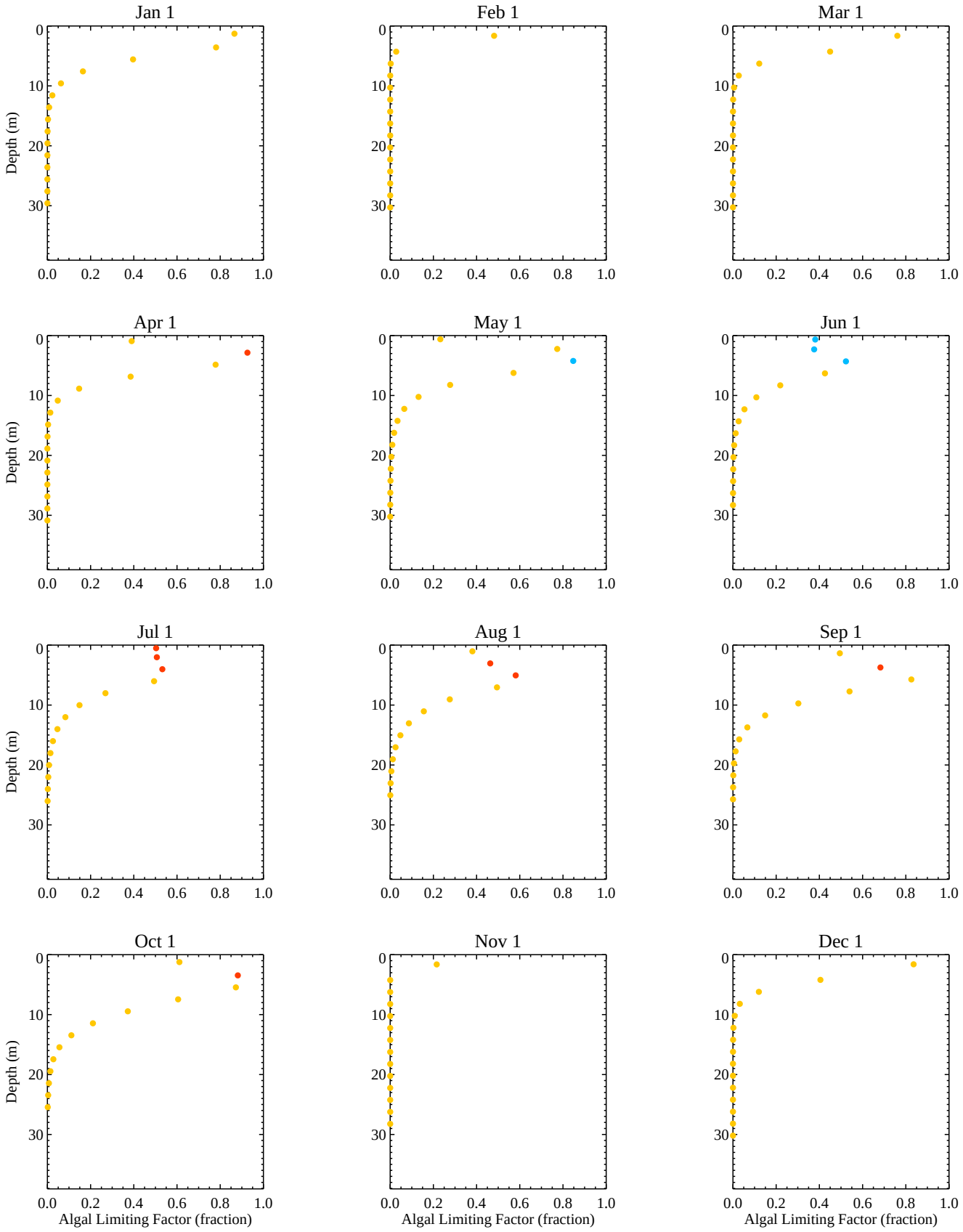

Figure J-23. Vertical profiles of algal limiting factor at Pace Bend (Segment 48) during 1998.

Profiles shown for first day of month.

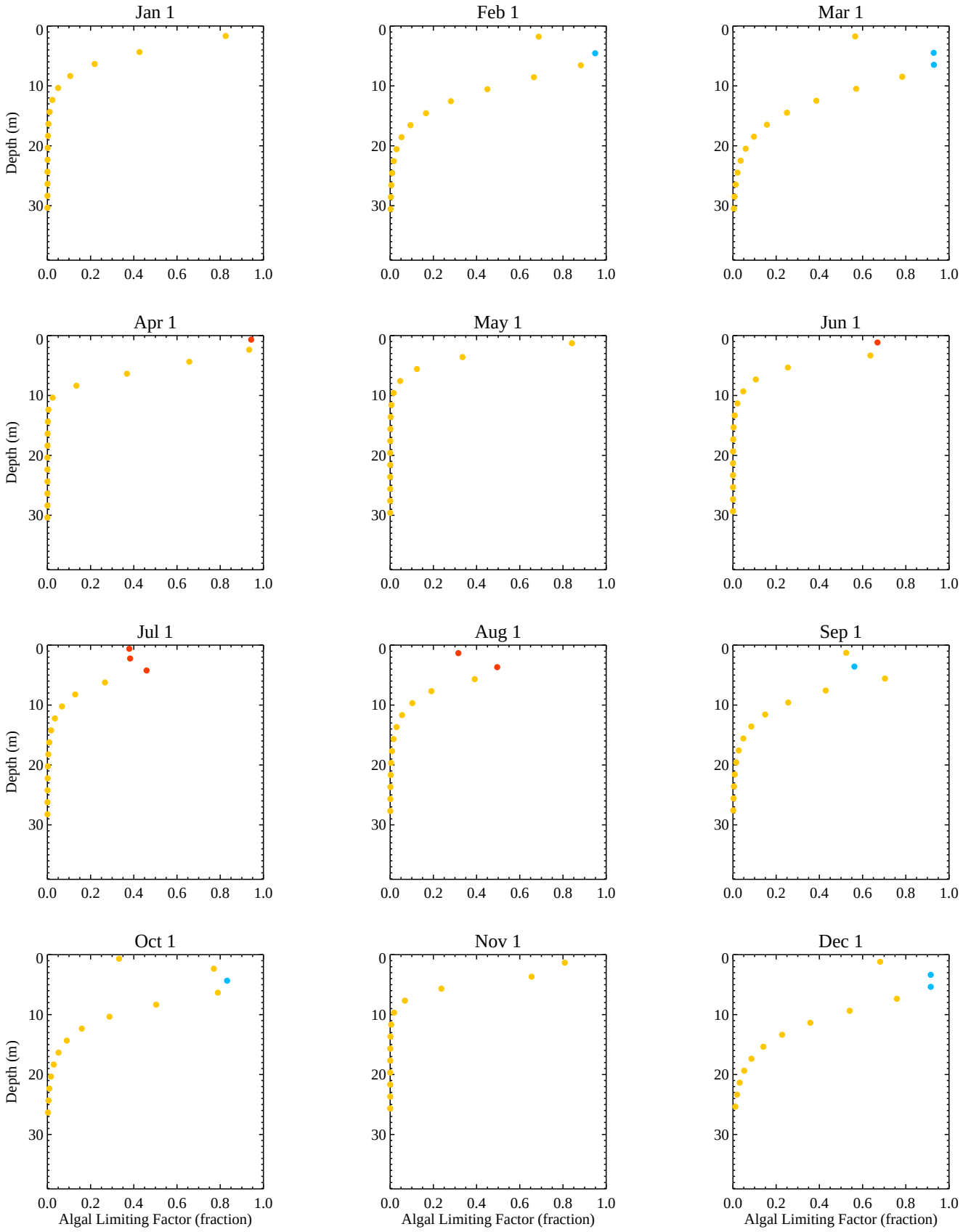

Figure J-23. Vertical profiles of algal limiting factor at Pace Bend (Segment 48) during 1999.

Profiles shown for first day of month.

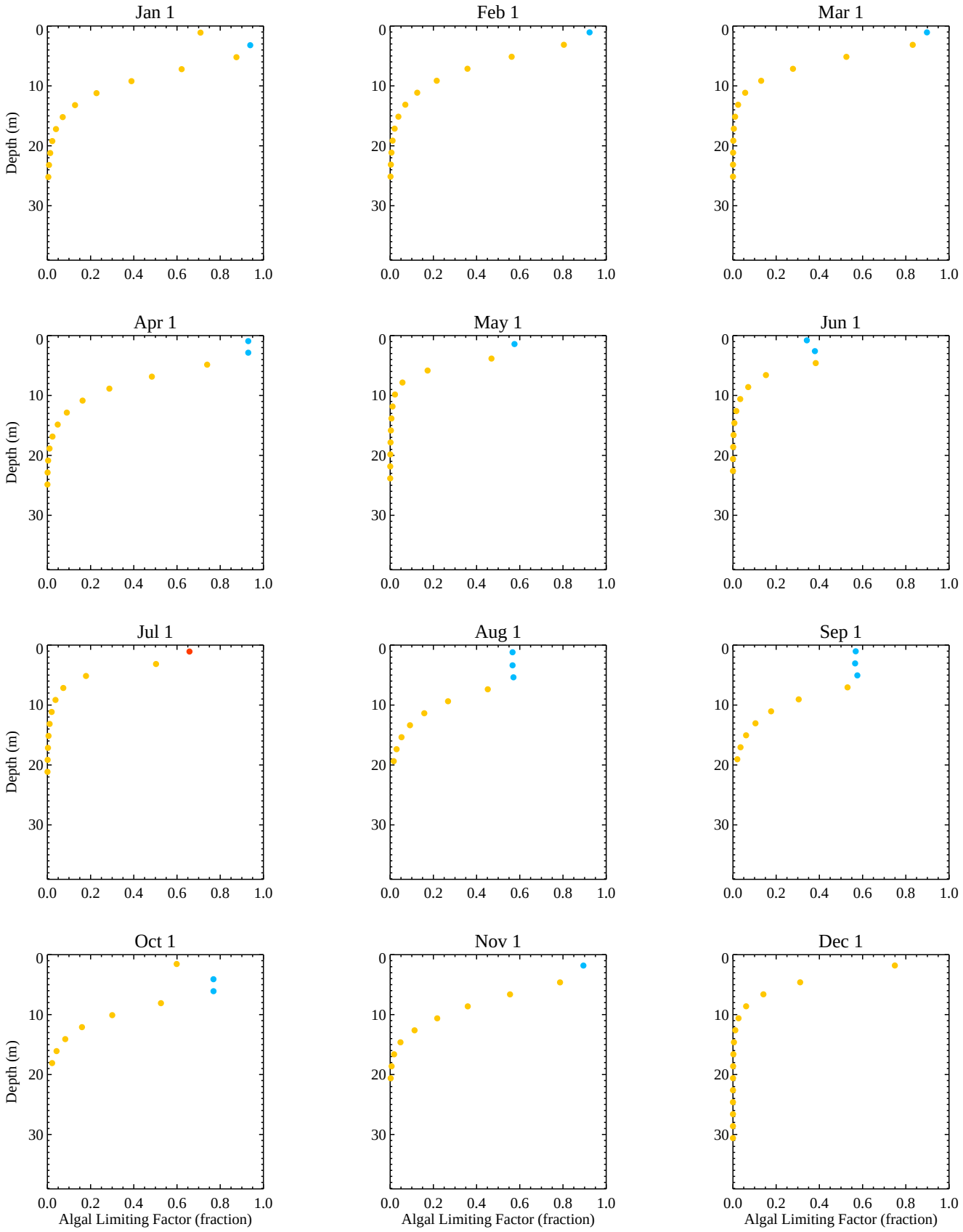

Figure J-23. Vertical profiles of algal limiting factor at Pace Bend (Segment 48) during 2000.

Profiles shown for first day of month.

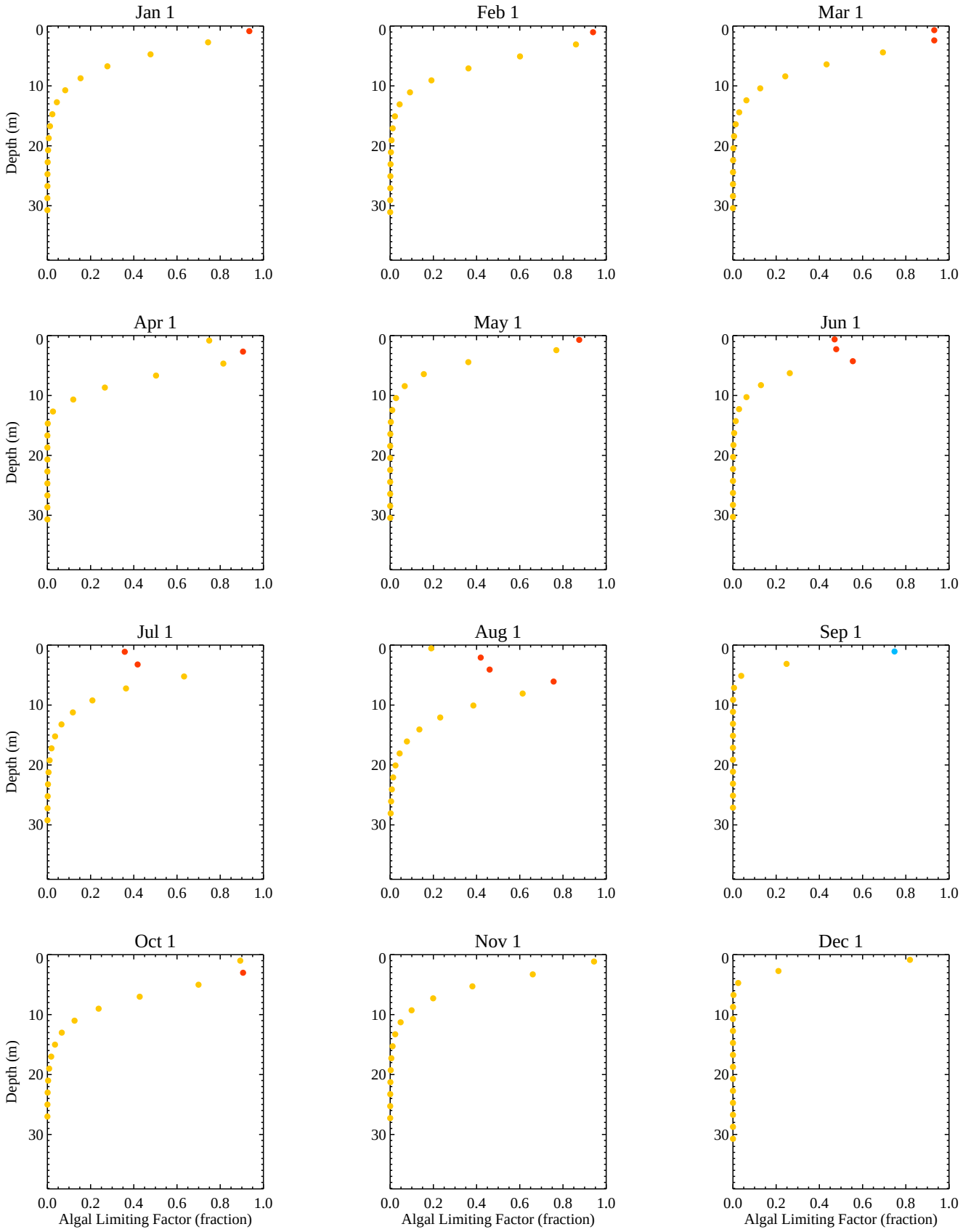

Figure J-23. Vertical profiles of algal limiting factor at Pace Bend (Segment 48) during 2001.

Profiles shown for first day of month.

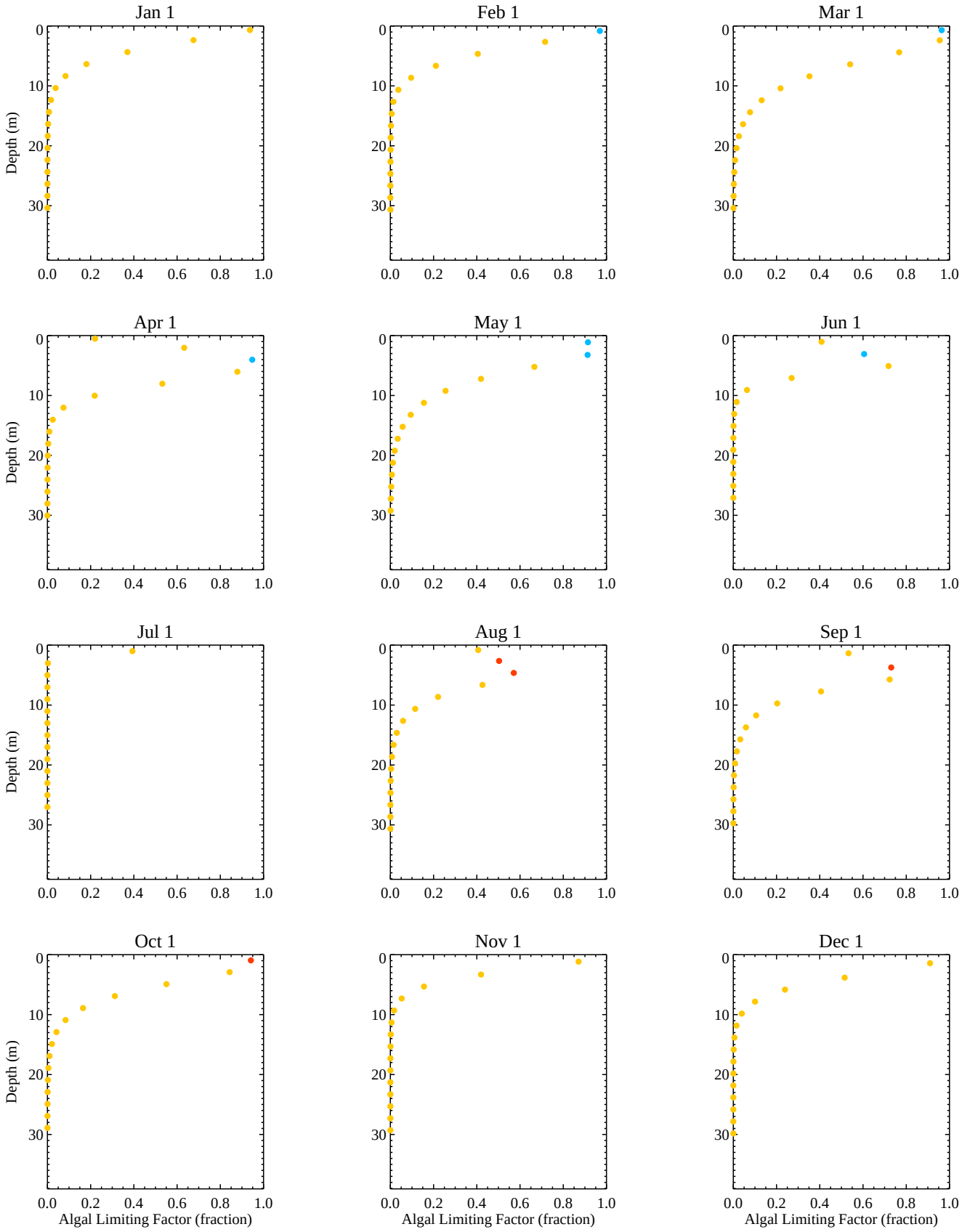

Figure J-23. Vertical profiles of algal limiting factor at Pace Bend (Segment 48) during 2002.

Profiles shown for first day of month.

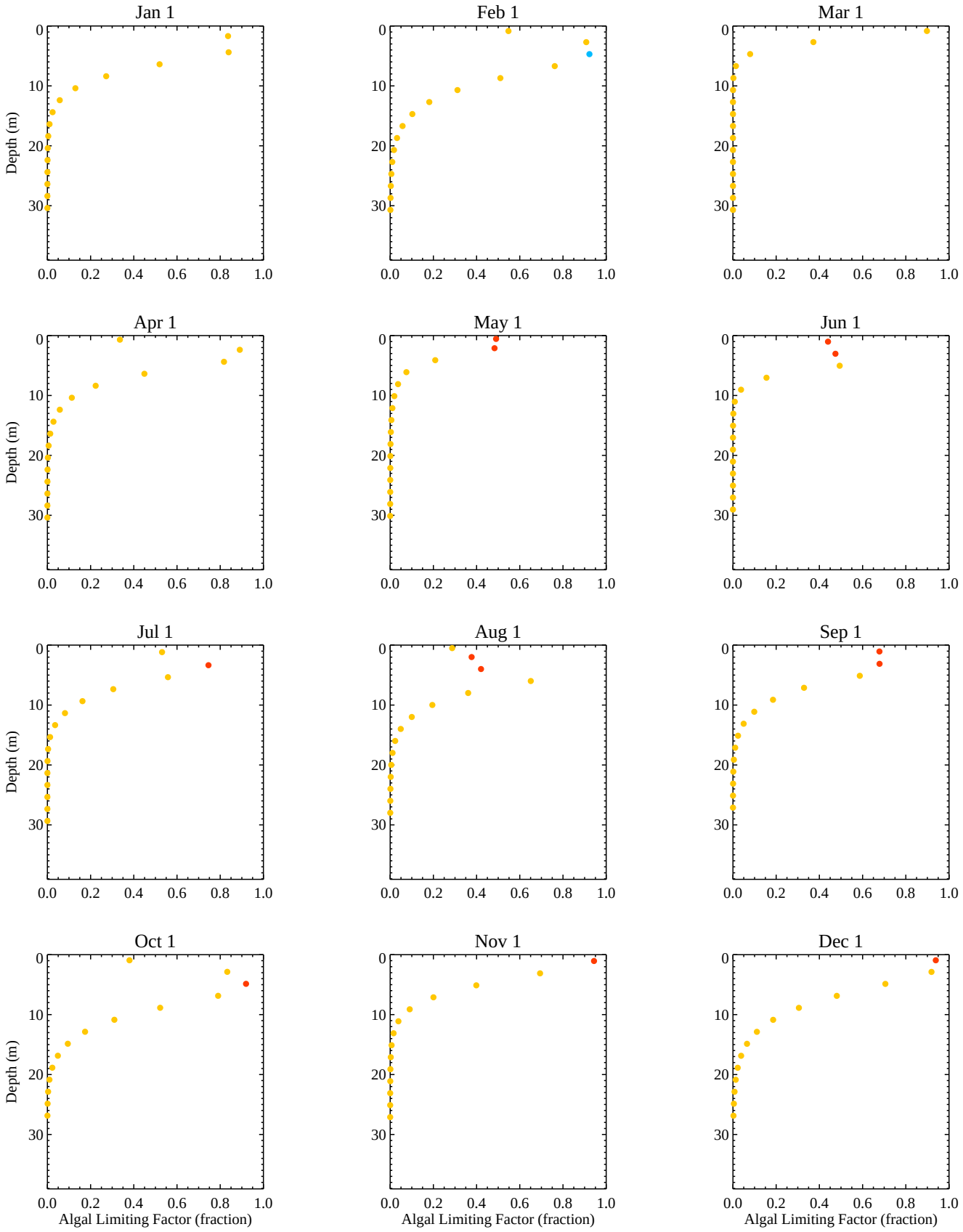

Figure J-23. Vertical profiles of algal limiting factor at Pace Bend (Segment 48) during 2003.

Profiles shown for first day of month.

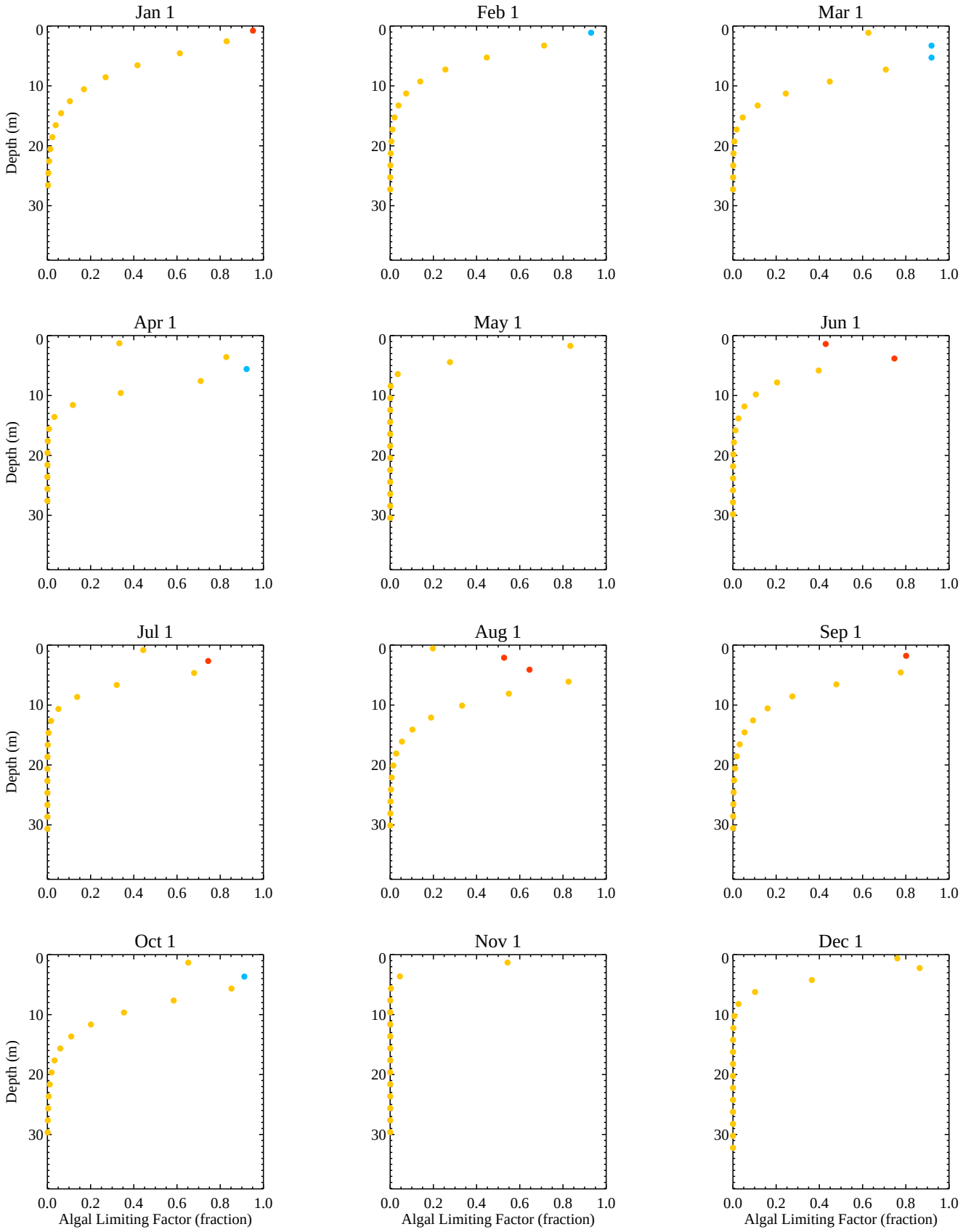

Figure J-23. Vertical profiles of algal limiting factor at Pace Bend (Segment 48) during 2004.

Profiles shown for first day of month.

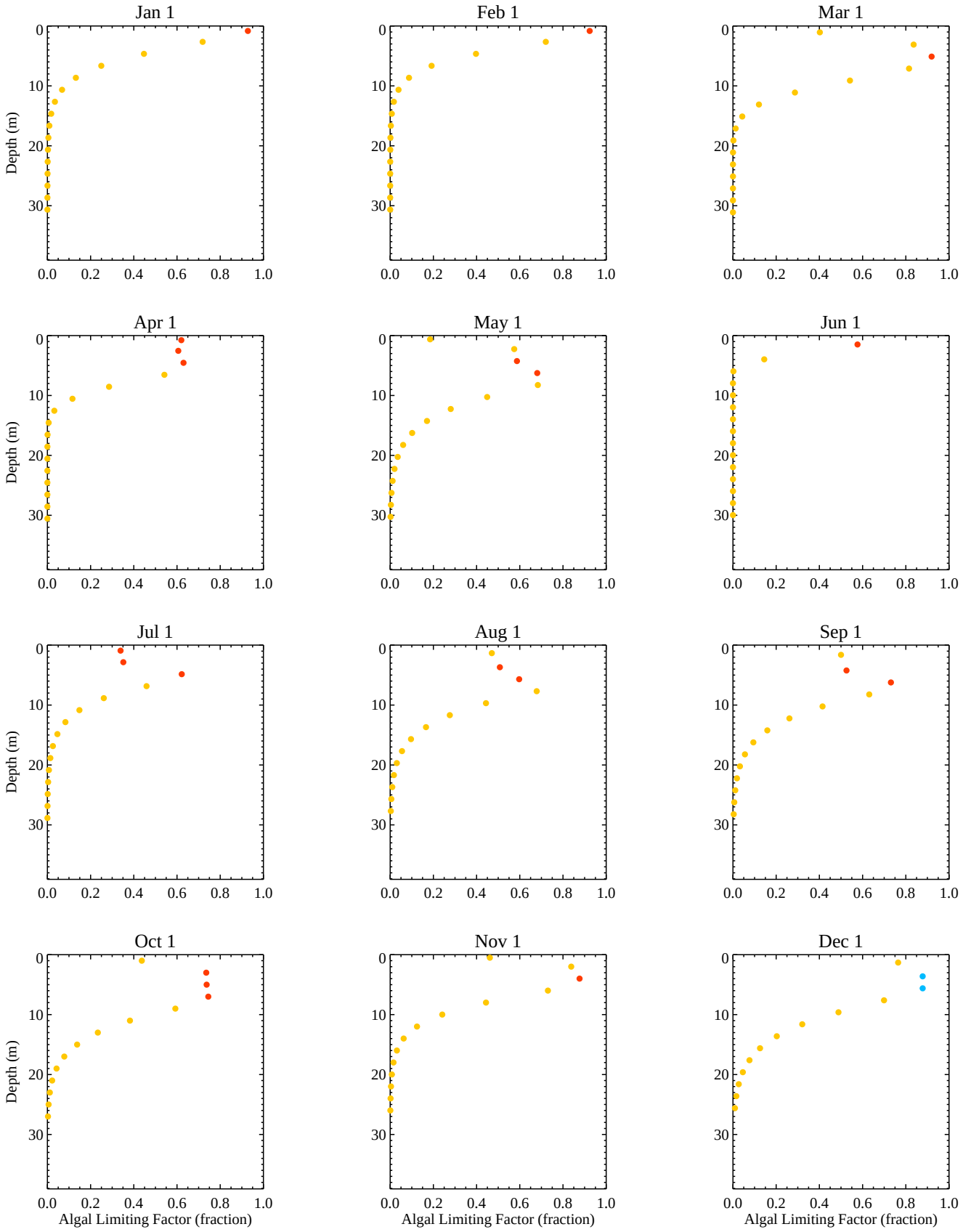

Figure J-23. Vertical profiles of algal limiting factor at Pace Bend (Segment 48) during 2005.

Profiles shown for first day of month.

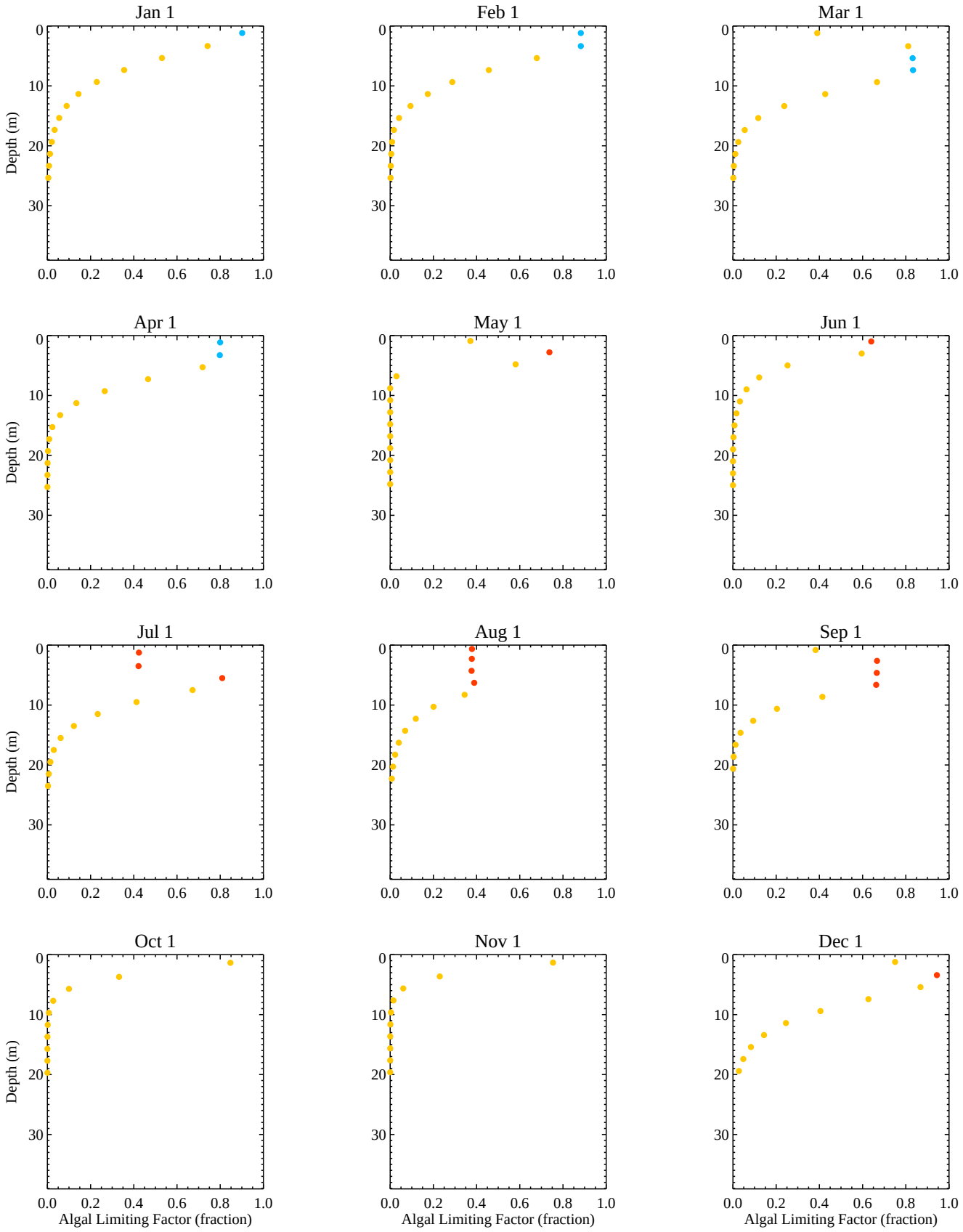

Figure J-23. Vertical profiles of algal limiting factor at Pace Bend (Segment 48) during 2006.

Profiles shown for first day of month.

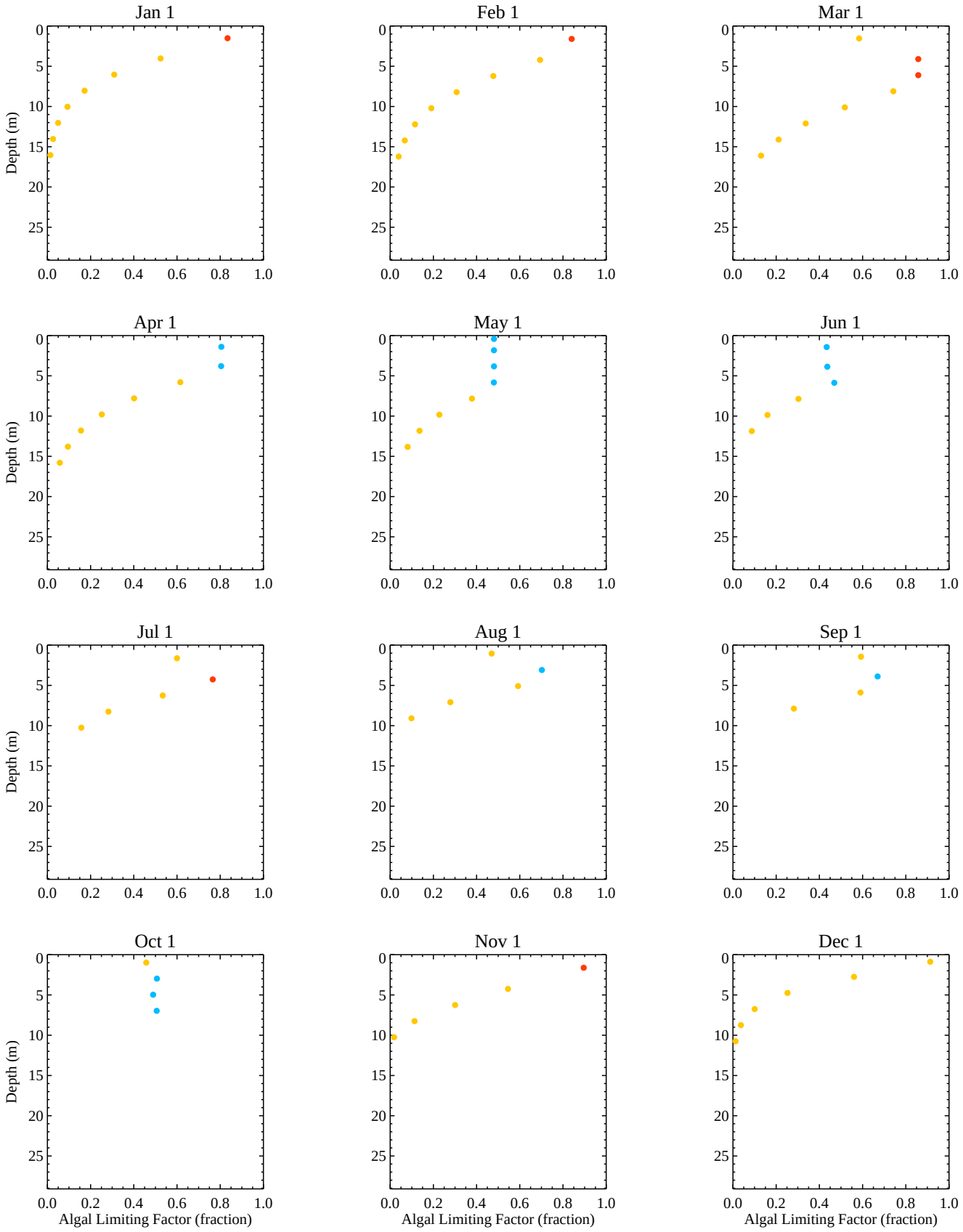

Figure J-24. Vertical profiles of algal limiting factor at Turkey Bend (Segment 28) during 1984.

Profiles shown for first day of month.

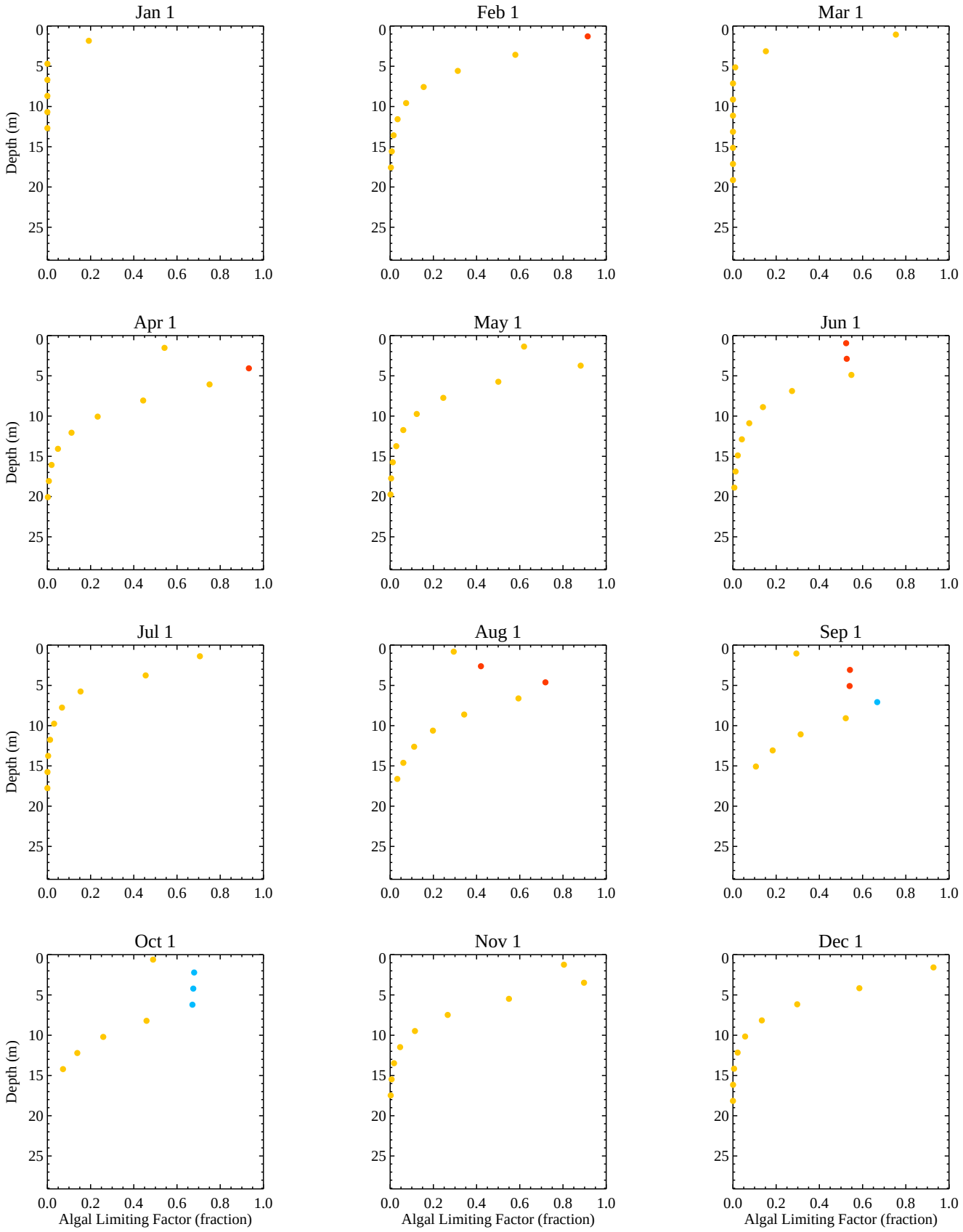

Figure J-24. Vertical profiles of algal limiting factor at Turkey Bend (Segment 28) during 1985.

Profiles shown for first day of month.

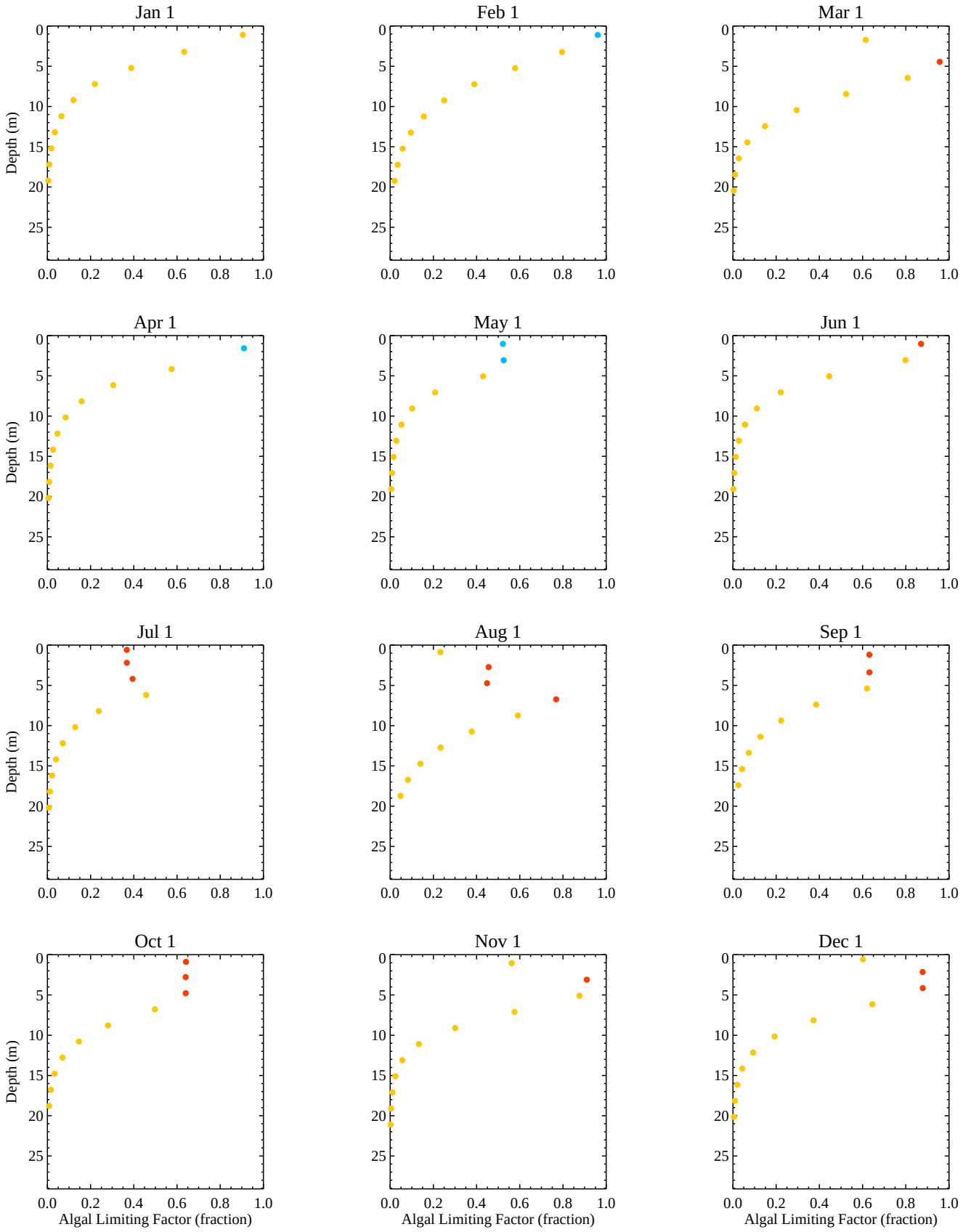

Figure J-24. Vertical profiles of algal limiting factor at Turkey Bend (Segment 28) during 1986.

Profiles shown for first day of month.

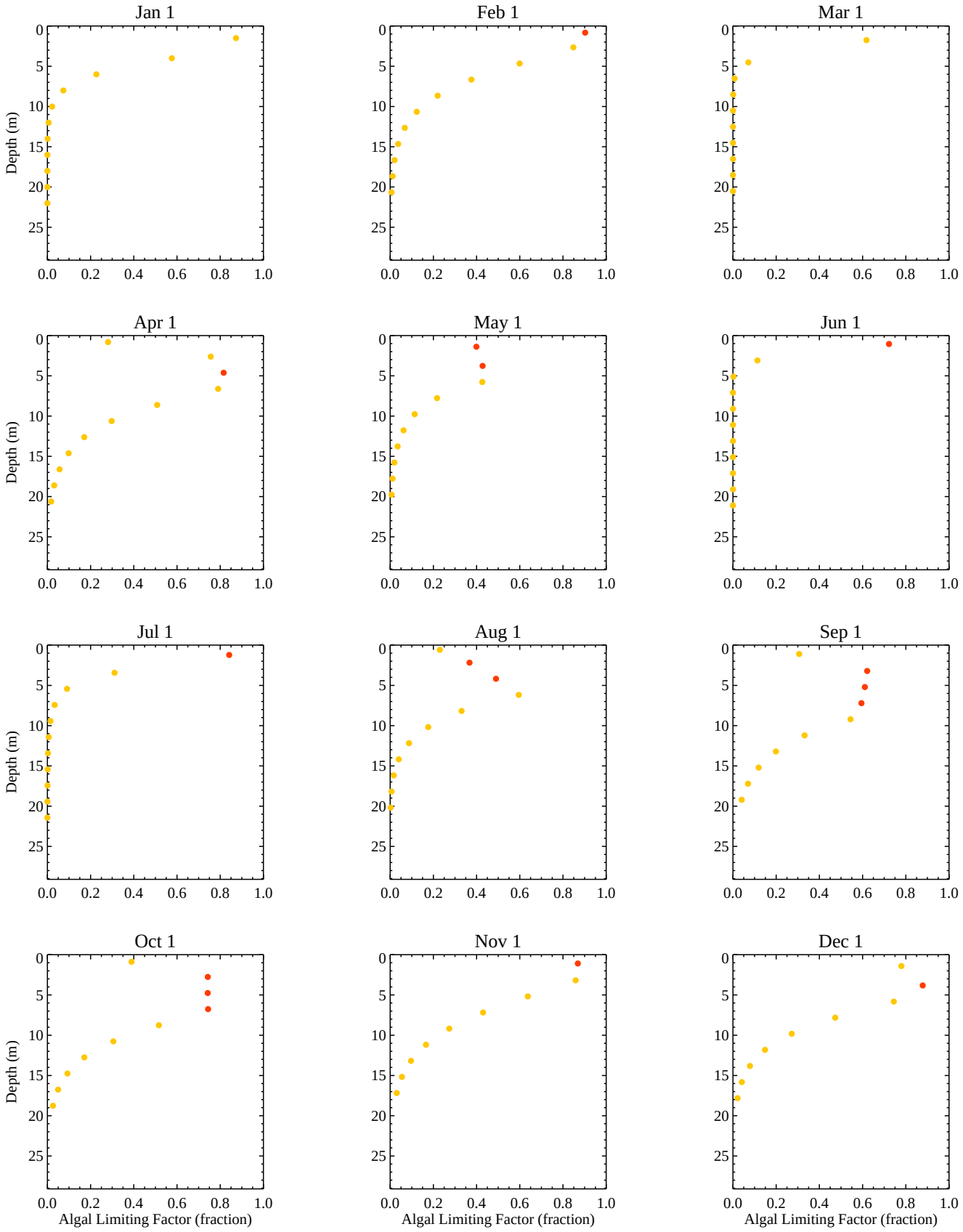

Figure J-24. Vertical profiles of algal limiting factor at Turkey Bend (Segment 28) during 1987.

Profiles shown for first day of month.

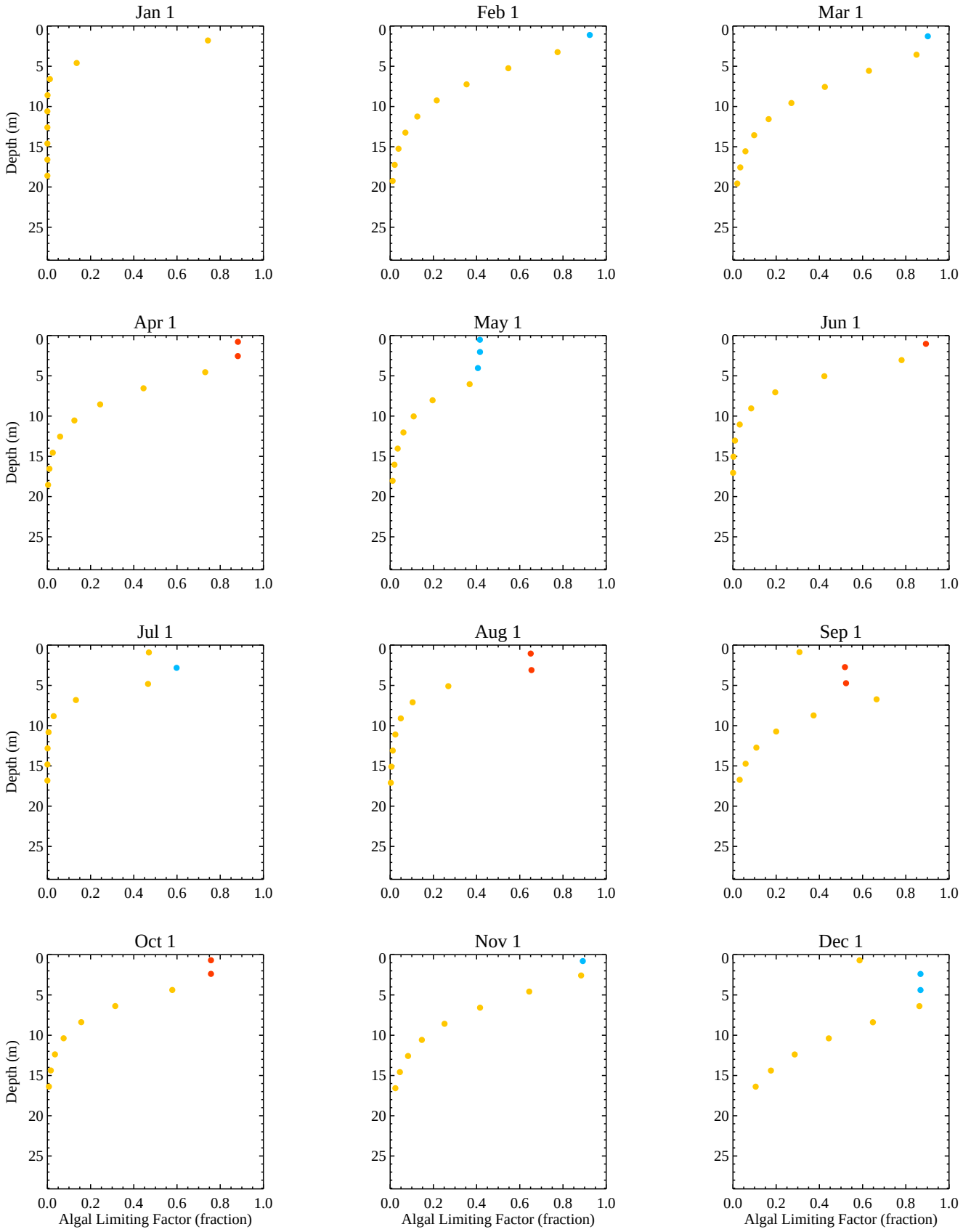

Figure J-24. Vertical profiles of algal limiting factor at Turkey Bend (Segment 28) during 1988.

Profiles shown for first day of month.

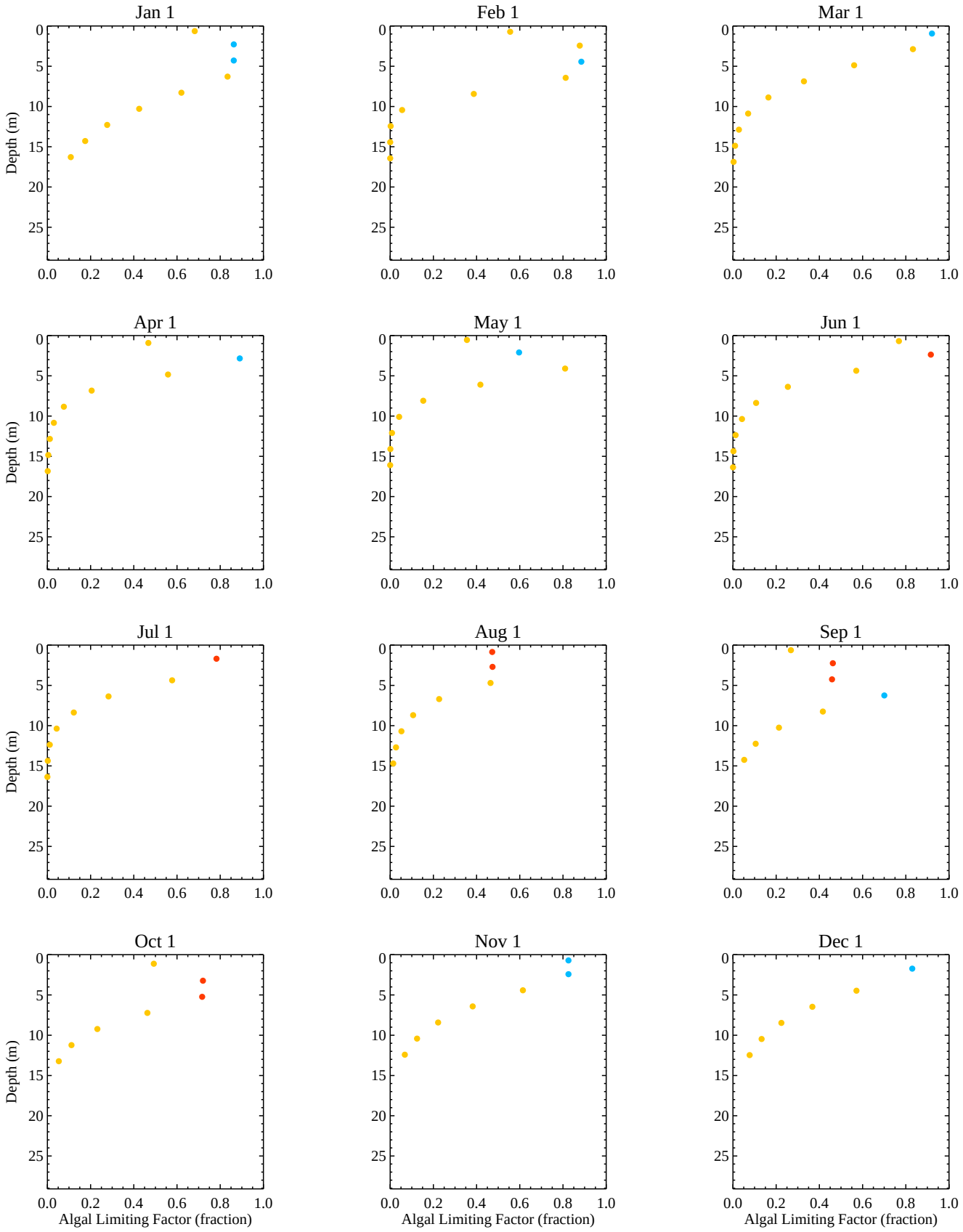

Figure J-24. Vertical profiles of algal limiting factor at Turkey Bend (Segment 28) during 1989.

Profiles shown for first day of month.

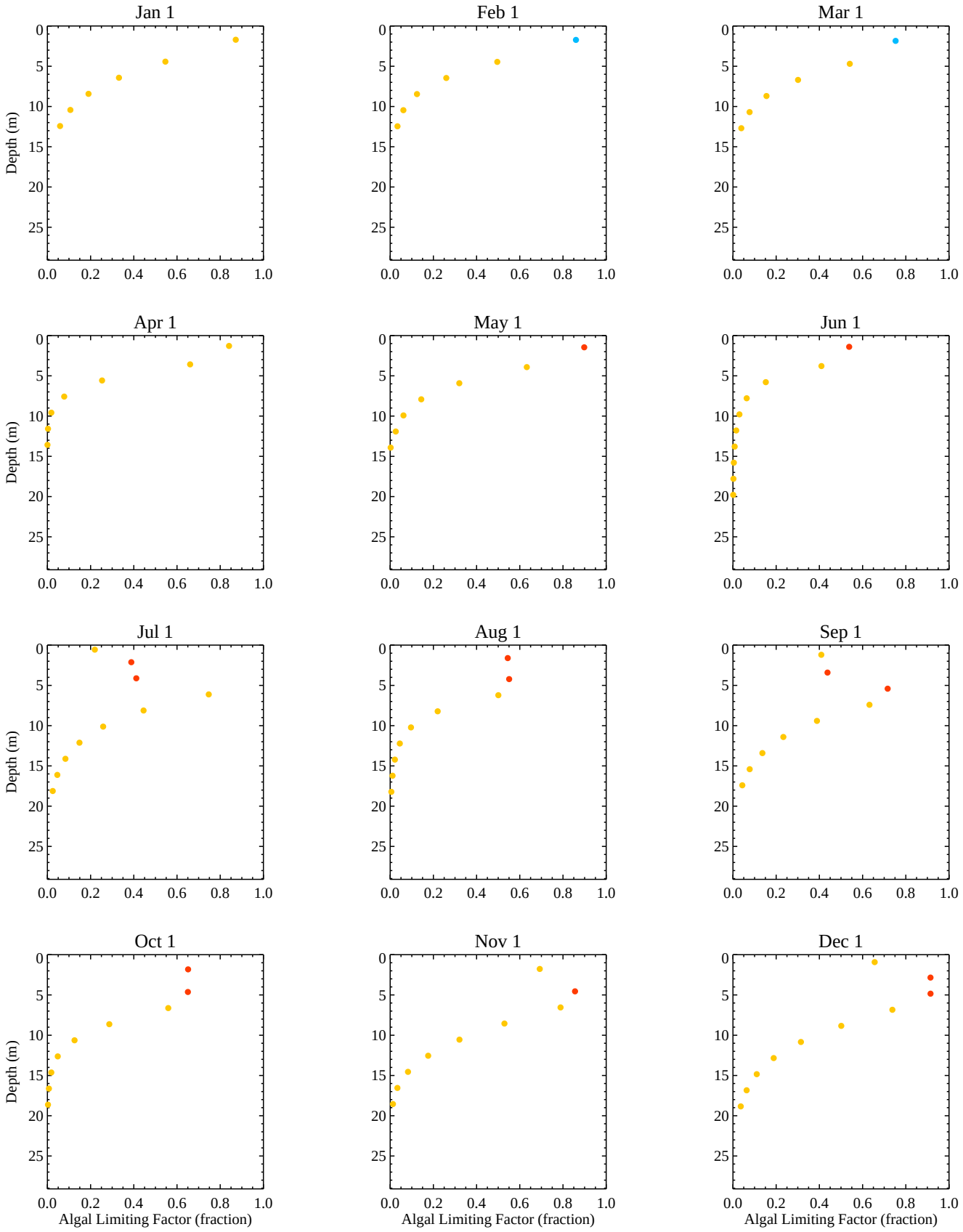

Figure J-24. Vertical profiles of algal limiting factor at Turkey Bend (Segment 28) during 1990.

Profiles shown for first day of month.

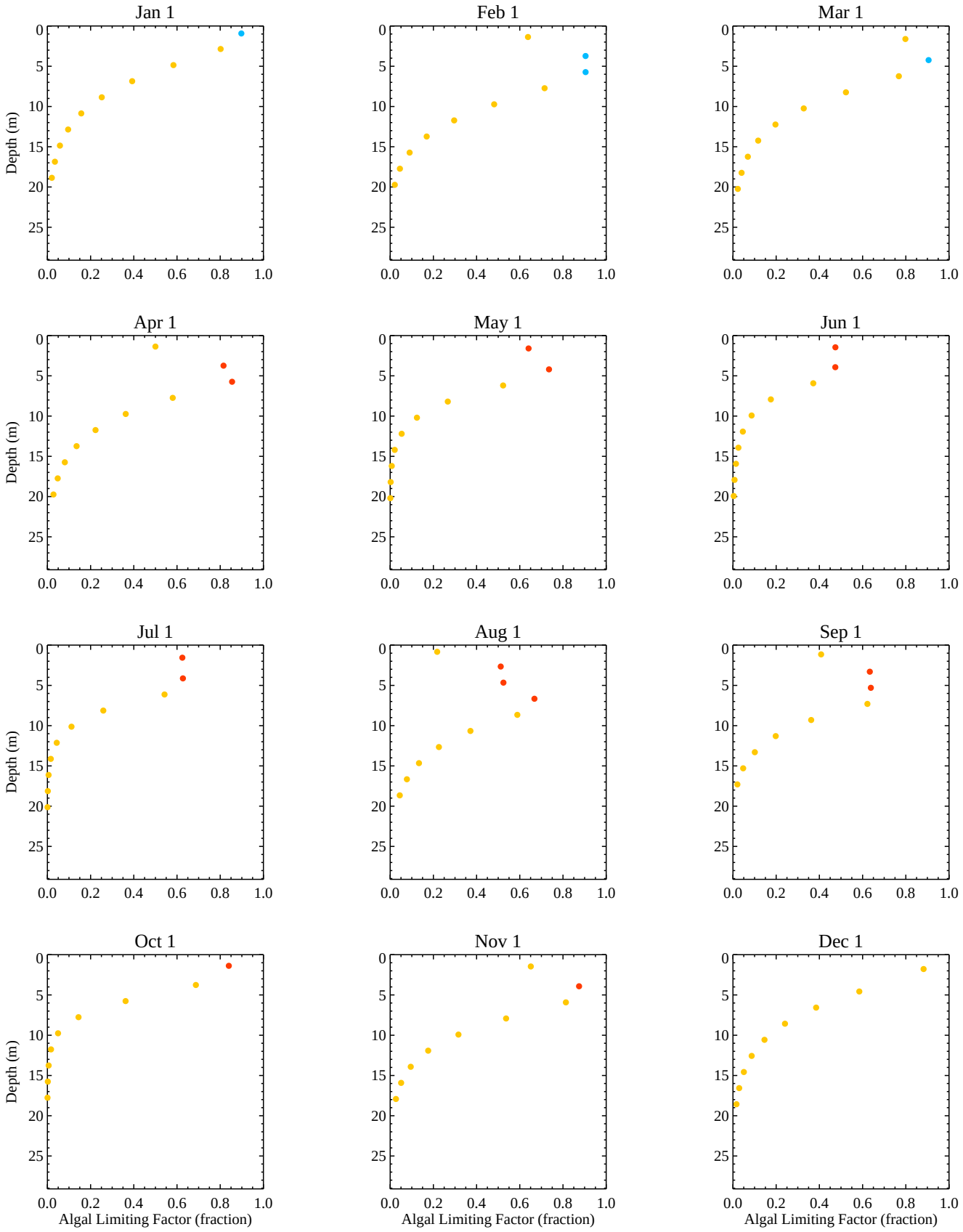

Figure J-24. Vertical profiles of algal limiting factor at Turkey Bend (Segment 28) during 1991.

Profiles shown for first day of month.

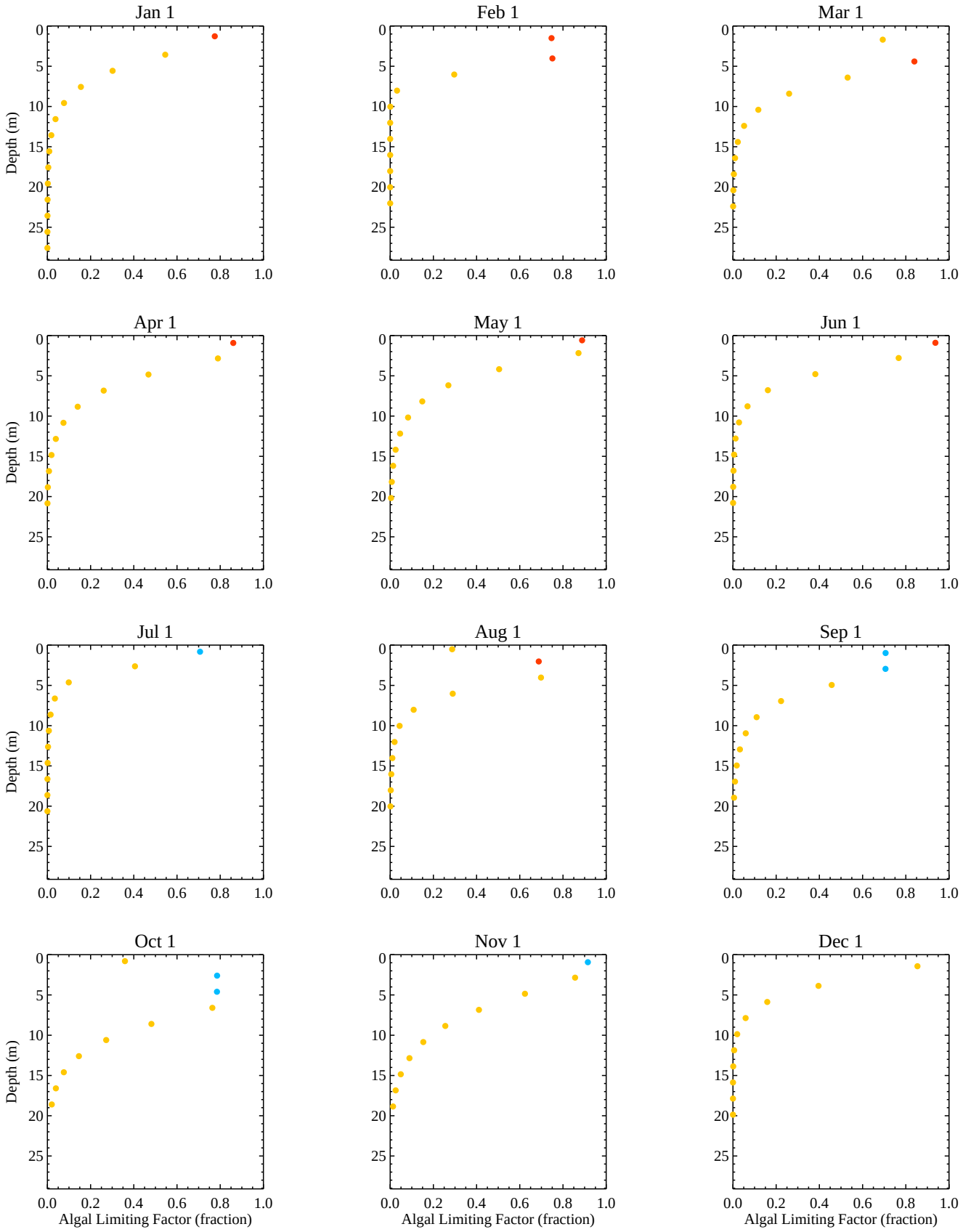

Figure J-24. Vertical profiles of algal limiting factor at Turkey Bend (Segment 28) during 1992.

Profiles shown for first day of month.

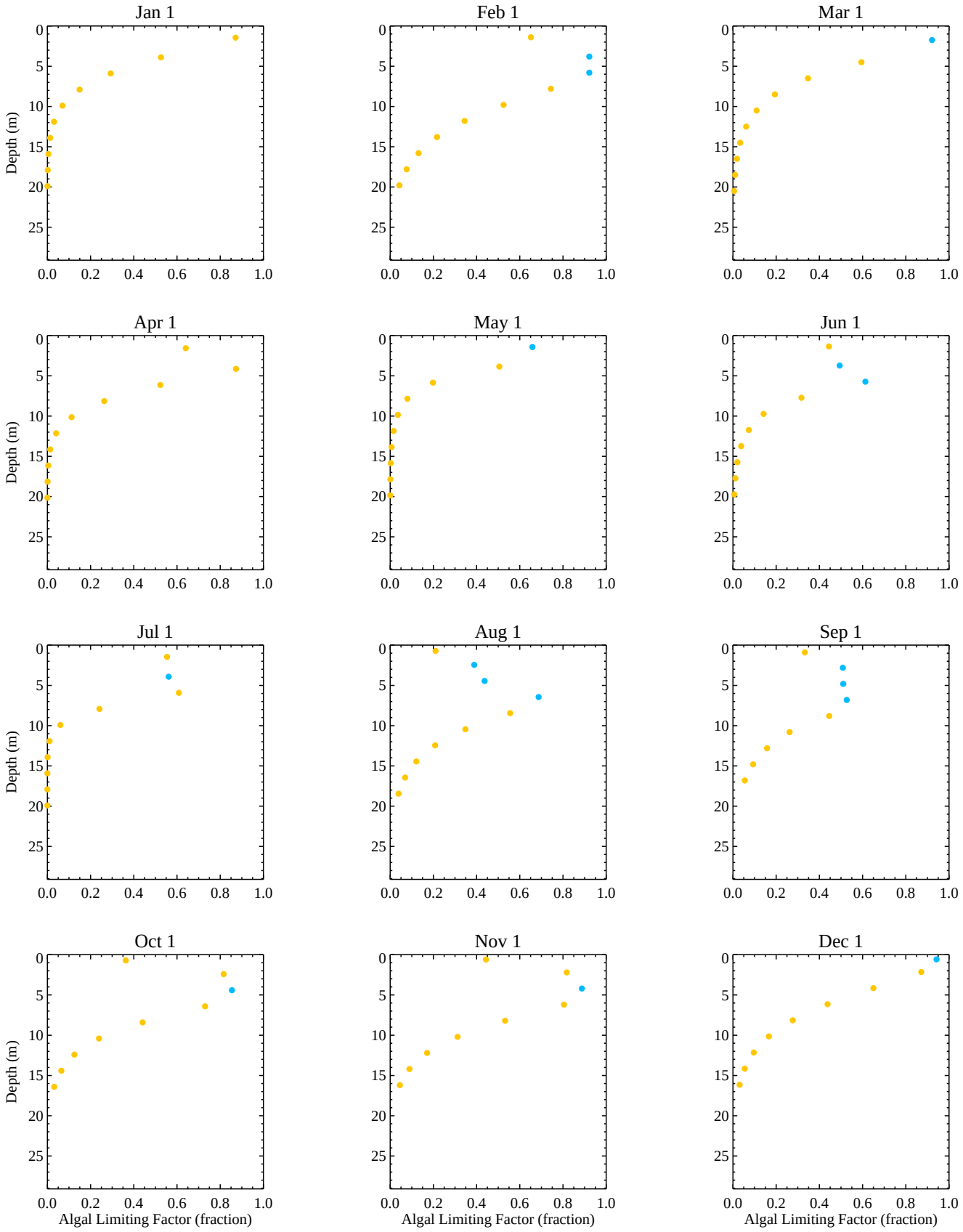

Figure J-24. Vertical profiles of algal limiting factor at Turkey Bend (Segment 28) during 1993.

Profiles shown for first day of month.

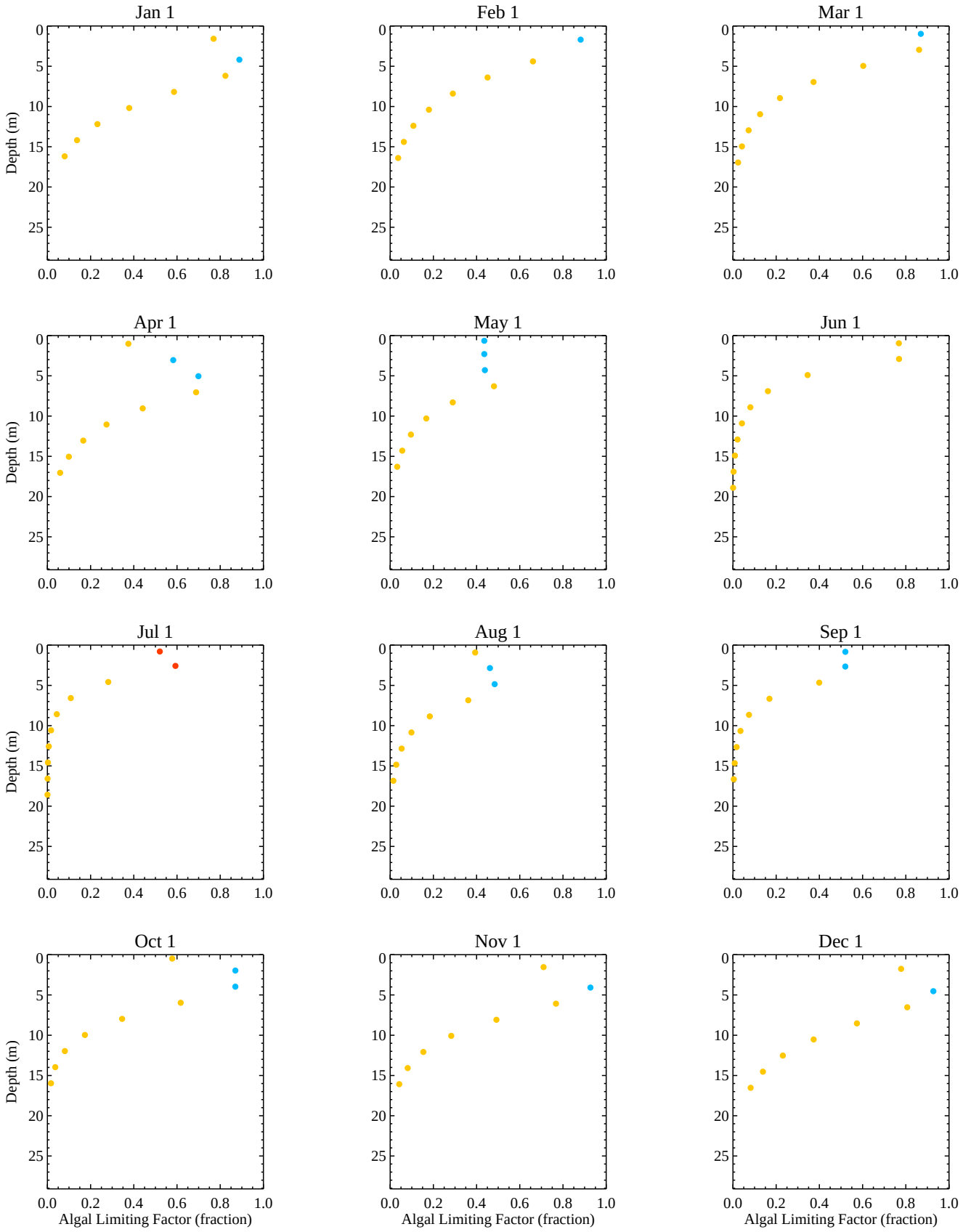

Figure J-24. Vertical profiles of algal limiting factor at Turkey Bend (Segment 28) during 1994.

Profiles shown for first day of month.

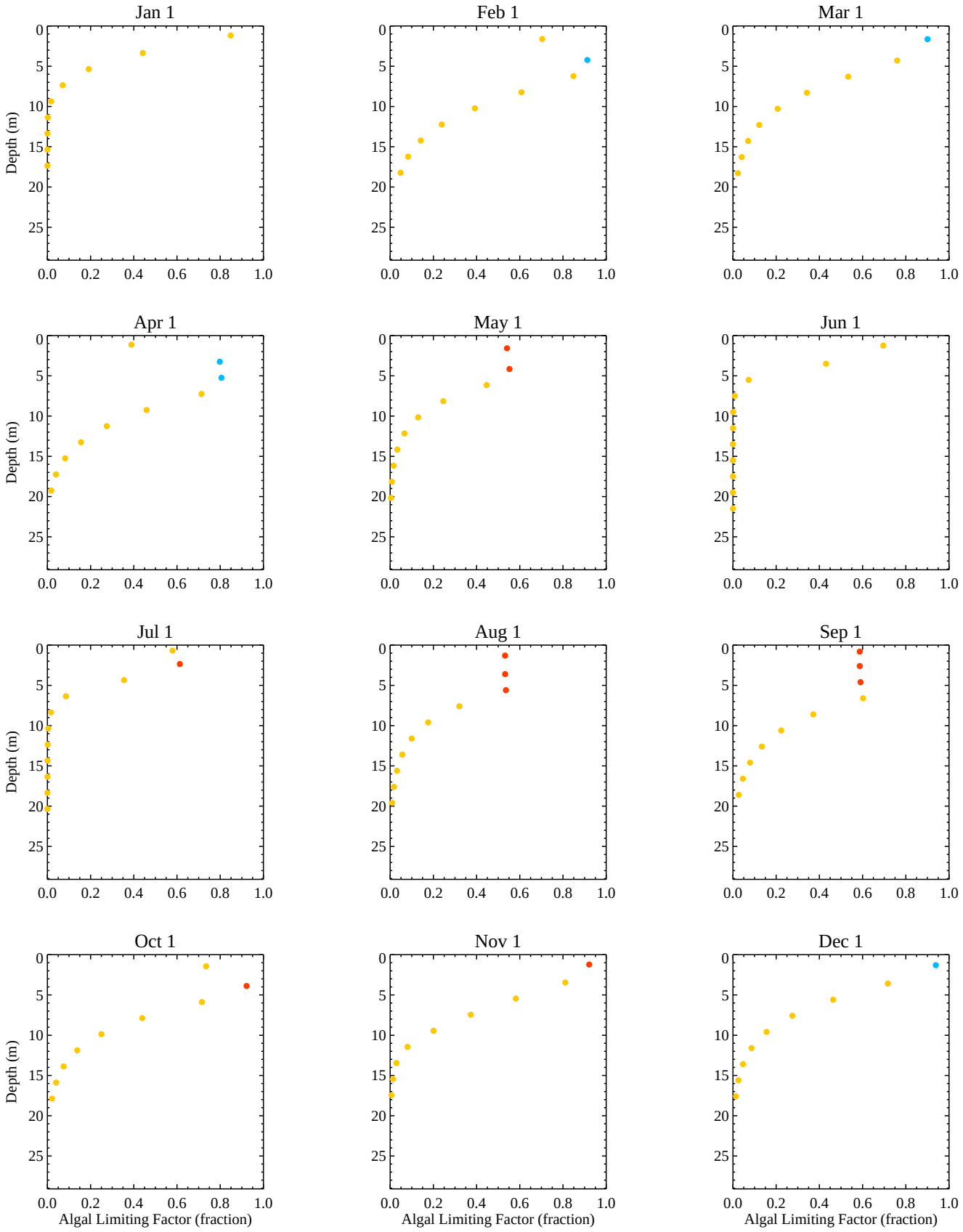

Figure J-24. Vertical profiles of algal limiting factor at Turkey Bend (Segment 28) during 1995.

Profiles shown for first day of month.

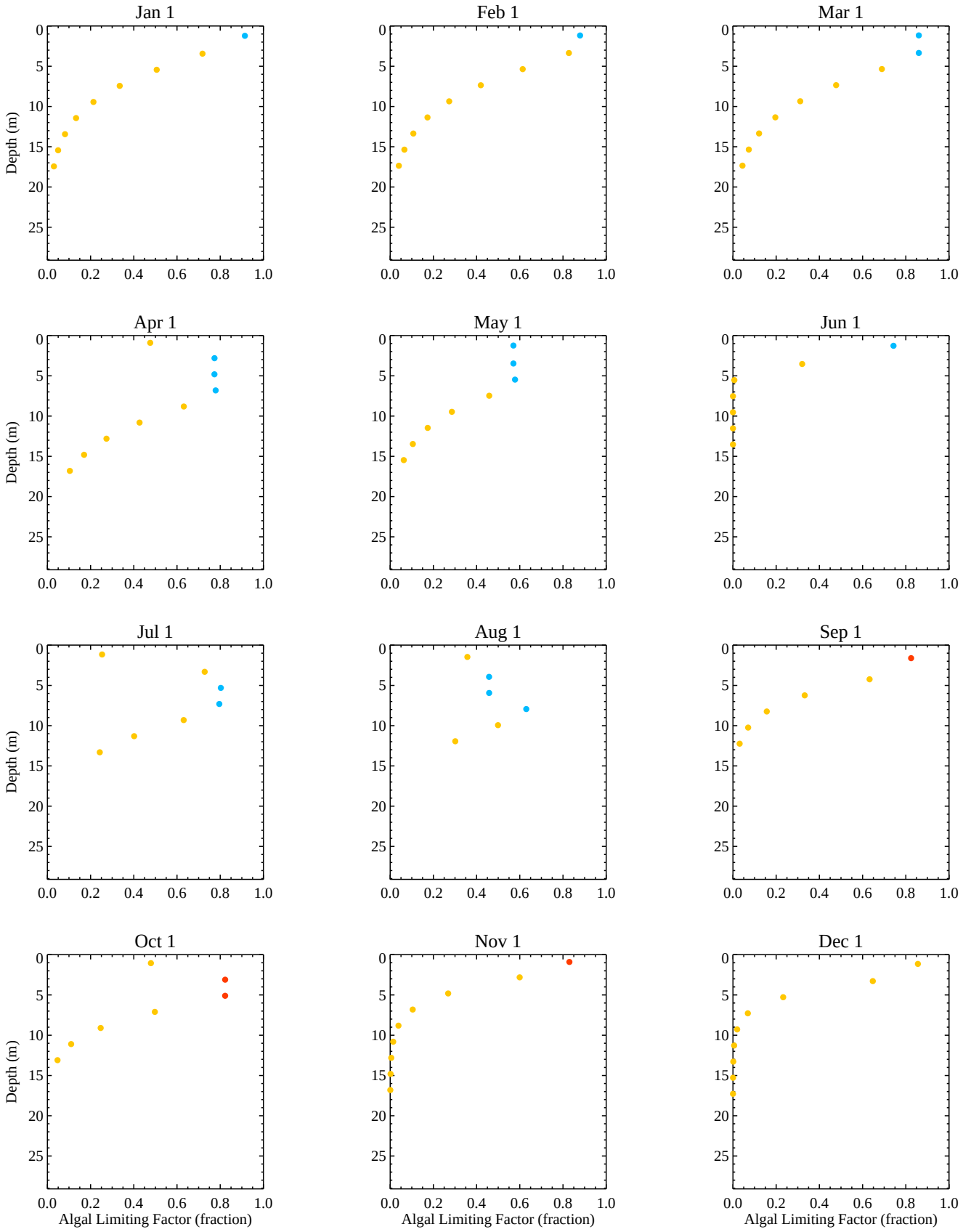

Figure J-24. Vertical profiles of algal limiting factor at Turkey Bend (Segment 28) during 1996.

Profiles shown for first day of month.

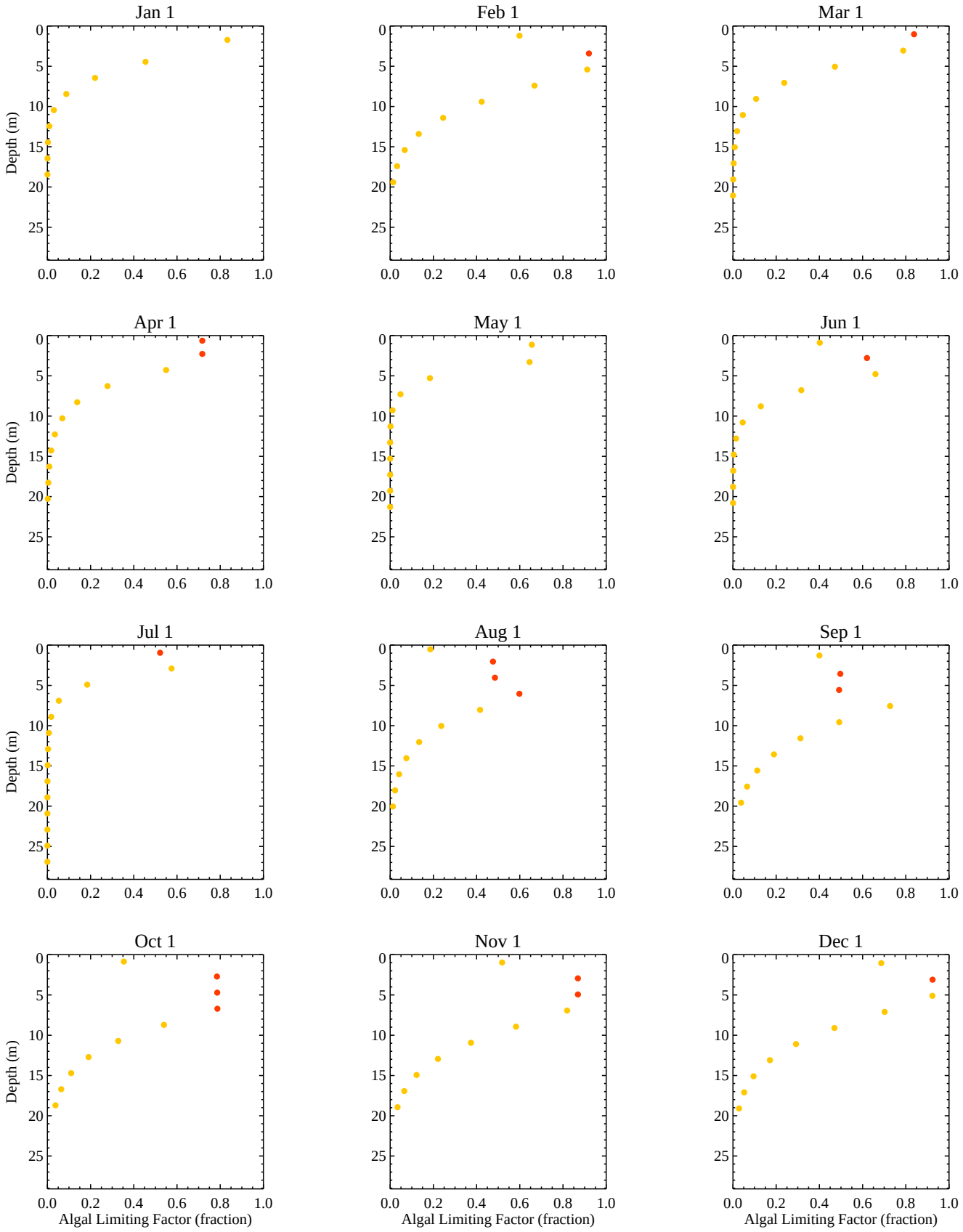

Figure J-24. Vertical profiles of algal limiting factor at Turkey Bend (Segment 28) during 1997.

Profiles shown for first day of month.

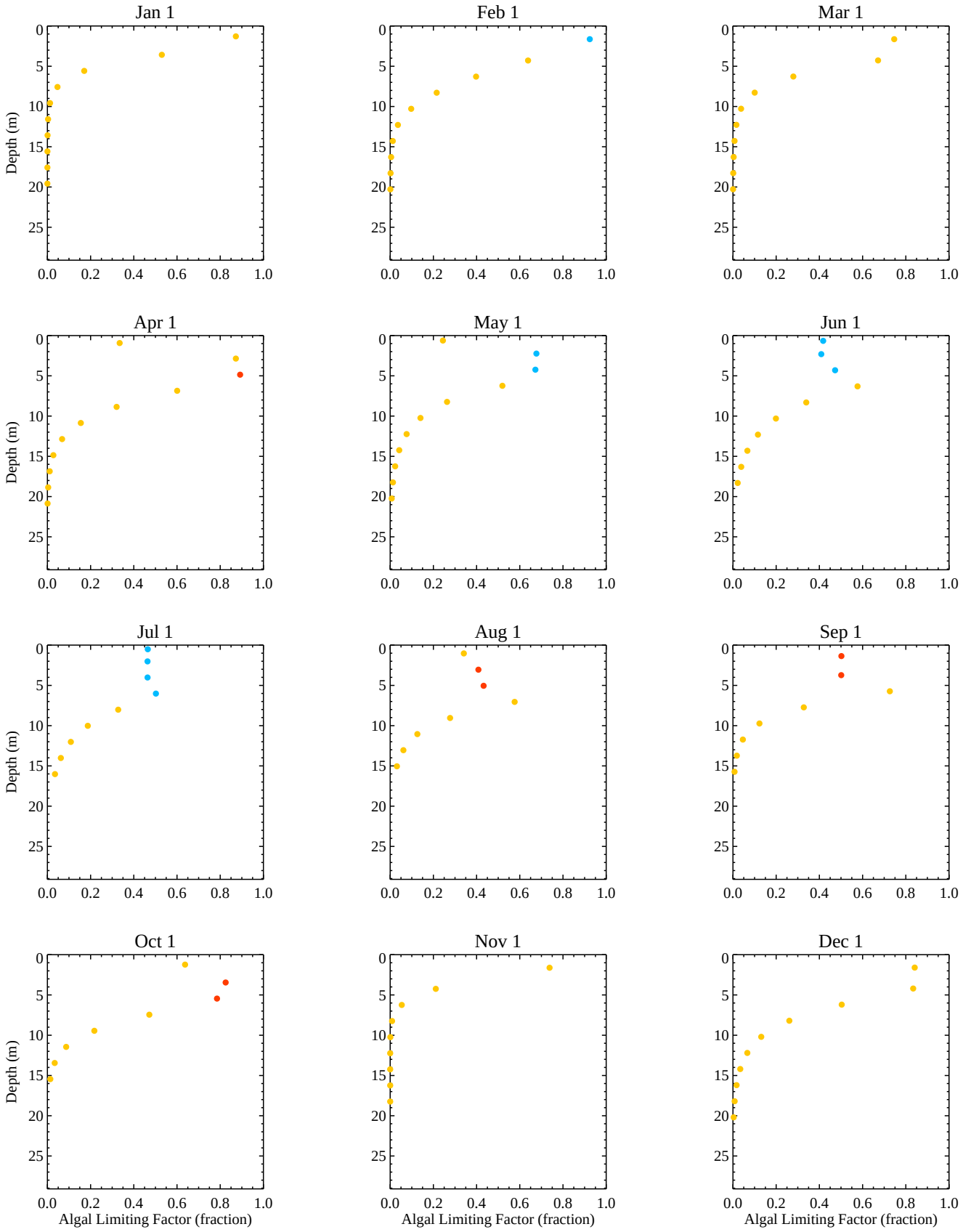

Figure J-24. Vertical profiles of algal limiting factor at Turkey Bend (Segment 28) during 1998.

Profiles shown for first day of month.

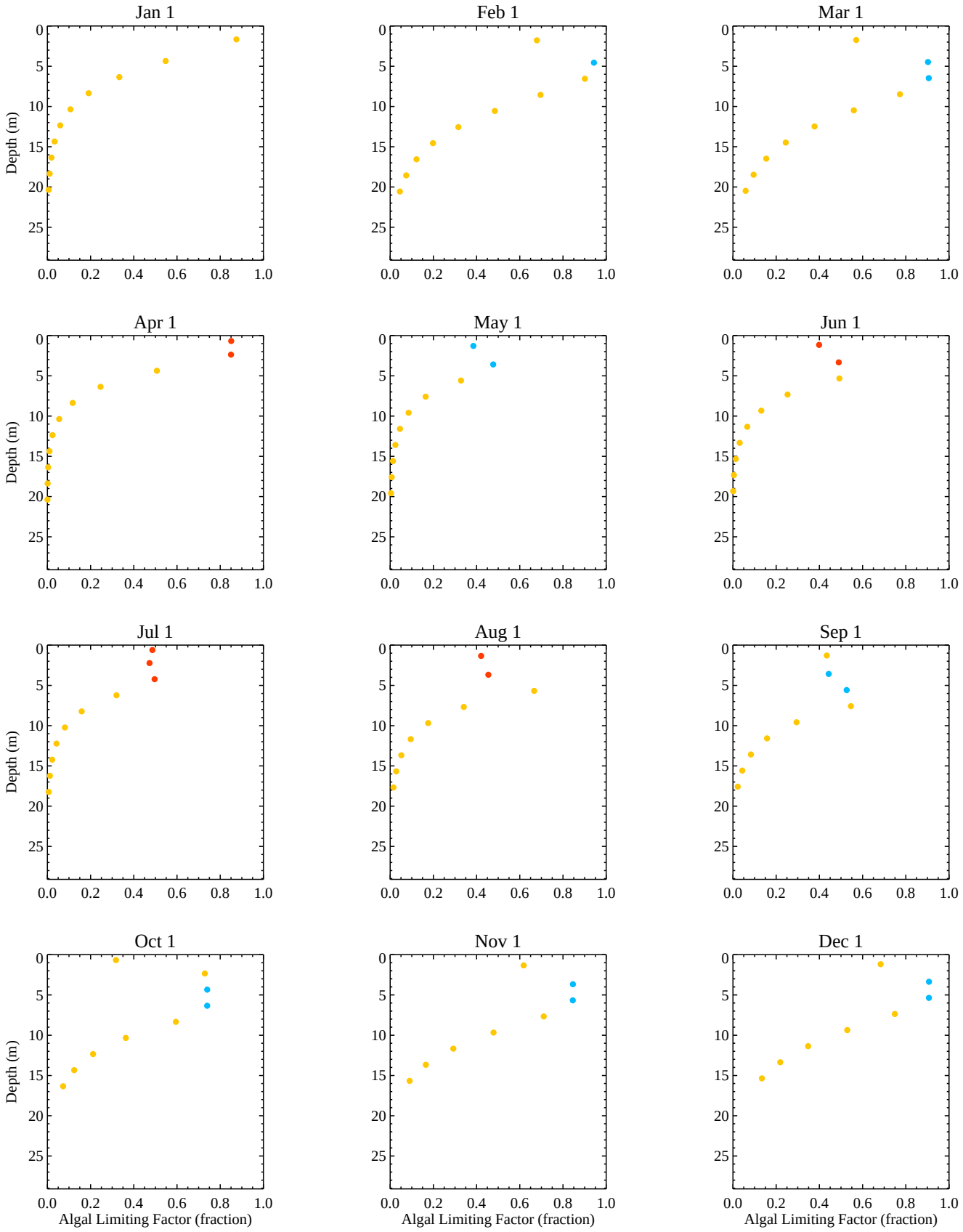

Figure J-24. Vertical profiles of algal limiting factor at Turkey Bend (Segment 28) during 1999.

Profiles shown for first day of month.

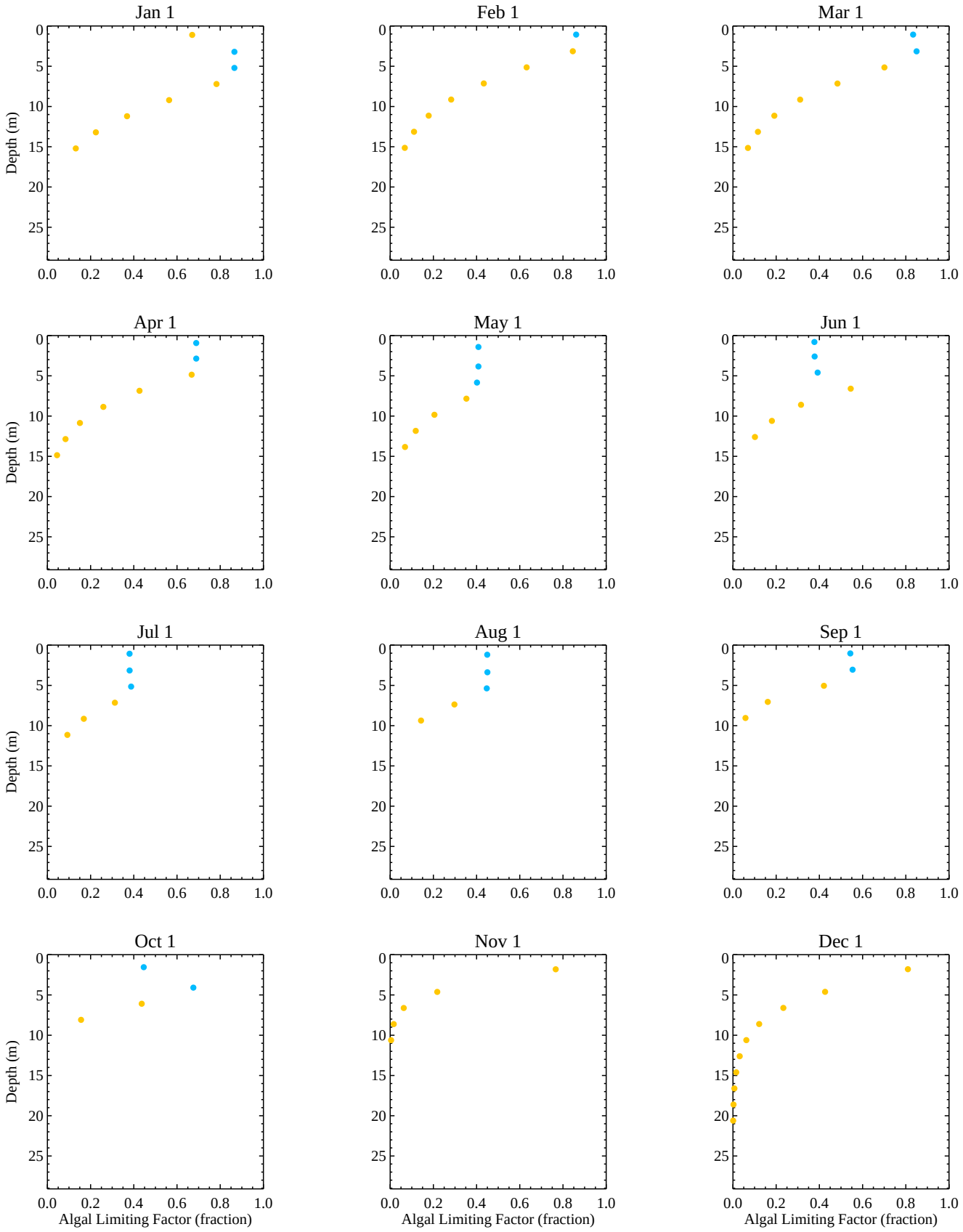

Figure J-24. Vertical profiles of algal limiting factor at Turkey Bend (Segment 28) during 2000.

Profiles shown for first day of month.

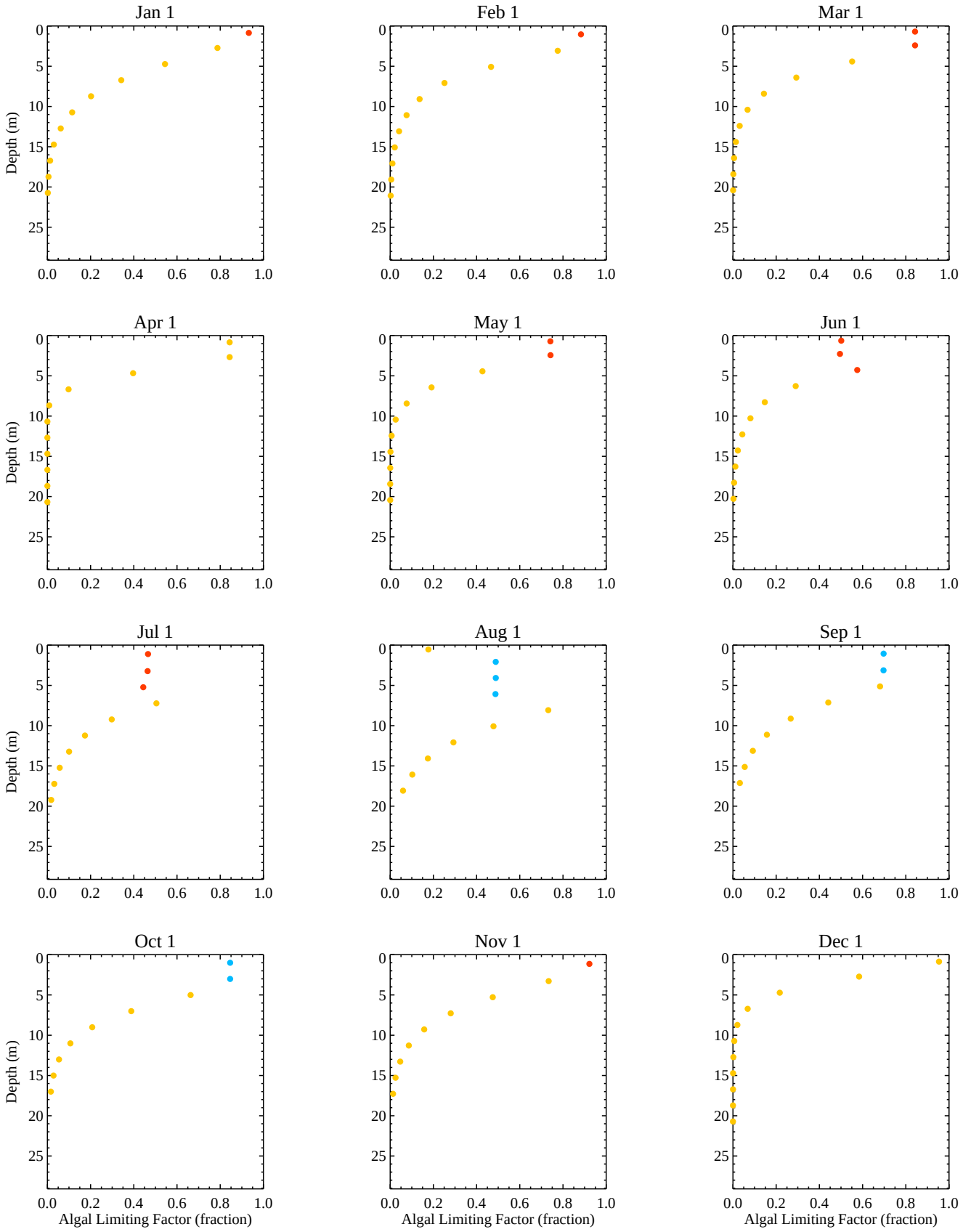

Figure J-24. Vertical profiles of algal limiting factor at Turkey Bend (Segment 28) during 2001.

Profiles shown for first day of month.

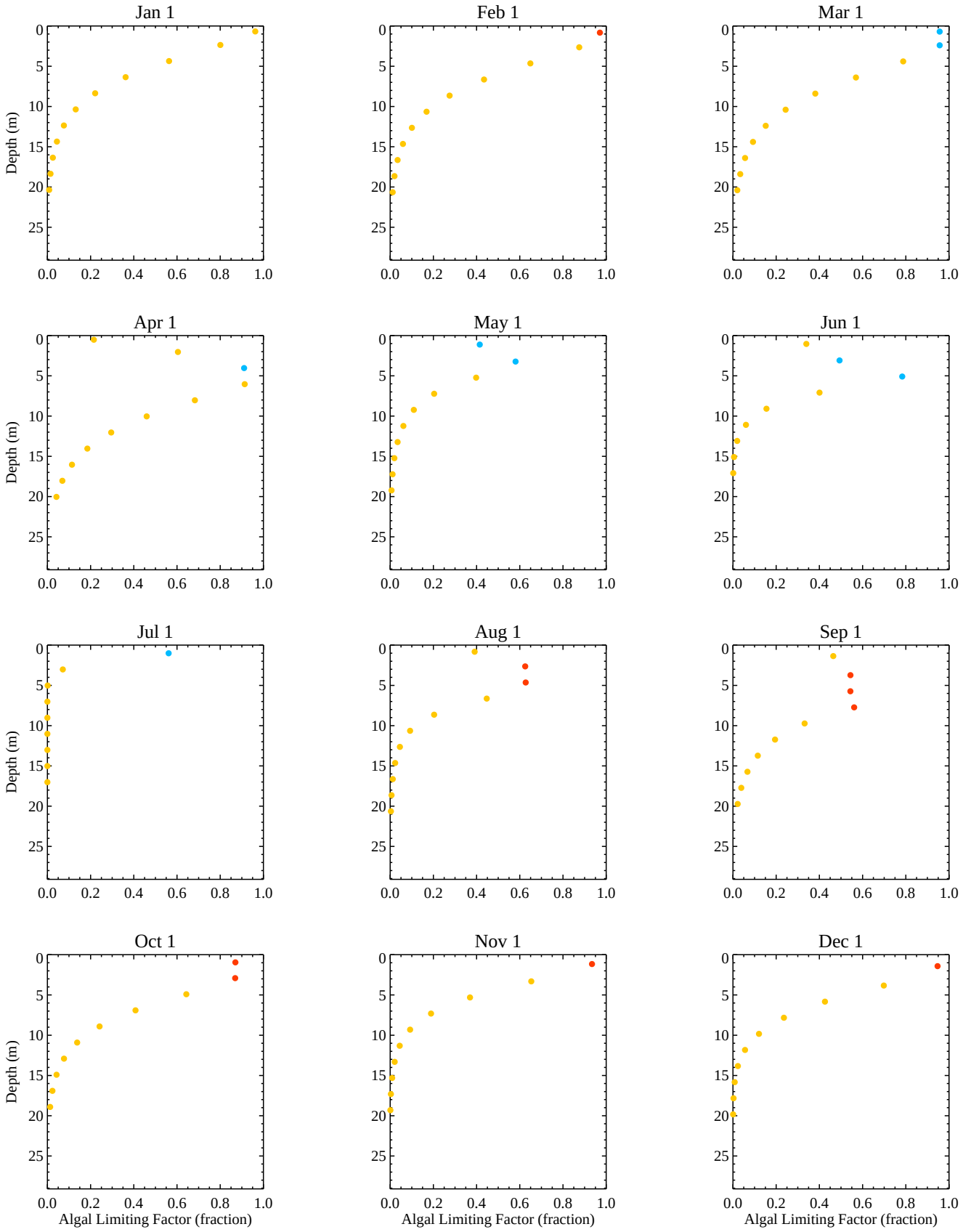

Figure J-24. Vertical profiles of algal limiting factor at Turkey Bend (Segment 28) during 2002.

Profiles shown for first day of month.

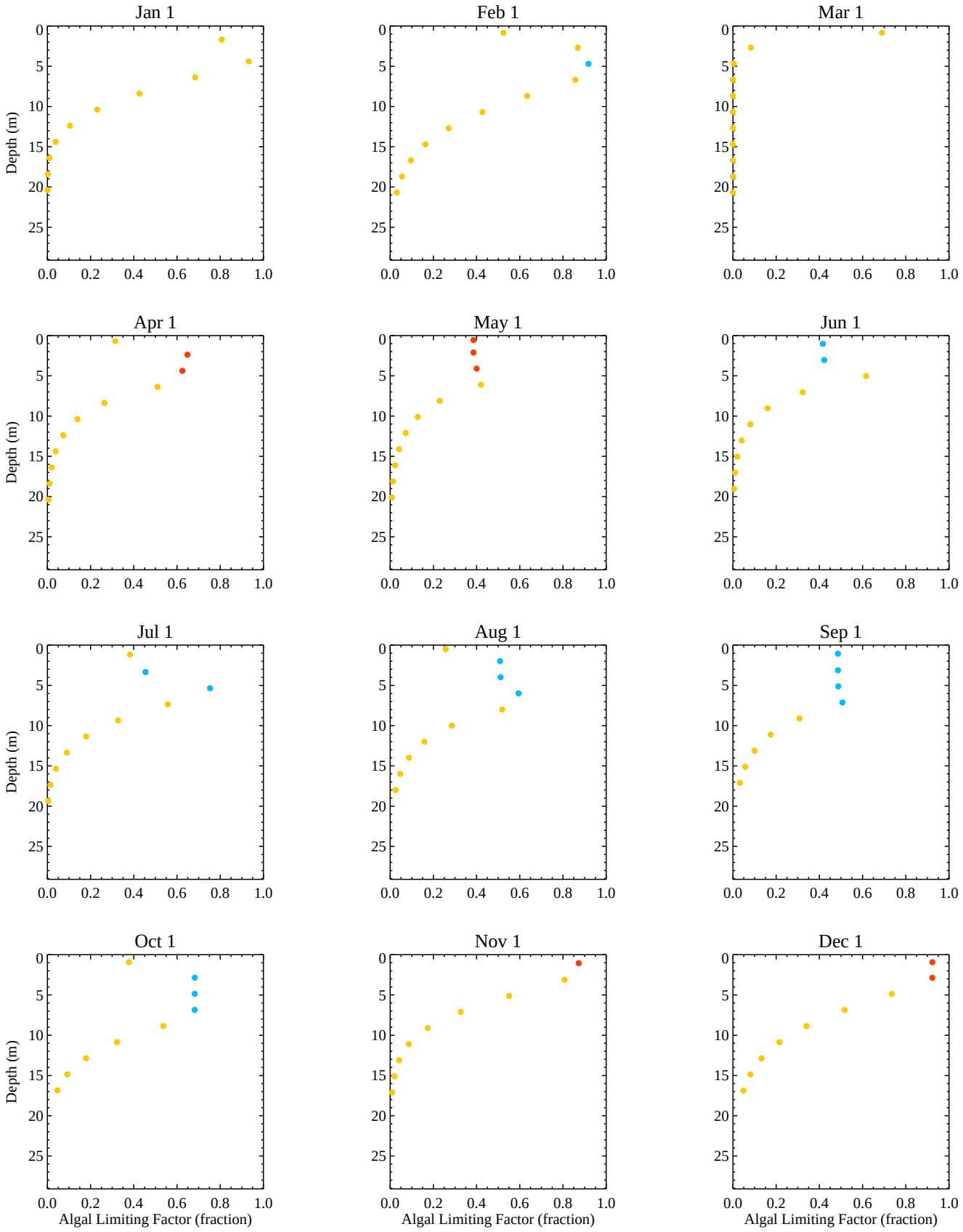

Figure J-24. Vertical profiles of algal limiting factor at Turkey Bend (Segment 28) during 2003.

Profiles shown for first day of month.

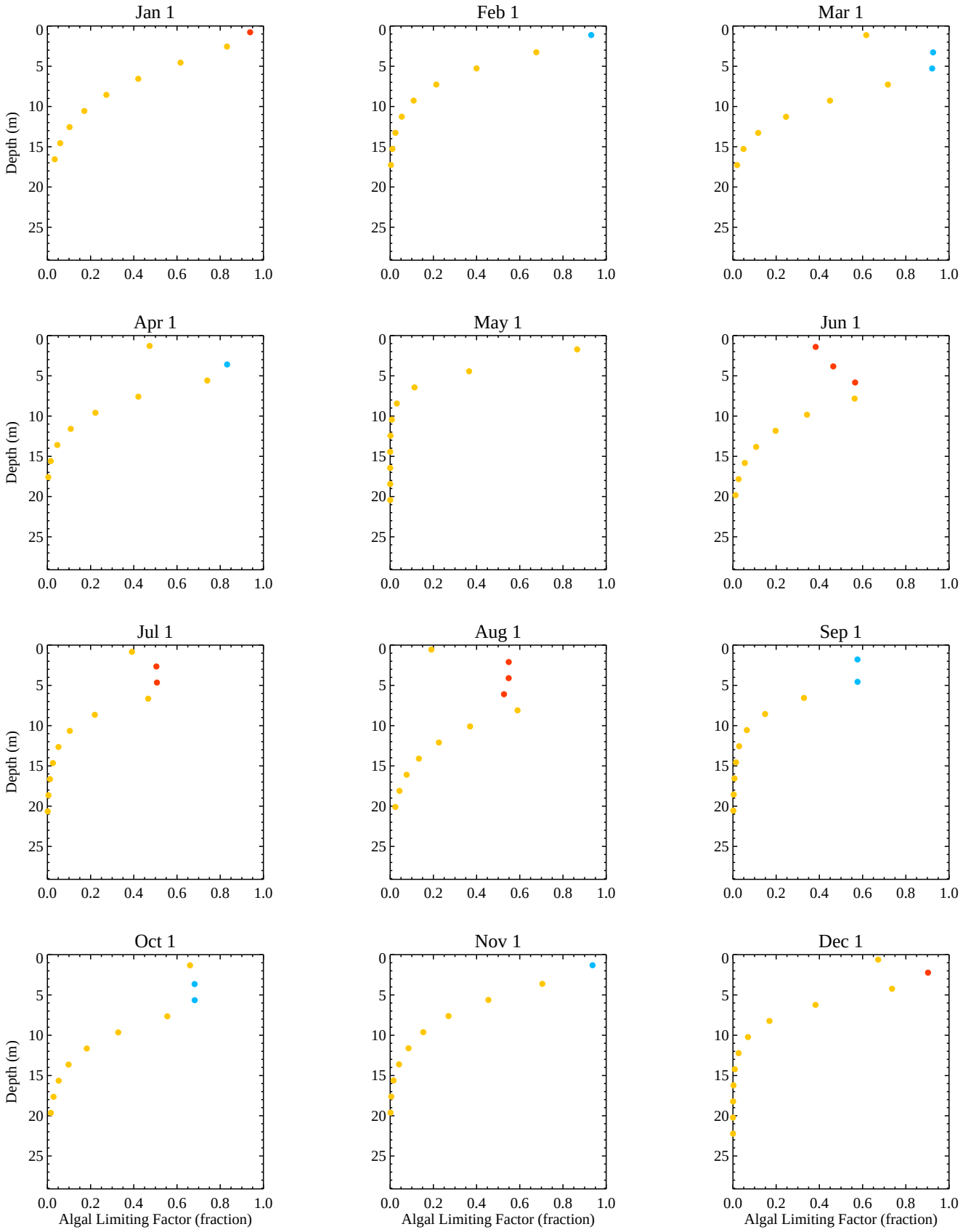

Figure J-24. Vertical profiles of algal limiting factor at Turkey Bend (Segment 28) during 2004.

Profiles shown for first day of month.

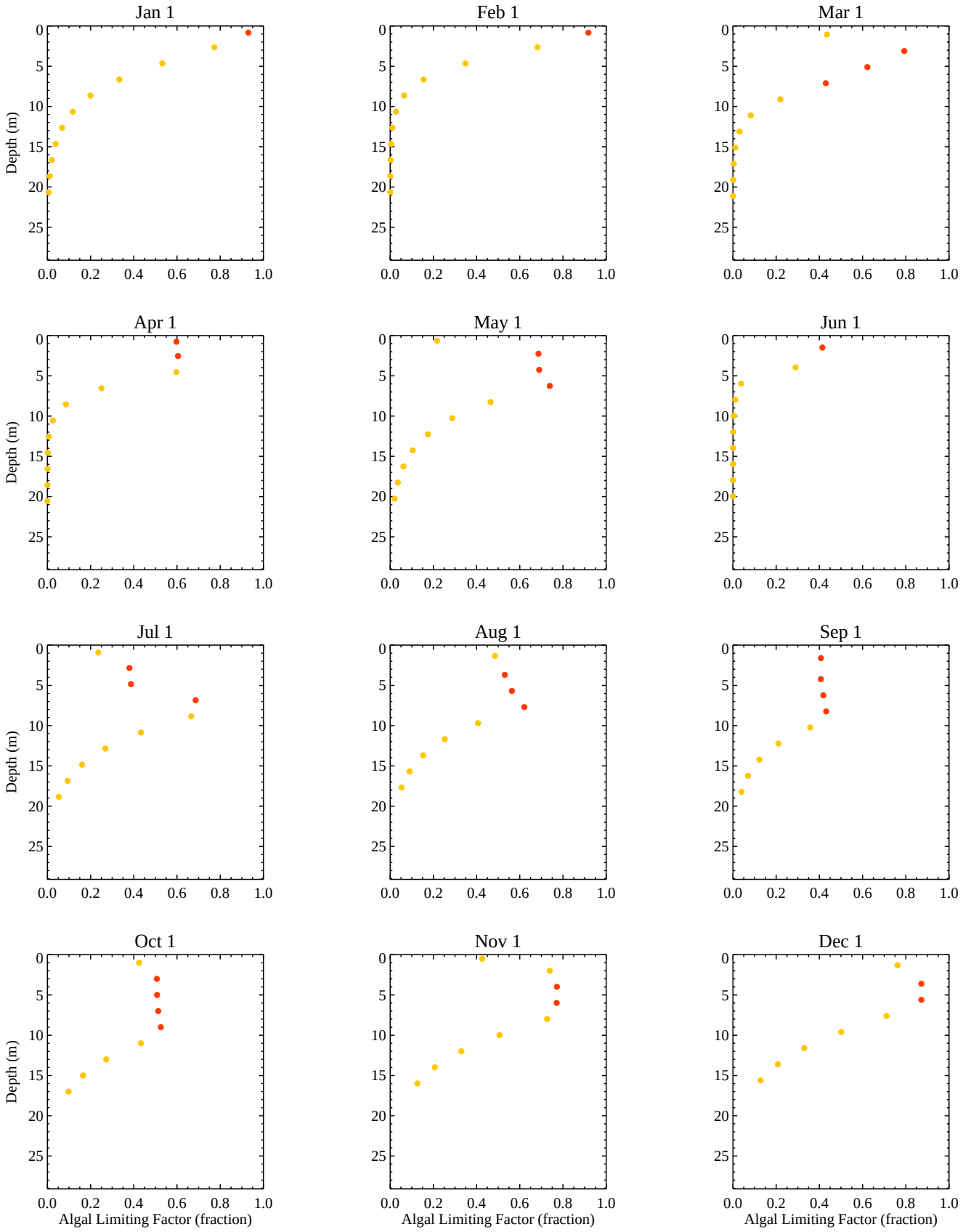

Figure J-24. Vertical profiles of algal limiting factor at Turkey Bend (Segment 28) during 2005.

Profiles shown for first day of month.

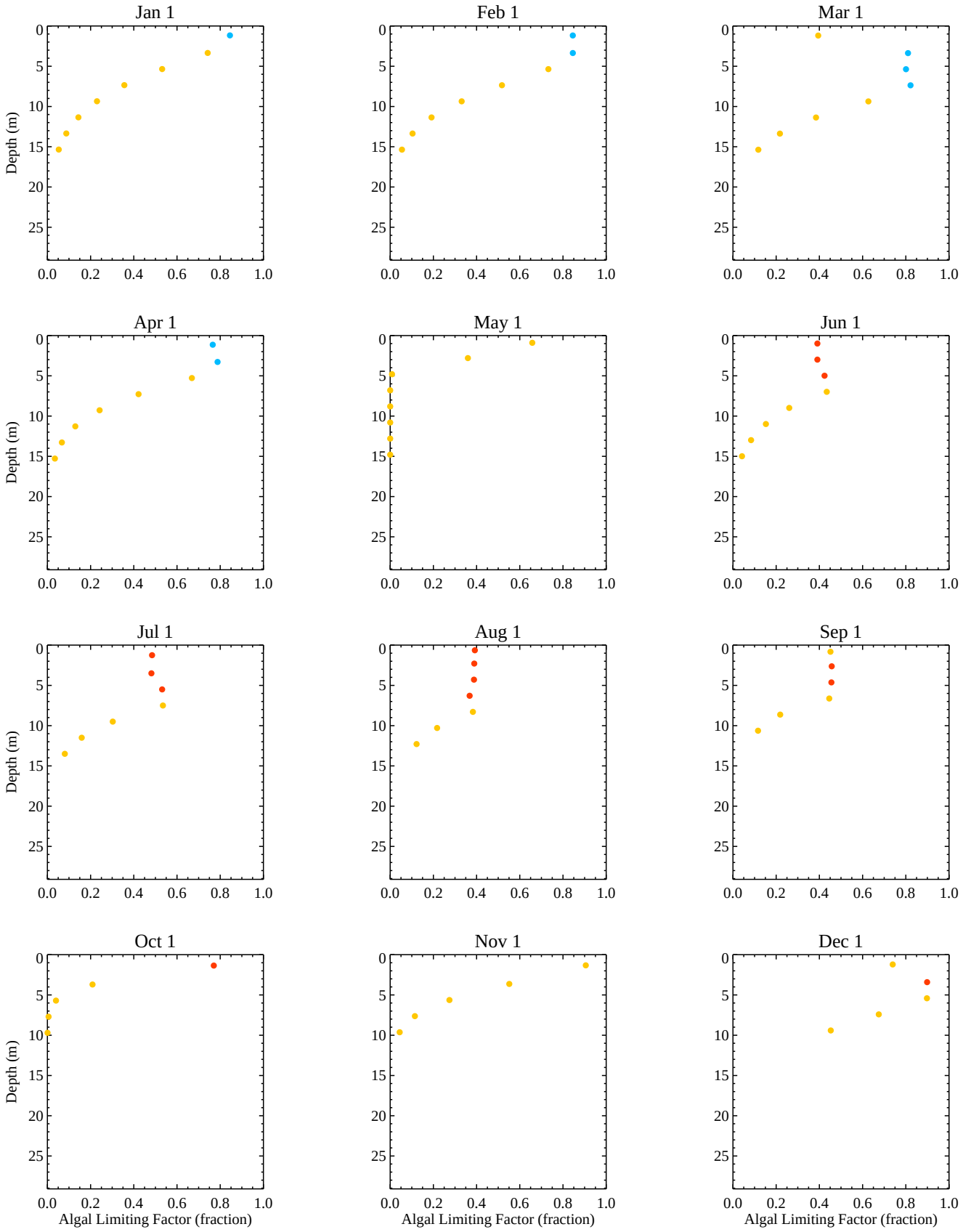

Figure J-24. Vertical profiles of algal limiting factor at Turkey Bend (Segment 28) during 2006.

Profiles shown for first day of month.

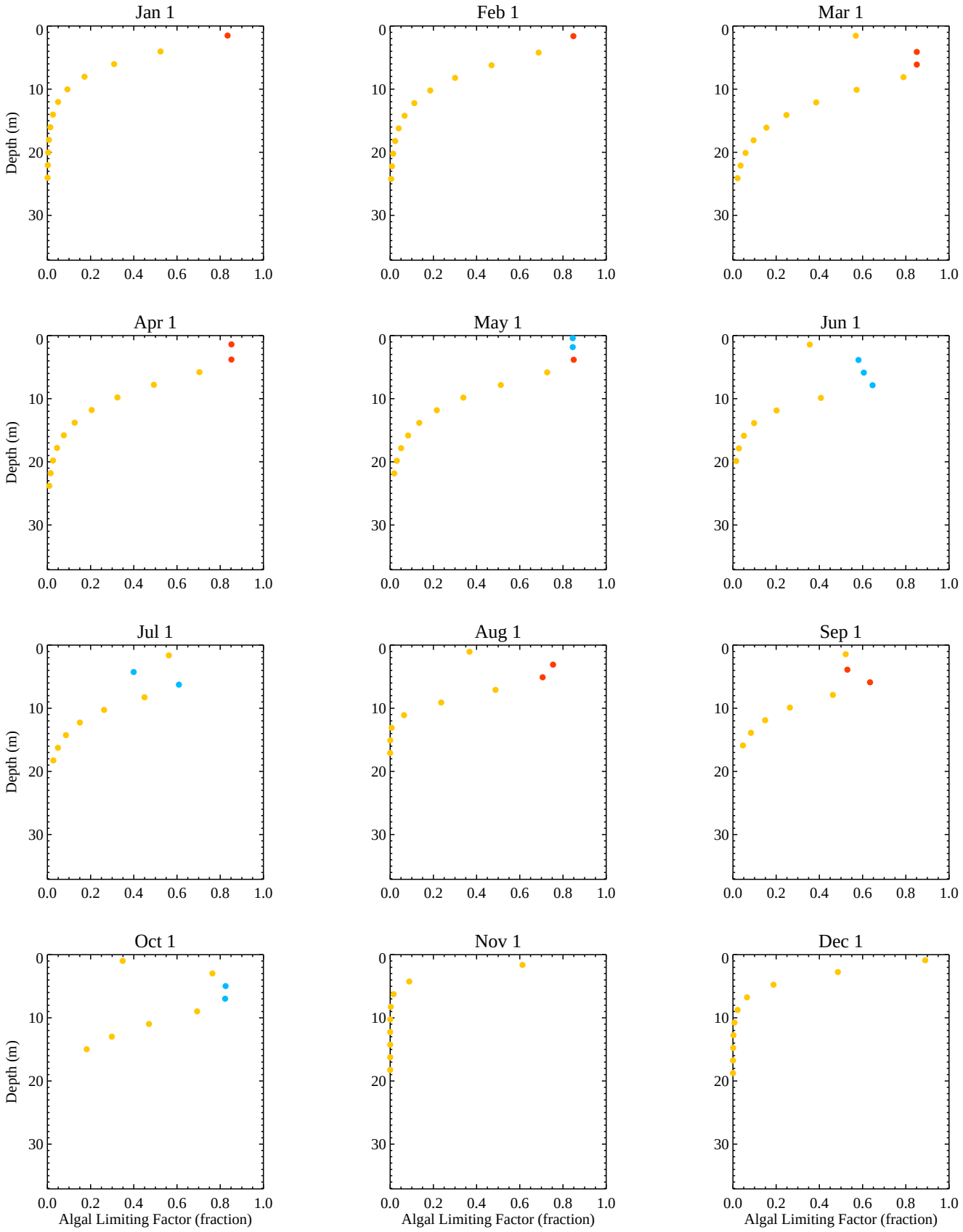

Figure J-25. Vertical profiles of algal limiting factor at Sandy Creek (Segment 161) during 1984.

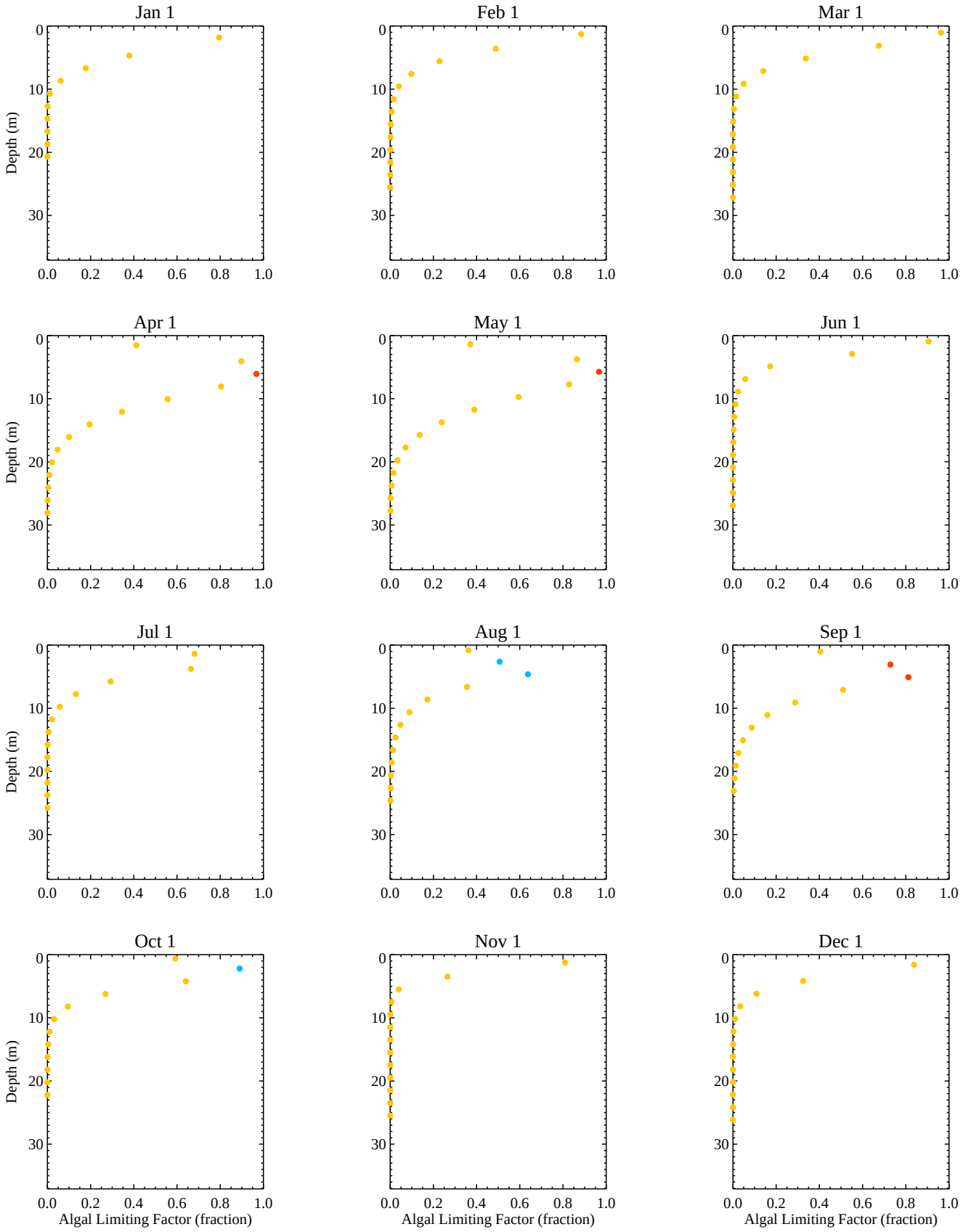

Figure J-25. Vertical profiles of algal limiting factor at Sandy Creek (Segment 161) during 1985.

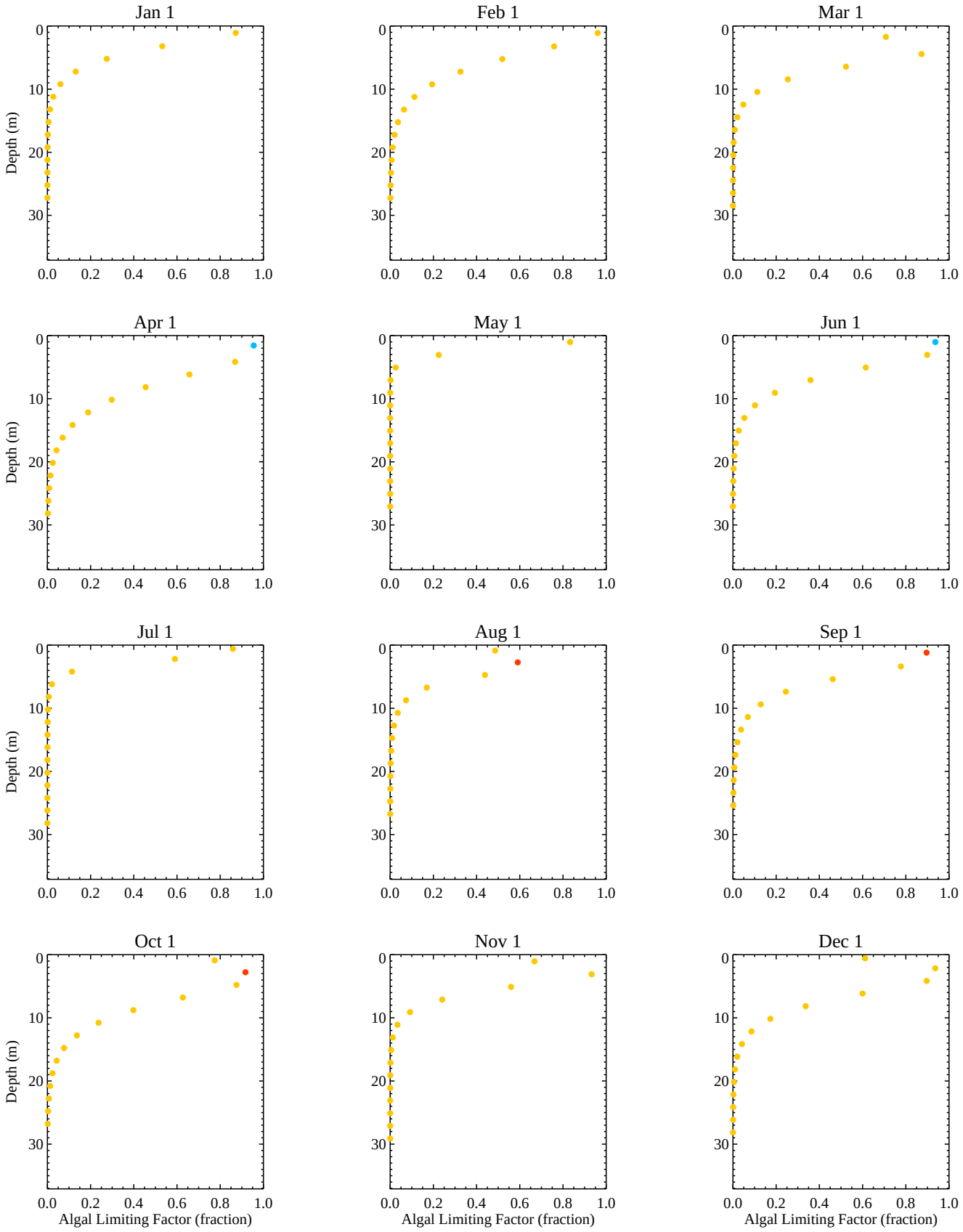

Figure J-25. Vertical profiles of algal limiting factor at Sandy Creek (Segment 161) during 1986.

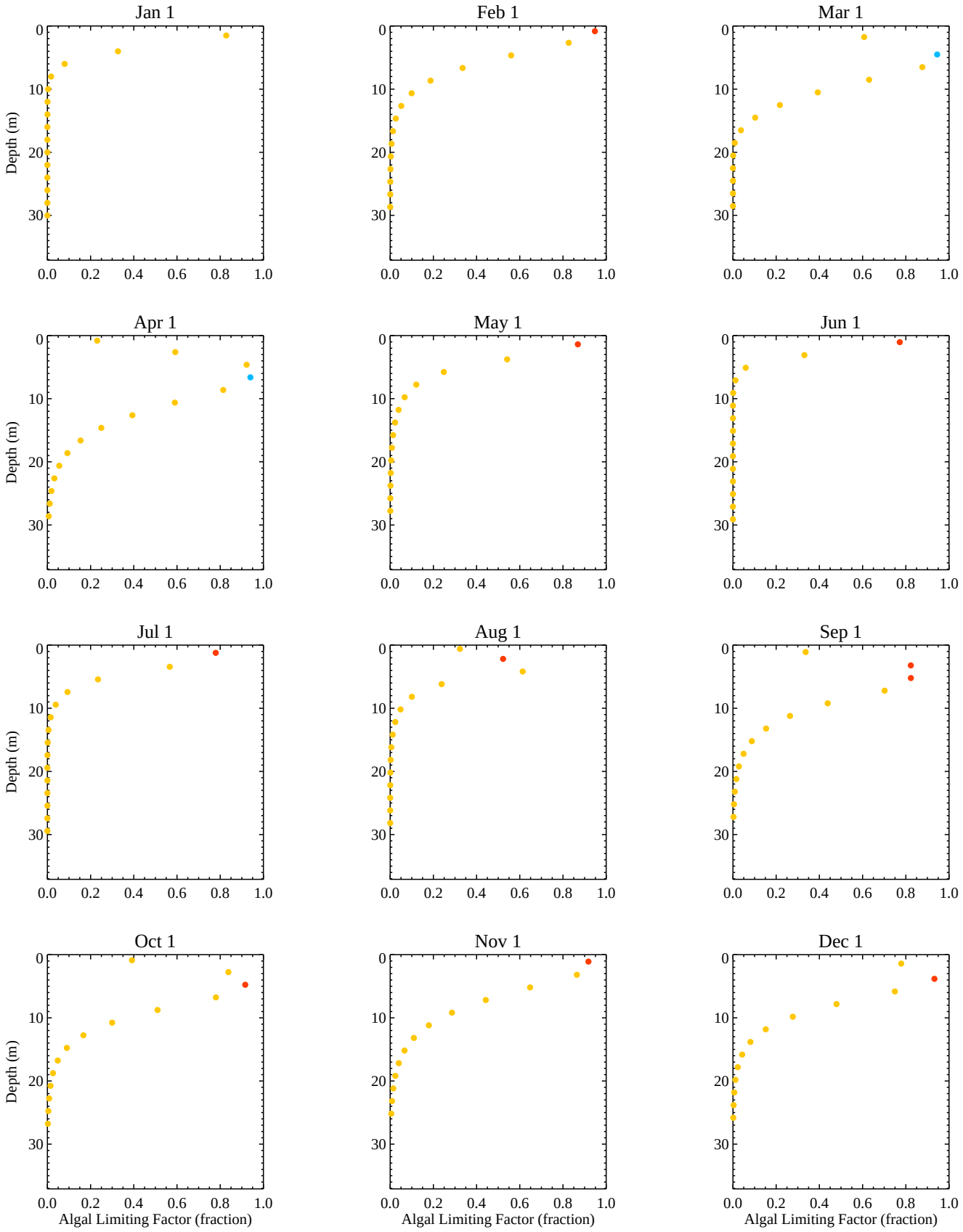

Figure J-25. Vertical profiles of algal limiting factor at Sandy Creek (Segment 161) during 1987.

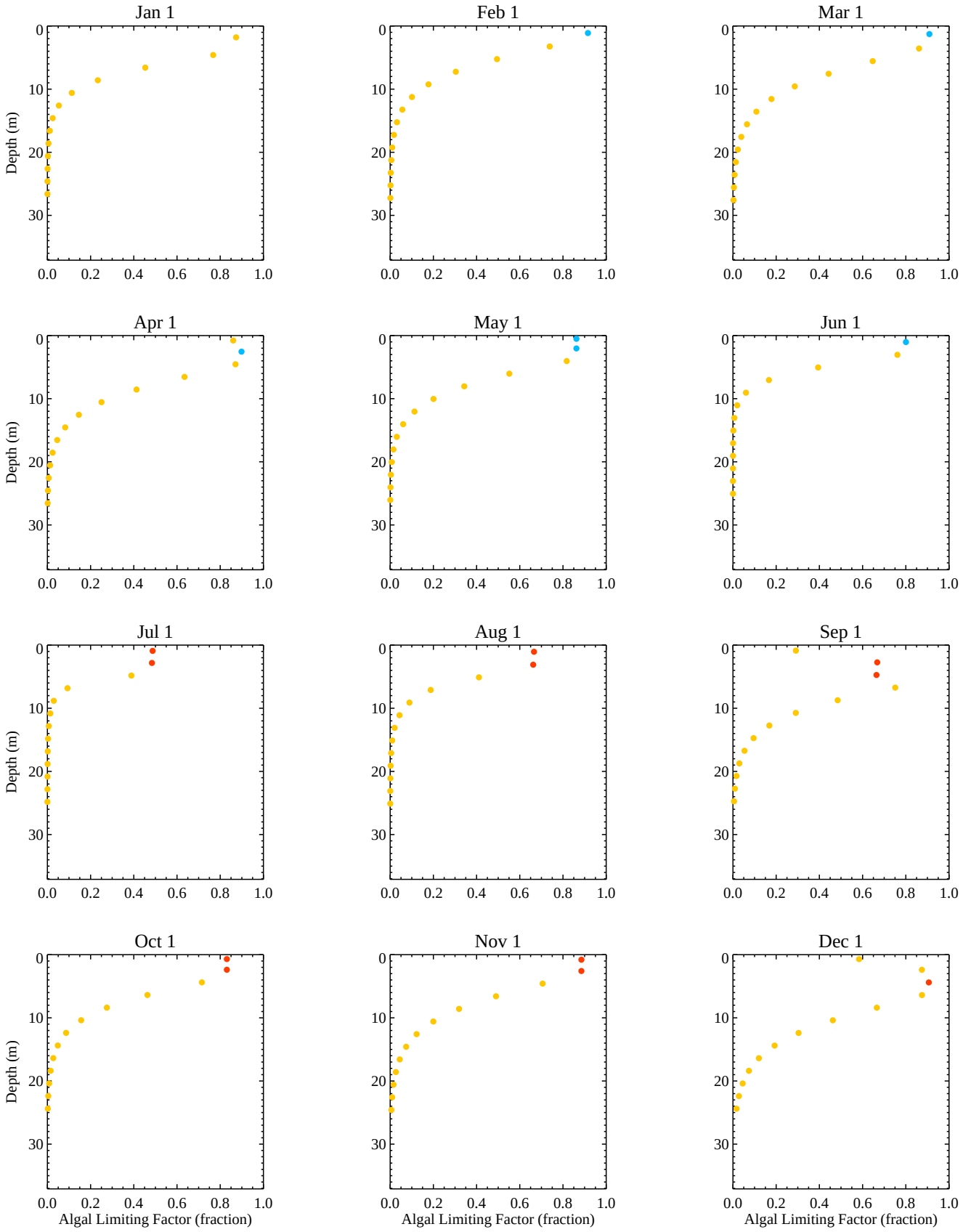

Figure J-25. Vertical profiles of algal limiting factor at Sandy Creek (Segment 161) during 1988.

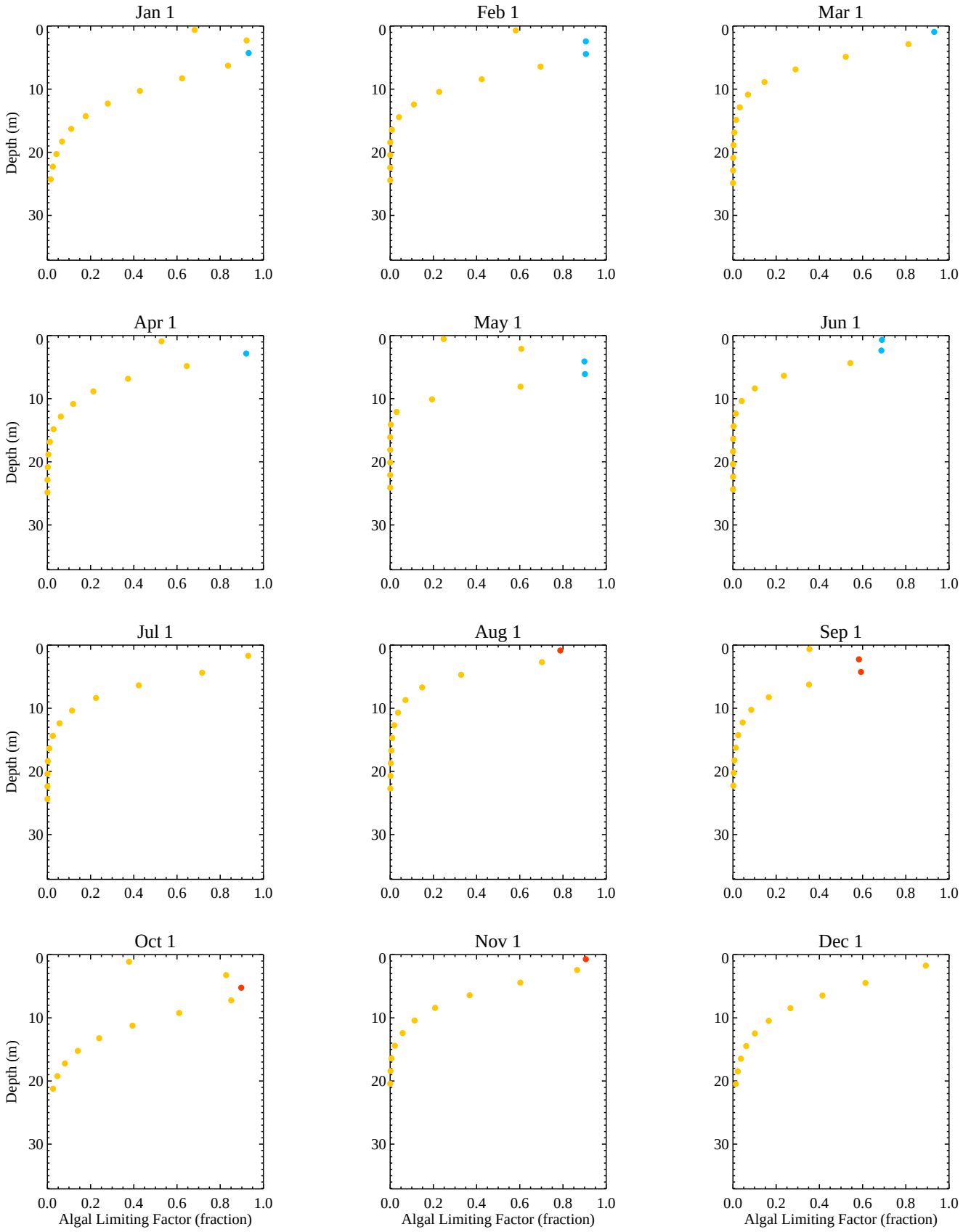

Figure J-25. Vertical profiles of algal limiting factor at Sandy Creek (Segment 161) during 1989.

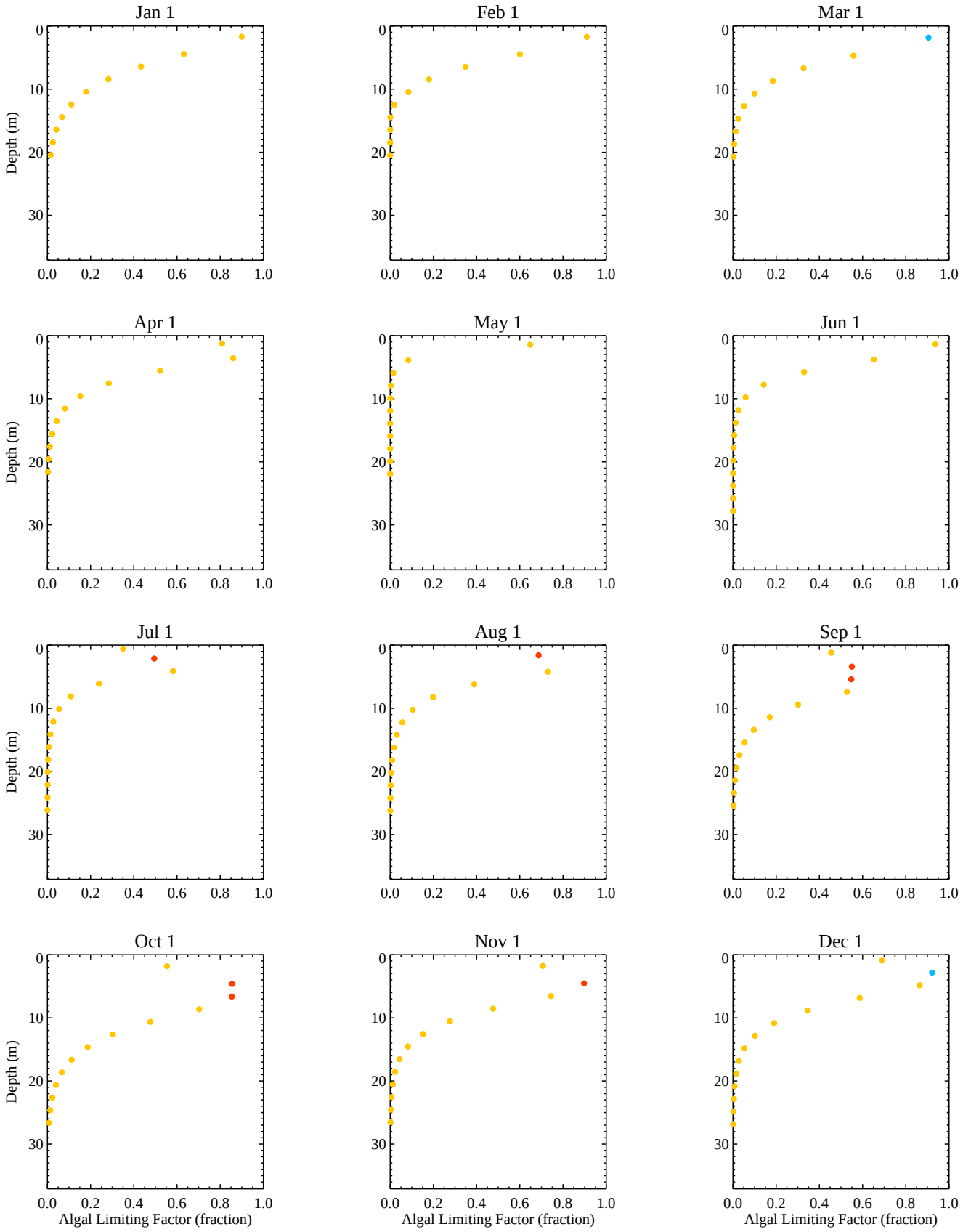

Figure J-25. Vertical profiles of algal limiting factor at Sandy Creek (Segment 161) during 1990.

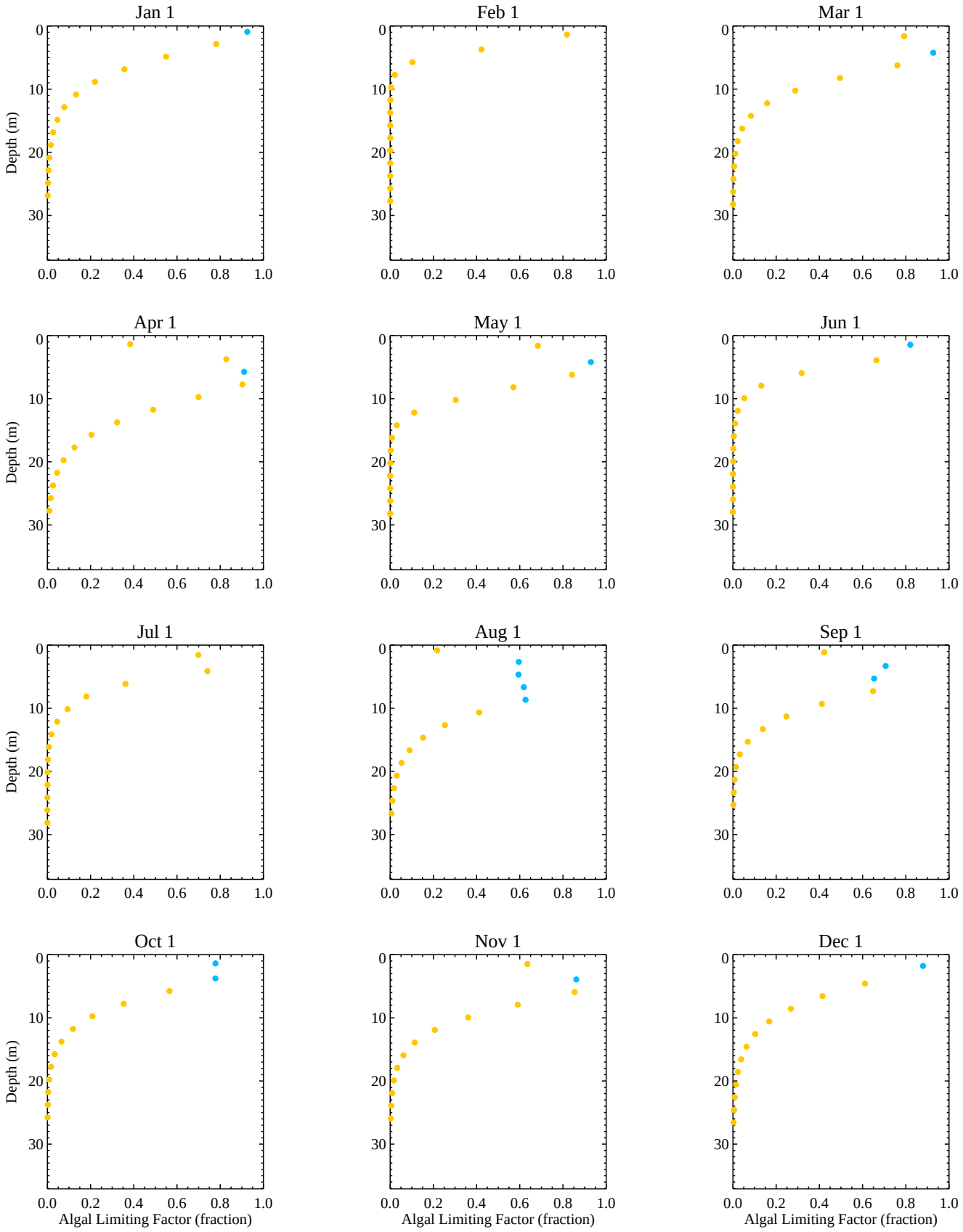

Figure J-25. Vertical profiles of algal limiting factor at Sandy Creek (Segment 161) during 1991.

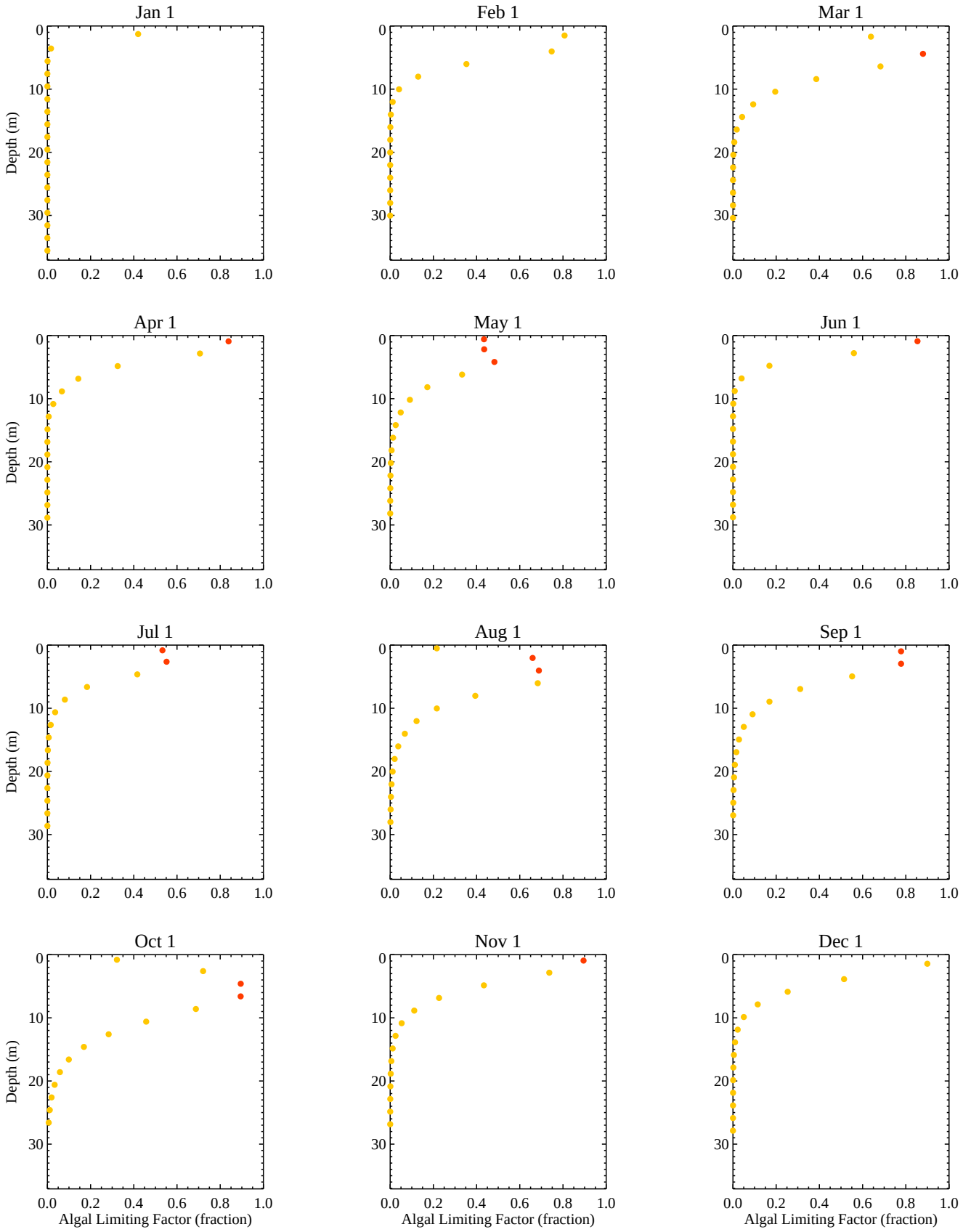

Figure J-25. Vertical profiles of algal limiting factor at Sandy Creek (Segment 161) during 1992.

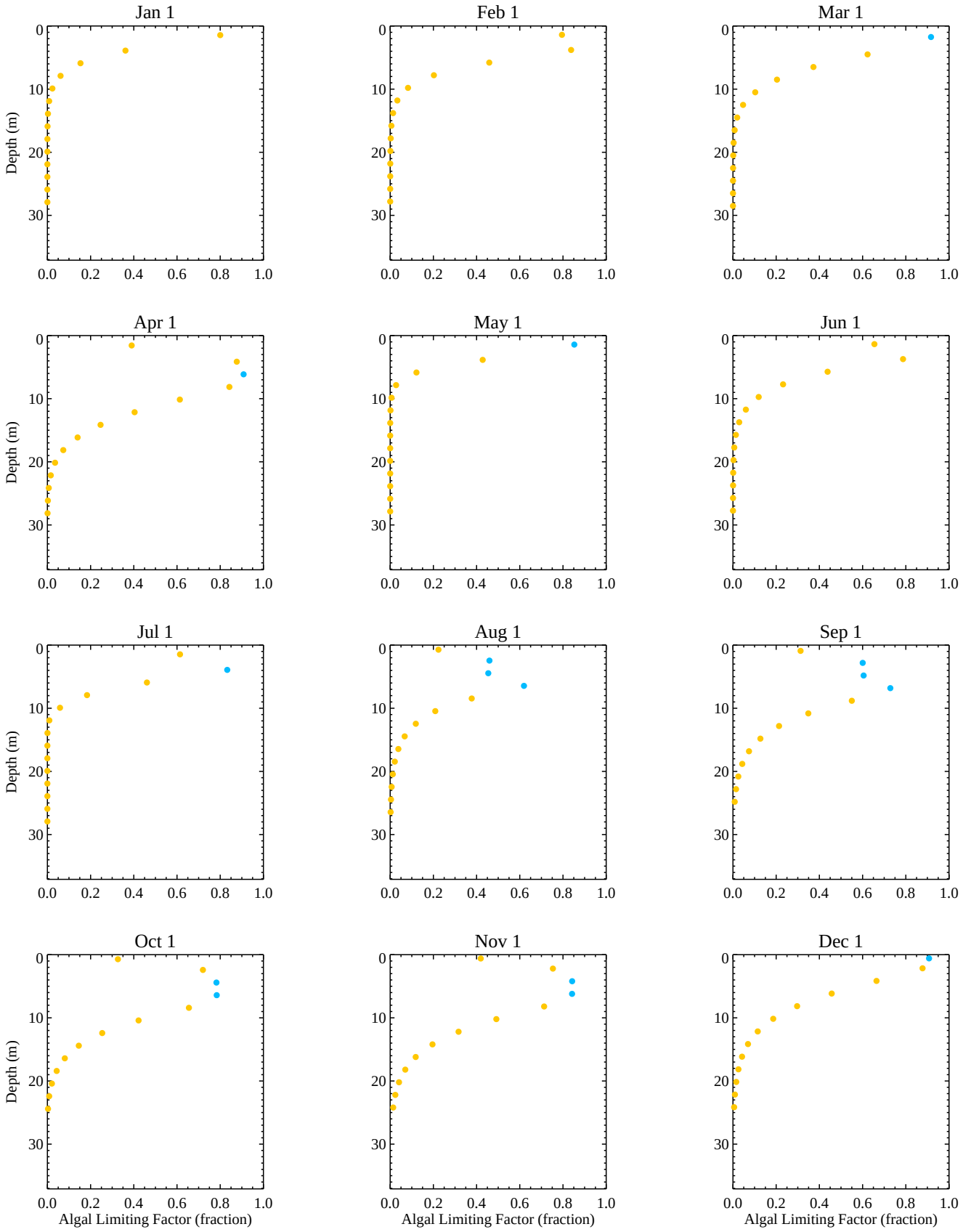

Figure J-25. Vertical profiles of algal limiting factor at Sandy Creek (Segment 161) during 1993.

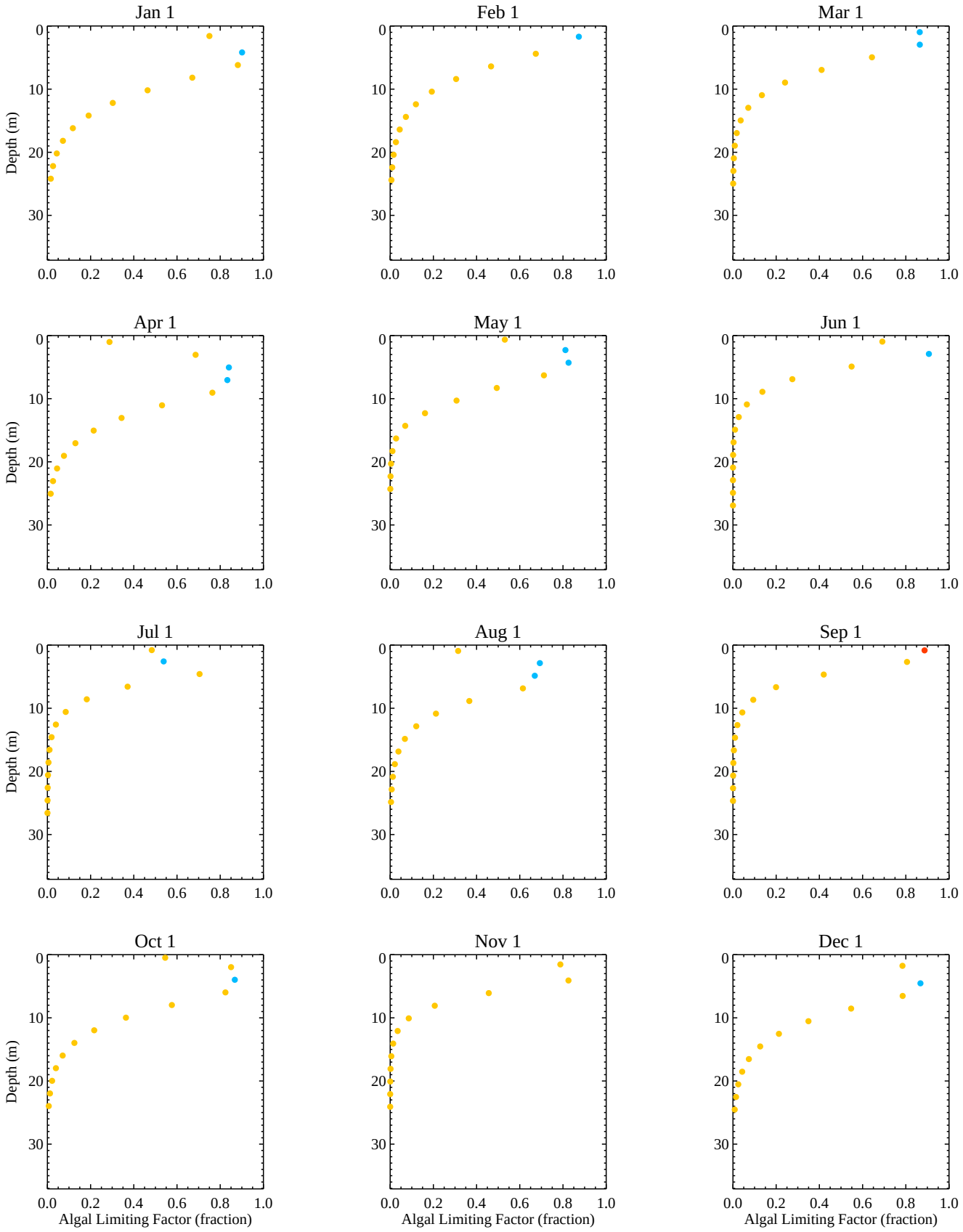

Figure J-25. Vertical profiles of algal limiting factor at Sandy Creek (Segment 161) during 1994.

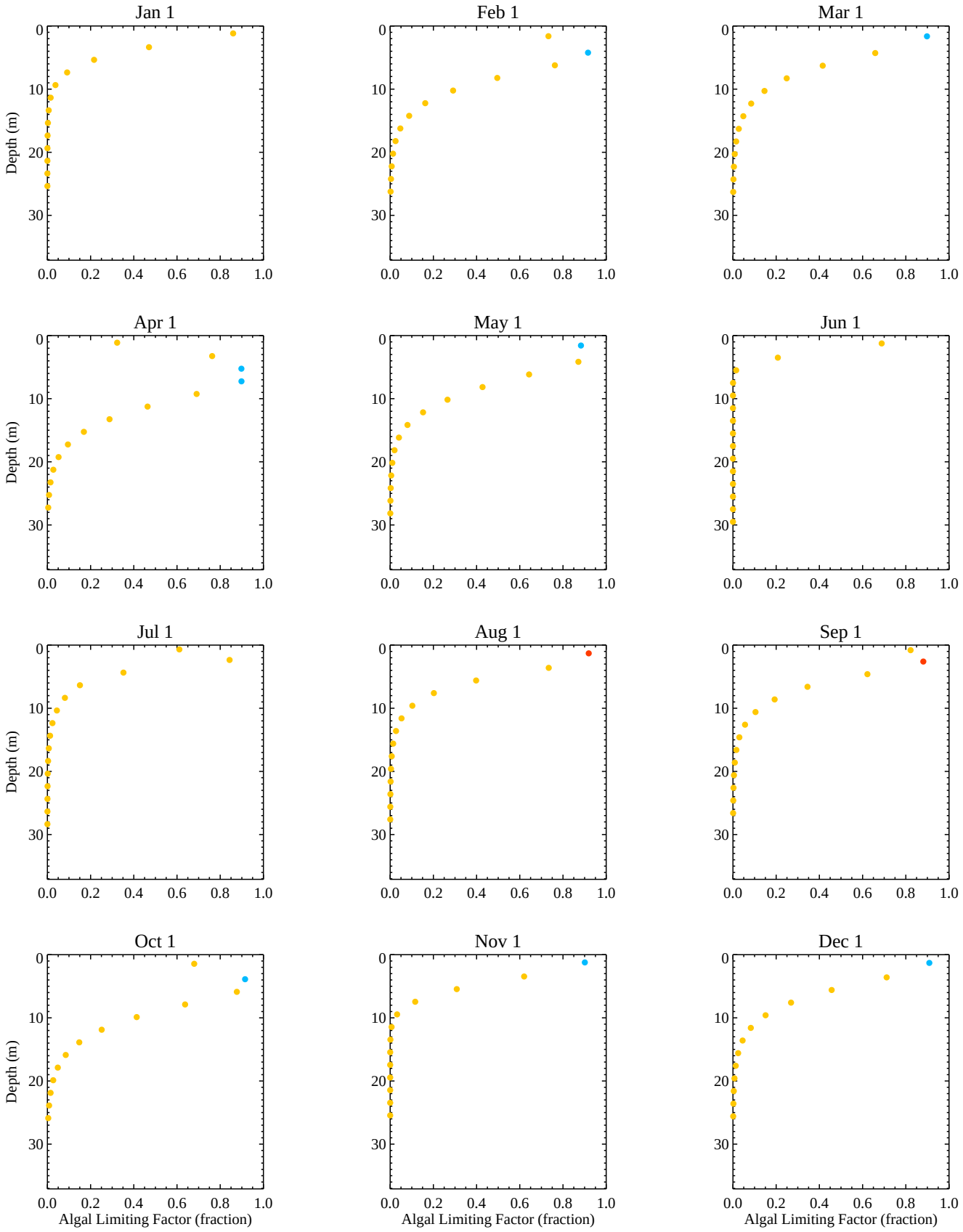

Figure J-25. Vertical profiles of algal limiting factor at Sandy Creek (Segment 161) during 1995.

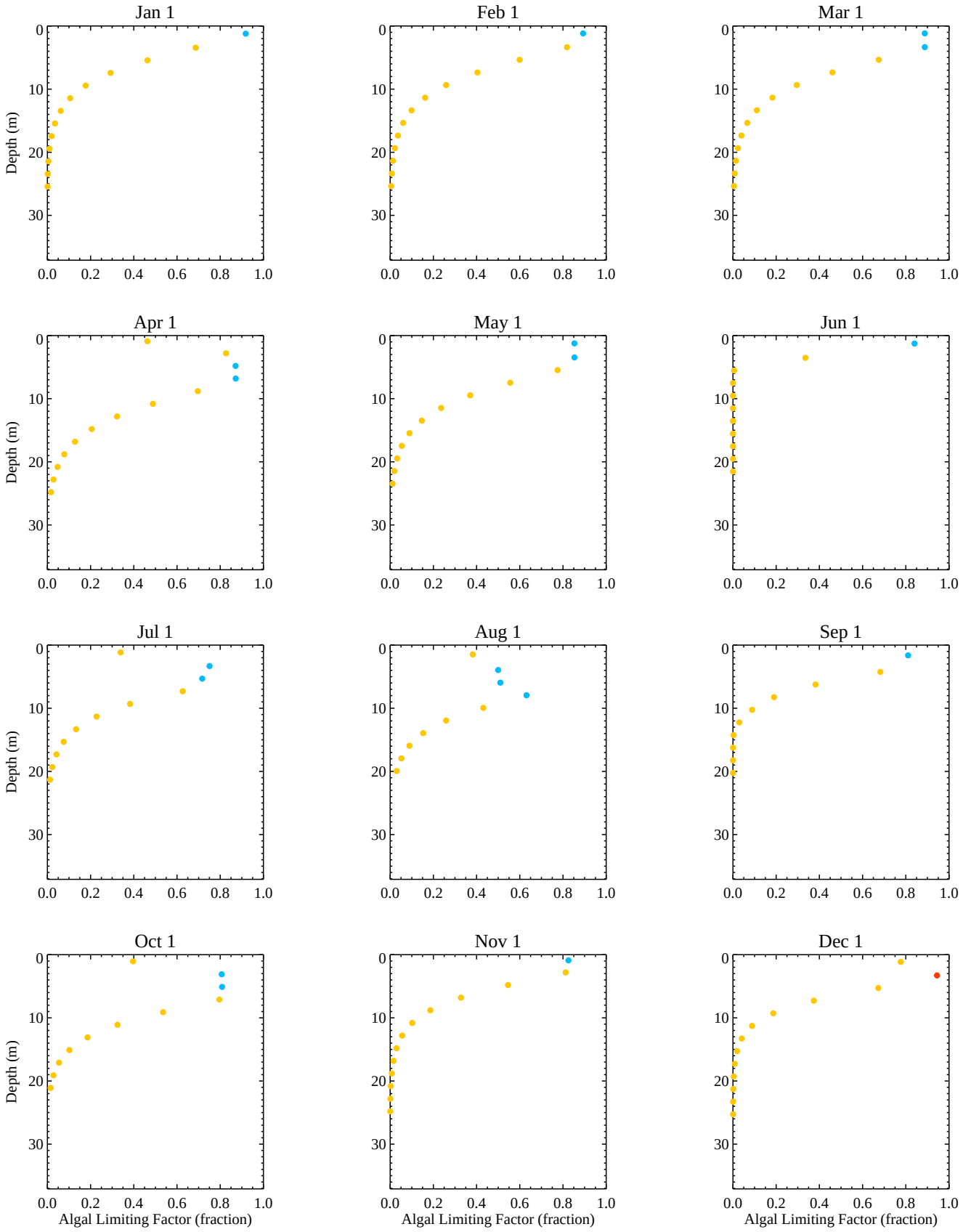

Figure J-25. Vertical profiles of algal limiting factor at Sandy Creek (Segment 161) during 1996.

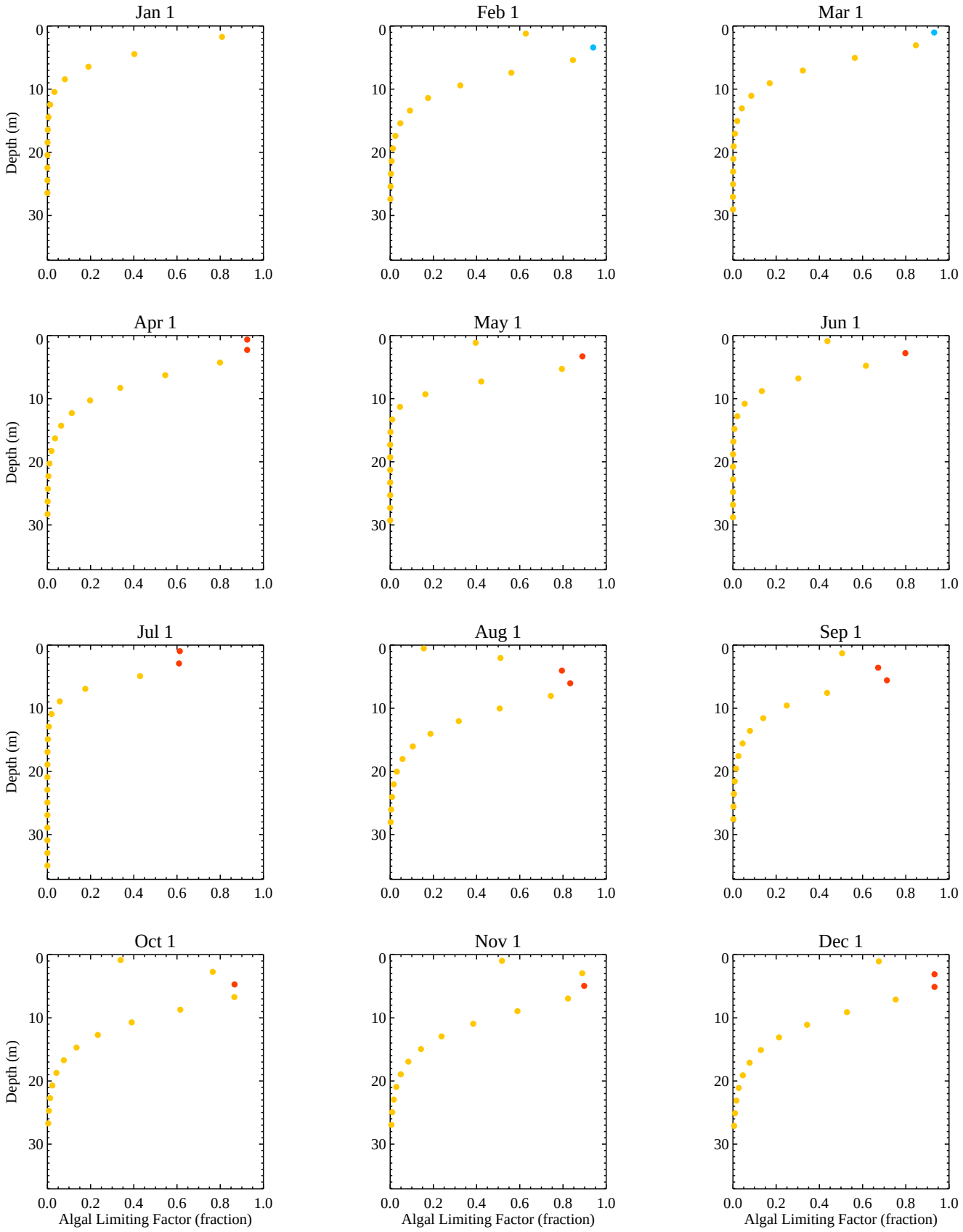

Figure J-25. Vertical profiles of algal limiting factor at Sandy Creek (Segment 161) during 1997.

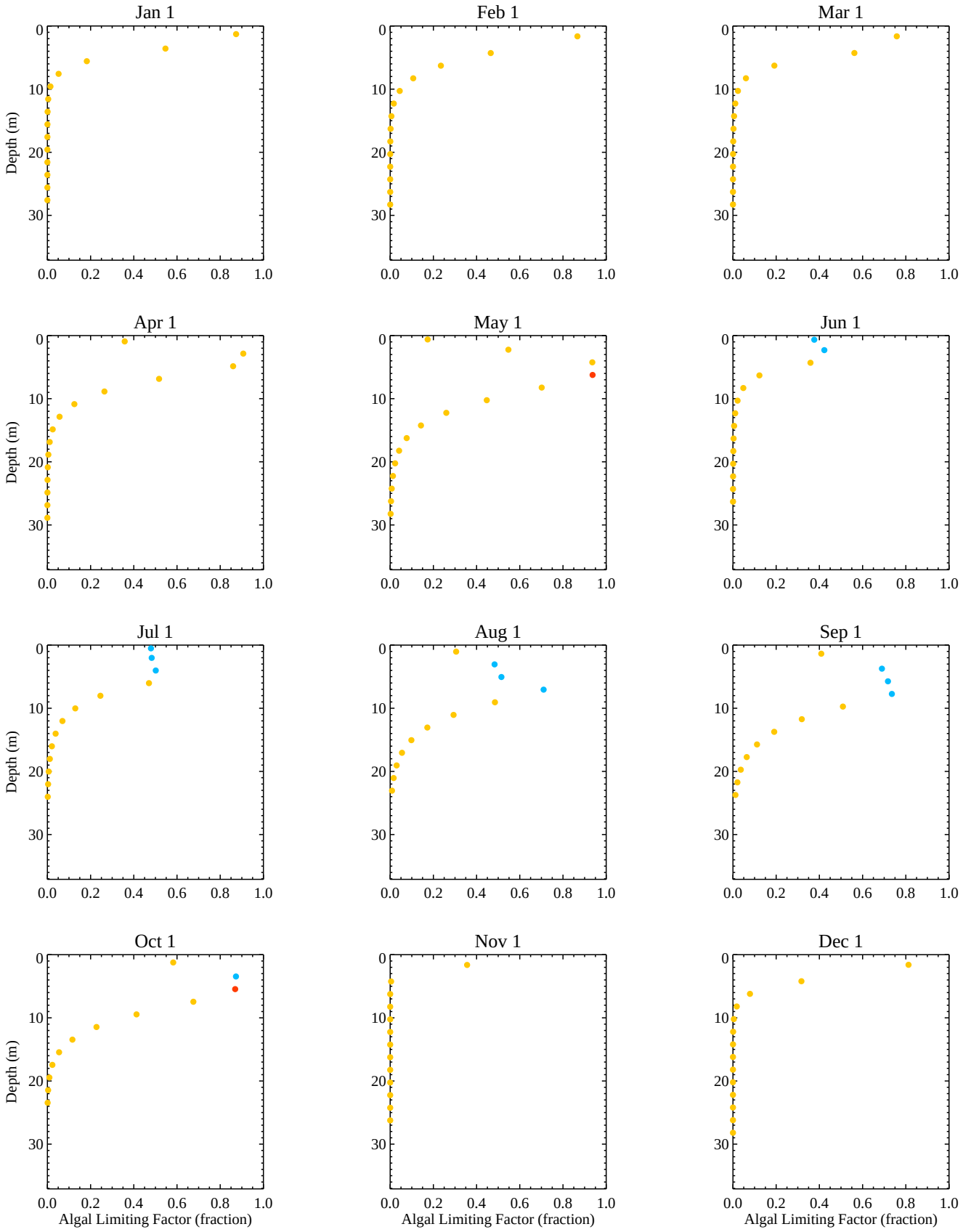

Figure J-25. Vertical profiles of algal limiting factor at Sandy Creek (Segment 161) during 1998.

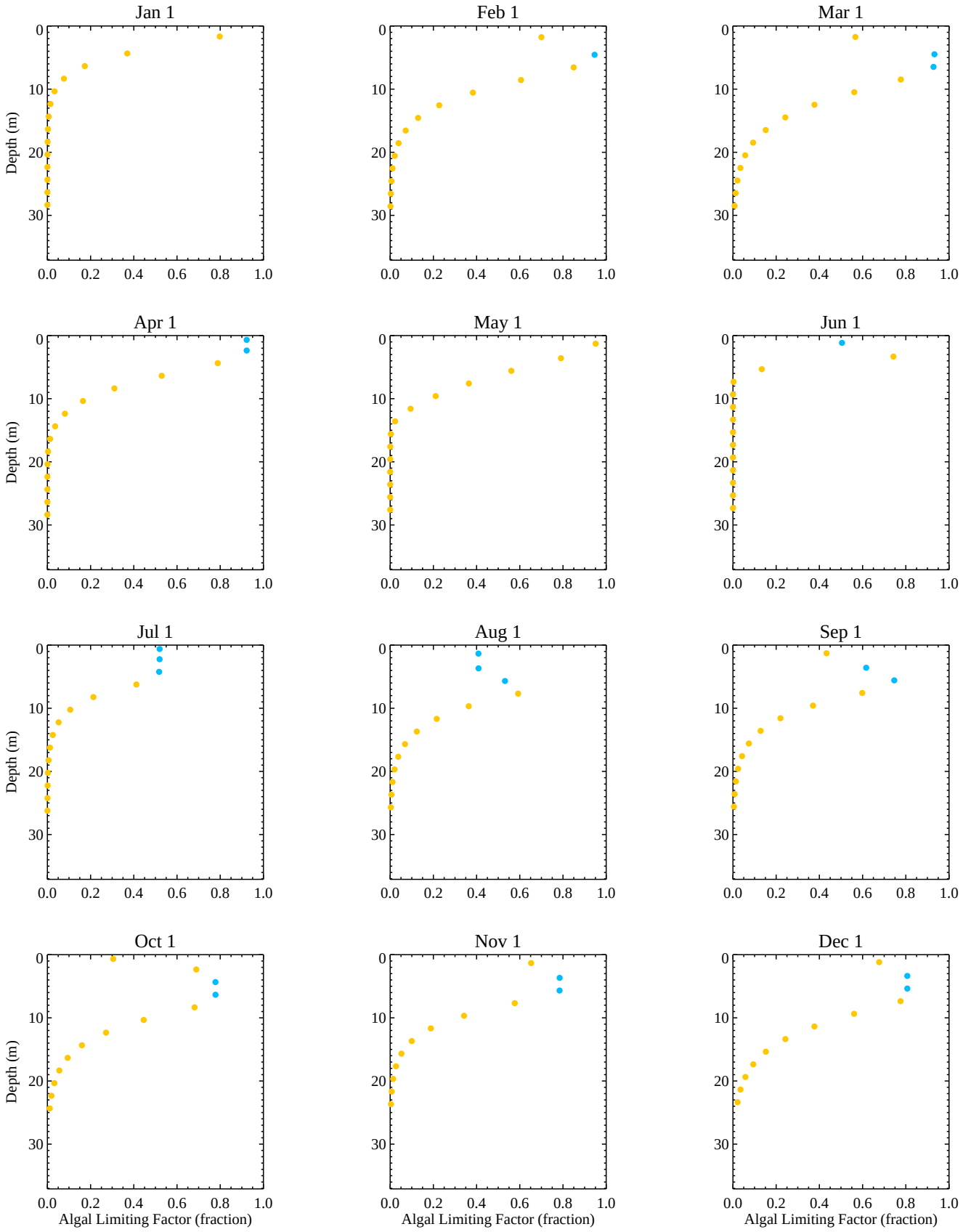

Figure J-25. Vertical profiles of algal limiting factor at Sandy Creek (Segment 161) during 1999.

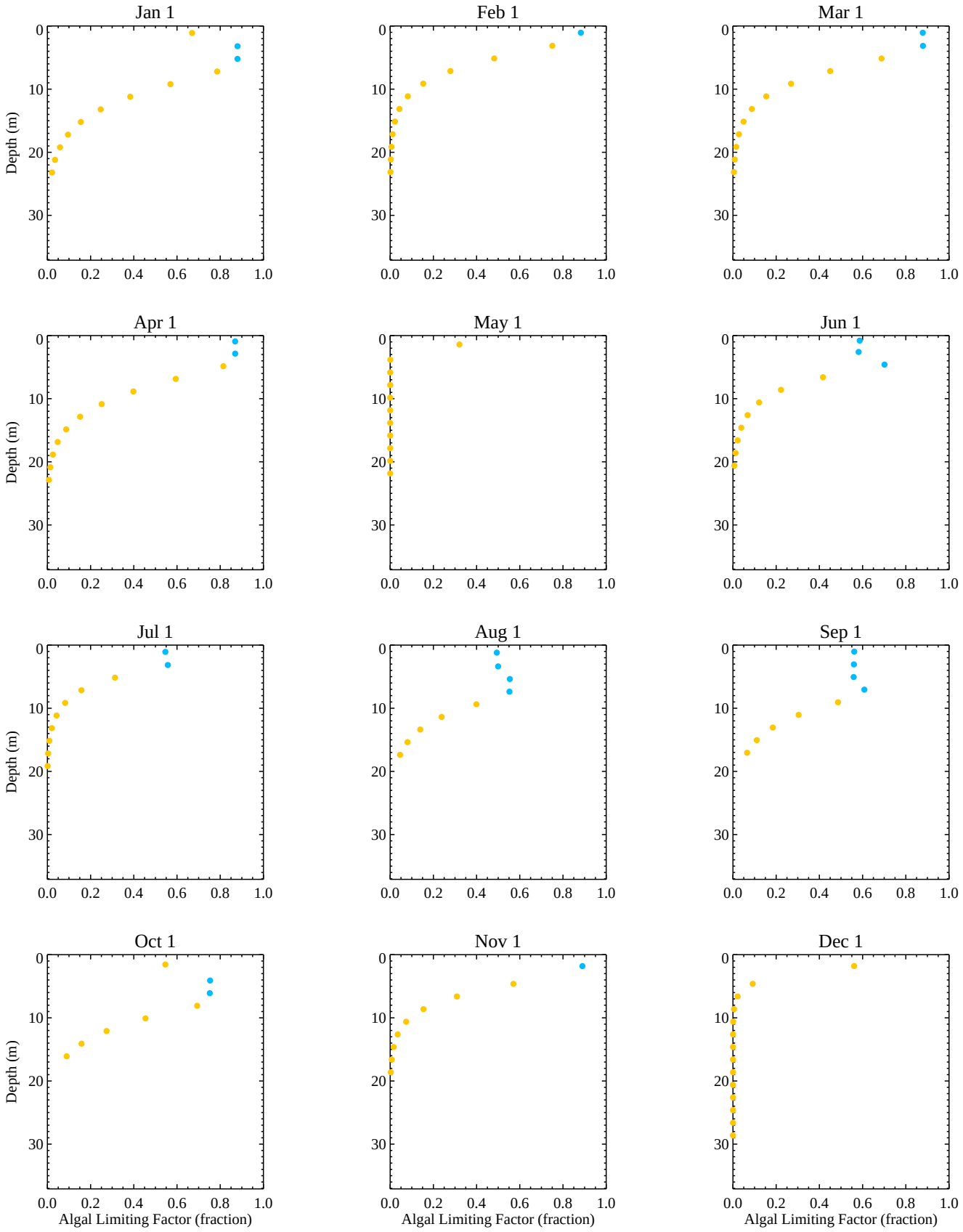

Figure J-25. Vertical profiles of algal limiting factor at Sandy Creek (Segment 161) during 2000.

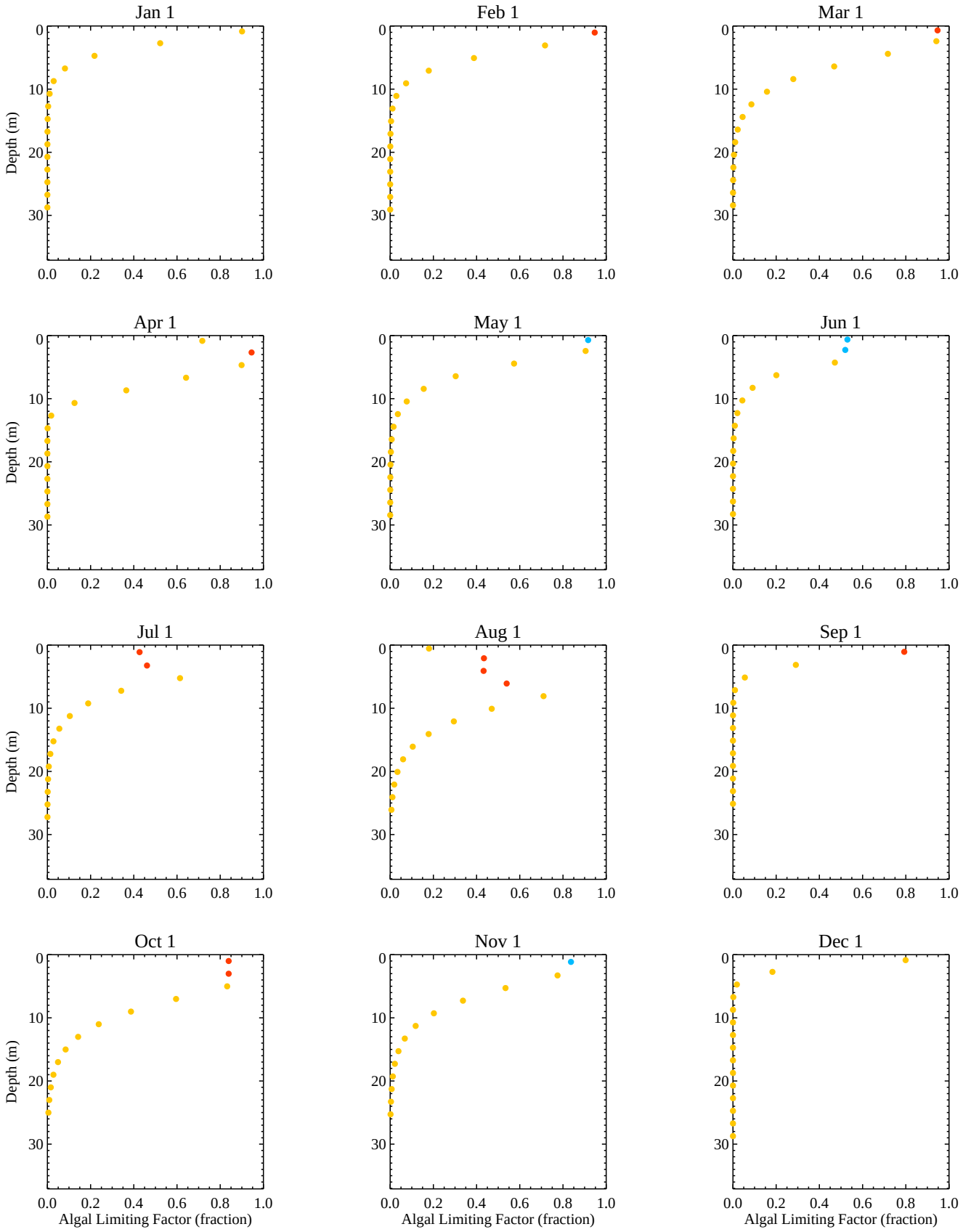

Figure J-25. Vertical profiles of algal limiting factor at Sandy Creek (Segment 161) during 2001.

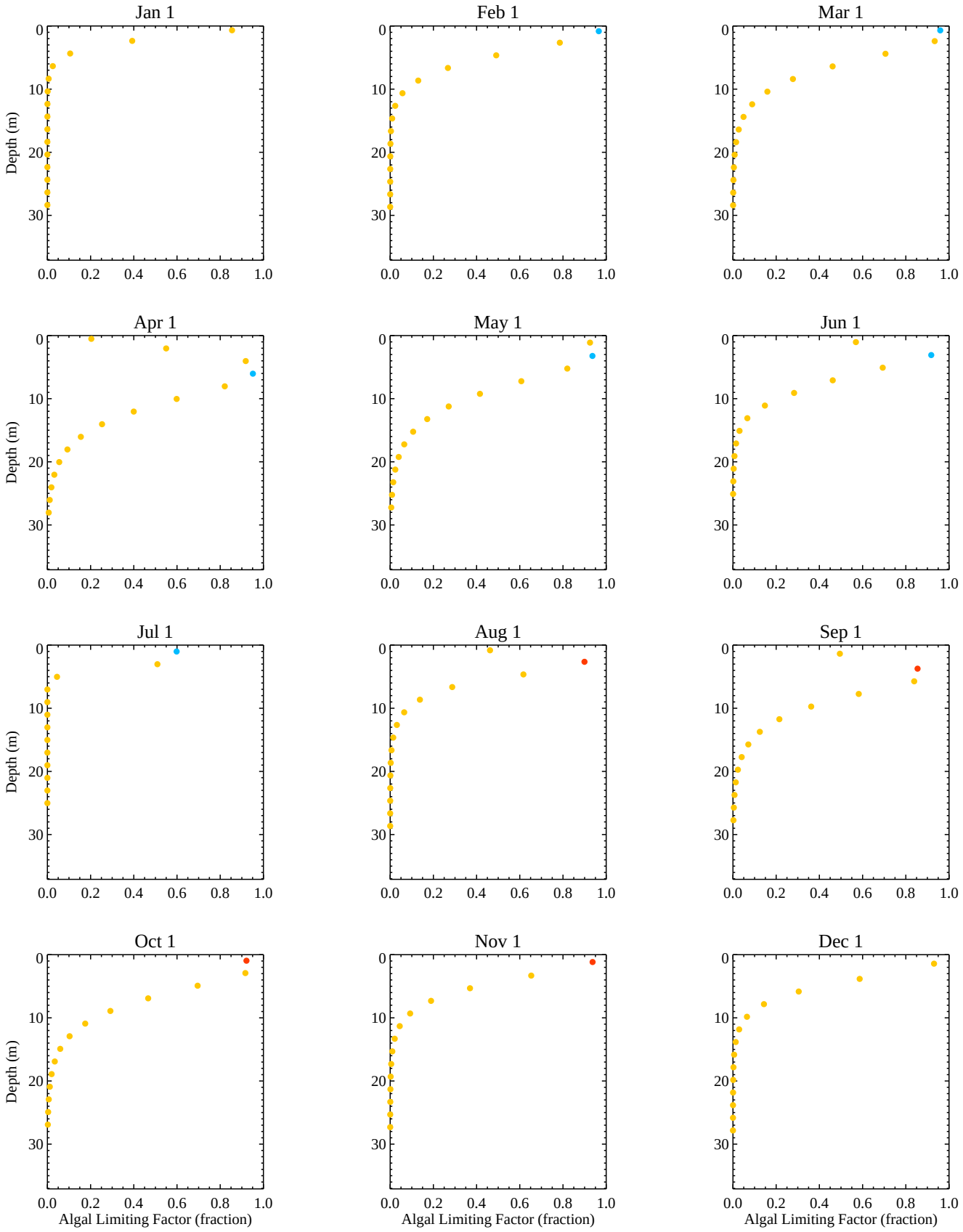

Figure J-25. Vertical profiles of algal limiting factor at Sandy Creek (Segment 161) during 2002.

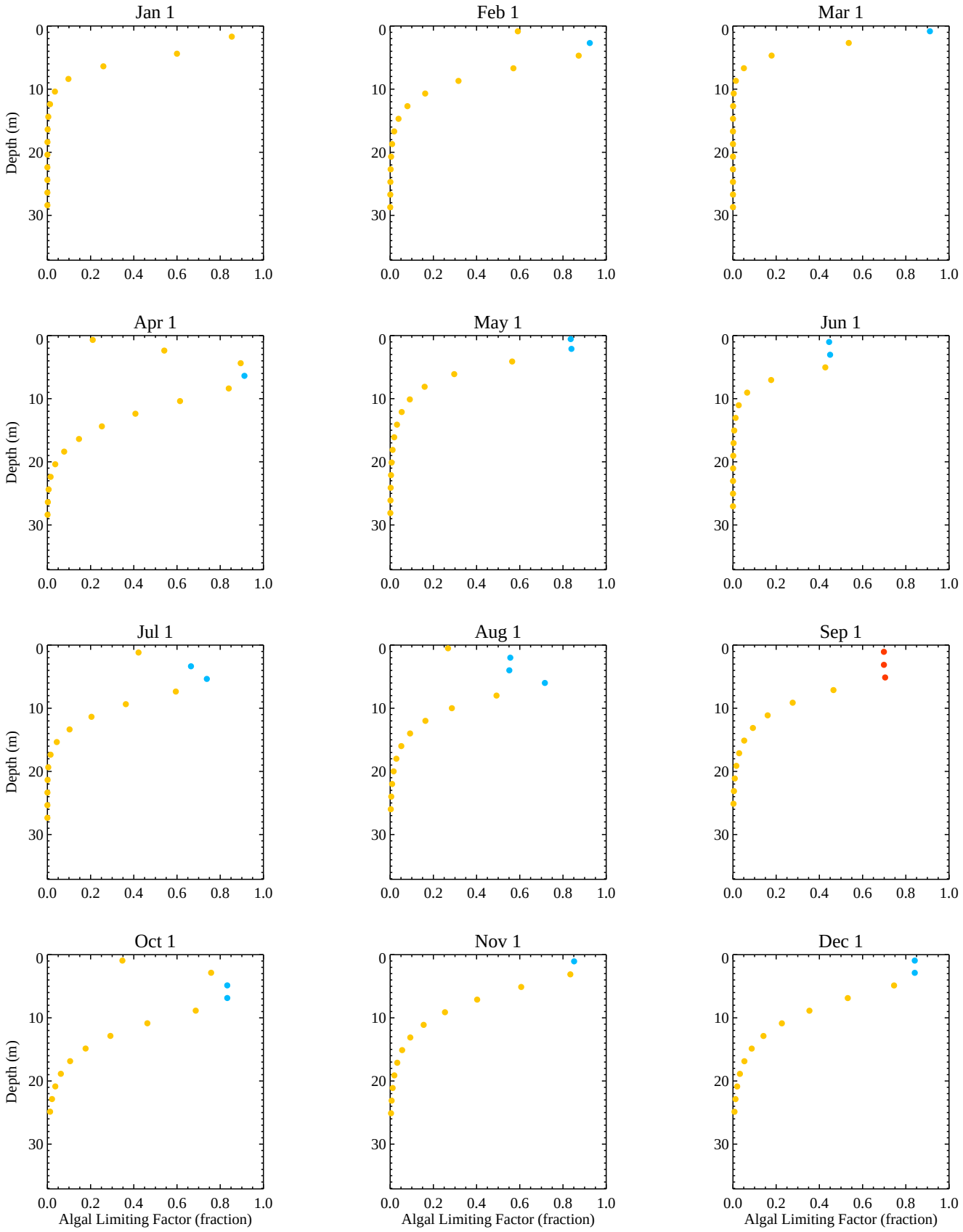

Figure J-25. Vertical profiles of algal limiting factor at Sandy Creek (Segment 161) during 2003.

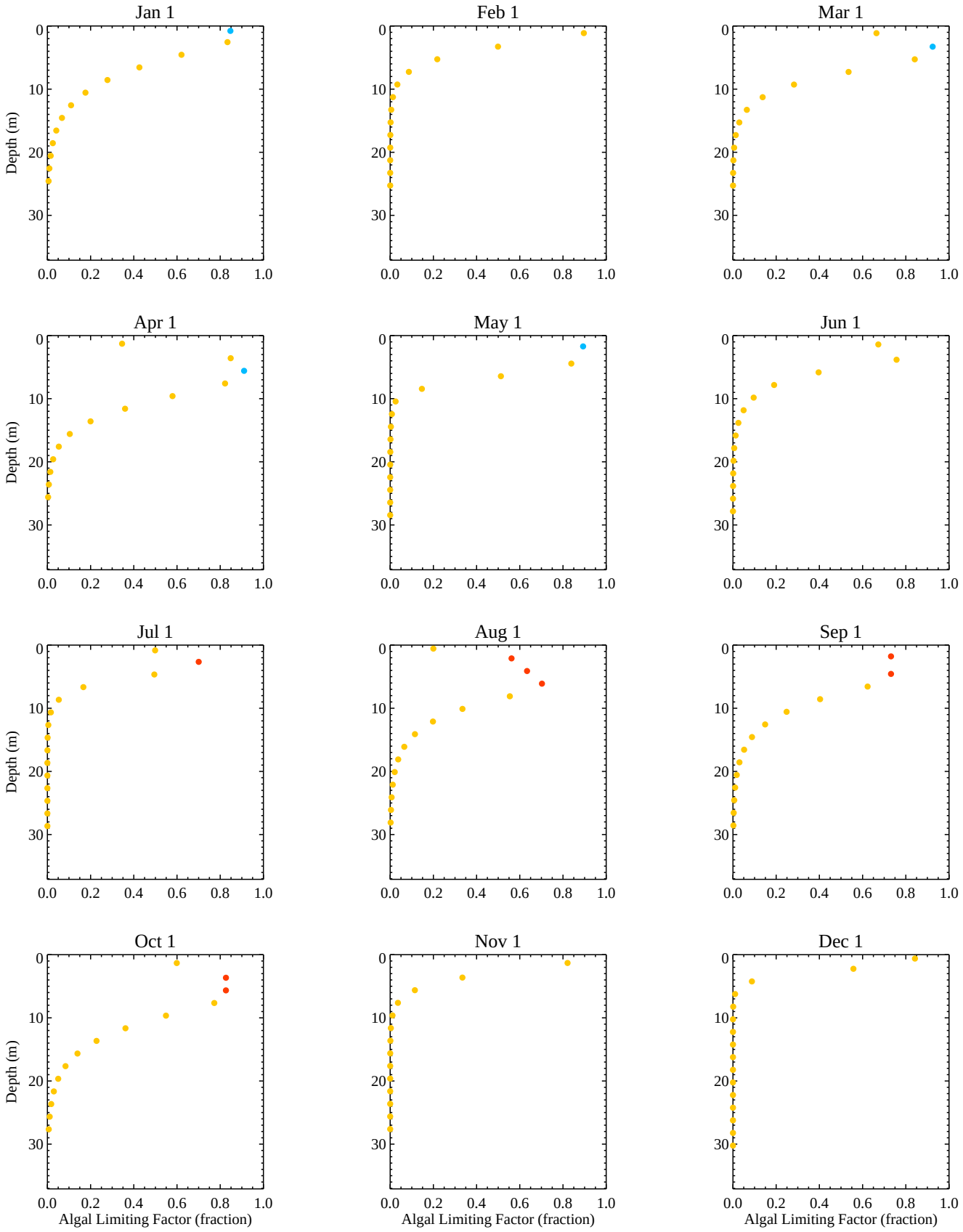

Figure J-25. Vertical profiles of algal limiting factor at Sandy Creek (Segment 161) during 2004.

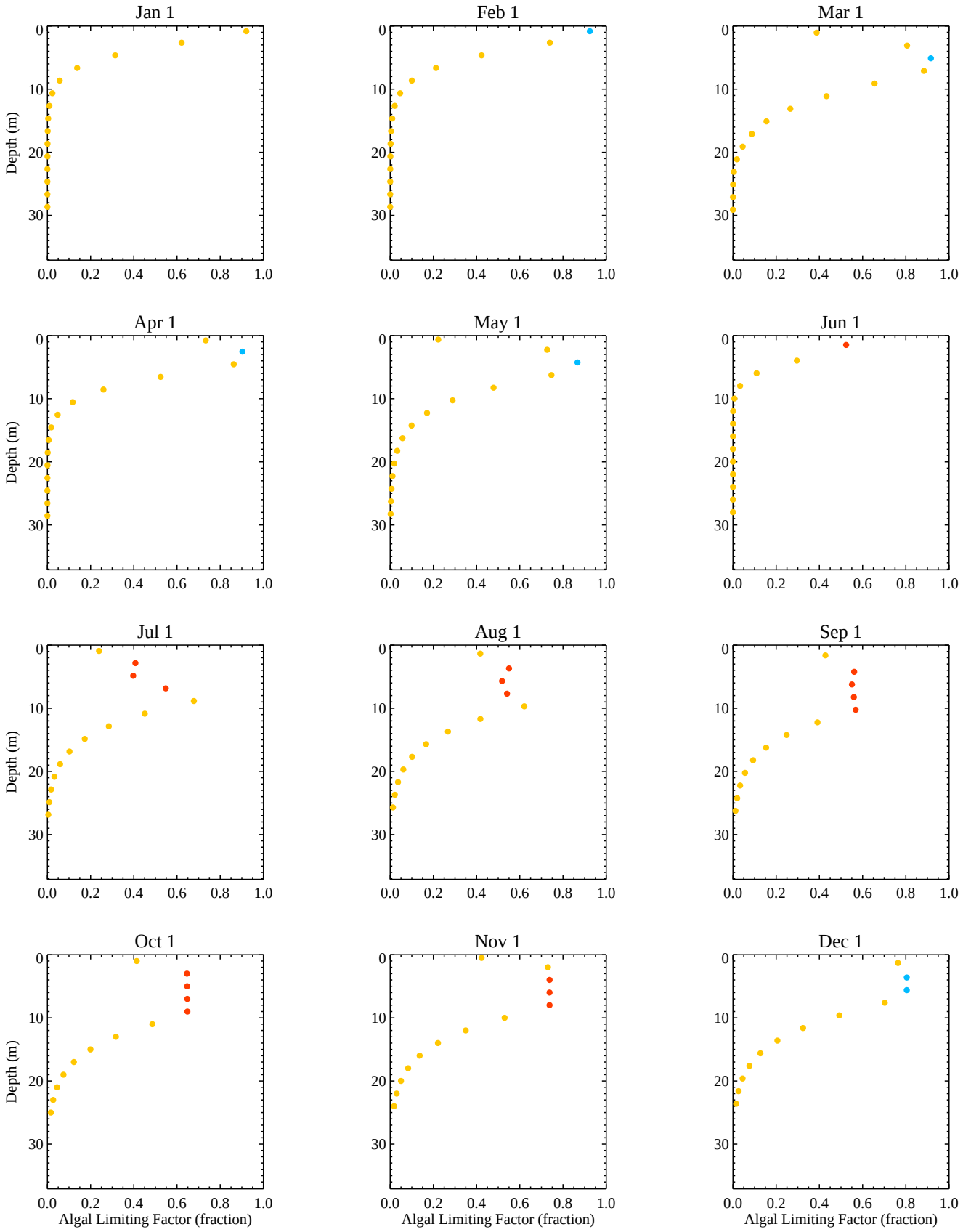

Figure J-25. Vertical profiles of algal limiting factor at Sandy Creek (Segment 161) during 2005.

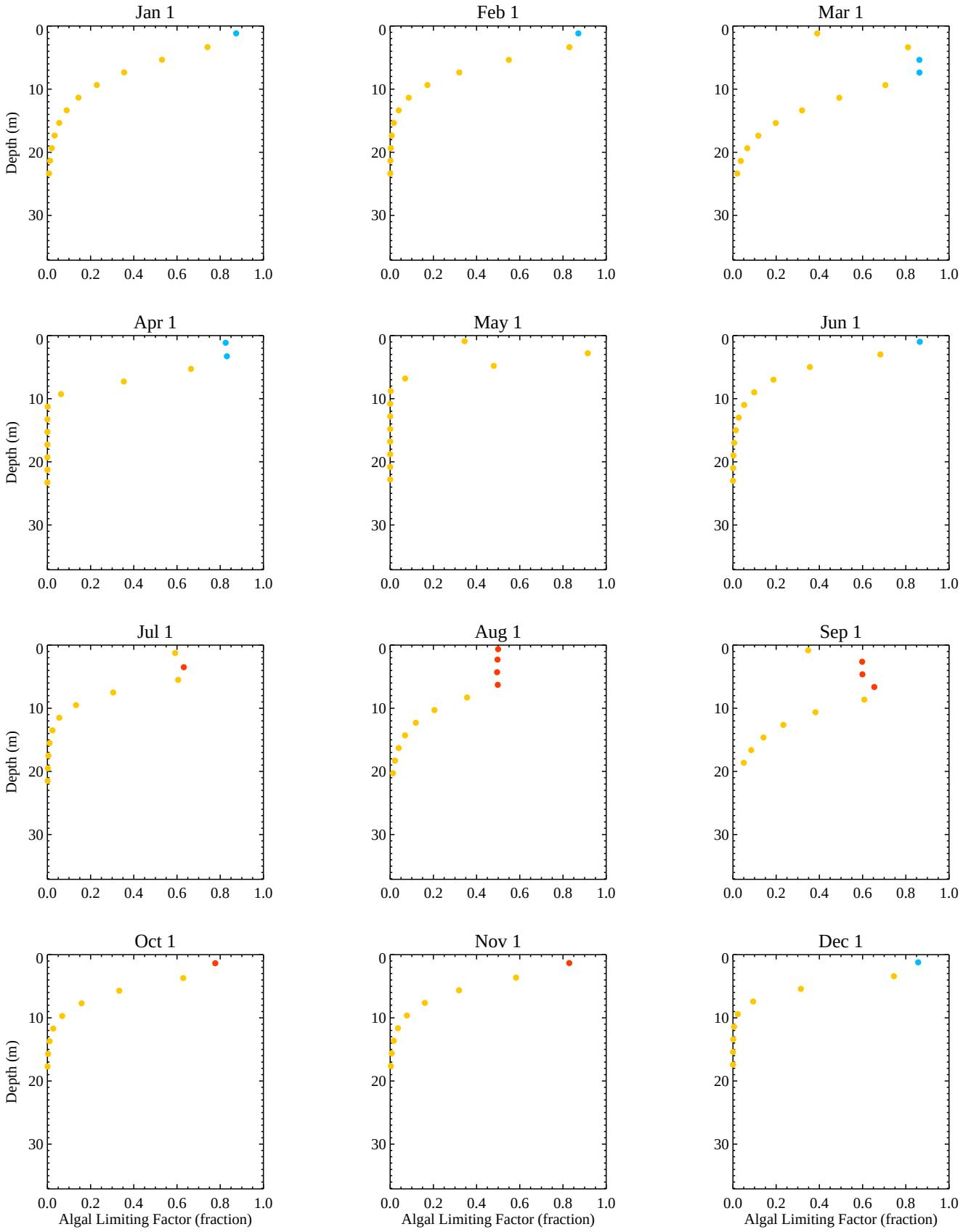

Figure J-25. Vertical profiles of algal limiting factor at Sandy Creek (Segment 161) during 2006.